Advances in Material Research and Technology

Sabu Thomas
Amadou Belal Gueye
Ram K. Gupta *Editors*

Nanostructured Materials for Supercapacitors

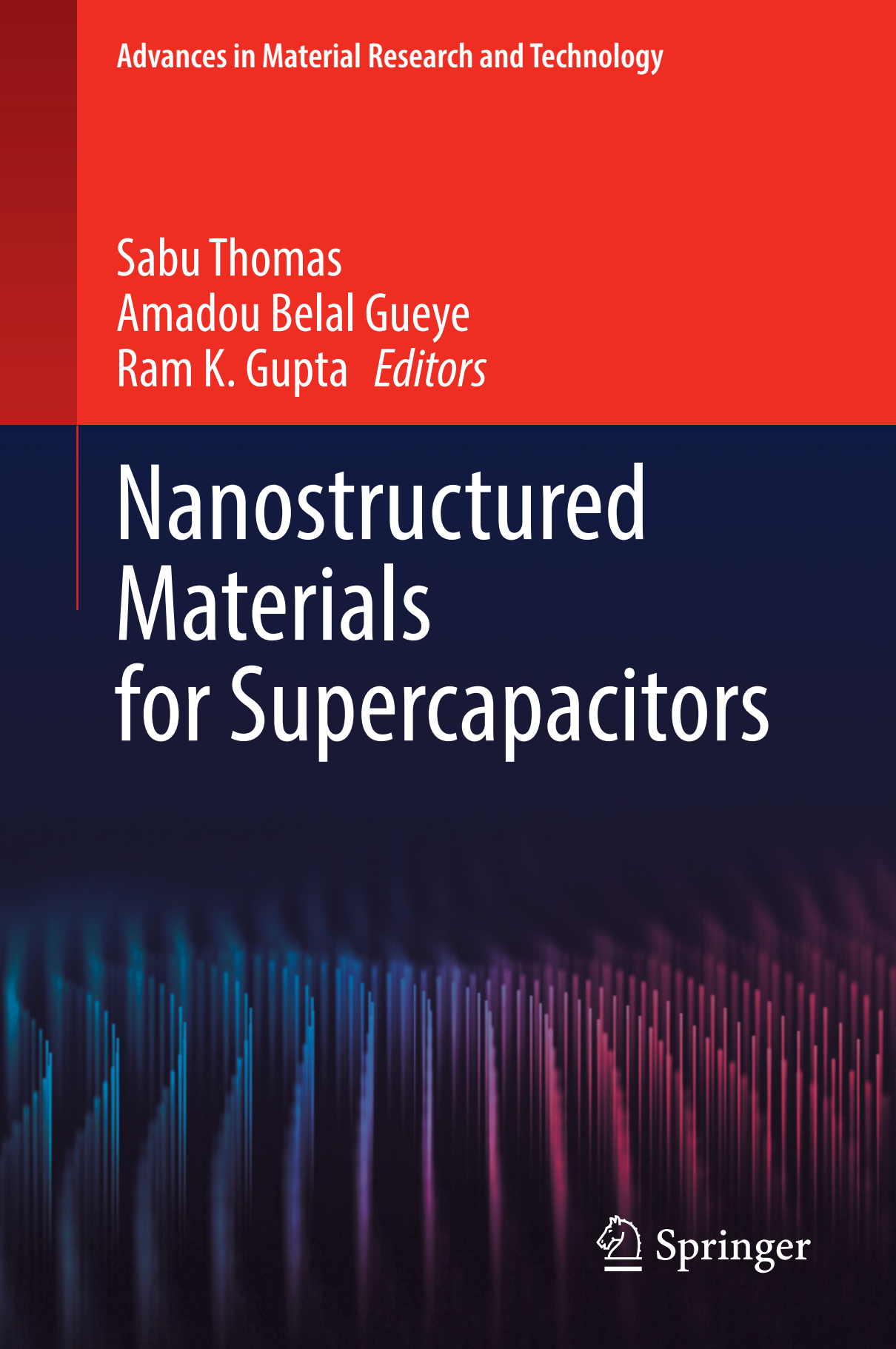

Springer

Advances in Material Research and Technology

This Series covers the advances and developments in a wide range of materials such as energy materials, optoelectronic materials, minerals, composites, alloys and compounds, polymers, green materials, semiconductors, polymers, glasses, nanomaterials, magnetic materials, superconducting materials, high temperature materials, environmental materials, Piezoelectric Materials, ceramics, and fibers.

More information about this series at https://link.springer.com/bookseries/16426

Sabu Thomas · Amadou Belal Gueye ·
Ram K. Gupta
Editors

Nanostructured Materials for Supercapacitors

Springer

Editors
Sabu Thomas
School of Chemical Science
Mahatma Gandhi University
Kottayam, Kerala, India

Amadou Belal Gueye
School of Chemical Science
Mahatma Gandhi University
Kottayam, Kerala, India

Ram K. Gupta
Department of Chemistry
Kansas Polymer Research Center
Pittsburg State University
Pittsburg, KS, USA

ISSN 2662-4761 ISSN 2662-477X (electronic)
Advances in Material Research and Technology
ISBN 978-3-030-99301-6 ISBN 978-3-030-99302-3 (eBook)
https://doi.org/10.1007/978-3-030-99302-3

This Springer imprint is published by the registered company Springer Nature Switzerland AG
The registered company address is: Gewerbestrasse 11, 6330 Cham, Switzerland

Preface

Supercapacitors are emerging as advanced energy storage devices which bridge the gap between batteries and conventional capacitors by providing high-power density (as of a capacitor) and high-energy density (as of a battery). Electrochemical double layer and redox process are two main charge storage mechanisms of supercapacitors. Approaches to combine both mechanisms in a supercapacitor to enhance its electrochemical properties are attracting considerable attention. The electrode materials used for the fabrication of supercapacitors can drastically affect the energy storage capacity of these devices. Many materials such as conducting polymers, carbon-based materials, layered structured materials, metal oxides, and sulfides are being used for supercapacitors. Types of materials and their morphology can affect the energy and power density of supercapacitors. This book reviews advances in this field in addition to presenting a brief history of supercapacitors as energy storage media and nanostructural materials. The nature of this technical book can serve as a very useful reference book or manual for a wide range of scientists, industrial practitioners, graduate and undergraduate students, and other professionals in the fields of science and education.

This book aims to cover the current cutting-edge advances in nanostructured materials for applications in supercapacitors. Nanoscale materials have many fascinating properties that are ideal for energy storage applications. In addition, approaches are aimed at their electronic, electrical, and morphological aspects to enhance their electrochemical performances. Many emerging nanomaterials such as aerogels, chalcogenides, and bio-derived carbons are covered. Novel approaches for the synthesis and tuning of their electrochemical properties are described in detail. This book consolidates information on synthesis and applications of nanomaterials for supercapacitors

with detailed characterization, mechanistic approaches, and theoretical consideration. Recent developments in advanced devices such as flexible and wearable supercapacitors using nanostructured materials are covered. This book provides fundamentals as well as advanced concepts to the readers for developing nanostructured materials for supercapacitors.

Ram K. Gupta
Associate Professor
Department of Chemistry
Kansas Polymer Research Center
Pittsburg State University
Pittsburg, KS, USA

Contents

Nanostructured Materials for Supercapacitors

Arun Thirumurugan, Kiruthiga Ramakrishnan, Ananthakumar Ramadoss, Prabhakaran Thandapani, Perarasu Thangavelu, R. Udayabhaskar, Mauricio J. Morel, Shanmuga Sundar Dhanabalan, N. Dineshbabu, K. Ravichandran, Radhamanohar Aepuru, R. V. Mangalaraja, and Ali Akbari-Fakhrabadi

Abstract A supercapacitor is considered to provide superior power density along with high energy density to overcome the issues of power density in a battery. The choice of electrode materials to achieve high power and energy densities is a crucial

A. Thirumurugan (✉) · K. Ramakrishnan
Sede Vallenar, Universidad de Atacama, Costanera 105, Vallenar, Chile
e-mail: arunthiruvbm@gmail.com; arun.thirumurugan@uda.cl

A. Ramadoss
Laboratory for Advanced Research in Polymeric Materials, Central Institute of Plastics Engineering and Technology, Bhubaneswar 751024, India

P. Thandapani
Materials and Low-Temperature Laboratory, Institute of Physics 'Gleb Wataghin', University of Campinas (UNICAMP), Campinas, São Paulo, Brazil

P. Thangavelu
Department of Chemical Engineering, Anna University, AC Tech, Chennai 600025, India

S. S. Dhanabalan
Functional Materials and Microsystems Research Group, RMIT University, Melbourne, Australia

N. Dineshbabu
1SSN Research Centre, SSN College of Engineering, Kalavakkam, Chennai, Tamilnadu 603110, India

K. Ravichandran
P.G, & Research Department of Physics, AVVM Sri Pushpam College (Autonomous), Thanjavur, India

R. Aepuru
Departamento de Ingeniería Mecánica, Facultad de Ingeniería, Universidad Tecnológica Metropolitana, Santiago, Chile

R. Udayabhaskar · M. J. Morel · R. V. Mangalaraja
Instituto de Investigaciónes Científicasy Tecnológicas (IDICTEC), Universidad de Atacama, Copayapu 485, Copiapo, Chile

R. V. Mangalaraja
Advanced Ceramics and Nanotechnology Laboratory, Department of Materials Engineering, Faculty of Engineering, University of Concepción, 4070409 Concepción, Chile

S. Thomas et al. (eds.), *Nanostructured Materials for Supercapacitors*,
Advances in Material Research and Technology,
https://doi.org/10.1007/978-3-030-99302-3_1

key point. However, several attempts have been done to achieve high power density, energy density, and long cyclic stability by attempting various electrode materials which include carbon-based materials, pseudocapacitive materials, new materials, and their composites. The tuning of morphology and composition was also attempted and showed significant improvements. This chapter deals with the new materials such as hydroxide, metal–organic framework, MXenes, nitrides, and their composites. The process and progress made on these novel materials are discussed with available recent literature.

Keywords Nanomaterials · Electrode materials · Supercapacitors · Nitrides · Hydroxides · Metal–Organic Frameworks · MXenes

1 Introduction

The high-performance electrochemical energy storage devices are becoming the cynosure of power backup technologies in automobiles such as hybrid electric vehicles and modern electronics as well. To achieve that, contemporary research has been engrossed in developing and improving efficient electrode materials. In recent times, better performance electrode materials such as carbon materials, metal oxides, hydroxides, carbides, sulfides, nitrides are being thoroughly investigated owing to their characteristics in the nano realms where nanotechnology enhances the device performance. Various things such as materials, fabrication routes, and many others affect the device's performance while enabling them to be potential energy-efficient materials. Therefore, developing some efficient ways to synthesize target material with required morphology and activity is crucial to get the potential for electrochemical applications which could be used for electronic devices. The development of nanocomposites with various combinations is important to utilize the characteristics of two or more materials in a single composite.

2 Nanocomposites for Supercapacitors

Several composites with carbon-based and pseudocapacitive materials have been attempted and found some interesting characteristics for the new nanocomposites. New novel materials such as MXenes, metal–organic frameworks, polymers, hydroxides, nitrides, and a few metal oxides along with conventional capacitive materials are attempted and obtained different kinds of results such as faradaic non-faradaic, a mixture of these two, and battery type behavior. Based on the electrochemical characteristics of the electrodes, the electrode materials are classified as capacitive

A. Akbari-Fakhrabadi
Advanced Materials Laboratory, Department of Mechanical Engineering, University of Chile, Santiago, Chile

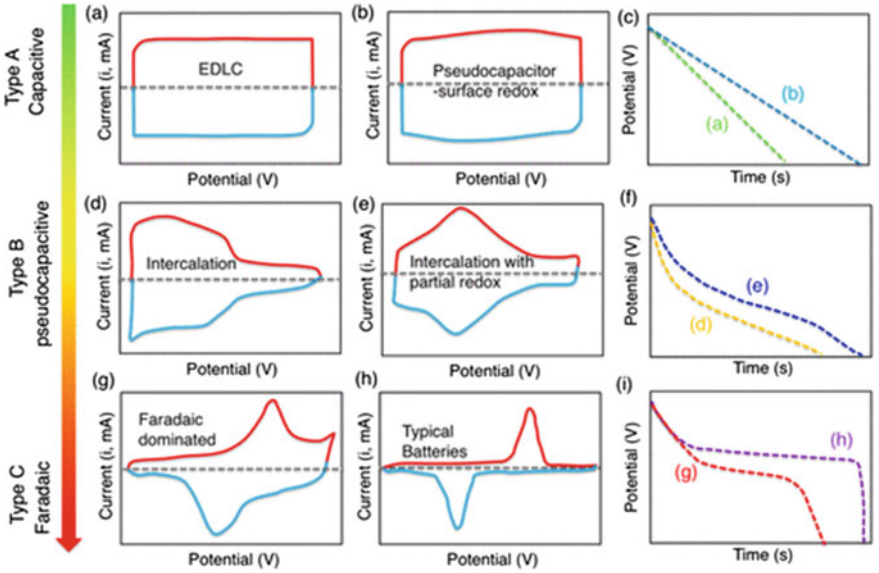

Fig. 1 The shape of cyclic voltammograms (**a**–**b**, **d**–**e**, **g**–**h**) and their corresponding GCD curves (**c**, **f**, and **i**) for different types of energy storage materials. Adapted with permission from reference [1], Copyright (2021), American Chemical Society

(EDLC), pseudocapacitive, and faradaic materials as shown in Fig. 1. Pseudocapacitive material may have the electrochemical properties of anyone, or a mixture of few among redox materials, intercalation-type materials.

2.1 Transition Metal Nitrides

Owing to its good electrical conductivity, high reactivity, and durable mechanical qualities, metal nitrides (MNs) are novel types of materials with features that can greatly improve performance. These materials are being used in energy storage devices, photocatalysis, sensors, and biological applications. To develop MNs, a variety of synthesis methods are available, based on the qualities and applications in which its synthetic frameworks are measured as the most important feature in defining the efficiency of nitrides. The size-dependent properties of MNs integrated with nanostructures, such as specific surface area, confirm the sufficient contact among active materials as well as electrolytes, allowing for a short dissemination path for ions transport and electrons resulting in improved performance. Furthermore, MNs have excellent mechanical stability, which helps to reduce the pulverization of electrode material during cycling [2–4].

Aside from the benefits mentioned above, the disadvantages of MNs that limit their practical application are also discussed. Synthesis of metal nitrides requires

multistep, high temperature (>800 °C) annealing with time to be synthesized in a controlled environment of specified crystalline plane phases, making their synthesis, complicated and uneconomical. The most important step in converting metal precursors into corresponding nitrides is a post ammonia reduction annealing. The structural features of the precursors can be well conserved, which is a major benefit of this conversion. Thereby the novel, cost-effective, and environmentally friendly methods are still necessary for producing high-quality MNs.

The bonding nature of nitrides determines their classification. Group I and II elements form nitrides with an ionic bond with excellent ionic conductivity, whereas group III and IV elements form a covalent bond with semiconducting or insulating nature and have a high melting point. Ionic, covalent, and metallic bonding contribute to metal-nitrogen bonding, which is necessary for its unique physicochemical properties. They are well suited for photoelectric applications, such as LEDs, laser diodes, and power electronics, due to their higher covalent nature [5–7].

Cui et. al prepared Nb_4N_5 nanochannels through Nb foil anodization followed by annealing for the first time, demonstrating their electrochemical performance as supercapacitor electrodes. In 1 $_M$ H_2SO_4 electrolytes, which are among the finest levels of nanostructured metal nitrides film electrodes, a capacitance of 226 mF cm^{-2} was achieved at 0.5 mA cm^{-2} of current density (CD). The electrochemical performance was ascribed to the Nb_4N_5 nanochannels with favorable structure, electrical conductivity, and good capacitive behavior. Mechanistic studies further confirmed its faradaic pseudocapacitance, which was derived from the proton integration as well as chemical adsorption caused by the abundance of valence ($_+5$) ions in Nb_4N_5. Furthermore, 70.9% of its initial capacitance remained, indicating good cycling stability. Even after 2000 CV cycles, 100% capacitance retention was achieved by coating a carbon layer on the Nb_4N_5@NC nanochannels electrode. The prepared Nb_4N_5 nanochannel structure can support the deposition of additional active capacitive materials to make hybrid electrode materials, also serve as a potential material for other energy-related applications [8].

Zhu et al. then investigated the assembly of nanostructured MNs on graphene for asymmetric supercapacitors (solid-state). By fully covering the graphene nanosheets and maintaining close contact among active nitride material and substrate, it ensured maximum use of conductive surfaces. The asymmetric supercapacitor made of TiN@GNSs and Fe_2N@ GNSs electrodes in (PVA)/LiCl electrolyte, delivered the SC of 58 F g^{-1} at CD of 4 A g^{-1} and was steady for ^{20,000} cycles. The device also demonstrated ED of 0.55 mWh cm^{-3} and PD of 220 mW cm^{-3} when examined at a high CD of 8 A g^{-1} [9].

Zhang et al. [10] studied lanthanum nitride (LAN) for energy storage application after calcining La_2O_3 in the NH_3 atmosphere. After 5000 cycles, 951 F cm^{-3} of capacitance was found in Na_2SO_4 (1 mol dm^{-3}) with CD of 1 A g^{-1} and 87% of the initial capacitance preserved at CD of 10 A g^{-1}. Long cycle life, as well as electrical charge transfer, were confirmed using a reversible electrode process. The use of nanoparticles (NPs) in aqueous electrolytes results in good capacitance. The symmetrical capacitor was also cycled and the obtained capacitance, lifetime, and ED were all good. The capacitance value obtained was 7–9.5 times more than that

of AC. During the charge–discharge process, the reversible reaction measured by diffusion and the electronic conductivity ensured longer cycle life and rate of charge transfer. The volumetric energy densities of the capacitor were extremely high, and it is expected that this capacitor will be used in the application of volumetric requirements. Additional research is being conducted to determine the exact charge storage mechanism of this material.

Wu et al. developed vanadium nitride/carbon (VN/C) membranes using a novel and simple approach. The VN/C (I) design was successfully prepared as a supercapacitor electrode material in this study, with carbon/VN networks with and porous structure. VN/C (I) showed a surface area of 523.5 m^2/g and exhibited outstanding electrochemical performance with low resistance value as well as good SC along with good cyclic stability. In 6 ^{M} KOH, VN/C (I) delivered a favorable rate ability at 30 A g^{-1} with 51% of capacitance retention and a capacitance value of 392 F g^{-1} at 0.5 A g^{-1}. Surprisingly, at PD of 800 W kg^{-1}, the assembled asymmetric device made of $Ni(OH)_2$/VN/C (I) produced a high ED of 43 Wh kg^{-1}, which fell to 32 Wh/kg at a higher PD of 4000 W/kg. Furthermore, after 8000 cycles, good cycle stability (82.9%) was achieved at 1 A g^{-1}. This simple method could be used to make other composite materials for hybrid supercapacitors by merging carbon-based metal oxide, nitride, and/or sulfide for various electrode materials [11].

Tan et al. [12] proposed an innovative method of combining polymerization as well as thermal treatment under NH_3/N_2 environment to make nanosheets of nitrogen-doped carbon/vanadium nitride NPs (N-CNS/VNNPs). In this synthesis method, pH value is significant for making the structure as well as improving the electrochemical behavior of N-CNS/VNNPs. This material was found to make of 2D nitrogen-doped carbon nanosheets and 0D vanadium nitride nanoparticles, according to the findings. The size of the carbon nanosheet and VN NPs both dropped when the pH was reduced from 2 to 0. This three electrodes system achieved a maximum SC of 280 F/g for the prepared electrode at a CD of 1 A/g. After 5000 cycles, the asymmetric device made of $Ni(OH)_2$ and N-CNS/VNNPs showed 89 F/g of capacitance value and 60% retention of capacitance at CD of 2.7 A/g. This asymmetric device exhibited a maximum ED of 29 Wh kg^{-1}. At CD of 0.5 A g^{-1}, N-CNS/VNNPs-0 delivered SC of 424 F g^{-1} (which is higher than N-CNS/VNNPs-1, N-CNS/VNNPs-2, and pristine VN). The asymmetric device showed ED of 29 Wh/kg and PD of 385 W/kg. Furthermore, after 5000 cycles, a maximum PD of 15 kW/kg with ED of 4.3 Wh/kg was achieved by maintaining 60% of SC at CD of 2.7 A g^{-1}. The surface of V_2O_5 xerogel, which served as both a template and an oxidative agent, in which (surface-initiated) reaction was carried out.

Using the phase-separation method intermediated by PAA-b-PAN-b-PAA (triblock copolymer), Ran et al. reported a hybrid electrode for supercapacitors. The block copolymer assembled on carbon nanofibers was used to adsorb NH_4VO_3 in the procedure of phase- separation. The treatment was carried out in an NH_3:N_2 (3:2) environment resulted in the development of vanadium nitride NPs that were consistently dispersed on the surface of nanofiber. The capacitance of 240 F/g was attained at a 0.5 A/g with good rate capability with 72% capacitance retention at CD of 5 A/g in 6 M KOH at the voltage range from −1.1 to 0 V. Furthermore, using

porous carbon fiber@VN and $Ni(OH)_2$ (as negative and positive) electrodes, the device (asymmetric supercapacitor) was assembled. This device produced a higher ED of 39 Wh kg^{-1} at a PD of 400 W kg^{-1}. It also demonstrated good electrochemical stability, suggesting that it could be served as a promising energy storage device [13].

Ouldhamadouche et al. demonstrated nano-structuration using vanadium nitride (VN) on a vertically aligned carbon nanotube (CNT) template (deposited by DC-sputtering). This led to the development of hierarchically composite electrodes for micro-supercapacitor applications made up of porous VN grown on CNTs. The electrodes performed well in K_2SO_4 (0.5 M) mild electrolyte, with an aerial capacitance value of 37 mF/cm^2 at 2 mV/s of scan rate. Furthermore, after 20,000 cycles, the capacitance decayed by only 15% and was found to increase with the thickness of the VN deposition. The formation of oxide layers on the vanadium nitride surface, which are favorable for energy storage behavior, was revealed by XPS analyses of the electrodes (before and after cycling). For micro-supercapacitors, such electrodes could contend with other MNs related electrodes. In comparison to other alkaline electrolytes reported, this work shows that the K_2SO_4 electrolyte can be used for VN to attain stability.

The supercapacitor device made of VN nanowire (NW) and VOx NW (as anode and cathode respectively) was reported by Lu et al. The asymmetric device displayed a stable potential range of 1.8 V and outstanding cycling stability, with only 13% decreased capacitance after 10,000 cycles. Furthermore, the asymmetric device produced 0.61 mWh cm^{-3} ED (at 0.5 mA/cm^2) and 0.85 W cm^{-3} PD (at 5 mA/cm^2). When compared to the reported quasi/solid-state supercapacitor devices, these values were significantly higher. This work was the first to show that VN NWs can be used as an anode, which could enhance the performance of supercapacitor devices. VN NWs can be used as a high-energy anode, which could help energy storage devices perform better [14].

Cao et al. synthesized Mo_5N_6 crystals through in-situ conversion of MoS_2. The method was expanded to synthesize W_5N_6 and TiN, demonstrating the adaptability of this general approach. They demonstrated a new way of conversion strategy from transition metal dichalcogenides (LTMDs) to their corresponding ultrathin nitrides. This facilitated the production of 2D crystalline MNs and opened the door to a previously inaccessible class of 2D materials. The in-situ conversion of MoS_2 to 2D Mo_5N_6 revealed a reduction in thickness after conversion. By converting a four-layer MoS_2 into a 2D Mo_5N_6 (as thin as 2.1 nm), electrical measurements revealed that the converted metallic Mo_5N_6 with good conductivity, with a low resistance value (100 Ω/square). The strategy proposed by the authors will enable the development of large, high-quality 2D MNs, which will meet the demands of high-performance energy storage devices [15].

Metal nitrides have many advantages over metal oxides, hydroxides, and conducting polymers. MNs, for example, have a long lifespan, high electrical conductivity, and a significant potential window. When compared to metal oxides, the physical, chemical, and electrochemical properties of MNs offer a lot of room for experimentation because their fundamental properties are in demand for a variety of energy

applications. In addition, to tailor nanostructure MNs with better performance, low-cost synthesis procedures are required. Finally, given the recent advancement in flexible electronics, the fabrication of advanced metal nitrides electrodes for energy storage application is a critical task that must be tackled right away.

2.2 Hydroxides

Due to the demand for advanced devices of electrochemical energy storage, supercapacitors with good charge–discharge rate, PD, and cycling stability have recently received a lot of attention, but they affect by low ED issues in real-time applications. As a result, much effort has gone into finding suitable electrode materials for supercapacitors, to boost ED while preserving PD as well as cycling stability [16, 17]. The electrochemical active surface area of electrode materials determines their SC. Metal oxides, hydroxides, nitrides, carbides, chalcogenides, and phosphates, among other layered materials with high surface area, have been widely explored as potential electrodes for supercapacitors [18].

Because of their superior electrochemical performance, metal hydroxides have gotten more attention. Due to their high capacitance, good electrolyte affinity, and ease of fabrication, they are being investigated in aqueous electrolytes. The development of layered hydroxide electrodes with pseudocapacitive behavior has been the focus of recent discoveries. Most of them have two crystalline structures (hydrotalcite or brucite) with open interlayers or open tunnels, allowing for ion insertion and extraction during redox reactions. Some hydroxides have charge-balancing intercalated anions in their layered structure, which are exchangeable and provide additional routes for tailoring the charge storage properties. Furthermore, the metal site in metal hydroxides acts as a redox-active center with various oxidation states, and its chemical property allows for enhanced charge storage behavior and optimal performance [19, 20].

Binary metal compounds have recently attained much interest. Owing to its intrinsic conductivity, environmental friendliness, and low cost. In this regard, $NiCo(OH)_2$ gained a lot of attention. However, due to faradic reactions, $NiCo(OH)_2$ usually suffered from unsatisfactory structural deterioration which reduced the duration of the cycling process. Previous reports have suggested that structural designs such as doping of heteroatom, coating of a protective layer, pores creation, particle size reduction, and morphology control are effective strategies for improving structural stability and electrochemical activity. Superior electron and ion transport kinetics will be induced by the improved electrical conductivity and high surface area, exposing vast active sites and stimulating electrochemical performance [21, 22]. The performance is mainly reliant on electrode materials. As a result, developing a suitable material with outstanding storage properties is critical. Dong et al. demonstrated nickel–cobalt hydroxide nanosheet arrays (with honeycomb-like structure), fully-fledged on nickel foam using a simple solvothermal process in this regard. At 20 mA cm^{-2}, the material delivered an areal capacitance of 267 mF/cm^2 than

$Ni(OH)_2$ (31 mF/cm^2) and $Co(OH)_2$ (88 mF cm^{-2}) electrodes. After 5000 cycles, the observed capacity retention was 83.8%, making it a viable electrode for energy storage applications [23].

Owing to their high theoretical capacity, layered double hydroxides (LDH) are appealing for supercapacitors as electrode materials. However, their structure frequently fails to withstand long charge/discharge cycles, resulting in a short lifespan. Wang et al. also reported using an inert Zn cation (electrochemically) as a sacrificial agent to enhance the cycling stability of Ni-Co LDH nanosheet for supercapacitors (Zn-Ni-Co LDH). The SC of 232 mAh g^{-1} at CD of 1 A g^{-1} along with an increase of capacity over 500% after 20,000 cycles at 20 A g^{-1} have been achieved with an optimal Zn content. A hybrid capacitor made of Zn-Ni-Co LDH material exhibited ED of 40 kW/kg and a PD of 16 kW/kg for practical applications, as well as exceptional cycling stability (20,000 cycles). The results of this study opened up a new avenue for developing durable electrodes for advanced supercapacitors with good ED value and cycling stability [24].

Power densities in supercapacitors are typically high but energy densities are low. It is critical to develop novel electrodes in terms of refining the energy densities of supercapacitors. Zhang et al. developed two redox-active electrode materials for dual pseudocapacitors, which included Ni-Co hydroxide/oxide hydroxide coated with reduced graphene oxide (hrGO) as cathode and rGO/Fe_2O_3 nanorods as an anode, respectively. The assembled device at 1.6 V delivered ED of 91 Wh/kg at 800 W/kg of PD with good cycling stability. The maximum PD of 24,008 W/kg was attained at 30 A/g. Thus, it can be performed as an efficient device for various applications [25]. For advanced battery type supercapacitors, Dai et al. investigated core–shell Fe_2O_3–Fe_3C–C nanochains as well as NiCo–CHH microspheres. The Fe_2O_3@Fe_3C@C anode they developed, showed an SC of 611 C/g with good rate capability. The fabricated cathode (NiCo–CHH) delivered a high SC of 814 C/g and good cycling stability. As a battery-type capacitor, the NiCo-CHH/Fe_2O_3–Fe_3C–C device delivered a high ED of 95 Wh kg^{-1} with good stability. Furthermore, Raman spectroscopy was used to demonstrate the reversibility of cathode as well as the synergistic effects of Ni and Co ions, showing its storage mechanism. Hence, the results revealed new information about high-performance battery-type supercapacitors [26].

2D materials such as layered metal hydroxides (LMHs), MXene, and graphene have attained more interest due to their extraordinary storage, electrical as well as optical properties. Ultrathin layered metal hydroxides (LMHs) nanosheets with active sites, high surface area, and ion-intercalation ability have been studied extensively in recent years. In catalysis, batteries, and supercapacitors, numerous LMHs have demonstrated outstanding performance. $Ni(OH)_2$, in particular, has been a competitive electrode for supercapacitors due to its very high theoretical capacitance (3750 F/g) and low cost. Their activity is still constrained by their lower rate and lack of cycle stability. In general, synthesizing LMHs along with desirable structures and performance is a difficult chore. Xia et al. proposed a novel synthesis method using a household microwave oven. $Ni(OH)_2$ NSAs exhibited a capacitance of 2516 and 1273 F g^{-1}, respectively at CD of 1 A/g and 20 A/g. Furthermore, a $Ni(OH)_2$/AC aqueous hybrid capacitor with a large ED of 67 Wh/kg at 400 W/kg and good

cycle stability of 85.2% was demonstrated. Other LMH NSAs, such as vertically aligned $Cu_2(OH)_3NO_3$ nanosheet arrays (NSAs), can also benefit from the low-cost microwave-assisted synthesis method. The exclusive nanostructure, development of binder-free electrodes, and highly efficient microwave aqueous method could all contribute to the outstanding electrochemical behavior of LMH NSAs. These findings showed that microwave-assisted synthesis has the potential to produce LMH NSAs simply and rapidly for a different range of applications. In comparison to traditional methods, the microwave-assisted synthesis route reported here has several benefits, together with rapid growth, ease of equipment as well as low cost, confirming it as a promising option for advanced fabrication of LMH NSAs on conductive foams. Furthermore, even after 5000 cycles, the hybrid capacitor showed cycling stability of 85.2%. This synthetic approach was found to have a less reaction time and excellent electrochemical performance. This research presented a novel synthesis method for obtaining LMH NSAs, as well as a cost-effective method for designing high-performance nanostructures for a variety of applications [27].

Cheng et al. also used a strategy to successfully prepare hollow spheres of Ni–Mn hydroxide [28]. In the first step, solid spheres of NiMn-glycerate were obtained as templates. The templates were etched to produce hollow spheres of Ni–Mn hydroxide after being treated in a mixture of N-methyl-pyrrolidone and water. This electrode material demonstrated SC of 1680 F/g at 2 A/g and was maintained at 1068 F/g at 15 A/g owing to the hollow structures and high surface area. Meanwhile, over 5500 cycles at 10 A g^{-1}, a decreased SC of only 3% was achieved. Furthermore, the fabricated device made of Ni-Mn hydroxide and activated carbon showed a specific ED of 43 Wh/kg at 1703 W/kg, indicating that it could be a promising electrode material. The specific ED (29 Wh/kg) at 12,747 W/kg) was also maintained. The observation showed that the hierarchical Ni-Mn hydroxides hollow spheres had a great deal of potential in the area of energy storage. Xia et al. developed a three-dimensional $Ni/Co(OH)_2$ composite film electrode for supercapacitors. The nano ramified walls of the 3D nano-Ni film served as a backbone for anchoring $Co(OH)_2$ nanoflakes, resulting in a composite electrode. The $Co(OH)_2$ nanoflake in the composite showed a specific capacitance of 1920 F/g at 40 A/g, corresponding to high ED of 80 Wh/kg at PD of 11 kW/kg. This composite film regarding supercapacitors with high ED, PD, and good stability, making it suitable electrode materials for advanced energy storage devices.

2.3 Metal–Organic Frameworks (MOFs)

Metal–organic frameworks- a new class of materials including metal ions and organic ligands along with porous nature suitable for various applications such as catalysis [29], gas storage and separation [30], electrochemical sensors [31], and energy storage [32]. The unique characteristics of high specific surface area, adjustable pore structure, functional groups attachment, and higher thermal and chemical stabilities make the MOF suitable for supercapacitor applications [33]. The opportunity to tune

the structure and morphology of MOF attracted researchers to attempt new morphologies of MOF adjusting simple experimental parameters. MOF has the highest theoretical specific surface area of around 14,600 m^2g^{-1} [34] and the experimentally achieved surface area of MOF is 7838 m^2g^{-1} [35]. Because of the versatility of MOF, the number of reports on the utilization of MOF for supercapacitor applications has increased every year [36].

Xu Zhang et al. developed Ni/Co-MOF various morphologies by just adjusting the molar ratio of the precursors. The schematic process for the development of various morphologies of MOF by tuning the molar ratio of precursors is shown in Fig. 2. Ni-MOF without Co showed a spherical morphology with a size of 3 μm containing needle shape on its spherical surface. The morphology was changed to a broken hollow sphere with a size of 300 nm was observed when the Co^{2+} ions were introduced in the MOF with a molar ratio of 5:1(Ni^{2+}: Co^{2+}) and the needle shape morphology on its surface got disappeared. These kinds of voids in the materials could be an advantage for supercapacitor applications as they could provide enough active

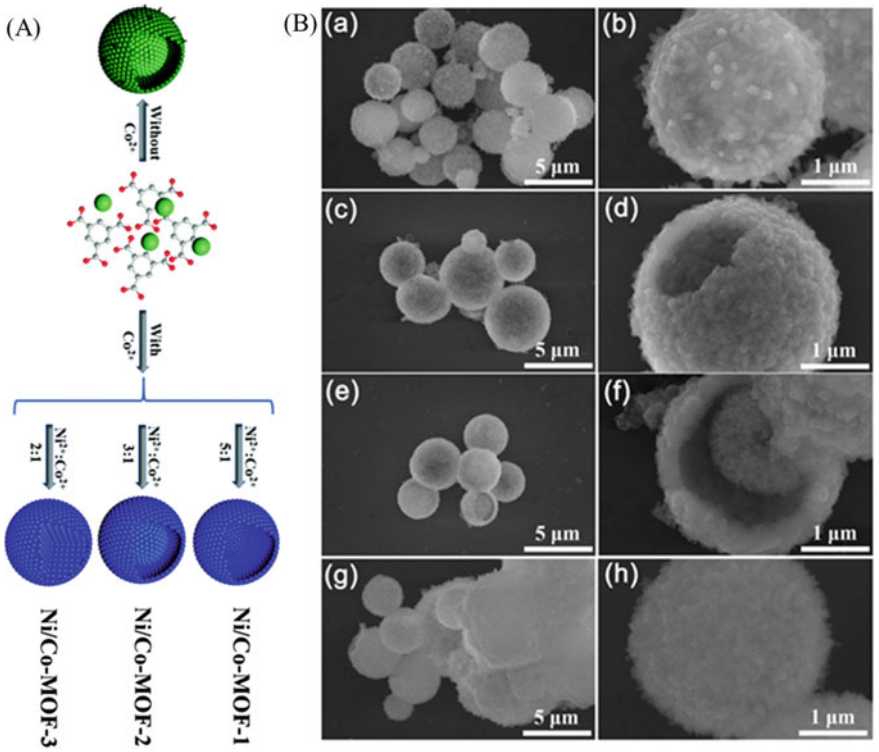

Fig. 2 **A** Schematic process of the fabrication process for Ni and Ni/Co-MOFs, **B** SEM Micrographs of MOFs with various magnifications-(**a**–**b**) Ni-MOF, **c**–**d** Ni/Co-MOF-1, **e**–**f** Ni/Co-MOF-2, and **g**–**h** Ni/Co-MOF-3. Adapted with permission from reference [37], Copyright (2021), Royal Society of Chemistry

contact area with electrolytes, and it could reduce the diffusion length of electrons and ions for the enhanced electrochemical activity. The yolk-shell morphology was observed by increasing the Co^{2+} ions to change the Ni/Co ratio to 5:3 (Ni_2^+: Co^{2+}) and further increasing Co^{2+} with Ni^{2+} ions as 5:1 ratio resulting in the solid spherical morphology. The obtained morphologies with a different molar ratio of Ni and Co are observed from the FESEM micrograph as shown in Fig. 2. The electrochemical performance of these morphologies of Ni–Co–MOF suggests that the hollow sphere morphology is best for the Ni/Co–MOF as it showed the highest specific capacitance of 1498 F/g with a current density of 1 A/g in a potential window of 0–0.6 V. Whereas the yolk-shell and solid sphere morphologies of MOF demonstrated the specific capacitance of 1244 and 1065 F/g, respectively. The study suggests that the small variation in the molar ratio of precursors or any other experimental parameter could strongly influence the resulting morphology and their characteristics.

It is also worth noting that the size of the MOF is important as the micro-supercapacitors are attracted highly as it is considered in present days due to the lightweight and foldability of wearable devices. Dai et al. reported the comparison for the effect of bulk and nanosheet (less than 10 nm) of MOF (Co_2(CoTCPP)($PZ)_2$). The lateral dimension of bulk MOF was observed as 2.6 μm and the thickness of nanosheet MOF was observed as 6.6 nm through transmission electron and atomic force microscopy. The BET surface area of bulk and nano MOF was estimated as 175 and 431 m^2/g, respectively. The pore size of both MOFs is lies between 2 and 2.75 nm. The electrochemical supercapacitor performance of bulk (MN-MSCs) and nano (MN-MSCs) MOF is shown in Fig. 3. It shows the areal capacitance with increasing scan rate and current density (Fig. 3a–b). The bulk MOF was tested with electrode thickness of bulk, 6, 12, 18, and 24 μm and the observed areal capacitance was increasing when the electrode thickness was reduced. The better areal performance was observed for nano MOF compared to bulk as seen from Figs. 3a–b. Similarly, the specific capacitance and capacitance retention were better for the nano MOF when it is compared with bulk MOF (Fig. 3c–d). Even with the larger scan rate of 1000 mV/s the MN-MSC showed the areal capacitance around 9 mF/cm^2, whereas the same was reduced to around 1 mF/cm^2 for MB-MSC. The capacitance retention of around 6 mF/cm^2 was observed for MN-MSC with a higher current density of 10 mA/cm^2 and the same has been reduced to the lowest of 1 mF/cm^2 for MB-MSC. The effect of CNT due to the addition in the electrode material is excluded by checking the performance of the micro supercapacitor with an increasing fraction of CNTs. The highest areal capacitance of around 28 mF/cm^2 was observed for MN-MSC and 96% of capacitance retention was observed for the same even till 10,000 cycles. The decreasing trend of capacitance retention was observed for the MB-MSC. The electrochemical performance was maintained up to 97% even with the bending states from 30 to 180° shows that the mechanical flexibility of MN-MSC and the MB-MSC could only be able to maintain 79% of its initial capacitance value. The electrochemical results along with the bending experiments suggest that the electrode of MOF with nanosheets could perform better the MOF in bulk form.

The only limitation of MOF for supercapacitor application is its low conductivity and weak electrolyte ion transport performance. The charge transfer process

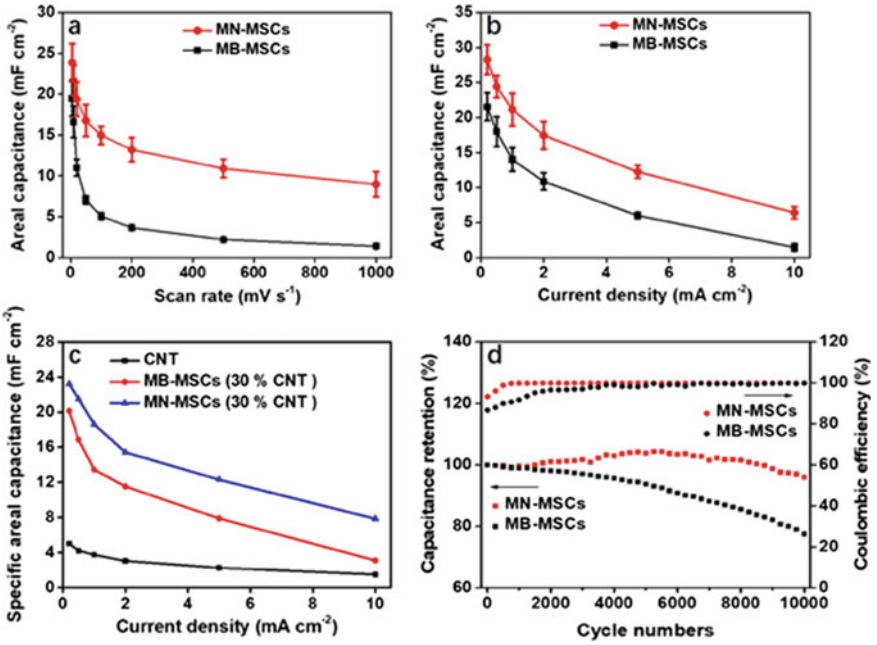

Fig. 3 The areal capacitance of MSCs at various **a** scan rates, **b** current densities, **c** Areal capacitance of bare CNT and MSCs (30% CNT) at various current densities. **d** capacitance retention and coulombic efficiency at 5 mA/cm^2. Adapted with permission from reference [38], Copyright (2021), Elsevier

is assumed from the process of hopping, through space, and bond [39]. To overcome these issues with MOF, good conducting materials could be coupled with MOF to develop hybrid composite materials of MOF. Materials belonging to the carbon family such as graphene, graphene oxide, carbon dots, carbon nanotubes, and carbon nanofiber are the best conducting materials among the other available materials for making composite materials. The composites of MOF with these carbon-based materials are attempted and demonstrated their successful characteristics for various applications including electrochemical applications. Among carbon-based materials, CNT is attractive because of its electrical conductivity and high surface area. Sreekanth et al. developed marigold flower-shaped Ni-MOFs decorated on multiwalled CNT through microwave irradiation and showed the formation of the microspheres with nanosheets. In MOF/MWCNTs, the composite formation was achieved without changing the microsphere and nanosheet morphology of MOF. The MOF microsphere was uniformly attached to the MWCNTs without any chemical treatment for the attachment. The morphology of MOF and its composites with MWCNT was observed from FESEM as shown in Fig. 4. Similarly, several composites of MOF with various materials with specific characteristics have been attempted

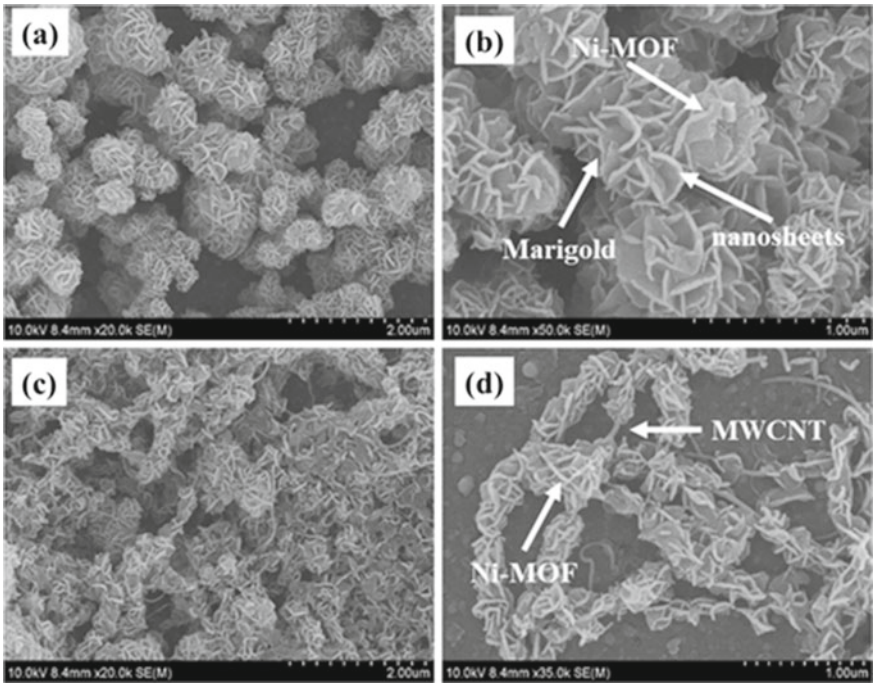

Fig. 4 SEM micrograph of bare Ni-MOF (**a**, **b**) and Ni-MOF@CNT (**c**, **d**) at different magnification. Adapted with permission from reference [40], Copyright (2021), Elsevier

and showed better performance compared to bare MOF. For the progress and comparison on MOF-based composites, the supercapacitor performances of a few MOF composites are given in Table 1.

From the table, it is understood that the composites of MOF showed significant improvement in the capacitance value and the capacitance retention. Further improvement could be achieved by developing a suitable combination of materials for the formation of composites.

2.4 MXenes

MXenes are the new group of two dimensional materials of transition metal carbides or nitrides utilized in energy storage [56], catalysis [57], water purification [58], electromagnetic interference shielding [59], lubricants [60], electrochemical actuators [61], solar cells [62], water splitting [63], electronic and photonic devices [64], wearable biosensor [65], and theranostic applications [66]. MXenes are synthesized typically by etching of A layer from the MAX (or $M_{n-1}AX_n$), (M—transition metal, A—elements from A group and X—carbon/nitrogen and n = 1–3). Few research

Table 1 Comparison of electrochemical performances MOF and their composites

Composites	Electrolytes	Specific capacitance (F/g)	Capacity retention	Cycles	Reference
rGO/Zn-MOF@PANI	$1MH_2SO_4$	371.91	82	5000	Le et al. [41]
AZIF8	0.5 M Na_2SO_4	107	91.2	5000	Boorboor Ajdari et al. [42]
2D Ni-HAB MOFs	1 m KOH	420	90	12,000	Feng et al. [43]
Zn/Ni MOF	3 M KOH	161.50	90	3000	Jiao et al. [44]
Zn-doped Ni-PTA (MOF-2)	6 m KOH	1620	91	3000	Yang et al. [45]
Cu-HHTP NW	3 m KCl	202	80	5000	Li et al. [46]
Tb^{III} MOF	2 M of KOH	346	93	2000	Xia et al. [47]
ZZIF	0.5 M of Na_2SO_4	500	94	5000	Boorboor Ajdari et al. [42]
MZIF	0.5 M of Na_2SO_4	315	95	5000	Boorboor Ajdari et al. [42]
manganese1,4- benzene dicarboxylate (Mn-BDC)	1 M Na_2SO_4	1590	82	3000	Sundriyal et al. [48]
ZIF–PPy	1 MNa_2SO_4	597.6	90.7	10,000	Xu et al. [49]
PANI-ZIF-67-CC	3 M KCl	371	80	2000	Wang et al. [50]
Co-MOF/rGO	1 M Na_2SO_4	1521.6	> 95	1500	Wang et al. [51]
PANI/UiO-66	6 M HNO_3	1015 F	91	5000	Shao et al. [52]
CNF@c-MOF	3 M KCl	125	99	10,000	Zhou et al. [53]
Ni-MOF with CNT	6 M KOH	1765	95	5000	Wen et al. [54]
Ni-MOF/Cabon nanowalls	1 M KOH	677	92.3	5000	Zhang et al. [55]

groups have done an enormous amount of effort to understand the MXene structure and its characteristics by theoretically and by developing new synthesis methods for various MXenes such as $Ti_3C_2T_x$, Ti_3CNT_x, Ti_2CT_x, Hf_3C_2Tz, V_2CT_x, Nb_2CT_x, $Nb_4C_3T_x$, $Ta_4C_3T_x$, $Ti_4N_3T_x$, etc., and still exploring new combinations. MXenes are having a metallic structure as well as semiconductor structures depending on the choice of metal, surface group, and carbon/ nitrogen. The better chemical multiplicity

and the variation in the structure make the MXenes attractive for various applications. The magnetic characteristics of the MXenes are also predicted and categorized as shown in Fig. 5. The required magnetic and electronic properties of the MXenes could be achieved from the suitable combination. The formation of MXene structure can be easily understood from the Fig. 5. The properties of MXenes could be tuned by the selection of transition metal and surface groups. The schematic band structure is also shown in Fig. 5. Thermal activation process could be adopted for the transition of semiconductor transport behavior to metallic for organic molecule intercalated MXenes [64]. MXenes are showing temperature dependent electrical characteristics and transition occurs between semiconductor and metallic natures. The conductivity of few MXene could be improved by vacuum annealing and the transition might be due to the removal of functional groups, intercalant, and water molecules. The surface treatment environment of MXenes is important as the surface might get oxidize and form oxide materials and by products [67]. Proper treatment has been demonstrated to achieve the better DC conductivity of 9880 S cm^{-1} for $Ti_3C_2T_x$. Further the physicochemical characteristics of the MXenes has been tuned or adjusted by developing MXene composites with various combinations of materials.

MXenes are found as new electrode materials for supercapacitor applications due to the architecture with open structure, high electronic conductivity, effective ion or electron transfer, and distinctive blend of conductive nature with hydrophilicity. One of the easy synthesis processes of MXene is the immersion of the MAX phase in hydrogen fluoric acid with sonication of certain times and this etching process results in the selective etching of aluminum layers and replaces them with OH and F surface

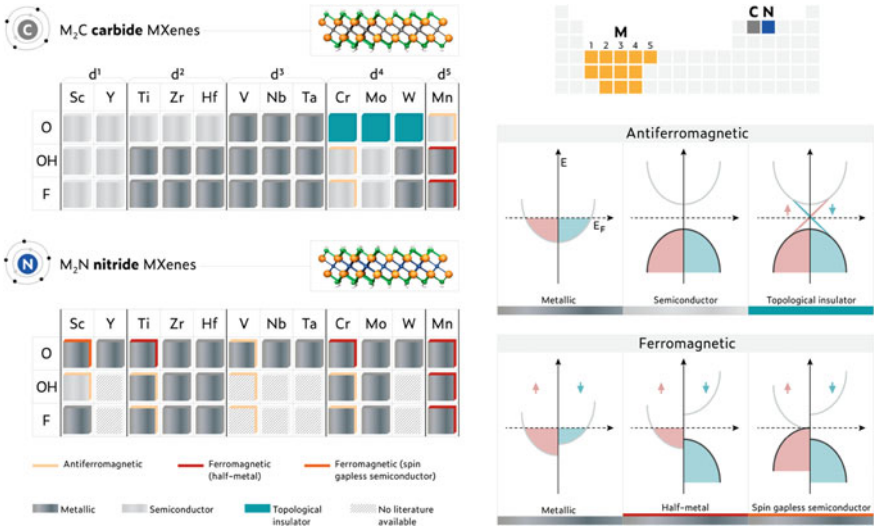

Fig. 5 Electronic and magnetic characteristics of M_2CTx and M_2NTx MXenes (Theoretical prediction). Adapted with permission from reference [64], Copyright (2021), American Chemical Society

groups. The schematic process for the simple synthesis process of MXene from the MAX phase is shown in Fig. 6a. Further, the restacking, metal oxide insertion and foam type structure formation are done with filtration and simple chemical treatment (Fig. 6b). It is also reported that 93% of transparency was achieved through a spin coating of $Ti_3C_2T_x$ colloidal solution with vacuum annealing at 200 °C [56]. The bare MXene itself shows better capacitive behavior than few available electrode materials for supercapacitor applications. But still, it is worth attempting the development of MXene composites with carbon-based or any other active electrode materials as the capacitance and capacitance retention may go further in a better way.

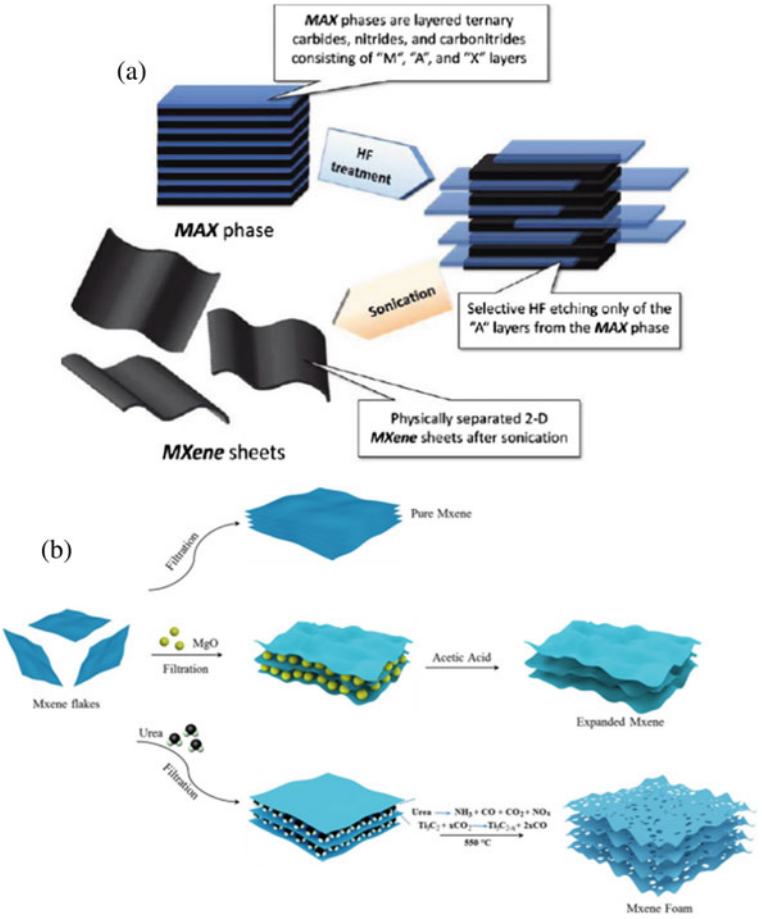

Fig. 6 **a** Schematic process for the synthesis of MXenes. Adapted with permission from reference [68], Copyright (2021), American Chemical Society. **b** Synthesis process schematic for the preparation of various forms of MXene. Adapted with permission from reference [69], Copyright (2021), Elsevier

The fraction of MXene in the nanocomposite is also important as the fraction of MXene plays a key part in electrochemical performance. The MXenes have the role for the capacitive performance even when it is in the composites, which is evaluated by forming the MXene composite with a layered double hydroxide (LDH). The electrochemical performance was evaluated with the LDH composites prepared with 20, 30, and 50 mg of MXene and shown in Fig. 7. The morphology of LDH covered on the exfoliated MXene was evidenced from the FESEM micrograph for the 30 mg

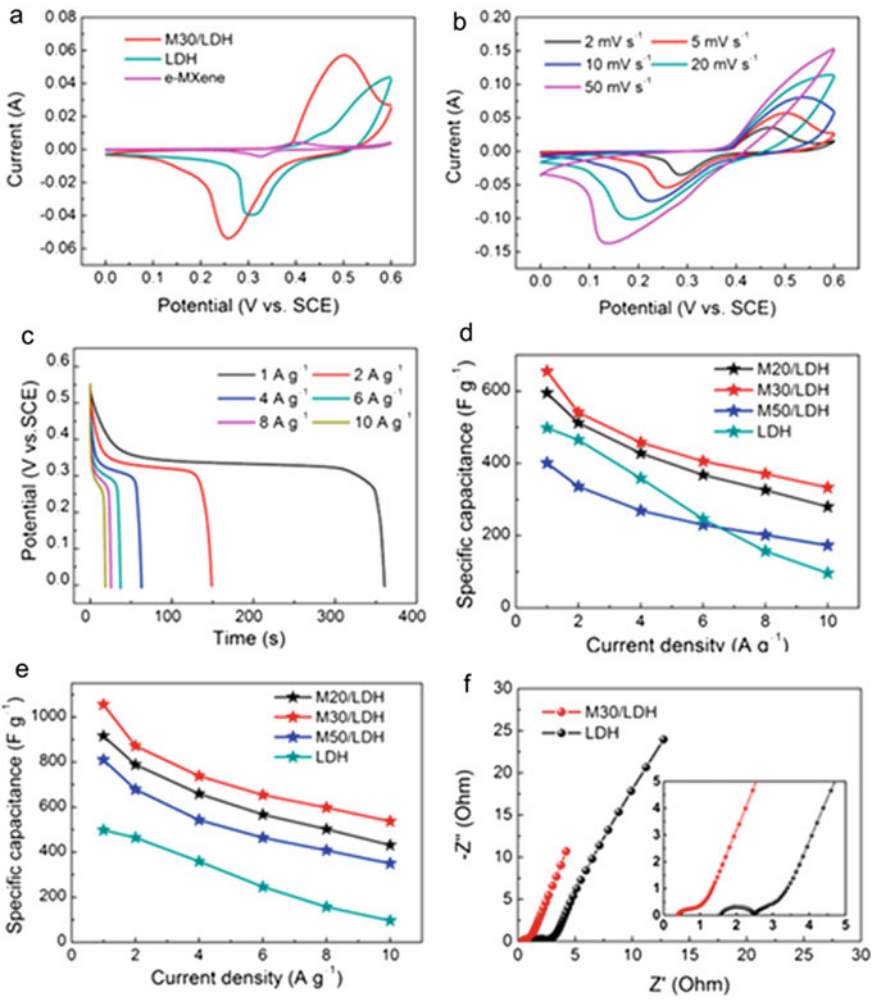

Fig. 7 **a** CV curves of e-MXene, LDH and M30/LDH (@5 mV s^{-1}) in 6 M of KOH, **b** CV curves of M30/LDH with the scan rates between 2 and 50 mV/s, **c** GCD curves of M30/LDH with current densities between 1 and 10A/g. The specific capacitance of samples with various current densities **d** corresponding to the mass of the composite **e** corresponding to LDH, and **f** Nyquist plots. Adapted with permission from reference [70], Copyright (2021), Elsevier

of MXene composites. The low fraction of MXene did not cover properly with LDH due to the limitation of available MXenes and a higher fraction of MXene also led to aggregation or over stacking of MXenes. Notably, the surface area of MXene composite with LDH was increased more than ten times than that of bare MXene. The bare MXene and MXene/LDH composite showed a pseudocapacitive behavior with a pair of redox peaks. The enhanced redox peak currents compared to bare MXene and LDH as shown in Fig. 7a confirm that proper composite formation could enhance the capacitive behavior with synergic effects. The less deviated redox peaks with increasing scan rate between 2 and 50 mV/s and the non-linear discharging characteristics with increasing current density between 1 and 10 A/g evidence good pseudocapacitive behavior of the nanocomposite. The increasing fraction of MXene in the composites showed the increasing tendency for the specific capacitance until a certain limit. The highest specific capacity of 1061 F/g was observed for LDH composite with 30 mg of MXene. The internal resistance of the composite was observed as less than that of bare LDH. The selection of electrode materials for the composite and the fraction of materials in the composites are playing a major role in electrochemical supercapacitor applications.

It is also important to select the suitable experimental procedure for the composite formation and the selection of electrolytes for electrochemical characteristics. A recent report demonstrated the simple process for the formation of Fe_3O_4/MXene/RGO hybrid magnetic nanocomposites through a modified chemical oxidation process [72] as seen from Fig. 8A. The cubic and octahedral-shaped

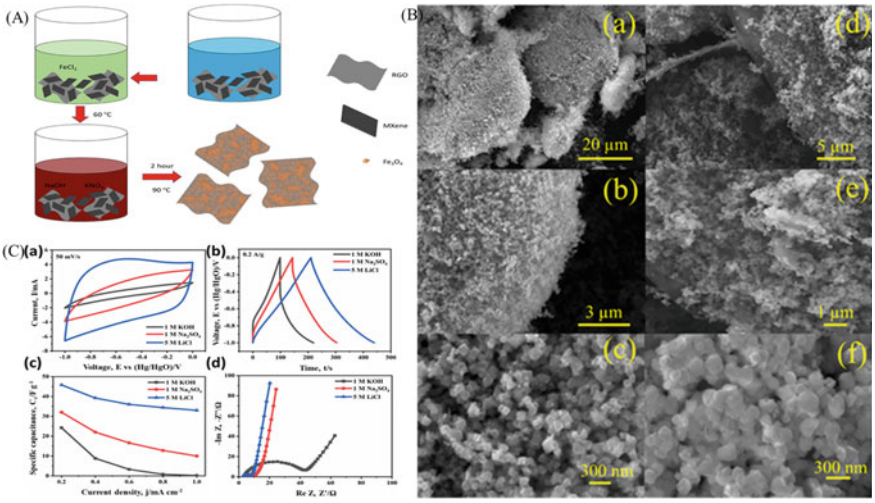

Fig. 8 **A** Schematic process for the formation of Fe_3O_4 /MXene/RGO, **B** FE-SEM micrographs of (**a**–**c**) Fe_3O_4/MXene and (**d**–**f**) Fe_3O_4 /MXene/RGO nanocomposites with various magnification, and **C** Comparison of **a** CV, **b** GCD, **c** Cs versus current density and **d** EIS plot of Fe_3O_4 /MXene/RGO electrodes in different electrolytes. Adapted with permission from Reference [71], Copyright (2021), Elsevier

Fe_3O_4 magnetic nanoparticles were surrounded on the MXene (Fig. 8). The individual Fe_3O_4 nanoparticles and the Fe_3O_4 covered MXenes on RGO sheets were developed by a simple chemical process and the morphology of the Fe_3O_4, MXene, and RGO was observed from the FESEM micrograph as shown in Fig. 8B. The electrochemical performance of the Fe_3O_4/MXene/RGO was evaluated by measuring the electrochemical characteristics and the performance of the material is shown in Fig. 8C. The performance of the Fe_3O_4/MXene/RGO in electrochemical was assessed employing Li^+, Na^+, and K^+ electrolyte ions. The observed results show that the performance of electrolytes varies as $LiCl > Na_2SO_4 > KOH$ which is also matched with the bare ion size in the same order. Similarly, more nanocomposites of MXene with materials such as reduced graphene oxide, CNTs, hydroxides, metal oxides, sulfides, nitrides, and polymers have been attempted and showed better performances. The electrochemical performance of a few nanocomposites is shown in Table 2.

3 Summary and Conclusion

Carbon-based materials, metal oxides, chalcogenides, polymers, and their composites have been continuously evaluated for electrochemical supercapacitor application through the faradaic and non-faradaic processes. But few materials like metal–organic framework, layered hydroxides, MXene, and nitrides are emerging as new electrode materials for electrochemical application due to the high theoretical capacity and high specific area. There are more opportunities for these materials in supercapacitor applications if we could be able to select suitable electroactive materials for the surface modification or composite formation. We have discussed the idea of the emerging electrode materials such as hydroxides, metal nitrides metal–organic frameworks, MXenes, and their composites for energy storage applications.

Table 2 Electrochemical performance of MXenes and their composites

Materials	Electrolyte	Specific capacitance (F/g)	Capacity retention (%)	Number of cycles	References
$Ti_3C_2T_x$	1 M H_2SO_4	892 (5 A/g)	100	10,000	Fu et al. [73]
$Ti_3C_2T_x$ aerogel	3 m H_2SO_4	404 (0.5A/g)	96	8000	Zhang et al. [74]
$Ti_3C_2T_x$/3D LDH	6 M KOH	1061 (1 A/g)	70	4000	Wang et al. [70]
Graphene-MXene Ti_2CT_x@polyaniline	1 M H_2SO_4	635 (1 A/g)	97.54	10,000	Fu et al. [75]
$Co_3O_4/Ti_3C_2T_x$/rGO	6 m KOH	345 (1 A/g)	85%	10,000	Liu et al. [76]
MXene/RGO	1 M H_2SO_4	233 (1A/g)	91.01	10,000	Shao et al. [77]
MXene/N-doped carbon foam	6 M KOH	332 (0.5A/g)	99.2	10,000	Sun et al. [78]
N&O co-doped C@Ti_3C_2 MXene	6 M KOH	250 (1A/g)	94	5000	Pan et al. [79]
Ti_3C_2/CNTs	6 M KOH	134 (1A/g)	100	10,000	Yang et al. [80]
MXene/CNT films	1 M H_2SO_4	300 (1A/g)	92	10,000	Chen et al. [81]
MnO_2@MXene/carbon nanotube fibers	1 M Na_2SO_4	181.8 (1A/g)	91	5000	Liu et al. [82]
NiMn-LDH/MXene	6 M KOH	1575 (0.5 A/g)	90.3	10,000	Zhang et al. [83]
Ti_3C_2/Ni − Co − Al LDH	1.0 M KOH	748.2 (1A/g)	97.8	10,000	Zhao et al. [84]
NiCo-MOF/T $Ti_3C_2T_x$	2 M KOH	815.2 (1 A/g)	82.3	10,000	Wang et al. [85]
$NiCo_2S_4$/MXene	3 M KOH	1028 (1A/g)	94.27	5000	Fu et al. [86]
MXene/NiS	2 M KOH	857.8 (1A/g)	99.49	3000	Liu et al. [87]
MXene/CoS_2	2 m KOH	1320 (1A/g)	98	5000	Liu et al. [88]
MXene/Polyaniline	1 M H_2SO_4	556.2 (0.5A/g)	91.6	5000	Xu et al. [89]

Acknowledgements The author T.A acknowledges Fondecyt postdoctoral project-3170696 ANID-SAI 77210070 and the University of ATACAMA Postdoctoral Project. Author K.R acknowledges FONDECYT Postdoctoral Project No.: 3200232, Government of Chile. The author M.J.M acknowledges Project PAI77190056.

References

1. Y. Gogotsi, R.M. Penner, Energy storage in nanomaterials—capacitive, pseudocapacitive, or battery-like? ACS Nano **12**, 2081–2083 (2018). https://doi.org/10.1021/acsnano.8b01914
2. M. Ghaemmaghami, R. Mohammadi, Carbon nitride as a new way to facilitate the next generation of carbon-based supercapacitors. Sustain. Energy Fuels **3**, 2176–2204 (2019). https://doi.org/10.1039/C9SE00313D
3. M.-S. Balogun, W. Qiu, W. Wang, P. Fang, X. Lu, Y. Tong, Recent advances in metal nitrides as high-performance electrode materials for energy storage devices. J. Mater. Chem. A. **3**, 1364–1387 (2014). https://doi.org/10.1039/C4TA05565A
4. B. Gao, X. Li, K. Ding, C. Huang, Q. Li, P.K. Chu, K. Huo, Recent progress in nanostructured transition metal nitrides for advanced electrochemical energy storage. J. Mater. Chem. A. **7**, 14–37 (2018). https://doi.org/10.1039/C8TA05760E
5. C. Qi Yi, J. Peng Zou, H. Zhi Yang, X. Leng, Recenst advances in pseudocapacitor electrode materials: transition metal oxides and nitrides. Trans. Nonferrous Met. Soc. China **28**, 1980–2001 (2018). https://doi.org/10.1016/S1003-6326(18)64843-5
6. X. Xiao, H. Wang, W. Bao, P. Urbankowski, L. Yang, Y. Yang, K. Maleski, L. Cui, S.J.L. Billinge, G. Wang, Y. Gogotsi, Two-dimensional arrays of transition metal nitride nanocrystals. Adv. Mater. **31**, 1902393 (2019). https://doi.org/10.1002/ADMA.201902393
7. J. Guo, Q. Zhang, J. Sun, C. Li, J. Zhao, Z. Zhou, B. He, X. Wang, P. Man, Q. Li, J. Zhang, L. Xie, M. Li, Y. Yao, Direct growth of vanadium nitride nanosheets on carbon nanotube fibers as novel negative electrodes for high-energy-density wearable fiber-shaped asymmetric supercapacitors. J. Power Sources **382**, 122–127 (2018). https://doi.org/10.1016/J.JPOWSOUR.2018.02.034
8. H. Cui, G. Zhu, X. Liu, F. Liu, Y. Xie, C. Yang, T. Lin, H. Gu, F. Huang, Niobium Nitride Nb4N5 as a new high-performance electrode material for supercapacitors. Adv. Sci. **2**, 1500126 (2015). https://doi.org/10.1002/ADVS.201500126
9. C. Zhu, P. Yang, D. Chao, X. Wang, X. Zhang, S. Chen, B.K. Tay, H. Huang, H. Zhang, W. Mai, H.J. Fan, All metal nitrides solid-state asymmetric supercapacitors. Adv. Mater. **27**, 4566–4571 (2015). https://doi.org/10.1002/ADMA.201501838
10. W.-B. Zhang, X.-J. Ma, A. Loh, X. Li, F.C. Walsh, L.-B. Kong, High volumetric energy density capacitors based on new electrode material lanthanum nitride. ACS Energy Lett. **2**, 336–341 (2017). https://doi.org/10.1021/ACSENERGYLETT.6B00636
11. Y. Wu, Y. Yang, X. Zhao, Y. Tan, Y. Liu, Z. Wang, F. Ran, A novel hierarchical porous 3D structured vanadium nitride/carbon membranes for high-performance supercapacitor negative electrodes. Nano-Micro Lett. **104**, 10, 1–11 (2018). https://doi.org/10.1007/S40820-018-0217-1
12. Y. Tan, Y. Liu, Z. Tang, Z. Wang, L. Kong, L. Kang, Z. Liu, F. Ran, Concise N-doped carbon nanosheets/vanadium nitride nanoparticles materials via intercalative polymerization for supercapacitors. Sci. Rep. **81**(8), 1–13 (2018). https://doi.org/10.1038/s41598-018-21082-w
13. F. Ran, Y. Wu, M. Jiang, Y. Tan, Y. Liu, L. Kong, L. Kang, S. Chen, Nanocomposites based on hierarchical porous carbon fiber@vanadium nitride nanoparticles as supercapacitor electrodes. Dalt. Trans. **47**, 4128–4138 (2018). https://doi.org/10.1039/C7DT04432A
14. X. Lu, M. Yu, T. Zhai, G. Wang, S. Xie, T. Liu, C. Liang, Y. Tong, Y. Li, High energy density asymmetric quasi-solid-state supercapacitor based on porous vanadium nitride nanowire anode. Nano Lett. **13**, 2628–2633 (2013). https://doi.org/10.1021/NL400760A
15. J. Cao, T. Li, H. Gao, Y. Lin, X. Wang, H. Wang, T. Palacios, X. Ling, Realization of 2D crystalline metal nitrides via selective atomic substitution, Sci. Adv. **6**, eaax8784 (2020). https://doi.org/10.1126/SCIADV.AAX8784
16. T. Nguyen, M. de F. Montemor, Metal oxide and hydroxide–based aqueous supercapacitors: from charge storage mechanisms and functional electrode engineering to need-tailored devices. Adv. Sci. **6**, 1801797 (2019). https://doi.org/10.1002/ADVS.201801797

17. S.J. Patil, N.R. Chodankar, R.B. Pujari, Y.K. Han, D.W. Lee, Core-shell hetero-nanostructured 1D transition metal polyphosphates decorated 2D bimetallic layered double hydroxide for sustainable hybrid supercapacitor. J. Power Sources. **466**, 228286 (2020). https://doi.org/10.1016/J.JPOWSOUR.2020.228286
18. D.S. Patil, S.A. Pawar, J.C. Shin, H.J. Kim, Layered double hydroxide based on ZnCo@NiCo-nano-architecture on 3D graphene scaffold as an efficient pseudocapacitor. J. Power Sources **435**, 226812 (2019). https://doi.org/10.1016/J.JPOWSOUR.2019.226812
19. Z. Pan, Y. Jiang, P. Yang, Z. Wu, W. Tian, L. Liu, Y. Song, Q. Gu, D. Sun, L. Hu, In Situ growth of layered bimetallic ZnCo hydroxide nanosheets for high-performance all-solid-state pseudocapacitor. ACS Nano **12**, 2968–2979 (2018). https://doi.org/10.1021/ACSNANO.8B00653
20. Y. Zhu, C. Huang, C. Li, M. Fan, K. Shu, H.C. Chen, Strong synergetic electrochemistry between transition metals of α phase Ni−Co−Mn hydroxide contributed superior performance for hybrid supercapacitors. J. Power Sources. **412**, 559–567 (2019). https://doi.org/10.1016/J.JPOWSOUR.2018.11.080
21. H. Ma, J. He, D.-B. Xiong, J. Wu, Q. Li, V. Dravid, Y. Zhao, Nickel Cobalt Hydroxide @reduced graphene oxide hybrid nanolayers for high performance asymmetric supercapacitors with remarkable cycling stability. ACS Appl. Mater. Interfaces. **8**, 1992–2000 (2016). https://doi.org/10.1021/ACSAMI.5B10280
22. R. Wang, A. Jayakumar, C. Xu, J.-M. Lee, Ni(OH)2 nanoflowers/graphene hydrogels: a new assembly for supercapacitors. ACS Sustain. Chem. Eng. **4**, 3736–3742 (2016). https://doi.org/10.1021/ACSSUSCHEMENG.6B00362
23. C. Dong, Q. Ge, Y. Li, J. Zhang, Boosting honeycomb-like layer double hydroxides nanosheets as advanced electrode for supercapacitors. Thin Solid Films **715**, 138439 (2020). https://doi.org/10.1016/J.TSF.2020.138439
24. T. Wang, F. Yu, X. Wang, S. Xi, K.J. Chen, H. Wang, Enhancing cycling stability of transition metal-based layered double hydroxides through a self-sacrificial strategy for hybrid supercapacitors. Electrochim. Acta. **334**, 135586 (2020). https://doi.org/10.1016/J.ELECTACTA.2019.135586
25. Y. Zhang, T. Zeng, D. Huang, W. Yan, Y. Zhang, Q. Wan, N. Yang, High-energy-density supercapacitors from dual pseudocapacitive nanoelectrodes. ACS Appl. Energy Mater. **3**, 10685–10694 (2020). https://doi.org/10.1021/ACSAEM.0C01747
26. S. Dai, Y. Bai, W. Shen, S. Zhang, H. Hu, J. Fu, X. Wang, C. Hu, M. Liu, Core-shell structured Fe2O3@Fe3C@C nanochains and Ni–Co carbonate hydroxide hybridized microspheres for high-performance battery-type supercapacitor. J. Power Sources. **482**, 228915 (2021). https://doi.org/10.1016/J.JPOWSOUR.2020.228915
27. G. Xia, S. Wang, Microwave-assisted facile and rapid synthesis of layered metal hydroxide nanosheet arrays towards high-performance aqueous hybrid supercapacitors. Ceram. Int. **45**, 20810–20817 (2019). https://doi.org/10.1016/J.CERAMINT.2019.07.068
28. C. Cheng, C. Wei, Y. He, L. Liu, J. Hu, W. Du, Etching strategy synthesis of hierarchical Ni-Mn hydroxide hollow spheres for supercapacitors. J. Energy Storage **33**, 102105 (2021). https://doi.org/10.1016/J.EST.2020.102105
29. J. Lee, O.K. Farha, J. Roberts, K.A. Scheidt, S.T. Nguyen, J.T. Hupp, Metal-organic framework materials as catalysts. Chem. Soc. Rev. **38**, 1450–1459 (2009). https://doi.org/10.1039/b807080f
30. M. Bonneau, C. Lavenn, P. Ginet, K.I. Otake, S. Kitagawa, Upscale synthesis of a binary pillared layered MOF for hydrocarbon gas storage and separation. Green Chem. **22**, 718–724 (2020). https://doi.org/10.1039/c9gc03561c
31. L. Liu, Y. Zhou, S. Liu, M. Xu, The applications of metal−organic frameworks in electrochemical sensors. ChemElectroChem **5**, 6–19 (2018). https://doi.org/10.1002/celc.201700931
32. Y. Li, Y. Xu, W. Yang, W. Shen, H. Xue, H. Pang, MOF-derived metal oxide composites for advanced electrochemical energy storage. Small **14**, 1704435 (2018). https://doi.org/10.1002/smll.201704435

33. A. Mohanty, D.P. Jaihindh, Y.P. Fu, S.P. Senanayak, L.S. Mende, A. Ramadoss, An extensive review on three dimension architectural metal-organic frameworks towards supercapacitor application. J. Power Sources **488** (2021). https://doi.org/10.1016/j.jpowsour.2020.229444
34. O.K. Farha, I. Eryazici, N.C. Jeong, B.G. Hauser, C.E. Wilmer, A.A. Sarjeant, R.Q. Snurr, S.T. Nguyen, A.Ö. Yazaydin, J.T. Hupp, Metal-organic framework materials with ultrahigh surface areas: is the sky the limit? J. Am. Chem. Soc. **134**, 15016–15021 (2012). https://doi.org/10.1021/ja3055639
35. I.M. Hönicke, I. Senkovska, V. Bon, I.A. Baburin, N. Bönisch, S. Raschke, J.D. Evans, S. Kaskel, Balancing mechanical stability and ultrahigh porosity in crystalline framework materials. Angew. Chemie - Int. Ed. **57**, 13780–13783 (2018). https://doi.org/10.1002/anie.201808240
36. R. Du, Y. Wu, Y. Yang, T. Zhai, T. Zhou, Q. Shang, L. Zhu, C. Shang, Z. Guo, Porosity engineering of MOF-based materials for electrochemical energy storage. Adv. Energy Mater. 2100154 (2021). https://doi.org/10.1002/aenm.202100154
37. X. Zhang, N. Qu, S. Yang, D. Lei, A. Liu, Q. Zhou, Cobalt induced growth of hollow MOF spheres for high performance supercapacitors. Mater. Chem. Front. **5**, 482–491 (2021). https://doi.org/10.1039/d0qm00597e
38. F. Dai, X. Wang, S. Zheng, J. Sun, Z. Huang, B. Xu, L. Fan, R. Wang, D. Sun, Z.S. Wu, Toward high-performance and flexible all-solid-state micro-supercapacitors: MOF bulk vs. MOF nanosheets. Chem. Eng. J. (2021). https://doi.org/10.1016/j.cej.2020.127520
39. M. Ko, L. Mendecki, K.A. Mirica, Conductive two-dimensional metal-organic frameworks as multifunctional materials. Chem. Commun. **54**, 7873–7891 (2018). https://doi.org/10.1039/c8cc02871k
40. T.V.M. Sreekanth, G.R. Dillip, P.C. Nagajyothi, K. Yoo, J. Kim, Integration of Marigold 3D flower-like Ni-MOF self-assembled on MWCNTs via microwave irradiation for high-performance electrocatalytic alcohol oxidation and oxygen evolution reactions. Appl. Catal. B Environ. **285**, 119793 (2021). https://doi.org/10.1016/j.apcatb.2020.119793
41. Q.B. Le, T.H. Nguyen, H. Fei, I. Sapurina, F.A. Ngwabebhoh, C. Bubulinca, L. Munster, E.D. Bergerová, A. Lengalova, H. Jiang, T.D. Tran, N. Bugarova, M. Omastova, N.E. Kazantseva, P. Saha, Electrochemical performance of composites made of rGO with Zn-MOF and PANI as electrodes for supercapacitors. Electrochim. Acta. **367** (2021). https://doi.org/10.1016/j.electacta.2020.137563
42. F. Boorboor Ajdari, M. Dashti Najafi, M. Izadpanah Ostad, H. reza Naderi, M. Niknam Shahrak, E. Kowsari, S. Ramakrishna, A symmetric ZnO-ZIF8//Mo-ZIF8 supercapacitor and comparing with electrochemical of Pt, Au, and Cu decorated ZIF-8 electrodes. J. Mol. Liq. **333**, 116007 (2021). https://doi.org/10.1016/j.molliq.2021.116007
43. D. Feng, T. Lei, M.R. Lukatskaya, J. Park, Z. Huang, M. Lee, L. Shaw, S. Chen, A.A. Yakovenko, A. Kulkarni, J. Xiao, K. Fredrickson, J.B. Tok, X. Zou, Y. Cui, Z. Bao, Robust and conductive two-dimensional metal-organic frameworks with exceptionally high volumetric and areal capacitance. Nat. Energy **3**, 30–36 (2018). https://doi.org/10.1038/s41560-017-0044-5
44. Y. Jiao, J. Pei, C. Yan, D. Chen, Y. Hu, G. Chen, Layered nickel metal-organic framework for high performance alkaline battery-supercapacitor hybrid devices. J. Mater. Chem. A **4**, 13344–13351 (2016). https://doi.org/10.1039/c6ta05384j
45. J. Yang, C. Zheng, P. Xiong, Y. Li, M. Wei, Zn-doped Ni-MOF material with a high supercapacitive performance. J. Mater. Chem. A **2**, 19005–19010 (2014). https://doi.org/10.1039/c4ta04346d
46. W.-H. Li, K. Ding, H.-R. Tian, M.-S. Yao, B. Nath, W.-H. Deng, Y. Wang, G. Xu, Supercapacitors: conductive metal-organic framework nanowire array electrodes for high-performance solid-state supercapacitors (Adv. Funct. Mater. 27/2017). Adv. Funct. Mater. **27** (2017). https://doi.org/10.1002/adfm.201770165
47. Z. Xia, C. Ren, W. Xu, F. Li, C. Qiao, Q. Wei, C. Zhou, S. Chen, S. Gao, Ultrasensitive Fe3+ luminescence sensing and supercapacitor performances of a triphenylamine-based TbIII-MOF. J. Solid State Chem. **282**, 121083 (2019). https://doi.org/10.1016/j.jssc.2019.121083

48. S. Sundriyal, V. Shrivastav, M. Sharma, S. Mishra, A. Deep, Redox additive electrolyte study of Mn–MOF electrode for supercapacitor applications. ChemistrySelect **4**, 2585–2592 (2019). https://doi.org/10.1002/slct.201900305
49. X. Xu, J. Tang, H. Qian, S. Hou, Y. Bando, M.S.A. Hossain, L. Pan, Y. Yamauchi, Three-dimensional networked metal-organic frameworks with conductive polypyrrole tubes for flexible supercapacitors. ACS Appl. Mater. Interfaces **9**, 38737–38744 (2017). https://doi.org/10.1021/acsami.7b09944
50. L. Wang, X. Feng, L. Ren, Q. Piao, J. Zhong, Y. Wang, H. Li, Y. Chen, B. Wang, Flexible solid-state supercapacitor based on a metal-organic framework interwoven by electrochemically-deposited PANI. J. Am. Chem. Soc. **137**, 4920–4923 (2015). https://doi.org/10.1021/jacs.5b01613
51. Z. Wang, C. Gao, Y. Liu, D. Li, W. Chen, Y. Ma, C. Wang, J. Zhang, Electrochemical performance and transformation of Co-MOF/reduced graphene oxide composite. Mater. Lett. **193**, 216–219 (2017). https://doi.org/10.1016/j.matlet.2017.01.121
52. L. Shao, Q. Wang, Z. Ma, Z. Ji, X. Wang, D. Song, Y. Liu, N. Wang, A high-capacitance flexible solid-state supercapacitor based on polyaniline and Metal-Organic Framework (UiO-66) composites. J. Power Sources **379**, 350–361 (2018). https://doi.org/10.1016/j.jpowsour.2018.01.028
53. S. Zhou, X. Kong, B. Zheng, F. Huo, M. Strømme, C. Xu, Cellulose nanofiber @ conductive metal-organic frameworks for high-performance flexible supercapacitors. ACS Nano **13**, 9578–9586 (2019). https://doi.org/10.1021/acsnano.9b04670
54. P. Wen, P. Gong, J. Sun, J. Wang, S. Yang, Design and synthesis of Ni-MOF/CNT composites and rGO/carbon nitride composites for an asymmetric supercapacitor with high energy and power density. J. Mater. Chem. A. **3**, 13874–13883 (2015). https://doi.org/10.1039/c5ta02461g
55. J. Zhang, Z. Wang, T. Deng, W. Zhang, Ni(OH)2 derived Ni-MOF supported on carbon nanowalls for supercapacitors. Nanotechnology **32**, 195404 (2021). https://doi.org/10.1088/1361-6528/abdf8e
56. C.J. Zhang, B. Anasori, A. Seral-Ascaso, S.H. Park, N. McEvoy, A. Shmeliov, G.S. Duesberg, J.N. Coleman, Y. Gogotsi, V. Nicolosi, Transparent, flexible, and conductive 2D titanium carbide (MXene) films with high volumetric capacitance. Adv. Mater. **29**, 1702678 (2017). https://doi.org/10.1002/adma.201702678
57. Z. Guo, Y. Li, B. Sa, Y. Fang, J. Lin, Y. Huang, C. Tang, J. Zhou, N. Miao, Z. Sun, M2C-type MXenes: promising catalysts for CO_2 capture and reduction. Appl. Surf. Sci. **521**, 146436 (2020). https://doi.org/10.1016/j.apsusc.2020.146436
58. Y.A.J. Al-Hamadani, B.M. Jun, M. Yoon, N. Taheri-Qazvini, S.A. Snyder, M. Jang, J. Heo, Y. Yoon, Applications of MXene-based membranes in water purification: a review. Chemosphere **254** (2020). https://doi.org/10.1016/j.chemosphere.2020.126821
59. F. Shahzad, M. Alhabeb, C.B. Hatter, B. Anasori, S.M. Hong, C.M. Koo, Y. Gogotsi, Electromagnetic interference shielding with 2D transition metal carbides (MXenes). Science (80-). (2016). https://doi.org/10.1126/science.aag2421
60. M. Marian, G.C. Song, B. Wang, V.M. Fuenzalida, S. Krauß, B. Merle, S. Tremmel, S. Wartzack, J. Yu, A. Rosenkranz, Effective usage of 2D MXene nanosheets as solid lubricant—influence of contact pressure and relative humidity. Appl. Surf. Sci. **531**, 147311 (2020). https://doi.org/10.1016/j.apsusc.2020.147311
61. D. Pang, M. Alhabeb, X. Mu, Y. Dall'Agnese, Y. Gogotsi, Y. Gao, Electrochemical actuators based on two-dimensional Ti3C2Tx (MXene). Nano Lett. **19**, 7443–7448 (2019). https://doi.org/10.1021/acs.nanolett.9b03147
62. X. Jin, L. Yang, X.F. Wang, Efficient two-dimensional perovskite solar cells realized by incorporation of Ti3C2Tx MXene as nano-dopants. Nano-Micro Lett. **13**, 1–13 (2021). https://doi.org/10.1007/s40820-021-00602-w
63. Z. Guo, J. Zhou, L. Zhu, Z. Sun, MXene: a promising photocatalyst for water splitting. J. Mater. Chem. A. **4**, 11446–11452 (2016). https://doi.org/10.1039/c6ta04414j
64. H. Kim, H.N. Alshareef, MXetronics: MXene-enabled electronic and photonic devices. ACS Mater. Lett. **2**, 55–70 (2020). https://doi.org/10.1021/acsmaterialslett.9b00419

65. Y. Lei, W. Zhao, Y. Zhang, Q. Jiang, J.H. He, A.J. Baeumner, O.S. Wolfbeis, Z.L. Wang, K.N. Salama, H.N. Alshareef, A MXene-based wearable biosensor system for high-performance in vitro perspiration analysis. Small **15**, 1901190 (2019). https://doi.org/10.1002/smll.201901190
66. H. Lin, Y. Wang, S. Gao, Y. Chen, J. Shi, Theranostic 2D tantalum carbide (MXene). Adv. Mater. **30**, 1703284 (2018). https://doi.org/10.1002/adma.201703284
67. I. Persson, J. Halim, T.W. Hansen, J.B. Wagner, V. Darakchieva, J. Palisaitis, J. Rosen, P.O.Å. Persson, How much oxygen can a mxene surface take before it breaks? Adv. Funct. Mater. **30**, 1909005 (2020). https://doi.org/10.1002/adfm.201909005
68. M. Naguib, O. Mashtalir, J. Carle, V. Presser, J. Lu, L. Hultman, Y. Gogotsi, M.W. Barsoum, Two-dimensional transition metal carbides. ACS Nano **6**, 1322–1331 (2012). https://doi.org/10.1021/nn204153h
69. Y. Zhu, K. Rajouâ, S. Le Vot, O. Fontaine, P. Simon, F. Favier, Modifications of MXene layers for supercapacitors. Nano Energy (2020). https://doi.org/10.1016/j.nanoen.2020.104734
70. Y. Wang, H. Dou, J. Wang, B. Ding, Y. Xu, Z. Chang, X. Hao, Three-dimensional porous MXene/layered double hydroxide composite for high performance supercapacitors. J. Power Sources **327**, 221–228 (2016). https://doi.org/10.1016/j.jpowsour.2016.07.062
71. T. Arun, A. Mohanty, A. Rosenkranz, B. Wang, J. Yu, M.J. Morel, R. Udayabhaskar, S.A. Hevia, A. Akbari-Fakhrabadi, R. V. Mangalaraja, A. Ramadoss, Role of electrolytes on the electrochemical characteristics of Fe_3O_4/MXene/RGO composites for supercapacitor applications. Electrochim. Acta. **367** (2021). https://doi.org/10.1016/j.electacta.2020.137473
72. T. Arun, K. Prabakaran, R. Udayabhaskar, R.V. Mangalaraja, A. Akbari-Fakhrabadi, Carbon decorated octahedral shaped Fe_3O_4 and α-Fe_2O_3 magnetic hybrid nanomaterials for next generation supercapacitor applications. Appl. Surf. Sci. **485**, 147–157 (2019). https://doi.org/10.1016/j.apsusc.2019.04.177
73. Q. Fu, J. Wen, N. Zhang, L. Wu, M. Zhang, S. Lin, H. Gao, X. Zhang, Free-standing Ti3C2Tx electrode with ultrahigh volumetric capacitance. RSC Adv. **7**, 11998–12005 (2017). https://doi.org/10.1039/c7ra00126f
74. X. Zhang, X. Liu, S. Dong, J. Yang, Y. Liu, Template-free synthesized 3D macroporous MXene with superior performance for supercapacitors. Appl. Mater. Today. **16**, 315–321 (2019). https://doi.org/10.1016/j.apmt.2019.06.013
75. J. Fu, J. Yun, S. Wu, L. Li, L. Yu, K.H. Kim, Architecturally robust graphene-encapsulated MXene Ti2CTx@Polyaniline composite for high-performance pouch-type asymmetric supercapacitor. ACS Appl. Mater. Interfaces. **10**, 34212–34221 (2018). https://doi.org/10.1021/acsami.8b10195
76. R. Liu, A. Zhang, J. Tang, J. Tian, W. Huang, J. Cai, C. Barrow, W. Yang, J. Liu, Fabrication of cobaltosic oxide nanoparticle-doped 3 D MXene/graphene hybrid porous aerogels for all-solid-state supercapacitors. Chem.—A Eur. J. **25**, 5547–5554 (2019). https://doi.org/10.1002/chem.201806342
77. L. Shao, J. Xu, J. Ma, B. Zhai, Y. Li, R. Xu, Z. Ma, G. Zhang, C. Wang, J. Qiu, MXene/RGO composite aerogels with light and high-strength for supercapacitor electrode materials. Compos. Commun. **19**, 108–113 (2020). https://doi.org/10.1016/j.coco.2020.03.006
78. L. Sun, G. Song, Y. Sun, Q. Fu, C. Pan, MXene/N-doped carbon foam with three-dimensional hollow neuron-like architecture for freestanding, highly compressible all solid-state supercapacitors. ACS Appl. Mater. Interfaces **12**, 44777–44788 (2020). https://doi.org/10.1021/acsami.0c13059
79. Z. Pan, X. Ji, Facile synthesis of nitrogen and oxygen co-doped C@Ti3C2 MXene for high performance symmetric supercapacitors. J. Power Sources **439** (2019). https://doi.org/10.1016/j.jpowsour.2019.227068
80. L. Yang, W. Zheng, P. Zhang, J. Chen, W.B. Tian, Y.M. Zhang, Z.M. Sun, MXene/CNTs films prepared by electrophoretic deposition for supercapacitor electrodes. J. Electroanal. Chem. **830–831**, 1–6 (2018). https://doi.org/10.1016/j.jelechem.2018.10.024
81. H. Chen, L. Yu, Z. Lin, Q. Zhu, P. Zhang, N. Qiao, B. Xu, Carbon nanotubes enhance flexible MXene films for high-rate supercapacitors. J. Mater. Sci. **55**, 1148–1156 (2020). https://doi.org/10.1007/s10853-019-04003-8

82. Q. Liu, J. Yang, X. Luo, Y. Miao, Y. Zhang, W. Xu, L. Yang, Y. Liang, W. Weng, M. Zhu, Fabrication of a fibrous MnO2@MXene/CNT electrode for high-performance flexible supercapacitor. Ceram. Int. **46**, 11874–11881 (2020). https://doi.org/10.1016/j.ceramint.2020.01.222
83. D. Zhang, J. Cao, X. Zhang, N. Insin, R. Liu, J. Qin, NiMn layered double hydroxide nanosheets In-situ anchored on Ti3C2MXene via chemical bonds for superior supercapacitors. ACS Appl. Energy Mater. **3**, 5949–5964 (2020). https://doi.org/10.1021/acsaem.0c00863
84. R. Zhao, M. Wang, D. Zhao, H. Li, C. Wang, L. Yin, Molecular-level heterostructures assembled from titanium carbide MXene and Ni-Co-Al layered double-hydroxide nanosheets for all-solid-state flexible asymmetric high-energy supercapacitors. ACS Energy Lett. **3**, 132–140 (2018). https://doi.org/10.1021/acsenergylett.7b01063
85. Y. Wang, Y. Liu, C. Wang, H. Liu, J. Zhang, J. Lin, J. Fan, T. Ding, J.E. Ryu, Z. Guo, Significantly enhanced ultrathin NiCo-based MOF nanosheet electrodes hybrided with Ti3C2Tx MXene for high performance asymmetric supercapacitors. Eng. Sci. (2020). https://doi.org/10.30919/es8d903
86. J. Fu, L. Li, J.M. Yun, D. Lee, B.K. Ryu, K.H. Kim, Two-dimensional titanium carbide (MXene)-wrapped sisal-Like NiCo2S4 as positive electrode for High-performance hybrid pouch-type asymmetric supercapacitor. Chem. Eng. J. **375**, 121939 (2019). https://doi.org/10.1016/j.cej.2019.121939
87. H. Liu, R. Hu, J. Qi, Y. Sui, Y. He, Q. Meng, F. Wei, Y. Ren, Y. Zhao, A facile method for synthesizing NiS nanoflower grown on MXene (Ti3C2Tx) as positive electrodes for "supercapattery." Electrochim. Acta. **353**, 136526 (2020). https://doi.org/10.1016/j.electacta.2020.136526
88. H. Liu, R. Hu, J. Qi, Y. Sui, Y. He, Q. Meng, F. Wei, Y. Ren, Y. Zhao, W. Wei, One-step synthesis of nanostructured CoS2 grown on titanium carbide MXene for high-performance asymmetrical supercapacitors. Adv. Mater. Interfaces **7**, 1901659 (2020). https://doi.org/10.1002/admi.201901659
89. H. Xu, D. Zheng, F. Liu, W. Li, J. Lin, Synthesis of an MXene/polyaniline composite with excellent electrochemical properties. J. Mater. Chem. A **8**, 5853–5858 (2020). https://doi.org/10.1039/d0ta00572j

Electrochemical Double Layer Capacitors

Stella Vargheese, R. T. Rajendra Kumar, and Yuvaraj Haldorai

Abstract Over the past decades, supercapacitors have created much attention and are considered promising energy storage devices owing to their high power density, wide potential range, and excellent cyclic stability. As a part of this renewed interest in electric double-layer capacitors (EDLCs), researchers began seeking new strategies to synthesize high surface area porous carbon-based materials as electrodes for EDLCs to obtain high specific capacitance and high energy density. This chapter provides a basic understanding of EDLCs and the choice of electrodes used in the EDLCs. In addition, the charge storage mechanism in EDLCs is discussed. Some key results are summarized relating to the above properties.

Keywords Electrochemical · Supercapacitor · Double layer · Energy storage

1 Introduction

Electrical energy is an inescapable thing of modern society. With the limited availability of fossil fuels and the increasing environmental pollution, there is an urgent need for renewable energy resources. The developed renewable energy resources like wind, solar, and ocean can generate a huge amount of electrical energy. However, we need energy storage devices to utilize these energy resources productively for various applications [1]. Different electrochemical energy storage devices are developed such as batteries, capacitors, supercapacitors, and fuel cells. Among these energy storage devices, supercapacitors or electrochemical capacitors created significant interest due to their high power density, long life cycle, and environmental safety. Supercapacitors possess higher power density than batteries but lower power density than capacitors. The energy density of conventional capacitors is lower than that of batteries but higher than that of capacitors [2]. Figure 1 shows the Ragone plot (energy density versus power density) of different energy storage systems. As noticed from the Ragone plot,

S. Vargheese · R. T. Rajendra Kumar · Y. Haldorai (✉)
Department of Nanoscience and Technology, Bharathiar University, Coimbatore, Tamil Nadu 641046, India
e-mail: yuvraj_pd@yahoo.co.in

S. Thomas et al. (eds.), *Nanostructured Materials for Supercapacitors*,
Advances in Material Research and Technology,
https://doi.org/10.1007/978-3-030-99302-3_2

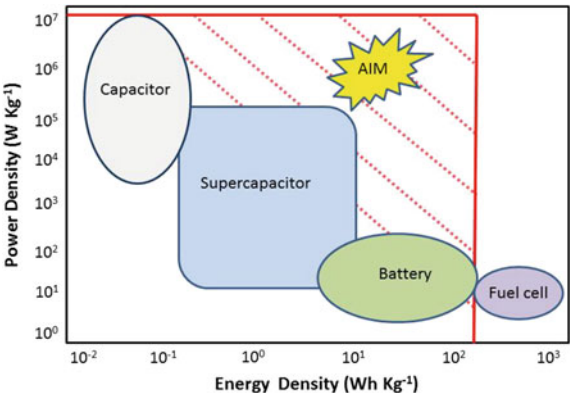

Fig. 1 Ragone plot of different electrochemical energy storage devices

the supercapacitor is an ideal storage device to overcome the gap between electrolyte capacitor and battery [3].

Supercapacitor stores energy based on different charge storage mechanisms, namely electric double-layer capacitor (EDLC), pseudocapacitor, and hybrid capacitor. Supercapacitor stores energy in the form of accumulation of charges at the electrode/electrolyte interface as a double layer. Generally, carbon-based materials are considered as electrodes for EDLCs because of their high surface area and porosity [4]. On the other hand, pseudocapacitor stores energy via faradic reaction (redox reaction). Transition metal oxides and conducting polymers are used as electrode materials [5]. In the case of a hybrid capacitor, both faradic and non-faradic reactions occur to store energy. The hybrid capacitor utilizes the advantages of both EDLC and pseudocapacitor [6].

In the batteries, the energy storage capacity is solely dependent on the chemical interconversion of electrode materials, resulting in visible phase change on the electrodes during charging and discharging. As a result, the cycle life of battery cells is shortened [7]. The non-faradic system of the supercapacitor, conversely, has a long cyclic life (10^5–10^6 times) due to the absence of phase alterations during the charge and discharge process. However, the specific energy of supercapacitors is lower than that of batteries because of the charge storage restriction on the surface of the electrode. Therefore, in recent years, several researchers have focussed on the fabrication of advanced functional materials as electrodes to improve the energy densities of supercapacitors comparable to the batteries without compromising the cyclic stability [8]. In this chapter, we focus on the general overview of the basic concept of EDLC and its charge storage mechanism. Also, the type of electrodes and electrolytes used in the high-performance EDLCs are discussed with literature reports. Owing to the considerable research paper in the EDLCs, a total survey was not possible. Therefore, more detailed explanations of the particular topics can be obtained from the related references.

2 Supercapacitor

Supercapacitors have been recognized as next-generation electrochemical energy storage devices owing to their long cycle life, wide potential windows, high power density, and fast charging and discharging. They are widely used in different electronic devices.

2.1 A Brief Overview of the History of Supercapacitor

In 1746, the capacitor technology begins when the Leyden jar was invented by Ewald Georg Von Kleist and Pieter Van Musschenhroek. The set-up of the Leyden jar was made to produce static energy [9]. In 1853, the electrostatic charge storage mechanism of the capacitor and the behavior of static electricity were clearly explained by Helmholtz using the electric double layer model [10]. In the early twentieth century, the electrolytic interaction at the electrode–electrolyte interface and the formation of a double-layer were described by Gouy-Chapman, Stern, and Grahame models [11].

In 1954, H. I. Becker has constructed an electrochemical energy storage device containing electrodes of activated charcoal with a small operating potential window.

It was the first patented electrochemical capacitor at General electric [12]. In 1969, the first non-aqueous electrolyte-based supercapacitor with large working window potential was invented by Robert Rightmire [13]. In 1971, B. E. Conway discovered ruthenium oxide (RuO_2) as an electrode material. The faradic charge storage mechanism indicates the pseudocapacitive nature of the RuO_2 [14]. In 1978, Nippon Electric Corporation patented Standard Oil Co. of Ohio constructed a double-layer capacitor and commercialized it in the name of a supercapacitor [13]. Pinnacle research institute began working on high-performance supercapacitors in 1980. In this project, the porous carbon was replaced by RuO_2 and tantalum oxide to increase the supercapacitor's performance and was named PRI ultracapacitors [15]. In 1989, the US Department of Energy and Maxwell Technologies Inc. have done collaboration work to improve the specific energy of the device. In that work, they introduced different types of supercapacitors (electrical double layer capacitor (EDLC), pseudocapacitor, and asymmetric capacitor) [16]. Later, new types of supercapacitors were created by ELTON, CAP-XX, Nippon chemicon, and Nesscap. Since 2000, the number of research projects has increased dramatically.

3 Classification of Supercapacitors

Supercapacitors are classified into three categories namely EDLCs, pseudocapacitors, and hybrid capacitors based on their charge storage mechanism.

3.1 Electric Double-Layer Capacitor (EDLC)

The EDLC capacitor consists of two carbon-based electrodes, a separator, and an electrolyte (Fig. 2a). When an external potential is applied to the electrodes, the charged ions are stored in the form of energy due to electrostatic interaction at the electrode/electrolyte interface [17]. The positively charged ions are diffused towards the negative electrode and the negatively charged ions are diffused towards the positive electrode. The storage is purely physical absorption and there is no ion exchange between the electrode material and electrolyte solution. The accumulation of charges in the double layer avoids the recombination of the ions at the surface of electrodes. The double-layer integrates to decrease the electrode distance and to increase the specific surface area. This enables the EDLC to achieve notable energy density [11]. Different carbon materials including porous carbon, activated carbon, carbon fiber, carbon nanotube, and graphene have been identified as suitable electrodes for EDLCs because of their large specific surface area, good thermal and chemical stabilities, and excellent conductivity [17]. The EDLC storage technique allows rapid energy intake, good power performance, and delivery. The capacitance of EDLC depends on the adsorption of charges on the electrode surface from the electrolyte and therefore the energy storage is highly reversible in EDLC [17]. Also, the EDLC performance can be altered by using various types of electrolytes such as aqueous and organic electrolytes. Compared to the organic electrolytes, the aqueous electrolytes exhibit lower series resistance. However, the potential window range becomes narrow in the case of aqueous electrolytes which limits the energy density of EDLC devices. Therefore, while selecting the electrolyte, electrochemical resistance, capacitance, and potential range must be considered.

3.2 Pseudocapacitor

Pseudocapacitors involve reversible oxidation and reduction reactions that take place at the electrode's surface to store energy when an external potential is applied to the cell (Fig. 2b). In pseudocapacitor, the charge/discharge process is not controlled by the diffusion and no phase transformation occurs on the active electrode material [18]. Generally, transition metal oxides and conducting polymers are utilized as effective electrode materials for pseudocapacitors. The faradic process of pseudocapacitors assists them to reach high specific capacitance and high energy density than EDLCs. The chemical redox reaction that takes place in the pseudocapacitor reduces its cyclic stability and power density due to the swelling of the electrode material. The electrochemical performance of pseudocapacitor is limited due to its poor conductivity, less accessibility of electrolyte, and short cyclic life [19].

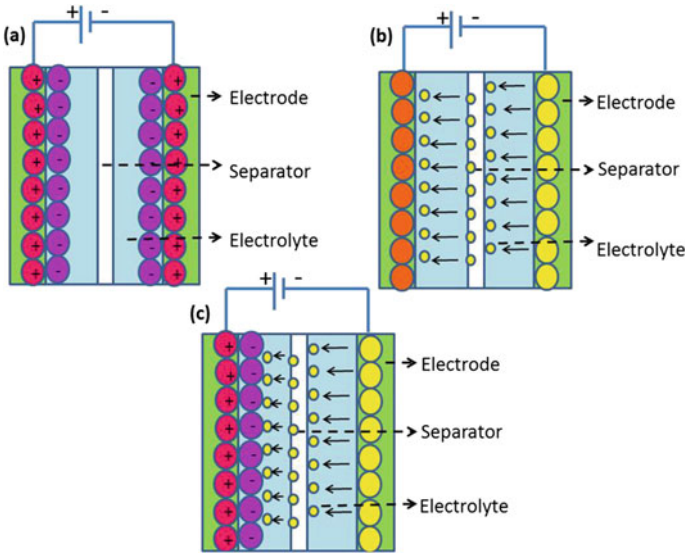

Fig. 2 Schematic representation of **a** EDLC, **b** pseudocapacitor, and **c** hybrid capacitor. Adapted with permission from Ref. [20], Copyright 2020, Elsevier

3.3 Hybrid Capacitor

The energy source of the pseudocapacitor and power source of EDLC combined to form a hybrid capacitor [20] to get the better of the limitation of EDLC and pseudocapacitor (Fig. 2c). This combination of electrode materials can increase the power density and energy density along with the cell voltage. According to the electrode alignment, the hybrid capacitor is classified into three types such as asymmetric, composite, and battery-type capacitors.

4 The Mechanisms of Energy Storage in EDLCs

Conventional capacitors are constructed by two conducting electrodes that are separated by a dielectric medium. The electrode's surface is accumulated with the oppositely charged ions due to the external electric field. The dielectric medium plays an important role to separate charges and produce an electric field to store energy on the capacitors.

The ratio between charges stored (Q) and applied potential (V) is called a capacitance (C).

$$C = \frac{Q}{V} \tag{1}$$

The capacitance of conventional capacitors is influenced by the electrode surface area (A) and electrode distance (D).

$$C = \varepsilon_o \varepsilon_r \frac{A}{D} \tag{2}$$

where ε_r and ε_o stand for the relative permittivity and vacuum permittivity.

In the case of EDLCs, the charged ions/molecules from the electrolyte are electrostatically attracted towards the electrode's surface to form a double-layer at the interface of the electrode and electrolyte. The double-layer at the electrode/electrolyte interface consisting of cations/anions and oriented solvent dipoles [21].

The EDLC process can be written as;

In the positive electrode

$$Es^+ + A^- \leftrightarrow Es^+//A^{-1} + e^{-1} \tag{3}$$

In the negative electrode

$$Es^- + C^+ + e^- \leftrightarrow Es^-//C^+ \tag{4}$$

Overall electrode reaction

$$Es^+ + Es^- + C^+A^- \leftrightarrow Es^+//A^{-1} + Es^-//C^+ \tag{5}$$

where C, A, E, and // represent the cation, anion, electrode, and a double-layer, respectively. During charging (Eqs. (3) and (4)), the electrons move from a positive to a negative electrode through an external circuit while charging supercapacitors. As a result, the cations and anions of the electrolyte are concentrated in the negative and positive electrodes, resulting in an electrical double-layer that compensated for imbalanced charges [22]. The cations and anions combined again during cell discharge due to the electron transport from the negative terminal to the positive terminal.

4.1 Helmholtz Model

Helmholtz's model reports the charge separation at the interface of electrode and electrolyte when an external potential is applied. Under this condition, the positive and negative ions diffuse through the electrolyte to form a condensed layer on the electrode surface called Helmholtz double-layer [23]. The double-layer is used to store electrical charges statically. For modeling the spatial charge distribution at the double-layer interface, this theory is the simplest approximation. At a specific distance from the electrode surface, the oppositely charged ions neutralized the charged electronic conductor. The Helmholtz double-layer capacitance equation

is as follows:

$$C_{\mathrm{H}} = \varepsilon_0 \varepsilon_r . \frac{1}{\mathrm{X_H}} \tag{6}$$

where C_H represents the Helmholtz double-layer capacitance and X_H is the distance between nearest charges. However, this model did not explain the interaction between the electrode and solvent dipole moment as well as the possibility of surface adsorption and ion diffusion in the solution.

4.2 Gouy-Chapman or Diffuse Model

Gouy and Chapman are the first to notice the effect of ionic concentration and applied potential on electrode capacitance. According to this model, the electrolyte contains the same amount of oppositely charged ions, and these ions are flexible and tend to diffuse into the liquid phase, forming a diffuse layer [24]. The kinetic energy of the ions has an impact on the diffuse layer thickness. The ionic concentration varies with distance from the electrode surface, although the capacitance is inversely proportional to the ion-to-electrode distance. Because of the highly charged double-layers, this model fails, and the predicted thickness value is less than the experimental result. In quantitative applications, this model has limitations and ignores ion radius and finite-sized ions.

4.3 Stern Model

To overcome the limitations of the Helmholtz model and Gouy-Chapman model, Stern integrated both models. According to the Stern model, ions of finite size are limited in their approach to the surface. As a result, the Stern model described finite-sized ions, and the ionic radius accounted for ion-electrode contact. The Stern layer or compact layer is termed as inner Helmholtz plane (HIP) and the outer Helmholtz plane (OHP) are the two layers of adsorbed ions. The electric double-layer capacitance (C_{DL}) is given by combining the diffuse layer (C_D) and compact layer (C_H) capacitances [25].

$$\frac{1}{C_{DL}} = \frac{1}{C_D} + \frac{1}{C_H} \tag{7}$$

The Stern model considered dielectric permittivity and fluid viscosity to be constant and this is the limitation of this model.

4.4 Grahame Model

The interaction of uncharged species with solvent molecules was proposed by Grahame. According to his model, the Stern layer permits uncharged species to penetrate even when solvent molecules are close to the electrodes. When ions leave the solvated shell, they may come into contact with the electrode. Three layers appear to be present in the model such as a diffuse layer, HIP, and OHP. Both Grahame and Stern models show linear potential fluctuation up to OHP and an exponential variation in the diffuse layer [26].

4.5 Brockri-Devanathan-Muller Model

Brockri-Devanathan-Muller (BDM) postulated the action of solvent molecules at the interface of the double-layer in 1963. This model describes how the electrode surface has a defined position for solvent molecules attaching to it. The first layer of adhering solvent molecules is strongly related to the electric field. This link has an impact on the solvent permittivity and it varies according to the field strength. The solvent molecules are allowed to flow through the IHP and the layer contains partially solvated ions as well as the ions that have been specially adsorbed. Outside the IHP, the electrolyte solvated ions are present. The diffuse layer is the area far away from OHP that passes through the solvated ions [26] (Fig. 3).

5 Electric Double-Layer in Supercapacitor

The aforementioned models discussed the establishment of the electric double-layer. They do not describe how the supercapacitor electrode materials distribute charges. Also, there is a lack of thorough understanding of the behavior of ions in the micropores. The mobility of ions in the electrode depends on the pore size of the electrode material and the accessibility of ions in the narrow pores is insufficient [27]. The charge storage capacitance is affected by the free space of broad pores, not by all pores. However, mesopores allowing a rapid supply of electrolyte ions can boost the supercapacitor's power capability.

$$\frac{C}{A} = \frac{1}{bln(b/b-d)} \times \varepsilon_o \varepsilon_r \tag{8}$$

$$\frac{C}{A} = \frac{1}{bln(b/a_0)} \times \varepsilon_o \varepsilon_r \tag{9}$$

$$\frac{C_{tot}}{2A} = \frac{C_s}{A} = \frac{1}{b-a_0} \times \varepsilon_o \varepsilon_r \tag{10}$$

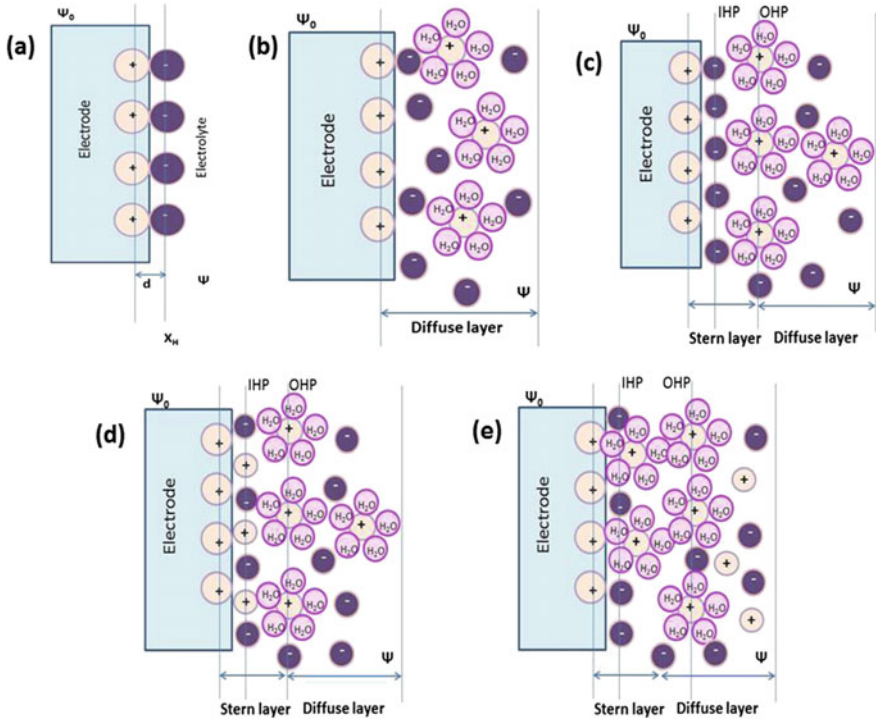

Fig. 3 Schematic models of double-layer **a** Helmholtz model, **b** Gouy-Chapman model, **c** Stern model, **d** Grahame model, and **e** BDM model

where a_0 is the ion size, b is the pore radius, and d is the distance between the ion and the electrode surface, C_S is the specific capacitance, and C_{tot} is the total capacitance.

6 Electric Field Across the Double-Layer

An electric field is created by the separation of electric charges. Coulomb's law and Poisson's equation are both related to the electric field, which is a fundamental property of the universe's electrical action [25]. The approximate electrical field (E) at an electrode interface with a 1.0 V potential difference over an electric double-layer is

$$E = 1.0/3.8 \times 10^{-8}\ \text{V cm}^{-1} \tag{11}$$

The double-layer has a thickness of 3.8 Å (0.38 nm). The thickness of the crystal is determined by the ionic radius of the crystal and the thickness of the solvation shell. For the double-layer capacitance, the solvated ions and the adsorbed solvent

molecules at the electrode interface operate as a dielectric medium. The molecular solvent (HCl or H_2O) dipole produces an interatomic field of 10^7 V cm^{-1}, and the interionic local field of ionic crystals is of the same magnitude. The ions have stable ionic states in the electric double-layer and as a result, there is no charge transfer breakdown when charges flow between the ions. The current leakage in the double-layer is caused thermodynamically by charge transfer at the interfacial field. The interfacial field at the electric double-layer can be calculated using the equation below.

$$E = \frac{-4\pi q}{\varepsilon} \tag{12}$$

where q is the charge density and ε is the dielectric constant. The maximum charge density renewable at the Hg electrode surface in an aqueous medium is 4.8×10^{-10} eus which is the charge of an electron. A compact Hg surface contains 3×10^{15} metal atoms per centimeter.

$$E = \frac{4\pi \times 4.8 \times 10^{-10}}{6} \times 0.17 \times 3 \times 10^{15} \text{ eus cm}^{-1} \tag{13}$$

$$E = 5 \times 10^5 \text{ eus cm}^{-1} \tag{14}$$

$$1 \text{ V} = 300 \times 1 \text{ eus} \tag{15}$$

$$E = 5 \times 10^5 \times 300 \text{ V cm}^{-1} \tag{16}$$

As result, E is value-dependent. The value of potential varies with the thickness d across the double-layer, but the magnitude is the same. The charge distribution, solvent dipole, and interphase region make up the double-layer. All these parameters are taken into account in the calculation of E.

7 Supercapacitor Parameter Evaluation

7.1 Capacitance

Capacitance is the measurement of a material's ability to store energy at various electrical potentials. Voltammetry and galvanometric techniques are used to determine the device's capacitance.

7.2 Voltammetry Capacitance

The specific capacitance of electrode materials is typically measured using the cyclic voltammetry (CV) technique in a three-electrode arrangement (working electrode, counter electrode, and reference electrode). The CV curve is generally rectangular in carbonaceous materials when capacitance is mainly derived from electrostatic interactions. Redox peaks with distortion, on the other hand, generally accompany a CV curve of a pseudocapacitive or battery-like substance. The specific capacitance of the active material is computed using the voltammetry charge integrated from the CV curves using the following equation:

$$C_V = \frac{\int i(V)dV}{2(v \times m \times \Delta V)} \tag{17}$$

$\int i(V)\, dV$—an integral area under the CV curve, v is the scan rate, m is the electrode mass, and ΔV is the potential window.

7.3 Galvanometric Capacitance

The electrode material's specific capacitance is calculated from the galvanostatic charge/discharge curve using the following equation. For the EDLC, the discharge curve is generally linear; however faradic contributions in pseudocapacitor and hybrid systems cause a substantial deviation from the linearity.

$$C_{sp} = \frac{I \times t}{m \times \Delta V} \tag{18}$$

where C_{sp}, I, t, are the specific capacitance of the electrode, discharge current (A), and discharge time (s), respectively.

7.4 Energy and Power Densities

In addition to capacitance, energy and power densities are two more significant factors to consider when evaluating the supercapacitor performance in a two-electrode setup. The energy density is the rate of energy supply per unit time, whereas the power density is the capacity to perform work. The cell voltage is built up between two electrodes when the supercapacitor is charged, and the conventional approach to estimating the maximum energy and power densities is as follows:

$$E = \frac{1}{2} \times \frac{C_{sp} \times \Delta V^2}{3.6} \tag{19}$$

$$P = \frac{3600 \times E}{t} \tag{20}$$

where E and P are the energy density and power density, respectively.

7.5 Cyclic Stability

The electrode material or device can provide reliable data regarding its stability after a certain number of charge/discharge cycles. The cyclic stability is often high (> 10,000 cycles) in EDLCs using carbon electrodes. Due to the non-ideal electrochemical reversibility of pseudocapacitive and faradic reactions, the cycle life of pseudocapacitors or hybrid capacitors is lower (800–8000 cycles). The parameters such as operating voltage, electrolyte, temperature, and current density affect the cyclic performance of electrode materials.

7.6 Coulombic Efficiency

The ratio of discharge capacity to the charge capacity within the cycle.

$$Coulombic\ efficiency(\%) = \frac{Discharge\ time}{Charge\ time} \times 100 \tag{21}$$

7.7 Thermal Stability

The temperature withstanding capacity of the electrode, electrolyte, and separator is called thermal stability.

7.8 Self-discharge Rate

It is associated with the gradual loss of potential and energy across the charged supercapacitor over a certain period when it is kept under the open-circuit condition.

7.9 Charge Balancing Equation

Charge storage ability varies for different materials, so the mass balancing equation optimizes the performance of the supercapacitor. It gives the mass ratios of positive and negative electrodes.

$$\frac{m+}{m-} = \frac{C+}{C-} \times \frac{\Delta E+}{\Delta E-} \tag{22}$$

where m^+ and m^- are the mass of positive and negative electrodes, C^+ and C^- are the capacitance of positive and negative electrodes, ΔE^+ and ΔE^- are the potentials of positive and negative electrodes.

8 Electrode Materials

Supercapacitor properties such a specific capacitance and charge storage are directly influenced by the electrode materials. The specific capacitance can be increased by increasing the surface area of the electrodes [28]. The pore size has a direct impact on the active surface area of electrode material because the electrolyte flows through the pores. Moreover, the pore size should be close to the size of the electrolyte ions for effective charge storage. The pore size must not be larger or smaller than the electrolyte ions because this reduces the capacitance. The smaller pore diameter (> 1 nm) lowers the accessibility of electrolyte ions leading to lower capacitance. In the case of larger pore size, the average distance between the center of ion and the pore wall increases, resulting in poor electrolyte contact which intern drops the capacitance. Therefore, with the right pore size distribution and retention can be improved to obtain higher capacitance. Owing to the good diffusion of electrolyte ions across the electrode material with an efficient pore size distribution, an ion sieving effect occurs [29].

The SOHIO was the first to patent a carbon-based electric double-layer capacitor in 1969. The most noteworthy properties of electrode materials in supercapacitor applications are their high surface area, variable pore size, pre-structure, electrical conductivity, surface functionality, and electrolyte ion accessibility [30]. The carbon-based materials are ideal electrodes for supercapacitors because of their unexpected chemical stability, thermal stability, low cost, environmental friendliness, and abundance. Carbon aerogels, carbon power, carbon composites, carbon sheets, carbon monoliths, carbon fibers, and carbon foams are just some of the carbon-based electrode materials we can work with. The carbon allotropes are also used as electrode materials in electrochemical capacitors.

8.1 Activated Carbon (AC)

AC materials are the most predominately used active materials in the EDLCs on account of their high electrical conductivity (10^{-8}–10^{10} S m^{-1}), high surface area (3000 m^2 g^{-1}), and low cost. The surface characteristics are established via the activated carbon manufacturing techniques [31] such as chemical or physical activation. In the physical activation process, pyrolysis of organic precursors takes place at high temperatures (600–1200 °C) in an inert environment to produce AC materials. On the other hand, in the chemical activation process, the AC materials are prepared at low temperatures (400–700 °C) by impregnating chemicals such as acid, alkali, and salts into the carbon source [32]. The activation processes produce large surface area carbon materials with different pore sizes. Macropores (> 50 nm), mesopores (2–50 nm), and micropores (less than 2 nm) are among the pore sizes accessible in the AC. The specific capacitance of the AC depends on various factors including pore size, pore shape, surface area, surface functionality, and conductivity [32]. The low electrochemical performance of AC is caused by insufficient activation and activation energy. The surface area, pore size, and pore size distribution of the AC materials depend on the types of organic precursors used and activation methods. The surface area of AC materials was observed in the range of 1000–2000 m^2 g^{-1} [33].

Xu et al. [34] prepared the AC from an apricot shell and activated it with NaOH delivered a specific capacitance of 339 F g^{-1}. In another study, Roldán et al. [35] synthesized the AC from coke and activated it with KOH showed capacitance of 351 F g^{-1}. Xu et al. [36] reported the free-standing AC/CNTs paper electrode exhibited capacitance of 267.7 F g^{-1}. Jung et al. [37] prepared flexible and transparent carbon nanocup (CNC) thin-film electrodes using a porous template (Fig. 4). The branched structure of the CNC electrode exhibited the capacitance of 409 mF cm^2 with a specific power and specific energy of 19 mW cm^{-3} and 47 mWh cm^{-3}, respectively. The capacitance (1220 mF cm^2) observed at 80 °C was three times higher than that of capacitance at room temperature. The electrode showed long cycle life even bending at 45°.

The mesoporous AC synthesized from rice husk and activated using CO_2 exhibited a surface area of 1357 m^2 g^{-1} with a specific capacitance of 114 F g^{-1} in organic electrolyte and 106 F g^{-1} in the aqueous electrolyte at 5 mV s^{-1} [38]. In a different work, the mesoporous carbon prepared by the activation of Polyacrylonitrile (PAN) using NaOH showed a specific capacitance of 187 F g^{-1} [39]. The AC materials also synthesized from olive pits [40] and rice husk [41] activated with KOH delivered a capacitance of 260 F g^{-1} and 250 F g^{-1}, respectively. Wang et al. [42] improved the capacitance from 17.68 to 171.2 F g^{-1} by increasing the surface area of AC materials from 621 to 2685 m^2 g^{-1}. The capacitance of AC electrodes in aqueous electrolytes is in the range of 100–300 F g^{-1}, which is higher than that in organic electrolytes (< 150 F g^{-1}) because of the smaller size of electrolyte ions [43]. Subramani et al. [44] prepared the porous carbon derived from the orange peel bio-waste and used it as an electrode for the flexible solid-state supercapacitor.

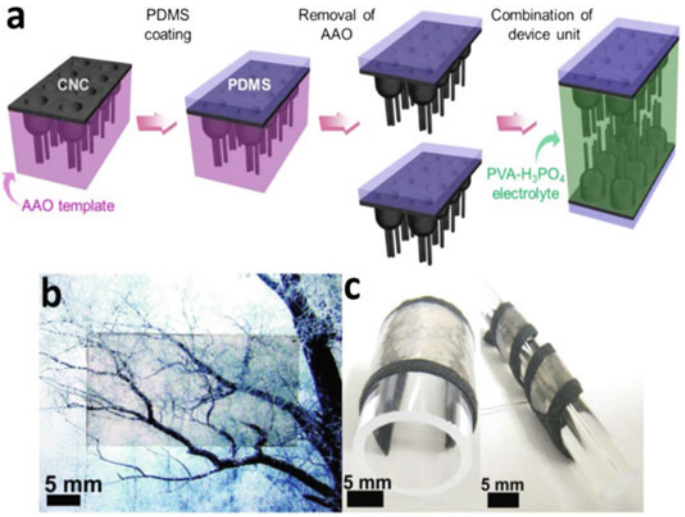

Fig. 4 Schematics of the fabrication process of a branched CNC-based supercapacitor and its optical images. **a** First, the CNC films are transferred to PDMS and released by dissolving AAO templates. Optical pictures demonstrating **b** transparent and **c** flexible natures of CNCs supercapacitor devices. Adapted with permission from Ref. [37], Copyright (2012), Nature Research

The high surface area (2160 $m^{2\,g-1}$) electrode delivered a capacitance, energy density, and power density of 460 F g^{-1}, 11.4 Wh kg^{-1}, and 6.6 KW kg^{-1}, respectively. They also fabricated a non-aqueous large size cylindrical device (Fig. 5)

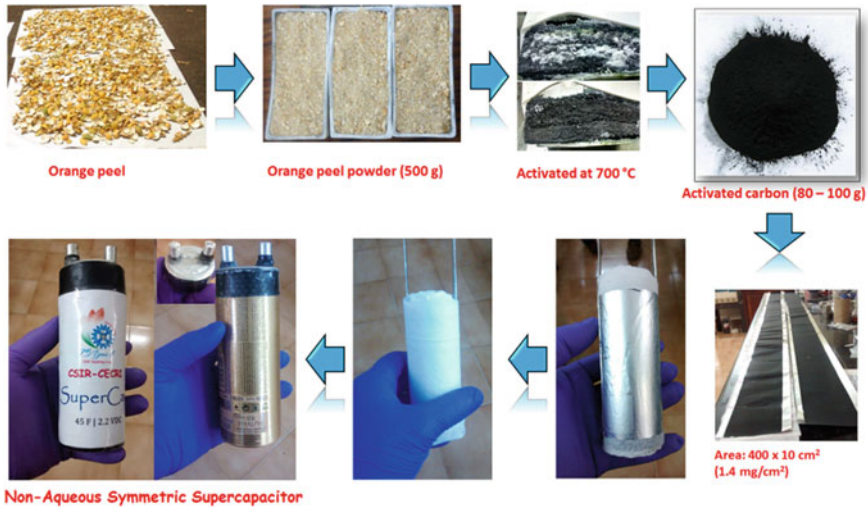

Fig. 5 Step-by-step fabrications of non-aqueous symmetric supercapacitor device. Adapted with permission from Ref. [45], Copyright (2019), Nature Research

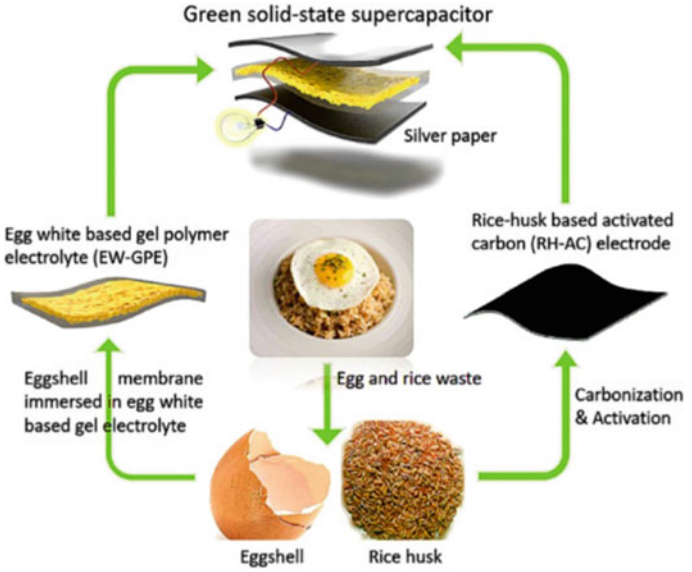

Fig. 6 Schematic of the fabrication of the green solid-state supercapacitor using the egg and rice waste (broken eggshell and rice husk). Adapted with permission from Ref. [46], Copyright 2018, Elsevier

by rolling two electrodes with a nonwoven foam as a separator and placed in an aluminum container filled with tetraethylammonium tetrafluoroborate in acetonitrile [45]. Na et al. [46] synthesized activated porous carbon from rice husk and egg white as the gel electrolyte (Fig. 6). The supercapacitor showed a high specific capacitance of 204.4 F g^{-1} at a current density of 1.0 A g^{-1} with good cyclic stability.

In recent years, covalent organic frameworks (COFs) created huge interest due to their high surface area, thermal and chemical stability, tunable pore size, and lost cost. Like organic biomass precursors, the COFs were used as precursor sources for the synthesis of porous carbon materials. Vargheese et al. [47] synthesized N-doped porous carbon from triazine-based COFs for high-performance supercapacitors. In a different study, polyimine-based COF was used as a precursor for the preparation of N-doped porous graphene delivered a capacitance of 460 F g^{-1} at a current density of 1.0 A g^{-1} [48]. Baumann et al. [49] synthesized hierarchical porous carbon derived from COFs for high mass loading supercapacitors. However, porous carbons derived from COFs as electrode materials for supercapacitors are scarce in the literature.

8.2 Carbon Nanotubes (CNTs)

The CNTs are an advanced form of carbon materials and can be classified as single-walled carbon nanotubes (SWCNTs), double-walled carbon nanotubes, and multi-walled carbon nanotubes (MWCNTs), which are used in different applications. The high electrical conductivity and high porosity of the tubular structured CNTs are used as new electrode materials for supercapacitors [50]. Owing to the mesoporous structure and low electrochemical series resistance, the CNT electrodes showed higher specific power than AC materials because of the faster diffusion of electrolyte ions. Du et al. [51] prepared CNT thin films using a colloidal suspension of CNTs to reduce the electrochemical series resistance. In another work, the CNTs were grown on nickel foam using the chemical vapor deposition (CVD) technique showed higher capacitance (127% higher) and lower electrochemical series than CNTs synthesized by the conventional method [52]. However, the surface area of CNTs is lower than that of AC which is the main drawback of CNTs in high-energy supercapacitors. To overcome this problem, the CNTs were treated with oxidative species to enlarging the porosity to increase specific surface area. Introducing a functional group into the CNTs matrix will increase the electrochemical performance. For example, the charge affinity of carbon is enhanced by doping nitrogen, and the wettability is increased by the addition of hydrophilic groups [53]. The aligned CNTs exhibited fast ionic transport than the entangled CNTs, which denotes the regular structures make way to migrate ions. Tips or walls of the CNTs are activated to improve the specific surface area. Pan et al. [50] synthesized tube-in-tube MWCNTs nanostructures by aluminum oxide-assisted template method. The average inner and outer diameters of MWCNTs were 1–3 nm and 50 nm, respectively. The electrode showed the specific capacitance of 315 F g^{-1} at 50 mV s^{-1} in 0.5 M H_2SO_4. Therefore, the capacitance depends on the pore size, pore-size distribution, structure, surface area, and conductivity of the electrodes. Frackowiak et al. [54] also synthesized MWCNTs and were used as electrode materials for high-performance supercapacitors. The MWCNTs exhibited capacitances in the range of 4–135 F g^{-1}, depending on their CNT types, pore size, surface area, and post-treatments. To enhance the surface area, several works have been developed to increase the active sites and conductivity of CNTs. Doping of heteroatoms on CNTs can also improve the active sites and conductivity [55]. The nitrogen-doped spherical particle of CNTs was prepared by emulsion-assisted method and showed three times higher specific capacitance than the pristine CNTs [56]. The dimension of CNTs changed from 1 to 3D by incorporating pseudocapacitive materials. In this type, the electrochemical properties are enhanced by a small diffusion path, fast redox reactions, and interconnected pores. The difficult synthesis process and high cost are still questionable for practical applications of CNT electrodes.

8.3 Graphene

The carbon allotrope 2D graphene is made of a polyaromatic honeycomb structure with sp^2 hybridized carbon atoms. The visible characteristics such as thermal conductivity (3000 W m K^{-1}), electrical conductivity, mechanical property (130 GPa), and high surface area (2600 m^2 g^{-1}) exhibited good electrochemical performance [57]. Graphene was discovered when the idea rises to utilize the fewer layer of graphite, so the synthesis of graphene is difficult. Mechanical exfoliation, chemical modification, and CVD methods were applied to synthesize graphene. The graphene was used as electrodes for high-performance supercapacitors because of its unique properties. The advantages of graphene electrodes in comparison with AC materials and CNTs are they do not depend on the pore size distribution in the electrode surface and also the accessibility of complete surfaces (interior and exterior) of the electrode by the electrolyte [58].

Even though the graphene was synthesized using different methods, the low agglomerated graphene exhibited improved specific capacitance. The surface functional group and open-pore system in graphene improve the ions transport which intern increases the capacitance. The re-stacking property of graphene leads to irreversible capacity loss and decreases the coulombic efficiency of the electrochemical device [59]. To reduce the re-stacking nature of graphene, Hummer's method is used to synthesize graphene or reduced graphene oxide (rGO) from graphite. The rGO exhibits surface functional groups such as –OH, –COOH, C=O, and epoxide. Also, the thermal exfoliation method is adopted to reduce the aggregation of rGO [60]. Among the different thermal exfoliation techniques, microwave irradiation reduces the time duration and reaction temperature, and thus showed increased specific capacitance. The ion transfer path is quite longer in grFaphene or rGO electrodes because the electrolyte ions transfer across the graphene sheets [61]. Xu et al. [62] minimized the ion transport path by holey graphene sheets, there is an ion-transfer between holes of graphene sheets and retaining effective electron-transport. Zhu et al. [63] reported that the activated graphene oxide using KOH exhibited the pore diameter and specific surface area of 1–10 nm and 3100 m^2 g^{-1}, respectively. Kim et al. [64] fabricated graphene-derived carbons by chemical activation of graphene with KOH. The carbon electrode showed both mesopores and micropores structure and exhibited a surface area of 3290 m^2 g^{-1}. The electrode delivered a high gravimetric capacitance of 174 F g^{-1}. The higher capacitance is due to the fast transfer of electrolyte ions on the surface of the porous electrode. As a result, the high specific power and specific energy of 338 KW kg^{-1} and 74 Wh kg^{-1}, respectively were observed. Also, the effective doping on graphene surfaces enhances its electrochemical behavior. To improve the capability of ion adsorption, the graphene aerogel and hydrogel were synthesized [65, 66] however, the graphene aerogel and hydrogel exhibited poor conductivity. Yang et al. [67] described the chemical converted graphene hydrogel films with increasing packing density by removing non-volatile and volatile electrolytes showed enhanced charge transport and exhibited volumetric energy densities of 60 Wh L^{-1}. Yoon et al.

[68] prepared vertically aligned rGO film electrodes for high-performance supercapacitors. The films with a packing density of 1.18 g cm^{-3} delivered a high volumetric capacitance of 171 F cm^{-3} in a 6.0 M KOH electrolyte. However, still there is a need to increase the energy density of supercapacitors.

8.4 Carbon Nanofibers

Carbon nanofibers are generally derived from polyacrylonitrile (PAN). Various synthetic techniques such as electrospinning, template-assisted solvothermal, and CVD produce carbon nanofibers using the PAN as a precursor [69]. Two steps are involved in the synthesis; nanofiber synthesis and carbonization. The conductivity of carbon nanofibers directly depends on the carbonization temperature. The conductivity and specific surface area of carbon nanofibers are lesser than that of the CNTs. However, high porosity and small-fiber diameter showed good electrochemical performance. Niu et al. [70] reported the synthesis of Inter-connected carbon nanofibers by electrospinning side-by-side polyvinylpyrrolidone (PVP) and (PAN), followed by carbonization. The carbon nanofibers showed higher capacitance than that of carbon fibers prepared from the PVP/PAN blend. They also investigated the effect of PVP and PAN ratios on the morphologies and surface area of the carbon fibers for supercapacitor applications. Nan et al. [71] prepared electrospun carbon nanofiber mats by electrospinning biochar and PAN mixture, followed by a pyrolysis process. The weight ratio of 4:10 biochar:PAN showed the higher gravimetric capacitance of 37.6 F g^{-1}.

8.5 Hybrid Carbon Materials

Two different types of carbon materials combined to produce hybrid carbon materials, which demonstrate a synergistic effect to enhance supercapacitor performance. Graphene sheet hybridized with carbon black and mesoporous carbon to minimize the aggregation and increase the specific capacitance value. When the CNTs were intercalated with the graphene sheets, the mechanical strength and electrical conductivity of the graphene were significantly improved. For instance, Yu et al. [72] reported the high specific surface area (396 m^2 g^{-1}) and electrical conductivity (102 S cm^{-1}) of graphene sheets that were developed by combining with the CNTs fibers. Cheng et al. [73] also prepared the Graphene/CNTs composite electrodes exhibited specific capacitance of 290.4 F g^{-1} with the power and energy densities of 263.2 kW kg^{-1} and 155.6 Wh kg^{-1}, respectively. They also prepared quaternary composites composed of AC/CB/CNTs/carbon nanofibers delivered a capacitance of 66.1 F cm^{-3}. The specific energy and specific power were calculated as 29.6 Wh L^{-1} and 101.7 kW L^{-1}, respectively. After 30,000 cycles, the electrode losses 8.6% of its original capacitance indicating its excellent stability.

In another study, Wang et al. [74] improved the electrochemical property of graphene sheets by incorporating carbon black (CB) as a spacer. Ogata et al. [75]

Table 1 Different carbon-based materials are used as electrodes in EDLCs

Electrode	Specific capacitance ($F\ g^{-1}$)	Power density ($W\ kg^{-1}$)	Energy density ($Wh\ kg^{-1}$)	Cyclic stability	References
Porous carbon	120 at 1 $A\ g^{-1}$	2827	74	100% after 100,000 cycles	[76]
B-doped rGO	200 at 0.1 $A\ g^{-1}$	10	5.5	95% after 4500 cycles	[77]
P-doped carbon/CNT monolith	220 at 1 $A\ g^{-1}$	226	10 $kWh\ kg^{-1}$	17% after 1000 cycles	[55]
CNTs grown on carbon cloth	210 at 1 $A\ g^{-1}$	–	27.8	97–95% after 10,000 cycles	[78]
N-doped porous carbon	185 at 0.4 $A\ g^{-1}$	1747	230	76.3% after 8000 cycles	[79]
SWCNT/rGO hybrid	222 at 1 $A\ g^{-1}$	1.19 $kW\ kg^{-1}$	106.6	99% after 1000 cycles	[80]
Carbon nanofiber paper	254 at 0.2 $A\ g^{-1}$	90	7.1	98% after 1000 cycles	[81]
Graphene/f-MWCNT	740.9 $\mu F\ cm^{-2}$ at 1 $\mu A\ cm^{-2}$	2.41 $W\ cm^{-3}$	0.107 $mWh\ cm^{-3}$	85% after 20,000 cycles	[82]
3D macro-mesoporous carbon	166 at 1 $A\ g^{-1}$	200	39	92.2% after 10,000 cycles	[83]
Vertically aligned CNTs	200 at 20 $A\ g^{-1}$	40	20	–	[84]
Onion-like carbon	0.9 $mF\ cm^{-2}$ at 100 $mV\ s^{-1}$	1 $kW\ cm^{-3}$	1×10^{-2} $Wh\ cm^{-3}$	100% after 10,000 cycle	[85]

developed rGO/GO/rGO composite electrode for supercapacitor and the device voltage was extended up to 1.5 V.

Even though it is very challenging to arrange a clear-cut comparison of the various carbon-based electrode materials used in EDLCs, we collected the data using different parameters such as specific capacitance, energy density, power density, and cyclic stability and presented in Table 1.

9 Self-discharge in Supercapacitors

When external sources are disconnected from EDLCs, voltage loss between the electrodes occurs spontaneously. Self-discharge is the term for this. As a result of the charge redistribution, the total capacitance of the electrode material rises [86]. Self-discharge is caused by three types of self-discharge mechanisms: charge redistribution, leakage current, and faradic reaction. In the case of the charge redistribution mechanism, the movement of charged ions is adsorbed on the electrode surface because of the concentration slope. On the other hand, the leakage current occurs owing to internal ohmic leakage between the oppositely charged electrodes. The Faradaic reaction mechanism outlines the redox reaction that takes place on the surface of the electrode due to excessive charging. The above self-discharge processes reduce the open circuit voltage followed by the energy loss in the EDLC devices [87]. There is some heat generated during the charge/discharge process in the EDLCs. This explains the voltage variations that are not caused by the energy loss. Owing to the galvanostatic and potentiostatic charging, the voltage changes in the device are slower in open circuits and with time, the voltage decay process slows down. The following equation is used to calculate the accumulated energy on EDLCs.

$$E = \frac{1}{2} C U^2 \tag{23}$$

where E is the energy accumulated by the EDLC and U is the voltage drop. Detailed explanations of the self-discharge mechanisms and the factors influencing the self-discharge processes can be obtained from the above references.

10 Applications of Supercapacitors

The fast charging-discharging nature of the supercapacitors is explored in the energy storage technology. The high power density and tunable energy density of supercapacitors show priority in portable electronics. The high-performance supercapacitor is playing a superior role in power supply, energy storage, power production, and memory backup [88]. A double layer electrical capacitor is used in a variety

of applications, including energy regenerating, compensation devices, and energy equalization.

Energy regeneration: in railways, regenerative breaks are used to recuperate the electricity utilized for acceleration. The electricity is stored in an electrical double-layer capacitor during the crane's ascension. It decreases the use of fossil fuels and decreases the efficiency of energy production.

Momentary voltage drop compensator: pose outages caused by lightning strikes can ruin equipment used in enterprises and hospitals. An electrical double layer capacitor is used to compensate for electricity until another source is connected.

The electrical double-layer capacitors utilized in energy fluctuation sources are known as energy equalization. Some power plants generate electricity using green energy, which is subject to natural changes. EDLCs keep electricity stable by holding inputs and delivering fewer outputs.

11 Conclusion

We have discussed briefly the overview of EDLCs including their history, electrodes fabrication, and applications. The preparation of EDLC materials such as AC, CNTs, graphene, and carbon nanofibers are described with a brief statement of their properties including the specific surface area, pore size, pore-size distribution, capacitance, and energy and power densities. The pore structures are closely associated with the types of precursors and how they are processed to obtain the electrode materials for EDLCs. To improve the performance of EDLCs, it is important to optimize the interface between electrode and electrolyte. The EDLC is a better replacement for many applications that needs storage of energy due to its fast charging/charging capability, long cycle life, and wide operating temperature range. With the continued growth of the capacitor market and the ongoing research on electrode materials and cell assembly, electrochemical capacitors emerging as new types of possible alternatives for batteries.

References

1. A. González, E. Goikolea, J.A. Barrena, R. Mysyk, Review on supercapacitors: technologies and materials. Renew. Sustain. Energy Rev. **58**, 1189–1206 (2016)
2. J. Zhao, A.F. Burke, Review on supercapacitors: technologies and performance evaluation. J. Energy Chem. **59**, 276–291 (2020)
3. B.K. Kim, S. Sy, A. Yu, J. Zhang, Electrochemical supercapacitors for energy storage and conversion, in *Handbook of Clean Energy Systems* (Wiley, Chichester, UK, 2015)
4. L. Shuai, L. Wei, W. Huai, Review on reliability of supercapacitors in energy storage applications. Appl. Energy **278**, 115436 (2020)
5. M.A.A.M. Abdah, N.H.N. Azman, S. Kulandaivalu, Y. Sulaiman, Review of the use of transition-metal-oxide and conducting polymer-based fibres for high-performance supercapacitors. Mater. Des. **186**, 108199 (2020)

6. D.P. Chatterjee, A.K. Nandi, A review on the recent advances in hybrid supercapacitors. J. Mater. Chem. A **9**, 15880–15918 (2021)
7. A. Allagui, T.J. Freeborn, A.S. Elwakil, B.J. Maundy, Reevaluation of performance of electric double-layer capacitors from constant-current charge/discharge and cyclic voltammetry. Sci. Rep. **6**, 38568 (2016)
8. R. Dubey, V. Guruviah, Review of carbon-based electrode materials for supercapacitor energy storage. Ionics **25**, 1419–1445 (2019)
9. Y. Shao, M.F. El-Kady, J. Sun, Y. Li, Q. Zhang, M. Zhu, H. Wang, B. Dunn, R.B. Kaner, Design and mechanisms of asymmetric supercapacitors. Chem. Rev. **118**, 9233–9280 (2018)
10. B.E. Conway, Behavior of the double layer in nonaqueous electrolytes and nonaqueous electrolyte capacitors, in *Electrochemical Supercapacitors*, Chap. 2 (Springer, New York, 1999)
11. O.Z. Stern, Theory of the electrical double layer. Electrochem. **30**, 508 (1924)
12. H.I. Becker, Low voltage electrolytic capacitor. US Patent 2800616 (1957)
13. R.A. Rightmire, Electrical energy storage apparatus. US Patent 3288641, 29 (1966)
14. S. Trasatti, G. Buzzanca, Ruthenium dioxide: A new interesting electrode material. Solid state structure and electrochemical behaviour. J. Electroanal. Chem. Interfacial. Electrochem. **29**, A1–A5 (1971)
15. G.L. Bullard, H.B. Sierra-Alcazar, H.L. Lee, J.L. Morris, Operating principles of the ultra capacitor. IEEE Trans. Magn. **25**, 102–106 (1989)
16. A.N. Neyagawa, I.T. Kadoma, A.Y. Hirakata, US Patent Number 4, 737, 889 "Ploarizable Electrode Body and Method for Its Making", April 12, (1988)
17. L.L. Zhang, X.S. Zhao, Carbon-based materials as supercapacitor electrodes. Chem. Soc. Rev. **38**, 2520–2531 (2009)
18. C. Zhong, Y. Deng, W. Hu, J. Qiao, L. Zhang, J. Zhang, A review of electrolyte materials and compositions for electrochemical supercapacitors. Chem. Soc. Rev. **44**, 7484–7539 (2015)
19. V. Augustyn, P. Simon, B. Dunn, Pseudocapacitive oxide materials for high-rate electrochemical energy storage. Energy Environ. Sci. **7**, 1597 (2014)
20. M.A. Scibioh, B. Viswanathan, *Materials for Supercapacitor Applications* (Elsevier, Amsterdam, 2020), pp. 15–33
21. J.P. Zheng, J. Huang, T.R. Jow, The limitations of energy density for electrochemical capacitors. J. Electrochem. Soc. **144**, 2026 (1997)
22. F. Stoeckli, T.A. Centeno, Pore size distribution and capacitance in microporous carbons. Phys. Chem. Chem. Phys. **14**(33), 11589–11591 (2012)
23. J.P. Zheng, T.R. Jow, in *Proceedings of The 5th International Seminar on Double Layer Capacitors and Similar Energy Storage Devices*, Florida Educational Seminars (1995)
24. V. Helmholtz, H.L.F. Ann. Physik, **89**, 211 (1853)
25. J.O'M. Bockris, M.A. Devanathan, K.Muller, On the structure of charged interfaces. Proc. R. Soc. **55** A274 (1963)
26. T.A. Centeno, F. Stoeckli, The volumetric capacitance of microporous carbons in organic electrolyte. Electrochem. Commun. **16**(1), 34–36 (2012)
27. B.E. Conway, *The Double Layer at Capacitor Electrode Interfaces: Its Structure and Capacitance*, Chap. 10 (Elsevier, Amsterdam, 1981)
28. O. Barbieri, M. Hahn, A. Herzog, R. Kötz, Capacitance limits of high surface area activated carbons for double layer capacitors. Carbon **43**, 1303–1310 (2005)
29. C. Largeot, C. Portet, J. Chmiola, P.-L. Taberna, Y. Gogotsi, P. Simon, Relation between the ion size and pore size for an electric double-layer capacitor. J. Am. Chem. Soc.**130**, 2730–2731 (2008)
30. H. Choi, H. Yoon, Nanostructured electrode materials for electrochemical capacitor applications. Nanomaterials **5**, 906–936 (2015)
31. P. Simon, A. Burke, Nanostructured carbons: double-layer capacitance and more. Electrochem. Soc. Interface **17**(1), 38–44 (2008)
32. P. Simon, Y. Gogotsi, Materials for electrochemical capacitors. Nat. Mater. **7**(11), 845–854 (2008)

33. M. Sevilla, R. Mokaya, Energy storage applications of activated carbons: supercapacitors and hydrogen storage. Energy Environ. Sci. **7**(4), 1250–1280 (2014)
34. B. Xu, Y. Chen, G. Wei, G. Cao, H. Zhang, Y. Yang, Activated carbon with high capacitance prepared by NaOH activation for supercapacitors. Mater. Chem. Phys. **124**(1), 504–509 (2010)
35. S. Roldán, I. Villar, V. Ruíz, C. Blanco, M. Granda, R. Menéndez, R. Santamaría, Comparison between electrochemical capacitors based on NaOH- and KOH-activated carbons. Energy Fuels **24**(6), 3422–3428 (2010)
36. G. Xu, C. Zheng, Q. Zhang, J. Huang, M. Zhao, J. Nie, X. Wang, F. Wei, Binder-free activated carbon/carbon nanotube paper electrodes for use in supercapacitors. Nano Res. **4**(9), 870–881 (2011)
37. H.Y. Jung, M.B. Karimi, M.G. Hahm, P.M. Ajayan, Y.J. Jung, Transparent, flexible supercapacitors from nano-engineered carbon films. Sci. Rep. **2**, 773 (2012)
38. S. Kumagai, M. Sato, D. Tashima, Electrical double-layer capacitance of micro- and mesoporous activated carbon prepared from rice husk and beet sugar. Electrochim. Acta. **114**, 617–626 (2013)
39. B. Xu, F. Wub, R. Chenb, G. Caoa, S. Chenb, Y. Yang, Mesoporous activated carbon fiber as electrode material for high-performance electrochemical double layer capacitors with ionic liquid electrolyte. J. Power Sourc. **195**, 2118–2124 (2010)
40. E. Redondo, J. Carretero-González, E. Goikolea, J. Ségalini, R. Mysyk, Effect of pore texture on performance of activated carbon supercapacitor electrodes derived from olive pits. Electrochim. Acta **160**, 178–184 (2015)
41. H. Xu, B. Gao, H. Cao, X. Chen, L. Yu, K. Wu, L. Sun, X. Peng, J. Fu, Nanoporous activated carbon derived from rice husk for high performance supercapacitor. J. Nanomater. **2014**, 1–7 (2014)
42. C.M. Wang, C.Y. Wen, Y.C. Chen, J.Y. Chang, C.W. Ho, K.S. Kao, W.C. Shih, C.M. Chiu, Y.A. Shen, in *Proceedings of the 2nd International Conference on Industrial Application Engineering*, Kitakyushu, Japan (2015), pp. 439–442
43. A. Ali, R. Jamal, W. shao, A. Rahman, Y. Osman, T. Abdiryim, Structure and properties of solid-state synthesized poly(3,4-propylenedioxythiophene)/nano-ZnO composite. Prog. Nat. Sci. Mater. Int. **23**, 524–531 (2013)
44. K. Subramani, N. Sudhan, M. Karnan, M. Sathish, Orange peel derived activated carbon for fabrication of high-energy and high-rate supercapacitors. Chem. Sel. **2**, 11384–11392 (2017)
45. K. Subramani, M. Sathish, Fabrication of 9.6 V high-performance asymmetric supercapacitors stack based on nickel hexacyanoferrate-derived $Ni(OH)_2$ nanosheets and bio-derived activated carbon. Sci. Rep. **9**, 1104 (2019)
46. R. Na, X. Wang, N. Lu, G. Huo, H. Lin, G. Wang, Novel egg white gel polymer electrolyte and a green solid-state supercapacitor derived from the egg and rice waste. Electrochim. Acta **274**, 316–325 (2018)
47. S. Vargheese, R.T.R. Kumar, Y. Haldorai, Synthesis of triazine-based porous organic polymer: a new material for double layer capacitor. Mater. Lett. **249**, 53–56 (2019)
48. J. Romero, D. Rodriguez-San-Miguel, A. Ribera, R. Mas-Ballesté, T.F. Otero, I. Manet, F. Licio, G. Abellán, F. Zamora, E. Coronado, Metal-functionalized covalent organic frameworks as precursors of supercapacitive porous N-doped graphene. J. Mater. Chem. A **5**, 4343–4351 (2017)
49. D. Baumann, C. Lee, C. Wan, H. Sun, X. Duan, Hierarchical porous carbon derived from covalent triazine frameworks for high mass loading supercapacitors. ACS Mater. Lett. **1**, 320–326 (2019)
50. H. Pan, C.K. Poh, Y.P. Feng, J. Lin, Supercapacitor electrodes from tubes-in-tube carbon nanostructures. Chem. Mater. **19**, 6120–6125 (2007)
51. C. Du, J. Yeh, N. Pan, High power density supercapacitors using locally aligned carbon nanotube electrodes. Nanotechnology **16**, 350 (2005)
52. H.-F. Li, F. Wu, C. Wang, P.-X. Zhang, H.-Y. Hu, N. Xie, M. Pan, Z. Zeng, S. Deng, M.H. Wu, K. Vinodgopal, G.-P. Dai, One-step chemical vapor deposition synthesis of 3D N-doped carbon nanotube/N-doped graphene hybrid material on nickel foam. J. Nanomater. **8**, 700 (2018)

53. A. Izadi-Najafabadi, S. Yasuda, K. Kobashi, T. Yamada, D.N. Futaba, H. Hatori, M. Yumura, S. Iijima, K. Hata, Extracting the full potential of single-walled carbon nanotubes as durable supercapacitor electrodes operable at 4 V with high power and energy density. Adv. Mater. **22**, E235–E241 (2010)
54. E. Frackowiak, K. Metenier, V. Bertagna, F. Beguin, Supercapacitor electrodes from multiwalled carbon nanotubes. Appl. Phys. Lett. **77**, 2421–2423 (2000)
55. J. Patiño, N. López-Salas, M.C. Gutiérrez, D. Carriazo, M.L. Ferrer, F. del Monte, Phosphorus-doped carbon–carbon nanotube hierarchical monoliths as true three-dimensional electrodes in supercapacitor cells. J. Mater. Chem. A **4**(4), 1251–1263 (2016)
56. D. Gueon, J.H. Moon, Nitrogen-doped carbon nanotube spherical particles for supercapacitor applications: emulsion-assisted compact packing and capacitance enhancement. ACS Appl. Mater. Interfaces **7**, 20083–20089 (2015)
57. P. Forouzandeh, V. Kumaravel, S.C. Pillai, Electrode materials for supercapacitors: a review of recent advances. Catalysts **10**, 969 (2020)
58. G.K. Sinniah, M.Z. Shah, H.C. Siong, The needs for changes in travel behaviour towards a low carbon society, in IBIMA, Madrid, Spain, pp. 3868–3876 (2015)
59. C. Liu, Z. Yu, D. Neff, A. Zhamu, B.Z. Jang, Graphene-based supercapacitor with an ultrahigh energy density. Nano Lett. **10**, 4863–4868 (2010)
60. X. Du, P. Guo, H. Song, X. Chen, Graphene nanosheets as electrode material for electric double-layer capacitors. Electrochim. Acta **55**, 4812–4819 (2010)
61. W. Lv, D.-M. Tang, Y.-B. He, C.-H. You, Z.-Q. Shi, X.-C. Chen, C.-M. Chen, P.-X. Hou, C. Liu, Q.-H. Yang, Low-temperature exfoliated graphenes: vacuum-promoted exfoliation and electrochemical energy storage. ACS Nano **3**, 3730–3736 (2009)
62. Y. Xu, Z. Lin, X. Zhong, X. Huang, N.O. Weiss, Y. Huang, X. Duan, Holey graphene frameworks for highly efficient capacitive energy storage. Nat. Commun. **5**, 4554 (2014)
63. Y. Zu, S. Murali, M.D. Stollerk, J. Ganesh, W. Cai, P.J. Ferreira, A. Pirkle, R.M. Wallace, K.A. Cychosz, A. Thommes, D. Su, E.A. Stach, R.S. Ruoff, Carbon-based supercapacitors produced by activation of graphene. Science **332**, 1537–1541 (2011)
64. T.Y. Kim, G. Jung, S. Yoo, K.S. Suh, R.S. Ruoff, Activated graphene-based carbons as supercapacitor electrodes with macro-and mesopores. ACS Nano **7**, 6899–6905 (2013)
65. Y. Liu, Y. Shen, L. Sun, J. Li, C. Liu, W. Ren, F. Li, L. Gao, J. Chen, F. Liu, Y. Sun, N. Tang, H.-M. Cheng, Y. Du, Elemental superdoping of graphene and carbon nanotubes. Nat. Commun. **7**, 10921 (2016)
66. Y. Zhao, C. Hu, Y. Hu, H. Cheng, G. Shi, L. Qu, A. Versatile, Ultralight, nitrogen-doped graphene framework. Angew. Chem. Int. Ed. **51**, 11371–11375 (2012)
67. X. Yang, C. Cheng, Y. Wang, L. Qiu, D. Li, Liquid-mediated dense integration of graphene materials for compact capacitive energy storage. Sci. **341**, 534–537 (2013)
68. Y. Yoon, K. Lee, S. Kwon, S. Seo, H. Yoo, S. Kim, Y. Shin, Y. Park, D. Kim, J.-Y. Choi, H. Lee, Vertical alignments of graphene sheets spatially and densely piled for fast ion diffusion in compact supercapacitors. ACS Nano **8**, 4580–4590 (2014)
69. H. Guanghua, S. Yonghai, C. Shuiliang, W. Li, Porous carbon nanofiber mats from electrospun polyacrylonitrile/polymethylmethacrylate composite nanofibers for supercapacitor electrode materials. J. Mater. Sci. **53**, 9721–9730 (2018)
70. H. Niu, J. Zhang, Z. Xie, X. Wang, T. Lin, Preparation, structure and supercapacitance of bonded carbon nanofiber electrode materials. Carbon **49**(7), 2380–2388 (2011)
71. W. Nan, Y. Zhao, Y. Ding, A.R. Shende, H. Fong, R.V. Shende, Mechanically flexible electrospun carbon nanofiber mats derived from biochar and polyacrylonitrile. Mater. Lett. **205**, 206–210 (2017)
72. D. Yu, K. Goh, H. Wang, L. Wei, W. Jiang, Q. Zhang, L. Dai, Y. Chen, Scalable synthesis of hierarchically structured carbon nanotube-graphene fibres for capacitive energy storage. Nat. Nanotechnol. **9**, 555–562 (2014)
73. F. Cheng, X. Yang, S. Zhang, W. Lu, Boosting the supercapacitor performances of activated carbon with carbon nanomaterials. J. Power Sources **450**, 227678 (2019)

74. G. Wang, X. Sun, F. Lu, H. Sun, M. Yu, W. Jiang, C. Liu, J. Lian, Flexible pillared graphene-paper electrodes for high-performance electrochemical supercapacitors. Small **8**, 452–459 (2012)
75. C. Ogata, R. Kurogi, K. Hatakeyama, T. Taniguchi, M. Koinuma, Y. Matsumoto, All-graphene oxide device with tunable supercapacitor and battery behaviour by the working voltage. Chem. Commun. **52**, 3919–3922 (2016)
76. W.-H. Qu, Y.-Y. Xu, A.-H. Lu, X.-Q. Zhang, W.-C. Li, Converting biowaste corncob residue into high value added porous carbon for supercapacitor electrodes. Bioresour. Technol. **189**, 285–291 (2015)
77. J. Han, L.L. Zhang, S. Lee, J. Oh, K.-S. Lee, J.R. Potts, J. Ji, X. Zhao, R.S. Ruoff, S. Park, Generation of B-doped graphene nanoplatelets using a solution process and their supercapacitor applications. ACS Nano **7**, 19–26 (2012)
78. Y-K Hsu, Y-C Chen, Y-GLin, L-C Chen, K-H Chen, High-cell-voltage supercapacitor of carbon nanotube/carbon cloth operating in neutral aqueous solution. J. Mater. Chem. **22**, 3383–3387 (2012)
79. B. Li, F. Dai, Q. Xiao, L. Yang, J. Shen, C. Zhang, M. Cai, Nitrogen-doped activated carbon for a high energy hybrid supercapacitor. Energy Environ. Sci. **9**(1), 102–106 (2016)
80. N. Jha, P. Ramesh, E. Bekyarova, M.E. Itkis, R.C. Haddon, High energy density supercapacitor based on a hybrid carbon nanotube-reduced graphite oxide architecture. Adv. Energy Mater. **2**, 438–444 (2012)
81. C. Ma, Y. Li, J. Shi, Y. Song, L. Liu, High-performance supercapacitor electrodes based on porous flexible carbon nanofiber paper treated by surface chemical etching. Chem. Eng. J. **249**, 216–225 (2014)
82. J. Yun, D. Kim, G. Lee, J.S. Ha, All-solid-state flexible micro-supercapacitor arrays with patterned graphene/MWNT electrodes. Carbon **79**, 156–164 (2014)
83. J. Li, N. Wang, J. Tian, W. Qian, W. Chu, Cross-coupled macro-mesoporous carbon network toward record high energy-power density supercapacitor at 4 V. Adv. Funct. Mater. **28**, 1806153 (2018)
84. B. Kim, H. Chung, W. Kim, Supergrowth of aligned carbon nanotubes directly on carbon papers and their properties as supercapacitors. J. Phys. Chem. C **114**, 15223–15227 (2010)
85. D. Pech, M. Brunet, H. Durou, P. Huang, V. Mochalin, Y. Gogotsi, P.-L. Taberna, P. Simon, Ultrahigh-power micrometre-sized supercapacitors based on onion-like carbon. Nat. Nanotechnol. **5**, 651–654 (2010)
86. Y.-Z. Wang, X.-Y. Shan, D.-W. Wang, H.-M. Cheng, F. Li, Mitigating self-discharge of carbon-based electrochemical capacitors by modifying their electric-double layer to maximize energy efficiency. J. Energy Chem. **38**, 214–218 (2019)
87. M. Xia, J. Nie, Z. Zhang, X. Lu, Z.L. Wang, Suppressing self-discharge of supercapacitors via electrorheological effect of liquid crystals. Nano Energy **47**, 43–50 (2018)
88. Z. Lei, H. Xiaosong, W. Zhenpo, S. Fengchun, G.D. David, A review of supercapacitor modeling, estimation, and applications: A control/management perspective. Renew. Sustain. Energy Rev. **81**, 1868–1878 (2018)

Pseudo-capacitors: Introduction, Controlling Factors and Future

M. Waqas Hakim, Sabeen Fatima, Syed Rizwan, and Asif Mahmood

Abstract Energy storage strategies are essential for addressing climate change and storing energy generated from renewable technologies. As a result, developing a highly efficient, affordable, and environmentally acceptable storage system has become a critical task for the scientific community. The introduction of pseudo-capacitors that exhibits higher charge storage capacity without losing their powerful output capability has provided a considerable advancement in the field of electrochemical energy storage (EES) systems. The fast surface redox kinetics provide an edge to pseudo-capacitors over batteries by providing high energy densities with much superior power densities. This chapter starts with clarifying the misconception between batteries and pseudocapacitive behaviors by briefing the basics of pseudo-capacitors in detail as well as their operating principle along with the various types of pseudo-capacitors and their fingerprint study based on different electrochemical phenomena involved. Furthermore, the chapter will conclude by discussing the various capacitance controlling parameters including energy density, power density, and specific capacitance, their connection to each other, and how they can be enhanced using different electrolytes and working materials.

Keywords Pseudo-capacitors · Energy density · Specific capacitance · Charge storage · Metal oxides

M. Waqas Hakim · S. Fatima · S. Rizwan
Physics Characterization and Simulation Lab (PCSL), Department of Physics, School of Natural Sciences (SNS), National University of Sciences and Technology (NUST), Islamabad 54000, Pakistan
e-mail: syedrizwan@sns.nust.edu.pk

A. Mahmood (✉)
School of Chemical and Biomolecular Engineering, The University of Sydney, Sydney, Australia
e-mail: asif.mahmood@sydney.edu.au

S. Thomas et al. (eds.), *Nanostructured Materials for Supercapacitors*,
Advances in Material Research and Technology,
https://doi.org/10.1007/978-3-030-99302-3_3

1 Introduction

The world's energy consumption is increasing at a breakneck speed. Economic growth, urbanization, rising per capita consumption, and the extension of energy access are all expected to drive up total energy demand significantly [1]. Society recognizes the importance of gathering renewable resources, storing them, and recovering them to fulfil both environmental and economic concerns [2]. In fulfilling the global energy needs supercapacitors play a vital role by providing smart, portable, and more efficient storage systems. Electrochemical energy storage (EES) has proven to be a highly effective way of storing energy because of the enhanced theoretical efficiency of transforming chemical energy to electrical with better energy and power densities [3]. EES comprises a variety of mechanisms, including the development of a non-faradaic electrical double layer (EDL), surface electron transfers redox reactions, ion insertion like in electrochemical intercalation, etc. [4]. The electrochemical ion insertion and transition satisfy Faraday's rule and include electron transport reactions across the electrochemical contact. Surface redox and certain ion-exchange processes are pseudocapacitive because their kinetics is similar to surface adsorption–desorption reactions.

Pseudo-capacitors have revolutionized the field of supercapacitors (Fig. 1) owing to distinct electrochemical features for high charge storage capability as well as enhanced energy density due to offering an efficient passage to charge transfer [5]. The study started in the late 90s using oxide materials mostly transition metal oxide and polymers, exhibiting high storage performance in comparison to EDLCs [6]. A lot of research is still going on pseudo-capacitors, but the reason for some energy loss during electrochemical reactions still needs to be investigated due to which their power density along with cyclic stability is compromised when put in comparison to other EDLCs [7]. In this chapter, an overview of the origin of pseudo-capacitance as well as the factors controlling pseudo-capacitance are discussed in detail.

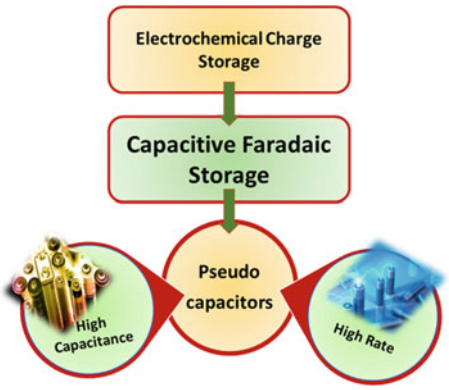

Fig. 1 Pseudo capacitors among electrochemical charge storage

2 Operating Principle of Pseudo-capacitors

The main source of energy storage in pseudo-capacitors is by the mean of faradaic reaction. Oxidation and reduction happen at or near the surface of the electrode. In supercapacitors with a pseudocapacitive electrode, a fast and reversible redox reaction occurs which increases overall capacitance. Due to the near and at surface phenomenon an electrode with high porosity or larger surface area plays an important role to exhibit pseudocapacitive behavior due to which mainly metal oxides based and carbon base materials with high surface area show good pseudocapacitive nature as an electrode. Faradaic and non-faradaic processes are the two types of reactions that any charge storage device electrode can go through. In the faradaic process after the application of constant current to the electrode, the charges on an electrode with voltage and the composition go to a new constant value. Whereas in non-faradaic process charge storage is a progressive way and after the layer of charge gets stored onto the surface of the electrode the reaction gets to a halt with no further storage to occur [8]. Faradaic processes electrode ions from electrolytes undergo charge transfer at the metal-electrolyte interface. Electrons transfer causes oxidation and reduction to occur. As shown in the equation below. In a complete faradaic reaction, reactants of this process come outside the bulk of the electrode and go back to the electrolyte. Figure 2 illustrates the schematic of the working of typical pseudo-capacitance.

$$\text{Oxidized specie} + \text{ne}^{-1} \rightleftharpoons \text{Reduced specie} \tag{1}$$

From a thermodynamics point of view whenever any property x is proportional to the charges passed there will be pseudocapacitive phenomena and their relation to the potential difference between a metal surface and the electrolyte solution can be expressed by equation.

$$\frac{\text{x}}{(1-\text{x})} = \text{K}\exp\left(\frac{\text{VF}}{\text{RT}}\right) \tag{2}$$

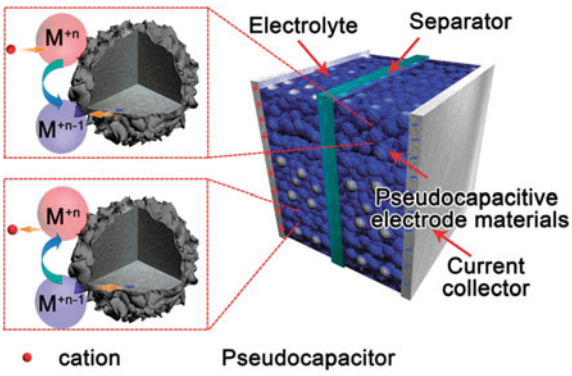

Fig. 2 Schematic on pseudo-capacitor. Reprinted with permission from Wiley-VCH Verlag GmbH & Co. KGaA, Weinheim [9]

In the equation the quantity x can be considered as occupancy fraction of the surface of the electrode, as a measure of fractional adsorption or some extent of fractional conversion of an oxide species to reduced species (or vice versa) in case of oxidation/reduction system and F is the faraday constant (96,485 C mol^{-1}) [10]. When synthesized in nanoscale forms, some material compositions that would in a bulk form display battery-type charge storage behavior appear capacitive. Indeed, certain faradaic electrodes when formed by using active material as nanosized or ultrathin films exhibit pseudocapacitive behavior, even though it is due to their morphology or electrode structure rather than any inherent features of the material itself [11]. Although both types of electrodes produce a capacitor-like electrochemical signature, we may distinguish between "intrinsic pseudo-capacitance" and "extrinsic pseudo-capacitance" by understanding the phenomenon occurring. Choice of active material and electrode design plays a very crucial role in the pseudocapacitive performance of the electrode.

A pseudo-capacitive material is the one that delivers linear or almost linear charge/discharge without producing a particularly prominent voltage plateau with broad and close to overlapping redox peaks not too prominent like in batteries but sufficient enough to be distinguished from EDLC [9]. Based on the materials used as active, this electrode can have intrinsically or extrinsically pseudocapacitive. Intrinsically pseudocapacitive materials include MnO_2, RuO_2, and other conducting polymers such as polypyrrole and polyaniline as their active material. Furthermore, several pseudocapacitive materials such as TiO_2 (B), α-MoO_3, T-Nb_2O_5, and $Li_4Ti_5O_{12}$ have been studied which has an extrinsic pseudocapacitive behavior, an example will be discussed later in this chapter. Another way of understanding the working of the pseudocapacitive electrode is by observation of its cyclic voltammogram (Fig. 3). Electrochemical signature analysis shows prominent oxidation and reduction peak in a single cycle which correspond to the phenomenon that charged species is going through redox reaction in a single cycle. Carbon-based

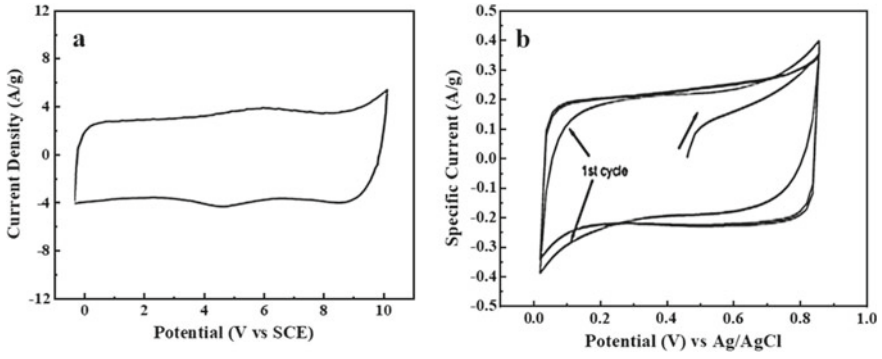

Fig. 3 CV Plots of **a** MnO_2 thin film in 2 M KCl electrolyte at a scan rate of 20 mV s^{-1}. Reprinted with permission from Elsevier [13]. **b** Powder-based MnO_2 electrode in 0.1 M K_2SO_4 at 2 mV s^{-1} Reprinted with permission from Elsevier [14]

electrode materials with induction of heteroatoms or with attached functional groups can also help in increasing the overall pseudo-capacitance of the electrode [12]. Pseudo-capacitance appears when the quantity Q that measures reaction extent, is a continuous function of the voltage difference (V), then the derivative dQ/dV will be capacitance like quantity.

The pseudocapacitors can also be categorized as intrinsic or extrinsic supercapacitors. Intrinsic pseudo-capacitance is generally related to the nature of the material as by the name the property is coming from the material itself. Intrinsic pseudocapacitive material will behave like a pseudocapacitive material regardless of its microstructure [9]. RuO_2 and MnO_2 electrodes are among the most prominent examples [13, 15]. A nanosize thin film or a micro-sized bulk powder both will be showing the same electrochemical signature when studied using cyclic voltammetry. Opposing that, extrinsic pseudocapacitive materials only show capacitor-like behavior when they are only in certain morphologies, structures, and sizes. The reason behind not expressing capacitive behavior is the phase transformation during ion storage. But when engineered with specific conditions they shift towards capacitive material due to shortening of diffusion distance, and some time due to their size limitation phase transformation effect gets suppressed. $LiCoO_2$ is among the list of such types of capacitive material. Commonly used as a positive electrode in Li-ion batteries, has no capacitive response in bulk form, but when the same material is synthesized in a way that we get nanometer thickness thin film of $LiCoO_2$ [16]. Material starts to behave like a capacitor. In Fig. 4, the extrinsic pseudo-capacitive nature of the electrode is shown that with a change in the size of the material as an electrode, capacitive behavior changes. With the increase in discharging time, pointing the device towards a battery-like charge storage system, a smaller crystal size plot is sloppy and the plateau region is decreasing with a decrease in size. This is due to an increase in the influence of surface Li-ion storage sites. Pseudocapacitive electrode exhibits some distinctive features which can be explained by using cyclic

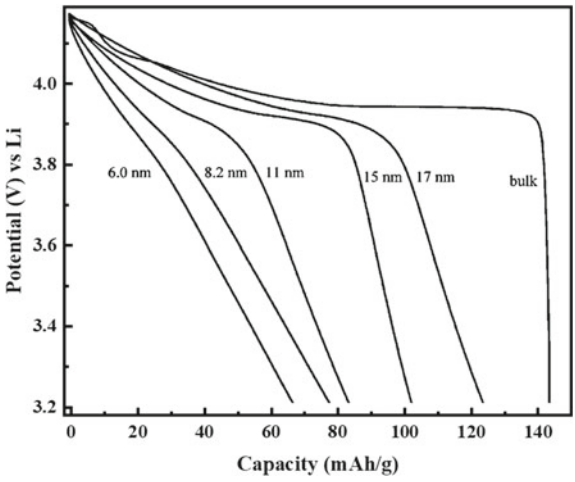

Fig. 4 Discharge curve for $LiCoO_2$ for 1 h charge–discharge. Reprinted with permission from the American Chemical Society [16]

voltammetry, response to voltage sweep, electrochemical impedance spectroscopy, and galvanostatic charge/discharge.

Figure 5 illustrates the electrochemical analysis of graphene hydrogel decorated with oxygen and nitrogen co-doped quantum dots are illustrated, four different concentrations for decoration used. In Fig. 5a CV curves of electrodes showing pseudo-capacitance with prominent redox peaks, where (GH is graphene hydrogel, GCD-2, GCD-3, GCD-4 are GO:CD concentration of 4:1, 3:1, 2:1 respectively).

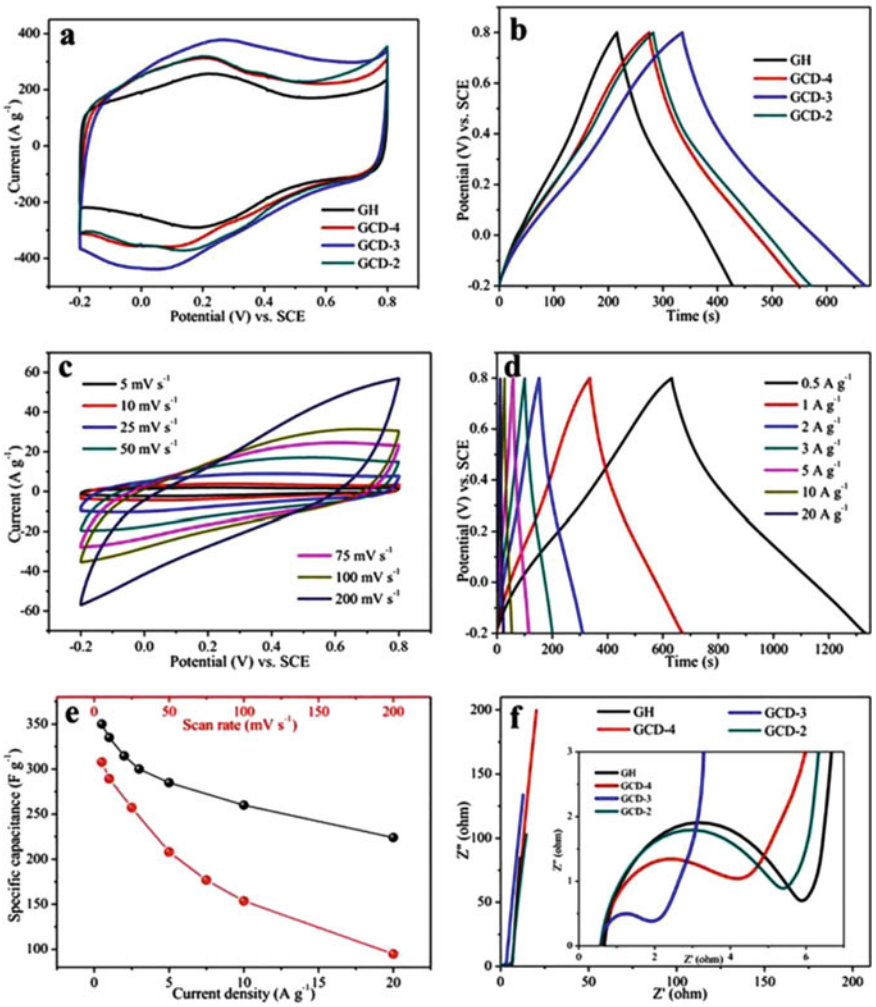

Fig. 5 **a** Cyclic voltammetry plots at the scan rate of 10 mV s^{-1}. **b** GCD of the electrodes at 1 A g^{-1} of current density. **c** CV curves for GCD-3 electrode. **d** Respective GCD plots for GCD-3 electrode. **e** Specific capacitance plot for GCD-3 electrode at different scan rates and current densities. **f** EIS (Nyquist) plots for every electrode. Reprinted with permission from IOP [17]

Figure 5b shows the triangular reversible behavior of these electrodes. Figure 5c and d indicate the stable behavior of GCD-3 at various scan rates and current densities respectively. And in Fig. 5e, the specific capacitance at various scan rates shows a decrease of specific capacitance with an increase in scan rate. Figure 5f shows the EIS Nyquist plots of the respective electrodes. In cyclic voltammetry, we apply a linear sweep voltage to an electrode at different scans rate. Capacitive material exhibits rectangular shape characteristic plots which show the charge storage and saturation of storage capability at a certain current limit when an external voltage is applied, similarly, batteries also show distinctive phenomenon when voltage is linearly swept across the working limit of the electrode, CV signature shows two distinguishable redox peaks in the plot. Capacitors exhibit fast charging and discharging capability with low energy density as compared to the batteries. When shifting towards pseudo-capacitors we compromise its energy density related to batteries with an increase in its power density. Pseudo-capacitors lie in between EDLC and batteries.

3 Phenomenon Occurring Inside Pseudo-capacitors

As already discussed, pseudo-capacitance is an electrochemical energy storage phenomenon in which faradaic charge transfer is taking place. Charge transfer occurs on the electrode–electrolyte interface is the main reason for pseudo-capacitance. The faradaic activity initiates due to a very fast faradaic reversible reaction taking place on the electrode surface. Figure 6 is a general representation of the reactions occurring on the electrode surface and the effect of that on the discharge curve of the respective electrode. EDLC uses an electrostatic charge storage mechanism which shows saturation in the curve. Pseudo-capacitor electrode allows slight bumps in the curve due to the presence of pseudocapacitance which shows additional charge storage. As the pseudocapacitance phenomenon is overcome by the faradaic processes its shows a battery-like CV curve with slow discharge.

Pseudo-capacitance phenomenon can be characterized into three main types depending upon the nature of faradaic reaction taking place at electrode–electrolyte interphase. Underpotential deposition, in which from the electrolyte a monolayer of atoms on the surface of the electrode gets deposited. Which normally involve H-atoms on the near-surface on noble metal oxides. Redox pseudo-capacitance is a phenomenon taking place near or at the surface of the electrode, and the third one is when ions intercalate into the place available or layers of material that exhibit redox activity, without changing the crystallographic nature of the material is known as intercalation pseudo-capacitance [19]. Schematics of the faradaic reactions corresponding to these phenomena are illustrated in Fig. 7.

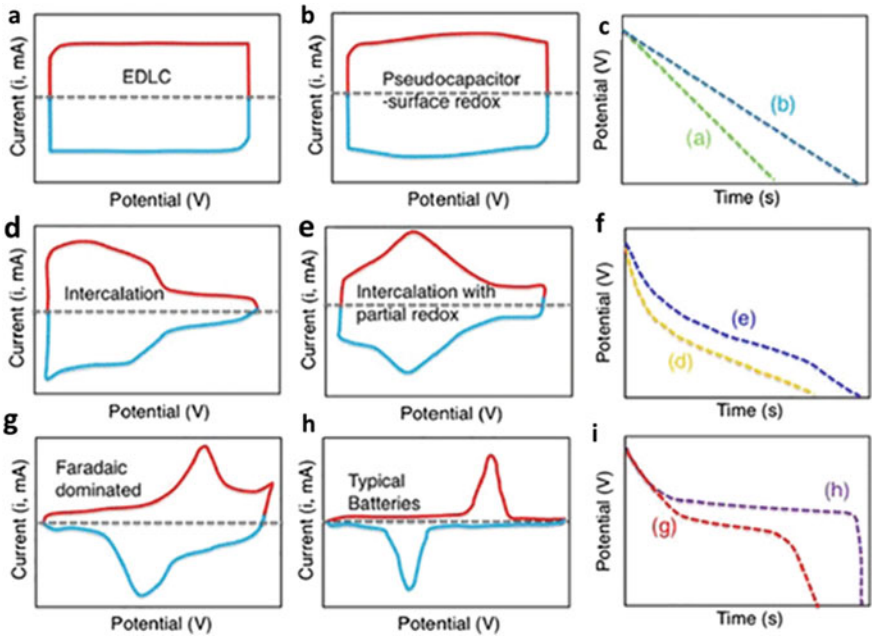

Fig. 6 Usual cyclic voltammetry plots of different energy storage devices. **a** Electrical double-layer capacitors. **b** Pseudo-capacitors. **c** Discharge curve of (**a**, **b**). **d**, **e** CV curves for the intercalation pseudocapacitance. **f** Electrodes discharge curve. **g** Pseudocapacitive electrode with dominated faradaic processes. **h** Batteries CV signature. **i** Discharge curves of (**g**, **h**). Reprinted with permission from the American Chemical Society [18]

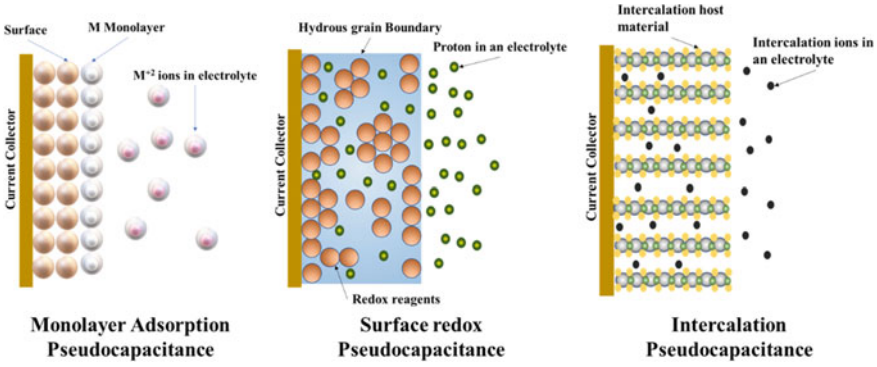

Fig. 7 Schematic of different faradaic processes that give rise to pseudo-capacitance

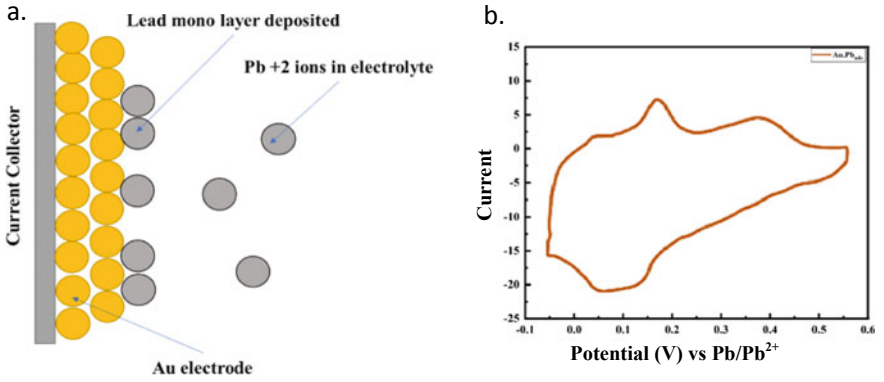

Fig. 8 **a** Pb coating on Au electrode and **b** its CV signature curve. Reprinted with permission from MDPI [20]

3.1 Adsorption or Underpotential Pseudo-capacitance

When a metal electrode is subjected to an external potential in an electrolyte, a monolayer gets deposited onto the surface of the metal due to surface adsorption and reduction of metal ions which results in a slight change in potential than its equilibrium potential. Adsorption of lead on the surface of Au electrode in an electrolyte of 1 mM PbF_2 + 10 mM $HClO_4$ is an example of adsorption pseudo-capacitance [20]. Schematic expression of this process is shown in Fig. 8a and the CV plot relative to the process is shown in Fig. 8b. In this process led mono layer gets deposited onto the surface of the electrode which creates an additional bulk phase for a charge species to interact to. This layer act as a charge storage site and the electrode behaves like a pseudocapacitive electrode as the CV curve clearly shows the capacitive nature with faradaic continuity. The chemical equation for underpotential deposition of led onto the Au electrode is expressed in the form of an electrochemical equation in Eq. 3.

$$Au + xPb^{2+} + 2xe^{-} \leftrightarrow Au.xPb_{ads} \tag{3}$$

3.2 Redox Pseudo-capacitance

Considered to be the most common type of pseudo-capacitance which is due to the electro-adsorption of active ions from electrolytes near or at the surface of electrode material which causes a faradaic reaction to start with continuous charge transfer. RuO_2 and MnO_2 are among electrode materials that show this kind of behavior due to the occurrence of fast redox reactions caused by the intercalation of H^+ ions or alkali metal cations. Ruthenium-based electrode material got a lot of attention because of its

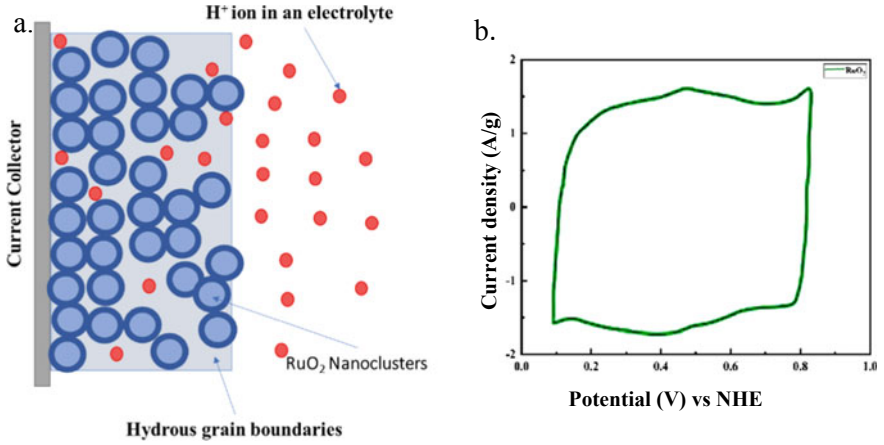

Fig. 9 **a** Redox pseudo-capacitance in RuO_2 schematics **b** CV signature curve. Reprinted with permission from the American Chemical Society [15]

high electrical conductivity and good thermal stability. The schematic of the charge store mechanism is shown in Fig. 9. In this process, no chemical changes happen to the surface of the electrode during charging/discharging because the functionalized molecular layer formed during the charging of the electrode gets removed during discharging as the process involves reversible redox faradaic reaction as shown in Eq. (4). Ruthenium oxide gets reduced during the charging cycle and gives rise to oxide with charge species attached to it and during the discharging of the capacitor, ion gets back to the electrolyte with balancing the potential difference between electrode and electrolyte resulting back to its original form. This process is responsible for the long-lasting cyclicity of these devices when compared with conventional batteries. An electrochemical reaction in the form of a chemical equation is shown in the following Eq. 4.

$$RuO_x(OH) + \delta H^+ + \delta e^- \leftrightarrow RuO_{x-\delta}(OH)_{y-\delta} \tag{4}$$

3.3 Intercalation Pseudo-capacitance

Intercalation pseudo-capacitance originates when ions from electrolyte intercalate into the layered or tunnels-like structure of the redox-active material due to which fast charge transfer of charge species of faradaic nature initiates. During this process, charge transfer does not change the crystallographic structure of the electrode material. As already mentioned, in other pseudo-capacitance phenomenon reaction occur only at or near the surface of the electrode but in this process, ions intercalate into the electrode. The reaction is fast enough that it behaves like an electrode reaction

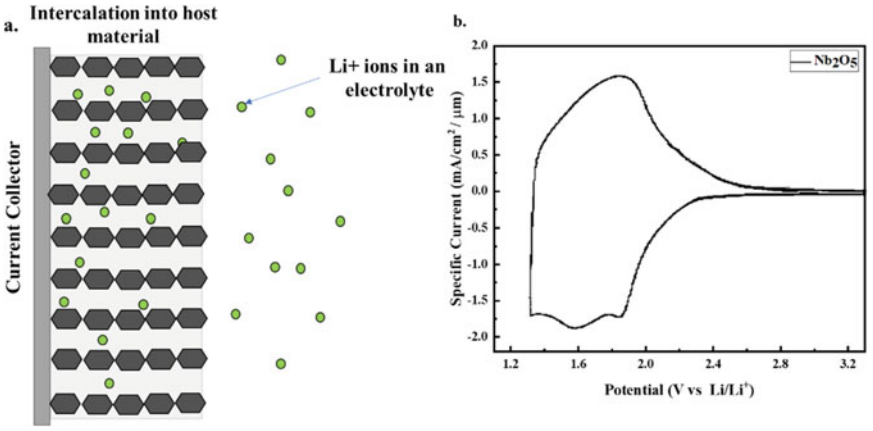

Fig. 10 **a** Intercalation pseudo-capacitance and **b** CV signature curve. Reprinted with permission from the American Chemical Society [21]

of supercapacitors. A chemical reaction in Eq. 5 is an example of such a reaction. Recently a newly developed class of materials called MXene are introduced as a unique host material for this type of pseudo-capacitance of these types of materials are already have a supporting structure for intercalation of electroactive ions into the material, which results in more surface area available to the electrolyte as compared to the other form of pseudocapacitive electrode materials (Fig. 10).

$$Nb_2O_5 + xLi^+ + xe^- \leftrightarrow Li_xNb_2O_5 \tag{5}$$

4 Parameters Governing Pseudo-capacitors

Pseudo-capacitance was originated with the birth of porous oxide materials and conductive polymers along with other sulfides, nitrides, and hydroxides. Scientific studies have suggested that physical properties including microstructure and surface morphology are the key determinants that decide the specific capacity of a material [22, 23]. Others point out, however, that chemical factors including the hydrous and valence state of material also control its capacitive performance [24, 25]. These dominant parameters need to be understood well before reaching optimum pseudo-capacitance because the physical and chemical properties of material often change at the same time, so a more extensive investigation is required to pinpoint the individual influence.

4.1 Active Material Growth and Morphology

The material's physical features play a crucial role in achieving good capacitive storage. Both crystalline rutile, as well as the hydrous phase of the material, participate very differently in the capacitive behavior of the same material [3]. The capacitance rapidly declines at the start of charge–discharge usage (about 100 cycles) and yet remains rather steady after that [26, 27]. Dissolution, detachment, structural collapse, anodization, and chemical deterioration of the active layer could all be factored in the capacitance decline. In early studies, the transition metal oxides were the prominent candidates involved in pseudo-capacitive charge storage. As the work started from the ruthenium oxide due to having high conductivity and thermal stability it was observed that the material behaves differently in its various states either conductive crystalline or the hydrated $RuO_2 \cdot H_2O$ [28]. In CV measurements it was demonstrated that films thermally produced or made from single-crystal RuO_2 have a rectangular reaction, whereas the others have a squiggly wave. Also, it was discovered that after multiple cycles of ruthenized electrodes, a rectangle CV response is formed in the anodic area [29]. Years later, it was proven that the storage responses of RuO_2 films vary depending on the film growth procedure, implying that the film structure also appears to be a key determinant [29, 30]. The hydrated form of material is formed due to physisorption or chemisorption of the water molecules over the grain surface. This addition and removal of water inside the material can vary the capacitive properties as in RuO_2 films the hydrated films provide higher specific capacitance in comparison to anhydrous form [31]. The investigations revealed that annealing leads to an extraction of confined water from the oxide layers resulting in the aggregation of large particles along with less contribution inside capacitive storage [32]. This also supports that the material's particle size is also important for achieving high pseudo-capacitance. Likewise, Manganese oxides are also very attractive electrode materials due to their high specific capacitance, relatively higher abundance, and eco-friendly nature. The Crystal morphology of manganese oxide exists in zero-dimensional core shells, one-dimensional tunnel structure, two-dimensional layers, and three-dimensional frameworks. This crystal diversity further influences significantly over the interlayer cationic insertion as well as transport, hence providing different storage capacitance with different tunnel sizes [33]. Many oxide materials also have a property to agglomerate which severely restrained the capacitive behavior due to which the good material dispersion is very essential while making the working electrode for capacitive measurement [34]. Moreover, the problems like poor conductivity, surface area, and high electrolyte dissolubility also suppress the performance of transition metal oxides in the charge storage field.

Material porosity is also a vital factor in determining the pseudo-capacitance of material as in ruthenium the presence of both meso as well as micropores will be responsible for its pseudo-capacitance [35]. The hydrous state of ruthenium provides higher specific capacitance due to micropore utilization. Moreover, the amorphous form of ruthenium also exhibited a higher storage capacity due to flexibility inside the lattice arrangement, inducing more active sites for electrolytic ion-exchange

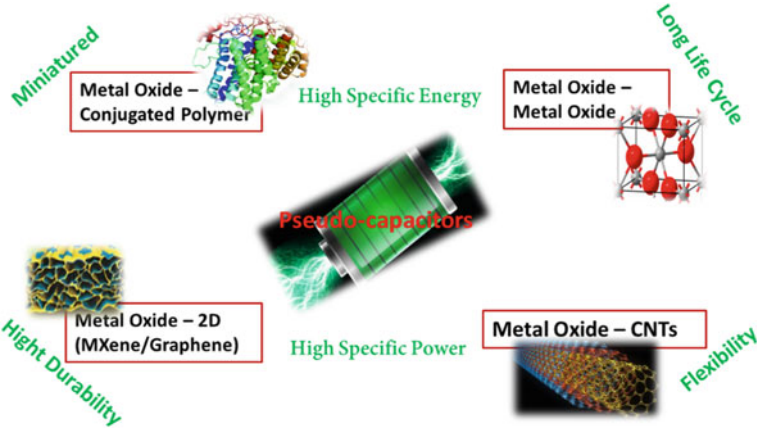

Fig. 11 Enhancement of pseudo-capacitive performance using different material hybridizations

inside the material [36]. The electrolyte may enter the porous surface more easily, a larger ionic conductivity in the oxide was predicted, resulting in improved reaction homogeneity. Which interns reduced the dissolution induced by electrochemical polarization. The great porosity, it is assumed, allows for substantial volume expansion/contraction of the oxide while charging and discharging, allowing the internal stress caused to be easily dissipated and therefore preventing physical damage to the electrode. The oxide dissolving rate was significantly reduced when the working electrode transitioned from a condensed to a porous fibrous structure during cycling [37]. Since the compact oxide nodules disintegrated quickly during CV cycling, the fibrous oxide remained extremely durable. Since the pores inside the working material will enhance its surface area, the fibrous electrodes were designed to have a large surface area, which increased the oxide's reactivity along with its reversibility. Furthermore, the researchers are doing work for minimizing the challenges faced by oxide materials via their hybridizations with other 2D materials like functionalized graphene and MXenes, conjugated polymers, or other metal oxides as shown in Fig. 11.

4.2 Electrolyte Interaction with the Active Material

While lying between the batteries and capacitor, pseudo-capacitors have an edge over processing both properties. Continuous work is going on for improving the key parameters including power as well as energy density along with durability for achieving the high capacitive performance. All these key parameters directly related to the interaction of active material with the electrolyte are illustrated in Fig. 12. So, for the optimization for getting efficient pseudo-capacitors, one needs a clear understanding of electrolyte working and its interaction with the active material. The

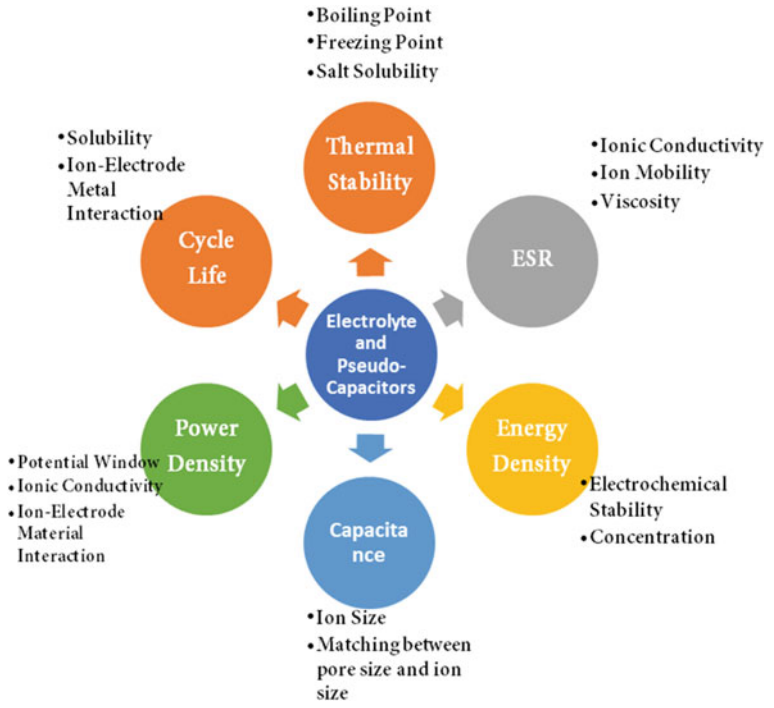

Fig. 12 Electrolyte role in regulating the key parameters to control capacitive performance in pseudo-capacitors

electrolyte is indeed an important constituent in supercapacitors, as it is responsible for transferring and regulating charges in between two electrodes [38]. There are several groups of electrolytes used in electrochemical supercapacitors. In all electrochemical processes, several electrolytes can be used but the electrode–electrolyte interplay has a substantial impact on the interface as well as the internal structure of active materials. Hence the electrolyte selection is critical for secure and high-performance capacitive devices. There is yet to be a perfect electrolyte that meets all the parameters of an electrochemical device. In cases when aqueous electrolytes are used, water is considered as a solvent for the salts. The ambient effect, ionic conductance, electrochemical behavior, ease of operation in the open climate, and cost-effectiveness are some of the reasons that make an aqueous electrolyte more preferable than an organic electrolyte.

The conductivity and capacitance of the aqueous electrolyte are higher but still are not used in commercial applications due to their low potential window; nonetheless, they are inexpensive and easier to produce than organic electrolytes. Electrolytic ion size, corrosive behavior, transportation, and ion conductivity all affect electrolyte performance. Aqueous electrolytes are classified chemically as acidic, alkaline, or neutral [39]. Materials with working potential lie between the O_2 as well as H_2

evolution potential are the exact match for these aqueous electrolytes. Different electrolytic cations such as H^+, Na^+, Li^+, and K^+ provide significant variation in specific capacitance during electrochemical performance only on a change of cation in the electrolyte solution which is mainly due to cationic radius, mobility, conductivity, ion exchange, and diffusion [40, 41]. Likewise, changing the anionic species inside the electrolyte has a similar effect on capacitive behavior. The size of the ionic hydration sphere also imparts in defining the capacitive performance as a bigger hydration sphere prohibits the entrance of electrolytic ions into pores resulting in low specific capacitance. The active electrode will corrode if the electrolyte has high molarity. Neutral electrolytes are more extensively employed than alkaline and acidic electrolytes because they are less corrosive, have a lower cost, and have a wider potential window [42]. If aqueous electrolytes are employed in the pseudo-capacitors, the power density will be high.

Organic electrolytes are typically made up of organic solvents with dissolved conducting salts. Organic electrolyte-based devices nowadays are ruling the commercial sector due to a high voltage window spanning from 2.6 to 2.9 V [43]. The nature of solvents, ionic size, their interaction, conductance, and viscosity, has substantial influences on the efficiency of organic electrolyte-based capacitive devices [44]. Contrarily, organic electrolytes have a higher resistance than aqueous electrolytes due to their big molecules, which necessitate large electrode pore sizes.

Ionic liquids are salts made up of ions (organic cation with organic/inorganic anion) having melting temperatures below 100 °C [45]. Ionic liquids have attracted a lot of attention as potential electrolytes due to their distinctive structures and capabilities [46]. The device's physical and chemical properties may be easily tweaked because of its wide range of cation and anion combinations. The capacitive performance can be increased (by adjusting the voltage window and operating temperature range) [47, 48]. When compared to other electrolytes, ionic liquids have several potential advantages, including nonflammability, improved thermal and chemical stability with a voltage window greater than 3 V, and low volatility [49].

Due to the constantly expanding demand for power in wearable, portable and printable electronics, solid-state electrolyte-based capacitive devices have piqued interest in recent years. Solid-state electrolytes also serve as electrode separators due to their ionic conducting media, lack of liquid leakage, and ease of packing and fabrication methods for capacitive storage media [50]. Gel phase polymer electrolytes offer the highest ionic conductivity among solid-state electrolytes. Attributed to the prevalence of a liquid phase, gel polymer electrolytes possess the maximum ionic conductivity. These electrolytes are now dominating the area of solid electrolyte capacitive devices due to their strong ionic conductivity, while the use of these solid electrolytes is quite limited [51]. However, due to water presence and low mechanical strength, gel polymer electrolytes may have a slim temperature range of operation. By inducing pseudocapacitive contribution from redox-active electrolytes, the capacitance can be enhanced. The pseudocapacitive material with redox mediator electrolyte can also contribute to the pseudo-capacitance, such as an iodide/iodine redox pair can act as the redox-active aqueous electrolyte in carbon-based supercapacitors [52, 53]. A

high capacitance can be produced owing to the electrolyte's pseudocapacitive contribution only at the positive electrode with a narrow potential range. Furthermore, as new electrolytes are developed, it is critical to optimize the compatibility of these electrolytes with new electrode materials. The reaction chemistry of different types of electrolytes, as well as their effects on electrochemical capacitive performance, have still to be thoroughly investigated to build better electrolytes to solve energy storage challenges.

5 Conclusions

In summary, the chapter provides proper terminology for pseudo-capacitive devices, as well as a thorough understanding of their architecture, fabrication, and charge storage mechanisms, as well as the phenomena involved in pseudo-capacitive behavior, as measured by CV and charge/discharge curves. The appropriate pseudocapacitive materials, their shape, the interaction between the electrolytes and electrode materials, and electrolytic parameters that affect electrochemical storage performance are also reviewed. Many aspects of the pseudo-capacitor field, however, have yet to be explored to overcome the difficulties and challenges.

References

1. T. Prasankumar, J. Jose, S. Jose, S.P. Balakrishnan, *Pseudo-capacitors* (IntechOpen, 2021)
2. A. Manthiram, Materials challenges and opportunities of lithium-ion batteries. Phys. Chem. Lett. **2**, 176–184 (2011)
3. A.J. Bard, G. Inzelt, F. Scholz, *Electrochemical Dictionary* (Springer Science & Business Media, 2008)
4. S. Fleischmann, J.B. Mitchell, R. Wang, C. Zhan, D. Jiang, V. Presser, V. Augustyn, Pseudocapacitance: from fundamental understanding to high power energy storage materials. Chem. Rev. **14**, 6738–6782 (2020)
5. G. Yu, X. Xie, L. Pan, Z. Bao, Y. Cui, Hybrid nanostructured materials for highperformance electrochemical capacitors. Nano Energy **2**, 213–234 (2013)
6. B.E. Conway, Transition from "supercapacitor" to "battery" behavior in electrochemical energy storage. J. Electrochem. Soc. **138**, 1539–1548 (1991)
7. Y. Zhang, H. Feng, X.B. Wu, L.Z. Wang, A.Q. Zhang, T.C. Xia, H.C. Dong, X.F. Li, L.S. Zhang, Progress of electrochemical capacitor electrode materials: a review. Int. J. Hydrogen Energy **34**, 4889–4899 (2009)
8. B. Maartein, P. Maarten, S. Porada, J.E. Dykstra, The difference between faradaic and nonfaradaic electrode processes. Chem. Phys. **2021**, 1–16 (2021)
9. J. Liu, J. Wang, C. Xu, H. Jiang, C. Li, C. Zhang, J. Lin, Z.X. Shen, Advanced energy storage devices: basic principles, analytical methods, and rational materials design. Adv. Sci. **5**, 1700322/1–19 (2017)
10. B.E. Conway, *Electrochemical Supercapacitors* (Springer, 1991)
11. D. Winny, R.R. Debra, D. Bruce, Electrochemical properties of high surface area vanadium oxide aerogels. Electrochem. Solid State Lett. **3**, 457–459 (2000)

12. Z. Cheng, Y. Deng, H. Wenbin, Q. Jinli, Z. Lei, Z. Jiujun, A review of electrolyte materials and compositions for electrochemical supercapacitors. Chem. Soc. Rev. **44**, 7484–7539 (2015)
13. T. Brousse, P.L. Taberna, O. Crosnier, R. Dugas, P. Guillemet, Y. Scudeller et al., Long-term cycling behavior of asymmetric activated carbon/MnO_2 aqueous electrochemical supercapacitor. J. Power Sources **173**, 633–641 (2007)
14. J.K. Chang, M.T. Lee, T.W. Tsai, In situ Mn K-edge X-ray absorption spectroscopic studies of anodically deposited manganese oxide with relevance to supercapacitor applications. J. Power Sources **166**, 590–594 (2007)
15. W. Dmowski, T. Egami, K.E. Swider-Lyons, C.T. Love, D.R. Rolison, Local atomic structure and conduction mechanism of nanocrystalline hydrous RuO_2 from X-ray scattering. J. Phys. Chem. B **106**, 12677–12683 (2002)
16. M. Okubo, E. Hosono, J. Kim, M. Enomoto, N. Kojima, T. Kudo, H. Zhou, I. Honma, J. Am, Nanosized effect on high-rate Li-Ion intercalation in $LiCoO_2$. Electrode Chem. Soc. **129**, 7444–7452 (2007)
17. S. Venkateshalu, A.N. Gracez, Review—heterogeneous 3D graphene derivatives for supercapacitors. J. Electrochem. Soc. **167**, 050509 (2020)
18. Y. Gogotsi, R.M. Penner, Energy storage in nanomaterials—capacitive, pseudocapacitive, or battery-like? ACS Nano **12**, 2081–2083 (2018)
19. J. Liu, *Graphene-Based Composites for Electrochemical Energy Storage* (Springer, Berlin, 2017), pp. 1–37
20. L. Bromberg, J. Xia, R. Rooney, N. Dimitrov, Enhanced adhesion of continuous nano porous Au layers by thermochemical oxidation of glassy carbon. Coatings **4**, 416–432 (2014)
21. S.O. Steinmueller, S.H. Tolbert, B.M. Smarsly, B. Dunn, T. Brezesinski, Pseudocapacitive contributions to charge storage in highly ordered mesoporous group V transition metal oxides with iso-oriented layered nanocrystalline domains. Am. Chem. Soc. **132**, 6982–6990 (2010)
22. M. Toupin, T. Brousse, D. Bélanger, Influence of microstructure on the charge storage properties of chemically synthesized manganese dioxide. Chem. Mater. **14**, 3946–3952 (2002)
23. M.T. Lee, J.K. Chang, W.T. Tsai, Effects of iron addition on material characteristics and pseudocapacitive behavior of Mn-oxide electrodes. J. Electrochem. Soc. **154**, A875–A881 (2007)
24. T. Liu, Y. Li, Addressing the Achilles' heel of pseudocapacitive materials: long-term stability. InfoMat **2**, 807–842 (2020)
25. H. Kim, B.N. Popov, Synthesis and characterization of MnO_2-based mixed oxides as supercapacitors. J. Electrochem. Soc. **150**, D56–D62 (2003)
26. C. Costentin, J.M. Savéant, Energy storage: pseudo-capacitance in prospect. Chem. Sci. **10**, 5656–5666 (2019)
27. Y.U. Jeong, A. Manthiram, Nanocrystalline manganese oxides for electrochemical capacitors with neutral electrolytes. J. Electrochem. Soc. **149**, A1419–A1422 (2002)
28. P. Ragupathy, H.N. Vasan, N. Munichandraiah, Synthesis and characterization of nano MnO_2 for the study of electrochemical supercapacitor studies. J. Electrochem. Soc. **155**, A34–A40 (2008)
29. S. Trasatti, G. Buzzanca, Solid state structure and electrochemical behaviour. J. Electroanal. Chem. **29**, A1–A5 (1971)
30. C.C. Huang, Y.H.H. Hu, Cyclic voltammetric deposition of hydrous ruthenium oxide for electrochemical capacitors. J. Electrochem. Soc. **146**, 2465–2471 (1999)
31. T.R. Jow, J.P. Zheng, Electrochemical capacitors using hydrous ruthenium oxide and hydrogen inserted ruthenium oxide. J. Electrochem. Soc. **145**, 49–52 (1998)
32. K.H. Chang, C.C. Hu, Oxidative synthesis of $RuOx \cdot nH_2O$ with ideal capacitive characteristics for supercapacitors. J. Electrochem. Soc. **151**, A958–A964 (2004)
33. N. Yoshida, Y. Yamada, S.I. Nishimura, Y. Oba, M. Ohnuma, A. Yamada, Unveiling the origin of unusual pseudo-capacitance of $RuO_2 \cdot nH_2O$ from its hierarchical nanostructure by small-angle X-ray scattering. J. Phys. Chem. C **117**, 12003–12009 (2013)
34. W.X.C. Wei, W. Chen, D.G. Ivey, Manganese oxide-based materials as electrochemical supercapacitor electrodes. Chem. Soc. Rev. **40**(3), 1697–1721 (2011)

35. J. Zhang, Y. Cui, G. Shan, Metal oxide nanomaterials for pseudo-capacitors. Appl. Phys. V **2**, 1–93 (2019)
36. W. Sugimoto, H. Iwata, K. Yokoshima, Y. Murakami, Y. Takasu, Proton and electron conductivity in hydrous ruthenium oxides evaluated by electrochemical impedance spectroscopy: the origin of large capacitance. J. Phys. Chem. B **109**, 7330–7338 (2005)
37. T.P. Gujar, V.R. Shinde, C.D. Lokhande, W.Y. Kim, K.D. Jung, O.S. Joo, Spray deposited amorphous RuO_2 for an effective use in electrochemical supercapacitor. Electrochem. Commun. **9**, 504–510 (2007)
38. J.K. Changa, C.H. Huang, M.T. Lee, W.T. Tsai, M.J. Deng, I.W. Sun, Physicochemical factors that affect the pseudo-capacitance and cyclic stability of Mn oxide electrodes. Electrochim. Acta **54**, 3278–3284 (2009)
39. I.W. Xu, Nonaqueous liquid electrolytes for lithium-based rechargeable batteries. Chem. Rev. **104**, 4303–4418 (2004)
40. B. Pal, S.G. Krishnan, B.L. Vijayan, M. Harilal, C.C. Yang, F.I. Ezema, M.M. Yusoff, R. Jose, In situ encapsulation of tin oxide and cobalt oxide composite in porous carbon for high-performance energy storage applications. J. Electroanal. Chem. **817**, 217–225 (2018)
41. M. Galiński, A. Lewandowski, I. Stepniak, Ionic liquids as electrolytes. Electrochim. Acta **51**, 5567–5580 (2006)
42. H. Kim, J. Hong, K.Y. Park, H. Kim, S.W. Kim, K. Kang, Aqueous rechargeable Li and Na ion batteries. Chem. Rev. **114**, 11788–11827 (2014)
43. B. Pal, S. Yang, S. Ramesh, V. Thangadurai, R. Jose, Electrolyte selection for supercapacitive devices: a critical review. Nanoscale Adv. **1**, 3807–3835 (2019)
44. A.R. Koh, B. Hwang, K.C. Roh, K. Kim, The effect of the ionic size of small quaternary ammonium BF4 salts on electrochemical double layer capacitors. Phys. Chem. Chem. Phys. **16**, 15146–15151 (2014)
45. J.K. McDonough, A.I. Frolov, V. Presser, J. Niu, C.H. Miller, T. Ubieto, M.V. Fedorov, Y. Gogotsi, Influence of the structure of carbon onions on their electrochemical performance in supercapacitor electrodes. Carbon **50**, 3298–3309 (2012)
46. R.D. Rogers, K.R. Seddon, Ionic liquids-solvents of the future. Science **302**, 7932–8793 (2003)
47. C.W. Liew, K.H. Arifin, J. Kawamura, Y. Iwai, S. Ramesh, A.K. Arof, Effect of halide anions in ionic liquid added poly (vinyl alcohol)-based ion conductors for electrical double layer capacitors. J. Non-Cryst. Solids **458**, 97–106 (2017)
48. M. Shi, S. Kou, X. Yan, Engineering the electrochemical capacitive properties of graphene sheets in ionic-liquid electrolytes by correct selection of anions. ChemSusChem **7**, 3053–3062 (2014)
49. Q. Dou, C. Lian, S. Lei, J. Chen, H. Liu, X. Yan, Silica-grafted ionic liquid for maximizing the operational voltage of electrical double-layer capacitors. Energy Storage Mater. **18**, 253–259 (2019)
50. B. Wu, K. Kuroda, K. Takahashi, E.W. Castner, Structural analysis of zwitterionic liquids vs. homologous ionic liquids. J. Chem. Phys. **148**, 193807-1-11
51. B.E. Francisco, C.M. Jones, S.H. Lee, C.R. Stoldt, Nanostructured all-solid-state supercapacitor based on Li_2S-P_2S_5 glass-ceramic electrolyte. Appl. Phys. Lett. **100**, 103902-1–103904 (2012)
52. M.L. Verma, M. Minakshi, N.K. Singh, Synthesis and characterization of solid polymer electrolyte based on activated carbon for solid state capacitor. Electrochim. Acta **137**, 497–503 (2014)
53. G. Lota, E. Frackowiak, Striking capacitance of carbon/iodide interface. Electrochem. Commun. **11**, 87–90 (2009)

Fundamentals, Mechanism, and Materials for Hybrid Supercapacitors

Son Qian Liew and Hieng Kiat Jun

Abstract With the advent of various electronic devices, energy storage systems have become one of the important components for the devices to have a long operating time. Supercapacitors are capable to provide fast charge when short-term power is required. However, the energy density of typical supercapacitors is lagging behind lithium-ion batteries. To improve the performance of energy density with good power density, hybrid supercapacitors are introduced. These groups of supercapacitors have the combination of the characteristics of electric double-layer capacitors and pseudocapacitors. Comparatively, hybrid supercapacitors have higher specific capacitance. In this chapter, the fundamental and storage mechanism of hybrid supercapacitors are presented. Their architecture, design, material selection, and characteristics are also explored. This chapter also gives an overview of recent development, challenges, and applications of hybrid supercapacitors, which can serve as guidelines for the next step of research and development.

Keywords Pseudocapacitor · Electric double-layer capacitor · Hybrid supercapacitor

1 Introduction and History

1.1 Brief History

Electrochemical supercapacitors (ESs) work under the concept of the presence of an electric double-layer (EDL) that is located at the interface between its contacting electrolyte solution and a conductor. In 1853, Hermann von Helmholtz presented the electric double-layer theory, and Gouy, Chapman, Grahame, and Stern bought further

S. Q. Liew · H. K. Jun (✉)
Department of Mechanical and Material Engineering, Lee Kong Chian Faculty of Engineering and Science, Universiti Tunku Abdul Rahman, Jalan Sungai Long, Bandar Sungai Long, 43000 Kajang, Selangor D.E., Malaysia
e-mail: junhk@utar.edu.my

S. Thomas et al. (eds.), *Nanostructured Materials for Supercapacitors*,
Advances in Material Research and Technology,
https://doi.org/10.1007/978-3-030-99302-3_4

advancement to it [1]. Numerous theories and technologies, including supercapacitors, batteries, and fuel cells, were created as a result of the invention of double-layer theory. Capacitors classified as first- and second-generation are electrostatic and electrolytic capacitors, respectively. Due to fast material advancements, the third-generation capacitor known as a supercapacitor was created [2–5]. ESs are sometimes referred to as supercapacitors, ultracapacitors, or double-layer electric capacitors (EDLCs). In 1971, the first commercially available supercapacitor devices manufactured by Nippon Electric Company (NEC) are called 'supercapacitors', which have become widely used. The term 'ultracapacitor' was also coined about low-resistance devices created in 1982 by the Pinnacle Research Institute (PRI) for military uses. Becker created and filed a patent for a low-voltage electrolytic capacitor that has electrodes that are made up of porous carbon in 1957. In his work, a high specific surface area carbon was coated on a metallic current collector in a sulfuric acid solution [6, 7]. In 1966, a device was created by R. A. Rightmire to allow energy storage in a double-layer interface when he was in Standard Oil of Ohio (an energy company) [8]. Then, Nippon Electronic Firm (NEC) of Japan developed aqueous-electrolyte capacitors for electronics power-saving units under a license from the Standard Oil of Ohio in 1971. This application is the origin of commercial electrochemical capacitors (ECs) [7]. Donald patented the first electrochemical capacitor in 1970 as 'Electrolytic Capacitor Having Carbon Paste Electrodes', following a few modifications [9]. The rapid development of mobile telephones, electronic equipment, and electric vehicles currently require novel, high-power electrochemical energy storage equipment. On the worldwide supercapacitors market, researchers have also been drawn to the development of energy collection applications that utilized supercapacitors (solar and wind power) and in the usage of supercapacitors in aircraft and trains. The Department of Energy in the United States established international awareness of the potentials of battery and supercapacitor research at the beginning of the 1990s. In 1992 Maxwell implemented the phrase ultracapacitors, termed 'Boots Caps', to be used in power applications, resulting in the design and development of revolutionary economically efficient electrode material and electrolytes to boost the performance in terms of electrochemical. The principal business of Maxwell is ultra-capacitors that have great-performance energy storage capability, as well as can load and discharge rapidly. Tesla announced the acquisition of Maxwell technologies from the established ultra-capacitor and storage materials company in an all-stock deal for $218 million in 2019. Various firms, including Panasonic, Maxwell Technologies, Tesla, Nesscap, ELNA, TOKIN, EPCOS, and, NEC are now investing extensively in developing electrochemical capacitors [10].

In 2018, the worldwide market of supercapacitors was valued at USD 685 million, with a CAGR of 21.8% anticipated in 2019–2024 of USD 2187 million by 2024. Supercapacitors replace ordinary automotive batteries with excellent temperature stability, power, and energy density. Soon, because of safety problems, supercapacitors could be a replacement for the lithium-ion battery. In addition, supercapacitors have better adaptability and stability than conventional batteries, therefore, they suit applications such as mobile devices, mobile media players, GPS, and laptops [10].

1.2 Introduction to Supercapacitors

The demand for efficient energy storage and sustainable energy alternatives is a significant issue today. For instance, energy storage technologies such as supercapacitors, batteries, and fuel cells can meet this demand. Supercapacitors are energy storage devices. They provide sufficient energy and power densities for intermediate to high power requiring applications (Fig. 1). They are storage devices that fall between capacitors and batteries [1]. Numerous alternative technologies have emerged to alleviate significant worries about the energy issue [11]. The emergence of this technology is to minimize greenhouse gas emissions from fossil fuels [12]. Supercapacitors are one such option, with high power densities, extended cycle lives, fast charge and discharge times, and clean and safe electrochemical energy storage [13]. Supercapacitors store energy via accumulating charge or reversible redox processes. Generally, they are classified into three categories: EDLC, pseudocapacitor, and hybrid supercapacitor. Electrochemical conversions are the basis for unconventional energy storage technologies, such as batteries, fuel cells, and supercapacitors. Supercapacitors have the advantage over batteries and fuel cells, such as long charge/discharge cycles and a wide operating temperature range [14]. Hybrid supercapacitors have high energy storage capability and also great capacitance. Due to their potential to combine the characteristics of their components (EDLC and pseudocapacitor), they have been given high attention recently [15]. There are several options for these combinations with a strong interest in those produced by conducting and electroactive components that possess energy storage [15].

The hybrid supercapacitor that combines EDLC and pseudocapacitor offers better features than those of the combined components. The energy storage at EDLC is dependent on the shell area and the partition length of the atomic charge [16]. The redox reactions between electroactive units resting on active electrode material and an electrolyte solution in the pseudocapacitor contribute to the storage of energy [17]. The integration of these two storage mechanisms results in the hybrid supercapacitors energy storage system, in which half of the system consists of a pseudocapacitor while the other half is EDLC. Compared to regular EDLC and pseudocapacitors,

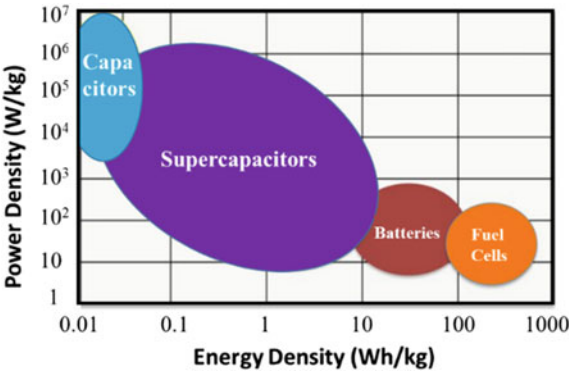

Fig. 1 Ragone plot for different energy storage devices

hybrid supercapacitors have greater power densities and higher energy densities, favoring their usage in energy-efficient systems [18]. Hybrid supercapacitors are still excelling as compared to fuel cells and batteries, although they have much lower power density than conventional capacitors depicted in the Ragone plot for different energy storage devices, as illustrated in Fig. 1.

The factor that distinguishes the supercapacitor from the ordinary capacitor is the absence of dielectric material [19]. The traditional capacitor uses dielectric plates to store electrostatic charge. A supercapacitor (hybrid) has electrodes immersed in electrolyte solution separated by a separator, allowing electrolytic ions diffusion while preventing electrode contact or short circuit [20]. In asymmetric or symmetric hybrid supercapacitors, two different electrodes are used. To be specific, the electrodes can be identical with different mass loadings or a combination between two electrodes that possess dissimilar characteristics of charge storage [21].

It has a higher power density than current rechargeable batteries due to reactions occurring on the outer layer of the electrode for charge storage without allowing ion dispersion into the active species [22]. Generally, the mechanism of the typical rechargeable batteries is due to the intercalation and deintercalation of cations regulated by diffusion limits, which also affects the charging and discharging rate or power density [23]. Moreover, hybrid supercapacitors can hold more charge than rechargeable batteries at higher power rates [24]. Thus, for high power delivery and rapid energy yield, hybrid supercapacitors may be an excellent alternative to rechargeable batteries [25]. However, unlike batteries, their energy density or capacity is limited because the charge stored on the surface limits their energy density or capacity. The specific capacitance of the active material and the net cell voltage dominate in hybrid supercapacitors [26].

The driving force behind hybrid supercapacitors is achieving high power levels, rapid kinetics, subordinate preparatory expenditure, increased safety, and extensive cycle life [27]. Recently, the hybrid supercapacitor systems made of non-aqueous redox materials have gained attention and are being explored and studied widely [28–32]. The significant provocative aspect in hybrid supercapacitors is discovering materials that demonstrate better energy density close to batteries without compromising their established high density and long cycling life [33].

Besides, the highly porous electrode made up of nano-scale material was developed to boost the capacity is one of the most efficient methods [34]. On the other hand, the performance of the overall cell voltage was effectively boosted with the construction of the hybrid supercapacitor using the potential gap between the two electrodes [35]. Therefore, a strategy is needed to magnify specific capacitance and cell voltage and boost performance. Enhancing the specific capacitance involves EDLCs and pseudo-capacitors electrodes, while hybrid substratum is associated with the latter strategy of increasing cell voltage [36]. This leads to significant improvements in performance and their applications.

The alternative technique includes developing nanomaterial electrodes to minimize the diffusion length and give a larger external layer area [37]. This technique focuses primarily on supercapacitors and rechargeable batteries. The higher energy density and voltages can be achieved with the interaction between the type of the

supercapacitor electrode and the type of battery to produce a hybrid supercapacitor. The period of recharge for hybrid supercapacitors compared to the standard platinum acid batteries and other rechargeable batteries are the significant factor to be taken into account [38]. The main objective now is to achieve the hybrid supercapacitors' energy density of 20–30 W h kg^{-1} [39].

2 Fundamental of Hybrid Supercapacitor and Its Storage Mechanism

2.1 Fundamental of Hybrid Supercapacitors

There are currently numerous capacitors available for energy storage that are classified according to the type of dielectric utilized or the physical state of the capacitor, as seen in Fig. 2 [40]. There are various applications and characteristics for capacitors, such as low-voltage trimming applications in electronics (regular capacitors) and supercapacitors that have high-voltage power factor correction [41]. The research on supercapacitors has accelerated dramatically over the last several decades to meet applications requiring attributes like greater specific energy, longer cycle life, and reliability. Supercapacitors that are subjected to electrochemical behavior have a configuration similar to that of a battery. The supercapacitor is composed of a bi-electrode configuration that is separated by an electrolyte-immersed separator. The supercapacitor assembly is composed of the following components: a pair of electrodes, separator, current collector, and electrolyte solution, as seen in Fig. 3

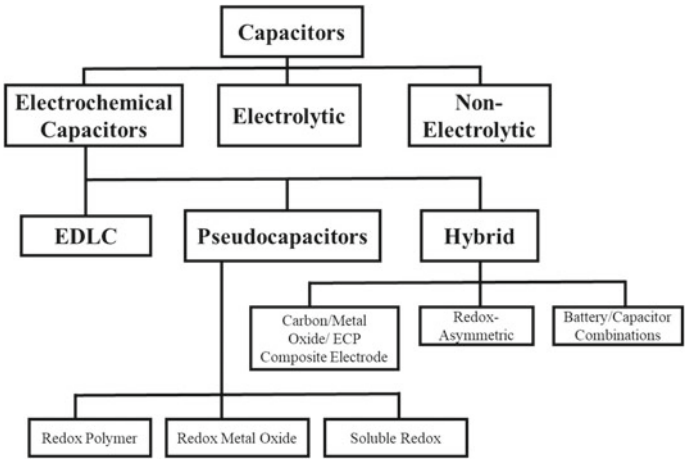

Fig. 2 Types of capacitors

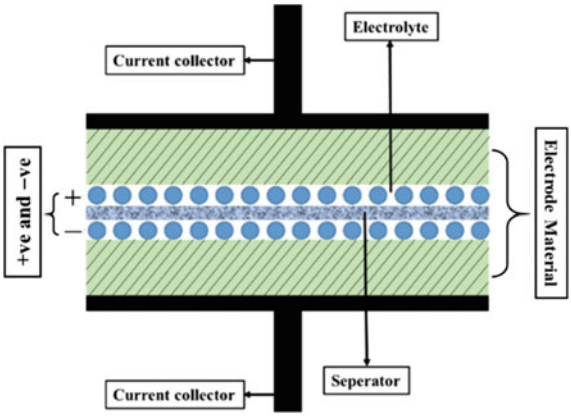

Fig. 3 Schematic diagram of a supercapacitor

[42]. These components contribute to the supercapacitor's properties. Supercapacitors are a form of the capacitor where the charging and discharging occur at the electrode–electrolyte contact that allows the storage of generated energy [43].

A hybrid supercapacitor is one type of supercapacitor that operates based on the following mechanisms:

- The capacitance of the EDL resulting from the adsorption of Coulombic charge that occurs near to the electrode–electrolyte contact
- The surface redox reactions which is related to their respective potentials, resulting in the pseudocapacitance
- The interaction between both types of supercapacitors formulates the concept for the hybrid supercapacitor operating mechanism

Although supercapacitors operate on the same principle as regular capacitors, they are preferred for rapid energy release and storage [44]. In comparison to regular capacitors, supercapacitors incorporate electrodes with a higher effective surface area, resulting in a factor of 10,000 increase in capacitance over conventional capacitors [45]. While typical capacitors have a charge storage range of micro- to millifarads, supercapacitors have a charge storage range of 100–1000 F per device and have low equivalent series resistance with high operational specific power time. Therefore, the supercapacitors can flexibly have a specific energy range and power with several variation orders through proper component design.

2.2 Storage Mechanism of Hybrid Supercapacitors

As mentioned earlier, the hybrid supercapacitors are a combination of both EDLC and pseudocapacitors. Therefore, this section discusses the storage mechanism for EDLC, pseudocapacitor, and hybrid supercapacitors separately for ease of understanding.

2.2.1 Storage Mechanism of an Electric Double Layer Capacitor (EDLC)

The capacitance mechanism of EDLC is alike to the conventional dielectric capacitor's mechanism [46]. Typical capacitors' capacitance depends on the separation between the two charged plates, which provides limited storage. However, in comparison with the ordinary capacitor, a supercapacitor is able to store more energy based on the EDL principle due to the characteristic of wide interface area of the electrodes. In EDLC, the reversible adsorption of electrolyte ions onto the electrochemically stable active material electrode causes the charge to be electrostatically stored [47]. The double-layer capacitance is generated due to the charge separation from polarization on the electric-electrolyte boundary. The capacitance is raised due to the true capacitance effect as the charging storage occurs directly across the electrode material's double-layer structure, and no charge transfer occurs across the boundary. The surface charging mechanism occurs in surface dissociation, ions adsorption from electrolyte, and flaws in the material's crystal lattice. To achieve electroneutrality, the opposing charged ions are produced in the electrolyte near the electrode–electrolyte boundary resulting from the deficiency or excessive charge formation at the surface of the electrode. The double layer's thickness depends on the concentration of the electrolyte and ion sizes and for concentrated electrolytes is of the order 5–10 Å.

Von Helmholtz illustrated the EDL charge storage mechanism during his study of the opposing charge distribution at the colloidal particle interface in the nineteenth century [48]. Based on Helmholtz's charge storage model, two layers with opposing charges are created simultaneously, and the separation at the electrode–electrolyte interface is maintained and equivalent to their atomic distance [49]. Nevertheless, after 1957, the concept became useful when H.I. Becker of General Electric patented the EDLC, where this is the first type of EDLC that has porous carbon electrode submerged in an aqueous electrolyte. An ion-permeable separator kept the electrodes apart [50].

Gouy and Chapman modified the Helmholtz model, which considers the distribution of the charge to be continuous throughout an electrolyte solution layer, also called the diffuse layer [39]. However, a more excellent capacitance estimation in EDL is a limiting factor for the model from Gouy and Chapman because of the inverse relationship between capacitance and distance. This model, therefore, offers larger capacitance on the electrode's outer layer as the presence of the ions near the electrode interface.

Apart from that, Stern's EDLC model combined two models relating to the EDL mechanism [51]. The Stern model describes some ions adhering to the internal electrode, while some charge distribution of ions follows according to the function of distance from the surface of the metal, which is called a compact layer (Stern layer) and diffuse layer, respectively [52]. The Stern layer is made up of firmly attached ions to an electrode. Unlike this, the diffuse layer suggested by the Gouy and Chapman models involves a continuous distribution of electrolytic ions supported by thermal motion [53]. Continuity to that, the distinction of ions in the compact layer is achieved by dividing it into two planes, the inner Helmholtz plane that is near to the electrode

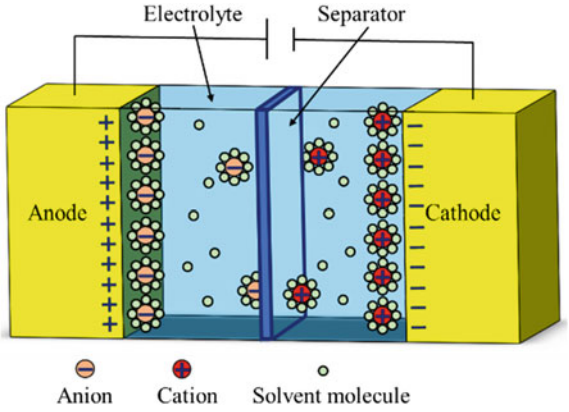

Fig. 4 Schematic diagram of an EDLC

core and the outer Helmholtz plane that in contact with the electrolyte. Therefore, the distinction of ions in the compact layer is achieved [54].

Two electrodes were attached to the metal collectors in the EDLC. Furthermore, the electrodes are arranged in the middle in an electrolyte solution with an ion-permeable separator, intended to avoid short circuits. The parameter such as the double layer's width at the electrode–electrolyte boundary significantly less than the separator thickness determines the capacitance in EDLC. The following general capacitance equation is used to measure the capacitance [55].

$$C = \frac{A \times \in_o}{d} \tag{2.1}$$

where C is the capacitance in farads, A indicates the surface area, ϵ_o indicates the permittivity of free space, while d is the Debye length which indicates the effectual width of the electrical double layer.

The energy generation of a conventional EDLC is due to the electrostatic interaction of ions at the electrode–electrolyte boundary [56]. The representation of an EDLC is illustrated in Fig. 4, where an EDLC consists of a simple configuration, with a separator and two electrodes in an electrolyte [57]. The energy density is one of the key characteristics for the application of supercapacitors. The low energy density restricts EDLC application in cars and other novel storage devices [46]. For instance, the current energy density of EDLC is between 5 and 10 W h^{-1} [15].

2.2.2 Storage Mechanism of Pseudocapacitor

Compared to the EDLC, the faradaic reactions are the key to the capacitance shown in pseudocapacitors, which envelop the pseudoelectrode energy elevation [58]. In fact, pseudocapacitance is not entirely electrostatic in nature and it becomes electrostatic

due to the electrochemical charge transfers and the presence of the active material (finite amount). The pseudocapacitor is to some extent analogous to a battery's behavior because the storage is based on redox reactions [59]. A pseudocapacitor structure is formed with a supercapacitor that has a double layer structure. The word pseudocapacitance is defined in electrochemistry as an electrochemical capacitive material with a linear reliance of the charge stored on a potential window width [60]. For instance, several reactions involved in the charge storage process and pseudocapacitance arise on the electrode's surface due to the faradic storing mechanism [61]. In a pseudocapacitor, a charge transfer is involved through the double layer and the amount of charge received and the changing potential result in the capacitance.

Generally, the pseudoelectrodes comprise metal oxides, metal-doped carbon, and polymers due to their conductive properties. The pseudocapacitance I can be described with the following equation:

$$C = \frac{d(\Delta q)}{d(\Delta V)} \tag{2.2}$$

where Δq is the derivative of charge acceptance and ΔV represents the changing potential.

The difference between EDLCs and pseudocapacitors is that the pseudocapacitors involve rapid and reversible redox reactions due to the thermodynamic nature of the electroactive material on the electrode–electrolyte interface [62]. The typical setup of a pseudocapacitor is illustrated in Fig. 5 [57]. Capacitance is generated at the pseudocapacitor electrode, which is caused by a faradaic current by electroabsorption or redox reactions of active materials (e.g. Co_3O_4 and RuO_2). The reaction that takes place at the surface of the electrode is the electrosorption process of electron-donating anions such as Cl^- and B^-, contributing to the electrosorption valence [57]. The charge exchange across the double layer causes redox reactions to occur rather than a static separation of charge. Generally, pseudocapacitance is shown in metal oxides such as ruthenium oxides [63], vanadium nitride [64], manganese oxide

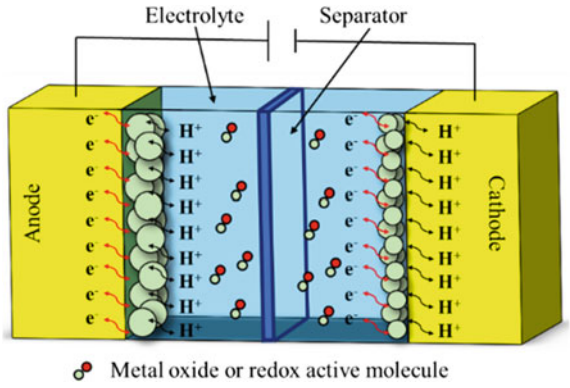

Fig. 5 Schematic diagram of a pseudocapacitor

[65], conducting polymers such as polyaniline (PANI) [66], carbon-based heteroatoms [67–71], other transition metal oxides [72, 73] and nanoporous carbons with electro-absorbed hydrogen [74, 75].

Pseudocapacitor has a higher capacitance value than EDLC (10–100 times higher) but its lower electrical conductivity results in low power density and weak cycling stability [70]. The pseudocapacitance of reversible redox reactions exists due to the faradaic charge shift and the intercalation and deintercalation processes, similar to batteries [73]. Typically, a pseudocapacitor consists of a pair of electrodes that are bonded with metallic current collectors, a separator, and immersed in an electrolyte solution [76]. The electrode potentials in pseudocapacitors are paired with the charge storage made of electroactive materials, resulting in a continuous logarithmic function of the sorption [74, 77]. Pseudocapacitor electrodes, therefore, demonstrate a linear charge dependency stored for charging potential. This linear dependency causes an electron-transfer-based charge storing mechanism rather than an accumulation of charges of the ions that occur in EDLC [78]. There is no pseudocapacitance without double-layer capacitance [79].

The transitional metal oxides RuO_2, Fe_3O_4, and MnO_2, in particular, undergo quick and reversible redox reactions, requiring improvement in long-term cyclability. The most popular electrode material used is RuO_2 because of its optimum capacitive behavior, theoretically providing a pseudocapacitance higher than 1300 g^{-1}. Nevertheless, according to recent reports, the maximal specific capacitance of 720 F g^{-1} has been obtained [63]. Its remarkable electrochemical reversibility and extensive cycling are the reasons for the high capacitance output. The following reactions show the electrochemical protonation of RuO_2, where the charge storage occurs in an aqueous electrolyte [80]:

$$RuO_2 + \delta H^+ + \delta e^- \leftrightarrow RuO_2 - \delta(OH)\delta \tag{2.3}$$

where $0 \leq \delta \leq 1$ over a voltage window of ~1.2 V.

The diffusion factor related to voltage is required for Faradaic reactions [81], where the desolvated ions are smaller than solvated ions [82]. The pseudocapacitance achieved is a linear function of the coverage area of adsorbed ions within a shorter limit [83]. Pseudocapacitance is dependent on the structure, pore diameters, and chemical affinity of the electrodes for surface adsorption [78]. It is not only redox reactions that produce pseudocapacitance but also various electrolyte chemisorption reactions [84–86]. So optimizing the pseudocapacitive electrode material to create beneficial redox sites increases the specific capacitance. In addition, based on the recent studies on pseudocapacitors, the materials reported to have the highest specific capacitance are PANI and RuO_2 [15].

2.2.3 Hybrid Supercapacitor

The hybrid supercapacitor concept was developed to increase the energy density to between 20–30 Wh kg^{-1} [39]. These efforts are focused on bringing the improvement

on the EDLC's energy density criteria by improving electrode and electrolyte materials or developing hybrid supercapacitors. The combinations of various EDLC and redox materials (metal oxides, activated carbon, graphene/graphite, and conducting polymer) form a hybrid supercapacitor [87–90]. To overcome the issue such as the energy density factor of typical pseudocapacitors and EDLCs, the coupling strategy was proposed through the use of hybrid systems consisting of a capacitor-like and a battery-like electrode, which are faradaic and non-faradaic, respectively [91]. The combination provides a more significant working potential and a capacitance two to three times that of traditional pseudocapacitors, EDLC, and capacitors.

The storage mechanism of hybrid supercapacitors combines the storage principle of EDLC and pseudocapacitor. The pseudocapacitor does not present the downside of the EDLC and vice versa. Therefore, the combination of two types of electrodes results in the advantage of providing higher capacitance by overshadowing the weaknesses of the components, respectively. Hybrid supercapacitors can be symmetrical or asymmetrical, which is based on the assembly configuration. Figure 6 illustrates the architecture of a hybrid supercapacitor that comprises a carbon electrode and a Li insertion electrode. When two different electrodes of different materials are combined to form a hybrid supercapacitor, the electrochemical behavior is superior to that of individual electrodes. The cycling stability and affordability are retained in hybrid supercapacitors serve as the limiting factors in developing the pseudocapacitor [89]. The hybrid supercapacitors show increased specific capacitance values and higher rated voltage than the symmetrical EDLC, corresponding to better specific energy.

The symmetric hybrid supercapacitor is constructed from two similar supercapacitor electrodes, which are similar to EDLC and pseudo-capacitive components. The typical hybrid supercapacitor is made of two alternating current electrodes dipped in an organic electrolyte with an electrical potential of up to 2.7 V [92]. An asymmetric hybrid supercapacitor is formed by the construction of two different electrodes, while the best candidates for the electrode's materials are the MnO_2 and AC as well as the AC−$Ni(OH)_2$ [93]. Generally, the hybrid supercapacitors that are commercially available are asymmetric, except for those having conducting polymer electrodes

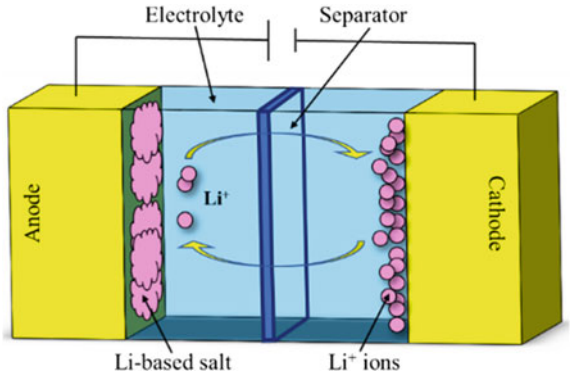

Fig. 6 Illustration of a hybrid supercapacitor

[94]. The redox reactions are carried out in conducting polymer to store and release charge in hybrid supercapacitor consisting of this electrode. When the polymer is oxidized or doped, the ions are transported to the polymer backbone; when the polymer is reduced or de-doped, the ions are returned to the solution. The charging process occurs in the polymer matrix's bulk volume rather than on the surface, as is the case with electrodes made of carbon. The usage of conducting polymers enables the achievement of increased specific capacitance. Mastragostino et al. demonstrated a hybrid supercapacitor with a specific capacitance of 39 F g^{-1}) based on conducting polymer [92].

Amatucci's group proposed a basic asymmetric hybrid supercapacitor that consists of a positive electrode of activated carbon (EDLC) and a negative electrode of $Li_4Ti_5O_{12}$ (Faradaic electrode) in an organic electrolyte [95]. In the hybrid system, high power density is provided by the EDLC electrode, while high energy density is provided by the psudoelectrode. As a result, dilapidation exceeding the limitations of the individual electrodes results in the formation of a hybrid component with increased parameters. It has also been reported that activated carbon can be assembled asymmetrically with potassium sulfate (K_2SO_4) and manganese dioxide (MnO_2) [96]. Rajkumar et al. recently reviewed the advancements of asymmetric supercapacitors with an aqueous electrolyte [97]. The study concluded that it is vital to investigate the physicochemical properties and mechanism of the charge storing process that occurs at the electrode and electrolyte boundary to improve electrochemical performance. Several strategies such as the development of components with high electronic conductivity, superior structures, a large surface area, and a high concentration of electrochemically active sites can improve the transportation of ions. On the other hand, the specific capacitance varies owing to the characteristics of the material type of electrode and electrolytes, as well as the fabrication technique.

Cericola and Kötz proposed a systematic approach to classifying hybrid supercapacitors based on material combinations [98]. As a result, the hybrid supercapacitor assembly can be formed using EDLC and pseudocapacitor electrodes and combining one of these components with a battery-type electrode. Hybrid systems, according to their research, can be symmetrical or asymmetrical, depending on the electrochemical behavior and types of material used to produce the electrodes. In addition, the symmetric systems outperform conventional EDLC or faradaic capacitors, yet asymmetric systems outperform all other forms of supercapacitors in every way. As a result, the asymmetric hybrid system is the optimal configuration for supercapacitors.

Internal resistance is the constraint on any supercapacitor's optimum capacitive operations. The power output is proportional to its internal resistance, which is defined as the resistance of the electrolyte, current collectors, and electrodes together referred to as equivalent series resistance (ESR) [99, 100]. By comparing to EDLC supercapacitors, hybrid supercapacitors exhibit a lower cyclability. Additionally, the electrodes and electrolyte material used will directly affect the performance and properties of a hybrid supercapacitor. Selecting the appropriate electrolyte for the electrode materials is critical to optimize the hybrid supercapacitor's overall performance.

3 Structure and Design of Hybrid Supercapacitors

3.1 Components and Architecture of Hybrid Supercapacitors

The schematic diagram of a hybrid supercapacitor has shown earlier in Fig. 6 in Sect. 2. Generally, a hybrid supercapacitor consists of electrolyte materials, separator, current collector, sealants, and a combination of two electrodes. In this section, the individual components of the hybrid supercapacitor are discussed.

3.1.1 Hybrid Electrodes

The term "hybrid supercapacitor" refers to a supercapacitor that contains electrodes made of two or more distinct materials. These electrodes will store energy via a combination of electric double-layer formations and pseudo-Faradaic reactions [101, 102]. Asymmetric electrode materials are utilized to store electrical energy in hybrid capacitors. The hybrid capacitor is designed to attain a high energy density. Compared to symmetric capacitors, hybrid capacitors have a large potential window and a high specific capacitance [103]. In general, hybrid capacitors employ three types of electrodes: composite electrodes, battery-type electrodes, and asymmetric electrodes. The types of hybrid electrodes are summarized in Fig. 7. In the first class of electrodes, carbon-based materials are combined with pseudocapacitive electrode material (conducting polymers or metal oxides) in composite electrodes [104]. As a result, the mutual charge storage in an electrode is enabled based on chemical and physical methods. The capacitive double layer made of carbon materials can perform the EDLC function while increasing the capacitance due to the large surface area [105]. The materials that show pseudocapacitance are conducting polymers or metal oxides. The increased surface area property facilitates contact between the electrolyte and the absorbed pseudo-material. In the following electrode category, one of the electrodes in a battery-type electrode will be carbon, while the other will be a battery electrode type [106]. In the third class of electrodes, both electrodes in an asymmetric capacitor are capacitive in nature; however, one will exhibit EDLC

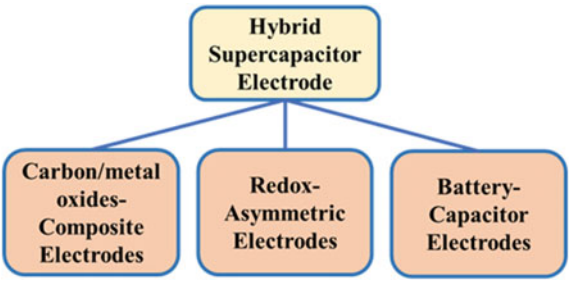

Fig. 7 Summary of types of hybrid supercapacitor electrodes

behavior while the other will be constructed of pseudocapacitive electrode material [107].

Composite electrodes have a significant effect on the phase structure, microstructure, and electrochemical performance. Notably, a porous nanocomposite (e.g., CoxNi1-x$(OH)_2$ disks@rGO) has shown exceptional specific capacities, rate capability, and cycling stability. When used in conjunction with a capacitive-type electrode (e.g., PPD/rGO), the hybrid supercapacitor demonstrated better energy and power density and consistent cycling performance over 20,000 cycles at 20 A g^{-1}. Furthermore, the hybrid supercapacitor with composite electrodes has outstanding electrochemical performance, and the straightforward preparation technique makes it a good candidate for commercial applications. Additionally, the straightforward preparation approach paves the way for creating cost-effective, high-performance supercapacitors based on transition metal hydroxides/composites for various applications [108].

Despite its asymmetry, battery-capacitor electrodes are distinct from typical "asymmetric supercapacitors" with two capacitive electrodes but an asymmetric capacitive charge storage mechanism. Given the complexity of electrode, electrolyte, and device configurations, there are several options to design diverse types of battery-capacitor hybrid supercapacitors, which are classified into the following categories: lithium-ion type, sodium ion type, acidic type, alkaline type, redox electrolyte type, and pseudocapacitive type [109].

It is worth noting that the term "asymmetric" or "hybrid" applies to devices, not electrodes. The term "hybrid capacitor" is widely understood to refer to a situation in which the two electrodes have two distinct charge-storage mechanisms: one capacitive and one battery-type Faradaic [29, 98, 110–113]. Furthermore, the theoretical range of asymmetric supercapacitors is more excellent. These devices may contain two distinct electrode materials (which may contain a hybrid device if the active materials have a different charge storage mechanism or a different ratio of redox-active sites on the electrode material), two distinct redox-active electrolytes, or even the same EDLC carbon material with distinct surface functional groups. In any case, hybrid devices are unquestionably a subcategory of asymmetric devices. Additionally, hybrid capacitor devices typically comprised of a Faradaic electrode (such as $Ni(OH)_2$ or Co_3O_4) and a carbon electrode [114]. The architecture and design of the hybrid supercapacitors with various electrodes are summarized in Fig. 8 [108, 109, 113].

3.1.2 Electrolyte Materials

The electrolyte composition dictates the power density of supercapacitors, as electrolyte resistance is a significant factor. The term 'electrochemical series resistance' refers to the collective resistances contained within a supercapacitor system. The power density is low if the resistance of the electrolyte is high. A variety of electrolytes can be employed in supercapacitors, including aqueous, organic, and ionic, which are classified as liquid or solid. Figure 9 illustrates the various types of liquid

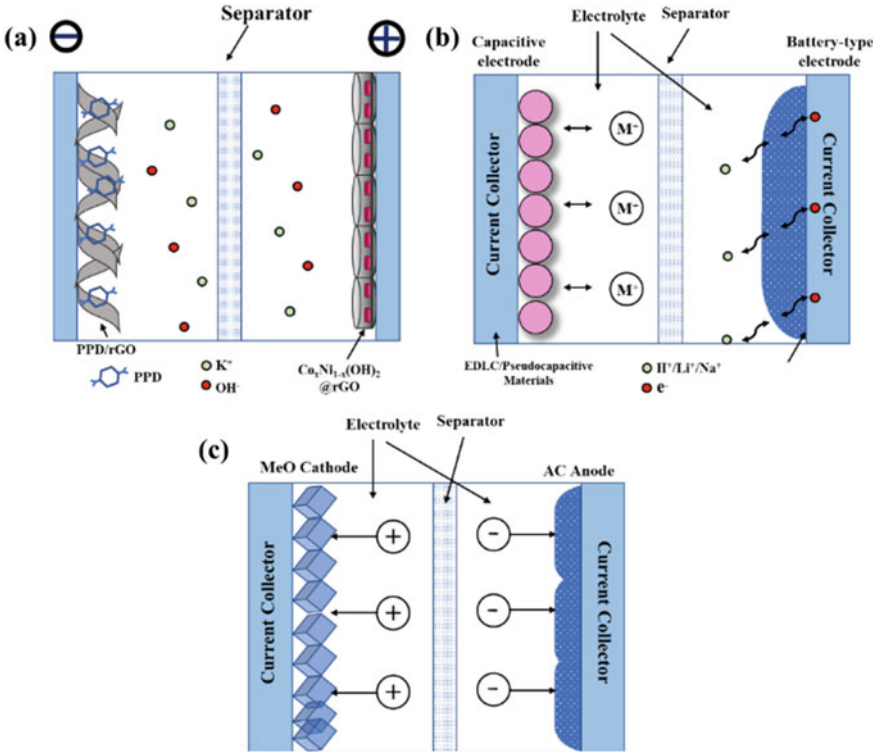

Fig. 8 Schematic diagram of hybrid supercapacitors with different types of electrodes: **a** composite electrode, **b** Asymmetric electrode, **c** Battery-capacitor electrode

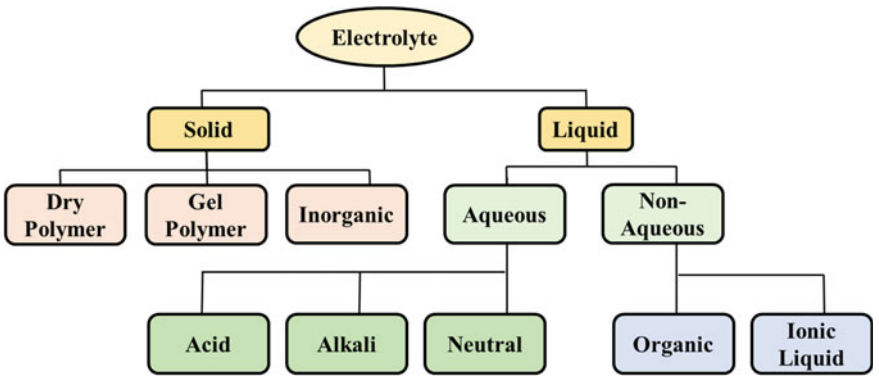

Fig. 9 Classification of liquid and solid electrolytes

and solid electrolytes [107]. The electrolyte is chosen depending on the stable potential range within which it operates. Aqueous electrolytes (acids, alkalis) have a low specific resistance, making them ideal for supercapacitor manufacture. Additionally, aqueous electrolytes are significantly less expensive than organic electrolytes, which is a significant advantage. It is worth noting that the organic electrolytes have a high specific resistance, which decreases the supercapacitor's power density [115]. Additionally, aqueous electrolytes have drawbacks, including instability at higher voltages, which results in electrode degradation, and are environmentally toxic. However, organic electrolytes are more stable at higher operating voltages but are also very poisonous and combustible. Aqueous electrolytes have low resistance because protons have a high mobility and a small size, which reduces the resistance.

On the other hand, the resistance of organic electrolytes is higher due to their large size. As a result, both the electrolyte and the porosity of the electrode architecture are critical for the supercapacitor to work optimally. As the supercapacitor functions for many thousand cycles, the electrolyte depletion increases the internal resistance, reducing the capacitance and thus the energy density. This is why both aqueous and organic electrolytes are not particularly well-suited for use in commercially available supercapacitors. Ionic liquids are used as electrolytes in commercial supercapacitors. These distinct classes of electrolytes are distinguished by their high conductivity and broad electrochemical potential window [116, 117]. Ionic liquids are naturally non-flammable, which makes them safe to handle. Electrolyte depletion can be minimized by increasing the concentration of ionic liquids.

Additionally, they exhibit excellent chemical and environmental stability, making them attractive candidates for application in supercapacitors. Due to their increased electrochemical properties, a new class of electrolytes known as gel polymer electrolytes has gained considerable popularity [118–120]. Gel polymer electrolytes can be utilized to build solid-state supercapacitors, which are particularly favorable for use in next-generation flexible and wearable electronic devices. Thus, a new class of electrolytes, dubbed ionic liquid-based gel polymer electrolytes are proposed by merging the properties of ionic liquids with gel polymer electrolytes [121, 122]. These combine all of the advantages of their individual counterparts and none of the disadvantages, but the cost aspect remains a significant issue.

3.1.3 Separator

An electrolyte separator membrane serves two purposes: (i) it allows electrolyte ions to pass through and (ii) it prevents the supercapacitor electrodes from short-circuiting. For supercapacitor applications, an electrolyte membrane that possesses excellent ionic conductivity is preferred. A simple piece of Xerox paper or a commercially available Whatman™ filter paper will suffice because these electrolyte membranes are inexpensive, making them accessible. Nanostructured electrolyte membranes have also been developed recently [123–125]. One such membrane is the Nafion™ membrane. Due to the nanoscale characteristics of Nafion™ membranes, they exhibit high ionic conductivities and are widely employed in commercial supercapacitors.

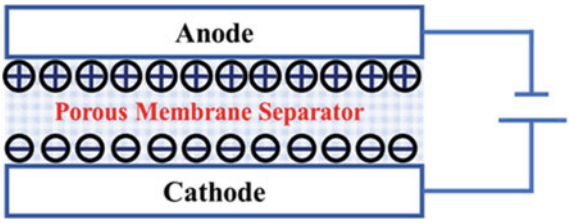

Fig. 10 Schematic diagram of porous membrane separator in a supercapacitor

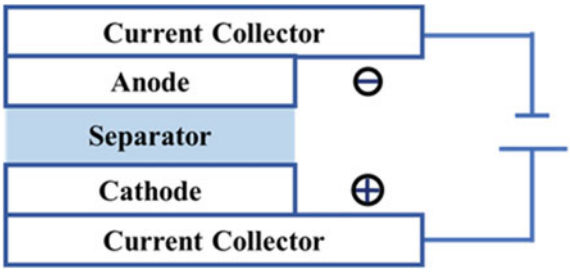

Fig. 11 Architecture of the current collector in supercapacitor

However, because Nafion™ is very expensive, developing innovative electrolyte membranes using less expensive polymers has gained attention [126, 127]. As illustrated in Fig. 10, the electrolyte membrane should have a porous structure to facilitate the transfer of ions from the electrolyte to the electrodes [107].

3.1.4 Current Collector

The current collector's function is to collect electrons from the electrode-active material and deliver them to the external circuit. Copper and aluminum plates are utilized for this purpose. Occasionally, alloys are used in the same way; one example is steel plates. Two current collectors are often utilized on supercapacitors' cathode and anode surfaces, as illustrated in Fig. 11 [107].

3.1.5 Sealants

Sealants support the configuration of a hybrid supercapacitor, preventing the system's loss in performance [128]. In addition, the sealant acts as a barrier to external contaminants such as air, chemicals, and water. Importantly, electrolyte degeneracy and oxidation of the electrode surface will occur with the presence of the contaminations. As a result, the effective sealing of the hybrid supercapacitor is critical. Shunt resistance between cells connected to the assembly will present due to the improper sealing, affecting the overall efficiency of the hybrid supercapacitor by stipulating alternate current pathways [129]. Due to their excellent moisture resistance and flexibility, polymeric materials are frequently utilized as sealants. A hermetic

seal is usually used as an appropriate sealing, based on the electrolyte material that prevents water and gas from entering the system. This sealing method is appropriate for monopolar arrangements, but improved edge sealing is necessary for bipolar arrangements to prevent the flow of shunt current [130]. This shunt current results in short-circuiting, self-discharging, and a reduction in charging efficiency.

3.2 Design of Hybrid Supercapacitors

A supercapacitor's design is related to the alignment of individual components within a larger configuration [131]. A hybrid supercapacitor is made up of two electrode sections that can be made of the same/different materials but with the exact dimensions, and a separator (microporous), all of which are immersed in a liquid electrolyte. While charging and discharging, the hybrid supercapacitor system is located between current collectors terminals [132]. Typically, when a non-aqueous electrolyte is used, the electrodes are close to 100 μm thick, and when an aqueous electrolyte is used, the thickness is slightly larger. Separators typically have a thickness of 24 μm, whereas current collectors have a thickness of 50 μm, which is a bipolar design [133]. The most often used design for supercapacitors is the organic electrolyte containing in the cell. The complete supercapacitor is depicted in a single cell, and the performance in DC applications can be significantly improved by combining such singular cells [134]. The purpose of combining such distinct cell components is to provide a higher level of reliability than the battery's cell combination. This provides the benefit that the parameters may be accurately evaluated at any point in time. The asymmetric design of the supercapacitor is gaining traction, particularly for the hybrid supercapacitor. Two different electrodes (EDLC and Faradaic) that operate independently are incorporated in the asymmetric design, which significantly increases the electrochemical capacitor's energy density while simultaneously decreasing the rate of self-discharge [131].

There are three types of supercapacitor cells: coin cells, cylindrical cells, and pouch cells, as schematically depicted in Error! Reference source not found.. As seen in Fig. 12a, the assembly of two electrodes and a separator in a metallic casing with the inclusion of an insulating polymer such as Teflon are presented in a coin cell made of SiO_2-Ppy composite [134]. The metallic case is made of conductive materials, while the insulating polymer is added to prevent short circuits and electrolyte leakage. The appropriate sealing of the system is achieved by applying sufficient pressure to the metallic shell [135]. The properties such as thin electrodes and a low active material concentration are being applied to this design.

For supercapacitors with a high mass of active material loading, cylindrical cell design is the most frequently used and recommended [63]. Figure 12b displays a schematic representation of a cylindrical design [136]. The electrodes are drawn as long rectangular sheets and then rolled to fit inside a cylindrical metal casing with identical dimensional separators. Solder is used to connect the current collector to the rolled electrode sheets. After the electrode-separator assembly is complete, the

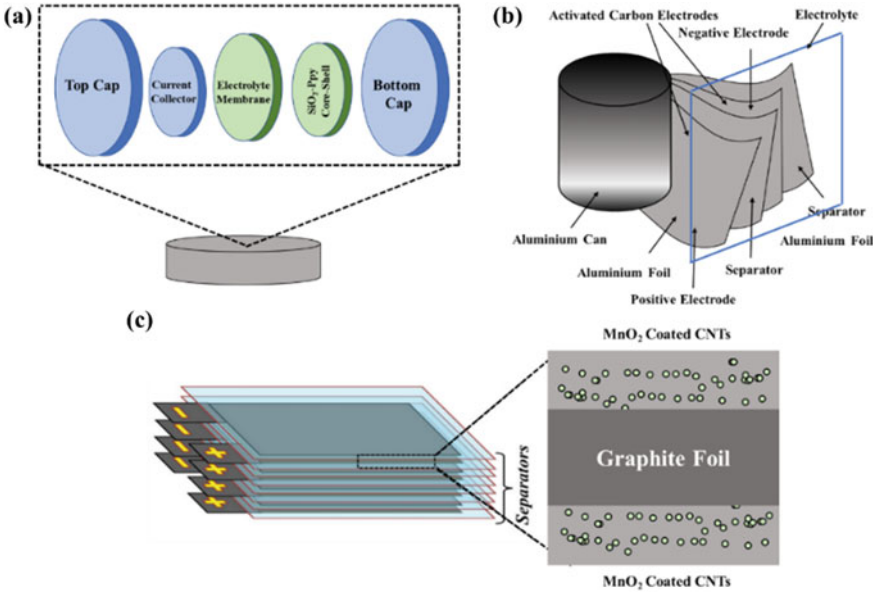

Fig. 12 Design of various supercapacitors: **a** Coin cell design, **b** cylindrical cell design, **c** pouch type cell design

electrolyte solution is poured into the casing. Finally, the entire cell is sealed, and safety vents are installed for added protection in the event of pressure build-up [15].

As with MnO_2 coated on CNT, the pouch type design includes the stacking of the electrode-separator-electrode layer by layer, which is critical for the arrangement of many electrode piles, as illustrated in Error! Reference source not found. **c**. The various electrodes are soldered to the current collectors respectively before being connected based on the desired configuration. To add flexibility to the system, the pouch design incorporates a polymer bag, rather than using an iron casing.

Manufacturing of the supercapacitor component includes various electrode fabrication and electrolyte preparation procedures [134]. The preparation of electrodes requires developing a paste (homogenized) or a slurry of active components in the presence of a binding agent in a solvent [135]. Hot pressing is used to press the past or slurry into a plate, which is then followed by drying, or it can be diluted further with solvent and sprayed on the current collector like paint [134]. The most often used fabrication process is printing, where the production of the substrate is directly applied to the electrode surface by spraying paint or printing, templates or ink-jet printing [137], and casting methods [135], among others. The surface coverage is increased with this printing approach and it allows the deposition on non-traditional surfaces such as polymers, paper, and flexible sheets. Then, the solvent is evaporated after the spraying of printable material, for example, the manufactured film (ink-jet printing) that covers a printed carbon nanotube network. On top of that,

dual-functional materials such as single-walled carbon nanotubes (SWCNTs) on a plastic substrate can be created using the spraying process [15].

Similarly, ink-jet printing is a frequently utilized manufacturing method for fabricating monowall carbon nanotubes on cloth and elastic surfaces for thin-film electrode configurations [138]. The controllable thickness, tunable electrical characteristics, and geometry preservation are achieved using an off-the-shelf ink-jet printer in this approach. Apart from that, ruthenium oxide/SWCNTs nanowire electrodes were also produced using a similar approach [137]. The alternative form of fabrication involves collateral lettering or depiction on cellulose paper using a graphite bar or pencil [139]. The advantage of this technology is that it does not require solvent, but the disadvantage is that it is not practicable for batch processing. Electrolyte preparation, which is entirely dependent on the electrolyte type, is simple compared to electrode preparation. For example, organic electrolytes are synthesized in a dry environment [15].

Material design plays a critical role in hybrid supercapacitor manufacture. For example, the ultra-centrifuging force (UCF) approach is used to design the hybrid assembly of $Li_4Ti_5O_{12}$ and AC [30, 64]. The nanostructure is made up of nanocrystalline composites of $Li_4Ti_5O_{12}$ particles that have been dissipated on activated carbon [140]. Therefore, the hybrid structure synthesized using the UCF approach was more conducive. Furthermore, by applying a positive electrode made of AC and a negative electrode made of composite material, the nano-hybrid capacitor can have increased power and energy density [140].

4 Characteristics of Hybrid Supercapacitors

To produce a good device of hybrid supercapacitors, the parameters of energy and power of the supercapacitors need to be taken into consideration. These two parameters are discussed in the following section. Although electrical parameters are not explained, this does not mean they are of lesser importance. Readers are advised to refer to other chapters on the discussion of other electrical parameters.

4.1 Energy Capacity

Typically, rated capacitance C_R is used to rate commercial capacitors. On the other hand, the amount of energy value provides the amount of the supercapacitors required in providing the maximum energy for the application [141]. The interaction between the capacitance value and the maximum energy is expressed in the following equation:

$$W_m = \frac{1}{2} C V_{max}^2 \tag{4.1}$$

where W_m is the maximum energy, C is the capacitance and V_{max} is the maximum voltage. The energy value of a supercapacitor is also known as energy capacity.

In theory, the supercapacitor has maximum stored energy as defined in Eq. 4.1. Unfortunately, in practical application, not all the stored energy is accessible. This is due to voltage drop and the time constant over the internal resistance. That means the effective energy W_{eff} is reduced as a result of voltage drop and it can be expressed as Eq. 4.2:

$$W_{eff} = \frac{1}{2}C(V_{max}^2 - V_{min}^2) \tag{4.2}$$

where V_{min} is the minimum voltage. Another way of quantifying this phenomenon is the discharge factor. Discharge factor, d is directly related to the minimum threshold voltage as expressed in Eq. 4.3

$$d = \frac{V_{min}}{V_{max}} \times 100 \tag{4.3}$$

The amount of energy stored in a supercapacitor usually is expressed in terms per mass. This term is called specific energy where it is measured gravimetrically in watt-hours per kilogram (Wh/kg). In some cases, the amount of stored energy is expressed in terms per volume. This term is designated as energy density. In some literature, it is also known as volumetric specific energy where the value is measured volumetrically in watt-hours per liter (Wh/l). Generally, the range of energy density for a hybrid supercapacitor is between 5 and 10 Wh/l.

4.2 Power

The power parameter of a supercapacitor is directly associated with the efficiency of the supercapacitor. As discussed earlier, supercapacitors have unfavorable energy capacity when compared with batteries. However, supercapacitors excel in high specific power. This parameter denotes the rate at which energy can be supplied to the load (during discharging). When voltage drop is taken into consideration, the effective power and maximum power for supercapacitors are represented in Eqs. 4.4 and 4.5, respectively.

$$P_{eff} = \frac{1}{8} \cdot \frac{V^2}{R_i} \tag{4.4}$$

$$P_{max} = \frac{1}{4} \cdot \frac{V^2}{R_i} \tag{4.5}$$

where V is the voltage applied and R_i is the internal resistance of the supercapacitor. For hybrid supercapacitors, the power density can range from 10 to 1000 kWh/kg even though there are different values reported in various literature [15].

Ragone chart (Fig. 1) is a valuable tool for a quick characterization of energy storage devices where the relationship between the specific energy and specific power can be compared.

5 Applications

Supercapacitors have been put to practical use in various sectors. The various fields of application are illustrated in Fig. 13. With the increasing demand for electric vehicles (and also hybrid vehicles), supercapacitors have become the important energy storage components in the transportation sector. They are used as instantaneous power providers during the startup of the internal combustion engine as demonstrated in Toyota's Yaris Hybrid-R car [142]. Besides passenger cars, supercapacitors are applied in buses and trolleybuses. Electric buses like e-buses which use supercapacitors as quick charging and storage devices have been introduced in China [143].

Application of supercapacitors in consumer products and computers peripheral is also gaining wide acceptance. For instance, a supercapacitor is used as a memory component where it serves as a memory backup system when there are power interruptions. In computer peripherals, supercapacitors are used as a backup power supply. Besides transport vehicles and electronic devices, supercapacitors are also applied in

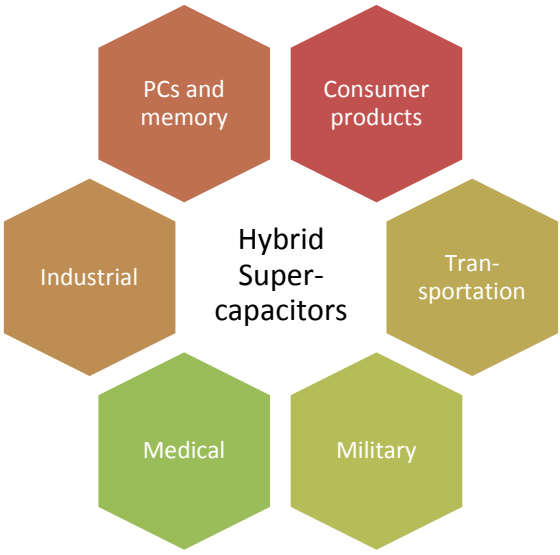

Fig. 13 Common application fields of hybrid supercapacitors

the area of military equipment, medical devices, and industrial products. A comprehensive list of supercapacitor applications can be referred to in the review study by Muzaffar et al. [15].

6 Conclusion

In this chapter, the concept of a hybrid supercapacitor is introduced. The background of electrochemical energy storage is first elaborated. As hybrid supercapacitor usually comprises partial EDLC and partial pseudocapacitor, their respective storage mechanisms are explained as well. The architecture and design of hybrid supercapacitors showed that suitable composition of materials used can yield good performance of the supercapacitors. As a high-performing energy storage device, hybrid supercapacitors have been applied in various sectors with automotive and consumer electronic products taking the bigger share. It is foreseen that the market of hybrid supercapacitors will continue to grow given the wide research and development interest from the scientific community and industry players. It is, therefore, paramount to understand and appreciate the fundamental concept of hybrid supercapacitors as presented in this chapter for better hybrid supercapacitors design.

References

1. BE Conway. Electrochemical supercapacitors: scientific fundamentals and technological applications. 2013 Springer Science & Business Media.
2. K.N. Hui, H.K. San, Z. Tang, V. Jadhav, Q.X. Xia, Hierarchical chestnut-like $MnCo_2O_4$ nanoneedles grown on nickel foam as binder-free electrode for high energy density asymmetric supercapacitors. J. Power Sources **330**, 195–203 (2016)
3. G. Oukali, E. Salager, M.R. Ammar, C.-E. Dutoit, V. Sarou-Kanian, P. Simon, E. Raymundo-Piñero, M. Deschamps, In situ magnetic resonance imaging of a complete supercapacitor giving additional insight on the role of nanopores. ACS Nano **13**, 12810–12815 (2019)
4. R. Sahoo, T.H. Lee, D.T. Pham, T.H.T. Luu, Y.H. Lee, Fast-charging high-energy battery–supercapacitor hybrid: anodic reduced graphene oxide–Vanadium (IV) Oxide Sheet-on-Sheet Heterostructure. ACS Nano **13**, 10776–10786 (2019)
5. Z. Chen, Y. Qin, D. Weng, Q. Xiao, Y. Peng, X. Wang, H. Li, F. Wei, Y. Lu, Design and synthesis of hierarchical nanowire composites for electrochemical energy storage. Adv. Func. Mater. **19**, 3420–3426 (2009)
6. H. Becker, Low voltage electrolytic capacitor. U.S. Patent 2,800,616, 14 April 1954 (1957)
7. R. Kötz, M. Carlen, Principles and applications of electrochemical capacitors. Electrochim. Acta **45**, 2483–2498 (2000)
8. R.A. Rightmire, Electrical energy storage apparatus. U.S. Patent 3,288,641, 7 June 1962 (1966)
9. D.L. Boos, Electrolytic capacitor having carbon paste electrodes. U.S. Patent 3,536,963, 27 October 1970 (1970)
10. V.V. Jadhav, R.S. Mane, P.V. Shinde, *Bismuth-Ferrite-Based Electrochemical Supercapacitors* (Springer Nature, 2020)

11. B.K. Kim, S. Sy, A. Yu, J. Zhang, Electrochemical supercapacitors for energy storage and conversion, in *Handbook of Clean Energy Systems* (Wiley, 2015)
12. N. Liu, K. Huo, M.T. McDowell, J. Zhao, Y. Cui, Rice husks as a sustainable source of nanostructured silicon for high performance Li-ion battery anodes. Sci. Rep. **3**, 1–7 (2013)
13. P. Simon, Y. Gogotsi, P. Rodgers (ed.). Materials for electrochemical capacitors, in *Nanoscience and Technology: A Collection of Reviews from Nature journals* (World Scientific, 2010)
14. S. Huang, X. Zhu, S. Sarkar, Y. Zhao, Challenges and opportunities for supercapacitors. APL Mater. **7**, 100901 (2019)
15. A. Muzaffar, M.B. Ahamed, K. Deshmukh, J. Thirumalai, A review on recent advances in hybrid supercapacitors: design, fabrication and applications. Renew. Sustain. Energy Rev. **101**, 123–145 (2019)
16. Z. Lu, Z. Chang, W. Zhu, X. Sun, Beta-phased $Ni(OH)_2$ nanowall film with reversible capacitance higher than theoretical Faradic capacitance. Chem. Commun. **47**, 9651–9653 (2011)
17. J. Xie, X. Sun, N. Zhang, K. Xu, M. Zhou, Y. Xie, Layer-by-layer β-Ni $(OH)_2$/graphene nanohybrids for ultraflexible all-solid-state thin-film supercapacitors with high electrochemical performance. Nano Energy **2**, 65–74 (2013)
18. M.D. Stoller, S. Park, Y. Zhu, J. An, R.S. Ruoff, Graphene-based ultracapacitors. Nano Lett. **8**, 3498–3502 (2008)
19. G. Wang, L. Zhang, J. Zhang, A review of electrode materials for electrochemical supercapacitors. Chem. Soc. Rev. **41**, 797–828 (2012)
20. X. Wang, Y.L. Yang, R. Fan, Y. Wang, Z.H. Jiang, TiO_x/N_y nanowire arrays: NH_3-assisted controllable vertical oriented growth and the electrophotochemical properties. J. Alloy. Compd. **504**, 32–36 (2010)
21. P.-C. Chen, G. Shen, Y. Shi, H. Chen, C. Zhou, Preparation and characterization of flexible asymmetric supercapacitors based on transition-metal-oxide nanowire/single-walled carbon nanotube hybrid thin-film electrodes. ACS Nano **4**, 4403–4411 (2010)
22. S.W. Lee, J. Kim, S. Chen, P.T. Hammond, Y. Shao-Horn, Carbon nanotube/manganese oxide ultrathin film electrodes for electrochemical capacitors. ACS Nano **4**, 3889–3896 (2010)
23. D. Zhang, H. Yan, Y. Lu, K. Qiu, C. Wang, C. Tang, Y. Zhang, C. Cheng, Y. Luo, Hierarchical mesoporous nickel cobaltite nanoneedle/carbon cloth arrays as superior flexible electrodes for supercapacitors. Nanoscale Res. Lett. **9**, 1–9 (2014)
24. H.-W. Wang, Z.-A. Hu, Y.-Q. Chang, Y.-L. Chen, H.-Y. Wu, Z.-Y. Zhang, Y.-Y. Yang, Design and synthesis of $NiCo_2O_4$–reduced graphene oxide composites for high performance supercapacitors. J. Mater. Chem. **21**, 10504–10511 (2011)
25. A.G. Pandolfo, A.F. Hollenkamp, Carbon properties and their role in supercapacitors. J. Power Sources **157**, 11–27 (2006)
26. I. Plitz, A. DuPasquier, F. Badway, J. Gural, N. Pereira, A. Gmitter, G. Amatucci, The design of alternative nonaqueous high power chemistries. Appl. Phys. A **82**, 615–626 (2006)
27. Y. Li, P. Hasin, Y. Wu, $Ni_xCo_{3-x}O_4$ nanowire arrays for electrocatalytic oxygen evolution. Adv. Mater. **22**, 1926–1929 (2010)
28. H. Chai, X. Chen, D. Jia, W. Zhou, Electrochemical deposition of Ni $(OH)_2$/CNTs electrode as electrochemical capacitors. Rare Met. **30**, 85–89 (2011)
29. K. Naoi, 'Nanohybrid capacitor': the next generation electrochemical capacitors. Fuel Cells **10**, 825–833 (2010)
30. S. Huang, Z. Wen, X. Zhu, Z. Gu, Preparation and electrochemical performance of Ag doped $Li_4Ti_5O_{12}$. Electrochem. Commun. **6**, 1093–1097 (2004)
31. L. Luo, J. Wu, J. Xu, V.P. Dravid, Tackling reversible conversion reaction mechanism for lithium based battery. Microsc. Microanal. **20**, 1618–1619 (2014)
32. M. Tachibana, T. Ohishi, Y. Tsukada, A. Kitajima, H. Yamagishi, M. Murakami, Supercapacitor using an electrolyte charge storage system. Electrochemistry **79**, 882–886 (2011)
33. J. Yan, Z. Fan, W. Sun, G. Ning, T. Wei, Q. Zhang, R. Zhang, L. Zhi, F. Wei, Advanced asymmetric supercapacitors based on $Ni(OH)_2$/graphene and porous graphene electrodes with high energy density. Adv. Func. Mater. **22**, 2632–2641 (2012)

34. V. Gupta, S. Gupta, N. Miura, Potentiostatically deposited nanostructured Co_xNi_{1-x} layered double hydroxides as electrode materials for redox-supercapacitors. J. Power Sources **175**, 680–685 (2008)
35. Z. Fan, J. Yan, T. Wei, L. Zhi, G. Ning, T. Li, F. Wei, Asymmetric supercapacitors based on graphene/MnO^2 and activated carbon nanofiber electrodes with high power and energy density. Adv. Func. Mater. **21**, 2366–2375 (2011)
36. A. Jorio, R. Saito, J. Hafner, C. Lieber, D. Hunter, T. McClure, G. Dresselhaus, M. Dresselhaus, Structural (n, m) determination of isolated single-wall carbon nanotubes by resonant Raman scattering. Phys. Rev. Lett. **86**, 1118 (2001)
37. H. Inoue, T. Morimoto, S. Nohara, Electrochemical characterization of a hybrid capacitor with Zn and activated carbon electrodes. Electrochem. Solid State Lett. **10**, A261 (2007)
38. W.-J. Zhou, J. Zhang, T. Xue, D.-D. Zhao, H.-L. Li, Electrodeposition of ordered mesoporous cobalt hydroxide film from lyotropic liquid crystal media for electrochemical capacitors. J. Mater. Chem. **18**, 905–910 (2008)
39. A. Burke, R&D considerations for the performance and application of electrochemical capacitors. Electrochim. Acta **53**, 1083–1091 (2007)
40. T. Pandolfo, V. Ruiz, S. Sivakkumar, J. Nerkar, General Properties of Electrochemical Capacitors. (Wiley, 2013)
41. J. Huang, B.G. Sumpter, V. Meunier, A universal model for nanoporous carbon supercapacitors applicable to diverse pore regimes, carbon materials, and electrolytes. Chem. A Eur. J. **14**, 6614–6626 (2008)
42. K. Dai, X. Wang, Y. Yin, C. Hao, Z. You, Voltage fluctuation in a supercapacitor during a high-g Impact. Sci. Rep. **6**, 38794 (2016)
43. S. Vivekchand, C.S. Rout, K. Subrahmanyam, A. Govindaraj, C. Rao, Graphene-based electrochemical supercapacitors. J. Chem. Sci. **120**, 9–13 (2008)
44. L.L. Zhang, X. Zhao, Carbon-based materials as supercapacitor electrodes. Chem. Soc. Rev. **38**, 2520–2531 (2009)
45. J. Huang, B.G. Sumpter, V. Meunier, Theoretical model for nanoporous carbon supercapacitors. Angew. Chem. **120**, 530–534 (2008)
46. G. Guidi, T.M. Undeland, Y. Hori, An interface converter with reduced volt-ampere ratings for battery-supercapacitor mixed systems. IEEJ Trans. Ind. Appl. **128**, 418–423 (2008)
47. P. Barrade, S. Pittet, A. Rufer, Series connection of supercapacitors, with an active device for equalizing the voltages (2000)
48. D. Petreus, D. Moga, R. Galatus, R. Munteanu, Modeling and sizing of supercapacitors. Adv. Electr. Comput. Eng. **8**, 15–22 (2008)
49. J. Kruusma, A. Tõnisoo, R. Pärna, E. Nõmmiste, I. Tallo, T. Romann, E. Lust, Influence of the negative potential of molybdenum carbide derived carbon electrode on the in situ synchrotron radiation activated X-ray photoelectron spectra of 1-ethyl-3-methylimidazolium tetrafluoroborate. Electrochim. Acta **206**, 419–426 (2016)
50. C.O. Ania, J. Pernak, F. Stefaniak, E. Raymundo-Piñero, F. Béguin, Polarization-induced distortion of ions in the pores of carbon electrodes for electrochemical capacitors. Carbon **47**, 3158–3166 (2009)
51. H. Helmholtz, Studien über electrische Grenzschichten. Ann. Phys. **243**, 337–382 (1879)
52. M. Endo, T. Takeda, Y.J. Kim, K. Koshiba, K. Ishii, High power electric double layer capacitor (EDLC's); from operating principle to pore size control in advanced activated carbons. Carbon. Sci. **1**, 117–128 (2001)
53. M. Gouy, Sur la constitution de la charge électrique à la surface d'un électrolyte. J. Phys: Theor. Appl. **9**, 457–468 (1910)
54. M.-W. Xu, S.-J. Bao, H.-L. Li, Synthesis and characterization of mesoporous nickel oxide for electrochemical capacitor. J. Solid State Electrochem. **11**, 372–377 (2007)
55. D.L. Chapman, A contribution to the theory of electrocapillarity. The London, Edinburgh, and Dublin Philosophical Magaz. J. Sci. **25**, 475–481 (1913)
56. Stern. The theory of the electrolytic double-layer. Zeitschrift für Elektrochemie **30** 1014–1020 (1924)

57. X. Chen, R. Paul, L. Dai, Carbon-based supercapacitors for efficient energy storage. Natl. Sci. Rev. **4**, 453–489 (2017)
58. Y. Zhao, M.-B. Zheng, J.-M. Cao, X.-F. Ke, J.-S. Liu, Y.-P. Chen, J. Tao, Easy synthesis of ordered meso/macroporous carbon monolith for use as electrode in electrochemical capacitors. Mater. Lett. **62**, 548–551 (2008)
59. B. Xu, F. Wu, S. Chen, C. Zhang, G. Cao, Y. Yang, Activated carbon fiber cloths as electrodes for high performance electric double layer capacitors. Electrochim. Acta **52**, 4595–4598 (2007)
60. A. Balducci, U. Bardi, S. Caporali, M. Mastragostino, F. Soavi, Ionic liquids for hybrid supercapacitors. Electrochem. Commun. **6**, 566–570 (2004)
61. Y. Fang, J. Liu, D.J. Yu, J.P. Wicksted, K. Kalkan, C.O. Topal, B.N. Flanders, J. Wu, J. Li, Self-supported supercapacitor membranes: Polypyrrole-coated carbon nanotube networks enabled by pulsed electrodeposition. J. Power Sources **195**, 674–679 (2010)
62. S. Banerjee, Y.C. Sharma, Equilibrium and kinetic studies for removal of malachite green from aqueous solution by a low cost activated carbon. J. Ind. Eng. Chem. **19**, 1099–1105 (2013)
63. H.P. Boehm, Surface oxides on carbon and their analysis: a critical assessment. Carbon **40**, 145–149 (2002)
64. E. Frackowiak, F. Beguin, Carbon materials for the electrochemical storage of energy in capacitors. Carbon **39**, 937–950 (2001)
65. T. Cottineau, M. Toupin, T. Delahaye, T. Brousse, D. Bélanger, Nanostructured transition metal oxides for aqueous hybrid electrochemical supercapacitors. Appl. Phys. A **82**, 599–606 (2006)
66. C.-C. Hu, K.-H. Chang, M.-C. Lin, Y.-T. Wu, Design and tailoring of the nanotubular arrayed architecture of hydrous RuO_2 for next generation supercapacitors. Nano Lett. **6**, 2690–2695 (2006)
67. D. Choi, G.E. Blomgren, P.N. Kumta, Fast and reversible surface redox reaction in nanocrystalline vanadium nitride supercapacitors. Adv. Mater. **18**, 1178–1182 (2006)
68. H. Zhang, G. Cao, Z. Wang, Y. Yang, Z. Shi, Z. Gu, Growth of manganese oxide nanoflowers on vertically-aligned carbon nanotube arrays for high-rate electrochemical capacitive energy storage. Nano Lett. **8**, 2664–2668 (2008)
69. L.-Z. Fan, Y.-S. Hu, J. Maier, P. Adelhelm, B. Smarsly, M. Antonietti, High electroactivity of polyaniline in supercapacitors by using a hierarchically porous carbon monolith as a support. Adv. Func. Mater. **17**, 3083–3087 (2007)
70. F. Béguin, M. Friebe, K. Jurewicz, C. Vix-Guterl, J. Dentzer, E. Frackowiak, State of hydrogen electrochemically stored using nanoporous carbons as negative electrode materials in an aqueous medium. Carbon **44**, 2392–2398 (2006)
71. C. Vix-Guterl, E. Frackowiak, K. Jurewicz, M. Friebe, J. Parmentier, F. Béguin, Electrochemical energy storage in ordered porous carbon materials. Carbon **43**, 1293–1302 (2005)
72. E. Raymundo-Pinero, V. Khomenko, E. Frackowiak, F. Beguin, Performance of manganese oxide/CNTs composites as electrode materials for electrochemical capacitors. J. Electrochem. Soc. **152**, A229 (2004)
73. M.J. Bleda-Martínez, J.M. Pérez, A. Linares-Solano, E. Morallón, D. Cazorla-Amorós, Effect of surface chemistry on electrochemical storage of hydrogen in porous carbon materials. Carbon **46**, 1053–1059 (2008)
74. K. Babeł, K. Jurewicz, KOH activated lignin based nanostructured carbon exhibiting high hydrogen electrosorption. Carbon **46**, 1948–1956 (2008)
75. B. Fang, M. Kim, J.H. Kim, J.-S. Yu, Controllable synthesis of hierarchical nanostructured hollow core/mesopore shell carbon for electrochemical hydrogen storage. Langmuir **24**, 12068–12072 (2008)
76. K. Naoi, P. Simon, New materials and new configurations for advanced electrochemical capacitors. Electrochem. Soc. Interface **17**, 34–37 (2008)

77. B.E. Conway, B.V. Tilak, Interfacial processes involving electrocatalytic evolution and oxidation of H_2, and the role of chemisorbed H. Electrochim. Acta **47**, 3571–3594 (2002)
78. G. Lota, K. Fic, E. Frackowiak, Carbon nanotubes and their composites in electrochemical applications. Energy Environ. Sci. **4**, 1592–1605 (2011)
79. M. Wu, J. Gao, S. Zhang, A. Chen, Synthesis and characterization of aerogel-like mesoporous nickel oxide for electrochemical supercapacitors. J. Porous Mater. **13**, 407–412 (2006)
80. J. Zheng, P. Cygan, T. Jow, Hydrous ruthenium oxide as an electrode material for electrochemical capacitors. J. Electrochem. Soc. **142**, 2699 (1995)
81. S. Sathyamoorthi, M. Kanagaraj, M. Kathiresan, V. Suryanarayanan, D. Velayutham, Ethyl viologen dibromide as a novel dual redox shuttle for supercapacitors. J. Mater. Chem. A **4**, 4562–4569 (2016)
82. S. Roldán, M. Granda, R. Menéndez, R. Santamaría, C. Blanco, Mechanisms of energy storage in carbon-based supercapacitors modified with a quinoid redox-active electrolyte. J. Phys. Chem. C **115**, 17606–17611 (2011)
83. K.H. An, K.K. Jeon, J.K. Heo, S.C. Lim, D.J. Bae, Y.H. Lee, High-capacitance supercapacitor using a nanocomposite electrode of single-walled carbon nanotube and polypyrrole. J. Electrochem. Soc. **149**, A1058 (2002)
84. P.-L. Taberna, G. Chevallier, P. Simon, D. Plée, T. Aubert, Activated carbon–carbon nanotube composite porous film for supercapacitor applications. Mater. Res. Bull. **41**, 478–484 (2006)
85. D.N. Futaba, K. Hata, T. Yamada, T. Hiraoka, Y. Hayamizu, Y. Kakudate, O. Tanaike, H. Hatori, M. Yumura, S. Iijima, Shape-engineerable and highly densely packed single-walled carbon nanotubes and their application as super-capacitor electrodes. Nat. Mater. **5**, 987–994 (2006)
86. A.L.M. Reddy, M.M. Shaijumon, S.R. Gowda, P.M. Ajayan, Multisegmented Au-MnO_2/carbon nanotube hybrid coaxial arrays for high-power supercapacitor applications. J. Phys. Chem. C **114**, 658–663 (2010)
87. Q. Wang, F.N. Yong, Z.H. Xiao, X.Y. Chen, Z.J. Zhang, Simply incorporating an efficient redox additive into KOH electrolyte for largely improving electrochemical performances. J. Electroanal. Chem. **770**, 62–72 (2016)
88. N.W. Duffy, W. Baldsing, A.G. Pandolfo, The nickel–carbon asymmetric supercapacitor—Performance, energy density and electrode mass ratios. Electrochim. Acta **54**, 535–539 (2008)
89. K. Machida, S. Suematsu, S. Ishimoto, K. Tamamitsu, High-voltage asymmetric electrochemical capacitor based on polyfluorene nanocomposite and activated carbon. J. Electrochem. Soc. **155**, A970 (2008)
90. Q. Wang, Y.F. Nie, X.Y. Chen, Z.H. Xiao, Z.J. Zhang, Controllable synthesis of 2D amorphous carbon and partially graphitic carbon materials: Large improvement of electrochemical performance by the redox additive of sulfanilic acid azochromotrop in KOH electrolyte. Electrochim. Acta **200**, 247–258 (2016)
91. Naoi, K., Nagano, Y., Béguin, F., Fraçowiak, E., (eds.) Li-Ion-based hybrid supercapacitors in organic medium, in *Supercapacitors* (Wiley-VCH Verlag GmbH, 2013)
92. M. Mastragostino, C. Arbizzani, F. Soavi, Conducting polymers as electrode materials in supercapacitors. Solid State Ionics **148**, 493–498 (2002)
93. Y.-G. Wang, L. Yu, Y.-Y. Xia, Electrochemical capacitance performance of hybrid supercapacitors based on $Ni(OH)_2$/carbon nanotube composites and activated carbon. J. Electrochem. Soc. **153**, A743 (2006)
94. P. Gómez-Romero, O. Ayyad, J. Suárez-Guevara, D. Muñoz-Rojas, Hybrid organic–inorganic materials: from child's play to energy applications. J. Solid State Electrochem. **14**, 1939–1945 (2010)
95. G.G. Amatucci, F. Badway, A. Du Pasquier, T. Zheng, An asymmetric hybrid nonaqueous energy storage cell. J. Electrochem. Soc. **148**, A930 (2001)
96. H. Yu, L. Fan, J. Wu, Y. Lin, M. Huang, J. Lin, Z. Lan, Redox-active alkaline electrolyte for carbon-based supercapacitor with pseudocapacitive performance and excellent cyclability. RSC Adv. **2**, 6736–6740 (2012)

97. M. Rajkumar, C.-T. Hsu, T.-H. Wu, M.-G. Chen, C.-C. Hu, Advanced materials for aqueous supercapacitors in the asymmetric design. Progress Nat Sci: Mater. Inter. **25**, 527–544 (2015)
98. D. Cericola, R. Kötz, Hybridization of rechargeable batteries and electrochemical capacitors: principles and limits. Electrochim. Acta **72**, 1–17 (2012)
99. V. Khomenko, E. Raymundo-Piñero, F. Béguin, High-energy density graphite/AC capacitor in organic electrolyte. J. Power Sources **177**, 643–651 (2008)
100. J.H. Park, O.O. Park, K.H. Shin, C.S. Jin, J.H. Kim, An electrochemical capacitor based on a $Ni(OH)_2$/activated carbon composite electrode. Electrochem. Solid-State Lett. **5**, H7–H10 (2002)
101. B. Senthilkumar, Z. Khan, S. Park, K. Kim, H. Ko, Y. Kim, Highly porous graphitic carbon and $Ni_2P_2O_7$ for a high performance aqueous hybrid supercapacitor. J. Mater. Chem. A **3**, 21553–21561 (2015)
102. N. Xu, X. Sun, X. Zhang, K. Wang, Y. Ma, A two-step method for preparing $Li_4Ti_5O_{12}$–graphene as an anode material for lithium-ion hybrid capacitors. RSC Adv. **5**, 94361–94368 (2015)
103. Z. Cheng, D. Yida, H. Wenbin, S. Daoming, H. Xiaopeng, Q. Jinli, Z. Jiujun, Compatibility of electrolytes with inactive components of electrochemical supercapacitors, in *Electrolytes for Electrochemical Supercapacitors* (CRC Press, 2016)
104. C. Lin, J.A. Ritter, B.N. Popov, Correlation of double-layer capacitance with the pore structure of sol-gel derived carbon xerogels. J. Electrochem. Soc. **146**, 3639–3643 (1999)
105. S. Ratchahat, S. Kodama, H. Sekiguchi, W. Tanthapanichakoon, K. Al-Ali, T. Charinpanitkul, A. Soottitantawat, A. Eiad-Ua, K. Faungnawakij, Mesoporous RF-xerogels by facile hydrothermal synthesis. Eng. J. **19**, 95–104 (2015)
106. Z. Zhou, Y. Zhu, Z. Wu, F. Lu, M. Jing, X. Ji, Amorphous RuO_2 coated on carbon spheres as excellent electrode materials for supercapacitors. RSC Adv. **4**, 6927–6932 (2014)
107. S. Banerjee, P. Sinha, K.D. Verma, T. Pal, B. De, J. Cherusseri, P.K. Manna, K.K. Kar, (ed.), Capacitor to supercapacitor, in *Handbook of Nanocomposite Supercapacitor Materials I: Characteristics* (Springer, Cham, 2020)
108. B. Zhao, D. Chen, X. Xiong, B. Song, R. Hu, Q. Zhang, B.H. Rainwater, G.H. Waller, D. Zhen, Y. Ding, Y. Chen, C. Qu, D. Dang, C.-P. Wong, M. Liu, A high-energy, long cycle-life hybrid supercapacitor based on graphene composite electrodes. Energy Storage Mater. **7**, 32–39 (2017)
109. W. Zuo, R. Li, C. Zhou, Y. Li, J. Xia, J. Liu, Battery-supercapacitor hybrid devices: recent progress and future prospects. Adv. Sci. **4**, 16005 (2017)
110. K. Naoi, W. Naoi, S. Aoyagi, J.-I. Miyamoto, T. Kamino, New generation "Nanohybrid Supercapacitor." Acc. Chem. Res. **46**, 1075–1083 (2013)
111. P. Simon, Y. Gogotsi, B. Dunn, Where do batteries end and supercapacitors begin? Science **343**, 1210–1211 (2014)
112. K. Naoi, S. Ishimoto, J.-I. Miyamoto, W. Naoi, Second generation 'nanohybrid supercapacitor': evolution of capacitive energy storage devices. Energy Environ. Sci. **5**, 9363–9373 (2012)
113. M.R. Lukatskaya, B. Dunn, Y. Gogotsi, Multidimensional materials and device architectures for future hybrid energy storage. Nat. Commun. **7**, 12647–12647 (2016)
114. Y. Shao, M.F. El-Kady, J. Sun, Y. Li, Q. Zhang, M. Zhu, H. Wang, B. Dunn, R.B. Kaner, Design and mechanisms of asymmetric supercapacitors. Chem. Rev. **118**, 9233–9280 (2018)
115. K.K. Kar, S. Rana, J. Pandey, *Handbook of Polymer Nanocomposites Processing, Performance and Application* (Springer, 2015)
116. M. Deschamps, E. Gilbert, P. Azais, E. Raymundo-Piñero, M.R. Ammar, P. Simon, D. Massiot, F. Béguin, Exploring electrolyte organization in supercapacitor electrodes with solid-state NMR. Nat. Mater. **12**, 351–358 (2013)
117. C. Zhong, Y. Deng, W. Hu, J. Qiao, L. Zhang, J. Zhang, A review of electrolyte materials and compositions for electrochemical supercapacitors. Chem. Soc. Rev. **44**, 7484–7539 (2015)
118. S.A. Hashmi, R.J. Latham, R.G. Linford, W.S. Schlindwein, Conducting polymer-based electrochemical redox supercapacitors using proton and lithium ion conducting polymer electrolytes. Polym. Int. **47**, 28–33 (1998)

119. X. Yang, F. Zhang, L. Zhang, T. Zhang, Y. Huang, Y. Chen, A high-performance graphene oxide-doped ion gel as gel polymer electrolyte for all-solid-state supercapacitor applications. Adv. Func. Mater. **23**, 3353–3360 (2013)
120. H. Yu, J. Wu, L. Fan, Y. Lin, K. Xu, Z. Tang, C. Cheng, S. Tang, J. Lin, M. Huang, Z. Lan, A novel redox-mediated gel polymer electrolyte for high-performance supercapacitor. J. Power Sources **198**, 402–407 (2012)
121. V. Dusastre (ed.), *Materials for Sustainable Energy: A Collection of Peer-Reviewed Research and Review Articles from Nature Publishing Group.* (World Scientific, 2010)
122. Y.J. Kang, H. Chung, C.-H. Han, W. Kim, All-solid-state flexible supercapacitors based on papers coated with carbon nanotubes and ionic-liquid-based gel electrolytes. *Nanotechnology 23,* 065401 (2012)
123. H. Dai, H. Zhang, H. Zhong, H. Jin, X. Li, S. Xiao, Z. Mai, Properties of polymer electrolyte membranes based on poly(Aryl Ether Benzimidazole) and sulphonated poly(Aryl Ether Benzimidazole) for high temperature PEMFCs. Fuel Cells **10**, 754–761 (2010)
124. Z. Mahmud, N. Zaki, R. Subban, A. Ali, M. Yahya, MG49-KOH-PC alkaline gel polymer electrolytes membrane for supercapacitors, in *2012 IEEE Colloquium on Humanities, Science and Engineering (CHUSER)*, (IEEE, 2012), pp. 621–626.
125. M. Rosi, M.P. Ekaputra, M. Abdullah, Khairurrijal, Synthesis and characterization of cross-linked polymer electrolyte membranes for supercapacitor, in *AIP Conference Proceedings,* vol 1 (American Institute of Physics, 2010), pp. 55–58
126. B. Soma, K.K. Kamal, Particulate filled polymer electrolyte membrane for fuel cell applications. Recent Patents Mater. Sci. **7**, 131–150 (2014)
127. B. Soma, K.K. Kamal, K.D. Malay, Electrolyte membranes for fuel cells: synthesis, characterization and degradation analysis. Recent Patents Mater. Sci. **7**, 173–203 (2014)
128. P. Tang, Y. Zhao, C. Xu, K. Ni, Enhanced energy density of asymmetric supercapacitors via optimizing negative electrode material and mass ratio of negative/positive electrodes. J. Solid State Electrochem. **17**, 1701–1710 (2013)
129. C. Liu, Z. Yu, D. Neff, A. Zhamu, B.Z. Jang, Graphene-Based Supercapacitor with an ultrahigh energy density. Nano Lett. **10**, 4863–4868 (2010)
130. G.A. Snook, P. Kao, A.S. Best, Conducting-polymer-based supercapacitor devices and electrodes. J. Power Sources **196**, 1–12 (2011)
131. A.S. Aricò, P. Bruce, B. Scrosati, J.-M. Tarascon, W. van Schalkwijk, Nanostructured materials for advanced energy conversion and storage devices. Nat. Mater. **4**, 366–377 (2005)
132. H.-C. Wu, Y.-P. Lin, E. Lee, W.-T. Lin, J.-K. Hu, H.-C. Chen, N.-L. Wu, High-performance carbon-based supercapacitors using Al current-collector with conformal carbon coating. Mater. Chem. Phys. **117**, 294–300 (2009)
133. Y. Wang, Y. Song, Y. Xia, Electrochemical capacitors: mechanism, materials, systems, characterization and applications. Chem. Soc. Rev. **45**, 5925–5950 (2016)
134. H. Han, S. Cho, Ex situ fabrication of polypyrrole-coated core-shell nanoparticles for high-performance coin cell supercapacitor. Nanomaterials **8**, 726 (2018)
135. S. Akbulut, M. Yilmaz, S. Raina, S.-H. Hsu, W.P. Kang, Advanced supercapacitor prototype using nanostructured double-sided MnO_2/CNT electrodes on flexible graphite foil. J. Appl. Electrochem. **47**, 1035–1044 (2017)
136. Y. Nishi, The development of lithium ion secondary batteries. Chem. Rec. **1**, 406–413 (2001)
137. G. Zheng, L. Hu, H. Wu, X. Xie, Y. Cui, Paper supercapacitors by a solvent-free drawing method. Energy Environ. Sci. **4**, 3368–3373 (2011)
138. D.A. McKeown, P.L. Hagans, L.P.L. Carette, A.E. Russell, K.E. Swider, D.R. Rolison, Structure of hydrous ruthenium oxides: Implications for charge storage. J. Phys. Chem. B **103**, 4825–4832 (1999)
139. M. Seyedsalehi, M. Goodarzi, H. Barzanouni, Use of carbon in increasing the quality of drinking water-case study: the wells of Savejbolagh villages. J. Biodivers. Environ. Sci. **4**, 102–111 (2014)
140. K. Naoi, S. Ishimoto, N. Ogihara, Y. Nakagawa, S. Hatta, Encapsulation of nanodot ruthenium oxide into KB for electrochemical capacitors. J. Electrochem. Soc. **156**, A52 (2009)

141. A. Burke, Ultracapacitors: why, how, and where is the technology. J. Power Sources **91**, 37–50 (2000)
142. Toyota Europe Newsroom, 2013 Frankfurt MS: Yaris Hybrid-R (2013) https://newsroom.toyota.eu/2019-2013-frankfurt-ms-yaris-hybrid-r/. Accessed 20 Oct 2021.
143. Aowei Technology – City bus (2018), http://www.aowei.com/en/program/applicationinfo-16.html. Accessed 20 Oct 2021.

Characterization Methods for Supercapacitors

Obinna Egwu Eleri, Fengliu Lou, and Zhixin Yu

Abstract High-performance qualification of supercapacitors is most often a consequence of favorable interactions in the electrode surface chemistry, electrode structural properties, and electrode/electrolyte interface. Supercapacitor performance can therefore be investigated by electrochemical characterization techniques which can individually access these interactions and factors contributing to its electrochemical performance, most commonly by using galvanostatic charge and discharge or cyclic voltammetry procedures. Different characterization techniques are discussed in this chapter, expatiating on the charge storage mechanism, electrode/electrolyte interactions, and accelerated aging procedures comparing long-term performance in addition to failure mechanisms.

Keywords Supercapacitors · Energy density · Power density · Cyclic voltammetry · Stability

1 Introduction

Technological progress made in the advancement from fossil fuel energy sources into renewable energy sources has necessitated an increased focus on the development of high-performance energy storage devices. These high-performance criteria are mostly a function of device properties such as high-energy–density, high-power density, low resistance, self-discharge, and long cycle life. Supercapacitors are exceptional due to their high-power densities and long cycle life and have thus been

O. E. Eleri · F. Lou (✉)
Beyonder AS, Stokkamyrveien 30, 4313 Sandnes, Norway
e-mail: fengliu@beyonder.no

O. E. Eleri
e-mail: obinna@beyonder.no

O. E. Eleri · Z. Yu
Department of Energy and Petroleum Engineering, University of Stavanger, 4036 Stavanger, Norway
e-mail: zhixin.yu@uis.no

S. Thomas et al. (eds.), *Nanostructured Materials for Supercapacitors*,
Advances in Material Research and Technology,
https://doi.org/10.1007/978-3-030-99302-3_5

applied extensively in high power applications such as regenerative braking in electric vehicles and trains, power grids load leveling, and wireless sensors. Incorporating supercapacitors effectively in these applications necessitates that their qualities are continuously improved with several optimizations being made on the active materials properties, current collectors, electrolytes, and device configuration. However, performance improvement can only be observed via the use of characterization methods capable of observing changes in the interactions between components, leading to favorable iterations facilitating the high-performance criteria. A comprehensive understanding of these device properties is needed firstly, after which characterization methods via which they are obtained, would then be discussed in this chapter.

2 Parameter Definition

2.1 Capacitance

Capacitance (measured in Farads) is the ratio of the amount of electric charge stored on a material to the difference in electric potential applied. The capacitance of a supercapacitor originates from surface electrostatic interactions and or faradaic reactions as in pseudocapacitors, based on the charge storage media undertaken [1]. Assuming no faradaic reactions and from first-order principles, the double-layer capacitance originating from surface interactions is expressed by Eq. 1.

$$C_{dl}(\mathrm{F}) = \varepsilon_r \varepsilon_0 \frac{s}{d} \tag{1}$$

where C_{dl} represents the double layer capacitance, ε_r, and ε_0 the relative permittivity of the dielectric material and vacuum permittivity respectively, s the electrode surface area and d the distance between the charge separation in the outer Helmholtz plane.

For pseudocapacitors with faradaic reactions, Eqs. 2 and 3 are used

$$R_{CT}(\Omega) = \frac{RT}{\propto nFi_0} \tag{2}$$

$$C_p(\mathrm{F}) = \frac{\theta(1-\theta)}{g\theta(1-\theta)-1}\frac{Z_F}{RT} \tag{3}$$

where R_{CT} represents the charge transfer resistance, Z_F the faradaic impedance and C_p the capacitance in series calculated as a function of the saturation coverage of the electrochemical sites θ and the repulsion factor g.

For comparison purposes, capacitance can also be expressed as gravimetric capacitance C_g and volumetric capacitance C_v considering the mass of active materials m

and volume of active materials v, using Eqs. 4 and 5 respectively.

$$C_g\left(\mathrm{F\ g^{-1}}\right) = \frac{C}{m} \tag{4}$$

$$C_v\left(\mathrm{F\ cm^{-3}}\right) = \frac{C}{v} \tag{5}$$

2.2 Specific Energy

Specific energy otherwise known as gravimetric energy density is a performance metric calculated from the gravimetric capacitance of the supercapacitor and its operating potential window. It is a metric value quantifying the amount of energy stored per unit mass of the supercapacitor (Eq. 6) or per unit volume (Eq. 7) when measured volumetrically.

$$E_g\left(\mathrm{Wh\ kg^{-1}}\right) = \frac{1}{2} C_g \Delta V^2 \tag{6}$$

$$E_v\left(\mathrm{Wh\ cm^{-3}}\right) = \frac{1}{2} C_v \Delta V^2 \tag{7}$$

where ΔV represents the operating potential window, E_g and E_v the gravimetric and volumetric specific energy, respectively.

2.3 Specific Power

Specific power is a measure of the speed at which energy can be stored or given off when needed. Supercapacitors electrostatic surface charge storage mechanism ensures that the latency associated with charge storage in batteries by virtue of chemical reactions is avoided, and thus the power is only affected by the internal resistance. Specific power is expressed gravimetrically using Eq. 8.

$$P_g\left(\mathrm{kW\ kg^{-1}}\right) = \frac{1}{4m} \frac{\Delta V^2}{R_i} \tag{8}$$

where R_i is the equivalent series resistance, m is the mass of active materials, and ΔV is the operating potential.

3 Electrochemical Characterization Methods

In the previous sections, we described the common parameters and performance attributes used in the characterization of supercapacitors. This section delves into electrochemical methods via which they can be obtained, beginning from cell configuration, and progressing with the description of the various electrochemical characterization methods.

3.1 Cell Configuration

Characterization of a supercapacitor cell begins with the electrode fabrication process where the active material is mixed with suitable binders (e.g., Polytetrafluoroethylene), with or often without the conductive additives and thereafter coated on suitable current collectors (e.g., Metal foils). Supercapacitor characterization and performance analysis are carried out using cells designed in either a two-electrode (Fig. 1a) or three-electrode configuration (Fig. 1b). Two-electrode systems are implemented to characterize cells while simulating real operating conditions. Symmetric or asymmetric cells are possible variations of the two-electrode configuration, where the working electrodes are identical as in the former or different as in the latter. The potential or changes observed in two-electrode systems are a summation of causative factors from the entire cell. Three electrodes configuration, on the other hand, are used in monitoring changes occurring in one electrode (working electrode) irrespective of processes occurring on the other (counter electrode) as against a reference electrode. They enable accurate observations of faradaic reactions, processes, and changes in the potential of the working electrode solely. Potentials recorded in three-electrode systems are referenced to a particular reference electrode connected to its appropriate terminal. Parameters such as mass and material changes in the counter and reference electrodes significantly affect the potential observed across the counter electrode and point of zero charge location [2]. Hence, three-electrode setups are highly sensitive, and values of capacitance obtained can significantly differ from two-electrode cell configurations as demonstrated in the works of Khomenko et al. [3]. Due to this high sensitivity, two-electrode cell configurations are mostly used in the characterization of the performance of an electrode material since large errors would be obtained using three electrodes. Nevertheless, three-electrode configurations are implemented in the study of faradaic reactions and other sensitive half-cell electrochemical processes occurring on the electrode.

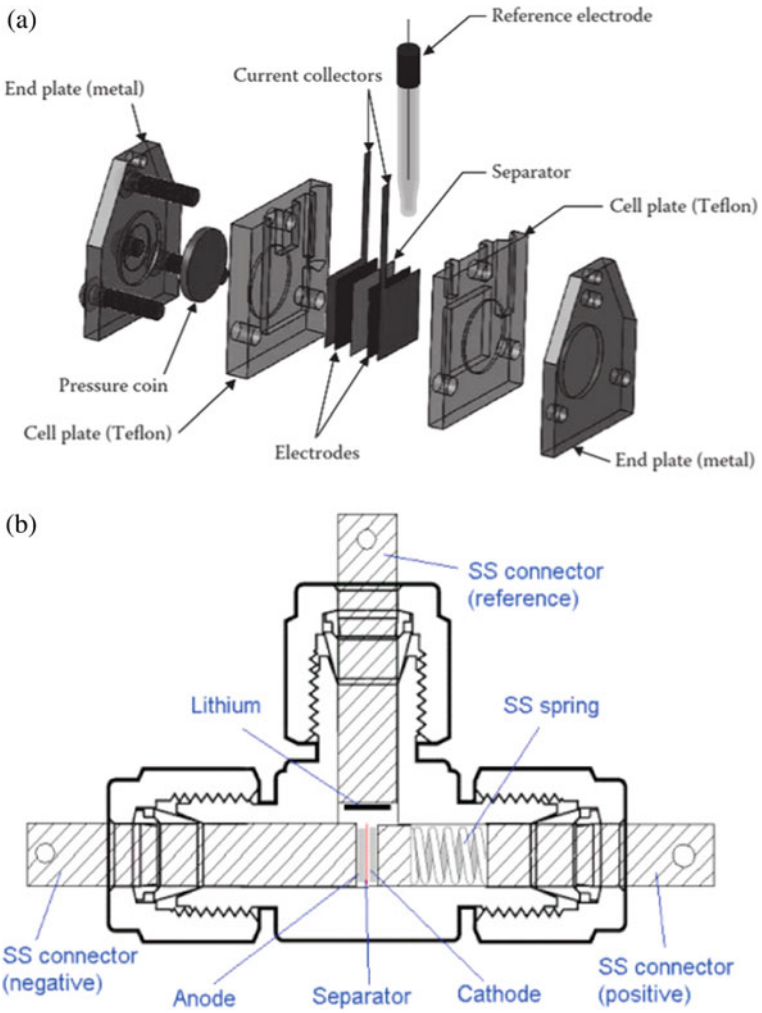

Fig. 1 **a** Two electrode **b** three electrode cell configurations. Reprinted from [4, 5], Copyright (2012) and (2016) with permission from Elsevier

3.2 Cyclic Voltammetry

Cyclic voltammetry (CV) is a versatile electrochemical technique capable of investigating changes in form of chemical reactions, mechanisms, electrocatalytic activity, degradations, and redox behavior in electrodes, electrolyte solutions as well as electrode/electrolyte interaction in cells over a set potential range. CV analyses are conducted using a potentiostat (example Metrohm Autolab) on a cell in a two or three-electrode configuration. In a typical CV scan, a potential is applied across the working electrode per unit of time (the scan rate in v s^{-1}) and the corresponding

current response is recorded as a function of the applied potential between the upper and lower limits. Measurements are typically conducted using a linear sweep pattern or cyclic staircase profile when multiple scans are recorded. In the former, the potential is applied linearly with time while in the latter, the potential is also applied linearly with time, but the sweep direction is reversed at the upper limit. A plot of the current response vs potential is obtained at a particular scan rate for each CV scan, providing detailed information about electrochemical changes occurring on the cell. By increasing the potential ranges in steps, the stability of the electrode/electrolyte can be monitored, and in the process, the safe operating potential window is determined. Degradation arising from electrode oxidation or electrolyte decomposition observed in form of irreversible anodic or cathodic peaks is noted by an increase in the current response when the applied potential is beyond the stability limit of the cell. The stability of the cell is influenced by reactions between the components of the electrodes and electrolytes when a set potential is applied. Other important criteria such as kinetic analysis and rate performance can be obtained by scanning with multiple scan rates while keeping the potential window constant.

3.2.1 Methodology

The principle of cyclic voltammetry borders on the current response obtained from a linear ramp of potential between the limits as shown in Fig. 2. The electrochemical signature in terms of the current response is expressed by Eq. 9 [1].

$$i(\mathrm{A}) = vC_{dl}\left[1 - \exp(-t/R_sC_{dl})\right] \tag{9}$$

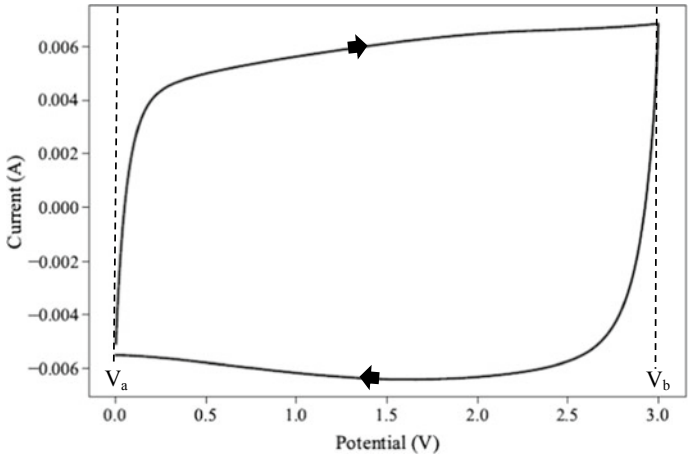

Fig. 2 Cyclic voltammetry of an activated carbon supercapacitor conducted at 25 °C using a scan rate of 10 mV s^{-1}, potential window from 0–3 V and 1 M $TEABF_4$ in PC electrolyte

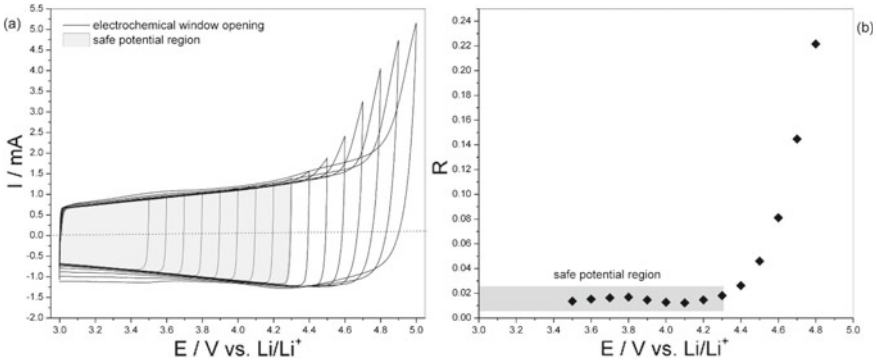

Fig. 3 **a** Cyclic voltammetry safe operating potential window determination on an AC electrode in 1 M $LiPF_6$ in EC/DMC (1:1) electrolyte; **b** Faradaic fraction vs upper potential limit. Reprinted from [6], Copyright (2015) with permission from Elsevier

where v represents the scan rate, C_{dl} the double layer capacitance and R_s the equivalent series resistance.

The cell is first connected to a potentiostat such as (Autolab from Metrohm) using appropriate terminals suitable for two-electrode or three-electrode cell configurations. The potential window to be investigated is thereafter set as the upper potential limit and lower potential limit as illustrated in Fig. 2 with the upper potential limit $V_b = 3.0$ V and the lower limit $V_a = 0$ V. An appropriate scan rate is thereafter chosen most commonly with a value between (5–20 mV s^{-1}). The CV scan is then conducted and the stability at various potential windows can be investigated by increasing the upper potential in steps of 0.1 V as illustrated in Fig. 3.

For supercapacitors, an ideal capacitive behavior is said to be exhibited when the observed shape of the obtained voltammogram is close to being rectangular. While in pseudocapacitors, the presence of reversible faradaic reactions distorts the shape of this curve, and most times, a not-so rectangular shape is obtained. In addition, a distorted rectangular shape characterized by a pronounced increase in current at the upper vertex potential in form of an irreversible anodic peak indicates that the cell has been subjected to the potential beyond its stability limit as shown in the unshaded region of Fig. 3a. The safe operating window/stability limit can also be determined from the plot of faradaic fraction R_f, calculated using Eq. 10 against the upper vertex potential as proposed by Weingarth et al. [7].

$$R_f = \frac{q_a}{q_c} - 1 \tag{10}$$

where q_a and q_c represent the anodic and cathodic charges. The safe operating window is indicated by the shaded region in Fig. 3b. Using the criterion by Weingarth et al.[7], an R_f value greater than 0.1 indicates greater than 10% faradaic contribution and thus implies electrolyte decomposition. Hence conclusions can be made that

electrolyte degradation, electrode oxidation, or undesirable faradaic reactions are occurring at such potential window.

3.2.2 Specific Capacitance Determination

The specific capacitance is determined from the relationship between charge transferred from the current vs time plot or the slope of the potential vs time plot shown in Fig. 4 in the desired operating potential window.

The charge passed during CV is equal to the area enclosed by the current vs time plot (Fig. 4) which can be obtained via integration of the curve using Eq. 11.

$$Q(\mathrm{C}) = \int_{Va}^{Vb} i\,dt \tag{11}$$

For supercapacitors with an ideal electrostatic surface capacitive charge storage mechanism, the average charge is used in obtaining the specific capacitance (Eq. 12). However, faradaic reactions are expected to occur mostly during charging, hence a more accurate value would be obtained by using the absolute value of charge obtained from an integration of the discharge portion.

$$C(\mathrm{F}) = \frac{Q}{\Delta V} \tag{12}$$

where Q represents the average charge, C the capacitance and ΔV the potential window. In instances where pseudocapacitive charge storage is dominant, Eq. 13 is used.

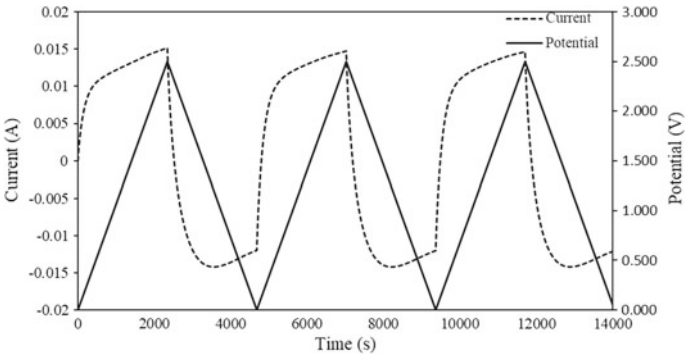

Fig. 4 Current vs time and potential vs time response obtained from CV analysis of an AC sample in $TEABF_4$/PC electrolyte, at 20 mV s^{-1} after 3 cycles at (0 −2.5 V)

$$C(\mathrm{F}) = \frac{\int_{V1}^{V2} i\,dt}{\int_{V1}^{V2} V\,dt} \tag{13}$$

The respective gravimetric or volumetric capacitance can thereafter be obtained using Eq. 4 or 5.

3.2.3 Rate Capability

Rate capability is determined by conducting a series of CV scans with a constant potential window (V_a to V_b) and a sequence of increasing scan rates. A quick observation of the shape of the voltammogram when plotted progressively from low scan rates to high scan rates describes the rate performance of the cell. Excellent rate capability is achieved when the device can maintain a rectangular voltammetric profile (as illustrated in Fig. 5), even at high scan rates in addition to minimizing losses in capacitance. Rate capability can also be determined using Galvanostatic charge and discharge analyses. Active materials in supercapacitors require an optimum balance between the volume of micropores and mesopores. Exclusive content of micropores without sufficient mesopores promotes ion trapping effect and subsequently increases their diffusion resistance, especially during higher scan rates or specific currents [8]. This increased diffusion resistance translates to poor rate capability and thus, mesopores are therefore needed to mitigate this effect and promote faster ion diffusion during charge and discharge processes. An illustration of excellent rate performance is presented in Fig. 5 where a rectangular profile is maintained even with a tenfold increase in the scan rate [9].

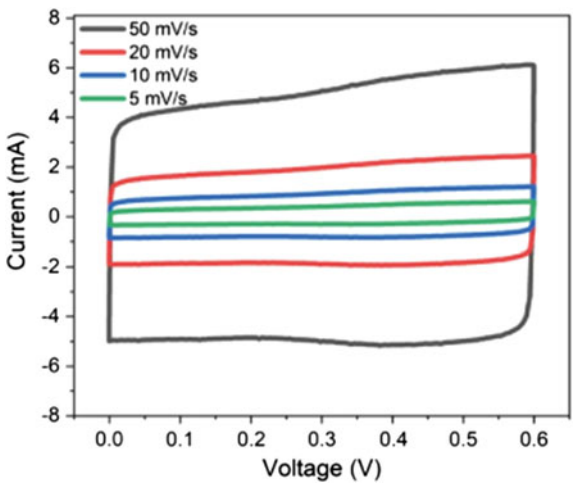

Fig. 5 CV curves obtained at different scan rates from carbon nanofiber spray coated paper electrode in hydroxyethyl cellulose:1-ethyl-3-methylimidazolium ethyl sulphate (HEC: EMIM-ES) gel electrolyte. Reprinted from [9]. Copyright (2020) with permission from Springer Nature

3.2.4 Limitations of Cyclic Voltammetry

Cyclic voltammetry is strongly affected by the cell configuration used and the nature of reference/counter electrodes in the three-electrode configuration. Capacitance values obtained differ with respect to the cell configurations and do not necessarily present the real-time performance when the active material is used in an actual cell.

3.3 Galvanostatic Charge and Discharge Analysis (GCD)

Galvanostatic charge and discharge analysis involve using battery testing equipment to apply a fixed current to a cell in form of a constant current charge and discharge (CCCD) and recording the corresponding change in voltage as a function of time in contrast to cyclic voltammetry where the current response is recorded. By recording the change in the voltage, parameters such as capacitance, coulombic efficiency, rate capability, and device resistance can be accurately determined.

3.3.1 Methodology

The device is first attached to the corresponding terminals of the battery tester. After determination of the operating potential window from CV analysis, this potential window (V_a – V_b) is entered in the software interface in addition to a constant charging current. In some instances, a rest period could be added between charging and discharge to investigate the relaxation potential of the cell. In most cases, this is omitted to properly observe the ohmic drop during the discharge sequence. A plot of potential vs time is obtained with a voltage expression given by Eq. 14. An illustration of a typical galvanostatic charge and discharge is presented in Fig. 6.

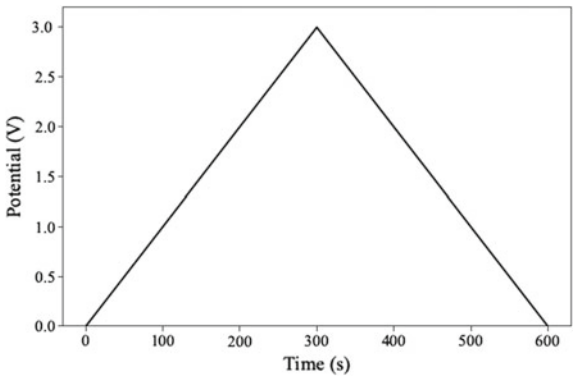

Fig. 6 GCD of an activated carbon supercapacitor coin cell

$$V(\mathrm{V}) = \frac{t}{C} i + Ri \tag{14}$$

where t represents the time, C is the capacitance, i is the set current and R is the resistance.

3.3.2 Specific Capacitance Determination

Specific capacitance can be determined from the slope using Eq. (15) if a linear discharge curve is obtained. For GCD plots with non-linear characteristics, integration of the discharge portion given by Eq. (16) is used.

$$C(\mathrm{F}) = \frac{i \Delta t}{\Delta V} \tag{15}$$

$$C(\mathrm{F}) = \int \frac{i \partial t}{\partial V} \tag{16}$$

The ΔV used in the capacitance determination from GCD is calculated from the difference in the operating potential window without the IR drop i.e., considering the upper limit as the voltage recorded at the beginning of the discharge. It is also necessary to ensure that the potential window (ΔV) being utilized in GCD analysis is within the operating potential window of the electrolyte used, which is typically less than 1.2 V for aqueous electrolytes and 0–2.7 V for organic electrolytes.

Considering that most GCD analysis is typically carried out in two-electrode cell configurations to emulate practical applications, the capacitance of a single electrode (C_m) is thus

$$C_m(\mathrm{F}) = 4 \times C \tag{17}$$

The multiplier 4 is used in normalizing the cellular capacitance arising from the mass/volume of the electrodes (which is two times less than the cellular value) and also the voltage window in a full cell which is two times greater than that of the electrode.

3.3.3 Rate Performance

Rate performance and cyclic stability are investigated by conducting a series of CCCD at a constant potential window while increasing currents or specific currents when comparing multiple samples. The capacitance can then be monitored as a function of a specific current via the corresponding GCD at a respective specific current (Fig. 7). The ability of the device to maintain high capacitance values even at high current densities indicates a very good rate capability. Rate capability is calculated in percentages using Eq. (18).

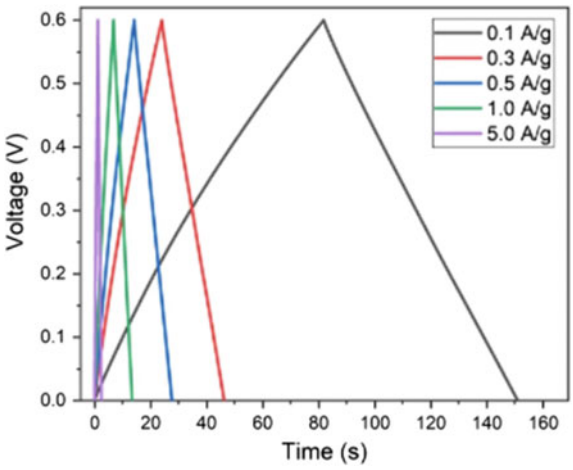

Fig. 7 Rate performance of carbon nanofiber spray coated paper electrode in hydroxyethyl cellulose:1-ethyl-3-methylimidazolium ethyl sulphate (HEC: EMIM-ES) gel electrolyte. Reprinted from [9]. Copyright (2020) with permission from Springer Nature

$$Rp = \frac{C_{g\,\max}}{C_{g\,\min}} \times 100\% \tag{18}$$

where $C_{g\min}$ and $C_{g\max}$ are the specific capacitance obtained using the lowest specific current, and the highest specific current, respectively.

3.3.4 Internal Resistance (IR)

Supercapacitors are advantageous in applications requiring energy storage devices with high power density. However, achieving such a high-power density is dependent on the supercapacitors internal resistance which is a combination of contributory factors such as ionic resistance from the bulk electrolyte, electrode resistance, faradaic reactions on the electrode surface, and resistance from active material, binder, and current collector interactions. The internal resistance R can be calculated from the AC impedance, or the IR drop (shown in Fig. 8) derived from the onset of a constant discharge during a GCD analysis. The internal resistance is calculated using Eq. 19.

$$R(\Omega) = \frac{V_{drop}}{2i} \tag{19}$$

where V_{drop} represents the IR drop estimated from the difference between the upper vertex potential and initial potential at the onset of a constant discharge using current i.

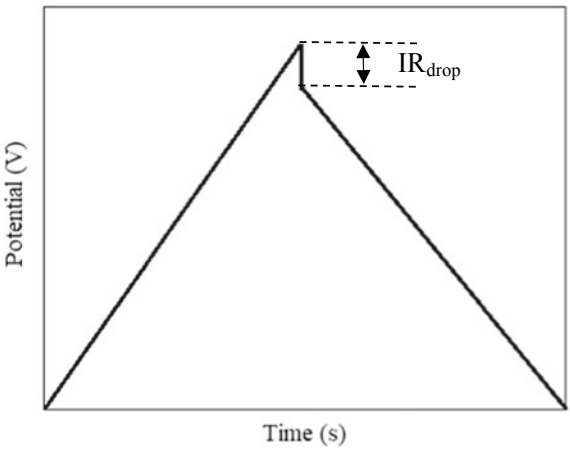

Fig. 8 Illustration of IR drop from GCD curve

3.3.5 Limitations and Special Considerations of GCD

Estimating the specific capacitance of a working electrode requires precise considerations on the operating potential window, charge and discharge currents, electrode thickness, and mass for accurate determination of its performance. Charging and discharging a cell using a potential window beyond its stability limit would result in an overestimation of capacitance value due to contributions from faradaic reactions. Additionally, the capacitance values obtained also vary with the potential and errors could arise when evaluating optimizations from different configurations. Likewise, using too small charge and discharge currents would also result in an overestimation of the capacitance from faradaic reactions and ohmic losses. Currents should therefore be estimated using specific units, where the current applied is calculated per mass of the active material and thus a more accurate comparison in optimization experiments. These specific currents should also reflect real-life applications where supercapacitors are charged and discharged in seconds. Furthermore, care should be taken in the dimensions of electrode thickness and mass of the active material, since very thin electrodes or small amounts of active materials would lead to an overestimation of the performance. However, ion mobility is significantly affected when using electrodes with very high thickness [10]. Hence, active material thickness and mass should be carefully controlled to correspond with optimized commercial standards.

3.4 *Stability Analysis: Long-Term Galvanostatic Charge and Discharge (GCD) Versus Floating Voltage Holds (FVH) for Aging Analysis*

Supercapacitors are spectacularly known for their long cycle life in comparison to batteries and are capable of undergoing millions of cycles of constant current charge and discharge (CCCD). It is therefore often necessary to compare the stability of cells while investigating influences of changes in electrolyte components, cellular or active material configuration. This is typically done by implementing a CCCD at appropriate current densities, (charging and discharging within 1 min) for at least 10,000 cycles.

GCD has traditionally been used in the analysis of the long-term stability and performance of electrode materials/electrolytes in supercapacitors and other energy storage devices. By subjecting the device to continue cycling for a prolonged period, degradations begin to occur, and this can be compared with other materials or electrolyte combinations to be analyzed. However, a certain exception could be made to using this technique as proven by Weingarth et al. [11] have shown that it is impossible to obtain accurate information concerning the stability of electrolytes via continuous GCD cycling. They attributed this to the limited cumulative holding time of the cell at high voltages in comparison to the duration of the entire cycling period. This is in addition to the extreme durations amounting to months from thousands of cycles which are necessary to simulate a normal continuous working life span of the device.

FVH on the other hand ensures that cells are kept at high voltages for prolonged periods to accurately monitor degradation, with consecutive capacity checks after each series to observe fades. A typical FVH (Illustrated in Fig. 9) consists of a 10 h FVH at a potential often at its stability limit or slightly beyond, after which a series of five CCCD cycles within the stable operating potential window is conducted as health checks to monitor the capacity of the cell. A 20% capacity fade in both the

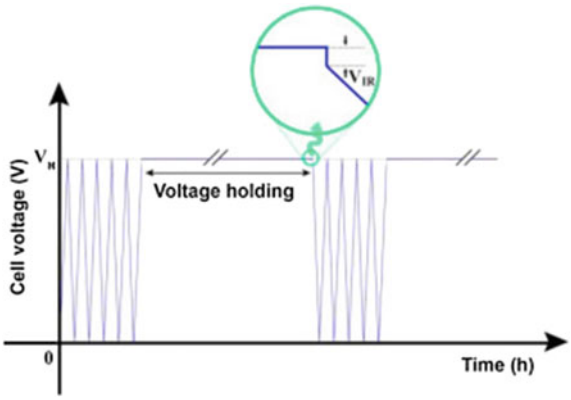

Fig. 9 Illustration of floating voltage hold experiment. Reprinted from [12], Copyright (2016) with permission from Elsevier

GCD and FVH is the threshold for comparison, and the number of cycles for the GCD and hours of FVH is recorded and compared with other devices.

3.5 Electrochemical Impedance Spectroscopy (EIS)

Electrochemical impedance spectroscopy (EIS) involves the measurement of changing properties of an AC signal as it is swept at a particular frequency between electrodes that are in contact with an electrolyte in an electrochemical cell. EIS has been broadly utilized in the characterization of diverse energy storage devices, giving detailed information about their impedance, internal resistance, current responses, and capacitance for supercapacitors. In a typical EIS analysis, an alternating current is generated in response to the applied potential and the signal characteristics/behavior is tagged as the impedance spectroscopy.

3.5.1 Procedure

In a typical EIS procedure, a potential of small amplitude (5–10 mV) is imposed on a working electrode and the time-dependant changes in the potential is recorded between a specified frequency range from the first applied frequency to the last applied frequency at a particular number of frequencies per decade. Nyquist plots of the imaginary impedance Z'' vs the real impedance Z' and others such as Bode plot of overall impedance Z versus frequency applied, phase transition (°) vs frequency, and oscillating (AC) current vs potential (AC) are recorded. These plots are thereafter analyzed to determine the contributors to the device resistance which are the bulk electrolyte, electrode, electrode/current collector contact, diffuse layer, charge transfer resistance and to estimate the double-layer capacitance.

3.5.2 Spectra Analysis

Analysis of impedance spectra begins with appropriate fitting of the obtained response behavior according to a stipulated equivalent-circuit model (ECM), whose complexity is dependent on the material, interface, and charge storage processes of the cell. The ECM attempts to simulate the impedance response obtained in an actual system and the calculation of a transfer function. Common elements of the equivalent circuit include double layer and pseudo capacitances (C_{dl}, C_p), resistors (R) and inductance (L), and Warburg impedance (W) in instances where diffusion resistance is present. Figure 10 shows a typical Nyquist plot for supercapacitors.

Where R_A, R_{AB}, R_B, R_{BC} have been attributed to the resistance of the electrodes, bulk electrolyte/charge transfer, the equivalent series resistance, and the diffuse layer respectively [13]. Analysis of respective plots of varying active material properties, electrolyte, and electrode fabrication techniques can be conducted to determine their

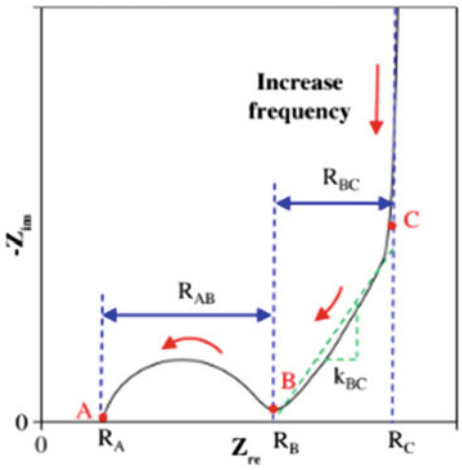

Fig. 10 Typical Nyquist plot for supercapacitors. Reprinted with permission from [13]. Copyright (2018) American Chemical Society

influence on the internal resistance of the device. Given that the impedance is recorded as a function of frequency through the imposition of an oscillating AC potential of low amplitude over a steady-state potential, specific capacitance can also be evaluated using the imaginary part of the impedance and the relation in Eq. (20).

$$C = \frac{-1}{2\pi f Z''} \tag{20}$$

where Z'' represents the imaginary part of the impedance, f the frequency, and C the capacitance.

3.6 Self-discharge

Supercapacitors are plagued with a self-discharge phenomenon whereby the open circuit voltage is seen to decrease during a fixed period under no load after it has been held at a constant voltage. This decrease in potential is caused by parasitic faradaic reactions between surface functionalities on the active material and the electrolyte, and the absence of leakage currents needed to hold the potential at the desired rating.

3.6.1 Procedure

The cell to be tested is connected to the terminals of the battery tester, charged to a value close to its maximum operating potential, and held at this potential for a duration (t_1) as shown in Fig. 11. Thereafter, the charging is stopped and the change in open circuit potential of the cell is recorded as time progresses. This is conducted for

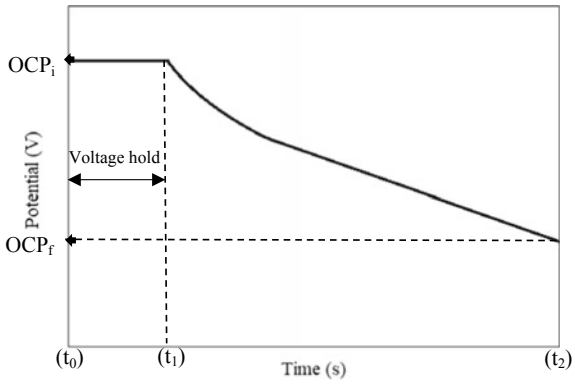

Fig. 11 Self-discharge determination

a determined duration (t_2) after which the self-discharge is calculated using Eq. (21).

$$Self\ discharge(\%) = \frac{OCP_f}{OCP_i} \times 100 \tag{21}$$

where OCP_i and OCP_f, represent the initial open circuit potential after the voltage hold and the final open circuit potential after a time (t).

4 Other Physical Characterization Methods

Electrochemical methods previously described, investigate performance in relation to electrochemical interactions. Consequentially, numerical quantitative metrics such as capacitance and resistance are obtained which enable comparison between different samples without typically expatiating on processes leading to such favorable interactions. Understanding these interactions, therefore, needs to be undertaken by other characterization methods which are capable of highlighting changes in electrodes structures, and electrolyte species that are responsible for charge storage processes as well as monitoring performance improvements and degradations. Critical understanding of the charge storage process would thereafter reveal further insights into improving the performance of active materials or provide reasons for failure while suggesting mitigating measures. The following sections highlight some in-situ characterization methods which have been used in a variety of advanced characterizations studies on supercapacitor devices, and brief instances where they have been applied.

4.1 In-Situ Nuclear Magnetic Resonance (NMR)

NMR spectroscopy is an advanced characterization technique capable of obtaining detailed information about the electrochemical interfaces, and the local environment around the electrodes via in-situ measurements or ex-situ analysis on electrolytes/active material samples. Individual distinct element-dependent resonance frequencies are obtained when nuclei capable of a spin are perturbed by a weak oscillating magnetic field. Examples of such nuclei are H^1, C^{13}, $F^{19,}$ and B^{11} corresponding to chemical species present in the commercially used electrolyte 1 M $TEABF_4$/ PC. Analysis of these non-zero spin Nuclei enables in-situ monitoring of anionic or cation species migration through observation of the respective resonance frequencies. By incorporating in-situ NMR during cycling, it becomes possible to probe the mechanism of charge storage by monitoring the adsorption of ionic moieties onto the surface of electrodes and ion transport in the pores. Forse et al. [14] implemented in-situ NMR in the direct monitoring of charge storing species during their investigation of ion dynamics and charge storage in ionic liquid supercapacitors. Wang et al. [15] also utilized in-situ NMR in their investigation of the charge and discharge mechanism of supercapacitors through quantification of isolated charge storage species and processes occurring in cathodes and anodes. Real-time migration of ions (BF_4^-) and binding within and unto the electrode surfaces during charge and discharge processes was observed. Figure 12 presents ^{19}F NMR spectra obtained from an isolated positive electrode during cyclic voltammetry of an overlaid supercapacitor cell consisting of a commercial AC electrode (YP50F) and 1.5 M NEt_4BF_4 in deuterated acetonitrile.

Ex-situ applications such as the investigation of behaviors of electrolyte species during electrochemical cycling with the objectives of probing the onset of degradations and interactions between organic electrolyte and functionalities present on the

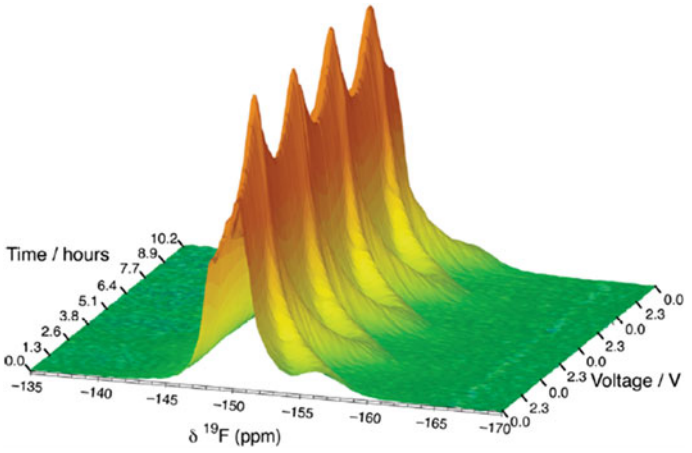

Fig. 12 In-situ ^{19}F NMR spectra of a supercapacitor positive electrode during CV. Reprinted with permission from [15]. Copyright (2013) American Chemical Society

electrode surface have also been reported. Lee et al. [16] used ex-situ NMR in the analysis of an extracted electrolyte from a disassembled cell, in their detailed studies of the behavior of tetrafluoroborate BF_4^- anion. Azais et al. [17] used NMR spectroscopy in the analysis of decomposition products from redox reactions between carbon functionalities and electrolytes ions, during aging studies of supercapacitors based on organic electrolytes.

Despite the advanced nature of NMR as a characterization technique, it is limited by the relative abundance of the respective nuclei in the chemical species to be analyzed. In addition, only samples containing elements with non-zero spin nuclei can be analyzed.

4.2 *In-Situ Electrochemical Quartz Crystal Microbalance (EQCM)*

EQCM is another technique used in examining the gravimetric behavior and interactions of electrodes with different systems of electrolytes during charge and discharge processes. A highly sensitive quartz crystal microbalance is used in measuring minute mass changes of materials in different mediums (air, water, and electrolytes, etc.). In electrochemical systems utilizing carbon electrodes, EQCM characterization enables the measurement of changes in ionic fluxes, concentration, and ionic transport which are dependent on the pore properties of the porous carbon material. In a typical EQCM characterization, a Pt/Au coated quartz crystal is sprayed with a composite active material and binder mixture in the desired ratios. Data in form of frequency shifts are obtained and thereafter converted into mass changes using the Sauerbrey equation (Eq. 22) [18].

$$\Delta m = -C_m * \frac{\Delta f}{n} \tag{22}$$

where Δm represents the mass changes of the coated electrode, C_m is the mass sensitivity factor, and Δf is the change in resonance frequency normalized by the overtone order. Investigations of dominant ionic species on particular electrodes through gravimetric comparisons can thereafter proceed after transforming the frequency shifts to masses. The first step involves the calculation of the change in ion populations of the coating Γ which is derived by dividing the mass changes in electrodes Δm by the molar masses of un-solvated ions. After which a relation between Q, the electrode charge densities estimated from faradays law can then be obtained to describe the gravimetric response of the active material during electrochemical cycling. Levi et al. [19] demonstrated the application of EQCM in the measurement of ionic fluxes of activated carbon electrodes in supercapacitors. Figure 13 illustrates the total mass changes observed due to adsorbed ions and solvents, and changes in the amount of species Γ.

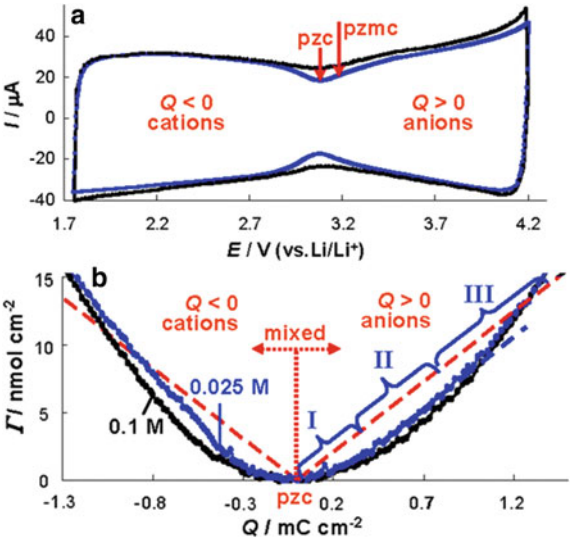

Fig. 13 CV obtained alongside in-situ EQCM characterization **a** CV of the carbon coated quartz crystal electrode **b** related EQCM responses. A carbon coated quartz crystal electrode was used in 0.1 M and 0.025 M $TEABF_4$/PC electrolyte. Reprinted with permission from [19]. Copyright (2010) American Chemical Society

Extensive reviews of the EQCM technique have been performed by Shpigel et al. [20] and Levi et al. [18] for applications in energy storage devices. EQCM is undisputedly a powerful characterization technique. However, it is limited to measurement of gravimetric changes only and can therefore be affected by the size of coating layer of active materials since larger coating masses would pose sensitivity issues and also negatively impact adhesion with the quartz substrate.

4.3 In-Situ X-ray Diffraction (XRD) Spectroscopy

Asymmetric supercapacitors utilizing nanostructured metal oxide materials are renowned for their excellent pseudocapacitive performances and thermal stabilities in comparison to single metal or bulk oxide materials. Factors contributing to these are enhanced electroactive sites and adequate interlayer spacing responsible for improved ionic transport. The charge storage capabilities of these electrodes are mainly via ion insertion in contrast with the typical surface adsorption processes in porous carbons. Consequently, interlayer spacing and crystal transformations are important parameters to be investigated. In-situ XRD has been used as a non-invasive technique to probe the interlaying spacing, transformation, and changes occurring in crystal structures of these electrodes during cycling. Specially constructed cells with x-ray permissible apertures having coverings made from beryllium disks [21], aluminum foils [22] and Kapton foils [23] have been utilized. Notably, Zhao et al. [24] probed the changes in the structure of free-standing MXene $Nb_4C_3T_x$ supercapacitor electrodes during electrochemical cycling using in-situ XRD. No change in interlayer spacing was observed during cycling (Fig. 14) hence confirming that

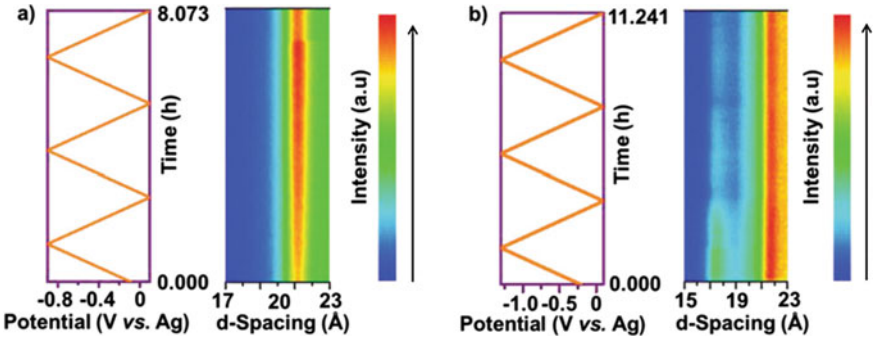

Fig. 14 Plot of the relationship between d-spacing and time during electrochemical cycling of MXene $Nb_4C_3T_x$ electrodes in **a** 1 M H_2SO_4 and **b** 1 M $MgSO_4$. Reprinted from [24], Copyright (2020) John Wiley and Sons

the space between the MXene layers was adequate for insertion and de-insertion of electrolyte ions. Sufficient interlayer spacing also meant that the stability of the electrode was guaranteed even at high charging and discharging rates.

In a similar form, Ghodbane et al. [25] implemented in-situ synchrotron XRD measurements in their investigation of the relationship between electrochemical properties of various MnO_2 crystalline structures and microstructural changes occurring during electrochemical cycling. The processes of ion intercalation and deintercalation were observed, which corresponded to "structural breathing" of the electrode (illustrated in Fig. 15) during the charge and discharge process, in addition to "metal–oxygen bond distance" changes [25].

It is, therefore, necessary to investigate structural changes in metal oxide electrodes as processes of intercalation and deintercalation induce swelling which can be detrimental to their long-term stability and performance. In-situ XRD characterization has been successfully used as highlighted by the references previously

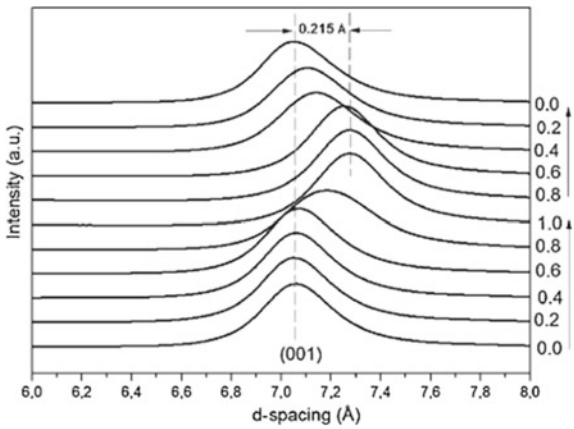

Fig. 15 In-situ XRD on MnO_2 electrodes in 1 M LiCl electrolyte during charge and discharge illustrating structural breathing phenomenon. Reprinted from [25], Copyright (2012), with permission from Elsevier

mentioned [21–25]. Nevertheless, this characterization technique is limited to application in metal oxide/crystalline materials and not the commonly used amorphous carbon. Other drawbacks include difficulty in the construction of specialized cell configurations and limitations in X-ray permissive aperture coverings with common issues such as cost, corrosion, toxicity for beryllium, and difficulties in achieving cell pressures most especially with large cell dimensions for aluminum and polymers [26].

4.4 In-Situ Atomic Force Microscopy (AFM)

In-situ AFM is a powerful characterization technique capable of examining electrode surfaces and interfaces with the electrolyte, to identify changes in the morphology of electrodes during cycling conditions. In-situ AFM experiments are conducted using AFM systems (e.g., Resolve by Bruker) in specially constructed three-electrode cell configurations and an attached potentiostat for the corresponding electrochemical cycling. During cycling, AFM tips are inserted into the test cell with a brief pause to probe morphological changes with respect to potentials applied. As mentioned previously, volume expansions and cracks during cycling are prominent occurrences in metal oxide electrodes, whose occurrences could be mitigated by a thorough understanding of relations between applied potentials and subsequent morphological change. Particularly, the morphology of MXene based electrodes utilized in supercapacitors undergo dynamic transformations during cycling, which are dependent on nanostructure configurations and nanocomposite matrixes utilized. Guan et al. [27] implemented in-situ AFM during electrochemical cycling to investigate changes in the morphology of $Ti_3C_2T_x$ nanosheets and $Fe_3O_4/Ti_3C_2T_X$ nanocomposites with applied potential. Figure 16 displays the obtained AFM images before and after several cycles, clearly portraying changes in the height profiles of the $Fe_3O_4/Ti_3C_2T_X$ electrode during potential cycling in 0.2 M KOH electrolyte.

Note that the protrusions present before cycling (position I) disappeared after two cycles as portrayed in Fig. 16 b. Also, a reversible fivefold increase in the size of protrusions in position (ii) occurred after cycling (Fig. 16b), indicating that deposits were present on the electrode surface which corresponded to volume expansion during cycling. These deposits were ascribed to the accumulation of FeOOH on the surface as determined from XRD and X-ray photoelectron spectroscopy (XPS) analysis [27]. Irreversible transformation of these FeOOH species was thereafter determined to be the cause of decreased specific capacitance with increasing cycle number, in addition to delamination of active materials from the electrode. Hence, the conclusion was made that increased loading of Fe_3O_4 nanoparticles in the composites could increase the specific capacitance and decrease the volume expansion observed by the in-situ AFM. Tao et al. [28] also observed similar volume expansion in supercapacitor electrodes using in-situ AFM.

With the applications mentioned previously, in-situ AFM has been effectively used in the characterization of the morphological changes of electrodes during cycling.

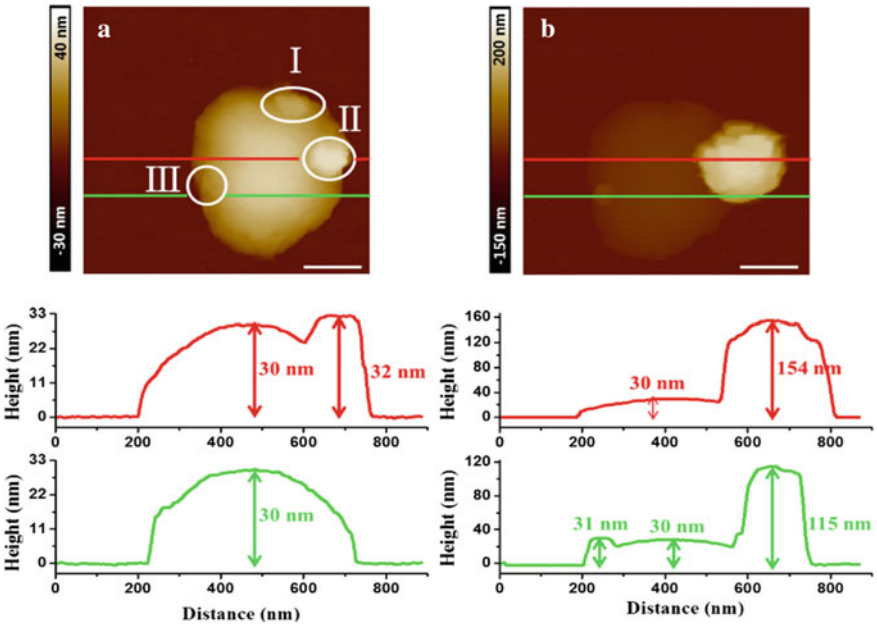

Fig. 16 Comparison of In-situ AFM images obtained before **a**, and after 2 cycles **b**, and corresponding height changes of the $Fe_3O_4/Ti_3C_2T_X$ nano composites with applied potential. Reprinted with permission from [27]. Copyright (2021) American Chemical Society

Notwithstanding, the AFM probe tip inserted into the cell during experiments could interfere with electrochemical processes in addition to solvent evaporation during insertion.

4.5 In-Situ Raman Spectroscopy

Raman spectroscopy is a non-destructive analytical technique used in examining the structural, chemical, and electronic changes occurring in materials. Materials exhibit distinctive vibrational features known as fingerprints from inelastic scattering of light beamed on them. These features arise from interactions of photons with chemical bonds and electronic configurations of molecules, leading to their polarization and subsequent electrons' excitement into higher virtual energy levels. Electrons at excited states are unstable and hence need to return to their virtual energy states, and in the process emit photons with information about their molecular characteristics [29]. Raman spectroscopy operates on this principle by focussing a laser beam of incident light rays on an object at a defined microscopic level, aperture opening, and magnification. A detector thereafter collects the scattered light and produces the record as a spectrometric graph. Upon analysis of the spectra, information about the

electrical conductivity of electrode materials, electronic state, stability of electrodes, and changes at the electrode/electrolyte interface can be obtained. Raman characterization can be obtained in-situ, using specially crafted Spectro-electrochemical cell enclosing the working electrode, reference, and counter electrode. In-situ measurements ensure that electrochemical processes in cells under operation could be related to changes in active materials structures under influence of various applied potentials. An interesting application could be in an aqueous electrolyte supercapacitor, whose potential windows are limited due to gas evolution from the decomposition of water at potentials beyond 1.23 V. Understanding the synergy between electrode structural variations under the influence of an applied potential would be vital towards expanding the operating potential windows of aqueous systems. In this regard, Abouelamaiem et al. [30] investigated the relationship between electrode structures and applied potentials using in-situ Raman spectrometry to study redox reactions on cathodes and anodes. Structural characterization illustrated in Fig. 17 was obtained at different potentials via a combination of chronoamperometry and Raman spectra at decreasing negative potentials to observe changes during electrochemical reduction.

From the spectra, it was observed that at decreasing negative potentials two new bands at 1110 cm^{-1} and 1500 cm^{-1} were introduced in addition to the original D 1330 cm^{-1} and G 1580 cm^{-1} observed in all experiments. These new bands were ascribed to C(sp^2)-H and C=C stretching vibrations arising from electrochemical hydrogen reduction storage. The appearance and disappearance of the bands as the potential was reversed, indicated that the process of hydrogen chemisorption was reversible. In complement with trends from other structural properties obtained from electrode characterization such as surface functional groups, pore volume, and surface area analysis, a trend in decreasing potentials where the onset of hydrogen chemisorption occurred as the activation intensity increased. Thus, emphasizing that attaining optimum performance in aqueous systems required a systemic

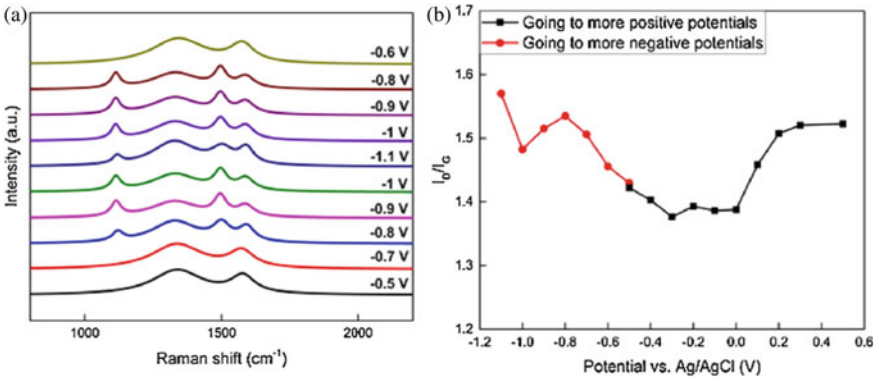

Fig. 17 In-situ Raman spectra obtained for different samples **a** KOH-1 **b** I_D/I_G vs applied potential obtained using a KOH activated carbon electrode and 6 M KOH electrolyte. Reprinted from [30], Copyright (2018) with permission from Elsevier

balance between structural properties impacted by activation methods and correlating maximum potentials at which hydrogen evolution occurred. Following this correlation, the operating potential window can therefore be expanded by structural optimizations made to prevent hydrogen evolution. In-situ Raman spectroscopy to monitor structural changes is therefore essential towards achieving this.

Nonetheless, Raman spectroscopy is prone to heat generation which could affect the electrochemical processes in cells during in-situ measurements.

4.6 In-Situ Fourier Transform Infrared (FTIR) Spectroscopy

The electrochemical interface between the surface of electrodes in contact with electrolytes in supercapacitors during cycling possesses vital information concerning the charge storage mechanism, ion molecular dynamics, and characteristic changes in the local environment of electrodes during cycling conditions. In-situ FTIR acquired during electrochemical cycling is capable of investigating the optical absorbance of electrolyte ion species in solution, in contact with electrodes, and reactional changes during the experiment. During operation, an IR beam is focused on the interface to be analyzed and a detector receives this reflection and records it as a plot of absorbance against the wavelength. Specially fabricated reflection units like the Bruker A530/x suitable for electrochemical cells are used in combination with required electrochemical characterizations such as CV [31] for in-situ monitoring of electrochemical processes. Electrode surfaces can then be analyzed with limited influence of the electrolytes using an internal reflection with an attenuated total reflection (ATR) setup, while the electrolyte and electrode surface can be analyzed using an external IR reflection absorbance spectroscopy[31]. Richey et al. [32] successfully utilized in-situ FTIR in monitoring and comparing ion dynamics in a supercapacitor consisting of porous carbon-derived carbide (CDC) and non-porous onion-like carbons(OLC) electrodes in 1-ethyl-3-methylimidazolium bis((trifluoromethyl)sulfonyl)imide (ETIm-TFSI) electrolyte. The normalized absorption spectra obtained during cyclic voltammetry are shown in Fig. 18.

The spectra revealed the entrance/exit of cation and anions into the pores of the CDC electrode during charge and discharge. In the OLC electrodes, on the other hand, ion motion was restricted to the OLC surface with no ion transport occurring in the pores. Thus, confirming the surface charge storage mechanism of non-faradaic supercapacitors experimentally which was originally postulated using computer simulations and theories. A detailed review of the application of in-situ FTIR in energy storage devices has been carried out by Li et al. [33].

Notwithstanding, acquiring in-situ FTIR spectra on the interface of electrolyte/electrolyte is plagued by absorption of a large proportion of the IR signal in the bulk of the electrolyte solvent. This is typically pronounced in an aqueous electrolyte incorporating water as the solvent [34]. Sensitivity issues are also prominent, which is related to the weak IR sources and IR detection mechanisms.

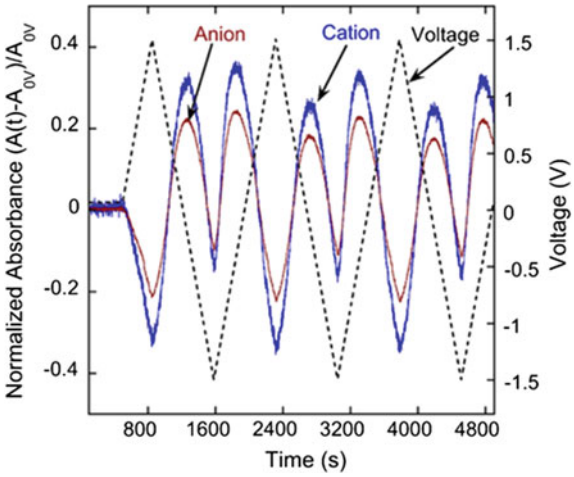

Fig. 18 Normalized absorbance obtained from In-situ FTIR spectra as a function of time during three CV cycles of CDC electrodes in EMIm-TFSI electrolyte. Reprinted with permission from [32]. Copyright (2013) American Chemical Society

5 Conclusion

Different characterization methods have been discussed in this chapter, spanning across electrochemical methods yielding performance metrics such as specific capacitance, resistance, energy, and power densities. In addition, physical characterization methods capable of identifying and monitoring charge storage mechanisms, and electrochemical processes occurring in supercapacitors which have previously been limited to theories and numerical simulations have also been discussed. A combination of these two techniques would ensure that performance metrics are not only determined but in-depth investigations into charge storage mediums and other electrochemically induced processes and changes occurring at the electrode/electrolyte interfaces are conducted. Critical insights unraveled from these techniques would ensure more effective optimizations towards producing high-performance supercapacitors.

References

1. M. Lu, Supercapacitors, *Materials, Systems, and Applications* (Wiley, 2013)
2. M.D. Stoller, R.S. Ruoff, Best practice methods for determining an electrode material's performance for ultracapacitors. Energy Environ. Sci. **3**(9), 1294–1301 (2010)
3. V. Khomenko, E. Frackowiak, F. Beguin, Determination of the specific capacitance of conducting polymer/nanotubes composite electrodes using different cell configurations. Electrochim. Acta **50**(12), 2499–2506 (2005)
4. K.-C. Tsay, L. Zhang, J. Zhang, Effects of electrode layer composition/thickness and electrolyte concentration on both specific capacitance and energy density of supercapacitor. Electrochim. Acta **60**, 428–436 (2012)
5. K. Kierzek, J. Machnikowski, Factors influencing cycle-life of full Li-ion cell built from Si/C composite as anode and conventional cathodic material. Electrochim. Acta **192**, 475–481 (2016)

6. S. Dsoke, B. Fuchs, E. Gucciardi, M. Wohlfahrt-Mehrens, The importance of the electrode mass ratio in a Li-ion capacitor based on activated carbon and $Li_4Ti_5O_{12}$. J. Power Sources **282**, 385–393 (2015)
7. D. Weingarth, H. Noh, A. Foelske-Schmitz, A. Wokaun, R. Kötz, A reliable determination method of stability limits for electrochemical double layer capacitors. Electrochim. Acta **103**, 119–124 (2013)
8. L.L. Zhang, X. Zhao, Carbon-based materials as supercapacitor electrodes. Chem. Soc. Rev. **38**(9), 2520–2531 (2009)
9. M.G. Say, R. Brooke, J. Edberg, A. Grimoldi, D. Belaineh, I. Engquist, M. Berggren, Spray-coated paper supercapacitors. npj Flex. Electron. **4**(1), 1–7 (2020)
10. Z. Li, S. Gadipelli, H. Li, C.A. Howard, D.J. Brett, P.R. Shearing, Z. Guo, I.P. Parkin, F. Li, Tuning the interlayer spacing of graphene laminate films for efficient pore utilization towards compact capacitive energy storage. Nat. Energy **5**(2), 160–168 (2020)
11. D. Weingarth, A. Foelske-Schmitz, R. Kötz, Cycle versus voltage hold–Which is the better stability test for electrochemical double layer capacitors? J. Power Sources **225**, 84–88 (2013)
12. A. Bello, F. Barzegar, M. Madito, D.Y. Momodu, A.A. Khaleed, T. Masikhwa, J.K. Dangbegnon, N. Manyala, Stability studies of polypyrole-derived carbon based symmetric supercapacitor via potentiostatic floating test. Electrochim. Acta **213**, 107–114 (2016)
13. B.-A. Mei, O. Munteshari, J. Lau, B. Dunn, L. Pilon, Physical interpretations of Nyquist plots for EDLC electrodes and devices. J. Phys. Chem. C **122**(1), 194–206 (2018)
14. A.C. Forse, J.M. Griffin, C. Merlet, P.M. Bayley, H. Wang, P. Simon, C.P. Grey, NMR study of ion dynamics and charge storage in ionic liquid supercapacitors. J. Am. Chem. Soc. **137**(22), 7231–7242 (2015)
15. H. Wang, A.C. Forse, J.M. Griffin, N.M. Trease, L. Trognko, P.-L. Taberna, P. Simon, C.P. Grey, In situ NMR spectroscopy of supercapacitors: insight into the charge storage mechanism. J. Am. Chem. Soc. **135**(50), 18968–18980 (2013)
16. S.-I. Lee, K. Saito, K. Kanehashi, M. Hatakeyama, S. Mitani, S.-H. Yoon, Y. Korai, I. Mochida, 11B NMR study of the BF4-anion in activated carbons at various stages of charge of EDLCs in organic electrolyte. Carbon **44**(12), 2578–2586 (2006)
17. P. Azaïs, L. Duclaux, P. Florian, D. Massiot, M.-A. Lillo-Rodenas, A. Linares-Solano, J.-P. Peres, C. Jehoulet, F. Béguin, Causes of supercapacitors ageing in organic electrolyte. J. Power Sources **171**(2), 1046–1053 (2007)
18. M.D. Levi, N. Shpigel, S. Sigalov, V. Dargel, L. Daikhin, D. Aurbach, In situ porous structure characterization of electrodes for energy storage and conversion by EQCM-D: a review. Electrochim. Acta **232**, 271–284 (2017)
19. M.D. Levi, N. Levy, S. Sigalov, G. Salitra, D. Aurbach, J. Maier, Electrochemical quartz crystal microbalance (EQCM) studies of ions and solvents insertion into highly porous activated carbons. J. Am. Chem. Soc. **132**(38), 13220–13222 (2010)
20. N. Shpigel, M.D. Levi, S. Sigalov, L. Daikhin, D. Aurbach, In situ real-time mechanical and morphological characterization of electrodes for electrochemical energy storage and conversion by electrochemical quartz crystal microbalance with dissipation monitoring. Acc. Chem. Res. **51**(1), 69–79 (2018)
21. M. Morcrette, Y. Chabre, G. Vaughan, G. Amatucci, J.-B. Leriche, S. Patoux, C. Masquelier, J. Tarascon, In situ X-ray diffraction techniques as a powerful tool to study battery electrode materials. Electrochim. Acta **47**(19), 3137–3149 (2002)
22. H. Wang, M. Yoshio, Graphite, a suitable positive electrode material for high-energy electrochemical capacitors. Electrochem. Commun. **8**(9), 1481–1486 (2006)
23. S.-L. Kuo, N.-L. Wu, Electrochemical characterization on MnFe2O4/carbon black composite aqueous supercapacitors. J. Power Sources **162**(2), 1437–1443 (2006)
24. S. Zhao, C. Chen, X. Zhao, X. Chu, F. Du, G. Chen, Y. Gogotsi, Y. Gao, Y. Dall'Agnese, Flexible Nb_4C_3Tx film with large interlayer spacing for high-performance supercapacitors. Adv. Func. Mater. **30**(47), 2000815 (2020)
25. O. Ghodbane, F. Ataherian, N.-L. Wu, F. Favier, In situ crystallographic investigations of charge storage mechanisms in MnO_2-based electrochemical capacitors. J. Power Sources **206**, 454–462 (2012)

26. W. Zhu, D. Liu, A. Paolella, C. Gagnon, V. Gariepy, A. Vijh, K. Zaghib, Application of operando X-ray diffraction and Raman spectroscopies in elucidating the behavior of cathode in lithium-ion batteries. Front. Energy Res. **6**, 66 (2018)
27. Y. Guan, M. Zhang, J. Qin, X. Guo, Z. Li, B. Zhang, J. Tang, Morphological evolutions of Ti_3C_2Tx nanosheets and Fe_3O_4/Ti_3C_2Tx nanocomposites under potential cycling investigated using in situ electrochemical atomic force microscopy. J. Phys. Chem. C (2021)
28. X. Tao, J. Du, Y. Sun, S. Zhou, Y. Xia, H. Huang, Y. Gan, W. Zhang, X. Li, Exploring the energy storage mechanism of high performance MnO2 electrochemical capacitor electrodes: an in situ atomic force microscopy study in aqueous electrolyte. Adv. Func. Mater. **23**(37), 4745–4751 (2013)
29. Z. Dong, H. Xu, F. Liang, C. Luo, C. Wang, Z.-Y. Cao, X.-J. Chen, J. Zhang, X. Wu, Raman characterization on two-dimensional materials-based thermoelectricity. Molecules **24**(1), 88 (2019)
30. D.I. Abouelamaiem, M.J. Mostazo-López, G. He, D. Patel, T.P. Neville, I.P. Parkin, D. Lozano-Castelló, E. Morallón, D. Cazorla-Amorós, A.B. Jorge, New insights into the electrochemical behaviour of porous carbon electrodes for supercapacitors. J. Energy Storage **19**, 337–347 (2018)
31. T. Tague Jr, *In-situ FT-IR Spectroelectrochemistry: Experimental Setup for the Investigation of Solutes and Electrode Surfaces* (Advanstar Communications INC 131 W 1ST Street, Duluth, MN 55802 USA, 2015)
32. F.W. Richey, B. Dyatkin, Y. Gogotsi, Y.A. Elabd, Ion dynamics in porous carbon electrodes in supercapacitors using in situ infrared spectroelectrochemistry. J. Am. Chem. Soc. **135**(34), 12818–12826 (2013)
33. J.-T. Li, Z.-Y. Zhou, I. Broadwell, S.-G. Sun, In-situ infrared spectroscopic studies of electrochemical energy conversion and storage. Acc. Chem. Res. **45**(4), 485–494 (2012)
34. J.K. Foley, S. Pons, In situ infrared spectroelectrochemistry. Anal. Chem. **57**(8), 945A-956A (1985)

Nanosupercapacitors

Khairunnisa Amreen and Sanket Goel

Abstract The enormous growth of industrialization has led to a prodigious dependence of humans on energy-consuming devices. Over the last few decades, the speedy upsurge of energy consumption and the environmental influence of conventional energy resources shave escalated the augmented research activities for finding alternate renewable resources. However, these renewable resources are usually geographically limited and intermittent, hence, there is a persistent requirement of developing energy storage devices like supercapacitors. There have been remarkable advances in strategic designs and development of supercapacitors which are preferred in comparison to other energy storage devices owing to their ultra-high power density, portability, and increased life spans. While the competence of supercapacitors hinges on variable factors, their overall performance depends on the structure and properties of the constituent materials used. The current expansion of nanotechnology has unlocked new pathways for fabricating novel materials like carbon nanotubes, graphene, MXenes, perovskites, and other nanostructures. Such nanomaterials have been leveraged to improve the performance of these supercapacitors, leading to a newer name, 'Nanosupercapacitors'. Since, electrodes mainly regulate the performance in terms of capacitance, power density, and energy storage, widespread efforts have been put forward to develop high-performing electrode materials. Due to the rapid increase in the applications daily, elevating the energy density and capacitance of nanosupercapacitors at an ultra-fast charging rate is essential. Hence, substantial research is being carried out in this context. The present chapter briefly gives an overview of recent advances and emerging trends in the fabrication, performance, and development of nanosupercapacitors.

Keywords Nanosupercapacitors · Nanomaterials · Power density · Capacitance

K. Amreen · S. Goel (✉)
MEMS, Microfluidics and Nanoelectronics Lab, Department of Electrical and Electronics Engineering, Birla Institute of Technology and SciencePilani, Hyderabad Campus, Hyderabad 500078, India
e-mail: sgoel@hyderabad.bits-pilani.ac.in

S. Thomas et al. (eds.), *Nanostructured Materials for Supercapacitors*,
Advances in Material Research and Technology,
https://doi.org/10.1007/978-3-030-99302-3_6

1 Introduction

The last few decades have witnessed tremendous development in industrialization globally. Parallelly, the growing population has escalated the energy usage and requirements worldwide. So far, petroleum and other non-renewable fossil fuel-based resources have been widely used which strain the present energy infrastructure and threaten the future. Hikes in fuel cost, environmental hazard, geopolitics, global warming are a few perils of a long-term dependence on these resources [1]. In this context, there is an extreme requirement for alternate renewable sources of power. There has been a significant effort in research and development on both industrial and academic levels for developing more efficient technologies to overcome the energy challenges. Several energy harvesting devices like fuel cells and energy storage devices like batteries, supercapacitors have been realized off lately. Supercapacitors, also regarded as electrochemical capacitors, exhibits high power and high-density energy storage than batteries. Furthermore, based upon the energy storage mechanism, a charge separation at the electrode–electrolyte interface, supercapacitors possess lesser internal resistance, enhanced capacity, and ease of storage and delivery of energy as compared to batteries, hence, attracted considerable interest [2].

The phenomenon of energy storage in carbon porous materials was first observed in 1957, later in 1966, the same effect was rediscovered when a group of researchers was working on the fuel cells. Finally in 1978, NEC developed supercapacitors based on these observations to give backup power supply to computers [3]. A typical supercapacitor is made up of two electrodes separated electrically by a separator and an electrolyte. The advantages like low maintenance, lightweight, portable packaging, high power, larger thermal range, and longer life make supercapacitors a better energy storage device [4]. Despite these advantages, there are certain limitations associated with the usage on a large and commercial scale-like, like less cost-effectivity, lower energy density, less voltage per cell, and more self-discharge. Significant research is being conducted to overcome these research gaps, maintain high power and energy density, faster charge/discharge cycle, and stability. One of the approaches is to use novel electrode materials. The material of the electrode plays a key role in giving high density and capacitance.

There are different types of materials being used for supercapacitor development, ranging from carbons, metal oxides, polymers, nanomaterials, redox mediators, etc. [5]. However, carbon-based materials are often used owing to their high surface areas. On the other hand, metal oxides increase energy and power density due to low resistance and high specific capacitance. In further, the redox reactions of conducting polymers are useful [6]. The basic principle behind the working of a supercapacitor and the energy storage is the electrode–electrolyte interface wherein the exchange of electrons takes place. Depending upon how the energy is stored, the supercapacitors are broad of three types: (a) Electrochemical double-layer capacitors (EDLC), (b) pseudocapacitors, and (c) hybrid supercapacitors. In further, each type utilizes different materials for the electrodes. Figure 1 gives the general classification of the

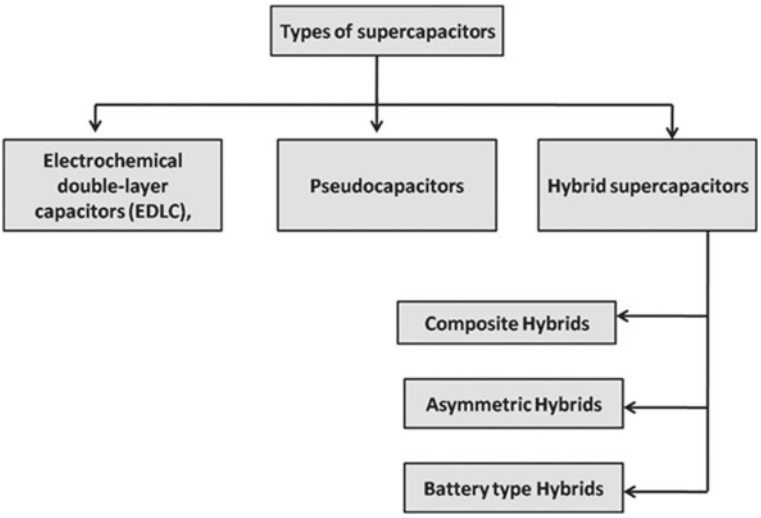

Fig. 1 Schematic representation of a broad classification of the types of supercapacitors

types of supercapacitors. Table 1 gives the common materials used for the fabrication of these various supercapacitors [7, 8]. However, the emerging trends suggest that these are not the only materials used, several novels, structurally engineered metals are also employed to improve the performance.

These highly efficient electrochemical supercapacitors provide solutions to the energy crisis as they have multiple applications in industry, commercial fields, military and defense, automobile industries, power companies, network and mobile

Table 1 This table describes various types of conducting materials used over electrodes for developing different types of supercapacitors

	EDLC	Pseudocapacitors	Hybrid supercapacitors
Electrode Materials	• Carbon Foam • Carbon nanotubes • Carbon aerogels carbide derived carbon • Activated carbon graphene • Carbon fibers	• Conducting polymers • Metal oxides	Asymmetric Composite Battery type } Carbon materials, polymers

industries, electric vehicles industry, eco-friendly devices, etc. Continual research and quest to improve the supercapacitor performance has made it a closer alternative to the batteries [9]. However, the downsizing of supercapacitors is still challenging. The development of nanoscale and miniaturized supercapacitors is of key importance. While reducing the size, parameters like energy output, power density, and capacitance are to be taken care of. Lithographic techniques have led to the development of miniaturized, thin-film electrodes for micro and nanosupercapacitors [10]. Off lately, there has been tremendous growth in miniaturizing the supercapacitors and embedding them on flexible micro-substrates [11]. Substrates like paper, fabric, textiles, etc. have been explored to integrate supercapacitors on a chip [12]. These miniaturized supercapacitors have been proven to be useful in many microelectronic applications. This chapter focuses on the emerging trends in fabricating, characterizing, and application of miniaturized micro-and-nanoscale supercapacitors. It also discusses the major research gaps and prospects of these miniaturized energy devices on a larger scale.

2 Working Principle

Based upon the working principle i.e.; energy storage mechanism of supercapacitors, they are of three types as mentioned above.

2.1 Electrochemical Double-Layer Capacitor (EDLC)

These comprise two electrodes, preferably carbon electrodes, an electrolytic solution, and a separator. EDLC stores charge through an electrostatic process. It is a non-faradic process wherein no transfer of charge takes place. The working principle behind the energy storage mechanism here is the formation of an electrochemical double layer. Upon supply of voltage to the electrodes, the charge is developed on the electrode surface, the oppositely charged ions from the electrolyte diffuse towards these charged electrode surface through pores of separators forming an electrostatic double layer. This double layer enhances the uptake of energy and storage. Figure 2a, gives a schematic representation of an EDLC working mechanism. The performance of a supercapacitor is decided by calculating the capacitance it offers. The capacitance in EDLC can be calculated with a standard equation below (Eq. 1)

$$C = (\varepsilon_0 \times \varepsilon_0 A)/d \tag{1}$$

Herein, ε_o is free surface permittivity,ε_r is dielectric materials relative permittivity, A = electrode surface area and d is the distance between two electrodes. Hence, by changing the dielectric materials, the capacitance of the supercapacitor can be improved [7].

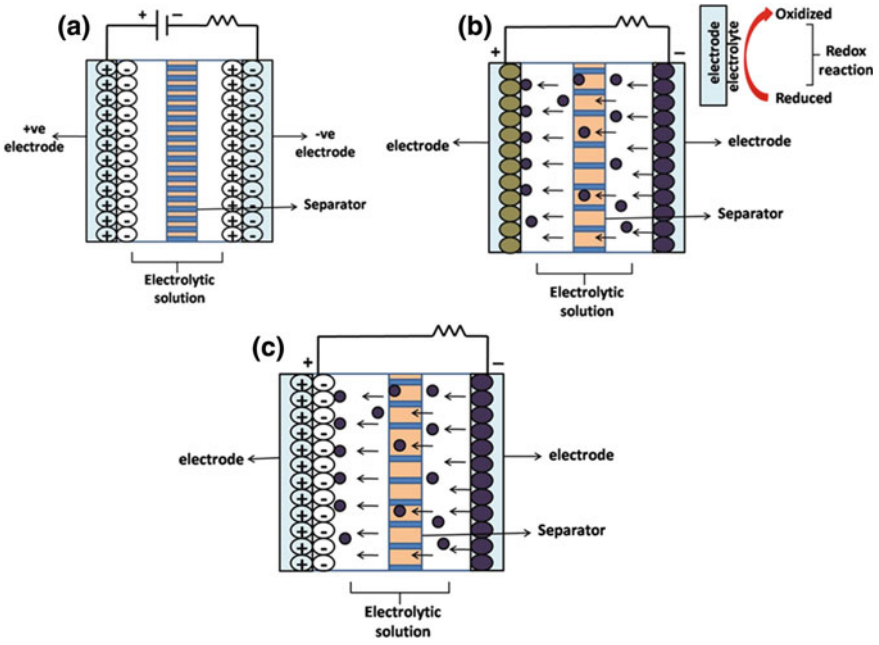

Fig. 2 Schematic representation of **a** Electrical double layer supercapacitor, **b** pseudocapacitor, **c** hybrid supercapacitor

2.2 *Pseudocapacitors*

The mechanism of energy storage in this is through a faradic process wherein, charge transfer between electrode and electrolyte occurs. Upon applying the potential to the electrodes, a redox reaction happens on the electrode material, which transfers charge across the double layer. Due to this mechanism, pseudocapacitors give higher energy density and specific capacitance than EDLC. For the ease of redox reaction to take place, the material used over the electrode is electroactive redox in nature like conducting polymers [13]. Figure 2b gives a schematic representation of the pseudocapacitor mechanism.

2.3 *Hybrid Supercapacitors*

These types of supercapacitors are a combination of both EDLC and pseudocapacitors. EDLC offers more cyclic stability and power whereas, pseudocapacitors offer higher specific capacitance. It has two types of electrodes, polarizable which is usually carbon electrode, non-polarizable which is a metal or conducting polymer electrode. It utilizes both faradic and non-faradic processes. This makes it like both

battery type and capacitor type [14] leading to provide better performance. Figure 2c gives the schematic representation of the hybrid supercapacitor. They are of further three types:

(a) *Composite hybrid*: In this, a single electrode will have a composite of carbon material with metal oxides or any conducting polymer. The carbon portion offers a capacitive double layer and greater surface area therefore, the contact between metal oxides or conducting polymers increases. The faradic reaction due to these pseudocapacitive materials enhances the capacitance. There are two designs in this; binary with a combination of two materials, ternary with a composite of three materials [15, 16].
(b) *Asymmetric hybrid*: Herein, two distant electrodes are combined. One acts as a faradic electrode and the other as a non-faradic thus, power and energy density are enhanced simultaneously. A carbon electrode is given a negative charge and metal oxide or conducting polymer electrode a positive charge. These are advantageous in terms of high cycling stability and good power density [17].
(c) *Battery-type hybrid*: This is a combination of two electrodes in which one is a supercapacitor electrode, other is a rechargeable battery type. This way, the properties of both supercapacitors and batteries are utilized in a single set-up hence offering better performance [16].

3 Electrode Preparation

Several approaches have been reported so far for the preparation of electrodes to be used in supercapacitors. Usually, carbon electrodes are used as the base or underlying electrodes which are further modified with various electrode materials like metal oxides, carbon nanomaterials, conducting polymers, etc. to enhance their energy storage capacity. Figure 3 summarizes the most commonly used electrode materials [3, 18–20].

The materials generally used have certain properties like high-temperature resistance, excellent conductivity, high chemical stability, eco-friendly, corrosion-resistant, and economic. The material should also be able to carry out a Faradic reaction. Thus, porous materials are preferred. The conventional bulk supercapacitors utilize bigger electrodes that are prepared using techniques like drop casting, spin coating, electrodeposition, physical adsorption, covalent adsorption, etc. of these materials. Figure 4 gives a summary of some of the approaches followed for the fabrication of these materials. The modern approach involves miniaturization of these supercapacitor electrodes. In this context, techniques like lithography, 3D-printing, screen printing, lamination, embossing are some of the recent advances specifically used for preparing miniaturized, micro and nanoelectrodes [18].

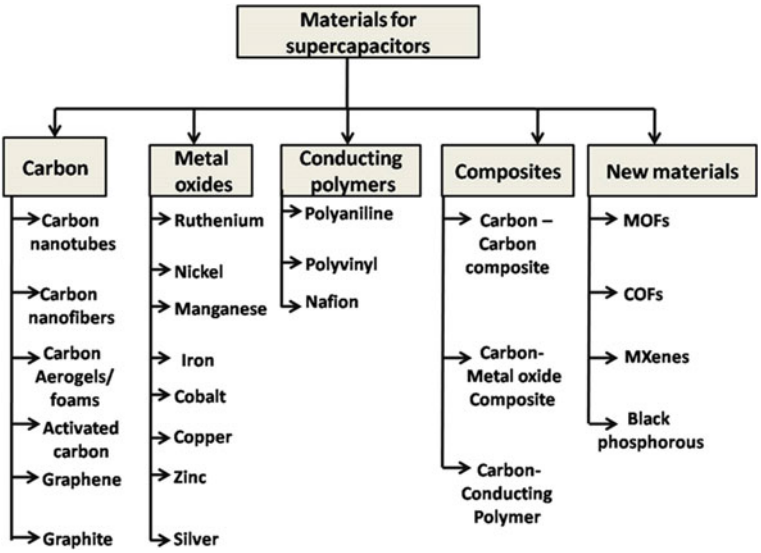

Fig. 3 Schematic summarizing various types of materials used on electrodes for preparing supercapacitors

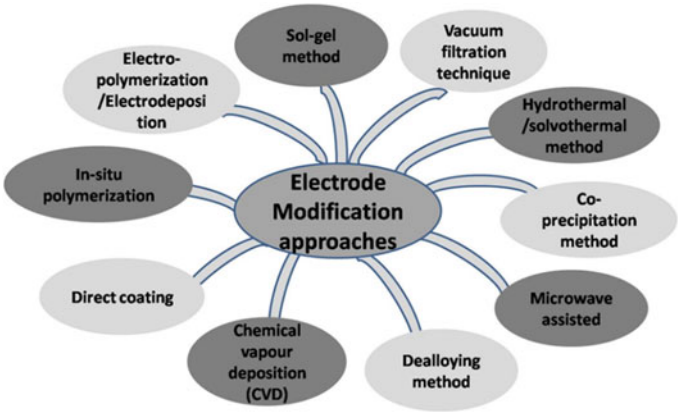

Fig. 4 Schematic representation summarizing various electrode modification methods

4 Miniaturized/Nanosupercapacitors

The plethora of the growing demand for wearable and portable electronics has increased the need for miniaturized energy storage devices. In this regard, micro-and-nanosupercapacitors with flexibility, safety, high power density, and longer lifespan i.e.; the capability of undergoing >100 000charge/discharge cycles, are preferred [21]. Fibers, textiles, papers, flexible substrates, etc. have been reported to be used as

a base in minuscule supercapacitor. Based on the type of substrate, various fabrication methods are adapted.

4.1 Miniaturized Supercapacitors(MSCs)

Various types of techniques are used and several miniature supercapacitors have been fabricated. Following are some of the reported miniature supercapacitors.

4.1.1 Photolithography Based MSCs

It is quite a popular technique of microfabrication wherein, a beam of photons like ultraviolet rays are used to engrave patterns on the substrates. Hence, also termed optical lithography. These patterns drawn over surfaces act like the electrodes of a supercapacitor and can be chemically modified with various electro-active materials using methods like spin coating, spray coating, electrodeposition, CVD, sputtering, etc. to increase their performance. For example, Si et al. developed a solid-state microsupercapacitor over a polyethylene terephthalate (PET) substrate. Herein, a total of 24 interdigitated fingers were designed using photolithography that was used as anode and cathode. In further, the electron beam evaporation technique was employed to deposit electrode materials and electrical contacts. The electrodes were deposited with multiple layers of MnO_x (Manganese oxide)/Au, with 50 nm thickness. Their device gave an energy density and power density of 1.75 mW h cm^{-3} and 3.44 W cm^3 respectively. It also displayed magnificent cycling stability of more than 15,000 times which is 74.1% higher than other bulk systems [22].

Similarly, Kim et al. reporteda3D porous, boron-doped carbon pattern using five-beam interference lithographic approach. The designed electrodes were carbonized under elevated temperatures(700–1000 °C) and argon. Boron doping was achieved by dipping the designed pattern into a boric acid solution followed by gold deposition over the electrode pattern through an interdigitated electrode mask. 50 nm thick Au layer was deposited. A gel electrolyte was used to experiment. The device showed capacitance of 7.15 mF/cm^2, an energy density of 7.1 mWh cm^{-3} and a power density of 66 W/cm^3 [23]. Likewise, Wang et al. prepared a reduced graphene oxide/TiO_2composite based micro-supercapacitor. The composite was deposited as thin films over the PET substrate. Using a photomask, interdigitated electrodes were patterned over these films using ultraviolet irradiation. Furthermore, a 45 nm gold layer was also deposited. Finally, a polymer gel electrolyte was dropped on the surface and dried. Their device gave a remarkable power density of 312 W cm^{-3}, the energy density of 7.7 mW h $cm^{-3,}$ and capacitance of 233.0 F cm^{-3}. Figure 5 is the reprint of their schematic representation of their device fabrication and real images of various electrode patterns designed by them reprinted with copyright (2017) publisher name (American chemical society), permission [24].

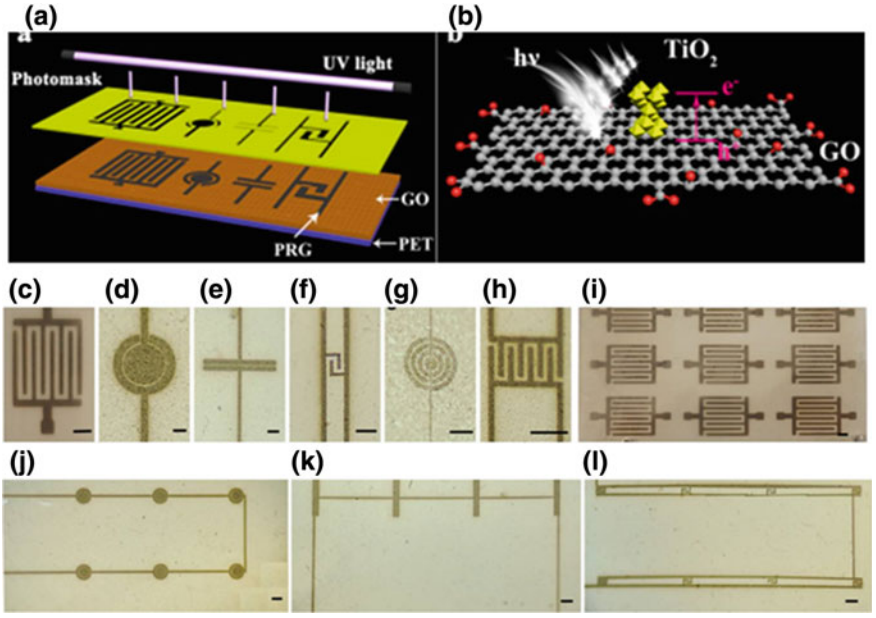

Fig. 5 **a** Schematic of photomask-based electrode pattern designing using UV. **b** Schematic of photoreduction of GO/TiO_2 film. (**c–l**) Real images of various designs patterned over PET/GO/TiO_2 film using photolithography. Reprinted with permission [24], copyright (2017) American Chemical Society

4.1.2 Ink-Jet Printing Based MSCs

This is a common technique employed for the fabrication of interdigitated arrays of electrodes. Herein, droplets of liquid electro-active materials are pushed through the nozzles and deposited over various substrates. Viscosity, chemical stability, solubility, particle size, and surface tension of the printing inks are used to play a key role in conductivity [25]. For instance, Wang et al. developed solid-state micro-supercapacitors using inkjet printing of δ-MnO_2 nanosheets. 5 layers of δ-MnO_2 ink were printed over glass and polyimide substrates. Over this, 2 additional layers of PEDOT polymer were printed. Annealing procedure at high temperatures was carried out post-printing to dry. The printed films were used as electrodes with polymer gel electrolytes of modified polyvinyl alcohol. The device showed good capacitance retention and cycling stability after 3600 charge–discharge cycles. The device exhibited an energy density of 1.8×10^{-4} $Whcm^{-3}$, power density of 0.018 $Wcm^{-3,}$ and capacitance of 2.4 Fcm^{-3} [25]. In another work, Choi et al. fabricated a paper-based miniature supercapacitor using ink-jet printing. Herein, a suspension of carbon nanofibers (CNF) was printed over an A4 size paper as a base electrode. Furthermore, a viscous conductive ink with a composite of single-walled carbon nanotube-activated carbon-silver nanowires was prepared as per standard procedure

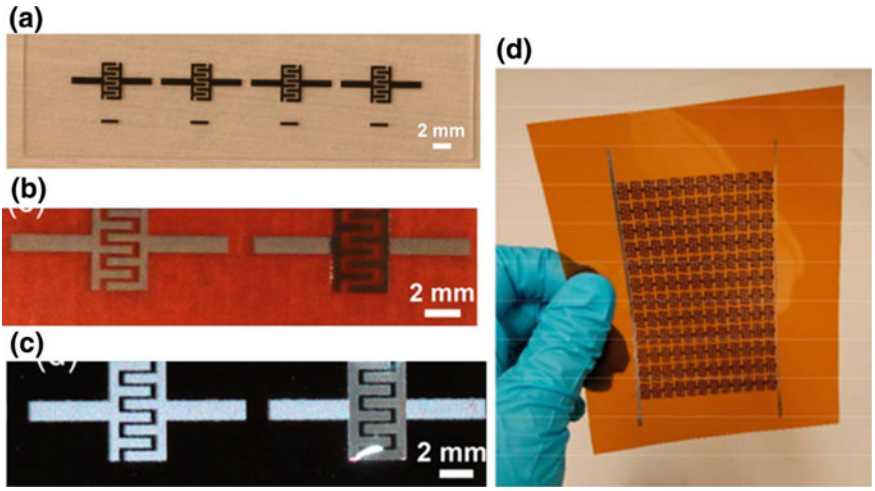

Fig. 6 A real image of a series of interdigitated arrays of graphene inkjet printed on **a** glass slide, **b** Kapton sheet, **c** wafer. **d** Real image of large-scale micro-supercapacitors ink-jetted with graphene over polyimide sheet. Reprinted with permission [27], copyright (2017) American Chemical Society

and ink-jet printed over CNF patterns. An ionic liquid-polymer gel electrolyte is used here as a medium. The device showed appreciable performance [26].

Li et al., designed graphene-based miniature supercapacitors through ink-jet printing. Graphene was exfoliated from graphite foil through the electrochemical exfoliation process. The obtained graphene was dispersed in DMF solvent to get viscous suspension as printable ink. This was fed into an ink-jet printer and printed over various substrates like a silicon wafer, glass, etc. in an interdigitated array format. Further, for the electrolyte polymer gel (poly(4-styrene sulfonic acid) ink was printed and dried. Figure 6 is the reprint of their fabricated device with copyright permission [27].

4.1.3 3D-Printing Based MSCs

3D printing or additive manufacturing is widely being used for making on-chip energy devices. It aids to design nanosupercapacitors with 3D structures that enhance power and energy density. This approach has been reported by quite a few researchers. For instance, Yang et al. fabricated an asymmetric miniature supercapacitor. The device was fabricated over a glass with electrodes and electrolyte ink printed. It gave an areal capacitance value of 208 mF cm^{-2} and an energy density of 73.9 μWh cm^{-2} [28].

In another interesting work, Zhang et al. reported a unique approach wherein they made stamps by using 3D printing which was further used to print electrodes on paper. Herein, they used polylactic acid conducting filament, fed into a 3D-printer,

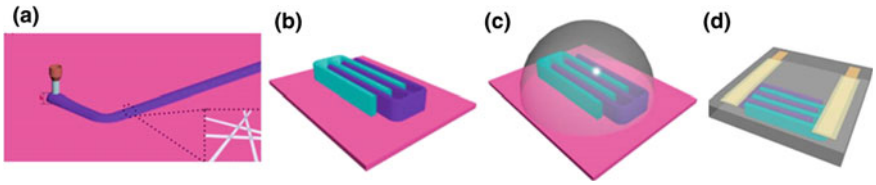

Fig. 7 Schematic representation of 3D printed microsupercapacitor device by Yu et al. reprinted copyright (2017) publisher name (American chemical society), permission. **a** Procedure of 3D-printing, **b** 3D-printed interdigitated electrodes, **c** pouring of gel electrolyte and **d** dried electrolyte and electrodes

the temperature was maintained at 200^0C to make filament molten and print. Various designs of stamps were printed like a spiral, interdigitated fingers, roller stamps, pad stamps, etc. Further, MXene ink was prepared and brushed on these stamps. The stamps were pressed firmly over A4 sheets to get printed and dried. These prints were used as electrodes and similarly, gel electrolytes were printed. The device showed an areal capacitance of 61 mF cm^{-2} at 25 μA cm^{-2} [29]. Yu et al., designed carbon nanotubes (CNT) based microsupercapacitors with 3D printing. In this work, the authors prepared CNT ink with solvent using standard procedure. These were fed into a 3D printer micronozzle with printing pressures of 10–30 kPa. Glass plates were employed as base substrates which were heated to remove the solvent. Later, annealing was carried out. Polyvinyl alcohol gel electrolyte was printed and dried to complete the microsupercapacitor. Figure 7 is the reprint of the schematic of their preparation method with copyright permission. Their device exhibited remarkable cycling stability and an areal capacitance value of 2.44 F cm^{-2} [30].

4.1.4 Screen-Printing Based MSCs

This is a modern approach of printing electrodes over various substrates like cloth, paper, glass, etc. Herein, a mesh supported by a stencil is used with desired patterns. The conductive ink of choice is poured over this stencil to obtain a print of the design over a substrate. Ink dries and adheres to the substrate. Since it is a simpler and more cost-effective way, it is substantially used. For example, Xie et al. reported copper electrodes in-situ modified with $Cu(OH)_2$@FeOOH nanotubes, interdigital array. A polyimide flexible substrate was used here over which conductive silver and copper electrodes were patterned using a mesh. Further, after drying, the designed substrate was immersed in an electroactive solution of copper and ferrous chloride to carry out electroless for in-situ electrodeposition of nanoparticles. Their device showed good specific capacitance at 0.1 mA cm^{-2}measuring about 58.0 mF cm^{-2} and an excellent energy density of 18.07 μWh cm^{-2} [31].

In another work, Wang et al. developed miniature supercapacitors with screen printing over PET substrate. Conductive silver ink was printed in the desired pattern followed by annealing. The MnO_2conductive ink was top coated over the silver

electrodes pattern and dried. Finally, a polyvinyl alcohol gel electrolyte was printed and dried. The procedure was also tried over glass and printing paper substrates. The device gave good cycling stability up to more than 1000 cycles, a capacitance of 7.04 mF $cm^{-2,}$ and a current density of 20 μA cm^{-2} [32].

4.1.5 Laser Writing Based MSCs

Direct laser scribing or writing has been employed to develop graphene-based nano, micro, miniaturized supercapacitors. Herein, various lasers, like UV, CO_2, Femto, pulsed, etc., can be used to directly engrave graphene and its derivatives over the flexible substrates. This can be used as electrodes [33]. For instance, Kady et al. reported large-scale production of graphene-based miniaturized supercapacitors over flexible substrates. Herein, they fabricated more than 100 miniature supercapacitors over graphite oxide films by direct laser writing with a light scribe DVD burner. Their device gave an areal capacitance, the volumetric capacitance of 2.32 mF cm^{-2}, 3.05 F cm^{-3} at 16.8 mA cm^{-3} respectively, and a power density of 200 W cm^{-3} [33]. Similarly, Lamberti et al. developed an approach of fabricating graphene electrodes over a flexible polyimide sheet using a CO_2 pulsed laser. These were transferred onto a PDMS substrate. In further, to avoid thermal loss and create a reservoir for electrolytes, glass and the PDMS layer were thermally bonded. Finally, the gel electrolyte of introduced through a syringe in the chamber created. The device gave an areal capacitance of 650 μF cm^{-2} at 50 mV s^{-1} [34]. In another work, Ye et al. demonstrated the deposition of graphene films via CVD over copper substrates. Multiple graphene layers were deposited. Further, these films were transferred over gold-coated substrates. Over these, laser scribing was done to obtain microelectrode patterns. This device showed good power density and energy density of 1860 W $cm^{-3}$and 23 mW h cm^{-3}respectively [35].

Kurra et al. reported the fabrication of 2D titanium carbide nanoparticles integrated MXene based interdigital electrode pattern over the paper. Herein, A4 papers were coated with gold nanoparticles through sputtering. MXene slurry with titanium carbide was poured and dried over the gold-coated paper. In further, CO_2 pulsed laser was employed to draw electrode patterns. Further, polyvinyl alcohol gel electrolyte was used. The device exhibited appreciable capacitance [36]. Lin et al., fabricated graphene-based electrodes over polyimide sheets and other polymer sheets using CO_2 laser. Interdigitated electrodes were designed and these gave remarkable specific capacitance of 4 mF cm^{-2} and a power density of 9 mWcm^{-2} [37]. Likewise, Zhang et al. developed on-chip 3D miniaturized supercapacitor. Herein, lignin film was used as a substrate over which graphene was scribed using a laser. Interdigitated electrode pattern was drawn and tested for energy storage application. This gave a good areal capacitance value of 25.1 mF cm^{-2}, an energy density of 1 mW h cm^{-3}, and a power density of 2 W cm^{-3} [38]. Overall, laser scribing is a simple and faster method but is restricted to certain materials only.

4.2 Fibrous MSCs

Various kinds of fibers, like carbon nanofiber, graphene fibers, composite fibers, polymer fibers, carbon nanotube fibers, etc., have been explored for miniature supercapacitor application. The fact that these are lightweight and flexible, makes them ideal for wearable electronics. Techniques like dry spinning, wet spinning, electrospinning, and hydrothermal have been used for fabricating these fibrous nanosupercapacitors. Xiao et al. used carbon fiber as base material to grow MnO_2particles via the electroless deposition method. These were used as two parallel electrodes mounted over the PET substrate. Furthermore, a PVA gel electrolyte was coated and made to solidify. This device gave a volume capacitance of 2.5 F cm^{-3}, an energy density of 2.2×10^{-4} Wh cm^{-3}. To further enhance the performance, the same device can be made by using up to 50 fibers [39]. Likewise, Sun et al. prepared reduced graphene oxide (rGO) fibers and incorporated them with transition metal nanomaterials to give hybrids. These were assembled with PVA gel electrolyte to give MSCs. The so prepared device exhibited volumetric capacitance of 1.5 F cm^{-3} [40]. Sun et al., developed an MXene/CNT helical fiber structure using Mxene nanosheets and a scaffold of carbon nanotube. These electrodes were placed over PET substrate and filled with PVA gel electrolyte to form a solid-state miniature supercapacitor. The device showed a current density of1.0 A cm^{-3}, volumetric capacitance of 22.7 F cm^{-3}, energy density of 2.55 mWh cm-^{3}, power density of 45.9 mW cm^{-3} [41].

In another work, Pan et al. used carbon nanotube fiber as a base electrode. Further, it was chemically modified by synthesizing an alloy of Co–Ni via electrochemical deposition. It was subsequently top coated with Au-MnOx. The electrodes were assembled over a prepared holy graphene paper with PVA gel electrolyte to make a compact miniature supercapacitor. The device showed an energy density of 15.1 mW h cm^{-3} and a power density of 7.28 W cm^{-3} [42]. Cai et al., developed micro supercapacitor wires using multiwalled CNT (MWCNT) fibers and conductive polymer composite. Herein, MWCNT fibers were dipped in the acidic solution of aniline so that it gets incorporated into the fibers. Further, the coated fibers were subjected to electrochemical polymerization to form polyaniline. A PVA gel electrolyte was coated and dried. The device gave 274 F g^{-1} gravimetric capacitance [43]. In another work, Shao et al. prepared PET fibers modified with Ni-Cu layer. These fibers were chemically modified with polyethylene oxide and MXene solution through electrospinning. These fibers were assembled over PET film and PVA gel electrolyte was poured over it and dried. The device gave an areal capacitance of 13.23 mF cm^{-2}, a current density of 0.25 mA cm^{-2} [44]. Overall, fiber-based supercapacitors have proven to be a potential candidate for fabricating nano capacitors.

4.3 Paper and Textile MSCs

Primarily, the paper-based supercapacitors are dependent upon the fact that the cellulose of paper forms a conductive network with electro-active material. There are three basic approaches for the integration of conductive materials over the paper. (i) Surface coating: herein, the slurry or dispersion of the conductive material can be either coated or printed over the surface of the paper and dried. (ii) Bulk mixing: also termed as soak and dry approach in which the paper is soaked in the solution of conductive material and dried. (iii) Molecular mixing: herein, the conductive materials are integrated at a molecular level. The cellulose fibers are mixed as composites with conductive material fibers and these are used to prepare a conductive paper that can be used as an electrode. Using these methods, several research groups have developed MSCs. For example, Cui et al. designed a single sheet of paper by printing single-walled carbon nanotubes (SWCNT) electrodes and newspaper as a separator over a single sheet of paper. To prevent SWCNT from seeping inside the paper, before modification, the paper was treated with polyvinylidene fluoride to make it impermeable for SWCNT. The device of 30 μM volume showed a specific capacitance of 33 F g^{-1} [45]. Zheng et al., reported a unique method in which they drew electrodes on a printing paper using a graphite rod. The electrodes were drawn on paper and a paper separator was kept. This device gave a capacitance of 2.3 mF cm^{-2} [46]. Bin et al. prepared a device over a printing paper wherein they used a pencil to draw graphite layer electrodes. Further, these electrodes were electrodeposited with polyaniline nanowire over these electrodes. A solid-state device was assembled using a PVA gel electrolyte. This device exhibited an energy density of 0.32 mW h cm^{-3}, a power density of 0.054 $^{W\ cm-3}$ [47]. Zhe et al. used graphene solution and cellulose paper with a soak and dry approach to develop a scalable approach for making MSCs. The device exhibited a capacitance of 46 mF cm^{-2} [48]. Longyan et al. developed solid-state MSCs using a simple printing paper. The paper was soaked in an acidic monomer solution of pyrrole and then dried in a fume hood. In further, this coated paper was soaked in PVA gel electrolyte and dried. The device was tested for supercapacitor application and showed an areal capacitance value of 0.42 F cm^2, power density, and energy density of 0.27 W cm^{-3} and 1 mW h cm^{-3} respectively [49].

Unlike paper, textile fibers and yarns have also been used as a base material for fabricating miniaturized supercapacitors. Several reports using cotton, polyester textile with carbon materials, and redox mediators have been reported for MSCs application. Dip coating, painting, and screen printing methods are adapted for this application. Substantial reports have been given in the literature. For example, Kristy et al. reported screen printing over cotton and polyester fabrics with carbon inks. Their device showed a capacitance of 210 mF cm^{-2} [50]. In an interesting work, Lihong et al. developed simple cotton t-shirts into highly carbonized fabrics and tested them for supercapacitor application. The device showed a capacitance of 112 mFcm^{-2} [51]. The same group also reported carbon fiber substrate modified with Zn_2SnO_4/MnO_2. This device gave an areal capacitance value of 288 mF cm^{-2} [52]. Jae et al. demonstrated redox supercapacitor using wearable, knottable, braidable, and

sewable yarns. CNT was incorporated into these yarns. The device gave volumetric capacitance of 179 F cm^{-3} [53]. Such type of paper and textile-based nano/micro-supercapacitors has proven to be excellent in wearable electronics.

5 Conclusion and Outlook

The present chapter discusses the emerging trends in nanosupercapacitors development. It gives a brief account of the types of supercapacitors, their working principle, the electrode preparation strategies reported, the electro-active materials used, the fabrication approaches employed for miniaturized supercapacitor fabrication like photolithography, screen printing, ink-jet printing, laser scribing, and 3D printing. In further, the recent advances in preparing microsupercapacitors using flexible substrates like fiber, paper, textile have also been discussed. Even though the growing need to fabricate next-generation smaller, wearable electronics has led to the miniaturization of energy storage devices. The development of micro and nanosupercapacitors has several challenges to be faced and is at an early stage. Due to their portability, bendability, and stretchability, the flexible substrates-based supercapacitors have seen remarkable growth off lately. These can be used as standalone power sources and applied in biomedical implantable devices, RFID tags, wireless smart sensors, and other MEMS devices associated with energy collecting and exchanging data. Several fabrication methods have been reported and significant research has been done to enhance the performance of these nanosupercapacitors. As the field continues to grow, the varied new applications of nanosupercapacitors are coming into existence. Limitations of nanosupercapacitors to be addressed in the future are especially in terms of performance, safety, more power, and energy density, and large-scale production at an economic cost. For this, several electro-active novel materials, substrates, and fabrication methods are being tested. Electrolytes used in these are mostly dry, gel electrolytes that have lesser conductivity as compared to liquid electrolytes. However, the liquid electrolytes if used faces issues like leakage and corrosion. Probably, better encapsulation strategies need to be developed to overcome this. Although many flexible substrates have been reported for MSCs, yet their capacitance is less satisfactory. Modification with nanomaterials with more conductivity, and improvement in design could be helpful to resolve this issue. A lot of improvement in terms of synthesizing solid electrolytes with improved properties has to be done. Considerable work has to be done to structurally engineer materials cost-effectively and at a large scale to be used for electrode modifications. In further, the development of rapid and controllable fabrication methods for flexible nanosupercapacitors assemblies is an urgent need. Though research is being carried out these nanosupercapacitors are still in infancy and have great potential in the future.

References

1. A. González, E. Goikolea, J.A. Barrena, R. Mysyk, Review on supercapacitors: technologies and materials. Renew. Sustain. Energy Rev. **58**, 1189–1206 (2016). https://doi.org/10.1016/j.rser.2015.12.249
2. M.D. Stoller, S. Park, Y. Zhu, J. An, R.S. Ruoff, *Graphene-Based Ultracapacitors* (2008), pp. 6–10
3. Z.S. Iro, C. Subramani, S.S. Dash, A brief review on electrode materials for supercapacitor. Int. J. Electrochem. Sci. **11**, 10628–10643 (2016). https://doi.org/10.20964/2016.12.50
4. Y. Wang, Z. Shi, Y. Huang, Y. Ma, C. Wang, M. Chen, Y. Chen, Supercapacitor devices based on graphene materials. J. Phys. Chem. C. **113**, 13103–13107 (2009). https://doi.org/10.1021/jp902214f
5. M.A. Pope, S. Korkut, C. Punckt, I.A. Aksay, Supercapacitor electrodes produced through evaporative consolidation of graphene oxide-water-ionic liquid gels. J. Electrochem. Soc. **160**, A1653–A1660 (2013). https://doi.org/10.1149/2.017310jes
6. P. Sharma, T.S. Bhatti, A review on electrochemical double-layer capacitors. Energy Convers. Manag. **51**, 2901–2912 (2010). https://doi.org/10.1016/j.enconman.2010.06.031
7. S. Najib, E. Erdem, Current progress achieved in novel materials for supercapacitor electrodes: mini review. Nanoscale Adv. **1**, 2817–2827 (2019). https://doi.org/10.1039/c9na00345b
8. M. Vangari, T. Pryor, L. Jiang, Supercapacitors: review of materials and fabrication methods. J. Energy Eng. **139**, 72–79 (2013). https://doi.org/10.1061/(asce)ey.1943-7897.0000102
9. R.R. Salunkhe, J. Lin, V. Malgras, S.X. Dou, J.H. Kim, Y. Yamauchi, Large-scale synthesis of coaxial carbon nanotube/$Ni(OH)_2$ composites for asymmetric supercapacitor application. Nano Energy **11**, 211–218 (2015). https://doi.org/10.1016/j.nanoen.2014.09.030
10. N.A. Kyeremateng, T. Brousse, D. Pech, Microsupercapacitors as miniaturized energy-storage components for on-chip electronics. Nat. Nanotechnol. **12**, 7–15 (2017). https://doi.org/10.1038/nnano.2016.196
11. Z.S. Wu, X. Feng, H.M. Cheng, Recent advances in graphene-based planar micro-supercapacitors for on-chip energy storage. Natl. Sci. Rev. **1**, 277–292 (2014). https://doi.org/10.1093/nsr/nwt003
12. M.J. Cima, Next-generation wearable electronics. Nat. Biotechnol. **32**, 642–643 (2014). https://doi.org/10.1038/nbt.2952
13. S. Mohapatra, A. Acharya, G.S. Roy, The role of nanomaterial for the design of supercapacitors. Lat. Am. J. Phys. Educ. **6**, 380–384 (2012)
14. A. Muzaffar, M. B. Ahamed, K. Deshmukh J. Thirumalai, A review on recent advances in hybrid supercapacitors: Design, fabrication and applications. Renew. Sust. Energ. Rev. **101**, 123–145 (2019)
15. A. Nag, S.C. Mukhopadhyay, J. Kosel, Sensing system for salinity testing using laser-induced graphene sensors. Sensors Actuators, A Phys. **264**, 107–116 (2017). https://doi.org/10.1016/j.sna.2017.08.008
16. J.C.E. Helpar, S. Marin, Related papers. Over Rim. **325**, 191–199 (2017). https://doi.org/10.2307/j.ctt46nrzt.12
17. H.D. Yoo, S.D. Han, R.D. Bayliss, A.A. Gewirth, B. Genorio, N.N. Rajput, K.A. Persson, A.K. Burrell, J. Cabana, "rocking-Chair"-type metal hybrid supercapacitors. ACS Appl. Mater. Interfaces **8**, 30853–30862 (2016). https://doi.org/10.1021/acsami.6b08367
18. Poonam, K. Sharma, A. Arora, S.K. Tripathi, Review of supercapacitors: materials and devices. J. Energy Storage **21**, 801–825 (2019). https://doi.org/10.1016/j.est.2019.01.010
19. A. Borenstein, O. Hanna, R. Attias, S. Luski, T. Brousse, D. Aurbach, Carbon-based composite materials for supercapacitor electrodes: a review. J. Mater. Chem. A. **5**, 12653–12672 (2017). https://doi.org/10.1039/c7ta00863e
20. Q. Ke, J. Wang, Graphene-based materials for supercapacitor electrodes—a review. J. Mater. **2**, 37–54 (2016). https://doi.org/10.1016/j.jmat.2016.01.001
21. P. Huang, Age, in which high-power delivery and uptake. Science (80-.), 3720, 3717–3720 (2015)

22. W. Si, C. Yan, Y. Chen, S. Oswald, L. Han, O.G. Schmidt, On chip, all solid-state and flexible micro-supercapacitors with high performance based on MnO_x/Au multilayers. Energy Environ. Sci. **6**, 3218–3223 (2013). https://doi.org/10.1039/c3ee41286e
23. C. Kim, D.Y. Kang, J.H. Moon, Full lithographic fabrication of boron-doped 3D porous carbon patterns for high volumetric energy density microsupercapacitors. Nano Energy **53**, 182–188 (2018). https://doi.org/10.1016/j.nanoen.2018.08.044
24. S. Wang, Z.S. Wu, S. Zheng, F. Zhou, C. Sun, H.M. Cheng, X. Bao, Scalable fabrication of photochemically reduced graphene-based monolithic micro-supercapacitors with superior energy and power densities. ACS Nano **11**, 4283–4291 (2017). https://doi.org/10.1021/acsnano.7b01390
25. Y. Wang, Y.Z. Zhang, D. Dubbink, J.E. ten Elshof, Inkjet printing of δ-MnO_2 nanosheets for flexible solid-state micro-supercapacitor. Nano Energy **49**, 481–488 (2018). https://doi.org/10.1016/j.nanoen.2018.05.002
26. K.H. Choi, J.T. Yoo, C.K. Lee, S.Y. Lee, All-inkjet-printed, solid-state flexible supercapacitors on paper. Energy Environ. Sci. **9**, 2812–2821 (2016). https://doi.org/10.1039/c6ee00966b
27. J. Li, S. Sollami Delekta, P. Zhang, S. Yang, M.R. Lohe, X. Zhuang, X. Feng, M. Östling, Scalable fabrication and integration of graphene microsupercapacitors through full inkjet printing. ACS Nano **11**, 8249–8256 (2017). https://doi.org/10.1021/acsnano.7b03354
28. K. Shen, H. Mei, B. Li, J. Ding, S. Yang, 3D printing sulfur copolymer-graphene architectures for Li-S batteries. Adv. Energy Mater. **8**, 1–6 (2018). https://doi.org/10.1002/aenm.201701527
29. C.J. Zhang, M.P. Kremer, A. Seral-Ascaso, S.H. Park, N. McEvoy, B. Anasori, Y. Gogotsi, V. Nicolosi, Stamping of flexible, coplanar micro-supercapacitors using MXene inks. Adv. Funct. Mater. **28**, 1–10 (2018). https://doi.org/10.1002/adfm.201705506
30. W. Yu, H. Zhou, B.Q. Li, S. Ding, 3D printing of carbon nanotubes-based microsupercapacitors. ACS Appl. Mater. Interfaces **9**, 4597–4604 (2017). https://doi.org/10.1021/acsami.6b13904
31. J.Q. Xie, Y.Q. Ji, J.H. Kang, J.L. Sheng, D.S. Mao, X.Z. Fu, R. Sun, C.P. Wong, In situ growth of Cu(OH) 2 @FeOOH nanotube arrays on catalytically deposited Cu current collector patterns for high-performance flexible in-plane micro-sized energy storage devices. Energy Environ. Sci. **12**, 194–205 (2019). https://doi.org/10.1039/c8ee01979g
32. Y. Wang, Y. Shi, C.X. Zhao, J.I. Wong, X.W. Sun, H.Y. Yang, Printed all-solid flexible micro-supercapacitors: towards the general route for high energy storage devices. Nanotechnology **25** (2014). https://doi.org/10.1088/0957-4484/25/9/094010
33. M.F. El-Kady, R.B. Kaner, Scalable fabrication of high-power graphene micro-supercapacitors for flexible and on-chip energy storage. Nat. Commun. **4** (2013). https://doi.org/10.1038/ncomms2446
34. A. Lamberti, F. Perrucci, M. Caprioli, M. Serrapede, M. Fontana, S. Bianco, S. Ferrero, E. Tresso, New insights on laser-induced graphene electrodes for flexible supercapacitors: tunable morphology and physical properties. Nanotechnology **28** (2017). https://doi.org/10.1088/1361-6528/aa6615
35. J. Ye, H. Tan, S. Wu, K. Ni, F. Pan, J. Liu, Z. Tao, Y. Qu, H. Ji, P. Simon, Y. Zhu, Direct laser writing of graphene made from chemical vapor deposition for flexible, integratable micro-supercapacitors with ultrahigh power output. Adv. Mater. **30**, 1–8 (2018). https://doi.org/10.1002/adma.201801384
36. N. Kurra, B. Ahmed, Y. Gogotsi, H.N. Alshareef, MXene-on-paper coplanar microsupercapacitors. Adv. Energy Mater. **6**, 1–8 (2016). https://doi.org/10.1002/aenm.201601372
37. J. Lin, Z. Peng, Y. Liu, F. Ruiz-Zepeda, R. Ye, E.L.G. Samuel, M.J. Yacaman, B.I. Yakobson, J.M. Tour, Laser-induced porous graphene films from commercial polymers. Nat. Commun. **5**, 5–12 (2014). https://doi.org/10.1038/ncomms6714
38. W. Zhang, Y. Lei, F. Ming, Q. Jiang, P.M.F.J. Costa, H.N. Alshareef, Lignin laser lithography: a direct-write method for fabricating 3D graphene electrodes for microsupercapacitors. Adv. Energy Mater. **8**, 1–9 (2018). https://doi.org/10.1002/aenm.201801840
39. X. Xiao, T. Li, P. Yang, Y. Gao, H. Jin, W. Ni, W. Zhan, X. Zhang, Y. Cao, J. Zhong, L. Gong, W.C. Yen, W. Mai, J. Chen, K. Huo, Y.L. Chueh, Z.L. Wang, J. Zhou, Fiber-based all-solid-state flexible supercapacitors for self-powered systems. ACS Nano **6**, 9200–9206 (2012). https://doi.org/10.1021/nn303530k

40. G. Sun, J. Liu, X. Zhang, X. Wang, H. Li, Y. Yu, W. Huang, H. Zhang, P. Chen, Fabrication of ultralong hybrid microfibers from nanosheets of reduced graphene oxide and transition-metal dichalcogenides and their application as supercapacitors. Angew. Chemie - Int. Ed. **53**, 12576–12580 (2014). https://doi.org/10.1002/anie.201405325
41. C. Yu, Y. Gong, R. Chen, M. Zhang, J. Zhou, J. An, F. Lv, S. Guo, G. Sun, A solid-state fibriform supercapacitor boosted by host-guest hybridization between the carbon nanotube scaffold and MXene nanosheets. Small **14**, 1–7 (2018). https://doi.org/10.1002/smll.201801203
42. Z. Pan, J. Zhong, Q. Zhang, J. Yang, Y. Qiu, X. Ding, K. Nie, H. Yuan, K. Feng, X. Wang, G. Xu, W. Li, Y. Yao, Q. Li, M. Liu, Y. Zhang, Ultrafast all-solid-state coaxial asymmetric fiber supercapacitors with a high volumetric energy density. Adv. Energy Mater. **8**, 1–10 (2018). https://doi.org/10.1002/aenm.201702946
43. Z. Cai, L. Li, J. Ren, L. Qiu, H. Lin, H. Peng, Flexible, weavable and efficient microsupercapacitor wires based on polyaniline composite fibers incorporated with aligned carbon nanotubes. J. Mater. Chem. A. **1**, 258–261 (2013). https://doi.org/10.1039/c2ta00274d
44. W. Shao, M. Tebyetekerwa, I. Marriam, W. Li, Y. Wu, S. Peng, S. Ramakrishna, S. Yang, M. Zhu, Polyester@MXene nanofibers-based yarn electrodes. J. Power Sources **396**, 683–690 (2018). https://doi.org/10.1016/j.jpowsour.2018.06.084
45. L. Hu, H. Wu, Y. Cui, Printed energy storage devices by integration of electrodes and separators into single sheets of paper. Appl. Phys. Lett. **96**, 94–97 (2010). https://doi.org/10.1063/1.3425767
46. G. Zheng, L. Hu, H. Wu, X. Xie, Y. Cui, Paper supercapacitors by a solvent-free drawing method. Energy Environ. Sci. **4**, 3368–3373 (2011). https://doi.org/10.1039/c1ee01853a
47. B. Yao, L. Yuan, X. Xiao, J. Zhang, Y. Qi, J. Zhou, J. Zhou, B. Hu, W. Chen, Paper-based solid-state supercapacitors with pencil-drawing graphite/polyaniline networks hybrid electrodes. Nano Energy **2**, 1071–1078 (2013). https://doi.org/10.1016/j.nanoen.2013.09.002
48. Z. Weng, Y. Su, D.W. Wang, F. Li, J. Du, H.M. Cheng, Graphene-cellulose paper flexible supercapacitors. Adv. Energy Mater. **1**, 917–922 (2011). https://doi.org/10.1002/aenm.201100312
49. L. Yuan, B. Yao, B. Hu, K. Huo, W. Chen, J. Zhou, Polypyrrole-coated paper for flexible solid-state energy storage. Energy Environ. Sci. **6**, 470–476 (2013). https://doi.org/10.1039/c2ee23977a
50. K. Jost, C.R. Perez, J.K. McDonough, V. Presser, M. Heon, G. Dion, Y. Gogotsi, Carbon coated textiles for flexible energy storage. Energy Environ. Sci. **4**, 5060–5067 (2011). https://doi.org/10.1039/c1ee02421c
51. L. Bao, X. Li, Towards textile energy storage from cotton T-shirts. Adv. Mater. **24**, 3246–3252 (2012). https://doi.org/10.1002/adma.201200246
52. L. Bao, J. Zang, X. Li, Flexible Zn_2SnO_4/MnO_2 core/shell nanocable-carbon microfiber hybrid composites for high-performance supercapacitor electrodes. Nano Lett. **11**, 1215–1220 (2011). https://doi.org/10.1021/nl104205s
53. J.A. Lee, M.K. Shin, S.H. Kim, H.U. Cho, G.M. Spinks, G.G. Wallace, M.D. Lima, X. Lepró, M.E. Kozlov, R.H. Baughman, S.J. Kim, Ultrafast charge and discharge biscrolled yarn supercapacitors for textiles and microdevices. Nat. Commun. **4** (2013). https://doi.org/10.1038/ncomms2970

Mesoporous Carbon for Supercapacitors

Hongzhen He, Yiyang Liu, Paul R. Shearing, Guanjie He, and Dan J. L. Brett

Abstract With the further advancement of electrification, supercapacitors (SCs) have garnered numerous attention as promising electrochemical energy storage (EES) devices, due to their favourable characteristics such as, high energy density, ultrahigh power density and long cycling stability. To fully exploit their potential as a platform for efficient energy storage devices, it is critical to gain a more in-depth understanding of the relationship between electrochemical performance and materials. Mesoporous carbon has arouse considerable interests as potential material for energy-related applications results from its large surface area, fast mass/charge transfer kinetics, and high abundance of active sites. In this chapter, we first provide a basic understanding of the classification of supercapacitors and the corresponding working principles. Then, the mainstream synthetic route of mesoporous carbon will be introduced, including templating and template-free methods. Next, an in-depth discussion of the representative mesoporous carbon for SCs is provided. Finally, insights into the major challenges and effective strategies for future developments are summarized.

Keywords Supercapacitors · Fundamental theories · Mesoporous carbon · Material synthesis · Electrode materials

H. He and Y. Liu: Authors have equal contributions.

H. He · Y. Liu · P. R. Shearing · G. He (✉) · D. J. L. Brett
Electrochemical Innovation Lab (EIL), Department of Chemical Engineering, University College London (UCL), London WC1 7JE, UK
e-mail: g.he@ucl.ac.uk

D. J. L. Brett
e-mail: d.brett@ucl.ac.uk

G. He
School of Chemistry, University of Lincoln, Brayford Pool, Lincoln LN6 7TS, UK

P. R. Shearing · D. J. L. Brett
The Faraday Institution, Quad One, Becquerel Avenue, Harwell Campus, Didcot OX11 ORA, UK

S. Thomas et al. (eds.), *Nanostructured Materials for Supercapacitors*,
Advances in Material Research and Technology,
https://doi.org/10.1007/978-3-030-99302-3_7

1 Introduction

As energy demands continue to grow, traditional energy sources, such as petroleum, natural gas and coal, are harder to meet human's ambition for carbon neutrality and net-zero emission. Therefore, efficient energy conversion and storage has become a grand challenge to society. Researchers and enterprises currently focus their efforts on developing new electrochemical energy storage (EES) devices, including secondary batteries, fuel cells, and supercapacitors (SCs). Secondary EES devices represented by Li-ion batteries (LIBs) generally have a high energy density (180 ~ 340 Wh kg^{-1}) and long durability, which dominates the EES market. However, their low power density (100 ~ 300 W kg^{-1}), high cost ($140 per kWh), limited raw material reserves and safety issues hindered their further development.

Although traditional capacitors could satisfy the high-power density demands, their low specific capacitance ($\leq$ 2.7 F g^{-1}) and energy density (0.01 ~ 0.3 Wh kg^{-1}) retards the further deployments. Supercapacitors (SCs) are the devices that possess ultrahigh power density (5 ~ 30 kW/kg), high energy conversion efficiency and long cycling durability (>100,000 cycles), which have become one of the most promising EES devices for high-power applications [4]. The electrochemical performance and characteristics of SCs sit between batteries and conventional capacitors; therefore, they have a much higher energy density (28 Wh kg^{-1}) than conventional capacitors. As illustrated in Fig. 1, it can be used as a starting source for vehicles and a power balance source for lifting devices. Additionally, it can be used as a source of traction energy for hybrid cars, internal combustion engines, trackless vehicles, and other equipment. Up to now, a wide range of materials have been reported as the electrodes

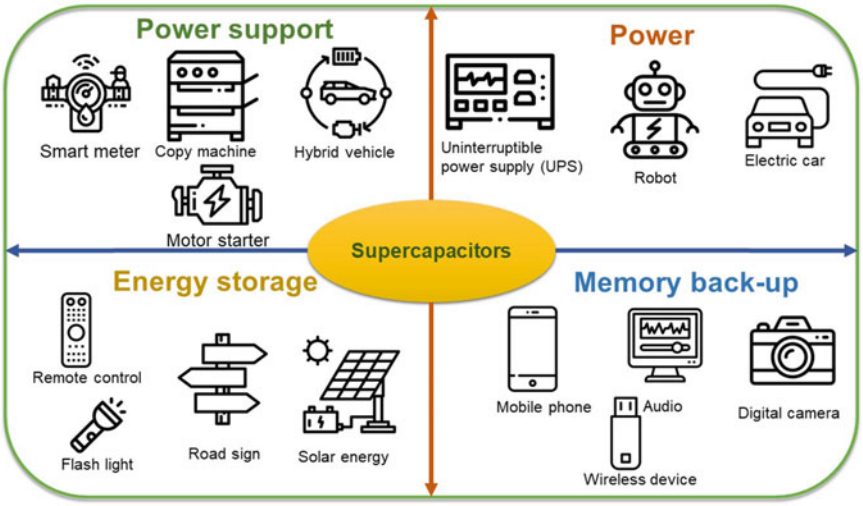

Fig. 1 Applications of supercapacitors

for SCs, such as carbon materials, covalent organic backbones (COFs), metal–organic backbones (MOFs), conductive polymers, transition metal compounds [20].

Mesoporous carbon materials have been widely investigated and used in many fields, including adsorption, separation, catalysis and EES applications. Mesoporous carbon materials are distinguished from conventional carbon materials by their controlled and superior properties in terms of synthetic routes, tunable pore structures and surface area. Compared to macroporous (> 50 nm) and microporous (<2 nm) carbon, the mesoporous (2 ~ 50 nm) carbon possess a more suitable pore size for application in SCs: the macroporous carbon can not provide a high specific surface area; while the micropores are hard for electrolyte penetration and diffusion. Despite the excellent performance offered by mesoporous carbon in energy-oriented applications, there are several challenges for their practical application in SCs. Firstly, it is challenging to achieve mass-production for mesoporous carbon. Secondly, scalable synthetic solutions with optimised structural and compositional parameters remain critical. Until now, very few control methods for mesoporous carbon synthesis have been reported, particularly for spherical materials with tunable pore size and hydrophilicity. Thirdly, modification of the surface of mesoporous carbon remains challenging.

To provide an informative and inspiring understanding for researchers in the mesoporous carbon and SC-related fields, this Chapter will provide an informative introduction and discussion covering: (a) the working mechanisms of SCs (Sect. 2); (b) synthesis route of mesoporous carbon (Sect. 3); (c) representative mesoporous carbon electrodes for SCs (Sect. 4); (d) conclusion and perspectives (Sect. 5).

2 Working Principle of SCs

The earliest capacitors date back to the invention of the ‘Leiden’ bottle by Prof. Pieter Van Musschenbroek at Leiden University in the Netherlands in 1746. A typical Leiden bottle is a glass container covered inside and outside with conductive metal foil to act as a pole plate. The bottle’s top end is connected to a circular electrode, while the bottom end is connected to the inner metal foil or water via a conductor (usually a metal locking chain). A vintage ‘Layden bottle’ can achieve a high voltage of 20 ~ 60 kV and a low specific capacitance of ~ 1 nF (per pint of volume).

In 1853, the German physicist Helmholtz proposed a theoretical model of an interfacial double layer: under the action of a certain voltage, the interface between the electrode material and the electrolyte solution generates two layers of charges of the same quantity and opposite charges, thus forming a double layer. In 1957, Becker from General Motors prepared a small capacitor with porous carbon electrodes based on the double layer capacitance theory mentioned above, and named it a “supercapacitor”, which was first developed and brought to market by SOHIO in 1969. The technology was subsequently transferred to NEC Japan and commercialised as an aqueous high-capacitance capacitor in battery starting systems for electric vehicles.

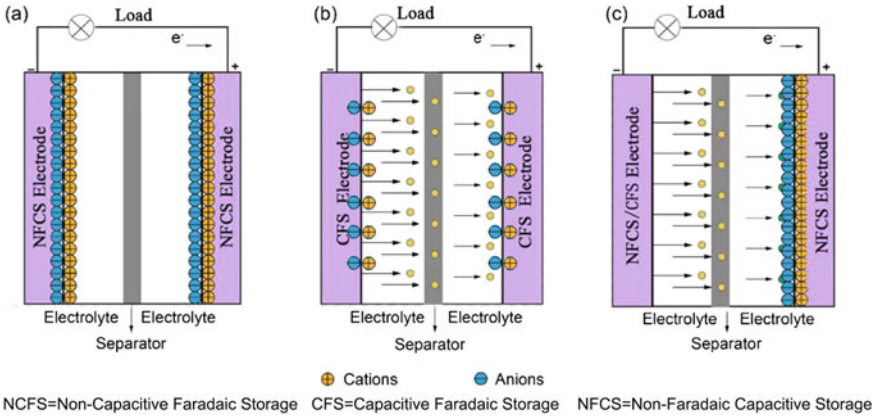

Fig. 2 Schematic illustration of **a** EDLC, **b** pseudocapacitor, and **c** Hybrid SC

Since then, SCs have attracted the attention of many countries, and comprehensive research has been carried out. In 1971, Sergio Trasatti and others discovered the outstanding capacitive properties of RuO_2, which led to a boom in the development of pseudocapacitors based on metal oxide electrodes. After 1975, Brian E. Conway carried out RuO_2-related research and commercial development attempts. Since then, pseudocapacitors with RuO_2 electrodes have been used in military applications. A wide range of inexpensive transition metal (hydro)oxides, heteroatom-doped carbon, conductive polymers, colvalent organic frameworks (COFs) and other materials have been extensively investigated since the 1990s. As shown in Fig. 2, SCs consist of cathodes, anodes, electrolytes and separators. SCs could be classified as three types depending on the charge and energy storage mechanisms: electric double-layer capacitors (EDLCs), pseudocapacitors, and hybrid SCs.

2.1 EDLCs

The working principle of an EDLC is shown in Fig. 2a. Under the action of an electric field, an equal number of anions and cations in the electrolyte move towards the cathodes and anodes, respectively; this will create an electric potential difference and an EDL between the electrode and the electrolyte. After the removal of this electric field, the layers and voltage can be stabilized due to the anisotropic attraction of the charges. After connecting EDLC to the external circuit, the charged ions adsorbed on the two electrodes will move directionally until the electrolyte becomes electrically neutral again.

The relationship among total capacitor capacitance is C_T and capacitance of both electrodes (C_1 and C_2) can be expressed by the formula:

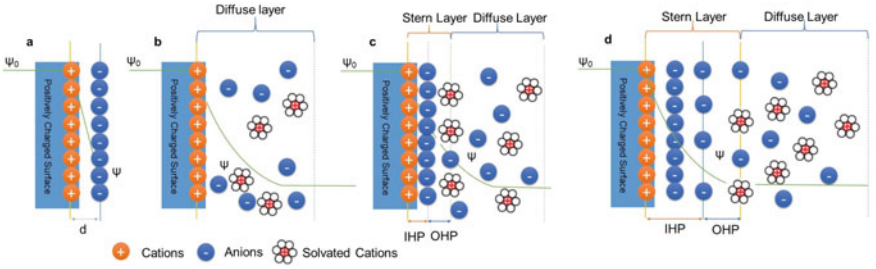

Fig. 3 Schematical diagram of EDL models. **a** Helmholtz model; **b** Gouy-Chapman (G-C) model; **c** Gouy-Chapman-Stern (G-C-S) model; **d** modified G-C-S model

$$\frac{1}{C_T} = \frac{1}{C_1} + \frac{1}{C_2} \tag{1}$$

Since 1853, numerous theories and models have been developed, the most notable ones include Helmholtz model, Gouy-Chapman (G-C) model, and Gouy-Chapman-Stern (G-C-S) model. The central concept of the Helmholtz model's is that opposite charges are distributed equally on both sides of the interface; additionally, this structure can be compared to a flat capacitor (Fig. 3a). Thus, Eq. (2) can be used to determine the unilateral charge density ($C \cdot m^{-3}$):

$$C = \frac{\varepsilon_r \varepsilon_0}{d} A \tag{2}$$

where C is the capacitance value, ε_r and ε_0 are the vacuum dielectric constant and the electrolyte dielectric constant, respectively; d is the effective thickness of the EDL; A is the specific surface area of the electrode material. Then, the capacitor capacitance (C_d) can be determined by:

$$C_d = \frac{\partial \sigma}{\partial V} = \frac{\varepsilon_r \varepsilon_0}{d} \tag{3}$$

It should be noted that C_d is a fixed value in the three formulas; however, C_d is actually affected by a series of factors, including relative potential, concentration of electrolyte, etc. Therefore, incorporating a diffuse layer model, The G-C model (Fig. 3b) was proposed. When the potential difference between two sides of the interface is large, more ions are compressed near the electrode; however, when the electrolyte concentration is high, the ions can also achieve charge equilibrium with the electrodes in a small space. In the G-C model, Helmholtz model's effective thickness (d) is converted into a variable, thereby allowing for a more accurate interpretation of the trend of C_d. Nevertheless, the C_d prediction in G-C model has several major shortages: (a) at both ends of the curve, C_d approaches infinity and contradicts actual tests; (b) could be significantly higher than the measured value; (c) low accuracy for capacitors with highly charged DLs. These deviations are inevitable since the

charges in G-C model are regarded as the mass points, which will be infinitely close to the surface of the electrodes under a large potential difference. Therefore, the distance between positive and negative charges will approach zero, which lead to a C_d approaching infinity [23].

Later on, based on G-C models, Otto Stern take ion size into condieration, and proposed the G-C-S model (Fig. 3c). At the electrode–electrolyte interface, the G-C-S model predicts two ion distribution regions: Helmholtz layer and Gouy-Chapman diffusion layer. The entire double-layer (C_{dl}) can be determined by capacitance generated in the diffusion layer (C_{diff}) and stern layer (C_H):

$$\frac{1}{C_{dl}} = \frac{1}{C_H} + \frac{1}{C_{diff}} \tag{4}$$

C_{dl} is always less than C_H and C_{diff}, according to Eq. (4). When the potential difference is small, C_{diff} has a negligible effect on C_{dl} and has a V-shaped curve versus potential difference; when the potential difference is large, C_{diff} has a large value and thus has a negligible effect on C_{dl}. The value of C_{dl} approaches C_H in this case. Nevertheless, there are serval drawbacks of the the G-C-S model: (a) the ions in the electrolyte will be surrounded by solvent ions, forming solvated ions; and (b) if the adsorption force at the interface exceeds the electrostatic force, even ions with similar charges will be stable at the interface.

David C. Grahame proposed a modification to the G-C-S model in 1947, arguing that certain ions or uncharged substances could penetrate the Stern layer. When approaching the electrode in the modified G-C-S model, the term "specifically absorbed ions" refers to the ions losing their solvation shell and coming into direct contact with the electrode. As illustrated in Fig. 3d, the modified model predicted the presence of three regions: the inner Helmholtz plane (IHP), the outer Helmholtz plane (OHP), and the diffuse layer. The IHP denotes the distance between specifically absorbed ions and the OHP denotes the distance between non-specifically absorbed ions [3]. Despite the increasing precision and sophistication of these theories and models, the debate and further exploration still exist.

2.2 Pseudocapacitors

The charge and energy storage mechanism of pseudocapacitors relies on the underpotential deposition on the surface or in the bulk phase of electrode materials with electrochemical activity in two or quasi-two dimensions. This results in highly reversible chemisorption or redox reaction that generates a capacitance related to the electrode charging potential. The voltage of this electrode system varies linearly with the amount of charge transferred and exhibits a capacitive characteristic, hence the term "pseudocapacitor", as a complementary form of EDLCs. Although they are not electrostatic in nature, they exhibit similar electrochemical properties to EDLC, such as cyclic voltammetry and charge/discharge curves. In general, pseudocapacitors tend

to have superior specific capacitance than traditional EDLCs. Nevertheless, with the occurrence of redox reactions during the cycling, the bulk phase of the active materials or the electrolyte composition is altered, which deteriorate the electrochemical stability of pseudocapacitors [5, 15, 18]. Take metal oxides as an example, the charging and discharging reaction process in an aqueous electrolyte is as follows:

When the electrolyte is acidic:

$$MO_x + H^+ + e^- \leftrightarrow MO_{x-1}(OH)$$

When the electrolyte is alkaline:

$$MO_x + OH^- - e^- \leftrightarrow MO_x(OH)$$

Alternatively, the pseudo-capacitance effect can be increased by adding ions with redox activities to the electrolyte [6]. Ren et al. reported a pseudocapacitor using a porous nanoflower polyaniline (PANI) electrode and redox-active electrolyte (1 M H_2SO_4 + 0.8 M Fe^{2+}/Fe^{3+}), which demonstrates a high specific capacitance of 1062 F g^{-1} (2 A g^{-1}) and remarkable capacitance retention of 93% at 5 A g^{-1} over 10,000 cycles (Ren et al. 2017). There are two redox systems in the as-assembled SC: (a) as shown in Eqs. (5) and (6), the conjugated double bonds in the PANI networks (P_m, m is the polymerization degree); (b) as shown in Eq. (7), the active Fe^{2+}/Fe^{3+} redox couples.

$$P_m^{x+}A_x^- + xe^- \Leftrightarrow P_m + xA^- \tag{5}$$

$$P_m^{y+}C_y^+ + ye^- \Leftrightarrow P_m + yC^+ \tag{6}$$

$$Fe^{3+} + e^- \Leftrightarrow Fe^{2+} \tag{7}$$

2.3 Hybrid SCs

The hybrid SCs combine the electrodes with different charge and energy storage mechanisms (Faradaic, capacitive, and capacitive-Faradaic processes), and increase the device energy density to 15–30 Wh kg^{-1}. The design of the components determines whether hybrid SCs are symmetrical or asymmetrical. When two separate electrodes comprised of different materials are combined in a hybrid supercapacitor, it exhibits better electrochemical behaviour than single electrodes. The hybrid technology preserves the level of cycle stability and affordability that has been a limiting factor in pseudocapacitor. The symmetric hybrid supercapacitor is made up of two same SC electrodes; while the asymmetric hybrid SC is made up of two different electrodes.

3 Synthesis of Representative Mesoporous Carbon

Numerous synthetic methodologies have been proposed, making it possible to prepare mesoporous carbon with various structures and morphologies. These methodologies could be classified as two categories: templating and template-free methods.

3.1 Templating Method

The templating method is the most widely studied methodology to prepare mesoporous carbon. Generally, the direct carbonisation of precursors is challenging to form mesoporous carbon with high surface area, which leads to limited electrochemical performance. In the templating methods, carbon is deposited on the surface of the template, thus forming a composite material, which can effectively generate carbon materials with desired structures and morphologies after removing the templates. In general, the templating method could be further classified as three types: hard templating, soft templating and hybrid templating.

3.1.1 Hard-Templating Method

Insoluble Templates

Although many metal/non-metal oxide and salt templates (*e.g.*, Al_2O_3, ZnO, MgO, and SiO_2) are insoluble in water, they could be removed under specific solutions. With a high melting point and exceptional thermal/chemical/mechanical stability, oxide and insoluble salt templates preserve their original structures and morphologies at elevated temperatures. As a result, the space occupied by the template is retained following its removal. Simultaneously, the morphology and structure of the resultant carbon substance are opposed to those of the templates. For instance, Seo and colleagues synthesised a mesoporous carbon using furfuryl alcohol (FA) and acidified mesoporous silica impregnated with phosphoric or sulphuric acid as precursors. This work avoided the formation of undesired carbon by using a weak acid to catalyze and slow down the FA polymerisation [10].

Soluble Templates

In contrast to insoluble templates, soluble templates can be removed directly with water, thus avoiding harmful reagents. In addition, soluble templates could be recycled during the synthesis process. De-templated wastewater could be processed to a suitably concentrated template solution that can be re-involved in the synthesis.

Lee's group prepared a mesoporous carbon with uniform pores (~10 nm) by using a mesoporous aluminosilicate foam template and in situ polymerisation of phenolic resin. Strong acid catalytic sites for the polymerisation of phenol and formaldehyde are created by impregnating aluminium into the silicate backbone. Several different mesoporous aluminium silicate foams with different cell and window sizes have been synthesised as templates for many other mesoporous carbon foams. For example, using aluminium silicate foams with 30 nm cells and 14 nm windows as a template, a mesoporous carbon foam was obtained. The mesoporous carbon foam possess an even mesopore size of approximately 3.5 nm, which was achieved by removing the aluminosilicate template [7].

Ice Templating Method

Distinct from other hard templating methods, the ice template will be removed before the carbonisation of the precursors. The ice template indirectly influences the carbon material structures via altering the structure and composition of the carbon precursor, whereas the other hard templates directly influence the carbon material structure. In general, a typical ice templating comprises three phases. Firstly, the aqueous carbon precursors are swiftly frozen and crystallised in the first stage, where water condenses into ice over time. The second phase involves sublimating the ice crystals directly into water vapour by freeze-drying, resulting in a loose and porous structure. Carbonisation of the freeze-dried carbon precursors is the third phase. Although ice templates can significantly increase the surface area, it is challenging to regulate the shape and size of the ice crystals at the nanoscale. Therefore, additional procedures, typical activation or porogenic agents, are required to control the nanostructure of carbon aerogels.

3.1.2 Soft Templating Method

Soft templates are usually the amphiphilic molecules that can form micelles by the self-assembly process. Then, the micelles could be disintegrated at high temperatures, thus forming pores in the space they occupy. Soft-templating has been widely used to synthesise various mesoporous materials, including zeolites, silica, inorganic metal oxides, and mesoporous carbons. To successfully synthesize the mesoporous carbon precursor by the soft template method, the following three requirements must be met: (a) can form nanostructures by self-assembly; (b) consists of at least one component that can stably form pores at high temperatures; (c) consists of at least one kind of carbon-producing components. Currently, only a few materials meet these requirements. Moriguchi et al. successfully synthesised an ordered mesoporous carbon, through the ageing of the intermediate phase assembled by phenolic resin and cetyltrimethylammonium bromide (CTAB) as a template. The lamellar, hexagonal, and disordered intermediate phases were synthesised by varying the ratio of phenol to CTAB from 1:1 to 6:1 [16]. Li's group has also investigated the use

of CTAB as a soft template for the synthesis of mesoporous carbon [9]. The carbon precursor they used was a solubilized pitch material with negatively charged terminal groups; this micelle-templating strategy resulted in forming carbon materials with a vesicular and hierarchical structure. Zhao et al. also reported another method to synthesise mesoporous carbon materials using alkyl chain-based (Brij) surfactants. Although highly ordered mesophases were obtained, the carbonised materials lacked mesoporous structures. This is because the residual carbon from surfactants used can occupy the mesopore-generating spaces. Therefore, it is recommended to remove the surfactant molecules prior to carbonization via solvent extraction [14].

3.2 Template-Free Method

3.2.1 Pyrolysis Route

The traditional mesoporous carbon synthesis route (*e.g.,* chemical vapour deposition and arc discharge) are generally cumbersome and expensive, limiting their practical applications. However, the rapid pyrolysis of biomass into functionalised mesoporous carbon via thermochemistry is an environmentally friendly approach without air pollution generated from open burning. Therefore, Yu et al. proposed a scalable "green" method (Fig. 4) for the synthesis of nanofibers/mesoporous carbon composites via pyrolysis of Fe(iii)-preloaded biomass, which is controllable through temperature adjustment and the addition of the $FeCl_3$ catalyst. In an in situ CVD process, the combined catalytic action of Fe and Cl species were able to effectively catalyse the growth of carbon nanofibers on mesoporous carbon and the formation of magnetic nanofibers/mesoporous carbon composites. Additionally, the as-prepared

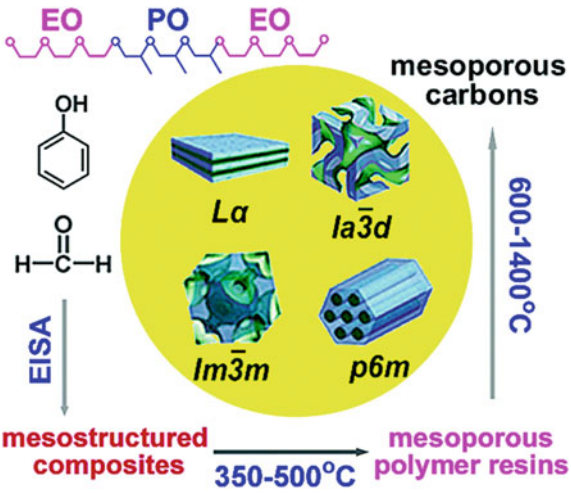

Fig. 4 Schematical illustration of mesoporous carbon materials synthesis using synthetic polymer precursor (Adapted with permission from Reference [14], Copyright (2006), ACS Publications)

material could be directly used as electrode materials for electrochemical energy storage without further separation and demonstrated a high specific capacitance of (128 F g^{-1} at 2 mV s^{-1}), remarkable cycling durability (98% capacitance retention over 10,000 cycles at 0.5 A g^{-1} [12].

3.2.2 Natural Biomass Precursors

Biomass is an ideal carbon precursor due to its porous structure, which simplifies the synthesis steps and reduces manufacturing costs. Also, the use of horticultural waste addresses solid waste management, lowers raw material costs, and addresses environmental concerns. Mesoporous carbon can be synthesised by high-temperature pyrolysis and physical/chemical activation of natural biomass. Currently, a variety of biomass precursors have been widely investigated, such as cellulose, chitin and lignin.

4 Mesoporous Carbon for Supercapacitors

4.1 Mesoporous Carbon (Pure Carbon)

Due to several favourable characteristics such as ease of synthesis, low cost and high electrical conductivity, activated carbon is widely used as the electrode material in EES devices. However, its low effective specific surface area hinders the practical deployment due to the presence of randomly connected micropores, which are difficult for electrolyte ions to access. To improve their performance, researchers have explored mesoporous carbon as electrodes for SCs. For example, mesoporous carbon synthesised by the carbonisation of a mixture of polyvinyl alcohol and inorganic salts exhibited a specific capacitance of 180 F g^{-1} at 100 mA cm^{-2} in H_2SO_4 [2]. The size and content of the mesopores will affect a wide range of electrochemical properties, including specific capacitance, energy/power density, and others. Wang et al. first prepared a mesoporous carbon nanofiber by restricting self-assembled triblock copolymers with soluble phenolic resins within the channels of anodic Al_2O_3 membranes. SEM and TEM observations revealed hexagonally arranged mesoporous channels coiled concentrically around the carbon nanofibers' longitudinal axis. The as-prepared high specific surface area (>1424 m^2 g^{-1}) carbon nanofiber was used as electrode materials in SCs with KOH and ethylene carbonate/diethyl carbonate (EC/DEC) electrolytes, which demonstrates constant value in the range of 152 F/g in sweep rates on 50 mV/s [19]. Pure mesoporous carbon generally possesses poor electrical conductivity and low capacitance, which cannot be used directly as SC electrodes. One effective strategy is to dope heteroatoms into mesoporous carbon, which will be discussed in the following parts.

4.2 N-doped Mesoporous Carbon

The presence of electron donor N in the mesoporous carbon can provide more active sites for fast redox reactions on the electrode surface, thus enhancing a variety of chemical/physical properties including wettability, electrical conductivity, surface affinity for electrolytes, etc.[10]. As illustrated in Fig. 4, Liu and colleagues proposed a template-catalyzed in situ polymerization and co-assembly method using urea formaldehyde (UF) as the precursor and the nitrogen source and polystyrene-block poly(acrylic acid) (PS-b-PAA) as a catalyst. The UF precursors can interact selectively with partially ionised poly(acrylic acid) segments via hydrogen bonding and electrostatic interactions, followed by in situ polymerisation of the UF resin/PS-b-PAA composite catalysed by acidic PAA chain segments. The resulting N-doped mesoporous carbon has a high N content of 19 wt%, a homogeneous and large pore size (9.5–17.2 nm), and a high surface area (458–476 m^2g^{-1}). Owning to these favourable properties, the as-fabricated SC exhibits a high specific capacitance of 252 $F\,g^{-1}$ at 0.2 $A\,g^{-1}$ [13]. In addition, Wu et al. developed a facile synthetic route for the N-doped ordered nanoporous carbon (NONCs) based on the in situ coating of polydopamine on the surface of SBA-15 pores. The carbonisation of polydopamine/silica nanocomposites in N_2 followed by removal of the silica template resulted in the formation of NONC materials with a BET surface area of 1013 m^2g^{-1} [11]. However, the poor crystallinity of the material deteriorated its electrical conductivity. To solve this issue, Yuan et al. synthesised a graphite-nitride ordered mesoporous carbon (G-OMC) by using mesoporous NiO as the template/catalyst and dopamine as the precursor. G-OMC possesses a higher degree of graphitisation than those prepared with dopamine and pure SBA-15, mainly due to the catalytic graphitisation induced by the NiO additives [22] (Fig. 5).

4.3 Other Non-Metal Doped Mesoporous Carbon Materials

Incorporating both N and other dopants (*e.g.*, S, P, F and B) in the carbon framework is becoming increasingly popular in the carbon research community due to the synergistic effects of co-doped atoms. For each application, the appropriate combination of co-dopants should be carefully chosen. For instance, the swollen carbon interlayer produced by S doping facilitates the adsorption of larger electrolyte ions; the highly electronegative F functional group significantly enhances polarisation and refines the pore structure/surface; doping P into carbon can modulate the formation of various N configurations [17]. While some literature suggests that surface co-doping has beneficial synergistic effects on capacitive properties, the underlying mechanisms require further investigation.

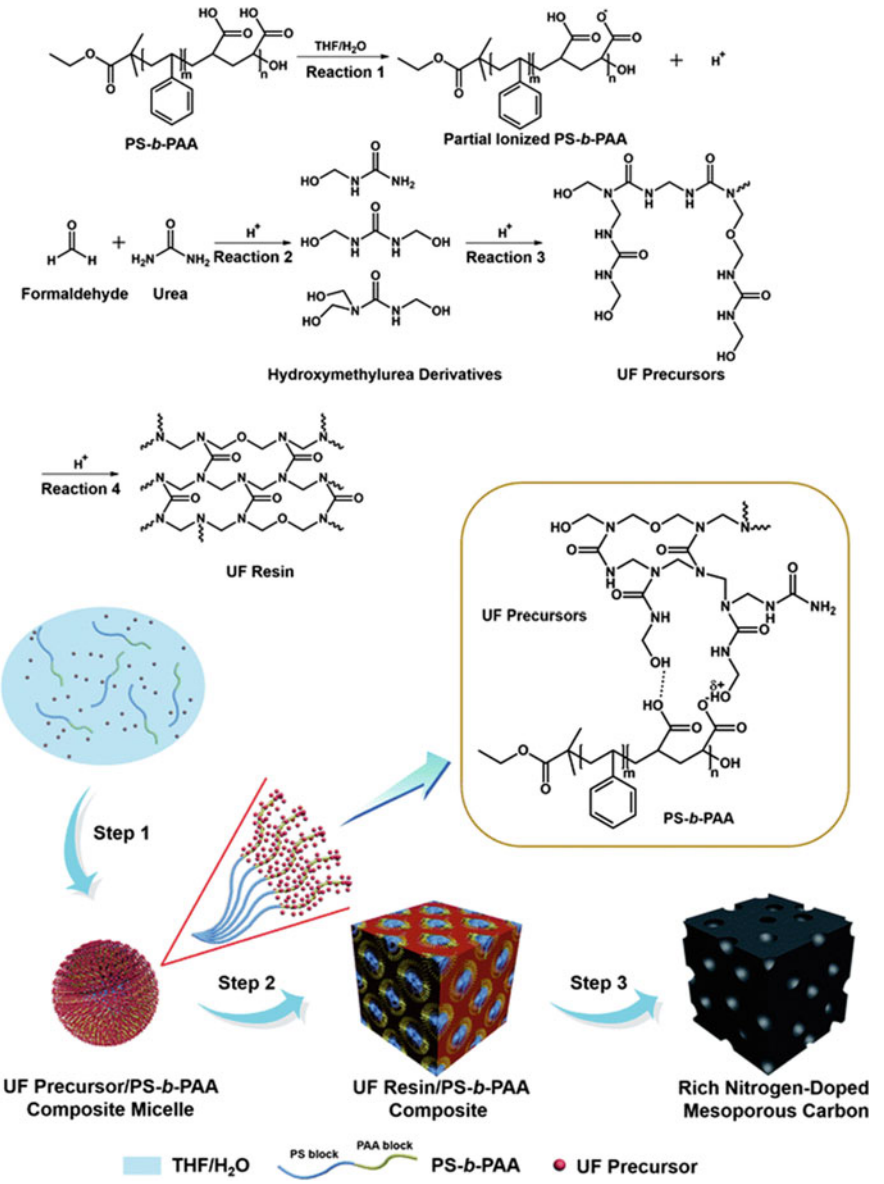

Fig. 5 The synthesis process of the abundant N-doped mesoporous carbon via in situ polymerization and co-assembly catalysed by a template (Adapted with permission from Reference [13], Copyright (2018), RSC Publications)

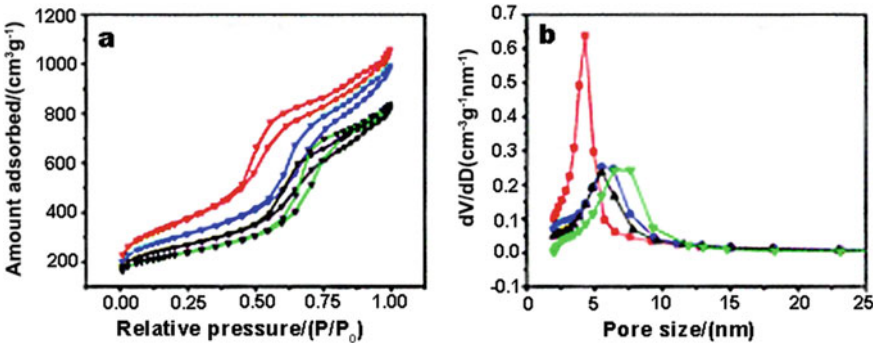

Fig. 6 **a** Nitrogen adsorption–desorption isotherms of ordered mesoporous carbon (OMC, red line), B-doped OMCs-1 (blue line), B-doped OMCs-2 (black line), and B-doped OMCs-3 (green line), **b** Pore size distributions of OMCs, B-doped OMCs-1, B-doped OMCs-2, and B-doped OMCs-3 (Adapted with permission from Reference [1], Copyright (2013), RSC Publications)

4.3.1 Boron-Doped Mesoporous Carbon

B doping will affect the electronic and electrical properties of the carbon nanostructures. As well as the thermal stability in the presence of nitrogen or air after substitution in the graphite skeleton. Coupling soft template and hydrothermal techniques, the evaporation-induced self-assembly (EISA) method using resorcinol and boric acid as precursors and Pluronic F127 as soft template was used to prepare B-OMC. However, the nitrogen adsorption data from three BOMCs in Fig. 6 demonstrate that the surface area and pore volume decrease as the B content increases. When B is incorporated into the OMC framework, micropores are lost, resulting in a decrease in the specific surface area and pore volume.

4.3.2 Phosphorus-Doped Mesoporous Carbon

Phosphorus is a member of the V group element in periodic table and shares the same number of valence electrons as nitrogen. Zhang's laboratory reported an ultra-convenient and energy-efficient microwave irradiation method for the fabrication of phosphorus-doped mesoporous carbon under ambient atmosphere. The prepared phosphorus-doped mesoporous carbon exhibits a high specific surface area (up to 2055 m^2g^{-1}), a large pore volume (up to 2.73 $cm^3\ g^{-1}$) and good electrical conductivity. It also has a specific capacitance of up to 210 F g^{-1}, maintains a capacitance of over 201 F g^{-1} even at high current densities of 20 A g^{-1} and achieves a capacitance retention rate of 97.39% after 10,000 charge/discharge cycles. Comparative studies showed that similar morphologies were obtained by microwave irradiation and conventional pyrolytic carbonisation, but a more developed porosity and higher

degree of graphitisation was obtained under microwave irradiation. The carbonisation process under microwave irradiation is completed in 1–3 min, whereas conventional pyrolysis typically takes more than 2 h at temperatures above 600 °C. No rapid increase in surface oxygen content was observed, even when produced under ambient atmosphere. Such samples have the potential to become cost-effective and high-performance electrode materials for commercial SCs [8].

4.4 Hierarchical Porous Carbon (HPC)

When used as electrode materials in EES devices, HPCs exhibit a multimodal pore size distribution of micro-, meso-, and/or macropores, resulting in a high electrochemically accessible surface area and mass transfer rate. Typically, HPCs are prepared using templating techniques or a combination of templating and activation techniques. After combination and chemical activation, Xing's team synthesised a series of HPCs. The pore structure analysis revealed that micropores could be generated in a controlled manner within the mesoporous walls of the mesoporous carbon during the activation process. The prepared HPCs exhibit better capacitive properties than the hard template ordered mesoporous carbon, maintaining a high capacitance of 180 F g^{-1} at high frequencies of 1 Hz. This can be attributed to the additional capacitance due to the generated micropores [21].

5 Conclusion and Perspective

SCs are promising EES devices to complement or even replace LIBs in various applications. This results from their favourable characteristics, including high power density, excellent cycle life, etc. This chapter presents and discusses the working principles, representative synthesis routes and optimisation of mesoporous carbon materials for SCs. Although many enlightening researches have been reported, more efforts are needed to bridge the large gap between laboratory-based research and commercial applications. Although these measurements are made using adsorption and theoretical models, the electrode pore structure is far more complex. Charge shielding, ion rearrangement, and sparse ionic pores will affect capacitance and ion dynamics. Therefore, more advanced characterization techniques such as micro/nano computerized tomography (CT) are recommended for further investigations. Also, future research could focus on improving carbon/electrolyte compatibility by adjusting micropore diameter/shape to accommodate larger electrolyte ions, adding meso/macropore pathways to transfer viscous media, and doping pseudo-active sites to improve interfacial interactions. For redox reactions and phase transitions, the improved device architecture must optimise carbon/electrolyte compatibility. Although challenges remain, we believe high-power, long-runtime

carbon-based supercapacitors will be developed soon for commercial applications in electronics and other fields.

Acknowledgements The authors would like to thank the Engineering and Physical Sciences Research Council (EPSRC, EP/533581/1), STFC Batteries Network (ST/R006873/1), RSC Mobility Grant (M19-7656) and Faraday Institution (EP/S003053/1) Degradation project (FIRG001) for financial support.

References

1. X. Bo, L. Guo, Ordered mesoporous boron-doped carbons as metal-free electrocatalysts for the oxygen reduction reaction in alkaline solution. Phys. Chem. Chem. Phys. **15**, 2459–2465 (2013). https://doi.org/10.1039/c2cp43541a
2. J.A. Fernández, T. Morishita, M. Toyoda, M. Inagaki, F. Stoeckli, T.A. Centeno, Performance of mesoporous carbons derived from poly(vinyl alcohol) in electrochemical capacitors. J. Power Sources **175**, 675–679 (2008). https://doi.org/10.1016/j.jpowsour.2007.09.042
3. D.C. Grahame, The electrical double layer and the theory of electrocapillarity. Chem. Rev. **41**, 441–501 (1947). https://doi.org/10.1021/cr60130a002
4. G. He, M. Ling, X. Han, D.I. Abou El Amaiem, Y. Shao, Y. Li, W. Li, S. Ji, B. Li, Y. Lu, R. Zou, F. Ryan Wang, D.J.L. Brett, Z. Xiao Guo, C. Blackman, I.P. Parkin, Self-standing electrodes with core-shell structures for high-performance supercapacitors. Energy Storage Mater. **9**, 119–125 (2017). https://doi.org/10.1016/j.ensm.2017.07.005
5. L. Hou, Y. Shi, C. Wu, Y. Zhang, Y. Ma, X. Sun, J. Sun, X. Zhang, C. Yuan, Monodisperse metallic NiCoSe2 hollow sub-microspheres: formation process, intrinsic charge-storage mechanism, and appealing pseudocapacitance as highly conductive electrode for electrochemical supercapacitors. Adv. Funct. Mater. **28**, 1705921 (2018). https://doi.org/10.1002/adfm.201705921
6. R. Kushwaha, S. Haldar, P. Shekhar, A. Krishnan, J. Saha, P. Hui, C.P. Vinod, C. Subramaniam, R. Vaidhyanathan, Exceptional capacitance enhancement of a non-conducting COF through potential-driven chemical modulation by redox electrolyte. Adv. Energy Mater. **11**, 2003626 (2021). https://doi.org/10.1002/aenm.202003626
7. J. Lee, K. Sohn, T. Hyeon, Fabrication of novel mesocellular carbon foams with uniform ultralarge mesopores. J. Am. Chem. Soc. **123**, 5146–5147 (2001). https://doi.org/10.1021/ja015510n
8. Y. Li, D. Zhang, M. Han, J. He, Y. Wang, K. Wang, Y. Wang, Fabrication of the phosphorus doped mesoporous carbon with superior capacitive performance by microwave irradiation under ambient atmosphere: an ultra-facile and energy-efficient method. Appl. Surf. Sci. **458**, 119–128 (2018). https://doi.org/10.1016/J.APSUSC.2018.07.089
9. Z. Li, W. Yan, S. Dai, A novel vesicular carbon synthesized using amphiphilic carbonaceous material and micelle templating approach. Carbon **42**, 767–770 (2004). https://doi.org/10.1016/j.carbon.2004.01.044
10. H.W. Liang, W. Wei, Z.S. Wu, X. Feng, K. Müllen, Mesoporous metal-nitrogen-doped carbon electrocatalysts for highly efficient oxygen reduction reaction. J. Am. Chem. Soc. **135**, 16002–16005 (2013). https://doi.org/10.1021/ja407552k
11. Y. Liang, H. Liu, Z. Li, R. Fu, D. Wu, In situ polydopamine coating-directed synthesis of nitrogen-doped ordered nanoporous carbons with superior performance in supercapacitors. J. Mater. Chem. A **1**, 15207–15211 (2013). https://doi.org/10.1039/c3ta13395h
12. W.J. Liu, K. Tian, Y.R. He, H. Jiang, H.Q. Yu, High-yield harvest of nanofibers/mesoporous carbon composite by pyrolysis of waste biomass and its application for high durability electrochemical energy storage. Environ. Sci. Technol. **48**, 13951–13959 (2014). https://doi.org/10.1021/es504184c

13. Y. Liu, Z. Wang, W. Teng, H. Zhu, J. Wang, A.A. Elzatahry, D. Al-Dahyan, W. Li, Y. Deng, D. Zhao, A template-catalyzed: In situ polymerization and co-assembly strategy for rich nitrogen-doped mesoporous carbon. J. Mater. Chem. A **6**, 3162–3170 (2018). https://doi.org/10.1039/c7ta10106f
14. Y. Meng, D. Gu, F. Zhang, Y. Shi, L. Cheng, D. Feng, Z. Wu, Z. Chen, Y. Wan, A. Stein, D. Zhao, A family of highly ordered mesoporous polymer resin and carbon structures from organic-organic self-assembly. Chem. Mater. **18**, 4447–4464 (2006). https://doi.org/10.1021/cm060921u
15. Y. Meng, K. Wang, Y. Zhang, Z. Wei, Hierarchical porous graphene/polyaniline composite film with superior rate performance for flexible supercapacitors. Adv. Mater. **25**, 6985–6990 (2013). https://doi.org/10.1002/adma.201303529
16. I. Moriguchi, A. Ozono, K. Mikuriya, Y. Teraoka, S. Kagawa, M. Kodama, Micelle-templated mesophases of phenol-formaldehyde polymer. Chem. Lett. 1171–1172 (1999). https://doi.org/10.1246/cl.1999.1171
17. J.P. Paraknowitsch, A. Thomas, Doping carbons beyond nitrogen: an overview of advanced heteroatom doped carbons with boron, sulphur and phosphorus for energy applications. Energy Environ. Sci. **6**, 2839–2855 (2013). https://doi.org/10.1039/c3ee41444b
18. H. Tang, J. Wang, H. Yin, H. Zhao, D. Wang, Z. Tang, Growth of polypyrrole ultrathin films on mos2 monolayers as high-performance supercapacitor electrodes. Adv. Mater. **27**, 1117–1123 (2015). https://doi.org/10.1002/adma.201404622
19. K. Wang, Y. Wang, Y. Wang, E. Hosono, H. Zhou, Mesoporous carbon nanofibers for supercapacitor application. J. Phys. Chem. C **113**, 1093–1097 (2009). https://doi.org/10.1021/jp807463u
20. Z.-S. Wu, Y. Zheng, S. Zheng, S. Wang, C. Sun, K. Parvez, T. Ikeda, X. Bao, K. Müllen, X. Feng, Z. Wu, S.H. Zheng, S. Wang, C.L. Sun, X.H. Bao, Y.J. Zheng, K. Parvez, K. Müllen, X.L. Feng, Stacked-layer heterostructure films of 2D thiophene nanosheets and graphene for high-rate all-solid-state pseudocapacitors with enhanced volumetric capacitance. Adv. Mater. **29**, 1602960 (2017). https://doi.org/10.1002/adma.201602960
21. W. Xing, C.C. Huang, S.P. Zhuo, X. Yuan, G.Q. Wang, D. Hulicova-Jurcakova, Z.F. Yan, G.Q. Lu, Hierarchical porous carbons with high performance for supercapacitor electrodes. Carbon **47**, 1715–1722 (2009). https://doi.org/10.1016/j.carbon.2009.02.024
22. D. Yuan, F. Zeng, J. Yan, X. Yuan, X. Huang, W. Zou, A novel route for preparing graphitic ordered mesoporous carbon as electrochemical energy storage material. RSC Adv. **3**, 5570–5576 (2013). https://doi.org/10.1039/c3ra40677f
23. L. Zhang, X.S. Zhao, Carbon-based materials as supercapacitor electrodes. Chem. Soc. Rev. **38**, 2520–2531 (2009). https://doi.org/10.1039/b813846j

Activated Carbon-Based Supercapacitors

Qi Zhang, E. Yi, Meng Jiang, Xin Chen, and Runfa Li

Abstract Supercapacitors (SCs) have been gaining significant attentions in the recent years due to their considerable power densities and long life cycles. Among the current supercapacitor electrode materials, activated carbons (ACs) have received extensive attention from researchers because of the fast ion/electron transport, low cost, high specific surface area and abundance. In this chapter, recent developments in different kinds of ACs, especially biomass based ACs, are presented and discussed. Moreover, the application status of AC materials as electrodes for SCs is summarized, and the possible future development directions of AC materials are also proposed, which will help AC materials to play more significant roles in wind farms, solar stations, electric vehicles, trains, ships, high buildings, etc., for solving the energy and environment problems of the world.

Keywords Supercapacitors · Activated carbon · Biomass · Electrochemical properties · Applications

1 Introduction

With the fast development of the worldwide economy, population increment, and extensive fossil fuel consumption, renewable energy technologies are urgently

Q. Zhang · E. Yi · M. Jiang · X. Chen (✉) · R. Li
Key Laboratory for Ultrafine Materials of Ministry of Education, and Shanghai Key Laboratory of Advanced Polymeric Materials, School of Materials Science and Engineering, East China University of Science and Technology, Shanghai 200237, P.R. China
e-mail: xinchen73@ecust.edu.cn

Q. Zhang
e-mail: zhangqimail1997@163.com

M. Jiang
e-mail: jiangmeng3706@163.com

R. Li
e-mail: lirunfa1996@163.com

S. Thomas et al. (eds.), *Nanostructured Materials for Supercapacitors*,
Advances in Material Research and Technology,
https://doi.org/10.1007/978-3-030-99302-3_8

needed for future energy generation, storage, and usage [1]. A range of energy conversion and storage technologies such as solar cells, wind power generators, fuel cells, supercapacitors (SCs), and lithium-ion batteries are being studied, to make full use of sustainable energy sources including solar, wind, biomass energy, etc. [2], among which, SCs, as a type of energy storage devices, have attracted great attentions in these years, owing to their long cycle life, high power density, superior pulse charge–discharge performance and low maintenance cost [3]. Compared with traditional capacitors, the energy densities of SCs are much higher because of the nanoporous electrode structure and the unique energy storage mechanisms. The energy stored in a traditional capacitor can be as high as the mF level, however, the capacitances of SCs can easily reach the ten, hundred, and even thousand-farad level [4]. Among the advanced energy storage technologies, the most prominent advantage of SCs is the quick charge/discharge response, which leads to their very high energy densities. SCs further have high reliabilities and can maintain excellent capacity even after thousands of charge/discharge cycles, which makes them very promising for being used in such as electric vehicles. To fully realize the potential of SCs, advanced electrode material development plays a key role, and many efforts have been undertaken on materials screening, structural design, and material preparation, to further improve the energy storage properties of the SC electrode materials [5, 6].

Among the electrode materials that have been researched, carbon materials have gained great interest. Advanced carbon materials such as activated carbon (AC), fullerene, carbon nanotubes, and graphene have attracted huge attention in the fields of energy storage, owing to of their excellent physicochemical properties, including high conductivity, high specific surface area, tunable porosity, outstanding chemical stability, and long cycle life [7]. Traditionally, the synthesis of advanced carbon materials relies on fossil fuel-based precursors (e.g. coal, phenol, methane, and pitch), and are based on energy-consuming synthetic processes (e.g. chemical vapor deposition, electric-arc discharge) [8], and the technology is relatively mature. Other than fossil fuels, biomass is another type of precursor for carbon material preparations. Differing from fossil fuels, biomasses are creature-based materials, which have the advantages of green resources, easiness to be obtained, and the potential of cost reduction [9], and recycling of the biomass-derived carbons used in the energy storage field may greatly improve the resource utilization efficiency.

Benefited from the natural biological precursor structures, different from graphite carbon, biomass-derived carbons are mainly composed of graphite-like micro crystallites, with the characteristics of smaller thicknesses and widths, more irregular shapes, lower crystallinities, and larger interlayer spacings, which not only increase the amount of active sites and material exchange channels but also provide 3-D structural stabilities, which are important for improving the charge/discharge cycle stabilities [4]. Overall, the advantages of biomass-derived carbons, used as SC electrode materials, have the advantages of (1) good chemical and physical stability [10]; (2) being intrinsically porous and/or hierarchically structured, that can promote the accessibility of electrolyte to an electrode and shorten the ion transport distance; (3) containing nitrogen, phosphorus, and other elements, which lead to the formation of extra-functional groups and active sites [9, 11].

For energy storage applications, a carbon material is generally activated, to become AC, to further optimize its performance. At present, a considerable number of works have been reviewed, on the preparation and application of biomass AC materials, e.g., (1) on introducing the precursor sources for biomass AC material preparations, such as lignocellulose precursors [12], oil palm [13], wood [14], agricultural waste, etc.; (2) on synthetic technologies for biomass AC preparations, such as microwave [15], hydrothermal conversion [16], chemical choices for thermochemical production [17] and preparation method comparison [18]; (3) on the of biomass AC applications, in such as hybrid electrochemical capacitor materials [19], adsorptions [20], and industrial contamination metal removal [21]. This review chapter is focused on the material choices for biomass AC preparations, as well as paying attention to the applications and future research trends of ACs.

2 Pure Biomass AC Materials

Biomass synthesis can provide the advantages of abundant sources, low price and easy availability. Biomass AC preparation can also alleviate environmental pollution caused by large amounts of biomass wastes. Efficient utilization of biomass is currently one of the important research topics. Biomass is the general term for substances derived from such as plants or animals, which can include all plants, animals, and microorganisms, and the wastes produced during their life cycles, thus, the main sources of biomass for the preparation of AC materials include plants, animals, and microorganisms, etc. [22, 23]. Among them, agricultural and forestry residues are considered to be the precursors of AC with commercial development potential due to their low price, renewability, and wide distribution, such as hemp straw, bamboo, bagasse wastes, reed straw, celery leaves, sunflower marrow, coconut shells, Pleurotus eryngii, etc. [24–31].

Jiang et al. [24] used hemp straw as the raw material, which is subjected to hydrothermal treatment at 120 °C for 4 h, and activated with KOH at 800 °C for 1 h, to obtain a specific surface area of 1964.46 m^2/g, and a specific capacitance of 221 F/g at a current density of 0.2 A/g. After 10,000 charging and discharging cycles, the specific capacitance still remains at the 96% level. The symmetrical SC can provide a high energy density of 18.14 Wh/kg and a power density of 450.37 W/kg. Zhang et al. [25] used bamboo as the raw material, carbonized at 700 °C for 3 h, and then activated with KOH at different temperatures to obtain AC electrode materials. At the optimized activation temperature of 900 °C, the specific surface area reaches 2221.1 m^2/g, and the specific capacitance is 293 F/g at a current density of 0.5 A/g. The assembled symmetrical SC can provide an energy density of 10.9 Wh/kg when the power density is 63 W/kg in an aqueous electrolyte, and the specific capacitance retention rate remains at 91.8% after 10,000 cycles.

Feng et al. [26] used hydrothermal carbonization combined with KOH activation to obtain AC material, from bagasse wastes, with a specific surface area of 2296 m^2/g and a pore volume of 1.34 cm^3/g. The specific capacitance reached 320 F/g at a

current density of 0.5 A/g. At a current density of 50 A/g, it can still maintain 70.8% of the original value, and kept a specific capacitance of 226 F/g. At a current density of 10 A/g, the retention rate of the specific capacitance exceeds 92.85% after 15,000 cycles. When assembled into a symmetrical SC, it can provide a maximum energy density of over 20 Wh/kg at 182 W/kg and have excellent long-term cycle stability after 10,000 cycles. Dai et al. [27] used reed straw to prepare AC, carbonized at 500 °C for 1 h, and then activated with KOH at 700 °C for 1 h. The resulted product had a specific surface area of 2387 m^2/g, and the specific capacitance reached 355 F/g at a current density of 1 A/g in 6 M KOH. Wang et al., [28] used waste celery leaves collected from the vegetable market to prepare porous carbon, which was carbonized at 600 °C in an argon atmosphere, and activated with KOH at 800 °C in an argon atmosphere for 1 h. The specific surface area reaches 3404 m^2/g, and the macropore volume is 1.88 cm^3/g. In a three-electrode system, at a current density of 0.5 A/g, the specific capacitance reached 421 F/g. At a current density of 5 A/g, the specific capacitance retention rate was 93.1% after 2000 cycles. In the two-electrode system, the specific capacitance is 273 F/g at a current density of 0.5 A/g.

Considering the wide availability, our group [29] used the platanus leaf as raw material, heated to 600 °C for 2 h in a nitrogen atmosphere, and activated it with potassium hydroxide solution at 800 °C for 1 h to synthesize biomass activated carbon. At a current density of 1 A/g, the specific capacitance reaches 266 F/g. After 2,000 cycles at a current density of 5 A/g, the specific capacity still retains 97.0%. Sun et al. [30] used sunflower marrow as the raw material and activated it by $ZnCl_2$ and $FeCl_3$ at 800 °C under nitrogen atmosphere for 2 h (Fig. 1). The specific surface area reached 1628.5 m^2/g, the macropore volume was 2.34 cm^3/g, and it had a 252.5 F/g specific capacitance at 0.5 A/g, and the specific capacitance was maintained at about 97% after 5000 cycles. The symmetrical SC produced with this kind of AC and a 0.5 M Na_2SO_4 aqueous electrolyte solution exhibits 12.4 Wh/kg energy density when the power density was 817 W/kg.

Sun et al. [31] used coconut shells to prepare porous graphene-like nanosheets with large surface areas. The raw material is mixed with $ZnCl_2$, $FeCl_3$ activators, dried at 100 °C to obtain a carbon precursor, and carbonized at 900 °C for 1 h. (Fig. 2) The specific surface area reached 1874 m^2/g, and the macropore volume was 1.21 cm^3/g. The specific capacitance reached 268 F/g at a current density of 1 A/g.

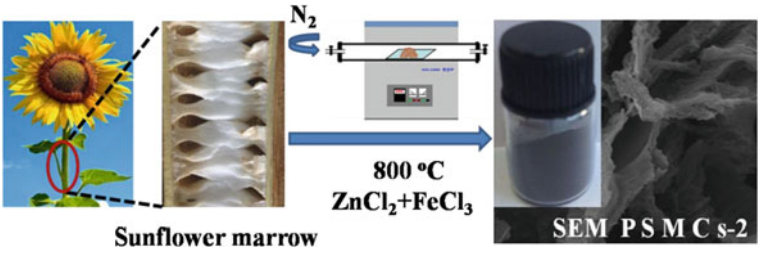

Fig. 1 Schematic route to prepare a biomass AC material. Adapted with permission from Reference [30]. Copyright 2016 International Journal of Electrochemical Science

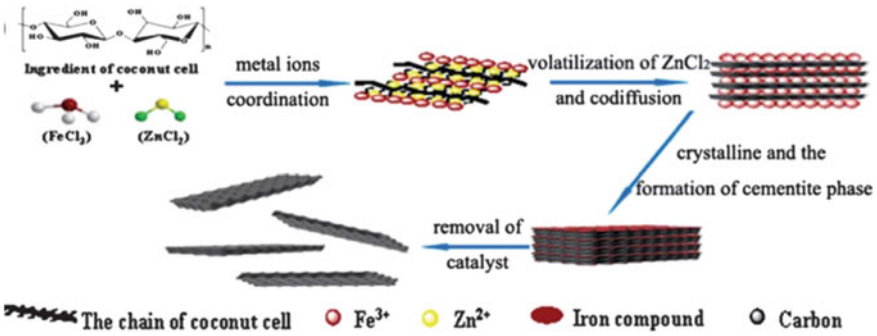

Fig. 2 Schematic diagram of the preparation process of porous graphene-like nanosheets. Adapted with permission from Reference [31]. Copyright 2013 Royal Society of Chemistry

It exhibits excellent cycle durability and coulomb efficiency, and after 5000 cycles, the specific capacitance retention rate exceeds 99.5%.

Yuan et al. [32] carbonized dried Pleurotus eryngii at 500 °C for 12 h in a nitrogen atmosphere, and then activated it with KOH at 600, 700, and 800 °C in a nitrogen atmosphere. For the AC activated at 700 °C, the specific surface area is 3255 m^2/g, and the specific capacitance measured at a current density of 2 A/g is 236 F/g. Assembled a symmetrical supercapacitor in 6 M KOH electrolyte, at a current density of 2 A/g, after 15,000 cycles. It has an excellent specific capacitance retention rate of about 93%.

3 Doped Biomass AC Materials

In recent years, studies have found that it is not only the specific surface area and pore structure that affect the performance of AC, heteroatom doping modification is a way to introduce heteroatoms into the carbon framework to improve the electrochemical performance of carbon materials by adjusting the electron donor properties and surface chemistry of carbon materials. Nitrogen, oxygen, sulfur, phosphorus, and other atoms can be incorporated into the carbon material framework separately or at the same time to obtain mono- or multi-element doped AC. When an AC material is doped, the resulting functional groups can improve the surface wettability, effectively reduce the diffusion resistance of electrolyte ions in the pores, and increase the surface area utilization rate. The incorporation of such as nitrogen, sulfur, phosphorus, etc., may further effectively improve the conductivity of carbon materials. There are two types of preparation methods for heteroatom-doped AC: one is to dope first, and then activate the doped carbon material, and the other is to perform post-treatment surface modification on the AC [33–36].

Khalafallah et al. [37] used potato skins to prepare porous AC co-doped with sulfur and phosphorus. The mixture containing sodium hypophosphite and thioacetamide

was heated at 180 °C for 15 h, then mixed with KOH, and heated at 750 °C for 3 h to obtain the product. The resulting heteroatom-doped porous AC has a specific surface area of 1911.5 m^2/g and a pore volume of 1.17 cm^3/g. The specific capacitance is 323 F/g at a current density of 1 A/g. At a current density of 10 A/g, the capacitance retention rate of the electrode after 5000 cycles was 98.2%. The symmetrical SC assembled by it showed a maximum energy density of 45.5 Wh/kg under a power density of 800 W/kg. Wang et al. [38] used durian shells to prepare activated porous carbon materials doped with N, O, and P heteroatoms. In the preparation process, $(NH_4)_2HPO_4$ is used as an activator and multiple heteroatoms are doped into the prepared AC material to modify the functional groups on the surface of the AC. (Fig. 3) The specific surface area of the obtained biomass AC was 823.9 m^2/g. The specific capacitance is 184 F/g at a current density of 0.5 A/g. At a current density of 10 A/g, the specific capacitance is 146 F/g. At a current density of 5 A/g, after 10,000 cycles, it showed a specific capacitance retention rate of about 88% and a Coulomb efficiency that is close to 100%.

Liu et al. [39] used bagasse as the raw material and urea as the nitrogen source, prepared a nitrogen-doped multi-level pores carbon material with a nitrogen concentration of 8.92%, a specific surface area of 805.6 m^2/g. (Fig. 4) The specific capacitance is 323 F/g at a current density of 1 A/g. When the current density reaches 30 A/g, the specific capacitance was 213 F/g. The symmetrical SC assembled from it has a capacitance retention rate of almost 100% after 10,000 cycles at a current density of 5 A/g.

Qian et al. [40] used human hair to prepare atom-doped biomass activated carbon. Human hair contains carbon, nitrogen, oxygen, hydrogen, sulfur, and other elements. The human hair is pre-carbonized and then mixed with KOH to produce AC. The

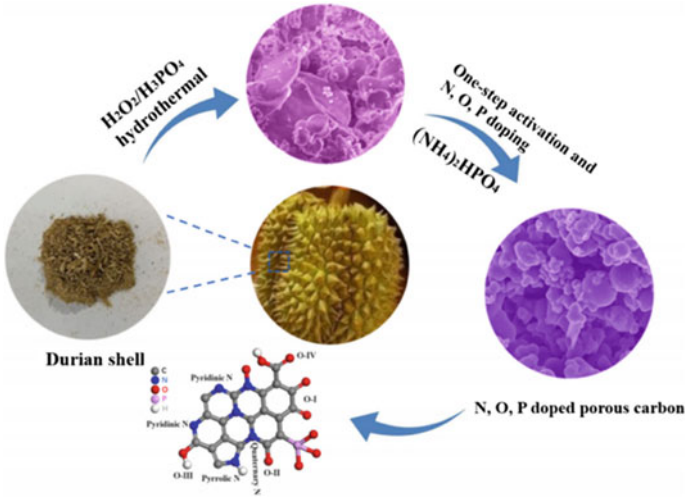

Fig. 3 The schematic preparation process of N, O, P co-doped porous carbon materials. Adapted with permission from Reference [38]. Copyright 2020 Springer Nature

Fig. 4 Schematic illustration of the synthesis of N-riched porous carbons. Adapted with permission from Reference [39]. Copyright 2016 American Chemistry Society

resulting product has a specific capacitance of 340 F/g at a current density of 1 A/g in 6 M KOH and a specific capacitance of 280 F/g after 20,000 cycles. Fu et al. [41] used plant waste grapefruit peel to produce nitrogen-doped graded porous carbon. The pomelo peel was dried and carbonized at 600 °C in a nitrogen atmosphere, and then activated with KOH. The obtained biomass AC has a nitrogen concentration as high as 4.47% and a BET (Brunauer, Emmett, and Teller) specific surface area of 1104 m^2/g. At a current density of 1 A/g, the specific capacitance is 208.7 F/g. At a current density of 20 A/g, the specific capacitance kept 166.9 F/g.

Zhou et al. [42] used dumpling powder to prepare nitrogen-doped porous carbon. First, stir a mixture of dumpling powder, KOH and urea vigorously, then the product was heated in a tube furnace at 800 °C under nitrogen atmosphere for 2 h. During the reaction, KOH is used to activate and provide pores. Urea is used both as a nitrogen source and a bulking agent. The resulting product exhibited a honeycomb-like porous structure. It has a specific surface area of 2853.6 m^2/g and a pore volume of 1.69 cm^3/g. The specific capacitance is 311 F/g at a current density of 1 A/g. When the current density reaches 50 A/g, the specific capacitance remained 200 F/g. At a current density of 10 A/g, the capacitance retention rate of the electrode after 10,000 cycles was 95.5%. The assembled symmetrical SC can provide an energy density of 15.92 Wh/kg at a current density of 0.5 A/g, and a power density of 358.28 W/kg. At a current density of 5 A/g, after 10,000 cycles, the capacitance retention rate was 97%. Yan et al. [43] used helianthus pallet to prepare N, S and O triple-doped AC. (Fig. 5) The sunflower tray was first dried at 100 °C, pre-carbonized in a nitrogen

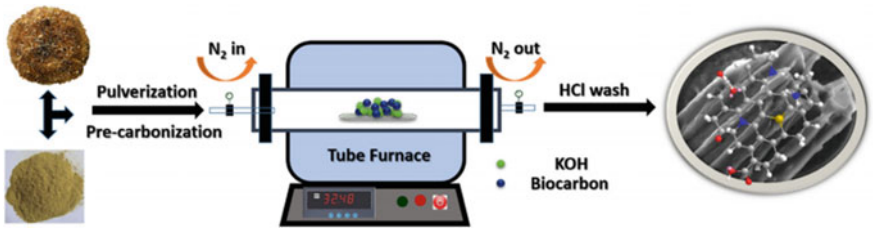

Fig. 5 Schematic of the procedures of template-like N, S, and O tri-doping AC derived from helianthus pallet. Adapted with permission from Reference [43]. Copyright 2020 Elsevier

atmosphere for 3 h, and then activated with KOH, and heated at 600 °C for 2 h. The resulting product has a specific capacitance of 357 F/g at a current density of 0.5 A/g. When the current density reaches 50 A/g, the specific capacitance kept 262 F/g. The symmetrical SC assembled by it can provide an energy density of 25.9 Wh/kg at a current density of 10 A/g and a power density of 951.4 W/kg. At a current density of 2 A/g, after 10,000 cycles, it showed an specific capacitance retention rate of about 98.4%.

Charoensook et al. [44] used rice straw to prepare nitrogen-doped porous AC. First, carbonize at 400 °C for 4 h, then add KOH and activate at 850 °C for 2 h. Finally, the AC is doped with nitrogen using melamine as the nitrogen source. The resulting product has a specific surface area of 25,376 m^2/g and a pore volume of 1.561 cm^3/g. The specific capacitance is 324 F/g at a current density of 0.5 A/g and undoped biomass activated carbon has a specific capacitance of 178 F/g. When the current density reaches 15 A/g, the specific capacitance value was still 237 F/g. The symmetrical SC assembled by it can provide an energy density of 45 Wh/kg when the power density is 250 W/kg. At a current density of 5 A/g, after 10,000 cycles, the capacitance retention rate reaches 95%.

4 Mixed Biomass AC Materials

Some of the biomass is in form of a mixture when collected, which is difficult and usually meaningless to separate into single substances. The examples may include fallen leaves, tea waste, sawdust, some other mixture of agricultural byproducts, waste papers, Trichoderma, and its culture medium. Using mixed biomass material for AC production can not only reduce the costs but also improve the AC material performance, which may arise from synergetic effects from the different components.

Peng et al. [45] have synthesized AC derived from the mixture of crab shells and rice husks. The mixture-derived AC showed better electrochemical performance than single biomass-derived ACs. The raw material was carbonized at 220 °C, with a hydrothermal method, and then activated with KOH at 700 °C. SEM image showed the AC has a unique 3D hierarchical porous morphology. This structure consists of a stacked sheet with abundant pores, which are mainly macropores. BET analysis showed the largest specific surface area of 3557 m^2/g of the AC. The electrochemical performance was also studied, showing the largest specific capacitance of 474 F/g. Yang et al. [46] reported a synthesis of mixed AC derived from sawdust with hierarchical porous morphology. Dry wood sawdust was mixed with KCl and KOH and then heated to 800 °C for 3 h to get the AC. According to the authors, KOH has strong oxidizability and will erode the carbon surface, letting the molten material flow into the pores of carbon under high temperatures, and by adjusting the KOH amount, the AC can change from hierarchical porous morphology to sheet structures. The resulting AC with plenty of micropores and mesopores showed the largest specific surface area of 1998 m^2/g. The AC sample showed the highest specific capacitance of 286 F/g and capacitance retention of 99.8% after 10,000 cycles. Eleri et al. [47]

reported a sawdust-derived AC with a honeycomb structure. The honeycomb structure may stem from the cell wall of the wood sawdust. The AC with honeycomb structure showed a specific surface area of 3083 m^2/g, a specific capacitance of 160 F/g, and an energy density of 49 Wh/kg.

Ma et al. [48] have reported wood waste-derived ACs with hollow fiber morphology. The precursor fibers were soaked in the acid solution for 5 h to obtain half-cured fibers. Then the half-cured fibers were treated with methanol solution and activated at a temperature range from 600–800 °C under N_2 atmosphere. Hollow fibers have the advantages of more activated sites, higher surface permeability, and better ion transport capability than solid fibers. BET analysis showed the largest specific surface area of 1873 m^2/g of the AC samples, with a specific capacitance of 295 F/g, excellent rate capability of 73.8% capacitance retention at 20 A /g, and cycling stability of 99.5% remaining over 10,000 cycles. Ruan et al. [49] have obtained Bean dregs derived AC with hierarchical pores and a specific capacitance of 482 F/g. The pre-treated materials were carbonized at 400 °C under Ar atmosphere and then activated by KOH at the specific activation temperature under Ar flow. In Fig. 6, the SEM image of an AC material, obtained with a large amount of KOH added, showed that there are interconnected cavities within the AC. While in the samples obtained with small amounts of KOH, the interconnected cavities are absent.

Jain et al. [50] have reported a synthesis of AC with acidic activate agents in mild experimental conditions. Leaves from European deciduous trees were collected and carbonized at a temperature range from 500–700 °C. A mixture of H_2SO_4 HNO_3 was used as the activating agent. The mixed leaves derived ACs showed hierarchical porous morphology, with a specific surface area of 614 m^2/g and a specific capacitance of 24 F/g. Our group [51] has reported a study to prepare mixed AC with microporous and wrinkled lamellar nanosheets morphologies. Different leaves were collected, carbonized, and activated by KOH. In Fig. 7, the FESEM images showed the AC samples from different leaves have quite different morphologies from each other, which may be due to the significant structural differences between land trees and the watery plant leaves. BET analysis showed the largest specific surface area

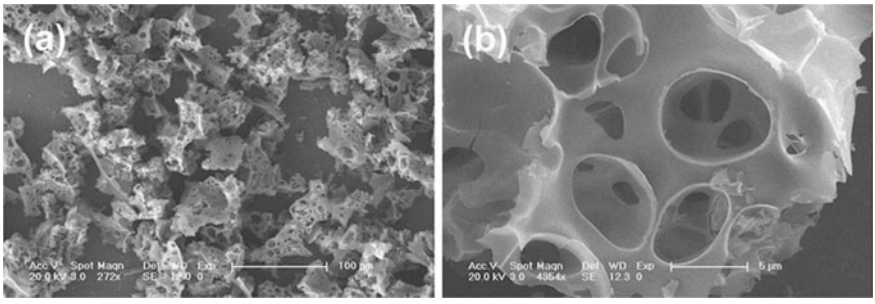

Fig. 6 SEM image of bean dregs derived ACs. Adapted with permission from Reference [49]. Copyright 2011 Royal Society of Chemistry

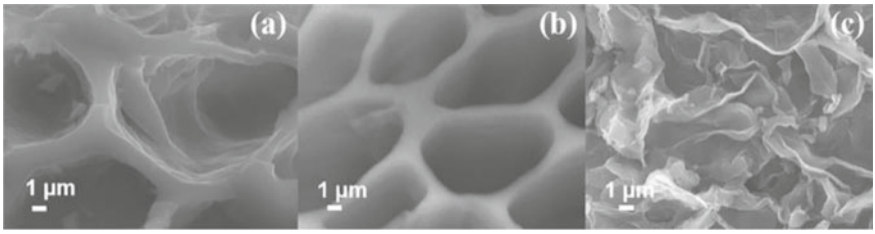

Fig. 7 FESEM image of platanus acerifolia, firmiana platanifolia, pistia stratiotes derived ACs. Adapted with permission from Reference [51]. Copyright 2011 John Wiley and Sons

of 1475.16 m^2/g of the AC, and the high specific capacitance was 246 F/g, 81.6% of which remained at 20 A/g, and a 100.0% capacitance retention was demonstrated over 1000 cycles.

Khan et al. [52] have reported a tea waste-derived AC with rod-like morphology. BET analysis showed a specific surface area of 1610 m^2/g, a specific capacitance of 332 F/g, and a rate capability of 66.9% at 100 A/g. Liu et al. [53] have reported the synthesis of AC from rice husk and some other food wastes with Trichoderma grown on them. This could be a new way for AC synthesis and biomass waste recycling. SEM image showed hierarchical porous morphology of the AC samples, with abundant mesoporous structures, which are controllable with the activation temperature. BET analysis showed the largest specific surface area of 3977.3 m^2/g, and a specific capacitance of 409.7 F/g.

5 Composite Materials with ACs

Although ACs have many advantages, it is generally viewed that some of their properties such as specific surface area and specific capacitance are not as good as such two dimensional (2D) materials and pseudocapacitance materials, thus in recent years, ACs derived from different biomass have been compounded with other materials to form higher performance electrode materials for capacitors. 2D graphene has excellent physical and chemical properties, such as ultra-high theoretical specific surface area, excellent mechanical strength, and conductivity, and has become a prominent candidate material for SC. The composite of AC and graphene can effectively prevent the agglomeration of graphene and improve the conductivity of AC. Xu et al. [54] have reported a composite of graphene and ACs. The ACs were derived from Ganoderma lucidum residues. Figure 8 shows the synthesis process. The raw materials were mixed with KOH and heated to 750 °C to achieve one-step carbonization and activation. BET analysis showed the composite has a specific surface area of 893.9 m^2/g. In electrochemical performance, the composite showed a specific capacitance of 176 F/g at 20 A/g and excellent cycling stability of 99.9% after 10,000 cycles.

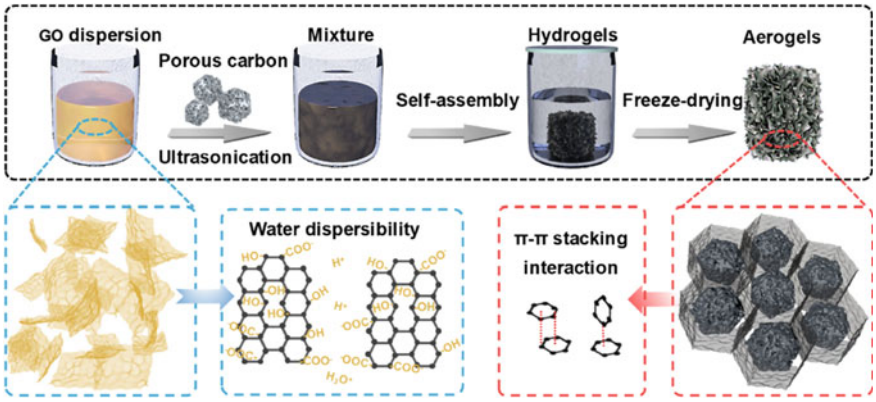

Fig. 8 Schematic illustration of the high-rate performance composite aerogels synthesis. Adapted with permission from Reference [52]. Copyright 2021 Elsevier

Guardia et al. [55] have reported the composite of grape seeds derived ACs and reduced graphene oxide. Grape seeds were solid wastes produced in the process of the wine industry. They were collected and grounded along with a KOH activating reagent, then heated to 1073 K under an N_2 atmosphere. BET analysis showed ACs have a large specific surface area of 1512 m^2/g. The prepared composite electrodes loaded with 20% rGO reached a specific capacitance of 260 F/g at 1mA/cm^2, and the composite electrode loaded with 20% rGO has eight times higher energy density and four times higer power density than the electrode without rGO.

Pseudocapacitance materials, such as transition metal oxides, have high theoretical specific capacitance and energy density, are usually considered as promising SC electrode materials. However, the low conductivity of such as manganese oxide (MnO_x) has limited its practical application. Compositing MnO_x with carbon materials may help charge transfer and improve the overall electrochemical performance of the SC devices. Zhou et al. [56] have reported a composite of MnO_x and radish-derived AC. The radish was cut into pieces and carbonized at 200 °C for 6h, then it was activated in the CO_2 atmosphere at 800 °C. MnO_x and ACs were composited by ultrasonic treatment and heating. BET analysis showed the composite has a specific surface area of 221.15 m^2/g. The porous structure of the ACs may be expanded when MnO_x nanoparticles grow, resulting in more microporous structures. However, excessive loading of MnO_x will lead to the agglomeration of nanoparticles. SEM image showed the composite has a hierarchical morphology. And the activation process not only resulted in the formation of a more porous structure but also kept the main structure of the carbon network. Besides, the composite shows a high specific capacitance of 557 F/g at 1 A/g and a high energy density of 248.2 Wh/kg.

Zhao et al. [57] have fabricated the composite of wasted litchi shell-derived ACs and MnO_x through a one-step method. The wasted litchi shells were grounded together with KOH and $KMnO_4$ and then heated at 800 °C for 2h. SEM images showed the ACs without MnO_x were micro-sized particles with smooth morphology,

while for the sample composited with MnO_x, the MnO_x nanoparticles were loaded on the cambered surface of ACs randomly. Meanwhile, the composite showed a high specific capacitance of 795.5 F/g at 0.5 A/g as the positive electrode, and a high energy density of 57.7 Wh/kg at 400 W/g. Besides, the composite electrode demonstrated good cycling stability of 93.5% after 5000 cycles. Shu et al. [58] have reported an apricot shell (AS) derived N-doped ACs/polyacrylonitrile (PAN) composite material. The steam activation method was used to activate the apricot shell, in a rotary tube furnace at 950 °C for 3 h. The AS-AC and PAN were composited at a certain weight ratio through a template-free approach to fabricate the 3D porous composite. The N-doped ACs showed 3D porous structure and were evenly dispersed on the PAN according to the SEM result. The 3D framework shrinked when the ACs content was larger than 30 wt%. In terms of electrochemical properties, the composite electrode showed a high specific capacitance of 442 F/g at 1 A/g, and cycling stability of 98% retention after 5000 cycles. Cao et al. [59] have synthesized RuO_2/coconut meat-derived ACs composite for high-performance flexible supercapacitor application. Waste coconuts were collected and cut into pieces, and the $RuCl_3$ and salicylic acid (SA) were dissolved and stirred to get $[Ru(SA)_3]$. The RuO_2/ACs were synthesized with a hydrothermal method. The resulting composite material showed a high Ru load of 9.2% and good Ru dispersion on the ACs base. The composite electrode showed a specific capacitance of 907.7 F/g and cycling stability of 98.2% after 10,000 cycles.

6 Applications of ACs in SCs

In 1957, General Electric (GE) applied for the first SC patent and then launched the first electric double-layer capacitor (EDLC) using carbon materials from Standard Oil Co. (Ohio) (SOHIO) [60]. AC is now widely used as the positive/negative electrode of SC devices. High-purity AC powder has a higher specific surface area, better-developed mesopores, reasonable pore structure distribution, and moderate apparent density, which are good for SC applications. Functionalization of the carbon materials has been used as an important way to improve the energy storage capacity, by improving the surface wettability of the active material, which helps the electrolyte to penetrate through the porous structure, thereby better forming an electrostatic double-layer [61, 62]. Currently, AC-based SCs are widely used in wind farms, electric vehicles, high buildings, industries, consumer electronics, telecommunications, medical equipment, national defense, aerospace, and other fields due to their large capacity, high energy density, and long lifetime.

Wind farm and solar station output power fluctuations create adverse effects on the voltage, frequency, and stability of the electric grid. Short-term wind farm power variations with high ramp rates can cause voltage instabilities, particularly if the farm is located in weak-grid areas. SCs and such as Li-ion capacitors can provide the advantages of fast responses, the long cycle life of more than 100,000 deep charge and discharge cycles, maintenance-free, and high reliability, thus providing a solution to

the problem faced by the wind farms. Okazaki et al. [63] used EDLCs to smooth the output of wind power generators. This paper studied charging methods of EDLCs to replace rechargeable batteries in wind power generation and discussed methods of realizing high charging efficiency. Esmaili et al. [64] further reported a system that parallelly connected AC-based Li-ion capacitors and zinc bromide flow battery as the proposed energy storage devices.

Electrochemical capacitors have been used in electric starting devices and energy regenerators for various large-scale loads, including vehicles, trains, and ships. Takahara et al. [65] studied the possible application of SCs to railway vehicles. The advantages of energy-saving, high-efficiency operation, as well as energy regeneration through the braking system, are discussed.

Mahon et al. [66] designed an SC based on AC with an organic electrolyte. Burke [67] reports some carbon/carbon ultracapacitance devices that are used in hybrid electric vehicles. Figure 9 shows two types of commercially available devices. The analysis showed that vehicles can be designed with carbon-based SCs (both carbon/carbon and hybrid carbon), which yield high fuel economy improvements for all of the driving cycles, and high volume produced SCs can be cost-competitive with lithium-ion batteries. The application of carbon/carbon devices in micro-hybrids is particularly attractive, for permitting engine operation near its maximum efficiency, using an electric motor of just 6 kW. In 2010, SC Buses were already demonstrated in Shanghai World Expo. The bus loaded aqueous hybrid SC from Aowel Technology's UCR. These buses do not need to be connected to the electric cable during motion, and only need to be charged for 30 s to 1 min while waiting for passengers at the bus station, and then it can travel about 5 km. Compared with traditional fuel buses, SC vehicles have lower energy consumption, much better power performance and are more comfortable [68, 69].

In 2016 China's first independently designed SC train rolled off the production line in Hunan province, and this train uses SC energy storage to operate, without external wires when running between stations, and can be fully charged during a 30 s stop and then run for 3–5 km. This tram uses graphene/AC composite SC from CRRC (CRRC Zhuzhou Locomotive) [70]. With the quick industrial development,

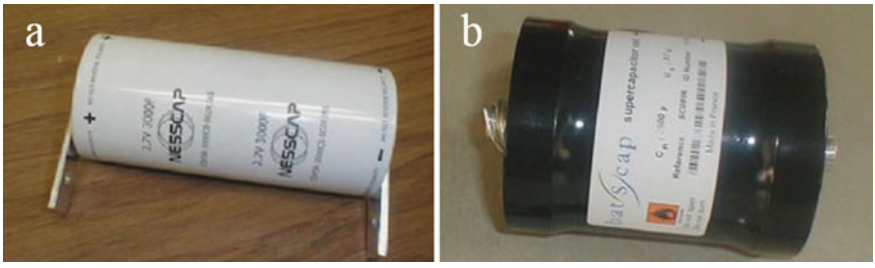

Fig. 9 Three types (**a** The NessCap 3000 F SC; **b** The Batscap 2700 F SC) of commercially available devices. Adapted with permission from Reference [67]. Copyright 2009 John Wiley and Sons

the SC market size in China is expected to reach 18.1 billion RMB in 2022, and the world SC market size is expected to reach 140 billion USD, with over 33% 5-year increase, which will greatly help solve the energy and environment problem of the world [71].

7 Conclusion and Outlook

In this chapter, we reviewed the recent development and application of ACs in SCs. Biomass-related AC preparations, such as pure biomass AC materials, doped biomass AC materials, mixed biomass AC materials, and composite materials containing biomass ACs, are extensively studied in laboratories, while for real SC applications, all types of AC can be considered. Currently, AC-based SCs are widely used in wind farms, solar stations, electric vehicles, trains, ships, high buildings, etc., and are expected to play a critical role in solving the energy and environmental problem of the world.

In today's era, green production and utilization of energy are the direction of modern industry. Extensive research efforts have been carried out on the development of wind and solar technologies to produce clean and green energy. However, the instability of wind blow and sunlight illumination require the development of energy storage systems. In this regard, AC application for energy storage such as SCs is very important. Bio-wastes, being used as raw materials for AC production, have the following advantages: environmental friendliness, low-cost and abundant varieties. An extremely larger amount of biomass waste is being made every day, and using them as the raw material for AC production not only helps solve the problem of waste disposal but also makes the AC preparation process less expensive. Working together with wind and solar technologies, it has the potential to replace fossil resources for energy production. Besides pure biomass-based AC materials, mixed biomass AC materials, doped biomass AC materials, and AC composited with other materials have carried out extensive research efforts. The development of these AC-based materials has involved raw material selection, and surface functionalization, cost reduction, composition modification, etc.

Although SCs using carbon materials have been commercialized, to further improve the performance of the capacitors, many problems have to be further solved. The performance improvement of the AC-based electrodes depends upon the surface area increment, the pore size distribution optimization, as well as performance enhancement by introducing surface functional groups and pseudocapacitive materials. Efforts have been made to prepare carbon materials with controllable pore sizes to achieve high specific capacitance and low impedance, composite with metal oxides or conductive polymers to increase the pseudocapacitance effect, etc.

Increasing the working voltage of the electrode, while not reducing the specific capacity, to increase the specific energy of the SC is one direction of future research. Another direction is to make sure the production processes of biomass-based AC are environmentally friendly. In the process of producing and activating AC, some

harmful gases such as NO_2 and SO_2 will inevitably be produced, and how to control the waste gas emission needs to be studied. The recycling and reuse of the other by-products generated during AC production also require scientific thinking and research. Besides the scientific studies in the laboratories, research work needs to be furthermore extended to the industrial or commercial level.

Acknowledgements The support from the National Natural Science Foundation of China (21875066), Shanghai Leading Academic Discipline Project (B502), and the Shanghai Key Laboratory Project (08DZ2230500) are acknowledged.

References

1. S.F. Huang, X.L. Zhu, S. Sarkar et al., Challenges and opportunities for supercapacitors. APL Mater. **7**(10), 100901 (2019)
2. V.A. Boicea, Energy storage technologies: the past and the present. Proc. IEEE **102**(11), 1777–1794 (2014)
3. B. Deng, Q. Huang, W. Zhang et al., Design high performance biomass-derived renewable carbon material for electric energy storage system. J. Clean. Prod. **309**(20), 127391 (2021)
4. X.Q. Li, L. Chang, S.L. Zhao et al., Research on carbon-based electrode materials for supercapacitors. Acta. Phys.-Chim. **33**(1), 130–148 (2017)
5. X.Q. Liang, M.H. Chen, G.X. Pan et al., New carbon for electrochemical energy storage and conversion. Funct. Mater. Lett. **12**(4), 1950049 (2019)
6. F. Beguin, V. Presser, A. Balducci et al., Carbons and electrolytes for advanced supercapacitors. Adv. Mater. **26**(14), 2219–2251 (2014)
7. A. Aqel, A.K.M.M. El-Nour, R.A.A. Ammar et al., Carbon nanotubes, science and technology part (I) structure, synthesis and characterisation. Arab. J. Chem. **5**(1), 1–23 (2012)
8. T.K. Enock, C.K. King'ondu, A. Pogrebnoi, et al. Status of biomass derived carbon materials for supercapacitor application. Int. J. Electrochem. (UK) **6453420**, 14 (2017)
9. J. Wang, P. Nie, B. Ding et al., Biomass derived carbon for energy storage devices. J. Mater. Chem. A **5**(6), 2411–2428 (2017)
10. Z. Zhang, Z. Zhu, B. Shen et al., Insights into biochar and hydrochar production and applications: a review. Energy **171**, 581–598 (2019)
11. C.E. Brewer, K. Schmidt-Rohr, J.A. Satrio et al., Characterization of biochar from fast pyrolysis and gasification systems. Environ. Prog. Sustain. **28**(3), 386–396 (2009)
12. P. González-García, Activated carbon from lignocellulosics precursors: a review of the synthesis methods, characterization techniques and applications. Renew. Sust. Energ Rev. **82**, 1393–1414 (2018)
13. M.O. Abdullah, I.A.W. Tan, L.S. Lim, Automobile adsorption air-conditioning system using oil palm biomass-based activated carbon: a review. Renew. Sust. Energ Rev. **15**(4), 2061–2072 (2011)
14. M. Danish, T. Ahmad, A review on utilization of wood biomass as a sustainable precursor for activated carbon production and application. Renew. Sust. Energ Rev. **87**, 1–21 (2018)
15. W. Ao, J. Fu, X. Mao et al., Microwave assisted preparation of activated carbon from biomass: a review. Renew. Sust. Energ Rev. **92**, 958–979 (2018)
16. A. Jain, R. Balasubramanian, M.P. Srinivasan, Hydrothermal conversion of biomass waste to activated carbon with high porosity: a review. Chem. Eng. J. **283**, 789–805 (2016)
17. K. Ukanwa, K. Patchigolla, R. Sakrabani et al., A review of chemicals to produce activated carbon from agricultural waste biomass. Sustainability **11**(22), 6204 (2019)

18. E. Taer, R. Taslim, Brief review: preparation techniques of biomass based activated carbon monolith electrode for supercapacitor applications, in 1st International Conference And Exhibition On Powder Technology Indonesia (ICEPTI) 2017. AIP Conference Proceedings, vol. 1927 (2018), pp. 020004
19. P. Dubey, V. Shrivastav, P.H. Maheshwari et al., Recent advances in biomass derived activated carbon electrodes for hybrid electrochemical capacitor applications: challenges and opportunities. Carbon **170**, 1–29 (2020)
20. V. Benedetti, F. Patuzzi, M. Baratieri, Characterization of char from biomass gasification and its similarities with activated carbon in adsorption applications. Appl. Energ. **227**, 92–99 (2018)
21. M. Bilal, J.A. Shah, T. Ashfaq et al., Waste biomass adsorbents for copper removal from industrial wastewater–a review. J. Hazard Mater. **263**(2), 322–333 (2013)
22. Y.Q. Zhao, M. Lu, P.Y. Tao et al., Hierarchically porous and heteroatom doped carbon derived from tobacco rods for supercapacitors. J. Power Sources **307**, 391–400 (2016)
23. Y. Gao, Q.Y. Yue, B.Y. Gao, High surface area and oxygen-enriched activated carbon synthesized from animal cellulose and evaluated in electric double-layer capacitors. RSC Adv. **5**(40), 31375–31383 (2015)
24. X. Jiang, G. Shi, G. Wang et al., A hydrothermal carbonization process for the preparation of activated carbons from hemp straw: an efficient electrode material for supercapacitor application. Ionics **25**(7), 3299–3307 (2019)
25. G. Zhang, Y. Chen, Y. Chen et al., Activated biomass carbon made from bamboo as electrode material for supercapacitors. Mater. Res. Bull. **102**, 391–398 (2018)
26. H. Feng, H. Hu, H. Dong et al., Hierarchical structured carbon derived from bagasse wastes: a simple and efficient synthesis route and its improved electrochemical properties for high-performance supercapacitors. J. Power Sources **302**, 164–173 (2016)
27. C. Dai, J. Wan, J. Shao et al., Hollow activated carbon with unique through-pore structure derived from reed straw for high-performance supercapacitors. Mater. Lett. **193**, 279–282 (2017)
28. R. Wang, P. Wang, X. Yan et al., Promising porous carbon derived from celtuce leaves with outstanding supercapacitance and CO_2 capture performance. ACS Appl. Mater. Interfaces **4**(11), 5800–5806 (2012)
29. W. Zhou, X. Chen, H. Cao et al., Preparation of platanus leaf-based activated carbon and its application to supercapacitors. CIESC J. **68**(7), 2918–2924 (2017)
30. K. Sun, High performance symmetric supercapacitor based on sunflower marrow carbon electrode material. Int. J. Electrochem. Sc. **12**(3), 2606–2617 (2017)
31. L. Sun, C. Tian, M. Li et al., From coconut shell to porous graphene-like nanosheets for high-power supercapacitors. J. Mater. Chem. A **1**(21), 6462–6470 (2013)
32. Y. Yuan, R. Yi, Y. Sun et al., Porous activated carbons derived from pleurotus eryngii for supercapacitor applications. J. Nanomater. **2018**, 1–10 (2018)
33. Q. Liang, L. Ye, Z.H. Hang et al., A honeycomb-like porous carbon derived from pomelo peel for use in high-performance supercapacitors. Nanoscale **6**(22), 13831–13837 (2014)
34. G. Ning, X. Ma, X. Zhu et al., Enhancing the Li storage capacity and initial coulombic efficiency for porous carbons by sulfur doping. ACS Appl. Mater. Interfaces **6**(18), 15950–15958 (2014)
35. X. Jia, G. Zhang, T. Wang et al., Monolithic nitrogen-doped graphene frameworks as ultrahigh-rate anodes for lithium ion batteries. J. Mater. Chem. A **3**(30), 15738–15744 (2015)
36. X. Wang, M. Lou, X. Yuan et al., Nitrogen and oxygen dual-doped carbon nanohorn for electrochemical capacitors. Carbon **118**, 511–516 (2017)
37. D. Khalafallah, X. Quan, C. Ouyang et al., Heteroatoms doped porous carbon derived from waste potato peel for supercapacitors. Renew. Energ **170**, 60–71 (2021)
38. K. Wang, Z. Zhang, Q. Sun et al., Durian shell-derived N, O, P-doped activated porous carbon materials and their electrochemical performance in supercapacitor. J. Mater. Sci. **55**(23), 10142–10154 (2020)
39. J. Liu, Y. Deng, X. Li et al., Promising nitrogen-rich porous carbons derived from one-step calcium chloride activation of biomass-based waste for high performance supercapacitors. ACS Sustain. Chem. Eng. **4**(1), 177–187 (2015)

40. W. Qian, F. Sun, Y. Xu et al., Human hair-derived carbon flakes for electrochemical supercapacitors. Energy Environ. Sci. **7**(1), 379–386 (2014)
41. G. Fu, Q. Li, J. Ye et al., Hierarchical porous carbon with high nitrogen content derived from plant waste (pomelo peel) for supercapacitor. J. Mater. Sci.-Mater. El **29**, 7707–7717 (2018)
42. J. Zhou, M. Wang, X. Li, Promising biomass-derived nitrogen-doped porous carbon for high performance supercapacitor. J. Porous. Mat. **26**(1), 99–108 (2018)
43. J. Yan, J. Shen, L. Li et al., Template-like N, S and O tri-doping activated carbon derived from helianthus pallet as high-performance material for supercapacitors. Diam. Relat. Mater. **102**, 107693 (2020)
44. K. Charoensook, C.L. Huang, H.C. Tai et al., Preparation of porous nitrogen-doped activated carbon derived from rice straw for high-performance supercapacitor application. J. Taiwan Inst. Chem. E **120**, 246–256 (2021)
45. L. Peng, Y. Liang, J. Huang et al., Mixed-biomass wastes derived hierarchically porous carbons for high-performance electrochemical energy storage. ACS Sustain. Chem. Eng. **7**, 10393–10402 (2019)
46. L. Yang, J. Qiu, Y. Wang et al., Molten salt synthesis of hierarchical porous carbon from wood sawdust for supercapacitors. J. Electroanal. Chem. **856**, 113673 (2020)
47. O.E. Eleri, K.U. Azuatalam, M.W. Minde et al., Towards high-energy-density supercapacitors via less-defects activated carbon from sawdust. Electrochim. Acta. **362**, 137152 (2020)
48. X. Ma, C. Ding, D. Li et al., A facile approach to prepare biomass-derived activated carbon hollow fibers from wood waste as high-performance supercapacitor electrodes. Cellulose **25**(8), 4743–4755 (2018)
49. C. Ruan, K. Ai, L. Lu, Biomass-derived carbon materials for high-performance supercapacitor electrodes. RSC Adv. **4**, 30887–30895 (2014)
50. A. Jain, M. Ghosh, M. Krajewski et al., Biomass-derived activated carbon material from native European deciduous trees as an inexpensive and sustainable energy material for supercapacitor application. J. Energy Storage **34**, 102178 (2021)
51. X. Yang, J. Xu, X. Chen et al., Preparation and characterization of porous carbon from mixed leaves for high-performance supercapacitors. Chinese J. Chem. **39**, 353–359 (2020)
52. A. Khan, R.A. Senthil, J. Pan et al., A new biomass derived rod-like porous carbon from tea-waste as inexpensive and sustainable energy material for advanced supercapacitor application. Electrochim. Acta. **335**, 135588 (2020)
53. Z. Liu, J. Hu, F. Shen et al., Trichoderma bridges waste biomass and ultra-high specific surface area carbon to achieve a high-performance supercapacitor. J. Power Sources **497**, 229880 (2021)
54. M. Xu, A. Wang, Y. Xiang et al., Biomass-based porous carbon/graphene self-assembled composite aerogels for high-rate performance supercapacitor. J. Clean Prod. **315**, 128110 (2021)
55. L. Guardia, L. Suárez, N. Querejeta et al., Biomass waste-carbon/reduced graphene oxide composite electrodes for enhanced supercapacitors. Electrochim. Acta. **298**, 910–917 (2019)
56. H. Zhou, Y. Zhan, F. Guo et al., Synthesis of biomass-derived carbon aerogel/MnO composite as electrode material for high-performance supercapacitors. Electrochim. Acta. **390**, 138817 (2021)
57. N. Zhao, L. Deng, D. Luo et al., One-step fabrication of biomass-derived hierarchically porous carbon/MnO nanosheets composites for symmetric hybrid supercapacitor. Appl. Surf. Sci. **526**, 146696 (2020)
58. Y. Shu, J. Maruyama, S. Iwasaki et al., Nitrogen-doped biomass/polymer composite porous carbons for high performance supercapacitor. J. Power Sources **364**, 374–382 (2017)
59. Z. Cao, R. Li, P. Xu et al., Highly dispersed RuO_2-biomass carbon composite made by immobilization of ruthenium and dissolution of coconut meat with octyl ammonium salicylate ionic liquid for high performance flexible supercapacitor. J. Colloid Interf. Sci. **606**(Pt 1), 424–433 (2021)
60. S. Balasubramaniam, A. Mohanty, S.K. Balasingam et al., Comprehensive insight into the mechanism, material selection and performance evaluation of supercapacitors. Nano-Micro. Lett. **12**(1), 85 (2020)

61. K. MacDermid-Watts, R. Pradhan, A. Dutta, Catalytic hydrothermal carbonization treatment of biomass for enhanced activated carbon: a review. Waste Biomass Valorization **12**(5), 2171–2186 (2020)
62. S. Saini, P. Chand, A. Joshi, Biomass derived carbon for supercapacitor applications: review. J. Energy Storage **39**, 102646 (2021)
63. Y. Okazaki, M. Yoshida, K. Fujiwara, Charging method of EDLCs by wind power generation in stand alone system, in International Power Electronics Conference (IPEC—Sapporo) (2010), pp. 2577–2584
64. A. Esmaili, B. Novakovic, A. Nasiri et al., A hybrid system of Li-ion capacitors and flow battery for dynamic wind energy support. IEEE T Ind. Appl. **49**(4), 1649–1657 (2013)
65. E. Takahara, T. Wakasa, J. Yamada, A study for electric double layer capacitor (EDLC) application to railway traction energy saving including change over between series and parallel modes, in Pcc-Osaka 2002: Proceedings of the Power Conversion Conference-Osaka, vol I–III (2002), pp. 855–860
66. P.J. Mahon, G.L. Paul, S.M. Keshishian et al., Measurement and modelling of the high-power performance of carbon-based supercapacitors. J. Power Sources **91**(1), 68–76 (2000)
67. A. Burke, Ultracapacitor technologies and application in hybrid and electric vehicles. Int. J. Energ Res. **34**(2), 133–151 (2010)
68. H. Li, E. Yang, Q. Liang, et al., Supercapacitor powertrain system used in shanghai expo 2010 for public transportation city bus and its popularization. China Acad. J. Electron. Publish. House (2011)
69. Xinhua News Agency, Supercapacitor bus service shanghai world expo (2010). http://www.gov.cn/jrzg/2010-05/04/content_1599079.htm
70. Xinhua News Agency, China's first home-made supercapacitor tram unveiled (2016). http://english.www.gov.cn/news/photos/2016/08/01/content_281475406499108.htm
71. WEFore, [world economic research] Operation status and future development trend of super capacitor industry (2021). https://www.sohu.com/a/442851208_530801

Carbon Aerogels for Supercapacitor Applications

Jingjing Cao, Mehran Asad Ayoubi, and Wei Wang

Abstract Carbon is a commonly used material in capacitors because it is inert and durable during charge–discharge cycles. With recent developments within the domains of nano and 2D materials, carbon materials have once again received attention in materials science. Carbon in different forms (such as graphite, graphene, and carbon nanotube) has a large specific surface area (SSA), which is essential for a material used in capacitors. Therefore, the application of the newly emerged carbon materials has been extensively explored. Carbon aerogel is a 3D material assembled by the aforementioned 1D or 2D carbon forms. Thus, carbon aerogels have remarkably high porosity and large SSA. In this chapter, we would like to present the recent progress of carbon aerogels in their application as electrode materials in supercapacitors. The chapter is organized into three sections. First, a brief introduction of supercapacitor and carbon aerogels is presented. In the second section, the common methods to synthesize carbon aerogels are summarized. In the last section, we present the application of different carbon aerogels in supercapacitors and compare the properties of different carbon aerogels, including capacitance, volumetric energy, porosity, etc.

Keywords Carbon · Aerogel · Supercapacitor · Carbonization · Cyclic charge–discharge

J. Cao
State Key Laboratory of Pollution Control and Resources Reuse, National Engineering Research Center for Organic Pollution Control and Resource Reuse, School of the Environment, Nanjing University, Nanjing 210023, China

M. A. Ayoubi
Shanghai Pubway Biotech, Shanghai 200333, China

W. Wang (✉)
Department of Chemistry, University of Bergen, 5020 Bergen, Norway
e-mail: wei.wang@uib.no

S. Thomas et al. (eds.), *Nanostructured Materials for Supercapacitors*,
Advances in Material Research and Technology,
https://doi.org/10.1007/978-3-030-99302-3_9

1 Introduction

The increasing consumption of fossil fuels pollutes the air and the soil and gives rise to the emission of large amounts of greenhouse gases [1]. Therefore, the development of environment-friendly means of energy generation and energy storage is of great significance [2]. In particular, the development of energy storage devices, including electrochemical supercapacitors (SCs) and batteries, has received a lot of attention [3–6]. Compared with batteries, the energy density of SCs is 3–30 times lower, but their power density is 100–1000 times higher [5, 7]. Besides, SCs are safer and more reliable than batteries, because SCs can withstand millions of charge–discharge cycles through a two-layer charge storage area that is not affected by chemical reactions, whereas excessive redox reactions during charge and discharge result in volumetric modulation and expansion of the active substance in the electrode of the batteries [8–10]. However, SCs are prone to electrolyte ageing and in order to avoid or at least minimize this phenomenon, the operating voltage of SCs must be lower than that of batteries [8]. For SCs with a high energy density, high working voltage is necessary. Thus, the optimization of working voltage is essential for high-performance SCs [10].

In SCs, a barrier separates the two electrodes. In symmetric SCs, the two electrodes are the same (Fig. 1a), but in asymmetric SCs (Fig. 1b and c), the two electrodes are different. Depending on the energy storage mechanism used, SCs can be divided into electrical double-layer capacitors (EDLCs), pseudocapacitors (PCs), and hybrid supercapacitors (HSCs), which are a combination of EDLC and PC [11, 12]. In EDLCs, the charge storage occurs between the electrolyte and the electrode interface (Fig. 1a). This means that the capacitance is proportional to the surface area accessed by the ion electrolytes. PCs involve reversible and fast Faraday redox reactions (Fig. 1b). Thus, a high reaction interfacial area is required for achieving high capacitance in PCs.

Suitable SC electrode materials should exhibit high capacitance, which is realized through a very large specific surface area (SSA). They should also withstand many charge–discharge cycles with little capacitance attenuation [14, 15]. Besides, preferably they should be nontoxic and cheap to produce. So far, carbon-based nanomaterials are the most promising electrode materials for SCs, due to their low cost, unique hierarchical structure, large specific surface and reaction interface area, and excellent electrochemical/mechanical properties [16, 17]. Among such materials, carbon aerogels are particularly attractive [17]. In addition to the excellent properties of aerogels, such as being lightweight, having high porosity, low density and high SSA, carbon aerogels also have the advantages of excellent electrical conductivity, relatively good mechanical properties, acid, and alkali resistance, etc. [13]. This chapter summarizes the progress in the research of carbon-based aerogels used in SCs and discusses the key elements of their synthesis and application.

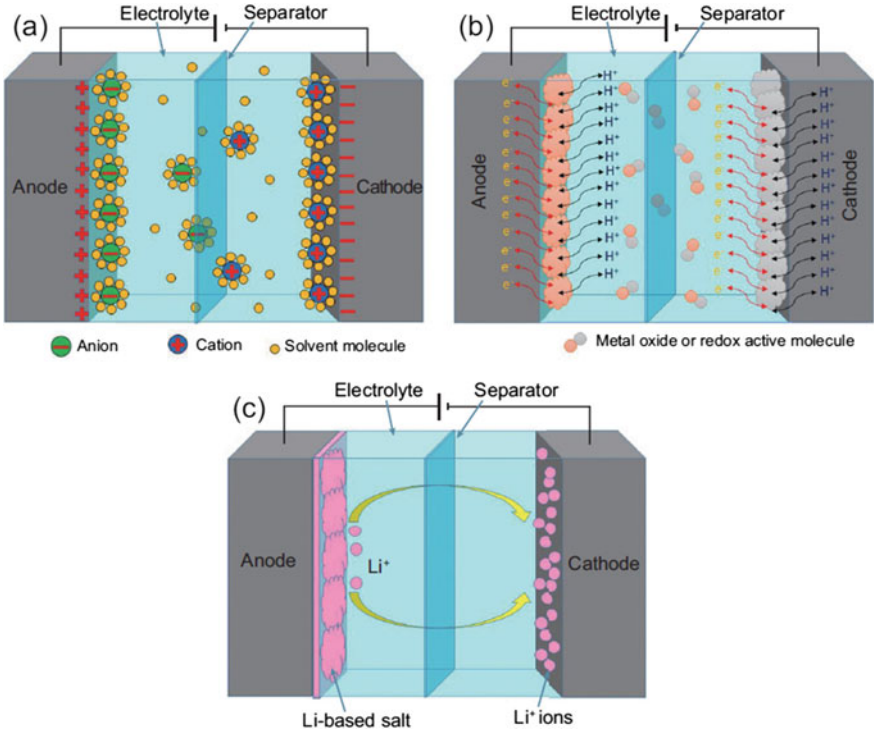

Fig. 1 **a** Schematic representation of electric double-layer capacitor (EDLC), **b** pseudo capacitor (PC), and **c** hybrid supercapacitor (HSC). Reprinted with permission from Ref. [13], Copyright © 2017, Oxford University Press

2 Synthesis of Carbon-Based Aerogels

Pekala produced the first example of a carbon aerogel by supercritical drying of resorcinol and formaldehyde that have undergone sol–gel reaction under the catalytic action of Na_2CO_3 catalyst [18]. Carbon aerogel is mainly obtained through drying of an organic gel to obtain an organic aerogel and then applying a carbonization treatment to retain the original spatial structure [14, 15]. Thus, compared to conventional aerogels, carbon aerogels require further carbonization after the drying process. At present, the two common carbonization methods are hydrothermal carbonization [19–22] and pyrolytic carbonization [23–27].

2.1 Hydrothermal Carbonization

Inspired by what happens in nature during the formation of coal, efforts have been put to achieve faster carbon formation from natural biomass. At the beginning of the twentieth century, Bergius first reported the conversion of cellulose into coal-like materials by hydrothermal method, and then Berl and Schmidt made further developments on this basis [19]. Hydrothermal carbonization is a form of conversion of organic matter into the inorganic matter under hydrothermal conditions. Hydrothermal transformation also includes hydrothermal gasification and hydrothermal liquefaction. Hydrothermal carbonization is a series of chemical reactions such as hydrolysis and hydropyrolysis of organic matter under suitable temperature and pressure conditions with water as the reaction medium, which converts macromolecules into small monomers and carbon substances. The process of hydrothermal carbonization is mainly divided into dehydration reaction, demethylation reaction, and decarboxylation reaction [20, 21]. Generally, the conditions of hydrothermal carbonization are relatively mild and this type of carbonization is commonly carried out within the temperature range of 180–250 °C and the pressure range of 2–10 MPa [22]. These hydrothermal conditions can be met in a reaction vessel (usually a reaction kettle), making the hydrothermal carbonization method a simple, efficient, economical, and environment-friendly preparation method.

2.2 Pyrolytic Carbonization

Compared with hydrothermal carbonization, pyrolytic carbonization degrades macromolecules in organic matter at high temperatures and decomposes them into small molecules, resulting in water vapor, carbon monoxide, and other carbon materials [14, 15]. Pyrolytic carbonization is carried out in isolation from the air commonly by filling the reaction vessel with inert gas, such as argon or nitrogen [23, 24]. The pyrolytic carbonization process generally includes crosslinking reaction, depolymerization, decomposition, etc., which means that the biomass undergoes irreversible chemical and physical reaction changes [25, 26]. When the temperature is lower than 500 °C, the main product is biomass carbon [26]. As the temperature increases, first, a depolymerization reaction begins, and afterward, a splitting reaction initiates, which results in the appearance of gases of small molecules [26]. The pyrolysis carbonization reaction is not only affected by the temperature, but also by the heating rate [25]. When the temperature is below 500 °C, the products are mainly biomass carbon under a slow heating rate [26]. However, as the heating rate speeds up, the output of biomass oil starts to increase, leading to the decrease of biomass carbon content [27]. Taking into account both the cost and the need for sustainable development, the pyrolytic carbonization of biomass is considered to be the most convenient, greenest, and simplest method for the preparation of carbon materials [25].

3 Applications of Carbon Aerogel Materials in Supercapacitors

The research and development of carbon nanomaterials in energy storage devices mainly focus on SCs, lithium-ion batteries, and other types of batteries [3]. Compared with batteries, SCs have higher power density, longer cycle stability, higher Coulombic efficiency, and shorter full charge–discharge cycles [5]. Therefore, SCs—especially those based on carbon nanotubes (CNTs), graphene, and mesoporous carbon electrodes—are becoming more and more popular [9, 13]. Using different synthetic methods, the carbon-based aerogel can be converted into a self-supporting carbon foam/aerogel, in which, the conductivity and capacitance have improved, while the original porous structure of the carbon foam/aerogel has been maintained. In this chapter, we discuss the following carbon aerogel-based electrode materials for SCs: (1) organic polymer-based aerogels, (2) biomass-derived aerogels, and (3) graphene-based aerogels.

3.1 Organic Polymer-Based Aerogels

The first preparation of carbon aerogel was carried out by decomposition of resorcinol–formaldehyde organic aerogel [18]. The decomposition of organic elements during the carbonization process does not destroy the original network structure but leaves behind a material with a rich porous structure (with a porosity of 80%–90%), high SSA (400–1000 $m^2\ g^{-1}$), and good electrical conductivity [28, 29]. Thus, the obtained carbon aerogel exhibits a high SSA and an ultra-high specific capacitance. In recent years, there have been reports in the literature on the influence of sub-nanometer pores on the electrochemical performance of SCs [30, 31]. The results show that micropores with a pore diameter of less than 1 nm can significantly increase the specific capacitance of electrode materials, where especially those micropores with a diameter of 0.5–1 nm are suitable for water-based electrolyte ions [30, 31]. Using phloroglucinol and p-benzodialdehyde as monomers, microporous organic polymers were prepared under solvothermal conditions, and a series of new ultramicroporous carbon microspheres (UCMs) and ultramicroporous carbon nanoparticles (UCNs) were fabricated by high-temperature carbonization using the polymer as the precursor. The synthesis process of ultramicroporous carbon is shown in Fig. 2 [30]. As a SC electrode material, an UCN sample with regular 0.54 nm ultramicropores [particle size ~ 30 nm; SSA = 842 $m^2\ g^{-1}$; pore volume = 0.73 $cm^3\ g^{-1}$] had a specific capacitance of 206 F g^{-1} (at a current density of 1.0 A g^{-1}), and exhibited excellent electrochemical cycling stability by showing a specific capacitance attenuation rate of only 2.4% after 5000 charge–discharge cycles [30]. Furthermore, when the current density was increased to 50 A g^{-1}, the specific capacitance of this sample still remained at 135 F g^{-1}, indicating that it still had good electric double

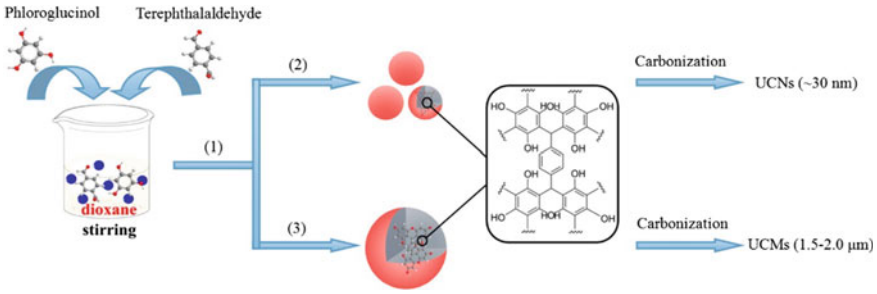

Fig. 2 Schematic of the procedure of synthesis of ultramicroporous carbon microspheres (UCMs) and ultramicroporous carbon nanoparticles (UCNs). Reprinted with permission from Ref. [30], Copyright © 2013 American Chemical Society

layer capacitance characteristics at a super high current density [30]. The excellent electrochemical performance of this sample came from its regular micropores that could accelerate the migration of electrolyte ions and improve its charge and discharge capabilities. The abundant pores provided a buffer area for accumulation of electrolyte ions and reduced their diffusion resistance. A large number of ultramicropores can shorten the transmission distance of electrolyte ions to the surface of the electrode, thereby greatly increasing the specific capacitance of the electrode material [30]. Therefore, as a new type of carbon material, UCNs/UCMs overcome the shortcoming of traditional microporous carbon materials in their inability to be charged and discharged under high currents, thus showing a very broad application prospect in the field of SC electrode materials [30].

Carbon aerogels have a 3D network of open pores, which offers a low resistance path for ion transport and is conducive to high power output. Drying—in particular in the atmospheric pressure—is normally accompanied by shrinkage of the pores, sometimes resulting in SSA values less than 800 $m^2\ g^{-1}$, which imposes a limit on the capacitance performance of the aerogel [32]. There are reports that activation can effectively increase the SSA of carbon aerogels and adjust their pore size distribution [32–34]. Nevertheless, the activator migrates from the outside of the carbon aerogel to the inside for activation. Thus, the internal space of carbon aerogel cannot be fully activated, which leads to low utilization of carbon aerogel [32]. In the presence of K_2CO_3, a hierarchical porous carbon aerogel was successfully prepared through the polymerization of resorcinol and formaldehyde and a one-step carbonization process [32]. This design takes advantage of K_2CO_3 in three capacities: (i) as a catalyst that effectively promotes the cross-linking of resorcinol and formaldehyde, (ii) as a shape-directing agent to adjust the generated carbon network, and (iii) as an in-situ activator to construct an interconnected layered porous framework during carbonization. The obtained aerogel had an SSA of 4568.9 $m^2\ g^{-1}$ and a pore volume of 4.92 $cm^3\ g^{-1}$. As an SC electrode material, the aerogel exhibited a specific capacitance of 173.6 $F\ g^{-1}$ (at a current density of 3 $A\ g^{-1}$; in $EMIMBF_4$ electrolyte), an ultrahigh energy density of 78.1 $Wh\ kg^{-1}$ at the power density of 2.7 $kW\ kg^{-1}$, and a specific capacitance attenuation rate of only 12% after 8000 charge–discharge cycles, indicative of an

excellent electrochemical cycling stability [32]. Due to the limitation in the length of the chapter, other organic polymer-based aerogels are summarized in Table 1 together with their performance as electrode materials in SCs [35–43].

3.2 Biomass-Derived Aerogel

Natural polymers are favored over synthetic polymers and carbon nanomaterials, because they are easy to obtain, are renewable, and are less likely to cause secondary pollution. Glucose, cellulose, bacterial cellulose, and lignin are the common natural polymer materials widely used in the preparation of carbon aerogels [44–48]. At present, a variety of biomass with high cellulose content, such as cotton, wood, waste paper, bamboo, and sisal, are used in the preparation of carbon aerogels [49–52]. In the process of high-temperature pyrolysis, some hydrophilic functional groups on the surface of biomass can be removed through some physical and chemical reactions, thus transforming it into graphitized carbon. Hao et al. used waste bagasse as raw material, carbonized it to produce biomass carbon aerogel, and further activated it [53]. The activated carbon aerogel showed a richer pore structure. The prepared porous carbon aerogel exhibited a specific capacitance of 142.1 F g^{-1} (at a current density of 0.5 A g^{-1}) and possessed a capacitance retention rate of 93.9% after 5000 charge–discharge cycles, thus showing excellent cyclic charge–discharge performance and cycling stability. Wright et al. used cheap banana peels to prepare a hierarchical carbon foam with a large number of biopolymer microporous structures and abundant pore surface functional groups [54]. The carboxyl and hydroxyl groups on the banana peel surface make complexes with zinc ions to form a zinc-containing complex similar to a metal–organic framework (MOF) polymer. Further on, the banana peel-based zinc complex was used as a template, which could be combined with additional carbon sources, such as aminophenol-furfural. Thus, a composite of phenolic resin-banana peel zinc-containing coordination polymer was synthesized and was directly carbonized to obtain hierarchical pore carbon foams (HPCFs) [54]. The obtained HPCFs had 3D interconnected macroporous cores, mesoporous channels, and microporous pores on the pore walls, with an SSA of up to 1650 m^2 g^{-1} and average pore size of 3.01 nm. As the electrode material for SC, the HPCFS electrode showed excellent electrochemical capacitance performance and high-rate characteristics. The specific capacitance of HPCFS electrode was 206 F g^{-1} when the current density was 1.0 A g^{-1} and remained 182 F g^{-1} when the current density was 10 A g^{-1}. Due to its ease of use, low production cost, and excellent electrochemical performance, this type of HPCFS synthesized based on banana peel composite has a wide range of application prospects in SCs. Xu et al. used watermelon as raw material and used freeze-drying technology to prepare aerogels on a large scale, and further carbonized them to prepare biomass-derived aerogels [55]. The activated carbon aerogel had a richer pore structure. As an SC electrode material, the obtained carbon aerogel exhibited excellent electrochemical capacitance performance with a

Table 1 A summary of carbon aerogels (CAs) and modified carbon aerogels as electrode materials in supercapacitors

Material	Preparation method	Electrolyte	SSA	Pore size	Pore volume	Capacitance (scan rate or current density)	Volumetric energy	Capacitance attenuation (cycle)	Ref
Mn_3O_4/CA	Supercritical CO_2	0.5 M Na_2SO_4	577 $m^2\ g^{-1}$	18 nm	1.182 $cm^3\ g^{-1}$	503 F g^{-1} (25 mV s^{-1})	48.5 kW kg^{-1} (500 mV s^{-1}) 21.6 Wh kg^{-1} (500 mV s^{-1})	1% (6000)	[35]
$NiCo_2O_4$/CA	Supercritical CO_2	1 M NaOH	206 $m^2\ g^{-1}$	16.7 nm	0.808 $cm^3\ g^{-1}$	1700 F g^{-1} (25 mV s^{-1})	/	2.4% (2000)	[36]
Polybenzoxazine-based CA	Air drying	/	368 $m^2\ g^{-1}$	3.67 nm	0.34 $cm^3\ g^{-1}$	55.78 F g^{-1}	/	/	[37]
MnO_2/CA	Air drying	1 M Na_2SO_4	120 $m^2\ g^{-1}$	~5 nm	/	515.5 F g^{-1} (2 mV s^{-1})	/	3% (1000)	[38]
Polyaniline/CA	Vacuum drying	/	13.35 $m^2\ g^{-1}$	1.358 nm	0.044 $cm^3\ g^{-1}$	710.7 F g^{-1} (1 mV s^{-1})	58.25 Wh kg^{-1}	43% (1000)	[39]
CA	Supercritical CO_2	1 M H_2SO_4	706 $m^2\ g^{-1}$	10.9 nm	/	197 F g^{-1} (5 mV s^{-1})	/	/	[40]
Nanowhisker-like NiO/CA microbead	Air drying	6 M KOH	/	/	/	356.2 F g^{-1} (1 A g^{-1})	/	0% (4000)	[41]
CAs	Air drying	6 M KOH	638 $m^2\ g^{-1}$	13.5 nm	0.26 $cm^3\ g^{-1}$	141.3 F g^{-1} (5 mV s^{-1})	/	/	[42]
Activated CA	Supercritical CO_2	6 M KOH	2119 $m^2\ g^{-1}$	4.8 nm	2.73 $cm^3\ g^{-1}$	250 F g^{-1} (0.5 A g^{-1})	4.71 Wh kg^{-1} (20 A g^{-1})	12% (4000)	[43]
Carbon nanotube aerogel	Air drying	5 M KOH	1059 $m^2\ g^{-1}$	1.41 nm	2.4 $cm^3\ g^{-1}$	524 F g^{-1}	/	/	[89]
3D/CNTS	Freeze-dried	1 M H_2SO_4	370 $m^2\ g^{-1}$	1.41 nm	1.2 $cm^3\ g^{-1}$	190 F g^{-1} (0.5 A g^{-1})	/	2% (3000)	[90]
Ni-microfiber-supported carbon nanotube aerogel	Air drying	5 M KOH	155 $m^2\ g^{-1}$	3.6 nm	0.138 $cm^3\ g^{-1}$	359 F g^{-1} (1 mV s^{-1})	/	5% (1000)	[91]
Carbon nanotube aerogel	Air drying	3 M H_2SO_4 6 M KOH	1059 $m^2\ g^{-1}$	1.44 nm	/	280 F g^{-1} 524 F g^{-1}	/	0% (5000)	[92]

(continued)

Table 1 (continued)

Material	Preparation method	Electrolyte	SSA	Pore size	Pore volume	Capacitance (scan rate or current density)	Volumetric energy	Capacitance attenuation (cycle)	Ref
N-doped CA	Air drying	6 M KOH	1626 $m^2 g^{-1}$	3.5 nm	1.69 $cm^3 g^{-1}$	354 F g^{-1} (0.2 A g^{-1})	/	15% (5000)	[93]
CNT sponges	CVD	1 M $EMIMBF_4$	100 $m^2 g^{-1}$	3.4 nm	/	28.5 F g^{-1} (1 mV s^{-1})	/	6% (15,000)	[94]
CNS/PEDOT	Vapor phase polymerization	1 M H_2SO_4	/	/	/	67 F g^{-1} (0.01mV s^{-1})	4391 kW kg^{-1}/37 Wh kg^{-1}	6% (5000)	[95]
CNFs/MWCNTs/HAs	Supercritical CO_2	6 M H_2SO_4	871 $m^2 g^{-1}$	2.6 nm	/	178 F g^{-1} (5 mV s^{-1})	13.6 mW cm^{-2} 20 mWh cm^{-2}	0.1% (1000)	[96]
Carbon coated-CNT	Freeze-dried	1 M H_2SO_4	605 $m^2 g^{-1}$	2.3 nm	/	214 F g^{-1} (10 mV s^{-1})	17 kW kg^{-1}/ 37 Wh kg^{-1}	5% (5000)	[97]
GO/aerogel	Freeze-dried	1 M H_2SO_4	/	/	/	172 F g^{-1} (1 A g^{-1})	/	1% (5000)	[74]
Graphene aerogel	Supercritical CO_2	[EMIM] TF_2N	867 $m^2 g^{-1}$	8.60 nm	1.90 $cm^3 g^{-1}$	153 F g^{-1} (0.1 A g^{-1})	21.4 Wh kg^{-1}	/	[75]
rGO aerogel	Supercritical CO_2	1 M H_2SO_4	830 $m^2 g^{-1}$	4.0 nm	/	278.6 F g^{-1} (0.2 A g^{-1})	<10 Wh kg^{-1}	1.5% (1000)	[98]
3D graphene-based frameworks	Freeze-dried	1 M H_2SO_4	350 $m^2 g^{-1}$	3.5 nm	0.810 $cm^3 g^{-1}$	226 F g^{-1} (1 mV s^{-1})	/	0% (5000)	[77]
Conductive graphene aerogel	Supercritical CO_2	6 M KOH	512 $m^2 g^{-1}$	/	2.48 $cm^3 g^{-1}$	128 F g^{-1} (0.05 A g^{-1})	/	/	[78]
3D Nitrogen and Boron Co-doped Graphene	Freeze-dried	1 M H_2SO_4	249 $m^2 g^{-1}$	8.5 nm	/	239 F g^{-1} (5 mV s^{-1})	1.65 kW kg^{-1}/ 8.7 Wh kg^{-1}	0% (1000)	[79]
3D interconnected graphene-based aerogels	Freeze-dried	1 M Na_2SO_4	364.5 $m^2 g^{-1}$	/	/	161.6 F g^{-1} (0.5 A g^{-1})	/	/	[80]

(continued)

Table 1 (continued)

Material	Preparation method	Electrolyte	SSA	Pore size	Pore volume	Capacitance (scan rate or current density)	Volumetric energy	Capacitance attenuation (cycle)	Ref
Alkali-treated graphene oxide	Supercritical CO_2	6 M KOH	763 $m^2 g^{-1}$	10–50 nm	3.8 $cm^3 g^{-1}$	122 F g^{-1} (0.05 A g^{-1})	/	/	[81]
Holey graphene/polypyrrole nanoparticle	Freeze-dried	1 M KOH	278 $m^2 g^{-1}$	0.7–2.7 nm	/	418 F g^{-1} (0.5 A g^{-1})	/	26% (2000)	[82]
DMQ@rGO	Air drying	1 M H_2SO_4	43 $m^2 g^{-1}$	3.38 nm	/	650 F g^{-1} (5 mV s^{-1})	/	1% (25,000)	[83]
Bacterial cellulose	Freeze-dried	0.5 M K_2SO_4	166.7 $m^2 g^{-1}$	7.95 nm	/	42 F g^{-1} (1 mV s^{-1})	/	/	[56]
Cellulose nanofiber–graphene	Supercritical CO_2	/	/	3.5 nm	/	207 F g^{-1} (5 mV s^{-1})	6 Wh kg^{-1}	0.9% (5000)	[57]
Bacterial cellulose–lignin	Supercritical CO_2	6 M KOH	199.4 $m^2 g^{-1}$	17.8 nm	/	124 F g^{-1} (0.5 A g^{-1})	/	2% (10,000)	[46]
Carbon Fiber	Air drying	6 M KOH	2307 $m^2 g^{-1}$	1.0–4.0 nm	1.18 $cm^3 g^{-1}$	283 F g^{-1} (1 A g^{-1})	/	3% (20,000)	[58]

specific capacitance of 333.1 F g^{-1} (at a current density of 1.0 A g^{-1}). It also exhibited excellent charge–discharge cycle performance and cycle stability by showing a capacitance retention rate of 96% after 1000 charge–discharge cycles. Other examples of utilization of biomass-derived aerogels as SC electrode materials can be found in Table 1 [46, 56–58].

3.3 Graphene-Based Aerogel

Graphene is a new type of ultrathin 2D crystal material with high electrical conductivity, high mechanical strength and elastic modulus, and high light transmittance. These excellent properties are specific to graphene sheets on a microscopic scale [59–61]. Macroscopic assembly structures in the form of graphene films, fibers, and aerogels, and other constructs are made to utilize these microscopic properties in practical applications [61–63]. Among these, the graphene aerogel structure can not only realize the conductivity and heat conduction properties of graphene but also has the characteristics of high porosity, large SSA, and low density, which makes it a flourishing research area [62, 63]. In traditional carbon aerogels, the pores are formed by the accumulation of many carbon nanoparticles, whereas in graphene aerogels pores are formed by stacking and overlapping 2D graphene nanosheets. Preparation methods of graphene aerogels are mainly hydrothermal reduction [64–66], cross-linking agent-induced assembly [67, 68], chemical reduction self-assembly [69–71], and template-guided method [72, 73].

The different arrangements of graphene sheets result in different effective electrochemical SSAs because liquid electrolyte ions can only diffuse through interlayer gaps and pores [62]. Thus, different reduced graphene oxide (rGO) structures and morphologies have different electrolyte ion diffusion lengths and diffusion paths [63]. 3D graphene networks have been used in EDLCs and PCs [64, 74–86]. Shi et al. found that when the concentration of the GO suspension is greater than 1 mg mL^{-1}, the GO suspension can be treated by the hydrothermal reduction method to form a stable 3D network hydrogel structure [84]. The shedding of graphene pieces of oxygen-containing functional groups reduces the repulsive force between the layers, which results in the assembly of overlapped nanosheets, thus the in-situ formation of a gel (Fig. 3) [64]. The formed aerogel showed excellent electrochemical capacitance and high ratio discharge property with specific capacitances of 175 F g^{-1} (at a scan rate of 10 mV s^{-1}) and 152 F g^{-1} (at a scan rate of 20 mV s^{-1}) [64]. SC electrodes based on 3D layered graphene/polypyrrole aerogel showed excellent electrochemical properties, including high specific capacitance up to 253 F g^{-1} (at a current density of 0.5 A g^{-1}), excellent rate performance, and excellent cycle stability (capacitance retention of 93% after 2000 cycles) [85]. Huang et al. used 3D porous graphene as the working electrode in the SC [86]. In the alkaline electrolyte, the measured capacitance was 341 F g^{-1} (at a scan rate of 1 mV s^{-1}) and the energy density was 16.2 Wh kg^{-1}, whereas in the organic electrolyte the measured values were 166 F g^{-1} (at a scan rate of 1 mV s^{-1}) and 52.5 Wh kg^{-1}, respectively [86]. Besides, due to the

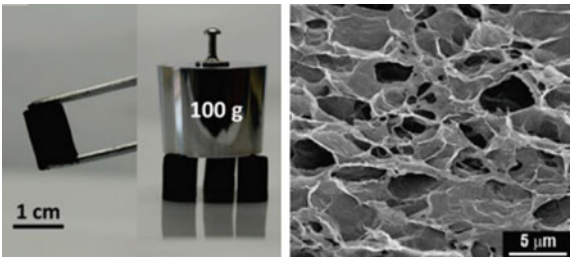

Fig. 3 Graphene oxide (GO) self-assembly results in a pyrotechnic graphene hydrogel. Reprinted with permission from Ref. [64], Copyright © 2010 American Chemical Society

high packing density of the 3D graphene network, higher volume power densities of 20.7 and 67.2 Wh L^{-1} were obtained in alkali and organic electrolytes, respectively [86]. After 1000 galvanostatic charge–discharge cycles, more than 96% and 86% of the original capacitance could be retained in alkaline and organic electrolytes, respectively [86]. 3D porous graphene electrode has better ion diffusion path and better electrochemical characteristics than traditional carbon-based electrode. The open pore structure improves the ion transport rate in EDLCs, reduces the ion diffusion resistance and eliminates the distributed charge storage behavior [87, 88]. Other examples of utilization of graphene-based aerogels as SC electrode materials can be found in Table 1 [74–83].

4 Conclusion

Carbon aerogels have found their way as electrode materials in supercapacitors. This is mostly due to their excellent electrical properties and high specific surface areas. In this chapter, the recent progress in the areas of the synthesis and application of carbon aerogels has been summarized, and the essential properties of carbon aerogels, including capacitance, volumetric energy, porosity, and capacitance attenuation during charge–discharge cycles have been discussed.

References

1. J. Artz, T.E. Müller, K. Thenert, J. Kleinekorte, R. Meys, A. Sternberg, A. Bardow, W. Leitner, Sustainable conversion of carbon dioxide: an integrated review of catalysis and life cycle assessment. Chem. Rev. **118**, 434–504 (2017)
2. G. Liu, M. Lee, S. Kwon, G. Zeng, J. Eichhorn, A.K. Buckley, F.D. Toste, W.A. Goddard, F.M. Toma, CO_2 reduction on pure Cu produces only H_2 after subsurface O is depleted: theory and experiment. Proc. Natl. Acad. Sci. (2021). https://doi.org/10.1073/PNAS.2012649118
3. Z. Yang, J. Ren, Z. Zhang, X. Chen, G. Guan, L. Qiu, Y. Zhang, H. Peng, Recent advancement of nanostructured carbon for energy applications. Chem. Rev. **2015**(115), 5159–5223 (2015). https://doi.org/10.1021/cr5006217
4. C. Tan, H. Zhang, Two-dimensional transition metal dichalcogenide nanosheet-based composites. Chem. Soc. Rev. **2015**(44), 2713–2731 (2015). https://doi.org/10.1039/c4cs00182f

5. P. Simon, Y. Gogotsi, B. Dunn, Where do batteries end and supercapacitors begin? Science **343**, 1210–1211 (2014)
6. L. Dai, D.W. Chang, J.B. Baek, W. Lu, Carbon nanomaterials for advanced energy conversion and storage. Small **8**, 1130–1166 (2012). https://doi.org/10.1002/smll.201101594
7. J.R. Miller, P. Simon, Materials science: electrochemical capacitors for energy management. Science **321**, 651–652 (2008)
8. M. Winter, R.J. Brodd, What are batteries, fuel cells, and supercapacitors? Chem. Rev. **104**, 4245–4270 (2004)
9. C. Zhong, Y. Deng, W. Hu, J. Qiao, L. Zhang, J. Zhang, A review of electrolyte materials and compositions for electrochemical supercapacitors. Chem. Soc. Rev. **2015**(44), 7484–7539 (2015). https://doi.org/10.1039/c5cs00303b
10. P. Simon, Y. Gogotsi, Materials for electrochemical capacitors. Nat Mater **7**, 845–854 (2008)
11. J. Cao, Q. Mei, R. Wu, W. Wang, Flower-like nickel e cobalt layered hydroxide nanostructures for super long-life asymmetrical supercapacitors. Electrochim. Acta. **321**, 134711 (2019)
12. J. Cao, T. Zhou, Y. Xu, Y. Qi, W. Jiang, W. Wang, P. Sun, A. Li, Q. Zhang, Oriented assembly of anisotropic nanosheets into ultrathin flowerlike superstructures for energy storage. ACS Nano **2021**(15), 2707–2718 (2021)
13. X. Chen, R. Paul, L. Dai, Carbon-based supercapacitors for efficient energy storage. Natl. Sci. Rev. **4**, 453–489 (2017)
14. H. Xie, J. Wang, W. Wang, Constructing porous carbon nanomaterials using redox-induced low molecular weight hydrogels and their application as supercapacitors. ChemistrySelect **2**, 9330–9335 (2017). https://doi.org/10.1002/slct.201701702
15. X. Qian, N. Li, M. Imerhasan, W. Wang, Conversion of low molecular weight hydrogel to nitrogen-doped carbon materials and its application as supercapacitor. Colloids Surf. A Physicochem. Eng. Asp. **573**, 255–261 (2019). https://doi.org/10.1016/j.colsurfa.2019.04.037
16. S. Bose, T. Kuila, A.K. Mishra, R. Rajasekar, N.H. Kim, J.H. Lee, Carbon-based nanostructured materials and their composites as supercapacitor electrodes. J. Mater. Chem. **2012**(22), 767–784 (2012). https://doi.org/10.1039/c1jm14468e
17. X. Cao, Z. Yin, H. Zhang, Three-dimensional graphene materials: preparation, structures and application in supercapacitors. Energy Environ. Sci. **2014**(7), 1850–1865 (2014). https://doi.org/10.1039/c4ee00050a
18. R.W. Pekala, Organic aerogels from the polycondensation of resorcinol with formaldehyde. J. Mater. Sci. **24**, 3221–3227 (1989). https://doi.org/10.1007/BF01139044
19. E. Berl, A. Schmidt, Über die Entstehung der Kohlen. II. Die Inkohlung von Cellulose und Lignin in neutralem Medium. Justus Liebigs Ann Chem (1932). https://doi.org/10.1002/jlac.19324930106
20. Z. Gao, Y. Zhang, N. Song, X. Li, Biomass-derived renewable carbon materials for electrochemical energy storage. Mater. Res. Lett. (2017). https://doi.org/10.1080/21663831.2016.1250834
21. Y. Shi, X. Zhang, G. Liu, Activated carbons derived from hydrothermally carbonized sucrose: remarkable adsorbents for adsorptive desulfurization. ACS Sustain. Chem. Eng. **2015**(3), 2237–2246 (2015). https://doi.org/10.1021/acssuschemeng.5b00670
22. M.M. Titirici, A. Thomas, M. Antonietti, Replication and coating of silica templates by hydrothermal carbonization. Adv. Funct. Mater. **17**, 1010–1018 (2007). https://doi.org/10.1002/adfm.200600501
23. A. Allahbakhsh, A.R. Bahramian, Self-assembled and pyrolyzed carbon aerogels: an overview of their preparation mechanisms, properties and applications. Nanoscale **17**, 1010–1018 (2015). https://doi.org/10.1039/c5nr03855c
24. H. Zhuo, Y. Hu, X. Tong, A supercompressible, elastic, and bendable carbon aerogel with ultrasensitive detection limits for compression strain, pressure, and bending angle. Adv. Mater. **2018**(30), 1706705 (2018). https://doi.org/10.1002/adma.201706705
25. N.A. Qambrani, M.M. Rahman, S. Won, S. Shim, C. Ra, Biochar properties and eco-friendly applications for climate change mitigation, waste management, and wastewater treatment: a review. Renew. Sustain. Energy Rev. **79**, 255–273 (2017)

26. F.X. Collard, J. Blin, A review on pyrolysis of biomass constituents: mechanisms and composition of the products obtained from the conversion of cellulose, hemicelluloses and lignin. Renew. Sustain. Energy Rev. **38**, 594–608 (2014)
27. S. Kang, X. Li, J. Fan, J. Chang, Characterization of hydrochars produced by hydrothermal carbonization of lignin, cellulose, d-xylose, and wood meal. Ind. Eng. Chem. Res. **51**, 9023–9031 (2012)
28. B. Li, Z. Guan, X. Yang, W.D. Wang, I. Hussain, K. Song, B. Tan, T. Li, Multifunctional microporous organic polymers. J. Mater. Chem. A. **2**, 11930–11939 (2014). https://doi.org/10.1039/c4ta01081g
29. R. Dawson, E. Stöckel, J.R. Holst, D.J. Adams, A.I. Cooper, Microporous organic polymers for carbon dioxide capture. Energy Environ. Sci. (2011). https://doi.org/10.1039/c1ee01971f
30. Y. Zhao, M. Liu, L. Gan, X. Ma, D. Zhu, Z. Xu, L. Chen, Ultramicroporous carbon nanoparticles for the high-performance electrical double-layer capacitor electrode. Energy Fuels **28**, 1561–1568 (2014)
31. B. Xu, S. Hou, H. Duan, G. Cao, M. Chu, Y. Yang, Ultramicroporous carbon as electrode material for supercapacitors. J. Power Sources **228**, 193–197 (2013)
32. F. Li, L. Xie, G. Sun, F. Su, Q. Kong, Q. Li, Y. Chao, X. Guo, C. Chen, Boosting the specific surface area of hierarchical porous carbon aerogel through the multiple roles of the catalyst for high-performance supercapacitors. ChemElectroChem **4**, 3119–3125 (2017)
33. N. Fechler, T.P. Fellinger, M. Antonietti, One-pot synthesis of nitrogen-sulfur-co-doped carbons with tunable composition using a simple isothiocyanate ionic liquid. J. Mater. Chem. A **1**, 14097–14102 (2013)
34. Z.Y. Jin, A.H. Lu, Y.Y. Xu, J.T. Zhang, W.C. Li, Ionic liquid-assisted synthesis of microporous carbon nanosheets for use in high rate and long cycle life supercapacitors. Adv. Mater. **26**, 3700–3705 (2014)
35. Y.H. Lin, T.Y. Wei, H.C. Chien, S.Y. Lu, Manganese oxide/carbon aerogel composite: an outstanding supercapacitor electrode material. Adv. Energy Mater. **1**, 901–907 (2011)
36. H.C. Chien, W.Y. Cheng, Y.H. Wang, S.Y. Lu, Ultrahigh specific capacitances for supercapacitors achieved by nickel cobaltite/carbon aerogel composites. Adv. Funct. Mater. **22**, 5038–5043 (2012)
37. P. Katanyoota, T. Chaisuwan, A. Wongchaisuwat, S. Wongkasemjit, Novel polybenzoxazine-based carbon aerogel electrode for supercapacitors. Mater. Sci. Eng. B Solid-State Mater. Adv. Technol. **167**, 36–42 (2010)
38. G.R. Li, Z.P. Feng, Y.N. Ou, D. Wu, R. Fu, Y.X. Tong, Mesoporous MnO_2/carbon aerogel composites as promising electrode materials for high-performance supercapacitors. Langmuir **26**, 2209–2213 (2010)
39. H. An, Y. Wang, X. Wang, N. Li, L. Zheng, The preparation of PANI/CA composite electrode material for supercapacitors and its electrochemical performance. J. Solid State Electrochem. **14**, 651–657 (2010)
40. Y.J. Lee, J.C. Jung, J. Yi, S.H. Baeck, J.R. Yoon, I.K. Song, Preparation of carbon aerogel in ambient conditions for electrical double-layer capacitor. Curr. Appl. Phys. **10**, 682–686 (2010)
41. X. Wang, X. Wang, L. Yi, L. Liu, Y. Dai, H. Wu, Preparation and capacitive properties of the core-shell structure carbon aerogel microbeads- Nanowhisker-like NiO composites. J. Power Sources **224**, 317–323 (2013)
42. G. Lv, D. Wu, R. Fu, Z. Zhang, Z. Su, Electrochemical properties of conductive filler/carbon aerogel composites as electrodes of supercapacitors. J. Non Cryst. Solids **354**, 4567–4571 (2008)
43. D. Liu, J. Shen, N. Liu, H. Yang, A. Du, Preparation of activated carbon aerogels with hierarchically porous structures for electrical double layer capacitors. Electrochim. Acta **89**, 571–576 (2013)
44. C. Li, Z.Y. Wu, H.W. Liang, J.F. Chen, S.H. Yu, Ultralight multifunctional carbon-based aerogels by combining graphene oxide and bacterial cellulose. Small **13**, 1700453 (2017). https://doi.org/10.1002/smll.201700453

45. C. Wan, J. Li, Synthesis and electromagnetic interference shielding of cellulose-derived carbon aerogels functionalized with α-Fe_2O_3 and polypyrrole. Carbohydr. Polym. **161**, 158–165 (2017). https://doi.org/10.1016/j.carbpol.2017.01.003
46. X. Xu, J. Zhou, D.H. Nagaraju, L. Jiang, V.R. Marinov, G. Lubineau, H.N. Alshareef, M. Oh, Flexible, highly graphitized carbon aerogels based on bacterial cellulose/lignin: catalyst-free synthesis and its application in energy storage devices. Adv. Funct. Mater. **25**, 3193–3202 (2015)
47. Z. Zeng, C. Wang, Y. Zhang, P. Wang, S.I. Seyed Shahabadi, Y. Pei, M. Chen, X. Lu, Ultralight and highly elastic graphene/lignin-derived carbon nanocomposite aerogels with ultrahigh electromagnetic interference shielding performance. ACS Appl. Mater. Interfaces. **10**, 8205–8213 (2018). https://doi.org/10.1021/acsami.7b19427
48. J. Zhang, B. Li, L. Li, A. Wang, Ultralight, compressible and multifunctional carbon aerogels based on natural tubular cellulose. J. Mater. Chem. A **4**, 2069–2074 (2016). https://doi.org/10.1039/c5ta10001a
49. H. Bi, Z. Yin, X. Cao et al., Carbon fiber aerogel made from raw cotton: a novel, efficient and recyclable sorbent for oils and organic solvents. Adv. Mater. (2013). https://doi.org/10.1002/adma.201302435
50. Y. Zhang, L. Zuo, L. Zhang, Y. Huang, H. Lu, W. Fan, T. Liu, Cotton wool derived carbon fiber aerogel supported few-layered $MoSe_2$ nanosheets as efficient electrocatalysts for hydrogen evolution. ACS Appl. Mater. Interfaces. **2016**(8), 7077–7085 (2016). https://doi.org/10.1021/acsami.5b12772
51. L. Li, B. Li, H. Sun, J. Zhang, Compressible and conductive carbon aerogels from waste paper with exceptional performance for oil/water separation. J. Mater. Chem. A **5**, 14858–14864 (2017). https://doi.org/10.1039/c7ta03511j
52. W. Li, J. Liu, D. Zhao, Mesoporous materials for energy conversion and storage devices. Nat. Rev. Mater. **1**, 16023 (2016). https://doi.org/10.1038/natrevmats.2016.23
53. P. Hao, Z. Zhao, J. Tian, H. Li, Y. Sang, G. Yu, H. Cai, H. Liu, C.P. Wong, A. Umar, Hierarchical porous carbon aerogel derived from bagasse for high performance supercapacitor electrode. Nanoscale **6**, 12120–12129 (2014)
54. Y. Lv, L. Gan, M. Liu, W. Xiong, Z. Xu, D. Zhu, D.S. Wright, A self-template synthesis of hierarchical porous carbon foams based on banana peel for supercapacitor electrodes. J. Power Sources **209**, 152–157 (2012)
55. X.L. Wu, T. Wen, H.L. Guo, S. Yang, X. Wang, A.W. Xu, Biomass-derived sponge-like carbonaceous hydrogels and aerogels for supercapacitors. ACS Nano **7**, 3589–3597 (2013). https://doi.org/10.1021/nn400566d
56. K.Y. Lee, H. Qian, F.H. Tay, J.J. Blaker, S.G. Kazarian, A. Bismarck, Bacterial cellulose as source for activated nanosized carbon for electric double layer capacitors. J. Mater. Sci. **48**, 367–376 (2013)
57. K. Gao, Z. Shao, J. Li, X. Wang, X. Peng, W. Wang, F. Wang, Cellulose nanofiber-graphene all solid-state flexible supercapacitors. J. Mater. Chem. A **1**, 63–67 (2013)
58. P. Cheng, T. Li, H. Yu, L. Zhi, Z. Liu, Z. Lei, Biomass-derived carbon fiber aerogel as a binder-free electrode for high-rate supercapacitors. J. Phys. Chem. C **120**, 2079–2086 (2016)
59. A.K. Geim, Graphene: status and prospects. Science **324**, 1530–1534 (2009)
60. T. Winzer, A. Knorr, E. Malic, Carrier multiplication in graphene. Nano Lett. **10**, 4839–4843 (2010). https://doi.org/10.1021/nl1024485
61. H. Chen, M.B. Müller, K.J. Gilmore, G.G. Wallace, D. Li, Mechanically strong, electrically conductive, and biocompatible graphene paper. Adv. Mater. **20**, 3557–3561 (2008). https://doi.org/10.1002/adma.200800757
62. V. Chabot, D. Higgins, A. Yu, X. Xiao, Z. Chen, J. Zhang, A review of graphene and graphene oxide sponge: material synthesis and applications to energy and the environment. Energy Environ. Sci. **7**, 1564–1596 (2014). https://doi.org/10.1039/c3ee43385d
63. S. Nardecchia, D. Carriazo, M.L. Ferrer, M.C. Gutiérrez, F. Monte, Three dimensional macroporous architectures and aerogels built of carbon nanotubes and/or graphene: synthesis and applications. Chem. Soc. Rev. **42**, 794–830 (2013). https://doi.org/10.1039/c2cs35353a

64. Y. Xu, K. Sheng, C. Li, G. Shi, Self-assembled graphene hydrogel via a one-step hydrothermal process. ACS Nano **4**, 4324–4330 (2010). https://doi.org/10.1021/nn101187z
65. Y. Bai, R.B. Rakhi, W. Chen, H.N. Alshareef, Effect of pH-induced chemical modification of hydrothermally reduced graphene oxide on supercapacitor performance. J. Power Sources **233**, 313–319 (2013)
66. Y. Wu, N. Yi, L. Huang, Three-dimensionally bonded spongy graphene material with super compressive elasticity and near-zero Poisson's ratio. Nat. Commun. (2015). https://doi.org/10.1038/NCOMMS7141
67. M. Chen, C. Zhang, X. Li, L. Zhang, Y. Ma, L. Zhang, X. Xu, F. Xia, W. Wang, J. Gao, A one-step method for reduction and self-assembling of graphene oxide into reduced graphene oxide aerogels. J. Mater. Chem. **1**, 2869–2877 (2013)
68. H. Bai, C. Li, X. Wang, G. Shi, A pH-sensitive graphene oxide composite hydrogel. Chem. Commun. **46**, 2376–2378 (2010)
69. W. Chen, L. Yan, In situ self-assembly of mild chemical reduction graphene for three-dimensional architectures. Nanoscale **3**, 3132–3137 (2011). https://doi.org/10.1039/c1nr10355e
70. H. Hu, Z. Zhao, W. Wan, Y. Gogotsi, J. Qiu, Ultralight and highly compressible graphene aerogels. Adv. Mater. **25**, 2219–2223 (2013)
71. H.-P. Cong, X.-C. Ren, P. Wang, S.-H. Yu, Macroscopic multifunctional graphene-based hydrogels and aerogels by a metal ion induced self-assembly process. ACS Nano **6**, 2693–2703 (2012)
72. X. Huang, K. Qian, J. Yang, J. Zhang, L. Li, C. Yu, D. Zhao, Functional nanoporous graphene foams with controlled pore sizes. Adv. Mater. **24**, 4419–4423 (2012)
73. Z. Chen, W. Ren, L. Gao, B. Liu, S. Pei, H.-M. Cheng, Three-dimensional flexible and conductive interconnected graphene networks grown by chemical vapour deposition. Nat. Mater. **10**, 424–428 (2011)
74. F. Liu, S. Song, D. Xue, H. Zhang, Folded structured graphene paper for high performance electrode materials. Adv. Mater. **24**, 1089–1094 (2012)
75. X. Wu, J. Zhou, W. Xing, G. Wang, H. Cui, S. Zhuo, Q. Xue, Z. Yan, S.Z. Qiao, High-rate capacitive performance of graphene aerogel with a superhigh C/O molar ratio. J. Mater. Chem. **22**, 23186–23193 (2012)
76. W. Si, X. Wu, J. Zhou, F. Guo, S. Zhuo, H. Cui, W. Xing, Reduced graphene oxide aerogel with high-rate supercapacitive performance in aqueous electrolytes. Nanoscale Res. Lett. **8**, 1–8 (2013)
77. Z.S. Wu, Y. Sun, Y.Z. Tan, S. Yang, X. Feng, K. Müllen, Three-dimensional graphene-based macro- and mesoporous frameworks for high-performance electrochemical capacitive energy storage. J. Am. Chem. Soc. **134**, 19532–19535 (2012)
78. X. Zhang, Z. Sui, B. Xu, S. Yue, Y. Luo, W. Zhan, B. Liu, Mechanically strong and highly conductive graphene aerogel and its use as electrodes for electrochemical power sources. J. Mater. Chem. **21**, 6494–6497 (2011)
79. Z.S. Wu, A. Winter, L. Chen, Y. Sun, A. Turchanin, X. Feng, K. Müllen, Three-dimensional nitrogen and boron co-doped graphene for high-performance all-solid-state supercapacitors. Adv. Mater. **24**, 5130–5135 (2012)
80. C.C. Ji, M.W. Xu, S.J. Bao, C.J. Cai, Z.J. Lu, H. Chai, F. Yang, H. Wei, Self-assembly of three-dimensional interconnected graphene-based aerogels and its application in supercapacitors. J. Colloid Interface Sci. **407**, 416–424 (2013)
81. F. Meng, X. Zhang, B. Xu, S. Yue, H. Guo, Y. Luo, Alkali-treated graphene oxide as a solid base catalyst: synthesis and electrochemical capacitance of graphene/carbon composite aerogels. J. Mater. Chem. **21**, 18537–18539 (2011)
82. Y. He, Y. Bai, X. Yang, J. Zhang, L. Kang, H. Xu, F. Shi, Z. Lei, Z.H. Liu, Holey graphene/polypyrrole nanoparticle hybrid aerogels with three-dimensional hierarchical porous structure for high performance supercapacitor. J. Power Sources **317**, 10–18 (2016)
83. M. Boota, C. Chen, M. Bécuwe, L. Miao, Y. Gogotsi, Pseudocapacitance and excellent cyclability of 2,5-dimethoxy-1,4-benzoquinone on graphene. Energy Environ. Sci. **9**, 2586–2594 (2016)

84. Y. Zhao, C. Hu, Y. Hu, H. Cheng, G. Shi, L. Qu, A versatile, ultralight, nitrogen-doped graphene framework. Angew. Chemie. Int. Ed. **51**, 11371–11375 (2012)
85. S. Ye, J. Feng, Self-assembled three-dimensional hierarchical graphene/polypyrrole nanotube hybrid aerogel and its application for supercapacitors. ACS Appl. Mater. Interfaces **6**, 9671–9679 (2014)
86. J. Hu, Z. Kang, F. Li, X. Huang, Graphene with three-dimensional architecture for high performance supercapacitor. Carbon **67**, 221–229 (2014)
87. Y. Zhao, J. Liu, Y. Hu, H. Cheng, C. Hu, C. Jiang, L. Jiang, A. Cao, L. Qu, Highly compression-tolerant supercapacitor based on polypyrrole-mediated graphene foam electrodes. Adv. Mater. **25**, 591–595 (2013). https://doi.org/10.1002/adma.201203578
88. J. Chen, K. Sheng, P. Luo, C. Li, G. Shi, Graphene hydrogels deposited in nickel foams for high-rate electrochemical capacitors. Adv. Mater. **24**, 4569–4573 (2012)
89. T. Bordjiba, M. Mohamedi, L.H. Dao, New class of carbon-nanotube aerogel electrodes for electrochemical power sources. Adv. Mater. **20**, 815–819 (2008)
90. J. Zhong, Z. Yang, R. Mukherjee, T.A. Varghese, K. Zhu, P. Sun, J. Lian, H. Zhu, N. Koratkar, Carbon nanotube sponges as conductive networks for supercapacitor devices. Nano Energy **2**, 1025–1030 (2013)
91. Y. Fang, F. Jiang, H. Liu, X. Wu, Y. Lu, Free-standing Ni-microfiber-supported carbon nanotube aerogel hybrid electrodes in 3D for high-performance supercapacitors. RSC Adv. **2**, 6562–6569 (2012)
92. T. Bordjiba, M. Mohamedi, Molding versus dispersion: effect of the preparation procedure on the capacitive and cycle life of carbon nanotubes aerogel composites. J. Solid State Electrochem. **15**, 765–771 (2011)
93. J. Zhang, G. Chen, Q. Zhang, F. Kang, B. You, Self-assembly synthesis of N-doped carbon aerogels for supercapacitor and electrocatalytic oxygen reduction. ACS Appl. Mater. Interfaces **7**, 12760–12766 (2015)
94. P. Li, C. Kong, Y. Shang, Highly deformation-tolerant carbon nanotube sponges as supercapacitor electrodes. Nanoscale **5**, 8472–8479 (2013)
95. J.A. Lee, M.K. Shin, S.H. Kim, S.J. Kim, G.M. Spinks, G.G. Wallace, R. Ovalle-Robles, M.D. Lima, M.E. Kozlov, R.H. Baughman, Hybrid nanomembranes for high power and high energy density supercapacitors and their yarn application. ACS Nano **6**, 327–334 (2012)
96. K. Gao, Z. Shao, X. Wang, Y. Zhang, W. Wang, F. Wang, Cellulose nanofibers/multi-walled carbon nanotube nanohybrid aerogel for all-solid-state flexible supercapacitors. RSC Adv. **3**, 15058–15064 (2013)
97. T. Tao, L. Zhang, H. Jiang, C. Li, Functional mesoporous carbon-coated CNT network for high-performance supercapacitors. New J. Chem. **37**, 1294–1297 (2013)
98. W. Si, X. Wu, J. Zhou, F. Guo, S. Zhuo, H. Cui, W. Xing, Reduced graphene oxide aerogel with high-rate supercapacitive performance in aqueous electrolytes. Nanoscale Res. Lett. **8**, 247 (2013). https://doi.org/10.1186/1556-276x-8-247

Carbon Nanofibers for Supercapacitors

Jiadeng Zhu, Hui Cheng, and Qiang Gao

Abstract Carbon nanofibers (CNFs) and their composites have been considered as promising candidates for the application in supercapacitors (SCs) due to their one-dimensional and high surface area features, offering shortened electron pathways and high ion-accessible sites. This chapter aims to provide an overview of research in the preparation and applications of CNFs and their composites in SCs. It starts with a brief introduction of SCs and CNFs, followed by their preparation, structure design, properties, and advantages. Applications of CNFs and their composites in SCs have been further discussed in detail. Perspectives regarding the broad applications of CNFs and their composites have also been presented at the end to give insightful comments in this area.

Keywords Carbon nanofibers · Supercapacitors · Electrospinning · Properties · Applications

1 Introduction

Supercapacitors (SCs) have attracted tremendous attention in the field of energy storage systems for electric vehicles, hybrid electric vehicles, as well as portable electronic devices recently because of their long cycle time and high power density [1–4]. Generally, there are two types of SCs, which are called electrical double-layer

J. Zhu (✉)
Chemical Sciences Division, Oak Ridge National Laboratory, Oak Ridge, TN 37831, USA
e-mail: zhujiadeng@gmail.com

Smart Devices and Printed Electronics Foundry, Brewer Science Inc., Springfield, MO 65806, USA

H. Cheng
Department of Textile Engineering, Chemistry and Science, Wilson College of Textiles, North Carolina State University, Raleigh, NC 27695-8301, USA

Q. Gao
School of Chemistry and Chemical Engineering, Yangzhou University, Yangzhou 225002, China

S. Thomas et al. (eds.), *Nanostructured Materials for Supercapacitors*,
Advances in Material Research and Technology,
https://doi.org/10.1007/978-3-030-99302-3_10

capacitors (EDLCs) and pseudocapacitors (PCs), respectively [5, 6]. The capacitance arises from the charge separation at the electro/electrolyte interface for EDLCs, while for PCs, it generates from surface redox reactions of active materials (i.e., metal oxides, conductive polymers, etc.) [7–9]. To achieve high capacitance and a high energy density, hybrids, which combine both EDLC and PC, have received remarkable interest, and the selection of electrode materials is extremely important in this regard [10–12].

Various carbon-based materials (i.e., graphene, carbon nanotubes, carbon nanoparticles, etc.) have been widely studied As the most used electrodes for EDLCs. Among them, carbon nanofibers (CNFs) via electrospinning, which has been considered as a most convenient method to prepare CNFs and their composites [13–18] due to its easy set-up, are receiving tremendous attention because of their high surface area, good electrical conductivity, surface functionality, etc. [19]. Additionally, elemental doping (i.e., nitrogen doping, phosphorus doping, etc.) and morphology control (i.e., porous structure, etc.) approaches have been performed to enhance the performance of CNFs [20–23]. For example, Barranco et al. [20] prepared amorphous CNFs, which were then applied as the electrode for SCs. The result indicated that the pristine CNFs could obtain a surface area of 448 $m^{2\,g-1}$, which was increased to 1520 m^2g^{-1} with the activation by KOH (KOH/CNF = 3/1 by weight). The corresponding capacitance of the cell reached 255 F g^{-1} in the acid electrolyte, which was significantly higher than that of the cell with pristine CNFs, resulting from new micropores, a higher content of oxygen-containing groups, and a larger surface area. Tian et al. [21] utilized NH_3 as the nitrogen provider to synthesize nitrogen-doped CNFs, which exhibited a high surface area of 763 m^2g^{-1} with good thermal and electrical conductivities, as well as rich surface functionalities. As a result, the cell with such unique electrodes could obtain a capacity of 251.2 F g^{-1} at a current density of 0.1 A g^{-1}, and capacity retention of 99% at 20 A g^{-1} even after 2000 cycles.

More recently, CNF composites have been prepared to further enhance the capacitance of SCs, especially for the materials with surface redox reactions [24–28]. For example, a highly conductive CNF/MnO_2 membrane was fabricated, which was then used for achieving high-performance SCs [29]. The cell with the resultant electrode could deliver a capacitance of 311 F g^{-1} at 2 $^{mV\,s-1}$ with good cycling stability. Other materials, like Co_3O_4, have also been widely utilized due to their high theoretical capacitance. Abouali et al. [30] successfully prepared the CNF/Co_3O_4 composite via electrospinning followed by the heat-treatment. The capacitance with such prepared electrode could be up to 586 F g^{-1} at a current density of 1 A g^{-1} with capacitance retention of 74% after 2000 cycles at 2 A g^{-1}, benefiting from the good electrical conductivity of the electrode and the uniform distribution of active particles in the CNF matrix.

In this chapter, we are mainly discussing the advantages of CNFs and their composites applied for SCs. It begins with a brief introduction of electrospinning and its working mechanism, followed by the fabrication and advantages of CNFs. More examples regarding the applications of CNFs and their composites for SCs will be

given and discussed in the following sections, aiming to provide an overall view of the CNFs and their composites in this area.

2 Overview of Electrospinning Derived CNFs

Electrospinning, highly versatile nanotechnology for nanofibers fabrication, has been widely utilized over the past decades [31–33]. This straightforward, incessant, and cost-effective method involves electrohydrodynamic phenomena to launch ultrathin fibers from an enormous number of materials including polymers, inorganic ceramics, composites, etc. [34–37]. So far, numerous research groups have contributed to the understanding of the electrospinning process, the characterization of electrospun nanofibers, and the identification of their potential applications, especially for CNFs.

2.1 Principle of Electrospinning

There are four main parts in a typical electrospinning apparatus (Fig. 1), including a high-voltage power supply, a metallic spinneret, a grounded collector, and an automatic syringe pump. In a conventional electrospinning process, the polymeric liquid is under an external high electric field, then the pendant droplet held by surface tension on the spinning tip can be charged with charges, which generates electrostatic force against the surface tension and forms a conical shape known as Taylor cone (Fig. 1). Once the electric field reaches a threshold value at which the repulsive electric force exceeds the surface tension, a thin charged jet is ejected from the tip of the Taylor cone [38, 39]. The jet then starts to elongate, bend and form 3D spiral loops simultaneously with solvent evaporating in traveling to the collector under a

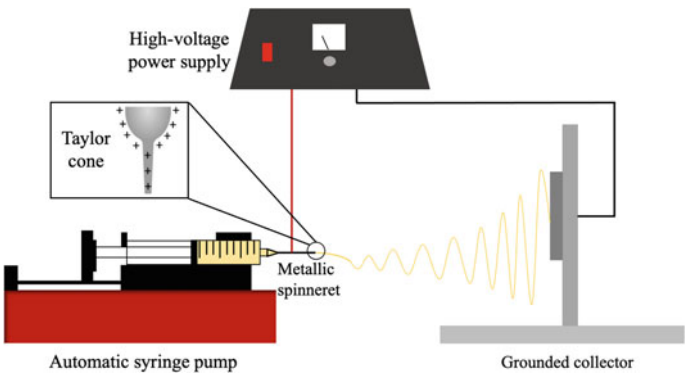

Fig. 1 Schematic drawing of elementary setup for electrospinning with inserted Taylor cone

high voltage [40]. Their small diameter provides a large surface-to-volume ratio, high length-to-diameter ratio, tunable porosity, and excellent malleability to achieve high-performance and multi-functional nanofibers with their 2D and 3D assemblies, which can be further treated to synthesize CNFs for their applications in SCs [41–43].

2.2 Structures of CNFs

As discussed earlier, CNFs can be prepared after treating the as-spun fibers. The resultant CNFs usually exhibit a unique morphologic structure featured with ultrafine diameters, extremely long length, large surface area per unit mass, and small pore size. Numbers of nanofiber structures and morphologies can be obtained via controlling parameters (i.e., spinning solutions, nozzle design, etc.). Generally, electrospun nanofibers are predominately cylindrically shaped (Fig. 2a) as a result of cylindrical fluid jet formation from the tip of the Taylor cone. For instance, Agyemang et al. [44] used polyacrylonitrile (PAN) as the precursor to obtaining the as-spun PAN nanofibers, which were then stabilized and carbonized to prepare CNFs. Later, a porous CNF membrane (Fig. 2b) was successfully fabricated with the help of poly(methyl methacrylate) (PMMA), which was decomposed during the heat treatment, performing as an activation agent to increase the surface area of the CNFs [45]. Moreover, with the design of the nozzle, hollow CNFs could also be synthesized, as shown in Fig. 2c [46]. The PAN and poly(vinyl pyrrolidone) (PVP) solutions were performed as the shell and core, respectively. The PVP could be fully decomposed during the pyrolysis, which generated a core–shell structure, as can be seen in Fig. 2c. Other morphological structures, like ribbon-shaped, helical, side-by-side nanofibers have also been successfully formed by electrospinning with required properties and performances.

2.3 Advantages of Electrospinning Derived CNFs

It has been considered that electrospun derived CNFs and their composites have been widely applied in SCs ascribed to their larger surface-to-volume area, tunable porosity, malleability to conform to a wide variety of sizes and shapes, and the ability to control the nanofiber composition to achieve the promising results from its properties and functionality. Besides, their desired nanostructures have exhibited unique electrical, optical, and catalytic properties than the bulk parts as well as nanomaterials synthesized through other approaches, which are discussed in detail in the following sections.

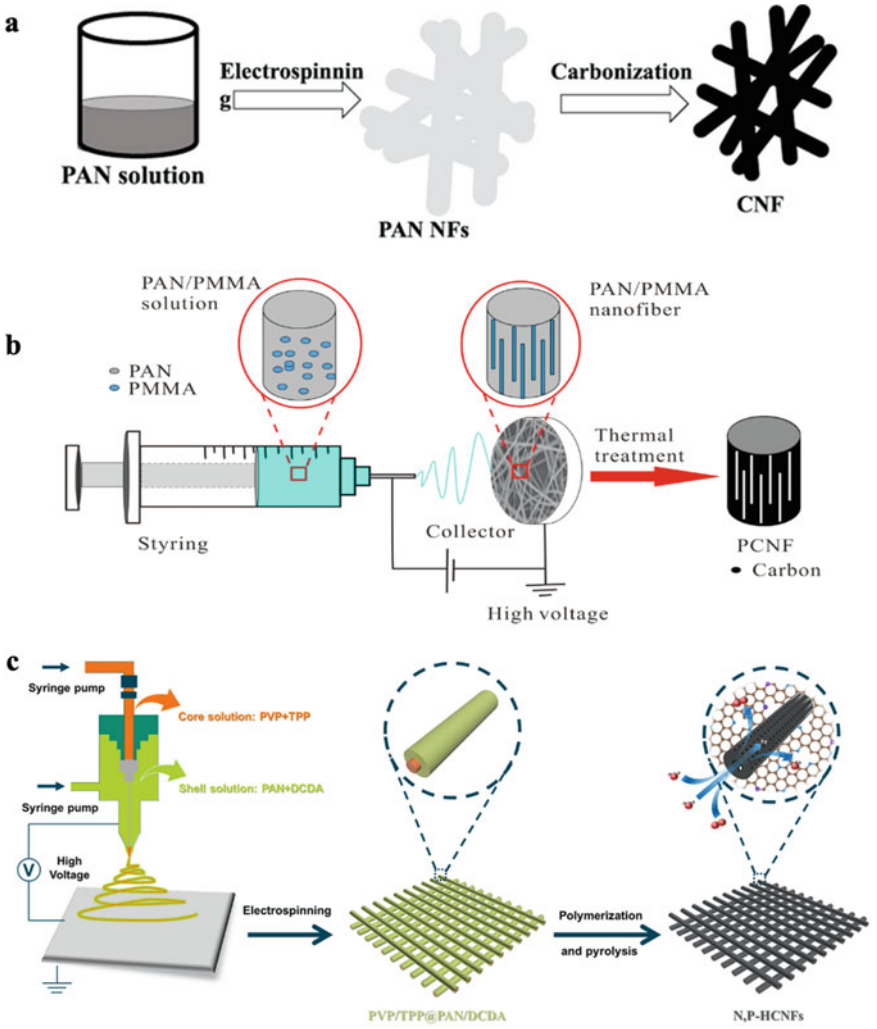

Fig. 2 The schematic illustration shows how to prepare CNFs with various structures: **a** solid CNFs. Adapted with permission from Reference [44], Copyright (2018), Elsevier; **b** porous CNFs. Adapted with permission from Reference [45], Copyright (2018), Elsevier; and **c** hollow CNFs. Adapted with permission from Reference [46], Copyright (2019), Elsevier

3 Applications in SCs

3.1 CNFs

CNFs are one of the common electrodes for SCs because they can provide the electrodes with high surface area, good electrical conductivity, surface functionalities,

etc. Thus, tremendous efforts, including elemental doping, porous structure design, biomass-derived carbon, etc., have been made in this area [47–51].

For instance, Hsu et al. [48] reported the preparation of interconnected CNFs for SCs by electrospinning the PAN and poly(acrylonitrile-*co*-butadiene) copolymer (PAN-*co*-PB) solution. The additional copolymer could prevent the polymer blends from the macrophase separation. The as-spun fibers were stabilized at 250 °C and carbonized at 800 °C, respectively, and the interconnected CNFs were prepared because of the decomposition of PB. It was also found that the diameter of the resultant CNFs was decreased with the increment of PAN-*co*-PB in blends since a large amount of melted PB caused the fusion of neighboring fibers (Fig. 3a–b). Figure 3f shows that the cell with the 90:10 PAN/PAN-*co*-PB derived CNFs could have a specific capacitance of 179.2 F g^{-1} at a scan rate of 5 mV s^{-1}, which was only 137.5 F g^{-1} for that of the cell with pristine PAN derived CNFs, benefiting from the increased electrical conductivity and microcrystallite size. While the surface area of CNFs (Fig. 3c–e) started to reduce with the further increment of PAN-*co*-PB contents, which was detrimental for the electrochemical performance of the prepared SCs (Fig. 3g).

Besides, elemental doping has been proved as a promising approach to enhance the overall performance of the CNFs based SCs because the extra pseudocapacitance

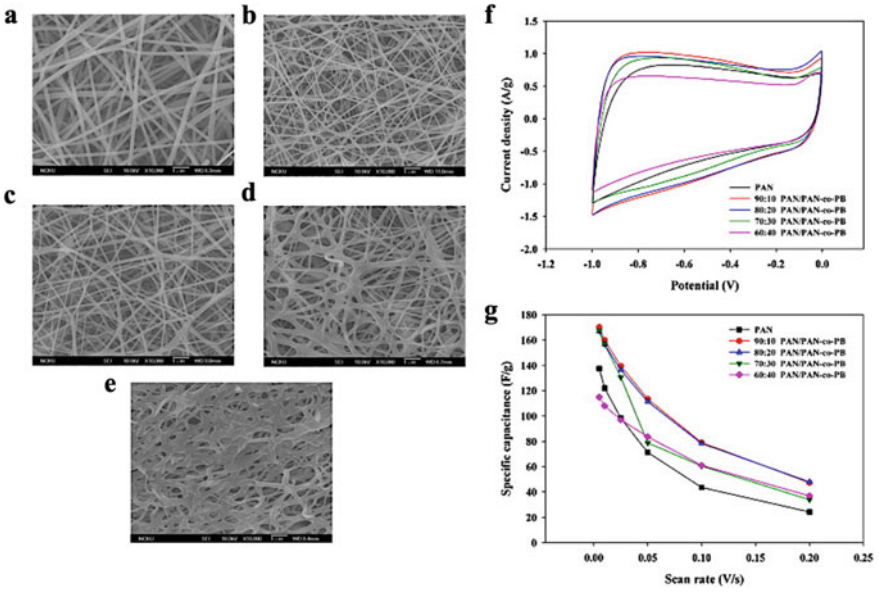

Fig. 3 SEM images of the CNFs as a function of PAN-*co*-PB composition: **a** PAN, **b** 90:10 PAN/PAN-*co*-PB, **c** 80:20 PAN/PAN-*co*-PB, **d** 70:30 PAN/PAN-*co*-PB and **e** 60:40 PAN/PAN-*co*-PB; **f** Cyclic voltammograms of the above-mentioned samples at a scan rate of 5 mV s^{-1} and **g** their corresponding rate capability. Adapted with permission from Reference [48], Copyright (2014), Elsevier

can arise from the fast Faradic redox reactions between the functional groups and the ions in the electrolytes. Tian et al. [21] successfully synthesized nitrogen-doped CNFs with remarkably enhanced capacitance. The procedure is shown in Fig. 4a. Briefly, the CNFs were firstly prepared, which were then activated at 800 °C under

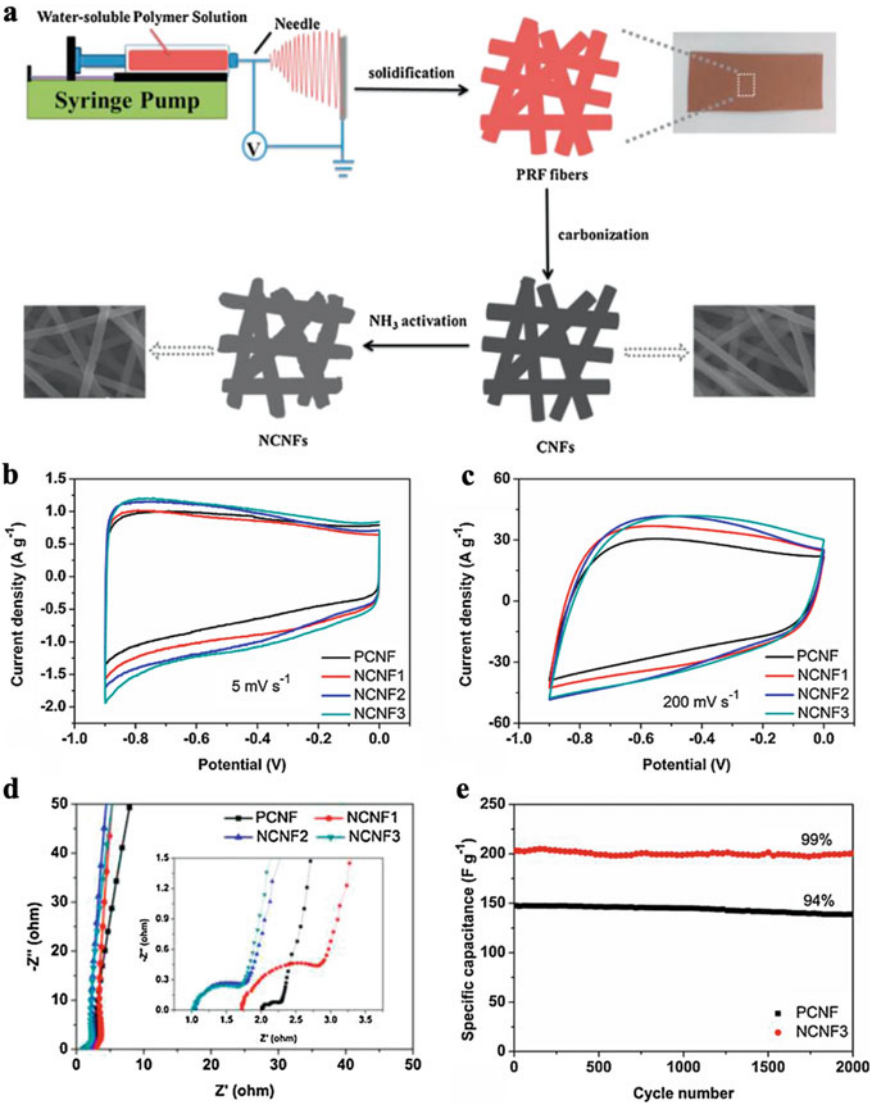

Fig. 4 **a** Schematic image showing the preparation process of n-doped CNFs; CV curves of PCNFs and NCNFs at a scan rate of **b** 5 mV s^{-1} and **c** 20 mV s^{-1}; **d** Nyquist plots of the prepared samples; **e** Cycling performance of the cells with PCNFs and NCNFs at 5 A g^{-1} for 2000 cycles. Adapted with permission from Reference [21], Copyright (2015), Elsevier

the NH_3 atmosphere for 1, 2, and 3 h to form nitrogen-doped CNFs (NCNFs). And the resultant NCNFs were denoted as NCNF1, NCNF2, and NCNF3, respectively. Upon the preparation of the samples, cyclic voltammetry (CV) at various scanning rates was performed to test their capacitance, as can be seen from Fig. 4b–c. It is obvious that the cell with NCNFs could deliver better capacitance compared with that of pristine CNFs (PCNFs) regardless of scanning rates, which was attributed to the heteroatom doping and the effective specific surface area. Additionally, the charge transfer resistance (R_{ct}) of the NCNFs was decreased with the increment of the carbonization time (Fig. 4d), which was lower than that of PCNFs, demonstrating the improvement of electrical conductivity via n-doping. Moreover, Fig. 4e exhibits that the cell with NCNF3 could have a capacitance of 201.1 F g^{-1} at 5 A g^{-1} even after 2000 cycles with high retention of 99%, which was superior compared with that of PCNF (94%). A similar trend was also found by Yan et al. [52], who fabricated the nitrogen/phosphorus co-doped CNFs for achieving high-performance SCs. As a result, the maximum specific capacitance could be up to 224.9 F g^{-1} at 0.5 A g^{-1} in 1 M H_2SO_4. A specific capacitance of 155.5 F g^{-1} even at a high current density of 30 A g^{-1} with a retention of 70% could be obtained, and no capacitance loss was observed over 8000 charge/discharge cycles. All those outstanding performances could be ascribed to the synergetic effect of nitrogen and phosphorus functionalities combined with the advantages of CNFs.

In contrast to the petroleum polymers including PAN, mesophase pitch, etc., biomass materials have also been extensively studied and developed to prepare CNFs mainly due to their low cost and environmentally friendly features [53–56]. For example, Cao et al. [57] proposed a facile phosphating process to fabricate lignin-cellulose-based CNFs, which were further utilized as the electrodes for SCs. As shown in Fig. 5a, the as-spun solution of lignin and cellulose acetate with/out H_3PO_4 was firstly prepared, which was then electrospun to obtain the precursor fibers. Finally, the CNFs could be obtained after the heat treatments. Six samples were prepared to study the effects of H_3PO_4 contents in this work, which were named as CF-1 (0 wt.% H_3PO_4), CF-2 (10 wt.% H_3PO_4), CF-3 (20 wt.% H_3PO_4), CF-4 (30 wt.% H_3PO_4), CF-5 (40 wt.% H_3PO_4), and CF-6 (50 wt.% H_3PO_4), respectively. Figure 5b–g exhibit the fiber could be not generated without H_3PO_4, which was attributed to the phase separation between the lignin molecule and cellulose acetate. The spinnability of the solution was significantly improved with the increment of H_3PO_4 contents because of the stable phospholipid bonds between lignin and cellulose acetate. However, more beads appeared with the excessive addition of H_3PO_4, which was mainly due to the formation of polyphosphate from the extra H_3PO_4. Figure 5h shows the CV curves at a scan rate of 5 mV s^{-1} of the cells with six specimens, and all of them displayed a typical rectangular shape. The enclosed area increased first and then decreased with the increment of the H_3PO_4 contents, which agreed with the charge/discharge curves shown in Fig. 5i. The cell with CF-5 (40 wt.% H_3PO_4) could have the highest capacitance of 346.6 F g^{-1} among the six samples at a current density of 0.1 A g^{-1}, which also had the smallest resistance (i.e., the intrinsic ohmic resistance R_s, the charge transfer resistance R_{ct}, the Warburg diffusion resistance R_w) based on the electrochemical impedance spectroscopy (EIS)

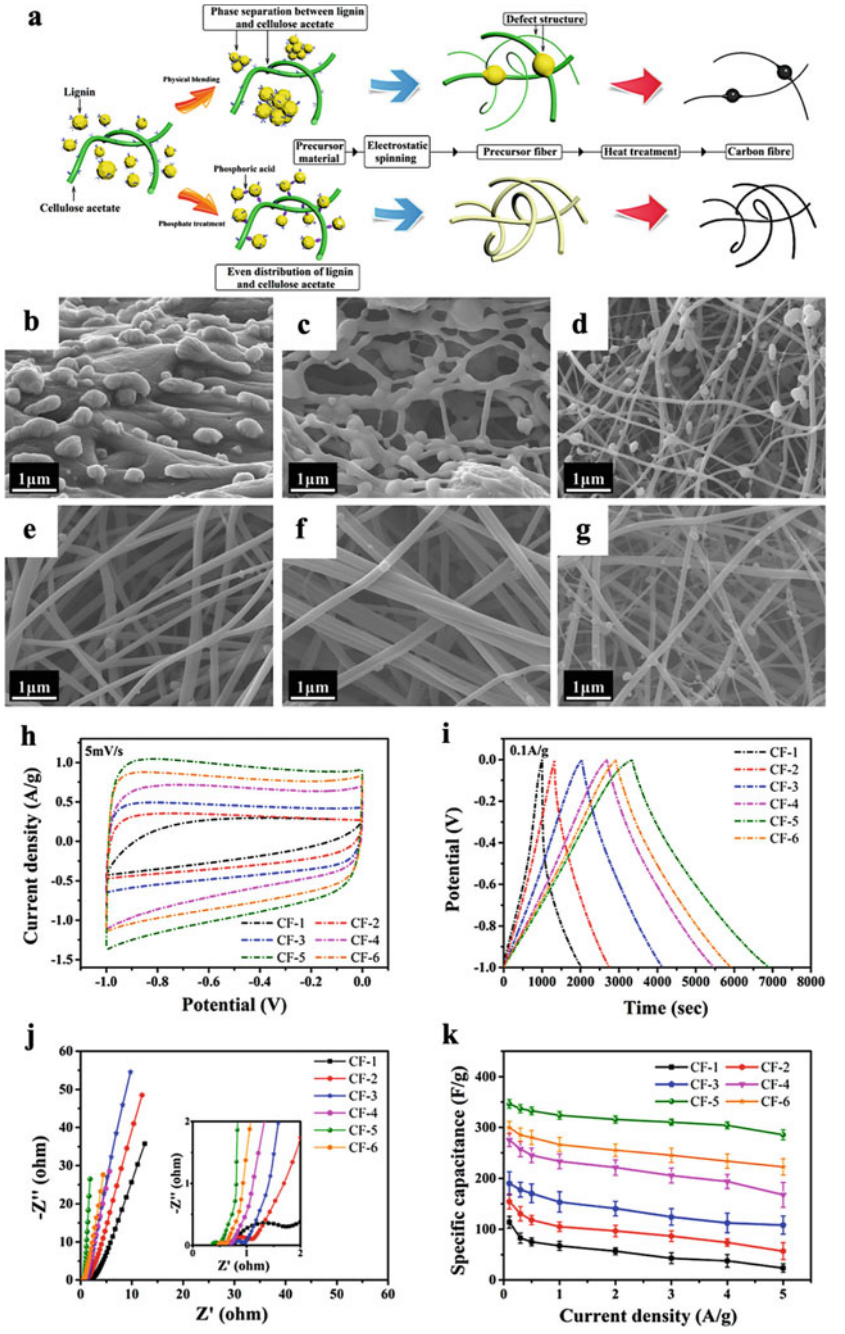
a
Phase separation between lignin and cellulose acetate
Physical blending
Lignin
Cellulose acetate
Phosphoric acid
Phosphate treatment
Even distribution of lignin and cellulose acetate
Defect structure
Precursor material
Electrostatic spinning
Precursor fiber
Heat treatment
Carbon fibre
b
c
d
e
f
g
1μm
h
5mV/s
Current density (A/g)
Potential (V)
CF-1
CF-2
CF-3
CF-4
CF-5
CF-6
i
0.1A/g
Potential (V)
Time (sec)
j
-Z'' (ohm)
Z' (ohm)
k
Specific capacitance (F/g)
Current density (A/g)

◀**Fig. 5** **a** Schematic illustration of the lignin-cellulose acetate derived CNFs; SEM images of CFs prepared by different weight ratios between H_3PO_4 and lignin: **b** 0/100, **c** 10/100, **d** 20/100, **e** 30/100, **f** 40/100 and **g** 50/100; **h** CV curves of the CFs at a scan rate of 5 mV s^{-1} and **i** their charge/discharge curves at a current density of 0.1 A g^{-1}; **j** EIS results of the cell with the prepared CFs and **k** the related rate capability. Adapted with permission from Reference [57], Copyright (2019), ACS Publications

results (Fig. 5j). Rate capability is another critical parameter for evaluating the electrochemical performance of SCs. As can be seen from Fig. 5k, the cell with the CF-5 had the best capacitance retention of 82.3% when the current density was increased from 0.1 to 5 A g^{-1}, which was remarkably better than the others, demonstrating its outstanding rate capability.

Very recently, Zhu et al. [4] reported that the lignin-derived CNFs could achieve a specific surface area of 2042.86 m^2g^{-1} via a simple modification and fractionation strategy design, which was able to effectively increase the molecular weight and reduce the heterogeneity of lignin, resulting in the reduction of carbon weight loss of the precursor fibers and the increment of graphitization degree as well as maintaining the morphology of CNFs. The cell with such prepared CNFs could deliver a capacitance of 442.2 F g^{-1} in 6 M KOH at a current density of 1 A g^{-1}, which was attributed to its high surface area and hierarchical porous structures. In addition, the heteroatoms on the CNF surface could provide extra pseudocapacitance, which has been considered as an effective strategy to prepare low-cost and high-quality lignin-derived CNFs, providing a great potential application in SCs. However, the effect of their molecular weight and intermolecular hydrogen bonding on the properties of lignin-based materials still needs further study.

3.2 Activated CNFs

It is well known that surface area is one of the crucial parameters of carbon electrodes for obtaining high-performance SCs according to the working mechanism of the EDLCs [58–61]. Therefore, many efforts have been made to improve surface area via different activation approaches (i.e., $ZnCl_2$, KOH, steam, CO_2, etc.) [62–64].

For instance, porous CNFs were prepared with the help of $ZnCl_2$ by Kim et al. [65] As shown in Fig. 6a–c, the diameter of CNFs could be decreased to ~100 nm without collapsing the fibrous morphology for all three samples. The combined physical and chemical reactions including carbon densification and gas evolution (e.g., CO, CO_2, H_2O, etc.) resulted in a tremendous volumetric change of the prepared nanofibers. Meanwhile, the trapped $ZnCl_2$ particles in the electrospun PAN nanofiber could transform into its hydrated form ($ZnCl_2{\cdot}nH_2O$), which was expected to hydrolyze and form an oxychloride in the subsequent stabilization step. As claimed in this study, the resultant zinc oxide might act as the catalyst for generating micropores on the outer surface of CNFs by etching carbon atoms. Figure 6d–f exhibits the CV curves

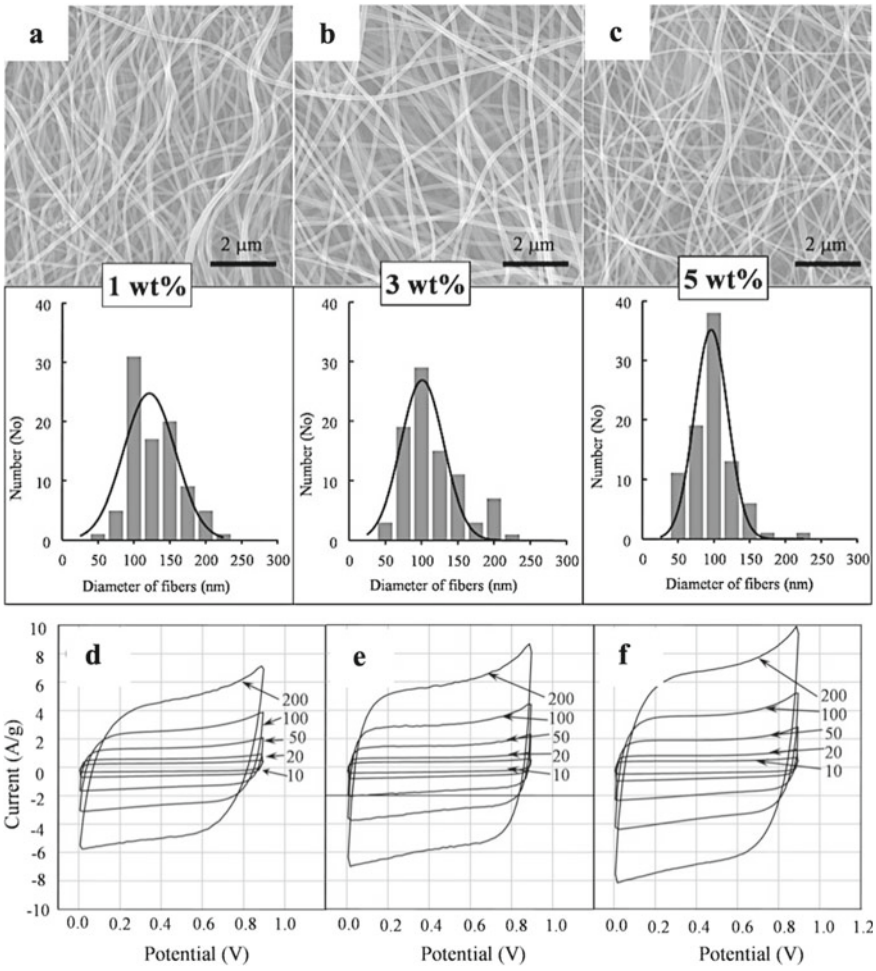

Fig. 6 SEM images of the CNFs and the corresponding diameter distributions: **a** 1 wt.%, **b** 3 wt.%, and **c** 5 wt.% $ZnCl_2$; CV curves of the cells with the resultant CNFs in 6 M KOH solutions at various scan rates: **d** 1 wt.%, **e** 3 wt.%, and **f** 5 wt.% $ZnCl_2$. Adapted with permission from Reference [65], Copyright (2017), Wiley Online Library

of the cells with the prepared CNFs in a 6 M KOH aqueous electrolyte solution at various scan rates of 10–200 mV s^{-1}. The potential range between 0 and 0.9 V was fixed, and no obvious redox peaks were originating from the functional groups. With the increment of $ZnCl_2$ content, the cell could deliver a higher capacitance (Fig. 6d–f), which was attributed to the enhancement of the surface area.

3D cross-linked nitrogen-enriched porous CNFs were also synthesized with the existence of $ZnCl_2$ [66]. The cell with the as-prepared CNFs could deliver a high capacitance of 214 F g^{-1} at a current density of 1 A g^{-1} in an acid electrolyte, good rate capability with current densities ranging from 1 to 60 A g^{-1}, as well as outstanding

cycling performance with high retention of 97.3% over 60,000 cycles at 2 A g^{-1} in alkaline electrolyte. The remarkable enhancement of the performance was caused by the synergistic effect of increased surface area for more charge accumulation and cross-linked architecture that enabled the electrons to fast transfer throughout the fibrous membrane.

In addition to $ZnCl_2$, microporous CNFs could also be prepared via using KOH, which can be utilized to adjust the diameter and improve the porous texture of nanofibers. The diameter could be controlled in the range of 252–666 nm with remarkable enhancement in terms of the microporous volume and specific surface by turning the contents of KOH in the spinning solution with pore size ranging from 0.7 to 1.2 nm [67]. The prepared CNF membrane could be then performed as a binder-free electrode by using the electrolyte of 6 M KOH aqueous solution, which exhibited higher specific capacitance, superior specific surface capacitance, and outstanding rate capability compared to the cell with the conventional microporous CNFs. Especially, the cell with the 20 wt.% KOH derived sample could obtain a specific capacitance of 256 F g^{-1} with a high specific surface capacitance of 0.51 F m^{-2} at a current density of 0.2 A g^{-1}. Moreover, a high specific capacitance of 170 F g^{-1} could remain at a current density of 20 A g^{-1} with a retention of 67%, which was ascribed to the optimized pore size (0.7–1.2 nm) and high surface area (597 m^2g^{-1}).

In contrast to the abovementioned strategies, in situ activation has also received lots of attention since it is a facile approach to prepare porous CNFs, which does not require an extra treatment process except for including a sacrificial agent into the precursor. For instance, Wang et al. [68] utilized polysulfone (PSF) as the decomposition agent to synthesize porous CNFs (Fig. 7a), which could achieve the highest surface area of 687 m^2g^{-1} with an optimal PSF content of 20 wt.% in precursor fibers. As can be seen from Fig. 7b–k, the diameters of CNFs decreased when the content of PSF increased, which was attributed to the PSF decomposition during the thermal treatment. While more interconnections happened when further increasing the amount of PSF because the PSF was melted during the carbonization process. As expected, the capacitance, power density, as well as energy density of the cell increased when the content of PSF was up to 20 wt.%, which was then started to decrease after that (Fig. 7l–p). EIS was also performed to analyze the charge and ion transport process of CNF electrodes in SCs, as shown in Fig. 7q. The charge transfer resistance (the semicircle at the high-frequency region) decreased remarkably for the SCs made of PAN/PSF-derived electrodes. In addition, the ion transfer resistance (the linear part at the low-frequency region) followed the same trend, demonstrating the enhancement of the capacitance of the cell with PAN/PSF-derived electrodes.

3.3 Hybrid CNFs

Even though CNFs have been widely studied and discussed earlier, they still suffer from low energy density because of the limited electrical charge separation at the

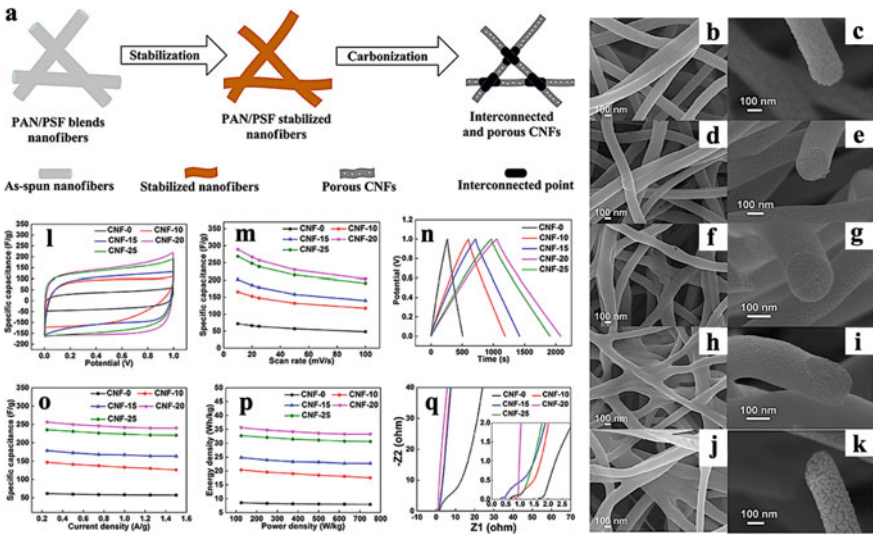

Fig. 7 **a** Schematic image showing the CNFs preparation. SEM images of the resultant CNFs containing different amounts of polysulfone (PSF) within the precursor nanofibers: **b**, **c** 0%, **d**, **e** 10%, **f**, **g** 15%, **h**, **i** 20% and **j**, **k** 25%; **l** CV curves and **m–o** rate capability of the prepared samples; **p** The relationship between power density and energy density of the assembled SCs and **q** their Nyquist plots. Adapted with permission from Reference [68], Copyright (2017), ACS Publications

interface of electrolyte and electrode materials, which tremendously hinders their practical applications in SCs [69]. Introducing pseudocapacitive materials (i.e., transition metal oxides, metal sulfides, metal hydroxides, etc.) is one of the promising methods since it can combine high-energy–density from themselves and the high-power density from CNFs [24, 70]. Zhao et al. [69] fabricated a freestanding MnO_x/CNF composite membrane with uniformly distributed MnO_x nanoparticles in CNFs. The resultant cell could have a specific capacitance of 174.8 F g^{-1} at a scan rate of 2 mV s^{-1} in 0.5 M Na_2SO_4 electrolyte and outstanding capability at even high current densities. Besides MnO_x, cobalt oxides have also been studied because of their high theoretical specific capacitance, which can be up to 3560 F g^{-1} [30]. It was reported that the cell with the optimum Co_3O_4/CNF composites (~68 wt.% active particles) possessed a high capacitance of 586 F g^{-1} at 1 A g^{-1}, which was ascribed to the uniform dispersion of active particles in CNFs.

Compared to an individual metal oxide, it has been demonstrated that the binary or multiple metal oxides can offer more stable redox chemical capability and broaden the potential window of the device, resulting in increasing their capacitance [70]. Both MnO_2 and Co_3O_4 could be homogeneously located on CNFs, as can be seen from Fig. 8a–c, e–j. The binary metal oxides at stable low current electrodeposition of on CNFs could also be prepared (Fig. 8d, k–n). Figure 8o shows that the cell with the binary electrode had the smallest resistance, indicating its efficient electron and mass transport. As a result, a high specific capacitance of 728 F g^{-1} in 6 M KOH

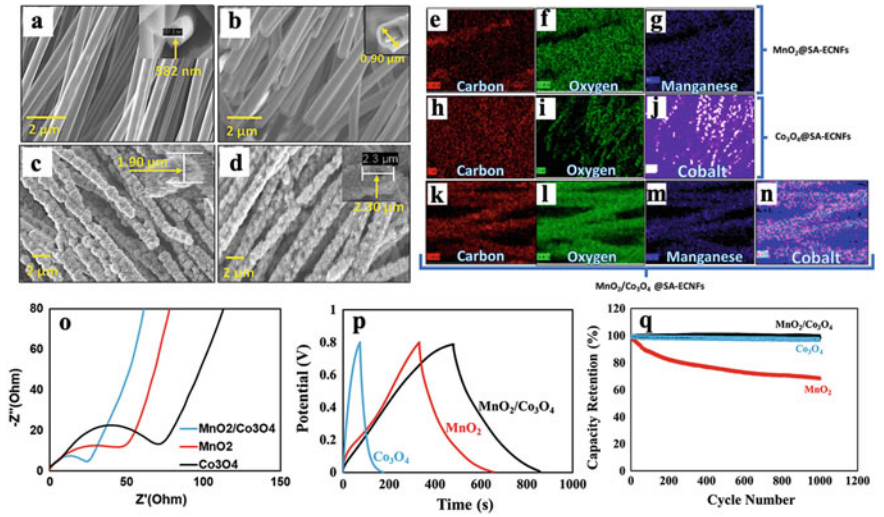

Fig. 8 SEM images of **a** the pristine CNFs, **b** MnO_2 coated CNFs, **c** Co_3O_4 coated CNFs, **d** MnO_2/Co_3O_4 coated CNFs and their corresponding EDS mapping images **e–f** MnO_2 coated CNFs, **h–j** Co_3O_4 coated CNFs, **k–n** MnO_2/Co_3O_4 coated CNFs; **o** EIS results; **p** charge/discharge profiles at 1 A g^{-1} and **q** cycling performance of the cell with the three samples at 1 A g^{-1}. Adapted with permission from Reference [70], Copyright (2021), ACS Publications

electrolyte could be achieved for the cell with the as-prepared MnO_2/Co_3O_4 coated CNF composite with better retention compared to that of the cells with individual oxides (Fig. 8p–q). Additionally, it could possess an energy density of 64.5 Wh kg^{-1} and a power density of 1276 W kg^{-1}, respectively, at a current density of 2 A g^{-1}.

Attributed to the high theoretical specific capacitances and fast multielectron surface Faradaic redox reactions, metal hydroxides have also attracted lots of attention [71, 72]. Multi-dimensional hybrids containing either Ni-Co layered double hydroxide nanorods or nanosheets on CNF were prepared [73], and the corresponding procedure is shown in Fig. 9a. Briefly, electrospun PAN nanofibers were stabilized and carbonized to obtain CNFs, which were then used as the substrate. Two different auxiliary agents were performed to grow Ni–Co layered double hydroxide with different morphologies on CNF membranes, as can be seen from Fig. 9b–g. The results indicated that the cells with Ni-Co layered double hydroxide nanorods and nanosheets could have high specific capacitances of 1378.2 F g^{-1} and 1195.4 F g^{-1} at a current density of 1 A g^{-1}, respectively, with excellent capability (Fig. 9h). What's more, cycling stabilities of both hybrid membranes could be significantly enhanced compared to the cells with the pure Ni-Co layered double hydroxide nanorod and nanosheet powders, which might be due to the uniform distribution of Ni-Co layered double hydroxide on CNFs, providing more active sites for electrochemical reaction as well as more efficient pathways for electron transport.

Overall, many materials, including but not limited to conductive polymers [74], MXene [9], graphene oxide [10], metal sulfides [75, 76], etc., have been successfully

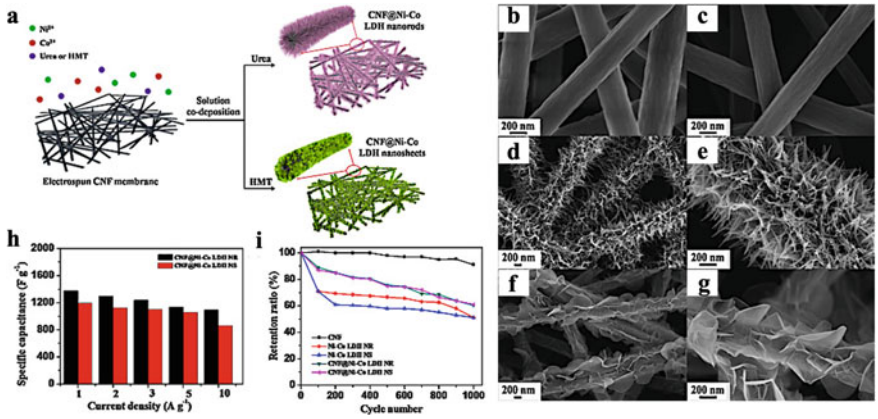

Fig. 9 **a** Schematic image showing the preparation of the Ni/Co layered double hydroxide nanorods/nanosheets. SEM images of **b** the as-spun PAN fibers, **c** CNFs, **d**, **e** Ni/Co layered double hydroxide nanorods coated CNFs and **f**, **g** Ni/Co layered double hydroxide nanosheets coated CNFs; **h** Rate capability and **i** cycling performance at 5 A g^{-1} of the cells with prepared samples. Adapted with permission from Reference [73], Copyright (2015), Elsevier

introduced to prepare CNF composites to achieve high-performance electrodes for SCs. How to scale them up becomes a big challenge, which remarkably limits their applications.

4 Conclusions and Perspectives

In this chapter, CNFs and their composites with designed structures and desired properties have been introduced and discussed in detail. The structure of those CNFs mainly depends on fabrication approaches, process conditions, as well as their compositions. Due to their unique properties (e.g., high surface area, large porosity, etc.), these CNFs and their composites have been widely performed in the applications of SCs. However, most of them are still on a lab scale, thus, more efforts need to make further improvements. Some perspectives are provided for the future development of CNFs and their composites in SC applications.

It is extremely important to discover environmentally friendly electrospun materials since tremendous organic solvents are currently used for the solution preparation, leading to economic and environmental concerns. Thus, more research should be focused on designing the electrospinning solution to not only have sustainable features but help to increase the diversity of materials that can be applicable for electrospinning. Meanwhile, advanced manufacturing technologies (i.e., multi-needle electrospinning, needle-less electrospinning, etc.) should be further developed to achieve mass production because of the limitation of lab-scale electrospinning set up, further accelerating the commercialization of electrospinning in this field.

Moreover, investigating new materials with various functionalities can enhance the overall electrochemical performance of the resultant CNFs and their composites, such as high electrical conductivity, good mechanical properties, etc. What's more, simulation models regarding the electrospinning process should be further optimized to better understand the system with a long-term goal of producing uniform fibers with high reproductivity at a large scale, while maintaining the desired morphology, size, as well as other exceptional properties.

In summary, CNFs and their composites have been considered as promising candidates for the applications of SCs, which play a crucial role in energy storage devices. Meanwhile, significant progress has been accomplished on the structure design and performance development. Future work should attract more researchers from different disciplines to comprehensively solve the real challenges and fulfill their practical applications in this area.

References

1. Q. Guo, X. Zhou, X. Li, S. Chen, A. Seema, A. Greiner, H. Hou, Supercapacitors based on hybrid carbon nanofibers containing multiwalled carbon nanotubes. J. Mater. Chem. **19**(18), 2810–2816 (2009)
2. M. Jiang, J. Zhu, C. Chen, Y. Lu, Y. Ge, X. Zhang, Poly (vinyl alcohol) borate gel polymer electrolytes prepared by electrodeposition and their application in electrochemical supercapacitors. ACS Appl. Mater. Interfaces **8**(5), 3473–3481 (2016)
3. N. He, O. Yildiz, Q. Pan, J. Zhu, X. Zhang, P.D. Bradford, W. Gao, Pyrolytic-carbon coating in carbon nanotube foams for better performance in supercapacitors. J. Power Sources **343**, 492–501 (2017)
4. M. Zhu, H. Liu, Q. Cao, H. Zheng, D. Xu, H. Guo, S. Wang, Y. Li, J. Zhou, Electrospun lignin-based carbon nanofibers as supercapacitor electrodes. ACS Sustain. Chem. Eng. **8**(34), 12831–12841 (2020)
5. C. Yang, D. Li, H. Gao, Q. Liu, J. Zhu, F. Wang, M. Jiang, Constructing high-energy-density aqueous supercapacitors with potassium iodide-doped electrolytes by a precharging method. ACS Appl. Energy Mater. **3**(3), 2674–2681 (2020)
6. Y. Wang, M. Wang, P. Wang, W. Zhou, Z. Chen, Q. Gao, M. Shen, J. Zhu, Urea-treated wet-spun PEDOT: PSS fibers for achieving high-performance wearable supercapacitors. Compos. Commun. **27**, 100885 (2021)
7. J. Li, E.-H. Liu, W. Li, X.-Y. Meng, S.-T. Tan, Nickel/carbon nanofibers composite electrodes as supercapacitors prepared by electrospinning. J. Alloy. Compd. **478**(1–2), 371–374 (2009)
8. M. Jiang, J. Zhu, C. Chen, Y. Lu, E.S. Pampal, L. Luo, P. Zhu, X. Zhang, Superior high-voltage aqueous carbon/carbon supercapacitors operating with in situ electrodeposited polyvinyl alcohol borate gel polymer electrolytes. J. Mater. Chem. A **4**(42), 16588–16596 (2016)
9. A.S. Levitt, M. Alhabeb, C.B. Hatter, A. Sarycheva, G. Dion, Y. Gogotsi, Electrospun MXene/carbon nanofibers as supercapacitor electrodes. J. Mater. Chem. A **7**(1), 269–277 (2019)
10. W. Chee, H. Lim, Y. Andou, Z. Zainal, A. Hamra, I. Harrison, M. Altarawneh, Z. Jiang, N. Huang, Functionalized graphene oxide-reinforced electrospun carbon nanofibers as ultrathin supercapacitor electrode. J. Energy Chem. **26**(4), 790–798 (2017)
11. U. Kurtan, H. Aydın, B. Büyük, U. Şahintürk, M. Almessiere, A. Baykal, Freestanding electrospun carbon nanofibers uniformly decorated with bimetallic alloy nanoparticles as supercapacitor electrode. J. Energy Storage **32**, 101671 (2020)

12. X. Xu, Y. Du, C. Wang, Y. Guo, J. Zou, K. Zhou, Z. Zeng, Y. Liu, L. Li, High-entropy alloy nanoparticles on aligned electronspun carbon nanofibers for supercapacitors. J. Alloys Compd. **822**, 153642 (2020)
13. Y. Ge, H. Jiang, K. Fu, C. Zhang, J. Zhu, C. Chen, Y. Lu, Y. Qiu, X. Zhang, Copper-doped Li4Ti5O12/carbon nanofiber composites as anode for high-performance sodium-ion batteries. J. Power Sources **272**, 860–865 (2014)
14. J. Zhu, C. Chen, Y. Lu, Y. Ge, H. Jiang, K. Fu, X. Zhang, Nitrogen-doped carbon nanofibers derived from polyacrylonitrile for use as anode material in sodium-ion batteries. Carbon **94**, 189–195 (2015)
15. C. Chen, G. Li, J. Zhu, Y. Lu, M. Jiang, Y. Hu, Z. Shen, X. Zhang, In-situ formation of tin-antimony sulfide in nitrogen-sulfur co-doped carbon nanofibers as high performance anode materials for sodium-ion batteries. Carbon **120**, 380–391 (2017)
16. J. Zhu, P. Zhu, C. Yan, X. Dong, X. Zhang, Recent progress in polymer materials for advanced lithium-sulfur batteries. Prog. Polym. Sci. **90**, 118–163 (2019)
17. S. Shanmugapriya, P.R. Kasturi, P. Zhu, J. Zhu, C. Yan, X. Zhang, R.K. Selvan, Hexanedioic acid mediated in situ functionalization of interconnected graphitic 3D carbon nanofibers as Pt support for trifunctional electrocatalysts. Sustain. Energy Fuels **4**(6), 2808–2822 (2020)
18. J. Zhu, E.S. Pampal, Y. Ge, J.D. Leary, X. Zhang, in *Fibers as Energy Materials*, Chapter 24, ed. by J. Hu, B. Kumar, J. Lu (Wiley Online Library, 2020), pp. 649–680
19. Y. Lu, K. Fu, S. Zhang, Y. Li, C. Chen, J. Zhu, M. Yanilmaz, M. Dirican, X. Zhang, Centrifugal spinning: a novel approach to fabricate porous carbon fibers as binder-free electrodes for electric double-layer capacitors. J. Power Sources **273**, 502–510 (2015)
20. V. Barranco, M. Lillo-Rodenas, A. Linares-Solano, A. Oya, F. Pico, J. Ibañez, F. Agullo-Rueda, J.M. Amarilla, J. Rojo, Amorphous carbon nanofibers and their activated carbon nanofibers as supercapacitor electrodes. J. Phys. Chem. C **114**(22), 10302–10307 (2010)
21. X. Tian, N. Zhao, Y. Song, K. Wang, D. Xu, X. Li, Q. Guo, L. Liu, Synthesis of nitrogen-doped electrospun carbon nanofibers with superior performance as efficient supercapacitor electrodes in alkaline solution. Electrochim. Acta **185**, 40–51 (2015)
22. Q. Xu, X. Yu, Q. Liang, Y. Bai, Z.-H. Huang, F. Kang, Nitrogen-doped hollow activated carbon nanofibers as high performance supercapacitor electrodes. J. Electroanal. Chem. **739**, 84–88 (2015)
23. Y.S. Yun, C. Im, H.H. Park, I. Hwang, Y. Tak, H.-J. Jin, Hierarchically porous carbon nanofibers containing numerous heteroatoms for supercapacitors. J. Power Sources **234**, 285–291 (2013)
24. K. Naoi, S. Ishimoto, Y. Isobe, S. Aoyagi, High-rate nano-crystalline Li4Ti5O12 attached on carbon nano-fibers for hybrid supercapacitors. J. Power Sources **195**(18), 6250–6254 (2010)
25. O. Pech, S. Maensiri, Electrochemical performances of electrospun carbon nanofibers, interconnected carbon nanofibers, and carbon-manganese oxide composite nanofibers. J. Alloy. Compd. **781**, 541–552 (2019)
26. S. Jeon, J.H. Jeong, H. Yoo, H.K. Yu, B.-H. Kim, M.H. Kim, RuO_2 nanorods on electrospun carbon nanofibers for supercapacitors. ACS Appl. Nano Mater. **3**(4), 3847–3858 (2020)
27. T. Mukhiya, G.P. Ojha, B. Dahal, T. Kim, K. Chhetri, M. Lee, S.-H. Chae, A. Muthurasu, A.P. Tiwari, H.Y. Kim, Designed assembly of porous cobalt oxide/carbon nanotentacles on electrospun hollow carbon nanofibers network for supercapacitor. ACS Appl. Energy Mater. **3**(4), 3435–3444 (2020)
28. S. Yang, J. Ai, Z. Han, L. Zhang, D. Zhao, J. Wang, C. Yang, B. Cao, Electrospun $ZnFe_2O_4$/carbon nanofibers as high-rate supercapacitor electrodes. J. Power Sources **469**, 228416 (2020)
29. M. Zhi, A. Manivannan, F. Meng, N. Wu, Highly conductive electrospun carbon nanofiber/MnO_2 coaxial nano-cables for high energy and power density supercapacitors. J. Power Sources **208**, 345–353 (2012)
30. S. Abouali, M. Akbari Garakani, B. Zhang, Z.-L. Xu, E. Kamali Heidari, J.-Q. Huang, J. Huang, J.-K. Kim, Electrospun carbon nanofibers with in situ encapsulated Co_3O_4 nanoparticles as electrodes for high-performance supercapacitors. ACS Appl. Mater. Interfaces **7**(24), 13503–13511 (2015)

31. J. Zhu, *Advanced Separator Selection and Design for High-Performance Lithium-Sulfur Batteries*. North Carolina State University (2016)
32. Y. Li, J. Zhu, R. Shi, M. Dirican, P. Zhu, C. Yan, H. Jia, J. Zang, J. He, X. Zhang, Ultrafine and polar ZrO_2-inlaid porous nitrogen-doped carbon nanofiber as efficient polysulfide absorbent for high-performance lithium-sulfur batteries with long lifespan. Chem. Eng. J. **349**, 376–387 (2018)
33. Y. Li, Q. Shen, J. Shen, X. Ding, T. Liu, J. He, C. Zhu, D. Zhao, J. Zhu, Multifunctional fibroblasts enhanced via thermal and freeze-drying post-treatments of aligned electrospun nanofiber membranes. Adv. Fiber Mater. **3**(1), 26–37 (2021)
34. B.-Y. Hsieh, J. Kim, J. Zhu, S. Li, X. Zhang, X. Jiang, A laser ultrasound transducer using carbon nanofibers–polydimethylsiloxane composite thin film. Appl. Phys. Lett. **106**(2), 021902 (2015)
35. C. Chen, G. Li, Y. Lu, J. Zhu, M. Jiang, Y. Hu, L. Cao, X. Zhang, Chemical vapor deposited MoS_2/electrospun carbon nanofiber composite as anode material for high-performance sodium-ion batteries. Electrochim. Acta **222**, 1751–1760 (2016)
36. P. Zhu, J. Zhu, C. Yan, M. Dirican, J. Zang, H. Jia, Y. Li, Y. Kiyak, H. Tan, X. Zhang, In Situ polymerization of nanostructured conductive polymer on 3D sulfur/carbon nanofiber composite network as cathode for high-performance lithium-sulfur batteries. Adv. Mater. Interfaces **5**(10), 1701598 (2018)
37. Y. Li, J. Zhu, H. Cheng, G. Li, H. Cho, M. Jiang, Q. Gao, X. Zhang, Developments of advanced electrospinning techniques: a critical review. Adv. Mater. Technol. 2100410 (2021)
38. J. Doshi, D.H. Reneker, Electrospinning process and applications of electrospun fibers. J. Electrostat. **35**(2–3), 151–160 (1995)
39. A.L. Yarin, S. Koombhongse, D.H. Reneker, Taylor cone and jetting from liquid droplets in electrospinning of nanofibers. J. Appl. Phys. **90**(9), 4836–4846 (2001)
40. S. Tripatanasuwan, Z. Zhong, D.H. Reneker, Effect of evaporation and solidification of the charged jet in electrospinning of poly (ethylene oxide) aqueous solution. Polymer **48**(19), 5742–5746 (2007)
41. D. Li, Y. Xia, Electrospinning of nanofibers: reinventing the wheel? Adv. Mater. **16**(14), 1151–1170 (2004)
42. C. Thompson, G.G. Chase, A. Yarin, D. Reneker, Effects of parameters on nanofiber diameter determined from electrospinning model. Polym. **48**(23), 6913–6922 (2007)
43. N. Bhardwaj, S.C. Kundu, Electrospinning: a fascinating fiber fabrication technique. Biotechnol. Adv. **28**(3), 325–347 (2010)
44. F.O. Agyemang, G.M. Tomboc, S. Kwofie, H. Kim, Electrospun carbon nanofiber-carbon nanotubes coated polyaniline composites with improved electrochemical properties for supercapacitors. Electrochim. Acta **259**, 1110–1119 (2018)
45. Y. Li, J. Zhu, P. Zhu, C. Yan, H. Jia, Y. Kiyak, J. Zang, J. He, M. Dirican, X. Zhang, Glass fiber separator coated by porous carbon nanofiber derived from immiscible PAN/PMMA for high-performance lithium-sulfur batteries. J. Membr. Sci. **552**, 31–42 (2018)
46. Y. Gao, Z. Xiao, D. Kong, R. Iqbal, Q.-H. Yang, L. Zhi, N, P co-doped hollow carbon nanofiber membranes with superior mass transfer property for trifunctional metal-free electrocatalysis, Nano Energy **64**, 103879 (2019)
47. C. Tran, V. Kalra, Fabrication of porous carbon nanofibers with adjustable pore sizes as electrodes for supercapacitors. J. Power Sources **235**, 289–296 (2013)
48. Y.-H. Hsu, C.-C. Lai, C.-L. Ho, C.-T. Lo, Preparation of interconnected carbon nanofibers as electrodes for supercapacitors. Electrochim. Acta **127**, 369–376 (2014)
49. C.-C. Lai, C.-T. Lo, Preparation of nanostructural carbon nanofibers and their electrochemical performance for supercapacitors. Electrochim. Acta **183**, 85–93 (2015)
50. R. Zhang, L. Wang, J. Zhao, S. Guo, Effects of sodium alginate on the composition, morphology, and electrochemical properties of electrospun carbon nanofibers as electrodes for supercapacitors. ACS Sustain. Chem. Eng. **7**(1), 632–640 (2018)
51. S. Tan, T.J. Kraus, K.D. Li-Oakey, Understanding the supercapacitor properties of electrospun carbon nanofibers from Powder River Basin coal. Fuel **245**, 148–159 (2019)

52. X. Yan, Y. Liu, X. Fan, X. Jia, Y. Yu, X. Yang, Nitrogen/phosphorus co-doped nonporous carbon nanofibers for high-performance supercapacitors. J. Power Sources **248**, 745–751 (2014)
53. C. Lai, Z. Zhou, L. Zhang, X. Wang, Q. Zhou, Y. Zhao, Y. Wang, X.-F. Wu, Z. Zhu, H. Fong, Free-standing and mechanically flexible mats consisting of electrospun carbon nanofibers made from a natural product of alkali lignin as binder-free electrodes for high-performance supercapacitors. J. Power Sources **247**, 134–141 (2014)
54. J. Zhu, C. Yan, X. Zhang, C. Yang, M. Jiang, X. Zhang, A sustainable platform of lignin: From bioresources to materials and their applications in rechargeable batteries and supercapacitors. Progr. Energy Combust. Sci. **76**, 100788 (2020)
55. Q. Cao, Y. Zhang, J. Chen, M. Zhu, C. Yang, H. Guo, Y. Song, Y. Li, J. Zhou, Electrospun biomass based carbon nanofibers as high-performance supercapacitors. Industrial Crops Prod. **148**, 112181 (2020)
56. G. Shi, C. Liu, G. Wang, X. Chen, L. Li, X. Jiang, P. Zhang, Y. Dong, S. Jia, H. Tian, Preparation and electrochemical performance of electrospun biomass-based activated carbon nanofibers. Ionics **25**(4), 1805–1812 (2019)
57. Q. Cao, M. Zhu, J. Chen, Y. Song, Y. Li, J. Zhou, Novel lignin-cellulose-based carbon nanofibers as high-performance supercapacitors. ACS Appl. Mater. Interfaces. **12**(1), 1210–1221 (2019)
58. H. Zhao, L. Wang, D. Jia, W. Xia, J. Li, Z. Guo, Coal based activated carbon nanofibers prepared by electrospinning. J. Mater. Chem. A **2**(24), 9338–9344 (2014)
59. J. Zhou, J. Chen, S. Han, H. Zhao, J. Bai, Z. Yang, X. Mu, Y. Liu, D. Bian, G. Sun, Constructing optimized three-dimensional electrochemical interface in carbon nanofiber/carbon nanotube hierarchical composites for high-energy-density supercapacitors. Carbon **111**, 502–512 (2017)
60. Y. Li, W. Ou-Yang, X. Xu, M. Wang, S. Hou, T. Lu, Y. Yao, L. Pan, Micro-/mesoporous carbon nanofibers embedded with ordered carbon for flexible supercapacitors. Electrochim. Acta **271**, 591–598 (2018)
61. H. Wang, W. Wang, H. Wang, Y. Li, X. Jin, H. Niu, H. Wang, H. Zhou, T. Lin, Improving supercapacitance of electrospun carbon nanofibers through increasing micropores and microporous surface area. Adv. Mater. Interfaces **6**(6), 1801900 (2019)
62. Z. Liu, D. Fu, F. Liu, G. Han, C. Liu, Y. Chang, Y. Xiao, M. Li, S. Li, Mesoporous carbon nanofibers with large cage-like pores activated by tin dioxide and their use in supercapacitor and catalyst support. Carbon **70**, 295–307 (2014)
63. W. Qian, X. Li, X. Zhu, Z. Hu, X. Zhang, G. Luo, H. Yao, Preparation of activated carbon nanofibers using degradative solvent extraction products obtained from low-rank coal and their utilization in supercapacitors. RSC Adv. **10**(14), 8172–8180 (2020)
64. M. Zhi, S. Liu, Z. Hong, N. Wu, Electrospun activated carbon nanofibers for supercapacitor electrodes. RSC Adv. **4**(82), 43619–43623 (2014)
65. C. Kim, B.T.N. Ngoc, K.S. Yang, M. Kojima, Y.A. Kim, Y.J. Kim, M. Endo, S.C. Yang, Self-sustained thin webs consisting of porous carbon nanofibers for supercapacitors via the electrospinning of polyacrylonitrile solutions containing zinc chloride. Adv. Mater. **19**(17), 2341–2346 (2007)
66. Q. Jiang, X. Pang, S. Geng, Y. Zhao, X. Wang, H. Qin, B. Liu, J. Zhou, T. Zhou, Simultaneous cross-linking and pore-forming electrospun carbon nanofibers towards high capacitive performance. Appl. Surf. Sci. **479**, 128–136 (2019)
67. C. Ma, Y. Song, J. Shi, D. Zhang, X. Zhai, M. Zhong, Q. Guo, L. Liu, Preparation and one-step activation of microporous carbon nanofibers for use as supercapacitor electrodes. Carbon **51**, 290–300 (2013)
68. H. Wang, W. Wang, H. Wang, X. Jin, H. Niu, H. Wang, H. Zhou, T. Lin, High performance supercapacitor electrode materials from electrospun carbon nanofibers in situ activated by high decomposition temperature polymer. ACS Appl. Energy Mater. **1**(2), 431–439 (2018)
69. X. Zhao, Y. Du, Y. Li, Q. Zhang, Encapsulation of manganese oxides nanocrystals in electrospun carbon nanofibers as free-standing electrode for supercapacitors. Ceram. Int. **41**(6), 7402–7410 (2015)
70. K. Allado, M. Liu, A. Jayapalan, D. Arvapalli, K. Nowlin, J. Wei, Binary MnO_2/Co_3O_4 metal oxides wrapped on superaligned electrospun carbon nanofibers as binder free supercapacitor electrodes. Energy Fuels **35**(9), 8396–8405 (2021)

71. L. Zhang, Q. Ding, Y. Huang, H. Gu, Y.-E. Miao, T. Liu, Flexible hybrid membranes with Ni(OH)2 nanoplatelets vertically grown on electrospun carbon nanofibers for high-performance supercapacitors. ACS Appl. Mater. Interfaces **7**(40), 22669–22677 (2015)
72. T. Mukhiya, B. Dahal, G.P. Ojha, D. Kang, T. Kim, S.-H. Chae, A. Muthurasu, H.Y. Kim, Engineering nanohaired 3D cobalt hydroxide wheels in electrospun carbon nanofibers for high-performance supercapacitors. Chem. Eng. J. **361**, 1225–1234 (2019)
73. F. Lai, Y. Huang, Y.-E. Miao, T. Liu, Controllable preparation of multi-dimensional hybrid materials of nickel-cobalt layered double hydroxide nanorods/nanosheets on electrospun carbon nanofibers for high-performance supercapacitors. Electrochim. Acta **174**, 456–463 (2015)
74. X. Yan, Z. Tai, J. Chen, Q. Xue, Fabrication of carbon nanofiber–polyaniline composite flexible paper for supercapacitor. Nanoscale **3**(1), 212–216 (2011)
75. Y. Liu, G. Jiang, S. Sun, B. Xu, J. Zhou, Y. Zhang, J. Yao, Growth of NiCo2S4 nanotubes on carbon nanofibers for high performance flexible supercapacitors. J. Electroanal. Chem. **804**, 212–219 (2017)
76. A. Rajapriya, S. Keerthana, C. Viswanathan, N. Ponpandian, Direct growth of MoS_2 hierarchical nanoflowers on electrospun carbon nanofibers as an electrode material for high-performance supercapacitors. J. Alloys Compd. **859**, 157771 (2021)

Graphene-Based Nanomaterial for Supercapacitor Application

Sanjeev Verma and Bhawna Verma

Abstract Graphene is a thick layer nanomaterial of carbon that plays an immense role in the areas of supercapacitor designing in the market of electric devices. Their two-dimensional structure, high electron movement, massive surface area, and high strength pay much attention to their electrical as well as thermal conductivity parameters in comparison to other carbon-based materials. Moreover, the easy admittance of electrolytes in pores of graphene along with not variable pore size distribution gives the most favorable condition for supercapacitors. In this chapter, we discuss the current scenario of research and development in the field of graphene-based nanomaterials as efficient supercapacitors. It involves graphene structure, synthesis of graphene, graphene derivatization, and graphene-based hybrid composites such as symmetric as well as asymmetric supercapacitors and also to be explored more chief domains of research for popularizing this nanomaterial.

Keywords Graphene · Carbon-based material · Nanomaterial · Conducting polymer · Metal oxide · Supercapacitor

1 Introduction

In today's advanced material world, besides other carbon-based materials (e.g. graphite, fullerenes, carbon nanotubes, carbon black), graphene and its family mainly graphene oxide (GO) and reduced graphene oxide (rGO) have attracted prominent regard because of their magnificent chemical, physical, electronic, optical and thermal properties such as higher chemical stability, huge reactive nature, larger area (~2600 $m^2\ g^{-1}$), a high value of young's modulus (~1 TPa), greater mobility of electron (~230,000 $cm^2\ V^{-1}\ s^{-1}$), higher transparency (~95%) of incident radiation and super thermal conductivity (~3000 $W\ m^{-1}\ K^{-1}$) at atmospheric conditions [1–4]. Graphene is a two-dimensional covalently bonded carbon atoms sheet containing

S. Verma · B. Verma (✉)
Department of Chemical Engineering and Technology, Indian Institute of Technology, Banaras Hindu University, Varanasi 221005, India
e-mail: bverma.che@iitbhu.ac.in

S. Thomas et al. (eds.), *Nanostructured Materials for Supercapacitors*,
Advances in Material Research and Technology,
https://doi.org/10.1007/978-3-030-99302-3_11

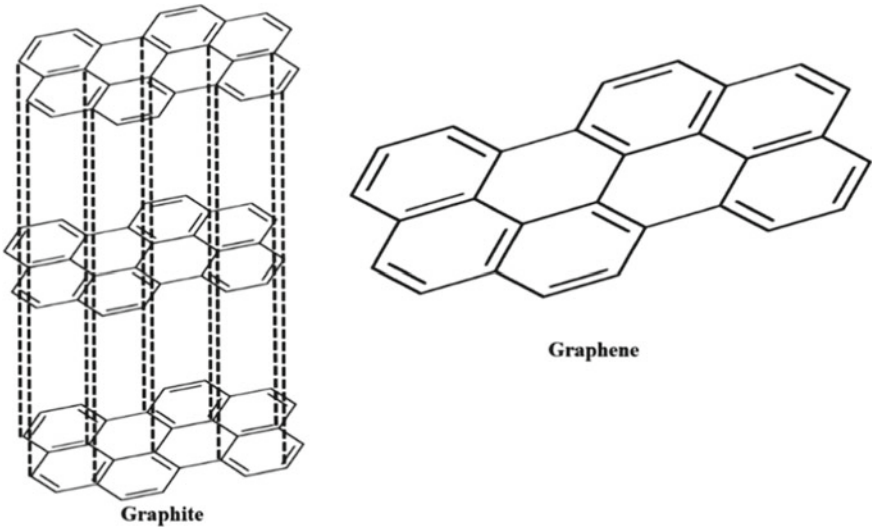

Fig. 1 Schematic structure representation of graphite and graphene

sp^2 hybridization. It is obtained from the graphite which contains many layers of graphene (Fig. 1) and arranged in a chicken wire hexagonal pattern which gives a perfect crystalline structure resulting in one of the strongest materials [5]. These all factors ensure that graphene is a play-field for researchers, especially in energy storage applications.

The existence of electrons in graphene gives massless particles and very high conducting capability as a relativistic particle. The zero-band gap of pristine graphene ensures that it behaves as a more metallic or semiconducting characteristic. The more metallic character shown due to their sheet sizes lies between microns to several nanometers. When the dimensions of the graphene layer are quite narrow around 1–2 nm, it generates a separate bandgap to exhibit semiconducting properties [6]. Due to increasing the need for energy, fewer resources availability, and high processing cost requires novel energy storage devices like supercapacitors, capacitors, fuel cells, solar cells, and batteries. Among all, supercapacitors pay much attention because of their rapid charging rate, magnificent power density, and longer stability. In the Ragone plot (Fig. 2), supercapacitors employ between the capacitors and batteries and display the higher power density compared to a battery and greater energy density compared to a capacitor. But less energy density than batteries and these less energy density could be improved with few advancements in supercapacitors mechanism as well as structure [7].

The three categories of supercapacitors are: electric double-layer capacitors (EDLCs), pseudocapacitors, and hybrid capacitors (Fig. 3). The storage of energy

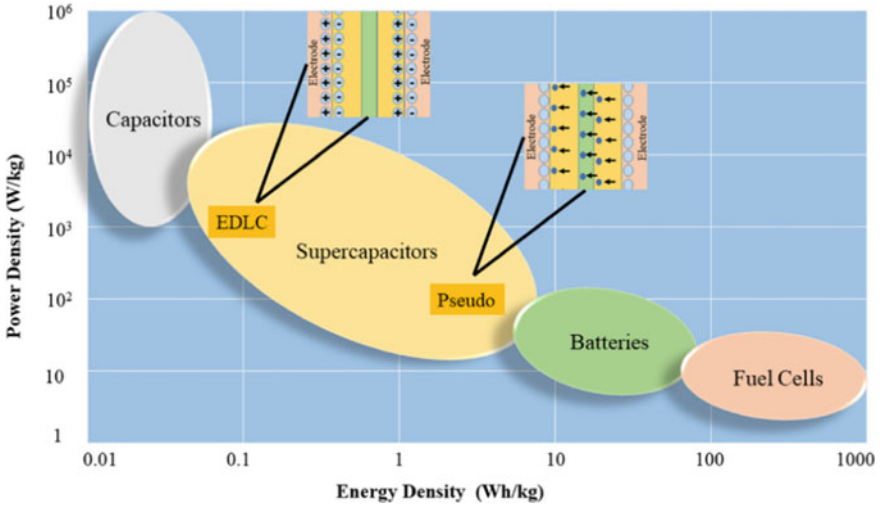

Fig. 2 Ragone plot for various energy devices

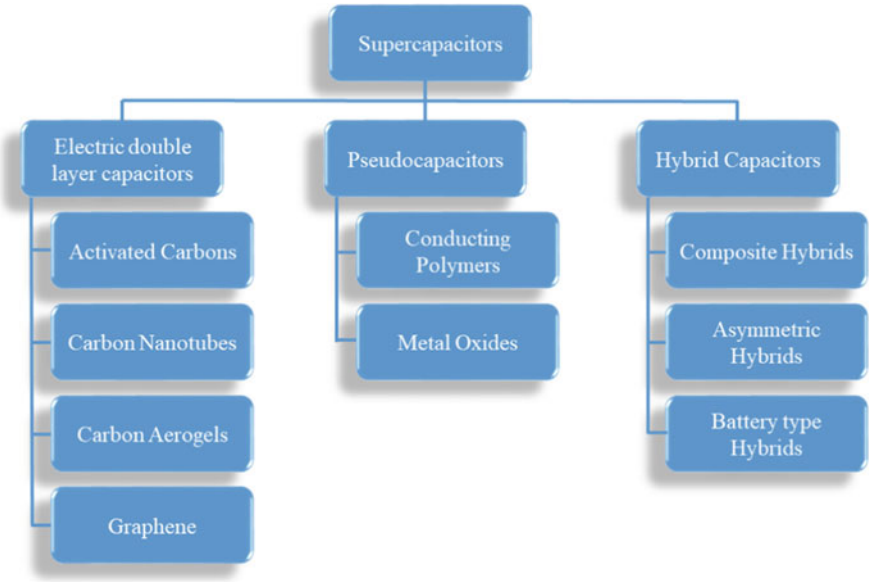

Fig. 3 Representation of supercapacitors classification

in EDLCs completely depends upon the electrostatic interface of electrode–electrolyte. Whereas, the energy storage in pseudocapacitors is due to charge transportation. Hybrid supercapacitors show by the combined nature of EDLC and pseudo mechanism.

The energy density along with power density are the two variables to define its performance. The energy density (E) is the quantity of the stored energy in supercapacitors and is represented as

$$E = \frac{1}{2}\mathrm{CV}^2 \text{ (Wh/kg)} \tag{1}$$

Whereas, power density (P) define as the speed of the energy that could be charged or discharged and it expressed as

$$P = \frac{E}{td} \text{ (W/kg)} \tag{2}$$

C = Capacitance; V = Voltage; td = Discharge time

$$\mathrm{C} = \varepsilon_0 \varepsilon_\mathrm{r} \frac{A}{d} \tag{3}$$

A = electrode area; d = space between two electrodes; ε_0 and ε_r = dielectric constant for free space and dielectric material.

Generally, supercapacitors have two electrodes separating by a semipermeable membrane and impregnating in an electrolyte, which sanction the flow of ions, as displayed in Fig. 4.

The non-faradic action of EDLC exhibits low capacitance. Pseudocapacitors store the energy in the form of faradic reactions with higher values of capacitance, high energy density, low stability, and having electrode material as conducting polymers and metal oxides. To overcome the lower capacitance, less energy density, and even low stability, the development of hybrid supercapacitors is a booming area in the current session [8].

2 Graphene Structure

The sixth element of the periodic table (i.e. carbon atom) has six proton-neutron in the nucleus. The outer shell of the carbon atom has six electrons, two in the K shell followed by four valence electrons in the L shell (Fig. 5a). These four valence electrons in the valence shell can be responsible for sp, sp^2, and sp^3 hybridization. Figure 5b displays the formation of sp^2 hybrids. The layered hexagonal planar is formed if sp^2 hybrid carbon atoms take part with others neighboring three carbon atoms. This layered honeycomb planar is called monolayer graphite or graphene. The electronic configuration of carbon is $1s^2 2s^2 2p_x{}^1 2p_y{}^1 2p_z{}^0$ in the ground state but when

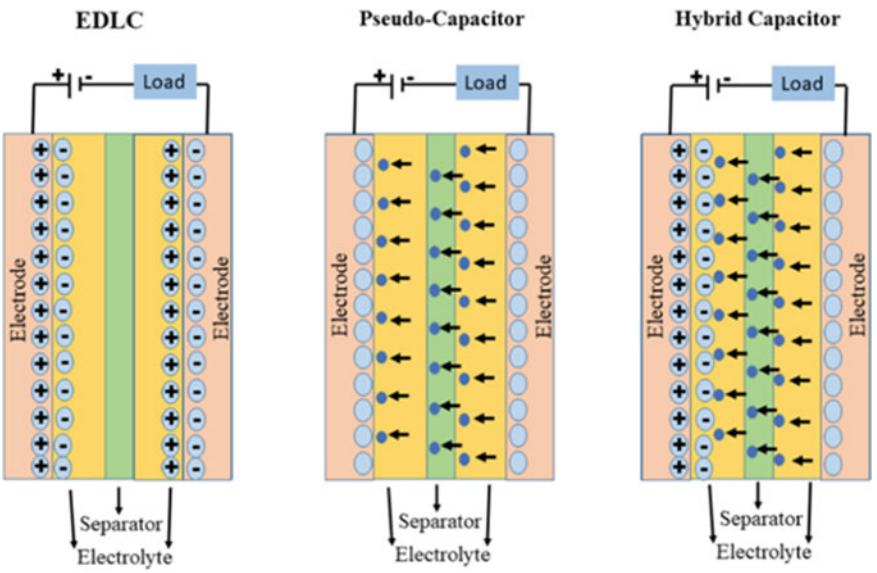

Fig. 4 Schematic representation of supercapacitors mechanism

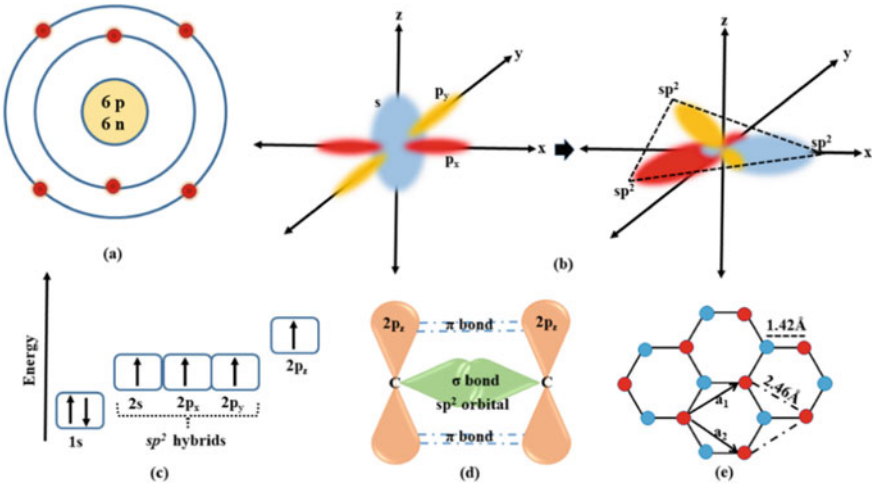

Fig. 5 **a** Carbon atomic structure. **b** sp^2 hybrid orbitals formation. **c** Energy level of carbon atoms. **d** sp^2 hybridized σ and π bond formation. **e** Crystal lattice structure of graphene

2*s* orbit gets sufficient energy then it's one electron jumped into $2p_z$ orbit. Due to this, $2p_z$ gets a higher energy level than $2p_x$, $2p_y$, and 2*s* orbit reach the energy level equal to $2p_x$ and $2p_y$. So orbit 2*s*, $2p_x$, and $2p_y$ form the sp^2 hybridization (Fig. 5c). Figure 5d illustrated that the strong σ bond form when two similar carbon atoms overlapped

with two sp^2 orbitals and un-hybridized $2p_z$ orbitals overlap with other neighboring $2p_z$ orbitals responsible for the formation of π bond. Generally, structural integrity is due to σ-bond and measurement of optical and electronic properties due to π-bond in graphene structure.

The crystal lattice of graphene is highlighted by a parallelogram marked with black dark and dotted lines (Fig. 5e). The two-unit cell vectors a_1 and a_2 with carbon–carbon spacing 1.42 Å and lattice constant 2.46 Å are also represented. The delocalization and resonance of electrons in π-orbitals, responsible for their extraordinary electrical properties and stability of the planar sheet [9, 10].

3 Graphene Synthesis

There are many methods based on physical and chemical routes for graphene synthesis, which are shown in Fig. 6.

3.1 Mechanical Exfoliation

In 1990, kurz and co-workers developed the scotch tape methodology for mechanical exfoliation. In 2010, Novoselov and co-workers designed a new method via the same procedure for graphene synthesis (single or few-layered) [11]. This method has several advantages such as

- Single-step and simple procedure.

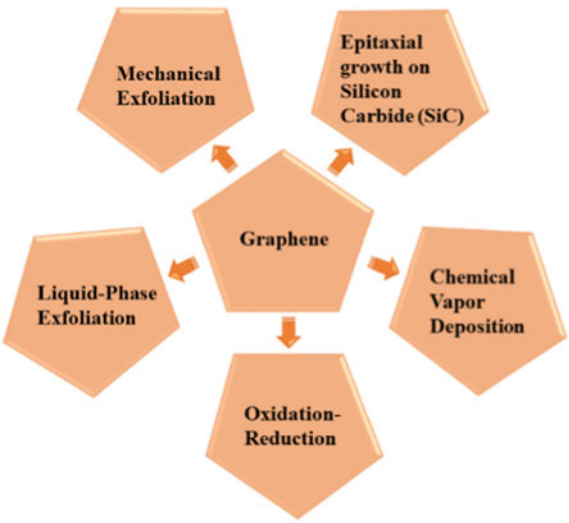

Fig. 6 Common graphene synthesis methods

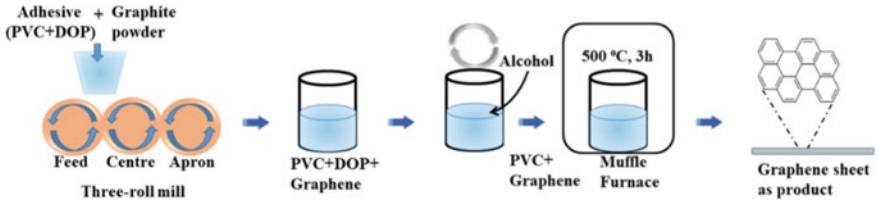

Fig. 7 Three-roll mill approach for continuous mechanical exfoliation of graphene

- Defect-free and non-functional graphene.
- Longer stability.

In a large production, this methodology fails because of high time consumption with higher costs. To overcome these factors, Chen and his teammates discovered a new mechanical exfoliation method via a three-roll mill (Fig. 7). This method is based on continuous mode whereas the scotch tape method is a batch mode.

3.2 Liquid-Phase Exfoliation

In this method, the conversion of graphite into monolayers or few-layered graphene occurs in liquid phase solvent via ultrasonication (Fig. 8). The following steps are involved in this process:

- Uniform distribution of graphite in a liquid solvent.
- Exfoliation of graphite by using ultrasonication.
- Purification of obtained graphene.

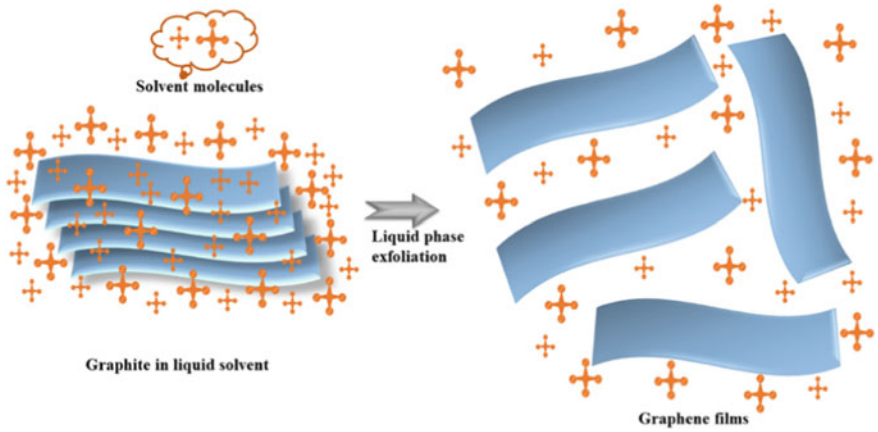

Fig. 8 Schematic illustration of liquid-phase exfoliation process

Fig. 9 Solvents for the liquid-phase exfoliation process

The degree of this exfoliation depends upon the mixing enthalpy per unit volume of solution [12] and derived as-

$$\frac{\Delta H_{mix}}{V_{sol}} \approx \frac{2}{T_g}(\sqrt{E_s} - \sqrt{E_g})^2 \phi_g \tag{4}$$

where $T_{g=}$ thickness of a graphene sheet, $E_{s=}$ surface energy of solvent, $E_{g=}$ surface energy of graphene layer, $\phi_{g=}$ graphene volume fraction, $\Delta H_{mix=}$ mixing enthalpy and V_{sol} = solution volume. The main standard of exfoliation process competition is the minimal mixing enthalpy which is performed by the equivalent of surface energies graphene and solvent. So, the lesser amount of mixing enthalpy resulted to obtain a higher degree of exfoliation. Solvent selection is another factor in this process. The solvent has low interfacial tension (less than 40 mJ m^{-2}). These solvents are NMP (N-methyl-2-pyrrolidone ~40 mJ m^{-2}), DCB (ortho-dichlorobenzene ~37 mJ m^{-2}) and DMF (N, N-dimethylformamide ~37.1 mJ m^{-2}) (Fig. 9).

3.3 Oxidation–Reduction

The most conventional method of graphene synthesis is oxidation–reduction. In this technique, the graphite powder is oxidized into graphene oxide/graphite oxide (GO) by using different oxidants. GO is then reduced by using different reducing agents to complete the synthesis of graphene/reduced graphene oxide (rGO). Graphite is a combination of various carbon atom layers joined with a weak covalent bond and oxidized graphite resulting to GO (Fig. 10).

After the reduction step of GO, we get rGO or graphene which is carbon atom sheets with negligible or less functional groups separately attached. Table 1 shows the various methods to get the oxidized form of graphite with some advantages and disadvantages.

Table 2 lists the various methods of reduction of GO to rGO. The complete removal of functional groups is very difficult but here most of the functional groups are reduced to form graphene.

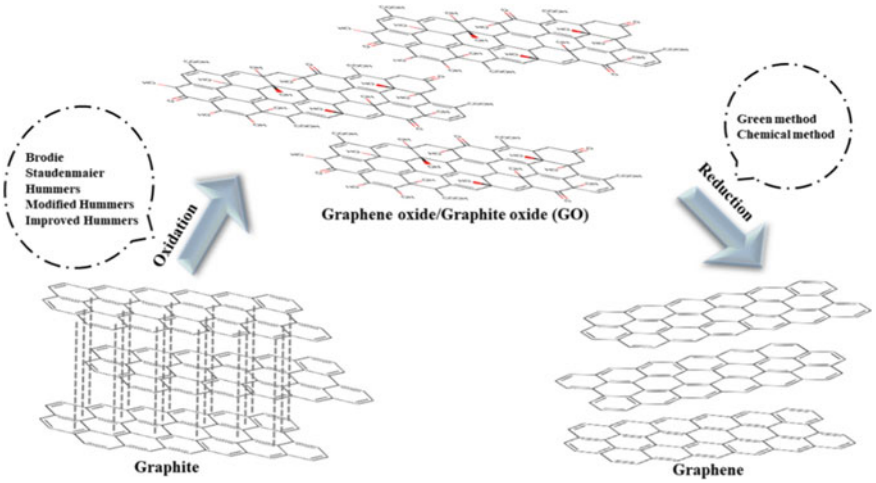

Fig. 10 Graphite to graphene synthesis using the oxidation–reduction method

Table 1 Different oxidation methods of GO synthesis

Method	Oxidant	Solvent	Additive	Advantages	Disadvantages	References
Brodie (1859)	$NaClO_3$, $KClO_3$	Fuming HNO_3	–	• Proper oxidation • Higher production	• Some chlorate left • Explosive nature	[13–17]
Staudenmaier (1898)	$KClO_3$, $NaClO_3$	H_2SO_4, Fuming HNO_3	KCl	• Commercial for large scale • Easily oxidation	• Time consuming process • Controlling of temperature	[18–21]
Hummers (1958)	$KMnO_4$	H_2SO_4	$NaNO_3$	• Higher degree of oxidation • Defect free product	• NO_x formation • Exothermic reaction nature	[22–25]
Modified Hummers (1999)	$KMnO_4$	H_2SO_4, H_3PO_4	$K_2S_2O_8$, P_2O_5	• Oxidation level boost up • Product performance enhanced	• Product purification • Time taking process	[26–29]
Improved Hummers (2010)	$KMnO_4$	H_2SO_4	K_2FeO_4, boric acid	• Improved oxidation states • Ecofriendly path	• Some difficulty in separation process • Highly costly	[30]

Table 2 Different reducing agents for rGO/graphene synthesis

Method	Reductant	Advantages	Disadvantages	References
Green method	Coconut water (*Cocos nucifera L*)	• Low cost • No harmful chemical use	• Lesser yield • Long reaction time	[31]
	Mango leaf (*Mangifera indica*), Pippala leaf (*Ficus religiosa*), Ashoka leaf (*Polyalthia longifolia*)			[32]
	Pomegranate juice			[33]
	Cow urine or urea			[34]
Chemical method	Sodium ascorbate	• High conductivity product • Less duration of reaction	• Some contamination contained • Toxicity of product	[35]
	$NaBH_4$			[36]
	Hydrobromic acid			[37]
	Dimethyl ketoxime			[38]

3.4 Chemical Vapor Deposition

In chemical vapor deposition (CVD) carbon atoms are deposited on the growth substrate (Cu, Ni) from a hydrocarbon source via chemical reactions. High-quality graphene formation with used at industrial level, continuous graphene film synthesis, ease of setup, and long term assessment attracted fundamental interest towards this method. The chemical reactions on growth substrate depend upon various parameters like CVD reactor setup, reactor pressure, furnace temperature, feedstock hydrocarbon availability, growth interval, and so on [39]. There are mainly two types of reactions in CVD reactor: first based on homogenous gas-phase reaction and another is based on a heterogeneous chemical reaction. Growth substrate can be Cu or Ni foils but Cu foil is the best applicant due to the small solubility of carbon atoms and uniformity of graphene film on Cu substrate surface. However, in the case of Ni foil, the uniform nature of carbon atoms on the Ni surface does not occur (Fig. 11) [40, 41].

3.5 Epitaxial Growth on Silicon Carbide (SiC)

The production of few-layer graphene on large scale with low defects has been done by using thermal decomposition on silicon carbide (SiC) substrate (Fig. 12). In thermal decomposition, the deposition of Si atoms from the SiC substrate is effectively performed in a furnace with high temperature (above 2000 °C) along with vacuum or argon atmosphere for uniform epitaxial graphene (carbon atoms) layer formation.

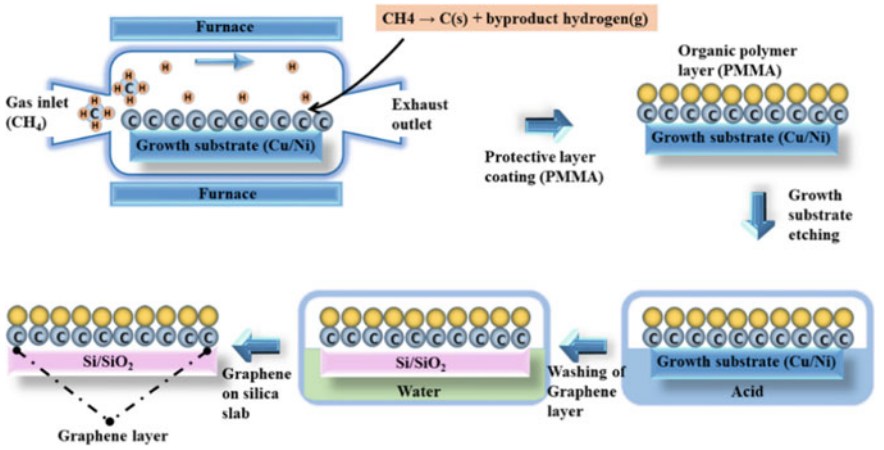

Fig. 11 Growth mechanism of graphene (carbon atoms) layer on metal growth substrate by using CVD technique

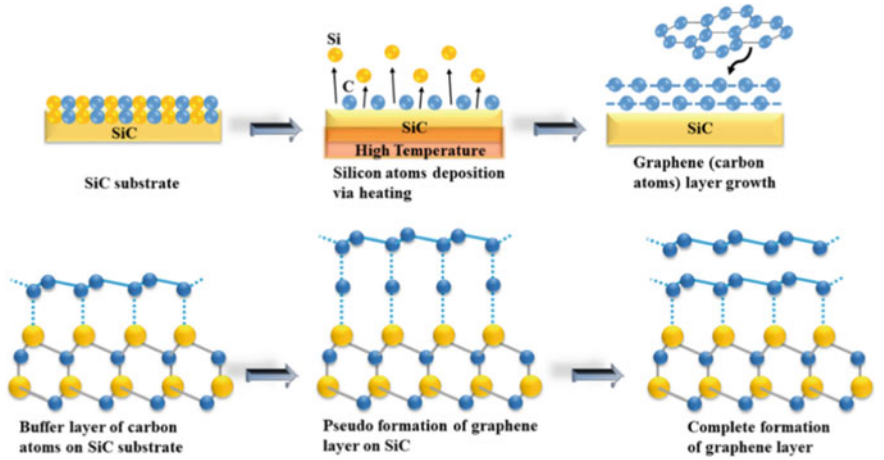

Fig. 12 Graphene layer formation sketch on silicon carbide (SiC) substrate

The primary advantage of this method is that no other device is needed till the complete growth of the graphene layer. There are two faces of polar substrate SiC, one is the Si face which corresponds to the (0001) polar surface and another tends to C face ($000\bar{1}$). When SiC substrate layer is subjected to high temperature, epitaxial graphene layer growth mechanism, and kinetics defined by few physical changes such as faster desorption of Si atoms because of high vapor pressure than carbon atoms and remaining carbon atoms left above on the SiC substrate layer [42, 43]. The different mechanisms and kinetics of Si and C atoms correspond to symmetry epitaxial graphene layer formation with excellent electronic properties. So due to the

various following benefits and ease of fabrication corresponds to the well suitable growth of graphene layer in large scale [44].

4 Graphene Derivatization

4.1 Graphene Oxide (GO)

It is a single-layered carbon atoms material with different functional groups like hydroxyl, carboxylic, epoxy, and ketone (Fig. 13). In the presence of these functional groups, GO exhibits dispersible nature in water and other solvents. This hydrophilic nature is responsible for enhancing the d-spacing from 0.3346 mm for graphite to 0.9794 mm for GO [45]. Moreover GO is a bad electrical conductor as compared to graphene. The mechanical, electrical, optical, and thermal properties of GO are not good as graphene. So for improving the properties, GO was reduced [46, 47]. The presence of huge chemical functionalities in GO surface makes a flexible chemical workplace for graphene-based nanomaterials in energy storage applications. There are various methods for GO synthesis such as Brodie, Staudenmaier, Hummers, and modified Hummers with some variations to get better oxidation product economically.

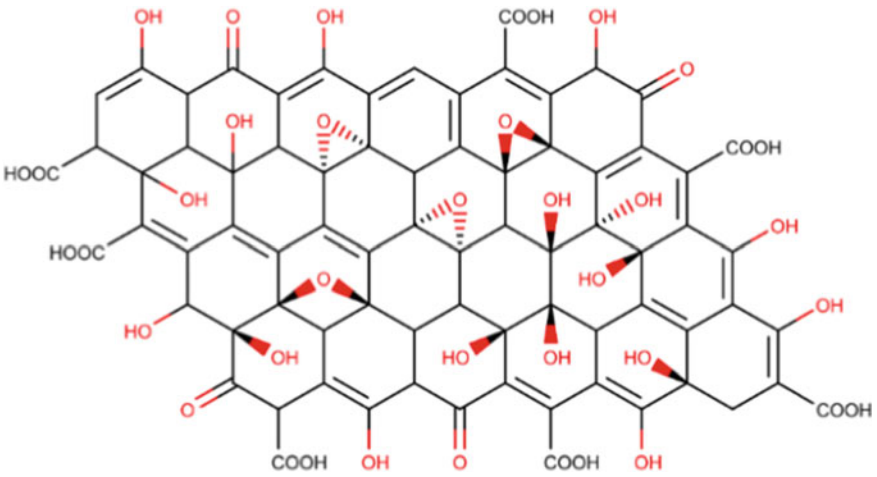

Fig. 13 Structure model of graphene oxide

4.2 Reduced Graphene Oxide (rGO)

rGO lies between graphene and GO because of restoring graphene-like properties like larger area and excellent electrical conductivity [48] (Fig. 14).

From a practical point of view, rGO can not be considered ideal graphene but it's not false to say "real Graphene". The degree of reduction is responsible for good quality, less interlayer spacing, and effective properties of rGO. There are various reduction methods with different reducing agents such as green methods, chemical methods, thermal methods, and electrochemical methods [33, 49]. Due to its incredible properties like graphene and ease of synthesis, rGO pays much attention to energy storage devices.

5 Graphene as Supercapacitor Material

Graphene and its derivatives based nanomaterials with other energetic materials like conducting polymers (CPs such as PANI (polyaniline), PPY (polypyrrole), etc.) and various metal oxides (MO_x i.e. RuO_2, MnO_2, NiO, Co_3O_4, Fe_3O_4, CuO) which enhance the redox actions and showing the combined behavior of EDLCs and pseudocapacitance. High faradic pseudocapacitance, superb conductivity, easy fabrication, reasonable cost, and high energy storage density of CPs are valuable in supercapacitor application. Polyaniline is used for supercapacitor application due to its enormous specific capacitance, cost-effectiveness, and high flexibility [50]. Among the composites synthesis methods, a hydrothermal method is a key method in most cases to fabricate the composites for energy storage devices, because of the refitting of surface morphologies by proper management of reactions temperature [51, 52]. Polypyrrole (PPY) is another conducting polymer for electrode material

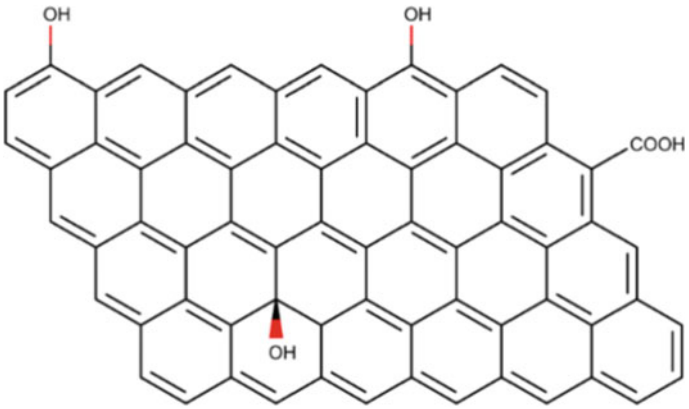

Fig. 14 Structure model of reduced graphene oxide

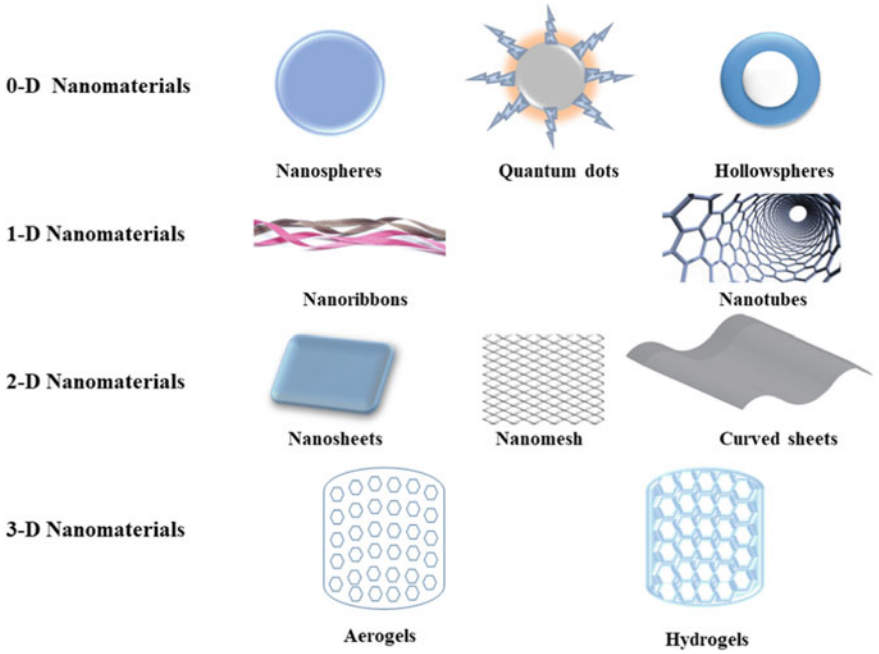

Fig. 15 Structure of graphene-based nanomaterials

after PANI due to its huge redox action, ecofriendly stable nature, high conductivity, and excellent volumetric capacitance. These properties exhibit good electrochemical performance with nanomaterials in supercapacitor applications [53, 54]. But some drawbacks are also associated with CPs like shrinkage problems during the doping/de-doping process, low strength, less processability, and limitations in stability [55, 56]. Moreover, metal oxides have higher specific capacitance, variable oxidation state, and rapid charge transfer mechanism which makes promising candidates for electrode materials [57]. The combination of graphene, CPs, and MO_x can intensify the performance of supercapacitors due to the synergistic effect. Graphene-based nanomaterial can be fabricated into a different dimensional structure such as 0-D (zero-dimensional) (i.e. nanospheres, quantum dots, and hollow spheres), 1-D (one-dimensional) (i.e. nanoribbons and nanotubes), 2-D (two-dimensional) (i.e. nanosheets, nanomesh, and curved sheets), and 3-D (three-dimensional) (i.e. aerogels, hydrogels, and nanocomposite) (Fig. 15).

5.1 0-D (Zero-Dimensional) Nanomaterials

Zhang and co-workers synthesized graphene quantum dots (GQDs) with uniform sizes by using nitric acid oxidant followed by sonication and hydrothermal process.

The electric double-layer behavior of GQD electrode is 296.7 F/g with 41.2 Wh/kg energy density at 1 A/g [58]. Fan et al., prepared nitrogen-doped graphene hollow spheres (NGHS) using layer-by-layer assembly of GO and PANI on polystyrene nanospheres by calcination and obtained 381 F/g specific capacitance at 1 A/g current density for NGHS with four bilayers [59]. Furthermore, Graphene nanospheres (GNS) were synthesized by the Yan and its teammates. GNS has a high energy density of 18.6 Wh/kg at 504 W/kg power density using a two-electrode symmetric system [60].

5.2 1-D (One-Dimensional) Nanomaterials

Saito et al., synthesized graphene nanoribbons (GNRs) from chemically reduced graphene oxide with different reduction times. The disorderly structure of GNR electrode has shown a high energy density of 5.54 Wh/kg at 313 kW/kg power density and 71% capacitance retention at 100 A/g [61]. Zhou and co-workers fabricated laser-induced bi-metallic sulfide on graphene (MoS_2/MnS/GR) nanoribbon for high performance of supercapacitors and having high areal energy density 7 $\mu Wh/cm^2$ at 50 $\mu A/cm^2$ with 93.6% capacitance retention up to 10,000 cycles [62]. Moreover, Ujjain et al. formed graphene nanoribbon wrapped with cobalt manganite particles for high-performance flexible supercapacitors. The synergic effect of pseudo and EDLCs showed the high energy density of 44.6 Wh/kg and 11.3 kW/kg power density with 95% retention after 10,000 loops [63]. Similarly, Ping et al. developed an Edge-riched graphene nanoribbon by longitudinal unzipping of carbon nanotubes and displayed larger capacitance as 202 F/g compared to GO and MWCNTs at a scan rate of 5 mV/s [64].

5.3 2-D (Two-Dimensional) Nanomaterials

Li et al. synthesized graphene nanosheets with KOH activation and showed the specific capacitance of 136 F/g, which was 35% higher than pristine graphene nanosheets [65]. While, Thirumal et al., prepared boron-doped graphene nanosheets using boric acid as a boron source through hydrothermal approach and displayed 113 F/g at 1 A/g current density when atomic doping was 2.56% [66]. Fan and co-workers, synthesized porous graphene nanosheets (PGNs) by the etching over graphene sheets by MnO_2 and showed the highest capacitance as 154 F/g at 500 mV/s after etching in 6 M KOH aqueous electrolyte, and obtained 88% capacitance retention after 5000 cycles [67]. Moreover, Cerium oxide is another type of metal oxide for supercapacitors because of its eco-friendly nature, economic and energetically redox actions, reported by Chakrabarty and co-workers [68]. They have developed CeO_2/Ce_2O_3-rGO nanocomposite hybrid with different weight fractions of rGO named CRGO1 (3 wt% rGO), CRGO2 (4.5 wt% rGO), CRGO3 (7 wt% rGO),

CRGO4 (9 wt% rGO), and got higher specific capacitance of 1027 F/g at 1 A/g for $CRGO_3$ while having 90% initial capacitance retention after 1000 cycles using 1 M NaOH electrolyte.

5.4 3-D (Three-Dimensional) Nanomaterials

Lee and co-workers [69] utilize an ambient pressure drying approach to produce reduced graphene oxide (rGO) aerogel for EDLCs behavior of supercapacitors. The low value of R_{ct} (2.52 Ω for 4 h sonicated rGO) indicates that proper communication is delivered between electrolyte and electrode. The 4 h-rGO exhibited high capacitance 182.0 F/g at 0.75 A/g current density, high surface area 190.40 m^2/g with 0.261 cm^3/g pore volume and 95.83% retention for 10,000 charge–discharge cycles. Zou et al., prepared N-doped graphene/PANI (GMPH7) binary hydrogel. The prepared GMPH7 hydrogel showed the higher specific capacitance 514.3 F/g while 375 F/g for graphene/PANI (GPH7) and 325 F/g for PANI at 1 A/g with 100% retention of its capacitance [70]. Hou et al., fabricate amine-functionalized graphene/polyaniline (F-rGO/PANI) and mesoporous graphene/polyaniline (PF-rGO/PANI) composite which exhibit high specific capacitance (597 F/g for F-rGO/PANI and 489 F/g for PF-rGO/PANI) at 0.5 A/g current density with 75% and 89% retention respectively [71]. MnO_2/rGO composite prepared using manganese sulfate monohydrate and exhibit capacitance around 759 F/g at 2 A/g current density with 88% capacitance retention for 3500 cycles [72]. Fu and co-workers presented a facile technique of V_2O_5/graphene composite formation. The high specific capacitance of formed hybrid exhibit 673.2 F/g at 1 A/g current density of V_2O_5/graphene-0.341 (where 0.341 was V_2O_5 mass proportion in composite) with 96.8% retention after 10,000 cycle life and excellent energy as well as power density such as 46.8 Wh/kg at 499.4 W/kg, 32.9 Wh/kg at 4746.0 W/kg in 1 M Na_2SO_4 electrolyte [73]**.** GCS@PANI@rGO were synthesized having a higher specific capacitance of 446.19 F/g at a current density of 2 A/g alongside 93.4% retention after 1000 cycles and even remained 88.7% retention after 5000 charge–discharge cycles, due to the synergic effect of GCS, PANI, and rGO [74]**.** Reduced GO/Fe_3O_4/PANI was synthesized and shown a higher specific capacitance of 610.4 F/g in comparison with rGO/Fe_3O_4 (212.6 F/g) with 87% capacitance because of synergic effect among rGO, Fe_3O_4, PANI as well and absence of agglomeration of Fe_3O_4 nanoparticles on the composite surface [75]. A ternary composite hydrogel PANI/Graphene/Fe_2O_3 was prepared using the microwave irradiation method as the first step. Furthermore, a polymerization process was carried out. The combination of PANI, Graphene, and Fe_2O_3 synergic action displays the high specific capacitance 1124 F/g at 0.25 A/g current density and 923 F/g at 7.5 A/g peak current density with 82.2% retention [76]**.** Another ternary rGO/Au/PANI nanocomposite was synthesized using *Cetraria Islandica L. ach.* extract as a green reducing agent [77]. This hybrid electrode material delivers a high specific capacitance of 212.8 F/g at 1 A/g current density and exhibits 86.9% retention after 5000 repeated charge–discharge cycles. The polyaniline-based ZnS/rGO/PANI ternary composite

exhibits a specific capacitance of 1045.3 F/g using three-electrode and 722.0 F/g capacitance using a two-electrode system at a current density of 1 A/g. Interestingly PANI based ternary composite holds 76.1% and 160% cycle stability for two-electrode and three-electrode systems respectively after 1000 charge–discharge loops [78].

A nanocomposite based on rGO/polypyrrole nanofiber was synthesized via microwave irradiation reduction of GO followed by in-situ polymerization of pyrrole. The higher specific capacitance of 227 F/g at 1 A/g using 1 M H_2SO_4 as an electrolyte and high energy density 38.5 Wh/kg at 500 W/kg power density [79]. Graphene/polypyrrole composite hydrogel prepared with good distribution and cross-linked of PPY on porous graphene structure showed specific capacitance of 295 to 240 F/g at 1–10 A/g current density withholds 80% capacitance retention cycle stability after 5000 cycles of charge–discharge [80]. Moreover, ternary hybrid nanocomposite NiO/Graphene/PPY was prepared [81]. This hybrid material on $Cu(OH)_2$/Cu foil substrate was used as a working electrode for electrochemical analysis. The flaky shape nanocomposite showed a high specific capacitance of 970.85 F/g using 6 M KOH aqueous electrolyte and 66.17 F/g for 1 M $TEABF_4$/AN organic electrolyte. Liang et al. synthesized Graphene/PPY/Ag hybrid nanocomposite [82]. The synergic nature of these three materials exhibits high areal capacitance 294.2 mF/cm^2 at 1 ^{mA}/cm^2 current density with capacitance retention around 80.1% after 5000 loops. The enhanced performance mainly from reversible Ag/Ag^+ redox action and complete wrapping of Ag nanoparticles by PPY on a graphene surface. Another novel hybrid nanocomposite PdPGO was synthesized [83]. This exhibits the highest capacitance as 595 F/g for PdPGO comparable to 335 F/g of binary PdO/PPY material at 1 A/g current density with 88% cycle stability after 5000 loops. Additionally, Xin et al. compared the supercapacitor material performance of MoO_3/Graphene aerogel/PPY, MoO_3/GA, and PPY, which exhibited the specific capacitance 1788 F/g, 1059 F/g, and 379 F/g at 1 A/g [84]. Based on the graphene ternary system, the insertion of PbO_2 nanoparticles has been displayed by Abraham and co-workers into the surface of PPY/rGO for the enhanced electrochemical nature of the supercapacitor [85].

6 Asymmetric Graphene-Based Materials for Supercapacitors

Asymmetric supercapacitors (ASC) have mainly two electrodes of two different positive and negative electrodes. The operating potential range boosted up and discharge times extended using asymmetric electrode materials, and also power and energy density were enhanced compared to symmetric supercapacitor because of fast charge transportation between electrode–electrolyte and combined effort of faradic with non-faradic actions [86–88]. Ashraf et al. developed asymmetric electrodes based on tungsten oxide, highly reduce-graphene oxide (HRG) as positive, and monoclinic

tungsten oxide (m-WO_3) as a negative electrode in 1 M H_2SO_4 electrolyte [89]. The ASC HRG//m-WO_3 showed high specific capacitance 389 F/g at 0.5 A/g and 1.6 V wide window with 93 Wh/kg energy density at 500 W/kg power density. The cyclic stability holds 92% capacitance retention after 5000 cycles. Based on asymmetric supercapacitors, Karimi and co-workers fabricated PPY/FeCoS-rGO//rGO ASC as positive pseudo and negative EDLC electrodes on nickel form current collector [90]. This asymmetric device showed high specific capacitance 94 F/g at 1 A/g and 28.3 Wh/kg energy density at 810 W/kg power density. The other ASCs assembly of PANI/NiO/SGO//Active carbon has 91.15% cycle stability after 10,000 loops, 308.8 F/g capacitance, and 109.8 Wh/kg energy density at 0.8 kW/kg power density [91]. The novel fabricated asymmetric device ASC rGO-S/MnO_2//AC-PS has a maximum 1.7 V potential and 99.6% efficient with 94.5% retention up to 10,000 continuous loops with 71.74 Wh/kg energy density corresponding to 850 W/kg power density [92]. Liu and teammates constructed NiCo-LDH hybrid on rGO surface was used asymmetric positive electrode and displayed excellent energy density 48.7 Wh/kg at 401 W/kg power density with 81% cycle stability correspond to 1.6 V voltage window [93].

7 Conclusion and Prospects

Graphene, a unit layered two-dimensional structures carbon sheet collects lots of reward due to its remarkable properties and is considered the most suitable material among all the carbon materials. So, graphene and its family members (GO and rGO) are widely used as electrode materials in energy storage devices. However, the deep research on graphene-based supercapacitors has reached to advance level by developing binary and ternary hybrid nanocomposites using conducting polymers and metal oxides. Hence we obtained advanced supercapacitors with a high value of capacitance, good cyclic stability, higher energy as well as power density. While pure synthesis of pristine graphene with the less costly and easy process is still the deepest research area for popularizing this material. But graphene can be a more efficient nanomaterial in every field of science and engineering with the proper support of the government. Therefore, we can say that there are wide ranges of research to boost up the supercapacitor performance with hybrid nanomaterials using graphene and its derivatives.

References

1. V. Singh, D. Joung, L. Zhai, S. Das, S.I. Khondaker, S. Seal, Graphene based materials: past, present and future. Prog. Mater. Sci. **56**, 1178–1271 (2011). https://doi.org/10.1016/j.pmatsci.2011.03.003

2. P. Blake, P.D. Brimicombe, R.R. Nair, T.J. Booth, D. Jiang, F. Schedin, L.A. Ponomarenko, S.V. Morozov, H.F. Gleeson, E.W. Hill, A.K. Geim, K.S. Novoselov, Graphene-based liquid crystal device. Nano Lett. **8**, 1704–1708 (2008). https://doi.org/10.1021/nl080649i
3. H.J. Choi, S.M. Jung, J.M. Seo, D.W. Chang, L. Dai, J.B. Baek, Graphene for energy conversion and storage in fuel cells and supercapacitors. Nano Energy **1**, 534–551 (2012). https://doi.org/10.1016/j.nanoen.2012.05.001
4. S. Verma, B. Verma, Synthesis of sulfur/phosphorous-doped graphene aerogel as a modified super capacitor electrode. Int. J. Chem. Stud. **6**, 111–117 (2018)
5. W. Du, X. Jiang, L. Zhu, From graphite to graphene: direct liquid-phase exfoliation of graphite to produce single- and few-layered pristine graphene. J. Mater. Chem. A **1**, 10592–10606 (2013). https://doi.org/10.1039/c3ta12212c
6. X. Xu, C. Liu, Z. Sun, T. Cao, Z. Zhang, E. Wang, Z. Liu, K. Liu, Interfacial engineering in graphene bandgap. Chem. Soc. Rev. **47**, 3059–3099 (2018). https://doi.org/10.1039/c7cs00836h
7. Y. Jiang, J. Liu, Definitions of pseudocapacitive materials: a brief review. Energy Environ. Mater. **2**, 30–37 (2019). https://doi.org/10.1002/eem2.12028
8. M. Vangari, T. Pryor, L. Jiang, Supercapacitors: review of materials and fabrication methods. J. Energy Eng. **139**, 72–79 (2013). https://doi.org/10.1061/(asce)ey.1943-7897.0000102
9. G. Yang, L. Li, W.B. Lee, M.C. Ng, Structure of graphene and its disorders: a review. Sci. Technol. Adv. Mater. **19**, 613–648 (2018). https://doi.org/10.1080/14686996.2018.1494493
10. M.K. Kavitha, M. Jaiswal, Graphene : a review of optical properties and photonic applications. Asian J. Phys. **25**, 809–831 (2016)
11. J.M. Raimond, M. Brune, Q. Computation, F. De Martini, C. Monroe, Electric field effect in atomically thin carbon films. **306**, 666–670 (2004)
12. Y. Hernandez, V. Nicolosi, M. Lotya, F.M. Blighe, Z. Sun, S. De, I.T. McGovern, B. Holland, M. Byrne, Y.K. Gun'ko, J.J. Boland, P. Niraj, G. Duesberg, S. Krishnamurthy, R. Goodhue, J. Hutchison, V. Scardaci, A.C. Ferrari, J.N. Coleman, High-yield production of graphene by liquid-phase exfoliation of graphite. Nat. Nanotechnol. **3**, 563–568 (2008). https://doi.org/10.1038/nnano.2008.215
13. T. Szabó, O. Berkesi, P. Forgó, K. Josepovits, Y. Sanakis, D. Petridis, I. Dékány, Evolution of surface functional groups in a series of progressively oxidized graphite oxides. Chem. Mater. **18**, 2740–2749 (2006). https://doi.org/10.1021/cm060258+
14. H.C. Schniepp, J.L. Li, M.J. McAllister, H. Sai, M. Herrera-Alonson, D.H. Adamson, R.K. Prud'homme, R. Car, D.A. Seville, I.A. Aksay, Functionalized single graphene sheets derived from splitting graphite oxide. J. Phys. Chem. B **110**, 8535–8539 (2006). https://doi.org/10.1021/jp060936f
15. C. Botas, P. Álvarez, P. Blanco, M. Granda, C. Blanco, R. Santamaría, L.J. Romasanta, R. Verdejo, M.A. López-Manchado, R. Menéndez, Graphene materials with different structures prepared from the same graphite by the Hummers and Brodie methods. Carbon **65**, 156–164 (2013). https://doi.org/10.1016/j.carbon.2013.08.009
16. A.V. Talyzin, G. Mercier, A. Klechikov, M. Hedenström, D. Johnels, D. Wei, D. Cotton, A. Opitz, E. Moons, Brodie versus Hummers graphite oxides for preparation of multi-layered materials. Carbon **115**, 430–440 (2017). https://doi.org/10.1016/j.carbon.2016.12.097
17. P. Feicht, J. Biskupek, T.E. Gorelik, J. Renner, C.E. Halbig, M. Maranska, F. Puchtler, U. Kaiser, S. Eigler, Brodie's or Hummers' method: oxidation conditions determine the structure of graphene oxide. Chem. Eur. J. **25**, 8955–8959 (2019). https://doi.org/10.1002/chem.201901499
18. H.L. Poh, F. Šaněk, A. Ambrosi, G. Zhao, Z. Sofer, M. Pumera, Graphenes prepared by Staudenmaier, Hofmann and Hummers methods with consequent thermal exfoliation exhibit very different electrochemical properties. Nanoscale **4**, 3515–3522 (2012). https://doi.org/10.1039/c2nr30490b
19. D.R. Dreyer, H.-P. Jia, C.W. Bielawski, Graphene oxide: a convenient carbocatalyst for facilitating oxidation and hydration reactions. Angew. Chem. **122**, 6965–6968 (2010). https://doi.org/10.1002/ange.201002160

20. G. Pavoski, T. Maraschin, F.D.C. Fim, N.M. Balzaretti, G.B. Galland, C.S. Moura, N.R.D.S. Basso, Few layer reduced graphene oxide: evaluation of the best experimental conditions for easy production. Mater. Res. **20**, 53–61 (2017). https://doi.org/10.1590/1980-5373-MR-2015-0528
21. M. Nováček, O. Jankovský, J. Luxa, D. Sedmidubský, M. Pumera, V. Fila, M. Lhotka, K. Klímová, S. Matějková, Z. Sofer, Tuning of graphene oxide composition by multiple oxidations for carbon dioxide storage and capture of toxic metals. J. Mater. Chem. A **5**, 2739–2748 (2017). https://doi.org/10.1039/c6ta03631g
22. I. Jung, D.A. Field, N.J. Clark, Y. Zhu, D. Yang, R.D. Piner, S. Stankovich, D.A. Dikin, H. Geisler, C.A. Ventrice, R.S. Ruoff, Reduction kinetics of graphene oxide determined by electrical transport measurements and temperature programmed desorption. J. Phys. Chem. C **113**, 18480–18486 (2009). https://doi.org/10.1021/jp904396j
23. N. Cao, Y. Zhang, Study of reduced graphene oxide preparation by Hummers' method and related characterization. J. Nanomater. 1–5 (2015). https://doi.org/10.1155/2015/168125
24. J. Guerrero-Contreras, F. Caballero-Briones, Graphene oxide powders with different oxidation degree, prepared by synthesis variations of the Hummers method. Mater. Chem. Phys. **153**, 209–220 (2015). https://doi.org/10.1016/j.matchemphys.2015.01.005
25. M.J. Yoo, H.B. Park, Effect of hydrogen peroxide on properties of graphene oxide in Hummers method. Carbon **141**, 515–522 (2019). https://doi.org/10.1016/j.carbon.2018.10.009
26. D.-W. Kang, H.-S. Shin, Control of size and physical properties of graphene oxide by changing the oxidation temperature. Carbon Lett. **13**, 39–43 (2012). https://doi.org/10.5714/cl.2012.13.1.039
27. N.I. Zaaba, K.L. Foo, U. Hashim, S.J. Tan, W.W. Liu, C.H. Voon, Synthesis of graphene oxide using modified Hummers method: solvent influence. Procedia Eng. **184**, 469–477 (2017). https://doi.org/10.1016/j.proeng.2017.04.118
28. T. Chen, B. Zeng, J.L. Liu, J.H. Dong, X.Q. Liu, Z. Wu, X.Z. Yang, Z.M. Li, High throughput exfoliation of graphene oxide from expanded graphite with assistance of strong oxidant in modified Hummers method. J. Phys.: Conf. Ser. **188** (2009). https://doi.org/10.1088/1742-6596/188/1/012051
29. A. Alkhouzaam, H. Qiblawey, M. Khraisheh, M. Atieh, M. Al-Ghouti, Synthesis of graphene oxides particle of high oxidation degree using a modified Hummers method. Ceram. Int. **46**, 23997–24007 (2020). https://doi.org/10.1016/j.ceramint.2020.06.177
30. H. Yu, B. Zha, B. Chaoke, R. Li, R. Xing, High-efficient synthesis of graphene oxide based on improved Hummers method. Sci. Rep. 1–7 (2016). https://doi.org/10.1038/srep36143
31. B. Kartick, S.K. Srivastava, I. Srivastava, Green synthesis of graphene. J. Nanosci. Nanotechnol. **13**, 4320–4324 (2013). https://doi.org/10.1166/jnn.2013.7461
32. P. Chamoli, R. Sharma, M.K. Das, K.K. Kar, Mangifera indica, Ficus religiosa and Polyalthia longifolia leaf extract-assisted green synthesis of graphene for transparent highly conductive film. RSC Adv. **6**, 96355–96366 (2016). https://doi.org/10.1039/c6ra19111h
33. F. Tavakoli, M. Salavati-niasari, F. Mohandes, Green synthesis and characterization of graphene nanosheets. Mater. Res. Bull. **63**, 51–57 (2015). https://doi.org/10.1016/j.materresbull.2014.11.045
34. P. Chamoli, T. Srivastava, A. Tyagi, K.K. Raina, K.K. Kar, Urea and cow urine-based green approach to fabricate graphene-based transparent conductive films with high conductivity and transparency. Mater. Chem. Phys. **242**, 122465 (2020). https://doi.org/10.1016/j.matchemphys.2019.122465
35. K.X. Sheng, Y.X. Xu, C. Li, G.Q. Shi, High-performance self-assembled graphene hydrogels prepared by chemical reduction of graphene oxide. New Carbon Mater. **26**, 9–15 (2011). https://doi.org/10.1016/S1872-5805(11)60062-0
36. W. Gao, L.B. Alemany, L. Ci, P.M. Ajayan, New insights into the structure and reduction of graphite oxide. Nat. Chem. **1**, 403–408 (2009). https://doi.org/10.1038/nchem.281
37. Y. Chen, X. Zhang, D. Zhang, P. Yu, Y. Ma, High performance supercapacitors based on reduced graphene oxide in aqueous and ionic liquid electrolytes. Carbon **49**, 573–580 (2011). https://doi.org/10.1016/j.carbon.2010.09.060

38. P. Su, H.L. Guo, L. Tian, S.K. Ning, An efficient method of producing stable graphene suspensions with less toxicity using dimethyl ketoxime. Carbon **50**, 5351–5358 (2012). https://doi.org/10.1016/j.carbon.2012.07.001
39. A.C. Ferrari, F. Bonaccorso, V. Fal'ko, K.S. Novoselov, S. Roche, P. Bøggild, S. Borini, F.H.L. Koppens, V. Palermo, N. Pugno, J.A. Garrido, R. Sordan, A. Bianco, L. Ballerini, M. Prato, E. Lidorikis, J. Kivioja, C. Marinelli, T. Ryhänen, A. Morpurgo, J.N. Coleman, V. Nicolosi, L. Colombo, A. Fert, M. Garcia-Hernandez, A. Bachtold, G.F. Schneider, F. Guinea, C. Dekker, M. Barbone, Z. Sun, C. Galiotis, A.N. Grigorenko, G. Konstantatos, A. Kis, M. Katsnelson, L. Vandersypen, A. Loiseau, V. Morandi, D. Neumaier, E. Treossi, V. Pellegrini, M. Polini, A. Tredicucci, G.M. Williams, B. Hee Hong, J.H. Ahn, J. Min Kim, H. Zirath, B.J. Van Wees, H. Van Der Zant, L. Occhipinti, A. Di Matteo, I.A. Kinloch, T. Seyller, E. Quesnel, X. Feng, K. Teo, N. Rupesinghe, P. Hakonen, S.R.T. Neil, Q. Tannock, T. Löfwander, J. Kinaret, Science and technology roadmap for graphene, related two-dimensional crystals, and hybrid systems. Nanoscale. **7**, 4598–4810 (2015). https://doi.org/10.1039/c4nr01600a
40. X. Li, W. Cai, J. An, S. Kim, J. Nah, D. Yang, R. Piner, A. Velamakanni, I. Jung, E. Tutuc, S.K. Banerjee, L. Colombo, R.S. Ruoff, Large-area synthesis of high-quality and uniform graphene films on copper foils. Science **324**, 1312–1314 (2009). https://doi.org/10.1126/science.1171245
41. R. Muñoz, C. Gómez-Aleixandre, Review of CVD synthesis of graphene. Chem. Vap. Deposition **19**, 297–322 (2013). https://doi.org/10.1002/cvde.201300051
42. J. Robinson, X. Weng, K. Trumbull, R. Cavalero, M. Wetherington, E. Frantz, M. LaBella, Z. Hughes, M. Fanton, D. Snyder, Nucleation of epitaxial graphene on SiC(0001). ACS Nano **4**, 153–158 (2010). https://doi.org/10.1021/nn901248j
43. N. Mishra, J. Boeckl, N. Motta, F. Iacopi, Graphene growth on silicon carbide: a review. Phys. Status Solidi (A) Appl. Mater. Sci. **213**, 2277–2289 (2016). https://doi.org/10.1002/pssa.201600091
44. G.G. Jernigan, B.L. VanMil, J.L. Tedesco, J.G. Tischler, E.R. Glaser, A. Davidson, P.M. Campbell, D.K. Gaskill, Comparison of epitaxial graphene on si-face and C-face 4H SiC formed by ultrahigh vacuum and RF furnace production. Nano Lett. **9**, 2605–2609 (2009). https://doi.org/10.1021/nl900803z
45. N.M.S. Hidayah, W. Liu, C. Lai, N.Z. Noriman, Comparison on graphite , graphene oxide and reduced graphene oxide : synthesis and characterization. 150002 (2017). https://doi.org/10.1063/1.5005764
46. O.C. Compton, S.T. Nguyen, Graphene oxide, highly reduced graphene oxide, and graphene: versatile building blocks for carbon-based materials. Small **6**, 711–723 (2010). https://doi.org/10.1002/smll.200901934
47. G. Eda, M. Chhowalla, Chemically derived graphene oxide: towards large-area thin-film electronics and optoelectronics. Adv. Mater. **22**, 2392–2415 (2010). https://doi.org/10.1002/adma.200903689
48. M. Iliut, A.M. Gabudean, C. Leordean, T. Simon, C.M. Teodorescu, S. Astilean, Riboflavin enhanced fluorescence of highly reduced graphene oxide. Chem. Phys. Lett. **586**, 127–131 (2013). https://doi.org/10.1016/j.cplett.2013.09.032
49. Y.U. Shang, D. Zhang, Y. Liu, C. Guo, Preliminary comparison of different reduction methods of graphene oxide. Bull. Mater. Sci. **38**, 7–12 (2015). https://doi.org/10.1007/s12034-014-0794-7
50. N. Kumari Jangid, S. Jadoun, N. Kaur, A review on high-throughput synthesis, deposition of thin films and properties of polyaniline. Euro. Polym. J. **125**, 109485 (2020). https://doi.org/10.1016/j.eurpolymj.2020.109485
51. H. Huang, R. Chen, S. Yang, L. Li, Y. Liu, J. Huang, Facile fabrication of MnO_2-embedded 3-D porous polyaniline composite hydrogel for supercapacitor electrode with high loading. High Perform. Polym. **32**, 286–295 (2020). https://doi.org/10.1177/0954008319860893
52. T. Das, B. Verma, Synthesis of polymer composite based on polyaniline-acetylene black-copper ferrite for supercapacitor electrodes. Polymer **168** (2019). https://doi.org/10.1016/j.polymer.2019.01.058

53. L.Z. Fan, J. Maier, High-performance polypyrrole electrode materials for redox supercapacitors. Electrochem. Commun. **8**, 937–940 (2006). https://doi.org/10.1016/j.elecom.2006.03.035
54. Y. Huang, H. Li, Z. Wang, M. Zhu, Z. Pei, Q. Xue, Y. Huang, C. Zhi, Nanostructured polypyrrole as a flexible electrode material of supercapacitor. Nano Energy **22**, 422–438 (2016). https://doi.org/10.1016/j.nanoen.2016.02.047
55. S. Lee, M.S. Cho, H. Lee, J. Do Nam, Y. Lee, A facile synthetic route for well defined multilayer films of graphene and PEDOT via an electrochemical method. J. Mater. Chem. **22**, 1899–1903 (2012). https://doi.org/10.1039/c1jm13739e
56. G. Wang, L. Zhang, J. Zhang, A review of electrode materials for electrochemical supercapacitors. Chem. Soc. Rev. **41**, 797–828 (2012). https://doi.org/10.1039/c1cs15060j
57. C. An, Y. Zhang, H. Guo, Y. Wang, Metal oxide-based supercapacitors: progress and prospectives, Nanoscale. Advances **1**, 4644–4658 (2019). https://doi.org/10.1039/c9na00543a
58. S. Zhang, L. Sui, H. Dong, W. He, L. Dong, L. Yu, High-performance supercapacitor of graphene quantum dots with uniform sizes. ACS Appl. Mater. Interfaces. **10**, 12983–12991 (2018). https://doi.org/10.1021/acsami.8b00323
59. W. Fan, Y.Y. Xia, W.W. Tjiu, P.K. Pallathadka, C. He, T. Liu, Nitrogen-doped graphene hollow nanospheres as novel electrode materials for supercapacitor applications. J. Power Sources **243**, 973–981 (2013). https://doi.org/10.1016/j.jpowsour.2013.05.184
60. Z. Yan, Z. Gao, Z. Zhang, C. Dai, W. Wei, P.K. Shen, Graphene nanosphere as advanced electrode material to promote high performance symmetrical supercapacitor. Small **17**, 1–12 (2021). https://doi.org/10.1002/smll.202007915
61. Y. Saito, M. Ashizawa, H. Matsumoto, Mesoporous hydrated graphene nanoribbon electrodes for efficient supercapacitors: effect of nanoribbon dispersion on pore structure. Bull. Chem. Soc. Jpn. **93**, 1268–1274 (2020). https://doi.org/10.1246/BCSJ.20200161
62. C. Zhou, M. Hong, Y. Yang, C. Yang, N. Hu, L. Zhang, Z. Yang, Y. Zhang, Laser-induced bimetal sulfide/graphene nanoribbon hybrid frameworks for high-performance all-in-one fiber supercapacitors. J. Power Sources **438**, 227044 (2019). https://doi.org/10.1016/j.jpowsour.2019.227044
63. S.K. Ujjain, P. Ahuja, R.K. Sharma, Graphene nanoribbon wrapped cobalt manganite nanocubes for high performance all-solid-state flexible supercapacitors. J. Mater. Chem. A **3**, 9925–9931 (2015). https://doi.org/10.1039/c5ta00653h
64. Y. Ping, Y. Zhang, Y. Gong, B. Cao, Q. Fu, C. Pan, Edge-riched graphene nanoribbon for high capacity electrode materials. Electrochim. Acta **250**, 84–90 (2017). https://doi.org/10.1016/j.electacta.2017.08.051
65. Y. Li, M. Van Zijll, S. Chiang, N. Pan, KOH modified graphene nanosheets for supercapacitor electrodes. J. Power Sources **196**, 6003–6006 (2011). https://doi.org/10.1016/j.jpowsour.2011.02.092
66. V. Thirumal, A. Pandurangan, R. Jayavel, R. Ilangovan, Synthesis and characterization of boron doped graphene nanosheets for supercapacitor applications. Synth. Met. **220**, 524–532 (2016). https://doi.org/10.1016/j.synthmet.2016.07.011
67. Z. Fan, Q. Zhao, T. Li, J. Yan, Y. Ren, J. Feng, T. Wei, Easy synthesis of porous graphene nanosheets and their use in supercapacitors. Carbon **50**, 1699–1703 (2012). https://doi.org/10.1016/j.carbon.2011.12.016
68. N. Chakrabarty, A. Dey, S. Krishnamurthy, A.K. Chakraborty, CeO_2/Ce_2O_3 quantum dot decorated reduced graphene oxide nanohybrid as electrode for supercapacitor. Appl. Surf. Sci. **536**, 147960 (2021). https://doi.org/10.1016/j.apsusc.2020.147960
69. S.P. Lee, G.A.M. Ali, H.H. Hegazy, H.N. Lim, K.F. Chong, Optimizing reduced graphene oxide aerogel for a supercapacitor. Energy Fuels **35**, 4559–4569 (2021). https://doi.org/10.1021/acs.energyfuels.0c04126
70. Y. Zou, Z. Zhang, W. Zhong, W. Yang, Hydrothermal direct synthesis of polyaniline, graphene/polyaniline and N-doped graphene/polyaniline hydrogels for high performance flexible supercapacitors. J. Mater. Chem. A **6**, 9245–9256 (2018). https://doi.org/10.1039/c8ta01366g

71. Z. Hou, S. Zou, J. Li, Morphology and structure control of amine- functionalized graphene/polyaniline composite for high-performance supercapacitors. J. Alloy. Compd. **827**, 154390 (2020). https://doi.org/10.1016/j.jallcom.2020.154390
72. S. Jadhav, R.S. Kalubarme, C. Terashima, B.B. Kale, V. Godbole, A. Fujishima, S.W. Gosavi, Manganese dioxide/reduced graphene oxide composite an electrode material for high-performance solid state supercapacitor. Electrochim. Acta **299**, 34–44 (2019). https://doi.org/10.1016/j.electacta.2018.12.182
73. M. Fu, Q. Zhuang, Z. Zhu, Z. Zhang, W. Chen, Q. Liu, H. Yu, Facile synthesis of V2O5/graphene composites as advanced electrode materials in supercapacitors. J. Alloy. Compd. **862**, 158006 (2021). https://doi.org/10.1016/j.jallcom.2020.158006
74. L. Liu, Y. Wang, Q. Meng, B. Cao, A novel hierarchical graphene/polyaniline hollow microsphere as electrode material for supercapacitor applications. J. Mater. Sci. **52**, 7969–7983 (2017). https://doi.org/10.1007/s10853-017-1000-2
75. S.R. Charandabinezhad, H. Asgharzadeh, N. Arsalani, Synthesis and characterization of reduced graphene oxide/magnetite/polyaniline composites as electrode materials for supercapacitors. J. Mater. Sci.: Mater. Electron. **32**, 1864–1876 (2021). https://doi.org/10.1007/s10854-020-04955-7
76. A. Gupta, S. Sardana, J. Dalal, S. Lather, A.S. Maan, R. Tripathi, R. Punia, K. Singh, A. Ohlan, Nanostructured polyaniline/graphene/Fe_2O_3 composites hydrogel as a high-performance flexible supercapacitor electrode material. ACS Appl. Energy Mater. **3**, 6434–6446 (2020). https://doi.org/10.1021/acsaem.0c00684
77. Z. Çıplak, A. Yıldız, N. Yıldız, Green preparation of ternary reduced graphene oxide-au@polyaniline nanocomposite for supercapacitor application. J. Energy Storage **32**, 101846 (2020). https://doi.org/10.1016/j.est.2020.101846
78. Z. Xu, Z. Zhang, H. Yin, S. Hou, H. Lin, J. Zhou, S. Zhuo, Investigation on the role of different conductive polymers in supercapacitors based on a zinc sulfide/reduced graphene oxide/conductive polymer ternary composite electrode. RSC Adv. **10**, 3122–3129 (2020). https://doi.org/10.1039/c9ra07842h
79. R. Ghanbari, M. Entezar Shabestari, E. Naderi Kalali, Y. Hu, S.R. Ghorbani, Electrochemical performance and complex impedance properties of reduced-graphene oxide/polypyrrole nanofiber nanocomposite. Ionics **27**, 1279–1290 (2021). https://doi.org/10.1007/s11581-021-03907-3
80. H. Zhou, T. Ni, X. Qing, X. Yue, G. Li, Y. Lu, One-step construction of graphene-polypyrrole hydrogels and their superior electrochemical performance. RSC Adv. **4**, 4134–4139 (2014). https://doi.org/10.1039/c3ra44647f
81. S.Z. Golkhatmi, A. Sedghi, H.N. Miankushki, M. Khalaj, Structural properties and supercapacitive performance evaluation of the nickel oxide/graphene/polypyrrole hybrid ternary nanocomposite in aqueous and organic electrolytes. Energy **214**, 118950 (2021). https://doi.org/10.1016/j.energy.2020.118950
82. C. Liang, C. Yang, L. Zang, Q. Liu, J. Qiu, Y. Li, W. Zuo, X. Liu, UV-assisted one-step synthesis of ternary graphene/polypyrrole/silver nanocomposites for supercapacitors. Energy Technol. **9**, 1–9 (2021). https://doi.org/10.1002/ente.202000966
83. J. Jose, S.P. Jose, T. Prasankumar, S. Shaji, S. Pillai, P. B. Sreeja, Emerging ternary nanocomposite of rGO draped palladium oxide/polypyrrole for high performance supercapacitors. J. Alloy. Compd. **855**, 157481 (2021). https://doi.org/10.1016/j.jallcom.2020.157481
84. Q. Xin, Z. Guo, Y. Zang, J. Lin, Graphene aerogel-coated MoO3 nanoparticle/polypyrrole ternary composites for high-performance supercapacitor. J. Mater. Sci.: Mater. Electron. **31**, 17110–17119 (2020). https://doi.org/10.1007/s10854-020-04271-0
85. S. Abraham, T. Prasankumar, K. Vinoth Kumar, S. Zh Karazhanov, S. Jose, Novel lead dioxide intercalated polypyrrole/graphene oxide ternary composite for high throughput supercapacitors. Mater. Lett. **273**, 127943 (2020). https://doi.org/10.1016/j.matlet.2020.127943
86. Z.S. Wu, W. Ren, D.W. Wang, F. Li, B. Liu, H.M. Cheng, High-energy MnO_2 nanowire/graphene and graphene asymmetric electrochemical capacitors. ACS Nano **4**, 5835–5842 (2010). https://doi.org/10.1021/nn101754k

87. C. Liu, F. Li, M. Lai-Peng, H.M. Cheng, Advanced materials for energy storage. Adv. Mater. **22**, 28–62 (2010). https://doi.org/10.1002/adma.200903328
88. X. Huang, Z. Zeng, Z. Fan, J. Liu, H. Zhang, Graphene-based electrodes. Adv. Mater. **24**, 5979–6004 (2012). https://doi.org/10.1002/adma.201201587
89. M. Ashraf, S.S. Shah, I. Khan, M.A. Aziz, N. Ullah, M. Khan, S.F. Adil, Z. Liaqat, M. Usman, W. Tremel, M.N. Tahir, A High-Performance asymmetric supercapacitor based on tungsten oxide nanoplates and highly reduced graphene oxide electrodes. Chem. Eur. J. **27**, 6973–6984 (2021). https://doi.org/10.1002/chem.202005156
90. A. Karimi, I. Kazeminezhad, L. Naderi, S. Shahrokhian, Construction of a ternary nanocomposite, polypyrrole/Fe-Co sulfide-reduced graphene oxide/nickel foam, as a novel binder-free electrode for high-performance asymmetric supercapacitors. J. Phys. Chem. C **124**, 4393–4407 (2020). https://doi.org/10.1021/acs.jpcc.9b11010
91. C. Huang, C. Hao, W. Zheng, S. Zhou, L. Yang, X. Wang, C. Jiang, L. Zhu, Synthesis of polyaniline/nickel oxide/sulfonated graphene ternary composite for all-solid-state asymmetric supercapacitor. Appl. Surf. Sci. **505**, 144589 (2020). https://doi.org/10.1016/j.apsusc.2019.144589
92. D.J. Tarimo, K.O. Oyedotun, A.A. Mirghni, N.F. Sylla, N. Manyala, High energy and excellent stability asymmetric supercapacitor derived from sulphur-reduced graphene oxide/manganese dioxide composite and activated carbon from peanut shell. Electrochim. Acta **353**, 136498 (2020). https://doi.org/10.1016/j.electacta.2020.136498
93. L. Liu, A. Liu, Y. Xu, H. Yu, F. Yang, J. Wang, Z. Zeng, S. Deng, Agglomerated nickel-cobalt layered double hydroxide nanosheets on reduced graphene oxide clusters as efficient asymmetric supercapacitor electrodes. J. Mater. Res. **35**, 1205–1213 (2020). https://doi.org/10.1557/jmr.2020.39

Nanocomposites of Carbon Nanotubes for Electrochemical Energy Storage Applications

Pranjal Saikia, Pranjit Barman, and Lakhya Jyoti Borthakur

Abstract Carbon nanotubes are tube-shaped molecules that are composed of plunged sheets of one or more layers of carbon atoms arranged in a honeycomb hexagonal fashion. Because of their structural features and well-conducting networks they are extensively used in many devices viz. supercapacitors, smart textiles as well as other energy conversion devices. Because of the superior flexibility and stretchable nature carbon nanotubes show enhanced cyclic stability to be used as active electrode material. Moreover, carbon nanotubes serve as an excellent additive for conducting polymers, metal oxides, and graphene-based supercapacitors by providing the best route for the propagation of charge by drastically reducing the cell resistance. This chapter will explore the use of carbon nanotubes in supercapacitors, batteries, and fuel cells.

Keywords Supercapacitors · Mesoporous structure · Metal oxide · Conducting polymers

1 Introduction

Carbon nanotubes (CNT) are a morphological texture of carbon with tube-shaped molecules arranged in a honeycomb hexagonal fashion where each carbon atom is sp^2 hybridized. Since its discovery by Sumio Iijjima in 1991 [1], CNTs have been able to find a wide range of applications in different fields because of their unique properties and structure [2–4]. CNT possesses high tensile strength, superior surface area, aspect ratio, and extraordinary thermal and electrical conductivity, chemical stability, and lightweight [5]. From the perspective of their mechanical properties CNTs are considered the strongest and the most buoyant materials in nature so far

P. Saikia · P. Barman
Department of Chemistry, NIT Silchar, Silchar, Assam 788010, India

L. J. Borthakur (✉)
Department of Chemistry, Nowgong College, Nagaon, Assam 782001, India
e-mail: lakhyab@gmail.com

S. Thomas et al. (eds.), *Nanostructured Materials for Supercapacitors*,
Advances in Material Research and Technology,
https://doi.org/10.1007/978-3-030-99302-3_12

[6]. Due to this unique nature, CNTs have many practical applications in chemical and bio-sensors, catalysis [7], field emission materials [8–9], and electronics [10]. Apart from these, CNTs and their composites are potential candidates in energy storage devices and are extensively used in supercapacitors, fuel cells, batteries as well as in hydrogen storage devices [11–13]. Owing to their exceptionally high electronic conductivity CNT has been used as an additive material in composite electrodes. These composites impart superior electrochemical activity to otherwise poorly conducting electrode materials. This chapter focuses on the use of CNTs in supercapacitors, alkali metal ion batteries, and fuel cells.

2 Structure and Properties of Carbon Nanotubes

There are two types of CNTs viz. single-walled carbon nanotubes (SWCNT) and multiwalled carbon nanotubes (MWCNT). SWCNT can be regarded as the wrapped up seamless cylinders of graphene sheets with a hexagonal honeycomb lattice structure whereas MWCNTs are made up of one to tens and hundreds of concentric shells of hexagonally arranged roll sheets of carbon atoms with a separating distance of ~0.3 nm [1, 6]. The electronic properties of CNTs may be associated with their geometrical structure which can be specified by a set of indexes called the chiral indexes (n, m). Based on this, CNTs are classified into three types viz chiral (n, m), zigzag (n, 0), and armchair (n, n). In the armchair structure of CNTs, single-layer graphene sheets are rolled up in such a way that the carbon–carbon bonds are aligned parallel to the axis of the tube. Zigzag is made by rolling the carbon sheets in a way that the tube axis is perpendicular to the carbon–carbon bond whereas for chiral structure the carbon–carbon bonds are inclined to the tube axis [6]. In CNTs, each carbon atom is covalently linked with the other three neighboring carbon atoms through sp^2 hybridized molecular orbitals in a hexagonal honeycomb lattice structure. Here, the fourth outermost electron of the P_Z orbital undergoes hybridization with other P_z orbitals and forms a delocalized π-band [14]. The chiral vector (C_h) defines the 2D lattice of CNTs. Here $C_h = na_1 + ma_2$, n and m are the two indices that define the configuration of CNTs that connects equivalent crystallographic sites of a two-dimensional graphene sheet, a_1 and a_2 are basis vector that corresponds to the graphene lattice structure [15]. Figure 1 shows the formation of single-walled CNTs by plunging a single graphene sheet in a different orientation.

3 Electronic Properties of CNTs

Depending on the values of n and m indexes CNTs may be metallic or semiconducting. The metallicity of SWCNT generally depends upon its chirality [14]. When $n - m \neq 3q$ (q being an integer), its electron density of states exhibits a remarkable bandgap close to the Fermi level, and the SWCNT will evince a semiconducting

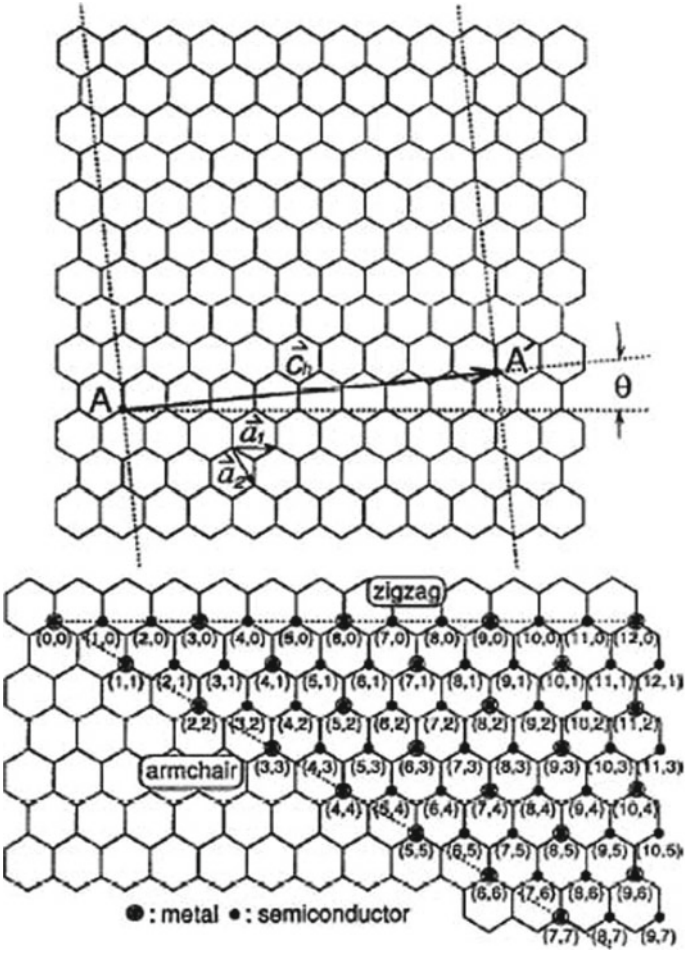

Fig. 1 Formation of SWCNT by wrapping graphene sheets into a cylindrical structure, the nature of wrapping is determined by the chiral vector C_h. "Adapted with permission from reference [14], Copyright (1993), AIP Publishing"

behavior at room temperature and will also exhibit a chirality dependent bandgap. If $n - m = 3q$, the conductance and valance band will overlap and thus will be purely metallic or semi-metallic. Zigzag (n, 0) SWCNT will show two distinct behaviors based on n/3 value. The tube will be metallic when n/3 is an integer and otherwise the tube will show semiconducting behavior. When C_h rotates from zigzag (n, 0) to chiral (n, m) the SWCNT will have the same electronic properties as zigzag SWCNT. When C_h rotates by 30° relative to (n, 0), it represents armchair CNTs that are expected to show metallic behavior [14, 16, 17].

The electrical conductivity of CNTs is determined by their carbon framework and one-dimensional property. CNTs have a current density of 10^9 A/cm^2 and they

also have improved rate capability to be used in electronic devices like supercapacitors, batteries, etc. The presence of strong carbon–carbon double bonds imparts high Young's modulus in the axial direction as well as the highest tensile strength to the CNTs. At room temperature, CNTs exhibit a thermal conductivity of about 6600 W/(mK) [18]. Owing to these favorable mechanical, electrical, and thermal properties they are extensively used in various energy storage and conversion devices.

4 Application of CNTs in Energy Storage Devices

4.1 Supercapacitors

The idea of a supercapacitor was first put forward by Becker in 1957 [19]. They are energy storage devices having much higher capacitance values. In comparison to conventional electrolytic capacitors, supercapacitors envy nearly 10–100 times more capacitance per unit mass. Based on their charge holding mechanism supercapacitors can be categorized as (a) Electrical double-layer capacitors (EDLC) and (b) Pseudocapacitors.

EDLC is typically composed of two porous electrodes separated by a thin separating medium soaked in an electrolytic solution [11]. In EDLC, the capacitance is due to the electrical charge separation, originated by the directional arrangement of the electrons and ions at the electrode–electrolyte interfaces [20, 21]. On charging the system, the cations move to the cathode and anions towards the anode. When electrons move in the external circuit from the cathode to the anode, an electrical double layer is generated at their interfaces. When charging is over, positive charges on the electrode attract the anions and negative charges attract the cations and this gives stability to the double layer. During the discharging process exactly the reverse happens. During the entire charging-discharging process the electrode material remains electrochemically inactive and accumulation of charge occurs only at the electrode/electrolyte interface. Therefore, electrical double layer capacitance is a surface phenomenon and the charging process in EDLC is a non-Faradaic one. The charge storage capacity therefore very much relies on the nature of the electrode material [21–24].

Pseudocapacitors mainly consist of electrodes of redox-active materials and the capacitance arises from the fast and reversible faradic reaction at the surface that involves passages of charge across the double layer [25, 26]. Figure 2 depicts the charge holding mechanism of (a) EDLC (b) Pseudocapacitors.

The relationship between the capacitance and energy stored in a supercapacitor is given by the equation

$$E = CV^2/2 \tag{1}$$

Here, C is capacitance and V represents the voltage of the cell. Power density is given by

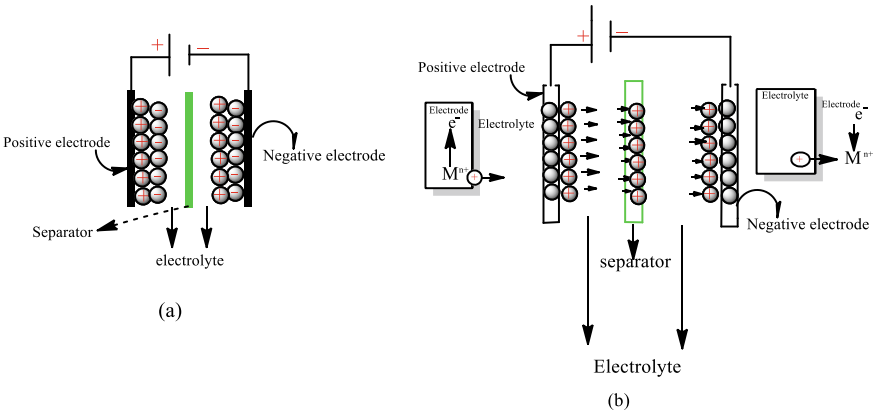

Fig. 2 **(a)** Electrical double-layer capacitor (EDLC) (**b)** Pseudocapacitor

$$P = V^2/4R_s \tag{2}$$

Here, R_s is the equivalent series resistance [11].

The capacitance of a supercapacitor is essentially determined by the physical properties of active electrode material. Based on specific surface area and porosity, a wide variety of materials like carbon aerogels, activated carbon, carbon fibers including oxides and their composites have been abundantly employed as active electrode material in supercapacitor devices [27–29]. For a supercapacitor to have high specific capacitance, there must be superior charge accumulation capacity of the electrode–electrolyte interface, that relies on the accessible surface area of the electrode to electrolyte to facilitate the rapid movement of ions at a higher current rate. However, the above-mentioned carbon materials have a poorly accessible surface area and it is a major hurdle in achieving the desired specific capacitance [30]. Most of these carbon materials have a surface area of less than 2 nm that resides in the scale of micropores [31, 32]. However, mesoporous materials are the most suitable contenders for the fabrication of any supercapacitor devices, and CNTs, owing to their high mesoporosity have earned extensive attention among the scientific communities for developing new generation supercapacitor devices.

Niu et al. [32] has pioneered the use of MWCNTs in fabricating EDLC electrode using 38% sulphuric acid solution as electrolyte. These CNTs have enviced a specific capacitance of 102 F/g with an energy density of 0.5 Wh/kg. An et al. [33] has employed SWCNT as active electrode material where they have attained a specific capacitance of 180 F/g. Niu et al. and Frackowiak and Beguin [32, 34] has reported the use of different types of SWCNT and MWCNT to fabricate supercapacitors and investigated its electrochemical properties. They found that in addition to mesopores present in the nanotube structure, high specific capacitance is also contributed by the central canal tube that facilitates the easy transport of the ions from the solution to the charged interface. For conventional carbon electrodes, capacitance decreases with an

increase in current densities. This may be attributed to the blockage of micropores with an increasing amount of current load. Thus the energy stored in such capacitors can be utilized only at a restricted discharge rate at a very low frequency. On the other hand, in the supercapacitors where CNTs are employed, fast charge integration and ejection can be observed. The frequency dependence of supercapacitors is usually assessed by "frequency Knee" in its impedance spectrum. Niu et al. [32] has observed a frequency Knee of 100 Hz for supercapacitors with CNT electrodes which means that energy stored in such capacitors are accessible at frequencies up to100 Hz.

Recent researches have revealed that vertically aligned CNTs are more appropriate structured materials than their arbitrarily intertwined counterparts. Zilli et al. [35] has observed that unlike randomly entangled CNT, the vertically aligned and unbundled CNT holds higher mesoporosity, high accessible surface area for the electrolyte ions and this in turn, provides better charge storage/delivery properties to the capacitors. This improvement in the properties of such capacitors can be attributed to the participation of each tube during the charging and discharging process indicating an integrated charge capacity from all the discrete tubes or the increased surface area of aligned CNTs. Huang and Dai [36] have applied the plasma etching method to remove the amorphous carbon layer that covers the aligned CNTs array. Based on this end cap opening of the aligned CNT, Frackowiak, and Begum [37] have concluded that the aligned CNTs with their open top end permit the ions from an electrolyte to access the internal voids present in the tubes. This distinctive arrangement with opened tip structure of the CNTs provides superior accessibility of the surface area to the electrolyte in comparison to it's arbitrarily intertwined counterparts (Fig. 3).

Based on the above-mentioned advantageous properties of aligned CNTs over arbitrarily intertwined CNTs, many scientists have utilized these CNTs in supercapacitor electrodes. Chen et al. [38] have made the use of aligned CNT array electrodes using the chemical vapor deposition method with porous aluminum oxide as

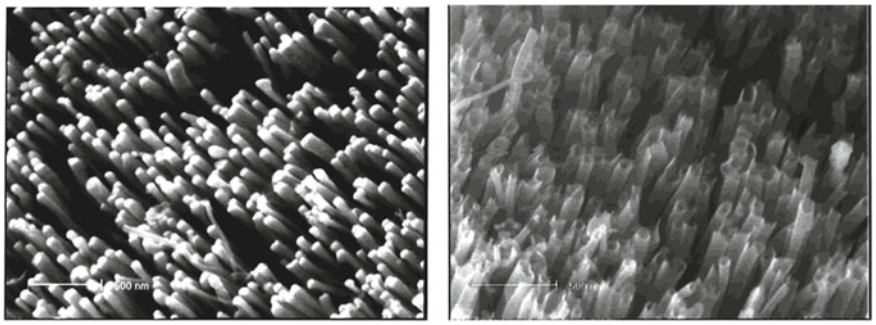

Fig. 3 Pictorial depiction of SEM morphologies of aligned CNTs (**a**) before and (**b**) after the plasma treatment to open the top end-caps of tubes. "Adapted with permission from reference [36], copyright (2002), American Chemical Society"

templates for the fabrication of supercapacitors and demonstrated a specific capacitance of 365 Fg^{-1} in one molar H_2SO_4 solution. Lu et al. [39] have reported a high specific capacitance of 440 Fg^{-1} for ionic liquid as electrolyte where CNTs were prepared by a template-free chemical vapor deposition method.

Functionalization or surface treatment of CNTs has also been observed to contribute significantly to the efficacy of CNT- based supercapacitors. Kim et al. [40] have conducted the functionalization of MWCNT using concentrated H_2SO_4/HNO_3 and $SOCl_2$ to have carboxylated and chlorinated MWCNTs. The oxidation treatment of MWCNT with strong acids has introduced oxygen-containing functional groups into the sidewalls of the MWCNTs, this results in the disruption of its graphene structure which in turn contributed to having 3.2 times higher specific capacitance of MWCNT due to increased hydrophilicity. In contrast to that chlorinated MWCNTs upon treatment with octanal/toluene, alkyl functionalized MWCNTs were obtained. These alkyl groups contributed to a significant loss in the specific capacitance of the MWCNT that can be attributed to the perfect blockage of protons/ions to access the surface area of CNTs due to extreme hydrophobicity (Fig. 4).

Liu et al. have investigated the influence of electrochemical treatment on the pore size distribution of SWCNT. They treated SWCNTs for 24 h at 1.5 V in an aqueous 6 M KOH solution and observed a specific surface area of 109.4 m^2/g [41]. Lee et al. has made use of fluorinated SWCNT in the fabrication of supercapacitor electrode. They found that even though the specific surface area of both SWCNT

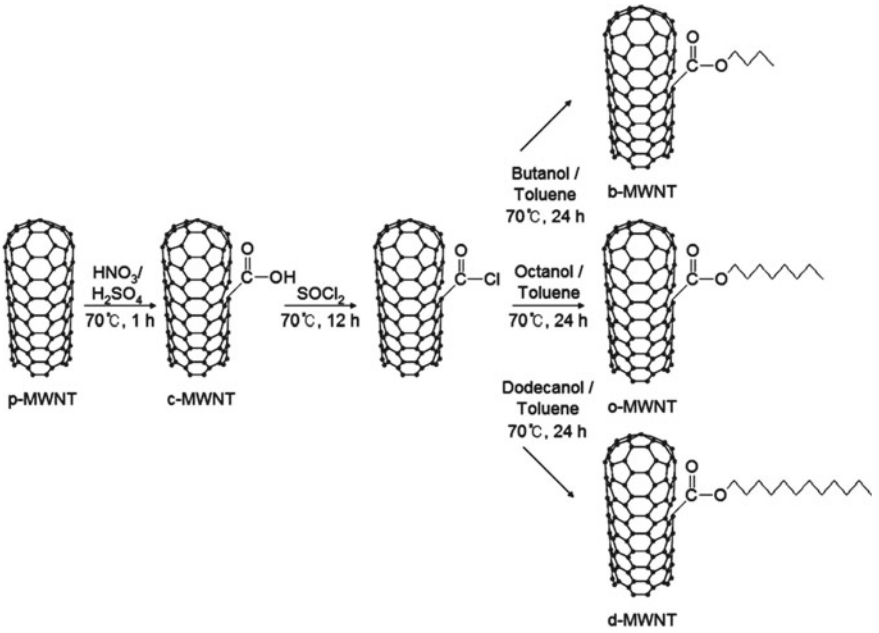

Fig. 4 Pictorial representation of synthetic pathway for the surface functionalization of CNTs. "Adapted with permission from reference [40], Copyright (2005),AIP Publishing"

and fluorinated SWCNT are quite similar, the specific capacitance of the fluorine atom functionalized SWCNT sample is quite lower than that of the bare SWCNT, particularly at a larger current density. However, at low discharge current density, the capacitance is almost similar for both samples. The lower specific capacitance of the fluorinated samples can be ascribed to the fact that micropores possessing small pore diameters are engulfed by fluorine ions and can get obstructed easily, at larger discharge currents. When the electrodes fabricated by fluorinated SWCNT are heated to 900 °C for 30 min under He, the fluorinated samples enviced a larger specific capacitance to those of pristine SWCNT. Here the micropores are assumed to develop due to the removal of fluorine atoms from the sidewalls of the SWCNTs upon heating. Here fluorine is supposed to be removed from the sidewalls of SWCNTs in the form of CF_4, C_2F_4, C_2F_6, and COF_2 forming chemically cut SWCNTs that in turn is expected to contribute to decreasing resistivity of the fluorinated samples to give consistently high specific capacitance than the raw SWCNT samples [42].

CNTs have found a wide range of applications in supercapacitor electrodes, nanocomposites form with activated carbon, graphene, electroactive polymers, and metal oxides to have improved electrochemical performances. Portet et al. [43] have reported an active electrode material composite, composed of a mixture of activated carbon and CNT in organic electrolytes. They evaluated the impact of CNT content on the equivalent series resistance (ESR) of the supercapacitor cell. No significant change was observed in the value of ESR at low content of CNT i.e. 5–10% in the composite. However, for the composite containing 15% and above the amount of CNT, a sharp decrease in the ESR from 0.8 to 0.65 Ω cm^2 has been observed. This reflects the proper equilibrium between the surface area and the porosity which contributes to the enhanced performance of these composite materials.

Physical and chemical activation of polyacrylonitrile or its co-polymers is usually employed for synthesizing activated carbon with superior surface area and porosity. Liu et al. has converted SWCNT/ PAN (polyacrylonitrile dimethylformamide) composite films into SWCNT/activated carbon composite electrode with CO_2 activation at 700 °C for twenty minutes. By investigating their electrochemical properties, they observed a specific capacitance of 380 Fg^{-1} which is significantly more than a specific capacitance of a pure SWCNT bucky paper electrode [44]. They observed that, though the specific capacitance of the heat-treated SWCNT/PAN composite film before the activation was quite similar to that of the bucky paper, the power density of the previous one is much superior to that of the latter.

Vinay Gupta and Norio Miura have reported the synthesis of PANI/SWCNT composite by electropolymerization of polyaniline onto SWCNT. They used the composite as active electrode material in a supercapacitor device using 1 molar H_2SO_4 solution as electrolyte and obtained a specific capacitance of 485 Fg^{-1} having power and energy density of 228 wh/kg and 2250 W/kg respectively having large cyclic stability up to 73 wt% deposits density of PANI onto SWCNT [45] (Fig. 5).

Dong et al. [46], has synthesized polyaniline/MWCNT composite, employing an in-situ chemical oxidative polymerization technique and investigated its electrochemical performances using 1 mol/L $NaNO_3$ solution as electrolytic medium and has obtained a specific capacitance of 328 Fg^{-1} for the as-prepared composite

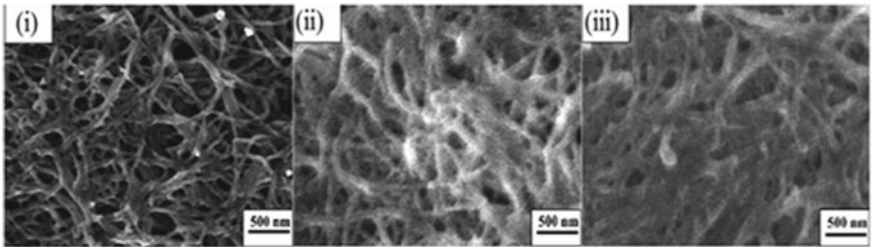

Fig. 5 SEM morphologies of the PANI/SWCNT composites with (i) 50 wt.% PANI; (ii) 70 wt.% PANI; (iii) 85 wt.% PANI. "Adapted with permission from reference [45], Copyright (2006), Elsevier"

whereas a capacitance of 193 Fg^{-1} observed for pure PANI. These results infer that MWCNT has offered an obvious contribution to the improvement of electrochemical properties of the sample by providing additional effectual regions for faradaic reaction and substantial specific surface area as compared to pure PANI. Kay Hyeok An et al. has synthesized a composite of SWCNT and polypyrrole in the weight ratio of 1:1 using 10 mmol of $FeCl_3$ and sodium p-toluenesulfonate as an oxidant for the polymerization of pyrrole. To reduce the internal resistance of the composite, acetylene black was added to the composite during the electrode fabrication. With 15 wt% of acetylene black, the composite because of its uniform covering by polypyrrole on the permeable and conductive support of SWNTs, envices an increased capacitance of 265 Fg^{-1} than pure polypyrrole and pristine SWNT electrodes [47].

Composites of noble metal oxides and CNTs have gained a remarkable interest among the scientific community to utilize it as an active electrode substance in supercapacitor devices. Jong Hyeok Park et al. have evaluated the electrochemical properties of RuO_2-CNT and RuO_2-HNO_3 treated CNT composite. They revealed that the electrostatic charge holding and pseuodofaradaic reaction of RuO_2 nanoparticles are influenced by the surface functionality of CNTs. The hydrophilicity of the surface-functionalized CNT contributes to the easy access of the solvated ions to the electrode/electrolyte interface. This not only magnifies the specific capacitance but also the number of faradaic reaction sites of RuO_2 nanocomposites. They obtained a specific capacitance of 120 Fg^{-1} (13 wt % loading of RuO_2) and 900 Fg^{-1} for RuO_2/hydrophilic CNT nanocomposites that relies on the integrated mass of RuO_2/hydrophilic CNT and the mass of RuO_2 respectively [48]. However, due to disadvantages like high cost, high toxicity, and non-availability of RuO_2 and IrO_2 the commercial utilization of such composites has become next to impossible. For this reason, the scientific community has diverted their interest towards the utilization of low-priced d-block metal oxides like nickel oxide, vanadium oxide (V_2O_5), and manganese oxide (MnO_2), to synthesize nanocomposite with CNTs to fabricate supercapacitor electrodes with superior electrochemical properties.

Vanadium oxide, owing to its non-poisonous, easy availability and high theoretical capacitance (590 mAh/g) has been extensively analyzed as an active electrode

substance for supercapacitor devices [49]. Various composites of V_2O_5 with carbonaceous substance and metal fibers have been synthesized to boost up its electrochemical performances. Reddy and Reddy [50] have synthesized nano-porous V_2O_5 by employing a sol–gel technique and observed a specific capacitance of 214 Fg^1 at a scan rate of 50 mVS^{-1} in two molar KCl solution and observed that its specific capacitance decreases rapidly after 100 cycles. It was reported that V_2O_5 possesses a limited electrical conductivity of 10^{-6}~10^{-7} S/cm) [51]. For this reason, electrodes of composites containing V_2O_5 with materials having high electrical conductivity have attracted lots of attention for pseudocapacitor applications. kim et al. [52] have synthesized thin films of $V_2O_5.xH_2O$ on a CNT film substrate by electrodeposition from an aqueous $VOSO_4$ solution and investigated their electrochemical performances in $LiClO_4$ in propylene carbonate. They observed a specific Li-ion capacitance of 910 Fg^{-1} from the as-prepared $V_2O_5.xH_2O$/CNT film electrode. The specific capacitance for the $V_2O_5.xH_2O$/CNT film electrode was 540 mAh/g at a current density of 10 Ag^{-1}. Based on the efficient semi-conductivity and redox properties of SnO_2, M. Jayalakshmi et. al has synthesized a nano-scale SnO_2-V_2O_5 mixed-oxide by employing a hydrothermal method. Carbon nanotubes and the oxides (both simple and mixed) were mixed thoroughly in the mole ratio of 1:10. After the evaluation of capacitive behavior of V_2O_5, V_2O_5—CNT, and SnO_2-V_2O_5-CNT electrodes using 0.1 M KCl solutions through CV analysis at a scan rate of 100 mV/s, they noticed that the electrode fabricated from SnO_2-V_2O_5-CNT composites has the highest specific capacitance [53].

Sofiane et al. has deposited vanadium oxide coating of different thicknesses on the internal surface of permeable CNT electrodes utilizing Atomic layer deposition through cyclic voltammetry technique and evaluated the effect of thickness of vanadium oxide coating on the electrochemical properties of the composite. They observed that vanadium-coated oxygenated CNT electrodes exhibit superb retention of capacitance at higher current density or scan rates and lowering the extent of thickness up to ~10 nm allows one to attain a magnified specific capacitance of about ~1550 Fg^{-1} at a current density of 1 Ag^{-1}. Their result indicates that the performances of electrodes are largely influenced by the uniformity and precise control over the conformity and thickness of the oxide coatings [54]. Manganese oxides, due to their cost effectiveness, moderate specific capacitance, and environmental compatibility too have emerged as one of the prominent candidates in this field. Electrodes with a high specific capacitance of composites containing manganese oxide, especially with a tiny load of manganese oxide disseminate uniformly over conductive and carbonaceous material with superior surface area have been widely studied. Ma et al. [55] has uniformly coated Birnessite type manganese oxide over CNT through a spontaneous redox reaction between CNT and $KMnO_4$. An initial specific capacitance of 250 Fg^{-1} was obtained at a current density of 1 Ag^{-1} and this is almost equal to 139 $mAhg^{-1}$, which directly depends on the entire weight of the electrode substance viz, (i) the electroactive substance (ii) the binder and (iii) the conducting medium. The specific capacitance of Manganese dioxide in the nanocomposite of MnO_2/CNT is 580 Fg^{-1} and is equivalent to 320 mA/g of MnO_2. The electrochemical properties of MnO_2 on the CNT can be ascribed to the

nanometre scale coating of MnO_2 on the CNT, the high interfacial area between the MnO_2 and electrolytic solution and the intertwined pores in the structure of CNTs. They also observed that the specific capacitance of the composite is also influenced by the pH of the beginning solution. Luman Zhang et al. have synthesized Flexible CNT-MnO_2 fiber composite by spontaneous deposition of MnO_2 on CNT fiber through direct redox reaction between an aqueous solution of $KMnO_4$ and CNTs to obtain a wire-shaped supercapacitor by fabricating two aligned CNT-MnO_2 fibers. The composite fiber showed hydrophilic nature that largely influenced the electrochemical properties of the fabricated supercapacitor with an enhanced specific capacitance of 231 Fg^{-1} in Na_2SO_4 electrolyte. In addition to that, they even synthesized a wire-shaped symmetric supercapacitor containing CNT-MnO_2 fiber electrodes and PVA/H_3PO_4 electrolyte with a magnified length specific capacitance of 621.8 uF/cm having high energy density and cycling stability over 1200 cycles. They observed that the fragility of the prepared composite depends upon the increasing concentration of $KMnO_4$ solution and the time of the reaction. This is due to the crumbled structure of CNT after being exposed to $KMnO_4$ solution [56]. Guo et al. have synthesized an electrode material that resembled the shape of a capacitor and a battery-type electrode material of CNTs@DNAMnO_2. They observed that the hydrophilic sugar-phosphate backbone of DNA enhances the dispersion of CNTs in water. In the CNT@DNAMnO_2 composite, the phosphate group on the DNA in the CNTs@DNA ideally holds the MnO_2. They perceived that CNTs@DNA bridges MnO_2 spheres to have a permeable structure of CNTs@DNAMnO_2 composite and for that reason the electrodes exhibit an energy density of 11.6 $Whkg^{-1}$ at a power density of 185.5 Wkg^{-1} with 4.2 mg cm^{-2}. mass loading of MnO_2 [57].

Nickel hydroxide is extensively used in various energy sources like alkaline rechargeable batteries, portable electronics, and electric vehicles. Numerous investigations regarding its use as active electrode material in supercapacitors have been reported. Crystalline β-$Ni(OH)_2$ have been extensively employed as supercapacitor electrodes because of their excessive staking density and stability in contrast to α-$Ni(OH)_2$. Sivalingam Ramesh et al. have synthesized a nanostructured composite that consists of MWCNT doped with a nitrogen atom and nickel hydroxide and evaluated its utilization in supercapacitors. They observed that the composites have specific capacitances of 350, 282, 240, 210, 160, and 140 Fg^{-1} at the current densities of 0.5, 1, 1.5, 2, 3, 4, and 5 A/g respectively and 90% of capacitance is retained even after five thousand cycles at a current density of 0.5 A/g. The composite also revealed an energy density of 43.75 wh/kg with a power density of 1500 w/kg at 0.5 A/g [58] (Fig. 6).

Multilayered composite papers combined with CNTs and nickel oxide were synthesized via a simple hydrothermal method by Lai et al. [59]. They first treated the CNTs with a mixture of sulphuric acid and nitric acid solution to create active sites on their surface to decorate the NiO materials. The fabrication of multilayer composite was carried out through layer by layer fabricating mode. Here, the composite paper utilizes the conductive network of CNTs as a holding framework as well as conduction route for the electrons whereas the NiO provides high pseudo-specific capacitance by the redox reaction. They have employed the synthesized multilayered CNTs/NiO

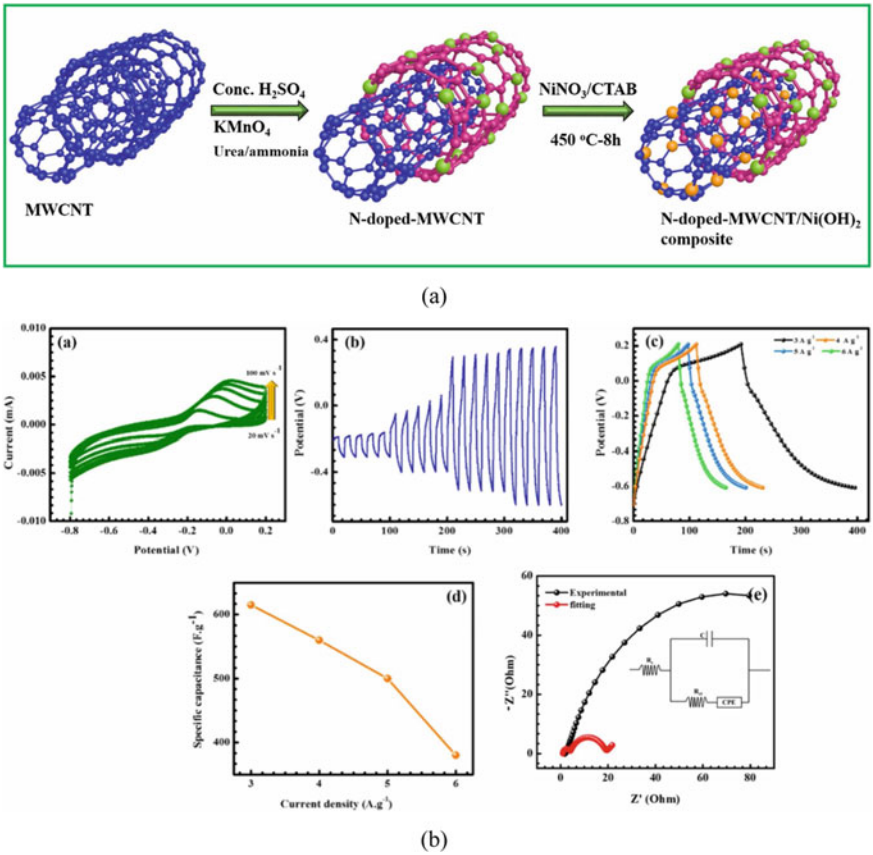

Fig. 6 (**a**) Pictorial representation of the route for the preparation of Ni $(OH)_2$@N-MWCNT hybrid composite. (**b**) (i) Cyclic voltammetry curves at various scan rates. (ii) Current versus time curve. (iii) Galvanostatic charge–discharge curve at different current densities. (iv) Graphical representation of impact current densities on the specific capacitance. (v) Nyquist impedance spectrum of $Ni(OH)_2$ @N-MWCNT. "Adapted with permission [58], Copyright the Authors, some right reserved, Exclusive License [Scientific reports] Distributed under a Creative Commons Attribution License 4.0 (CC BY)"

composite as the anode and an activated carbon/CNTs composite as the cathode in an asymmetric supercapacitor with a 6 molar potassium hydroxide solution. The capacitor had a high specific capacitance of 713.9 Fg^{-1} at a scan rate of 200 mV/s having power and energy densities of 698.6 w/kg and 23.9 wh/kg respectively with excellent cycling stability of 88% retention after 3000 cycles. Wang et al. have synthesized a novel composite of highly conductive nickel cobalt oxide and single-walled CNTs with –COOH functional group ($NiCo_2O_4$-SWCNT composite). The composite showed a specific capacitance of 1642 Fg^{-1} with the retention of the capacitance of about 94.1% after 2000 cycles [60]. Kumar et al. have prepared a nanocomposite of Co_3O_4 and CNTs (Co_3O_4/CNT) and used it in the fabrication of a supercapacitor

electrode material through the electrophoretic deposition method (binder-free electrode deposition). Upon investigation of electrochemical properties of composite in an aqueous electrolyte-based system with 1 M potassium hydroxide solution, they observed that when the concentration of precursor is taken as 2 mmol the composite envice a specific capacitance of 705 Fg^{-1} at a current density of 3 A/g [61].

Recently, graphene, based on its interesting belongings like high electrical conductivity, mechanical strength, high specific surface area (2630 m^2/g), and excellent theoretical specific capacitance (550 Fg^{-1}), has been able to find a wide range of its application in various energy storage devices. Graphene also possesses some drawbacks to be used directly as active electrode materials in any energy storage devices. It generally tends to form irreversible clusters by the reason of π–π and vanderwaal's interconnection within its adjacent layers that contributes highly to decrease its surface area and obstructs its possibility for doable implementation. To overcome this hurdle different approaches like the introduction of MnO_2 and RuO_2 onto the plane of graphene sheets, functionalization of graphene sheets with various hydrophilic groups, and incorporation of SWCNT and MWCNT as splitters between sheets of the graphene layers have been extensively studied by the scientific community. Among the above-mentioned techniques, the utilization of CNTs between the sheets of graphene layers has been widely accepted as the most suitable, low cost and environmentally benign approach. Cheng et al. have synthesized a composite film, containing graphene and SWCNT and observed a specific capacitance of 290.6 Fg^{-1} and 201.0 Fg^{-1} for aqueous and organic electrolytes, respectively [62]. Moreover, they observed an increased energy density of 23% with the introduction of SWCNT to graphene powder and a 31% increase in the value of power density. Imran Shakir has put forward an approach of constructing thin film of high-density flexible electrodes for supercapacitor using layer by layer framework of MWCNT and graphene sheets to prevent the agglomeration between each graphene layer. They observed that the as-prepared layer by layer assembled electrode envised a magnified electrochemical capacitance of 390 Fg^{-1} and showed superior cycling stability of about 97% retention even after 25,000 charge–discharge cycles [63] (Fig. 7).

Borthakur et al. have prepared a nanocomposite of carboxylic acid-functionalized MWCNTs and reduced graphene oxide sheets and utilized them as active electrode materials in supercapacitors with enhanced electrochemical properties. First, pristine MWCNT were functionalized with a carboxylic acid group using concentrated H_2SO_4 and HNO_3 in the ratio 3:1. The final composite was prepared by the reduction of graphene oxide powder employing an in-situ method in the presence of MWCNTs that were functionalised with carboxylic acid group and hydrazine hydrate. They reported a high specific capacitance of 302 Fg^{-1} with energy and power density of 41.65 wh/kg and 496.49 w/kg respectively [64].

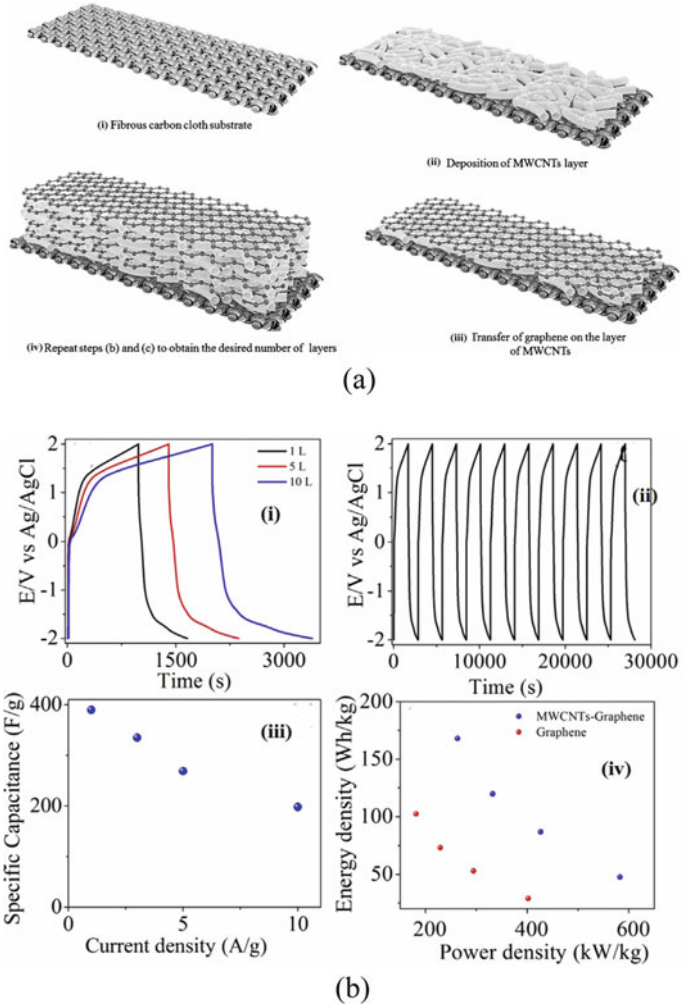

Fig. 7 (**a**) Pictorial demonstration of the route for the synthesis of the layer by layer (LBL) framework of MWCNTs and graphene on fibrous carbon cloth substrate in order to utilize it in a flexible supercapacitor. (**b**) (i) Galvanostatic charge–discharge plot of layer by layer assembled electrode with one, five, and upto ten layers of MWCNTs and graphene at a current density of 1 Ag^{-1}, (ii) typical charge–discharge plot for layer by layer assembled electrode with ten layers of MWCNTs and graphene sheets with a current density of 1 Ag^{-1}, (iii) variation of specific capacitance layer by layer assembled electrode with ten layers of MWCNTs and graphene as a function of different current densities, (iv) Ragone plot of layer by layer assembled electrode upto ten layers of MWCNTs and graphene obtained from the discharge curves studied at various constant current densities. "Adapted with permission from reference [63], Copyright (2014) Elsevier"

4.2 CNTs in Alkali Metal Ion Batteries

CNTs, based on their advantageous belongings like superior electrical conductivity, mechanical robustness, and structural properties enviced excellent performance as positive electrode materials and as negative electrode additives for alkali metal ion batteries. CNT has earned enormous interest among the scientific community as an electrode substance in batteries. Recently, various modifications in the CNTs have been reported regarding its use as a favorable electrode material concerning alkali metal ion intercalations, adsorption, and diffusion. In Li^+ ion Batteries, lithium ions are stored following two pathways (i) through intercalation and (ii) alloying. The effective loading of Li^+ ion directly depends on the surface morphologies of CNTs, especially on its voids (defects) and diameters [65].

Defects (i.e. n rings) in CNTs are seen to occur naturally or via acid treatment. To investigate detailed energetic adsorption of Li^+ ion on the defective sidewalls of CNTs theoretical studies like density functional theory (DFT), total-energy calculations using local-density approximation (LDA) and the generalized-gradient approximation (GGA) were performed [66]. It was observed that the effective diffusion of lithium ions into the inside CNTs is promoted by the existence of voids on the sidewalls of the CNTs that result in the reduction of the diffusion path length. It has also been reported that the end cap opening of CNTs can also contribute to the effective penetration of Li^+ through the ends of the open end. From theoretical studies, Kumar et al. [67] has reported that there exists a capacitance difference of almost 120 $mAhg^{-1}$ between opened and closed carbon nanotubes. For effective ionic motion and to free intercalation/de-intercalation of Li^+ ions, the size of CNTs must be small. Wang et al. have reported that the capacity of short (300 nm) CNTs is much higher than that of longer CNTs with length in micrometer [68]. Since the last 20 years both SWCNT and MWCNTs have found extensive use in lithium-ion batteries either as anode materials or as a conductive additive in the composite electrode. As compared to conventional graphitic carbons, CNTs have a higher potential to store a larger amount of lithium ions depending on their structure, morphology, and defect concentrations. Scientists have established effective utilization of both SWCNT and MWCNT for the intercalation of lithium-ion in batteries with a maximum specific capacitance of around 8500 $mAhg^{-1}$ for multi-walled CNTs at a decreased current rate of 0.1 mA cm^{-2} [69]. Seung woo lee et al. has synthesized a different class of electrode for lithium storage using carboxylated and $–NH_2$ functionalized MWCNT by employing a layer by layer (LBL) assembling technique. They observed that the as-prepared additive-free LBL assembled MWCNT electrode reveals high gravimetric energy of 200 Wh $kg_{electrode}{}^{-1}$ with gravimetric power of ~100 kW $kg_{electrode}{}^{-1}$ [70]. Li et al. has prepared nitrogen-doped carbon nanotubes and utilized them as cathode material for lithium-air batteries. They observed that the newly fabricated cathode material has shown a specific discharge capacity of 866 $mAhg^{-1}$ [71]. Hemalatha et al. have used TiO_2 to uniformly coat over CNTs surface and utilized this TiO_2 coated CNTs in lithium storage. The composite electrode enviced a specific capacity of 470 $mAhg^{-1}$ [72]. Keeping given recent trends

of excessive usage of Lithium-ion batteries in most of the power devices, recently researchers have diverted the attention towards the use of an appropriate alternative to overcome the storage of Li sources. Among all the potential candidates Na^+ ions have been able to seek much importance to be utilized as one of the most prominent elements replacing Li^+ ions due to its high easy availability, low price, and environmental benign characteristics. In this aspect, Yan et al. have proposed a composite of carboxylated based organic, sodium trimesic (Na_3TM) with three-dimensional conductive networks of CNTs to be utilized as an anode material. They observed that the composite material enviced a reversible capacity of 214.6 $mAhg^{-1}$ at 0.1 Ag^{-1} having superb rate capability with specific capacitance 149 $mAhg^{-1}$ and 87.5 $mAhg^{-1}$ at 1 and 10 Ag^{-1} [73].

4.3 CNTs in Fuel Cells

Generally in a fuel cell, electrical energy is obtained directly from chemical energy with superior energy transformation efficiency and low emissions. Generally, Pt is used as a catalyst in fuel cells. Although it has good catalytic efficiency, due to its high-cost commercial viability is a major concern. Various materials like carbon black, graphene, CNTs, etc. have been used as catalyst support in fuel cells to reduce the use of platinum catalysts. Jha et al. [74] used functionalized SWCNTs as catalyst support in proton exchange membrane fuel cell (PEMFC) and found that the Pt loading may be reduced to 0.06 mg Pt/m^2. Grish Kumar et al. [75]. has reported that CNT is a better Pt catalyst support in fuel cells than carbon black. CNTs are also used as support in fuel cells for Pt-Ru alloy catalysts [76–78]. MWCNTs have been used as support to synthesize Pt/MWCNTs, PtNi/MWCNTs, PtRu/MWCNTs, PtRuNi/MWCNTs, etc., catalysts to be used in fuel cells with better electrocatalytic activity [79].

Many attempts have been made to use cheaper alternatives of Pt catalysts and in this regard, CNTs play a pivotal role. Sheng et al. [80] found that MWCNT supported Cu/Cu_xO catalysts have higher activity than Pt nanoparticles. Wang et al. [81] used polyelectrolyte functionalized CNTs as a catalyst that is free of any metal ion for oxidation–reduction reactions and has found a similar catalytic property to that of Pt catalyst in a fuel cell. Reddy et al. [82] have reported the use of cobalt-polypyrrole-MWCNT catalysts for hydrogen and alcohol fuel cells. Matsumoto et al. [83] have reported the use of CNTs supported Mo_2C catalyst as anode material in fuel cells and they found that it has a higher overvoltage than Pt-based electrode. Composite of MWCNT and SnO_2 has been used as anode for microbial fuel cells with large maximum power density. Ru decorated Pt nanoparticles on nitrogen-doped MWCNT have been used in methanol fuel cells with high performance and dispersion [84].

5 Conclusion

For the last 20 years, CNTs have been explored as one of the most ideal electroactive materials for energy storage devices. CNTs possess superior electrical conductivity, lightweight, excessive physical robustness than conventional materials like carbon black, activated carbon, and other carbon-based materials. However, direct utilization of CNTs in electrodes is not always feasible enough to meet the desired electrochemical performances like high power and energy densities of the fabricated devices. For this reason, CNTs are assembled to their composites with other compounds with varying configurations to fabricate new generation electrochemical devices. It has been observed that modification in the structure of CNTs like defect creation, atom dopping, and managing pore size distribution plays a key role in manufacturing binder-free electrodes. CNTs can be directly grown on current collectors that offer effective networks for short electron transport pathways and eliminate the need for binder and conductive additives for electrode fabrication. Electrodes with CNT and their composite with nanostructured composites of oxides, polymers, and other carbon-based materials exploit the benefits of high surface area and excellent conductivity. This in turn imparts high stability, better ion transport, enhanced specific capacitance, and acceptable high rate capability. Relying on its excellent mechanical strength, CNTs have now been accepted as the most strong contender to be employed as the active electrode substance for next-generation wearable and flexible energy storage appliances.

References

1. V.N. Popov, Carbon nanotubes: properties and applications. Mater. Sci. Eng. R **431**, 61–102 (2004)
2. S. Lijima, Helical microtubules of graphitic carbon. Nature **354**, 56–58 (1991)
3. S. Lijima, P.M. Ajayan, T. Ichihashi, Growth model for carbon nanotubes. Phys. Rev. Lett. **69**(21), 3100–3103 (1992)
4. S. Lijima, T. Ichihashi, Single-shell carbon nanotubes of 1nm diameter. Nature **363**, 603–605 (1993)
5. B.I. Yakobson, R.E. Smalley, Fullerene nanotubes, $C_{1,000,000}$ and beyond. Am. Sci. **85**, 324–337 (1997)
6. C. Du, N. Pan, Nanotechnol. Law Bus. **4**, 569–576 (2007)
7. Y. Zhang, B.R. Bunes, N. Wu, A. Ansari, S. Rajabali, L. Zang, Sensing methamphetamine with chemiresistive sensors based on polythiophene blended single-walled carbon nanotubes. Sens. Actuators, B Chem. **255**, 1814–1818 (2018)
8. L.R. Shobin, S. Manivannan, Silver nanowires-single walled carbon nanotubes heterostructure chemiresistors. Sens. Actuators, B Chem. **256**, 7–17 (2018)
9. R.B. Rakhi, K. Sethupathi, S. Ramaprabhu, Electron field emission properties of conducting polymer coated multi walled carbon nanotubes. Appl. Surf. Sci. **254**(21), 6770–6774 (2008)
10. S. Saito, Carbon nanotubes for next-generation electronics devices. Science **278**(5335), 77 (1997)
11. H. Pan, J. Li, Y. Feng, Carbon nanotubes for supercapacitor. Nanoscale, Res. Lett. **5**, 654–668 (2010)

12. E. Akbari, Z. Buntat, Benefits of using carbon nanotubes in fuel cells. Int. J. Energy Res. **41**(1), 92–102 (2014)
13. B.J. Landi, M.J. Ganter, C.D. Cress, R.A. DiLeo, R.P. Raffaelle, Carbon nanotubes for lithium ion batteries. Energy Environ. Sci. **2**(6), 638–654 (2009)
14. R. Saito, M. Fujita, G. Dresselhaus, M.S. Dresselhaus, Electronic structure of chiral graphene tubules. Appl. Phys. Lett. **60**, 2204–2206 (1992)
15. T.W. Odom, J. Huang, P. Kim, C.M. Lieber, Atomic structure and electronic properties of single-walled carbon nanotubes. Nature **391**, 62–64 (1998)
16. P.M. Ajayan, Nanotubes from carbon. Chem. Rev. **99**, 1787–1799 (1999)
17. B. Wu, D. Geng, Y. Liu, Evaluation of metallic and semiconducting single-walled carbon nanotube characteristics. Nanoscal **3**, 2074–2085 (2011)
18. J. Hone, B. Batlogg, Z. Benes, A.T. Johnson, J.E. Fischer, Quantized photon spectrum of single-wall carbon nanotubes. Science **289**(5485), 1730 (2000)
19. R. Kötz, M. Carlen, Principles and applications of electrochemical capacitors. Electrochim. Acta **45**(15–16), 2483–2498 (2000)
20. Y. Soneda, Carbons for supercapacitors, in *Handbook of Advance Ceramics* (Second Edition) (Elsevier, 2013), pp. 211–222
21. Y. Shao, M.F. El-Kady, L.J. Wang, Q. Zhang, Y. Li, H. Wang, M.F. Mousavi, R.B. Kaner, Graphene-based materials for flexible supercapacitors. Chem. Soc. Rev. **44**, 3639–3665 (2015)
22. K. Jost, G. Dion, Y. Gogotsi, Textile energy storage in perspective. J. Mater. Chem. A **2**, 10776–10787 (2014)
23. C.C. Hu, K.H. Chang, M.C. Lin, Y.T. Wu, Design and tailoring of the nanotubular arrayed architecture of hydrous RuO_2 for next generation supercapacitors. Nano Lett. **6**, 2690–2695 (2006)
24. A. Burke, Ultracapacitors: why, how, and where is the technology. J. Power Sources **91**(1), 37–50 (2000)
25. Y. Zhou, P. Jin, Y. Zhou, Y. Zhu, High performance symmetric supercapacitors based on carbon nanotube/graphite nanofiber nanocomposites. J. Sci. Rep. **8**, 9005 (2018)
26. S. Zhu, L. Li, J. Liu, H. Wang, T. Wang, Y. Zhang, L. Zhang, R.S. Ruoff, F. Dong, Structural directed growth of ultrathin parallel birnessite on β-MnO_2 for high-performance asymmetric supercapacitors. ACS Nano **12**, 33–42 (2018)
27. D. Kalpana, K.S. Omkumar, S.S. Kumar, N.G. Renganathan, A novel high power symmetric ZnO/carbon aerogel composite electrode for electrochemical supercapacitor. Electrochimca. Acta **52**, 1309–1315 (2006)
28. M. Min, K. Machida, J.H. Jang, K. Naoi, Hydrous RuO/carbon black nanocomposites with 3D porous structure by novel incipient wetness method for supercapacitors. J. Electrochem. Soc. **153**, A334–A338 (2006)
29. J.M. Miller, B. Dunn, Morphology and electrochemistry of ruthenium/carbon aerogel nanostructures. Langmuir **15**, 799–806 (1999)
30. P.J. Mahon, G.L. Paul, S.M. Keshishian, A.M. Vassallo, Measurement and modelling of the high-power performance of carbon-based supercapacitors. J. Power Sources **91**, 68–76 (2000)
31. B.E. Conway, *Electrochemical Supercapacitor, Scientific Fundamentals and Technologicals Applications* (Kluwer Academic/Plenum Publishers, New York, 1999)
32. C. Niu, E.K. Sichel, R. Hoch, D. Moy, H. Tennent, High power electrochemical capacitors based on carbon nanotube, electrodes. Appl. Phys. Lett **70**, 1480–1482 (1997)
33. K.H. An, W.S. Kim, Y.S. Park, J.M. Moon, D.J. Bae, S.C. Lim, Y.S. Lee, Y.H. Lee, Electrochemical properties of high-power supercapacitors using single-walled carbon nanotube electrodes. Adv. Funct. Mater **11**(5), 387–392 (2001)
34. E. Frackowiak, F. Beguin, Carbon materials for the electrochemical storage of energy in capacitors. Carbon **39**, 937–950 (2001)
35. D. Zilli, P.R. Bonelli, A.L. Cukierman, Effect of alignment on adsorption characteristics of self-oriented multi-walled carbon nanotube arrays. Nanotechnology **17**(20), 5136–5141 (2006)
36. S. Huang, L. Dai, Plasma etching for purification and controlled opening of aligned carbon nanotubes. J. Phys. Chem. B **106**, 3543–3545 (2002)

37. E. Frackowiak, F. Béguin, Electrochemical storage of energy in carbon nanotubes, and nanostructured carbons. Carbon **40**(10), 1775–1787 (2002)
38. Q.L. Chen, K.H. Xue, W. Shen, F.F. Tao, S.Y. Yin, W. Xu, Fabrication and electrochemical properties of carbon nanotube array electrode for supercapacitors. Electrochim. Acta **49**(24), 4157–4161 (2004)
39. W. Lu, L. Qu, K. Henry, L. Dai, High performance electrochemical capacitors from aligned carbon nanotube electrodes and ionic liquid electrolytes. J. Power Sources **189**(2), 1270–1277 (2009)
40. Y.T. Kim, Y. Ito, K. Tadai, T. Mitani, U. Kim, H.S. Kim, B.W. Cho, Drastic change of electric double layer capacitance by surface functionalization of carbon nanotubes. Appl. Phys. Lett. **87**, 234106-1–234106-3 (2005)
41. C.G. Liu, H.T. Fang, F. Li, M. Liu, H.M. Cheng, Single-walled carbon nanotubes modified by electrochemical treatment for application in electrochemical capacitors. J. Power Sources **160**, 758–761 (2006)
42. Y.J. Lee, K.H. An, J.K. Heo, Y.H. Lee, Fabrication of supercapacitor electrodes using fluorinated single-walled carbon nanotubes. J. Phys. Chem. B **107**, 8812–8815 (2003)
43. C. Portet, P.L. Taberna, P. Simon, E. Flahaut, Influence of carbon nanotubes addition on carbon–carbon supercapacitor performances in organic electrolyte. J. Power Sources **139**, 371–378 (2005)
44. T. Liu, T.V. Sreekumar, S. Kumar, R.H. Hauge, R.E. Smalley, SWNT/PAN composite film-based supercapacitors. Carbon **41**, 2427–2451 (2003)
45. V. Gupta, N. Miura, Polyaniline/single-wall carbon nanotube (PANI/SWCNT) composites for high performance supercapacitors. Electrochim. Acta **52**, 1721–1726 (2006)
46. B. Dong, B.L. He, C.L. Xu, H.L. Li, Preparation and electrochemical characterization of polyaniline/multi-walled carbon nanotubes composites for supercapacitor. Mater. Sci. Eng., B **143**, 7–13 (2007)
47. K.H. An, K.K. Jeon, J.K. Heo, S.C Lim, D.J. Bae, Y.J. Lee, High-capacitance supercapacitor using a nanocomposite electrode of single-walled carbon nanotube and polypyrrole. J. Electrochem. Soc. **149**(8), A1058–A1062 (2002)
48. J.H. Park, J.M. Ko, O.O. Park, Carbon nanotube/RuO_2 nanocomposite electrodes for supercapacitors. J. Electrochem. Soc. **150**(7), A864–A867 (2003)
49. D.B. Le, S. Passerini, J. Guo, J. Ressler, B.B. Owens, W.H. Smyrl, High surface area V_2O_5 aerogel intercalation electrodes. J. Electrochem. Soc. **143**(7), 2099–2104 (1996)
50. R.N. Reddy, R.G. Reddy, Porous structured vanadium oxide electrode material for electrochemical capacitors. J. Power Sources **156**, 700–704 (2006)
51. M. Benmoussa, E. Ibnouelghazi, A. Bennouna, E.L. Ameziane, Structural, electrical and optical properties of sputtered vanadium pentoxide thin films. Thin Solid Films **265**(1–2), 22–28 (1995)
52. I.H. Kim, J.H. Kim, B.W. Cho, Y.H. Lee, K.B. Kim, Synthesis and electrochemical characterization of vanadium oxide on carbon nanotube film substrate for pseudocapacitor applications. J. Electrochem. Soc. **153**(6), A989–A996 (2006)
53. M. Jayalakshmi, M.M. Rao, N. Venugopal, K.B. Kim, Hydrothermal synthesis of SnO_2–V_2O_5 mixed oxide and electrochemical screening of carbon nano-tubes (CNT), V_2O_5, V_2O_5–CNT, and SnO_2–V_2O_5–CNT electrodes for supercapacitor applications. J. Power Sources **166**, 578–583 (2007)
54. S. Boukhalfa, K. Evanoff, G. Yushin, Atomic layer deposition of vanadium oxide on carbon nanotubes for high-power supercapacitor electrodes. Energy Environ. Sci. **5**, 6872–6879 (2012)
55. S.B. Ma, K.W. Nam, W.S. Yoon, X.Q. Yang, K.Y. Ahn, K.H. Oh, K.B. Kima, Electrochemical properties of manganese oxide coated onto carbon nanotubes for energy-storage applications. J. Power Sources **178**, 483–489 (2008)
56. L. Zhang, X. Zhang, J. Wang, D. Seveno, J. Fransaer, J.P. Locquet, J.W. Seo, Carbon nanotube fibers decorated with MnO_2 for wire-shaped supercapacitor. Molecule **26**(3479), 1–19 (2021)
57. C.X. Guo, A.A. Chitre, X. Lu, DNA-assisted assembly of carbon nanotubes and MnO_2 nanospheres as electrode for high-performance asymmetricsupercapacitors. Phys. Chem. Chem. Phys **16**, 4672–4678 (2014)

58. S. Ramesh, K. Karuppasamy, H.M. Yadav, J.J. Lee, H.S. Kim, H.S. Kim, J.H. Kim, $Ni(OH)_2$-decorated nitrogen doped MWCNT nanosheets as an efficient electrode for high- performance supercapacitors. J. Sci. Rep. **9**, 6034 (2019)
59. Y.H. Lai, S. Gupta, C.H Hsiao, C.Y. Lee, N.H. Tai, Multilayered nickel oxide/carbon nanotube composite paper electrodes for asymmetric supercapacitors, J. Electrochimica Acta **354**, 136744 (2020)
60. X. Wang, X. Han, M. Lim, N. Singh, C.L. Gan, M. Jan, P.S. Lee, Nickel cobalt oxide-single wall carbon nanotube composite material for superior cycling stability and high-performance supercapacitor application. J. Phys. Chem. C **116**, 12448–12454 (2012)
61. N. Kumar, Y.C. Yu, Y.H. Lu, T.Y. Tseng, Fabrication of carbon nanotube/cobalt oxide nanocomposites via electrophoretic deposition for supercapacitor electrodes, Springer. J. Mater. Sci. **51**, 2320–2329 (2016)
62. Q. Cheng, J. Tang, J. Ma, H. Zhang, N. Shinya, L. Qinc, Graphene and carbon nanotube composite electrodes for supercapacitors with ultra-high energy density. J. Phys. Chem Phys **13**, 17615–17624 (2011)
63. I. Shakir, High energy density based flexible electrochemical supercapacitors from layer by layer assemble multiwalled carbon nanotubes and graphene. J. Electrochem. Acta **124**, 13 (2014)
64. P. Saikia, K. Dutta, A.K. Guha, S.K. Dolui, P. Barman, L.J. Borthakur, High-performance aqueous electrolyte based supercapacitor of carboxylic acid functionalized carbon-nanotubes and graphene nano composite. J. Mater. Chem. Phys. **258**, 123786 (2021)
65. C. de las Casas, W. Li, A review of application of carbon nanotubes for lithium ion battery anode material. J. Power Sources **208**, 74–85 (2012)
66. K. Nishidate, M. Hasegawa, Energetics of lithium ion adsorption on defective carbon nanotubes. Phys. Rev. B **71**(24), 245418 (2005)
67. T.P. Kumar, R. Ramesh, Y.Y. Lin, G.T. Fey, Tin-filled carbon nanotubes as insertion anode materials for lithium ion batteries. Electrochem. Commun. **6**(6), 520–525 (2004)
68. X.X. Wang, J.N. Wang, L.F. Su, Preparation and electrochemical performance of ultra-short carbon nanotubes. J. Power Sources **186**(1), 194–200 (2009)
69. R. Carter, L. Oakes, A.P. Cohn, J. Holzgrafe, H.F. Zarick, S. Chatterjee, R. Bardhan, C.L. Pint, Solution assembled single-walled carbon nanotube foams: superior performance in supercapacitors, lithium-ion, and lithium-air batteries. J. Phys. Chem. C **118**(35), 20137–20151 (2014)
70. S.W. Lee, N.Y. Betar, M. Gallant, S. Chen, B.S. Kim, P.T. Hammond, Y. Shao-Horn, High-power lithium batteries from functionalized carbon-nanotube electrodes. Nat. Nanotechnol. **5**, 531–537 (2010)
71. Y. Li, J. Wang, X. Li, J. Liu, D. Geng, J.Y.R. Li, X. Sun, Nitrogen-doped carbon nanotubes as cathode for lithium–air batteries. Electrochem. Commun. **13**, 668–672 (2011)
72. K. Hemalatha, A.S. Prakash, K. Guruprakash, M. Jayakumar, TiO_2 coated carbon nanotubes for electrochemical energy storage. J. Mater. Chem. A **2**, 1757–1766 (2014)
73. X. Yan, H. Ye, X.L. Wu, Y.P. Zhen, F. Wan, M. Liu, X.H. Zhang, J.P. Zhang, Y.G. Guo, Three-dimensional carbon-nanotube networks enhanced sodium trimesic: a new anode material for sodium ion batteries and Na-storage mechanism revealed by ex-situ studies. J. Mater. Chem. A 1–3 (2013)
74. N. Jha, P. Ramesh, E. Bekyarova, X. Tian, F. Wang, M.E. Itkis, R.C. Haddon, Fuctionalized single-walled carbon nanotubes-based fuel cell benchmarked against US DOE 2017 technical targets. J. Sci. Rep. **3**, 2257 (2013)
75. G. Girishkumar, M. Rettker, R. Underhile, D. Binz, K. Vinodgopal, P. McGinn, P. Kamat, Single-wall-carbon nanotube-based proton exchange membrane assembly for hydrogen fuel cells. Langmuir **21**(18), 8487–8494 (2005)
76. N. Jha, A.L.M. Reddy, M.M. Shaijumon, N. Rajalakshmi, S. Ramaprabhu, Pt-Ru/multi-walled carbon nanotubes as electrocatalysts for direct methanol fuel cell. J. Hydrogen Energy **33**(1), 427–433 (2008)

77. L. Li, Y.C. Xing, Pt-Ru nanoparticles supported on carbon nanotubes as methanol fuel cell catalysts. J. Phys. Chem. C **111**(6), 2803–2808 (2007)
78. H. Wang, X. Wang, J. Zheng, F. Peng, H. Yu, Enhanced activity and durability of nanosized Pt-SnO2/IrO2/CNTs catalyst for methanol electro-oxidation. J. Nanosci. Nanotechnol. **15**(5), 3662–3669 (2015)
79. Y. Zhao, L. Fan, J. Ren, B. Hong, Electrodeposition of Pt–Ru and Pt–Ru–Ni nanoclusters on multi-walled carbon nanotubes for direct methanol fuel cell. Int. J. Hydrogen Energy **39**(9), 4544–4557 (2014)
80. X. Sheng, B. Wouters, T. Breugelmans, A. Hubin, I.F.J. Vankelecom, P.P. Pescarmona, Cu/CuxO and Pt nanoparticles supported on multi-walled carbonnanotubes as electrocatalysts for the reduction of nitrobenzene. Appl. Catal. B **147**, 330–339 (2014)
81. S. Wang, D. Yu, L. Dai, Polyelectrolyte functionalized carbon nanotubes as efficient metal-free electrocatalysts for oxygen reduction. J. Am. Chem. Soc. **133**(14), 5182–5185 (2011)
82. T. Matsumoto, Y. Nagashima, T. Yamazaki, J. Nakamura, Fuel cell anode composed of Mo_2C catalyst and carbon nanotube electrodes. J. Electrochem. Solid-State Lett. **9**(3), A160–A162 (2006)
83. A.C. Johansson, R.B. Yang, K.B. Haugshøj, J.V. Larsen, L.H. Christense, E.V. Thomsen, Ru-decorated Pt nanoparticles on N-dopedmulti-walled carbon nanotubes by atomic layer deposition for direct methanol fuel cell. J. Hydrogen Energy **38**(26), 11406–11414 (2013)
84. A. L. M. Reddy, N. Rajalakshmi, S. Ramaprabhu, Cobalt-polypyrrole-multiwalled carbon nanotube catalysts for hydrogen and alcohol fuel cells. Carbon 46(1), 2-11 (2008). https://doi.org/10.1016/j.carbon.2007.10.021

Transition Metal Oxides for Supercapacitors

S. Chandra Sekhar, Bhimanaboina Ramulu, and Jae Su Yu

Abstract Active materials are the core components of energy storage devices, which usually determine the potential window and capacity. Among the developed active materials, transition metal oxides (TMOs) have been fascinated as electrode candidates in supercapacitors (SCs) due to their high theoretical capacity, excellent redox chemistry, multivalence states, and affordable cost. In this chapter, firstly, different types of TMOs and their charge storage mechanism are discussed. Furthermore, combining the TMOs in a composite form leads to an improvement in the energy storage performance of SCs, and hence, different combinations of TMOs are elucidated broadly. The impact of hybridizing the different metal oxides with other materials like graphene, conductive polymers, etc. is also comprehensively discussed. On the other hand, versatile preparation methods to design the hierarchical/porous architectured nanostructures of TMOs are discussed in this chapter. Recently, metal–organic frameworks (MOFs) have emerged as a new class of materials and attracted a great deal of interest in a variety of fields because of their captivating features. This chapter also focussed on the development of highly porous MOF-based/derived TMOs and their contribution to the energy storage field. Considering next-generation flexible electronic gadgets, the proximity of TMOs in the fabrication of flexible energy storage devices is also described in this chapter.

Keywords Transition metal oxides · Synthesis methods · Hybridization of TMOs · MOF-derived TMOs · Supercapacitors

S. Chandra Sekhar · B. Ramulu · J. S. Yu (✉)
Department of Electronic Engineering, Institute for Wearable Convergence Electronics, Kyung Hee University, 1732 Deogyeong-daero, Gihung-gu, Yongin-si, Gyeonggi-do 17104, Republic of Korea
e-mail: jsyu@khu.ac.kr

S. Thomas et al. (eds.), *Nanostructured Materials for Supercapacitors*,
Advances in Material Research and Technology,
https://doi.org/10.1007/978-3-030-99302-3_13

1 Introduction

Active materials are major decisive parameters in the energy storage performance of supercapacitors (SCs). So far, versatile active materials such as carbon-related materials, conducting polymers, and hydroxides/oxides of transition metals, and some noble metals have been investigated as electrode candidates for SCs. Although carbon-related materials offer high power density, long durability, and high structural stability, they can not deliver high capacity owing to the non-faradaic-type reactions involved in their charge storage process. Conducting polymers and transition metal hydroxides have recently attracted special interest as electrode materials due to their advanced properties compared to those of the above-mentioned materials because the charge storage process in those materials involves reversible faradaic-type reactions with electrolyte ions. However, poor crystallinity and agglomeration of metal hydroxides, and meager structural rigidity of conductive polymers further hinder the development of cost-effective and high-performance SCs [1, 2]. Whereas, transition metal oxides (TMOs) have captivated exclusive attention owing to their high theoretical capacity, decent electrical conductivity, multi-oxidation states of the elements, and affordable cost.

In this chapter, versatile TMOs which are in two classifications are discussed comprehensively. More importantly, some misconceptions regarding the type of charge storage process in different TMOs and the metrics used to measure their capacity performance are interpreted with graphical demonstrations. The effect of a combination of multiple TMOs and their hybridization with carbon-related or conductive polymers is also discussed in this chapter. The merits involved in the development of TMOs from the recently evolved state-of-the-art metal–organic frameworks (MOFs) are also elaborated. In the end, the proximity of TMOs in the design of flexible/wearable SCs is also unveiled by reviewing the recently reported literature.

2 Types of TMOs

According to the charge storage process, the TMOs can be distinguished into two types, i.e., pseudocapacitor (PC)-type and battery-type.

2.1 Pseudocapacitor-Type TMOs

As well known, electric double-layer capacitor (EDLC)-type materials accumulate the charge in a non-faradaic process. Therefore, these materials (typically carbon-based materials) usually do not exhibit oxidation–reduction peaks in their cyclic voltammetry (CV) response within the defined potential window, as shown in Fig. 1a–

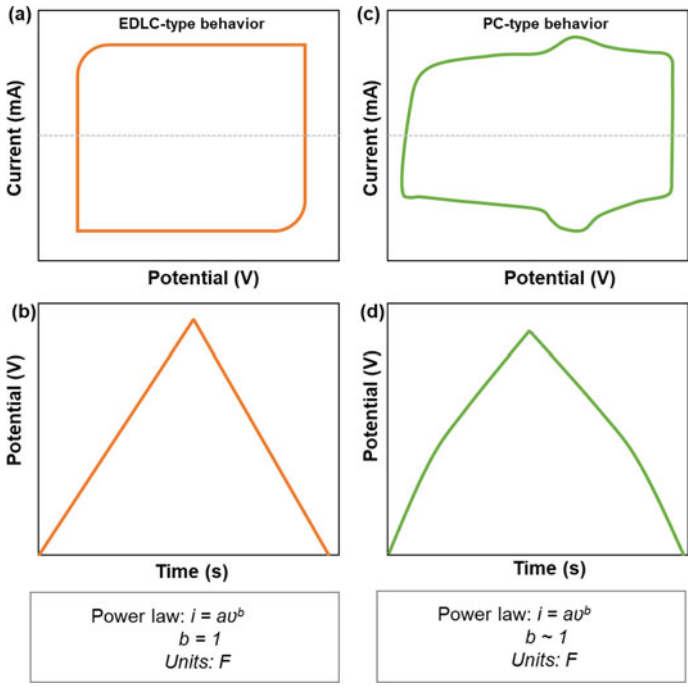

Fig. 1 Typical, **a** and **c** CV and **b** and **d** GCD responses of EDLC-type and PC-type electrode materials in the SC study

b. Differently, PC-type materials show slight redox peaks in the forward and backward sweeps in the CV response as they execute reversible faradaic reactions. The word "pseudocapacitance" is perhaps standardized by joining the prefix "pseudo" to the word "capacitance" [3]. The word "pseudocapacitance" defines "(a) nearly impending, or trying to be" and "(b) not really but in the appearance of". The latter phrase is well suited to this type of behavior because the CV and galvanostatic charge–discharge (GCD) outlines of PC-type materials are similar to those of EDLC-type materials, as displayed in Fig. 1c–d. However, the electrode materials indeed demonstrate reversible electrochemical reactions [4]. The diffusion coefficient (b) values of the EDLC- and PC-type materials are 1 and nearly 1, respectively. The generated charge during the measurement is constant within the defined potential window. Therefore, the electrochemical performance of these materials should be estimated in capacitance with the unit of a Farad (F).

Ruthenium oxide: RuO_2 in crystalline or amorphous state has gained the most promising attraction as a positive electrode among different PC-type materials because of its high electrochemical activity, redox reversibility, metallic conductivity, and thermal/chemical stability [5–7]. Although this material was broadly studied as a PC electrode candidate, the underlying faradaic process that corresponds to the pseudocapacitance further needs to be explored in an attempt to design benefit-enriched

RuO_2 materials. Some previous studies have proposed that the charge storage process in RuO_2 takes place due to the proton-electron reaction as described in the following equation [8, 9]:

$$RuO_2 + \delta H^+ + \delta e^- \leftrightarrow RuO_{2-\delta}(OH)_\delta \quad (1)$$

Here, δ varies between 0 and 2. This equation signifies that the valency of Ru changes from 2 to 4 in the oxidation process and vice versa in the reduction process. Nevertheless, the demerits of the RuO_2 such as high cost, formation of nanoparticle clusters, instability of power density especially at high current rates impede its extensive usage as an electrode candidate in SCs [10]. Therefore, the RuO_2 material must be synthesized in the hydrous form (designated as $RuO_2{\cdot}xH_2O$) with the structural features of a thin layer and porosity to attain the exalted capacitance performance [11–13]. For instance, Changzhou Yuan et al. prepared hydrous ruthenium oxides/mesocarbon microbeads ($RuO_2{\cdot}H_2O$/MCMB) by hydrothermal method [14]. The resultant material exhibited almost EDLC behavior, but small redox humps in CV analysis and nearly triangular shape-like charge–discharge lines in the GCD analysis, as shown in Fig. 2a–b. These outlines of CV and GCD measurements endorse the PC-type of the $RuO_2{\cdot}H_2O$/MCMB material. At a starting current density of 0.5 A/g, this material demonstrated a high specific capacitance of 1084 F/g and remained 74% of this capacitance, i.e., 812 F/g even at a high current density of 5 A/g, as illustrated in Fig. 2c.

Manganese oxides: As an alternative to RuO_2, manganese oxides have garnered great attention because of their several characteristics such as non-noble metals, broad divergence in its valency (Mn (0) to Mn (VII)), wide operating potential window (∼1 V), and admirable capacitive performance (∼1400 F/g), and eco-benignity. Besides, the manganese element is situated at the tenth place in the abundantly available elements on the Earth's surface, which describes its cheaper cost than RuO_2 [15]. Moreover, the facile oxidizing property of the manganese element makes it promising in the derivation of versatile and stable polymorphs such as manganese monoxide (MnO), dimangaese trioxide (Mn_2O_3), trimanganese tetroxide (Mn_3O_4), and manganese dioxide (MnO_2) with α-, β-, and δ-phases. In analogy to the RuO_2 material, the above manganese oxides also demonstrate the faradaic-type charge storage process with PC-type behavior in their CV and GCD analyses. For instance, the CV and GCD curves of MnO_2@vapor grown carbon fiber electrode are displayed in Fig. 3 [16].

Each polymorph differs from others due to its crystal structure, chemical configuration, and diverge physical and chemical properties, which leads to the differences in the capacity performance. The MnO_2 displays disparate polymorphs of α-MnO_2, β-MnO_2, R-MnO_2, γ-MnO_2, δ-MnO_2, and λ-MnO_2, which have hollandite-, pyrolusite-, Ramsdellite-, nsutite-, birnessite-, and spinel-type crystal structures, respectively (Fig. 4) [17, 18]. Besides the morphological and other properties, these crystal struc-

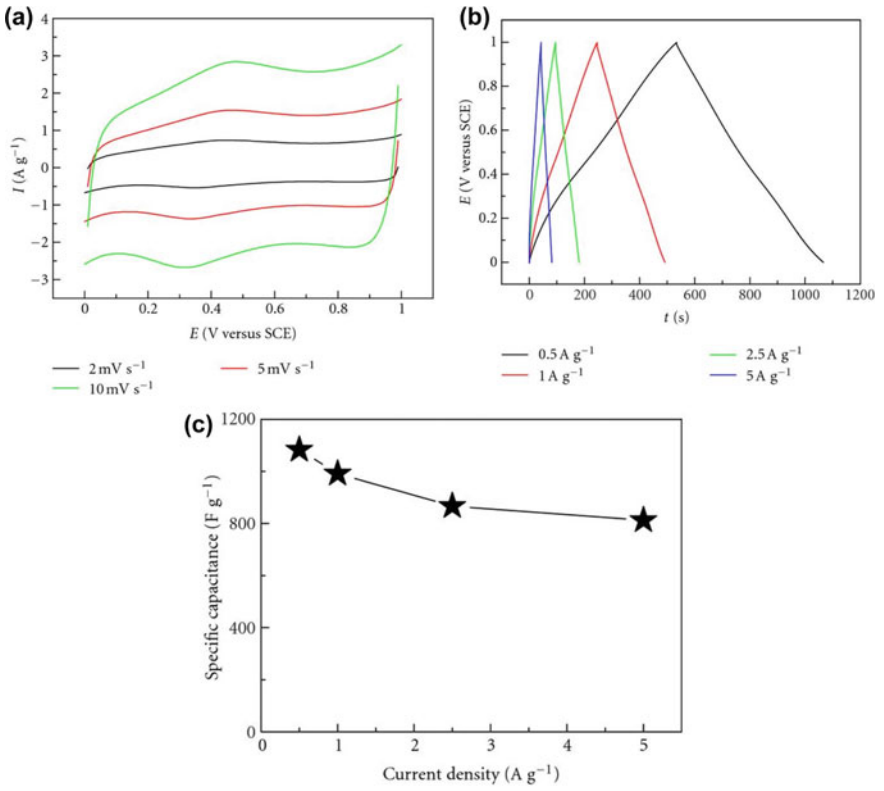

Fig. 2 Electrochemical properties of $RuO_2 \cdot H_2O$/MCMB composite electrode. **a** CV curves, **b** GCD curves, and **c** specific capacitance values at different current densities. Adapted with permission from reference [14], Copyright © 2012 Changzhou Yuan et al. Published under the terms of Creative Commons Attribution License

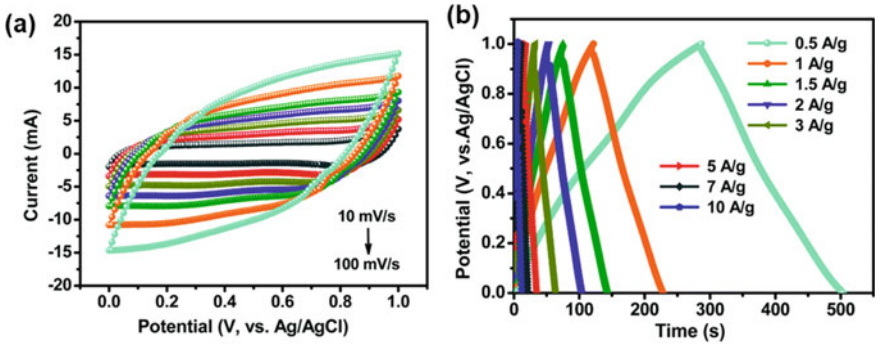

Fig. 3 **a** CV curves and **b** GCD curves of the MnO_2@VGCF electrode measured at different test conditions, revealing PC-type charge-storage behavior. Adapted with permission from reference [16], Copyright (2016), Royal Society of Chemistry

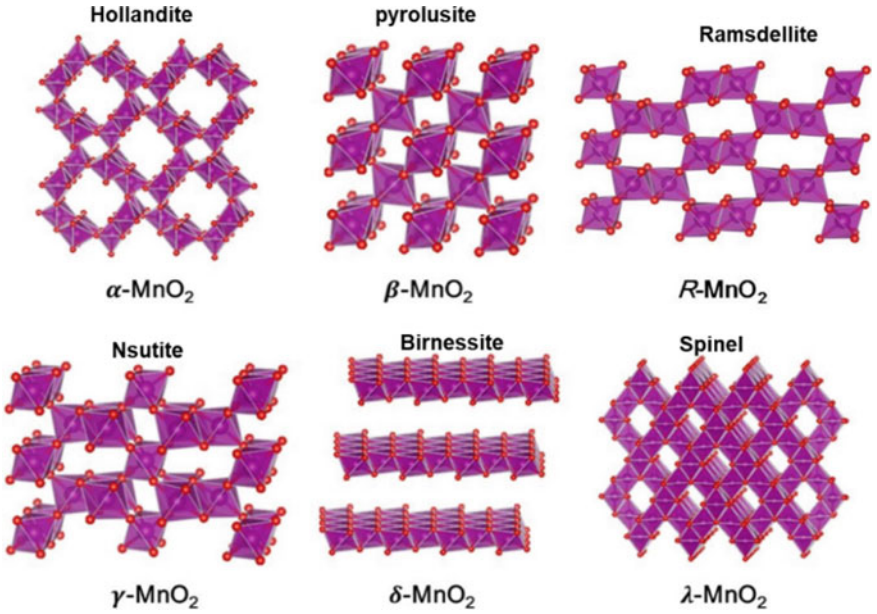

Fig. 4 Crystal structures of MnO_2 polymorphs. Adapted with permission from reference [17], Copyright (2020), Taylor & Francis

tures also play a major role in implementing redox reactions by offering intercalation/deintercalation of electrolyte ions, followed by the accumulation of generated charge.

Although MnO_2 and RuO_2 demonstrate a noteworthy capacity performance, they lag behind other electrode materials due to some of the constraints like relatively low electrochemical activity, and high cost and eco-scarcity of RuO_2, respectively. Therefore, developing more advanced TMOs with enriched redox activity, higher electrical conductivity, low-cost features would be a propitious strategy to achieve better energy storage performance.

2.2 Battery-Type TMOs

Recently, battery-type TMOs have attracted much attention due to their superior characteristics of high redox chemistry, high electrical conductivity, exalted capacity performance. Owing to the involvement of diffusion or intercalation of electrolyte ions, the battery-type TMOs exhibit apparent and distinct redox peaks in the CV measurement and non-linear charge–discharge curves with clear plateau behavior in the GCD measurement, as illustrated in Fig. 5. The diffusion constant (b) value is

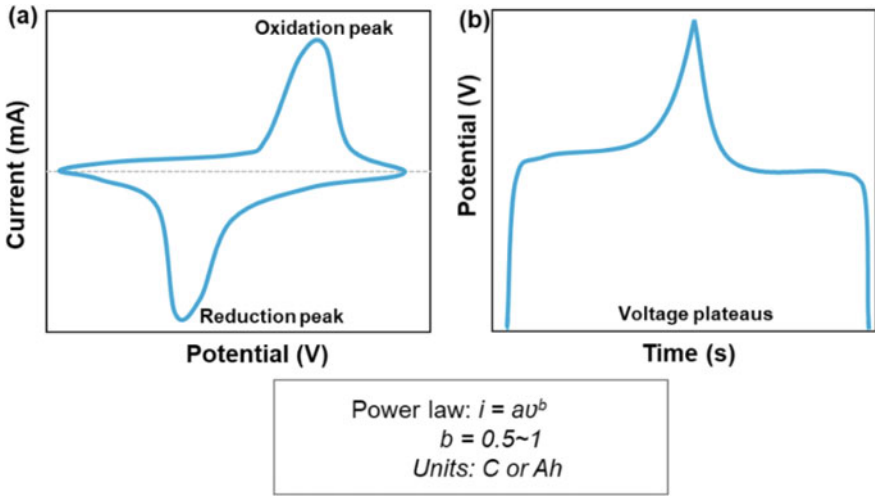

Fig. 5 Typical, **a** CV response and **b** GCD response of battery-type TMOs

close to 0.5 for this type of behavior. Since the generated charge during the measurement is not constant within the defined potential window, the capacity of battery-type materials which specifically exhibit the above-mentioned behavior should be calculated in coulomb (C) or Ah. Some of battery-type TMOs and their electrochemical behavior are explained in the following section.

So far, disparate battery-type TMOs such as nickel oxide, cobalt oxide, copper oxide, iron oxide, zinc oxide, molybdenum oxide, etc. have been explored for use as electrode candidates in SCs.

Nickel oxide: Among the above-mentioned battery-type TMOs, nickel oxide (NiO) has received unprecedented attraction as an SC electrode material due to its remarkable theoretical capacitance of $\sim$ 3750 F/g, high electrochemical activity, eco-friendly nature, and affordable cost. The alkaline solution, i.e., potassium hydroxide (KOH), is usually used as an electrolyte because of its high ionic conductivity. Here, the charge transfer process ensues during the conversion of NiO into NiOOH. The NiO gets oxidized by reacting with hydroxyl ions (OH^-) and releases one electron in the oxidation process, whereas the NiOOH is reduced to NiO by taking an electron in the reduction process. The corresponding reversible redox reactions of the NiO material in the charge storage process are given below:

$$NiO + OH^- \leftrightarrow NiOOH + e^- \tag{2}$$

$$NiO + H_2O \leftrightarrow NiOOH + H^+ + e^- \tag{3}$$

Figure 6 displays the electrochemical properties of the NiO active material prepared by a solvothermal method [19]. Owing to the high redox response of NiO

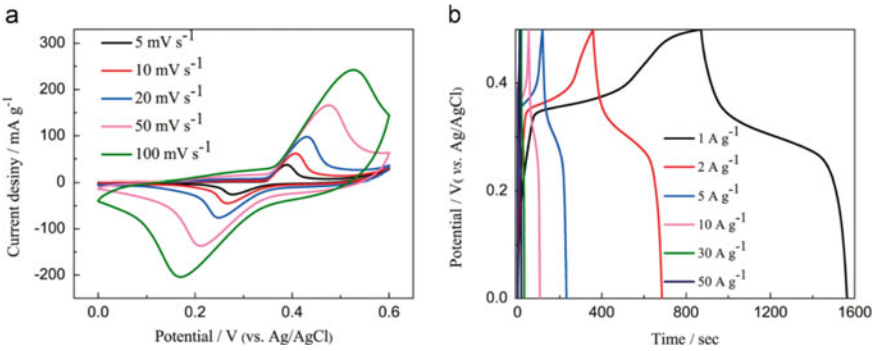

Fig. 6 **a** CV curves and **b** GCD curves of the NiO electrode material recorded at various scan rates and current densities, respectively. Adapted with permission from reference [19], Copyright (2015), Elsevier

material, it exhibited profound redox peaks in the CV measurement and voltage plateaus in the GCD measurement, as displayed in Fig. 6.

Cobalt oxide: Similar to NiO, different cobalt oxides such as cobalt monoxide (CoO), cobalt dioxide (CoO_2), dicobalt trioxide (Co_2O_3), and tricobalt tetroxide (Co_3O_4) have also received considerable interest as electrode materials of SCs [20, 21]. Among these, CoO and Co_3O_4 have captivated more attention because of their disparate physical and chemical properties, high theoretical capacity (~3500 F/g), good thermal stability, affordable cost, and natural abundance [22, 23]. These materials also exhibit reversible redox reactions by reacting with alkaline electrolytes and the corresponding charge storage process is explained by the following equations [24, 25]:

$$Co_3O_4 + OH^- + H_2O \leftrightarrow 3CoOOH + e^- \tag{4}$$

$$CoOOH + OH^- \leftrightarrow CoO_2 + H_2O + e^- \tag{5}$$

Owing to the low ionic and electronic conductivities, the rate capability of this material is usually low. However, other properties like high electric conductivity and chemical stability of Co_3O_4 promote its usage as electrode materials in SC application. For instance, Fangyan Liu et. al. synthesized ultrafine Co_3O_4 nanoparticles [26]. Exploiting structural and redox properties, the Co_3O_4 material exhibited a high electrochemical response with battery-type behavior, as displayed in Fig. 7. At 0.5 A/g, this electrode showed a maximum specific capacitance of 523 F/g and also demonstrated good cycling stability after 1500 cycles.

Besides the above two materials, several other TMOs like TiO_2 [27], VO_x [28], ZnO [29], Nb_xO_y [30], MoO_x [31], WO_x [32], etc. have also been investigated as SC electrode materials. The major limitations of TMOs are relatively low electrical conductivity and moderate energy density regarding the energy storage performance

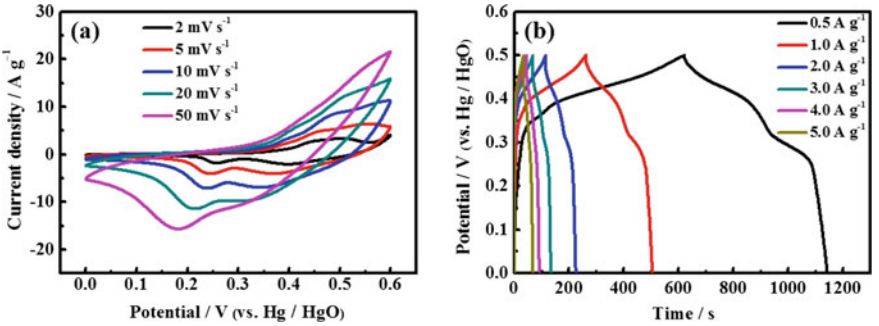

Fig. 7 **a** CV curves and **b** GCD curves of Co_3O_4 electrode (sample-II) at different test conditions. Adapted with permission from reference [26], Copyright (2017), Elsevier

of SCs. To overcome these hurdles, the possible solutions are described in the next sections.

3 Combinations of TMOs

To overcome the limitations of TMOs mentioned above, one of the potential strategies is combining more than one TMO in a composite form. Here, one TMO can compensate for the limitations of another TMO by its intriguing aspects and vice versa. Consequently, these TMOs in a composite form synergistically endow their respective redox chemistry to deliver improved energy storage performance. Currently, binary/ternary TMOs have been fascinated because of their enriched redox chemistry, improved conductivity, widened potential window, and good structural and charge-transfer abilities. Binary TMOs with especially spinel structure with a formula of $A_xB_{2x}O_4$, where A and B are transition metals (Ni, Mn, Zn, Cu, Co, Fe, etc.) have gained more attention owing to their high capacity, rate capability, and long-term stability. Mostly, all of these metals exhibit bivalency in the oxide form, and some even show trivalency and tetravalency. As a result, numerous charges can be transferred during the electrochemical reactions, which leads to capacity boosting. For instance, M. Nagaraju et. al. prepared spinel-type manganese cobaltite ($MnCo_2O_4$) via a single-step solvothermal method [33]. The prepared $MnCo_2O_4$ material exhibited fine nanoparticles with $\leq$100 nm size, as displayed in Fig. 8a. To investigate the synergistic effect of both transition metals, i.e., Mn and Co, the authors also prepared solitary manganese and cobalt oxides by keeping all the synthesis conditions the same. As shown in Fig. 8b–c, the $MnCo_2O_4$ electrode demonstrated a higher electrochemical response in CV and GCD analyses than the solitary manganese and cobalt oxides owing to the involvement of high redox-active Mn and Co elements.

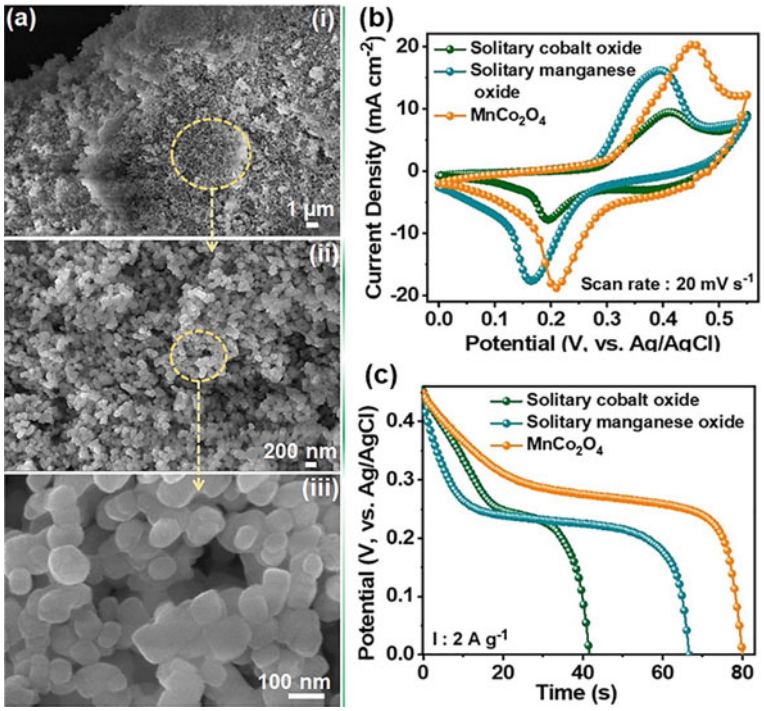

Fig. 8 **a** Morphology of $MnCo_2O_4$ material. **b** CV and **c** GCD profiles of solitary manganese oxide, solitary cobalt oxide, and $MnCo_2O_4$ composite electrodes compared at a fixed scan rate and current density, respectively. Adapted with permission from reference [33], Copyright (2020), Elsevier

With this synergistic redox chemistry and improved conductivity, the $MnCo_2O_4$ electrode was able to attain a higher specific capacity of 44.8 mAh/g than the solitary manganese (∼23 mAh/g) and cobalt oxides (∼37 mAh/g).

In another report, Chun We et. al. synthesized Zn–Ni–Co ternary oxide (ZNCO) with mesoporous nanowire morphology by hydrothermal process, followed by calcination [34]. In this literature, the authors systematically revealed the combination effect of different TMOs. They prepared solitary Co_3O_4, binary $ZnCo_2O_4$, and ternary Zn–Ni–Co oxides. Their electrochemical response was recorded at a constant scan rate of 2 mV/s and current density of 1 A/g, as shown in Fig. 9a–b. The ZNCO electrode demonstrated higher redox response in CV and longer charge–discharge times in GCD analyses than the other two electrodes (CO and ZCO) owing to efficient exploitation of all respective features of Zn, Ni, and Co elements synergistically. In detail, the Zn element provides electrical conductivity, whereas the Ni and Co elements are highly redox-active and also have good electrical conductivity. Owing to these benefit-enriched aspects, the ZNCO electrode delivered a higher capacitance at all the measured current densities than solitary CO electrode and even binary ZCO electrode, as illustrated in Fig. 9c. However, the ZCO electrode exhibited higher

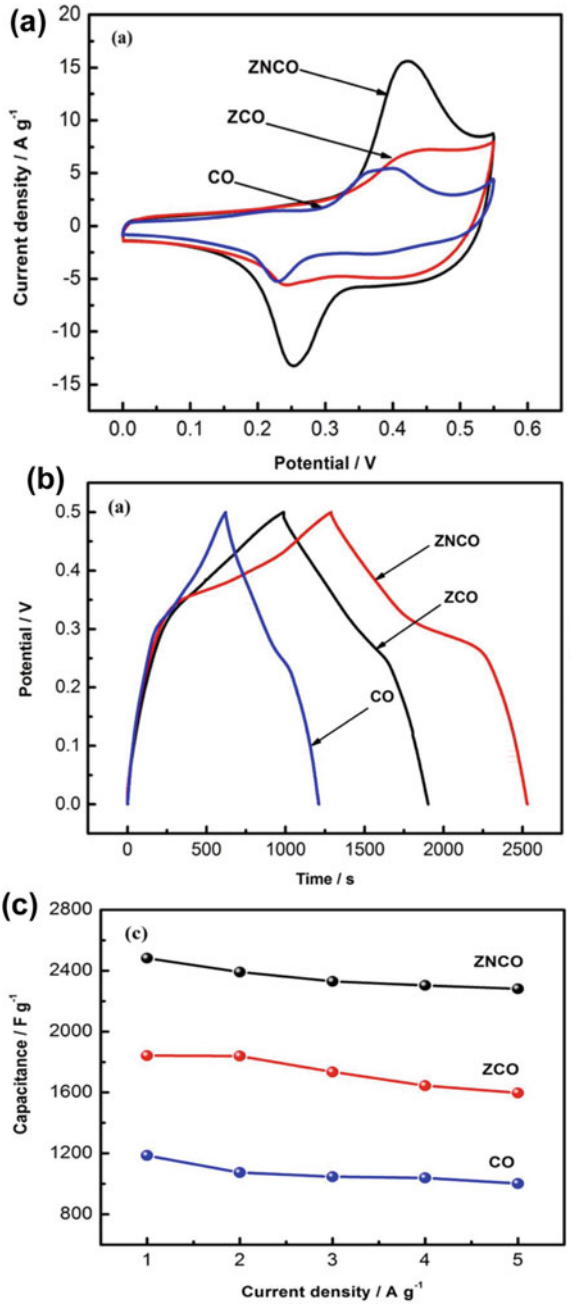

Fig. 9 **a** CV profiles, **b** GCD profiles, and **c** capacitance values compared among the solitary Co_3O_4 (CO), binary $ZnCo_2O_4$ (ZCO), and ternary Zn–Ni–Co (ZNCO) oxide electrodes. Adapted with permission from reference [34], Copyright (2020), American Chemical Society

capacitance performance than the solitary CO electrode due to the involvement of binary TMOs.

In addition to the number of TMOs in the composite form, the specific surface area and conductivity are two main aspects that can enhance the SC performance. Therefore, downsizing the morphology to the nanoscale, for example, one-dimensional structures or thin two-dimensional structures probably are the appropriate approach to achieve a high surface area. Another engaging strategy is synthesizing TMOs with the aid of MOFs whose architecture typically comprises the above-mentioned characteristics. Regarding the electrical conductivity, slightly modifying or creating vacancies in the architecture of core material by adding/doping other TMOs can also enhance the conductivity. Although noteworthy development has been made in the binary/ternary TMOs for SC application, there is still room to overcome some obstacles like binder-assisted synthesis and limited yield.

4 Hybridization of TMOs

Hybridizing TMOs with other materials like carbon-related materials, conductive polymers, and noble metals is also considered as one of the potential strategies to overcome the demerits of TMOs. For example, the carbon-related materials integrated with TMOs not only offer mechanical support but also boost the charge-kinetics, power density, and rate-capability properties. In the previous literature, Jae Su Yu et. al. fabricated a hybrid material of reduced graphene oxide (rGO) sheathed Co_2VO_4 (rGO@Co_2VO_4) porous nanospheres for bifunctional applications [35]. Scanning electron microscope (SEM) and transmission electron microscope (TEM) images in Fig. 10a–b unveil the wrapping of Co_2VO_4 nanospheres by rGO nanosheets. The rGO can effectively suppress the volume changes in the nanostructures of TMOs owing to its high mechanical flexibility. Thus, the rGO@Co_2VO_4 hybrid material was able to maintain excellent cycling stability without a capacity loss (from the second cycle) after 100 cycles in the lithium-ion battery (LIB) study, as displayed in Fig. 10c. Meanwhile, the Co_2VO_4 material without having rGO shielding was not able to form a solid electrolyte interphase layer until nearly 10 cycles, leading to more capacity loss as shown in Fig. 10d. In the SC study, the comparative CV and GCD curves revealed the higher electrochemical response of rGO@Co_2VO_4 hybrid material than the Co_2VO_4 material. Moreover, the rGO@Co_2VO_4 hybrid material demonstrated higher capacity values at all the measured current densities than those of the Co_2VO_4 material obtained at the same current densities.

In addition to the carbon-based materials, conductive polymers such as polypyrrole (PPY), polyaniline, poly(3,4-ethylenedioxythiophene) -poly(styrenesulfonate) possessing the notable features of high electrical conductivity, good redox-activity, good flexibility, noteworthy capacitance, low cost, and easy synthesis have also attracted more attention in the fabrication of electrode materials for SCs. Moreover, the conductive polymers enable the solvent/electrolyte uptake property owing to having hydrophilic functional groups, which promotes potential ion diffusion and

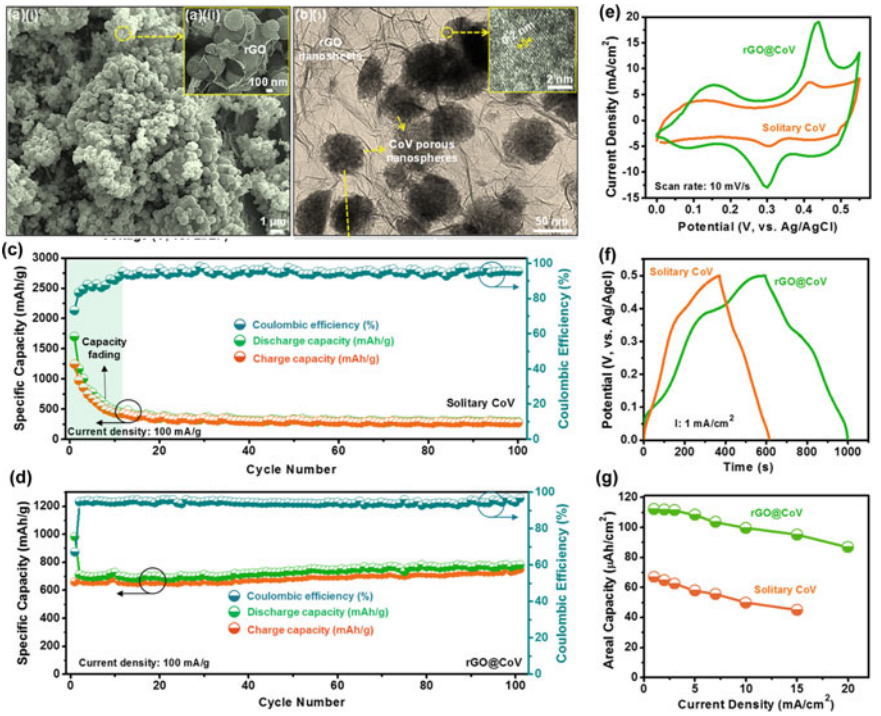

Fig. 10 **a** SEM and **b** TEM images of the rGO@Co_2VO_4 hybrid material. Cycling test of **c** solitary Co_2VO_4 and **d** rGO@Co_2VO_4 materials measured at 100 mA/g. Comparative **e** CV and **f** GCD curves of rGO@Co_2VO_4 and Co_2VO_4 materials at fixed test conditions. **g** Areal capacity values of both materials. Adapted with permission from reference [35], Copyright (2020), Americal Chemical Society

enhances the ion-accessible area. Like carbon matrix, the nanolayers of conductive polymers can also alleviate extreme volume changes because of their high flexibility [36]. In the previous report, Xinyi He et. al. prepared $FeCo_2O_4$ nanowires on the flexible carbon cloth (Fig. 11a–c) [37]. Next, the authors decorated PPY nanolayer over these nanowires to enhance the conductivity and redox activity, as shown in Fig. 11d–f. Compared to pristine $FeCo_2O_4$ material, an optimized PPY coated $FeCo_2O_4$ ($FeCo_2O_4$@PPY) material showed a higher electrochemical response in both CV and GCD tests because of boosted conductivity and redox properties, as displayed in Fig. 11g–h, respectively. Moreover, the shell-like PPY nanolayer protects $FeCo_2O_4$ nanowires from destruction during the long-term cycling process. As a result, the $FeCo_2O_4$@PPY hybrid material demonstrated remarkable cycling stability over 5000 cycles with 90.2% retention compared to the pristine $FeCo_2O_4$ material (84.5%), as illustrated in Fig. 11i.

The hybridization strategy is, therefore, more effective to maximize the energy storage performance and the lifetime of TMOs-based energy storage devices. Here,

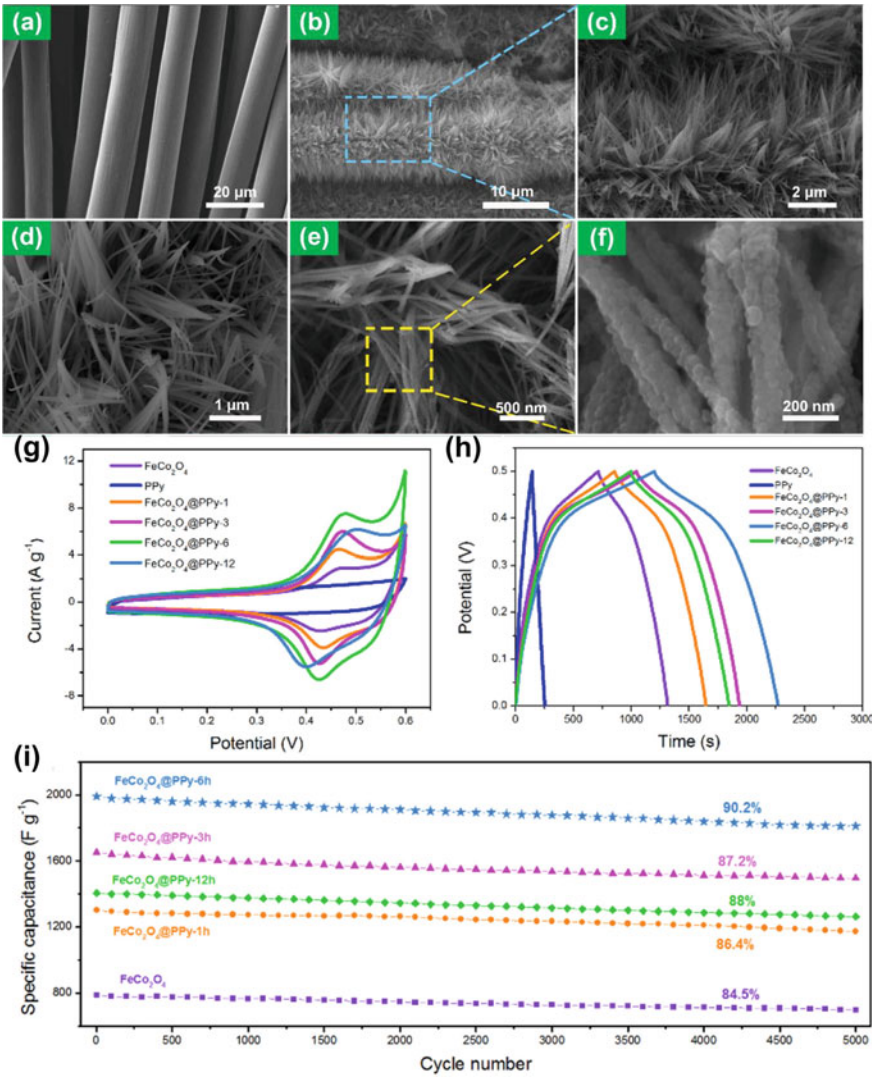

Fig. 11 SEM images of **a–c** pristine $FeCo_2O_4$ and **d–f** $FeCo_2O_4$@PPY materials. Comparative **g** CV curves and **h** GCD curves of pristine $FeCo_2O_4$ with different $FeCo_2O_4$@PPY electrodes. **i** Cycling results of pristine $FeCo_2O_4$ and different $FeCo_2O_4$@PPY electrodes Adapted with permission from reference [37], Copyright (2020), Americal Chemical Society

the additives that are integrated with TMOs not only contribute their inherent capacity but also extend the lifetime of designed electrode materials.

5 Preparation Methods of TMOs

The preparation method is another crucial factor of SC electrode materials. As of now, versatile synthesis methods such as chemical vapor deposition, sputtering, atomic layer deposition, template-assisted method, sonochemical processing, etc. have been utilized in the development of TMOs. However, almost all of the above-mentioned methods generally use high energy-consuming equipment or require expensive templates and arduous operation. These factors make the SC electrodes more expensive. Alternatively, several wet-chemical methods such as sol–gel, hydro/solvothermal, and co-precipitation have gained particular interest because of their easy processing, cost-effectiveness, controllability of chemicals/surfactants/solution concentrations, morphology tailoring, reproducibility, high yield, etc. [38]. For instance, Apurba Ray et. al. chose a sol–gel method to prepare the spinel $NiMn_2O_4$ nanoparticles by considering its effective characteristics such as fine nanoparticle formation, reproducibility, low-temperature process, and controllability [39]. Figure 12a–b displays the SEM and TEM images of the $NiMn_2O_4$ material. From the TEM image, semi-transparent nanoparticles can be observed, which suggests the porous behavior of the prepared material. The surface area and porosity analyses estimated their values as 43.6 m^2/g and 13.3 nm, respectively (Fig. 12c).

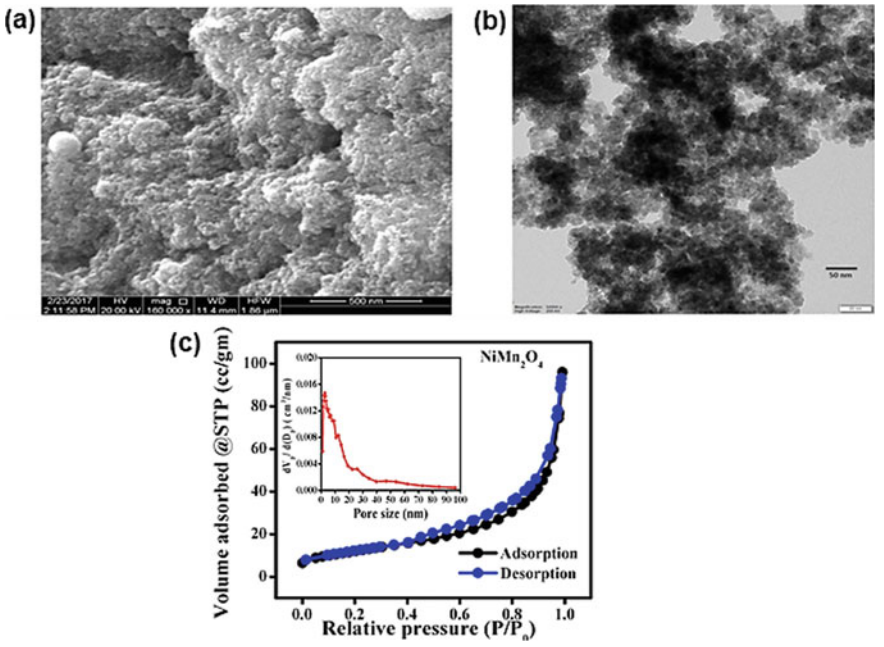

Fig. 12 **a** SEM image and **b** TEM image of the $NiMn_2O_4$ electrode prepared by a sol–gel method. **c** Surface area and pore-size analysis results of the $NiMn_2O_4$ electrode. Adapted with permission from reference [39], Copyright (2019), Elsevier

Owing to the fine nanoparticle morphology with high surface area and porosity, the $NiMn_2O_4$ material demonstrated a high specific capacitance of 875 F/g at an initial scan rate of 2 mV/s.

In another report, Jae Su Yu et al. utilized hydrothermal and coprecipitation methods to design the core-shell-like TMOs [40]. Both methods are cost-effective, can produce large-scale yield, and require simple instruments. The other features such as repeatability, uniform growth, and controllability also make these methods more promising in the synthesis of versatile electrode materials. These two methods can also grow the active material directly on the selected current collectors without the aid of binders. Therefore, the authors *in-situ* deposited core-like NiO-Co_3O_4 fish thorns-like nanostructures by the hydrothermal process. The hierarchical shell-like NiO nanosheets were then wrapped on these NiO-Co_3O_4 nanostructures by employing the coprecipitation method, as described in the schematic (Fig. 13a–c). By measuring morphological and electrochemical characteristics, the NiO-Co_3O_4-NiO composite material exhibited excellent energy storage performance in three- and two-electrode systems.

Even though the electrode materials comprised the pack of several electrochemical (high redox chemistry and multivalency) and physical (high redox chemistry, high surface area, and large porosity) features, their electrochemical performance is likely to be partly due to the presence of binders. Therefore, the important factor that should be considered in the fabrication of SC electrode is whether it is prepared with or without binders. Because the binders that are normally employed are electrically non-conductive and electrochemically inactive. As a consequence, the electric resistance of the electrode will upsurge, which leads to poor electrokinetics while performing the electrochemical reactions as demonstrated in Fig. 14. Moreover, the binders, auxiliary solvents, and conductive additives increase the production cost. Although these components will not participate in the electrochemical reactions, they increase the total weight of the SC device, which affects the volumetric capacitance. However, the binder-free preparation overcomes all the above-stated constraints by eradicating all auxiliary components. Besides, this preparation promotes rapid charge transportation, which results in relatively higher energy storage performance. The features of the binder-free preparation are illustrated in Fig. 14. Therefore, adopting the binder-free process using cost-effective methods to synthesize TMOs is a captivative approach.

6 Metal–organic Frameworks (MOFs)-Derived/Based TMOs

Recently, MOFs comprising transition metals and organic linkers have attracted a great deal of interest in versatile research fields owing to their several intrinsic factors of high porosity, high specific surface area, and tunability in pore distribution. Especially, the involvement of transition metals in the MOF matrix makes them extremely promising in the energy storage field as they are key components to execute redox

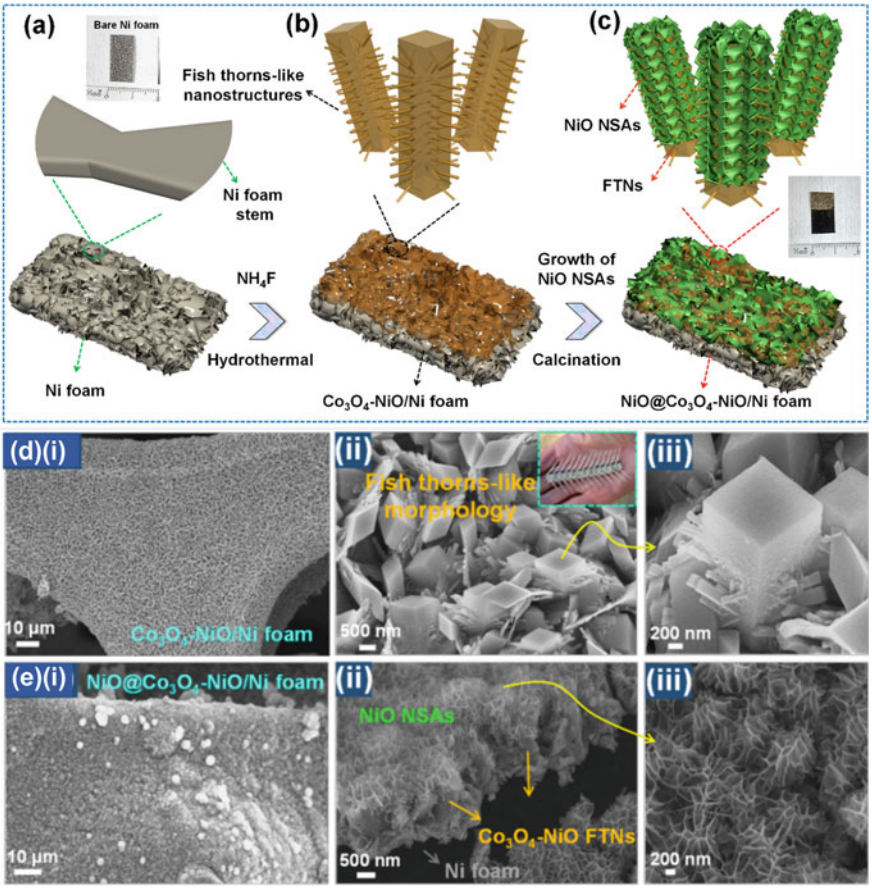

Fig. 13 **a**–**c** Schematic representation for the synthesis of the NiO-Co_3O_4-NiO composite material using successive hydrothermal and oven-based wet-chemical approaches. SEM images of **d** core-like NiO-Co_3O_4 and **e** core–shell-like NiO-Co_3O_4-NiO samples. Adapted with permission from reference [40], Copyright (2018), Elsevier

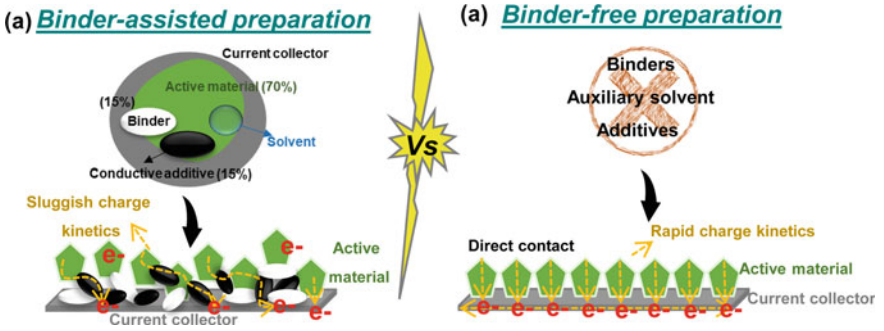

Fig. 14 Merits of binder-free preparation over the binder-assisted preparation of the SC electrodes

reactions. Comprising organic linkers is another benefit in a different aspect. They, of course, do not participate in any electrochemical reactions, but can be converted in the form of carbon in an inert atmosphere. Since pure TMOs usually have lower electrical conductivity and stability issues, this converted carbon is likely to enhance these aspects efficiently. Therefore, developing MOFs-derived/based TMOs using facile preparation routes is a prominent strategy to enhance the electrochemical performance of energy storage devices. For instance, Jae Su Yu et al. employed Co-MOF nano hexagonal prisms as a starting material and derived $Co_3V_2O_8$ in successive room-temperature ion-exchange methods, followed by calcining in an inert atmosphere (Fig. 15a–c) [41]. These $Co_3V_2O_8$ nano hexagonal prisms were grafted on CuV_2O_6 nanorod arrays to make the $Co_3V_2O_8$@CuV_2O_6 composite material (Fig. 15d). Especially, the porous nature of $Co_3V_2O_8$ nanoparticles can be seen from the TEM image as displayed in Fig. 15e. The $Co_3V_2O_8$@CuV_2O_6-based LIB showed a higher capacity of 1477.5 mAh/g at the first discharge cycle, and also exhibited excellent cycling stability over 150 cycles (Fig. 15f). Additionally, highly porous carbon was also derived from the Co-MOF material by the carbonization, followed by acid treatment. A hybrid SC device was then fabricated with $Co_3V_2O_8$@CuV_2O_6 and MOF-derived carbon materials as illustrated in Fig. 15g. By exploiting the benefits of both positive and negative electrodes, the SC device revealed superior energy and power densities (0.092 mWh/cm^2 and 24.40 mW/cm^2, respectively), as shown in Fig. 15h.

In another report, Yingxi Zhang et. al. designed hollow $Co(VO_3)_2$-$Co(OH)_2$ leaf-like arrays based on the Co-MOF materials [42]. As shown in Fig. 16a, the Co-MOF nanostructures were initially grown on carbon cloth substrate. The VO_3^- ion-exchange reaction was then carried out at room temperature to produce $Co(VO_3)_2$-$Co(OH)_2$ composite material. The SEM images in Fig. 16b show the smooth surface of the Co-MOF leaf-like nanostructure. This surface became rough after performing the VO_3^- ion-exchange reactions as presented in Fig. 16c. Benefitting from the composite active material and structural features, the $Co(VO_3)_2$-$Co(OH)_2$ electrode was able to deliver a higher areal capacitance of 522 mF/cm^2 at 0.5 mA/cm^2 than the other electrodes. Besides, it exhibited noteworthy capacitance retention of 90% over 15,000 cycles.

However, the impediments in the preparation of MOFs such as low-scale production, multiple preparation steps, and compromised electrical conductivity still limit their extensive applicability in the energy storage field. On the other side, the development of MOF-based electrode materials is still at the laboratory level. Therefore, novel and cost-effective synthesis routes with high yield have to be explored to address these issues. Moreover, incorporating two or more transition metals in the MOF matrix without deteriorating its core structure is highly desirable to exalt redox chemistry and electrokinetics.

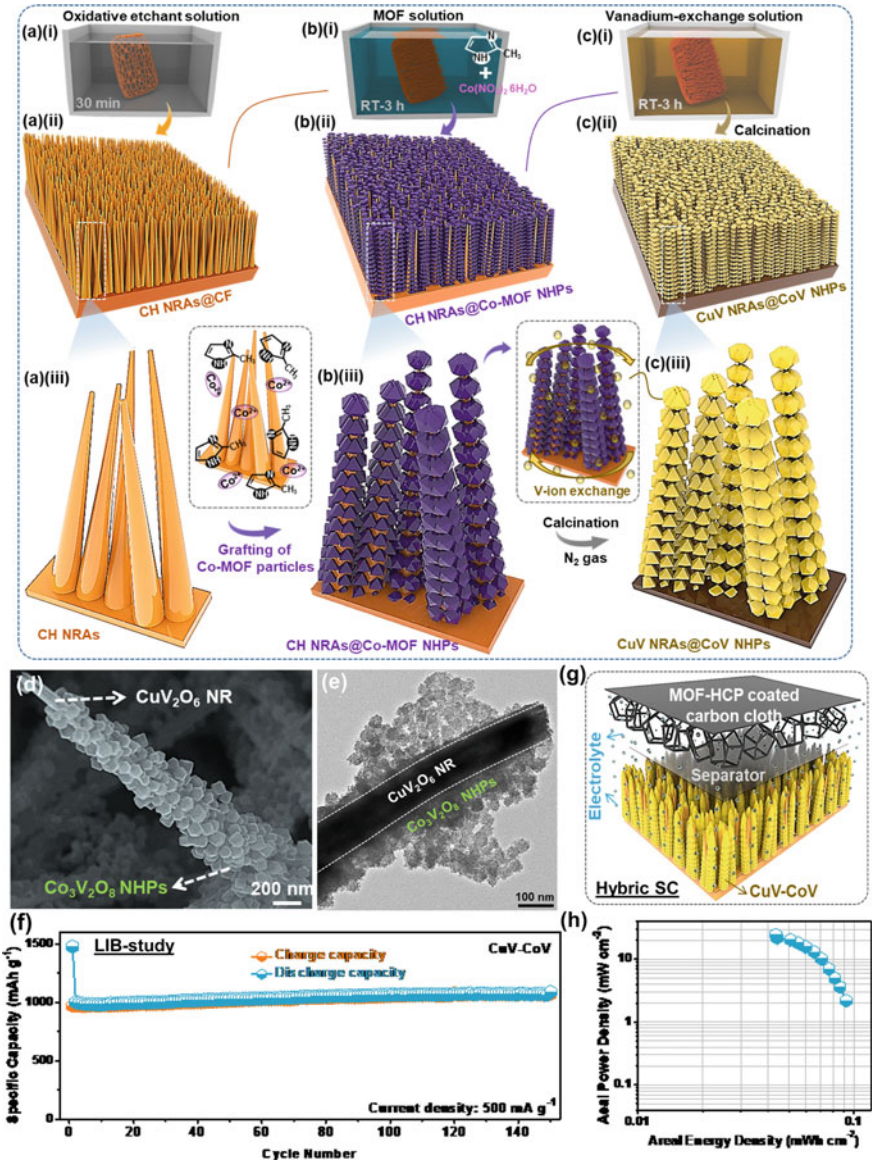

Fig. 15 **a–c** Scheme for the synthesis of $Co_3V_2O_8$@CuV_2O_6 material, **d** SEM and **e** TEM images of the $Co_3V_2O_8$@CuV_2O_6 material, and **f** LIB performance of the $Co_3V_2O_8$@CuV_2O_6 material. **g** Fabrication of hybrid SC and its **h** Ragone diagram. Adapted with permission from reference [41], Copyright (2020), Wiley

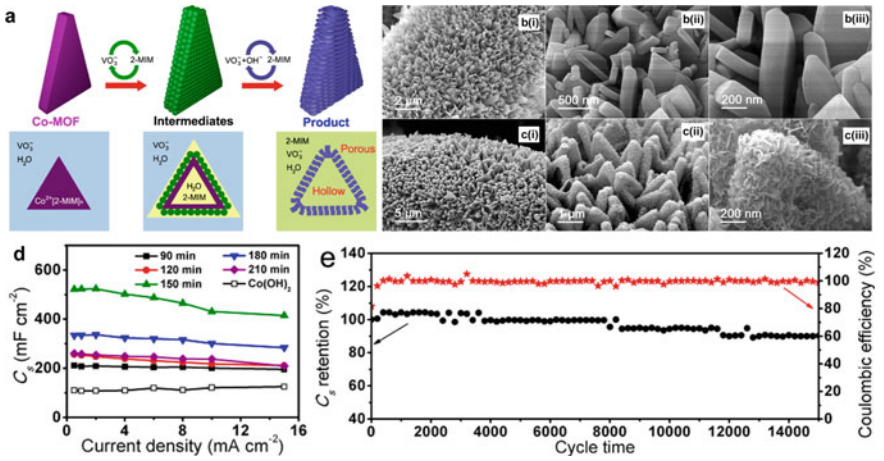

Fig. 16 **a** Synthesis process of $Co(VO_3)_2$-$Co(OH)_2$ material. SEM images of **b** Co-MOF and **c** $Co(VO_3)_2$-$Co(OH)_2$ materials. **d** Capacitance and **e** cycling performance of $Co(VO_3)_2$-$Co(OH)_2$ electrode. Adapted with permission from reference [42], Copyright (2018), American Chemical Society

7 TMOs Towards Flexible SCs

The recent advancement in the emergence of portable/wearable electronics and electric vehicles has accelerated the research community to develop flexible, renewable, and compatible SCs. The crucial component in the development of flexible/wearable SCs is the current collector, which should exhibit disparate flexibility conditions. Some conductive substrates like nickel foam/foil, fluorine-doped tin oxide substrate, copper foam/foil, stainless steel foil, and titanium foil could not serve as efficient current collectors in the fabrication of flexible/wearable SCs due to their physical rigidity and inelasticity issues. In contrast, fabrics/cloths, cellulose papers, and thin metal wires demonstrate excellent flexibility conditions such as bending, rolling, folding, and even twisting. Until now, different TMOs have been synthesized on various flexible conductive fabrics/textiles. Among these, carbon fabric has captivated a great deal of interest due to its excellent flexibility, high mechanical, chemical, and thermal stabilities, high electrical conductivity, and lightweight. Considering these properties, Hui Jiang et al. synthesized Mn_3O_4 material on the carbon cloth using the two-step hydrothermal method, as displayed in Fig. 17a [43]. From Fig. 17b–c, the uniform coating of Mn_3O_4 nanoparticles can be seen. The asymmetric SC was then fabricated with the Mn_3O_4/CC as a positive electrode and activated carbon as a negative electrode (Fig. 17d). The flexibility of this SC device was studied under physical deformations like bending and twisting, as shown in Fig. 17e. The CV curves of the device measured for 200 cycles under bending and twisting conditions are almost overlapped, which unveiled its excellent flexibility (Fig. 17f–g).

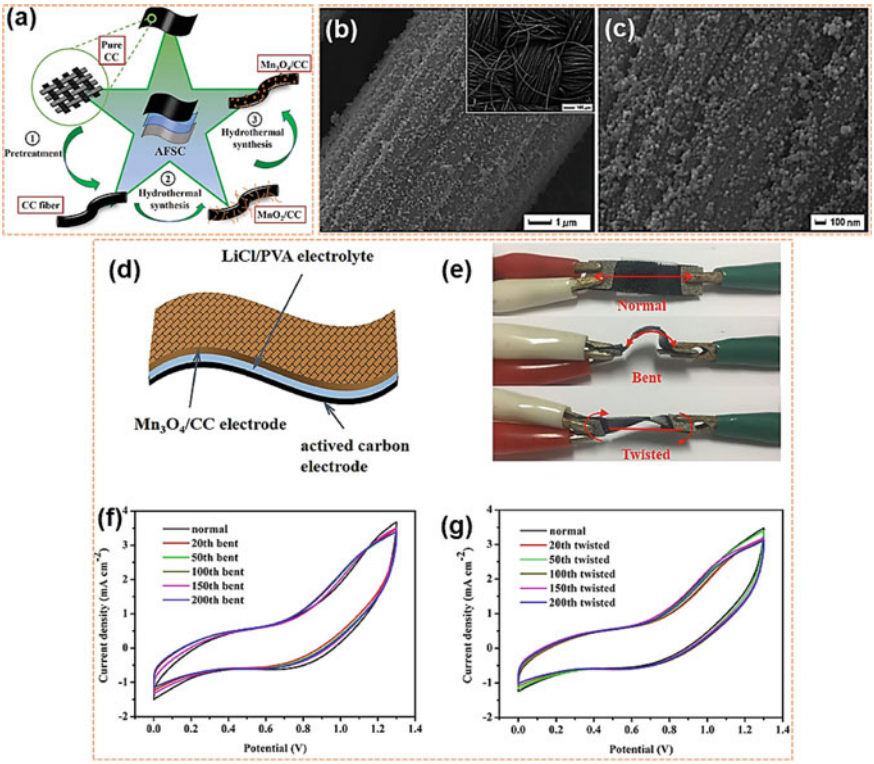

Fig. 17 **a** Scheme for the preparation of Mn_3O_4/CC sample. **b** and **c** SEM images of the Mn_3O_4/CC electrode. **d** Fabrication of the SC device. **e** Photographic representation of the SC device under normal, bending, and twisting conditions. CV cycling of the SC device under **f** bending and **g** twisting conditions. Adapted with permission from reference [43], Copyright (2020), Elsevier

Other substrates like cellulose paper [44], 3D spacer fabric [45], cellulose filter membrane [46], etc. have also unveiled their potency as current collectors in the fabrication of flexible SCs. The SC devices employing all these substrates demonstrated a stable performance under different flexible conditions, as displayed in Fig. 18.

Furthermore, TMOs have been also fabricated on flexible yarns/wires/cables. The SCs fabricated with these substrates can be more easily sew into human textiles/fabrics because of their tiny size and high flexibility. However, the loading of TMOs or any other active materials on these substrates is somewhat difficult by the binder-assisted process, which may result in the nonuniform coating or unwanted lumps. These factors limit the redox process and hinder the expose of inner active material to electrolyte ions, respectively. Therefore, the TMOs should be prepared directly without the assistance of binders or conductive additives. For instance, Jae Su Yu et al. fabricated NiO@CNTs@CuO composite material in situ on the discarded Cu fiber using facile wet-chemical processes, as presented in Fig. 19a [47]. Then, the solid-state hybrid SC was fabricated with this electrode as a positive electrode and

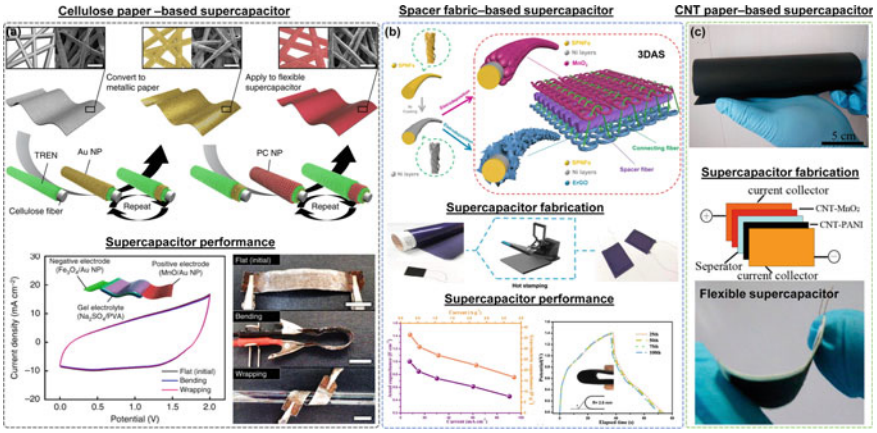

Fig. 18 Flexible SCs fabricated by the **a** cellulose paper. Adapted with permission from reference [44], Copyright (2017), Nature with slight modifications, **b** spacer fabric. Adapted with permission from reference [43], Copyright (2020), Elsevier with slight modifications, and **c** CNT paper substrates. Adapted with permission from reference [45], Copyright (2020), Elsevier

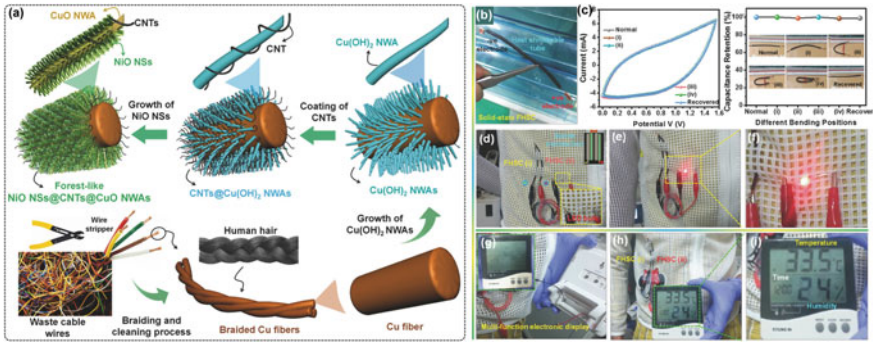

Fig. 19 **a** Synthesis of NiO@CNTs@CuO composite material on Cu fibers. **b** Fiber-shaped solid-state hybrid SC. **c** CV performance of solid-state hybrid SC under various bending conditions. **d–i** Real-time applicability of solid-state hybrid SC. Adapted with permission from reference [47], Copyright (2017), Wiley

activated carbon as a negative electrode, and inserted into the heat-shrinkable tube (Fig. 19b). The device showed a noteworthy electrochemical performance and especially showed a stable CV response under different flexible conditions (Fig. 19c). Furthermore, the wearability of these fiber-based SCs was also disclosed by being woven into a shirt, followed by power electronic components, as shown in Fig. 19d–i.

Most of the TMOs require a heat-treatment process at elevated temperatures to obtain the oxide phase. As a result, some substrates such as conductive polyester textiles and cellulose papers are unable to be employed as current collectors to synthesize TMOs since they become brittle at elevated temperatures. To tackle this

constraint, novel fabrication methods should be evolved in the design of TMOs on these substrates at low temperatures, which not only promotes the usage of the above-stated substrates but also diminishes the fabrication cost of SC electrodes.

8 Summary

This chapter described the significance of TMOs in SCs. The charge storage concepts in EDLC-type materials and PC- and battery-type TMOs are elaborated. Importantly, the capacity/capacitance metrics that have been used to measure the performance of the above-stated materials are interpreted clearly with corresponding graph models, which could enlighten the readers more about these concepts. Considering some demerits of solitary TMOs, designing the combination of multiple TMOs in a composite form is promoted in this chapter with proper examples. Although the EDLC-type materials and conductive polymers provide lower capacity, they can enhance the structural and cycling stabilities of TMOs by suppressing the volume changes. This chapter explained the benefits that result from the hybridization of TMOs with these materials. Various synthesis methods in the fabrication of TMOs are also discussed and some of the benefit-enriched methods are deliberated comprehensively. Especially, the merits of the binder-free synthesis over the binder-assisted synthesis of TMOs are exemplified. Since MOFs typically exhibit high porosity and surface area characteristics, the preparation of TMOs based on MOF materials is introduced and their physical properties for high performance are also elucidated. Finally, the fabrication of TMOs-based flexible SCs is also explained by stating the suitable current collectors. At the end of almost every section, the hurdles that usually exist in that specified section are discussed and their probable solutions are unraveled.

References

1. J.P. Cheng, J. Zhang, F. Liu, Recent development of metal hydroxides as electrode material of electrochemical capacitors. RSC Adv. **4**(73), 38893–38917 (2014)
2. Y. Luo, Y. Li, D. Wang, C. Zhai, T. Yang, M. Zhang, Hierarchical α-$Ni(OH)_2$ grown on CNTs as a promising supercapacitor electrode. J. Alloy. Compd. **743**, 1–10 (2018)
3. Z. Wu, L. Li, J.-M. Yan, X.-B. Zhang, Materials design and system construction for conventional and new-concept supercapacitors. Adv. Sci. **4**(6), 1600382 (2017)
4. K. Zhang, X. Han, Z. Hu, X. Zhang, Z. Tao, J. Chen, Nanostructured Mn-based oxides for electrochemical energy storage and conversion. Chem. Soc. Rev. **44**(3), 699–728 (2015)
5. Q. Jiang, N. Kurra, M. Alhabeb, Y. Gogotsi, H.N. Alshareef, All pseudocapacitive MXene-RuO_2 asymmetric supercapacitors. Adv. Energy Mater. **8**(13), 1703043 (2018)
6. C.-C. Hu, K.-H. Chang, M.-C. Lin, Y.-T. Wu, Design and tailoring of the nanotubular arrayed architecture of hydrous RuO_2 for next generation supercapacitors. Nano Lett. **6**(12), 2690–2695 (2006)

7. W. Wang, S. Guo, I. Lee, K. Ahmed, J. Zhong, Z. Favors, F. Zaera, M. Ozkan, C.S. Ozkan, Hydrous ruthenium oxide nanoparticles anchored to graphene and carbon nanotube hybrid foam for supercapacitors. Sci. Rep. **4**(1), 4452 (2014)
8. M. Manuraj, J. Chacko, K.N. Narayanan Unni, R.B. Rakhi, Heterostructured MoS_2-RuO_2 nanocomposite: a promising electrode material for supercapacitors. J. Alloys Comp. **836**, 155420 (2020)
9. M.-Y. Chung, C.-T. Lo, High-performance binder-free RuO_2/electrospun carbon fiber for supercapacitor electrodes. Electrochim. Acta **364**, 137324 (2020)
10. X. Li, W. Gan, F. Zheng, L. Li, N. Zhu, X. Huang, Preparation and electrochemical properties of RuO_2/polyaniline electrodes for supercapacitors. Synth. Met. **162**(11), 953–957 (2012)
11. Y.-T. Kim, K. Tadai, T. Mitani, Highly dispersed ruthenium oxide nanoparticles on carboxylated carbon nanotubes for supercapacitor electrode materials. J. Mater. Chem. **15**(46), 4914–4921 (2005)
12. B.J. Lee, S.R. Sivakkumar, J.M. Ko, J.H. Kim, S.M. Jo, D.Y. Kim, Carbon nanofibre/hydrous RuO_2 nanocomposite electrodes for supercapacitors. J. Power Sources **168**(2), 546–552 (2007)
13. V. Subramanian, S.C. Hall, P.H. Smith, B. Rambabu, Mesoporous anhydrous RuO_2 as a supercapacitor electrode material. Solid State Ionics **175**(1), 511–515 (2004)
14. C. Yuan, L. Hou, D. Li, L. Yang, J. Li, Enhanced supercapacitance of hydrous ruthenium oxide/mesocarbon microbeads composites toward electrochemical capacitors. Int. J. Electrochem. **2012**, 714092 (2012)
15. S.K. Ghosh, Diversity in the family of manganese oxides at the nanoscale: from fundamentals to applications. ACS Omega **5**(40), 25493–25504 (2020)
16. S.C. Sekhar, G. Nagaraju, S.M. Cha, J.S. Yu, Birnessite-type MnO_2 nanosheet arrays with interwoven arrangements on vapor grown carbon fibers as hybrid nanocomposites for pseudocapacitors. Dalton Trans. **45**(48), 19322–19328 (2016)
17. J. Shin, J.K. Seo, R. Yaylian, A. Huang, Y.S. Meng, A review on mechanistic understanding of MnO_2 in aqueous electrolyte for electrical energy storage systems. Int. Mater. Rev. **65**(6), 356–387 (2020)
18. D.A. Kitchaev, S.T. Dacek, W. Sun, G. Ceder, Thermodynamics of phase selection in MnO_2 framework structures through alkali intercalation and hydration. J. Am. Chem. Soc. **139**(7), 2672–2681 (2017)
19. G. Cai, X. Wang, M. Cui, P. Darmawan, J. Wang, A.L.-S. Eh, P.S. Lee, Electrochromo-supercapacitor based on direct growth of NiO nanoparticles. Nano Energy **12**, 258–267 (2015)
20. G.-S. Jang, S. Ameen, M.S. Akhtar, H.-S. Shin, Cobalt oxide nanocubes as electrode material for the performance evaluation of electrochemical supercapacitor. Ceram. Int. **44**(1), 588–595 (2018)
21. M. Aadil, S. Zulfiqar, M.F. Warsi, P.O. Agboola, I. Shakir, Free-standing urchin-like nanoarchitectures of Co_3O_4 for advanced energy storage applications. J. Market. Res. **9**(6), 12697–12706 (2020)
22. R.B. Rakhi, W. Chen, D. Cha, H.N. Alshareef, Substrate dependent self-organization of mesoporous cobalt oxide nanowires with remarkable pseudocapacitance, Nano Lett. **12**(5)
23. J. Mei, T. Liao, G.A. Ayoko, J. Bell, Z. Sun, Cobalt oxide-based nanoarchitectures for electrochemical energy applications. Prog. Mater. Sci. **103**, 596–677 (2019)
24. R. Kumar, A. Soam, V. Sahajwalla, Carbon coated cobalt oxide (CC-Co_3O_4) as electrode material for supercapacitor applications. Mater. Adv. **2**(9), 2918–2923 (2021)
25. K. Deori, S.K. Ujjain, R.K. Sharma, S. Deka, Morphology controlled synthesis of nanoporous Co_3O_4 nanostructures and their charge storage characteristics in supercapacitors. ACS Appl. Mater. Interfaces. **5**(21), 10665–10672 (2013)
26. F. Liu, H. Su, L. Jin, H. Zhang, X. Chu, W. Yang, Facile synthesis of ultrafine cobalt oxide nanoparticles for high-performance supercapacitors. J. Colloid Interface Sci. **505**, 796–804 (2017)
27. H. Zhou, Y. Zhang, Electrochemically self-doped TiO_2 nanotube arrays for supercapacitors. J. Phys. Chem. C **118**(11), 5626–5636 (2014)

28. S. Chen, H. Jiang, Q. Cheng, G. Wang, S. Petr, C. Li, Amorphous vanadium oxides with metallic character for asymmetric supercapacitors. Chem. Eng. J. **403**, 126380 (2021)
29. A. Kumar, Sol gel synthesis of zinc oxide nanoparticles and their application as nano-composite electrode material for supercapacitor. J. Mol. Struct. **1220**, 128654 (2020)
30. X. Wang, C. Yan, J. Yan, A. Sumboja, P.S. Lee, Orthorhombic niobium oxide nanowires for next generation hybrid supercapacitor device. Nano Energy **11**, 765–772 (2015)
31. L. Huang, B. Yao, J. Sun, X. Gao, J. Wu, J. Wan, T. Li, Z. Hu, J. Zhou, Highly conductive and flexible molybdenum oxide nanopaper for high volumetric supercapacitor electrode. J. Mater. Chem. A **5**(6), 2897–2903 (2017)
32. S. Yoon, E. Kang, J.K. Kim, C.W. Lee, J. Lee, Development of high-performance supercapacitor electrodes using novel ordered mesoporous tungsten oxide materials with high electrical conductivity. Chem. Commun. **47**(3), 1021–1023 (2011)
33. M. Nagaraju, S. Chandra Sekhar, S. Junied Arbaz, J. Su Yu, Solvothermal-derived nanoscale spinel bimetallic oxide particles rationally bridged with conductive vapor-grown carbon fibers for hybrid supercapacitors. Appl. Surf. Sci. **563**, 150223 (2021)
34. C. Wu, J. Cai, Q. Zhang, X. Zhou, Y. Zhu, P.K. Shen, K. Zhang, Hierarchical mesoporous zinc–nickel–cobalt ternary oxide nanowire arrays on nickel foam as high-performance electrodes for supercapacitors. ACS Appl. Mater. Interfaces. **7**(48), 26512–26521 (2015)
35. S. Chandra Sekhar, G. Nagaraju, D. Narsimulu, B. Ramulu, S.K. Hussain, J.S. Yu, Graphene matrix sheathed metal vanadate porous nanospheres for enhanced longevity and high-rate energy storage devices. ACS Appl. Mater. Interfaces **12**(24), 27074–27086 (2020)
36. X. He, Q. Liu, J. Liu, R. Li, H. Zhang, R. Chen, J. Wang, High-performance all-solid-state asymmetrical supercapacitors based on petal-like $NiCo_2S_4$/Polyaniline nanosheets. Chem. Eng. J. **325**, 134–143 (2017)
37. X. He, Y. Zhao, R. Chen, H. Zhang, J. Liu, Q. Liu, D. Song, R. Li, J. Wang, Hierarchical $FeCo_2O_4$@polypyrrole core/shell nanowires on carbon cloth for high-performance flexible all-solid-state asymmetric supercapacitors. ACS Sustain. Chem. Eng. **6**(11), 14945–14954 (2018)
38. C. Tan, H. Zhang, Wet-chemical synthesis and applications of non-layer structured two-dimensional nanomaterials. Nat. Commun. **6**(1), 7873 (2015)
39. A. Ray, A. Roy, M. Ghosh, J. Alberto Ramos-Ramón, S. Saha, U. Pal, S.K. Bhattacharya, S. Das, Study on charge storage mechanism in working electrodes fabricated by sol-gel derived spinel $NiMn_2O_4$ nanoparticles for supercapacitor application. Appl. Surf. Sci. **463,** 513–525 (2019)
40. S. Chandra Sekhar, G. Nagaraju, J.S. Yu, High-performance pouch-type hybrid supercapacitor based on hierarchical NiO-Co_3O_4-NiO composite nanoarchitectures as an advanced electrode material. Nano Energy **48**, 81–92 (2018)
41. S.C. Sekhar, B. Ramulu, D. Narsimulu, S.J. Arbaz, J.S. Yu, Metal-organic framework-derived $Co_3V_2O_8$@CuV_2O_6 hybrid architecture as a multifunctional binder-free electrode for li-ion batteries and hybrid supercapacitors. Small **16**(48), 2003983 (2020)
42. Y. Zhang, H. Chen, C. Guan, Y. Wu, C. Yang, Z. Shen, Q. Zou, Energy-saving synthesis of MOF-derived hierarchical and hollow $Co(VO_3)_2$-$Co(OH)_2$ composite leaf arrays for supercapacitor electrode materials. ACS Appl. Mater. Interfaces. **10**(22), 18440–18444 (2018)
43. H. Jiang, C. Zhou, X. Yan, J. Miao, M. You, Y. Zhu, Y. Li, W. Zhou, X. Cheng, Effects of various electrolytes on the electrochemistry performance of Mn_3O_4/carbon cloth to ultra-flexible all-solid-state asymmetric supercapacitor. J. Energy Storage **32**, 101898 (2020)
44. Y. Ko, M. Kwon, W.K. Bae, B. Lee, S.W. Lee, J. Cho, Flexible supercapacitor electrodes based on real metal-like cellulose papers. Nat. Commun. **8**(1), 536 (2017)
45. J. Wen, B. Xu, J. Zhou, Towards 3D knitted-fabric derived supercapacitors with full structural and functional integrity of fiber and electroactive materials. J. Power Sources **473**, 228559 (2020)
46. Y. Jin, H. Chen, M. Chen, N. Liu, Q. Li, Graphene-patched CNT/MnO_2 nanocomposite papers for the electrode of high-performance flexible asymmetric supercapacitors. ACS Appl. Mater. Interfaces. **5**(8), 3408–3416 (2013)

47. G. Nagaraju, S.C. Sekhar, J.S. Yu, Utilizing waste cable wires for high-performance fiber-based hybrid supercapacitors: an effective approach to electronic-waste management. Adv. Energy Mater. **8**(7), 1702201 (2018)

Novel 3D Hierarchical Porous Carbon/Metal Oxides or Carbide Composites

Li Sun and Chunxu Pan

Abstract The performance of supercapacitors is highly related to the microstructures of electrode materials, such as components, morphology, configurations, etc. In recent years, a kind of three-dimensional (3D) hierarchical porous carbon-based composite has been attracted intensive interest due to its advantages, such as highly porous architecture, high surface area, good electrical conductivity, and high mechanical strength. 3D porous structure facilitates the electrolyte access to the interior of the electrode, and supplies electric ways for the anchored active materials, thereby improving the electric double-layer capacitance and pseudocapacitance. Additionally, the hierarchical porosity with a combination of the macro/meso/micropores be conducive to reducing internal resistance, improving ion diffusion/transport, ion storage, so as to achieve higher rate capabilities. In this chapter, we are concerned with some novel structures of the 3D hierarchical porous carbon/metal oxides or carbide composites together with their preparation methods, properties, and applications. Also, the dare of the 3D hierarchical porous carbon/metal oxides or carbide composites is also proposed.

Keywords Novel composites · 3D · Hierarchical porous carbon · Metal oxides · Carbide

1 Introduction

Supercapacitors are deemed to be one of the most potential energy storage technologies in renewable energy systems owing to their excellent characteristics such as fast charging speed, long service life, high power density, and wide operating temperature range [1, 2]. Supercapacitors storage charge through a double-layer capacitance on the electrode surface or a pseudocapacitor process based on a rapidly reversible two-dimensional redox reaction near the surface or a rapid three-dimensional intercalation

L. Sun · C. Pan (✉)
MOE Key Laboratory of Artificial Micro- and Nano-Structures, School of Physics and Technology, Wuhan University, Wuhan 430072, China
e-mail: cxpan@whu.edu.cn

S. Thomas et al. (eds.), *Nanostructured Materials for Supercapacitors*,
Advances in Material Research and Technology,
https://doi.org/10.1007/978-3-030-99302-3_14

process in an extremely thin surface layer, which is the main obstacle to implementing the full commercial capacity of the method [3]. Many factors will affect the capability of supercapacitors. Among these factors, the structure of electrode material is considered to be one of the pivotal elements.

In the development of supercapacitors, carbon materials have attracted more and more attention due to their large specific surface area, high stability, good stability, and other characteristics, and they are good candidates for electrode materials for supercapacitors [4, 5]. Carbon materials have been extensively studied over the past few decades, and great efforts have been made in their development and diversity. For example, CNT electrodes with unique tubular porous structures and excellent electrical properties can increase the energy density, however, high production costs limit their wide application [6]. The application of graphene in double-layer capacitors has aroused great interest. As a two-dimensional (2D) material, graphene shows great potential owing to its high specific surface area and electrical conductivity [7]. In practical applications, the energy density of the currently obtained pure graphene-based supercapacitors ranges from 15 to 35 Wh kg^{-1}, far lower than the theoretical value of less than 60 Wh kg^{-1} [8]. In addition, the planar two-dimensional structure has a high barrier to the decoration of other pseudocapacitor materials on the graphene sheet, which usually requires electrochemical inert additives and binders to design the graphene-based electrode, which affects the performance of the electrode.

In order to adequately exploit the high surface area of carbon materials, 3D porous structure has aroused extensive interest among researchers, which can the unique properties of carbon materials to a large extent, including honeycomb hierarchical porous carbon, carbon foam, carbon aerogel, carbon nanotube network, and carbon fiber network [9–13]. Moreover, due to the special porous structure (high specific surface area and pore volume), as well as inherent characteristics, such as high electronic conductivity, good thermal stability, and excellent mechanical strength, 3D interconnected porous carbon materials have aroused strong interest in the application of supercapacitors. As far as we know, due to the channels in the porous structure, the 3D porous structure carbon material can transmit electrons and ions very quickly and can be self-supporting, which means that when used as a supercapacitor electrode material, there is no need to add a binder. In addition, carbon materials can endure abominable environments due to their excellent thermal and chemical stability. However, pure carbon electrode materials offer a limited energy density, and cannot fulfill the growing needs of people. Except for designing a 3D porous structure, the functionalization of electrode materials also has an important impact on it. The integration of heteroatoms into carbon substrates can effectively regulate their intrinsic activity, which has high practicability and reference value for carbon electrodes. According to reports in the literature, symmetry can be broken by doping adjacent 2p or 3p elements (N, S, P, B, O, etc.) to change the carbon structure π-π conjugation, changing the intrinsic bandgap, leads to adjustable functions in energy storage scopes [14]. Zhu and his group discovered the wettability and conductivity can be enhanced by N atom in N-doped porous carbon, and obtained 292 F g^{-1} capacitance value [15]. Ma and his group prepared S-doped mesoporous carbon fibers. Due to the electron absorption properties of S, the resulting material

has a wider bandgap, achieving 221 F g^{-1} capacitance value [16]. In addition, multi-heteroatomic doping has better properties than mono-heteroatomic carbon materials. Zhou and his group studied hierarchical polyporate carbon materials with multi-heteroatomic doping (N/S) and N/P co-doped polyporate carbon/siphonate carbon heterojunctions. Due to the synergistic effect of multiple heteroatoms, their capacitance values reached 302 and 324 F g^{-1}, respectively [17, 18]. Exhilarating, porous structural carbon materials are a potential foothold material for doping diverse inorganic, metal oxides or organics to make up for the deficiency of pure carbon materials, which offers an opportunity to construct three-dimensional carbon-based composites with synthetic electrochemical properties. Thence, the construction of porous carbon materials has achieved all-time development in the past few years. To satisfy the claim of new technologies, the unceasing renewal of self-knowledge has to turn into a certain tendency of scientific progress. Zhang and his group designed a new flexible electrode consisting of $NiCo_2S_4$ nanosheets and N-doped carbon foam (NCF) for supercapacitors to strengthen the energy density [19]. Due to the composition characteristics and 3D structure of the electrode, the high capacitance of 877 F g^{-1} is achieved. Ma and his group synthesized 3D porous N-doped carbon frame *in-situ* clad NiO nanoparticles, showing large specific capacitance (1074 F g^{-1} at 1.0 A g^{-1}), good rate property (820 F g^{-1} at 20 A g^{-1}), and salient cycling performance (almost no attenuation) [19]. Yue and his group prepared self-healing MXene-rGO aerogel composites with 3D structure as electrode materials for micro-supercapacitors, which had 34.6 mF cm^{-2} capacitance value at 1 mV s^{-1}, and the capacitance value remained 91% after 15,000 cycles [20].

In this chapter, the latest advances in some 3D porous heteroatom doped carbon matrix composites are reviewed, and their energy storage mechanisms, structure-performance relationships are investigated, while their unique potential as supercapacitors is explored. In the following, a variety of newly designed 3D porous heteroatom doped carbon/metal oxide or carbide composites and new preparation methods, such as zero dimension (0D)/3D, 0D/2D/3D, 2D/3D, and one dimensional (1D)/2D, are introduced, and highly compressible or flexible carbon/metal carbide composites are designed and prepared according to bionics principles. Finally, some dares facing the progress of 3D porous carbon-based composite materials for supercapacitors are summarized, and the probable developing tendency is predicted.

2 Carbon Materials/Metal Oxides Composites with 3D Hierarchical Porous Structure

For pseudocapacitance materials, metal oxides (Co_3O_4, MnO_2, Mn_3O_4, NiO, and RuO_2) are intensively studied for supercapacitors [19, 21–23]. Among them, Mn_3O_4 has been widely studied for sixpenny, plentiful natural resources, salient environmental compatibility, and preeminent capacitance value [21]. Nevertheless, poor conductivity (10^{-5}–10^{-6} S cm^{-1}) and unstoppable stability make its application

limited. At present, the preparation of 3D porous micro/nanostructured materials and composites are considered a promising approach for elevating the overall property of Mn_3O_4.

2.1 3D Hierarchical Porous Composites Constructed by 0D and 3D

In this part, a 3D N/P co-doped hierarchical polyporate carbon skeleton "in situ" armored Mn_3O_4 nanoparticles (NPCM/Mn_3O_4) with 0D and 3D construction was synthesized by one-step pyrolysis [24]. Chitosan is mixed with $Mn(NO_3)_2$ solution and dilute phosphoric acid, then freeze-dried and pyrolyzed at high temperature to obtain NPCM/Mn_3O_4-1. (The preparation process is shown in Fig. 1a) NPCM/Mn_3O_4 applied to supercapacitors has excellent specific capacitance and good cycling ability. The symmetrical supercapacitor assembled from this sample exhibits a large energy density. Furthermore, all solid-state symmetrical supercapacitors assembled from this sample can withstand mechanical bending, and the salient capacitance performance and steadiness can still be maintained.

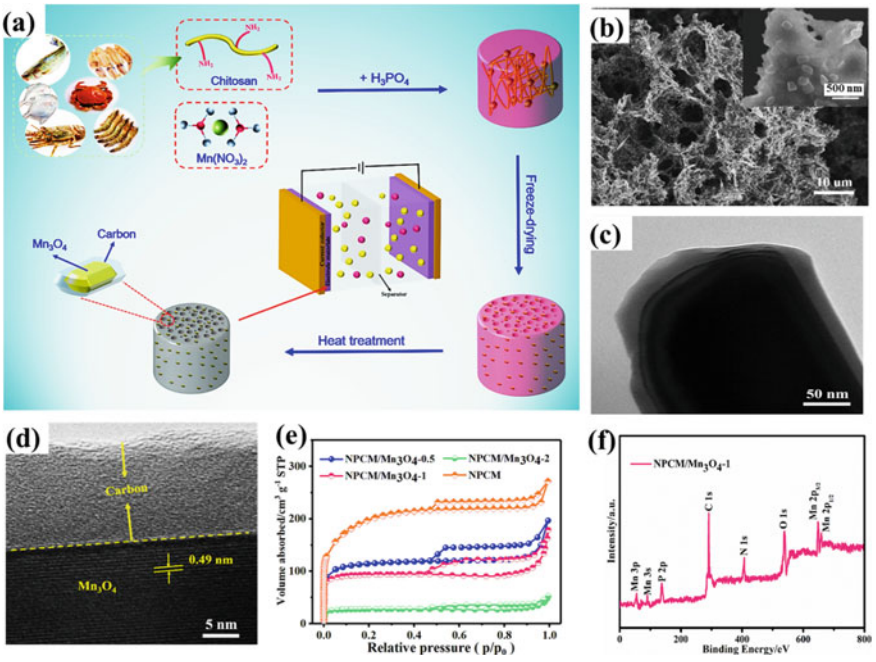

Fig. 1 **a** Preparation process for NPCM/Mn_3O_4. **b** SEM morphologies. **c** and **d** TEM micrographs of NPCM/Mn_3O_4-1. **e** N_2 adsorption/desorption isotherms. **f** XPS survey spectrum. Adapted with permission from Reference [24], Copyright (2020), Elsevier

2.1.1 Morphology, Structure, and Composition of Composites

The scanning electron microscope (SEM) images show NPCM/Mn_3O_4-1 presents a 3D pore construction in Fig. 1b, which can reduce the spread journey of ions, similar to an ion buffer pool [9]. Moreover, the Mn_3O_4 nanoparticles are evenly let into the carbon (inset of Fig. 1b). In Fig. 1c, transmission electron microscope (TEM) image presents the coated carbon layer on the surface of the single Mn_3O_4 nanoparticle. The clear lattice fringe spacing (0.49 $_{nm}$) exists in the high-resolution TEM, which echoes the (101) plane of Mn_3O_4, and the wrapped carbon layer is an irregular graphitic carbon material (Fig. 1d).

In Fig. 1e, the N_2 adsorption_desorption isotherm of NPCM/Mn_3O_4-1 indicates hierarchical pore construction [25]. The specific surface area can reach 338 $m^2\ g^{-1}$. Based on the energy storage mechanism, micropores are used to accumulate most of the charge or electrolyte ions, and electrolyte ions can be transported into the micropores through macropores and mesopores, thereby enhancing the conduction efficiency. More active sites can exist owing to the prominent surface area, and the pervasion of ions is promoted by rich porosity, thereby effectively enhancing the performance of supercapacitors [24]. In addition, the X-ray photoelectron spectroscopy (XPS) of NPCM/Mn_3O_4-1 shows the main constituent elements are P (6.58 at.%), C, N (5.35 at.%), O, and Mn (8.93 at.%) in Fig. 1f.

2.1.2 Capacitance Performance of Composites

In Fig. 2a, an aligned symmetric redox peak appears in the cyclic voltammetry (CV) curve of NPCM/Mn_3O_4-1, indicating the existence of a reversible redox reaction between the electrode and the electrolyte interface [26]. Although the current response increases with the increase of the scan rate, the curve has no obvious shape distortion, indicating the outstanding magnification performance of the electrode material. Surprisingly, there is no polarization phenomenon in all the CV curves of the sample in the potential of 1.3 V [27]. Furthermore, the similar shape of the galvanostatic charge/discharge (GCD) curve and the almost symmetrical potential platform at different current densities in Fig. 2b indicate typical pseudocapacitance behavior (Fig. 2b). Figure 2c shows that the highest specific capacitance of NPCM/Mn_3O_4-1 can reach 384 Fg^{-1}, and even at 20 A g^{-1}, the capacitance value still presents 204 Fg^{-1} and negligible IR drop. The enhancement of the capacitance performance of NPCM/Mn_3O_4-1 is due to the 3D interworking polyporate construction and high specific surface area, which prominently reduces the ion transmission journey to promote ion storage and rapid access to the active site. Figure 2d shows that the sample can maintain a capacitance of 98.2% after 5000 cycles and almost coincides with the CV curve before and after 5000 cycles (the inset of Fig. 2d), indicating excellent stability. [22] Mn_3O_4 nanoparticles are coated with a carbon layer to enhance the conductivity of NPCM/Mn_3O_4-1, while preventing the migration/aggregation of Mn_3O_4 [28].

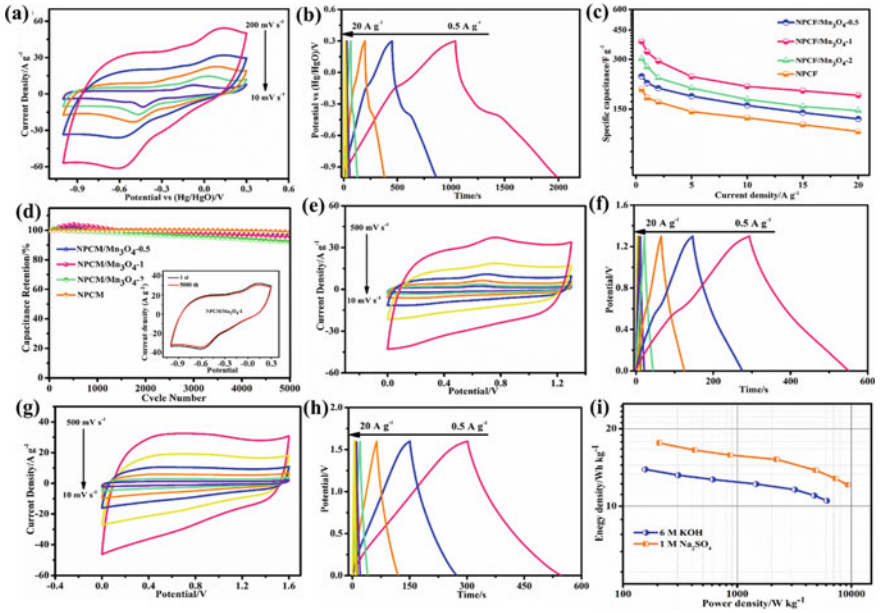

Fig. 2 Electrochemical tests (6 M KOH electrolyte): **a** CV curves of NPCM/Mn_3O_4-1; **b** GCD curves of NPCM/Mn_3O_4-1; **c** Capacitance value at different current densities; **d** Cycling stability. Electrochemical tests of the NPCM/Mn_3O_4-1 in two-electrode system; **e** CV and **f** GVD curves in 6 M KOH; **g** CV and **h** GVD curves in 1 M Na_2SO_4; **i** Ragone plot. Adapted with permission from Reference [24], Copyright (2020), Elsevier

The voltage window of the CV curve and GCD curve for NPCM/Mn_3O_4-1 based symmetrical supercapacitors (6 M KOH as electrolytes) in Fig. 2e and f can reach 1.3 V. The form of CV curves is almost unchanged, even at 500 mV s^{-1}, indicating that the capacitance behavior and magnification performance are excellent. The shape of the GCD curve of various current density tests is similar to a symmetrical triangle, indicating that the capacitance is excellent in reversibility. The specific capacitance of this device can achieve 237 F g^{-1}, and the rate property (75.5%) is outstanding in the range of 0.5–20 A g^{-1}. In the 1 M Na_2SO_4 electrolyte, the potential window of the CV curve of NPCM/Mn_3O_4-1 is as high as 0–1.6 V, as shown in Fig. 2g. The highest capacitance value can reach 186 F g^{-1}, and the capacitance retention rate is still 70.4% at 20 A g^{-1} (Fig. 2h). In addition, the energy density of 13.9 and 16.5 Wh kg^{-1} achieve in the device in 6 M KOH and 1 M Na_2SO_4 electrolytes, respectively.

2.1.3 Application for Flexible Supercapacitors

The CV curve area of the all-solid flexible symmetrical supercapacitor device under different bending states changes slightly (Fig. 3a and **inset**), indicating that the resistivity of the device changes very little in the bending state, and it has a perfect

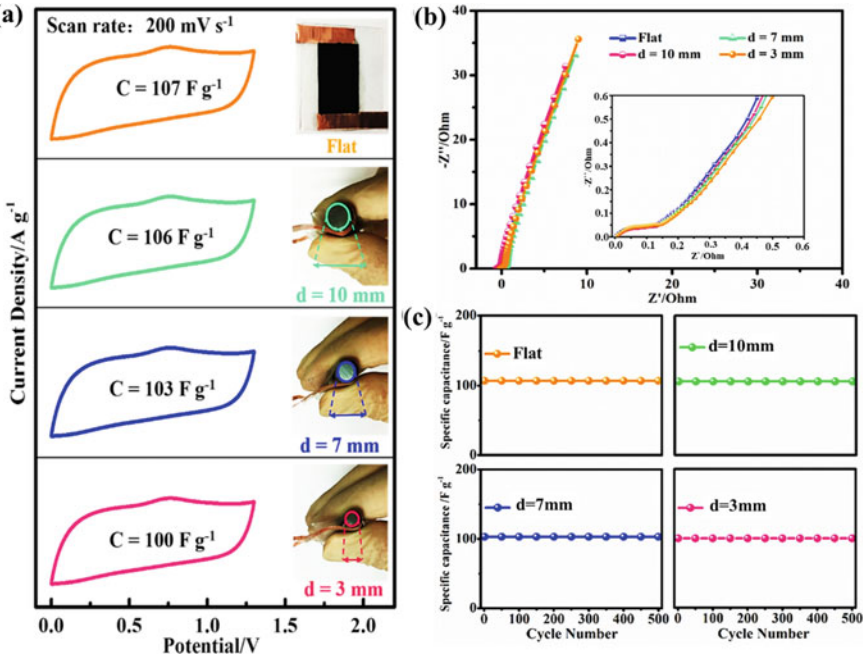

Fig. 3 Electrochemical tests of all-solid-state supercapacitors (6 M KOH gel electrolyte) under mechanical deformation: **a** CV curves; **b** EIS; **c** Capacitance value after cycles. Adapted with permission from Reference [24], Copyright (2020), Elsevier

capacitance answer. The EIS test under different bending conditions (Fig. 3b) shows that the resistance of the device changes only slightly, which is consistent with the above conclusions. In addition, more than 95% of the capacitance retention after 500 cycles of mechanical deformation (Fig. 3c) confirms the good mechanical stability and practical application potential of the device.

2.2 3D Hierarchical Porous Composites Constructed by 0D, 2D, and 3D

In this part, a 3D hierarchical porous heteroatom-doped carbon foam composite material with a combination of 0D/2D/3D structure is prepared [29]. Chitosan is reacted with dilute phosphoric acid to prepare [Chit][H_2PO_4], and then $Mn(NO_3)_2$ solution is added. After fully immersing the commercial melamine sponge in the above solution, freeze-drying, and high-temperature pyrolysis, the Mn_3O_4 embedded 3D multi-heteroatom codoped carbon sheets/carbon foams (Mn_3O_4-NPCN/CF) composites are obtained. The preparation process is shown in Fig. 4a. Mn_3O_4-NPCN/CF has a 3D transparent porous structure, and Mn_3O_4 is embedded in N/P co-doped carbon

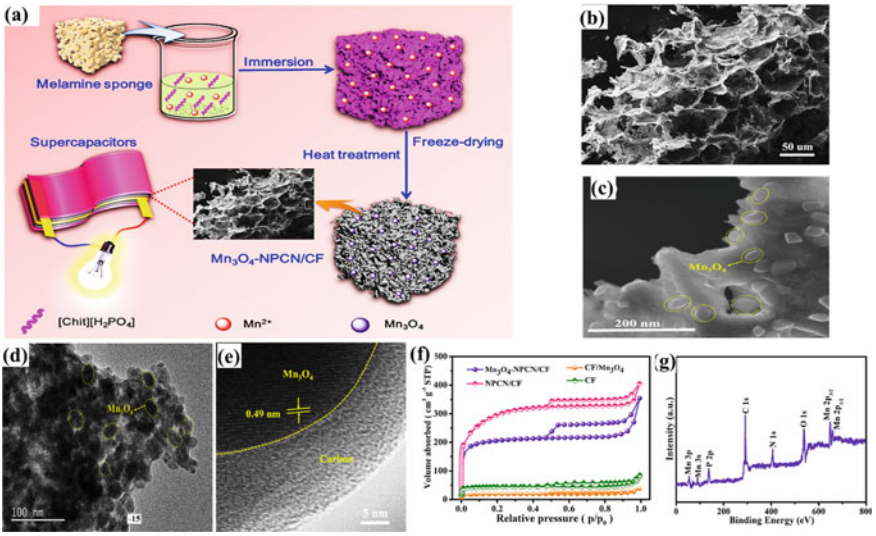

Fig. 4 **a** Schematic for preparing Mn_3O_4-NPCN/CF. **b** and **c** SEM morphologies. **d** and **e** TEM micrographs of Mn_3O_4-NPCN/CF. **f** N_2 adsorption/desorption isotherms. **g** XPS survey spectrum. Adapted with permission from Reference [29], Copyright (2020), Elsevier

sheets. Excellent capacitance performance exists in Mn_3O_4-NPCN/CF-based supercapacitors. In addition, high energy and power density are present in all-solid-state symmetrical supercapacitors devices based on Mn_3O_4-NPCN/CF in different electrolytes. During this period, it has excellent flexibility and can be used in a wide temperature environment.

2.2.1 Morphology, Structure, and Composition of Composites

Figure 4b shows that the porous interconnection framework decorated by carbon sheets is present in the Mn_3O_4-NPCN/CF composites, which promotes the transport of electrons. High-resolution SEM (Fig. 4c) and TEM images (Fig. 4d) showed that many nanoparticles (average particle size of 19.5 nm) were embedded on the surface of the carbon sheet, and the graphite carbon material was wrapped in the nanoparticles (Fig. 4e). This structure efficaciously enhances the conductivity and steadiness of the composites.

In Fig. 4f, the apparent H2-type hysteresis loop in the N_2 adsorption_desorption isotherm of Mn_3O_4-NPCN/CF confirms the hierarchical porous feature. The S_{BET} values of Mn_3O_4-NPCN/CF reach 783 $cm^2\ g^{-1}$. More micropores can achieve more charge or ion accumulation, and the rapid transport of ions to the micropores can be achieved through macropores and mesopores so that the conductivity efficiency is improved [30]. XPS in Fig. 4g shows that the Mn_3O_4-NPCN/CF composites are mainly composed of P (5.64 at. %), C, N (6.82 at. %), O, and Mn (9.87 at.%).

2.2.2 Capacitance Performance of Composites

The redox peaks and voltage plateaus are shown in all CV curves and GCD curves of Mn_3O_4-NPCN/CF composites, respectively, which are typical pseudocapacitance behaviors (Fig. 5a and b). And there is no obvious change in the shape of the curve with the scan rate, indicating that the capacitance performance is good [26]. The capacitance value of 519 F g^{-1} (Fig. 5c) realizes in the composites, and the IR drop is small under high current conditions, which is the combined effect of high S_{BET}, high content of N/P co-doping, 3D interconnection framework, and special structure [24, 31, 32]. In addition, the 96% retention rate and the overlap of the CV curve before and after 5000 cycle test (Fig. 5d) confirm the excellent steadiness of the composites.

Mn_3O_4-NPCN/CF-based symmetrical supercapacitors show excellent capacitance performance in both 6 M KOH and 1 M Na_2SO_4 electrolytes and exhibit a broad potential of 1.4 and 1.7 V [28]. The capacitance values of 305 and 208 F g^{-1} can be realized in two electrolytes with this device. Mn_3O_4-NPCN/CF-based all-solid-state symmetrical supercapacitors also have an excellent performance by CV and GVD curves (Fig. 6a–d) in PVA/KOH or Na_2SO_4 gel electrolytes, achieving a capacitance value of 207 and 141 F g^{-1}, respectively. Moreover, the energy densities of 20.7 and 20.9 Wh kg^{-1} can be achieved during this period (Fig. 6e).

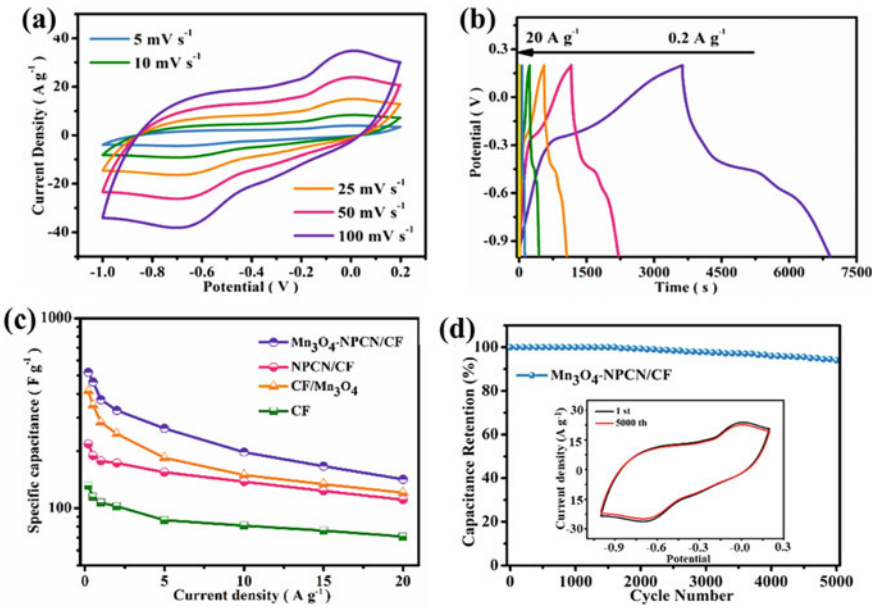

Fig. 5 Electrochemical tests in 6 M KOH: **a** CV curves of Mn_3O_4-NPCN/CF; **b** GCD curves of Mn_3O_4-NPCN/CF; **c** Capacitance value; **d** Cycling test. Adapted with permission from Reference [29], Copyright (2020), Elsevier

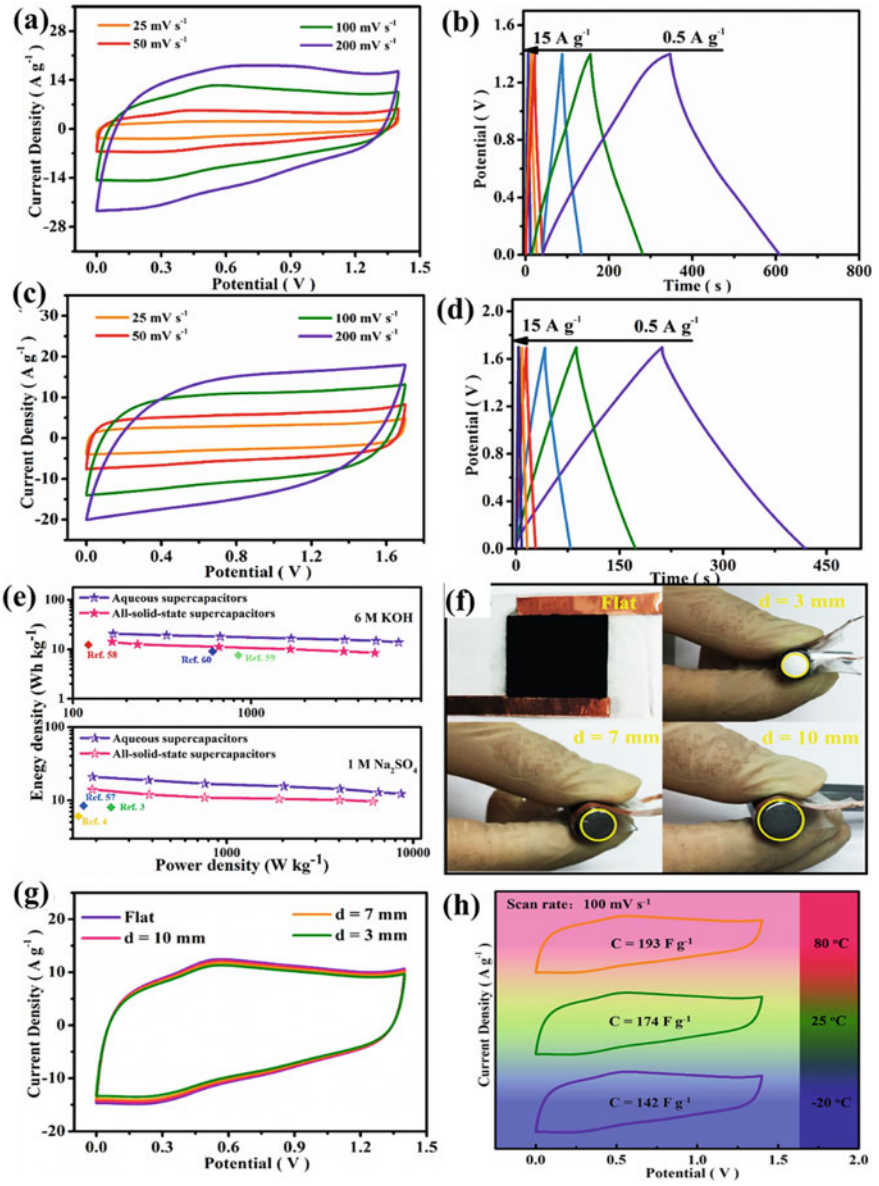

Fig. 6 Electrochemical tests of the Mn_3O_4-NPCN/CF in the two-electrode system. 6 M KOH: **a** CV and **b** GVD curves. 1 M Na_2SO_4: **c** CV and **d** GVD curves. **e** Ragone plot. All-solid-state supercapacitors under mechanical deformation: **f** Photographs tested, **g** CV curves. **h** CV curves under different temperatures. Adapted with permission from Reference [29], Copyright (2020), Elsevier

2.2.3 Application for Flexible Supercapacitors

There are only slight changes in the shape and area of the CV curve of the all-solid-state symmetrical supercapacitors device based on Mn_3O_4-NPCN/CF under different mechanical deformations (Fig. 6f and g). Even 500 times of continuous deformation means excellent capacitance behavior and stability. The unique 3D interconnection frame structure of 2D carbon sheet decoration reduces the change of resistivity during mechanical deformation. [32] In addition, the device can tolerate a wide ambient temperature (−20 to 80 °C), and the capacitance value does not change much, even after 500 cycles of testing. This is due to the steady 3D construction, high specific surface area, and prominent conductivity. Reduced charge transfer resistance [33]. These outstanding properties mean that Mn_3O_4-NPCN/CF possesses tremendous latent capacity in flexible energy storage territory.

3 Carbon Materials/Metal Carbide Composites with 3D Hierarchical Porous Structure

In recent years, 2D layered transition metal carbide/nitride MXene becomes a new type of hot material due to its exciting conductivity, stability, and mechanical properties in various fields [34]. In addition, the redox-active surface and excellent conductivity have high capacitance, so MXene has potential characteristics of electrode materials, such as Ti_3C_2Tx electrode material in the sulfuric acid electrolyte can achieve a high capacitance value (380 F g^{-1}) and outstanding cycle characteristics [34]. However, the influence of forces between 2D nanosheets, self-stacking, and aggregation are usually inevitable [35]. As a result, the specific surface area is small, the ion transport channel is limited, and the active site is unreachable [35]. According to reports, 3D structure electrodes are a possible solution. However, the porous MXene prepared by the multi-step method and template method has an unstable structure and is easily broken under the action of external mechanical strain, and its elasticity is small [20]. Secondly, the crafting procedure is complicated, high-cost, and non-eco-friendly [35]. Thence, a simple and environmentally friendly preparation process for producing an excellent performance of 3D porous MXene is the key to large-scale applications.

3.1 3D Hierarchical Porous Composites Constructed by 2D and 3D

This section proposes a simple and environmentally friendly method to prepare highly compressible 3D hollow “neuron-like” structure MXene/N doped carbon

foam (MXene/NCF) composites that combine 2D and 3D structures [36]. Commercial melamine foam is fully immersed in MXene solution, then freeze-dried and pyrolyzed at high temperature to obtain MXene/NCF composite. The preparation process is shown in Fig. 7a. This structure not only inherits the excellent mechanical stability of melamine foam, and effectively abates the accumulate and aggregation of MXene nanosheets, but also the 3D hierarchical porous hollow "neuron-like" structure and good specific surface area can be used for ion diffusion/electron transmission and highly stable and efficient channel to improve electrode dynamics and mass transmission. The composite material effectively utilizes the large-conductance and hydrophilicity of MXene and combines the 3D polyporate neuron-like construction of NCF. The composite endure 80% of the compression deformation, and the volume

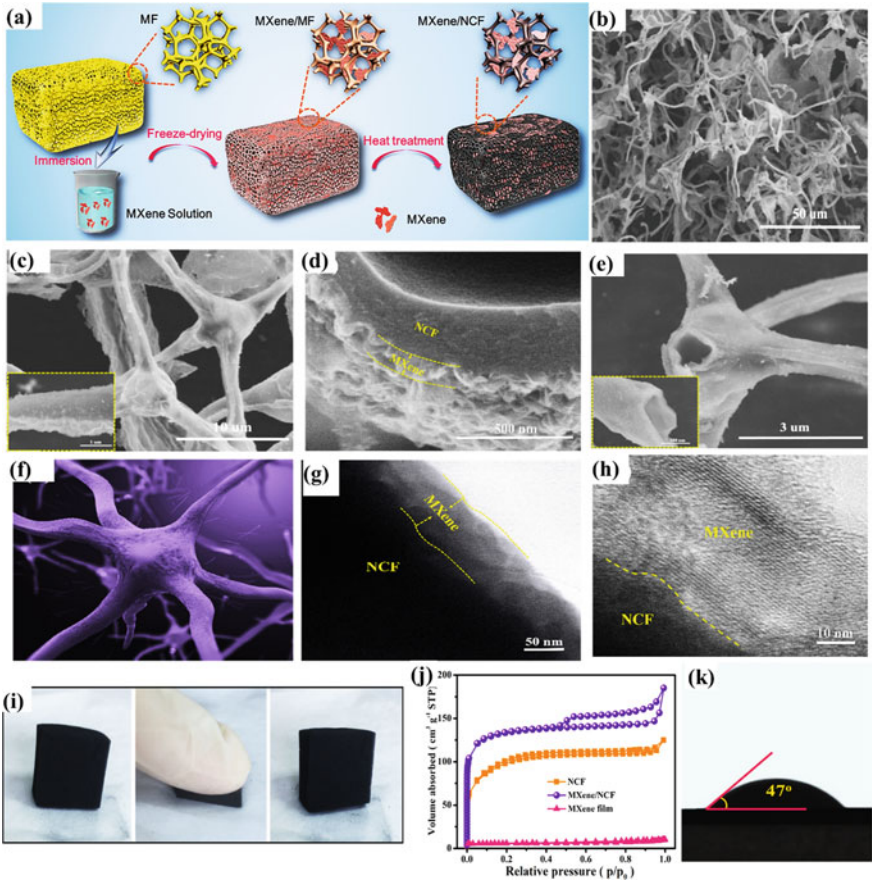

Fig. 7 **a** Schematic illustration of the fabrication processes for MXene/NCF. **b–e** SEM images. **f** Cartoon of the neuron structure. **g** and **h** TEM micrographs. **i** Digital images showing compressibility. **j** N_2 adsorption/desorption isotherms. **k** Contact angle of MXene/NCF. Adapted with permission from Reference [36], Copyright (2021), American Chemical Society

does not decrease significantly after being compressed 500 times under a constant strain of 60%. Compressible all-solid-state supercapacitor with the self-supporting electrodes of MXene/NCF still exhibits excellent electrochemical performance and stability.

3.1.1 Morphology, Structure, and Composition of Composites

The SEM image in Fig. 7b shows that MXene/NCF has a 3D porous interconnected tetrapod skeleton. In addition, there are many MXene nanosheets between and on the surface of the 3D porous tetrapod framework (Fig. 7c and inset, Fig. 7d). The surface of the irregular graphitic carbon NCF is enclosed with MXene (about 75 nm) through the TEM image (Fig. 7g and h). Most of the joints of the composite material have become hollow spheres (Fig. 7c), and the quadruped arms have a tubular structure through SEM (Fig. 7e and inset), resembling the neuron construction (Fig. 7f). Compared with the solid structure, the hollow structure is more conducive to energy storage [26]. In addition, the repeated compression test of the composite material reflects the excellent flexibility and elasticity, and severe compression has only a small effect on the composite material (Fig. 7i).

The N_2 adsorption–desorption confirmed hierarchical porous characteristics of composite (Fig. 7j), and the specific surface area can reach 517 $m^2\ g^{-1}$. In addition, the composite material can achieve a contact angle of only 47° (Fig. 7k), confirming high hydrophilicity, which effectively promotes the electrolyte to penetrate electrode material, thus effectively strengthening the energy storage performance of the double-layer capacitor [24].

3.1.2 Mechanical Property of Composites

The MXene/NCF composite material can not only tolerate a weight of 100 g but the shape and size are immediately restored to the original state as the weight decreases (digital photo in Fig. 8a). The 20, 40, 60, and 80% stress–strain curves in Fig. 8b show that there is no plastic deformation in the composite material from deformation to recovery deformation. Moreover, the stress–strain curve (Fig. 8c) of the composite material before and after 500 cycles of compression (60% strain) only slightly changed, and the relative height (Fig. 8d) remained almost unchanged [37]. SEM images under different compression levels are shown in Fig. 8e–j. In addition, the contact between the porous framework of the composite material increases the conductive path under different strains, so that the conductivity (Fig. 8k) increases with the increase of strain.

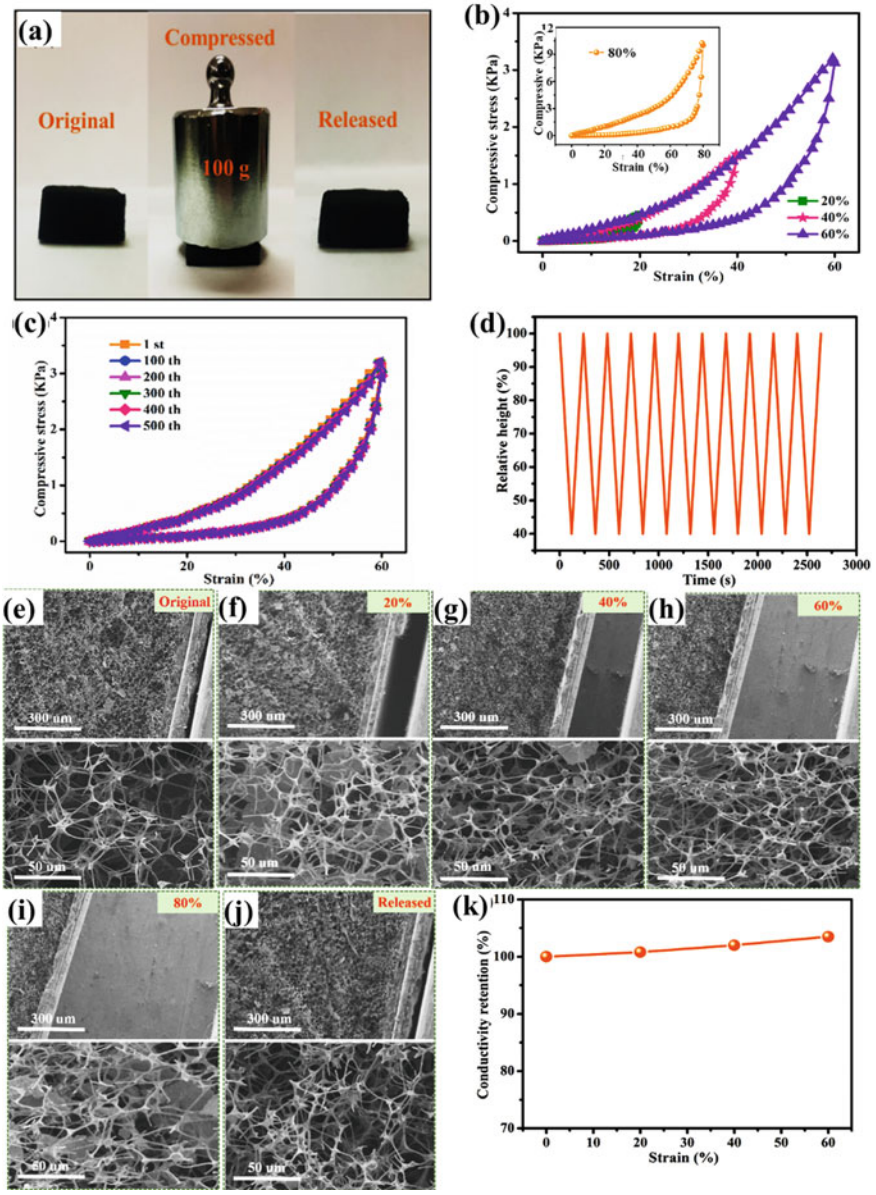

Fig. 8 Compressibility tests: **a** Digital photo, **b** Stress–strain curves at different strain, **c** Stress–strain curves by 500 cycles, **d** Height change, **e**–**j** SEM morphologies under varied compression. **k** Conductivity retention. Adapted with permission from Reference [36], Copyright (2021), American Chemical Society

3.1.3 Capacitance Performance of Composites

The shape of the CV curve of the MXene/NCF composite in the 6 M KOH electrolyte (Fig. 9a) is rectangular, even at 1000 mV s^{-1}, confirming fast ion answer and excellent rate property. The triangular GCD curve (Fig. 9b) confirms exceptional invertibility and prominent coulomb efficiency [38]. In addition, the capacitance value of 332 F g^{-1} can be realized, and the capacitance can still maintain 64% even at 100 A g^{-1} (Fig. 9c). These results are due to the synergistic effect of large specific surface area (increasing accessible sites), N atom doping (providing additional pseudocapacitance), 3D hollow interconnected neuron structure (short-range vertical transmission of ions), and the introduction of MXene (increasing electron transfer rate) [17, 39].

Under the conditions of 20, 40, 60 and 80% compressive strain, the specific capacitance of the MXene/NCF electrode still achieved 99.5, 98.6, 97.5 and 95.7% retention, respectively (Fig. 9d). During the deformation process, the contact between adjacent skeletons of MXene/NCF reduces the actual contact sites of ions and reduces the capacitance [10]. However, the capacitance under different compression conditions is reversible, even with 80% strain. In addition, the MXene/NCF electrode can still achieve 99.2% capacitance retention after 10,000 cycles (Fig. 9e), confirming outstanding stability.

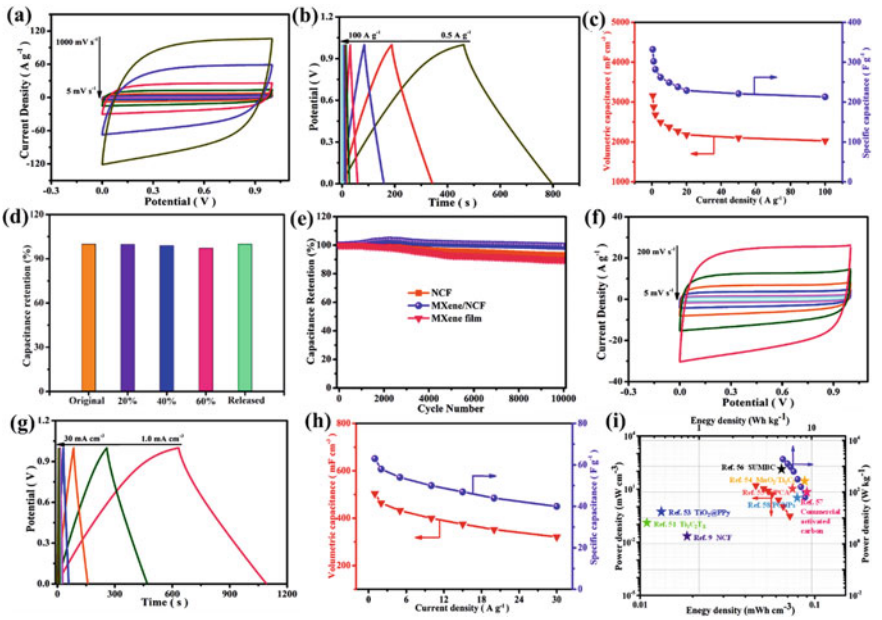

Fig. 9 Electrochemical tests: **a** CV curves; **b** GCD curves; **c** Calculated capacitance value; **d** Capacitance retention at different compression; **e** Cycling performance. Electrochemical measurements of the device; **f** CV curves; **g** GVD curves; **h** Calculated capacitance value; **i** Ragone plot. Adapted with permission from Reference [36], Copyright (2021), American Chemical Society

The CV curve (Fig. 9f) and GCD curve (Fig. 9g) of the all-solid-state supercapacitor device (SSC) both confirmed the excellent electrochemical behavior of the device. The device can achieve capacitance values of 63 F g^{-1} (Fig. 9h), even at 30 A g^{-1}, which can still reach 40 F g^{-1}. In addition, the maximum energy density of 8.75 Wh kg^{-1} is realized in this device.

3.1.4 Application for Freestanding, Highly Compressible Supercapacitors

The MXene/NCF-based SSC device does not leak electrolytes under different compression conditions, and the shape can be restored immediately after the stress is removed (Fig. 10a). The CV and GCD curves of the device have only minor differences under different compression conditions (Fig. 10b and c), and the capacitance attenuation is less than 3% (Fig. 10d), confirming the excellent structure and performance stability. In addition, the gel electrolyte layer prevents the touching between the neighboring skeleton under deformation conditions, so that the EIS curves (Fig. 10e) of the devices under different deformation conditions are almost the same in the high plateau area, confirming a constant internal contact resistance [36]. In addition, the capacitance of the device still achieved 96% after 2500 cycles under different mechanical deformation (Fig. 10f), confirming good durability, which is owing to the steady conductance, salient mechanical properties, and endurance of the MXene/NCF electrode. Moreover, two devices can light up the LED (rated voltage of 1.8 V) (Fig. 10g), and the brightness of the light-emitting diode is almost unchanged under compression and subsequent recovery conditions (Fig. 10g), further confirming the MXene/NCF-based SSC devices have great potential in compressible and durable wear-resistant electronic products.

3.2 3D Hierarchical Porous Composites Constructed by 1D and 2D

According to the principle of bionics, a new type of flexible 3D hierarchical porous "skin/bone" structure composite material, namely: MXene/biomass-derived carbon fiber (MXene/CF) heterogeneous structure was constructed [40]. Commercial cotton fiber wiper is fully immersed MXene solution, then freeze-dried and pyrolyzed at high temperature to obtain MXene/CF composite. The preparation process is shown in Fig. 11a. The experimental results show that: (1) This newly designed structure effectively weakens the accumulation of MXene nanosheets, with a specific surface area of up to 386 m^2 g^{-1}; (2) The 3D layered porous structure can promote electrolyte penetration, allowing ions to quickly enter the electrode to achieve energy storage; (3) MXene nanosheets are distributed in the carbon fiber gap to act as a bridge,

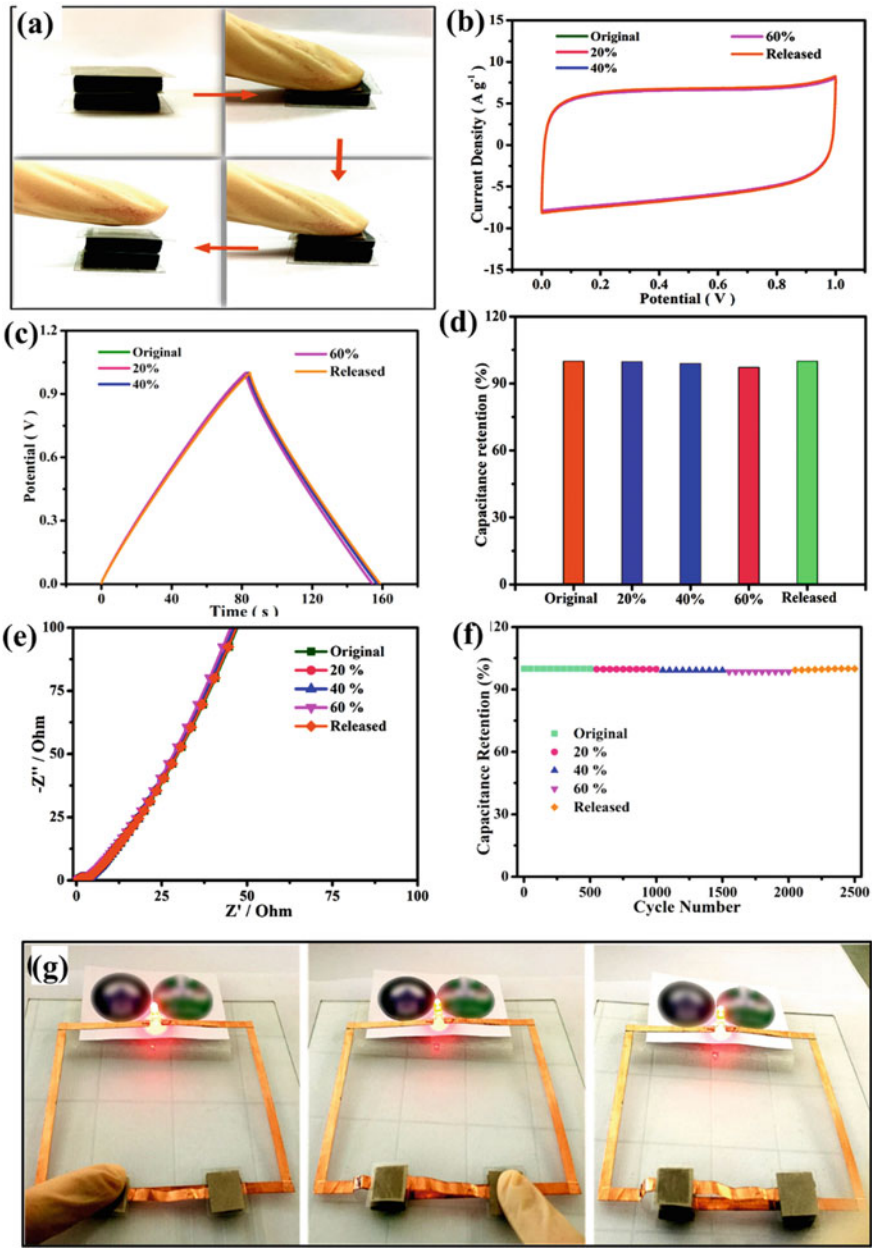

Fig. 10 Electrochemical tests of the compressible device: **a** Digital photographs; **b** CV and **c** GCD curves; **d** Capacitance retention; **e** The Nyquist impedance plot; **f** Cycling performance; **g** Photos of the device driving LED light in different states. Adapted with permission from Reference [36], Copyright (2020), American Chemical Society

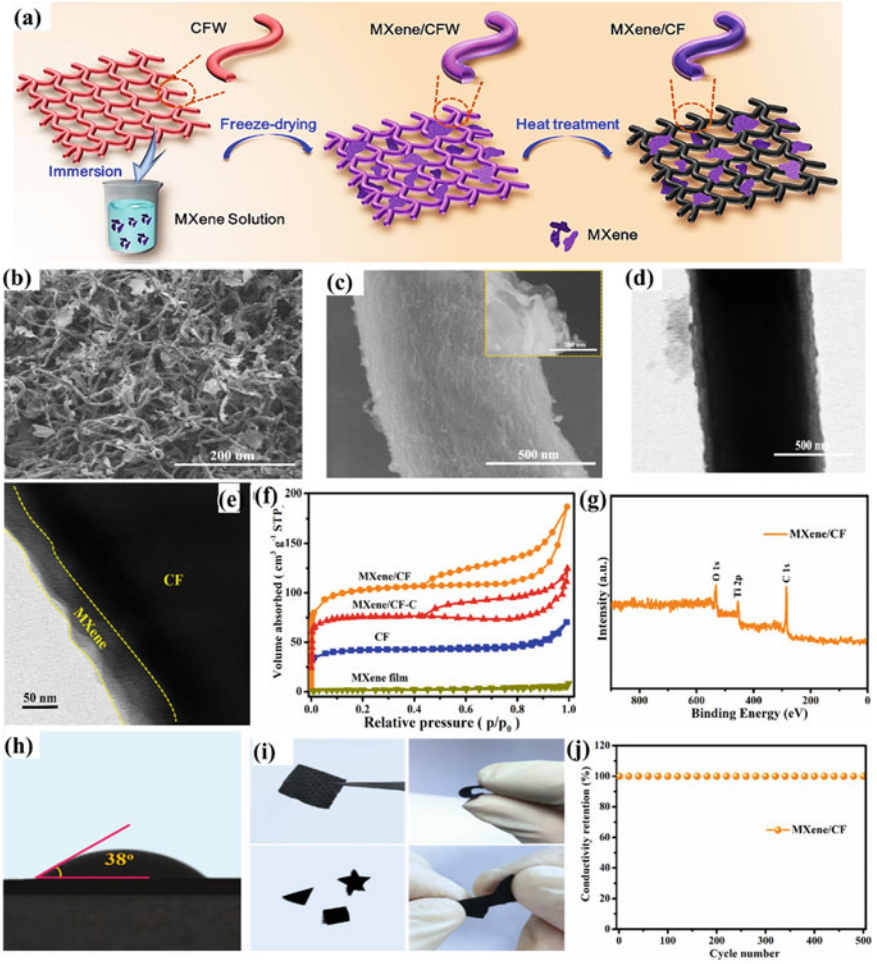

Fig. 11 **a** Schematic illustration of the fabrication processes for MXene/CF. **b–c** SEM morphologies. **d–e** TEM micrographs of MXene/CF. **f** N_2 adsorption/desorption isotherms. **g** XPS survey spectrum. **h** Contact angle of MXene/CF. **i** Digital images of mechanical properties for the MXene/CF. **j** Conductivity retention under bending conditions. Adapted with permission from Reference [40], Copyright (2021), Elsevier

providing a more efficacious and steady channel for electron transfer; (4) The existence of heterogeneous structure effectively reduces internal resistance and improves the mechanical and mechanical properties of composite materials. Cycle stability; (5) the composite material as a self-supporting electrode presents high volume-specific capacitance, excellent rate characteristics, and cycle stability.

3.2.1 Morphology, Structure, and Composition of Composites

The porous network structure formed by interlacing CF is shown in the SEM image of MXene/CF (Fig. 11b and c), and the fiber surface is wrapped with loose, porous, and wrinkled MXene (the inset of Fig. 11c), similar to the "skin/skeleton" structure. The aggregation of 2D nanosheets on the surface is effectively alleviated. The MXene nanosheets scattered between the CF networks are similar to bridges, increasing the transfer channels of electrons and ions. Therefore, the accumulation is well weakened. In the TEM image, the diameter of MXene/CF is about 790 nm (Fig. 11d), and the thickness of MXene wrapped on the CF surface is about 65 nm (Fig. 11e). The N_2 absorption–desorption curve with a typical H3 hysteresis loop (Fig. 11f) confirms the MXene/CF hierarchical porous characteristics (providing a steady and efficient aisle for ion/electron conveyance) and achieves 386 $m^2\ g^{-1}$ surface area to provide more contact sites for energy storage, thus significantly improving capacitance and Magnification performance [9, 20].

C, Ti, and O constitute the main constituent elements of MXene/CF through XPS (Fig. 11g), and have a contact angle of 36° (Fig. 11h), confirming the high hydrophilicity. In addition, different shape cutting and arbitrary deformation can be realized in MXene/CF, and the shape and size will be restored to the original state immediately after the deformation stress is relieved (Fig. 11i). The electrical conductivity changes very little during the 500 bending repetitions (Fig. 11j), confirming the high structural stability and high electrical conductivity.

3.2.2 Capacitance Performance of Composites

The rectangular-like CV curve of the self-supporting electrode MXene/CF, even at 1000 mV s^{-1} (Fig. 12a), confirms the low internal resistance, better rate performance, and ion responsiveness. [41] The high coulombic efficiency can be confirmed by the almost symmetrical GCD curve with different current densities (Fig. 12b) [30]. In addition, the hierarchical porous framework and large specific surface area enable the large capacitance value of 357 F g^{-1} to be achieved, while maintaining 63.9% at 100 A g^{-1} (Fig. 12c). Furthermore, the good stability can be confirmed by 99.8% capacitance retention after 5000 cycles (Fig. 12d) and no change in microstructure by SEM image after cycles (Fig. 12e).

The MXene/CF-based all-solid symmetrical supercapacitor device (MXene/CF-SSC) has a rectangular CV curve shape (Fig. 12f) and a symmetrical GCD curve (Fig. 12g) from 10 to 500 mV s^{-1}, confirming good rate capability, reversibility, and high Coulomb efficiency [42]. The capacitance value of 76 F g^{-1} at 0.5 A g^{-1} and 51 F g^{-1} at 50 A g^{-1} are realized (Fig. 12h), respectively. In addition, the device achieves the highest energy density of 10.6 Wh kg^{-1}), which is higher than the recently reported MXene-based SSC (Fig. 12i) [43–46].

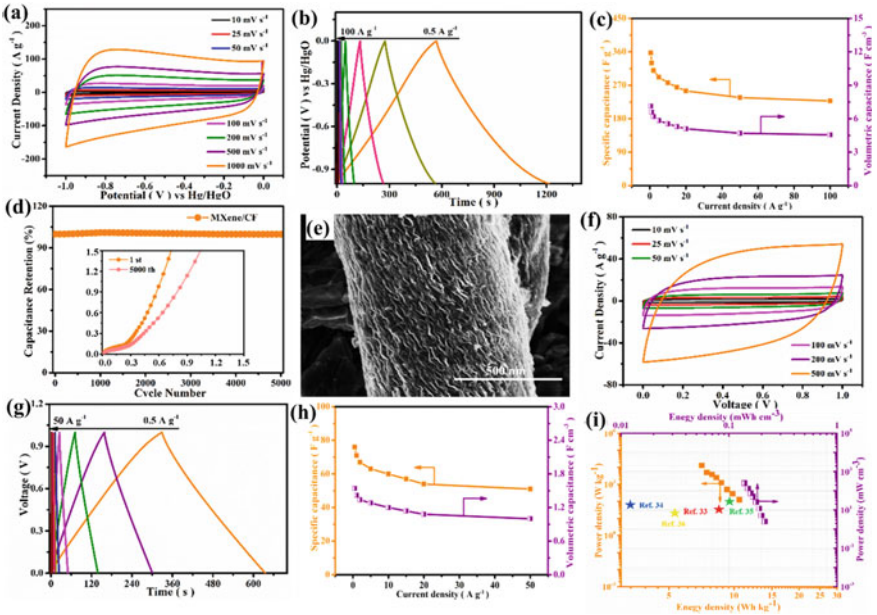

Fig. 12 Electrochemical measurements of MXene/CF in 6 M KOH: **a** CV curves; **b** GCD curves; **c** Capacitance value; **d** Cycling test. **e** SEM images after cycle stability test. Electrochemical measurements of the device; **f** CV curves; **g** GVD curves; **h** Capacitance value; **i** Ragone plot. Adapted with permission from Reference [40], Copyright (2021), Elsevier

3.2.3 Application for Flexible Supercapacitors

The CV and GCD curves of the device with little variation under mechanical deformation (Fig. 13a and b) confirm the excellent flexibility and stability. Under the maximum mechanical deformation, the capacitance attenuation is only less than 1.9% (Fig. 13c), and the capacitance value is completely restored immediately as the deformation is removed. The almost completely coincident EIS curves (Fig. 13d) in the high-frequency region under different mechanical deformations prove that the internal contact resistance changes very little. In addition, the 2.3% capacitance decay after 2500 cycles of mechanical deformation further proves the outstanding durability of the device (Fig. 13e). The above results are closely related to the stability, flexibility, and conductivity of the electrode material's microstructure. Two devices in series can illuminate a light-emitting diode with a working voltage of 1.8 V (Fig. 13f), and there is almost no change in brightness under mechanical change and recovery, indicating the huge application potential of MXene/CF in the field of wearable electronic devices.

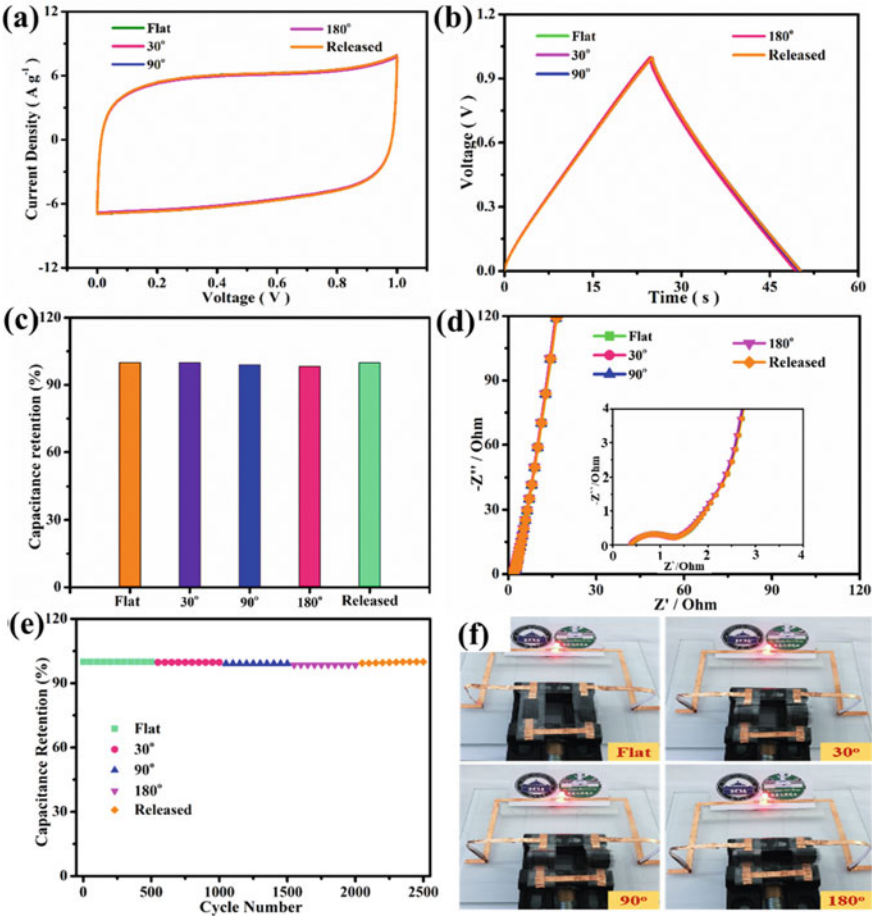

Fig. 13 Electrochemical properties of the device under mechanical deformation: **a** CV curves; **b** GCD curves; **c** Capacitance retention; **d** Nyquist impedance plot; **e** Cycling performance; **f** Photos of the device driving LED light. Adapted with permission from Reference [40], Copyright (2021), Elsevier

4 Prospects and Challenge

3D hierarchical porous carbon/metal oxides or carbide composite has become more and more popular in the research field due to many excellent characteristics. Moreover, a hierarchical porous structure helps prevent the re-accumulation of metal oxides or carbides to obtain a large charge contact area, so it is particularly popular. Abundant ion adsorption/active sites can be achieved through micropores, and ions can quickly diffuse into the electrode material through mesopores and macropores to generate electrochemical reactions, thereby achieving high power density [47]. Therefore, it is important to make full use of the unique porous structure. So far,

only moderate specific surface area, specific capacitance, and energy density can be achieved in three-dimensional hierarchical porous carbon/metal oxide or carbide composite materials, which is still far behind the theoretical value. Before further exploration can be made to fully utilize the synergistic effects of the components of three-dimensional porous carbon/metal oxide or carbide composites, the optimal 3D hierarchical porous structure must be designed first. At present, The following main challenges remain: (i) How to develop low-cost, environmentally friendly technologies; (ii) How to precisely control the pore structure distribution; (iii) How to balance the proportion of different pore sizes.

In addition, there are still challenges in obtaining 3D hierarchical porous carbon/metal oxide or carbide composite materials. While maintaining the porous properties, it is the key to giving full play to the role of other ingredients besides the carbon material. A significant increase in the energy density of carbon materials can be achieved by the introduction of metal oxide or carbide materials. However, due to the introduction of metal oxide or carbide materials into the composite material, the internal resistance and weight will increase, thereby reducing the power density of the composite material, and making it difficult to achieve the goal of light electrode materials for the development of portable electronic products. Therefore, balancing the two is the key. In the future, the focus of research may focus on the following points: (i) How to dominate the percentage of both; (ii) How to maintain the vintage architecture of porous carbon materials when other architecture in drafted; (iii) The complex hybrid structure also makes the true mechanism of charge storage difficult to understand.

This chapter is focused on the novel 3D hierarchical porous carbon/metal oxide or carbide composite electrode materials. From this review, it can be inferred that the 3D hierarchical porous carbon/metal oxide or carbide composite material has broad prospects in the future development of supercapacitors. Although some reported achievements increase confidence, the exploration of new generation supercapacitors should not stop at the initial stage. There is still a long way to go before mass production is achieved: (1) To control the interface reaction between the electrode and the electrolyte, it is necessary to understand the energy storage mechanism in depth. In the process of exploration, advanced simulation and modeling studies are added to reveal the nano-scale electrochemical mechanism. (2) "Technology is always limited by available materials", this applies in the past, or today, or the future. In recent years, a series of new two-dimensional materials with unique electronic, chemical, and surface properties have been successfully developed to meet the needs of new materials, such as germanene, silicone, butene and borene, and they have shown tremendous latent capacity in supercapacitors. The combination of carbon materials and these nanomaterials to construct three-dimensional hierarchical porous composite materials is expected to produce a new generation of supercapacitor electrodes with high energy and power density shortly. As we all know, the high-purity mass production of new nanomaterials is the ultimate challenge. (3) The rapid popularization of intelligent electronic technology needs the ongoing evolution of intelligent power with integrated stimulus responses. It will be very interesting to integrate more functions into an energy storage device.

References

1. P. Simon, Y. Gogotsi, Materials for electrochemical capacitors. Nat. Mater. **7**, 845–854 (2008)
2. Q. Wang, F. Liu, Z. Jin, X. Qiao, H. Huang, X. Chu, D. Xiong, H. Zhang, Y. Liu, W. Yang, Hierarchically divacancy defect building dual-activated porous carbon fibers for high-performance energy-storage devices. Adv. Funct. Mater. **30**, 2002580 (2020)
3. Z. Yu, L. Tetard, L. Zhai, J. Thomas, Supercapacitor electrode materials: nanostructures from 0 to 3 dimensions, energ. Environ. Sci. **8**, 702–730 (2015)
4. S. Kumar, G. Saeed, L. Zhu, K.N. Hui, N.H. Kim, J.H. Lee, 0D to 3D carbon-based networks combined with pseudocapacitive electrode material for high energy density supercapacitor: A review. Chem. Eng. J. **403**, 126352 (2021)
5. L. Sun, Y. Yao, Y. Zhou, L. Li, H. Zhou, M. Guo, S. Liu, C. Feng, Z. Qi, B. Gao, Solvent-free synthesis of N/S-codoped hierarchically porous carbon materials from protic ionic liquids for temperature-resistant, flexible supercapacitors. ACS Sustain. Chem. Eng. **6**, 13494–13503 (2018)
6. M. Sarno, Chapter 22—Nanotechnology in energy storage: the supercapacitors, in *Studies in Surface Science and Catalysis*, ed. by A. Basile, G. Centi, M. De Falco, G. Iaquaniello (Elsevier, 2020)
7. S. Sahoo, C.S. Rout, Facile electrochemical synthesis of porous manganese-cobalt-sulfide based ternary transition metal sulfide nanosheets architectures for high performance energy storage applications. Electrochim. Acta **220**, 57–66 (2016)
8. M.F. El-Kady, Y. Shao, R.B. Kaner, Graphene for batteries, supercapacitors and beyond. Nat. Rev. Mater. **1**, 1–14 (2016)
9. L. Sun, Y. Zhou, L. Li, H. Zhou, X. Liu, Q. Zhang, B. Gao, Z. Meng, D. Zhou, Y. Ma, Facile and green synthesis of 3D honeycomb-like N/S-codoped hierarchically porous carbon materials from bio-protic salt for flexible, temperature-resistant supercapacitors. Appl. Surf. Sci. **467–468**, 382–390 (2019)
10. K. Xiao, L.X. Ding, G. Liu, H. Chen, S. Wang, H. Wang, Freestanding, hydrophilic nitrogen-doped carbon foams for highly compressible all solid-state supercapacitors. Adv. Mater. **28**, 5997–6002 (2016)
11. S. Long, Y. Feng, F. He, J. Zhao, T. Bai, H. Lin, W. Cai, C. Mao, Y. Chen, L. Gan, J. Liu, M. Ye, X. Zeng, M. Long, Biomass-derived, multifunctional and wave-layered carbon aerogels toward wearable pressure sensors, supercapacitors and triboelectric nanogenerators. Nano Energy **85**, 105973 (2021)
12. T.P. Mofokeng, Z.N. Tetana, K.I. Ozoemena, Defective 3D nitrogen-doped carbon nanotube-carbon fibre networks for high-performance supercapacitor: transformative role of nitrogen-doping from surface-confined to diffusive kinetics. Carbon **169**, 312–326 (2020)
13. L. Fan, L. Yang, X. Ni, J. Han, R. Guo, C. Zhang, Nitrogen-enriched meso-macroporous carbon fiber network as a binder-free flexible electrode for supercapacitors. Carbon **107**, 629–637 (2016)
14. J.P. Paraknowitsch, A. Thomas, Doping carbons beyond nitrogen: an overview of advanced heteroatom doped carbons with boron, sulphur and phosphorus for energy applications. Energ. Environ. Sci. **6**, 2839 (2013)
15. D. Zhu, J. Jiang, D. Sun, X. Qian, Y. Wang, L. Li, Z. Wang, X. Chai, L. Gan, M. Liu, A general strategy to synthesize high-level N-doped porous carbons via Schiff-base chemistry for supercapacitors. J. Mater. Chem. A **6**, 12334–12343 (2018)
16. X. Ma, G. Ning, Y. Kan, Y. Ma, C. Qi, B. Chen, Y. Li, X. Lan, J. Gao, Synthesis of S-doped mesoporous carbon fibres with ultrahigh S concentration and their application as high performance electrodes in supercapacitors. Electrochim. Acta **150**, 108–113 (2014)
17. L. Sun, H. Zhou, L. Li, Y. Yao, H. Qu, C. Zhang, S. Liu, Y. Zhou, Double soft-template synthesis of nitrogen/sulfur-codoped hierarchically porous carbon materials derived from protic ionic liquid for supercapacitor. ACS Appl. Mater. Interfaces **9**, 26088–26095 (2017)

18. L. Li, Y. Zhou, H. Zhou, H. Qu, C. Zhang, M. Guo, X. Liu, Q. Zhang, B. Gao, N/P codoped porous carbon/one-dimensional hollow tubular carbon heterojunction from biomass inherent structure for supercapacitors. ACS Sustain. Chem. Eng. **7**, 1337–1346 (2018)
19. L. Shen, J. Wang, G. Xu, H. Li, H. Dou, X. Zhang, $NiCo_2S_4$ nanosheets grown on nitrogen-doped carbon foams as an advanced electrode for supercapacitors. Adv. Energy Mater. **5**, 1400977 (2015)
20. Y. Yue, N. Liu, Y. Ma, S. Wang, W. Liu, C. Luo, H. Zhang, F. Cheng, J. Rao, X. Hu, J. Su, Y. Gao, Highly Self-healable 3D microsupercapacitor with MXene-graphene composite aerogel. ACS Nano **12**, 4224–4232 (2018)
21. S. Yang, X. Song, P. Zhang, L. Gao, Crumpled nitrogen-doped graphene-ultrafine Mn3O4 nanohybrids and their application in supercapacitors. J. Mater. Chem. A **1**, 14162 (2013)
22. L. Ma, G. Sun, J. Ran, S. Lv, X. Shen, H. Tong, One-pot template-free strategy toward 3D hierarchical porous nitrogen-doped carbon framework in situ armored homogeneous NiO nanoparticles for high-performance asymmetric supercapacitors. ACS Appl. Mater. Interfaces **10**, 22278–22290 (2018)
23. R. Xie, H. Huang, X. Qi, G. Wei, Significant enhancement of the electrochemical performance of hierarchical Co_3O_4 electrodes for supercapacitors via architecture design and training activation. J. Energy Storage **35**, 102258 (2021)
24. L. Sun, G. Song, Y. Sun, Q. Fu, C. Pan, One-step construction of 3D N/P-codoped hierarchically porous carbon framework in-situ armored Mn_3O_4 nanoparticles for high-performance flexible supercapacitors. Electrochim. Acta **333**, 135496 (2020)
25. G. Zhao, C. Chen, D. Yu, L. Sun, C. Yang, H. Zhang, Y. Sun, F. Besenbacher, M. Yu, One-step production of O-N-S co-doped three-dimensional hierarchical porous carbons for high-performance supercapacitors. Nano Energy **47**, 547–555 (2018)
26. H. Jia, Z. Wang, C. Li, X. Si, X. Zheng, Y. Cai, J. Lin, H. Liang, J. Qi, J. Cao, J. Feng, W. Fei, Designing oxygen bonding between reduced graphene oxide and multishelled Mn_3O_4 hollow spheres for enhanced performance of supercapacitors. J. Mater. Chem. A **7**, 6686–6694 (2019)
27. D. Hulicova-Jurcakova, A.M. Puziy, O.I. Poddubnaya, F. Suarez-Garcia, J.M.D. Tascon, G.Q. Lu, Highly stable performance of supercapacitors from phosphorus-enriched carbons. J. Am. Chem. Soc. **131**, 5026–5027 (2009)
28. H.-P. Feng, L. Tang, G.-M. Zeng, J. Tang, Y.-C. Deng, M. Yan, Y.-N. Liu, Y.-Y. Zhou, X.-Y. Ren, S. Chen, Carbon-based core-shell nanostructured materials for electrochemical energy storage. J. Mater. Chem. A **6**, 7310–7337 (2018)
29. L. Sun, Q. Fu, C. Pan, Mn_3O_4 embedded 3D multi-heteroatom codoped carbon sheets/carbon foams composites for high-performance flexible supercapacitors. J. Alloys Comp. **849**, 156666 (2020)
30. Y. Wang, N. Xiao, Z. Wang, Y. Tang, H. Li, M. Yu, C. Liu, Y. Zhou, J. Qiu, Ultrastable and high-capacity carbon nanofiber anodes derived from pitch/polyacrylonitrile for flexible sodium-ion batteries. Carbon **135**, 187–194 (2018)
31. X. Wang, F. Wan, L. Zhang, Z. Zhao, Z. Niu, J. Chen, Large-area reduced graphene oxide composite films for flexible asymmetric sandwich and microsized supercapacitors. Adv. Funct. Mater. **28**, 1707247 (2018)
32. W. Li, X. Xu, C. Liu, M.C. Tekell, J. Ning, J. Guo, J. Zhang, D. Fan, Ultralight and binder-free all-solid-state flexible supercapacitors for powering wearable strain sensors. Adv. Funct. Mater. **27**, 1702738 (2017)
33. F. Lai, J. Feng, R. Yan, G.-C. Wang, M. Antonietti, M. Oschatz, Breaking the limits of ionic liquid-based supercapacitors: mesoporous carbon electrodes functionalized with manganese oxide nanosplotches for dense, stable, and wide-temperature energy storage. Adv. Funct. Mater. **28**, 1801298 (2018)
34. F. Bu, M.M. Zagho, Y. Ibrahim, B. Ma, A. Elzatahry, D. Zhao, Porous MXenes: Synthesis, structures, and applications. Nano Today **30**, 100803 (2020)
35. X. Zhang, X. Liu, S. Dong, J. Yang, Y. Liu, Template-free synthesized 3D macroporous MXene with superior performance for supercapacitors. Appl. Mater. Today **16**, 315–321 (2019)

36. L. Sun, G. Song, Y. Sun, Q. Fu, C. Pan, MXene/N-doped carbon foam with three-dimensional hollow neuron-like architecture for freestanding, highly compressible all solid-state supercapacitors. ACS Appl. Mater. Interfaces **12**, 44777–44788 (2020)
37. X. Lu, M. Yu, G. Wang, Y. Tong, Y. Li, Flexible solid-state supercapacitors: design, fabrication and applications. Energ. Environ. Sci. **7**, 2160 (2014)
38. L. Shen, X. Zhou, X. Zhang, Y. Zhang, Y. Liu, W. Wang, W. Si, X. Dong, Carbon-intercalated $Ti_3C_2T_x$ MXene for high-performance electrochemical energy storage. J. Mater. Chem. A **6**, 23513–23520 (2018)
39. A.E. Allah, J. Wang, Y.V. Kaneti, T. Li, A.A. Farghali, M.H. Khedr, A.K. Nanjundan, B. Ding, H. Dou, X. Zhang, B. Yoshio, Y. Yamauchi, Auto-programmed heteroarchitecturing: Self-assembling ordered mesoporous carbon between two-dimensional $Ti_3C_2T_x$ MXene layers. Nano Energy **65**, 103991 (2019)
40. L. Sun, Q. Fu, C. Pan, Hierarchical porous "skin/skeleton"-like MXene/biomass derived carbon fibers heterostructure for self-supporting, flexible all solid-state supercapacitors. J. Hazard. Mater. **410**, 124565 (2021)
41. K. Wang, B. Zheng, M. Mackinder, N. Baule, H. Qiao, H. Jin, T. Schuelke, Q.H. Fan, Graphene wrapped MXene via plasma exfoliation for all-solid-state flexible supercapacitors. Energy Storage Mater. **20**, 299–306 (2019)
42. Q. Yang, Z. Xu, B. Fang, T. Huang, S. Cai, H. Chen, Y. Liu, K. Gopalsamy, W. Gao, C. Gao, MXene/graphene hybrid fibers for high performance flexible supercapacitors. J. Mater. Chem. A **5**, 22113–22119 (2017)
43. A.M. Navarro-Suárez, K.L. Van Aken, T. Mathis, T. Makaryan, J. Yan, J. Carretero-González, T. Rojo, Y. Gogotsi, Development of asymmetric supercapacitors with titanium carbide-reduced graphene oxide couples as electrodes. Electrochim. Acta **259**, 752–761 (2018)
44. K. Krishnamoorthy, P. Pazhamalai, S. Sahoo, S.-J. Kim, Titanium carbide sheet based high performance wire type solid state supercapacitors. J. Mater. Chem. A **5**, 5726–5736 (2017)
45. W. Liu, Z. Wang, Y. Su, Q. Li, Z. Zhao, F. Geng, Molecularly Stacking manganese dioxide/titanium carbide sheets to produce highly flexible and conductive film electrodes with improved pseudocapacitive performances. Adv. Energy Mater. **7**, 1602834 (2017)
46. X. Wang, Q. Fu, J. Wen, X. Ma, C. Zhu, X. Zhang, D. Qi, 3D $Ti_3C_2T_x$ aerogels with enhanced surface area for high performance supercapacitors. Nanoscale **10**, 20828–20835 (2018)
47. C. Xiong, B. Li, X. Lin, H. Liu, Y. Xu, J. Mao, C. Duan, T. Li, Y. Ni, The recent progress on three-dimensional porous graphene-based hybrid structure for supercapacitor. Compos. B. Eng. **165**, 10–46 (2019)

Nanostructured 2D Transition Metal Dichalcogenides (TMDs) as Electrodes for Supercapacitor

Raheela Naz, Tahir Rasheed, Suleman Khan, and Muhammad Bilal

Abstract To satisfy the increasing global demand for energy, it is urgent to develop new energy sources and energy storage devices. In this respect, supercapacitors are potential energy storage devices due to their properties of high-power density, long cyclic stability, and rapid charge/discharge ability. The performance of the supercapacitors mainly relies on the electrode materials with high electrical conductivity, easy charge (ion/electron) transportation, adequate porosity, and high surface area. To date, 2D materials such as transition metal dichalcogenides (TMDs), reduced graphene oxide (RGO), transition metal oxides (TMOs), and their composites have been investigated as commendable electrode materials for high-performance supercapacitors due to their outstanding merits including high specific surface area, additional electrochemical active sites, high conductivity, and single-layer morphology.

Keywords Transition metal dichalcogenides · 1T-molybdenum disulfide · Supercapacitors

1 Introduction

For several decades, two-dimensional (2D) transition metal dichalcogenides (TMDs) have been known as layered material, but their hi-tech properties have not been recognized until the discovery of graphene, a 2D carbon allotrope [1]. Now, 2D-TMDs

R. Naz · S. Khan
Institute of Engineering and Technology, NFC, Multan, Pakistan

T. Rasheed (✉)
Interdisciplinary Research Center for Advanced Materials, King Fahd University of Petroleum and Minerals (KFUPM), Dhahran 31261, Saudi Arabia
e-mail: tahir.rasheed@hotmail.com

M. Bilal (✉)
School of Life Science and Food Engineering, Huaiyin Institute of Technology, Huaian 223003, China
e-mail: bilaluaf@hotmail.com

S. Thomas et al. (eds.), *Nanostructured Materials for Supercapacitors*,
Advances in Material Research and Technology,
https://doi.org/10.1007/978-3-030-99302-3_15

have arisen as attractive materials with their exotic physicochemical properties, like good semiconducting nature, excellent chemical stability, exceptional mechanical properties, large surface area, high catalytic activity, and low cost [2, 3]. Recently, 2D TMDs have been investigated in several applications, such as batteries, supercapacitors, solar cells, transistors, electrocatalysts, and optical display [2]. In electrochemical applications, 2D TMDs with abundant active edge sites can perform excellent catalytic activities [4] and their 2D layered structure having large surface area and interlayer space can help in easy ion transportation/intercalation, which is beneficial for energy storage devices [5]. However, the easy restacking possibility of the layered structure, low electrical conductivity, and poor electrical contact of 2D TMDs prohibit their electrochemical performance [6]. To overcome these challenges, the hybridization of 2D TMDs with highly conductive materials and inducing defects or holes on the sheets of TMDs have become attractive routes for improving their electrochemical performance [7].

The increasing demand for global energy and the depletion of available energy sources are motivating scientists to explore other energy sources and develop energy storage devices with high performance, low cost, and environment-friendly behavior [8]. Numerous electrochemical energy conversion and storage devices, like Li-ion batteries, hydrogen evolution reaction, solar cell, and supercapacitor are becoming attractive techniques to solve the global energy problems [9]. As one of the energy storage devices, supercapacitors have great importance due to their rapid charge/discharge ability, high power density, long service life, and environmental friendliness [10]. To develop a supercapacitor, one of the key factors is to explore electrode materials with superior performance.

2 2-Dimensional Transition Metal Dichalcogenides (2D TMDs)

TMDs are layered materials having the general formula (MX_2), in which transition metal (M = Mo, W, V, Re, Ta, and Ti) layer is sandwiched between two chalcogen (X = S, Se, and Te) atomic layers. Each layer is attracted by a neighboring layer due to weak van der Waals forces. On the base of atomic configuration, 2D TMDs have different crystal phases, such as hexagonal (2H), trigonal (1T), and distorted phase (T') [11]. The atomic ratio in layered TMDs is one transitional metal to two chalcogen atoms (MX_2) except in some cases of quintuple layers (M_2X_3) and metal chalcogenides (MX) [12].

2D TMDs family covers a wide range of bandgap including visible and infrared range, as shown in Fig. 1. Most of the semiconducting 2D TMDS in monolayer, such as MoS_2, $MoSe_2$. $MoTe_2$, WS_2, and WSe_2 reveal a direct bandgap, but this direct band can transit to indirect bandgap in bulk form. Depending on the crystal phase, most 2D TMDs could be metallic, semiconducting, and superconducting. For example, 1T-phase (metallic phase) of MoS_2 is 10^7 times more conductive than 2H MoS_2

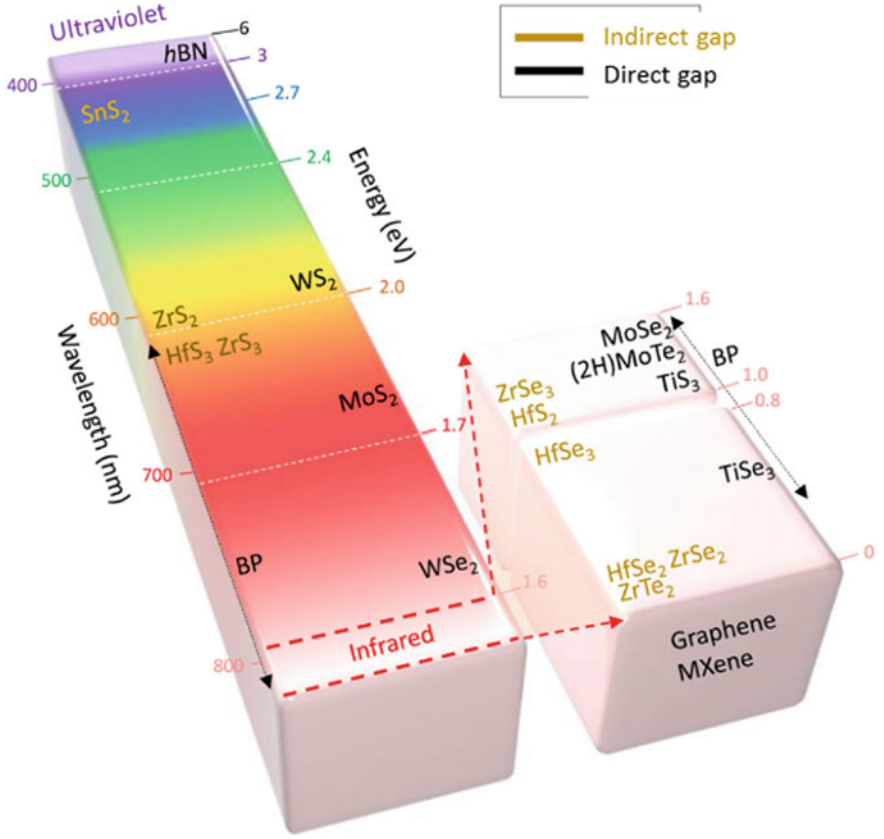

Fig. 1 The bandgap of different 2D layered materials. Adapted from Reference [2] copyright 2017, Elsevier

(semiconducting phase) [13]. The stability of the 2D TMDs phases is different in different materials. Mostly the stable phase of MX_2 is a 2H phase, such as MoS_2 has a more stable 2H-phase compared to 1T-phase [13] and WTe_2 has a more stable 1T and 1T′ phase than the 2H phase [14].

As elastic properties, single-layered (SL) MoS_2, $MoSe_2$, WS_2, and WSe_2 show outstanding elastic performance due to the low modulus values as compared to graphene materials [15]. Additionally, 2D TMDs show excellent electronic properties with high carrier mobility of 200 cm^2/VS (demonstrated by MoS_2 transistors) [16] and high thermal conductivity (27.9–88.8 W mK^{-1}) [17].

3 Advantages of 2D TMDs Nanostructures

2D TMDs nanostructured materials with their exotic properties like excellent chemical stability, positive lattice thermal expansion coefficient, and good thermal stability, have become popular among researchers for electronic applications [18]. The high surface area and wide range of oxidation states of transition metals in 2D TMDs, make these materials favorable for energy storage devices [19]. Due to the low cost, high density of electroactive sites along the edges of sheets, and electrochemical stability of 2D TMDs, they offer promise to use in electrocatalyst applications especially for HER [20]. In addition, the sheet-like structured 2D TMDs with larger interlayer spacing and weak van der Waal interaction between layers offer easy ion and molecular intercalation, making 2D TMDs attractive materials for several electrochemical applications [21].

In view of the interesting structure and properties of 2D TMDs, their applications cover numerous fields, such as sensors, energy conversion systems, electronic devices, and energy storage technology as shown in Fig. 1.3 [22]. To date, the main challenges related to the synthesis of 2D TMDs are the low electrical conductivity and restacking of layers, compromise of their applications due to the reduction of active sites, and high charge transfer resistance [23]. To overcome the above problems, the development of heterostructure of 2D TMDs with highly conductive materials having a large surface area (graphene) is the main compulsory step for future applications.

4 Molybdenum Disulfide (MoS_2) as 2D TMDs

Among various 2D TMDs, MoS_2 has more attraction for researchers due to its unique properties. MoS_2 has a layered structure, in which S-Mo-S layers have weak van der Waals interactions with an interlayer spacing of 0.615 nm, obviously larger than that of graphite 0.335 nm [24]. The atomic structure, properties, and synthetic strategies have been discussed in detail in the next sections.

4.1 Atomic Structure of MoS_2

According to the arrangement of Mo atoms in a single layer, the MoS_2 structure can be classified into two classes: hexagonal MoS_2 (2H) and tetragonal MoS_2 (1 and 1T′, Fig. 2a) [25]. In 2H-MoS_2, the Mo atoms have trigonal prismatic coordination in the Mo layer, and this layer is sandwiched between two S layers and this phase is semiconductor [26]. In comparison, the tetragonal MoS_2 including ordered 1T- and distorted 1T′-MoS_2 is a metallic phase, the arrangement of Mo atoms in octahedral coordination [27]. The study of scanning transmission electron microscope (STEM)

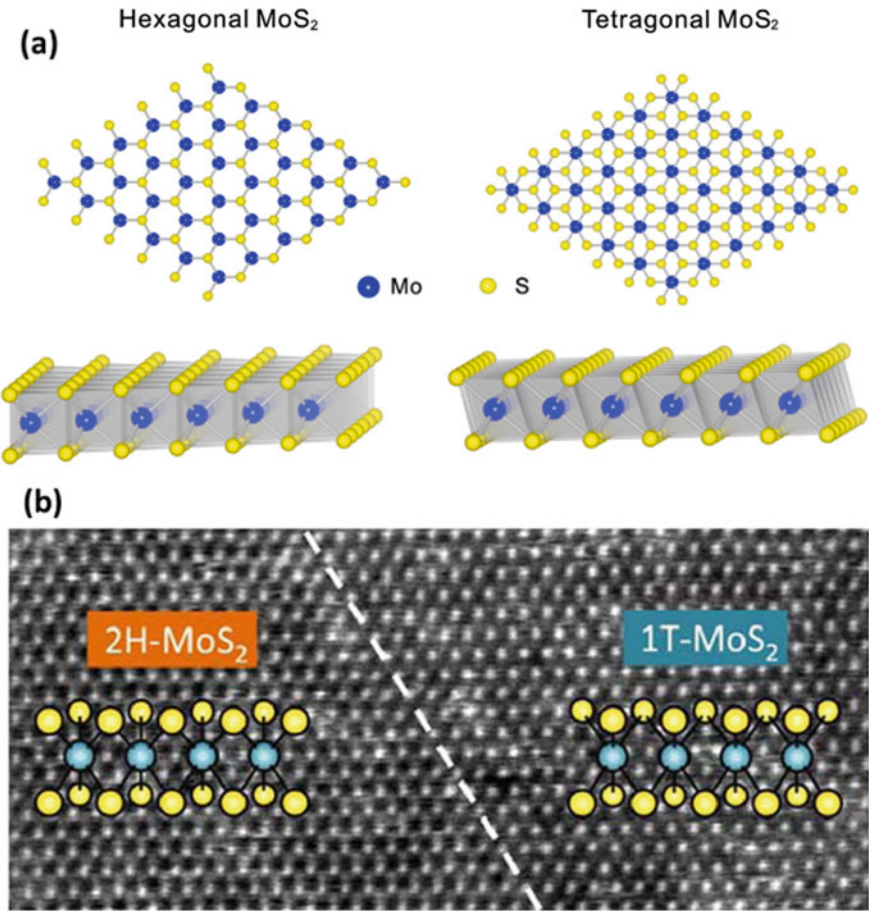

Fig. 2 **a** Schematic of different polytypes of MoS2. Adapted from reference [25] copyright 2016, Elsevier. **b** STEM images of 2H- MoS2 and 1T- MoS2. Adapted from reference [28] copyright 2012, American Chemical Society

image reveals that the 2H-MoS_2 possesses honeycomb-like lattice and metallic MoS_2 (1T-MoS_2) has hexagonal lattice as shown in Fig. 2b [28].

4.2 Preparation of 2D MoS_2

MoS_2 has a diversity of structures and a wide range of properties. Extensive research has been done to synthesize low-cost and large-scale MoS_2 nanostructures with exotic properties and superior performance. Mostly, two kinds of preparation approaches

have been used: A top-down approach (like exfoliation of bulk material); and a bottom-up approach (including hydrothermal and solvothermal methods).

(1) **Top-down approach**

The top-down approach includes various methods such as mechanical, microwave-assisted exfoliation, chemical, liquid-phase, and electrochemical intercalation and exfoliation. Like graphene, MoS_2 nanosheets have been obtained by mechanical exfoliation of bulk MoS_2 powder material. Novoselov et al. achieved single-layer MoS_2 nanosheets with a good quality crystalline structure, but the low yield is the main hindrance for practical applications [29]. To improve the yield, chemical and liquid phase exfoliation methods have been developed. These methods involve the intercalation of ions like Li-ion by using n-butyllithium in an inert atmosphere. Then the exfoliation of intercalated MoS_2 sheets can be done by sonication, microwave, and ball-milling processes. Li-ion intercalation can also be done by using a Li-ion battery system, in which lithium foil and bulk MoS_2 were used as anode and cathode, respectively [30]. Other alkali metals have also been used for the exfoliation of bulk MoS_2. During the metal ion-intercalation, these alkali metals act as electron donors and induce strain force leading to the phase transition of MoS_2 from 2H to 1T phase [31].

The other top-down approach such as mechanical ball milling has been used to prepare MoS_2 nanosheets without any additives or any special treatment. The size of nanosheets and phases (2H and 1T) of MoS_2 have been controlled by milling time. Recently, Xu and coworkers used supercritical CO_2 gas for the exfoliation of bulk MoS_2 [32]. Similar to alkali metals, the introduction of CO_2 between MoS_2 layers induces strain forces into MoS_2 sheets, leading to exfoliation of sheets and transition of phase from 2H to 1T.

(2) **Bottom-up approach**

The bottom-up approach includes hydrothermal, solvothermal processes, and chemical vapor deposition (CVD) for the synthesis of MoS_2 nanosheets [33]. In hydrothermal and solvothermal processes, the different precursors of Mo and S elements have been used. These precursors were thermally treated at 180–220 ℃ for 18–24 h. The obtained MoS_2 nanosheets have a 200 nm lateral size and thickness of 2–5 layers. The temperature and composition ratio of precursors are the critical factors for the control of the MoS_2 phase. Lui et al. found that the metallic content of MoS_2 was significantly influenced by precursor ratio [33]. In CVD process, a thin film of MoS_2 has been developed by the chemical reaction of vapors over the substrate on a large scale as shown in Fig. 3. In this method, three different types of precursors have been utilized namely, ammonium thiomolybdate solution, molybdenum trioxide powder, and elemental molybdenum. Balendhran et al. reported a bulk synthesis CVD method for MoS_2, in which MoO_3 precursor is evaporated on a substrate followed by the sulfurization process in a quartz tube [34].

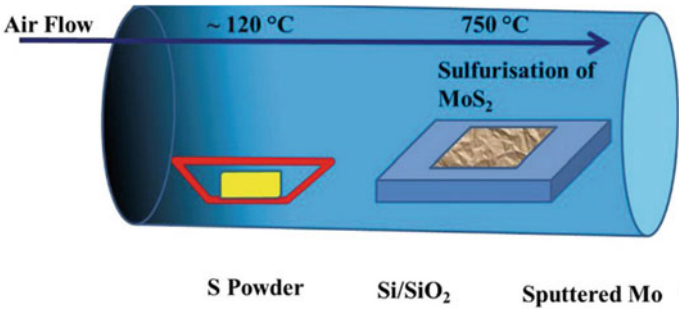

Fig. 3 The schematic diagram for the Chemical vapor deposition method. Adapted from reference [35] copyright 2019, Elsevier

4.3 Hybrid Nanostructures of MoS_2

However, there are two basic challenges in the synthesis of MoS_2: (1) the restacking of the MoS_2 nanosheets; (2) the low electrical conductivity of MoS_2, leading to the hindrance in electrochemical applications. Therefore, the hybridization of MoS_2 with conductive materials, like conductive polymers, carbonaceous materials, and metals, is the effective step to overcome the above-mentioned problems.

(1) **Hybrids of MoS_2 and graphene**

Various carbonaceous nanomaterials including, carbon nanofibers, carbon nanotubes (CNTs), activated carbon, and graphene have been reported as auspicious materials for MoS_2 hybridization. These carbonaceous materials have attractive properties like superior electrical conductivity, low toxicity, lightweight, and easy fabrication methods. Considering the graphene, the integration of graphene with MoS_2 leads to the following advantages for energy storage applications; (i) the high electrical conductivity of graphene improves the low electrical conductivity of MoS_2. (ii) The hierarchical 3D structure of graphene aerogel boosts the structural integrity of MoS_2, leading to improve cyclic stability for energy storage devices. (iii) The dispersion of graphene can alleviate the aggregation of MoS_2 sheets, which leads to improving the electrochemical/catalytic performance. (iv) Graphene as a template for MoS_2 growth provides a conducting network for the transportation of ions/charges [36]. In contrast, MoS_2 is also advantageous for improving the properties of graphene; (i) MoS_2 anchored onto the surface of graphene provides electrocatalytically active sites for the reduction of tri-iodide-like species, giving applications in dye-sensitized solar cells (DSSCs) as counter electrodes. (ii) 2D MoS_2 can also lessen the aggregation of graphene sheets and increase its surface area [37].

The key synthetic route for MoS_2/graphene hybrid is the hydrothermal method. A solvothermal method was also used to prepare reduced graphene oxide doped with S/N and decorated with MoS_2 nanosheets by using L-cysteine and ethylene glycol [38]. Flower-like MoS_2/N-doped graphene hybrid has been prepared by one-pot hydrothermal method for supercapacitor applications. In this method, sodium

molybdate, graphene oxide, L-cysteine, and urea were used as starting materials [39]. Initially, MoS_2/graphene hybrids were synthesized $_{via}$ mechanical exfoliation and dry transfer of graphene and MoS_2 layers [40]. The main disadvantages of this manual approach are; (1) unwanted gaps or wrinkles, (2) residual contamination between connecting 2D layers leading to detrimental performance of the devices [41]. Another approach is the direct growth of 2D-MoS_2 on graphene substrate by chemical vapor deposition (CVD). In this approach, MoS_2 and WS_2 sheets were grafted on the surface of graphene by co-evaporation CVD or by the MOCVD process [42]. The hexagonal flakes of MoS_2 were grown on graphene substrate by a CVD process, in which $(NH_4)_2MoS_4$ precursor self-assembled to form MoS_2 flakes by thermal decomposition at a lower growth temperature of 400 ºC [43].

(2) **Hybrids of MoS_2 and conductive polymers**

Numerous conductive polymers (CP) have been employed as electrode materials for energy storage/conversion applications owing to their low cost, high electrical conductivity, high energy density, facile synthesis, and biodegradability. However, CP materials have inherent disadvantages like mechanical degradation and low heat resistance, leading to poor electrochemical performance. It has been demanded to prepare hybrid materials to overcome these drawbacks and improve their properties. Several approaches have been employed to prepare MoS_2 hybrids with polymers including physical mixing of 2D MoS_2 and polymers, covalent functionalization of MoS_2 and polymers, and in-situ polymerization process. Eksik et al. exfoliated bulk MoS_2 and then mechanically mixed 2D MoS_2 with epoxy polymers [44]. Similarly, Song et al. synthesized MoS_2/PEDOT-PSS composite by dispersing the 2D MoS_2 in the aqueous solutions of poly(3,4-ethylenedioxythiophene) and poly (styrenesulfonate) [45].

The major problem of this approach is the restacking of 2D MoS_2 layers in polymer solutions. In an alternate approach of in-situ polymerization, many conducting polymers including polyaniline (PANI), polypyrrole (PPy), and poly(3,4-ethylenedioxythiophene) (PEDOT) were polymerized with 2D MoS_2. Ma et al. reported PPy/MoS_2 nanocomposite by in-situ oxidation polymerization of pyrrole in 2D MoS_2 suspension [46]. Huang et al. synthesized PANI/MoS_2 composite by using an in-situ polymerization approach and reported this nanocomposite as electrode material for supercapacitors [47]. Sha et al. reported MoS_2/PANI/graphene ternary nanocomposite by using a two-step approach, giving superior supercapacitor performance [48].

(3) **Hybrids of MoS_2 and transition metal oxides (TMOs)**

2D MoS_2 hybrids have also been reported with TMOs as energy storage and electrocatalytic HER applications. The most commonly used TMOs are iron oxide (Fe_2O_3, Fe_3O_4), cobalt oxide (Co_3O_4), manganese oxide (MnO_2), tin oxide (SnO_2), tungsten oxide (WO_3), and ruthenium oxide (RuO_2). The main roles of TMOs in their hybrids with MoS_2 are high redox activity, superior specific capacitance, and preventing the restacking of 2D MoS_2. In contrast, 2D MoS_2 acts as a supporting template for the growth of TMOs and restricts the volumetric change of

TMOs during charge/discharge cycles. The most extensively used synthetic strategy for MoS_2/TMOs hybrids is a hydrothermal process. For example, a heterojunction composite of MoS_2 nanoflake arrays (MNFs) and WO_3 nanorod arrays was synthesized on a copper substrate via a simple hydrothermal method [49].

Figure 4a–b shows the TEM images of MNFs-WNRs composite heterojunction. Another heterojunction composite of MoS_2 QDs/WO_3 was synthesized and used as photoelectrode. In this process, WO_3 nanoplates were prepared by hydrothermal process, and MoS_2 QDs were prepared by exfoliation process, then MoS_2 QDs were deposited on WO_3 nanoplates via dipping-/drop casting-annealing process [50]. Figure 4c shows the energy level structure and the principle of separation of charge carriers in MoS_2/WO_3 DA NPAs. In another study, MoS_2 nanosheets were implanted on TiO_2 nanobelts by sequential hydrothermal processes [51]. Figure 4d shows the SEM images of bare TiO_2 nanobelts (left) and MoS_2/TiO_2 hybrid (right).

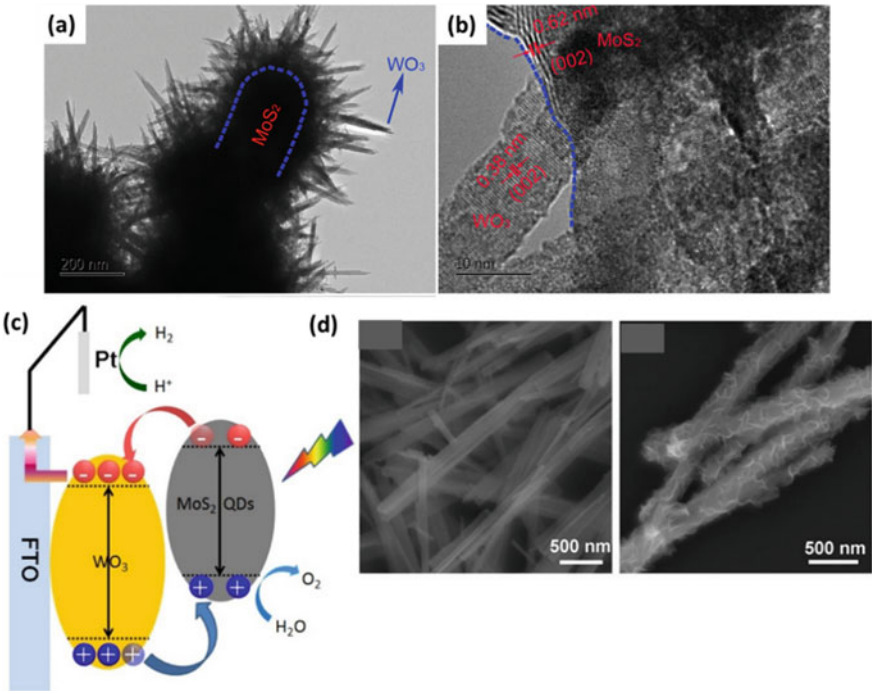

Fig. 4 **a** TEM image **b** HRTEM image of MNFs-WNRs composite heterojunction. Adapted from reference [49] copyright 2018, Elsevier. **c** Depiction of the energy level diagram of MoS_2/WO_3 DA NPAs and the charge separation process. Adapted from reference [50] copyright 2017, Elsevier. **d** SEM image of TiO_2 nanobelts (left) and 2D MoS_2 coated-TiO_2 hybrid (right). Adapted from reference [51] copyright 2018, Elsevier

4.4 Metallic MoS_2 (1T-MoS_2) as 2D TMDs

Among MoS_2 phases, the metallic 1T phase shows conspicuous physical and chemical properties. Compared to the 2H phase of MoS_2, the 1T phase has 10^7 times higher electrical conductivity, which enhances the electron transfer capability of 1T-MoS_2. Moreover, it has been studied that the basal plane of 1T-MoS_2 has rich electrocatalytically active sites for HER as compared to 2H-MoS_2. These properties make 1T-MoS_2 (metallic) a more promising material for energy generation, conversion, and storage applications.

4.5 Fabrication Methods for Metallic MoS_2 (1T-MoS_2)

1T MoS_2 (metallic phase) does not occur in nature. Mostly, the Li-ion intercalation strategy is used to convert stable 2H-MoS_2 (semiconducting) to metastable 1T-MoS_2 (metallic). The hydrothermal and solvothermal processes have also been reported for the synthesis of 1T-MoS_2. These fabrication methods are categorized into two approaches; (1) top-down approach includes the intercalation and exfoliation of bulk MoS_2; (2) bottom-up approach includes hydrothermal and solvothermal processes.

(1) **Lithium-ion intercalation method**

The most traditional method used for the synthesis of 1T-MoS_2 is the chemical intercalation and exfoliation of bulk MoS_2. The mechanism of this method consists of two steps; the first step is the intercalation of Li-ion by mixing the bulk MoS_2 powder in the presence of some strong reducing agents like *n*-butyllithium/$LiBH_4$ and organic solvent, resulting in the formation of unstable Li_xMoS_2 species; the second step is the exfoliation of 2D MoS_2 by ultrasonication of the obtained Li_xMoS_2 resulting in the transition of 2H-MoS_2 to 1T-MoS_2 [52]. Eda et al. reported the synthesis of metallic MoS_2 by mixing bulk MoS_2 with *n*-butyllithium and hexane for two days in an inert atmosphere of Ar gas [52]. Similarly, Acerce et al. synthesized 1T-MoS_2 monolayer nanosheets by intercalation of organolithium in bulk MoS_2 followed by exfoliation process [53]. Moreover, Voiry et al. also reported the chemical intercalation process for the synthesis of monolayer 1T-MoS_2 [54].

Furthermore, electrochemical intercalation of Li-ion is another process to synthesize metallic MoS_2. Cui et al. successfully achieved metallic MoS_2 by electrochemical Li-ion intercalation [55]. They assembled 2H-MoS_2 film as an anode in a Li-ion battery semi-cell and applied a certain voltage to charge the cell. Raman and XPS analysis were used to confirm the conversion of the 2H phase to the 1T phase of MoS_2. Zhang et al. reported the synthesis of 1T MX_2 QDs by electrochemical Li-ion intercalation [56]. They observed the effect of applied discharge current on the transition of MoS_2 phases and the size of obtained MoS_2 sheets. The small discharge current allowed high Li content intercalation, leading to 2H to 1T phase transition and formation of QDs. But this process has limitations of low yield and time taking process.

(2) **Solvothermal and hydrothermal process**

In the bottom-up strategy, solvothermal and hydrothermal are two typical fabrication methods for metallic MoS_2. Wei et al. synthesized a mixture of 2H- and 1T-MoS_2 by a solvothermal process of 2H-MoS_2 in ethanol at 220 ℃ for 8 h [57]. N, N-dimethylformamide (DMF) has been reported as an excellent solvent for the fabrication of metallic MoS_2 by the solvothermal process. Song et al. achieved metallic MoS_2 by the solvothermal process of molybdate tetrahydrate and thiourea in DMF and water (1:4) mixture at 220 ℃ for 72 h as shown in Fig. 5a [58]. The interlayer distance of obtained MoS_2 is 0.98 $_{nm}$. This group reported that the metallic MoS_2 can also be fabricated by the reaction of molybdenum chloride and thioacetamide using only DMF as solvent.

Pan et al. reported the reaction of $Na_2MoO_4.2H_2O$ and L-cysteine in the mixture of DMF and water of 1.5:1 ratio for metallic MoS_2 fabrication as shown in Fig. 5b [59]. Chen et al. reported another hydrothermal method, in which MoO_3 reacts with thioacetamide in water to give metallic MoS_2 with dispersion stability of around 1 month in water and metallic phase stability is more than 90 days [60]. The study of fabrication of metallic MoS_2 has been proved that 1T-MoS_2 could be achieved by autoclave method using proper chemicals under a certain pressure. This method does not require any specific facilities and can give a good yield.

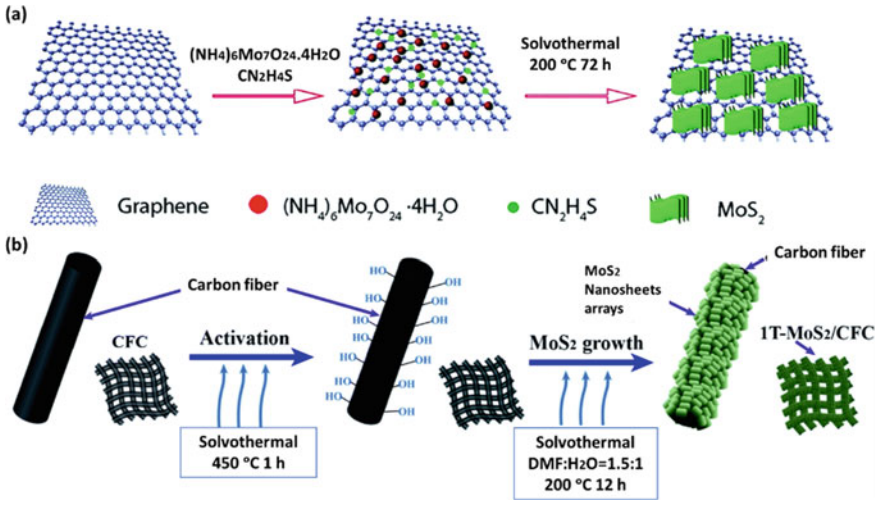

Fig. 5 Schematic of the fabrication of Metallic MoS2 in the mixture of **a** DMF and water with 1:4 ratio. Adapted from reference [58] copyright 2017, RSC. **b** DMF:H2O = 1.5:1. Adapted from reference [59] copyright 2017, RSC

5 Applications of 2D TMDs Nanostructures

2D TMDs nanomaterials have diverse applications in the field of photonics, electronics, energy storage, and sensing devices (Fig. 6). The exceptional properties of 2D materials including high mechanical strength, excellent electrostatic efficiency, tunable electronic structure, good sensor behavior, and optically transparent, make them attractive for these applications, particularly for flexible nanotechnology.

5.1 Electrical and Optoelectronic Applications

Due to some limitations of standard silicon technology, it has been suggested from the last few decades that 2D semiconducting TMDs might be proved excellent materials for future electronic technology and solve the fabrication and integration problems. So, China has released its first market product of graphene-based smartphone touch display, in 2014. Meanwhile, 2D TMDs have been reviewed related to their innovations and applications. Akinwande et al. reported high-performance flexible thin-film transistors (TFTs) based on the CVD-grown MoS_2 with electron mobility of 50 $cm^2\ V^{-1}\ s^{-1}$ and current density of 250 $\mu A/\mu m$ [61]. This device also achieved high intrinsic transit frequencies of 5 GHz and oscillation frequencies of 3.3 GHz. Gao et al. proposed novel strategies for high-performance monolayer MoS_2/PNC hybrid photodetectors (HPs) [62]. The high photoresponsivity of 6.40×10^5 mA W^{-1} and quantum efficiency of 1.50×10^5% have been demonstrated by these HPs. Wu et al. reported high-performance radio frequency transistors based on CVD-grown bilayer MoS_2 [63]. These transistors deliver an extrinsic high cut-off frequency of 7.2 GHz and an extrinsic maximum oscillation frequency of 23 GHz.

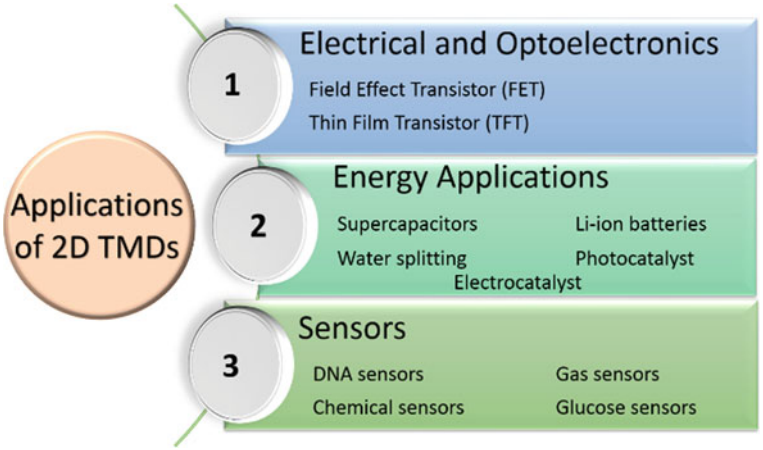

Fig. 6 Different application areas for 2D TMDs

5.2 Energy Applications

2D TMDs have become attractive electrode materials for energy storage devices. This is attributed to their high surface area, atomically thin layered structure, superior electrochemical properties, and mechanical stability. However, some problems related to its applications are low yield, small flake size, the thickness of sheets, and uncontrollable defects [64]. Tour et al. reported the fabrication of edge-oriented MoS_2 nanosheets with large interlayer space and additional edge active sites providing superior capacitive properties [65]. Among 2D TMDs, MoS_2 has known as attractive anode material for Li-ion batteries due to large interlayer space for ease intercalation of Li-ions, no obvious volume change, and no degradation of material during charge/discharge cycles, and high theoretical capacitance of 670 mAh g^{-1} [66].

5.3 MoS_2 as Supercapacitor Electrodes

As new power supply devices, supercapacitors are considered a bridge for the gap between capacitors and batteries due to their special properties of high power density, cyclic stability, rapid charge/discharge process, and ecofriendly. As a two dimensional (2D) transition metal dichalcogenide, MoS_2 is promising for electrochemical storage due to.

(1) **Layered structure** with intralayer Van der Waals interactions having an interlayer spacing of 0.615 nm significantly larger than that of graphite (0.335 nm) [67]. The layered morphology of MoS_2 provides a high specific surface area and short charge (ion/electron) transfer distance for double layers and pseudocapacitor charge storage [38].
(2) **High theoretical capacity** due to high surface area, sheet-like morphology, and intrinsic bandgap [68],.
(3) **A wide range of oxidation numbers** of Mo atoms from + 2 to + 6 causes pseudocapacitor nature and results in superior specific capacity [69].
(4) **Good cyclic stability** owing to low degradation and low volumetric expansion during the charging/discharging process [70].

Various nanostructures of MoS_2 have been reported for supercapacitors applications. Choudhary et al. fabricated a high-performance supercapacitor electrode based on a thin film of MoS_2 by a direct magnetron sputtering technique. This electrode showed a specific capacitance of 330 F g^{-1} at 10 mV s^{-1} and capacitance retention of 97% after 5000 cycles [71]. Karade and coworkers reported a successful synthesis of ultrathin MoS_2 nanoflakes and fabricated an electrode for supercapacitors. This electrode showed excellent supercapacitance performance with a high specific capacity of 576 F g^{-1} at 5 mV s^{-1} and good capacitance retention of 82% over 300 cycles [72].

5.3.1 1T-MoS_2 as Supercapacitor Electrodes

The intrinsic semiconducting nature of the 2H-MoS_2 prevents it from being an ideal electrode material for supercapacitors. So, 1T-MoS_2 has become a more attractive electrode material due to:

(1) **High electrical conductivity**: 1T phase is 10^7 times more conductor than that of 2H phase with enhanced electron transfer capability of 1T-MoS_2.
(2) **High electrochemical activity:** 1T phase has rich active sites even on basal plane benefiting for higher reaction kinetics.

Hongli et al. reported 2D water-coupled metallic MoS_2 nanochannels by using a simple hydrothermal process [73]. The high electrical conductivity of metallic MoS_2 and nanochannels are beneficial for electron transport and ion adsorption. This M-MoS_2-H_2O based supercapacitor exhibited a specific capacitance of 380 F g^{-1} at 5 mV s^{-1}. The best capacitive behavior of M-MoS_2 is in the Li_2SO_4 electrolyte due to easy Li-ion intercalation between the nanochannels. Tarpin et al. reported the chemical synthesis of 2D M-MoS_2 and observed that the stability of the metallic phase of MoS_2 is associated with the adsorbed monolayer of water between the nanosheets of MoS_2, leading to prevent the restacking and aggregation [60]. Chhowalla et al. reported the fabrication of 1T monolayer MoS_2 by chemical exfoliation method and observed the volumetric capacitance of 400–650 F cm^{-3} at 20 mV s^{-2} in various aqueous electrolytes [53]. They also investigated the capacitive behavior of 1T MoS_2 film in the nonaqueous electrolyte ($TEABF_4$). This electrode exhibited the volumetric capacitance of 180 F cm^{-3} with capacitance retention of 90% over 5000 cycles at 1 A g^{-1}. Thus, metallic MoS_2 shows better supercapacitor performance due to the hydrophilic and conductive nature leading to rapid ion diffusion as compared to semiconducting 2H MoS_2.

5.3.2 MoS_2/Graphene Hybrids as Supercapacitor Electrodes

The modest capacitive performance of 2H MoS_2 due to the semiconducting nature, the hybrid composites of 2H-MoS_2 with other highly conductive materials (like graphene and polyaniline) are used to improve the electrical properties and capacitive behavior. Xiao et al. reported MoS_2/graphene hollow microsphere delivering high specific capacitance of 218 F g^{-1} at a current density of 1 A g^{-1} [74].

Additionally, these microspheres exhibited capacitance retention of 91.8% over 1000 cycles. Sun and coworkers fabricated MoS_2 microstructures on a 3D graphene network by hydrothermal process. This 3DG/MoS_2 composite showed the high specific capacitance of 410 F g^{-1} at 1 A g^{-1} with capacitance retention of 80.3% over 10,000 cycles at 2 A g^{-1} [75]. The superior capacitance performance can be attributed to the synergetic effect of 3DG and flower-like MoS_2 microstructures that provide easy electronic transportation and additional ion diffusion channels. San et al. reported an electrode for supercapacitor based on MoS_2/PANI/rGO aerogel with a high specific capacitance of 618 F g^{-1} and good capacitance retention of 78% after

2000 cycles [48]. Xi and coworkers reported a one-pot hydrothermal process for the fabrication of MoS_2 and N-doped Graphene composite (MoS_2/NG). The MoS_2/NG composite exhibited the specific capacitance of 245 F g^{-1} at 0.25 A g^{-1} and good cyclic stability of 91.3% after 1000 cycles at 2 A g^{-1} [39]. Thangappan et al. fabricated a composite of MoS_2 nanosheets and graphene $_{via}$ a hydrothermal process. The MoS_2/G composite delivered a higher specific capacitance of 270 F g^{-1} compared with the pure MoS_2 C_{sp} value of 162 F g^{-1}. Moreover, this composite exhibited an energy density of 12.5 Wh kg^{-1} and power density of 2500 W kg^{-1} [76].

5.3.3 MoS_2/TMOs Hybrids as Supercapacitor Electrodes

Wang et al. fabricated a composite of layered MoS_2 and Mn_3O_4 nanoparticles (MoS_2/Mn_3O_4) by using a simple hydrothermal process [77]. The MoS_2/Mn_3O_4 composite showed the specific capacitance of 115.7 F g^{-1} at 5 mV s^{-1} with capacitance retention of 69.3% at 1 A g^{-1}. Samo et al. reported a hybrid nanostructure of MoS_2 nanosheets with Fe_3O_4 nanoparticles and physically exfoliated graphene (MoS_2/Fe_3O_4/PHG). This composite MoS_2/Fe_3O_4/PHG delivered a high C_{sp} value of 830 F g^{-1} at 1 A g^{-1} with cyclic stability of 96% over 2200cycles [78]. Ling and coworkers synthesized MoS_2/Co_3O_4 composite by using laser ablation technique and applied as supercapacitor electrode delivering a specific capacitance of 69 mAh g^{-1} at 0.5 A g^{-1} and cyclic stability of 87% after 500 cycles [79]. Wang and coworkers reported the heterostructures of 2D MoS_2 nanosheets and various TMOs like NiO, Fe_3O_4, and Co_3O_4. They found that MoS_2-NiO heterostructure delivered a higher C_{sp} value of 1080 F g^{-1} at 1 A g^{-1} with excellent cyclic stability of 101.9% capacitance retention over 9000 cycles for 1 A g^{-1} [80]. Li et al. developed of 3D core–shell structure with MoS_2 nanosheets and CeO_2 hollow spheres by using a wet chemistry method that delivered a superior specific capacitance of 90 mF cm^{-2} at 2.55 mA cm^{-2} with capacitance retention of 98%.

6 Challenges of 2D TMDs Electrode Materials

The intensive study of 2D TMD heterostructures made them attractive materials for energy storage and energy conversion systems due to their exotic properties. These studies revealed that the synthesis of monolayer TMD nanostructures has been achieved successfully. However, the achievement of high-quality TMD nanostructures on large scale is still a big challenge. Although the pseudocapacitor behavior of most of TMDs delivers high specific capacitance, the low conductivity and poor cyclic stability are the main hindrances for their practical applications as energy storage devices. Additionally, the practical applications for successfully synthesized highly crystalline TMD nanostructure are still a challenge. As the following key aspects, the performance and efficiency of 2D TMD electrode material can be enhanced.

- Controllable Fabrication Methods: The properties of TMDs mainly depends on the crystalline phase and morphologies. Various synthetic strategies have been reported including top-down and bottom-up approaches. But these methods have various issues like low stability and low purity of phase. The development of an effective, controllable, and ecofriendly synthetic method for 2D TMDs nanostructures is thus highly demanded.
- Restacking: The restacking of nanosheets of TMDs is the main hindrance in energy storage and energy conversion applications. To reduce the restacking, various approaches can be applied like introducing a water monolayer between the nanosheets, functionalization of TMDs, and making hybrids with 2D materials (graphene).
- Conductivity: In electrochemical applications, the electrical conductivity of electrode materials is the key factor. So, the low conductivity of 2D TMDs limits its application in energy storage and energy conversion applications. To enhance the conductivity, numerous methods can be used including, hybridization with graphene and conductive polymers, alloying of different TMDs, and doping of graphene or TMDs with inorganic elements.
- Mass production: The low yield of synthetic methods for 2D TMDs causes hindrance for their applications on an industrial scale. So, the production of stable and pure 2D TMDs on large scale is still a challenge. Further modification methods like autoclave methods can be used for large-scale production.
- Cost production: For practical utilization of supercapacitor, the cost of electrode materials is also an important aspect with all other characteristics. So, it is also a challenge to fabricate the electrode material for enhanced supercapacitor performance at a low cost.

7 Conclusion

The unique nanostructures and properties of 2D-TMDs open a new venue of great research concern to the development of novel functional materials for a variety of applications. Although the synthetic strategies of large-scale and uniform atomic layers of 2D TMDs have developed, the quality of 2D TMDs has not yet met the mechanical exfoliation strategy of 2D TMDs. To meet the practical applications with the advanced synthesis of 2D TMDs, key issues should be addressed, including single-layer growth, defect controllability, and doping of TMDs. Considering the exotic properties like high surface area, atomic-layered structure, and excellent electrochemical properties, TMDs have found huge applications in energy storage, sensor, electrical and optoelectronic devices. Despite the excellent applications of 2D TMDs, there is more room for research for the development and advancement in interdisciplinary areas. Hence, more study is still needed to explore the tunable properties of nanostructured 2D TMDs materials.

References

1. M.J. Allen, V.C. Tung, R.B. Kaner, H. carbon, a review of graphene. Chem. Rev. **110**(1), 132–145 (2010)
2. W. Choi, N. Choudhary, G.H. Han, J. Park, D. Akinwande, Y.H. Lee, Recent development of two-dimensional transition metal dichalcogenides and their applications. Mater. Today **20**(3), 116–130 (2017)
3. X. Huang, Z. Zeng, H. Zhang, Metal dichalcogenide nanosheets: preparation, properties and applications. Chem. Soc. Rev. **42**(5), 1934–1946 (2013)
4. J. Wang, J. Liu, B. Zhang, X. Ji, K. Xu, C. Chen, L. Miao, J. Jiang, The mechanism of hydrogen adsorption on transition metal dichalcogenides as hydrogen evolution reaction catalyst. Phys. Chem. Chem. Phys. **19**(15), 10125–10132 (2017)
5. J. Feng, X. Sun, C. Wu, L. Peng, C. Lin, S. Hu, J. Yang, Y. Xie, Metallic few-layered VS2 ultrathin nanosheets: high two-dimensional conductivity for in-plane supercapacitors. J. Am. Chem. Soc. **133**(44), 17832–17838 (2011)
6. K. Leng, Z. Chen, X. Zhao, W. Tang, B. Tian, C.T. Nai, W. Zhou, K.P. Loh, Phase restructuring in transition metal dichalcogenides for highly stable energy storage. ACS Nano **10**(10), 9208–9215 (2016)
7. Y. Sun, S. Gao, F. Lei, Y. Xie, Atomically-thin two-dimensional sheets for understanding active sites in catalysis. Chem. Soc. Rev. **44**(3), 623–636 (2015)
8. P. Xiong, J. Zhu, L. Zhang, X. Wang, Recent advances in graphene-based hybrid nanostructures for electrochemical energy storage. Nanoscale Horizons **1**(5), 340–374 (2016)
9. G. Zhang, H. Liu, J. Qu, J. Li, Two-dimensional layered MoS 2: rational design, properties and electrochemical applications. Energy Environ. Sci. **9**(4), 1190–1209 (2016)
10. D. Wang, Y. Xiao, X. Luo, Z. Wu, Y.-J. Wang, B. Fang, Swollen ammoniated MoS2 with 1T/2H hybrid phases for high-rate electrochemical energy storage. ACS Sustain. Chem. Eng. **5**(3), 2509–2515 (2017)
11. X. Qian, J. Liu, L. Fu, J. Li, Quantum spin Hall effect in two-dimensional transition metal dichalcogenides. Science **346**(6215), 1344–1347 (2014)
12. X. Zhou, J. Cheng, Y. Zhou, T. Cao, H. Hong, Z. Liao, S. Wu, H. Peng, K. Liu, D. Yu, Strong second-harmonic generation in atomic layered GaSe. J. Am. Chem. Soc. **137**(25), 7994–7997 (2015)
13. R. Kappera, D. Voiry, S.E. Yalcin, W. Jen, M. Acerce, S. Torrel, B. Branch, S. Lei, W. Chen, S. Najmaei, Metallic 1T phase source/drain electrodes for field effect transistors from chemical vapor deposited MoS2. Apl Mater. **2**(9), 092516 (2014)
14. K.-A.N. Duerloo, Y. Li, E.J. Reed, Structural phase transitions in two-dimensional Mo-and W-dichalcogenide monolayers. Nat. Commun. **5**, 4214 (2014)
15. Z. Fan, Z. Wei-Bing, T. Bi-Yu, Electronic structures and elastic properties of monolayer and bilayer transition metal dichalcogenides MX2 (M= Mo, W; X= O, S, Se, Te): a comparative first-principles study. Chinese Physics B **24**(9), 097103(2015)
16. B. Radisavljevic, A. Radenovic, J. Brivio, I.V. Giacometti, A. Kis, Single-layer MoS 2 transistors. Nat. Nanotechnol. **6**(3), 147 (2011)
17. Z. Zhang, Y. Xie, Y. Ouyang, Y. Chen, A systematic investigation of thermal conductivities of transition metal dichalcogenides. Int. J. Heat Mass Transf. **108**, 417–422 (2017)
18. C. Muratore, V. Varshney, J.J. Gengler, J.J. Hu, J.E. Bultman, T.M. Smith, P.J. Shamberger, B. Qiu, X. Ruan, A.K. Roy, A.A. Voevodin, Cross-plane thermal properties of transition metal dichalcogenides. Appl. Phys. Lett. **102**(8), 081604 (2013)
19. J.M. Soon, K.P. Loh, Electrochemical double-layer capacitance of MoS2 nanowall films. Electrochem. Solid-State Lett. **10**(11), A250–A254 (2007)
20. H. Pan, Metal dichalcogenides monolayers: novel catalysts for electrochemical hydrogen production. Sci. Rep. **4**, 5348 (2014)
21. X. Chia, A. Ambrosi, Z. Sofer, J. Luxa, M. Pumera, Catalytic and charge transfer properties of transition metal dichalcogenides arising from electrochemical pretreatment. ACS Nano **9**(5), 5164–5179 (2015)

22. T.D. Thanh, N.D. Chuong, H. Van Hien, T. Kshetri, N.H. Kim, J.H. Lee, Recent advances in two-dimensional transition metal dichalcogenides-graphene heterostructured materials for electrochemical applications. Prog. Mater. Sci. **96**, 51–85 (2018)
23. W. Li, Q. Liu, Y. Sun, J. Sun, R. Zou, G. Li, X. Hu, G. Song, G. Ma, J. Yang, MnO 2 ultralong nanowires with better electrical conductivity and enhanced supercapacitor performances. J. Mater. Chem. **22**(30), 14864–14867 (2012)
24. Z. Wu, B. Li, Y. Xue, J. Li, Y. Zhang, F. Gao, Fabrication of defect-rich MoS 2 ultrathin nanosheets for application in lithium-ion batteries and supercapacitors. J. Mater. Chem. A **3**(38), 19445–19454 (2015)
25. H. Huang, Y. Cui, Q. Li, C. Dun, W. Zhou, W. Huang, L. Chen, C.A. Hewitt, D.L. Carroll, Metallic 1T phase MoS2 nanosheets for high-performance thermoelectric energy harvesting. Nano Energy **26**, 172–179 (2016)
26. R. Ganatra, Q. Zhang, Few-layer MoS2: a promising layered semiconductor. ACS Nano **8**(5), 4074–4099 (2014)
27. G. Gao, Y. Jiao, F. Ma, Y. Jiao, E. Waclawik, A. Du, Charge mediated semiconducting-to-metallic phase transition in molybdenum disulfide monolayer and hydrogen evolution reaction in new 1T′ phase. J. Phys. Chem. C **119**(23), 13124–13128 (2015)
28. G. Eda, T. Fujita, H. Yamaguchi, D. Voiry, M. Chen, M. Chhowalla, Coherent atomic and electronic heterostructures of single-layer MoS2. ACS Nano **6**(8), 7311–7317 (2012)
29. K.S. Novoselov, D. Jiang, F. Schedin, T. Booth, V. Khotkevich, S. Morozov, A.K. Geim, Two-dimensional atomic crystals. Proc. Natl. Acad. Sci. **102**(30), 10451–10453 (2005)
30. Z. Zeng, Z. Yin, X. Huang, H. Li, Q. He, G. Lu, F. Boey, H. Zhang, Single-layer semiconducting nanosheets: high-yield preparation and device fabrication. Angew. Chem. Int. Ed. **50**(47), 11093–11097 (2011)
31. S. Shi, Z. Sun, Y.H. Hu, Synthesis, stabilization and applications of 2-dimensional 1T metallic MoS 2. J. Mater. Chem. A **6**(47), 23932–23977 (2018)
32. Y. Qi, Q. Xu, Y. Wang, B. Yan, Y. Ren, Z. Chen, CO2-induced phase engineering: protocol for enhanced photoelectrocatalytic performance of 2D MoS2 nanosheets. ACS Nano **10**(2), 2903–2909 (2016)
33. Q. Liu, X. Li, Q. He, A. Khalil, D. Liu, T. Xiang, X. Wu, L. Song, Gram-scale aqueous synthesis of stable few-layered 1T-MoS2: applications for visible-light-driven photocatalytic hydrogen evolution. Small **11**(41), 5556–5564 (2015)
34. S. Balendhran, J.Z. Ou, M. Bhaskaran, S. Sriram, S. Ippolito, Z. Vasic, E. Kats, S. Bhargava, S. Zhuiykov, K. Kalantar-Zadeh, Atomically thin layers of MoS 2 via a two step thermal evaporation–exfoliation method. Nanoscale **4**(2), 461–466 (2012)
35. U. Krishnan, M. Kaur, K. Singh, M. Kumar, A. Kumar, A synoptic review of MoS2: synthesis to applications. Superlattices Microstruct. (2019).
36. Y. Liu, X. He, D. Hanlon, A. Harvey, J.N. Coleman, Y. Li, Liquid phase exfoliated MoS2 nanosheets percolated with carbon nanotubes for high volumetric/areal capacity sodium-ion batteries. ACS Nano **10**(9), 8821–8828 (2016)
37. F. Bonaccorso, L. Colombo, G. Yu, M. Stoller, V. Tozzini, A.C. Ferrari, R.S. Ruoff, V. Pellegrini, Graphene, related two-dimensional crystals, and hybrid systems for energy conversion and storage. Science **347**(6217), 1246501 (2015)
38. J. Huo, Y. Xue, X. Zhang, S. Guo, Hierarchical porous reduced graphene oxide decorated with molybdenum disulfide for high-performance supercapacitors. Electrochim. Acta **292**, 639–645 (2018)
39. B. Xie, Y. Chen, M. Yu, T. Sun, L. Lu, T. Xie, Y. Zhang, Y. Wu, Hydrothermal synthesis of layered molybdenum sulfide/N-doped graphene hybrid with enhanced supercapacitor performance. Carbon **99**, 35–42 (2016)
40. R. Moriya, T. Yamaguchi, Y. Inoue, S. Morikawa, Y. Sata, S. Masubuchi, T. Machida, Large current modulation in exfoliated-graphene/MoS2/metal vertical heterostructures. Appl. Phys. Lett. **105**(8), 083119 (2014)
41. Y. Liu, Y. Guo, S. Sonam, S.K. Hong, M.H. Nai, C.T. Nai, L. Gao, J. Chen, B.J. Cho, C.T. Lim, Large-area, periodic, hexagonal wrinkles on nanocrystalline graphitic film. Adv. Func. Mater. **25**(34), 5492–5503 (2015)

42. Y.-C. Lin, R.K. Ghosh, R. Addou, N. Lu, S.M. Eichfeld, H. Zhu, M.-Y. Li, X. Peng, M.J. Kim, L.-J. Li, Atomically thin resonant tunnel diodes built from synthetic van der Waals heterostructures. Nat. Commun. **6**, 7311 (2015)
43. Y. Shi, W. Zhou, A.-Y. Lu, W. Fang, Y.-H. Lee, A.L. Hsu, S.M. Kim, K.K. Kim, H.Y. Yang, L.-J. Li, van der Waals epitaxy of MoS2 layers using graphene as growth templates. Nano Lett. **12**(6), 2784–2791 (2012)
44. O. Eksik, J. Gao, S.A. Shojaee, A. Thomas, P. Chow, S.F. Bartolucci, D.A. Lucca, N. Koratkar, Epoxy nanocomposites with two-dimensional transition metal dichalcogenide additives. ACS Nano **8**(5), 5282–5289 (2014)
45. D. Song, M. Li, Y. Jiang, Z. Chen, F. Bai, Y. Li, B. Jiang, Facile fabrication of MoS2/PEDOT–PSS composites as low-cost and efficient counter electrodes for dye-sensitized solar cells. J. Photochem. Photobiol., A **279**, 47–51 (2014)
46. G. Ma, H. Peng, J. Mu, H. Huang, X. Zhou, Z. Lei, In situ intercalative polymerization of pyrrole in graphene analogue of MoS2 as advanced electrode material in supercapacitor. J. Power Sources **229**, 72–78 (2013)
47. K.-J. Huang, L. Wang, Y.-J. Liu, H.-B. Wang, Y.-M. Liu, L.-L. Wang, Synthesis of polyaniline/2-dimensional graphene analog MoS2 composites for high-performance supercapacitor. Electrochim. Acta **109**, 587–594 (2013)
48. C. Sha, B. Lu, H. Mao, J. Cheng, X. Pan, J. Lu, Z. Ye, 3D ternary nanocomposites of molybdenum disulfide/polyaniline/reduced graphene oxide aerogel for high performance supercapacitors. Carbon **99**, 26–34 (2016)
49. H. Gong, F. Zheng, J. Xu, C. Sun, L. Gao, P. Hu, Y. Li, Y. Gong, Q. Zhen, S. Bashir, Preparation and supercapacitive property of molybdenum disulfide (MoS2) nanoflake arrays-tungsten trioxide (WO3) nanorod arrays composite heterojunction: a synergistic effect of one-dimensional and two-dimensional nanomaterials. Electrochim. Acta **263**, 409–416 (2018)
50. Y.-H. Xiao, W.-D. Zhang, MoS2 quantum dots interspersed WO3 nanoplatelet arrays with enhanced photoelectrochemical activity. Electrochim. Acta **252**, 416–423 (2017)
51. W. Zhou, Z. Yin, Y. Du, X. Huang, Z. Zeng, Z. Fan, H. Liu, J. Wang, H. Zhang, Synthesis of few-layer MoS2 nanosheet-coated TiO2 nanobelt heterostructures for enhanced photocatalytic activities. Small **9**(1):140–147 (2013)
52. G. Eda, H. Yamaguchi, D. Voiry, T. Fujita, M. Chen, M. Chhowalla, Photoluminescence from chemically exfoliated MoS2. Nano Lett. **11**(12), 5111–5116 (2011)
53. M. Acerce, D. Voiry, M. Chhowalla, Metallic 1T phase MoS 2 nanosheets as supercapacitor electrode materials. Nat. Nanotechnol. **10**(4), 313 (2015)
54. D. Voiry, A. Goswami, R. Kappera, C.D.C.C. e Silva, D. Kaplan, T. Fujita, M. Chen, T. Asefa, M. Chhowalla, Covalent functionalization of monolayered transition metal dichalcogenides by phase engineering. Nat. Chemm **7**(1), 45 (2015)
55. H. Wang, Z. Lu, S. Xu, D. Kong, J.J. Cha, G. Zheng, P.-C. Hsu, K. Yan, D. Bradshaw, F.B. Prinz, Electrochemical tuning of vertically aligned MoS2 nanofilms and its application in improving hydrogen evolution reaction. Proc. Natl. Acad. Sci. **110**(49), 19701–19706 (2013)
56. W. Chen, J. Gu, Q. Liu, R. Luo, L. Yao, B. Sun, W. Zhang, H. Su, B. Chen, P. Liu, Quantum dots of 1T phase transitional metal dichalcogenides generated via electrochemical Li intercalation. ACS Nano **12**(1), 308–316 (2017)
57. L. Cai, J. He, Q. Liu, T. Yao, L. Chen, W. Yan, F. Hu, Y. Jiang, Y. Zhao, T. Hu, Vacancy-induced ferromagnetism of MoS2 nanosheets. J. Am. Chem. Soc. **137**(7), 2622–2627 (2015)
58. T. Xiang, Q. Fang, H. Xie, C. Wu, C. Wang, Y. Zhou, D. Liu, S. Chen, A. Khalil, S. Tao, Vertical 1T-MoS 2 nanosheets with expanded interlayer spacing edged on a graphene frame for high rate lithium-ion batteries. Nanoscale **9**(21), 6975–6983 (2017)
59. M. Wu, J. Zhan, K. Wu, Z. Li, L. Wang, B. Geng, L. Wang, D. Pan, Metallic 1T MoS 2 nanosheet arrays vertically grown on activated carbon fiber cloth for enhanced Li-ion storage performance. J. Mater. Chem. A **5**(27), 14061–14069 (2017)
60. X. Geng, W. Sun, W. Wu, B. Chen, A. Al-Hilo, M. Benamara, H. Zhu, F. Watanabe, J. Cui, T.-P. Chen, Pure and stable metallic phase molybdenum disulfide nanosheets for hydrogen evolution reaction. Nat. Commun. **7**, 10672 (2016)

61. H.Y. Chang, M.N. Yogeesh, R. Ghosh, A. Rai, A. Sanne, S. Yang, N. Lu, S.K. Banerjee, D. Akinwande, Large-area monolayer MoS2 for flexible low-power RF nanoelectronics in the GHz regime. Adv. Mater. **28**(9), 1818–1823 (2016)
62. L. Zhang, S. Shen, M. Li, L. Li, J. Zhang, L. Fan, F. Cheng, C. Li, M. Zhu, Z. Kang, Strategies for air-stable and tunable monolayer MoS2-based hybrid photodetectors with high performance by regulating the fully inorganic trihalide perovskite nanocrystals. Adv. Optic. Mater. **7**, 1801744 (2019)
63. Q. Gao, Z. Zhang, X. Xu, J. Song, X. Li, Y. Wu, Scalable high performance radio frequency electronics based on large domain bilayer MoS 2. Nat. Commun. **9**(1), 4778 (2018)
64. H. Li, J. Wu, Z. Yin, H. Zhang, Preparation and applications of mechanically exfoliated single-layer and multilayer MoS2 and WSe2 nanosheets. Acc. Chem. Res. **47**(4), 1067–1075 (2014)
65. Y. Yang, H. Fei, G. Ruan, C. Xiang, J.M. Tour, Edge-oriented MoS2 nanoporous films as flexible electrodes for hydrogen evolution reactions and supercapacitor devices. Adv. Mater. **26**(48), 8163–8168 (2014)
66. J. Zhou, J. Qin, X. Zhang, C. Shi, E. Liu, J. Li, N. Zhao, C. He, 2D space-confined synthesis of few-layer MoS2 anchored on carbon nanosheet for lithium-ion battery anode. ACS Nano **9**(4), 3837–3848 (2015)
67. Z. Wu, B. Li, Y. Xue, J. Li, Y. Zhang, F. Gao, Fabrication of defect-rich MoS2 ultrathin nanosheets for application in lithium-ion batteries and supercapacitors. J. Mater. Chem. A **3**(38), 19445–19454 (2015)
68. C. Zhao, Y. Zhou, Z. Ge, C. Zhao, X. Qian, Facile construction of MoS2/RCF electrode for high-performance supercapacitor. Carbon **127**, 699–706 (2018)
69. H. Tang, J. Wang, H. Yin, H. Zhao, D. Wang, Z. Tang, Growth of polypyrrole ultrathin films on MoS2 monolayers as high-performance supercapacitor electrodes. Adv. Mater. **27**(6), 1117–1123 (2015)
70. Y. Li, K. Yin, L. Wang, X. Lu, Y. Zhang, Y. Liu, D. Yan, Y. Song, S. Luo, Engineering MoS2 nanomesh with holes and lattice defects for highly active hydrogen evolution reaction. Appl. Catal. B **239**, 537–544 (2018)
71. N. Choudhary, M. Patel, Y.-H. Ho, N.B. Dahotre, W. Lee, J.Y. Hwang, W. Choi, Directly deposited MoS 2 thin film electrodes for high performance supercapacitors. J. Mater. Chem. A **3**(47), 24049–24054 (2015)
72. S.S. Karade, D.P. Dubal, B.R. Sankapal, MoS 2 ultrathin nanoflakes for high performance supercapacitors: room temperature chemical bath deposition (CBD). RSC Adv. **6**(45), 39159–39165 (2016)
73. X. Geng, Y. Zhang, Y. Han, J. Li, L. Yang, M. Benamara, L. Chen, H. Zhu, Two-dimensional water-coupled metallic MoS2 with nanochannels for ultrafast supercapacitors. Nano Lett. **17**(3), 1825–1832 (2017)
74. W. Xiao, W. Zhou, T. Feng, Y. Zhang, H. Liu, L. Tian, Simple synthesis of molybdenum disulfide/reduced graphene oxide composite hollow microspheres as supercapacitor electrode material. Materials **9**(9), 783 (2016)
75. T. Sun, Z. Li, X. Liu, L. Ma, J. Wang, S. Yang, Facile construction of 3D graphene/MoS2 composites as advanced electrode materials for supercapacitors. J. Power Sources **331**, 180–188 (2016)
76. R. Thangappan, S. Kalaiselvam, A. Elayaperumal, R. Jayavel, M. Arivanandhan, R. Karthikeyan, Y. Hayakawa, Graphene decorated with MoS 2 nanosheets: a synergetic energy storage composite electrode for supercapacitor applications. Dalton Trans. **45**(6), 2637–2646 (2016)
77. M. Wang, H. Fei, P. Zhang, L. Yin, Hierarchically layered MoS2/Mn3O4 hybrid architectures for electrochemical supercapacitors with enhanced performance. Electrochim. Acta **209**, 389–398 (2016)
78. M. Sarno, A. Troisi, Supercapacitors based on high surface area MoS2 and MoS2–Fe3O4 nanostructures supported on physical exfoliated graphite. J. Nanosci. Nanotechnol. **17**(6), 3735–3743 (2017)

79. D. Liang, Z. Tian, J. Liu, Y. Ye, S. Wu, Y. Cai, C. Liang, MoS2 nanosheets decorated with ultrafine Co3O4 nanoparticles for high-performance electrochemical capacitors. Electrochim. Acta **182**, 376–382 (2015)
80. K. Wang, J. Yang, J. Zhu, L. Li, Y. Liu, C. Zhang, T. Liu, General solution-processed formation of porous transition-metal oxides on exfoliated molybdenum disulfides for high-performance asymmetric supercapacitors. J. Mater. Chem. A **5**(22), 11236–11245 (2017)

Recent Development in Chalcogenides for Supercapacitor Applications

G. M. Lohar, O. C. Pore, R. K. Kamble, and A. V. Fulari

Abstract The electrochemical supercapacitor, due to their rapid charge-discharge rates, good cyclic stability, high energy density, and power density are considered an ideal candidate for energy storage devices. For the high efficiency, improvement in performance, and electrochemical properties of supercapacitors; different nanostructured electrode materials have been studied. The efforts have been carried out to develop state-of-the-art high capacitive electrode materials for supercapacitors which enable high specific capacitance using rapid Faradaic redox reactions and provide ultra-high cyclic stability. Recent progress studies demonstrated that the transition metal chalcogenides especially NiX (X = S, Se, Te) are noteworthy candidates for highly efficient supercapacitor application because of their promising properties such as thermal stability, mechanical stability, superior intrinsic conductivity as compared to transition metal oxides and good cyclability. In the present chapter, we discussed the NiX (X = S, Se, Te) based materials for electrochemical supercapacitor application. Furthermore, we have summarized the supercapacitor performance of NiX (X = S, Se, Te) based nanomaterials. Lastly, the benefits and challenges of NiX (X = S, Se, Te) based materials for upcoming energy storage are discussed.

Keywords Metal chalcogenides · Supercapacitor · Specific capacitance

G. M. Lohar (✉) · O. C. Pore · R. K. Kamble
Department of Physics, Lal Bahadur Shastri College of Arts, Science and Commerce, Satara, M.S 415002, India
e-mail: gauravlohar24@gmail.com

O. C. Pore · R. K. Kamble
Holography and Materials Research Laboratory, Department of Physics, Shivaji University, Kolhapur, M.S. 416004, India

A. V. Fulari
Division of Physics and Semiconductor Science, Dongguk University, Seoul 04620, Republic of Korea

S. Thomas et al. (eds.), *Nanostructured Materials for Supercapacitors*,
Advances in Material Research and Technology,
https://doi.org/10.1007/978-3-030-99302-3_16

1 Introduction

The rapidly growing energy demand, energy consumption, and its consequences such as depletion of fossil fuels, pollution, and global warming, etc. attract the use of highly efficient, clean, energy consumption technologies and renewable energy resources. In recent years, different energy storage devices for example conventional capacitors, fuel cells, batteries, and supercapacitors receiving more attention from researchers. Among these devices, supercapacitors with their promising properties such as low maintenance costs, fast charging-discharging rate, high power density, high cyclic stability, and safe operation play a crucial role in electrochemical energy storage devices [1–3]. Based on charge storage mechanism, supercapacitors are of two types viz electric double-layer capacitors (EDLCs) and pseudocapacitors. The EDLCs store charges electrostatically at the electrode and electrolyte interface. Carbon-based materials are the EDLC type supercapacitors and they are suitable in the field of electronic equipment. But their relatively lower energy density restricts its application where high energy storage capability is required. In pseudocapacitors, reversible redox reactions are responsible for the charging-discharging process [4–6].

Different Metal oxides (MnO_2, Co_3O_4, Fe_2O_3, RuO_2, NiO, CuO), metal chalcogenides (NiS, MoS_2, VS_2, NiSe, NiTe, Cu_2S, CoS_2, and $NiCo_2S_4$), metal nitrides (RuN, VN, TiN, MoN), and conducting polymers have been utilized as pseudocapacitive electrode materials [4, 7]. The metal chalcogenides exhibit a better electrochemical supercapacitor performance as compared to metal oxides and replacing oxygen with chalcogenides is responsible for more flexibility for material organization. Out of these many materials transition metal chalcogenides; especially Sulphides, Selenides, and Tellurides have received more research interests as potential applications in supercapacitors. The better electrochemical supercapacitor performance of these transition metal chalcogenides is because of their unique crystal structures, tunable stoichiometric compositions, and redox-rich sites. Also, its higher electrical conductivity in comparison to respective transition metal oxide makes them a suitable candidate for supercapacitor application as compared to transition metal oxides [3, 8, 9].

Recently, the transition metals such as Ni, Co, Mn, Ti, and Fe and their compounds (oxides, hydroxides, and sulfides) have been extensively studied for electrochemical supercapacitor application. Among these transition metal base compounds, transition metal sulfides especially nickel sulfides resemble suitable candidates for supercapacitor application because of the slight difference in electronegativity of Ni ($\nu =$ 1.91 eV) and S ($\nu = 2.58$ eV), high specific capacitance value, high redox activity, high electrical conductivity, easy as well as low-cost preparation [10–12]. Selenium (Se) is the nearest element of sulfur (S) in the VI A group of the periodic table and exhibits the same oxidation states and valance electrons as sulfur. Hence, the electrochemical activities of metal selenides and metal sulfides almost resemble. The lower electronegativity of Te ($\nu = 2.1$ eV) as compared to S and Se ($\nu = 2.55$ eV) also attracting attention of researchers for their use in Ni-based metal chalcogenides [3, 13–15]. In the present chapter the NiX (X = S, Se, Te) based electrode materials,

their characterizations (XRD, FT-IR, Raman, XPS spectra), and their use in supercapacitor application are discussed. NiX (X = S, Se, Te) based electrode materials have been unveiled as cheap, promising, and eco-friendly materials for the development of supercapacitors.

2 Characterizations of NiX (X = S, Se, Te) Based Materials

Some characterizations such as X-ray diffraction (XRD), Fourier transform infrared spectroscopy (FT-IR), Fourier transforms Raman spectroscopy (FT-Raman), and X-ray photoelectron spectroscopy (XPS) of NiX (X = S, Se, Te) based materials for electrochemical supercapacitor application are mentioned. Parveen et al. [16] synthesized flower-like NiS nanostructures by solvothermal method. The XRD pattern (Fig. 1a) of as optimized NiS_10h electrode shows the characteristic peaks at 30.15°, 34.63°, 45.86°, 53.55°, 60.8°, 62.68°, 65.31°, 70.64°, and 73.13° which are corresponding to the planes (100), (101), (102), (110), (103), (200), (201), (004), and (202) respectively. These all peaks are related to JCPDS card number 10-075-0613 of NiS. Wu et al. [17] synthesized $Ni_{0.85}Se$ nanoparticles by tuning morphologies by using different solvents by simple solvothermal method. Figure 1b shows the XRD spectra of $Ni_{0.85}Se$ different NiSe nanostructures synthesized by using different solvents. The peaks at 33.3°, 45.0°, 50.7°, 60.3°, 62.5°, and 70.5° are assigned to planes (101), (102), (110), (103), (201), and (202) of $Ni_{0.85}Se$ JCPDS card number 18-0888. These results indicated the formation of high crystallinity and purity of $Ni_{0.85}Se$ nanostructures. Zhou et al. [18] developed NiTe directly deposited on NF for supercapacitor application for the first time. Figure 1c depicts the XRD spectrum of the NiTe electrode. The peaks at 58.61°, 46.52°, 43.41°, 31.54°, and in the XRD pattern of NiTe are correspond to the crystalline plane (103), (110), (102), (101) and respectively. These peaks are corresponding to the JCPDS card number 38–1393 corresponding to the hexagonal crystalline structure of NiTe. Karthikeyan et al. [19] synthesized NiS nanoparticles with a precursor hot-injection method. The FT-IR study reveals that the peaks at 2921/2852, 3400, and 1653 cm^{-1} are related to the C-H stretching, N-H stretching, and rocking vibrations respectively. Li et al. [20] prepared a composite of graphene and NiS_2 (graphene/NiS_2) by using a simple solvothermal reaction.

Figure 1d presents the FT-Raman spectrum of as-synthesized graphene/NiS_2 composite. The peak at 1580 and 1349 cm^{-1} corresponds to the G and D band of rGO respectively. Song et al. [21] developed Nickel selenide nanoparticles on carbon nanowires ($NiSe_2$/C NWs) by simple hydrothermal method and salinization strategy. Figure 1e shows the Raman spectra of $NiSe_2$/C electrode. The Raman shift in Fig. 1e at 1576 and 1349 cm^{-1} present the G and D band of carbon respectively. Inset of Fig. 1e shows the Raman spectra with an enlarged scale of $NiSe_2$/C NWs showing the peaks at 151.86, 169.24, 209.20, and 231.75 cm^{-1}. Kim et al. [22] prepared Ni_3S_2/Ni electrode with the help of a two-step electrodeposition method for supercapacitor application. Figure 1f and g presents the Ni 2p and S 2p spectrum of Ni_3S_2/Ni electrode. The two peaks in Ni 2p spectrum at 855.4 eV and 873.2 eV are

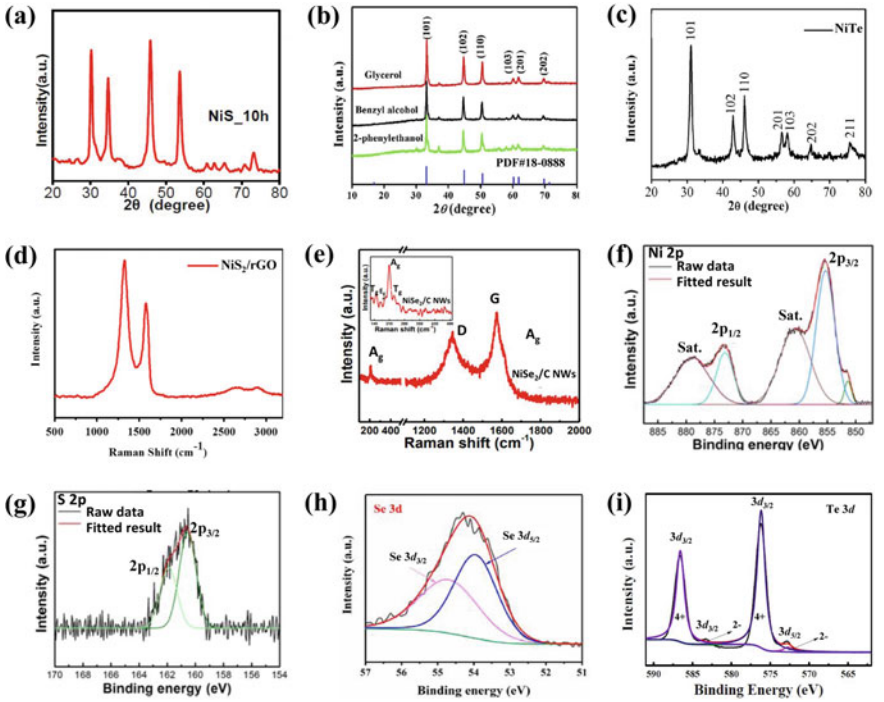

Fig. 1 **a** XRD pattern of NiS. Adapted with permission from [16], Copyright (2018), Elsevier. **b** XRD spectra of $Ni_{0.85}Se$ synthesized by using different solvents. Adapted with permission from [17], Copyright (2019), Elsevier. **c** XRD spectrum of NiTe. Adapted with permission from [18], Copyright (2016), Elsevier. **d** Raman spectrum of NiS_2/rGO. Adapted with permission from [20], Copyright (2015), Elsevier. **e** Raman spectrum of $NiSe_2$/C NWs (Inset: enlarged view of Raman spectra). Adapted with permission from [21], Copyright (2017), Elsevier. **f** the Ni 2p spectrum of Ni_3S_2/Ni 6 min electrode. Adapted with permission from [22], Copyright (2018), American Chemical Society. **g** and S 2p spectrum. Adapted with permission from [22], Copyright (2018), American Chemical Society. **h** XPS spectra of Se. Adapted with permission from [23], Copyright (2020), Elsevier. **i** XPS spectra of Te 3d spectrum. Adapted with permission from [24], Copyright (2019), Elsevier

related to Ni $2p_{3/2}$ and Ni $2p_{1/2}$ respectively. The peaks at 162.1 eV and 160.5 eV in S 2p spectra confirm the presence of Ni_3S_2. Zhao et al. [23] developed hierarchical Ni_3Se_2 nanodendrite arrays by a solvothermal method by a binder-free approach. Figure 1h shows the Se 3d spectrum of as-synthesized Ni_3Se_2. The peaks in Se 3d spectrum at 53.95 and 54.69 eV are related to Se $3d_{5/2}$ and Se $3d_{3/2}$ respectively which confirms the existence of Se^{2-}. Ye et al. [24] prepared cobalt-doped NiTe electrode (NiTe: Co) via the single-step hydrothermal method for electrochemical supercapacitor application. Figure 1i presents Te 4d spectrum. The characteristic bands at 583.3 eV as well as 572.8 eV are related to the Te^{2-}, while the peaks at 586.6 eV and 576.2 eV are related to Te^{4+}.

3 Recent Development in NiX (X = S, Se, Te) Based Electrode Materials for Supercapacitor Application

3.1 Nickle Sulfides

Zhang et al. [25] developed different β-NiS morphologies by two-step solvothermal method by varying volume ratios of a solvent such as ethanol, deionized water, and glycol. Out of different morphologies, flowerlike β-NiS electrode achieved 2425.89 F g^{-1} specific capacitance at 1 A g^{-1}. The better supercapacitor results of β-NiS flower-like electrode as compared to other morphologies (coral-like, urchin-like, and flake-like) raised due to its special pore structures and enlarge surface area as compared to other morphologies. These observations confirm that the flower-like β-NiS electrode performs a crucial role in achieving better specific capacitance. The as-synthesized β-NiS//Activated Carbon (β-NiS//AC) electrode achieved a maximum specific capacitance of 32.90 F g^{-1}. Kim et al. [22] developed Ni_3S_2/Ni electrodes with a two-step electrodeposition process. Figure 2a presents the synthesis process of Ni_3S_2/Ni electrode by electrodeposition method. The optimized Ni_3S_2/Ni electrode shows flaky morphology. The prepared electrode exhibited 786.5 C g^{-1} specific capacitance at 10 mA cm^{-2} as well as good capacity retention of 88.6% over 1000 cycles. Also, they have prepared (Asymmetric supercapacitor device) ASC device (Ni_3S_2/Ni 6 min//AC) which achieved a specific capacitance of 103.2 F g^{-1} at 1 A g^{-1} and cyclic stability of 93.9% after 6000 cycles. Darsara et al. [26] developed Ni_3S_4–NiS and Ni_3S_4–NiS@rGO hybrid by one-step hydrothermal method. SEM study of Ni_3S_4–NiS reveal the formation of starfish-like morphology with various dimensions (Fig. 2b). In the case of Ni_3S_4–NiS@rGO hybrid, starfish-like morphology of Ni_3S_4–NiS observed to be anchored on graphene surface plate. The Ni_3S_4–NiS and Ni_3S_4–NiS@rGO samples showed a BET surface area of 220 and 270 m^2 g^{-1} respectively. The prepared Ni_3S_4–NiS and Ni_3S_4–NiS@rGO electrodes achieved 1005 and 1578 F g^{-1} specific capacitance at 0.5 A g^{-1}.

The Ni_3S_4–NiS@rGO electrode exhibited 9% more stability as compared to Ni_3S_4–NiS electrode. The Ni_3S_4–NiS@rGO electrode exhibited more specific capacitance and stability as compared to Ni_3S_4–NiS electrode because the rGO in Ni_3S_4–NiS@rGO provides more surface area for electrolyte interaction and higher conductivity. Guan et al. [27] synthesized NiS-MoS_2 on carbon cloth having morphology hetero-nanosheet arrays (HNSAs) as shown in (Fig. 2c). The maximum specific capacity calculated for NiS-MoS_2 HNSAs//CC electrode was 271.7 mAh g^{-1} at 2.5 mA cm^{-2}. Also, it showed better cyclic stability of 78% over 3000 GCD cycles. Xu et al. [28] developed carbon nanofibers (CNFs) wrapped with NiS nanoparticles via electrospinning, calcination, and in situ sulfurization method. As shown in Fig. 2d CNFs-NiS show a netlike structure. This netlike structure is observed to be made up of many pores spread on a rough surface. It exhibited the highest 177.1 mAh g^{-1} specific capacity at 1 A g^{-1} with 88.7% cyclic stability after 5000 cycles.

Tan et al. [29] developed cabbage-like α-NiS using facile solvothermal method then annealing treatment. The CVs of α-NiS electrode at 5 to 50 mV s^{-1} scan rates are

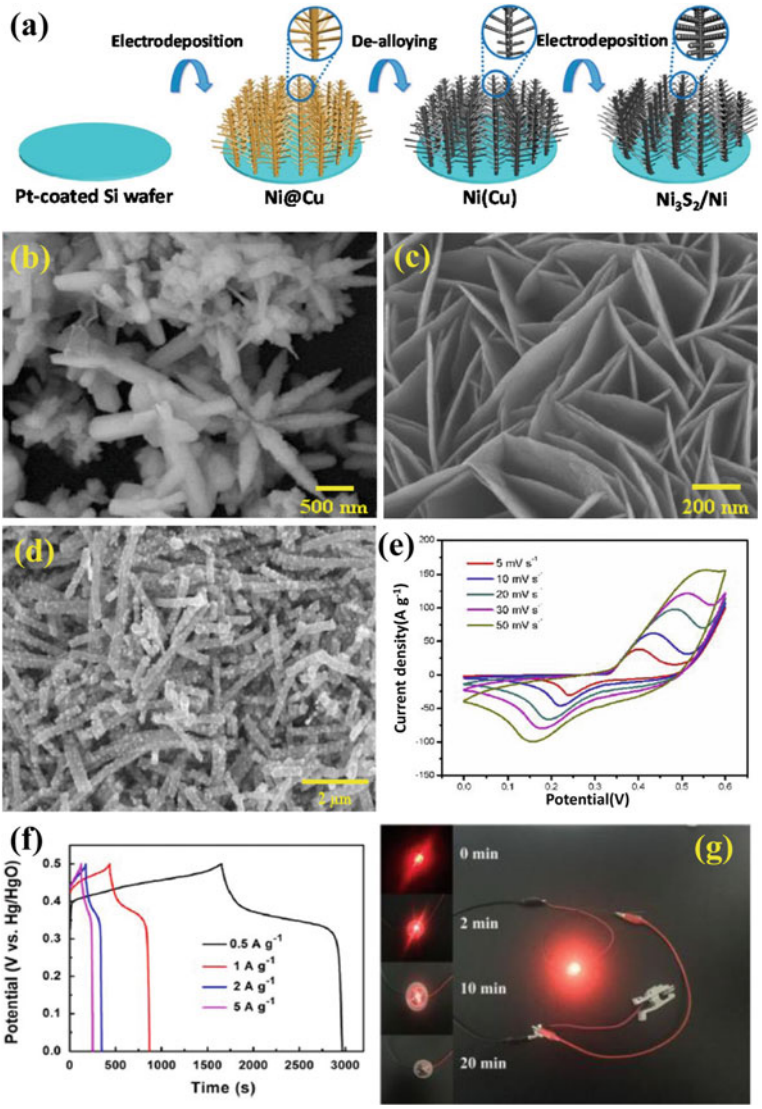

Fig. 2 **a** Schematic presentation of preparation of Ni_3S_2/Ni electrode. Adapted with permission from [22], Copyright (2018), American Chemical Society. **b** SEM image of Ni_3S_4–NiS. Adapted with permission from [26], Copyright (2021), Elsevier. **c** SEM image of NiS-MoS_2. Adapted with permission from [27], Copyright (2019), American Chemical Society. **d** SEM image of CNFs-NiS. Adapted with permission from [28], Copyright (2018), Elsevier. **e** CV curves of α-NiS electrode at various scan rates (5–50 mV s^{-1}). Adapted with permission from [29], Copyright (2019), Elsevier. **f** GCD curves of NiS/rGO composites at various current densities (0.5–5 A g^{-1}). Adapted with permission from [30], Copyright (2014), Elsevier. **g** LED indicator lighted up by two CNFs-NiS//CNFs Asymmetric Supercapacitor device cells. Adapted with permission from [28], Copyright (2018), Elsevier

depicted in Fig. 2e. The electrode achieved a specific capacity of 235.88 mAh g^{-1} at 1 A g^{-1} and cyclic stability of 87.1% over 2000 cycles. Yang et al. [30] synthesized NiS/rGO composite in which NiS nanorods anchored on rGO via hydrothermal method. Figure 2f displays the GCD curves of NiS/rGO composite at 0.5–5 A g^{-1} current densities. The NiS/rGO electrode achieved 905.30 F g^{-1} specific capacitance at 0.5 A g^{-1} and exhibited cyclic stability of 90.9% over 1000 cycles. Figure 2g shows the LED indicator lighted up by two CNFs-NiS//CNFs Asymmetric Supercapacitor device cells synthesized by Xu et al. [28]. It showed an energy density of 13.32 mWh cm^{-3} and about 89.5% of cyclic stability after 5000 cycles. The NiS based electrode materials are a promising candidate in the field of electrochemical supercapacitor application.

3.2 Nickel Selenide

Zhao et al. [31] developed NiSe@Ni_3Se_2/NF nanostructure by hydrothermal method followed by electrodeposition method. The schematic presentation of synthesis of NiSe@Ni_3Se_2/NF nanostructure is shown in Fig. 3a. The NiSe@Ni_3Se_2/NF nanostructure is made up of NiSe nanowire arrays core and thin Ni_3Se_2 nanosheets shell. Figure 3b shows the NiSe nanowire arrays and such morphology favorable for better electric conductivity and indirectly better theoretical specific capacitance. The prepared NiSe@Ni_3Se_2/NF electrode achieved 1260 F g^{-1} specific capacitance at 10 A g^{-1} and capacity retention of 92.5% after 4000 cycles. The ASC device exhibited an energy density of 45.5 Wh kg^{-1} (at power density 1.600 kW kg^{-1}). Also, it showed capacity retention of 96.1% over 12,000 cycles. Zhao et al. [23] developed binder-less Ni_3Se_2 nanodendrite arrays grown on NF with a one-step solvothermal approach for advanced positive electrodes for supercapacitors. Figure 3c shows the morphology and dendrite-shaped features of Ni_3Se_2 electrodes. Such morphology of Ni_3Se_2 makes it highly electronically conductive, able to provide a more surface area and large number of electrochemical active sites. The as synthesized electrode achieved 1234 F g^{-1} specific capacitance at 1 A g^{-1}. Arul et al. [32] prepared $NiSe_2$/$Ni(OH)_2$ nanocomposites with hydrothermal method followed by ultrasonication method. Figure 3d depicts the FESEM image of hexapod-like $NiSe_2$ microstructure. Such Hexapod-like microstructures are made up of less than ~10 nm nanoparticles.

The prepared electrode exhibited 2212 F g^{-1} specific capacitance at 2 mA cm^{-2} with cyclic stability of 95% for 5000 cycles. Tian et al. [33] prepared NiSe nanorod arrays on a NF current collector with a one-pot hydrothermal method. Figure 3e depicts the GCD curves of NiSe NRA/NF electrode at 5–50 mA cm^{-2} current densities. The NiSe electrode achieved 6.81 F cm^{-2} specific capacitance at 5 mA cm^{-2}. The assembled ASC device (NiSe NRA/NF//RGO) retained 90.09% initial capacitance over 3000 cycles. Wang et al. [34] developed truncated cube-like crystals of $NiSe_2$ via a simple hydrothermal method. Figure 3f presents estimated specific capacitance from the galvanostatic charge-discharge curve versus applied current density of the $NiSe_2$ electrode. The cube-like $NiSe_2$ electrode shows a maximum 1044 F

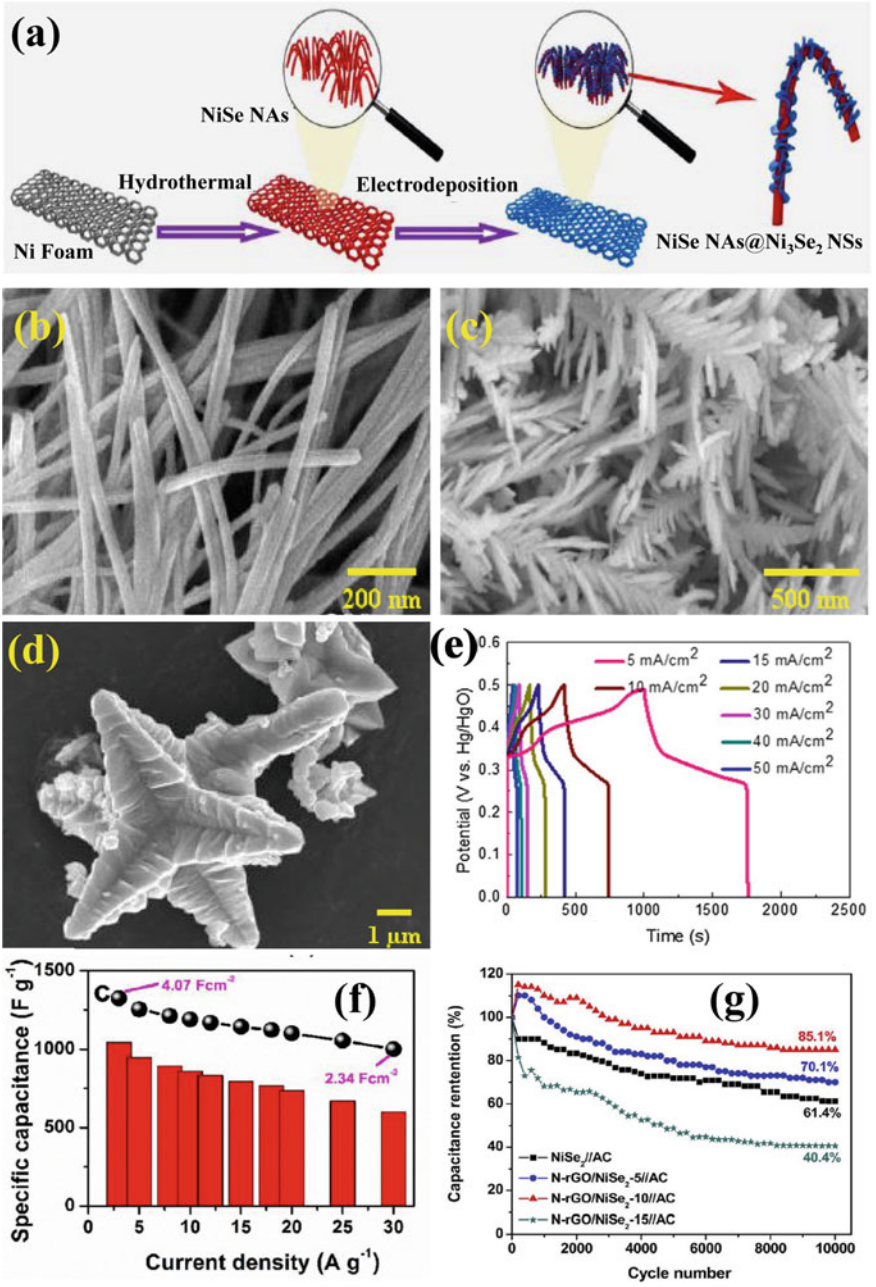
(a)
NiSe NAs
Hydrothermal
Electrodeposition
Ni Foam
NiSe NAs@Ni3Se2 NSs
(b)
200 nm
(c)
500 nm
(d)
1 µm
(e)
5 mA/cm2
10 mA/cm2
15 mA/cm2
20 mA/cm2
30 mA/cm2
40 mA/cm2
50 mA/cm2
Potential (V vs. Hg/HgO)
Time (s)
(f)
4.07 Fcm-2
2.34 Fcm-2
Specific capacitance (F g-1)
Current density (A g-1)
(g)
85.1%
70.1%
61.4%
40.4%
NiSe2//AC
N-rGO/NiSe2-5//AC
N-rGO/NiSe2-10//AC
N-rGO/NiSe2-15//AC
Capacitance rentention (%)
Cycle number

◀**Fig. 3** **a** Schematic presentation of synthesis of NiSe nanowire arrays (NWAs) @ Ni_3Se_2 nanosheets (NSs) composites by hydrothermal method followed by electrodeposition method. Adapted with permission from [31], Copyright (2021), Elsevier. **b** SEM image of NiSe NWAs. Adapted with permission from [31], Copyright (2021), Elsevier. **c** SEM image of Ni_3Se_2 electrode. Adapted with permission from [23], Copyright (2020), Elsevier. **d** FESEM image of $NiSe_2$ electrode. Adapted with permission from [32], Copyright (2019), Elsevier. **e** GCD curves of NiSe NRA/NF electrode at various current densities (5–50 mA cm^{-2}). Adapted with permission from [33], Copyright (2017), Elsevier. **f** Graph of specific capacitance vs current density of $NiSe_2$ electrode. Adapted with permission from [34], Copyright (2017), Elsevier. **g** cyclic stability test of for $NiSe_2$//AC, N-rGO/$NiSe_2$-5//AC, N-rGO/$NiSe_2$-10//AC and N-rGO/$NiSe_2$-15//AC asymmetric supercapacitors at a current density of 5 A g^{-1}. Adapted with permission from [35], Copyright (2019), Elsevier

g^{-1} specific capacitance at 3 A g^{-1}. The prepared $NiSe_2$//AC ASC device shows 87.4% capacity retention over 20,000 cycles. Gu et al. [35] prepared N-rGO/$NiSe_2$ composite with the help of a two-step method. In actual experimental firstly $Ni(OH)_2$ synthesized by simple hydrothermal method and then N-rGO/$NiSe_2$ nanocomposites with different content of N-rGO by solvothermal method. The amount of GO used in the synthesis of composites were 0, 5, 10, and 15 mg. Accordingly, the obtained composites were named $NiSe_2$, N-rGO/$NiSe_2$-5, N-rGO/$NiSe_2$-10, and N-rGO/$NiSe_2$-15 which exhibited higher specific capacitance of 720.8, 1270.4, 2451.4, and 616.0 F g^{-1} at 1 A g^{-1}. Also, they prepared an ASC device with prepared composites and AC. Out of different ASC devices, the N-rGO/$NiSe_2$-10//AC device shows maximum specific capacitance of 113.8 F g^{-1} at a current density of 1 A g^{-1}. Figure 3g shows the cyclic stability test for $NiSe_2$//AC, N-rGO/$NiSe_2$-5//AC, N-rGO/$NiSe_2$-10//AC, and N-rGO/$NiSe_2$-15//AC ASC device at a current density of 5 A g^{-1}. The N-rGO/$NiSe_2$-10//AC ASC device showed better capacity retention of 85.1% after 10,000 cycles. The study reveals that the NiSe based electrodes are promising materials for supercapacitor application.

3.3 Nickel Telluride

Deshagani et al. [36] synthesized selenide dopped nickel telluride (NiTe: Se) flakes by facile hydrothermal method. The experimental procedure of synthesis of NiTe:Se@NF, synthesis of AC from dried coconut shell, and synthesis of poly(N-methyl pyrrole) (PMP) is depicted in Fig. 4a. The SEM study shows the compositional transformation i.e. doping of NiTe with Se produces NiTe:Se, and morphology changes from fiber-like to flakelike morphology. The as-prepared electrode achieved a 634 F g^{-1} specific capacitance at 1 A g^{-1}. The prepared PMP@AC//PMP@NiTe:Se supercapacitor exhibited a capacity of 404 C g^{-1}. Zhou et al. [18] developed NiTe rods on NF by simple hydrothermal method. Figure 4b shows the FESEM image of the NiTe electrode shows a maximum specific capacitance of 804 F g^{-1} (at 1 A g^{-1}). The fabricated ASC device with NiTe as anode and AC as a cathode (NiTe//AC) achieved

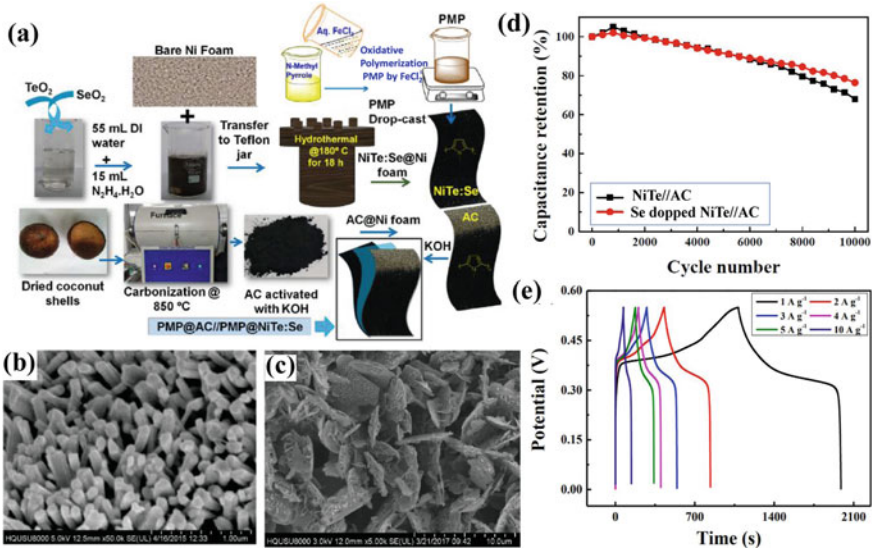

Fig. 4 **a** Schematic diagram of the synthesis of PMP@AC//PMP@ NiTe:Se device. Adapted with permission from [36], Copyright (2020), Elsevier. **b** FESEM images of NiTe rods. Adapted with permission from [18], Copyright (2016), Elsevier. **c** FESEM images of Se doped NiTe with 9:100 doping ratio of Se:Te. Adapted with permission from [37], Copyright (2018), Elsevier. **d** Cycling performances of NiTe and Se doped NiTe electrodes at a current density of 2 A g^{-1}. Adapted with permission from [37], Copyright (2018), Elsevier. **e** GCD curve of NiTe:Co electrode at current densities (1–10 A g^{-1}). Adapted with permission from [24], Copyright (2019), Elsevier

a maximum energy density of 33.6 Wh kg^{-1} and power density of 807.9 W kg^{-1}. It exhibited cyclic stability of about 81% over 3000 cycles. Ye et al. [37] prepared Se doped NiTe electrode materials by using a hydrothermal method on Ni-foam. Figure 4c shows the FESEM image of Se doped NiTe with a 9:100 doping ratio of Se:Te. Such electrode showed 603.6 F g^{-1} specific capacitance at a current density of 1 A g^{-1}. Figure 4d shows the cyclic stability of Se doped NiTe and pristine NiSe electrodes.

The estimated capacitance of the NiTe with Se doped electrode after 1000 cycling is almost constant. The pristine NiTe without Se doping also exhibited better capacity retention of 93.2% over 1000 cycles. The fabricated ASC device achieved a 119.9 F g^{-1} specific capacitance at 1 A g^{-1} and excellent cyclic stability of 76.4% after 10,000 cycles. Ye et al. [24] also synthesized Co-doped NiTe on NF by one-step hydrothermal method. The doping of Co ions in NiTe changes the original microstructure of NiTe as well as improves the electrochemical properties. Figure 4e shows the GCD curve of NiTe: Co electrode at different current densities (1–10 A g^{-1}). The estimated maximum specific capacitance of NiTe: Co electrode is 1445.6 F g^{-1} at 1 A g^{-1}. The as fabricated NiTe: Co//AC device provided an energy density of 36.8 Wh kg^{-1} than the NiTe//AC device (24.4 Wh kg^{-1}).

4 Concluding Remark

This chapter describes a brief overview of NiX (X = S, Se, Te) electrode materials for their electrochemical supercapacitor application. Such electrode materials have been unveiled as cost-effective, promising, and environmentally friendly materials for the fabrication of scalable and flexible supercapacitors. In the beginning, we discussed some characterizations of NiX based electrodes. We have summarized the electrochemical supercapacitor performance of NiX based electrodes and their composites. The approaches towards modifying the physical and chemical parameters of NiX based electrodes for cheap, highly efficient, and renewable energy devices are still in demand. The NiX based electrodes are still far from commercialization even though they show better results. To complete this target, continued and dedicated research efforts should be needed for the improvement of its mechanisms, electrochemical performance, and electrochemical reactions for commercial applications. Despite all the challenges, ongoing research should be more focused to develop highly conductive binder-less NiX based electrodes and their composites.

Table 1 Literature review on nanostructured NiX (X = S, Se, Te) based electrodes

Sr. No	Electrode material	Morphology	KOH Electrolyte	Specific capacitance	Stability	Ref
1	α-NiS	Cabbage-like	6 M	235.88 mAh g^{-1} at 1 A g^{-1}	87.1% after 2000 cycles	[29]
2	NiS	Flower-like	6 M	603.97 F g^{-1} at 1 A g^{-1}	88.57% after 5000 cycle	[16]
3	NiS	Nanowires	3 M	2187.5 F g^{-1} at 3 mV s^{-1}	78.7% after 8000 cycles	[38]
4	β-NiS	Flower-like	6 M	2425.89 F g^{-1} at 1 A g^{-1}	~100% after 5000 cycles	[25]
5	NiS	Nanoparticles	2 M	177.1 mAh g^{-1} at 1 A g^{-1}	88.7% after 5000 cycles	[28]
6	NiS	Forest-like	1 M	342.1 mA h g^{-1} at 4 mA cm^{-2}	89.4% after 3000 cycles	[39]

(continued)

Table 1 (continued)

Sr. No	Electrode material	Morphology	KOH Electrolyte	Specific capacitance	Stability	Ref
7	Ni_3S_2	Flacky	1 M	786.5 C g^{-1} at 10 mA cm^{-2}	88.6% after 1000 cycles	[22]
8	NiS/NiO	Nanoparticles	2 M	1260 F g^{-1} at 0.5 A g^{-1}	–	[40]
9	NiS-MoS_2	Hetero-nanosheet arrays	6 M	271.7 mAh g^{-1} at 2.5 mA cm^{-2}	78% after 3000 cycles	[27]
10	Ni_3S_4–NiS@rGO	Starfish like	2 M	1073 F g^{-1} at 0.5 A g^{-1}	91% after 5000 cycles	[26]
11	NiS/rGO	Porous microstructures	6 M	305 F g^{-1} at 1.1 A g^{-1}	91% after 3000 cycles	[41]
12	Gaphene@NiS	Graphene wrapped nanoprisms	2 M	1000 F g^{-1} at 5 A g^{-1}	71% after 2000 cycles	[42]
13	NiS/rGO	Nanorods anchored on rGO	2 M	905.30 F g^{-1} at 0.5 A g^{-1}	90.9% after 1000 cycles	[30]
14	NiS/rGO	Nanorods anchored on graphene	2 M	744 C g^{-1} at 1 A g^{-1}	89% after 20,000 cycles	[43]
15	Ni_xS_y/rGO	Nanoflakes	2 M	2074 F g^{-1} at 1 A g^{-1}	80% after 5000 cycles	[44]
16	Ni_3Se_2	Nanodendrite arrays	2 M	1234 F g^{-1} at 1 A g^{-1}	Good cyclic stability	[23]
17	Ni_3Se_2	Nanowires	2 M	2.6 C cm^{-2} at 5 mA cm^{-2}	93.1% after 2000 cycles	[45]
18	Ni_3Se_2	Nanosheets	3 M	854 F g^{-1} at 1 A g^{-1}	87.23% after 2000 cycles	[46]

(continued)

Table 1 (continued)

Sr. No	Electrode material	Morphology	KOH Electrolyte	Specific capacitance	Stability	Ref
19	$Ni_{0.85}Se$	Honeycomb like nanosheets	3 M	3105 F g^{-1} at 1 A g^{-1}	90.1% after 5000 cycles	[47]
20	$NiSe_2$	Spheres	2 M	1144.1 F g^{-1} at 0.5 A g^{-1}	Good cyclic stability	[48]
21	$NiSe_2$	Hollow spheres	2 M	341 F g^{-1} at 1 A g^{-1}	Good cyclic stability	[49]
22	$NiSe_2$	2D nanosheets	1 M	466 F g^{-1} at 5 mV s^{-1}	81.3% after 1000 cycles	[50]
23	NiSe	Nanorod arrays	6 M	6.81 F cm^{-2} at 5 mA cm^{-2}	78.9% after 2000 cycles	[33]
24	$NiSe_2$	Truncated cube-like	4 M	1044 F g^{-1} at 3 A g^{-1}	67% after 2000 cycles	[34]
25	$NiSe_2$	Pyramid-like	3 M	240.83 mAh g^{-1} at 1 A g^{-1}	52.7% after 1000 cycles	[51]
26	NiSe-$Ni_{0.85}Se$	Irregular nanoparticle	2 M	669 C g^{-1} at 1 A g^{-1}	–	[52]
27	NiSe@Ni_3Se_2	Nanosheet nanowire arrays	3 M	1260 F g^{-1} at 10 A g^{-1}	92.5% after 4000 cycles	[31]
28	$NiSe_2$/$Ni(OH)_2$	Hexapod-like	3 M	2212 F g^{-1} at 2 mA cm^{-2}	95% after 5000 cycles	[32]
29	NiSe	Microspheres	2 M	492 F g^{-1} at 0.5 A g^{-1}	84.6% after 200 cycles	[53]
30	N-rGO/$NiSe_2$	GO decorated with nanoparticle	3 M	2451.4 F g^{-1} at 1 A g^{-1}	–	[35]
31	$Ni_{0.85}Se$@C/rGO	Nanosheets on the surface of rGO	2 M	1160 F g^{-1} at 1 A g^{-1}	88.8% after 1000 cycles	[54]

(continued)

Table 1 (continued)

Sr. No	Electrode material	Morphology	KOH Electrolyte	Specific capacitance	Stability	Ref
32	$NiSe_2$/rGO	Nanoparticles supported on GO	2 M	137.7 mAh g^{-1} at 1 A g^{-1}	82% after 2500 cycles)	[55]
33	NiTe	Rod like	3 M	804 F g^{-1} at 1 A g^{-1}	91.3% after 1000 cycles	[18]
34	NiTe	Fiber-like	6 M	634 F g^{-1} at 1 A g^{-1}	–	[36]
35	NiTe: Se	Flake-like	6 M	943 F g^{-1} at 1 A g^{-1}	–	[36]
36	NiTe	Nanorods	3.5 M	618 F g^{-1} at 1 A g^{-1}	75% after 5000 cycles	[56]
37	NiTe: Co	Nanoparticles	3 M	1645.6 F g^{-1} at 1 A g^{-1}	90% after 1000 cycles	[24]
38	NiTe	Flake shaped	3 M	872.7 F g^{-1} 1 A g^{-1}	85% after 1000 cycles	[24]
39	Se-doped NiTe	Flake-like	3 M	998.2 F g^{-1} at 1 A g^{-1}	Good cyclic stability over 1000 cycles	[37]
40	NiTe	–	3 M	603.6 F g^{-1} at 1 A g^{-1}	93.2% after 1000 cycles	[37]

Acknowledgements Dr. G. M. Lohar is thankful to DST-SERB, Government of India, for providing funds under the ECRA scheme File No: ECR/2017/002099.

References

1. U.M. Patil, V. V. Patil, A.S. Patil, S.J. Marje, J.L. Gunjakar, C.D. Lokhande, Nanoporous Transition metal oxide-based electrodes for supercapacitor application. Chem. Depos. Nanocrystalline Met. Oxide Thin Film. 623–672 (2021)

2. J. Theerthagiri, A.P. Murthy, S.J. Lee, K. Karuppasamy, S.R. Arumugam, Y. Yu, M.M. Hanafiah, H.S. Kim, V. Mittal, M.Y. Choi, Recent progress on synthetic strategies and applications of transition metal phosphides in energy storage and conversion. Ceram. Int. **47**, 4404–4425 (2021)
3. H. Yuan, L. Kong, T. Li, Q. Zhang, A review of transition metal chalcogenide/graphene nanocomposites for energy storage and conversion. Chinese Chem. Lett. **28**, 2180–2194 (2017)
4. O.C. Pore, A.V. Fulari, R.V. Shejwal, V.J. Fulari, G.M. Lohar, Review on recent progress in hydrothermally synthesized MCo2O4/rGO composite for energy storage devices, Chem. Eng. J. **426**, 131544 (2021)
5. M. Sajjad, F. Cheng, W. Lu, Research progress in transition metal chalcogenide based anodes for K-ion hybrid capacitor applications: a mini-review. RSC Adv. **11**, 25450–25460 (2021)
6. C. Xia, Q. Jiang, C. Zhao, P.M. Beaujuge, H.N. Alshareef, Asymmetric supercapacitors with metal-like ternary selenides and porous graphene electrodes. Nano Energy **24**, 78–86 (2016)
7. J. Theerthagiri, K. Karuppasamy, G. Durai, A. ul H.S. Rana, P. Arunachalam, K. Sangeetha, P. Kuppusami, H.S. Kim, Recent advances in metal chalcogenides (MX; X = S, Se) nanostructures for electrochemical supercapacitor applications: a brief review. Nanomaterials **8**, 256 (2018)
8. G.A. Muller, J.B. Cook, H.-S. Kim, S.H. Tolbert, B. Dunn, High performance pseudocapacitor based on 2D layered metal chalcogenide nanocrystals. Nano Lett. **15**, 1911–1917 (2015)
9. H. Chauhan, S. Deka, Supercapacitors based on two-dimensional transition metal dichalcogenides and their hybrids, Fundam. Supercapacitor Appl. 2D Mater. 159–191 (2021)
10. M.J. Crane, M.B. Lim, X. Zhou, P.J. Pauzauskie, Rapid synthesis of transition metal dichalcogenide–carbon aerogel composites for supercapacitor electrodes. Microsystems Nanoeng. **3**, 17032 (2017)
11. Y. Wang, Y. Zhao, X. Ding, L. Qiao, Recent advances in the electrochemistry of layered post-transition metal chalcogenide nanomaterials for hydrogen evolution reaction. J. Energy Chem. **60**, 451–479 (2021)
12. N.M. Santhosh, K.K. Upadhyay, P. Stražar, G. Filipič, J. Zavašnik, A.M. de Ferro, R.P. Silva, E. Tatarova, M. de F. Montemor, U. Cvelbar, Advanced carbon–nickel sulfide hybrid nanostructures: extending the limits of battery-type electrodes for redox-based supercapacitor applications. ACS Appl. Mater. Interfaces. **13**, 20559–20572 (2021)
13. M. Manikandan, K. Subramani, S. Dhanuskodi, M. Sathish, One-pot hydrothermal synthesis of nickel cobalt telluride nanorods for hybrid energy storage systems. Energy Fuels **35**, 12527–12537 (2021)
14. O. Maurya, S. Khaladkar, M.R. Horn, B. Sinha, R. Deshmukh, H. Wang, T. Kim, D.P. Dubal, A. Kalekar, Emergence of Ni-based chalcogenides (S and Se) for clean energy conversion and storage. Small **17**, 2100361 (2021)
15. R.N.A.R. Seman, M.A. Azam, M.H. Ani, Graphene/transition metal dichalcogenides hybrid supercapacitor electrode: status, challenges, and perspectives. Nanotechnology **29**, 502001 (2018)
16. N. Parveen, S.A. Ansari, S.G. Ansari, H. Fouad, N.M. Abd El-Salam, M.H. Cho, Solid-state symmetrical supercapacitor based on hierarchical flower-like nickel sulfide with shape-controlled morphological evolution. Electrochim. Acta. **268**, 82–93 (2018)
17. S. Wu, Q. Hu, L. Wu, J. Li, H. Peng, Q. Yang, One-step solvothermal synthesis of nickel selenide nanoparticles as the electrode for high-performance supercapacitors. J. Alloys Compd. **784**, 347–353 (2019)
18. P. Zhou, L. Fan, J. Wu, C. Gong, J. Zhang, Y. Tu, Facile hydrothermal synthesis of NiTe and its application as positive electrode material for asymmetric supercapacitor. J. Alloys Compd. **685**, 384–390 (2016)
19. R. Karthikeyan, D. Thangaraju, N. Prakash, Y. Hayakawa, Single-step synthesis and catalytic activity of structure-controlled nickel sulfide nanoparticles. CrystEngComm **17**, 5431–5439 (2015)
20. X. Li, J. Shen, N. Li, M. Ye, Template-free solvothermal synthesis of NiS2 microspheres on graphene sheets for high-performance supercapacitors. Mater. Lett. **139**, 81–85 (2015)
21. D. Song, H. Wang, X. Wang, B. Yu, Y. Chen, NiSe2 nanoparticles embedded in carbon nanowires as highly efficient and stable electrocatalyst for hydrogen evolution reaction. Electrochim. Acta. **254**, 230–237 (2017)

22. D. Kim, P.K. Kannan, S. Mateti, C.-H. Chung, Indirect nanoconstruction morphology of Ni3S2 electrodes renovates the performance for electrochemical energy storage. ACS Appl. Energy Mater. **1**, 6945–6952 (2018)
23. L. Zhao, P. Zhang, Y. Zhang, Z. Zhang, L. Yang, Z.G. Chen, Facile synthesis of hierarchical Ni3Se2 nanodendrite arrays for supercapacitors. J. Mater. Sci. Technol. **54**, 69–76 (2020)
24. B. Ye, M. Huang, L. Fan, J. Lin, J. Wu, Co ions doped NiTe electrode material for asymmetric supercapacitor application. J. Alloys Compd. **776**, 993–1001 (2019)
25. Y. Zhang, J. Zhang, D. Ding, Y. Gao, Controllable synthesis of three-dimensional β-NiS nanostructured assembly for hybrid-type asymmetric supercapacitors. Nanomater **10**, 487 (2020)
26. S. Azizi Darsara, M. Seifi, M.B. Askari, M. Osquian, Hierarchical 3D starfish-like Ni3S4–NiS on reduced graphene oxide for high-performance supercapacitors. Ceram. Int. **47**, 20992–20998 (2021)
27. S. Guan, X. Fu, Z. Lao, C. Jin, Z. Peng, NiS-MoS2 hetero-nanosheet arrays on carbon cloth for high-performance flexible hybrid energy storage devices. ACS Sustain. Chem. Eng. **7**, 11672–11681 (2019)
28. J. Xu, L. Zhang, G. Xu, Z. Sun, C. Zhang, X. Ma, C. Qi, L. Zhang, D. Jia, Facile synthesis of NiS anchored carbon nanofibers for high-performance supercapacitors. Appl. Surf. Sci. **434**, 112–119 (2018)
29. Y. Tan, W.D. Xue, Y. Zhang, D.X. He, W.J. Wang, R. Zhao, Solvothermal synthesis of hierarchical α-NiS particles as battery-type electrode materials for hybrid supercapacitors. J. Alloys Compd. **806**, 1068–1076 (2019)
30. J. Yang, X. Duan, W. Guo, D. Li, H. Zhang, W. Zheng, Electrochemical performances investigation of NiS/rGO composite as electrode material for supercapacitors. Nano Energy **5**, 74–81 (2014)
31. J. Zhao, L. Yang, H. Li, T. Huang, H. Cheng, A. Meng, Y. Lin, P. Wu, X. Yuan, Z. Li, Ni3Se2 nanosheets in-situ grown on 3D NiSe nanowire arrays with enhanced electrochemical performances for supercapacitor and efficient oxygen evolution. Mater. Charact. **172**, 110819 (2021)
32. N.S. Arul, J.I. Han, Enhanced pseudocapacitance of NiSe2/Ni(OH)2 nanocomposites for supercapacitor electrode. Mater. Lett. **234**, 87–91 (2019)
33. Y. Tian, Y. Ruan, J. Zhang, Z. Yang, J. Jiang, C. Wang, Controllable growth of NiSe nanorod arrays via one-pot hydrothermal method for high areal-capacitance supercapacitors. Electrochim. Acta. **250**, 327–334 (2017)
34. S. Wang, W. Li, L. Xin, M. Wu, Y. Long, H. Huang, X. Lou, Facile synthesis of truncated cube-like NiSe2 single crystals for high-performance asymmetric supercapacitors. Chem. Eng. J. **330**, 1334–1341 (2017)
35. Y. Gu, L.Q. Fan, J.L. Huang, C.L. Geng, J.M. Lin, M.L. Huang, Y.F. Huang, J.H. Wu, N-doped reduced graphene oxide decorated NiSe2 nanoparticles for high-performance asymmetric supercapacitors. J. Power Sources **425**, 60–68 (2019)
36. S. Deshagani, P. Ghosal, M. Deepa, Altered crystal structure of nickel telluride by selenide doping and a poly(N-methylpyrrole) coating amplify supercapacitor performance. Electrochim. Acta **345**, 136200 (2020)
37. B. Ye, M. Huang, S. Jiang, L. Fan, J. Lin, J. Wu, In-situ growth of Se-doped NiTe on nickel foam as positive electrode material for high-performance asymmetric supercapacitor. Mater. Chem. Phys. **211**, 389–398 (2018)
38. Y. Xu, W. Du, L. Du, W. Zhu, W. Guo, J. Chang, B. Zhang, D. Deng, Monocrystalline NiS nanowire arrays supported by Ni foam as binder-free electrodes with outstanding performances, RSC Adv. **7**, 22553–22557 (2017)
39. G.S.R. Raju, E. Pavitra, G. Nagaraju, S.C. Sekhar, S.M. Ghoreishian, C.H. Kwak, J.S. Yu, Y.S. Huh, Y.-K. Han, Rational design of forest-like nickel sulfide hierarchical architectures with ultrahigh areal capacity as a binder-free cathode material for hybrid supercapacitors. J. Mater. Chem. A. **6**, 13178–13190 (2018)

40. H. Wang, J. Wang, M. Liang, Z. He, K. Li, W. Song, S. Tian, W. Duan, Y. Zhao, Z. Miao, Novel dealloying-fabricated NiS/NiO nanoparticles with superior cycling stability for supercapacitors. ACS Omega **6**, 17999–18007 (2021)
41. N.A. Marand, S.M. Masoudpanah, S. Alamolhoda, M.S. Bafghi, Solution combustion synthesis of nickel sulfide/reduced graphene oxide composite powders as electrode materials for high-performance supercapacitors, J. Energy Storage **39**, 102637 (2021)
42. A.A. AbdelHamid, X. Yang, J. Yang, X. Chen, J.Y. Ying, Graphene-wrapped nickel sulfide nanoprisms with improved performance for Li-ion battery anodes and supercapacitors. Nano Energy **26**, 425–437 (2016)
43. C. Qu, L. Zhang, W. Meng, Z. Liang, B. Zhu, D. Dang, S. Dai, B. Zhao, H. Tabassum, S. Gao, H. Zhang, W. Guo, R. Zhao, X. Huang, M. Liu, R. Zou, MOF-derived α-NiS nanorods on graphene as an electrode for high-energy-density supercapacitors. J. Mater. Chem. A. **6**, 4003–4012 (2018)
44. S. Dai, B. Zhao, C. Qu, D. Chen, D. Dang, B. Song, B.M. deGlee, J. Fu, C. Hu, C.P. Wong, M. Liu, Controlled synthesis of three-phase NixSy/rGO nanoflake electrodes for hybrid supercapacitors with high energy and power density. Nano Energy **33**, 522–531 (2017)
45. W. Li, T. Chen, A. Li, P. Shi, M. Wu, T. Li, H. Yue, Y. Chen, B. Huang, X. Lou, High energy density hybrid supercapacitors derived from novel Ni3Se2 nanowires in situ constructed on porous nickel foam. Inorg. Chem. Front. **8**, 1093–1101 (2021)
46. S. Jiang, J. Wu, B. Ye, Y. Fan, J. Ge, Q. Guo, M. Huang, Growth of Ni3Se2 nanosheets on Ni foam for asymmetric supercapacitors. J. Mater. Sci. Mater. Electron. **29**, 4649–4657 (2018)
47. L. Du, W. Du, H. Ren, N. Wang, Z. Yao, X. Shi, B. Zhang, J. Zai, X. Qian, Honeycomb-like metallic nickel selenide nanosheet arrays as binder-free electrodes for high-performance hybrid asymmetric supercapacitors. J. Mater. Chem. A. **5**, 22527–22535 (2017)
48. J. Yang, Z. Sun, J. Wang, J. Zhang, Y. Qin, J. You, L. Xu, Hierarchical NiSe2 spheres composed of tiny nanoparticles for high performance asymmetric supercapacitors. CrystEngComm **21**, 994–1000 (2019)
49. M. Lu, X.-P. Yuan, X.-H. Guan, G.-S. Wang, Synthesis of nickel chalcogenide hollow spheres using an L-cysteine-assisted hydrothermal process for efficient supercapacitor electrodes. J. Mater. Chem. A. **5**, 3621–3627 (2017)
50. A. Chang, C. Zhang, Y. Yu, Y. Yu, B. Zhang, Plasma-assisted synthesis of NiSe2 ultrathin porous nanosheets with selenium vacancies for supercapacitor. ACS Appl. Mater. Interfaces. **10**, 41861–41865 (2018)
51. L. Meng, Y. Wu, T. Zhang, H. Tang, Y. Tian, Y. Yuan, Q. Zhang, Y. Zeng, J. Lu, Highly conductive NiSe2 nanostructures for all-solid-state battery–supercapacitor hybrid devices. J. Mater. Sci. **54**, 571–581 (2019)
52. Y. Bai, W. Shen, K. Song, S. Zhang, Y. Wang, T. Xu, J. Xu, S. Dai, X. Wang, Controlled synthesis of NiSe-Ni0.85Se nanocomposites for high-performance hybrid supercapacitors. J. Electroanal. Chem. **880**, 114795 (2021)
53. K. Guo, F. Yang, S. Cui, W. Chen, L. Mi, Controlled synthesis of 3D hierarchical NiSe microspheres for high-performance supercapacitor design. RSC Adv. **6**, 46523–46530 (2016)
54. Z. Sun, F. Liu, J. Wang, Y. Hu, Y. Fan, S. Yan, J. Yang, L. Xu, Tiny Ni0.85Se nanosheets modified by amorphous carbon and rGO with enhanced electrochemical performance toward hybrid supercapacitors. J. Energy Storage **29**, 101348 (2020)
55. S. Wu, T. Cui, Q. Hu, F. Yin, Q. Feng, S. Zhou, Q. Su, L. Wu, Q. Yang, Mixing solvothermal synthesis nickel selenide on the surface of graphene for high-efficiency asymmetric supercapacitors. Synth. Met. **268**, 116490 (2020)
56. M. Manikandan, K. Subramani, M. Sathish, S. Dhanuskodi, NiTe nanorods as electrode material for high performance supercapacitor applications. ChemistrySelect **3**, 9034–9040 (2018)

Chalcogenide Based 2D Nanomaterials for Supercapacitors

Raja Noor Amalina Raja Seman and Mohd Asyadi Azam

Abstract To overcome the depletion of fossil fuels, current cutting-edge research is focusing on the future engineering and technologies in any energy generating devices. A supercapacitor is one of the most promising among them, with very fast charging and discharging times and good cyclic stability. Supercapacitors have been rapidly developing to meet the demand to solve energy and environmental problems. The electrochemical parameters of supercapacitor devices, such as specific capacitance, rate, cycling stabilities, energy, and power densities, are greatly influenced by the electrode materials used. Metal chalcogenide nanomaterials are highly demanded in the research of various electrodes to meet the ever-increasing energy source demands. Metal chalcogenides are strongly scrutinized as an emerging competitor due to their distinctive physical and chemical features. These materials have a lot of potential as electrode materials in supercapacitor devices. In this chapter, the outstanding performance of metal chalcogenides nanomaterials in the field of supercapacitors is summarized in terms of their electrochemical performances, demonstrating them as a very efficient electrode for supercapacitors.

Keywords Supercapacitor · Chalcogenides · Power density · Energy density

1 Introduction

Nowadays, due to tremendous population growth and industrial development, environmental and energy obstacles are currently one of the most major concerns [1]. These devices have improved the energy efficiency, dependability, flexibility of electrical systems, and the performance of manufacturing systems. This topic has attracted a lot of interest due to the expectation of a high level of renewable energy integration in electrical networks [2]. However, there are still a lot of requirements to meet to develop more modern technologies that can simultaneously deliver a

R. N. A. Raja Seman · M. A. Azam (✉)
Fakulti Kejuruteraan Pembuatan, Universiti Teknikal Malaysia Melaka, Hang Tuah Jaya, Durian Tunggal, 76100 Melaka, Malaysia
e-mail: asyadi@utem.edu.my

S. Thomas et al. (eds.), *Nanostructured Materials for Supercapacitors*,
Advances in Material Research and Technology,
https://doi.org/10.1007/978-3-030-99302-3_17

high energy and power density. Also, due to their extremely high cost, the usage of rechargeable devices is restricted [3].

Supercapacitors have sparked rising scrutiny as the most convincing storage devices due to their outstanding features such as high power [4], high specific capacitance [5], fast charge–discharge rate [6], and long lifespan [7]. Supercapacitors are made up of electrode and electrolyte materials, as well as current collectors, separators, and sealants, all of which contribute to the device's electrochemical performance [8]. Furthermore, because the electrodes must be able to provide a large specific surface area, the electrode materials are chosen and their design is crucial in boosting the capacitance performance of supercapacitors [9]. Also, they must be both environmentally friendly and economical [10]. Supercapacitors are classified into two types based on their storage mechanism which are electrical double-layer capacitors (EDLCs) and/or pseudocapacitors [11, 12]. In EDLCs, ion electrosorption and the occurrence of an electrochemical double layer are used to store charge. Meanwhile, the faradic reactions store the charges in the pseudocapacitors (redox reactions). The electrode materials for supercapacitors can be divided into three main categories such as carbon-based materials (e.g., graphene, activated carbon (ACs), and carbon nanotubes (CNTs)) [13], transition metal oxides (e.g., manganese oxide (MnO_2)), [14], and conducting polymers (e.g., polyaniline (PANI), and polypyrrole (PPy)) [15].

Currently, the electrochemical performance of supercapacitors has considerably increased, there are still various areas where they can be improved. The electrochemical performance of supercapacitors can be revamped by altering or changing the electrode material [16]. Latterly, the synthesis of two-dimensional (2D) materials opens the door for the research of materials science and technology, which had previously been difficult to achieve due to the controlled structure of 2D materials [17]. Through the interlayer gap, 2D materials with strong in-plane covalent bonding and weak van der Waals interaction out-of-plane across the interlayer gap materials offer a varied spectrum of material sciences with customizable properties for energy conversion and storage devices [18]. Novel 2D materials have demonstrated various applications including transition metal dichalcogenides (TMDs) [19], transition metal carbides (TMCs) [20], graphene [21], black phosphorous (BP) [22], and MXenes [23]. TMDs especially MoS_2 has many of the same physical features as graphenes, such as high charge carrier transfer and high wear resistance. Also, MoS_2 outperforms graphene in terms of cost, abundance, and a tunable bandgap with well visible light absorption capability.

This chapter mainly focuses on recent endeavors towards the electrochemical performances of chalcogenide-based 2D nanomaterials as supercapacitor electrodes. We have compiled a list of the most recent advancements in 2D materials, as well as how they can be used in the field of supercapacitors. The hybrid electrode which is composed of 2D materials with a highly conductive and capacitive nature outperforms the limited performances due to their remarkable structural properties allowing better electrochemical behavior. It also includes the advancement of 2D materials, such as asymmetric supercapacitors with high energy and power densities. The summary of electrochemical performance of the reported chalcogenide-based 2D nanomaterials

Table 1 Specific capacitances from CV at different scan rates

Scan rate (V/s)	Specific capacitance (F g^{-1})			
Sample code	MoSGMn-1	MoSGMn-2	MoSGMn-3	MoSGMn-4
0.001	980	788	527	310
0.005	520	460	134	120
0.01	208	190	76	70
0.05	91	90	34	31
0.1	50	39	27	25
0.5	37	20	15	13

Reproduced with permission from reference [27]. Copyright (2021) Elsevier

electrodes used in supercapacitor in terms of specific capacitances and energy density are tabulated in Table 1.

2 Chalcogenide-Based Carbonaceous Materials for Supercapacitors

Chalcogenide-based carbonaceous materials are favorable contenders in the field of energy storage, particularly as electrodes for supercapacitors applications, because of their unique combination of tunable physical properties [24] and metallic conductivity [25]. Carbonaceous materials can be found in a variety of places, including activated carbon, graphene, carbon nanotube, and so on, because of their ability to store charges through EDLC mechanisms, they can be employed as electrode materials for supercapacitors. Kumar et al. have used a simple hydrothermal technique to nucleate the hexagonal $NiCo_2S_4$ hierarchical nanostructure on reduced graphene oxide (rGO) sheets (Fig. 1). The hybrid composites showed a higher specific capacitance (972 F g^{-1}) than the bare electrode at 1 A g^{-1} [26]. The supremacy of hybrid rGO-$NiCo_2S_4$ composites includes expanded electrolyte diffusion channels, fast electron transport, and a sufficient number of active sites, which take advantage of the synergistic effects between the hierarchical architecture of $NiCo_2S_4$ and the remarkable conductivity of rGO. The synergistic effects of the hierarchical architecture of $NiCo_2S_4$ and the remarkable conductivity of rGO have benefited the hybrid composites by providing enhanced electrolyte diffusion channels, quick electron transport, and sufficient active sites.

Furthermore, the fabricated supercapacitor device made by modified MoS_2 deposited graphene oxide rolled MnOx nanocomposite has shown large supercapacitance values of 980 F g^{-1}, and 788 F g^{-1}, respectively [27]. As the amount of MoS_2 counted is reduced from 100 to 15 mg (MoSGMn-4), its efficiency gradually diminishes. MoS_2 particles integrated into manganese oxide fibers with a fibrous needle and nanotube-like morphology have the potential to change the energy levels of

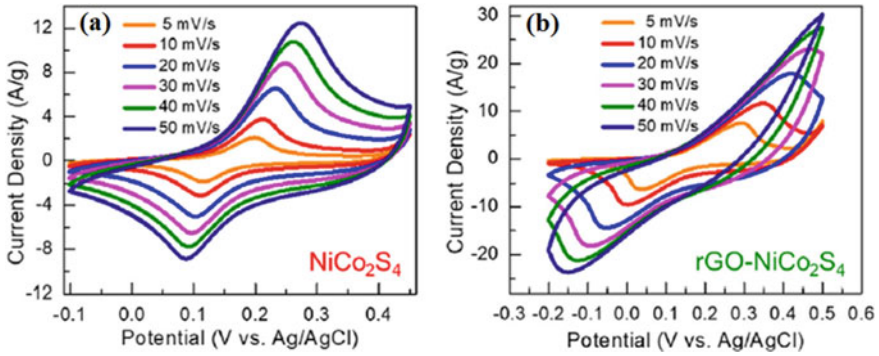

Fig. 1 CV curves at various scan rates (5–50 mV/s) of the **a** $NiCo_2S_4$ and **b** rGO-$NiCo_2S_4$. Reproduced with permission from reference [26]. Copyright (2021) Elsevier

manganese oxide's pseudocapacitance nature. Graphene intercalation also improves the porous conductivity of manganese oxide during charge and discharge, which is one of the most important elements affecting the specific capacitance values. Table 1 lists the capacitance values for four distinct samples.

Also, VS_2 supported MWCNTs made by a simple hydrothermal technique have been reported by Meyer et al. [28] for their structure, morphological features, and prospective application as an electrode in supercapacitors. The supercapacitor has a capacitance of approximately 33 F g^{-1} at 1 mA^{-1} current density. At lower current densities, the increased capacitance results from a stronger and more effective interaction between the electrode and the electrolyte, resulting in a more efficient charge transfer. In contrast, only minimum interaction occurs at higher current densities, resulting in reduced charge transfer and poor capacitance. Increased carbon content results in higher capacitance and charge transfer due to good electrical conductivity and a larger surface area for electrolyte ion adsorption.

For instance, Ji et al. [29] have prepared a ball-milling the heterogeneous layered materials of bulk MoS_2 and GO powders followed by the hydrazine-reducing method yielded the binder-free MoS_2/rGO composites. The MoS_2/rGO composites electrodes of symmetric supercapacitor revealed high specific capacitance of 365, 283, 267, 230, and 227 F g^{-1} at a current rate of 0.5, 1, 2, 4, and 10 A g^{-1}, respectively being much higher than those of MoS_2 electrodes (253, 213, 199, 198 and 181 F g^{-1}) (Fig. 2). Furthermore, the rate capability of MoS_2/rGO composites electrodes (227 F g^{-1}) is higher than MoS_2 electrode even at a high rate of current density. Also, MoS_2/rGO composites electrode maintains a high specific capacitance of 260 10 F g^{-1} at a relatively high current density of 4 A g^{-1} compared to pure MoS_2 electrode which is 144 $\pm$ 10 F g^{-1}. The resultant MoS_2/rGO composites electrode showed a maximum energy density of 125.0 Wh kg^{-1} at a power density of 1.6 kW kg^{-1}.

In another study, Xu et al. [30] synthesized a new type of 3D NiS/MoS_2@N-rGO hybrid composites by using an easy and cost-effective hydrothermal method. The

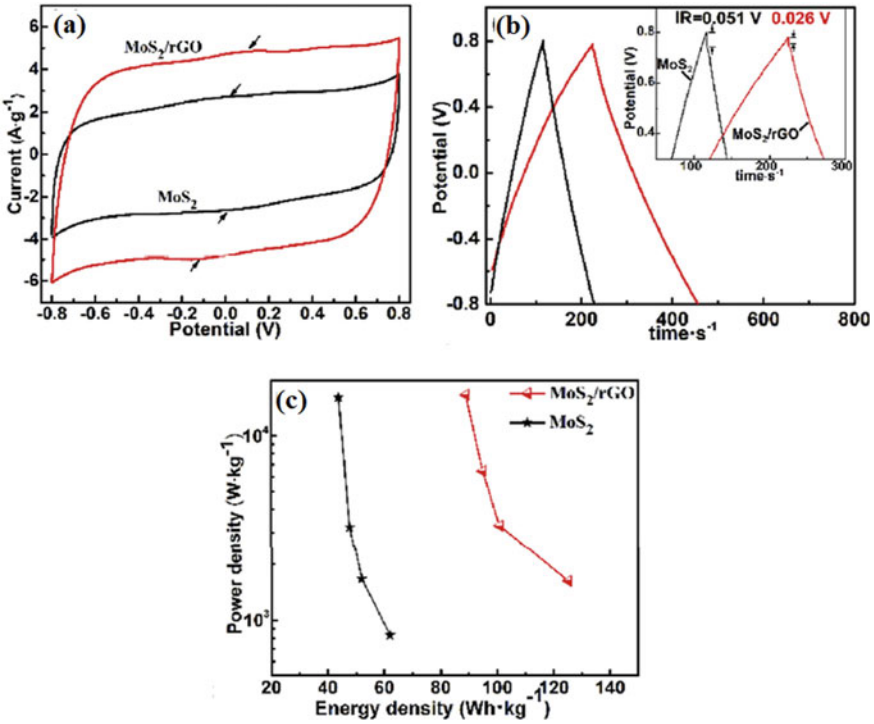

Fig. 2 **a** Cyclic voltammetry curves of MoS_2/rGO and MoS_2 electrodes at a scan rate of 50 mV s^{-1}. **b** Galvanostatic charge–discharge curves of MoS_2/rGO and MoS_2 electrodes at a current density of 1 A g^{-1}, within a potential range of −0.8–0.8 V. **c** Ragone plot of MoS_2/rGO and MoS_2 electrodes. Reproduced with permission from reference [29]. Copyright (2019) Elsevier

hybrid electrodes for these supercapacitors have been nickel sulfide and molybdenum disulfide with N-reduced graphene oxide. The fabricated NiS/MoS_2@N-rGO hybrid composites delivered a high specific capacitance of about 1028 F g^{-1} at 1 A g^{-1}. In addition, the hybrid electrodes remained stable up to 50,000 charging and discharging cycles. Based on the Ragone plot, the hybrid device showed high energy and power densities of 35.69 Wh kg^{-1} and 601.8 W kg^{-1}, respectively (Fig. 3).

Naz et al. have demonstrated the hybrid electrode of highly defective MoS_2 nanosheets of 1 T phase and on a three-dimensional rGO network through a one-pot hydrothermal method [31]. This electrode exhibited very outstanding specific capacitance (442.0 F g^{-1} at 1 A g^{-1}, in a three-electrode system, in 1 M H_2SO_4 electrolyte), and cycling performances of 84.5% capacitance retention after 3000 cycles, 5 A g^{-1}.

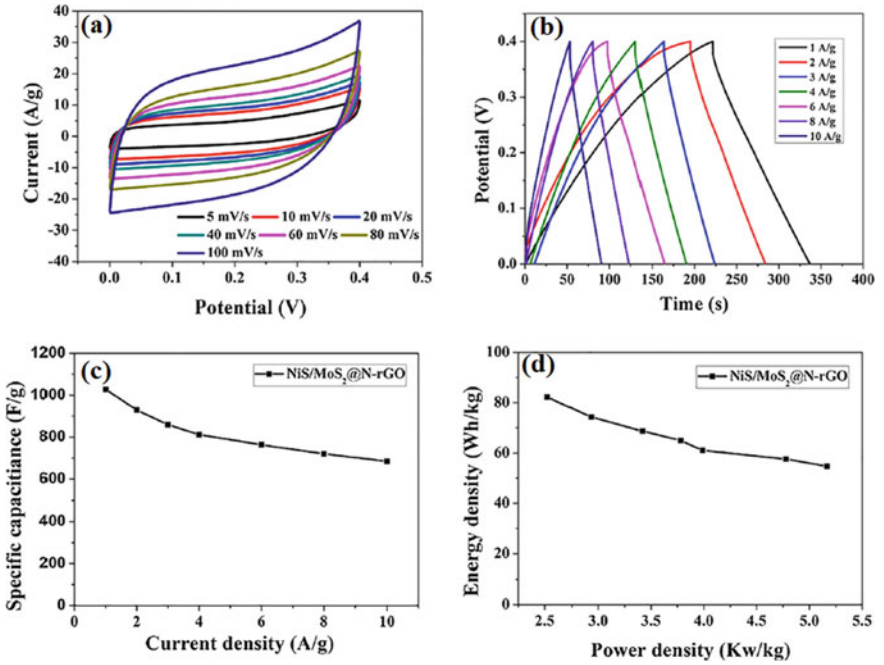

Fig. 3 **a** CV curves of the NiS/MoS_2@N-rGO electrode at various scan rates from 5 to 100 mV s^{-1}. **b** Galvanostatic harge-discharge curves of the NiS/MoS_2@N-rGO electrode different current densities in the range of 1–10 A g^{-1}. **c** Specific capacitances of NiS/MoS_2@N-rGO electrode at different current densities. **d** Ragone plots of the NiS/MoS_2@N-rGO electrode. Reproduced with permission from reference [30]. Copyright (2019) Elsevier

3 Chalcogenide Hybrids with Other 2D Analogues for Supercapacitors

Farag et al. [32] have prepared nano $CuCo_2O_4$/CuS nanocomposite samples using the hydrothermal procedure. $CuCo_2O_4$/CuS nanocomposite possess a larger surface area compared with $CuCo_2O_4$. The area of $CuCo_2O_4$/CuS nanocomposite increases with increasing the amount of CuS from 0 to 25%. Meanwhile, the area of $CuCo_2O_4$/CuS nanocomposite decreases with the addition of doping. In addition, the 0.75 $CuCo_2O_4$/0.25CuS nanocomposite provides a larger surface area compared with other nanocomposites. The high rate capabilities and improved specific capacitance of $CuCo_2O_4$/CuS nanocomposite may be attributed to the synergistic effect of $CuCo_2O_4$ and CuS. This finding suggested that the new 0.75 $CuCo_2O_4$/0.25 CuS composite is a promising active material for supercapacitors.

For instance, Manikandan et al. [33] have developed the selenium reinforced hybrid $NiSe_2$@Fe_3Se_4 (NFS) nanocomposites deposited on Ni-foam via chemical bath deposition (CBD) method. Figure 4 illustrates the electrochemical performances of Ni foam, SeO_2, and hybrid electrodes at 10 mV s^{-1} of scan rate. The electrode

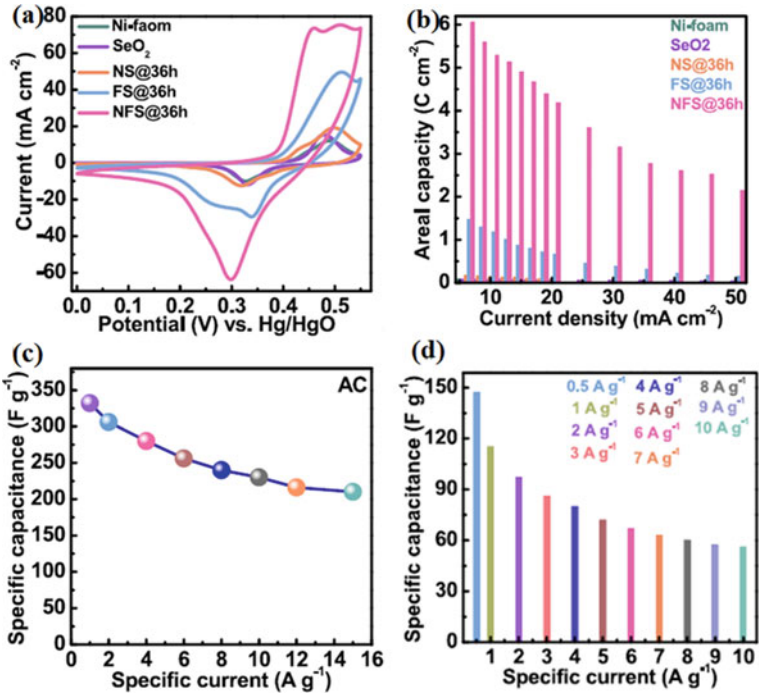

Fig. 4 **a** CV curves of five different electrodes at a scan rate of 10 mV s^{-1}. **b** Areal capacitance of the electrodes at different discharge current densities, **c** The capacitance values of the ONAC electrode at different currents from 1 to 15 A g^{-1}, and **d** Calculated capacitance values of the HSC device at different currents from 0.5 to 10 A g^{-1}. Reproduced with permission from reference [33]. Copyright (2021) Elsevier

delivered a good areal capacity at a current density of 6 mA cm^{-2}. These findings show that a large contact space for rapid electrolyte ion transport across electrode material/electrolyte interfaces can be created by effectively depositing NFS nanocomposites on a Ni-foam surface. In addition, from the GCD curves, O, N enriched activated carbon (ONAC) derived from bio-waste as a negative electrode showed specific capacitance values in the range of 210–332 F g^{-1}, at 1–15 A g^{-1} current densities. The specific capacitance value of the as-synthesized ONAC sample was higher than that of recently published activated carbon materials generated from diverse bio-wastes.

In another study, Gowrisankar et al. [34] have demonstrated different Mo and W-based dichalcogenides as a bifunctional electrode material for supercapacitor application. the examples of dichalcogenides include MoS_2, tungsten sulfoselenide (WSSe), molybdenum sulfoselenide (MoSSe), molybdenum diselenide ($MoSe_2$), tungsten diselenide (WSe_2), and tungsten disulfide (WS_2) nanostructures (Fig. 5). Based on the CV results, MoSSe loaded electrode showed high specific capacitances in the range of 101–314 F g^{-1} at 1–50 A g^{-1}. Furthermore, the hybrid capacitor

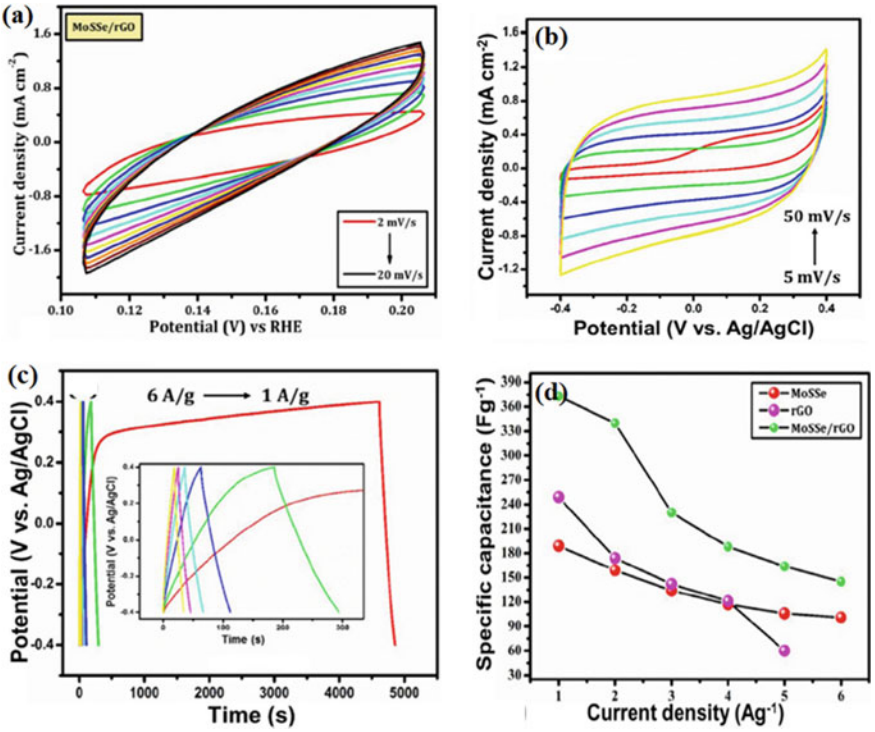

Fig. 5 **a** Cyclic voltammetry of WSSe/rGO composites, **b** The CV of MoSSe/rGO loaded electrodes at different scan rates, **c** GCD profiles of MoSSe/rGO loaded electrodes at different current densities (1–6 A/g), and **d** Specific capacitance vs current density plots. Reproduced with permission from reference [34]. Copyright (2021) Elsevier

material resulted by incorporating rGO into MoSSe composites. Further, the specific capacitance values for MoSSe/rGO composites are 373, 340, 230, 188, 164, and 145 F g^{-1}, respectively. The increase in capacitance value may be attributed to the insertion of MoSSe onto rGO. It should be noted that as current density has increased, the specific capacitance has gradually decreased.

Several recent studies have incorporated 2D MoS_2 layers into Ni_3S_2 to fabricate supercapacitors. For example, Liu et al. designed a hierarchical MoS_2/Ni_3S_2 structure grown on nickel foam via a simple one-pot hydrothermal method [35]. From GCD curves, the specific capacitance value of hybrid structure was 1.033 (1 mA cm^{-2}), 1.018 (2 mA cm^{-2}), 0.993 (3 mA cm^{-2}), 0.973 (4 mA cm^{-2}), 0.926 (6 mA cm^{-2}) and 0.894 C cm^{-2} (8 mA cm^{-2}), respectively (Fig. 6). The strong interaction between MoS_2 and Ni_3S_2 endowed the MoS_2/Ni_3S_2 hybrid structure with high long-term cycling stability. Capacitance retention up to 62.5% was achieved after 10,000 charging and discharging repeatedly at the current density of 20 mA cm^{-2}.

Alternatively, Lokhande et al. direct coating of ternary chalcogenide-based nanostructured Cu_4SnS_4 (CTS) thin film electrodes for the energy storage application [36].

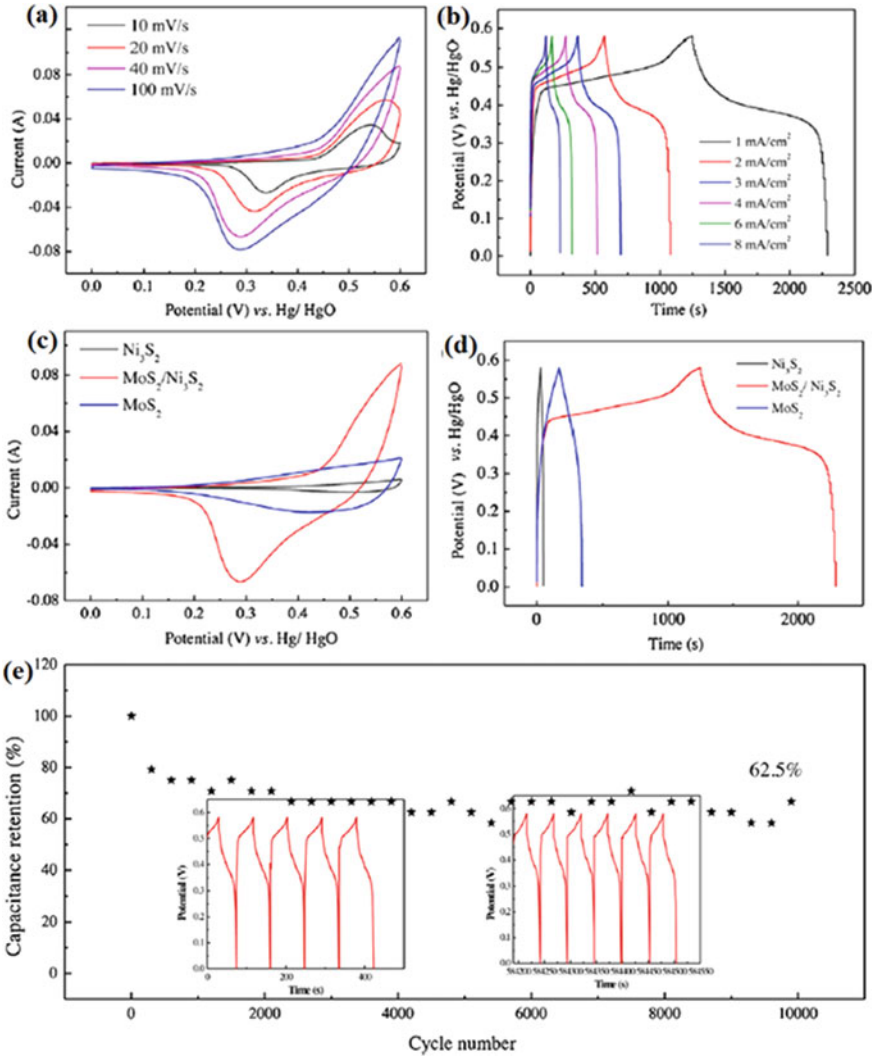

Fig. 6 **a** CV curves at 10–100 mV/s. **b** GCD curves at various current densities. **c** CV curves of different electrodes at 40 mV s^{-1}. **d** GCD curves of different electrodes at 1 mA cm^{-2}, and **e** Capacitance retention of the hybrid up to 10,000 cycles at 20 mA cm^{-2}. Reproduced with permission from reference [35]. Copyright (2019) Elsevier

The Cu-rich Cu_4SnS_4 (CTS) nanoparticle thin film was found to provide an ionic transfer via an effective conducting pathway. From electrochemical measurement, a specific capacitance of the fabricated CTS electrode was 704 F g^{-1} in 1 M NaOH aqueous electrolyte. Furthermore, a higher concentration of aqueous electrolyte influenced the performance of the fabricated CTS electrode. 3 M NaOH exhibited lower specific capacitance compared to 2 M NaOH with the specific capacitance value

of 585 F g^{-1} and 663 F g^{-1} for 3 M NaOH and 2 M NaOH aqueous electrolytes, respectively. The fabricated CTS electrode revealed a maximum energy density of 27.77 Wh kg^{-1} and a power density of and 7.14 kW kg^{-1} at an applied current density of 40 mA cm^{-2}.

4 Recent Development of Chalcogenides for Asymmetric Supercapacitors

As a typical example, Yang et al. constructed a flower-like $CoNi_2S_4$/multi-walled carbon nanotube (MWCNT) nanosheet arrays on Ni foam through a facile and cheap hydrothermal process [37]. The sulfur source was thioglycerol (TA). The synergistic effect between MWCNT and $CoNi_2S_4$ endowed the $CoNi_2S_4$/MWCNT/Ni hybrid electrode with high long-term cycling stability. The $CoNi_2S_4$/MWCNT/Ni hybrid retains up to 109% after 2000 repeatedly charging and discharging at 10 mA cm^{-2}. Moreover, $CoNi_2S_4$/MWCNT hybrid also showed superior rate performance. The $CoNi_2S_4$/MWCNT/Ni hybrid delivered a high capacitance of 5.65 C cm^{-2} at current densities of 10 mA cm^{-2}. The $CoNi_2S_4$/MWCNT hybrid microstructure changing after long-term charging and discharging repeatedly exposing new redox-active sites at the electrode/electrolyte interface, increasing capacitance retention.

AC as the negative electrode and $CoNi_2S_4$/MWCNT/Ni as the positive electrode was built-in asymmetric supercapacitor (ASC) to investigate the practical application of $CoNi_2S_4$/MWCNT/Ni hybrid. This ASC delivered up to 56.6% of the areal capacitance at a scan rate of 10 mA cm^{-2}. It was suggested that the excellent rate capability of this ASC remain up to 85% of its initial areal capacity after 2000 charging and discharging, repeatedly for excellent cycling stability. The ASC delivered maximum specific energy of 60.83 Wh kg^{-1} at a specific power of 284.9 W kg^{-1} and a maximum energy density of 3.6 Wh m^{-2} at a power density of 16.9 Wh m^{-2} (Fig. 7).

Furthermore, $NiCo_2S_4$ with a special structure on nickel foam for ASC using hydrothermal and co-sulfurization methods were demonstrated by Gong et al. [38] who reported an outstanding specific capacitance value of 850.2 F g^{-1} at 1 A g^{-1}. The capacitance retention was 93.6% based on charging and discharging repeatedly. The NCS-A1 electrode was used as the cathode, while AC was used as the anode. The 3 M KOH was used as an aqueous electrolyte. It was found that the value of the specific capacitance of NCS-A1//AC device is 140 (1 A g^{-1}), 134.9 (2 A g^{-1}), 117.4 (3 A g^{-1}), 105 (5 A g^{-1}), and 58.6 F g^{-1} (10 A g^{-1}), respectively. The NCS-A1//AC ASC delivered remarkable cyclic stability with capacitance retention that can reach 84.3% after 5000 charging and discharging repeatedly. The calculated energy density was 38.1 (700 W kg^{-1}), 36.7 (1400 W kg^{-1}), 32 (2100 W kg^{-1}), 28.6 (3500 W kg^{-1}) and 16 Wh kg^{-1} (7000), respectively.

Tiwari et al. [39] fabricated an ASC with MoS_2/CNT as a negative electrode and MnO_2/CNT as a positive electrode. For MoS_2 and MnO_2 thin films, the areal capacitance values were evaluated to be 2.8 and 9.6 mF cm^{-2}, respectively (Fig. 8).

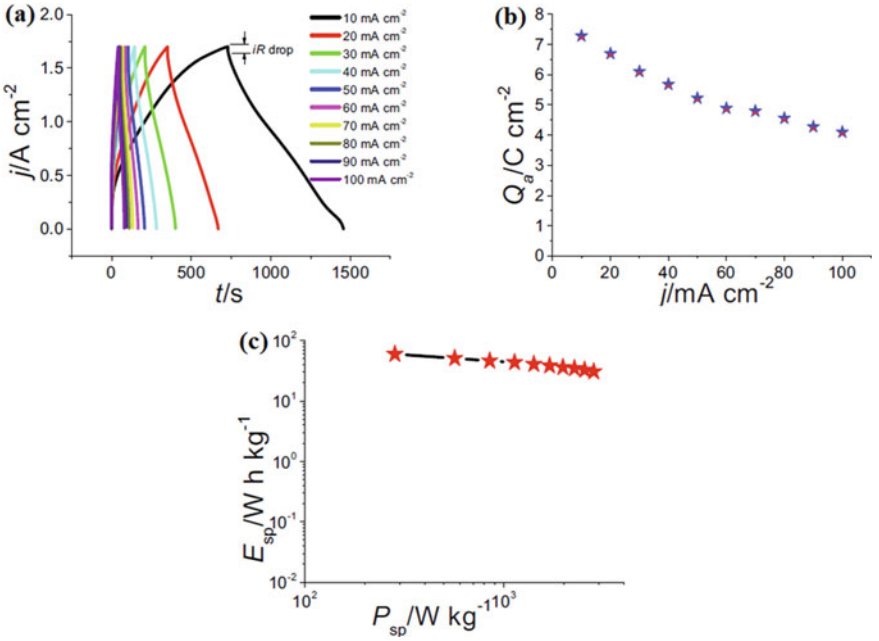

Fig. 7 **a** GCD curves of $CoNi_2S_4$/MWCNT/Ni//AC ASC in 2 M KOH aqueous electrolyte at different current densities from 10 to 100 mA/cm^2, **b** Areal capacity of the ASC versus current densities from 10 to 100 mA/cm^2, and **c** Ragone plot of the ASC. Reproduced with permission from reference [37]. Copyright (2021) Elsevier

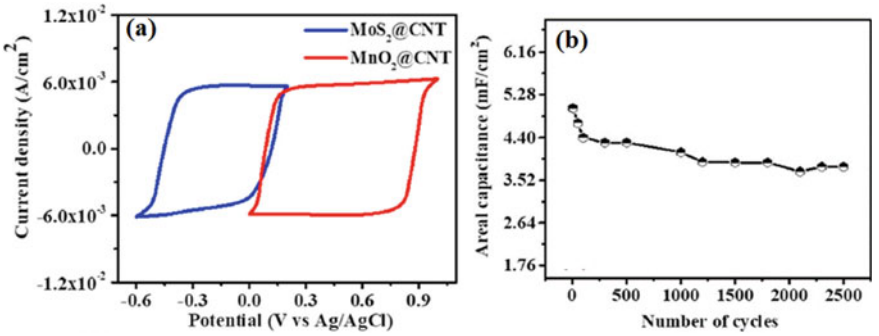

Fig. 8 **a** CV curves of two different electrodes and **b** Capacitive retention of MoS_2/CNT//MnO_2//CNT asymmetric supercapacitor up to 2500 charge–discharge cycles. Reproduced with permission from reference [39]. Copyright (2021) Elsevier

The fabricated MoS_2/CNT//MnO_2//CNT ASC device showed remarkable cycling stability up to 98.3% over 2500 charging and discharging repeatedly. The areal capacitance of the fabricated MoS_2/CNT//MnO_2//CNT ASC device was 0.25 F cm^{-2}. Meanwhile, the fabricated MoS_2/CNT//MnO_2//CNT ASC device possesses a high energy density of 88.8 mWh cm^{-2} a power density of 227 mW cm^{-2}, respectively.

Recently, Vidhya et al. [40] have synthesized $MnSe_2$-$CoSe_2$ by hydrothermal process by varying the amount of Mn. Different amount of Mn was used which are 0.05 as Mn1, 0.1 as Mn2, and 0.15 as Mn3 wt.%, respectively. The influence of amount Mn usage improved the electrochemical properties. Based on the electrochemical measurements in 1 M KOH, the electrode delivered a specific capacitance value of 373 F g^{-1} (Mn3), 182 F g^{-1} (Mn2), and 295 F g^{-1} (Mn1), respectively. The capacitance retention of up to 99% was achieved over 5000 charging and discharging. Moreover, the specific energy density and specific power density values are 73, 62, 55, 53, 25 Wh kg^{-1} and 75, 1499, 2250, 4500, 5625 W kg^{-1}, respectively (Table 2).

5 Conclusions

The main focus of this chapter was to bring about a broad outlook of recent progress and development in chalcogenide-based 2D nanomaterials based on their potential usage as a supercapacitor electrode. The research and development of chalcogenide-based electrode materials for high-performance electrochemical energy storage devices are gaining traction. In terms of supercapacitors, electrochemical energy devices are a fast expanding thrust area in which these materials showed considerable promise to compete with traditional energy sources.

Furthermore, combining a 2D material with a large volume material successfully eliminates the restacking problem of 2D material. On the other hand, 2D materials including 2D conductive polymers, 2D transition metal oxides/hydroxides, and single-element 2D material have been revealed to have a wide variety of applications for high-performance energy devices. The selection of electrode material plays an important role in the developing study of 2D nanomaterials. Thus, the produced composites/hybrids combining various 2D materials may collect their own merits, it could pave the way for 2D materials to be used in high-performance electrochemical energy device applications. In addition, it is highly desirable to design cost-effective materials that are efficient and ecologically friendly approaches to achieve good performance. As a result, focusing future research on the development of low-cost 2D electrode materials with high charge capacity and stability will be tremendously useful. The supercapacitor is predicted to become a promising energy storage device in the future.

The advantages of electrochemical supercapacitors include high power density, longevity, cycle efficiency, operating temperatures, environmental friendliness, and safety. However, the challenges of focusing on supercapacitors are numerous such as energy density, cost-effectiveness, and self-discharge rate. A high energy density

Table 2 Comparison of capacitances and energy density of the reported chalcogenide-based 2D nanomaterials electrodes for supercapacitor

Materials	Method	Specific capacitance	Energy density/power density	References
rGO-$NiCo_2S_4$ composites	Hydrothermal technique	972 F g^{-1} (1 A g^{-1})	–	[26]
MoSGMn-1	Modified MoS_2 deposited graphene oxide rolled MnOx Nanocomposite	980 F g^{-1} 5 mV s^{-1}	–	[27]
VS_2 supported MWCNTs	Hydrothermal technique	33 F g^{-1} (1 mA^{-1})	–	[28]
MoS_2/rGO composites	Ball-milling with reducing process	356 F g^{-1} (0.5 A g^{-1})	125.0 Wh kg^{-1}/ 1.6 kW kg^{-1}	[29]
3D NiS/MoS_2@N-rGO hybrid composites	Hydrothermal technique	1028 F g^{-1} (1 A g^{-1})	35.69 Wh kg^{-1}/ 601.8 W kg^{-1}	[30]
MoS_2/rGO	Hydrothermal technique	442.0 F g^{-1} (1 A g^{-1})	–	[31]
$CuCo_2O_4$/CuS nanocomposite	Hydrothermal technique	-	–	[32]
$NiSe_2$@Fe_3Se_4 (NFS) nanocomposites	Chemical bath deposition technique	332 F g^{-1} (1 A g^{-1})	–	[33]
MoSSe/rGO composites	Hydrothermal technique	373 F g^{-1} (1 A g^{-1})	–	[34]
MoS_2/Ni_3S_2 structure	Hydrothermal technique	1.033 C cm^{-2} 1 mA cm^{-2}	–	[35]
Cu_4SnS_4	Direct coating	704 F g^{-1}	27.77 Wh kg^{-1}/ 7.14 kW kg^{-1}	[36]
$CoNi_2S_4$/MWCNT hybrid	Hydrothermal technique	5.65 C cm^{-2} (10 mA cm^{-2}) ASC $CoNi_2S_4$/MWCNT/ Ni//AC	– 60.83 Wh kg^{-1}/ 284.9 W kg^{-1}	[37]
$NiCo_2S_4$	Hydrothermal and co-sulfurization processes	850.2 F g^{-1} (1 A g^{-1}) ASC NCS-A1//AC 140 F g^{-1} (1 A g^{-1})	38.1 Wh kg^{-1}/ 700 W kg^{-1}	[38]
MoS_2/CNT//MnO_2//CNT	Unique combination of chemical and DC magnetron sputtering techniques	0.25 F cm^{-2}	88.8 mWh cm^{-2}/ 227 mW cm^{-2}	[39]

(continued)

Table 2 (continued)

Materials	Method	Specific capacitance	Energy density/power density	References
$MnSe_2$-$CoSe_2$	Hydrothermal technique	373 F g^{-1} (Mn3), 182 F g^{-1} (Mn2), and 295 F g^{-1} (Mn1) at 1 A g^{-1}	73 Wh kg^{-1}/ 750 W kg^{-1}	[40]

electrochemical system is required for practical application. Because of this, electrochemical supercapacitors have a lower energy density than batteries. The most typically used electrode materials, such as carbon materials with a large porous surface area are more expensive. Furthermore, the expense of organic electrolytes is not insignificant. Lastly, self-discharge rates of 10–40% per day are common in electrochemical supercapacitors.

References

1. P. Forouzandeh, S.C. Pillai, Two-dimensional (2D) electrode materials for supercapacitors. Mater. Today: Proc. **41**, 498–505 (2021)
2. G. Navarro, J. Torres, M. Blanco, J. Nájera, M. Santos-Herran, M. Lafoz, Present and future of supercapacitor technology applied to powertrains, renewable generation and grid connection applications. Energies **14**(11), 3060 (2021)
3. D. Tie, S. Huang, J. Wang, J. Ma, J. Zhang, Y. Zhao, Hybrid energy storage devices: advanced electrode materials and matching principles. Energy Storage. Mater. **21**, 22–40 (2019)
4. W. Yang, M. Ni, X. Ren, Y. Tian, N. Li, Y. Su, X. Zhang, Graphene in supercapacitor applications. Curr. Opin. Colloid Interface Sci. **20**(5–6), 416–428 (2015)
5. M.A. Azam et al., Activated carbon and single-walled carbon nanotube based electrochemical capacitor in 1 M LiPF6 electrolyte. Mater. Res. Bull. **69**, 20–23 (2015)
6. S. Arunachalam, B. Kirubasankar, D. Pan, H. Liu, C. Yan, Z. Guo, S. Angaiah, Research progress in rare earths and their composites based electrode materials for supercapacitors. Green Energy Environ. **5**(3), 259–273 (2020)
7. M.A. Azam, N. Dorah, R.N.A.R. Seman, N.S.A. Manaf, T.I.T. Kudin, Electrochemical performance of activated carbon and graphene based supercapacitor. Mater. Technol.: Adv. Funct. Mater. **30**(A1), A14–A17 (2015)
8. M.A. Azam, N.E. Safie, M.F.A. Aziz, R.N.A.R. Seman, M.R. Suhaili, A.A. Latiff et al., Structural characterization and electrochemical performance of nitrogen doped graphene supercapacitor electrode fabricated by hydrothermal method. Int. J. Nanoelectronics Mater. **14**(2), 127–136 (2021)
9. M.A. Azam, N.N. Zulkapli, N. Dorah, R.N.A.R. Seman et al., Review—Critical considerations of high quality graphene synthesized by plasma-enhanced chemical vapor deposition for electronic and energy storage devices. ECS J. Solid State Sci. Technol. **6**(6), M3035–M3048 (2017)
10. H. Tang, Q. Hu, M. Zheng, Y. Chi, X. Qin, H. Pang, Q. Xu, MXene–2D layered electrode materials for energy storage. Prog. Nat. Sci.: Mater. Int. **28**(2), 133–147 (2018)
11. B. Raj, A.K. Padhy, S. Basu, M. Mohapatra, Futuristic direction for R&D challenges to develop 2D advanced materials based supercapacitors. J. Electrochem. Soc. **167**(13), 136501 (2020)

12. M.A. Azam, A. Fujiwara, T. Shimoda, Direct growth of vertically-aligned single-walled carbon nanotubes on conducting substrates using ethanol for electrochemical capacitor. J. New Mater. Electrochem. Syst. **14**(3), 173–178 (2011)
13. T. Palaniselvam, J.B. Baek, Graphene based 2D-materials for supercapacitors. 2D Mater. **2**(3), 032002 (2015)
14. R. Liang, Y. Du, P. Xiao, J. Cheng, S. Yuan, Y. Chen, J. Yuan, J. Chen, Transition metal oxide electrode materials for supercapacitors: a review of recent developments. Nanomaterials **11**(5), 1248 (2021)
15. X. Jian, S. Liu, Y. Gao, W. Tian, Z. Jiang, X. Xiao, H. Tang, L. Yin, Carbon-based electrode materials for supercapacitor: progress, challenges and prospective solutions. J. Electr. Eng. **4**(2), 75–87 (2016)
16. R.N.A.R. Seman, M.A. Azam, Hybrid heterostructures of graphene and molybdenum disulfide: The structural characterization and its supercapacitive performance in 6M KOH electrolyte. J. Sci.: Adv. Mater. Devices **5**(4), 554–559 (2020)
17. K.S. Kumar, N. Choudhary, Y. Jung, J. Thomas, Recent advances in two-dimensional nanomaterials for supercapacitor electrode applications. ACS Energy Lett. **3**(2), 482–495 (2018)
18. M.A. Azam, N.S.N. Ramli, N.A.N.M. Nor, T.I.T. Nawi, Recent advances in biomass-derived carbon, mesoporous materials, and transition metal nitrides as new electrode materials for supercapacitor: a short review. Int. J. Energy Res. **45**, 8335–8346 (2021)
19. N.K. Chaudhari, H. Jin, B. Kim, D. San Baek, S.H. Joo, K. Lee, MXene: An emerging two-dimensional material for future energy conversion and storage applications. J. Mater. Chem. A **5**(47), 24564–24579 (2017)
20. A.S. Levitt, M. Alhabeb, C.B. Hatter, A. Sarycheva, G. Dion, Y. Gogotsi, Electrospun MXene/carbon nanofibers as supercapacitor electrodes. J. Mater. Chem. A **7**(1), 269–277 (2019)
21. C.J. Zhang, V. Nicolosi, Graphene and MXene-based transparent conductive electrodes and supercapacitors. Energy Storage Mater. **16**, 102–125 (2019)
22. R. Garg, A. Agarwal, M. Agarwal, A review on MXene for energy storage application: effect of interlayer distance. Mater. Res. Express **7**(2), 022001 (2020)
23. X. Li, Z. Huang, C. Zhi, Environmental stability of MXenes as energy storage materials. Front. Mater. **6**, 312 (2019)
24. Q. Yun, L. Li, Z. Hu, Q. Lu, B. Chen, H. Zhang, Layered transition metal dichalcogenide-based nanomaterials for electrochemical energy storage. Adv. Mater. **32**(1), 1903826 (2020)
25. J. Theerthagiri, K. Karuppasamy, G. Durai, A.U.H.S. Rana, P. Arunachalam, K. Sangeetha, P. Kuppusami, H.S. Kim, Recent advances in metal chalcogenides (MX; X= S, Se) nanostructures for electrochemical supercapacitor applications: a brief review. Nanomaterials **8**(4), 256 (2018)
26. S. Kumar, S. Sekar, A.K. Kaliamurthy, S. Lee, Bifunctional rGO-$NiCo_2S_4$ MOF hybrid with high electrochemical and catalytic activity for supercapacitor and nitroarene reduction. J. Mater. Res. Technol. **12**, 2489–2501 (2021)
27. J.R. Rajabathar, H.A. Al-lohedan, P. Arunachalam, Z.A. Issa, M.K. Gnanamani, J.N. Appaturi, S.N. Ibrahim, W.M. Dahan, Synthesis and characterization of metal chalcogenide modified graphene oxide sandwiched manganese oxide nanofibers on nickel foam electrodes for high performance supercapacitor applications. J. Alloy. Compd. **850**, 156346 (2021)
28. E. Meyer, A. Bede, D. Mutukwa, R. Taziwa, N. Zingwe, Optimization, and analysis of carbon supported VS2 nanocomposites as potential electrodes in supercapacitors. J. Energy Storage **27**, 101074 (2020)
29. H.M. Ji, A.L. Luan, C.C. Dai, M. Li, G. Yang, W.H. Hou, Highly active free-standing and flexible MoS_2/rGO sandwich-structured films for supercapacitor applications. Solid State Commun. **297**, 45–49 (2019)
30. X. Xu, W. Zhong, X. Zhang, J. Dou, Z. Xiong, Y. Sun, T. Wang, Y. Du, Flexible symmetric supercapacitor with ultrahigh energy density based on NiS/MoS_2@ N-rGO hybrids electrode. J. Colloid Interface Sci. **543**, 147–155 (2019)

31. R. Naz, M. Imtiaz, Q. Liu, L. Yao, W. Abbas, T. Li, I. Zada, Y. Yuan, W. Chen, J. Gu, Highly defective 1T-MoS_2 nanosheets on 3D reduced graphene oxide networks for supercapacitors. Carbon **152**, 697–703 (2019)
32. N.M. Farag, M.A. Deyab, A.M. El-naggar, A.M. Aldhafiri, M.B. Mohamed, Z.K. Heiba, Exploring the functional properties of $CuCo_2O_4$/CuS nanocomposite as improved material for supercapacitor electrode. J. Mater. Res. Technol. **10**, 1415–1426 (2021)
33. R. Manikandan, C.J. Raj, G. Nagaraju, R. Velayutham, S.E. Moulton, J. Puigdollers, B.C. Kim, Selenium enriched hybrid metal chalcogenides with enhanced redox kinetics for high-energy density supercapacitors. Chem. Eng. J. **414**, 128924 (2021)
34. A. Gowrisankar, A.L. Sherryn, T. Selvaraju, In situ integrated 2D reduced graphene oxide nanosheets with MoSSe for hydrogen evolution reaction and supercapacitor application. Appl. Surf. Sci. Adv. **3**, 100054 (2021)
35. Y. Liu, D. Zhao, H. Liu, A. Umar, X. Wu, High performance hybrid supercapacitor based on hierarchical MoS_2/Ni_3S_2 metal chalcogenide. Chin. Chem. Lett. **30**(5), 1105–1110 (2019)
36. A.C. Lokhande, A. Patil, A. Shelke, P.T. Babar, M.G. Gang, V.C. Lokhande, D.S. Dhawale, C.D. Lokhande, J.H. Kim, Binder-free novel Cu_4SnS_4 electrode for high-performance supercapacitors. Electrochim. Acta **284**, 80–88 (2018)
37. Y.J. Yang, C. Yao, S. Chen, N. Wang, P. Yang, C. Jiang, M. Liu, Y. Cheng, A 3D flower-like $CoNi_2S_4$/carbon nanotube nanosheet arrays grown on Ni foam as a binder-free electrode for asymmetric supercapacitors. J. Electroanal. Chem. **888**, 115217 (2021)
38. J. Gong, J. Yang, J. Wang, L. Lv, W. Wang, L. Pu, H. Zhang, Y. Dai, A dual NiCo metal-organic frameworks derived $NiCo_2S_4$ core-shell nanorod arrays as high-performance electrodes for asymmetric supercapacitors. Electrochim. Acta **374**, 137794 (2021)
39. P. Tiwari, D. Janas, R. Chandra, Self-standing MoS_2/CNT and MnO_2/CNT one dimensional core shell heterostructures for asymmetric supercapacitor application. Carbon **177**, 291–303 (2021)
40. M.K. Vidhya, R. Yuvakkumar, G. Ravi, E.S. Babu, B. Saravanakumar, O. Nasif, S.A. Alharbi, D. Velauthapillai, Demonstration of 1.5 V asymmetric supercapacitor developed using $MnSe_2$-$CoSe_2$ metal composite. Ceram. Int. **47**(8), 11786–11792 (2021)

Chalcogenides Based Nano Composites for Supercapacitors

A. Rajapriya, S. Keerthana, and N. Ponpandian

Abstract The hybrid structured nanocomposite materials possess outstanding electro-capacitance behavior because of the synergistic effects from different composite materials. Environmental pollution, ecological damage, and energy crises consume severely hampered the future transition to a sustainable society and consequently of the prompt growth of the economy and widespread usage of conventional fossil fuels. Synthesizing novel nanomaterials with relatively low cost, high efficiency, and exceptional characteristics is essential for the effective use of energy conversion and storage (ECS) devices. Depending on individual physical and chemical characteristics, such as conductivity, mechanical and thermal stability, and cyclability, nanostructured transition metal chalcogenides (TMCs) have recently been shown to be very promising candidates for effective ECS systems. In supercapacitor applications, the TMCs and their nanocomposites have been systematically summarized due to their great successful cases.

Keywords Supercapacitor · Hybrid material · Nanocomposites · Transition metal chalcogenides · Sulfides · Selenides · Tellurides

1 Introduction

Two-dimensional transition metal chalcogenides (TMCs) consist of more than 40 compounds with the general formula of MX_2, M represents the transition metal (group 4–7) and X represents chalcogenides (S, Se, Te) [1]. Significant advancement in large-scale-based approaches to the production of 2D TMC nanosheets and their incorporation with other innovative materials used to produce functional composites. They propose 2D TMD-based composites with metal oxides, noble metals, metal–organic frameworks, metal chalcogenides, organic molecules, and polymers for supercapacitors, batteries, electronics, electro- and photocatalysis, sensors, and biomedicine [2].

A. Rajapriya · S. Keerthana · N. Ponpandian (✉)
Department of Nanoscience and Technology, Bharathiar University, Coimbatore 641046, India
e-mail: ponpandian@buc.edu.in

S. Thomas et al. (eds.), *Nanostructured Materials for Supercapacitors*,
Advances in Material Research and Technology,
https://doi.org/10.1007/978-3-030-99302-3_18

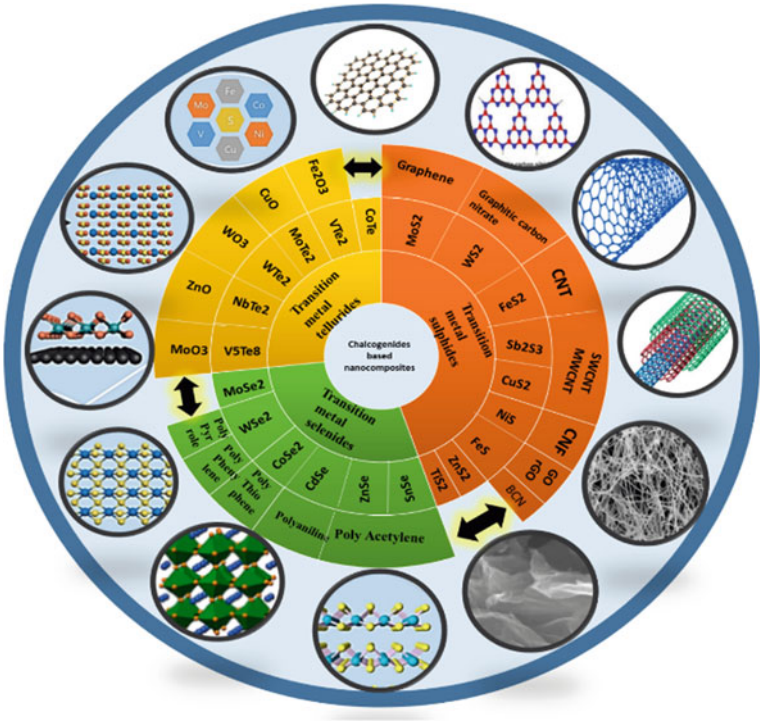

Fig. 1 Classification of transition metal chalcogenides with various composite materials

TMCs have attained plenty of contemplation over years as a result of their extensive theoretical specific power, limited volume shifts besides higher surface area, high electrical conductivity, and multiple oxidation states. TMCs establishing substantial attention in energy devices including Li-ion batteries, fuel cells, supercapacitors, solar cells, sensors, light-emitting diodes, memory devices, and thermoelectric devices. Due to these facilitated properties, TMCs could store a substantial amount of energy by electrical double layer. To demand the high energy density, necessities of contemporary electronic devices, the hybrid electrodes are designed with TMCs and other materials and further hybrid configurations are implemented. Over the past few years, TMCs advanced electrochemical hybrid energy storage schemes to overcome the drawbacks of cycle life and power density of Li-ion batteries and low energy density of supercapacitors (Fig. 2). TMCs can be embodied as an anode for battery through the electrochemical intercalation of ions and as a cathode material for capacitor through physical adsorption of metal ions in electrolyte [3].

TMCs have numerous charge storage properties in hybrid capacitors: (1) Due to high surface area TMCs, the duration of ion diffusion is inadequate (2) Have multiple exposed active areas. (3) TMCs are two-dimensional materials the ion transport is rapid. (4)) Two-dimensional channels can be simply expanded and contracted. (5) The electrical conductivity, electrode dynamics, and cycle stability of TMCs (6) Surface

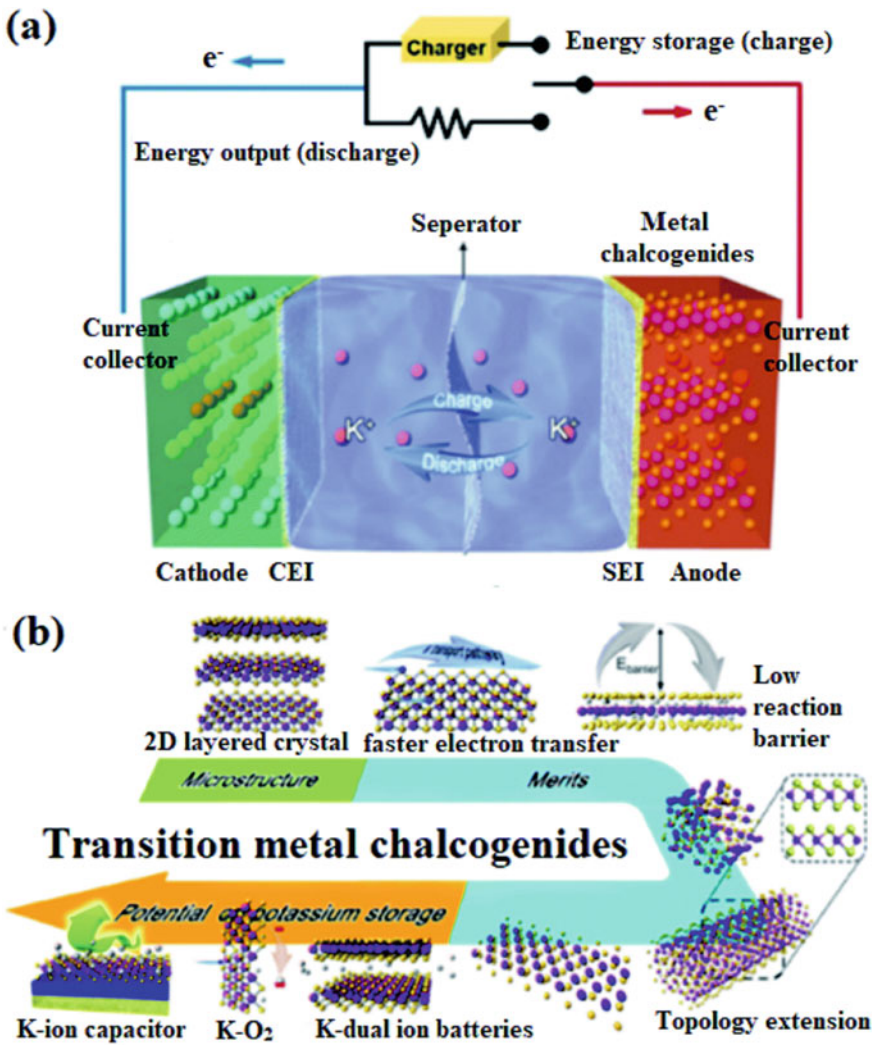

Fig. 2 Schematics of working of supercapacitor and structures of metal chalcogenides [3]. Adapted from an Open Access Article is licensed under a Creative Commons Attribution-NonCommercial 3.0 Unported Licence ((OC) BY-NC)

redox pseudocapacitance or intercalation can be obtained readily using TMCs. (7) TMC structures have outstanding steadiness and mechanical capability [4]. These significant properties urge that transitional metal-based chalcogenides materials can be used as pioneering electrodes for potassium ion hybrid capacitors.

2 Transition Metal Sulfides (TMSs) Based Nanocomposites for Supercapacitor

2.1 Metal Sulfide/Metal Oxides Composite Material

Because the composite prevents both $NiFe_2O_4$ and MoS_2 from restacking, the $NiFe_2O_4/MoS_2$ could be a superior choice for energy storage. Furthermore, 2D MoS_2 can offer a homogeneous and extensive surface area for electrolyte permeability and additional networks for ions and electrons transport. Initially, the CV analysis of nickel foam was measured to clarify the capacitance contribution under the same condition in an alkaline medium. When compared with the nickel foam, $NiFe_2O_4/MoS_2$ composite has attributed to the synergistic effect with the significant specific capacitance [5]. The two pairs of intense redox peaks were witnessed for $NiFe_2O_4/MoS_2$ composite materials, which leads to the reversible responses to M-S/M-S-OH and M–O/M-OOH where M is Ni, Fe or Mo ions. The electrode's redox mechanism may be expressed as follows. The CV curves' pattern does not change at any of the examined scan rates, and the current density increases as the scan rate increases, indicating perfect capacitive behavior. Additionally, when scan rates improve, peak current densities migrate to a wider potential window, which can be interpreted a Charge transfer-limited kinetics and diffusion-limited redox reactions [6].

$$NiFe_2O_4 + H_2O + OH^- \leftrightarrow NiOOH + 2FeOOH + e^- \quad (1)$$

$$MoS_2 + OH^- \leftrightarrow MoS_2OH + e^- \quad (2)$$

The GCD curves of $NiFe_2O_4/MoS_2$ electrode material at different current densities 1, 2, 3, 4, 5, 6, and 7 A/g were studied and the capacitance may be estimated as 506, 426, 373, 331, 300, 253, and 207 F/g, respectively. The electrode can operate at a high current density, indicating the composite material's excellent electrochemical performance. It's worth mentioning that the $NiFe_2O_4/MoS_2$ particles are deposited was not constantly functional during the first cycle, but after a long period of charging and discharging, the electrode has significant contact with the electrolyte, resulting in improved capacitive performance.

2.2 Metal Sulfide/Quantum Dot Hybrids

Si nanoparticles have garnered considerable attention as a consequence of their great research value in both fundamental theory and practical applications. When the particle size of a-Si nanocrystal is limited to the Bohr excitons radius, the quantum confinement effect occurs and it is called a Silicon quantum dot (Si-QD) [7]. The

mobility of electrons or holes in three-dimensional space in Si QDs is restricted by the circumstance that the restricted carrier can only be found at the isolated bound level, and the motion is quantized, reducing the momentum conservation requirement. The use of Si QDs as the nucleation center enhances the nucleation of MoS_2 and improves up the reaction rates. The Si/MoS_2 composite crisscross each other, forming a flower-like structure. This structure allows the active material to make absolute contact with the electrolyte, resulting in a redox reaction. Furthermore, the structure minimizes the changes in the material's microstructure induced by the charging and discharging process to some extent. When the electrochemical performance of the two types of electrodes (MoS_2 and Si/MoS_2 composite) is compared, the Si/MoS_2 composite electrode outperforms the MoS_2 electrode in terms of specific capacitance and cyclic stability. MoS_2 prefers to build in the direction with the lowest binding potential energy without Si-QDs [8]. The MoS_2 nanosheets got larger and more stacked as the reaction time was extended. Only a tiny portion of MoS_2 nanosheets can resist partial binding potential energy squeezing or quasi-upright growth. The TEM analysis of Si/MoS_2 provides the high resolution image clearly illustrates the highly ordered lattice fringes with the inter-planar distance of 0.61 nm which corresponds to the plane (002) of MoS_2 is illustrated in Fig. 3.

The electrochemical performance of pure MoS_2 and Si/MoS_2 composite were compared with a sweep rate of 100 mV/s. The integrated area in the CV curves of

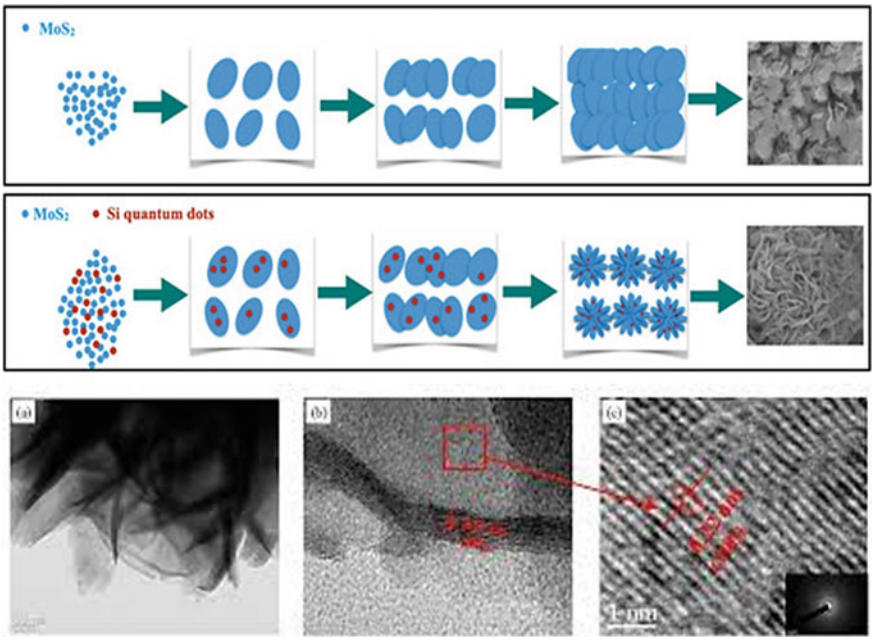

Fig. 3 Schematic illustration of the formation for MoS_2 and Si/MoS_2 composite and their HR-TEM images [8]. This article is an open-access article distributed under the terms and conditions of the Creative Commons Attribution (CC BY) license

Si/MoS_2 is larger when than the pure MoS_2, which significantly corresponds to the better specific capacitance of the composite material. The GCD plateaus constitute the pseudocapacitance behavior and the composite Si/MoS_2 provides the larger discharge time when compare with MoS_2 with enhanced specific capacitance. For the following three reasons, the specific capacitance of Si/MoS_2 composite is greater than that of MoS_2: (i) Si-QDs is added and it acts as the nucleation center to support the nanosheets MoS_2 which readily increases the ion transport channel, (ii) the diffusion path of ions and electrons which improves the electrochemical performances with porous and microflower structure of Si/MoS_2 and (iii) the robust electrolytic ions supply the sufficient oxidation and reduction reactions have open space in composite microflower [9]. In the CV curves of MoS_2 and Si/MoS_2 composite, the peak of the current increased gradually when the scanning rate was increased, and the curve form remained essentially unchanged. The composite Si/MoS_2 materials improve the electrochemical characteristics and have the specific capacitance of 574.4 F/g at 5 A/g with 84.5% retention after 1000 cycles.

2.3 Nickel Sulfide Nanohybrids

In recent decades, nickel sulfide (NiS) garnered extensive attention because of its unique properties in hybrid capacitor applications. The arrangement of electrochemically active sites, on the other hand, dramatically reduces their electrochemical performance. Building coordinated structures with conductive substrates, increasing active sites through nanocrystallization, and establishing nanohybrid architecture combining different electrode materials have all resulted in substantial improvements [10]. This section overviews the advancement in the practical preparation and reasonable designing of NiS and their composite materials as an electrode combined with several bifunctional EDLC based materials and pseudocapacitive materials.

Reaction mechanism of NiS: The oxidation–reduction reaction of NiS in alkaline electrolytes are represented as follows [11].

$$NiS_x + OH^- \leftrightarrow NiS_xOH + e^- \tag{3}$$

$$Ni_3S_2 + 3OH^- \leftrightarrow Ni_3S_2(OH)_3 + 3e^- \tag{4}$$

The electrochemical reactions of active electrode materials are verified using quasi- diffusion-limited kinetics to distinguish between the redox mechanism of pseudocapacitance or battery-type electrodes, where the kinetic operation of the electrode and the flow of electrons in redox reactions are controlled by a semi-discrete diffusion. However, in most cases, NixSy's poor cycle performance is followed by irreversible reactions [12]:

$$NiS_x + H_2O + 0.5O_x \rightarrow Ni(OH)_2 + xS \tag{5}$$

$$Ni_3S_4 + 3H_2O + 1.5O_x \rightarrow 3Ni(OH)_2 + 4S \quad (6)$$

$$Ni(OH)_2 + OH^- \rightarrow NiOOH + H_2O + e^- \quad (7)$$

According to earlier findings, NixSy electrodes' battery-type redox process, as well as their reduced rate performance and poor cyclic stability, would severely restrict their applicability. Due to its fast-decaying capacitance at increased rates, which is caused by its low inherent electrical conductivity and insufficient quantity of active sites. Constructed synthesis of nanostructured materials, binder-free electrodes produced on conductive substrates, and manufacturing of nano-hybrids (nanocomposites) with good conductive reinforcements such as graphene, porous carbons, and conducting polymers are some of the strategic priorities to resolve the challenges mentioned above. The shape and surface area of electrode materials are well recognized to influence electrochemical performance and hence controlled synthesis of NiS nanoparticles with a steady structure and greater surface area is essential.

NiS pristine: Among the various NixSy structures, NiS holds the easiest stoichiometry occurring in two possible phases of α-NiS (hexagonal) and β-NiS (rhombohedral). NiS is especially suitable for hybrid capacitors due to its large theoretical capacity, low cost, excellent electrical conductivity, environment sustainability, and simple production method. NiS as an electrode material has some primary disadvantages such as low rate capability and slow electron transport rate. These issues can be rectified by constructing NiS with different dimensions such as nanoplates, porous nanomaterials, nanorods, nanowires as well as hierarchical designs such as core–shell, complex hollow [13].

NiS covered on N-doped hollow carbon spheres (NHCS) composites: The assembly of functional materials on carbon materials such as graphene, carbon nanotube, and carbon nanofiber is an inspiring approach to boost the electrochemical behavior designated with cycling life and rate capability by combining carbonaceous materials and pseudocapacitive materials. The synthesis and the structure of NiS coated NHCS through the template-assisted method. The core–shell NiS/NHCS structures template for nickel silicates follows the formation of NiS nanosheets reinforced on the NHCS hollow structure. The GCD profile of NiS/NHCS electrode favors the capacitance of 1150 F/g at 1 A/g current density with the capacitance retention of 76% at 5 A/g over 4000 cycles of charge–discharge. The hybrid capacitor of NiS/NHCS//AC performed a specific capacitance of 120 F/g at 0.2 A/g current density.

Composite material $CoNi_2S_4/Ni_3S_2$: The Ni_3S_2 composite with $CoNi_2S_4$ demonstrates the distinctive pseudocapacitive behavior because it shows a redox peak in CV curves. When the scan rate increases, the integrated area increases indicating that the fabricated materials promote electron transfer and fast ion rate. The GCD curves of composite material $CoNi_2S_4/Ni_3S_2$ hold a specific capacitance at the current density (1 A/g) of 997.2 F/g and the electrode exhibited reduced contact and greater charge transfer resistance than other metal oxides. This $CoNi_2S_4/Ni_3S_2$ hybrid structure has

outstanding electrochemical performance. The electrochemical device is arranged using the active carbon (negative electrode) and $CoNi_2S_4/Ni_3S_2$ nanowires (positive electrode) to further evaluate the functional application of the as-prepared electrode. The CV curves were operated at a current density of 50 mV/s and with the potential range of 0–0.6 V and −1 to 0 V that the device has the total potential of 1.6 V. The fabricated $CoNi_2S_4/Ni_3S_2$ electrode exhibits CV curves at different scan rate from 2 to 50 mV/s. The electrocapacitive device at various potential windows at the scan rate of 50 mV/s showed the prolonged working voltage is shown in Fig. 4. The device has a stable capacitive behavior with both EDLC and pseudocapacitance performance at

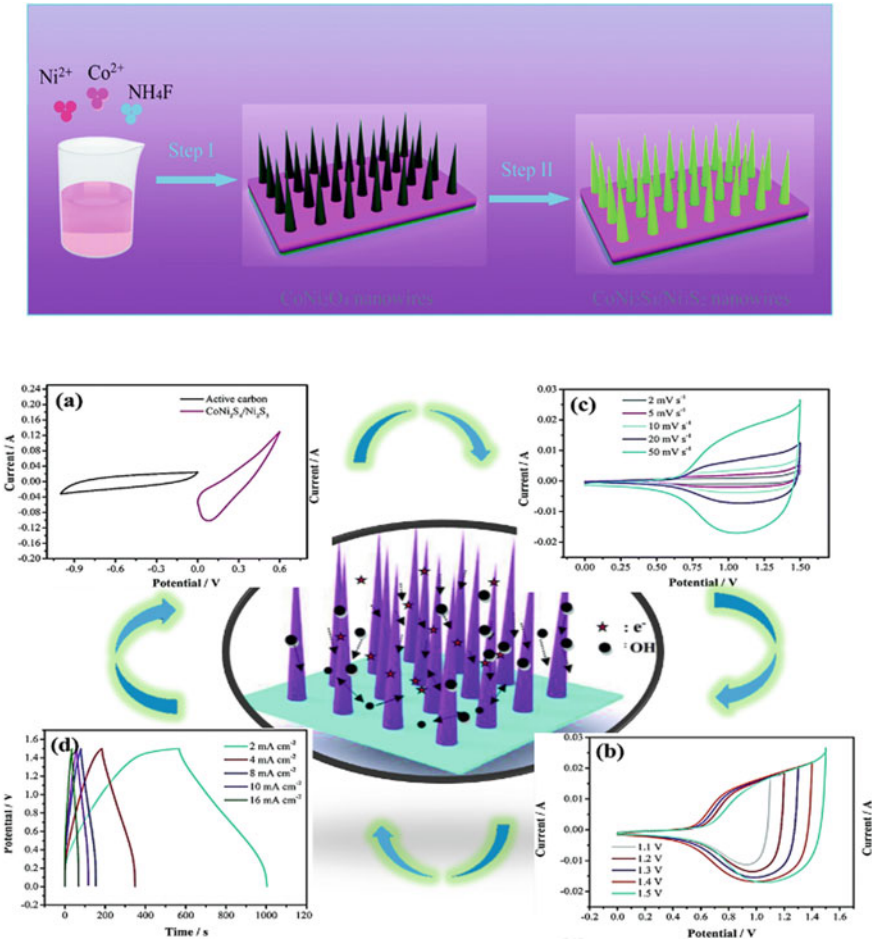

Fig. 4 The synthesis and electrochemical characteristics of fabricated $CoNi_2S_4/Ni_3S_2$ electrode [14]. Article is licensed under a Creative Commons Attribution-Non Commercial 3.0 Unported Licence (BY-NC)

the voltage of 1.5 V. The GCD curve demonstrated the areal capacitance of 136.05 mF/cm at 2 mA/cm current density [14].

3 Transition Metal Selenides (TMSes) Based Nanocomposites Electrode for Supercapacitor

TMCs have recently received a lot of attention in the energy storage sector due to their high theoretical capacity. TMSes are layered compounds made up of a hexagonal arrangement of transition metal atoms which is sandwiched between two layers of group six chalcogen atom-like Se. In these materials, metals and chalcogen atoms are connected by strong covalent bonds and intra-layers are connected via weak van der Waals forces. Moreover, this sandwich structure is favorable for insertion and desertion of electrolyte ions [15, 16]. Even though TMSes is a metal chalcogen molecule with a high pseudocapacitance, there have been few studies on the usage of metal selenides in supercapacitors. Particularly TMSes, have recently received a lot of attention as effective electrocatalysts for a variety of electrochemical applications. Especially, due to their unique electronic conductivity, interesting electrocatalytic activity, higher conductive nature, relatively high energy density, and binding affinity mark them promising materials for supercapacitors [17]. According to published studies, selenide has a high theoretical specific capacitance and excellent electrochemical performance. Other advantages of TMSes are their low cost, abundant earth, and ease of manufacturing; these qualities are highly advantageous for their use in electrical devices. Remarkably, $MoSe_2$ is a layered structure (Se–Mo–Se) with a narrow bandgap that might be a suitable candidate for the electrode material for supercapacitors. Moreover, $MoSe_2$ has a wider interlayer spacing (0.646 nm) than graphite (0.335 nm) and MoS_2 (0.615 nm). As a result, $MoSe_2$ is considered as one of the supreme electrode materials for supercapacitors, and some research has been conducted on the electrochemical performance of supercapacitors utilizing $MoSe_2$ [18]. For instance, a group developed, mushroom-like $NiSe_2$ for the flexible supercapacitors and it delivers remarkable properties like mechanical flexibility. These findings open up a new initiative to build flexible, smart, and portable electronic products [19].

3.1 Combination of Metals Selenides Hybrids for Supercapacitor

However, the electrocatalytic activity of metals selenide is limited by relatively weak conductivity and aggregation of the material. So, there is a need for hybrid TMSes to be developed using nano-structural engineering to adjust their electrical and structural characteristics for the ideal architecture, which may increase conductivity and

enhance the capacitance of electrode materials for charge storage. The combined effect of metal selenides strengthens supercapacitor performance due to their synergistic contact that emerges from the number of active sites, enhancing electrical conductivity, rising higher surface area, and narrowing the networks to assure superior catalytic activity and higher storage efficiencies [20]. In relation, $WSe_2/CoSe_2$ hybrid composites with improved electrochemical performances were developed using a hot-injection method by making $CoSe_2$ well dispersed in WSe_2 by altering their conducting property and boosting the active sites on the interfaces between the two components. Furthermore, the proposed $WSe_2/CoSe_2$ has a higher specific capacitance of 2720 F g^{-1} for 1 A g^{-1}, as well as a higher cycle life of 93.75% [21]. Likewise, a group prepared polyhedron structured $NiSe_2@MoSe_2$ by hydrothermal synthesis is shown in Fig. 5. The fabricated asymmetric device shows outstanding capacitance of 305 Fg^{-1} at 1 Ag^{-1} with good cycling stability. Herein, the combination of Ni and Mo delivers the greater redox activity, which is beneficial to the higher electrochemical performance [22]. The two-electrode cell setup was built by $NiSe_2@MoSe_2$ and activated carbon as positive and negative electrodes and the two electrodes and both possess different potential windows is shown in Fig. 5. The

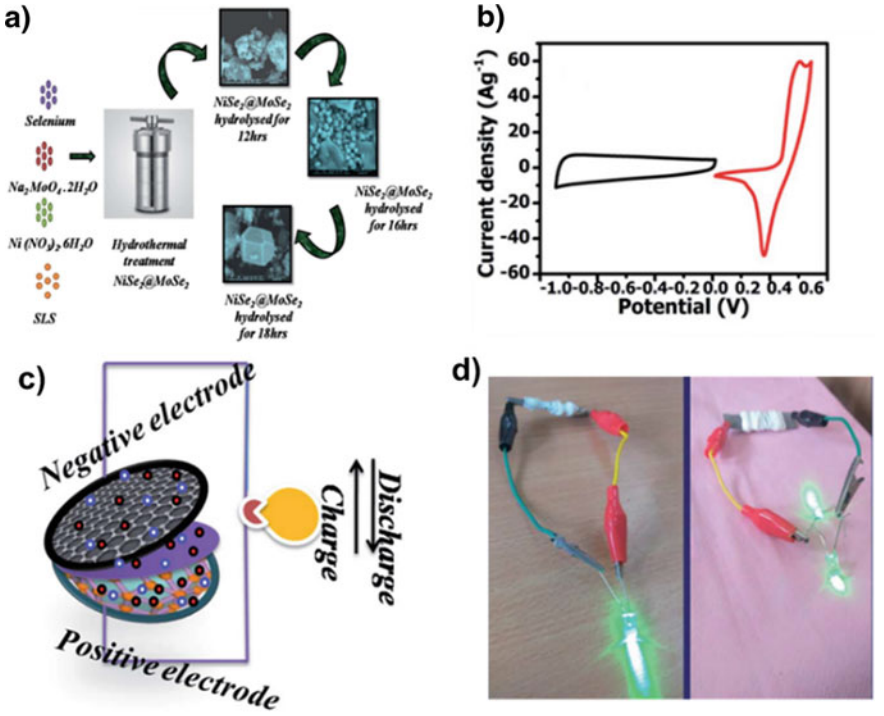

Fig. 5 Synthesis procedure, CV profile, and the schematics of an asymmetric device [22]. Adapted from an Open Access Article is licensed under a Creative Commons Attribution-Non Commercial 3.0 Unported Licence (BY-NC)

device fabrication and the response was shown in Fig. 5. Accordingly, the device works well, hence the polarization achieved at the voltage of 0–1.5 V, demonstrating the appropriate potential range of the asymmetric super capacitor should be 0–1.5 V.

The coexistence of various transition metals in bimetallic compounds improves electronic conductivity and redox activity, thereby improving rate performances in electrochemical reactions by sharing and combining their individual electronic properties. Based on this, a group designed $CoSe_2$ by incorporating transition metals (V, Zn, Mn, and Cu) to tune its rate capability towards supercapacitors. V-$CoSe_2$, Zn-$CoSe_2$, Mn-$CoSe_2$, and Cu-$CoSe_2$ were developed directly on nickel foam in this study. This binder-free direct growth facilitates the abundance of active sites and lowers the interfacial resistance between the conductive substrate and active material. As a result of this, V-$CoSe_2$ consumes a higher capacitance of 1830.2 F/g. The specific capacitance of V-$CoSe_2$ is related to the morphology of nanosheets with defects on the basal plane, which provides additional active sites and increases their electron transfer kinetics [23]. Table 1 comprises the list of a variety of hybrid-metal chalcogenides used for making hybrid supercapacitors.

4 Transition Metal Tellurides (TMTs) and Their Composites Based Supercapacitor

TMTs have recently received considerable attention as important members of TMCs due to their various crystal structures and unique electronic configuration. Due to its distinct phase transition properties, electron strong-correlated phenomenon, and ferromagnetism, TMTs open up new avenues for fundamental research and novel device applications. For example, the crystal structure transition between T′ and H phases of $MoTe_2$ is easier to trigger due to lower energy differences. Group VB metal tellurides have been considered as a potential framework for initiating its physical parameters such as superconductivity, electro-catalytic activity, and quantum spin hall-effect. Tellurium (Te) is an intriguing p-type semiconductor with important supercapacitor properties, owing to its high electrical conductivity and material density. It is widely used in a variety of energy storage systems, including Li-Te batteries [24]. Recently, metal tellurides like CoTe, NiTe, La_2Te_3, $MoTe_2$, and Sm_2Te_3 have been used as electrode materials for energy storage devices. Because of its thermal, electrical, and magnetic properties, CoTe has a wide range of applications, including electro-catalysis, water splitting, solar cells, batteries, photo-catalysis, and biosensors. Cobalt telluride nanomaterials materials have shown promise in a variety of applications, most notably in energy production and storage. High temperatures and a limiting atmosphere are required for the synthesis of cobalt telluride-based 2-D nanomaterials, making large-scale production and fabrication of supercapacitors difficult and expensive. Thus, a group prepared CoTe nanorods by hydrothermal method and it exhibits the high specific capacitance 170 Cg^{-1} at 0.5 Ag^{-1} and the prepared CoTe nanorods retain 85% of its initial capacitance is shown in Fig. 6 [25].

Table 1 Synthesis method, specific capacitance, and retention of a variety of hybrid-metal chalcogenides

Material	Synthesis method	Specific capacity or specific capacitance	Retention	Ref
Graphene wrapped copper sulfide hollow spheres	Solvothermal method	2317.8 F g^{-1} at 1 Ag^{-1}	96.2% after 1200 cycles	[36]
NiS micro-flowers	Sulfurization method	1122.7 Fg^{-}1 at 1 Ag^{-1}	97.8% after 1000 cycles	[37]
Manganese-cobalt sulfide-core–shell nanostructures	Hydrothermal method	2067 F g^{-1} at 1 Ag^{-1}	89% after 5000 cycles	[38]
Hollow structured $Cu(Co–Ni)_2S_4$ NTs/Ni foam	Template method	903.9 Fg^{-1} at 2 Ag^{-1}	96.2% after 5000 cycles	[39]
Hierarchical cobalt-molybdenum selenide hollow spheres	Gas bubbled template method	211.97 mAh g^{-1} at 1 Ag^{-1}	93% after 10,000 cycles	[40]
Molybdenum selenide nanosheets	Electrodeposition	325.92 mAh g^{-1}	80% after 1000 cycles	[41]
Cobalt–nickel selenides	Selenization method	447 C g^{-1} at 1 A g^{-1}	97% after 2000 cycles	[42]
Hierarchical-sea urchin-like bimetallic zinc–cobalt selenide	Hydrothermal method	1419 Cg^{-1} at 2 A g^{-1}	80% after 10,000 cycles	[43]
Cobalt zinc selenide @CNTs–CNFs	Electrospinning	1891 Fg^{-1} at 1 A g^{-1}	88.6% after 8000 cycles	[44]
Urchin-like manganese –cobalt Selenide	Hydrothermal method	1656 Fg^{-1} at 1 A g^{-1}	91.8% after 8000 cycles	[45]

Despite the fact that tellurium has significantly higher electronic conductivity, it is estimated that supercapacitors fabricated on a composite of metal tellurides and carbon-based materials will have great capacitance and conspicuous electrochemical performances by aiding better electron transfer and delivering lower electric series resistance. In response to this exciting research, we created a simple one-step method for fabricating $MoTe_2$/graphene electrodes in which $MoTe_2$ are grown on graphene using a microwave-synthesis method. To further evaluate the supercapacitor behavior, galvanostatic charge–discharge was performed and it exhibits the capacitance of 434 Fg^{-1} at 1 Ag^{-1} [26]. TMTes research for energy storage applications, on the other hand, is still in its initial stages. Furthermore, Te has lower electronegativity, higher electronic conductivity, and greater atomic size than S and Se, allowing for the acceptance of more electrolyte ions with enhanced diffusion kinetics. Given these critical issues, it is expected that the fabrication of composite materials composed of distinct but complementary components will provide opportunities resulting from the

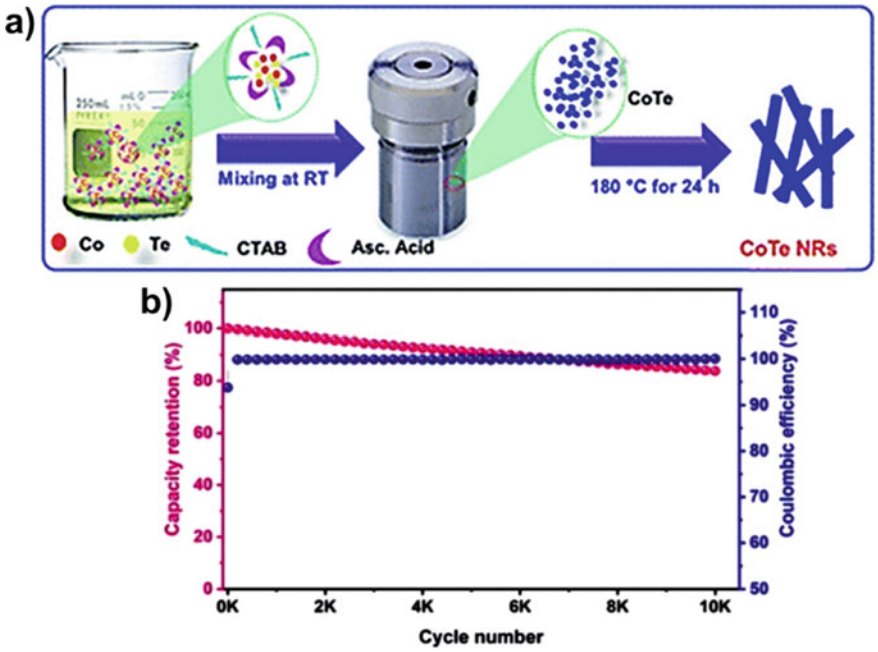

Fig. 6 Schematic illustration for the growth and their capacity retention of CoTe nano-rods [22]. Adapted from an Open Access Article is licensed under a Creative Commons Attribution-Non Commercial 3.0 Unported Licence (OC-BY)

synergistic performance of each component, resulting in improved electrochemical performance. A group demonstrates how to design and fabricate a highly porous CoTe@C–NiF composite material derived from a Co–MOF structure rationally. The CoTe@C–NiF composite material is unique and significant in that it can be used as a working electrode in a variety of potential ranges, specifically (0.8–0) V as a negative electrode and (0–0.5) V as a positive electrode. Also, the assembled device delivers an energy density of 43.84 Wh kg^{-1} at a power density of 738.88 W kg^{-1} [27].

A group developed, NiCoTe nanotubes directly on nickel foam by Solvothermal method and successive ion-exchange reaction. It delivers the higher specific capacity of 131. 2 mAh g^{-1} at 1 Ag^{-1} and satisfactory cyclic stability with the retention of 92% after 5000 cycles. Bimetallic Ni-Co tellurides may have high electrical conductivity, allowing electron transfer and faradaic redox reactions to occur at high charge/discharge rates. As a result, although this has rarely been reported, Ni-Co tellurides are highly possible to provide agreeable energy storage performances as electrode materials. Furthermore, the morphology and microstructure of electro-active materials would influence the accessible surface and structural stability, and thus the electrochemical performances. As a result, we intend to develop Ni–CoTe with controllable structures for use as high-performance electrode materials [28].

Still, there is scope for enhancing the action of TMTes by identifying appropriately mixed metals and enabling the greatly conductive networks by adorning by noble metals such as silver (Ag), gold (Au), platinum (Pt), and so on. Fe-based materials have received a great deal of attention for the fabrication of SCs due to their rich redox activity, which is advantageous for high specific capacitance and Fe is the most abundant element in the Earth's crust, so it is inexpensive. Furthermore, Fe-based materials are safer for the environment than other transition metal-based electrodes. As a result, increasing conductivity by a combination of conductive materials. Because of the above-said clearness, a group created the first Ag-decorated NiFeTe hierarchical nanorods (AMMT HNRs) on nickel foam (NF) by wet chemical method. Their HSC device shows an energy density of 0.669 mWh cm^{-2} and a power density of 64 mW cm^{-2} at current densities of 4 mA cm^{-2}. Also, it retains its capacity of 86% after 5000 cycles [29].

5 TMCs/Carbon-Based Nanocomposites Material for Hybrid Capacitor Applications

Carbonaceous Materials Hybrids, such as graphene, carbon nanotubes (CNTs), carbon aerogel, and others, typically have high electrical conductivity and surface area. Designing TMD hybrids- or making composite with carbon-based materials results in a complementary effect of the two materials; carbon provides conductive channels and improves interfacial contact, while TMD improves overall electrochemical performance. Likewise, a group synthesized MoS_2/rGO hollow microspheres by a hydrothermal method by using SiO_2/GO hollow microsphere as a pattern. MoS_2/rGO hollow spheres deliver a capacitance of 218 Fg^{-1}. Whereas, the HRTEM images indicate the structure of MoS_2 nanosheets anchored rGO microspheres with the complete removal of SiO_2 pattern, where the lattice fringes are noticeable and their d-spacing is corresponding to the crystal plane (002) of MoS_2 in Fig. 7.

In this way, another group prepared directly grown MoS_2 nanowalls on MWCNTs by simple hydrothermal method without the use of any binder and surfactant for surface modification [30]. Herewith, plenty of active sites were obtained in MoS_2 layers by the growth taking place in acidic conditions. Furthermore, the capacitive contribution of the system was analyzed and found that the maximum capacitance was attributed to the diffusion-controlled process comes from the intercalation of K^+ ions into the MoS_2 layers is shown in the following equation.

$$MoS_2 + K^+ + e^- \leftrightarrow MoS - SK \tag{8}$$

Similarly, compared with single nickel chalcogenides, nanocomposites can make full use of the synergistic and complementary effects among components, which makes them have superior advantages in applications. Likewise, nickel sulfides/graphene composites are belonging to the pseudocapacitance material and

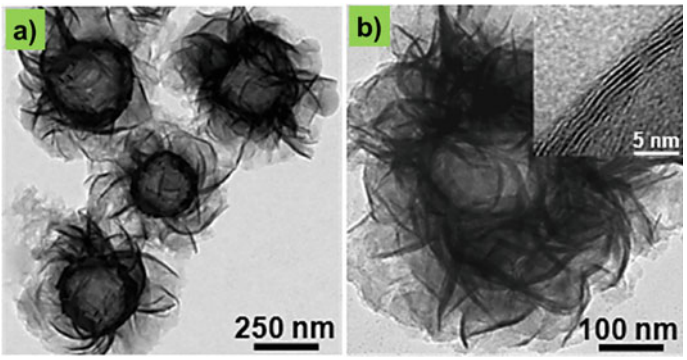

Fig. 7 HR-TEM images of MoS_2/rGO hollow spheres [30]. Adapted from an article is licensed under a Creative Commons Attribution 4.0 International License, provide a link to the Creative Commons license, and indicate if changes were made (CC-BY)

it facilitates the fast electron transfer leads to electrochemical performance. So that, a group developed composites of NiS_2 and $NiSe_2$ with graphene by simple hydrothermal synthesis [31]. In the benefit of synergetic effect, the composite of $NiCo_2S_4$/carbon spheres proposed for high energy density supercapacitors was prepared by a hydrothermal method is shown in Fig. 8. With this, carbon spheres

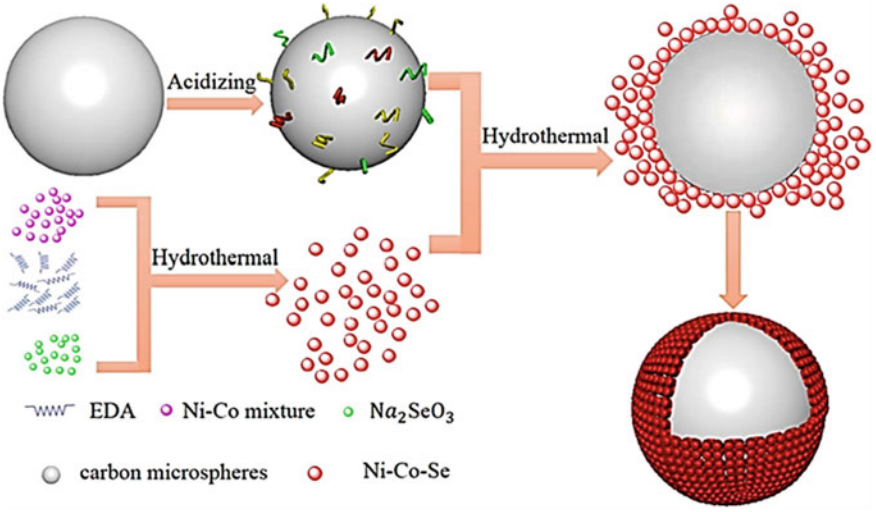

Fig. 8 Schematic illustration of the fabrication of $NiCo_2S_4$/carbon spheres [32]. Adapted from an open access article distributed under the terms of the Creative Commons Attribution Non-Commercial No Derivatives 4.0 License (CC BY-NC-ND)

were uniformly shielded with $NiCo_2S_4$ promoting the enhancement of the supercapacitor, and its shows the energy density of 101Wh Kg^{-1} at a power density of 0.749 kW kg^{-1} [32].

5.1 Metal Sulfide/Carbon Hybrids as a Nanocomposite

Because of its 2D structure, new semiconductor characteristics, and inventiveness to be a good substitute for carbonaceous materials. MoS_2 is one of the best among transition metal dichalcogenides in the future. In MoS_2, wide interlayer gap causes double-layer capacitance due to the high surface area, while pseudocapacitance is caused by the many oxidation states of the central Mo atom. Furthermore, the enhancement of the specific capacitance is strongly influenced by differentiating features of current collectors such as conductivity, working area of the electrode, decreased electrode-material resistance, and high adhesive forces [33]. Current collectors utilized in the creation of supercapacitors include stainless steel, nickel foam, carbon textiles, and different metal mesh.

The pore size of the material, which is equivalent to the hydrated ion size, has the potential to increase the capacitance. Hence, the pore diameter of MoS_2 and MoS_2/CNF was determined to be 3.68 and 5.35 nm, respectively, which is larger than the radius of the hydrated K^+ ion size of 0.33 nm [34]. The asymmetric GCD curves of both MoS_2 and MoS_2/CNF, as well as the irregular triangular form, reveal the material's pseudocapacitive nature. At a current density of 1 A/g, the developed MoS_2/CNF nanostructures have a capacitance of 903.9 F/g and withstand 94% of their capacitance after 5000 cycles. The void area between the nanosheets of MoS_2/CNF and MoS_2 nanoflowers facilitates the insertion of electrolyte ions, which enhances the capacitance [35]. As a result, the suggested composite could be paving the way for the development of highly efficient supercapacitors composed of 2D and 1D materials.

5.2 Metal Selenides/Graphene Composites

Moreover, structural defects provide a new direction for boosting the inherent catalytic activity of materials, particularly 2D-TMDs. Sulphur (S) vacancies in TMDs like MoSSe or WSSe are stable and aid in the absorption of protons in the electrolyte. Also, adding of S atom can modify the electronic structure of the MoSe/WSe. For that, a group demonstrated the use of a hydrothermal method to prepare sulfur-introduced tungsten selenide (WSSe) or molybdenum selenide (MoSSe). The CV and GCD responses MoSSe and MoSSe/rGO at different sweep rates from 5 to 50 mV s^{-1} and current densities from 1 to 6 Ag^{-1} are shown in Fig. 9. The improved performance of MoSSe/rGO supercapacitor applications can be determined by various factors: the complementary interaction of MoSSe/2D-rGO nanosheets possess edge active sites

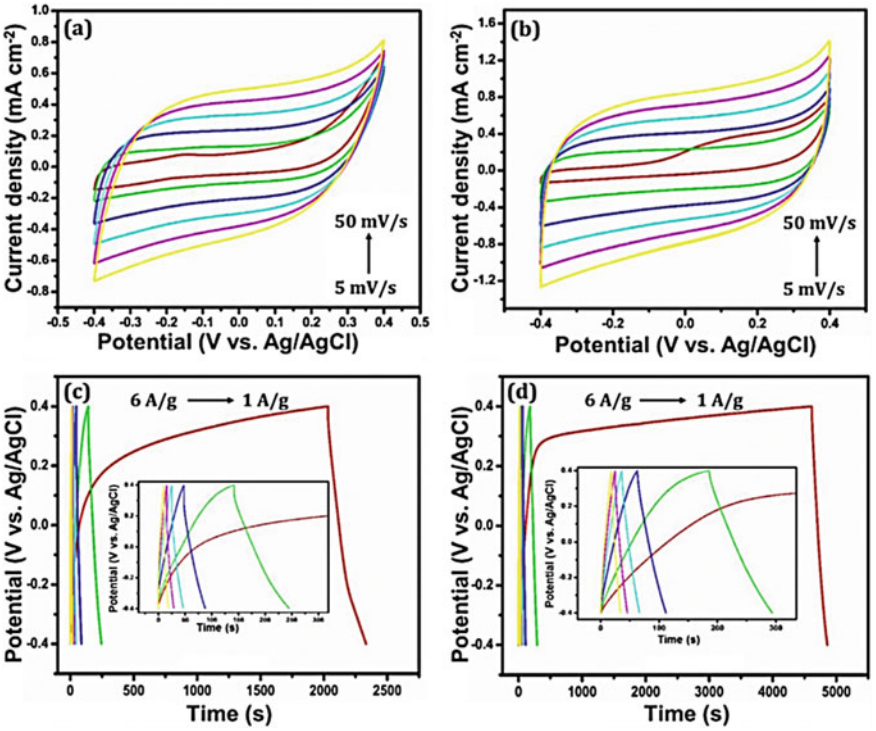

Fig. 9 The CV and GCD profiles of MoSSe and MoSSe/rGO [46]. Adapted from an open article is available under the Creative Commons CC-BY-NC-ND license and permits non-commercial use of the work as published, without adaptation or alteration provided the work is fully attributed

to facilitate the charge transfer and redox reaction resulting in increased contact of electrolyte ions during the charge–discharge process [46].

Two-dimensional TMCs have gained attention for energy storage devices due to their physicochemical properties and strong theoretical ability. And their excellent mechanical performance, electrical conductivity, and thermal stability than metal oxides make them a promising aspirant for HIC anode. Nitrogen-doped MoSe/graphene composites with good pseudocapacitive behavior were designed [47]. Diatomite templates were joint with sodium molybdate, Se powder, and graphene oxide and treated in hydrothermal. The SEM and TEM images depict that the resultant diatomic derived nitrogen-doped MoSe/G is a 3D biomorphic formed with voids and porous structure. Further, it was employed as the anode material for potassium ion-based hybrid capacitor in conjunction with carbon black as the cathode. The distinctive hierarchical 3D nanostructure tends to enhance the electrode/electrolyte interfacial connectivity, fast electron/ion transport, and improved surface area, resultant in an obvious pseudo-capacitance with a high energy density of 119 Wh kg^{-1} and a high power density of 7212 W kg^{-1} along with a period of 3000 cycles. Ge J demonstrated ED-MoS_2@CT hybrids where MoS_2 nanosheets are

anchored on hollow tubular carbon. The interlayer spacing of MoS_2 is controlled by the intercalation of dopamine (DA) and ethylene glycol (EG) in a step-by-step manner [35]. The unique morphology of MoS_2@CT with broad layer spacing efficiently improves the mechanical strain and provides a large area for fast ion/electron diffusion and transition. N_C doped $FeSe_2$ formed by the assembly of micro rods into the hierarchical 3D structure over a diameter of about 100 nm. N–C/$FeSe_2$ enhances the electron conductivity by providing high active sites, minimizing the electron transport path, and lowering the volume expansion [48]. This 3D structure attained an energy density of 230 W hKg^{-1}, a higher strength density of 920 W kg^{-1}, and superior cycling endurance over 1100 cycles at 500 mA g^{-1}.

6 TMCs for Hybrid Ion Capacitors

Advancing technology of Hybrid ion capacitors (HICs) is in haste generating immense energy densities at high rates throughout a long period by integrating both batteries and supercapacitors' premier features. By the mass of the active materials, HICs could stream energy within 60 and 200 Wh kg^{-1} which are higher than that of traditional supercapacitors, and consider their strength varies from 200 to 20,000 W kg^{-1} superior in relative to batteries. Potassium ion (K^+) storage devices are receiving momentum in the commercialization of renewable energy storage systems as potassium (K) is abundant in Earth's crust and also belongs to a similar group to that of Li exhibiting related physicochemical assets [49]. Furthermore, these storage devices have higher ionic conductivity and, a more operating voltage in electrolytes in contrast to sodium ion (Na^+) storage devices that is the redox pair of K/K^+ has a higher potential of 2.93 V in comparison with Na/Na^+ (2.71 V) and alike to Li/Li^+ (3.3 V), preserving the efficient viability of high energy density. Altogether designing both high-energy anode and cathode electrode materials with stable structure and better energy values for fascinating performance is an exceptional challenge [50].

7 Strategies to Increase the Performance of the TMCs-Based Supercapacitor

Layered TMCs-based nanostructures with semiconducting and metallic states have caught researchers' curiosity for application in supercapacitors. The inter-sheet and intra-sheet double-layers over individual TMCs sheets enable layered TMCs nanomaterials to store charges due to their sheet-like morphology and high specific surface area. Furthermore, the varied oxidation states of transition metal atoms, such as + 2 to + 6 of Mo atoms in MoS_2, permit layered TMCs nanomaterials to store energy via Faradaic charge transport processes. However, the poor electrical conductivity and semi-insulating nature of TMCs diminish the cycling stability of supercapacitors.

The feasible ways to improve its specific capacitance, TMCs are entrenched with carbonaceous materials and the modification of its electronic structure. So that, the metallic 1_T MoS_2 electrode exhibits higher pseudo-capacitive behavior in aqueous H_2SO_4, Li_2SO_4, Na_2SO_4, and K_2SO_4 electrolytes, suggesting that it may electrochemically intercalate ions such as H^+, Li^+, K^+, and Na^+ with great efficiency [51]. Carbon materials, including graphene, carbon nanotubes (CNTs), carbon nanofibers (CNFs), and activated carbon are ideal supplements for loading $MoSe_2$ to strengthen its electro-catalytic activity due to its specific physicochemical characteristics and excellent conductivity. Energy storage devices, as an essential part of this wearable system, should be smaller, more flexible, and portable without losing energy storage capacity. Because of their excellent temperature and corrosion resistance, carbon fibers are frequently utilized in flexible electronic devices. With the concession of mechanical flexibility, and the fabric structure can lower the current density of the electrodes. Cotton fabric, on the other hand, offers exceptional benefits such as elasticity, corrosion resistance, lightweight, cheap cost, and seamless integration into clothes, but its weak conductivity severely limits its employment as a conductive collector. In this case, a flexible conductive collector with excellent conductivity may be produced by electroplating a conductive metal layer, such as a nickel layer with good corrosion resistance, on its surface. So that, a group developed Ni-Co selenide nanostructure grown nickel-plated cotton cloth as cathode and it provides the higher specific capacity of 1333 Cg^{-1} at 1.2 Ag^{-1}. Herewith, Ni-Co selenide nanostructures electrode offers more active sites, higher surface area, and higher electrical conductivity [52].

8 Summary and Future Perspectives

Transition metal chalcogenides have been extensively considered due to their outstanding assets for numerous applications such as energy storage systems and energy conversion. TMCs demonstrated exceptional achievement in the synthesis and fabrication of supercapacitors. However, the pursuit of high quality in mass synthesis continues to be a challenge. Despite their high specific capacitance, pseudocapacitors' low conductivity and reduced cycling stability destined their real-world use of energy storage devices. Most studies only focus on making different nanostructures for TMCs, with little attention paid to refining the entire production method of the supercapacitor device. Boosting the engineering process and lowering production costs are also essential for achieving extensive construction for industrial claims, and scheming yields based on market requests can more efficiently stimulate the practical development of supercapacitors. Temporarily, a thorough appreciative relationship between the performance of these TMDs for supercapacitors should be established. The improvement of theoretical and mathematical modeling is also greatly expected to study the complete energy storage mechanism and the rational scheme of electrode materials, leading to the determined design of simple, low-cost, large-scale research of TMCs with excellent electrochemical performance. It is essential to investigate

non-aqueous electrolytes to obtain higher energy/power density, which will overlay the way for the practical manufacture of supercapacitors. To completely maximize the potential of TMCs -based electrode materials for supercapacitors, both synthesis parameters, and material properties must be adjusted. In the future, the production factors of electrodes, such as current collectors, electrolytes, and packaging, will require a deeper study from fundamental research. Overall, with prolonged and devoted research efforts, these attractive TMCs nanomaterials will provide a new way for commercializing the appealing electrochemical supercapacitors.

References

1. M. Chhowalla, Z. Liu, H. Zhang, Two-dimensional transition metal dichalcogenide (TMD) nanosheets. Chem. Soc. Rev. **44**, 2584–2586 (2015)
2. J. Zhou, Y. Liu, S. Zhang, T. Zhou, Z. Guo, Metal cha lcogenides for potassium storage. InfoMat **2**, 437–465 (2020)
3. M. Sajjad, F. Cheng, W. Lu, Research progress in transition metal chalcogenide based anodes for K-ion hybrid capacitor applications: a mini-review. RSC Adv. **11**, 25450–25460 (2021)
4. Z. Hai, S. Zhuiykov, Functionalizing new intercalation chemistry for sub-nanometer-scaled interlayer engineering of 2D transition metal oxides and chalcogenides. Adv. Mater. Interfaces **5**, 1–17 (2018)
5. Y. Zhao, L. Xu, J. Yan, W. Yan, C. Wu, J. Lian, Y. Huang, J. Bao, J. Qiu, L. Xu, Y. Xu, Facile preparation of $NiFe_2O_4/MoS_2$ composite material with synergistic effect for high performance supercapacitor. J. Alloys Compd. **726**, 608–617 (2017)
6. G. Tong, J. Guan, Q. Zhang, In situ generated gas bubble-directed self-assembly: synthesis, and peculiar magnetic and electrochemical properties of vertically aligned arrays of high-density Co3O4 nanotubes. Adv. Funct. Mater. **23**, 2406–2414 (2013)
7. N.M. Park, T.S. Kim, S.J. Park, Band gap engineering of amorphous silicon quantum dots for light-emitting diodes. Appl. Phys. Lett. **78**, 2575–2577 (2001)
8. J. Zheng K. Cheng, R. Zhang, Y. Yang, Y. Wu, P. Yu, Si quantum dots assist synthesized microflower-like Si/MoS_2 composites for supercapacitors. Curr. Comput.-Aided Drug Des. **10**, 1–11 (2020)
9. H. Huo, Y. Zhao, C. Xu, 3D Ni3S2 nanosheet arrays supported on Ni foam for high-performance supercapacitor and non-enzymatic glucose detection. J. Mater. Chem. A **2**, 15111–15117 (2014)
10. R. Pothu, R Bolagam, Q.H. Wang, W. Ni, J.F. Cai, X.X. Peng, Y.Z. Feng, J.M. Ma, Nickel sulfide-based energy storage materials for high-performance electrochemical capacitors. Rare Met. **40**, 353–373 (2021)
11. J. Lin, X. Zheng, Y. Wang, H. Liang, H. Jia, S. Chen, J. Qi, J. Cao, W. Fei, J. Feng, Rational construction of core-shell Ni3S2@Ni(OH)2 nanostructures as battery-like electrodes for supercapacitors. Inorg. Chem. Front. **5**, 1985–1991 (2018)
12. H. Wang, M. Liang, D. Duan, W. Shi, Y. Song, Z. Sun, Rose-like Ni_3S_4 as battery-type electrode for hybrid supercapacitor with excellent charge storage performance. Chem. Eng. J. **350**, 523–533 (2018)
13. J. Wen, S. Li, T. Chen, Y. Yue, N. Liu, Y. Gao, B. Li, Z. Song, L. Xiong, Z. Chen, Y. Guo, Three-dimensional hierarchical NiCo hydroxide@Ni_3S_2 nanorod hybrid structure as high performance positive material for asymmetric supercapacitor. Electrochim. Acta **222**, 965–975 (2016)
14. X. Liu, Q. Li, X. Zhang, Y. Jiang, Hybrid structured $CoNi_2S_4/Ni_3>S_2$ nanowires with multifunctional performance for hybrid capacitor electrodes and overall water splitting. RSC Adv. **10**, 33428–33435 (2020)

15. J. Theerthagiri, K. Karuppasamy, G. Durai, H. Sarwar, K. Sangeetha, Recent advances in metal chalcogenides (MX; X = S, Se) nanostructures for electrochemical supercapacitor applications : a brief review. Nanomater. **8**(4), E256 (2018)
16. M.R. Gao, Y.F. Xu, J. Jiang, S.H. Yu, Nanostructured metal chalcogenides: synthesis, modification, and applications in energy conversion and storage devices. Chem. Soc. Rev. **42**, 2986–3017 (2013)
17. Y. Zhang, Q. Zhou, J. Zhu, Q. Yan, S.X. Dou, W. Sun, Nanostructured metal chalcogenides for energy storage and electrocatalysis. Adv. Funct. Mater. **27**, 1–34 (2017)
18. Y.P. Gao, X. Wu, K.J. Huang, L.L. Xing, Y.Y. Zhang, L. Liu, Two-dimensional transition metal diseleniums for energy storage application: a review of recent developments. Cryst. Eng. Comm. **19**, 404–418 (2017)
19. Y. Gu, W. Du, Y. Darrat, M. Saleh, Y. Huang, Z. Zhang, S. Wei, In situ growth of novel nickel diselenide nanoarrays with high specific capacity as the electrode material of flexible hybrid supercapacitors. Appl. Nanosci. **10**, 1591–1601 (2020)
20. M. Sajjad , M. Amin, M.S. Javed, M. Imran, W. Hu, Z. Mao, W. Lu, Recent trends in transition metal diselenides (XSe2: X = Ni, Mn, Co) and their composites for high energy faradic supercapacitors. J. Energy Storage **43**, 103176 (2021)
21. M. Muska, J. Yang, Y. Sun, J. Wang, Y. Wang, Q. Yang, CoSe2 nanoparticles dispersed in WSe2 nanosheets for efficient electrocatalysis and supercapacitance applications. ACS Appl. Nano Mater. **4**, 5796–5807 (2021)
22. M.S. Vidhya, R. Yuvakkumar, G. Ravi, B. Saravanakumar, D. Velauthapillai, Asymmetric polyhedron structured $NiSe_2$@$MoSe_2$ device for use as a supercapacitor. Nanoscale Adv. **3**, 4207–4215 (2021)
23. M. Sakthivel, S. Ramaraj, S.M. Chen, K.C. Ho, Bimetallic vanadium cobalt diselenide nanosheets with additional active sites for excellent asymmetric pseudocapacitive performance: comparing the electrochemical performances with M–CoSe 2 (M= Zn, Mn, and Cu). J. Mater. Chem. A. **7**(20), 12565–12581 (2019)
24. J. Su, K. Liu, F. Wang, B. Jin, Y. Guo, G. Liu, H. Li, T. Zhai, Van der Waals 2D transition metal tellurides. **1900741**, 1–17 (2019)
25. M. Manikandan, K. Subramani, M. Sathish, S. Dhanuskodi, Hydrothermal synthesis of cobalt telluride nanorods for a high performance hybrid asymmetric supercapacitor. RSC Adv. **10**, 13632–13641 (2020)
26. S. Sarwar, Z. Liu, J. Li, Y. Wang, R. Wang, X. Zhang, High performance hybrid-capacitor based on $MoTe_2$/graphene through ultra-fast, facile microwave-initiated synthesis. J. Alloys Compd. **846**, 155886 (2020)
27. T. Kshetri, T.I. Singh, Y.S. Lee, D.D. Khumujam, N.H. Kim, J.H. Lee, Metal organic framework-derived cobalt telluride-carbon porous structured composites for high-performance supercapacitor. Compos. Part B Eng. **211**, 108624 (2021)
28. S. Zhang, D. Yang, M. Zhang, Y. Liu, T. Xu, J. Yang, Z.Z. Yu, Synthesis of novel bimetallic nickel cobalt telluride nanotubes on nickel foam for high-performance hybrid supercapacitors. Inorg. Chem. Front. **7**, 477–486 (2020)
29. N. Jayababu, S. Jo, Y. Kim, D. Kim, Novel conductive ag-decorated NiFe mixed metal telluride hierarchical nanorods for high-performance hybrid supercapacitors. ACS Appl. Mater. Interfaces **13**, 19938–19949 (2021)
30. F. Nur, I. Sari, J. Ting, Direct growth of MoS_2 nanowalls on carbon nanofibers for use in supercapacitor. Sci. Rep. **7**, 1–14 (2017)
31. M. Lu, M. Sun, X. Guan, G. Wang, Graphene for efficient supercapacitor electrodes **I7**, 11786–11792 (2021)
32. Y. Li, L. Xu, M. Jia, L.L. Cui, J. Gao, X.J. Zin, Hydrothermal synthesis and characterization of litchi-like $NiCo_2Se_4$ @carbon microspheres for asymmetric supercapacitors with high energy density. J. Electrochem. Soc. **165**, E303–E310 (2018)
33. S.K. Balasingam, J.S. Lee, Y. Jun, Molybdenum diselenide/reduced graphene oxide based hybrid nanosheets for supercapacitor applications. Dalt. Trans. **45**, 9646–9653 (2016)

34. C. Kanade, S. Arbuj, K. Kanade, K.S. Kim, G.Y. Yeom, B. Kale, Hierarchical nanostructures of nitrogen-doped molybdenum sulphide for supercapacitors. RSC Adv. **8**, 39749–39755 (2018)
35. A. Rajapriya, S. Keerthana, C. Viswanathan, N. Ponpandian, Direct growth of MoS_2 hierarchical nanoflowers on electrospun carbon nanofibers as an electrode material for high-performance supercapacitors. J. Alloys Compd. **859**, 1–8 (2021)
36. H. Gu, Y. Huang, L. Zuo, W. Fan, T. Liu, Graphene sheets wrapped carbon nanofibers as a highly conductive three-dimensional framework for perpendicularly anchoring of MoS_2: advanced electrocatalysts for hydrogen evolution reaction. Electrochim. Acta **219**, 604–613 (2016)
37. B. Guan, Y. Li, B. Yin, K. Liu, D. Wang, H. Zhang, C.Cheng, Synthesis of hierarchical NiS microflowers for high performance asymmetric supercapacitor. Chem. Eng. J. **308**, 1165–1173 (2017)
38. S. Liu, S.C. Jun, Hierarchical manganese cobalt sulfide core–shell nanostructures for high-performance asymmetric supercapacitors. J. Power Sources **342**, 629–637 (2017)
39. S. Goli Nagaraju, V. Chandra Sekhar, N. Himanaboina Ramulu, High-performance hybrid supercapacitors based on MOF-derived hollow ternary chalcogenides. Energy Storage Mater. **35**, 750–760 (2021)
40. J. Lu, L. Pu, W. Wang, Y. Dai, Journal of colloid and interface science construction of hierarchical cobalt-molybdenum selenide hollow nanospheres architectures for high performance battery-supercapacitor hybrid devices. J. Colloid Interface Sci. **563**, 435–446 (2020)
41. P. Pazhamalai, K. Krishnamoorthy, S. Sahoo, S.J. Kim, Two-dimensional molybdenum diselenide nanosheets as a novel electrode material for symmetric supercapacitors using organic electrolyte. Electrochim. Acta **295**, 591–598 (2019)
42. Y. Hu, C. Huang, S. Jiang, Y. Qin, H.C. Chen, Journal of colloid and interface science hierarchical nickel-cobalt selenide nanoparticles/nanosheets as advanced electroactive battery materials for hybrid supercapacitors. J. Colloid Interface Sci. **558**, 291–300 (2020)
43. L. Cheng, S. Chen, Q. Zhang, Y. Li, C. Y. bing, Hierarchical sea-urchin-like bimetallic zinc—cobalt selenide for enhanced battery-supercapacitor hybrid device. J. Energy Storage **31**, 101663 (2020)
44. L.P. Lv, C. Zhi, Y. Gao, X. Yin, Y. Hu, D. Crespy, Y. Wang, Hierarchical "tube-on-fiber" carbon/mixed-metal selenide nanostructures for high-performance hybrid supercapacitors **45**, 13996–14009 (2019)
45. C. Miao, P. Xu, J. Zhao, K. Zhu, K.Cheng, K. Ye, J. Yan, D. Cao, G. Wang, X. Zhang, Binder-free hierarchical urchin-like manganese—cobalt selenide with high electrochemical energy storage performance (2019)
46. A. Gowrisankar, A.L. Sherryn, T. Selvaraju, Applied Surface Science Advances In situ integrated 2D reduced graphene oxide nanosheets with MoSSe for hydrogen evolution reaction and supercapacitor application. Appl. Surf. Sci. Adv. **3**, 100054 (2021)
47. Y. Yi, Z. Sun, C. Li, Z. Tian, C. Lu,Y. Shao, J. Li, J. Sun, Z. Liu, Designing 3D biomorphic nitrogen-doped $MoSe_2$/Graphene composites toward high-performance potassium-ion capacitors. Adv. Funct. Mater. **30**, 1–10 (2020)
48. J. Ge, B. Wang, J. Wang, Q. Zhang, B. Lu, Nature of $FeSe_2$/N-C anode for high performance potassium ion hybrid capacitor. Adv. Energy Mater. **10**, 1–9 (2020)
49. A. Eftekhari, Z. Jian, X. Ji, Potassium secondary batteries. ACS Appl. Mater. Interfaces **9**, 4404–4419 (2017)
50. X. Wu, D.P. Leonard, X. Ji, Emerging non-aqueous potassium-ion batteries: challenges and opportunities. Chem. Mater. **29**, 5031–5042 (2017)
51. Q. Yun, L. Li, Z. Hu, Q. Lu, B. Chen, H. Zhang, Layered transition metal dichalcogenide-based nanomaterials for electrochemical energy storage. Adv. Mater. **32**, 1–29 (2020)
52. C. Wang, Z. Song, H. Wan, X. Chen, Q. Tan, Y. Gan, P. Liang, J. Zhang, H. Wang, Y. Wang, X. Peng, Ni-Co selenide nanowires supported on conductive wearable textile as cathode for flexible battery-supercapacitor hybrid devices. Chem. Eng. J. **400**, 125955 (2021)

Chalcogenides and Phosphides for High-Performance Supercapacitors

Emad S. Goda, Ahmed Al-Shahat Eissa, Bidhan Pandit, and Mahmoud H. Abu Elella

Abstract Recently, extraordinary attention has been directed to transition metal derivatives, especially, transition metal chalcogenides (sulfides and selenides) and phosphides in the energy storage devices field as supercapacitor electrodes. Because of their outstanding features such as excellent conductivity, low cost, high surface area, and their metalloid electrochemical features. This chapter aimed to show recent researches that have been done on the usage of both chalcogenides and phosphides for designing the supercapacitors electrodes, illustrating their preparation approaches. Furthermore, we illustrated several approaches for fabricating the chalcogenides and phosphides which can adjust their thickness and size diameter. Additionally, it exhibits different routes for improving their drawbacks to achieve good cycle life, energy/power densities, and retention rate, which increased the number of global scientific researchers to apply them as supercapacitors.

Keywords Chalcogenides · Phosphides · Energy storage devices · Supercapacitor

E. S. Goda (✉)
Organic Nanomaterials Lab, Department of Chemistry, Hannam University, Daejeon 34054, Republic of Korea
e-mail: emadzidan630@gmail.com

Fire Protection Laboratory, National Institute of Standards, 136, Giza 12211, Egypt

A. A.-S. Eissa
Graduate School of Energy Science and Technology, Chungnam National University, 99 Daehak-ro, Yuseong-gu, Daejeon 34134, Republic of Korea

Department of Chemistry, School of Science, South Valley University, Qena 83523, Egypt

B. Pandit
Department of Materials Science and Engineering and Chemical Engineering, Universidad Carlos III de Madrid, Avenida de la Universidad 30, 28911 Leganés, Madrid, Spain

M. H. Abu Elella (✉)
Chemistry Department, Faculty of Science, Cairo University, Giza 12613, Egypt
e-mail: mahmoudhussien3766@yahoo.com

S. Thomas et al. (eds.), *Nanostructured Materials for Supercapacitors*,
Advances in Material Research and Technology,
https://doi.org/10.1007/978-3-030-99302-3_19

1 Introduction

Energy is considered the bottleneck for all advanced technologies playing a vital role in our current life. Meanwhile, the continuous exhaustion of fossil fuels releases various environmental dilemmas and can endanger sustainability in world development [1, 2]. To overcome these aspects, there is an urgent need for developing green energy technologies like tidal, wind, solar energies [3]. However, these renewal energy techniques still need help from the energy storage systems. Energy storage devices such as supercapacitors (SCs) and rechargeable batteries are extensively applied in smart grids, electronics, and running electric vehicles [4]. The batteries usually offer high energy density over the supercapacitors because they are carried out through faradic interactions between electrodes leading to high capacity capability, and enlarged potential windows as shown in Fig. 1. Nevertheless, those materials have lower power density due to the limited kinetics of mass diffusion. Comparably, the traditional dielectric capacitors store the electrical energy by the mechanism of fast separation and recombination of charge on the interface between the metal-based electrodes and dielectric materials showing higher power densities. Therefore, SCs can connect the gab presented between these capacitors and batteries by the discovery of new materials that can be used as electrodes with outstanding electrochemical properties [5].

SCs can be grouped into three types; pseudo-capacitors, electric double-layer capacitors (EDLCs), and hybrid supercapacitors (HSCs) based on the mechanism applied for storing the energy [6, 7]. Interestingly, the various mechanisms of energy storage, their related materials, and cyclic voltammetry are depicted in Fig. 2. Firstly, EDLCs materials are worked by adsorbing and desorbing the ions physically at the interfaces that existed between electrolyte and electrodes without any redox reactions giving a fast discharge process and ultrahigh power density. EDLCs have a rectangular CV curve and the capacitance can be estimated based on the following equation.

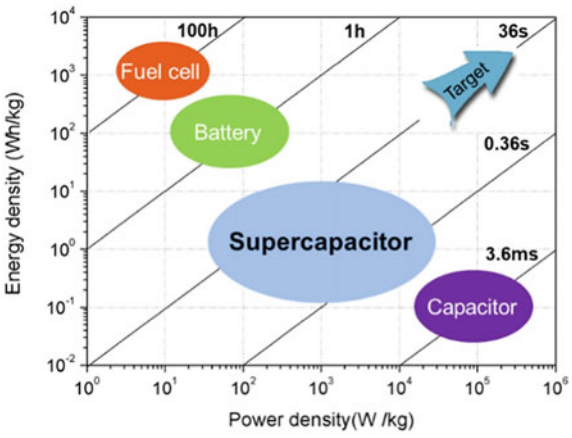

Fig. 1 Ragone plot for the widely used energy storage devices. Adapted with permission from Ref. [5], Copyright (2021), Elsevier

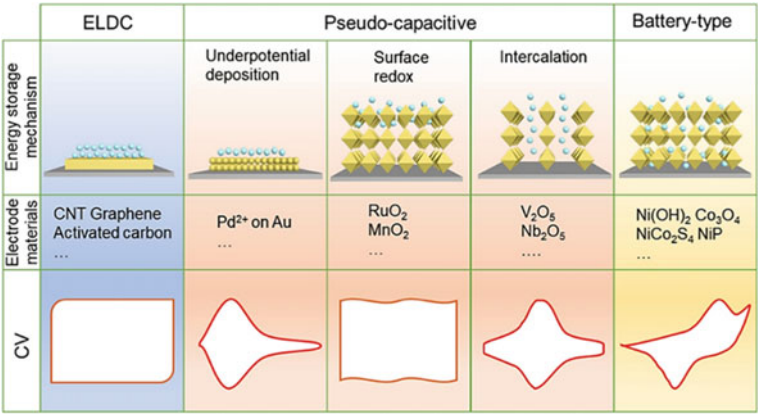

Fig. 2 Schematic representation for the mechanisms of energy storage, and their related materials, and CV patterns. Adapted with permission from Ref. [5], Copyright (2021), Elsevier

$$C = \frac{\mathcal{E}_r \mathcal{E}_o A}{d} \tag{1}$$

where the dielectric constants of electrolyte, and vacuum are represented by $\mathcal{E}_r$, $\mathcal{E}_o$, respectively. While d is the distance of charge separation, and A is the area [8].

The surface features and surface areas could affect the electronic properties of EDLCs electrodes. While pseudo-capacitors are worked by prompt and reversible redox reactions that occurred nearby or on the electrode surface yielding higher energy density and capacitance values when compared with traditional EDLCs. These materials are typically categorized into three kinds depending on the redox behavior including *underpotential deposition*, surface redox, and *intercalation* pseudo-capacitances. Underpotential deposition phenomenon is usually performed due to the *electrodeposition* of metal ions by adjusting a voltage that is lower than its redox value as a result of the sturdy binding that can happen between the substrate and metal such as Pd^{2+} on Au. The operating potential is very narrow because the potential value should be lower than that required for the redox reaction of metal cations. In the surface pseudocapacitors, the storage of energy is carried out via a redox reaction that happened on the surface of the electrode such as MnO_2, PPy, and RuO_2. In general, these active materials have characteristic rectangular CV curves that are the same as EDLCs. Whereas the intercalation pseudocapacitors are usually run when the electrolyte ions are reversibly inserted and extracted into electrode structure without performing any phase changes such as Nb_2O_5, and V_2O_5. The CV of former materials appeared with clear faradic peaks, however, the capacitive reactions are largely driving the kinetics of the whole process [5].

Transition metal phosphides (TMPs) involve the integration of transition metals with phosphorus in material with outstanding conductivity, metalloid electrochemical features [5]. In comparison, TMPs manifest higher specific capacity and rate capability than TMOs because phosphorous has a lower electronegativity than oxygen

leading to improved physicochemical features [9]. Additionally, transition metal chalcogenides (TMCs, MX, X = S, Se) have been widely utilized as SCs electrodes and are also known to exhibit higher electronic properties compared to TMOs. In this chapter, the recent advances in the utilization of chalcogenides and metal phosphides as supercapacitor electrodes. Also, an overview was extensively introduced for their synthesis methods. The structural properties were also related to the electrochemical properties for understanding the whole performance of their electrodes.

2 Synthesis of Transition Metal Chalcogenides

The capability to adjust the thickness and size diameter of transition metal chalcogenides allows recognizing new phenomena related to their characteristics. Moreover, expanding the scope of the practical applicability of the TMCs can be achieved by modulating their properties through synthetic strategies. There are several approaches for fabricating the TMCs which will be discussed in the following sections:

2.1 Sonication Based Exfoliation Approach

Liquid-phase exfoliation (LPE) is a straightforward approach that includes the sonication of layered bulks in organic solvents. The factors for adjusting the characteristics of the product are selecting the solvent, sonication time/power, and centrifugation circumstances [10]. In the LPE, the ultrasonication produces jet cavitation which works on large blocks to stimulate breaking down into small sheets, and hence achieving the proper exfoliation [11]. Choosing the convenient dispersant is considered fundamentally for decreasing the potential energy found between the neighboring layers [12]. The sonication power/time and initial mass were altered to realize their influence on the yield [13].

2.2 Size Sorting of As-Exfoliated Nanosheets

Size sorting is a compulsory precondition designated for all practical applications of the TMCs because their physicochemical properties rely on their size confinement effect. The techniques of sedimentation separation and density-gradient ultracentrifugation are being used for sorting the exfoliated TMCs flakes [14]. In the sedimentation-based separation strategy, the specific components are isolated based on their shape, size, and density that are yielded from a heterogeneous mixture. Particles of diverse sizes reveal different rates of sedimentation operated at various

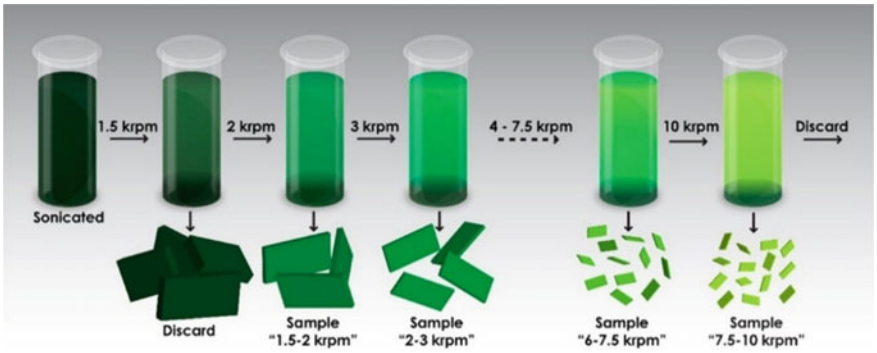

Fig. 3 Scheme demonstrating the cascade centrifugation approach. Size selectivity is achieved by the removal of sediments by increasing the centrifugation rates. Adapted with permission from Ref. [15], Copyright (2016), American Chemical Society

speeds of centrifugation, where the weighty large nanoflakes are precipitated under-doing centrifugation, meanwhile the small ultrathin ones which possess light weights remain to disperse in the solution. For example, the size selection of a monolayer-enriched solution was obtained by performing the repetitive cycles of centrifugation and discarding (Fig. 3) [15].

2.3 Intercalation of Alkali Metals and Gaseous Molecules for Exfoliation

The yield and monodispersity have been improved by modifying the intercalation approaches and chemical reagents. An efficient alternative method to overcome the significant thermodynamic energy barrier for carrying out the intercalation of Li^{2+} is the solvothermal reaction-based intercalation of *n*-BuLi at 100 °C. For example, the lithiation of Li_xTaS_2 at 0.55 was observed to be ideal for setting the manual shaking exfoliation into submillimeter-sized TaS_2 monolayers within small periods [16]. The intercalation of the TMCs could also be achieved electrochemically [17] by utilizing Li as the anode and the bulk TMC as the cathode (Fig. 4). By employing this route, large-scale manufacture of single-layer TMC nanosheets has been accomplished in different chemical compositions of WS_2, TaS_2, MoS_2, and TiS_2. Controlling the exfoliation of the TMCs to give trilayered nanosheets was characterized through the stoichiometric interaction of *n*-BuLi and MoS_2 for undergoing the exfoliation in a mixture of 45% (v/v) of ethanol/water solution [18].

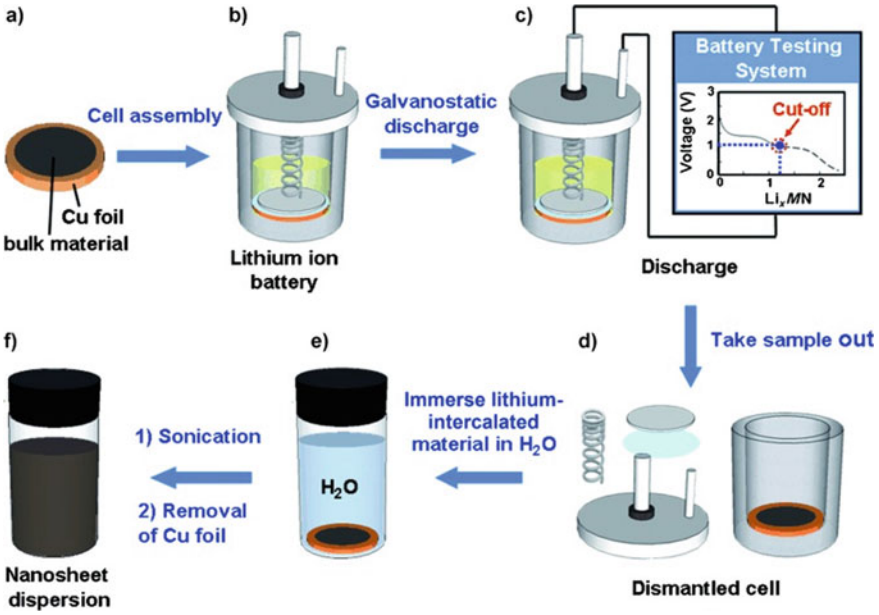

Fig. 4 Lithium intercalation process electrochemically to the transformation of layered and bulky materials into 2D nanosheets from layered bulk material. Adapted with permission from Ref. [14], Copyright (2017), American Chemical Society

2.4 Hot Injection Strategy

This method is among the most discernible synthetic strategies for fabricating single-crystal and adjusting the shape of nanocrystals, where an anionic precursor is usually added to a hot mixture containing the capped surfactants with the metal precursors. Controlling the reaction factors such as molar ratio, time, temperature, and surfactants, as well as selecting the convenient precursor is important for the successful fabrication of 2D layered TMCs. For example, metal-acetylacetonate, -carbonyl, -chloride, and -carboxylate precursors were used as efficient metal precursors [19, 20].

2.5 One-Pot Heat-Up Strategy

In this technique, all precursors are initially agitated below 120 °C, then thermally heated to enhance the chemical reactions and growth of nanosheets. This synthetic approach has been utilized for fabricating all members of group IV, V, and VI 2D TMCs [21], where metal chlorides and elemental S and Se powder chalcogen precursors are used. TiS_2 nanosheets with a dimension of about 500 nm and thickness of

about 5 nm have been fabricated by injecting $TiCl_4$ into a oleylamine containing S at 100 °C, then heating to 300 °C [22]. It has been reported that the usage of elemental S results in poor quality 2D layered TMC nanosheets compared to nanosheets produced using alternative chalcogen sources like CS_2 [23]. In contrary to the troubles related to the usage of elemental S, elemental Se could be used for synthesizing the metal selenides of groups IV and V [24].

2.6 Hydro/Solvothermal Strategy

Hydrothermal synthesis is a process in which the growth of the crystals happens in a sealed autoclave at high temperatures and pressures. The reaction parameters are the organic additives, pressure, pH, reducing agents, concentration, and reaction time. The hydrothermal process of 2D layered TMCs generated 3D radially oriented nanospheres and corrugated nanoflowers [25–28]. The hydrothermal strategy is appropriate to produce the TMCs of only group VI, where group IV and V would oxidize to metal oxides during the fabrication process.

3 Synthesis of Transition-Metal Phosphides

Transition-metal phosphides (TMPs) are a complex and several family (such as Ni_xP (x = 2–12), Fe_yP, W_dP and Co_zP (y, d and z = 1 and 2), InP, MoP, etc.) and have different properties [29]. TMPs can be prepared via different preparation methods including (a) metal-organic precursors decomposition method [30], (b) solvothermal/hydrothermal method [31, 32], (c) solid-state reaction method [33, 34], and gas–solid phase reaction [35, 36]. Metal-phosphide preparation methods play a vital role in distributing P inside the TMPs structure and their shaping, as well. Additionally, the various preparation conditions such as heating rate and preparation time affect their surface area and pore size [37].

3.1 Metal–Organic Precursors Decomposition

The decomposition of metal-organic precursors is one of the most popular approaches to prepare TMPs by using different metal sources (such as metal oxides, metal carbonyl, metal nanoparticles, and bulk metal precursors) and organic phosphorus sources such as tributylphosphine (TBP) and trioctylphosphine (TOP) while the letter one is widely used because it is happened under moderate temperatures and reduces the problems that presented in traditional phosphide preparation methods. Notably, TOP facilitates the phosphatization reaction thanks to its strong coordination effect and easy decomposition of its covalent C–P bond through 250–350 °C.

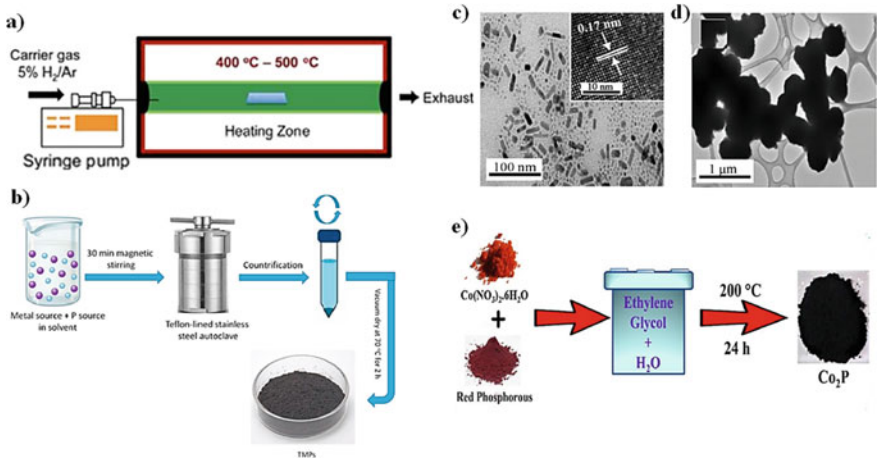

Fig. 5 Schematic illustrations for the preparation of TMPs by using **a** the decomposition of metal-organic precursors method. Adapted with permission from Ref. [30], Copyright (2016), American Chemical Society. **b** The solvothermal/hydrothermal process. Adapted with permission from Ref. [37], Copyright (2021), Elsevier. TEM images of **c** Fe_2P NPs include inserting an image for its high resolution and **d** FeP microspheres. Adapted with permission from Ref. [39], Copyright (2022), Elsevier. **e** Schematic diagram of the one-pot solvothermal preparation of Co_2P. Adapted with permission from Ref. [40], Copyright (2021), Elsevier

In this method, the organic phosphorus is mixed with a metal-organic precursor to produce an organometallic complex. After that, the organometallic complex exposes to thermal decomposition to fabricate TMPs [29, 37]. For example, Read et al. [30], reported the preparation of different TMPs by reacting various metal foils such as Co, Cu, Ni, Fe, and NiFe with TOP or TBP as organic phosphorus sources via metal-organic precursor decomposition method by using a syringe pump (Fig. 5a). In Fig. 5a, organic phosphorus source as vapor was inserted within a quartz tube which includes metal foils, and heated at a moderate temperature similar to the low boiling temperature of TOP and TBP as 291 and 240 °C, respectively. They showed that all products of TMPs were prepared in a highly pure form. However, the remaining TOP and TBP ligands in the device surface were removed with a 5% H_2/Ar heating process.

3.2 Solvothermal/Hydrothermal Method

Solvothermal and hydrothermal processes are widely applied for fabricating TMP nanoparticles according to the illustrated diagram in Fig. 5b. In the hydrothermal route, water can be used as the solvent medium, conversely, in the solvothermal approach, the organic solvents medium such as oleylamine and 1-octadecene can be applied. In Fig. 5b, generally, definite amounts of phosphorus sources (white or

red phosphorous) are mixed with metal sources by using either distilled water (for hydrothermal route) as a solvent or organic solvents as oleylamine, ethylenediamine, and 1-octadecene (for solvothermal route). After that, the above mixture is moved into a tightly sealed-stainless steel autoclave and conducted at different temperatures in the range of 120–350 °C and the reaction time. Subsequently, after finishing the reaction time, the autoclave is cooled and the as-obtained black precipitate product is washed by ethanol/water mixture. Finally, the final TMP product is dried under vacuum at 70 °C. Moreover, in this method, the crystallinity and morphology of TMPs nanoparticles can be controlled by different factors including tuning the growth/nucleation process at various temperatures, phosphorus sources/metal sources molar ratio, and incorporation of additional coordinating solvents [37, 38]. Chouki et al. [39], reported the preparation of iron phosphides (FeP and Fe_2P) via solvothermal route by the reaction of iron pentacarbonyl ($Fe(CO)_5$ with triphenylphosphine (TPP) precursor at elevated temperatures; 300 °C for Fe_2P and 350 °C for FeP. The TEM data for the as-prepared iron phosphides (Fig. 5c, d) showed that the presence of two different NPs morphology including nanospheres (less than 20 nm) and nanorods in the range of 15–40 nm. A facile one-pot solvothermal method to prepare cobalt phosphide (Co_2P) NP_S in the presence of cobalt nitrate hexahydrate, ethylene glycol (EG) and phosphorous source (red phosphorous) has been developed by Jebaslinhepzybai et al. [40] according to Fig. 5e. In this study, they used cobalt nitrate hexahydrate/red phosphorous molar ratio of 1:10 and then injected to autoclaved at 200 °C for 24 h to obtain Co_2P NPs.

3.3 Solid–Solid-State Reaction

The Solid–solid state reaction process is another approach to synthesize TMPs. In this method, the solid metal source including metal oxides, metal NPs, or metal hydroxide, is mixed with phosphorus sources such as ammonium phosphate, or red phosphorous under a thermal condition in the presence of inert gas or vacuum at various temperatures. Notably, metal sources and P sources are mixed with stoichiometric ratios. Subsequently, they are kept in an evacuated silica tube, and then heated up to high elevated temperatures for long time to obtain TMPs. On the other hand, various metal sources and temperature reactions fabricate diverse crystalline phases of TMPs with uniform size and shape distribution (Fig. 6a) [37]. For example, Li et al. [41] designed a series of Ni TMPs (Ni_xP_z) by solid-state reaction of Ni hydroxide and sodium ammonium phosphate with a stoichiometric ratio of 1:5 under inert argon gas. They found that Nickel hydroxide nanoplates converted to Ni_xP_z NPs after the solid phosphatization approach (Fig. 6b, c). Also, they studied the effect of temperature on the obtained controlled phases of TMPs, for instance, at 275 °C, a pure Ni_2P phase was prepared, while, both Ni_5P_4 and NiP_2 have been obtained at a higher temperature of 325 °C and 475 °C for the former and letter one, respectively.

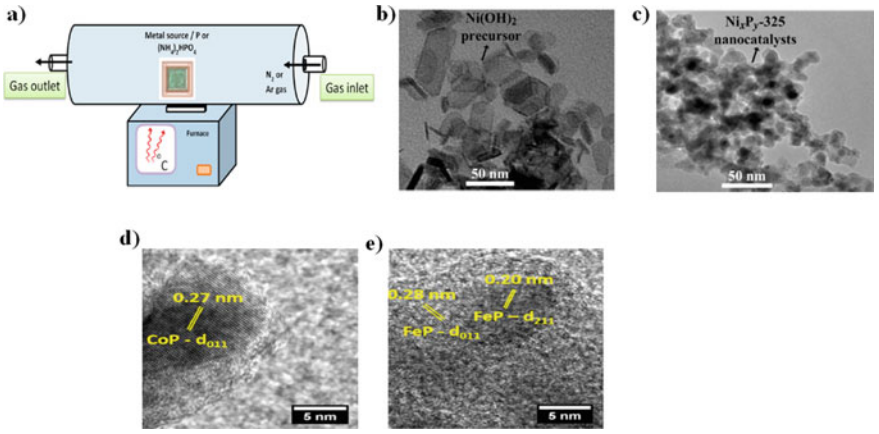

Fig. 6 **a** Schematic diagram of the solid–solid reaction process for preparation TMPs. Adapted with permission from Ref. [37], Copyright (2021), Elsevier. TEM image of **b** nickel hydroxide nanoplates and **c** Ni_xP_y NPs by solid–solid phase method at 325 °C. Adapted with permission from Ref. [41], Copyright (2016), American Chemical Society. TEM image of **d** CoP nanostructures and **e** FeP nanostructures, Adapted with permission from Ref. [42], Copyright (2021), Elsevier

3.4 Solid–Gas Phase Method

TMPs can be prepared by solid–gas phase reaction between PH_3 phosphorization gas and metal sources (including metal oxides, metal hydroxides, metal-organic framework, and bulk metals) at different temperatures. Phosphorization gas can be produced via thermal decomposition of its hypophosphites such as sodium and ammonium hypophosphites at 250 °C. The solid–gas phase method includes a surfactant-free method that maintains the dimensions and morphology of the precursor material. Conversely, direct reduction of metal orthophosphates via hydrogen gas at higher temperatures (above 650 °C) leads to preparing TMPs [29]. For instance, most recently, Murali et al. [42] have cited the conversion of metal oxalate to TMPs nanostructures via solid–vapor phase method using sodium hypophosphite and their application for rechargeable Li, Na, and K-ion batteries as an anode. Cobalt phosphide and iron phosphide have been prepared by reacting sodium hypophosphite with cobalt oxalate and iron oxalate under Ar/H_2 atmosphere. After that, the mixture was maintained in a single sealed tube at 400 °C for 2 h, and their TEM images are shown in Fig. 6d, e.

4 Metal Chalcogenides for Electrochemical SCs

The technically substantial and industrially scalable metal chalcogenides (MCs) have drawn great attention in the past couple of years because of their properties such as

tunable band-gap, unique morphology, environmental stability, low solubility in most electrolytes, anisotropic property, and easy availability of precursors [43]. Generally, MCs involve forming compounds from the binding of metal ions with elements such as S, Se, and Te [44]. These layered nanomaterials owe the formula of MX_2, where M is a transition element (Ni, Sc, Zr, Ti, Hf, Ta, Nb, Cr, V, W, Mo, Mn, Re, Tc, Fe, Co) and X can be any of the above-mentioned chalcogen atom [45]. Normally, the bandgap is almost zero for pristine graphene whereas the bandgap depends on the number of layers, elemental combination, and adopting atoms influence in transition MCs, coinciding the band gap values from 0 to 2 eV. So, various transition MC structures are tunable by adjusting bandgap, advantageous for industrial applications [46].

4.1 Transition Metal Sulfides

4.1.1 Cobalt Sulfides

Cobalt-based sulfides have received great attention because of salient features of associated metal sulfide materials. Chen et al. [47] synthesized Co_3S_4 nanosheet arrays on Ni-foam using simples anion exchange reaction route. When compared to Co_3O_4, Co_3S_4 electrode shows improved specific capacitance of 1081 F/g at 1.61 A g and areal capacitance of 1.81 F/cm^2 at 24 mA/cm^2. On the other hand, Wang et al. established 3D hierarchical $CoS_{1.097}$ via a simple solvothermal route. The electrode shows excellent specific capacitances of 464 and 555 F/g at 100 and 5 mA/cm^2, respectively [48]. The high-quality Co_9S_8 films have been coated on Ni foam by physical method (atomic layer deposition) and employed as SC electrode which possesses a high capacitance of 1645 F/g at 3 A/g [49] (Fig. 7).

4.1.2 Copper Sulfide

Copper sulfide is one of the earth-abundant compounds which can be easily employed for supercapacitor applications. Peng et al. synthesized CuS with various morphologies by adopting the solvothermal method. The flower-like CuS structure with a high surface area shows excellent capacitance of 597 F/g with good cycling stability [50]. The CuS@PPy composite has also been prepared by an in situ oxidation polymerization method [51]. The morphology of the composite shows uniform spheres (average thickness 1 m) composed of intertwined sheet-like subunits, advantageous for excellent electrochemical activities. The electrode exhibits a high capacitance of 427 F/g at 1 A/g with 88% capacitive retention after 1000 cycles. The as-prepared CuS electrode exhibits a specific capacitance of 222 F/g and an excellent power density of 1.75 kW/kg in 1 M $LiClO_4$ electrolyte [52].

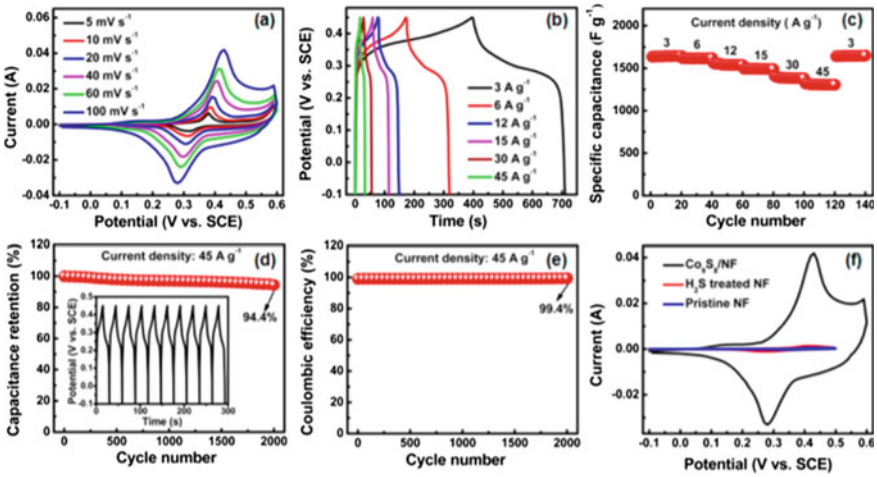

Fig. 7 **a**, **b**, **c** CV at various scan rates, GCD at different current densities, rate performance against the current density, cycle life at 45 A/g for 2000 cycles (inset shows the first GCD 10 cycles), **d** coulombic efficiency, and **f** comparable CV curves for the Co_9S_8/NF electrode, H_2S treated NF electrode and pristine NF electrode at a scan rate of 100 mV/s. Adapted with permission from Ref. [49], Copyright (2015), American Chemical Society

4.1.3 Nickel Sulfides

Nickel-based sulfides are the most reported metal sulfides due to their different phases and structures with excellent electrochemical. Among various nickel sulfides, the Ni_3S_2 structure displays an advanced energy storage performance because of its advantageous and versatile morphologies including easy, low cost, and remarkable capacitance properties. Krishnamoorthy et al. [53] prepared Ni_3S_2 on Ni foam by using a hydrothermal method to improve the electrochemical properties. The electrode offers a high capacitance of 1293 F/g at 5 mA/cm^2. Similarly, Wang et al. prepared 1D NiS nanorods electrode which exhibits a high capacitance of 1403.8 F/g at 1 A/g, resulting from large specific surface area and 1D charge transport pathways of NiS [54]. Similarly, successful SC performances of α-NiS and β-NiS were reported by Wei et al. via adopting the Kirkendall effect with various hydrothermal conditions [55].

4.2 Transition Metal Selenides and Tellurides

Though transition metal sulfides are more studied as compared to corresponding selenides and tellurides, there is considerable interest in these components nowadays. Wang et al. [56] prepared truncated cube-like single crystals of $NiSe_2$ by using a hydrothermal method. The electrode shows a high capacitance of 1044 F/g at 3 A/g

with an exceptional rate capability study. Furthermore, 2D $NiSe_2$ hexapod single crystals have been developed; the fabricated electrode delivers a high specific capacitance of 75 F/g at 1 mA/cm^2 with a capacitance retention rate of 94% after cycles [57]. The binder-free $CuSe_2$/Cu electrode prepared by the hydrothermal method shows a high capacitance of 1037.5 F/g at 0.25 mA/cm^2 [58]. Furthermore, copper selenide CuSe nanosheet with vertical orientation has been recently grown and it exhibited capacitance of 209 F/g when used for flexible solid-state SCs [59]. Balasingam et al. prepared layered structured $MoSe^2$ for the fabrication of two-electrode configuration by using H_2SO_4 electrolyte, in which the electrode shows capacitance of 199 F/g at 2 mV/s [60]. Xia et al. investigated that $(Ni, Co)_{0.85}$ Se electrode was capable to show a high areal capacitance of 2.33 F/cm^2 at 4 mA/cm^2 [61]. The as-prepared iron selenide electrode capacitance of 671.7 F/g at 2 mV/s with 91.9% capacitance retention at 4000 cycles [62]. The cerium selenide electrode was able to provide a capacitance of 285 F/g at 2 mA/cm^2 in a potential window of 0.9 V [63].

Recently, metal tellurides are also being reported for energy storage application by adopting their layered structures and unique morphologies [64]. For example, Sankapal and coworkers have reported vanadium telluride (VxTey) nanostructures onto multi-walled carbon nanotubes (MWCNTs) to fabricate a composite for supercapacitor application [65]. The V_xTe_y/MWCNTs electrode showed capacitance of 470 F/g with excellent capacitive retention up to 10,000 cycles. Zhou et al. adopted a hydrothermal route to prepare NiTe electrode which showed a specific capacitance of 804 F/g at 1 A/g in 3 M KOH electrolyte [66]. The nanostructured cobalt telluride was reported to deliver a capacity of 170 C/g at a current density of 0.5 A/g with exceptional cyclic stability [67]. The Sm_2Te_3 electrode prepared by the simple chemical bath deposition (CBD) method can deliver a high capacitance of 207 F/g including a good power density of 14.18 kW/kg [68]. Siddique et al. prepared a GaTe electrode which showed a moderate capacitance of 14 F/g with exceptional 96% charge retention after 10,000 cycles [69]. The synthesized 1 T′-$MoTe_2$ nanosheets prepared by Liu et al. can be used as an efficient electrode with capacitances of 714 F/g and 1393 F/g at current densities of 100 A/g and 100 A/g [70].

5 Transition Metal Phosphides for Electrochemical SCs

Recently, TMPs were widely used in the fields of metallurgy, photocatalytic degradation, and hydro-processing catalysts. TMPs have particularly received interest in establishing SCs, electrocatalysts, and lithium-ion batteries owing to their unexceptional physicochemical properties. Various metal phosphide systems such as FeP, CoP, and Ni_2P are being discovered for energy storage devices [71].

5.1 Nickel Phosphide

Since the introduction of nickel phosphide (Ni_2P) to the vapor phase catalysis done in 1950, it was used globally for more than half a century [72]. In particular, Ni_2P is considered a smart candidate for making new pseudocapacitors because of its natural abundance, higher theoretical capacitance, and inferior resistance. Many cathodes were fabricated based on nickel phosphide with different crystalline morphologies. For instance, Liu et al. [73] was efficiently fabricated nickel phosphide with different crystalline structures from honeycomb-like biphasic Ni_5P_4–Ni_2P (Ni_xP_y) nanosheets by applying hydrothermal followed by phosphorylation method as shown in Fig. 8. The hydrothermal method was used to obtain first, $Ni(OH)_2$ nanosheets on a substrate from nickel foam subsequent by phosphorylation process. During this step, the amount of phosphorous source was varied at 10, 20, and 30 mmol to give samples coded as Ni_xP_y-1, Ni_xP_y-2, Ni_xP_y-3, respectively.

As can be seen from SEM images in Fig. 9a, Ni_xP_y-1 was formed in nanosheets shape that is constructed by the interconnection of small nanoparticles of diameter 20 nm. TEM images in Fig. 9 further confirmed the existence of numerous interspaces with the size range of 10–30 nm beside the HR-TEM reveals that the material contains lattice fringes related to Ni_2P and Ni_5P_4. When the mass of the phosphorous source was increased, the material of Ni_xP_y-2 reveals rough sheets with more increased interspacing (Fig. 9b, e, h). The further increase of sodium hypophosphite causes the randomness of the interconnected nanoparticles and overcrowding the interspace between the nanoparticles that limits the movement of electrolyte ion accessibility results in depressed, electrochemical performance when used as supercapacitor electrode (Fig. 9c, f, i). Such mechanism was clearly explained by the authors as seen in Fig. 9j.

The authors found that the Ni_xP_y electrodes appeared with superior energy capacity compared to the precursor $Ni(OH)_2$ electrode where Ni_xP_y-2 electrode could specifically achieve a capacity of 1272 C/g more than Ni_xP_y-1 electrode (1009 C/g)

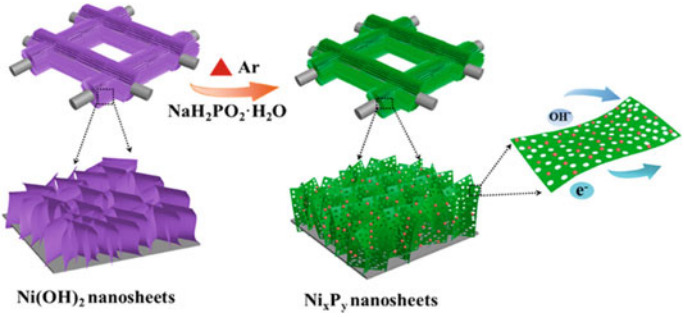

Fig. 8 **a** The preparation of Ni_xP_y nanosheets by the related two steps of hydrothermal precipitation and phosphorization. Adapted with permission from Ref. [73], Copyright (2017), American Chemical Society

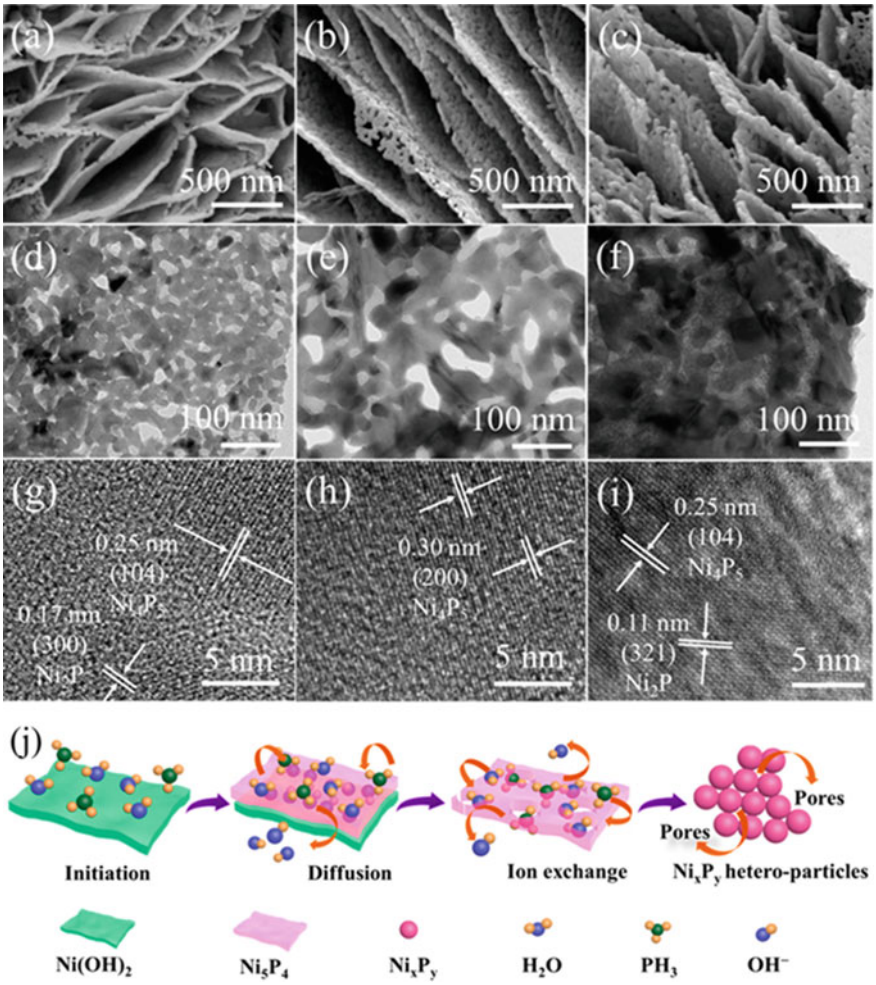

Fig. 9 SEM images of the Ni_xP_y prepared at a phosphorus source with the amounts of **a** 10 mmol, **b** 20 mmol, and **c** 30 mmol. TEM and HRTEM images of the **d**, **g** 10 mmol, **e**, **h** 20 mmol, and **f**, **i** 30 mmol. **j** Scheme showing the phosphorization mechanism and its changed morphology for preparing Ni_xP_y nanosheets. Adapted with permission from Ref. [73], Copyright (2017), American Chemical Society

and Ni_xP_y-3 electrode (1140 C/g) when applying current density of 2 A/g. Inspired by the impressive properties of such electrode, it was assembled with activated carbon in an asymmetrical device giving a higher power density of 67.2 Wh/kg at the power density of 0.75 kW/kg. To overcome the poor conductivity, Ni_2P was also composited with the conductive graphene to yield a porous network that could attain a specific capacitance of 1912 F/g at an operated current density of 5 mA/cm^2 [74]. By following the same concept, the carbon fiber was mixed with NiP_x which

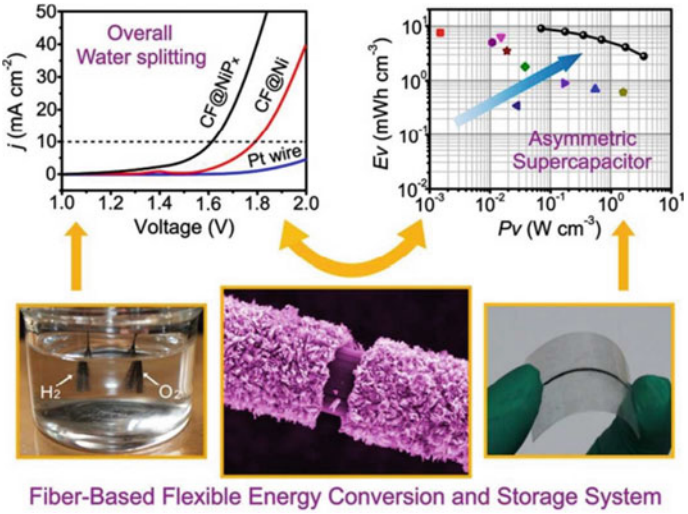

Fig. 10 Scheme representation showing the performance of the developed NiP_x/carbon fiber. Adapted with permission from Ref. [75], Copyright (2016), Royal Society of Chemistry

was prepared by Zhang et al. [75] through electrodeposition method and followed by the phosphatization process for getting 3D porous nanoarchitecture with effective synergism properties. The electrode could give a volumetric capacitance value of 817 F/cm^3. Moreover, the NiP_x decorated on carbon fiber can work as an electrolyzer for alkaline water efficiently as it can produce a current of 10 mA/cm^2 by using only 1.61 V with higher stability. The electrode was further assembled with a negative electrode from reduce graphene oxide attached on CF@Ni to reveal device with energy density of 8.97 mWh/cm^3, and longer cycle life (Fig. 10).

5.2 Cobalt Phosphide

There is a variety of cobalt derivatives such as cobalt oxides, phosphides, and hydroxides that are operating as smart electrocatalysts. Particularly, cobalt phosphide (CoP) is one member of the TMPs family and has been recently used as an efficient SCs electrode because of its low cost, high theoretical capacitance, and availability. CoP undergoes a redox reaction for Co^{2+}/Co^{3+} by doing two related charge and discharge processes. Due to the lower specific capacitance, there are limited reports about their SCs application compared to the Ni_2P-based materials. Lately, rod and flower shapes from Co_2P were designed by Chen et al. [76] as electrodes for SCs by utilizing the thermal decomposition approach. The electrode with nanoflower morphology was expected to have a 3D porous framework allowing specious contact area and decreased agglomeration of the material. Therefore, its morphology was observed to

obtain specific capacitance of 416 F/g which is relatively superior to that prepared with rod-like structure electrode, besides it could deliver high energy density up to 8.8 Wh/kg with outstanding life stability of 97% after spending 6000 cycles. This is important for enlarging the application of CoP in the field of SCs by discovering novel nanoporous materials with higher surface area for enhancing the specific features of the electrode.

Also, the doping of cobalt phosphide is another approach for improving the conductivity of the electrode. For instance, Elshahawy et al. [77] have deposited hollow S-doped CoP on carbon cloth through a further sulfidation process performed for the as-obtained CoP leading to a capacity which is 1.78 times than the undoped cobalt phosphide as seen in Fig. 11. Also, the as-formed electrode could withstand up to 10,000 with a more remarkable capacity retention of 99%. When HSCs were established with a negative electrode from previously prepared porous carbon polyhedron to receive ultrahigh energy density of 39 Wh/kg obtained at a power density of 800 W/kg. In addition, the whole device can stay for 50,000 cycles with a considerable capacitance remaining of nearly 86.4%.

5.3 Iron Phosphides

Another metal phosphide is iron phosphide (FeP) that is continuously attracting great concern due to its durable chemical stability, low cost, less toxic, and ultrahigh catalytic activity. Various FeP nanomaterials have been lately prepared for electrochemical applications such as FeP nanowires, FeP/carbon cloth, and porous FeP nanosheets [78]. For achieving higher electrochemical properties of the electrodes, the porous and hollow nanostructures from FeP should be designed as a consequence of their huge surface area and highly allowable active sites for the electrochemical reaction with electrolyte ions. For example, Liang et al. [79] studied the usage of FeP nanotubes arrays for the asymmetrical supercapacitors with an areal capacity of 142 mF/cm^2. The FeP nanotubes were prepared by the deposition of sacrificial template from ZnO on carbon cloth which followed by phosphatization process, and their electrode was identified to give capacitance of 149.11 F/g. The conducting polymer can modify the FeP for enhancing the conductivity and the whole properties of the final electrode. Following the same strategy, Luo et al. [80] abled to coat the hydrothermally prepared FeP with PEDOT on carbon cloth through the electrochemical polymerization of EDOT monomer at 1 V for 1 min as found in Fig. 12. Such material was used as an efficient negative electrode (operating window from 0 to −0.8 V) with electrochemically synthesized MnO_2 as a positive electrode for obtaining asymmetric cell with a volumetric capacity of 4.53 F/g and an energy density of 1.61 mWh/cm^3.

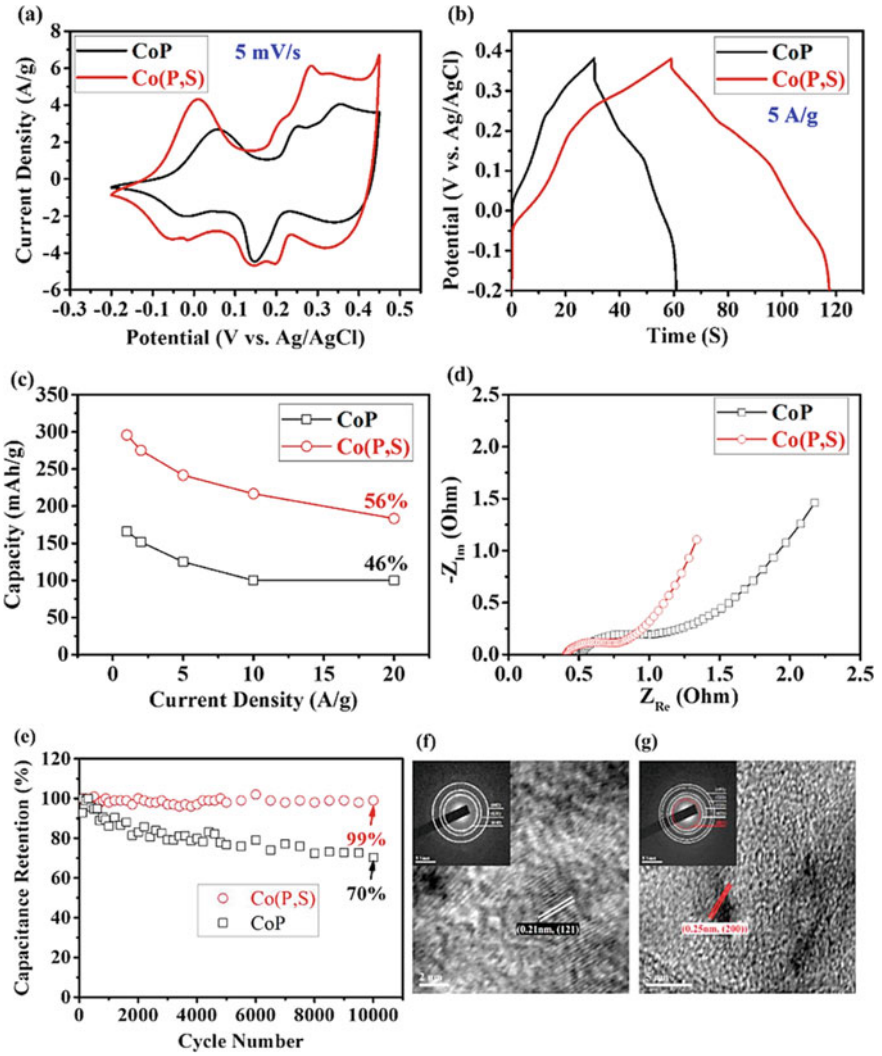

Fig. 11 **a** CV, and GCD patterns achieved at 5 mV/s, 5 A/g for CoP/CC and Co(P, S)/CC, respectively, **c**, **d** specific capacities versus current density, and EIS for CoP/CC and Co(P, S)/CC, respectively, **e** cycling life test operated at 10.0 A/g for 10,000 times, and **f**, **g** HRTEM images done for the electrodes of CoP/CC and Co(P, S)/CC after finishing the cyclic test. Adapted with permission from Ref. [77], Copyright (2017), Elsevier

6 Concluding Remarks

Transition metal chalcogenides and phosphides are considered a new technology for electricity generation, particularly, for energy storage devices such as supercapacitors thanks to their excellent specific capacitance, cycle life, and power/energy

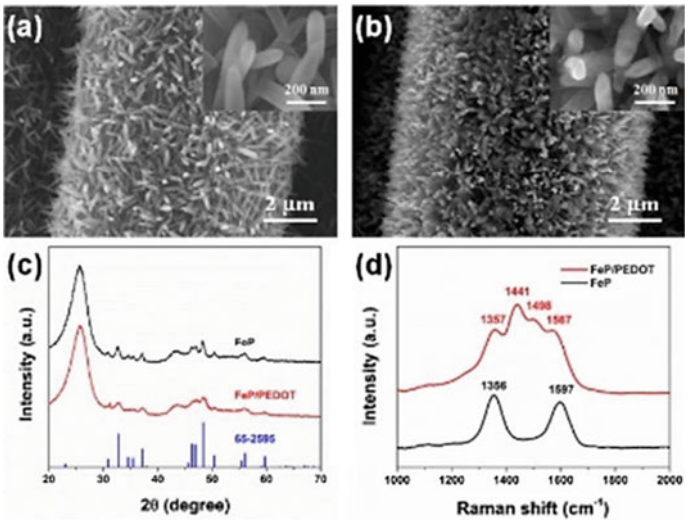

Fig. 12 FE-SEM images for **a** FeP, and **b** FeP/PEDOT nanorods (insets refers for high resolution SEM), while **c** and **d** their related XRD, Raman spectra, respectively. Adapted with permission from Ref. [80], Copyright (2018), Royal Society of Chemistry

densities. Therefore, they can be used to design supercapacitor electrodes owing to their simple synthesis, high surface area, cost-effectiveness, and electrochemical features. The present chapter overviewed the recent works that achieved on both transition metal chalcogenides (sulphide and selenide) and phosphides in the field of supercapacitors, their various preparation approach. Moreover, it showed how the synthesis method can affect the thickness, porosity, stability, and size diameter of the obtained chalcogenides and phosphides. Besides, chalcogenides and phosphides could be also hybridized with graphene as EDLCs materials or with conducting polymers as PEDOT and PPy, in addition to metal oxides derivatives including MnO_2 and RuO_2 for enhancing their electrochemical behavior.

References

1. W. Raza, F. Ali, N. Raza, Y. Luo, K.-H. Kim, J. Yang, S. Kumar, A. Mehmood, E.E. Kwon, Recent advancements in supercapacitor technology. Nano Energy **52**, 441–473 (2018)
2. S.-W. Zhang, B.-S. Yin, X.-X. Liu, D.-M. Gu, H. Gong, Z.-B. Wang, A high energy density aqueous hybrid supercapacitor with widened potential window through multi approaches. Nano Energy **59**, 41–49 (2019)
3. C.V.V. Muralee Gopi, R. Vinodh, S. Sambasivam, I.M. Obaidat, H.-J. Kim, Recent progress of advanced energy storage materials for flexible and wearable supercapacitor: from design and development to applications. J. Energy Storage **27**, 101035 (2020)
4. L.E. Blanc, D. Kundu, L.F. Nazar, Scientific challenges for the implementation of Zn-Ion batteries. Joule **4**(4), 771–799 (2020)

5. Q. Zong, C. Liu, H. Yang, Q. Zhang, G. Cao, Tailoring nanostructured transition metal phosphides for high-performance hybrid supercapacitors. Nano Today **38**, 101201 (2021)
6. V. Gupta, A.M. Kannan, S. Kumar, Graphene foam (GF)/manganese oxide (MnO_2) nanocomposites for high performance supercapacitors. J. Energy Storage **30**, 101575 (2020)
7. Q. Zhang, Z. Liu, B. Zhao, Y. Cheng, L. Zhang, H.-H. Wu, M.-S. Wang, S. Dai, K. Zhang, D. Ding, Y. Wu, M. Liu, Design and understanding of dendritic mixed-metal hydroxide nanosheets@N-doped carbon nanotube array electrode for high-performance asymmetric supercapacitors. Energy Storage Mater. **16**, 632–645 (2019)
8. J. Jiang, Y. Zhang, P. Nie, G. Xu, M. Shi, J. Wang, Y. Wu, R. Fu, H. Dou, X. Zhang, Progress of nanostructured electrode materials for supercapacitors. Adv. Sustain. Syst. **2**(1), 1700110 (2018)
9. N. Zhang, Y. Li, J. Xu, J. Li, B. Wei, Y. Ding, I. Amorim, R. Thomas, S.M. Thalluri, Y. Liu, G. Yu, L. Liu, High-performance flexible solid-state asymmetric supercapacitors based on bimetallic transition metal phosphide nanocrystals. ACS Nano **13**(9), 10612–10621 (2019)
10. X. Zhang, Z. Lai, C. Tan, H. Zhang, Solution-processed two-dimensional MoS_2 nanosheets: preparation, hybridization, and applications. Angew. Chem. Int. Ed. **55**(31), 8816–8838 (2016)
11. F. Bonaccorso, A. Lombardo, T. Hasan, Z. Sun, L. Colombo, A.C. Ferrari, Production and processing of graphene and 2d crystals. Mater. Today **15**(12), 564–589 (2012)
12. M. Wang, X. Xu, Y. Ge, P. Dong, R. Baines, P.M. Ajayan, M. Ye, J. Shen, Surface tension components ratio: an efficient parameter for direct liquid phase exfoliation. ACS Appl. Mater. Interfaces **9**(10), 9168–9175 (2017)
13. A. O'Neill, U. Khan, J.N. Coleman, Preparation of high concentration dispersions of exfoliated MoS_2 with increased flake size. Chem. Mater. **24**(12), 2414–2421 (2012)
14. J. Kang, V.K. Sangwan, J.D. Wood, M.C. Hersam, Solution-based processing of monodisperse two-dimensional nanomaterials. Acc. Chem. Res. **50**(4), 943–951 (2017)
15. C. Backes, B.M. Szydłowska, A. Harvey, S. Yuan, V. Vega-Mayoral, B.R. Davies, P.-L. Zhao, D. Hanlon, E.J.G. Santos, M.I. Katsnelson, W.J. Blau, C. Gadermaier, J.N. Coleman, Production of highly monolayer enriched dispersions of liquid-exfoliated nanosheets by liquid cascade centrifugation. ACS Nano **10**(1), 1589–1601 (2016)
16. J. Peng, J. Wu, X. Li, Y. Zhou, Z. Yu, Y. Guo, J. Wu, Y. Lin, Z. Li, X. Wu, C. Wu, Y. Xie, Very large-sized transition metal dichalcogenides monolayers from fast exfoliation by manual shaking. J. Am. Chem. Soc. **139**(26), 9019–9025 (2017)
17. G. Zhu, J. Liu, Q. Zheng, R. Zhang, D. Li, D. Banerjee, D.G. Cahill, Tuning thermal conductivity in molybdenum disulfide by electrochemical intercalation. Nat. Commun. **7**(1), 13211 (2016)
18. P.L. Cullen, K.M. Cox, M.K. Bin Subhan, L. Picco, O.D. Payton, D.J. Buckley, T.S. Miller, S.A. Hodge, N.T. Skipper, V. Tileli, C.A. Howard, Ionic solutions of two-dimensional materials. Nat. Chem. **9**(3), 244–249 (2017)
19. W. Zhao, B. Dong, Z. Guo, G. Su, R. Gao, W. Wang, L. Cao, Colloidal synthesis of VSe_2 single-layer nanosheets as novel electrocatalysts for the hydrogen evolution reaction. Chem. Commun. **52**(59), 9228–9231 (2016)
20. H. Quan, Y. Hu, Z. Huang, D. Wenmeng, Preparation and property evaluation of a hydrophobically modified xanthan gum XG-C16. J. Dispersion Sci. Technol. **41**(5), 656–666 (2020)
21. X. Qian, S. Shen, T. Liu, L. Cheng, Z. Liu, Two-dimensional TiS_2 nanosheets for in vivo photoacoustic imaging and photothermal cancer therapy. Nanoscale **7**(14), 6380–6387 (2015)
22. V.V. Plashnitsa, F. Vietmeyer, N. Petchsang, P. Tongying, T.H. Kosel, M. Kuno, Synthetic strategy and structural and optical characterization of thin highly crystalline titanium disulfide nanosheets. J. Phys. Chem. Lett. **3**(11), 1554–1558 (2012)
23. S. Jeong, D. Yoo, J.-T. Jang, M. Kim, J. Cheon, Well-defined colloidal 2-D layered transition-metal chalcogenide nanocrystals via generalized synthetic protocols. J. Am. Chem. Soc. **134**(44), 18233–18236 (2012)
24. P. Sekar, E.C. Greyson, J.E. Barton, T.W. Odom, Synthesis of nanoscale $NbSe_2$ materials from molecular precursors. J. Am. Chem. Soc. **127**(7), 2054–2055 (2005)
25. K. Yang, X. Wang, H. Li, B. Chen, X. Zhang, S. Li, N. Wang, H. Zhang, X. Huang, W. Huang, Composition- and phase-controlled synthesis and applications of alloyed phase heterostructures of transition metal disulphides. Nanoscale **9**(16), 5102–5109 (2017)

26. X. Geng, W. Sun, W. Wu, B. Chen, A. Al-Hilo, M. Benamara, H. Zhu, F. Watanabe, J. Cui, T.-P. Chen, Pure and stable metallic phase molybdenum disulfide nanosheets for hydrogen evolution reaction. Nat. Commun. **7**(1), 10672 (2016)
27. Q. Liu, X. Li, Z. Xiao, Y. Zhou, H. Chen, A. Khalil, T. Xiang, J. Xu, W. Chu, X. Wu, J. Yang, C. Wang, Y. Xiong, C. Jin, P.M. Ajayan, L. Song, Stable metallic 1T-WS_2 nanoribbons intercalated with ammonia ions: the correlation between structure and electrical/optical properties. Adv. Mater. **27**(33), 4837–4844 (2015)
28. Z. Liu, Z. Gao, Y. Liu, M. Xia, R. Wang, N. Li, Heterogeneous nanostructure based on 1T-phase MoS_2 for enhanced electrocatalytic hydrogen evolution. ACS Appl. Mater. Interfaces **9**(30), 25291–25297 (2017)
29. J. Su, J. Zhou, L. Wang, C. Liu, Y.J.S.b. Chen, Synthesis and application of transition metal phosphides as electrocatalyst for water splitting. Sci. Bull. **62**(9), 633–644 (2017)
30. C.G. Read, J.F. Callejas, C.F. Holder, R.E. Schaak, General strategy for the synthesis of transition metal phosphide films for electrocatalytic hydrogen and oxygen evolution. ACS Appl. Mater. Interfaces **8**(20), 12798–12803 (2016)
31. E.J. Popczun, J.R. McKone, C.G. Read, A.J. Biacchi, A.M. Wiltrout, N.S. Lewis, R.E. Schaak, Nanostructured nickel phosphide as an electrocatalyst for the hydrogen evolution reaction. J. Am. Chem. Soc. **135**(25), 9267–9270 (2013)
32. S. Msp, G. Gnanasekaran, P. Pazhamalai, S. Sahoo, M.M. Hossain, R.M. Bhattarai, S.-J. Kim, Y.S. Mok, Engineering, hierarchically porous nanostructured nickel phosphide with carbon particles embedded by dielectric barrier discharge plasma deposition as a binder-free electrode for hybrid supercapacitors. ACS Sustain. Chem. Eng. **7**(17), 14805–14814 (2019)
33. D. Wang, X. Zhang, D. Zhang, Y. Shen, Z. Wu, Influence of Mo/P ratio on CoMoP nanoparticles as highly efficient HER catalysts. Appl. Catal. A: Gen. **511**, 11–15 (2016)
34. T. Wu, S. Chen, D. Zhang, J. Hou, Facile preparation of semimetallic MoP_2 as a novel visible light driven photocatalyst with high photocatalytic activity. J. Mater. Chem. A **3**(19), 10360–10367 (2015)
35. J. Tian, Q. Liu, A.M. Asiri, X. Sun, Self-supported nanoporous cobalt phosphide nanowire arrays: an efficient 3D hydrogen-evolving cathode over the wide range of pH 0–14. J. Am. Chem. Soc. **136**(21), 7587–7590 (2014)
36. J. Kibsgaard, T.F. Jaramillo, Molybdenum phosphosulfide: an active, acid-stable, earth-abundant catalyst for the hydrogen evolution reaction. Angew. Chem. Int. Ed. **53**(52), 14433–14437 (2014)
37. T. Jayaraman, A.P. Murthy, S.J. Lee, K. Karuppasamy, S.R. Arumugam, Y. Yu, M.M. Hanafiah, H.-S. Kim, V. Mittal, M. Choi, Recent progress on synthetic strategies and applications of transition metal phosphides in energy storage and conversion. Ceram. Int. **47**(4), 4404–4425 (2021)
38. V. Tallapally, R.J.A. Esteves, L. Nahar, I. Arachchige, Multivariate synthesis of tin phosphide nanoparticles: temperature, time, and ligand control of size, shape, and crystal structure. Chem. Mater. **28**(15), 5406–5414 (2016)
39. T. Chouki, M. Machreki, S. Emin, Solvothermal synthesis of iron phosphides and their application for efficient electrocatalytic hydrogen evolution. Int. J. Hydrogen Energy **45**(41), 21473–21482 (2020)
40. B.T. Jebaslinhepzybai, T. Partheeban, D.S. Gavali, R. Thapa, M. Sasidharan, One-pot solvothermal synthesis of Co_2P nanoparticles: an efficient HER and OER electrocatalysts. Int. J. Hydrogen Energy (2021)
41. J. Li, J. Li, X. Zhou, Z. Xia, W. Gao, Y. Ma, Y. Qu, Highly efficient and robust nickel phosphides as bifunctional electrocatalysts for overall water-splitting. ACS Appl. Mater. Interfaces **8**(17), 10826–10834 (2016)
42. A.S. Murali, D.S. Baji, S. Nair, D. Santhanagopalan, Vapour phase conversion of metal oxalates to metal phosphide nanostructures and their use as anode in rechargeable Li, Na and K-ion batteries. Electrochim. Acta **388**, 138643 (2021)
43. S. Chandrasekaran, L. Yao, L. Deng, C. Bowen, Y. Zhang, S. Chen, Z. Lin, F. Peng, P. Zhang, Recent advances in metal sulfides: from controlled fabrication to electrocatalytic, photocatalytic

and photoelectrochemical water splitting and beyond. Chem. Soc. Rev. **48**(15), 4178–4280 (2019)
44. R. Barik, P.P. Ingole, Challenges and prospects of metal sulfide materials for supercapacitors. Curr. Opin. Electrochem. **21**, 327–334 (2020)
45. D. Ghosh, C.K. Das, Hydrothermal growth of hierarchical Ni_3S_2 and Co_3S_4 on a reduced graphene oxide hydrogel@Ni foam: a high-energy-density aqueous asymmetric supercapacitor. ACS Appl. Mater. Interfaces **7**(2), 1122–1131 (2015)
46. R. Kötz, M. Carlen, Principles and applications of electrochemical capacitors. Electrochim. Acta **45**(15), 2483–2498 (2000)
47. Q. Chen, H. Li, C. Cai, S. Yang, K. Huang, X. Wei, J. Zhong, In situ shape and phase transformation synthesis of Co_3S_4 nanosheet arrays for high-performance electrochemical supercapacitors. RSC Adv. **3**(45), 22922–22926 (2013)
48. Q. Wang, L. Jiao, H. Du, J. Yang, Q. Huan, W. Peng, Y. Si, Y. Wang, H. Yuan, Facile synthesis and superior supercapacitor performances of three-dimensional cobalt sulfide hierarchitectures. CrystEngComm **13**(23), 6960–6963 (2011)
49. H. Li, Y. Gao, Y. Shao, Y. Su, X. Wang, Vapor-phase atomic layer deposition of Co_9S_8 and its application for supercapacitors. Nano Lett. **15**(10), 6689–6695 (2015)
50. H. Peng, G. Ma, J. Mu, K. Sun, Z. Lei, Controllable synthesis of CuS with hierarchical structures via a surfactant-free method for high-performance supercapacitors. Mater. Lett. **122**, 25–28 (2014)
51. H. Peng, G. Ma, K. Sun, J. Mu, H. Wang, Z. Lei, High-performance supercapacitor based on multi-structural CuS@polypyrrole composites prepared by in situ oxidative polymerization. J. Mater. Chem. A **2**(10), 3303–3307 (2014)
52. C. Justin Raj, B.C. Kim, W.-J. Cho, W.-G. Lee, Y. Seo, K.-H. Yu, Electrochemical capacitor behavior of copper sulfide (CuS) nanoplatelets. J. Alloy. Compd. **586**, 191–196 (2014)
53. K. Krishnamoorthy, G.K. Veerasubramani, S. Radhakrishnan, S.J. Kim, One pot hydrothermal growth of hierarchical nanostructured Ni_3S_2 on Ni foam for supercapacitor application. Chem. Eng. J. **251**, 116–122 (2014)
54. Z. Wang, C. Nan, D. Wang, Y. Li, Fabrication of 1D nickel sulfide nanocrystals with high capacitances and remarkable durability. RSC Adv. **4**(88), 47513–47516 (2014)
55. C. Wei, C. Cheng, J. Zhao, Y. Wang, Y. Cheng, Y. Xu, W. Du, H. Pang, NiS hollow spheres for high-performance supercapacitors and non-enzymatic glucose sensors. Chem. Asian J. **10**(3), 679–686 (2015)
56. S. Wang, W. Li, L. Xin, M. Wu, Y. Long, H. Huang, X. Lou, Facile synthesis of truncated cube-like $NiSe_2$ single crystals for high-performance asymmetric supercapacitors. Chem. Eng. J. **330**, 1334–1341 (2017)
57. N.S. Arul, J.I. Han, Facile hydrothermal synthesis of hexapod-like two dimensional dichalcogenide $NiSe_2$ for supercapacitor. Mater. Lett. **181**, 345–349 (2016)
58. P. Pazhamalai, K. Krishnamoorthy, S.J. Kim, Hierarchical copper selenide nanoneedles grown on copper foil as a binder free electrode for supercapacitors. Int. J. Hydrogen Energy **41**(33), 14830–14835 (2016)
59. L. Li, J. Gong, C. Liu, Y. Tian, M. Han, Q. Wang, X. Hong, Q. Ding, W. Zhu, J. Bao, Vertically oriented and interpenetrating CuSe nanosheet films with open channels for flexible all-solid-state supercapacitors. ACS Omega **2**(3), 1089–1096 (2017)
60. S.K. Balasingam, J.S. Lee, Y. Jun, Molybdenum diselenide/reduced graphene oxide based hybrid nanosheets for supercapacitor applications. Dalton Trans. **45**(23), 9646–9653 (2016)
61. C. Xia, Q. Jiang, C. Zhao, P.M. Beaujuge, H.N. Alshareef, Asymmetric supercapacitors with metal-like ternary selenides and porous graphene electrodes. Nano Energy **24**, 78–86 (2016)
62. B. Pandit, S.R. Rondiya, S. Shegokar, L.K. Bommineedi, R.W. Cross, N.Y. Dzade, B.R. Sankapal, Combined electrochemical and DFT investigations of iron selenide: a mechanically bendable solid-state symmetric supercapacitor. Sustain. Energy Fuels **5**(19), 5001–5012 (2021)
63. B. Pandit, A. Agarwal, P. Patel, B.R. Sankapal, The electrochemical kinetics of cerium selenide nano-pebbles: the design of a device-grade symmetric configured wide-potential flexible solid-state supercapacitor. Nanoscale Adv. **3**(4), 1057–1066 (2021)

64. R.A. Hussain, I. Hussain, Metal telluride nanotubes: synthesis, and applications. Mater. Chem. Phys. **256**, 123691 (2020)
65. B. Pandit, S.R. Rondiya, R.W. Cross, N.Y. Dzade, B.R. Sankapal, Vanadium telluride nanoparticles on MWCNTs prepared by successive ionic layer adsorption and reaction for solid-state supercapacitor. Chem. Eng. J. **429**, 132505 (2022)
66. P. Zhou, L. Fan, J. Wu, C. Gong, J. Zhang, Y. Tu, Facile hydrothermal synthesis of NiTe and its application as positive electrode material for asymmetric supercapacitor. J. Alloy. Compd. **685**, 384–390 (2016)
67. M. Manikandan, K. Subramani, M. Sathish, S. Dhanuskodi, Hydrothermal synthesis of cobalt telluride nanorods for a high performance hybrid asymmetric supercapacitor. RSC Adv. **10**(23), 13632–13641 (2020)
68. V.S. Kumbhar, A.C. Lokhande, N.S. Gaikwad, C.D. Lokhande, One-step chemical synthesis of samarium telluride thin films and their supercapacitive properties. Chem. Phys. Lett. **645**, 112–117 (2016)
69. S. Siddique, C.C. Gowda, R. Tromer, S. Demiss, A.R.S. Gautam, O.E. Femi, P. Kumbhakar, D.S. Galvao, A. Chandra, C.S. Tiwary, Scalable synthesis of atomically thin gallium telluride nanosheets for supercapacitor applications. ACS Appl. Nano Mater. **4**(5), 4829–4838 (2021)
70. M. Liu, Z. Wang, J. Liu, G. Wei, J. Du, Y. Li, C. An, J. Zhang, Synthesis of few-layer 1T′-$MoTe_2$ ultrathin nanosheets for high-performance pseudocapacitors. J. Mater. Chem. A **5**(3), 1035–1042 (2017)
71. Z. Fang, L. Peng, Y. Qian, X. Zhang, Y. Xie, J.J. Cha, G. Yu, Dual tuning of Ni–Co–A (A = P, Se, O) nanosheets by anion substitution and holey engineering for efficient hydrogen evolution. J. Am. Chem. Soc. **140**(15), 5241–5247 (2018)
72. N.P. Sweeny, C.S. Rohrer, O.W. Brown, Dinickel phosphide as a heterogeneous catalyst for the vapor phase reduction of nitrobenzene with hydrogen to aniline and water. J. Am. Chem. Soc. **80**(4), 799–800 (1958)
73. S. Liu, K.V. Sankar, A. Kundu, M. Ma, J.-Y. Kwon, S.C. Jun, Honeycomb-like interconnected network of nickel phosphide heteronanoparticles with superior electrochemical performance for supercapacitors. ACS Appl. Mater. Interfaces **9**(26), 21829–21838 (2017)
74. J. Theerthagiri, G. Durai, K. Karuppasamy, P. Arunachalam, V. Elakkiya, P. Kuppusami, T. Maiyalagan, H.-S. Kim, Recent advances in 2-D nanostructured metal nitrides, carbides, and phosphides electrodes for electrochemical supercapacitors—a brief review. J. Ind. Eng. Chem. **67**, 12–27 (2018)
75. Z. Zhang, S. Liu, J. Xiao, S. Wang, Fiber-based multifunctional nickel phosphide electrodes for flexible energy conversion and storage. J. Mater. Chem. A **4**(24), 9691–9699 (2016)
76. X. Chen, M. Cheng, D. Chen, R. Wang, Shape-controlled synthesis of Co_2P nanostructures and their application in supercapacitors. ACS Appl. Mater. Interfaces **8**(6), 3892–3900 (2016)
77. A.M. Elshahawy, C. Guan, X. Li, H. Zhang, Y. Hu, H. Wu, S.J. Pennycook, J. Wang, Sulfur-doped cobalt phosphide nanotube arrays for highly stable hybrid supercapacitor. Nano Energy **39**, 162–171 (2017)
78. W. Jin, G. Maduraiveeran, Recent advances of porous transition metal-based nanomaterials for electrochemical energy conversion and storage applications. Mater. Today Energy **13**, 64–84
79. B. Liang, Z. Zheng, M. Retana, K. Lu, T. Wood, Y. Ai, X. Zu, W. Zhou. Synthesis of FeP nanotube arrays as negative electrode for solid-state asymmetric supercapacitor. Nanotechnology **30**(29), 295401 (2019)
80. J. Luo, Z. Zheng, A. Kumamoto, W.I. Unah, S. Yan, Y.H. Ikuhara, X. Xiang, X. Zu, W. Zhou, PEDOT coated iron phosphide nanorod arrays as high-performance supercapacitor negative electrodes. Chem. Commun. **54**(7), 794–797 (2018)

Nanostructured Metal Phosphides and Chalcogenides for Supercapacitor Application

Ajay D. Jagadale and Surendra K. Shinde

Abstract Recently, supercapacitor (SC) has received great attention as an energy storage device owing to its high-power density, rapid charge-discharge, and long cycle life. Various electrode materials have been explored for SC application including carbon, metal oxides/hydroxides, conducting polymers, metal chalcogenides, and metal phosphides. Amongst, nanostructured metal chalcogenides and phosphides have gained much interest because of their relatively high conductivity and high theoretical capacities/capacitances. Herein, brief information on SCs and the discussion on important contributions on nanostructured metal chalcogenides and phosphides have been provided. Different influencing factors including morphology, synergic effect, and hybridization have been discussed. The literature of metal phosphides and chalcogenides has been reviewed based on the nanostructure of an electrode, charge storage mechanism, device configuration, and supercapacitive performance. This chapter will be beneficial for researchers around the world to have a better idea of the potential of metal phosphides and chalcogenides as SC electrodes.

Keywords Metal chalcogenide · Metal phosphide · Nanostructure · Supercapacitor · Hybrid energy storage

1 Introduction

The electrochemical energy storage (EES) devices exhibit an imperative role in achieving the development of sustainable energy technology [1]. These devices store the energy generated by renewable energy sources such as solar, wind, etc., and supply

A. D. Jagadale (✉)
Centre for Energy Storage and Conversion, School of Electrical and Electronics Engineering, SASTRA Deemed University, Tamil Nadu, Thanjavur 613401, India
e-mail: jagadaleajay99@gmail.com

S. K. Shinde
Department of Biological and Environmental Science, College of Life Science and Biotechnology, Dongguk University, Biomedical Campus, 32 Dongguk-ro, Ilsandong-gu, Siksa-dong, Goyang-si, Gyeonggi-do 10326, South Korea

S. Thomas et al. (eds.), *Nanostructured Materials for Supercapacitors*,
Advances in Material Research and Technology,
https://doi.org/10.1007/978-3-030-99302-3_20

wherever necessary. There have been two types of EES devices primarily available; supercapacitors (SCs) and batteries [2]. SCs are high power density devices, whereas, batteries provide high energy density. SCs have several advantages over batteries such as rapid charge-discharge, high power performance, and long cycle life. Depending on the material and structure of the electrode, SCs store a charge via two principles; electrical double layer capacitance (EDLC) and pseudocapacitance [3]. The EDLC achieves electrostatic storage of energy via separation of charge at the electrode-electrolyte interface as shown in Fig. 1a. The pseudocapacitance results from electrochemical redox reactions and intercalation processes on the surface of the electrode. Pseudocapacitance involves three storage mechanisms; (i) underpotential deposition, (ii) redox pseudocapacitance and (iii) intercalation pseudocapacitance. The mechanism of underpotential deposition can be understood using a process of adsorption of hydrogen atoms on noble metals such as platinum and rhodium (Fig. 1b). With this mechanism, a maximum capacitance of ~2200 $\mu F\ cm^{-2}$ can be obtained. However, the operational potentials range from 0.3 to 0.6 V, limiting the capacitance values [4]. In the case of redox pseudocapacitive materials such as RuO_2 and MnO_2, fast redox reactions occur at the electrode surface (Fig. 1c). The maximum capacitance achieved through this mechanism is much higher than that of EDLC materials. Pseudocapacitance is also observed in the process of ion insertion/intercalation into layered crystalline materials as shown in Fig. 1d. The intercalation happens along with the change of the oxidation states of the metal for maintaining electric neutrality.

Previously, a variety of different materials with various charge storage mechanisms have been studied for SC application, mainly carbon, metal oxides/hydroxides, conducting polymers, metal chalcogenides, metal phosphides, carbides, and nitrides [5]. Amongst, metal phosphides and chalcogenides have attracted great attention due to their semi-metallic nature, high electrical conductivity, and numerous electrochemically active sites [6]. In the present chapter, we have briefly discussed a hydrothermal

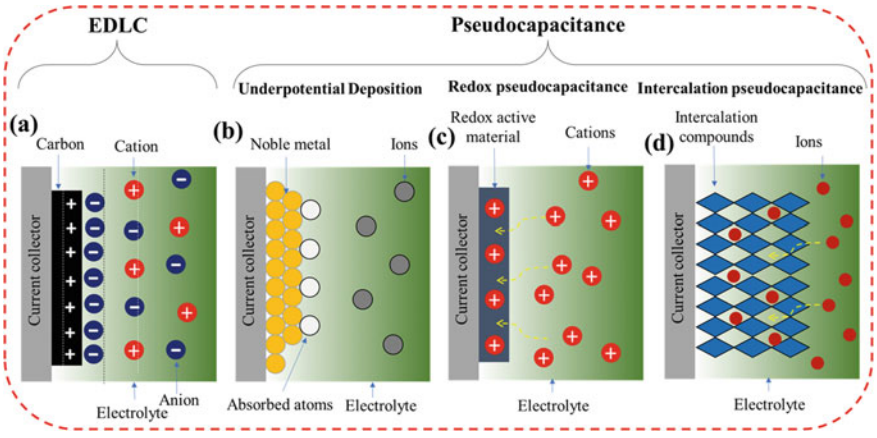

Fig. 1 Schematic of charge storage mechanism of EDLC and pseudocapacitor

synthesis route for preparing phosphides and chalcogenides along with the formation mechanism. Moreover, different influencing factors such as morphology, synergic effect, and hybridization have been thoroughly explained with the help of important contributions. Metal phosphides and chalcogenides have been classified based on the type of the components used such as pristine and composites with carbon, metal oxides/hydroxides, conducting polymers, etc. Furthermore, the SC performance of these materials has been discussed based on the morphology, nanostructure, and compositional synergy.

2 Synthesis of Phosphide and Chalcogenides

The nanostructured metal phosphides have been prepared with a variety of different methods including thermal decomposition, hydrothermal, solvothermal, microwave-assisted hydrothermal, co-electrodeposition, and solid-state reaction. However, metal phosphides prepared with the hydrothermal method have been frequently reported for SC application. The hydrothermal method is primarily used to prepare metal precursors such as metal hydroxides, oxides, metal-organic frameworks, etc., and later on, these precursors are phosphorized using a phosphorous source. For SC application, to avoid an additional weight of binders and conducting additives, these metal precursors are preferentially coated on conducting supports such as stainless steel, Ni foam, etc., and further phosphorized in the inert atmosphere using a gas solid-reaction approach. In this method, a gaseous phosphine (PH_3) is effectively used for the phosphorization process, however, due to its toxic and lethal nature, its *in situ* generation via ammonium ($NH_4H_2PO_2$) or sodium (NaH_2PO_2) hypophosphites is recommended. A typical reaction can be given as $2NaH_2PO_2 = PH_3\uparrow + Na_2HPO_4$ [7]. As shown in Fig. 2a, hypophosphite powder is placed at the upstream side and metal precursors are downstream of the inert atmosphere furnace, leading to a thorough phosphorization of the metal precursor. Since the microstructure doesn't change

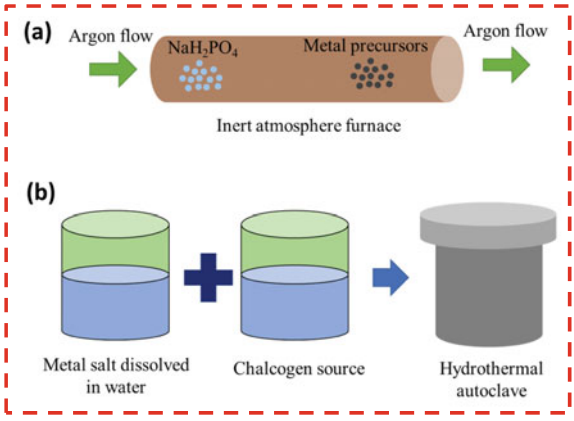

Fig. 2 Hydrothermal synthesis of metal phosphides and chalcogenides

significantly after the phosphorization process, materials with different morphologies can be obtained.

Metal chalcogenides can be prepared with various methods such as liquid exfoliation, hot injection, hydrothermal, solvothermal, etc. Amongst, hydrothermal and liquid exfoliation methods are widely used. The liquid exfoliation is used to prepare layered transition metal chalcogenides (TMDs) such as MoS_2, WS_2, and VS_2. However, these layered TMDs cannot be directly utilized for SC application without the binder and conductive additives. The hydrothermal method has great potential to prepare nanostructured metal chalcogenides both in film and powder forms, therefore, it is reported widely to prepare binder and conductive additive-free electrodes for SC application. As shown in Fig. 2b, the hydrothermal method uses water as a reaction medium in which metal salts are dissolved, to this solution chalcogen source is added. This solution is further transferred to a Teflon-lined steel autoclave which is heated to a designated temperature to react. Until now, various nanostructures of metal chalcogenides have been prepared via the hydrothermal method including hollow microspheres/cubic cages, nanoflowers, nanocrystals, nanoparticles, etc.

3 Influencing Factors

3.1 Morphology

It is seen that major technological progress has been made due to the advances in materials. The morphology, size, and shape of materials have great control over supercapacitive properties and can be effectively tuned to achieve enhanced performance. The functionalities of the materials are largely affected by the morphologies and the electrochemically active surface area. As shown in Fig. 3a–i, phosphides and chalcogenides have been reported with variety of different morphologies including nanorods [8, 9], nanoflowers [8], nanowires [10, 11], nanoshuttles [12], nanoparticles [13, 14], nanoprisms [15], nanotubes [16, 17], nanosheets [18, 19], nanospheres [20], nanobelts [21], nanocages [22], etc. Amongst, phosphides and chalcogenides with nanosheets-like morphology have been reported frequently for SC application. The nanosheets-like morphology has several advantages such as it offers a low ion-diffusion barrier, excellent durability, and the ability to accommodate volume variations during cycling. Besides, efforts have been made to prepare phosphides and chalcogenides with one-dimensional nanowires-like morphology that facilitates an efficient transport pathway for both electrons and ions, leading to a high-rate capability. Interestingly, the way material is grown or the kind of surface morphology is formed affects the supercapacitive performance of the material. For instance, Chen et al. [8] prepared the Co_2P with nanorod and nanoflower-like morphologies by controlling the decomposition process of Tris(acetylacetonato) cobalt(III) in oleylamine system using a triphenylphosphine phosphorus source. It is observed that the heating rate influences the morphology of the material. At the rapid heating rate,

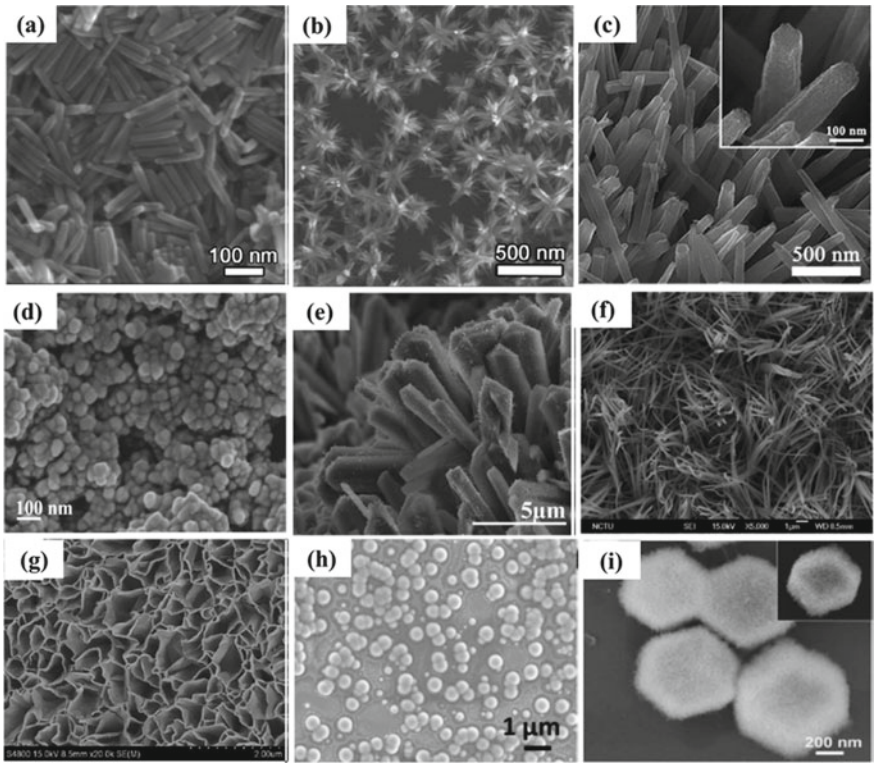

Fig. 3 Different morphologies of metal phosphides and chalcogenides such as **a** Co_2P nanorods, **b** Co_2P nanoflowers, **a**–**b** adapted with permission from reference [8] Copyright 2016, American Chemical Society, **c** $NiCo_2S_4$ nanowires, adapted with permission from reference [11] Copyright 2019, Elsevier, **d** CoP nanoparticles, adapted with permission from reference [13] Copyright 2017, Guo-Qun Zhang et al. some rights reserved; exclusive licensee Hindawi. Distributed under a Creative Commons Attribution License 4.0 (CC BY) https://creativecommons.org/licenses/by/4.0/, **e** CoP nanoprisms, adapted with permission from reference [15] Copyright 2017, Elsevier, **f** Cu_3P nanotubes, adapted with permission from reference [16] Copyright 2017, American Chemical Society, **g** NiCo-S nanosheets, adapted with permission from reference [19] Copyright 2018, Elsevier, **h** Ni_xP nanospheres, adapted with permission from reference [20] Copyright 2018, Elsevier and **i** NiCoP nanocages, adapted with permission from reference [22] Copyright 2019, Liang et al. some rights reserved; exclusive licensee Wiley-VCH. Distributed under a Creative Commons Attribution License (CC BY) https://creativecommons.org/licenses/

nanorods (∼18 nm) were formed and at a sluggish heating rate, the nanoflowers were formed. The nanoflower-like Co_2P demonstrated a specific capacitance of 416 F g^{-1} at a current density of 1 A g^{-1} that was far better than that of nanorod-like morphology (284 F g^{-1}).

Recently, hollow nanoarchitectures have gained great attention as a promising material for SC application owing to their enhanced active surface area and shorter diffusion pathways, leading to a high rate capability. Hollow structures are prepared

via a template route in which organic solvents are used to remove the polymer template. Besides, to avoid organic solvents, SiO_2 is also used as the template to obtain a hollow structure [23]. Phosphides and chalcogenides with different types of hollow structures have been prepared for SCs including nanoflowers, microspheres, nanocages, microcubes, etc. For instance, Gao et al. [24] synthesized urchin-like NiCoP hollow spheres via mild hydrothermal method followed by phosphorization. The urchin-like structure is originated due to the gas bubble templating mechanism of urea. This electrode demonstrated an excellent specific capacity of 761 C g^{-1} at a current density of 1 A g^{-1} and the rate capability of 91.1% when the current density was increased to 20-fold. Therefore, it is highly desirable to prepare these materials with various shapes, sizes and morphologies for SC application.

3.2 Synergic Effect

The composition of multi-metallic phosphides and chalcogenides greatly influences the SC performance. The synergic effect between different elements in multi-metallic phosphides modifies the electronic structure of the metal sites, facilitating enhanced ion adsorption capability for rapid energy storage. For instance, Liang et al. [22] carried out DFT calculations to understand the synergic effect between Co and Ni in NiCoP. It is observed that the OH^- absorption energy of Ni sites in NiCoP (−2.63 eV) was lower than that in NiP (−2.35 eV), implying simplistic ionic transport in multi-metal phosphide electrodes. These nanocages-like NiCoP demonstrated excellent specific capacity of 894 C g^{-1} at 1 A g^{-1} and rate capability.

3.3 Hybrids

Although phosphides and chalcogenides exhibit better electrical conductivity than oxides, the conductivity is still limited to achieving the acceptable values of rate capability. Besides, most of the phosphides and chalcogenides usually depict poor cyclic stability due to their battery-type charge storage mechanism. Recently, many efforts have been devoted to improving the rate capability and the cyclic stability of phosphides and chalcogenides by combining them with electrical double layer type-carbon materials. These composites are referred as hybrids. For example, Zhou et al. [25] prepared NiCoP/C nanohybrid materials via in-situ calcination/phosphorization of MOF precursor. This electrode showed an excellent specific capacity of 775.7 C g^{-1} at 1 A g^{-1} and a rate capability of 75.1% along with excellent cyclability up to 10000 cycles. These values were superior when compared with the bare NiCoP. Therefore, the preparation of hybrid materials is a promising approach to enhance the rate capability and the cyclic life of phosphides and chalcogenides.

4 Metal Phosphides

Metal phosphides, especially, transition metal phosphides have gained much attention in the field of catalysis and energy storage [26]. As shown in Fig. 4, phosphides can be classified as pristine, phosphide-metal oxide/hydroxide/chalcogenide/phosphide composites, phosphide-carbon composite and phosphide-polymer composite as discussed below.

4.1 Pristine Phosphides

Cobalt phosphides: Cobalt phosphides have been widely explored due to their interesting magnetic, electronic, electrochemical, and catalytic properties. As a SC electrode, two important phases of cobalt phosphides have been reported such as CoP and Co_2P. As observed from the cyclic voltammograms (Fig. 5a), a pseudocapacitive CoP stores charge via following electrochemical reactions in alkaline solution, CoP $+ 2H^+ \leftrightarrow Co^{2+} + PH_2$, $Co^{2+} + 2OH^- \leftrightarrow Co(OH)_2$, $Co(OH)_2 + OH^- \leftrightarrow CoOOH + H_2O + e^-$ and $CoOOH + e^- \leftrightarrow Co_3O_4 + H_2O + OH^-$. The research of pristine cobalt phosphides mostly focuses on preparing various morphologies and evaluating their influence on storage performance. For instance, Zheng et al. [10] prepared 3D cobalt phosphide (CoP) nanowire arrays on a carbon cloth via hydrothermal and subsequent phosphatization methods. This binder-free 3D CoP electrode demonstrated an areal capacitance of 571.3 mF cm^{-2} at 1 mA cm^{-2}. Furthermore, an asymmetric flexible

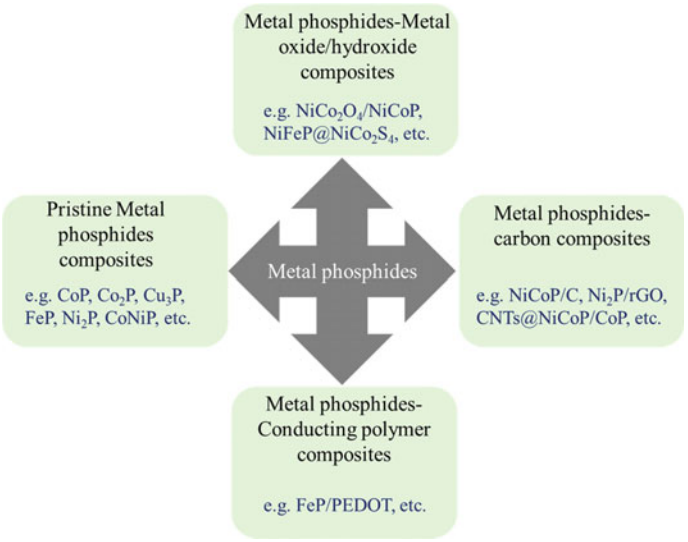

Fig. 4 Classification of metal phosphides

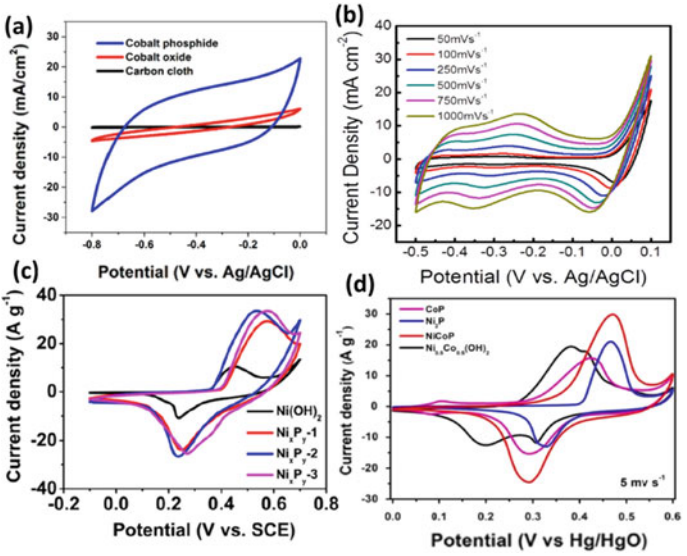

Fig. 5 CV curves of **a** cobalt phosphide, cobalt oxide and carbon cloth, adapted with permission from reference [10] Copyright 2017, American Chemical Society, **b** Cu_3P nanotubes at various scan rates, adapted with permission from reference [16] Copyright 2017, American Chemical Society, **c** $Ni(OH)_2$ and nickel phosphides at 5 mV s^{-1}, adapted with permission from reference [28] Copyright 2017, American Chemical Society and **d** CoP, Ni_2P, NiCoP and $Ni_{0.5}Co_{0.5}(OH)_2$ at 5 mV s^{-1}, adapted with permission from reference [30] Copyright 2020, Elsevier

solid-state SC was fabricated by combining CoP as a negative electrode and MnO_2 as a positive electrode that showed a high volumetric energy density of 0.69 mWh cm^{-3} and a high-power density of 114.2 mW cm^{-3}.

Copper phosphide: Chen et al. [16] fabricated binder-free and conducting additive-free copper foil-supported 1D Cu_3P nanotube arrays electrode via electro-oxidation and phosphatization processes. As shown in cyclic voltammetry (CV) curves (Fig. 5b), this 1D Cu_3P electrode acts as a negative pseudocapacitive electrode that showed maximum specific capacitance of 300.9 F g^{-1} at 2.5 mA cm^{-2} in 1M H_2SO_4. The charge storage mechanism can be revealed from the following reactions, $Cu(I)_3P + xH^+ + xe^- \leftrightarrow H_x\{Cu(0)_xCu(I)_{3-x}\}P$ and $Cu(I)_3P + H_2O \leftrightarrow Cu(II)_yO_yCu(I)_{3-y}P + 2yH^+ + 2ye^-$. A hybrid SC fabricated with carbon nanotubes (CNTs) negative electrode demonstrated excellent energy density (44.6 Wh kg^{-1}), power density (17045.7 W kg^{-1}), and cyclability (81.9% after 5000 cycles).

Iron phosphide: Owing to its abundance and low cost, iron phosphide has attracted great attention in different energy-related applications. For instance, Liang et al. [27] synthesized FeP nanotube arrays on carbon cloth via the phosphatization process. The ZnO nanorod arrays were used as the sacrificial templets. The diameter of FeP nanorods was found to be about 200 nm and the wall thickness was in the range of 50–100 nm. The FeP acts as a negative electrode and shows a quasi-rectangular shape in a 1M LiCl electrolyte. This nanotube-like FeP demonstrated a maximum

specific capacitance of 149.11 F g^{-1} at 1 mA cm^{-2}. The superior performance was attributed to the tubular structure of FeP nanotubes, facilitating easy ion pathway and reducing inactive parts of the material.

Nickel phosphide: Different phases of nickel phosphide have been reported so far, for instance, Ni_2P, Ni_5P_4, Ni_7P_3, $Ni_{12}P_5$, and Ni_3P. Amongst, Ni_2P is frequently reported due to its excellent storage performance. The Ni_2P depicts a battery-type charge storage mechanism with clear redox peaks in the CV curve (Fig. 5c). The electrochemical process during charging-discharging in the alkaline solution can be described by the following reactions, $Ni_2P+2OH^- \leftrightarrow Ni_2P(OH)_2 + 2e^-$, and $Ni_5P_4 + 5OH^- \leftrightarrow Ni_5P_4(OH)_5 + 5e^-$ [28]. Efforts have been made to prepare pristine nickel phosphides with different nanostructures by applying various synthetic routes. For example, Zhou et al. [29] prepared nanosheets of Ni_2P on the surface of Ni foam via phosphorization of hydrothermally synthesized $Ni(OH)_2$ nanosheets. This electrode depicted excellent specific capacitance of 2141 F g^{-1} at a sweep rate of 50 mV s^{-1} which is far greater than $Ni(OH)_2$ (1592 F g^{-1}) and NiO (1180 F g^{-1}) electrodes. Therefore, it is recommended to prepare nickel phosphides with different nanostructures, morphologies, phases, and porosity for hybrid SCs.

Multi-metal phosphide: To benefit from the improved electrical conductivity and the synergic effect between different metal species, mixed metal phosphides have become one of the important classes of materials. Recently, a variety of binary and ternary mixed metal phosphides have been employed for SC application. The binary NiCoP has been reported frequently with different morphologies prepared with various synthesis routes. The NiCoP shows a battery-like charge storage mechanism with clear distinct peaks corresponding to Ni^{2+}/Ni^{3+} and Co^{2+}/Co^{3+} faradaic redox reactions (Fig. 5d) [30]. It is observed that the electrochemical activity and stability of monometallic phosphide can be significantly improved by preparing multi-metallic phosphide. For instance, Liang et al. [31] demonstrated that the electrochemical performance of Ni_2P increased significantly after the incorporation of Co. Besides, the hollow structured NiCoP provides a number of redox-active sites and simplifies ion diffusion and charge transport. Recently, Gao et al. [24] prepared urchin-like hollow spheres via mild hydrothermal method followed by phosphorization that showed a specific capacity of 761 C g^{-1} at 1 A g^{-1} [24]. Previously, various hollow structures of NiCoP have been successfully prepared such as hollow nanocages, spheres, microcubes and nanocubes. Therefore, when compared with single metal phosphides, multi-metal phosphides can be considered as a promising SC electrode.

4.2 Metal Phosphide-Metal Oxide/Hydroxide/Chalcogenide/Phosphide Composite

Phosphide-metal oxide/hydroxide composites: Basically, phosphides have been considered to be poor electrochemically stable electrodes. Integrating phosphides

with metal oxides/hydroxides can be an effective way to boost capacitive performance. Recently, Wen et al. [32] prepared CoP@$Ni(OH)_2$ core-shell composite electrodes via electrodeposition and vapor phase phosphatization methods. As shown in Fig. 6a, the $Ni(OH)_2$ nanosheets were uniformly grown on the nanosheets arrays of CoP. This composite electrode demonstrated the longest discharging time when compared with individual CoP and $Ni(OH)_2$ electrodes (Fig. 6b). The maximum specific capacitance of the composite electrode was found to

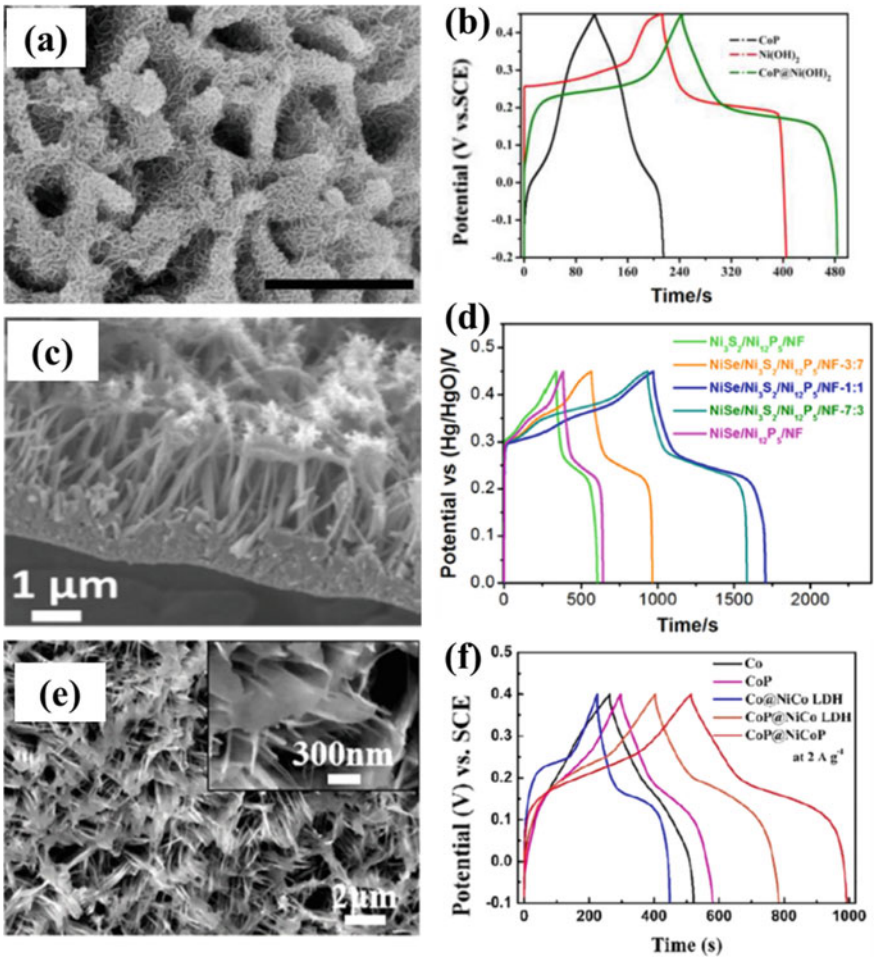

Fig. 6 **a** SEM image of CoP@$Ni(OH)_2$ porous composite, **b** GCD curves of CoP, $Ni(OH)_2$ and CoP@$Ni(OH)_2$ at 4 A g^{-1}, **a–b** adapted with permission from reference [32] Copyright 2017, Elsevier **c** SEM image and **d** GCD curves of $NiSe/Ni_3S_2/Ni_{12}P_5$ composites, **c–d** adapted with permission from reference [33] Copyright 2019, Elsevier **e** SEM image of CoP@NiCoP and **f** GCD curve of CoP@NiCoP and its comparison with other electrodes at 2 A g^{-1}. **e–f** adapted with permission from reference [34] Copyright 2020, Elsevier

be 1989 F g^{-1} at 2 A g^{-1} which was far better than the bare CoP (645 F g^{-1}) and $Ni(OH)_2$ (1659 F g^{-1}) electrodes. Similarly, different phosphide-metal oxide/hydroxide composites have been used for SC such as Ni-P@NiCo LDH, $NiCo_2O_4$/NiCoP, CoP@$Ni(OH)_2$, FeNiP@CoNi-layered double hydroxide, T-Nb_2O_5@Ni_2P, CoP_x/CoO, CuCo-P@$Ni(OH)_2$

Metal phosphide-metal chalcogenide composites: It was highly desirable to improve the capacitive performance of phosphides by hybridizing them with metal chalcogenides such as nickel sulfide and selenide, cobalt sulfide, and vanadium sulfide. Different composites such as NiFeP@$NiCo_2S_4$, NiVS/NiCuP, Ni-Mo-S@Ni-P have been prepared so far. For instance, Tao et al. [33] grew $Ni_{12}P_5$ nanoparticles on the surface of NiSe/Ni_3S_2 nanofibers as shown in Fig. 6c. This heterostructured electrode showed a large mass-loading of 8.5 mg cm^{-2} that could provide a high areal capacity of 2.04 mA h cm^{-2} at 10 mA cm^{-2} along with the superior cyclic life which was quite comparable with other compositions (Fig. 6d).

Phosphide-phosphide composites: Although the phosphide-phosphide composite materials have been reported for SC, much work is devoted to preparing core/shell heterostructured nanocomposites owing to their high surface area and relatively good electrical conductivity that offers a number of electrochemically active sites for faradaic reactions and rapid charge transfer, respectively. For instance, Wang et al. [34] synthesized CoP@NiCoP composite on Ni foam via facile two-step hydrothermal and phosphorization methods (Fig. 6e). As depicted in Fig. 6f, this composite electrode showed the longest discharging time than other composites. The corresponding specific capacitance was found to be 1911.6 F g^{-1} at 2 A g^{-1}.

4.3 Metal Phosphide-Carbon Composites

Metal phosphides have been considered as good conducting material as compared with their oxide counterpart. However, the conductivity of the bare phosphide material is not up to the mark to facilitate high-rate capability. Also, the rate capability does not only depend on the conductivity of the electrode but also depends on the specific surface area and the porosity of the electrode. Bare metal phosphides still suffer due to their poor specific surface area and compact microstructure. Therefore, it is anticipated to combine them with highly conducting and porous carbon materials. For instance, Shao et al. [35] synthesized 3D hierarchical $Ni_xCo_{1-x}O$/$Ni_yCo_{2-y}P$@C hybrid electrode via phosphorization treatment of hierarchical $Ni_xCo_{1-x}O$@C grown on Ni foam (Fig. 7a). This hybrid electrode demonstrated the longest discharging time as compared with other bare phosphide and oxide electrodes (Fig. 7b). This 3D, nanostructured, and highly stable hybrid electrode depicted a maximum specific capacitance of 2638 F g^{-1} at 1 A g^{-1}. Similarly, different phosphide-carbon composite materials have been prepared for SC application including, NiCoP/C, Ni_2P@N-C, CoP/C, CoP–CoNC/CC, Ni-Ni_xP_y@C, MoP/NPC, C-doped Co–Mn–Fe-P, Ni_2P-C, $Ni_{1.4}Co_{0.6}P$@C, etc.

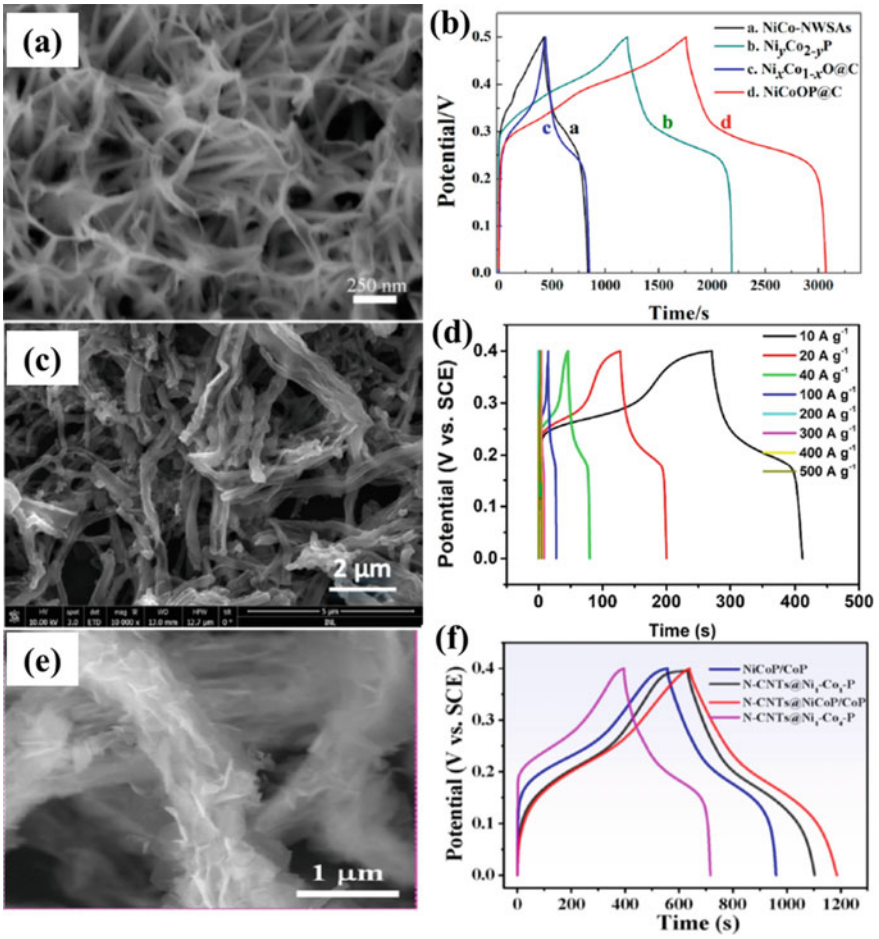

Fig. 7 **a** FESEM image of $Ni_yCo_{2-y}P$, **b** GCD curves of all samples at current density 1 A g^{-1}, **a–b** adapted with permission from reference [35] Copyright 2016, American Chemical Society, **c** SEM image of $Co_{0.1}Ni_{0.9}P$/CNF sample, **d** GCD curves of $Co_{0.1}Ni_{0.9}P$/CNF electrode at different current densities, **c–d** adapted with permission from reference [36] Copyright 2019, American Chemical Society **e** SEM image of N-CNTs@NiCoP/CoP nanosheets and **f** GCD curves of different electrodes at 1 A g^{-1}, **e–f** adapted with permission from reference [37] Copyright 2020, Elsevier

Research and development of flexible SC devices have received great attention in recent years due to their unexceptional role in emerging consumer electronic devices. One of the important components to develop high-performance flexible devices is a flexible and robust current collector. Different current collectors have been recently employed for this purpose including, thin metal foils, carbon paper, graphene paper, carbon fiber cloth, etc. Amongst, the carbon cloth exhibits several advantages such as high flexibility, large surface area, lightweight, and good electronic conductivity. Recently, single and mixed metal phosphides have been coated on carbon cloth for

flexible SC applications. For instance, as shown in the SEM image (Fig. 7c), Zhang et al[36] grew bimetallic $Co_xNi_{1-x}P$ ultrafine nanocrystals on carbon nanofibers and used them as a positive battery-type electrode for hybrid flexible solid-state-SC. The optimized electrode depicted a maximum specific capacity of 1405.6 C g^{-1} (3514 F g^{-1}) at 5 A g^{-1} which outperforms almost all transition metal phosphide-based electrodes (Fig. 7d). Recently, various metal phosphide-based flexible SCs have been reported including AC//NiCoP@NiCoP@CC, $NiCo_2Py$@CC// $NiCo_2Py$@CC, etc.

Although CNTs are expensive, they are widely used for flexible and stretchable SCs. Both single and double-walled CNTs have attracted much research interest due to their excellent electrical conductivity, facile charge transport, good chemical stability, and huge surface area (2000–3000 m^2 g^{-1}). Recently, metal phosphides have been combined with CNTs to improve their rate capability. For instance, Dang et al. [37] deposited NiCoP/CoP nanosheets on the surface of N-doped CNTs via one-step phosphorization of hydroxide precursors (Fig. 7e). As shown in the GCD plots (Fig. 7f), this composite electrode demonstrated the longest discharging time and thereby the maximum specific capacity of 152 mAh g^{-1} at 1 A g^{-1}. Likewise, different CNTs and metal phosphides-based hybrid electrode materials have been fabricated for SCs.

Graphene-based electrodes have been proved to be a promising electrode for electrochemical energy storage devices such as batteries and SCs due to their interesting properties including tunable surface area, good electrical conductivity, and excellent chemical stability. Earlier, An et al. [38] grew Ni_2P nanoparticles on reduced graphene oxide via the low-temperature solid-state reaction method for SCs. This hybrid Ni_2P/rGO electrode demonstrated a maximum capacitance of 2266 F g^{-1} and excellent cyclic stability. This performance is far better than the bare Ni_2P electrode. Recently, different graphene-metal phosphide-based electrodes have been prepared for SC applications, especially, metal phosphides nanostructures are strategically anchored on the graphene surface. Therefore, the preparation of metal phosphide-carbon composites can be a promising strategy to improve the rate capability as well as the cyclic stability of electrodes.

4.4 Metal Phosphide-Conducting Polymer Composite

Metal phosphides have been mostly reported as positive electrode materials in asymmetric SCs. Since, iron-based electrodes such as Fe_2O_3, Fe_3O_4, and FeOOH have been reported as negative electrodes, they can be a good substitute for carbon electrodes. To address the poor conductivity issue of the iron oxide, iron phosphides have been prepared and applied for SC. Besides, the poor stability performance of the iron-based electrodes can be addressed by coating conducting polymers on their surfaces. Luo et al. [39] recently prepared a FeP/PEDOT composite electrode that demonstrated the highest areal capacitance of 790.59 mF cm^{-2} and excellent cyclic stability of 82.12% after 5000 cycles. The stability performance was quite acceptable when compared with the bare FeP electrode. Similarly, different conducting polymers

such as polyaniline, polypyrrole, etc. have been combined with metal phosphides to enhance the SC performance.

5 Metal Chalcogenides

Metal chalcogenides such as sulfides, selenides, and tellurides have been emerged as an important class of materials and successfully explored for energy storage applications including SCs and batteries. The stable chalcogenide crystal structures are formed by combining main group metals, especially, transition metals with VIA group elements (S, Se, and Te). These metal chalcogenides exhibit excellent electrical conductivity and numerous electrochemically active sites as compared to their oxide counterparts. As shown in Fig. 8, metal chalcogenides can be classified into sulfides, selenides, and tellurides. Each of these chalcogenides can be further classified into pristine and their composites with carbon or conducting polymers as discussed below.

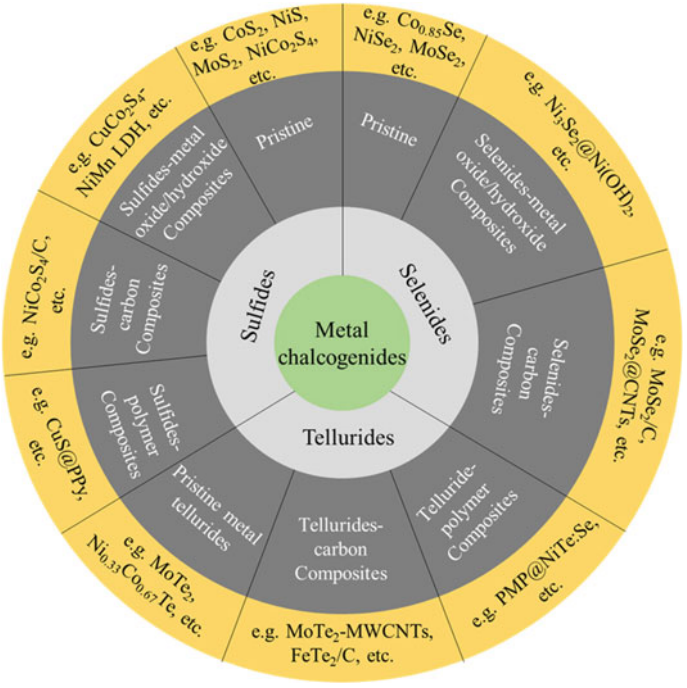

Fig. 8 Classification of metal chalcogenides

5.1 Metal Sulfides

Transition metal sulfides have been considered as promising electrode materials for SCs due to their unique electronic and electrochemical properties. Recently, different types of metal sulfide-based electrodes have been reported which can be classified as pristine metal sulfides, metal sulfide-metal oxide/hydroxide composites, metal sulfide-carbon composites, and metal sulfide-polymer composites as discussed below.

5.1.1 Pristine Metal Sulfides

To understand the intrinsic electrochemical properties of bare metal sulfides, previously various bare sulfides have been prepared and employed for SC application. Pristine sulfides and mixed metal sulfides based on cobalt, nickel, molybdenum, copper, tungsten, etc. have been the prime focus of research.

Cobalt sulfide: The cobalt sulfide has been reported mainly with phases such as CoS, CoS_2, Co_4S_3, Co_3S_4, and Co_9S_8 for SC applications. As shown in CV curves (Fig. 9a), these electrodes show battery-type storage behavior in which charge is stored via reversible faradaic reactions in alkaline electrolytes. General possible electrochemical reactions of cobalt sulfide can be written as $CS + OH^- \leftrightarrow CSOH + H_2O + e^-$ and $CSOH + OH^- \leftrightarrow CSO + H_2O + e^-$, where CS is different phases of cobalt sulfide such as CoS, CoS_2, Co_4S_3, Co_3S_4, Co_9S_8, etc. Since the SC performance highly depends on the morphology and the nano/microstructure of the electrode, similar efforts have been made previously, for instance, Wan et al. [40] performed the size-controlled synthesis of nanotubes-like cobalt sulfide via the hydrothermal method. The effect of reaction temperature on the size of nanostructure and corresponding SC performance has been investigated. The cobalt sulfide nanotubes prepared at 80 °C showed excellent specific capacitance of 285 F g^{-1} at 0.5 A g^{-1}. Similarly, various nanostructures of bare cobalt sulfide have been reported so far.

Nickel sulfide: Recently, pristine nickel sulfide electrodes are widely used in SCs due to their attractive merits such as natural abundance, high capacitance, good conductivity, and environmental benignity. The nickel sulfide has been prepared with different stoichiometric forms such as NiS, NiS_2, Ni_3S_2, Ni_3S_4, Ni_6S_5, Ni_7S_6, and Ni_9S_8. The nickel sulfide electrode is found to be a battery-like electrode with clear oxidation and reduction peaks in the cyclic voltammogram. As a representative example, the Ni_3S_2 store a charge via reversible faradaic reaction in the alkaline electrolyte as shown by the reaction $Ni_3S_2 + 3OH^- \leftrightarrow Ni_3S_2(OH)_3 + 3e^-$ [41]. The pristine nickel sulfide with different morphologies has been reported for SC application.

Molybdenum sulfide: The molybdenum sulfide, especially 2D form, has emerged as a promising material for SC application owing to its interesting electrical, mechanical, and optical properties. It exhibits a graphite-like layered structure with the weak

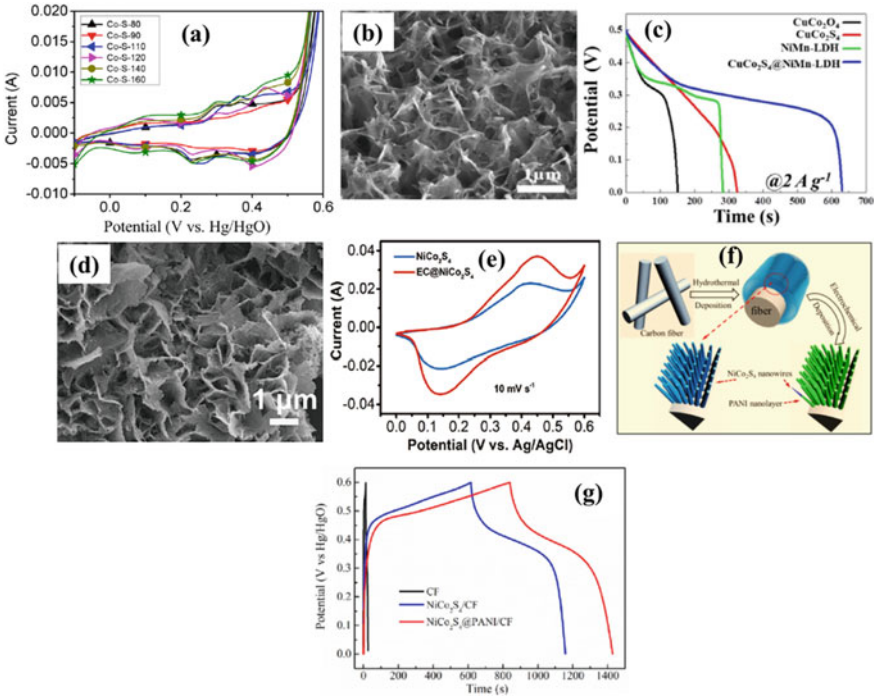

Fig. 9 **a** CV curves of cobalt sulfide electrodes prepared at various temperatures at 10 mV s^{-1}, adapted with permission from reference [40] Copyright 2013, Elsevier, **b** SEM image of $CuCo_2S_4$@NiMn-LDH, **c** GCD curves of different electrodes at 2 A g^{-1}, **b–c** adapted with permission from reference [46] Copyright 2018, Elsevier, **d** SEM image and **e** CV curves of eggplant derived carbon@$NiCo_2S_4$ composite, **d–e** adapted with permission from reference [47] Copyright 2019, Elsevier, **f** Schematics of synthesis of $NiCo_2S_4$@PANI/CF composite and **g** GCD curves of carbon fiber, $NiCo_2S_4$/carbon fiber and $NiCo_2S_4$@PANI/carbon fiber at 2 mA cm^{-2}, **f–g** adapted with permission from reference [51] Copyright 2017, Elsevier

van der Waals force of attraction between the S-Mo-S sandwiched layers. Each layer has a thickness of ~0.65 nm which is double the thickness of graphite layers (0.335 nm). The molybdenum sulfide is a polytypic material that exists in three different phases such as hexagonal (2H), trigonal (3R), and synthetic octahedral (1 T) [42]. The MoS_2 stores charge via both faradaic and non-faradaic processes as described by the reactions $MoS_2 + Na^+ + e^- \leftrightarrow MoS - SNa$ and $(MoS_2) + Na^+ + e^- \leftrightarrow (MoS_2{}^- - Na^+)$, respectively [43]. Recently, MoS_2 is effectively used for flexible SCs, for instance, Javed et al. [44] used MoS_2 to fabricate a solid-state flexible SC that demonstrated a maximum capacitance of 368 F g^{-1} and a high power density of 128 W kg^{-1} at the energy density of 5.42 Wh kg^{-1}.

Mixed metal sulfide: Due to the synergic effect between different elements in the sulfide, it is desirable to prepare multi-metal sulfides for SCs. Recently, various mixed metal sulfides have been prepared, for instance, copper-cobalt, copper-tungsten, iron-cobalt, nickel-cobalt, zinc-cobalt, etc. Among these, nickel-cobalt sulfide has

attracted great attention due to its high conductivity and rich redox-active sites. Owing to the high theoretical specific capacitance (2111 F g^{-1}), the $NiCo_2S_4$ phase is predominantly reported for SCs. Previously, various morphologies of $NiCo_2S_4$ have been reported including nanoflakes, nanoparticles, nanosheets, nanotubes, and nanowires. The hollow structure of $NiCo_2S_4$ shows additional benefits for electrochemical applications. For instance, Shen et al. [45] prepared complex ball-in-ball hollow spheres of $NiCo_2S_4$ via an anion exchange method for pseudocapacitor. Interestingly, this electrode demonstrated a maximum specific capacitance of 1,036 F g^{-1} at 1.0 A g^{-1}. A hybrid SC combined with graphene/carbon negative electrode showed an excellent energy density of 42.3 Wh kg^{-1} at a power density of 476 W kg^{-1}. The nanosheets of $NiCo_2S_4$ have been frequently reported for SC due to their high surface area and numerous active sites. Therefore, it is seen that the mixed metal sulfide are promising electrodes when compared with single metal sulfides.

5.1.2 Metal Sulfide-Metal Oxide/Hydroxide Composites

Apart from the pristine metal sulfides, metal sulfides composited with other metal oxides/ hydroxides have been a focus of research. The metal oxide/hydroxide normally exhibits poor electrical conductivity. To improve their electrical conductivity and enhance the surface area, metals oxides/hydroxides are composited with metal sulfides. Recently, most of the research is focused on preparing core/shell heterostructures by using metal sulfide core and oxide/hydroxides shell materials. For instance, Lin et al. [46] hydrothermally prepared a hybrid structure on nickel foam which consists of $CuCo_2S_4$ core and NiMn-layered double hydroxide (LDH) shell. As shown in Fig. 9b, NiMn LDH was conformally coated on the surface of $CuCo_2S_4$. This hybrid core-shell structured electrode depicted the longest discharging time when compared with bare oxide ($CuCo_2O_4$), sulfide ($CuCo_2S_4$), and LDHs (NiMn LDH) electrodes (Fig. 9c). The maximum specific capacitance was reported to be 2520 F g^{-1} at 2 A g^{-1}. It is seen that the merits of highly conductive sulfide and high surface area hydroxides can be combined by simply preparing core-shell heterostructures. Besides, to get benefitted from the structural and compositional merits, recently, metal sulfides have been composited with different single metal and mixed metal chalcogenides for SC application.

5.1.3 Metal Sulfide-Carbon Composite

Although various nanostructures and compositions of metal sulfides have been reported so far, they still face issues such as unsatisfactory unitization of active material, low specific surface area, and poor conductivity. These issues can be addressed by combining them with carbonaceous materials including porous carbon, CNTs, graphene, etc. Much research is focused on preparing composites with carbon, graphene, and CNTs. For instance, Liu et al. [47] derived high surface area (3608.4 m^2 g^{-1}) carbon flakes material from eggplant and used them as substrates for depositing

$NiCo_2S_4$ nanosheets. This kind of architecture (Fig. 9d) may facilitate high active surface area, accelerating ionic and electronic transport. As shown in Fig. 9e, the area under the CV curve of the composite electrode was greater than that of the bare $NiCo_2S_4$ electrode. Moreover, this composite showed an excellent specific capacitance of 1394.5 F g^{-1} at 1 A g^{-1} which was quite higher than that of the bare metal sulfide electrode. It is observed that the hybrid electrode made of metal sulfide-carbon composite increases the capacitance value by almost 2-folds [48]. This is mainly because of the reduced equivalent series resistance and high surface area nanostructured carbon materials. In this way, the rate performance of metal sulfides can be effectively improved by combining them with cost-effective carbon materials.

CNTs are considered to be one of the most fascinating carbonaceous materials due to their unique 1D tubular structure and ultra-high conductivity. When CNTs-based materials are used as SC electrodes, they do not only improve the conductivity but also upgrade the stability of the electrode materials. Dai et al. [49] prepared a hybrid electrode by growing Ni_3S_2 nanoparticles on multi-walled CNTs (MWCNTs). This electrode demonstrated excellent capacitive performance as compared with the bare Ni_3S_2 and MWCNTs electrodes. The improved capacitive and stability performance was attributed to the synergic effect, lower charge transfer resistance, and the better diffusion of the hybrid electrode.

Metal sulfides are also combined with graphene, for instance, Liu et al. [50] prepared a sandwich-like composite by embedding $Co_{0.33}Fe_{0.67}S_2$ nanoparticles into the graphene nanosheets via one-step hydrothermal method. This robust electrode showed an excellent specific capacity of 310.2 C g^{-1} at 2 mV s^{-1} and an exceptional rate capability of 61.8% at 200 mV s^{-1}.

5.1.4 Metal Sulfide-Conducting Polymer Composites

Conducting polymers such as polyaniline, polypyrrole, polythiophene, and derivatives of polythiophene have been commonly used for SC applications. These pseudocapacitive conducting polymers have attracted great attention due to their high theoretical capacitance, good chemical stability, excellent conductivity, low cost, and easy preparation. Recently, to benefit from the high conductivity, metal sulfides have been combined with conducting polymers including polypyrrole and polyaniline. For instance, Liu et al. [51] synthesized carbon fiber supported, polyaniline-coated $NiCo_2S_4$ nanowires via hydrothermal and potentiostatic deposition methods as illustrated in the schematic (Fig. 9f). As shown in the GCD plots (Fig. 9g), this composite electrode demonstrated the longest discharging time and therefore the capacitance (823 F g^{-1} at 2 mA cm^{-2}) as compared to their counterparts.

5.2 Metal Selenides

Since selenide is the nearest neighbor of sulfide in the VI group, it has the same valence electrons and oxidation number as sulfur. Therefore, most of the chemical and electrochemical properties of metal selenides are similar to that of metal sulfides. In the following section, we have discussed the SC properties of metal selenides. These metal selenides have been classified into pristine metal selenides, metal selenide-metal oxide/hydroxide composites, metal selenide-carbon composites, and metal selenide-conducting polymer composites.

5.2.1 Pristine Metal Selenides

Previously, much research work was focused on synthesizing pristine single metal or multi-metal selenides for SC applications. Pristine selenides based on cobalt, nickel, molybdenum, manganese, copper, and cerium have been reported so far. Besides, multi-metallic selenides, especially binaries and ternaries of the aforementioned elements have also been prepared for SC application. SC properties of some important pristine metal selenides have been discussed below.

Cobalt selenide: Cobalt selenide has attracted great attention due to its inexpensiveness and high reversibility. In alkaline electrolyte, it shows battery-type behavior with two distinct oxidation and reduction peaks in the cyclic voltammogram. Cobalt selenides can be prepared with different phases such as $Co_{0.85}Se$, Co_3Se_4, $CoSe_2$, Co_2Se_3, and CoSe. However, among these phases, the $Co_{0.85}Se$ $CoSe_2$, and CoSe have been frequently reported for SC application owing to their high electrochemical activity. As a typical example, $Co_{0.85}Se$ stores charge via reversible redox processes described by the reactions $Co_{0.85}Se + OH^- \leftrightarrow Co_{0.85}SeOH + e^-$ and $Co_{0.85}SeOH + OH^- \leftrightarrow Co_{0.85}SeO + H_2O + e^-$. To improve the storage performance of the cobalt selenide, different nanostructures have been prepared, for instance, Rabani et al. [52] grew 1D-$CoSe_2$ nanoarrays on Ti foil via wet chemical ion-exchange method. This electrode was employed to fabricate symmetric SC that showed an excellent energy density of 21.1 Wh kg^{-1} at a power density of 0.5 kW kg^{-1}.

Nickel selenide: The nickel selenide shows a battery-type storage mechanism, leading to a very high specific capacity. Recently different phases of nickel selenide have been reported for SC application including $Ni_{0.85}Se$, $NiSe_2$, NiSe, Ni_3Se_2, etc. Amongst, the $Ni_{0.85}Se$ exhibits numerous electrochemical active sites and rapid charge-transfer channels [53]. The possible reversible reaction during the charging-discharging process can be given as $Ni_{0.85}Se+OH^- \leftrightarrow Ni_{0.85}SeOH+e^-$ and $Ni_{0.85}SeOH+OH^- \leftrightarrow Ni_{0.85}SeO + H_2O+e^-$. It is observed that the phase NiSe prepared via electrodeposited method depicted superior capacitive performance (1644.7 F g^{-1}) as compared to the phase Ni_3Se_2 (581.1 F g^{-1}) [54]. Since the performance of nickel sulfide is mainly attributed to the surface morphology, the nickel sulfide has been prepared with different microstructures. As shown in Fig. 10a, the nanoflowers of $Ni_{0.85}Se$ were prepared by Kuai et al. [55] via a two-step

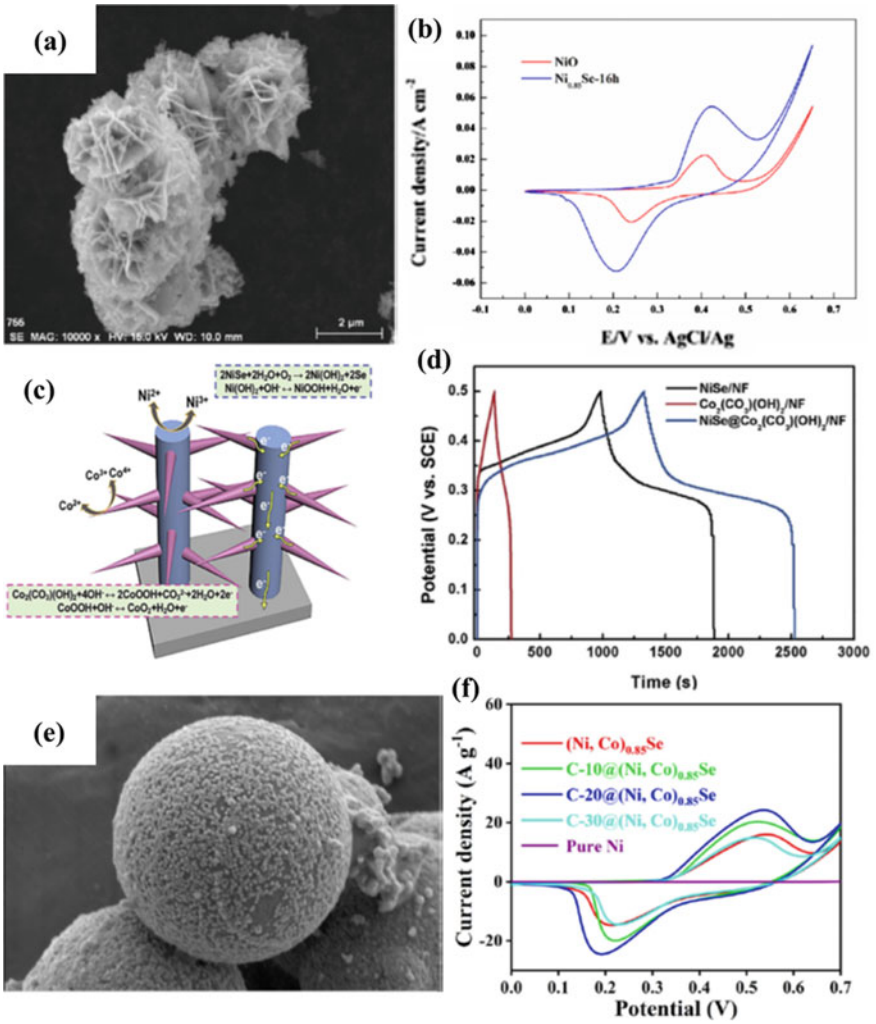

Fig. 10 **a** SEM image of $Ni_{0.85}Se$ sample, **b** CV curves of NiO and $Ni_{0.85}Se$ electrodes, **a–b** adapted with permission from reference [55] Copyright 2019, Elsevier, **c** Schematic of storage mechanism of $NiSe@Co_2(CO_3)(OH)_2$ nanowire arrays, **d** GCD curves of all electrodes at 4mA cm^{-2}, **c–d** adapted with permission from reference [61] Copyright 2019, Elsevier **e** SEM image of C-20@(Ni, $Co)_{0.85}Se$ composite and **f** CV curves of composites with different masses of carbon microspheres, **e–f** adapted with permission from reference [64] Copyright 2021, Elsevier

hydrothermal method. This nanostructure provides intimate contact between electrode and electrolyte for the electrochemical process, leading to longer discharging time as compared to its oxide counterpart (Fig. 10b). The areal capacitance estimated for this electrode was 3.6-fold greater than that of NiO. Besides, the porosity of the electrode highly impacts the capacitive performance, some efforts have been

made to enhance the porosity of the nickel sulfide electrode. For instance, Yu et al. [56] prepared a porous nanosheet network of NiSe via selenylation/pickling of as prepared manganese-doped α-$Ni(OH)_2$. This porous battery-type electrode showed a high specific capacity of 443 mAh g^{-1} at 3.0 A g^{-1}. Therefore, it is concluded that most of the research work was focused on preparing different morphologies, phases and porous structures of nickel selenides.

Molybdenum selenide: The $MoSe_2$ is considered to be a promising SC electrode due to its layered structure and high electrical conductivity as compared with its sulfide counterpart. It has strong in-plane bonding and weak out-of-plane interactions, leading to an exfoliation into 2D layers. Due to its battery-type nature, the $MoSe_2$ stores charge via reversible faradaic redox reaction through the electrochemical reaction, $MoSe_2 + Na^+ + e^- \leftrightarrow$ Na-$MoSe_2$ in an alkaline electrolyte [57]. The theoretical capacity of the $MoSe_2$ is 422 mA h g^{-1} [58]. Previously, the $MoSe_2$ has been prepared with different morphologies and structures for SC application. For instance, Zhang et al. [59] synthesized flower-like $MoSe_2$ via the facile hydrothermal method. This electrode showed a maximum capacity of 641.5 mAh g^{-1} at 0.1 A g^{-1} with excellent rate capability by retaining the capacity of 380.3 mAh g^{-1} at a high current density of 5 A g^{-1}. Furthermore, a hybrid lithium-ion capacitor ($MoSe_2$//AC) demonstrated an ultra-high energy density of 78.75 Wh kg^{-1} at 3600 W kg^{-1}.

5.2.2 Metal Selenide-Metal Oxide/Hydroxide Composite

It is well accepted that metallic doping enhances the electrical conductivity of the materials. Recently, metal selenides have been doped with different metals such as Ni, Co, Mn, Sn, and W and employed for SCs. Particularly, the isoelectronic (having the same number of electrons) doping in metal selenide causes modification in the electrical and optical properties. Bhat et al. [60] recently prepared tungsten-doped molybdenum selenide (W-$MoSe_2$). The $MoSe_2$ doped with 2M % of W showed a maximum specific capacitance of 147 F g^{-1}.

To improve the conductivity and the rate capability of the oxide/hydroxide materials, metal selenide has been considered as a promising choice. For instance, Yuan et al. [61] synthesized hierarchical NiSe@$Co_2(CO_3)(OH)_2$ heterogeneous nanowire arrays onto the Ni foam via a two-step soft-chemical approach. As depicted in the schematic (Fig. 10c), the NiSe serves as a bridge for electronic transport between $Co_2(CO_3)(OH)_2$ and the current collector. Interestingly, this nanostructure prevents the agglomeration of $Co_2(CO_3)(OH)_2$ and offers high mass loading as well as efficient utilization of active materials. As illustrated in the GCD curves (Fig. 10d), the NiSe@$Co_2(CO_3)(OH)_2$ electrode demonstrated the longest discharging time and the areal capacitance (9.56 F cm^{-2}) as compared with their counterparts. To integrate the benefits of metal selenides and oxides, different composites have been prepared for SC application.

Besides, as compared with individual metal selenides, the co-existence of active sites of mixed-phase metal selenides may facilitate an additional number of multi-electron redox reactions. For instance, Ye et al. [62] prepared NiSe/ZnSe mixed-phase nanostructure via co-electrodeposition method on nickel foam. It is observed that the Ni/Zn ratio significantly influences the SC performance. The Ni/Zn ratio of 2:1 was found suitable that provided a specific capacity of 651.5 mAh g^{-1} at 1 A g^{-1}. Previously, various mixed-phase metal selenides have been prepared for SC application including $MnSe_2$-$CoSe_2$, Cu_2Se@Co_3Se_4, NiSe-$Ni_{0.85}Se$, Cu_7Se_4-$Cu_xCo_{1-x}Se_2$, $NiCoSe_2$/$Ni_{0.85}Se$, etc. Recently, metal selenides have also been combined with Mxene to enlarge the spacing and prevent the agglomeration and stacking of the layers [63].

5.2.3 Metal Selenide-Carbon Composites

To improve the electronic/ionic diffusion, conductivity, and electrochemically active surface area, metal selenides have been combined with different carbonaceous materials such as carbon, CNTs, and graphene. For instance, Wu et al. [64] prepared a core-shell structure by growing cobalt and nickel selenide nanoparticles on a carbon microsphere. As shown in Fig. 10e, nanoparticles of $(Ni, Co)_{0.85}Se$ were uniformly coated on the surface of the carbon microsphere. In this work, carbon-$(Ni, Co)_{0.85}Se$ composites were prepared with different amounts of carbon ranging from 0 to 30 mg. The composite formed at 20 mg of carbon demonstrated the highest area under the CV curve as compared with other compositions and bare components (Fig. 10f). The maximum specific capacitance was found to be 960 F g^{-1} along with excellent stability of 85% after 2000 cycles. In another work, the $MoSe_2$ nanotubes were combined with carbon net and the ratio between selenide and carbon was optimized. The ratio of 3:1 showed excellent SC performance as compared with other compositions [17]. Similar efforts have been made previously [65, 66].

As an imperative carbonaceous material, CNTs do not only facilitate high electrical conductivity but also serve as a framework for growing various nanostructured metal selenide materials. For instance, Liu et al. [67] grew $MoSe_2$ nanoflakes on a vertically aligned CNT array by combining chemical vapor deposition and solvothermal methods. This kind of nanostructure provides a rapid transfer of ions and reduces the effect of volume changes during the charging-discharging process. Apart from nanostructuring, CNTs can also be simply combined with metal selenides for the enhancement of capacitive performance.

Graphene is considered one of the important carbonaceous materials due to its high conductivity and high specific surface area. Recently, much work was executed on combining metal selenides with graphene for SCs. The metal selenide-graphene nanocomposite needs to be optimized to achieve a proper synergic effect between them. It is observed that nitrogen-doped graphene also enhances the performance of metal selenide-based composites [68]. Besides, to achieve structural benefits, graphene, along with metal selenide has been used to develop hollow 3D structures. For instance, Zardkhoshoui et al. [69] prepared graphene encapsulated multi-shelled

zinc-cobalt selenide hollow nanospheres and graphene encapsulated yolk-double shell cobalt iron selenide hollow nanospheres, as positive and negative electrodes, respectively for SC. Preparation of 3D graphene scaffolds offers large specific surface area, excellent porosity, and superior physicochemical stability. Recently, efforts have been made on developing metal selenide-3D graphene composites for SCs [70].

5.3 Metal Tellurides

Recently, metal tellurides have become one of the important classes of materials owing to their superior optical, electronic, catalytic, and biological properties. Previously, a significant number of metal tellurides have been prepared and successfully employed for SCs. As described below, these metal tellurides can be classified as pristine, metal telluride-carbon composites, and metal telluride-polymer composites.

5.3.1 Pristine

As compared with other metal chalcogenides (sulfides and selenides), very little but a significant amount of work has been reported on the synthesis and electrochemical characterization of metal tellurides. Most of the reports focus on synthesizing pristine metal tellurides with various morphologies for SCs. For instance, cobalt, gallium, lanthanum, molybdenum, nickel, samarium, and tantalum tellurides have been prepared for SCs. Most of the pristine metal tellurides have been prepared with nanosheets-like morphology that showed excellent electrochemical properties. Besides, as depicted in Fig. 11a, rod-like NiTe was grown onto Ni foam via a simple hydrothermal route by Zhou et al. [71] This electrode showed a battery-type sluggish charge storage mechanism with distinct redox peaks as shown in Fig. 11b. For this electrode, the maximum specific capacitance was reported to be 804 F g^{-1} at 1 A g^{-1}. It is noteworthy that the synthesis of ultrathin $MoTe_2$ nanosheets is quite difficult as compared with molybdenum sulfide/selenides due to the lesser electronegativity difference between Te and Mo (0.3 eV). Liu et al. [72] synthesized ultrathin nanosheets of 1T'-$MoTe_2$ via a colloidal chemical strategy. In this work, the shape of the 1T'-$MoTe_2$ was controlled by altering the molybdenum precursors and the reaction atmosphere. The optimized 1T' -$MoTe_2$ nanosheets demonstrated a high specific capacitance of 1393 F g^{-1} at 1 A g^{-1}. Besides, it can be observed that metal tellurides have been reported as both pseudocapacitive and battery-like materials. For instance, metal tellurides based on Co, Ni, and Mo have been reported mainly as the battery-like positive electrode in alkaline electrolytes, whereas, tellurides based on rare earth elements such as samarium and lanthanum depict pseudocapacitive characteristics.

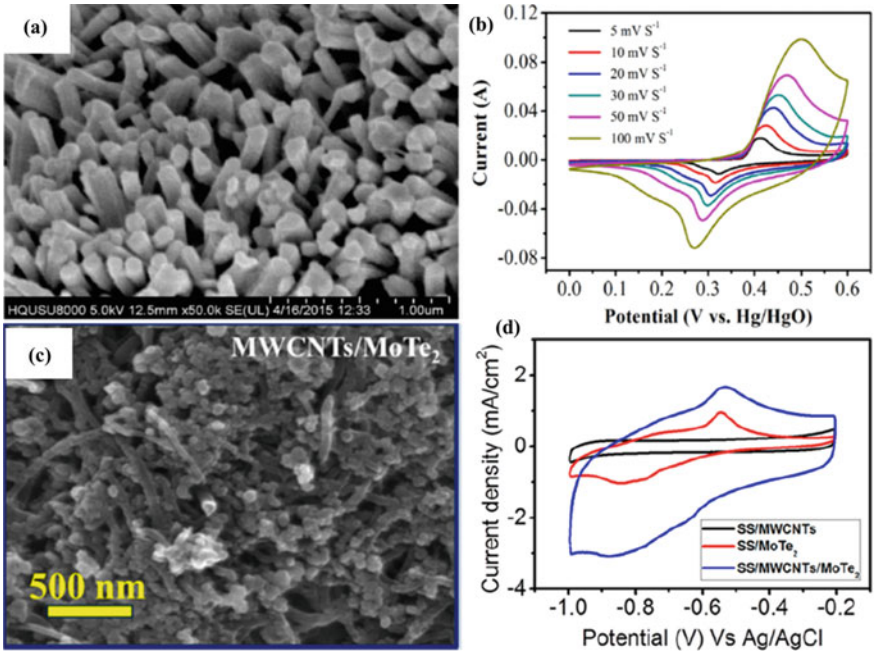

Fig. 11 **a** FESEM image of NiTe rods, **b** CV curves of NiTe rods at different scan rates, **a–b** adapted with permission from reference [71] Copyright 2016, Elsevier, (c) SEM image of $MoTe_2$-MWCNTs composite and **d** CV curves of $MoTe_2$-MWCNTs composite, bare $MoTe_2$ and MWCNTs at 100 mV s^{-1}, **c–d** adapted with permission from reference [73] Copyright 2018, American Chemical Society

5.3.2 Metal Telluride-Carbon Composite

In metal sulfides and selenides, almost all of the important carbon materials have been composited to achieve superior SC performance. However, metal tellurides have been combined with very few selected carbon materials. For instance, Karade et al. [73] prepared $MoTe_2$-MWCNTs composite via successive ionic layer adsorption and reaction (SILAR) method. As shown in Fig. 11c, the $MoTe_2$ and MWCNTs were thoroughly mixed which is quite imperative to achieve synergy between them. This composite electrode demonstrated the largest area under the CV curve when compared with bare $MoTe_2$ and MWCNTs electrodes (Fig. 11d). The composite depicted a maximum specific capacitance of 502 F g^{-1} at the sweep rate of 2 mV s^{-1}. Moreover, the flexible solid-state symmetric SC formed of this composite electrode demonstrated excellent flexibility.

5.3.3 Metal Telluride-Conducting Polymer Composite

Conducting polymers not only provides highly conducting frameworks but also helps in storing charge via doping/de-doping. Although conducting polymers exhibit superior properties such as high specific capacitance, good rate capability and facile synthesis, to achieve synergic between metal tellurides and the conducting polymers, a significant amount of work has not been done yet in this field. Very few researches have been reported so far, for instance, Deshagani et al. [74] prepared selenide doped nickel telluride material as battery-type positive electrode and AC as negative electrode for hybrid SC. Furthermore, both electrodes were coated with poly(N-methyl pyrrole) (PMP) polymer. This PMP@AC//PMP@NiTe:Se SC demonstrated a maximum energy density of 90 Wh kg^{-1}, at 400 W kg^{-1}.

6 Conclusions

In this chapter, initially, the construction and charge storage mechanism of the SC are briefly discussed. Since the nanostructured metal phosphides and chalcogenides have been prepared with various methods, one of the important protocols such as hydrothermal synthesis has been explained. The important factors influencing the SC performance have been discussed in great detail such as morphology, synergy, and hybridization. Based on the components used, phosphides and chalcogenides have been classified into pristine and their composites with metal oxide/hydroxide, carbon, and conducting polymers. Each of these types is thoroughly described based on the nanostructure, charge storage mechanism, and SC performance. It is seen that efforts have been made to synthesize pristine phosphides and chalcogenides with different morphologies and nanoarchitecture. Due to the compositional synergic effect, the multi-metallic phosphides and chalcogenides attract great attention. The rate and cyclic stability of phosphides and chalcogenides can be effectively improved by preparing their composites with carbonaceous materials such as carbon, CNTs, and graphene. In summary, phosphides and chalcogenides are found to be cost-effective, reliable, and stable electrode materials for fabricating high-performance supercapacitors.

References

1. Z. Yang, J. Zhang, M.C.W. Kintner-Meyer, X. Lu, D. Choi, J.P. Lemmon, J. Liu, Electrochemical energy storage for green grid. Chem. Rev. **111**, 3577–3613 (2011)
2. A. Jagadale, X. Zhou, R. Xiong, D.P. Dubal, J. Xu, S. Yang, Lithium-ion capacitors (LICs): Development of the materials. Energy Storage Mater. **19**, 314–329 (2019)
3. A. Borenstein, O. Hanna, R. Attias, S. Luski, T. Brousse, D. Aurbach, Carbon-based composite materials for supercapacitor electrodes: a review. J. Mater. Chem. A. **5**, 12653–12672 (2017)

4. Y. Shao, M.F. El-Kady, J. Sun, Y. Li, Q. Zhang, M. Zhu, H. Wang, B. Dunn, R.B. Kaner, Design and mechanisms of asymmetric supercapacitors. Chem. Rev. **118**, 9233–9280 (2018)
5. E.E. Miller, Y. Hua, F.H. Tezel, Materials for energy storage: review of electrode materials and methods of increasing capacitance for supercapacitors. J. Energy Storage **20**, 30–40 (2018)
6. A. Agarwal, B.R. Sankapal, Metal phosphides: topical advances in the design of supercapacitors. J. Mater. Chem. A. **9**, 20241–20276 (2021)
7. Y. Shi, B. Zhang, Recent advances in transition metal phosphide nanomaterials: synthesis and applications in hydrogen evolution reaction. Chem. Soc. Rev. **45**, 1529–1541 (2016)
8. X. Chen, M. Cheng, D. Chen, R. Wang, Shape-controlled synthesis of Co2P nanostructures and their application in supercapacitors. ACS Appl. Mater. Interfaces. **8**, 3892–3900 (2016)
9. K. Narthana, G. Durai, P. Kuppusami, J. Theerthagiri, S. Sujatha, S.J. Lee, M.Y. Choi, One-step synthesis of hierarchical structured nickel copper sulfide nanorods with improved electrochemical supercapacitor properties. Int. J. Energy Res. **45**, 9983–9998 (2021)
10. Z. Zheng, M. Retana, X. Hu, R. Luna, Y.H. Ikuhara, W. Zhou, Three-dimensional cobalt phosphide nanowire arrays as negative electrode material for flexible solid-state asymmetric supercapacitors. ACS Appl. Mater. Interfaces. **9**, 16986–16994 (2017)
11. N. Liu, Z. Pan, X. Ding, J. Yang, G. Xu, L. Li, Q. Wang, M. Liu, Y. Zhang, In-situ growth of vertically aligned nickel cobalt sulfide nanowires on carbon nanotube fibers for high capacitance all-solid-state asymmetric fiber-supercapacitors. J. Energy Chem. **41**, 209–215 (2020)
12. F. Liang, L. Huang, L. Tian, J. Li, H. Zhang, S. Zhang, Microwave-assisted hydrothermal synthesis of cobalt phosphide nanostructures for advanced supercapacitor electrodes. CrystEngComm. **20**, 2413–2420 (2018)
13. G.-Q. Zhang, B. Li, M.-C. Liu, S.-K. Yuan, L.-Y. Niu, Liquid phase synthesis of CoP nanoparticles with high electrical conductivity for advanced energy storage. J. Nanomater. e9728591 (2017)
14. K. Krishnamoorthy, P. Pazhamalai, S.J. Kim, Ruthenium sulfide nanoparticles as a new pseudocapacitive material for supercapacitor. Electrochimica Acta. **227**, 85–94 (2017)
15. Q. Zhang, W.-B. Zhang, P. Hei, Z. Hou, T. Yang, J. Long, CoP nanoprism arrays: Pseudocapacitive behavior on the electrode-electrolyte interface and electrochemical application as an anode material for supercapacitors. Appl. Surf. Sci. **527**, 146682 (2020)
16. Y.-C. Chen, Z.-B. Chen, Y.-G. Lin, Y.-K. Hsu, Synthesis of copper phosphide nanotube arrays as electrodes for asymmetric supercapacitors. ACS Sustain. Chem. Eng. **5**, 3863–3870 (2017)
17. M. Ojha, M. Deepa, Molybdenum selenide nanotubes decorated carbon net for a high performance supercapacitor. Chem. Eng. J. **368**, 772–783 (2019)
18. C. Zhou, T. Gao, Y. Wang, Q. Liu, D. Xiao, Through a hydrothermal phosphatization method synthesized NiCo and Fe-based electrodes for high-performance battery-supercapacitor hybrid device. Appl. Surf. Sci. **475**, 729–739 (2019)
19. D. Zha, Y. Fu, L. Zhang, J. Zhu, X. Wang, Design and fabrication of highly open nickel cobalt sulfide nanosheets on Ni foam for asymmetric supercapacitors with high energy density and long cycle-life. J. Power Sources **378**, 31–39 (2018)
20. X. Cao, D. Jia, D. Li, L. Cui, J. Liu, One-step co-electrodeposition of hierarchical radial NixP nanospheres on Ni foam as highly active flexible electrodes for hydrogen evolution reaction and supercapacitor. Chem. Eng. J. **348**, 310–318 (2018)
21. Y. Jin, C. Zhao, L. Wang, Q. Jiang, C. Ji, X. He, Preparation of mesoporous Ni2P nanobelts with high performance for electrocatalytic hydrogen evolution and supercapacitor. Int. J. Hydrogen Energy. **43**, 3697–3704 (2018)
22. Z. Liang, C. Qu, W. Zhou, R. Zhao, H. Zhang, B. Zhu, W. Guo, W. Meng, Y. Wu, W. Aftab, Q. Wang, R. Zou, Synergistic effect of Co–Ni hybrid phosphide nanocages for ultrahigh capacity fast energy storage. Adv. Sci. **6**, 1802005 (2019)
23. J. Wei, X. Li, H. Xue, J. Shao, R. Zhu, H. Pang, Hollow structural transition metal oxide for advanced supercapacitors. Adv. Mater. Interfaces **5**, 1701509 (2018)
24. M. Gao, W.-K. Wang, X. Zhang, J. Jiang, H.-Q. Yu, Fabrication of metallic nickel-cobalt phosphide hollow microspheres for high-rate supercapacitors. J. Phys. Chem. C. **122**, 25174–25182 (2018)

25. Q. Zhou, Y. Gong, K. Tao, Calcination/phosphorization of dual Ni/Co-MOF into NiCoP/C nanohybrid with enhanced electrochemical property for high energy density asymmetric supercapacitor. Electrochimica Acta. **320**, 134582 (2019)
26. Y. Shi, M. Li, Y. Yu, B. Zhang, Recent advances in nanostructured transition metal phosphides: synthesis and energy-related applications. Energy Environ. Sci. **13**, 4564–4582 (2020)
27. B. Liang, Z. Zheng, M. Retana, K. Lu, T. Wood, Y. Ai, X. Zu, W. Zhou, Synthesis of FeP nanotube arrays as negative electrode for solid-state asymmetric supercapacitor. Nanotechnology **30**, 295401 (2019)
28. S. Liu, K.V. Sankar, A. Kundu, M. Ma, J.-Y. Kwon, S.C. Jun, Honeycomb-like interconnected network of nickel phosphide heteronanoparticles with superior electrochemical performance for supercapacitors. ACS Appl. Mater. Interfaces **9**, 21829–21838 (2017)
29. K. Zhou, W. Zhou, L. Yang, J. Lu, S. Cheng, W. Mai, Z. Tang, L. Li, S. Chen, Ultrahigh-performance pseudocapacitor electrodes based on transition metal phosphide nanosheets array via phosphorization: a general and effective approach. Adv. Funct. Mater. **25**, 7530–7538 (2015)
30. P. Li, M. Zhang, H. Yin, J. Yao, X. Liu, S. Chen, Hierarchical mesoporous NiCoP hollow nanocubes as efficient and stable electrodes for high-performance hybrid supercapacitor. Appl. Surf. Sci. **536**, 147751 (2021)
31. H. Liang, C. Xia, Q. Jiang, A.N. Gandi, U. Schwingenschlögl, H.N. Alshareef, Low temperature synthesis of ternary metal phosphides using plasma for asymmetric supercapacitors. Nano Energy. **35**, 331–340 (2017)
32. J. Wen, S. Li, T. Chen, B. Li, L. Xiong, Y. Guo, G. Fang, Porous nanosheet network architecture of CoP@Ni(OH)2 composites for high performance supercapacitors. Electrochimica Acta. **258**, 266–273 (2017)
33. K. Tao, Y. Gong, J. Lin, Epitaxial grown self-supporting NiSe/Ni3S2/Ni12P5 vertical nanofiber arrays on Ni foam for high performance supercapacitor: matched exposed facets and re-distribution of electron density. Nano Energy **55**, 65–81 (2019)
34. X. Wang, C. Jing, W. Zhang, X. Wang, X. Liu, B. Dong, Y. Zhang, One-step phosphorization synthesis of CoP@NiCoP nanowire/nanosheet composites hybrid arrays on Ni foam for high-performance supercapacitors. Appl. Surf. Sci. **532**, 147437 (2020)
35. Y. Shao, Y. Zhao, H. Li, C. Xu, Three-dimensional hierarchical NixCo1–xO/NiyCo2–yP@C hybrids on nickel foam for excellent supercapacitors. ACS Appl. Mater. Interfaces **8**, 35368–35376 (2016)
36. N. Zhang, Y. Li, J. Xu, J. Li, B. Wei, Y. Ding, I. Amorim, R. Thomas, S.M. Thalluri, Y. Liu, G. Yu, L. Liu, High-performance flexible solid-state asymmetric supercapacitors based on bimetallic transition metal phosphide nanocrystals. ACS Nano **13**, 10612–10621 (2019)
37. T. Dang, D. Wei, G. Zhang, L. Wang, Q. Li, H. Liu, Z. Cao, G. Zhang, H. Duan, Homologous NiCoP/CoP hetero-nanosheets supported on N-doped carbon nanotubes for high-rate hybrid supercapacitors. Electrochimica Acta **341**, 135988 (2020)
38. C. An, Y. Wang, Y. Wang, G. Liu, L. Li, F. Qiu, Y. Xu, L. Jiao, H. Yuan, Facile synthesis and superior supercapacitor performances of Ni2P/rGO nanoparticles. RSC Adv. **3**, 4628–4633 (2013)
39. J. Luo, Z. Zheng, A. Kumamoto, W.I. Unah, S. Yan, Y.H. Ikuhara, X. Xiang, X. Zu, W. Zhou, PEDOT coated iron phosphide nanorod arrays as high-performance supercapacitor negative electrodes. Chem. Commun. **54**, 794–797 (2018)
40. H. Wan, X. Ji, J. Jiang, J. Yu, L. Miao, L. Zhang, S. Bie, H. Chen, Y. Ruan, Hydrothermal synthesis of cobalt sulfide nanotubes: the size control and its application in supercapacitors. J. Power Sources **243**, 396–402 (2013)
41. B. Wu, H. Qian, Z. Nie, Z. Luo, Z. Wu, P. Liu, H. He, J. Wu, S. Chen, F. Zhang, Ni3S2 nanorods growing directly on Ni foam for all-solid-state asymmetric supercapacitor and efficient overall water splitting. J. Energy Chem. **46**, 178–186 (2020)
42. X. Li, H. Zhu, Two-dimensional MoS2: properties, preparation, and applications. J. Materiomics **1**, 33–44 (2015)
43. D. Sarkar, D. Das, S. Das, A. Kumar, S. Patil, K.K. Nanda, D.D. Sarma, A. Shukla, Expanding interlayer spacing in MoS2 for realizing an advanced supercapacitor. ACS Energy Lett. **4**, 1602–1609 (2019)

44. M.S. Javed, S. Dai, M. Wang, D. Guo, L. Chen, X. Wang, C. Hu, Y. Xi, High performance solid state flexible supercapacitor based on molybdenum sulfide hierarchical nanospheres. J. Power Sources **285**, 63–69 (2015)
45. L. Shen, L. Yu, H.B. Wu, X.-Y. Yu, X. Zhang, X.W. (David) Lou, Formation of nickel cobalt sulfide ball-in-ball hollow spheres with enhanced electrochemical pseudocapacitive properties. Nat. Commun. **6**, 6694 (2015)
46. J. Lin, H. Jia, H. Liang, S. Chen, Y. Cai, J. Qi, C. Qu, J. Cao, W. Fei, J. Feng, Hierarchical CuCo2S4@NiMn-layered double hydroxide core-shell hybrid arrays as electrodes for supercapacitors. Chem. Eng. J. **336**, 562–569 (2018)
47. Y. Liu, Z. Li, L. Yao, S. Chen, P. Zhang, L. Deng, Confined growth of NiCo2S4 nanosheets on carbon flakes derived from eggplant with enhanced performance for asymmetric supercapacitors. Chem. Eng. J. **366**, 550–559 (2019)
48. Q. Li, W. Lu, Z. Li, J. Ning, Y. Zhong, Y. Hu, Hierarchical MoS2/NiCo2S4@C urchin-like hollow microspheres for asymmetric supercapacitors. Chem. Eng. J. **380**, 122544 (2020)
49. C.-S. Dai, P.-Y. Chien, J.-Y. Lin, S.-W. Chou, W.-K. Wu, P.-H. Li, K.-Y. Wu, T.-W. Lin, Hierarchically structured Ni3S2/Carbon nanotube composites as high performance cathode materials for asymmetric supercapacitors. ACS Appl. Mater. Interfaces **5**, 12168–12174 (2013)
50. W. Liu, H. Niu, J. Yang, K. Cheng, K. Ye, K. Zhu, G. Wang, D. Cao, J. Yan, Ternary transition metal sulfides embedded in graphene nanosheets as both the anode and cathode for high-performance asymmetric supercapacitors. Chem. Mater. **30**, 1055–1068 (2018)
51. X. Liu, Z. Wu, Y. Yin, Hierarchical NiCo2S4@PANI core/shell nanowires grown on carbon fiber with enhanced electrochemical performance for hybrid supercapacitors. Chem. Eng. J. **323**, 330–339 (2017)
52. I. Rabani, S. Hussain, D. Vikraman, Y.-S. Seo, J. Jung, A. Jana, N.K. Shrestha, M. Jalalah, Y.-Y. Noh, S.A. Patil, 1D-CoSe2 nanoarray: a designed structure for efficient hydrogen evolution and symmetric supercapacitor characteristics. Dalton Trans. **49**, 14191–14200 (2020)
53. S. Wu, Q. Hu, L. Wu, J. Li, H. Peng, Q. Yang, One-step solvothermal synthesis of nickel selenide nanoparticles as the electrode for high-performance supercapacitors. J. Alloys Compd. **784**, 347–353 (2019)
54. H. Li, J. Gong, J.-C. Li, X. Zhang, C. Tang, H. Yao, Q. Ding, Synthesis of nickel selenide thin films for high performance all-solid-state asymmetric supercapacitors. Chin. Chem. Lett. **31**, 2275–2279 (2020)
55. Y. Kuai, T. Wang, M. Liu, H. Ma, C. Zhang, Flower-like Ni0·85Se nanosheets with enhanced performance toward hybrid supercapacitor. Electrochimica Acta **321**, 134701 (2019)
56. D. Yu, Z. Li, G. Zhao, H. Zhang, H. Aslan, J. Li, F. Sun, L. Zhu, B. Du, B. Yang, W. Cao, Y. Sun, F. Besenbacher, M. Yu, Porous ultrathin NiSe nanosheet networks on nickel foam for high-performance hybrid supercapacitors. ChemSusChem. **13**, 260–266 (2020)
57. L. Xu, L. Ma, T. Rujiralai, Y. Ling, Z. Chen, L. Liu, X. Zhou, Molybdenum selenide nanosheets with enriched active sites supported on titanium mesh as a superior binder-free electrode for electrocatalytic hydrogen evolution and supercapacitor. J. Taiwan Inst. Chem. Eng. **107**, 35–43 (2020)
58. S. Hu, Q. Jiang, S. Ding, Y. Liu, Z. Wu, Z. Huang, T. Zhou, Z. Guo, J. Hu, Construction of hierarchical MoSe2 hollow structures and its effect on electrochemical energy storage and conversion. ACS Appl. Mater. Interfaces **10**, 25483–25492 (2018)
59. H.-J. Zhang, Y.-K. Wang, L.-B. Kong, A facile strategy for the synthesis of three-dimensional heterostructure self-assembled MoSe2 nanosheets and their application as an anode for high-energy lithium-ion hybrid capacitors. Nanoscale **11**, 7263–7276 (2019)
60. K.S. Bhat, H.S. Nagaraja, Effect of isoelectronic tungsten doping on molybdenum selenide nanostructures and their graphene hybrids for supercapacitors. Electrochimica Acta **302**, 459–471 (2019)
61. Y. Yuan, R. Chen, H. Zhang, Q. Liu, J. Liu, J. Yu, C. Wang, Z. Sun, J. Wang, Hierarchical NiSe@Co2(CO3)(OH)2 heterogeneous nanowire arrays on nickel foam as electrode with high areal capacitance for hybrid supercapacitors. Electrochimica Acta **294**, 325–336 (2019)

62. B. Ye, X. Cao, Q. Zhao, J. Wang, Coelectrodeposition of NiSe/ZnSe hybrid nanostructures as a battery-type electrode for an asymmetric supercapacitor. J. Phys. Chem. C. **124**, 21242–21249 (2020)
63. X. Chen, J. Zhu, J. Cai, Y. Zhang, X. Wang, Nanosheets assembled layered MXene/MoSe2 nanohybrid positive electrode materials for high-performance asymmetric supercapacitors. J. Energy Storage **40**, 102721 (2021)
64. S. Wu, Y. Xue, Q. Yang, Q. Hu, T. Cui, Q. Su, F. Yin, Y. Wang, H. Zhan, Conductive carbon spheres-supported nickel-cobalt selenide nanoparticles as a high-performance and long-life electrode for supercapacitors. Diamond Related Mater. **111**, 108187 (2021)
65. P. Sun, J. Zhang, J. Huang, L. Wang, P. Wang, C. Cai, M. Lu, Z. Yao, Y. Yang, Bimetallic MOF-derived (CuCo)Se nanoparticles embedded in nitrogen-doped carbon framework with boosted electrochemical performance for hybrid supercapacitor. Mater. Res. Bull. **137**, 111196 (2021)
66. L.-P. Lv, C. Zhi, Y. Gao, X. Yin, Y. Hu, D. Crespy, Y. Wang, Hierarchical "tube-on-fiber" carbon/mixed-metal selenide nanostructures for high-performance hybrid supercapacitors. Nanoscale **11**, 13996–14009 (2019)
67. Y. Liu, W. Li, X. Chang, H. Chen, X. Zheng, J. Bai, Z. Ren, MoSe2 nanoflakes-decorated vertically aligned carbon nanotube film on nickel foam as a binder-free supercapacitor electrode with high-rate capability. J. Colloid Interface Sci. **562**, 483–492 (2020)
68. S.Y. Ahmed, S.G. Mohamed, S.Y. Attia, Y.F. Barakat, M.A. Shoeib, N.S. Tantawy, High electrochemical energy-storage performance promoted by SnSe nanorods anchored on rGO nanosheets. J. Electroanal. Chem. **883**, 115063 (2021)
69. A.M. Zardkhoshoui, S.S.H. Davarani, Boosting the energy density of supercapacitors by encapsulating a multi-shelled zinc–cobalt-selenide hollow nanosphere cathode and a yolk–double shell cobalt–iron-selenide hollow nanosphere anode in a graphene network. Nanoscale **12**, 12476–12489 (2020)
70. Y. Wang, W. Zhang, X. Guo, K. Jin, Z. Chen, Y. Liu, L. Yin, L. Li, K. Yin, L. Sun, Y. Zhao, Ni–Co Selenide Nanosheet/3D Graphene/Nickel foam binder-free electrode for high-performance supercapacitor. ACS Appl. Mater. Interfaces. **11**, 7946–7953 (2019)
71. P. Zhou, L. Fan, J. Wu, C. Gong, J. Zhang, Y. Tu, Facile hydrothermal synthesis of NiTe and its application as positive electrode material for asymmetric supercapacitor. J. Alloys Compd. **685**, 384–390 (2016)
72. M. Liu, Z. Wang, J. Liu, G. Wei, J. Du, Y. Li, C. An, J. Zhang, Synthesis of few-layer 1T′-MoTe2 ultrathin nanosheets for high-performance pseudocapacitors. J. Mater. Chem. A. **5**, 1035–1042 (2017)
73. S.S. Karade, B.R. Sankapal, Materials Mutualism through EDLC-Behaved MWCNTs with Pseudocapacitive MoTe2 Nanopebbles: Enhanced Supercapacitive Performance. ACS Sustain. Chem. Eng. **6**, 15072–15082 (2018)
74. S. Deshagani, P. Ghosal, M. Deepa, Altered crystal structure of nickel telluride by selenide doping and a poly(N-methylpyrrole) coating amplify supercapacitor performance. Electrochimica Acta **345**, 136200 (2020)

Carbon Nanocomposite-Based SCs as Wearable Energy Storage

Mujtaba Ikram, Ali Raza, Muhammad Ikram, and Asif Mahmood

Abstract The demand for highly efficient energy storage devices having high energy and power densities is increasing exponentially. In this regard, supercapacitors (SCs) have got great attention due to fast power generation and longer cyclic life. A range of electrodes has been explored for SCs applications including C-carbon, metal/carbon hybrids, metal oxides, etc. Among these, carbon-based electrodes have shown tremendous potential because of their hierarchical structure, electrical conductivity, and large surface areas. Still, carbon-based SCs offer limited energy density which strongly limits its application to a broader scale. A range of strategies was presented to boost the energy density of C-based SCs like developing highly porous nanostructures, introducing heteroatoms for pseudocapacitance, compositing with other forms of carbon, etc. Very recently, carbon-based electrodes have found great applications in wearable electronics owing to the fact that thin and flexible carbon electrodes chemistries can be readily obtained. This has opened new avenues in energy harvesting and utilization. In this chapter, we will provide insights into synthesis strategies of carbon-based wearable electrodes and their potential applications.

Keywords SC · Carbon-based electrode · Capacitance · High energy-power density · Pseudocapacitors

M. Ikram
Department of Chemical Engineering, University of Punjab, Lahore, Punjab 54590, Pakistan

A. Raza
Department of Physics, University of Sialkot (USKT), 1-Km Main Daska Road, Sialkot, Punjab 51311, Pakistan

A. Raza · M. Ikram · A. Mahmood (✉)
Solar Cell Applications Research Lab, Department of Physics, Government College University, Lahore, Punjab 54000, Pakistan
e-mail: asif.mahmood@sydney.edu.au

M. Ikram · A. Raza · M. Ikram · A. Mahmood
School of Chemical and Biomolecular Engineering, University of Sydney, Sydney 2006, Australia

S. Thomas et al. (eds.), *Nanostructured Materials for Supercapacitors*,
Advances in Material Research and Technology,
https://doi.org/10.1007/978-3-030-99302-3_21

1 Introduction

The ever-increasing rate of fossil fuel burning and associated skyrocketing prices have raised severe worries headed for rapid diminution of current fossil fuel supplies along with worrisome greenhouse discharge of gas and pollution in the air. Consequently, renewable energy generation and storage systems are vital for sustaining life on earth. Several renewable energy technologies have been explored in this regard including solar, wind, geothermal, and electrochemical, etc. Among these, the electrochemical energy storage technologies like electrochemical SCs (ESCs) and rechargeable batteries present the most promising renewable energy technologies owing to long life, high storage capability, easy portability, etc. [1–4]. ESCs have a power density 100–1000 times that of batteries, however a lower energy density of 3–30 times that of batteries [5]. The assessment regarding various energy storage devices for definite power versus definite energy is shown in the Ragone plot (Fig. 1) [6]. The ESCs are best suited for great-power bursts, such as those used to accelerate/brake high-speed transportation systems [6]. Additionally, ESCs can withstand millions of charge/discharge cycles owing to the chemical reaction absence in the electric double-layer charge storage [5, 7, 8]. ESCs may be classified (Sect. 2) as electric double-layer capacitors (EDLCs), which can store charge at the interfaces among the electrolyte or electrodes or pseudocapacitors (PCs), that can store charge through reversible and fast Faradaic redox processes. A SC can store charge with the combination of capacitive carbon electrodes utilizing a lithium insertion electrode or a pseudocapacitive; therefore the SC is stated as hybrid SC (HSC).

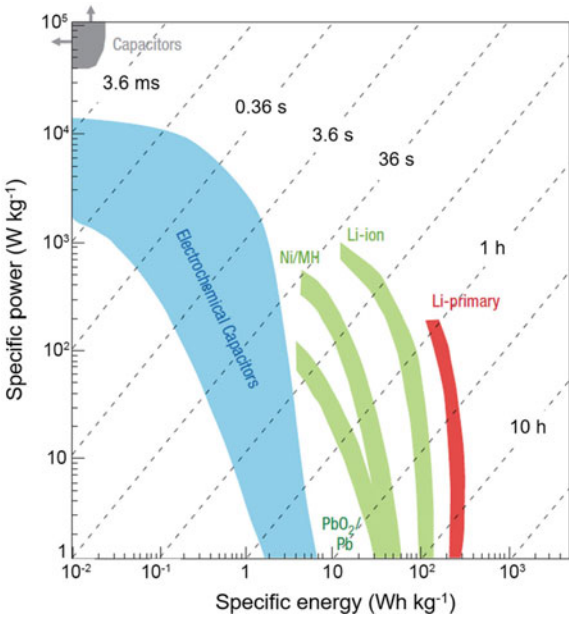

Fig. 1 Definite power contrary to definite energy (Ragone plot), for many electrical energy storage components (i.e. exceptional power, definite energy, time constants). Reproduced with permission from ref. [6] Copyright 2008 Springer Nature

In recent years, the increasing growth of wearable or flexible electronics produces a serious demand for integrated power roots that entirely depend upon flexible and even stretchy electrodes. As a result, SCs with flexible as well as stretchy fiber-shaped that are also termed as ultrathin SCs have garnered considerable interest recently [7, 9, 10]. The carbon nanotubes (CNTs) and graphene (GR) have been recognized as quality electrode materials because of their great bending power, and outstanding mechanical stability that leads to the fabrication of flexible and stretchy ESCs. There was an enormous quantity of research published on carbon-based ESCs, and the number of papers continues to grow at a rapid pace each year. It is extremely desirable to conduct a timely evaluation of such a quickly emerging area of such importance. The purpose of this chapter is to give a timely, succinct, and critical analysis of recent significant work on the subject by reviewing recent work and highlighting essential concerns relating to electrode design or material fabrication and explanation for energy-storage devices.

2 Classification of Carbon-Based SCs

SCs store energy via two distinct capacitive processes: Firstly, electric double-layer (EDL) capacitance, which stemmed due to various accumulation of electrostatic charges at the electrode/electrolyte interface; and secondly, pseudocapacitance owing to fast and reversible redox reactions. Figure 2 indicates many SC types categorized of energy storage devices together with electrode species [11].

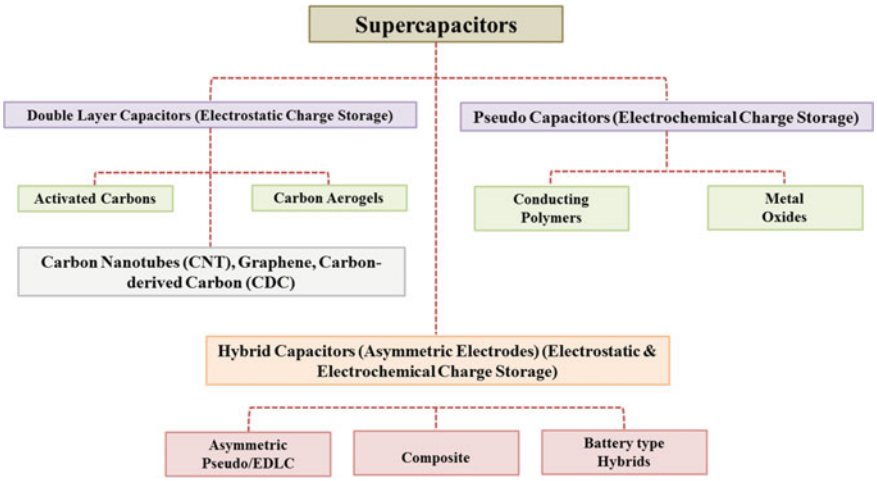

Fig. 2 SCs taxonomy with many electrode materials

2.1 Electric Double-Layer Capacitors

Von Helmholtz pioneered the indication and EDL model in 1853 when he conducted a detailed investigation of colloidal suspension [12]. This model detailed the formation of two electrically layers opposed charges at the electrode/electrolyte interface and their division into a monoatomic distance that was remarkably comparable to the structure of a conventional capacitor. Then, Gouy and Chapman [13, 14] updated this straightforward EDL model by taking an electrolyte in which both anions and cations were considered as a continuous distribution that created a diffuse layer when thermal motion was applied. When ions that were not been tightly bonded to the surface were considered, the number of opposite ionic charges became equal to that of charged solid while distributed in the electrolyte. Moreover, the thickness of diffuse layers is somewhat dependent on the ion's kinetic energy. Furthermore, this model resulted in an EDL capacitance overestimation; as generally the capacitance (C) of capacitor seemed inversely proportional to the distance between two distinct charges; therefore, a large C value has been produced whenever point charge approached the surface of the corresponding electrode. Later, Stern [15] updated Gouy–Chapman model by merging it with the Helmholtz model. He distinguished two charge distribution regions: the diffuse and stern layers. Charges (often hydrated) were absorbed extremely powerfully on the electrode in the Stern layer that comprised of: firstly, specifically absorbed charges (SACs) and secondly, nonspecifically absorbed countercharges (nSACs). These SACs and nSACs were respectively represented by IHP and OHP. The EDL models show that charge storage happens through electrostatic adsorption at the electrode/electrolyte interface, however, no charge transfer exists during charge/discharge processes. Due to the physical electrostatic reactions, the charge/discharge processes of EDLCs are quick, allowing them to respond swiftly to prospective changes. Calculation of the C value of an EDLCs electrode can be done using the following Eq. 1 [16, 17]:

$$C = \frac{\varepsilon_r \varepsilon_0}{d} A \tag{1}$$

where ε_r and ε_0 denote relative and vacuum permittivity respectively, A represents operative contact area, and d corresponds to the thickness of EDL. Zhang and Zhao [16] examined the evolution of the three above-mentioned modeling mechanisms for EDL, as depicted in Fig. 3.

2.2 Pseudo-Capacitors

Unlike EDL, PCs are determined through the thermodynamic component and are related to charges acceptance (Δq) and potential changes (ΔU) [16, 17]. The primary

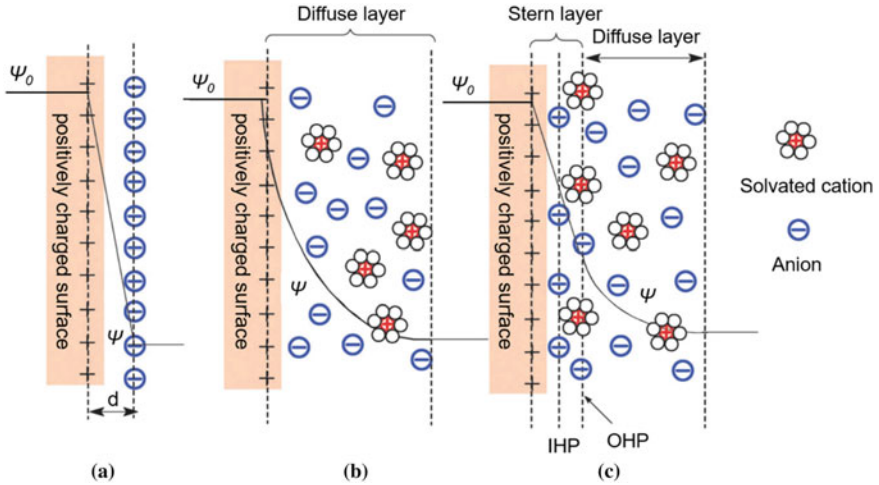

Fig. 3 EDLCs: Models **a** Helmholtz model, **b** Gouy–Chapman model, and **c** Stern model, where Ψ *and* Ψ_o represent potential at electrode/electrolyte interface and electrode potential respectively, **d** Helmholtz distance, where IHP relates to inner and OHP define outer Helmholtz plane, respectively. Reproduced with permission from ref. [16] Copyright 2009 Royal Society of Chemistry

electrochemical characteristic is the Faraday reaction that is followed by PCs electrode materials for instance oxidation–reduction reaction through the process of charging or discharging operations, implying that the valence state changes in charge/discharge operations [18, 19]. Figure 4 illustrates the charge storage methods in PCs [20]. The term "under-potential deposition" refers to the process for noble metals through which atoms were adsorbed via electro-deposition potential which is usually less negative compared to the cation reduction equilibrium potential. In addition, redox processes produce redox PCs. These reactions occur in the presence of adsorbed cations on the electrode species, which resulted in reversible and rapid transmission of charge towards the contact of electrolyte/electrode [6]. Further, PC may also be generated by the insertion/extraction of cations inside tunnels or crystalline layer materials. During insertion/extraction, the crystal may stay electrically neutral. Intercalation PC could be regarded using a "transitional" characteristic among the SCs and Li-ion [21]. Although PC electrode may achieve far greater capacitance values than EDL electrodes, it has poor electrical conductivity and cycle stability.

2.3 Carbon-Based Hybrid SCs

Initially, to bridge the gap amongst extraordinary command hybrid SCs (HSCs) might be utilized however lower energy ESCs and higher energy with less power batteries. Moreover, in many cases, HSCs were composed of carbon capacitive electrode materials joined with either a lithium-insertion or a pseudocapacitive material (Fig. 5a,

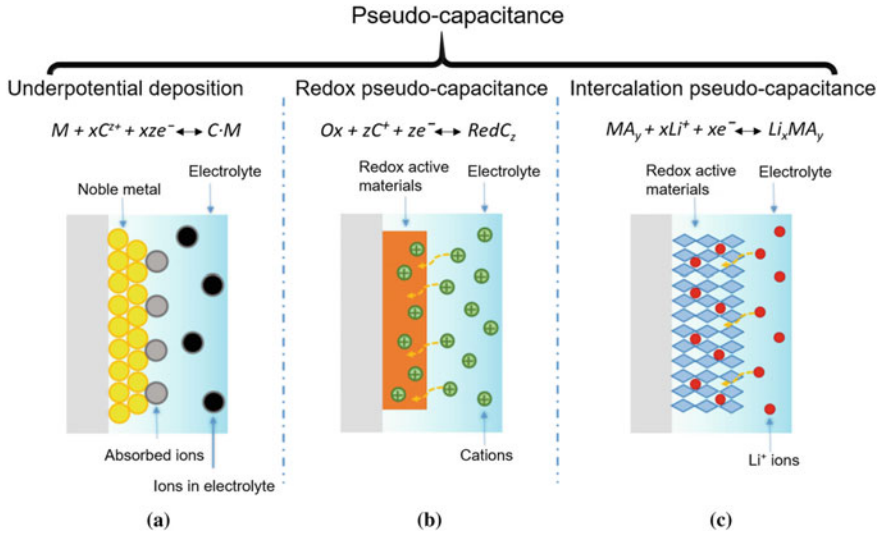

Fig. 4 Illustration of charge storage in PCs: **a** under potential deposition, **b** redox reactions, **c** ion insertion/extraction [20] Copyright 2018 American Chemical Society

b) [6, 22, 23]. Grouping of Faradaic surface reaction and non-Faradaic intercalation on cathode and anode respectively, (Fig. 5c) offers a chance to attain enormous energy and power densities with no effects on its cost and cycle stability. Up to this point, in HFCs the published carbon-based electrodes employed for cathode including GR, graphite, CNTs, 3D mesoporous C as well as many MO/polymer-based C-nanomaterials [24]. In the same context, 3D-GR or MnO_2 nanocomposite does seem to have a greater specific capacitance (1145 F/g), with roughly 83% theoretical capacitance and mass 13% MnO_2 mass loading [23]. Conversely, HSCs have been manufactured through a simple Solvothermal method using Fe_3O_4 NPs or GR nanocomposite. Fe_3O_4 NPs or GR-based composite half-cell revealed an enormous flexible specific tendency within an excellent capability and cycle stability rate, surpassing 1000 mAh/g at 90 mA/g current density [25]. Furthermore, Li-ion-based HSCs that are recognized as $LiPF_6$ can be joined with this composite and attain energy- and power densities in the order 204 to 65 Wh/kg and 55 to 4600 W/kg respectively [25]. Apart from that, Lim et al. explained HSCs depend upon mesoporous Nb_2O_5 or carbon nanocomposite cathode and (AC MSP-20) anode, describing energy power (18,510 W/kg) and power densities (74 Wh/kg) by 90% capacitance retention at 1000 mA/g in the electrolyte combination of ($LiPF_6$) 1.0 M/ethylene or dimethyl carbonate with volume ratio of 1:1 after 1000 cycles [26]. Hybrid-based SCs which depend upon N-doped AC were structured by Li et al. [27] signifying large substance-level energy densities of 230 Wh/kg through 76.3% capacity retention and power density of 1747 W/kg after 8000 cycles.

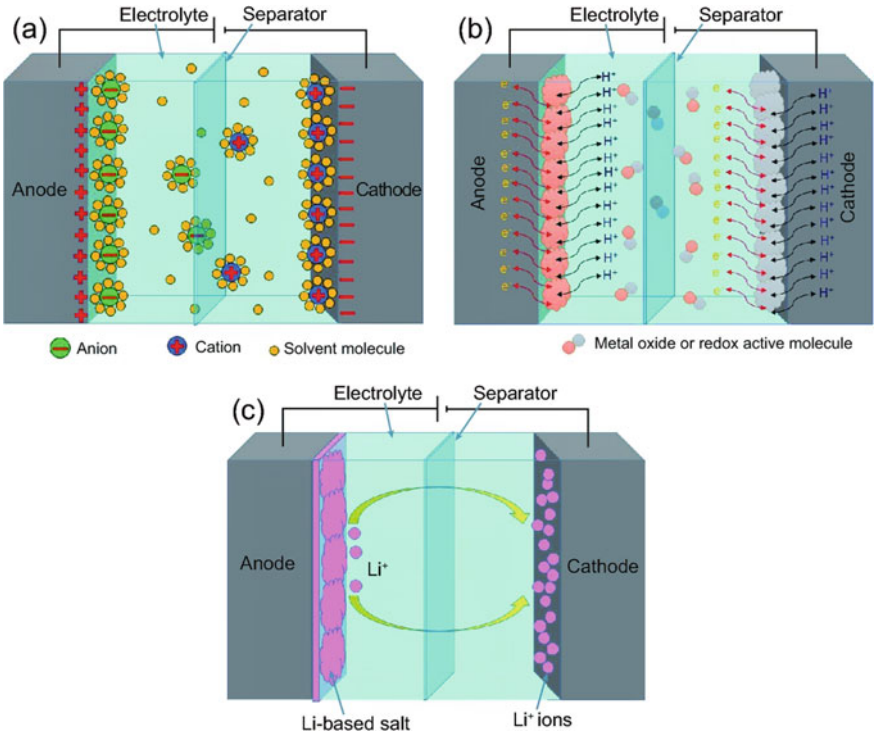

Fig. 5 Illustration of **a** EDLC-electrical double-layer capacitor, **b** PCs, and **c** hybrid SC (HSC). Reproduced with permission from ref. [5] Copyright 2017 Oxford University Press

3 Carbon-Based Nanocomposites for SCs

3.1 Carbon Nanotubes

Carbon nanotubes (CNTs) are a 1-D nanocomposite entirely formed of carbon sp^2-bonded hexagonal networks that have been rolled into a tubular form [28]. CNTs were extensively researched as electrodes in SCs due to greater mechanical power, structure strength along with stability, and conductivity, which all make them attractive choices for modification and inclusion of other active materials [29, 30]. Chen et al. [31], for example, synthesized a hierarchically organized carbon microfiber composed of an aligned and linked SWNTs net structure and introduced N-doped rGO nanosheets. From two parallel fiber electrodes, ASS-micro-SCs were prepared which demonstrated an exceptional volumetric energy density (6.3 $mWcm^3$) owing to large surface area for ions adsorption provided by rGO and low interlayer and contact resistance provided by SWNTs. Conversely, the surface wettability of hybrid fiber was increased using oxygen functional groups and nitrogen heteroatoms. Peng et al. [32] created GR/CNT hybrid fibers by inserting GR sheets

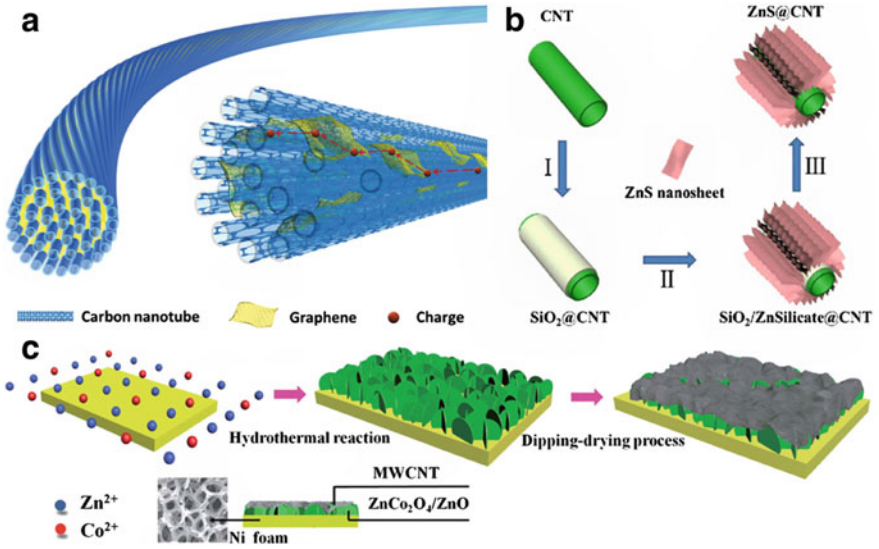

Fig. 6 **a** Schematic view of the structure of the GR/CNT fiber composite. Reproduced with permission from ref. [32] Copyright 2014 John Wiley & Sons. **b** Illustration for the production of the ZnS@CNT composites with a multistep conversion process. Reproduced with permission from ref. [38] Copyright 2017 Springer Nature. **c** Representation of the fabrication routes of Zn1Co2@MWCNT nanocomposite electrode using a laminated structure. Reproduced with permission from ref. [40] Copyright 2017 Royal Society of Chemistry

between neighboring carbon nanotubes (Fig. 6a). Because of the strong reaction among GR sheets and carbon nanotubes, the GR sheets acted as conducting "bridges, " facilitating charge movement and lowering contact resistances. Thus, the new composite fibers exhibited the required conductivity and essential electrochemical properties simultaneously. In addition, Wallace et al. [33] synthesized extremely flexible CNTs/MgO hybrid nanocomposite fibers through wet spinning scrutinized with MnO_2 electrode position onto the carbon nanotube fibers. The internal nanonetwork of CNTs and mesoporous MnO_2 nanoflakes promoted the degree of ion transfer and consequently increased electrochemical characteristics. The dopant concentration of different metal oxides/hydroxides/sulfides to enhance the electrical efficiency of carbon nanotubes has sparked widespread public attention as carbon nanotubes not just respond as a conductive backbone for metallic particles to increase conductivity but enable the electrolyte ions diffusion with the electrode substances [34].

Additionally, several redox processes happening mostly close to the surface or on the surface of the metal oxide (MO)/hydroxide/sulfide may cause to boost in the energy density of SCs [35]. A chemical co-precipitation approach to synthesize coaxial CNT/$Ni(OH)_2$ [36]. The ASCs were constructed using and rGO as −ve and CNT/$Ni(OH)_2$ as +ve electrodes, respectively. Furthermore, constructed ASCs had power density (1.8 $kWkg^{-1}$) and energy density (35 $Whkg^{-1}$), which exhibits the

coating of $Ni(OH)_2$ on the surface of CNT improved matrix conductivity and dual-storage processes significantly. Multiwall CNT (MWCNT) hybrid fibers were synthesized by Chen et al. [37] with MoS_2-rGO by embedding the 2-D nanosheets into well-ordered MWCNT and finally curving them consecutively. The constructed asymmetric device from MoS_2-rGO/MWCNT and rGO/MWCNT demonstrated excellent electrochemical properties. Similarly, an ultrathin ZnS@CNT was prepared by Luo et al. [38] by the decoration of hierarchical ultrathin Zinc sulfide nanosheets onto MWCNTs, as presented in Fig. 6b. The growth of three-layer sandwiched CNT/Fe_2O_3@C arrays on carbon cloth was described by Zhang et al. [39] using CVD and magnetron sputtering techniques. The CNT/Fe_2O_3@C composite demonstrated good electrochemical properties that were attributed mostly to the carbon shell's ability to effectively shield the internal Fe_2O_3 and prevent dissemination of Fe-based oxide/hydroxide between the layers. A novel method for fabricating $ZnCo_2O_4$/ZnO@MWCNT hybrids was conveyed by Zhao et al. [40]. The technique entailed the synthesizing of $ZnCo_2O_4$/ZnO (Zn_1Co_2) on Ni foam via hydrothermal scheme and covering MWCNTs on Zn_1Co_2 using a dipping-drying process at 25 °C (Fig. 6c). The resulting sandwich structure provided large electrode/electrolyte contact that give rise to boosting electrochemical progress. Thus, the $ZnCo_2$@MWCNTs nanocomposite demonstrated excellent SCs of 2069 Fg^{-1} at 1 Ag^{-1}, while the full device consisting of $ZnCo_2$@MWCNTs//AC exhibited a high energy density of 48.1 W h kg^{-1} at a corresponding power density of 900 Wkg^{-1}.

3.2 Graphene/Graphene Oxide

Graphene is a 2-D material that comprises of a honeycomb-like lattice structure, consisting of monolayers of hexatomic rings [41, 42]. GR has found extensive applications in electrochemical energy storage systems also has fascinating properties of higher surface area, superior thermal and significant electrical conductivity, and mechanical properties [43, 44]. Thus far, the research has established its successful utilization as an electrode for SCs. However, the electrochemical activity of GR strongly depends on the active surface area [45]. The individual GR layers can provide high active area and electrochemical performance [42]. That being said, because highly cohesive interactions (i.e. van der Waals) and intense reaction among planar basal planes and GR layers demonstrate a greater ability to restack, that also occurs during the manufacturing and cycling of both electrodes. The restacking causes loss of active surface and eventually results in loss of performance. Numerous techniques have been investigated to inhibit GR layer aggregation to improve the surface area, decrease internal resistance, and promote electrolyte distribution to the inner section during the production of SCs [42, 46]. According to Liu et al. [47], micro-SCs (MSC) of flexible GR/CNT were manufactured utilizing the laser-scribing method. CNTs acted as spacers, preventing GR layers from restacking resulting in increasing ion-accessible surface area. The laser-scribed GR/SWCNT MSC had the greatest electrochemical characteristics when utilizing SWCNTs with sizes of 1–2 nm.

Computational analysis and experimental testing were described by Deng et al. [48] to study the relationship between capacitive performance and electrode structure about GR sheet orientation. Simulation results demonstrated that GR sheets' oriented structure and shape had a considerable effect on the capacity to transport ions and accumulate charges. Furthermore, the experimental data recommended that the areal capacitive vertical GR value was approximately 38% greater than that of lateral GR and 6 times greater for graphite paper electrode, which corresponds to effective ion transfer stations; whereas higher field development influenced the capacitance of vertical GR nanosheets (VGNS) (Fig. 7a, b). Ostrikov et al. [28] manufactured VGNS by breaking down natural precursors into a well-organized graphic form along with the growth of CNTs directly on VGNS. The resulting VGNS/CNT 3D/1D nanoarchitecture exhibited superior electrochemically active material density and high stability. Kim et al. [44] through coexisting GR nanosheets and nanoscrolls, produced hierarchically interconnected carbon nanoarchitecture with a scalable technique using large-temperature molten salt. Through catalytic gasification, they proposed multifunctional micro-level GR nanomesh (GNMs) with greater-density nano perforation. The production procedure induced selective GR disintegration next to the metal catalyst that leads to the formation of nanoperforations. GNMs pore density distribution, pore size, and aperture size might be ordered by altering GR metal oxide size and portion. The developed hierarchical linked carbon nanocomposite and GNMs all displayed extraordinary rate capability, exceptional cycle ability, and large reversible specific capacity towards SC applications [49]. Although previous tactics are operational to progress GR electrochemical application, the energy density is quite inadequate concerning high demand and rapid expansion in place of future generation energy storage systems (EEs) devices.

Given their exceptional capacitive performance, conductive polymers and MOs/hydroxides were integrated headed for GR nanosheets to suit the needs of high-energy storage systems. For example, a GR-covered, Co_3O_4-inserted hybrid was prepared by Oh et al. [50] by way of microwave irradiation technique (in situ) (Fig. 7c). Moreover, an as-prepared product was enveloped with GR nanosheets and hence mechanically protected which helped to avoid the Co_3O_4 aggregation and the collapse or deterioration of electrode material in successive cycles. Likewise, Co_3O_4 NPs hybrid electrode substances are oriented vertically on GR nanosheets maintained through carbon fabric were effectively fabricated with good electrochemical progress (Fig. 7d–f) [46]. In addition, α-Fe_2O_3/GR nanostructures were produced by Zhang et al. [51] by adopting solvothermal technique along with annealing action. Resulted crystalline uniform α-Fe_2O_3 nanoparticles offered extensive electrolyte contact surfaces. Meanwhile, the perfect coupling of α-Fe_2O_3 and linked GR nanosheets offered fast electrical and ion transport, making α-Fe_2O_3/GR composite a promising rapid energy storage material. Among manganese oxides, metal oxides are regarded as an intriguing alternative that, due to their pseudocapacitive characteristics, can give a superior specific capacitive property. Furthermore, mixed value manganese (Mn) oxide nanoparticles bound with rGO were prepared by Yang et al. [52] through a solution-phase assembly combined via hydrazine vapor reduction treatment. The GO performed as a template to direct MnO_x's final product

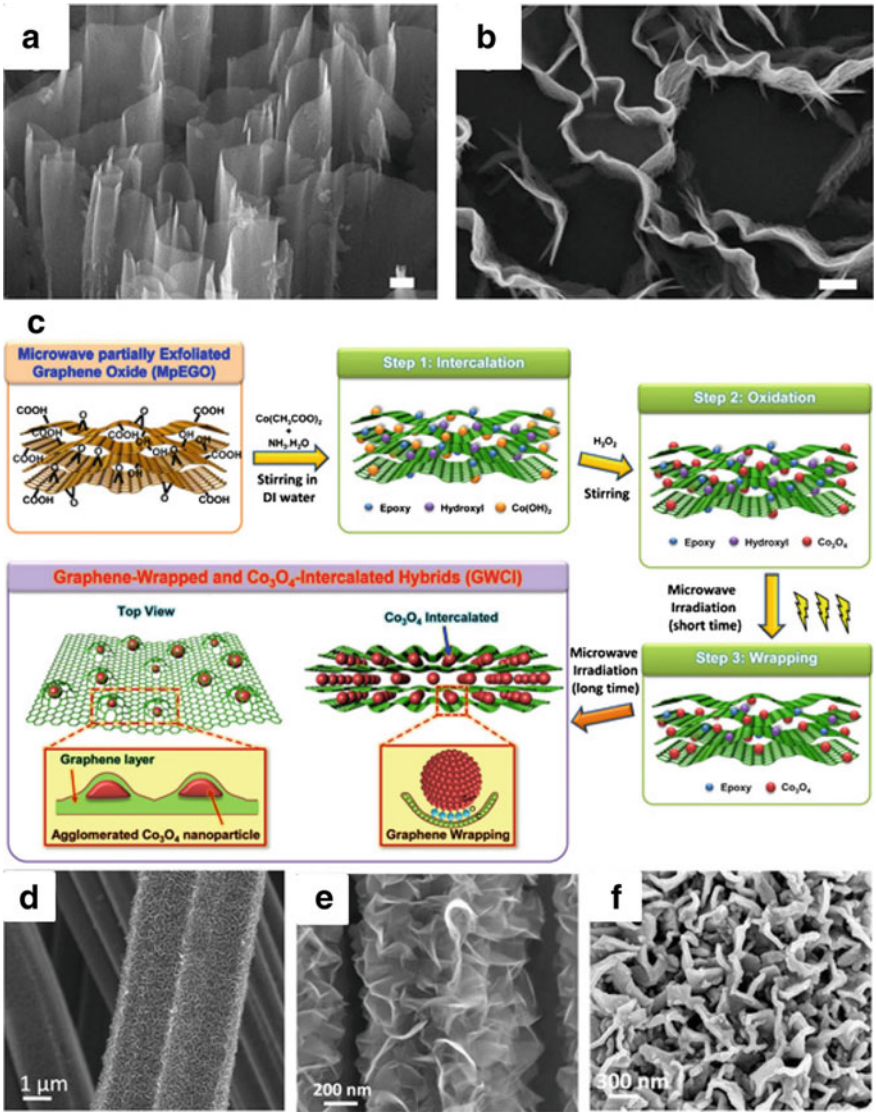

Fig. 7 Vertically oriented SEM micrograph of GR sheets (scale 100 nm) **a** Tilt-view, **b** top-view. Reproduced with permission from ref. [48] Copyright 2016 American Chemical Society. **c** Illustration of a three-step route for the production of GWCI hybrid. Reproduced with permission from ref. [50] Copyright 2014 Elsevier B.V. **d** LR-SEM micrograph of the VAGN. **e** HR-SEM micrograph of the VAGN, and **f** HR-SEM micrograph of Co_3O_4-H. Reproduced with permission from ref. [46] Copyright 2015 American Chemical Society

production and uniform distribution. The rGO/MnO_x electrode displayed improved capacitance, speed performance, and notably extended cycle. It might be ascribed to numerous characteristics, such as the good network of ion and electron percolation with the mixed-valence Mn cations coexistence and synergistic impact among the composite section. Joining 2-D GR using MOs/hydroxide for instance MnO is a realistic approach to reconcile critical energy density and large GR cost.

4 Carbon-Based Flexible SCs with Planar Structures

The carbon nanotubes and GR are two broadly utilized C-allotropes for electrochemical energy storage [53, 54]. This section discusses the development of advanced-progress flexible SCs with planar CNT, GR, and hybrid electrode structures.

4.1 CNT-Based Flexible SCs

CNTs were extensively employed as electrode species in the field of flexible SCs that owns both liquid and gel as electrolytes [1, 53]. They can be directly deposited on nonconductive substrates (like plastic film, cellulose paper, and office paper) [55–57] or onto conductive substrates to act as a current electrode and collector as electrode materials [58]. Printable thin film SCs were developed by Kaempgen and colleagues [55] with spray-coated SWCNTs on PET sheets as charge collectors as well as electrodes (Fig. 8a). To entirely printable the device, they combined the electrolyte and separator into a mono sheet of gel electrolyte (PVA/H_3PO_4). Thin film SCs have been sandwiched between carbon nanotube electrodes and the gel electrolyte (Fig. 8b). Figure 8c, d demonstrates CV and GCD curves of SSSCs made in this way, from which a specific capacitance of 36 Fg^{-1} was determined. Various cost benefits, low-weight substrates (office paper, bacterial nanocellulose) were used as electrodes in flexible SCs in addition to plastic sheets [57, 59]. Kang et al., for example, utilized vacuum filtration to deposit carbon nanotubes onto a bacterial nanocellulose substrate, yielding sheets with outstanding flexibility, huge specific surface area (SSA), and chemical durability [59]. The ASSSCs in this study had a specific capacitance (46.9 Fg^{-1}) and were stable after 5000 charge–discharge cycles at a high current density (10 Ag^{-1}). Higher efficiency of pure carbon nanotube-based flexible EDLCs was achieved using carbon nanotube composites including transition metal oxides (TMO) or conductive polymers with pseudocapacitance into flexible SC [60, 61]. Meng et al. [62] formed flexible all-solid-state supercapacitors (ASSSCs) utilizing PANI-coated carbon nanotube networks as electrodes (Fig. 8e). The electrode materials (Fig. 8f, g) had a high 350 Fg^{-1} specific capacitance, whereas the whole specific capacitance of the device was 31.4 Fg^{-1}, demonstrating outstanding stability with 8.1% specific capacitance degradation after 1000 charge–discharge cycles. Vertically

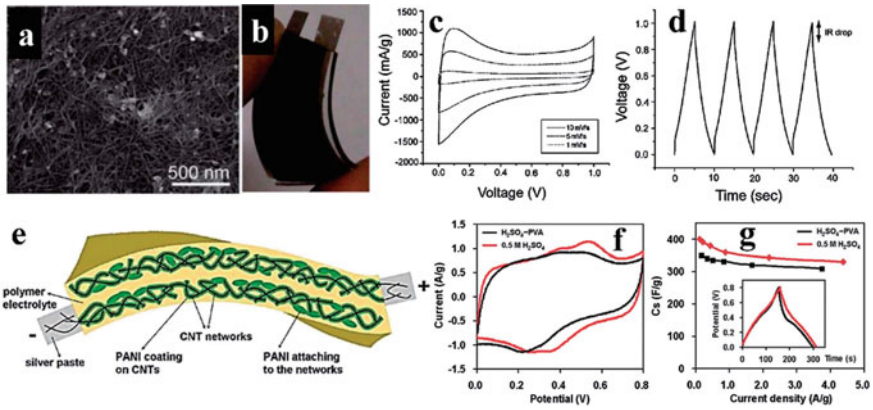

Fig. 8 **a** SWCNT networks SEM image; **b** PVA/H_3PO_4-based polymer electrolyte in sprayed SW carbon nanotube films on PET; **c** CV and **d** thin film SC (GCD curves). Reproduced with permission from ref. [55] Copyright 2009 American Chemical Society. **e** PANI/carbon nanotube nanocomposite electrode in a polymer gel electrolyte, schematically represent. **f** CV at 5 mVs^{-1} and **g** Flexible PANI/carbon nanotube nanocomposite thin film electrodes discharge characteristics in H_2SO_4–PVA gel and 0.5 M H_2SO_4 aqueous. 1 Ag^{-1} galvanostatic charge–discharge curves in H_2SO_4–PVA gel electrolyte and 0.5 M H_2SO_4 aqueous solution are shown in inset (g). Reproduced with permission from ref. [62] Copyright 2010 American Chemical Society

aligned carbon nanotube (VA-CNT) networks provide excellent inter-tube distance along with associated porous structural features, resulting in advanced electrolyte reachable surface area for the gain of charge transport and storage. [63, 64]. SCs constructed with VA-CNTs can discharge 50% of their stored energy in <0.76 ms than SCs produced of random CNT networks, according to theoretical models and actual evidence [64]. Furthermore, plasma etching [65, 66] can be utilized to expose the top end-caps of VA-CNTs, enabling the electrolyte access to the VA-CNTs' interior chamber for charge storage. The current study suggests that a 3-electrode configuration and a liquid electrolyte may be used to get the upgraded efficiency of VA-CNTs as compared to random carbon nanotubes [63, 65, 67]. Furthermore, using a template-free CVD technique, a VA-CNT array electrode obtained a high capacitance of 365 Fg^{-1} in 1 M H_2SO_4 [68] and 440 Fg^{-1} in ionic liquid electrolytes [65, 69]. In contrast, VA-CNTs have received minimal attention for use in two-electrode ASSSC lead to an increase in the flexible device performance.

4.2 Graphene-Based Flexible SCs

It was previously utilized to create other graphitic carbon forms, such CNTs, in a variety of applications where CNTs were employed. Graphene, like CNTs, has a huge SSA, decent electromechanical characteristics, and at last chemically stable [70–72]. Chemical reduction of graphene oxide (GO) [76, 77], CVD [78], and ball

milling [79] were only a few known methods for producing GR. Graphene materials produced as a consequence have been reported to be broadly employed as electrodes in liquid electrolyte SCs [75, 80]. A single electrode supercapacitance of 200 Fg^{-1} has been obtained using two-electrode SCs with large surface area GR electrode materials (3100 m^2g^{-1}) [80]. Flexible ASSSCs with GR electrodes were reported to have a range of interesting characteristics [81, 82], in addition to GR-based SCs development with liquid electrolytes. El-Kady et al. [82], for example, employed a standard LightScribe DVD optical drive to generate GR electrodes via conducting the laser-induced reduction of GO sheets for SCs (Fig. 9a–f). These flexible ASSSCs also exhibited a high energy density (1.36 mW h cm^{-3}, twice that of activated carbon) and outstanding stability when bent from 0° to 180° (Fig. 9g–i). The majority of SSSCs based on free-standing GR materials have specific capacitances (80–118 Fg^{-1}) that is expressively lower compared to the theoretical value (550 Fg^{-1}) [83], due to GR sheet restacking to decrease the GR active surface area and slowed ion transport/diffusion within the active mat. Porous three-dimensional GR networks, like GR hydrogels and aerogels, were created as suitable electrodes for electrochemical energy storage devices to solve this issue [84, 85]. Moreover, freeze dehydration of a chemically reduced GR dispersion [86] or uninterrupted CVD on Ni-foam [84, 87]

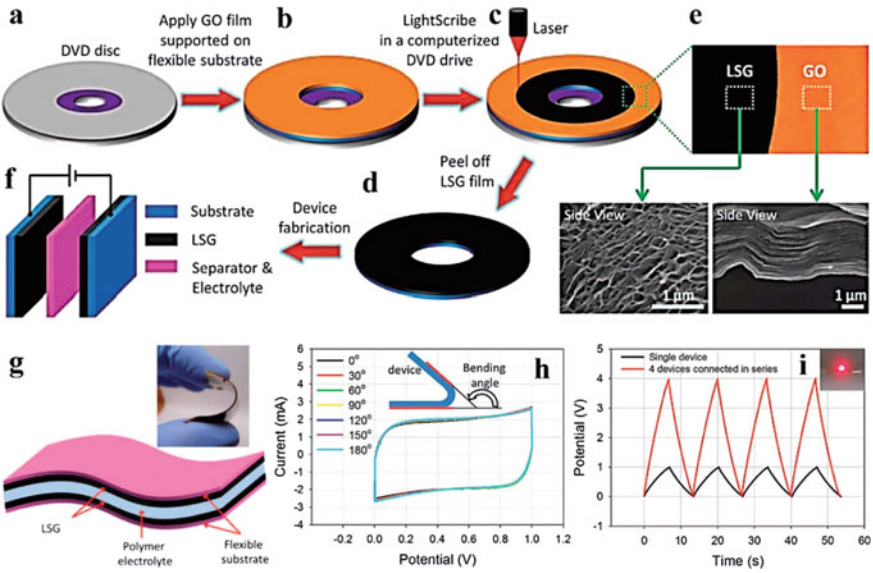

Fig. 9 **a–f** The manufacturing of laser-scribed GR-based electrochemical capacitors is depicted schematically (EC), **e** GO film photograph as converted to laser-scribed GR. **g** ASS-LSG–EC demonstrates how the gelled electrolyte may double as an electrolyte and a separator shown schematically. The inset is a digital image demonstrating the device's adaptability. **h** CV curves obtained when the device was bent at various angles at a scan rate of 1000 mVs^{-1}. I Galvanostatic charge–discharge curves for 4-devices linked in series; an LED has been used to power the charge–discharge curves (the inset image). Reproduced with permission from ref. [82] Copyright 2012 AAAS

are both used to generate porous three-dimensional GR materials. Graphene sheets were effectively prevented from restacking in both cases, and electrolyte transport throughout the GR network was much improved. Consequently, 3-electrode SCs based on 3D GR hydrogels demonstrated enhanced electrochemical efficiency, with specific capacitances (up to 220 Fg^{-1}) for a single electrode at 1 Ag^{-1} in an aqueous solution containing 5 M KOH.

Highly deformable SCs were created using 3D GR foams. Zhao et al. [89] used hydrothermal reduction of aqueous GR dispersions to make 3D GR foam and GR/polypyrrole composite foam (Fig. 10e–h). Under manual compression, these foams can resist significant strain deformation (50% strain) and recover to their innovative figure deprived of structural variation in 10 s. After 1000 compression-decompression cycles at a 50% compressed strain, the CV curves for SCs based on these 3D GR foams remained stable (Fig. 10i). Ball milling of graphite powders has resulted in the production of EFGRs-edge-functionalized GR sheets with a range of edge groups (–H, –N, –Br, –Cl, –I, –COOH, and $–SO_3H$) [79, 90, 91]. By using

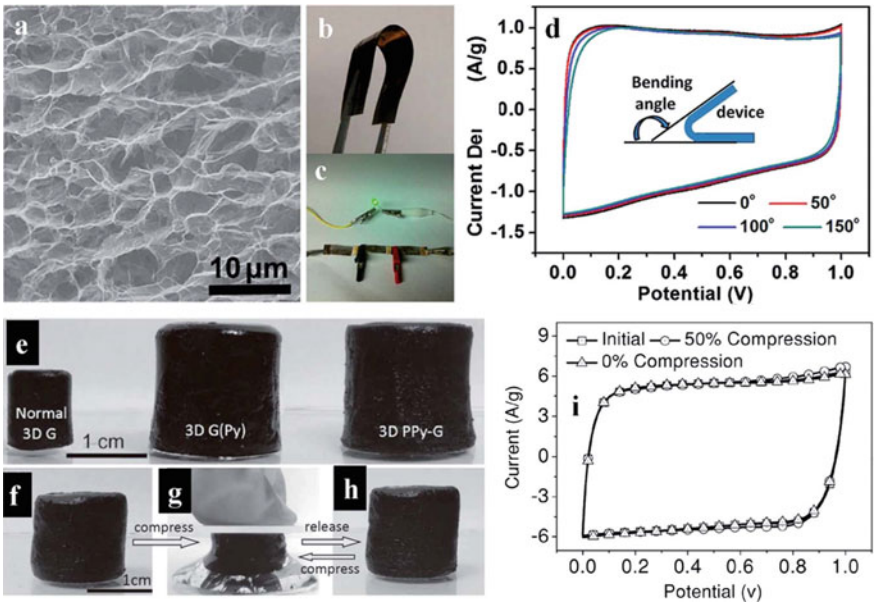

Fig. 10 **a** SEM image of GR hydrogel; **b** flexible SSSCs made of GR hydrogel photograph. **c** A green LED driven by 3-series-connected SCs photograph. **d** CV curves for the flexible SSSCs at 10 mV/s for various bending angles Permission granted by ref. [88] American Chemical Society. All rights reserved. **e** Photographs of as-prepared conventional 3-D GR, 3-D GR-pyrrole (GR-Py), and 3-D GR-polypyrrole (PPy-GR) (from left to right). **f–h** PPy-G foam compression-decompression procedures. I–V curves of compressible SC cells based on PPy-GR foam electrodes at 0 and 50% compression for one cycle at a scan rate of 30 mVs^{-1}. Permission granted by ref. [89] 2013 John Wiley & Sons

a wide range of solution processing/self-assembling methods, large-area hierarchically structured GR films can be produced that can be used as electrodes in a range of various energy-related devices, including fuel cells and flexible SCs, due to the availability of solution-processable EFGRs [79, 92].

4.3 3D Pillared CNT/Graphene Architectures for Flexible SCs

As mentioned previously, some recent achievements in manufacturing randomly oriented carbon nanotube/GR hybrid electrodes for SCs were obtained. Furthermore, controlling the porosity and hole distribution inside randomly oriented carbon nanotube/GR hybrid materials is challenging, if not unachievable, due to the random assembly of the component carbon nanotubes and GR sheets [93–95]. Recent theoretical studies [95, 96] demonstrate that three-dimensional pillared architectures (Fig. 11a) [93], composed of parallel GR layers supported by VA-carbon nanotubes in between, exhibit a high degree of structural tunability. VA-carbon nanotubes will provide some ideal transport and mechanical characteristics for effective energy storage within the pillared structure. In three dimensions, there are excellent conductive pathways for efficient charges transport, resulting in high capacitance and rate capability. According to theoretical predictions, 3-D pillared carbon nanotube/GR hybrid structure with modifiable pore diameters and surface areas may be constructed [94, 95]. Three-dimensional pillared VA-carbon nanotube/GR structures with alternating VA-carbon nanotubes of various NTs lengths/packing densities and GR layers (Fig. 11b) were produced through intercalated CVD growth [93]. They possessed a specific capacitance of around 110 Fg^{-1} when employed as electrodes in a three-electrode system [93]. After $Ni(OH)_2$ coating, a high specific capacitance (1065 Fg^{-1}) has been obtained (Fig. 11c), together with exceptional rate capability and durable electrochemical stability. This value is 10 times including of big surface area activated carbons (100 Fg^{-1}), and is comparable to 953–1335 Fg^{-1} for GR-supported single-crystalline $Ni(OH)_2$ hexagonal nanoplates [98]. Lin et al. [99] recently explained the fabrication in situ of 3-D CNR/GR micro-SCs (Fig. 11d–h). The volumetric energy density of the ionic liquid has been reported to be 2.42 $mWhcm^{-3}$ (Fig. 11i), which is higher than LSG–DLC49 and Al–electrolytic capacitors [100]. Additionally, the ultrahigh rate capability of 400 Vs^{-1} enables to achieve a maximum power density of 115 and 135 Wcm^{-3} in aqueous and BMIM–BF_4 electrolyte, respectively (Fig. 11j). These findings demonstrate conclusively that the 3D pillared carbon nanotube/GR hybrid designs provided great performance for liquid electrolyte SCs, which is consistent with theoretical models. As a result, they should be interesting choices for use as electrode materials in high-performance flexible ASSSCs, though this has not yet been shown experimentally.

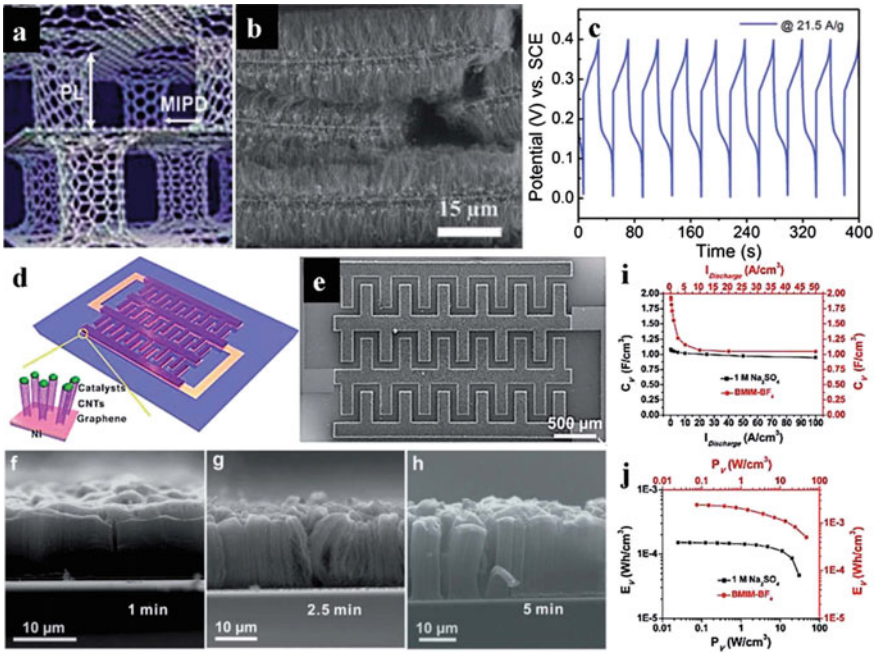

Fig. 11 **a** Schematic of a three-dimensional pillared VA-carbon nanotube/GR nanostructure. **b** A representative SEM image of 3-D pillared VA-carbon nanotube/GR architecture. **c** Galvanostatic charge and discharge curves for the $Ni(OH)_2$-coated VA-carbon nanotube/GR electrode at 21.5 Ag^{-1}. Permission required for reproduction of ref. [93] 2011 American Chemical Society. All rights reserved. **d** Schematic of GR/carbon nanotube Cs–MCs structure. Inset: enlarged diagram of the Ni–GR– carbon nanotube-Cs pillar structure without the Al_2O_3 on top of the carbon nanotube-Cs. **e** SEM micrograph of GR/carbon nanotube Cs–MC produced in the laboratory. **f**–**h** SEM micrograph of cross-sectioned carbon nanotube-Cs grown for 1, 2. 5, and 5 **min**. **i** Comparing CV and discharge volumetric current densities; **j** A comparison of the PV and energy density in the Ragone plots (EV). Reproduced with permission from ref. [99] Copyright 2013 American Chemical Society

4.4 Free-Standing CNT/Graphene Hybrid Films for Flexible SCs

There seems to be a lack of control over the film architecture/properties when employing 3D GR foams as electrodes in SCs. One appealing approach is to utilize 1D carbon nanotubes to physically divide 2D GR sheets to retain GR's large surface area and to create well-controlled designs for effective charge/electrolyte transport in CNT conducting networks [101, 102]. Free-standing CNT/GR composite films were produced using a variety of techniques, such as LBL self-assembling, vacuum filtering, and solution casting [102, 103]. Yu and Dai [101] produced CNT/GR hybrid films with well-defined nanopores using LBL self-assembling poly(ethyleneimine)-modified GR sheets and acid-oxidized carbon nanotubes. Even at an extremely high scan rate of 1 Vs^{-1}, the resultant free-standing multilayered carbon nanotube/GR

hybrid film displayed a virtually rectangular CV with an average specific capacitance of 120 Fg^{-1} (3-electrode). Furthermore, the TMOs were included in a carbon nanotube, GR, and their hybrid materials to enhance the electrochemical performance of the resulting flexible SC [102, 103]. Cheng et al., developed free-standing carbon nanotube/MnO_2/GR composite films with MnO_2 loading of 71 wt% and outstanding mechanical characteristics (tensile strength of 48 MPa) using a vacuum filtering technique and showed their application as flexible electrodes in liquid electrolyte SCs (1 M of Na_2SO_4). Due to the existence of conducting carbon nanotube networks, a specific capacitance of 372 Fg^{-1} was attained with a high rate capability. Gao et al. [104] created an asymmetric ASSSC utilizing a free-standing carbon nanotube/GR paper as the negative electrode and GR/Mn_3O_4 paper as the positive electrode in a slightly related but independent study (Fig. 12a). Both composite sheets were produced by filtering their respective mixed solutions. In Fig. 12b, a photograph of the as-prepared carbon nanotube/GR composite paper with a diameter (4 cm) as displayed, while in Fig. 12c, a cross-section SEM image of the paper is displayed, revealing the CNTs interposed between the GR layers. The specific capacitance of

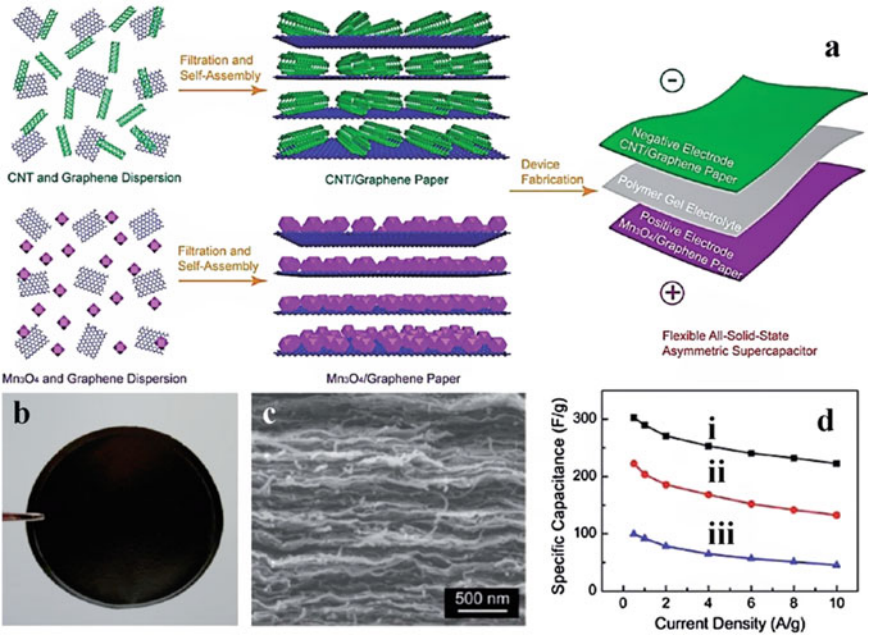

Fig. 12 **a** Process schematic for fabricating flexible ASSSCs using free-standing carbon nanotube/GR and MnO_2/GR paper electrodes. **b** Photograph of 4 cm diameter carbon nanotube graphen-40 paper. **c** SEM image of carbon nanotube GR-40 paper in cross-section. **d** Specific capacitance values for CNTG-40 I CNTG-20 (ii), and rGO (iii) papers as a function of discharge current densities. (carbon nanotube GR-40 and carbon nanotube GR-20 denote carbon nanotube/GR papers having a carbon nanotube mass ratio of 40% and 20%, respectively.). Reproduced with permission from ref. [104] Copyright 2012 American Chemical Society

the carbon nanotube/GR paper electrodes improved from 99.7 to 212.9 and 302 Fg^{-1} (3-electrode) with an increase in CNT mass ratio (Fig. 12d). The asymmetric ASSCs' total capacitance reached 72.6 Fg^{-1} (2-electrode) at a current density of 0.5 Ag^{-1}, resulting in high energy density (32.7 $Whkg^{-1}$) and good cycling stability.

4.5 Carbon Fiber-Based SCs

As mentioned previously, several SCs with planar topologies have been created [105], such as based on cotton/textile electrodes coated with carbon nanotubes or GR. Moreover, the rapid growth of wearable electronics [106] necessitates the creation of flexible and wearable SCs in fibers shape. As a result, wearable fiber-shaped SCs have gained growing interest [107, 108], and a variety of fiber materials were used as substrates, for example, Kevlar fiber [107], metal fiber [108], C-fiber [109], CNT-fiber [110], and GR-fiber [111]. CNT fibers were widely investigated because of their high electrical conductivity, great mechanical characteristics, and exceptional flexibility [110, 112, 113]. Ren et al. [110] innovated the incorporation of carbon nanotubes into fiber-shaped SCs with a twisted structure and a low specific capacitance (0.006 $mFcm^{-1}$). The specific capacitance of a single electrode subsequently increased to 294 Fg^{-1} or 282 $mFcm^{-1}$ via a pseudocapacitance originating from PANI [113]. Similarly, Lee et al. [112] developed a fast-ion-transport yarn (Fig. 13a, b) by scrolling MWCNT with conductive polymer (PEDOT-poly(3,4-ethylenedioxythiophene)). The capacitance of the plied yarn SCs increased linearly with scan rate up to 80 Vs^{-1} for liquid electrolytes and 20 Vs^{-1} for solid electrolytes. The resulting fiber-shaped SCs were extremely stable, and exhibited high capacitance retention upon bending as shown in Fig. 13d–e.

4.6 Carbon-Based Bendable and Transparent SCs

Besides the recent advancement in SCs and towards flexible, wearable electronics using thin-film/fiber type (textile, fabric, and coating, etc.) were garnered increased interest as improved power sources. Owing to their outstanding electrochemical stability, enormous surface area, outstanding electric and mechanical properties; C-nanoparticles are recognized as favorable electrode substances for flexible SCs. Within the same context, transparent and flexible SCs focused on (In_2O_3) nanowire or CNT heterogeneous layers were devolved by Chen et al. that shows raised specific capacitance degree (64 F/g) as the number of (In_2O_3) nanowire up to 0.007 mg distributed on carbon NT films increased [114].

Alternative work revealed that a film-based 2 mm-thick FSCs composed of MnO_2 nanosheets doped with carbon electrodes nanofiber had a gravimetric capacitance (142 F/g) at 10 mV/s slow scan rate when interfaced through PVA-$H_4SiW_{12}O_{40} \cdot nH_2O$ [115]. Additionally, TiO_2/MWNT/PEDOT nanocomposite C-fibers and

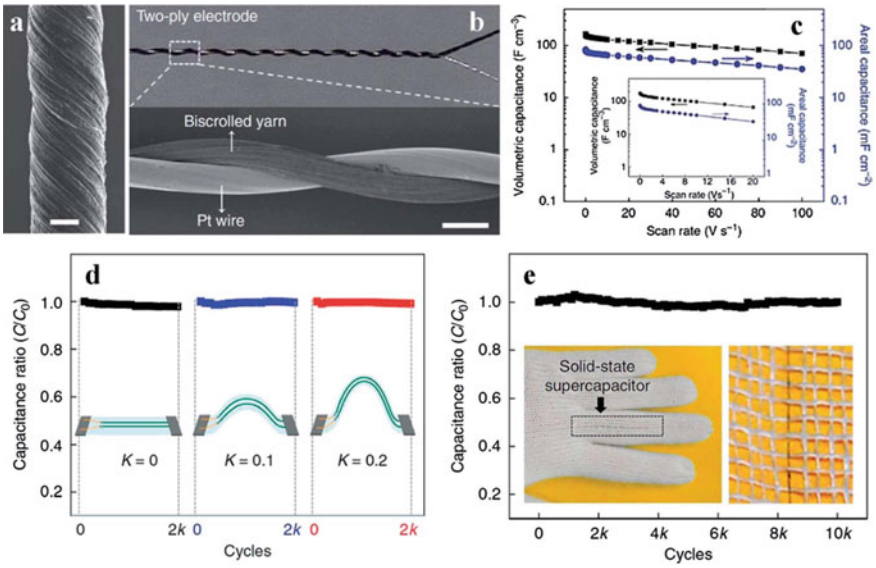

Fig. 13 **a** SEM-images of a 37° biscrolled yarn. **b** SEM-images of PEDOT/MWCNT biscrolled yarn. **c** Capacitance in volume against scan rate. **d** Bending a flexible PET film. **d** Producing a glove (the yarn SC was 5 cm long). Permission to reproduce from [112] Nature Publishing Group

different C-papers composed of nanotubes, fiber, and aerogel have been employed as electrodes in FSCs [116]. Liu et al. [117] used an electrospinning technology in conjunction with a Co ion-assisted acid corrosion procedure to create extremely flexible porous carbon nanofibers (PCNFs) films. The resulting fibers exhibit excellent mechanical flexibility and electrical conductivity with no resistance change after repetitive bending up to 180°. The PCNFs electrode demonstrated a specific capacity rate (104.5 F/g) in 0.5 M H_2SO_4 around 0.2 A/g current markedly increased constancy of cycling process with 94% specific capacity after 2000 charging/discharging cycles, as well as after 500 bending cycles, 89.4% capacitance rate was observed. Such exceptional properties correspond to P-high CNF's graphitization degree and its distinct hierarchical pore structure [117].

It is usually desired to have a low processing cost while producing flexible electrodes. Du et al. [118] created an economical, flexible, and highly efficient hybrid electrode using a vacuum-filtered MnO_2-NT and CNT nanocomposite layer (Fig. 14a). The dynamical effects among carbon conductive nanotubes and pseudocapacitive MnO_2-NT, the hierarchical freestanding porous layer structure, and the superior MnO_2 mass loading with 4 mg/cm^2, the MnO_2-nanotube or carbon nanotube as electrodes demonstrated significant electrochemical plus mechanical strength using the volumetric capacity rate in polyvinyl alcohol (5.1 F/cm^3) because of ultra-lengthy 1D-NT morphology. Due to the self-activation effect, the capacitance retention is about 105% of initial capacitance with (PVA)/LiCl gel electrolyte having a great energy density value (0.45 mWh/cm^3) for entire FSCs volume after

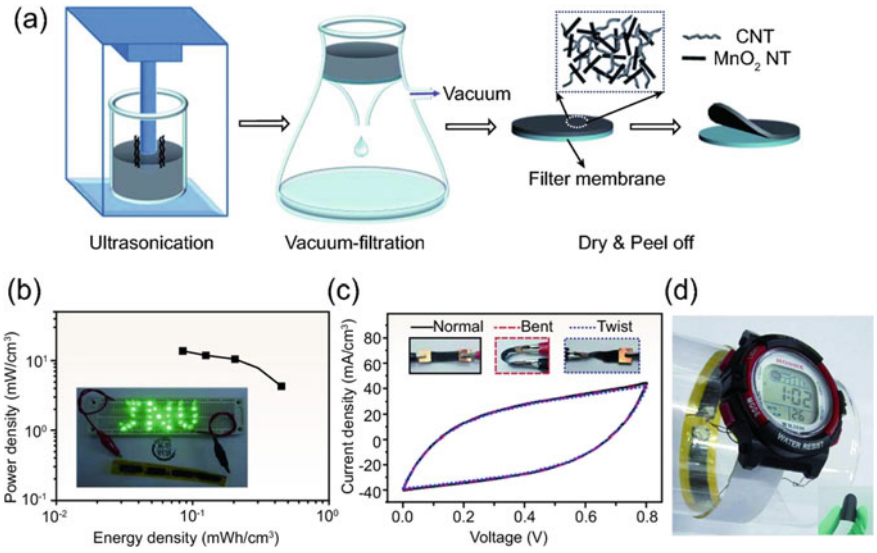

Fig. 14 **a** Representation for the synthesis of flexible free-standing CNT/MnO_2-NT hybrid film, **b** Ragone plots of the flexible SSSCs device (Inset indicates a LEDs group), **c** CV curves collected under normal, bent, and twisted conditions (insets represents digital micrograph under various tests environments), **d** an electronic watch wrapped around a transparent glass tube. Reproduced with permission from ref. [118] Copyright 2014 Royal Society of Chemistry

6000 cycles. Resulted in SCs can be utilized in a source of flexible power such as wearable electronic systems for watches and LEDs as can be seen in Fig. 14b–d.

As with traditional ESCs, composites of CNT/GR and conductive polymers were frequently employed in FSCs. Polyacrylic acid/polyaniline (PAA/PANI) nanocomposites were synthesized by Wang et al. with N-decorated GR (NG) (NG-PAA/PANI) [119] and indicated the CC electrodes comprising 32 wt% PANI and 1.3 wt% NG had a high capacitance (521 F/g) in (1 M) H_2SO_4 electrolyte at 0.5 A/g (Fig. 15). A symmetric SC 20% PANI-CC electrodes composition demonstrated a 68 F/g capacitance at 1 A/g that was four times from earlier described SCs composed of flexible PANI-CNT nanocomposites. With 5.8 Wh/kg energy density, 1.1 kW/kg power density, 81% capability rate at 10 A/g, and (83.2% retention) after 2000 cycles, the NG-PAA/PANI electrode preserved its entire capacitance through significant bending angles [119].

Chen et al. produced the first CNT-based electrodes with good transparency (up to 78% at 550 nm) and stretchability that increased electrical resistance by just 80% when coated with a layer of PVA–H_3PO_4 electrolyte [120]. On the other hand, these scientists suggested transparent and stretchy ASSSCs (Fig. 16a, b) by directly pressing two PDMS-supported carbon nanotube electrodes with the separator inserted in between [120]. The device (Fig. 16b) exhibited transmittance of ~75% (Fig. 16c), equal to a single-layer carbon nanotube. However, a similar device with a parallel constructed arrangement (Fig. 16a) showed a transmittance of 64%.

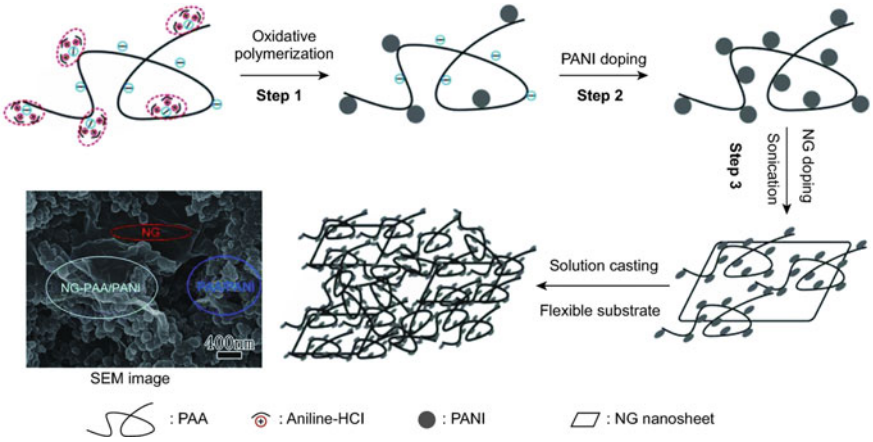

Fig. 15 Illustration of a synthesis route for attaining an NG-PAA/PANI composite coating on CC. Reproduced with permission from ref. [119] Copyright 2016 Springer Nature

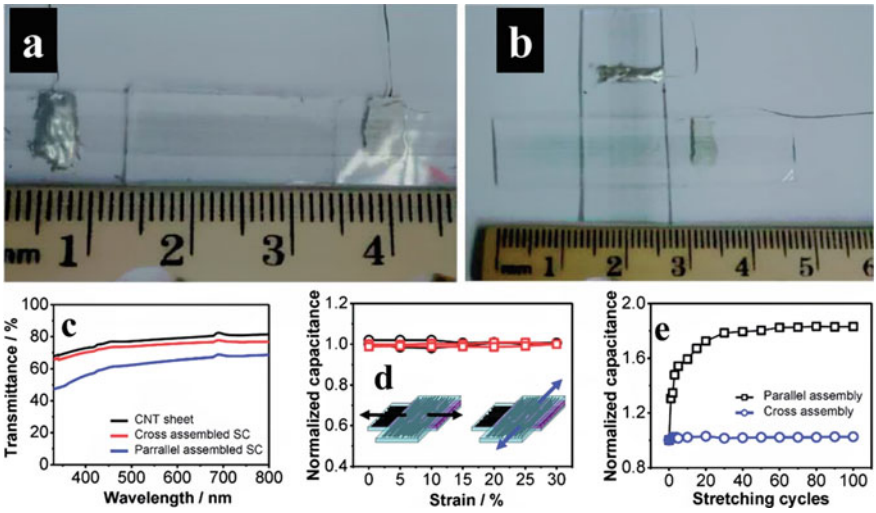

Fig. 16 **a**, **b** Photographs of parallel and cross configurations of SCs. **c** Transmittance spectra of a single layer CNT. **d** As a function of biaxially stretched tensile strain, the normalized specific capacitance of a SC with cross assembly is shown. **e** Specific capacitance of two SCs normalized as a function of stretching cycles. Reproduced with permission from ref. [124] Copyright 2014 Nature Publishing Group

The device demonstrated excellent biaxial stretchability (Fig. 16d). Further, it was demonstrated that the cross-constructed SC is more stable than its parallel equivalent (Fig. 16e). By comparison, the parallel constructed SC had a capacitance rise of almost 70% over the initial 20-stretching cycles before stabilizing. The increase

in capacitance can be attributed to the combined effects of a stretching-induced increase in the active sites of the carbon nanotube sheet and contact loss between nanotubes [120]. Both types of SCs demonstrated excellent stability even after several hundreds of stretching cycles, indicating a high degree of practical application potential. Besides the transparent carbon nanotube electrodes, GR was already utilized for the same purpose due to its superior optical and electrical characteristics [121–123].

Even though some GR-based stretchable electrodes and electronic devices were published [121, 125], their effectiveness is still severely constrained by the GR sheet's susceptibility to damage when stretched. For example, when a GR sheet was placed onto a pre-strained elastic substrate, the electrical resistance jumped by a factor of more than one order [121]. Furthermore, it is challenging to transfer as-grown GR with a surface area (22 cm^{-2}) to a pre-strained substrate since the GR sheet frequently cracks or breaks during the transfer process. Therefore, only a small amount of work was being focused on developing transparent and stretchy GR electrodes, as this is extremely difficult, if not impossible. One-atom-thick and/or few-layered GR sheets exhibit excellent stretchable and transparent optoelectronics properties resulting in high conductivity and transparency (up to 95% for a 2 nm thick film [77]). To enable this potential, the world's first wrinkled few-layer GR sheet was designed, which served as the basis for the fabrication of transparent and stretchy ASSSCs [126]. Owing to its distinctive structure, the coated wrinkled multilayered GR sheet has been observed to be extremely stretchable, with an increase in electrical resistance of only 170% under 40% strain [126], which is significantly better than any previously reported stretchable planar GR electrode [121]. The resulting wrinkled GR was flexible and had a 60% transmittance at 550 nm. They show that SCs with wrinkled GR electrodes have excellent optical transparency and mechanical stretchability, which is useful for portable energy storage components in stretchy integrated systems. The low SSA of the horizontally layered GR sheets and the lack of a metal current collector both limit the effectiveness of these recently found transparent and stretchable SCs based on wrinkled GR electrodes. As a consequence, conductive polymers and/or metal oxides can significantly enhance the electrochemical activity of carbonaceous nanomaterials.

4.7 Carbon-Based Stretchable and Twistable SCs

As the FSCs discussed before, twisted and stretchy FSCs are necessary for innovative electronics, for instance, self-powered polymer sensors, polymer LEDs as well as solar cells, and sharp matrix demonstrations [127]. Using early findings on twisted SCs, buckling SWNT or polydimethylsiloxane (PDMS) electrodes have garnered broad interest owing to their tendency to withstand strains of a maximum of 140% without negotiating resistance [128, 129]. The use of crumpled GR nanosheets simplified and lowered the cost of creating flexible, highly efficient electrodes for SCs [130]. During 1000 stretch/relax cycles, the crumpled GR nanosheets electrode paper displayed potential stretchability of around 300% linear strain and 800% aerial

strain, as well as great specific capacitance (196 F/g) in H_3PO_4-PVA electrolyte and dependability [130]. Additionally, Kim et al. [131] demonstrated a delamination-free stretched SCs in which all of the components have been arranged using a single matrix made of an ionic liquid, 1-ethyl-3-methylimidazolium bis(trifluoromethylsulfonyl)-imide, and a polymer, poly(vinylidene fluoridehexafluoropropylene), as a supporting film and an electrode. The electrode film can be formed via integrating carbon nanotubes into a common (polymer) matrix and then dissolving the composite's surface with acetone to form a single body. The operating voltage of cell was a high as 3 V due to utilization of ionic liquid-based gel electrodes. The areal cell capacitance was 12.7 D/cm^2, and specific electrode capacitance was 67.2 F/g. Standard deviations for capacitance were observed to be 1.4 and 2.1% respectively, after radial stretches at 0.5 strains and 500 lateral cycles. MnO_2 nanoparticles with PPy-coating were placed on the textile CNT-decorated SCs electrode, increasing the electrochemical energy storing capacity of MnO_2 or CNT-based flexible (13% bend) and stretchable (21% tensile strain) SCs by 38% (Fig. 17) [132].

A specific capacitance (461 F/g) has been found in H_3PO_4-PVA electrolyte at 0.2 A/g current density, which has been ascribed to the delamination anticipation of MnO_2 NPs via PPy coating. Additionally, 96.2% of capacitance is being retained after 750,000 bending (13%) cycles [132]. The identical deformable substrate is shown in Fig. 18 [133]. Using PANI-wrapped MWNTs and an ion-gel electrolyte composed of poly(ethylene glycol) diacrylate and 1-ethyl-3-methylimidazolium bis (trifluoromethylsulfonyl) imide, the MSCs patterns have been made which demonstrated exceptional electrochemical efficiency when subjected to a 50% uniaxial strain and a 40% biaxial strain; their initial performance. Additionally, the GR sensor patterns have been identified NO_2 gas for around an hour when integrated with MSCs through serpentine interconnections, even when uniaxially stretched by 50%. For near-term applications, such a hybrid mixing of SCs and other practical electrical systems is extremely required. However, considerably greater emphasis must be placed on significantly enhancing the capacitive storage capacity of flexible and stretchy SCs [134], buckled carbon nanotube films were also studied for use as stretchable electrodes in SCs. A comparison of PANI composites of buckled carbon nanotubes with and without nitric acid action found that acid-treated buckling carbon nanotube@PANI electrodes had a maximum specific capacitance (1147.12 mF/cm^2) at 10 mV/s in H_3PO_4-PVA electrolyte [134]. This finding is consistent with the creation of stronger interfacial bonds among acid-treated carbon nanotubes and PANI. The acid-treated electrode likewise demonstrated an energy density ranging (31.56–50.98) Wh/cm^2, and a power density of (2.294–28.404) mW/cm^2 with a scan rate of 10–200 mV/s. The comparable SC withstood a 200% omnidirectional strain. Subsequently, yarn-based stretchable and twistable SCs were produced, consisting of core–shell nanostructured coiled electrodes by pseudocapacitive carbon NT cores and MnO_2 core-shells [135].

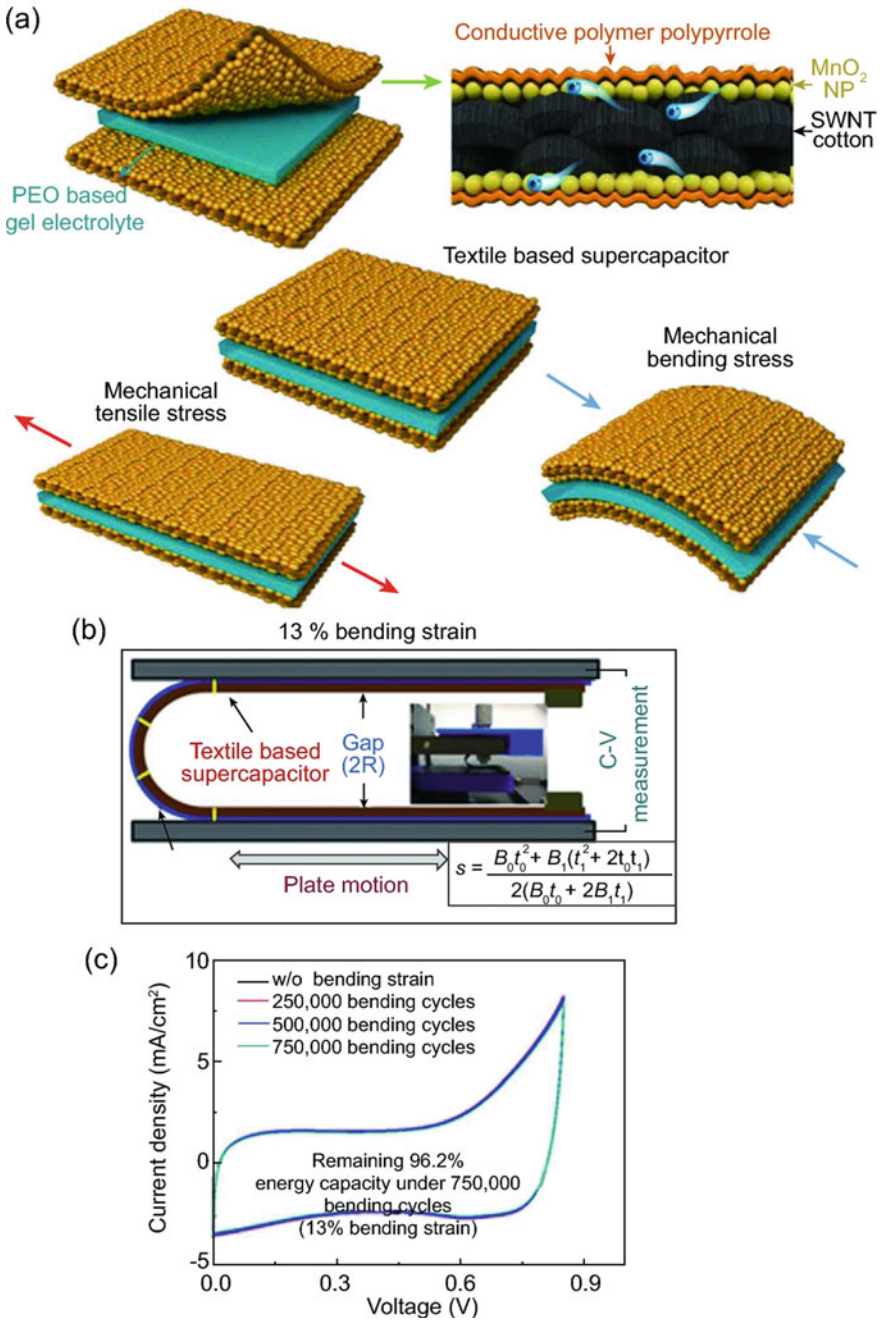

Fig. 17 **a** Schematic view of the polypyrrole—MnO_2-fabrication coated textile SC, **b** illustration for bending test performed on polypyrrole—MnO_2-coated SC, **c** cyclic voltammetry of SC under 13% bending strain. Reproduced with permission from ref. [132] Copyright 2015 American Chemical Society

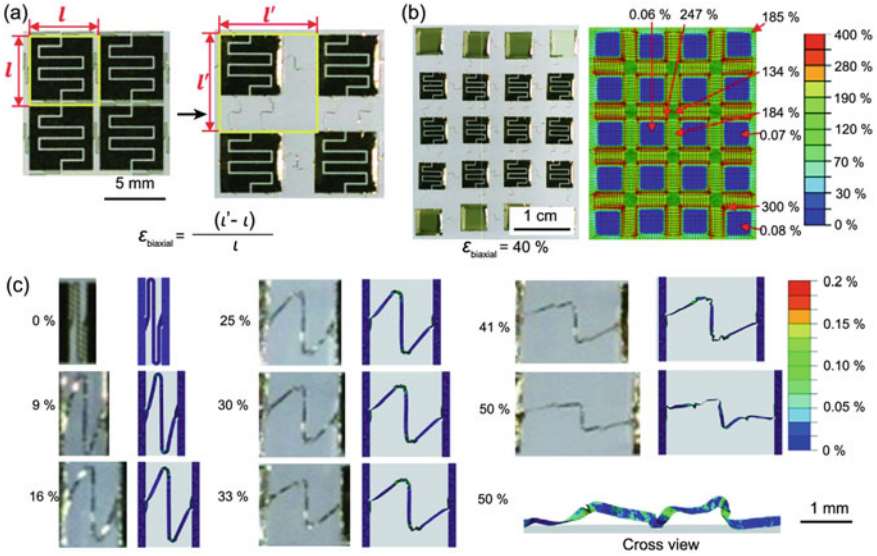

Fig. 18 **a** Schematic view of the biaxial strain $\varepsilon_{biaxial}$, **b** optical microscope micrographs of MSC array (left) and the strain distribution estimated with FEM analysis (right) under a biaxial strain of 40%, **c** optical images (left) and the results received from FEM analysis (right) of a serpentine interconnection in different uniaxial stretching states. The cross-sectional view shown is for a strain of 50%. Reproduced with permission from ref. [133] Copyright 2016 Elsevier

5 Conclusion(s) and Summary

The current chapter has presented summarized overview related to recent advances owing to various dimensional carbonaceous architectures/composites towards applications of SCs. In this regard, dimensional carbonaceous nanoarchitecture, such as carbonaceous nanotubes, GR nature nanostructures, and carbon-based nanosheets, porous carbons; carbide derivatives, MOF derivatives, carbon aerogels, and all other possible nanostructures have been discussed associated with employed synthetic strategies. Main exploring advantages are natural abundance, approachable availability, low-cost property, reliable stability, due to which carbonaceous nanostructures are widely implemented as electrodes owing to SCs. These carbonaceous materials possess a large surface area site for ions, defined pore structures for ionic transportation, and significant electrical conductivity for transferring electrons. To achieve these goals, a variety of strategies were employed for developing sensible as well as controllable carbonaceous structures. Moreover, various carbonaceous composites/nanostructures were developed enhancing capacitive efficiency along with energy densities regarding SCs. In addition to significant researches, attractive efforts in favor of dimensional carbonaceous nanoarchitectures towards novel applications of SCs were achieved recently. Furthermore, designing and fabrication of attractive nanoarchitectures inheriting excellent performance towards increasing

demand of energy storage devices are considered still a pending challenge. In addition, future carbonaceous materials may be excavated depending upon various aspects to be discussed in this work. Firstly, the existence of a high specific area provides necessary space with respect to ion accessibility and also charge accumulation. Secondly, normally optimized pore diameter along with size distribution may vary porous structure hierarchically. Microporous diameter is compared with ion size for accelerating electrolytic ions accessibility. Mesopores may function as ion channels for accelerating transportation of ions existing in the electrolyte into electrode materials, whereas macropores perform their role as ion-buffering reservoirs, shortening the space of the ions diffusion mechanism. Thirdly, a balanced state of pore structure with conductivity may significantly accelerate electrolytic ionic diffusion as well as electron transfer, because the rising temperature may result in improved graphitization degree, thereby generating reasonable conductivity, though may cause collapsed pore structure. Fourthly, the formation of capacitively hybrid carbonaceous nanostructure associated with pseudo-capacitive components, in turn presenting faradaic redox reactions, thereby increasing capacitance efficiency along with energy densities. Moreover, wettability lying between electrode materials as well as aqueous media of electrolytes with production has been taken into consideration for developed carbonaceous electrode materials towards novel application relevant to SCs. With unremitting endeavors, it is believed that the applications owing to carbon-based nanomaterials for future generations of EESs, particularly SCs, are expected to meet flourishing age.

References

1. L. Dai, D.W. Chang, J.-B. Baek, W. Lu, Carbon nanomaterials for advanced energy conversion and storage. Small **8**, 1130–1166 (2012)
2. X.-Y. Luo, Y. Chen, Y. Mo, A review of charge storage in porous carbon-based SCs. New Carbon Mater. **36**, 49–68 (2021)
3. Y. Han, Z. Lai, Z. Wang, M. Yu, Y. Tong, X. Lu, Designing carbon based SCs with high energy density: a summary of recent progress. Chem. A Eur. J. **24**, 7312–7329 (2018)
4. Y. Wang, Z. Chang, M. Qian, Z. Zhang, J. Lin, F. Huang, Enhanced specific capacitance by a new dual redox-active electrolyte in activated carbon-based SCs. Carbon **143**, 300–308 (2019)
5. X. Chen, R. Paul, L. Dai, Carbon-based SCs for efficient energy storage. Natl. Sci. Rev. **4**, 453–489 (2017)
6. P. Simon, Y. Gogotsi, Materials for electrochemical capacitors. Nat. Mater. **7**, 845–854 (2008)
7. S.-W. Xu, M.-C. Zhang, G.-Q. Zhang, J.-H. Liu, X.-Z. Liu, X. Zhang, D.-D. Zhao, C.-L. Xu, Y.-Q. Zhao, Temperature-dependent performance of carbon-based SCs with water-in-salt electrolyte. J. Power Sour. **441**, 227220 (2019)
8. A. Borenstein, O. Hanna, R. Attias, S. Luski, T. Brousse, D. Aurbach, Carbon-based composite materials for SC electrodes: a review. J. Mater. Chem. A **5**, 12653–12672 (2017)
9. J. Cherusseri, R. Sharma, K.K. Kar, Helically coiled carbon nanotube electrodes for flexible SCs. Carbon **105**, 113–125 (2016)
10. M. Yu, D. Lin, H. Feng, Y. Zeng, Y. Tong, X. Lu, Boosting the energy density of carbon-based aqueous SCs by optimizing the surface charge. Angew. Chem. Int. Ed. **56**, 5454–5459 (2017)
11. R. Dubey, V. Guruviah, Review of carbon-based electrode materials for SC energy storage. Ionics **25**, 1419–1445 (2019)

12. H. Helmholtz, Ueber einige Gesetze der Vertheilung elektrischer Ströme in körperlichen Leitern, mit Anwendung auf die thierisch-elektrischen Versuche (Schluss.). Ann. Phys. **165**, 353–377 (1853)
13. G. Guoy, Constitution of the electric charge at the surface of an electrolyte. J. Physique **9**, 457–467 (1910)
14. D.L. Chapman, LI. A contribution to the theory of electrocapillarity. London Edinburgh Dublin Philos. Mag. J. Sci. **25**, 475–481 (1913)
15. O. Stern, The theory of the electrolytic double-layer. Z. Elektrochem **30**, 1014–1020 (1924)
16. L.L. Zhang, X.S. Zhao, Carbon-based materials as SC electrodes. Chem. Soc. Rev. **38**, 2520–2531 (2009)
17. Y. Wang, L. Zhang, H. Hou, W. Xu, G. Duan, S. He, K. Liu, S. Jiang, Recent progress in carbon-based materials for SC electrodes: a review. J. Mater. Sci. **56**, 173–200 (2021)
18. B.E. Conway, V. Birss, J. Wojtowicz, The role and utilization of pseudocapacitance for energy storage by SCs. J. Power Sour. **66**, 1–14 (1997)
19. V. Augustyn, P. Simon, B. Dunn, Pseudocapacitive oxide materials for high-rate electrochemical energy storage. Energ. Environ. Sci. **7**, 1597–1614 (2014)
20. Y. Shao, M.F. El-Kady, J. Sun, Y. Li, Q. Zhang, M. Zhu, H. Wang, B. Dunn, R.B. Kaner, Design and mechanisms of asymmetric SCs. Chem. Rev. **118**, 9233–9280 (2018)
21. V. Augustyn, J. Come, M.A. Lowe, J.W. Kim, P.-L. Taberna, S.H. Tolbert, H.D. Abruña, P. Simon, B. Dunn, High-rate electrochemical energy storage through Li+ intercalation pseudocapacitance. Nat. Mater. **12**, 518–522 (2013)
22. D.P. Dubal, O. Ayyad, V. Ruiz, P. Gómez-Romero, Hybrid energy storage: the merging of battery and SC chemistries. Chem. Soc. Rev. **44**, 1777–1790 (2015)
23. M.F. El-Kady, M. Ihns, M. Li, J.Y. Hwang, M.F. Mousavi, L. Chaney, A.T. Lech, R.B. Kaner, Engineering three-dimensional hybrid SCs and microSCs for high-performance integrated energy storage. Proc. Natl. Acad. Sci. **112**, 4233 (2015)
24. Y. Ma, H. Chang, M. Zhang, Y. Chen, Graphene-based materials for lithium-ion hybrid SCs. Adv. Mater. **27**, 5296–5308 (2015)
25. F. Zhang, T. Zhang, X. Yang, L. Zhang, K. Leng, Y. Huang, Y. Chen, A high-performance SC-battery hybrid energy storage device based on graphene-enhanced electrode materials with ultrahigh energy density. Energ. Environ. Sci. **6**, 1623–1632 (2013)
26. E. Lim, H. Kim, C. Jo, J. Chun, K. Ku, S. Kim, H.I. Lee, I.-S. Nam, S. Yoon, K. Kang, J. Lee, Advanced hybrid SC based on a mesoporous niobium pentoxide/carbon as high-performance anode. ACS Nano **8**, 8968–8978 (2014)
27. B. Li, F. Dai, Q. Xiao, L. Yang, J. Shen, C. Zhang, M. Cai, Nitrogen-doped activated carbon for a high energy hybrid SC. Energ. Environ. Sci. **9**, 102–106 (2016)
28. D.H. Seo, S. Yick, Z.J. Han, J.H. Fang, K. Ostrikov, Synergistic fusion of vertical graphene nanosheets and carbon nanotubes for high-performance SC electrodes. Chemsuschem **7**, 2317–2324 (2014)
29. T. Lv, Y. Yao, N. Li, T. Chen, Highly stretchable SCs based on aligned carbon nanotube/molybdenum disulfide composites. Angew. Chem. Int. Ed. **55**, 9191–9195 (2016)
30. J. Wu, W.-W. Liu, Y.-X. Wu, T.-C. Wei, D. Geng, J. Mei, H. Liu, W.-M. Lau, L.-M. Liu, Three-dimensional hierarchical interwoven nitrogen-doped carbon nanotubes/Co_xNi_{1-x}-layered double hydroxides ultrathin nanosheets for high-performance SCs. Electrochim. Acta **203**, 21–29 (2016)
31. D. Yu, K. Goh, H. Wang, L. Wei, W. Jiang, Q. Zhang, L. Dai, Y. Chen, Scalable synthesis of hierarchically structured carbon nanotube–graphene fibres for capacitive energy storage. Nat. Nanotechnol. **9**, 555–562 (2014)
32. H. Sun, X. You, J. Deng, X. Chen, Z. Yang, J. Ren, H. Peng, Novel graphene/carbon nanotube composite fibers for efficient wire-shaped miniature energy devices. Adv. Mater. **26**, 2868–2873 (2014)
33. Z. Lu, Y. Chao, Y. Ge, J. Foroughi, Y. Zhao, C. Wang, H. Long, G.G. Wallace, High-performance hybrid carbon nanotube fibers for wearable energy storage. Nanoscale **9**, 5063–5071 (2017)

34. H.-W. Chang, Y.-R. Lu, J.-L. Chen, C.-L. Chen, J.-F. Lee, J.-M. Chen, Y.-C. Tsai, C.-M. Chang, P.-H. Yeh, W.-C. Chou, Y.-H. Liou, C.-L. Dong, Nanoflaky MnO_2/functionalized carbon nanotubes for SCs: an in situ X-ray absorption spectroscopic investigation. Nanoscale **7**, 1725–1735 (2015)
35. W. Jiang, D. Yu, Q. Zhang, K. Goh, L. Wei, Y. Yong, R. Jiang, J. Wei, Y. Chen, Ternary hybrids of amorphous nickel hydroxide-carbon nanotube-conducting polymer for SCs with high energy density, excellent rate capability, and long cycle life. Adv. Func. Mater. **25**, 1063–1073 (2015)
36. R.R. Salunkhe, J. Lin, V. Malgras, S.X. Dou, J.H. Kim, Y. Yamauchi, Large-scale synthesis of coaxial carbon nanotube/$Ni(OH)_2$ composites for asymmetric SC application. Nano Energ. **11**, 211–218 (2015)
37. G. Sun, X. Zhang, R. Lin, J. Yang, H. Zhang, P. Chen, Hybrid fibers made of molybdenum disulfide, reduced graphene oxide, and multi-walled carbon nanotubes for solid-state, flexible, asymmetric SCs. Angew. Chem. Int. Ed. **54**, 4651–4656 (2015)
38. X. Hou, T. Peng, J. Cheng, Q. Yu, R. Luo, Y. Lu, X. Liu, J.-K. Kim, J. He, Y. Luo, Ultrathin ZnS nanosheet/carbon nanotube hybrid electrode for high-performance flexible all-solid-state SC. Nano Res. **10**, 2570–2583 (2017)
39. Z. Zhang, H. Wang, Y. Zhang, X. Mu, B. Huang, J. Du, J. Zhou, X. Pan, E. Xie, Carbon nanotube/hematite core/shell nanowires on carbon cloth for SC anode with ultrahigh specific capacitance and superb cycling stability. Chem. Eng. J. **325**, 221–228 (2017)
40. J. Sun, P. Zan, L. Ye, X. Yang, L. Zhao, Superior performance of $ZnCo_2O_4$/ZnO@multiwall carbon nanotubes with laminated shape assembled as highly practical all-solid-state asymmetric SCs. J. Mater. Chem. A **5**, 9815–9823 (2017)
41. R. Raccichini, A. Varzi, S. Passerini, B. Scrosati, The role of graphene for electrochemical energy storage. Nat. Mater. **14**, 271–279 (2015)
42. Y. Shao, M.F. El-Kady, L.J. Wang, Q. Zhang, Y. Li, H. Wang, M.F. Mousavi, R.B. Kaner, Graphene-based materials for flexible SCs. Chem. Soc. Rev. **44**, 3639–3665 (2015)
43. H.-P. Cong, X.-C. Ren, P. Wang, S.-H. Yu, Flexible graphene–polyaniline composite paper for high-performance SC. Energ. Environ. Sci. **6**, 1185–1191 (2013)
44. H.-K. Kim, A.R. Kamali, K.C. Roh, K.-B. Kim, D.J. Fray, Dual coexisting interconnected graphene nanostructures for high performance SC applications. Energ. Environ. Sci. **9**, 2249–2256 (2016)
45. H. Jiang, P.S. Lee, C. Li, 3D carbon based nanostructures for advanced SCs. Energ. Environ. Sci. **6**, 41–53 (2013)
46. Q. Liao, N. Li, S. Jin, G. Yang, C. Wang, All-solid-state symmetric SC based on Co_3O_4 nanoparticles on vertically aligned graphene. ACS Nano **9**, 5310–5317 (2015)
47. F. Wen, C. Hao, J. Xiang, L. Wang, H. Hou, Z. Su, W. Hu, Z. Liu, Enhanced laser scribed flexible graphene-based micro-SC performance with reduction of carbon nanotubes diameter. Carbon **75**, 236–243 (2014)
48. Y. Zhang, Q. Zou, H.S. Hsu, S. Raina, Y. Xu, J.B. Kang, J. Chen, S. Deng, N. Xu, W.P. Kang, Morphology effect of vertical graphene on the high performance of SC electrode. ACS Appl. Mater. Interfaces. **8**, 7363–7369 (2016)
49. H.-K. Kim, S.-M. Bak, S.W. Lee, M.-S. Kim, B. Park, S.C. Lee, Y.J. Choi, S.C. Jun, J.T. Han, K.-W. Nam, K.Y. Chung, J. Wang, J. Zhou, X.-Q. Yang, K.C. Roh, K.-B. Kim, Scalable fabrication of micron-scale graphene nanomeshes for high-performance SC applications. Energ. Environ. Sci. **9**, 1270–1281 (2016)
50. R. Kumar, H.-J. Kim, S. Park, A. Srivastava, I.-K. Oh, Graphene-wrapped and cobalt oxide-intercalated hybrid for extremely durable super-capacitor with ultrahigh energy and power densities. Carbon **79**, 192–202 (2014)
51. H. Zhang, Solvothermally induced α-Fe_2O_3/graphene nanocomposites with ultrahigh capacitance and excellent rate capability for SCs. J. Mater. Chem. A **3**, 22005–22011 (2015)
52. Y. Wang, W. Lai, N. Wang, Z. Jiang, X. Wang, P. Zou, Z. Lin, H.J. Fan, F. Kang, C.-P. Wong, C. Yang, A reduced graphene oxide/mixed-valence manganese oxide composite electrode for tailorable and surface mountable SCs with high capacitance and super-long life. Energ. Environ. Sci. **10**, 941–949 (2017)

53. S. Park, M. Vosguerichian, Z. Bao, A review of fabrication and applications of carbon nanotube film-based flexible electronics. Nanoscale **5**, 1727–1752 (2013)
54. Y. He, W. Chen, C. Gao, J. Zhou, X. Li, E. Xie, An overview of carbon materials for flexible electrochemical capacitors. Nanoscale **5**, 8799–8820 (2013)
55. M. Kaempgen, C.K. Chan, J. Ma, Y. Cui, G. Gruner, Printable thin film SCs using single-walled carbon nanotubes. Nano Lett. **9**, 1872–1876 (2009)
56. L. Hu, M. Pasta, F. La Mantia, L. Cui, S. Jeong, H.D. Deshazer, J.W. Choi, S.M. Han, Y. Cui, Stretchable, porous, and conductive energy textiles. Nano Lett. **10**, 708–714 (2010)
57. Y.J. Kang, H. Chung, C.-H. Han, W. Kim, All-solid-state flexible SCs based on papers coated with carbon nanotubes and ionic-liquid-based gel electrolytes. Nanotechnology **23**, 065401 (2012)
58. V.L. Pushparaj, M.M. Shaijumon, A. Kumar, S. Murugesan, L. Ci, R. Vajtai, R.J. Linhardt, O. Nalamasu, P.M. Ajayan, Flexible energy storage devices based on nanocomposite paper. Proc. Natl. Acad. Sci. **104**, 13574 (2007)
59. Y.J. Kang, S.-J. Chun, S.-S. Lee, B.-Y. Kim, J.H. Kim, H. Chung, S.-Y. Lee, W. Kim, All-solid-state flexible SCs fabricated with bacterial nanocellulose papers, carbon nanotubes, and triblock-copolymer ion gels. ACS Nano **6**, 6400–6406 (2012)
60. L. Hu, W. Chen, X. Xie, N. Liu, Y. Yang, H. Wu, Y. Yao, M. Pasta, H.N. Alshareef, Y. Cui, Symmetrical MnO_2–carbon nanotube-textile nanostructures for wearable pseudocapacitors with high mass loading. ACS Nano **5**, 8904–8913 (2011)
61. G. Yu, X. Xie, L. Pan, Z. Bao, Y. Cui, Hybrid nanostructured materials for high-performance electrochemical capacitors. Nano Energ. **2**, 213–234 (2013)
62. C. Meng, C. Liu, L. Chen, C. Hu, S. Fan, Highly flexible and all-solid-state paperlike polymer SCs. Nano Lett. **10**, 4025–4031 (2010)
63. J.-S. Ye, H.F. Cui, X. Liu, T.M. Lim, W.-D. Zhang, F.-S. Sheu, Preparation and characterization of aligned carbon nanotube-ruthenium oxide nanocomposites for SCs. Small **1**, 560–565 (2005)
64. T. Chen, L. Dai, Flexible SCs based on carbon nanomaterials. J. Mater. Chem. A **2**, 10756–10775 (2014)
65. W. Lu, L. Qu, K. Henry, L. Dai, High performance electrochemical capacitors from aligned carbon nanotube electrodes and ionic liquid electrolytes. J. Power Sour. **189**, 1270–1277 (2009)
66. S. Huang, L. Dai, Plasma etching for purification and controlled opening of aligned carbon nanotubes. J. Phys. Chem. B **106**, 3543–3545 (2002)
67. H. Zhang, G. Cao, Z. Wang, Y. Yang, Z. Shi, Z. Gu, Growth of manganese oxide nanoflowers on vertically-aligned carbon nanotube arrays for high-rate electrochemical capacitive energy storage. Nano Lett. **8**, 2664–2668 (2008)
68. Q.-L. Chen, K.-H. Xue, W. Shen, F.-F. Tao, S.-Y. Yin, W. Xu, Fabrication and electrochemical properties of carbon nanotube array electrode for SCs. Electrochim. Acta **49**, 4157–4161 (2004)
69. W. Lu, L. Qu, L. Dai, K. Henry, Superior capacitive performance of aligned carbon nanotubes in ionic liquids. ECS Trans. **6**, 257–261 (2019)
70. K.S. Novoselov, V.I. Fal′ko, L. Colombo, P.R. Gellert, M.G. Schwab, K. Kim, A roadmap for graphene. Nature **490**, 192–200 (2012)
71. A.K. Geim, K.S. Novoselov, The rise of graphene, in *Nanoscience and Technology.* (Co-Published with Macmillan Publishers Ltd, UK, 2009), pp. 11–19
72. A.K. Geim, Graphene: status and prospects. Science **324**, 1530 (2009)
73. L.L. Zhang, R. Zhou, X.S. Zhao, Graphene-based materials as SC electrodes. J. Mater. Chem. **20**, 5983–5992 (2010)
74. J. Hou, Y. Shao, M.W. Ellis, R.B. Moore, B. Yi, Graphene-based electrochemical energy conversion and storage: fuel cells, SCs and lithium ion batteries. Phys. Chem. Chem. Phys. **13**, 15384–15402 (2011)
75. C. Xu, B. Xu, Y. Gu, Z. Xiong, J. Sun, X.S. Zhao, Graphene-based electrodes for electrochemical energy storage. Energ. Environ. Sci. **6**, 1388–1414 (2013)

76. D. Li, M.B. Müller, S. Gilje, R.B. Kaner, G.G. Wallace, Processable aqueous dispersions of graphene nanosheets. Nat. Nanotechnol. **3**, 101–105 (2008)
77. G. Eda, G. Fanchini, M. Chhowalla, Large-area ultrathin films of reduced graphene oxide as a transparent and flexible electronic material. Nat. Nanotechnol. **3**, 270–274 (2008)
78. X. Li, W. Cai, J. An, S. Kim, J. Nah, D. Yang, R. Piner, A. Velamakanni, I. Jung, E. Tutuc, S.K. Banerjee, L. Colombo, R.S. Ruoff, Large-area synthesis of high-quality and uniform graphene films on copper foils. Science **324**, 1312 (2009)
79. I.-Y. Jeon, Y.-R. Shin, G.-J. Sohn, H.-J. Choi, S.-Y. Bae, J. Mahmood, S.-M. Jung, J.-M. Seo, M.-J. Kim, D. Wook Chang, L. Dai, J.-B. Baek, Edge-carboxylated graphene nanosheets via ball milling. Proc. Natl. Acad. Sci. **109**, 5588 (2012)
80. Y. Zhu, S. Murali, M.D. Stoller, K.J. Ganesh, W. Cai, P.J. Ferreira, A. Pirkle, R.M. Wallace, K.A. Cychosz, M. Thommes, D. Su, E.A. Stach, R.S. Ruoff, Carbon-based SCs produced by activation of graphene. Science **332**, 1537 (2011)
81. B.G. Choi, J. Hong, W.H. Hong, P.T. Hammond, H. Park, Facilitated ion transport in all-solid-state flexible SCs. ACS Nano **5**, 7205–7213 (2011)
82. M.F. El-Kady, V. Strong, S. Dubin, R.B. Kaner, Laser scribing of high-performance and flexible graphene-based electrochemical capacitors. Science **335**, 1326 (2012)
83. M.D. Stoller, S. Park, Y. Zhu, J. An, R.S. Ruoff, Graphene-based ultracapacitors. Nano Lett. **8**, 3498–3502 (2008)
84. Z. Chen, W. Ren, L. Gao, B. Liu, S. Pei, H.-M. Cheng, Three-dimensional flexible and conductive interconnected graphene networks grown by chemical vapour deposition. Nat. Mater. **10**, 424–428 (2011)
85. Y. Xu, K. Sheng, C. Li, G. Shi, Self-assembled graphene hydrogel via a one-step hydrothermal process. ACS Nano **4**, 4324–4330 (2010)
86. Y. Xue, J. Liu, H. Chen, R. Wang, D. Li, J. Qu, L. Dai, Nitrogen-doped graphene foams as metal-free counter electrodes in high-performance dye-sensitized solar cells. Angew. Chem. Int. Ed. **51**, 12124–12127 (2012)
87. Y. Xue, D. Yu, L. Dai, R. Wang, D. Li, A. Roy, F. Lu, H. Chen, Y. Liu, J. Qu, Three-dimensional B, N-doped graphene foam as a metal-free catalyst for oxygen reduction reaction. Phys. Chem. Chem. Phys. **15**, 12220–12226 (2013)
88. Y. Xu, Z. Lin, X. Huang, Y. Liu, Y. Huang, X. Duan, Flexible solid-state SCs based on three-dimensional graphene hydrogel films. ACS Nano **7**, 4042–4049 (2013)
89. Y. Zhao, J. Liu, Y. Hu, H. Cheng, C. Hu, C. Jiang, L. Jiang, A. Cao, L. Qu, Highly compression-tolerant SC based on polypyrrole-mediated graphene foam electrodes. Adv. Mater. **25**, 591–595 (2013)
90. I.-Y. Jeon, H.-J. Choi, S.-M. Jung, J.-M. Seo, M.-J. Kim, L. Dai, J.-B. Baek, Large-scale production of edge-selectively functionalized graphene nanoplatelets via ball milling and their use as metal-free electrocatalysts for oxygen reduction reaction. J. Am. Chem. Soc. **135**, 1386–1393 (2013)
91. A. Raza, J.Z. Hassan, M. Ikram, S. Ali, U. Farooq, Q. Khan, M. Maqbool, Advances in liquid-phase and intercalation exfoliations of transition metal dichalcogenides to produce 2D framework. Adv. Mater. Interfaces **8**, 2002205 (2021)
92. L. Dai, Functionalization of graphene for efficient energy conversion and storage. Acc. Chem. Res. **46**, 31–42 (2013)
93. F. Du, D. Yu, L. Dai, S. Ganguli, V. Varshney, A.K. Roy, Preparation of tunable 3D pillared carbon nanotube-graphene networks for high-performance capacitance. Chem. Mater. **23**, 4810–4816 (2011)
94. G.K. Dimitrakakis, E. Tylianakis, G.E. Froudakis, Pillared graphene: a new 3-D network nanostructure for enhanced hydrogen storage. Nano Lett. **8**, 3166–3170 (2008)
95. Y. Mao, J. Zhong, The computational design of junctions by carbon nanotube insertion into a graphene matrix. New J. Phys. **11**, 093002 (2009)
96. V. Varshney, S.S. Patnaik, A.K. Roy, G. Froudakis, B.L. Farmer, Modeling of thermal transport in pillared-graphene architectures. ACS Nano **4**, 1153–1161 (2010)

97. O. Barbieri, M. Hahn, A. Herzog, R. Kötz, Capacitance limits of high surface area activated carbons for double layer capacitors. Carbon **43**, 1303–1310 (2005)
98. H. Wang, H.S. Casalongue, Y. Liang, H. Dai, $Ni(OH)_2$ Nanoplates grown on graphene as advanced electrochemical pseudocapacitor materials. J. Am. Chem. Soc. **132**, 7472–7477 (2010)
99. J. Lin, C. Zhang, Z. Yan, Y. Zhu, Z. Peng, R.H. Hauge, D. Natelson, J.M. Tour, 3-dimensional graphene carbon nanotube carpet-based MicroSCs with high electrochemical performance. Nano Lett. **13**, 72–78 (2013)
100. D. Pech, M. Brunet, H. Durou, P. Huang, V. Mochalin, Y. Gogotsi, P.-L. Taberna, P. Simon, Ultrahigh-power micrometre-sized SCs based on onion-like carbon. Nat. Nanotechnol. **5**, 651–654 (2010)
101. D. Yu, L. Dai, Self-assembled graphene/carbon nanotube hybrid films for SCs. J. Phys. Chem. Lett. **1**, 467–470 (2010)
102. Y. Cheng, S. Lu, H. Zhang, C.V. Varanasi, J. Liu, Synergistic effects from graphene and carbon nanotubes enable flexible and robust electrodes for high-performance SCs. Nano Lett. **12**, 4206–4211 (2012)
103. S.-Y. Yang, K.-H. Chang, H.-W. Tien, Y.-F. Lee, S.-M. Li, Y.-S. Wang, J.-Y. Wang, C.-C.M. Ma, C.-C. Hu, Design and tailoring of a hierarchical graphene-carbon nanotube architecture for SCs. J. Mater. Chem. **21**, 2374–2380 (2011)
104. H. Gao, F. Xiao, C.B. Ching, H. Duan, Flexible all-solid-state asymmetric SCs based on free-standing carbon nanotube/graphene and Mn_3O_4 nanoparticle/graphene paper electrodes. ACS Appl. Mater. Interfaces **4**, 7020–7026 (2012)
105. L. Hu, Y. Cui, Energy and environmental nanotechnology in conductive paper and textiles. Energ. Environ. Sci. **5**, 6423–6435 (2012)
106. T. Chen, L. Qiu, Z. Yang, H. Peng, Novel solar cells in a wire format. Chem. Soc. Rev. **42**, 5031–5041 (2013)
107. J. Bae, M.K. Song, Y.J. Park, J.M. Kim, M. Liu, Z.L. Wang, Fiber SCs made of nanowire-fiber hybrid structures for wearable/flexible energy storage. Angew. Chem. Int. Ed. **50**, 1683–1687 (2011)
108. Y. Fu, X. Cai, H. Wu, Z. Lv, S. Hou, M. Peng, X. Yu, D. Zou, Fiber SCs utilizing pen ink for flexible/wearable energy storage. Adv. Mater. **24**, 5713–5718 (2012)
109. X. Xiao, T. Li, P. Yang, Y. Gao, H. Jin, W. Ni, W. Zhan, X. Zhang, Y. Cao, J. Zhong, L. Gong, W.-C. Yen, W. Mai, J. Chen, K. Huo, Y.-L. Chueh, Z.L. Wang, J. Zhou, Fiber-based all-solid-state flexible SCs for self-powered systems. ACS Nano **6**, 9200–9206 (2012)
110. J. Ren, L. Li, C. Chen, X. Chen, Z. Cai, L. Qiu, Y. Wang, X. Zhu, H. Peng, Twisting carbon nanotube fibers for both wire-shaped micro-SC and Micro-battery. Adv. Mater. **25**, 1155–1159 (2013)
111. Y. Meng, Y. Zhao, C. Hu, H. Cheng, Y. Hu, Z. Zhang, G. Shi, L. Qu, All-graphene core-sheath microfibers for all-solid-state, stretchable fibriform SCs and wearable electronic textiles. Adv. Mater. **25**, 2326–2331 (2013)
112. J.A. Lee, M.K. Shin, S.H. Kim, H.U. Cho, G.M. Spinks, G.G. Wallace, M.D. Lima, X. Lepró, M.E. Kozlov, R.H. Baughman, S.J. Kim, Ultrafast charge and discharge biscrolled yarn SCs for textiles and microdevices. Nat. Commun. **4**, 1970 (2013)
113. Z. Cai, L. Li, J. Ren, L. Qiu, H. Lin, H. Peng, Flexible, weavable and efficient microSC wires based on polyaniline composite fibers incorporated with aligned carbon nanotubes. J. Mater. Chem. A **1**, 258–261 (2013)
114. P.-C. Chen, G. Shen, S. Sukcharoenchoke, C. Zhou, Flexible and transparent SC based on In_2O_3 nanowire/carbon nanotube heterogeneous films. Appl. Phys. Lett. **94**, 043113 (2009)
115. S.K. Nataraj, Q. Song, S.A. Al-Muhtaseb, S.E. Dutton, Q. Zhang, E. Sivaniah, Thin, flexible SCs made from carbon nanofiber electrodes decorated at room temperature with manganese oxide nanosheets. J. Nanomater. **2013**, 272093 (2013)
116. C. Chien, S.S. Deora, P. Chang, D. Li, J.G. Lu, Flexible symmetric SCs based on TiO_2 and carbon nanotubes. IEEE Trans. Nanotechnol. **10**, 706–709 (2011)

117. L. Zhang, Q. Ding, Y. Huang, H. Gu, Y.-E. Miao, T. Liu, Flexible hybrid membranes with $Ni(OH)_2$ nanoplatelets vertically grown on electrospun carbon nanofibers for high-performance SCs. ACS Appl. Mater. Interfaces **7**, 22669–22677 (2015)
118. L. Du, P. Yang, X. Yu, P. Liu, J. Song, W. Mai, Flexible SCs based on carbon nanotube/MnO_2 nanotube hybrid porous films for wearable electronic devices. J. Mater. Chem. A **2**, 17561–17567 (2014)
119. Y. Wang, S. Tang, S. Vongehr, J. Ali Syed, X. Wang, X. Meng, High-performance flexible solid-state carbon cloth SCs based on highly processible N-graphene doped polyacrylic acid/polyaniline composites. Sci. Rep. **6**, 12883 (2016)
120. S. Zeng, H. Chen, F. Cai, Y. Kang, M. Chen, Q. Li, Electrochemical fabrication of carbon nanotube/polyaniline hydrogel film for all-solid-state flexible SC with high areal capacitance. J. Mater. Chem. A **3**, 23864–23870 (2015)
121. K.S. Kim, Y. Zhao, H. Jang, S.Y. Lee, J.M. Kim, K.S. Kim, J.-H. Ahn, P. Kim, J.-Y. Choi, B.H. Hong, Large-scale pattern growth of graphene films for stretchable transparent electrodes. Nature **457**, 706–710 (2009)
122. S. Bae, H. Kim, Y. Lee, X. Xu, J.-S. Park, Y. Zheng, J. Balakrishnan, T. Lei, H. Ri Kim, Y.I. Song, Y.-J. Kim, K.S. Kim, B. Özyilmaz, J.-H. Ahn, B.H. Hong, S. Iijima, Roll-to-roll production of 30-inch graphene films for transparent electrodes. Nat. Nanotechnol. **5**, 574–578 (2010)
123. X. Li, Y. Zhu, W. Cai, M. Borysiak, B. Han, D. Chen, R.D. Piner, L. Colombo, R.S. Ruoff, Transfer of large-area graphene films for high-performance transparent conductive electrodes. Nano Lett. **9**, 4359–4363 (2009)
124. T. Chen, H. Peng, M. Durstock, L. Dai, High-performance transparent and stretchable all-solid SCs based on highly aligned carbon nanotube sheets. Sci. Rep. **4**, 3612 (2014)
125. A. Yu, I. Roes, A. Davies, Z. Chen, Ultrathin, transparent, and flexible graphene films for SC application. Appl. Phys. Lett. **96**, 253105 (2010)
126. T. Chen, Y. Xue, A.K. Roy, L. Dai, Transparent and stretchable high-performance SCs based on wrinkled graphene electrodes. ACS Nano **8**, 1039–1046 (2014)
127. H. Xu, X. Hu, H. Yang, Y. Sun, C. Hu, Y. Huang, Flexible asymmetric Micro-SCs based on Bi_2O_3 and MnO_2 nanoflowers: larger areal mass promises higher energy density. Adv. Energ. Mater. **5**, 1401882 (2015)
128. C. Yu, C. Masarapu, J. Rong, B. Wei, H. Jiang, Stretchable SCs based on buckled single-walled carbon-nanotube macrofilms. Adv. Mater. **21**, 4793–4797 (2009)
129. Z. Niu, H. Dong, B. Zhu, J. Li, H.H. Hng, W. Zhou, X. Chen, S. Xie, Highly stretchable, integrated SCs based on single-walled carbon nanotube films with continuous reticulate architecture. Adv. Mater. **25**, 1058–1064 (2013)
130. J. Zang, C. Cao, Y. Feng, J. Liu, X. Zhao, Stretchable and high-performance SCs with crumpled graphene papers. Sci. Rep. **4**, 6492 (2014)
131. W. Kim, W. Kim, 3 V omni-directionally stretchable one-body SCs based on a single ion–gel matrix and carbon nanotubes. Nanotechnol. **27**, 225402 (2016)
132. T.G. Yun, B.I. Hwang, D. Kim, S. Hyun, S.M. Han, Polypyrrole–MnO_2-coated textile-based flexible-stretchable SC with high electrochemical and mechanical reliability. ACS Appl. Mater. Interfaces **7**, 9228–9234 (2015)
133. J. Yun, Y. Lim, G.N. Jang, D. Kim, S.-J. Lee, H. Park, S.Y. Hong, G. Lee, G. Zi, J.S. Ha, Stretchable patterned graphene gas sensor driven by integrated micro-SC array. Nano Energ. **19**, 401–414 (2016)
134. J. Yu, W. Lu, S. Pei, K. Gong, L. Wang, L. Meng, Y. Huang, J.P. Smith, K.S. Booksh, Q. Li, J.-H. Byun, Y. Oh, Y. Yan, T.-W. Chou, Omnidirectionally stretchable high-performance SC based on isotropic buckled carbon nanotube films. ACS Nano **10**, 5204–5211 (2016)
135. C. Choi, H.J. Sim, G.M. Spinks, X. Lepró, R.H. Baughman, S.J. Kim, Elastomeric and dynamic MnO_2/CNT core-shell structure coiled yarn SC. Adv. Energ. Mater. **6**, 1502119 (2016)

Conducting Polymers Based Nanocomposites for Supercapacitors

Syed Shaheen Shah, Md. Abdul Aziz, Wael Mahfoz, and Abdul-Rahman Al-Betar

Abstract Among the unconventional electrically powered devices (supercapacitors, batteries, and fuel cells), supercapacitors have received significant interest due to their better electrochemical performance, exceptional cycle life, outstanding specific power, and rapid charging/discharging rate. Furthermore, supercapacitors based on conducting polymers (CPs) have higher power density and specific energy, giving them a more versatile and less expensive energy storage option. CPs have been the subject of intensive research over the years due to their potential use in various disciplines such as sensors, fuel cells, and supercapacitors. Several novel techniques have been developed to enhance the characteristics of CPs, including CPs-based nanocomposites, which combine CPs with other nanomaterials. Due to their high capacitances and ability to endure multiple charge/discharge cycles, CPs-based nanocomposites have become more popular as supercapacitor electrodes. We summarize essential topics in this study field following a discussion of the obstacles that CPs-based nanocomposites must overcome to become technologically feasible. This chapter will help readers understand the benefits and drawbacks of using the CPs-based nanocomposites in supercapacitors and identify topics for further research.

Keywords Conducting polymers · Polyaniline · Polypyrrole · Polythiophene · Poly(3,4-ehtylenedioxythiophene) · Nanocomposites · Carbonaceous materials · Metallic composites · Supercapacitors

S. S. Shah · Md. A. Aziz (✉) · A.-R. Al-Betar
Interdisciplinary Research Center for Hydrogen and Energy Storage (IRC-HES), King Fahd University of Petroleum and Minerals, KFUPM Box 5040, Dhahran 31261, Saudi Arabia
e-mail: maziz@kfupm.edu.sa

S. S. Shah
Physics Department, King Fahd University of Petroleum and Minerals, KFUPM Box 5047, Dhahran 31261, Saudi Arabia

W. Mahfoz · A.-R. Al-Betar
Chemistry Department, King Fahd University of Petroleum and Minerals, Dhahran 31261, Saudi Arabia

S. Thomas et al. (eds.), *Nanostructured Materials for Supercapacitors*,
Advances in Material Research and Technology,
https://doi.org/10.1007/978-3-030-99302-3_22

1 Introduction

Electrochemical energy storage technologies, for example, supercapacitors and batteries, have shown to be highly reliable in enabling the utilization of renewable energy. It is essential to consider the development of efficient electrochemical energy storage devices. The design of active electrode materials for elevated electrochemical performance is the essential component of an energy storage system [1, 2]. Conducting polymers (CPs), among the numerous materials used in energy storage devices, have piqued the interest of researchers all over the globe because of their low-cost, simple tunability of arrangements, rich redox chemistry, flexibility, structure, and morphology [3, 4]. As a result, CPs appear to be a viable option for next-generation supercapacitors. However, cycle stability is a bottleneck restriction for practical applications of CPs-based energy storage systems. As a result, research into developing next-generation CPs-driven energy storage has been ongoing to provide practically feasible solutions. CPs-based energy storage devices appear to have a bright future, but additional research and development studies are needed before they can be commercialized on a larger scale. Nanotechnology is an endeavor to achieve engineering and production of materials at the level of the nanoscale. The latest materials science and engineering developments have brought about the fast growth of nanoscale materials, which draw much interest and excitement for study. The focus is on nanoporous CPs from maximal uses in catalysis, adsorption, the transmission of pharmaceuticals, sensors, and energy storage/conversion [5–7]. CPs nanocomposites have superior physicochemical and biological characteristics. CPs with secondary component increases various features beneficial for supercapacitor applications. A nanocomposite's intended aspects are regulated by its shape, size, and distribution of the dispersed phase [8]. Nanocomposites comprising CPs with metals or metal oxides, carbon-based nanomaterials, and their ternary nanocomposites were synthesized using in-situ, one-pot, and vapor-phase polymerization [9–12]. This chapter investigates the latest developments in CPs-based nanocomposites for supercapacitor applications. It provides a brief overview of current advancements in CPs and their nanocomposites, synthetic methods, and applications in supercapacitors. As a result, improving CPs-based supercapacitor performance involves increasing the CPs surface area. CPs must be mixed with other materials to minimize ion diffusion length, allowing composites where CPs are coated onto the second materials. Also, CPs undergo significant volume changes during redox, causing capacitance loss during charging/discharging. Using porous carbons as templates might help decrease this detrimental effect. To produce high-performance nanocomposites, the host materials must meet specific criteria. They must be highly porous, have a large specific area, and give enough electrical conductivity [13, 14]. Carbon-related materials, such as activated carbon, carbon nanotubes (CNTs), and graphene, appear to be the best options to fulfill these problems. Advanced literature has been summarized on CPs-based nanocomposites, including binary and ternary nanocomposites, and recent advances in using these nanocomposites in supercapacitors are emphasized.

2 CPs and Their Nanocomposites

Polymers are macromolecules made up of many monomers or repeated subunits. Polymer is derived from two Greek words: *poly*, which means many, and *mer*, which means parts or units. Monomers are small molecules that serve as the building blocks of polymers, whereas polymers make up large molecules. CPs represent an important class of functional organic materials for next-generation electronic and optical devices. CPs conduct electricity due to π electron delocalization. These compounds could be considered as either metallic conductors or semiconductors. Organic synthesis and advanced dispersion techniques can be used to fine-tune the electrical properties. CPs synthesized as nanomaterials are especially interesting because their properties differ significantly from their bulk counterparts [15]. CPs include polyaniline (PANI), polypyrrole (PPy), polythiophene (PTh), and poly(3,4-ehtylenedioxythiophene) (PEDOT) display huge theoretical specific capacitances, which allow them to act as better electrode materials for supercapacitors. Advances in nanotechnology allow for the fabrication of various conducting polymer nanocomposites with different methods. CPs-based nanocomposites featuring high surface area, small dimensions, and exhibit unique physical and chemical properties; therefore, they have been widely used for various purposes such as supercapacitors.

CPs-based nanocomposites have attracted significant interest in recent research due to their remarkably enhanced dielectric, electrochemical, and electrical properties, allowing their applications in electrochemical lithium-ion batteries, stretchable electronics, sensors, and supercapacitors. Compared to other conductive materials (i.e., transition metal nanoparticles, CNTs, or carbon black), nanostructured CPs have better tunability, processability, and moldability, meaning that they are more easily processed into various forms such as powder, thin-films, hydrogels, and coatings to efficiently establish dynamic interfaces inside the nanocomposites and enrich their essential electrical functions. CPs and their nanocomposites can be formed using chemical and electrochemical methods [14]. Chemical synthesis of CPs is achieved by oxidation of the monomers using an oxidizing agent such as iron chloride or ammonium persulfate, while electrochemical synthesis involves anodic polymerization on an electrode in the presence of the counter-ion species. The chemical synthesis of CPs nanocomposites consists of mixing a conducting polymer's monomer with the supporting material (which can be charged or discharged) before the oxidation step. When forming a nanocomposite with an uncharged supporting material, supporting electrolytes are also required in the reaction mixture. Electrochemical synthesis of CPs nanocomposites can proceed in two ways, either by polymerization on a preformed layer of the support material on an electrode or by co-electrodeposition. The electrochemical deposition of the CPs and the adhesion of the supporting material to the deposited CPs occurs simultaneously. During CPs nanocomposite formation, chemical or electrochemical oxidation of the monomers leads to precipitation of the polymers from solution.

3 Importance of CPs-Based Nanocomposites

Although pure CPs own many unique properties, they are not appropriate to be utilized as active electrode materials alone. The CPs have a common weakness that limits their use in supercapacitors alone, i.e., their structures are degraded during repeated redox cycles. This occurs due to the associated ion and solvent transfer across the interface of the CPs and electrolytes, which causes shrinkage and swelling of CPs [13]. The instability of CPs towards repeated redox cycling shows that just a porous structure alone is insufficient to make these materials into high-performing electrode materials. To improve the CPs-based electrochemical performances and supercapacitors' stabilities, researchers have tried to synthesize binary and even ternary nanocomposites with other active materials, including carbon materials and metal oxides, and the progress of which will be discussed hereinafter.

A range of CPs nanocomposites containing nanoarchitecture materials has been developed to impart mechanical strength and porosity to CPs to improve the redox cycling stability [4, 16]. Higher capacitance values for the CPs can be achieved by forming composite structures with carbon and/or metal oxides. In current research developments, the studies on CPs and their nanocomposites using carbonaceous materials [4, 17] and transition metal oxides (TMOs) [18] as the electrodes for supercapacitor devices are quite promising due to ease of fabrication, higher stability, and high flexibility. Carbon-based nanocomposites typically enhance the surface area of an electrode, increasing the contribution of double-layer capacitance [19], while composites with TMOs introduce additional charge storage mechanisms to the system [20]. Furthermore, CPs nanocomposites can also improve an electrode's material utilization efficiency, conductivity, or cycling stability. Experimental capacitance values for various CPs and CPs-based nanocomposites are summarized in Fig. 1.

4 CPs-Based Binary Nanocomposites

A nanocomposite is a multiphase solid substance in which one of the phases has one, two, or three dimensions less than 100 nm, or structures with nanoscale repetition intervals between the distinct phases that comprise the material. Due to their constituents' synergistic effect, composite materials possess more significant advantages, including high mechanical stability and improved electrochemical behavior. CPs nanocomposites are solid-phase materials (metals/ceramics) with a CP falling within nanometer range (1–100 nm) at least in one of its dimensions. Researchers have focused on merging nanomaterials with CPs for the past two decades because of their efficient electronic behavior through electronic interactions or structural modifications in the binary components. In the following subsections, we will provide research progress of different kinds of CPs-based binary nanocomposites for supercapacitor applications.

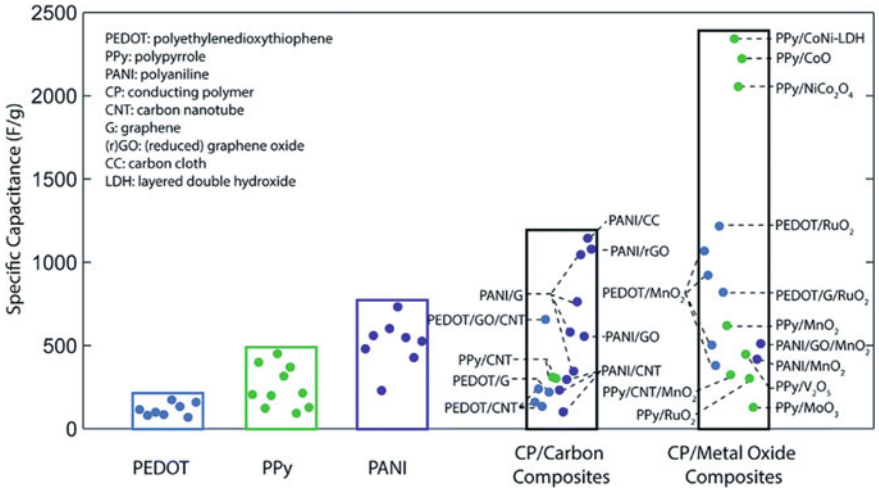

Fig. 1 Specific capacitance comparison of various CPs and their nanocomposites. Adapted with permission from reference [20]. Copyright The Authors, some rights reserved; exclusive licensee Royal Society of Chemistry. Distributed under a Creative Commons Attribution License 3.0 (CC BY)

4.1 CPs and Carbon-Based Binary Nanocomposites

CPs have attracted a lot of investigation in the previous decade due to their unique characteristics. The main challenges in their supercapacitor applications are volumetric shrinkage and severe aggregation. On the other hand, carbon materials have excellent electrical conductivity, large specific surface areas, cyclic stability, and mechanical characteristics but exhibit low capacitance. To overcome these challenges, CPs are commonly mixed with carbonaceous materials to produce nanocomposites. Many investigations have demonstrated that compared with pure CPs, CPs/carbon nanocomposites show better electrochemical properties. Carbon materials are ideal fillers for CPs-based supercapacitors. Various CPs/carbon nanocomposites have been studied, such as CPs/CNTs [21], CPs/graphene [22], CPs/carbon nanofibers [23], CPs/carbon spheres [24], and CPs/carbon particles [4].

4.1.1 CPs/CNTs Nanocomposites

Over the last decade, there has been much research interest in CPs/CNTs nanocomposites for supercapacitors. Because of their large surface area, high mechanical strength, and high conductivity, CPs/CNTs composites are very appealing for supercapacitor applications. The main requirements for materials used in supercapacitor applications are high specific capacitance and high electrochemical stability. CNTs have been shown to act as a perfect backbone for a homogeneous distribution of

CPs in the nanocomposite. Because pure CPs are mechanically weak, CNTs protect the CPs active material from mechanical changes (breaking/shrinkage) over long periods of charge–discharge performance. Aside from having excellent conducting and mechanical properties, the presence of CNTs improves charge transfer, allowing for a high charge/discharge rate [25].

Aswathy et al. [2] recently reported flexible substrate electrodes based on PANI/CNTs for supercapacitor applications. A solid-state flexible supercapacitor made of PANI/CNTs-based flexible substrate electrodes and a PVA-based gel electrolyte achieved an aerial capacitance of 8.4 mF/cm^2 at 25 mV/s and good capacitance retention. The current strategy has paved the way for CPs/CNTs-based nanocomposites with high porosity and flexibility as sustainable electrode materials for energy storage applications. Wu et al. [26] fabricated a high-performance supercapacitor using PANI/CNTs nanocomposite electrodes, with vertically aligned CNTs generated by electrochemical induction at 0.75 V. The CNTs structure also play an important role in the development of PANI/CNTs nanocomposites. As illustrated in Fig. 2a, the disordered CNTs (D-CNTs) were randomly aggregated, requiring a lengthy route for charges (ions), resulting in less charge buildup in electrodes and low capacitance. However, after the disordered structure was vertically oriented (VA-CNTs), the constantly conductive channels of the produced VA-CNTs enabled charge direct and rapid transit. The comparative electrochemical results of the developed PANI/CNTs nanocomposite are shown in Fig. 2b–e. The PANI/CNTs supercapacitor will have a lot of potential for portable and wearable electronic applications because of these extraordinary results. Zhang et al. [8] reported PANI/CNTs core–shell nanocomposites electrodes for supercapacitors with large specific capacitance and high capacitance retention owing to the hierarchically porous structure of electrode materials,

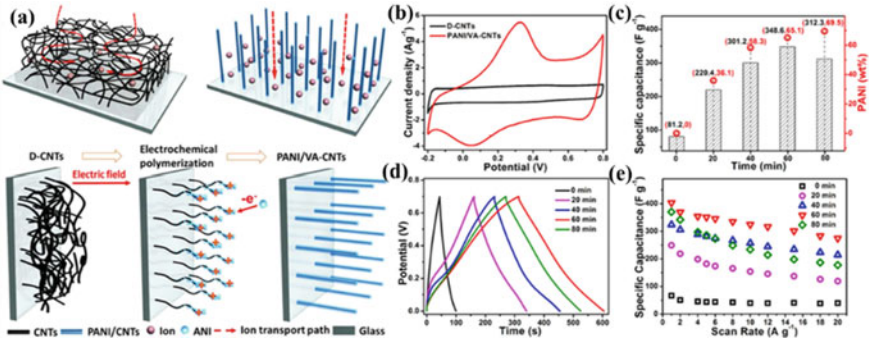

Fig. 2 **a** Schematic illustration for the development of PANI/CNTs nanocomposite electrode. **b** CV curves of the pure CNTs (D-CNTs) and PANI/CNTs nanocomposite at a scan rate of 10 **mV**/s. **c** The corresponding specific capacitances and weight percentages of PANI in the PANI/CNTs nanocomposite electrodes with different electrochemically induced time at a scan rate of 10 **mV**/s. **d** GCD profiles of the PANI/CNTs nanocomposite electrode at a current density of 1 A/g. **e** The obtained specific capacitances at various current densities. Adapted with permission from reference [26]. Copyright The Authors, some rights reserved; exclusive licensee Springer Nature. Distributed under a Creative Commons Attribution License 4.0 (CC BY)

decreased ions diffusion length, and effectual charge transport. They then prepared a series of core–shell structured PANI/CNTs composites to investigate the effect of the microstructures [27]. Despite extensive research into the connection between PANI loading/thickness and characteristics, the concept of rational design of hierarchically organized electrodes with good performance is still in its early stages, which is an important issue that must be addressed.

PPy is one of the most widely studied CPs owing to its solid environmental stability, low-cost, significant mechanical characteristics, high capacitance, and easy solubility in aqueous media [28]. Through a combination of the high conductivity and EDLC behaviors of CNTs, as well as the high pseudocapacitance of redox-active PPy, PPy has been coated on pure and/or functionalized CNTs to produce nanocomposite electrode materials with better electrochemical performance [13, 25]. Several studies have demonstrated that supercapacitors based on PPy/CNTs nanocomposite have higher specific capacitances [29]. Lin et al. [30] even reported an unusually high result of 890 F/g for the PPy/CNTs nanocomposite. Fang et al. [31] reported that strong stacking between the conjugated backbone of PPy and the graphitic sidewall of CNTs is responsible for the microstructural homogeneity, high specific capacitance, and conductivity of PPy/CNTs nanocomposite in supercapacitor. CNTs can be used as reinforcing material to overcome the PPy shrinkage/swelling during the doping/undoping process. The innovative binder-free direct growing method is responsible for the overall excellent cycle stability and performance of the produced PPy/CNTs nanocomposite-based flexible electrode. Specific capacitance, energy density, and cycle life are often used to describe the capacitive performance of PPy/CNTs nanocomposites-based supercapacitors. It is important to note that the ultimate capacitive properties of PPy/CNTs nanocomposites for supercapacitors are influenced by a variety of factors such as surface morphologies, fabrication techniques, PPy/CNTs ratios, and experimental conditions such as current densities, scan rates, and electrolyte.

The electrochemical performance of PEDOT as electrode material for supercapacitor was also highly improved by forming nanocomposites with CNTs. The capacitance of an electrochemically synthesized PEDOT/CNTs nanocomposite was more than twice that of pristine PEDOT synthesized using the same deposition charge. Peng et al. [13] prepared nanocomposite films of PEDOT and CNTs by electrochemical co-deposition of solutions comprising the PEDOT monomer and acid-treated CNTs. CNTs were used as charge carriers during electrodeposition, acting as the backbone of a three-dimensional micro- and nano-porous structure and the effective charge-balancing dopant inside the polymer. Unlike pure PEDOT, the PEDOT/CNTs nanocomposite retained the capacitance of the as-prepared film considerably better in continuous potential cycling experiments. The PEDOT monomer is only soluble in acetonitrile, whereas the oxidized CNTs could be dispersed in the aqueous solutions. However, the chemically synthesized PEDOT/CNTs nanocomposites can easily be soluble in aqueous solutions [9]. In situ chemical polymerization synthesized the homogenously grafted PEDOT/CNTs nanocomposite, which showed better electrochemical performance as a supercapacitor electrode [9]. A controlled and simple technique was used to develop free-standing 3D electrodes PEDOT/CNTs sponge

nanocomposites, and a symmetric all-solid-state supercapacitor cell was fabricated [32]. The considerably increased capacitance of the PEDOT/CNTs nanocomposites compared to pure PEDOT and CNTs electrodes might be attributed to pseudocapacitance resulting from the rapid redox process occurring in each component's unique connection and porous structure. The schematic representation for the synthesis of PEDOT/CNTs sponge nanocomposite and the corresponding FESEM images are shown in Fig. 3a. During the charge/discharge, the redox process is described in Eq. 1 and schematically represented in Fig. 3b. The negative and positive electrodes undergo n-doping and p-doping during charging. The n− and p− doped electrodes adsorb opposite ions from the electrolyte, such as anions of SO_4^{2-} and cations of H^+. Accordingly, such doping mechanism, the adsorbed charges are released during the discharging process [33]. When the cell is entirely discharged, both electrodes become undoped.

$$2PEDOT + tC_x^{m+}A_y^{n-} \rightleftarrows [PEDOT]^{tn+}tA_y^{n-} + [PEDOT]^{tm-}tC_c^{m+} \quad (1)$$

4.1.2 CPs/Biomass-Derived Carbon Nanocomposites

Because of their combined functionality of faradic reactions and electrostatic charging processes, carbon and CPs nanocomposites are promising electrode materials for high-performance supercapacitors. However, traditionally produced nanocarbon compounds for wide-ranging purposes are not advised because of their costly nanocarbon precursors and complicated synthesis methods. Instead, the use of low-cost biomass precursors and the development of a more efficient and ecologically friendly approach to technological development are appealing. Biomass-derived carbonaceous nanomaterials are produced from natural resources in labs, including jute sticks/fibers [5, 34–38], banana leaves [39], *Syzygium cumini* leaves [40], *Albizia proccera* leaves [41–43], nettle fibre [44], coal [45], tal palm [46], and *Pithophora polymorpha* [4].

Shah et al. [4] reported nanocomposite of PANI and *Pithophora polymorpha* derived nanocarbon as efficient electrode material for supercapacitor, which displayed a pseudocapacitor behavior and exhibited high areal capacitance and good cyclic stability. The unique redox-active behavior of PANI, the active framework of porous heteroatoms-enriched hierarchical nanocarbon and enhanced electrical conductivity of the composite electrode may be ascribed to its advanced electrochemical energy storage capabilities. The schematic representation for the synthesis of PANI/nanocarbon via electrochemical deposition and the corresponding supercapacitor performance is shown in Fig. 4. The use of boron-doped activated wood-derived nanocarbon to support and scatter PANI for the application as supercapacitor electrode materials were reported by Liu et al. [12]. Due to the synergetic effect between PANI/nanocarbon, the as-prepared PANI/nanocarbon nanocomposite had considerably increased specific capacitance compared to pure PANI and

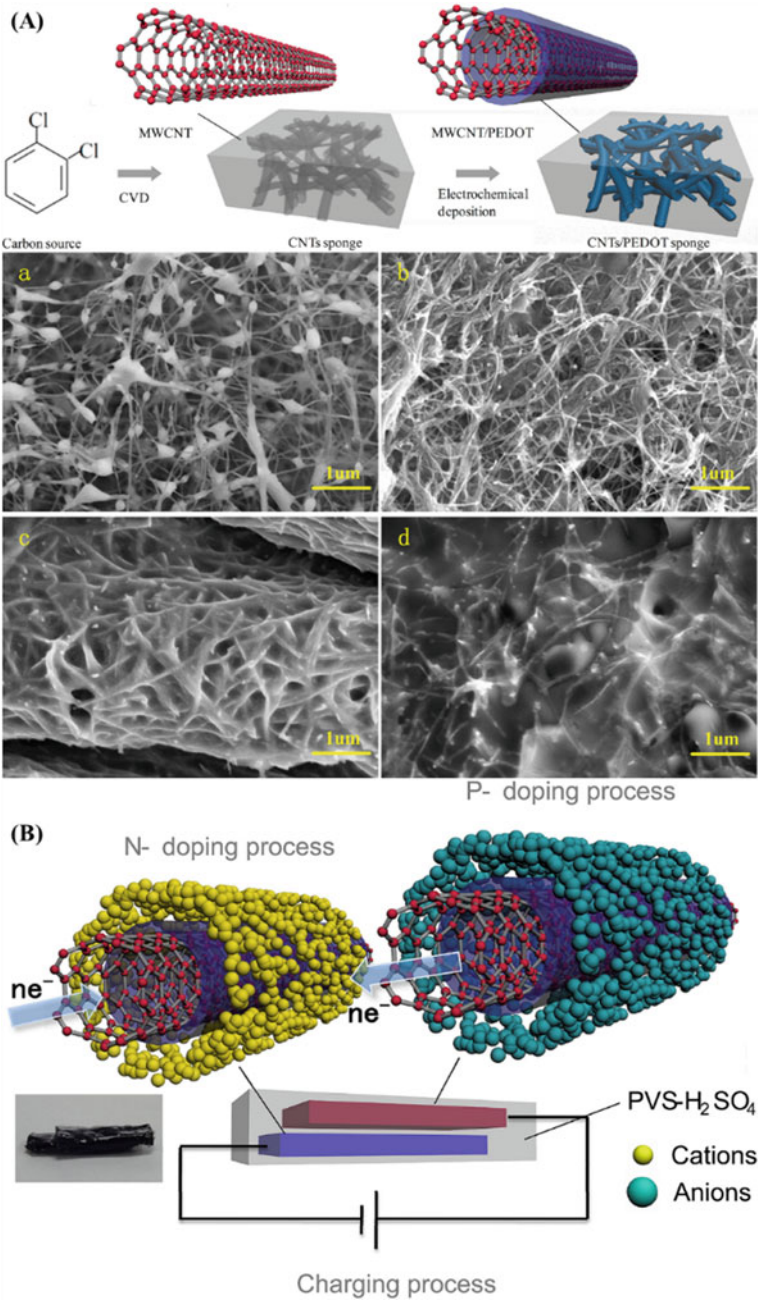

Fig. 3 (A) A schematic illustration for synthesizing PEDOT/CNTs sponge nanocomposite and (**a**–**d**) the corresponding FESEM images. (B) A schematic illustration for the charging mechanism of the PEDOT/CNTs sponge nanocomposite-based symmetric supercapacitors. Adapted with permission from reference [32], Copyright (2018), Elsevier

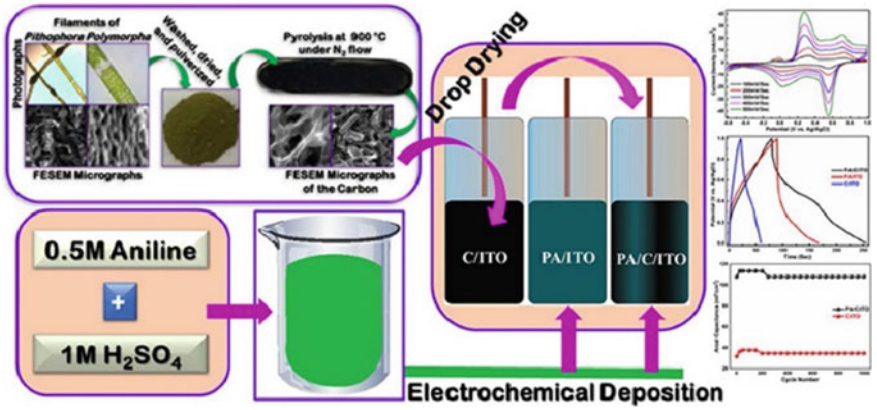

Fig. 4 Schematic representation for the synthesis of PANI/carbon via electrochemical deposition and the corresponding supercapacitor performance. Adapted with permission from reference [4], Copyright (2020), Elsevier

nanocarbon. A simple two-step synthesis method was used to produce biomass-derived three-dimensional nanocarbon fiber aerogels containing PPy nanoparticles [47]. The 3D carbon aerogels made from biomass and its nanocomposite with PPy exhibited excellent capacitance and long-term stability, making them ideal for supercapacitors. Peng et al. [48] prepared the lignosulfonate/PPy hydrogel by hydrothermally treating a combination of porous nanocarbon nanospheres/lignosulfonate/PPy. This study contributes to building electroactive biomass-based hydrogels and a new way of improving hydrogel characteristics. A promising nanocomposite of PEDOT and bamboo shoot shells derived nitrogen/sulfur co-doped porous carbons were synthesized for supercapacitor electrodes [49].

4.1.3 CPs/Graphene Nanocomposites

Over the last decade, there has been a surge in interest in nanocomposite materials. Graphene, graphene analogs, and CPs are increasingly being used as nanocomposite materials for supercapacitor applications. Combining graphene and CPs materials at the nanoscale allows for the creation of efficient nanocomposites with unique and, in many cases, improved characteristics. Fan et al. [50] developed a low-cost and high-efficiency technique to produce free-standing PANI/graphene nanocomposite sheets. PANI was evenly intercalated into the sulfonated graphene layers of the nanocomposite paper. Individual graphene sheets were covered with nanostructured PANI. The PANI/graphene nanocomposite sheets were thin, light, and flexible, and their supercapacitors performed well electrochemically, with high cycle stability. The in situ polymerization produced a micro-spherical PANI/graphene nanocomposite with a porous structure [51]. The 3D framework of graphene microspheres

made of pure few-layer graphene nanosheets was utilized to load PANI, significantly improving its conductivity. In terms of electrochemical performance, the PANI/graphene nanocomposite demonstrated good cycle stability, indicating significant promise for high-power electrical sources. Liu et al. [52] developed a simple method for preparing PPy/graphene nanocomposites for supercapacitors. The in-situ one-pot method reduced graphene oxide and intercalated PPy into graphene nanosheets sequentially to avoid graphene aggregation. The PPy/graphene nanocomposites had the greatest electrical conductivity of 1980 S/m and specific capacitance of 650 F/g at 0.45 A/g. Khasim et al. [53] reported the excellent performance of free-standing films of PEDOT/graphene nanocomposites by secondary graphene doping for supercapacitors utilizing a simple bar coating process. Table 1 summarizes the capacitive properties of CPs/carbon-based binary nanocomposites as electrodes for supercapacitors.

4.2 CPs/TMOs-Based Binary Nanocomposites

Supercapacitors based on TMOs operate by fast charging/discharging processes because of the fast-faradaic redox reactions at the electrode–electrolyte interface. Thus, compared with electric double-layer capacitors, TMOs based pseudocapacitors have high specific capacity and energy density. Its weak conductivity and limited surface area, however, hindered its further use in supercapacitors. Therefore, a synergistic impact of TMOs and CPs for developing composite electrodes for supercapacitors was recognized to enhance conduction and surface area without decreasing the corresponding pseudocapacitive performance. The development of electrochemical accessibility of redox sites for supercapacitors of the high-performance processing processes may be achieved by the CPs/TMOs nanocomposite electrodes. Therefore, this section presents a detailed overview of the preparation, structural features, electrical characteristics, and supercapacitor performance of CPs/TMOs-based binary nanocomposites for supercapacitors.

4.2.1 PANI/TMOs-Based Nanocomposites

A range of chemical and electrochemical processes are used to prepare PANI nanocomposites with varying TMOs for supercapacitor applications. Metal oxide nanoparticles from a salt solution are commonly deposited on the conducting surface of PANI (used as an electrode) by electrochemical deposition. Metal ions are reduced at the working electrode when a sufficient current is passed through the salt solution. The size and morphology of TMOs can be precisely controlled in this method by adjusting the electrochemical parameters. Singu et al. [57] synthesized PANI/NiO nanocomposites by in situ aqueous oxidative polymerization for supercapacitor applications. The study demonstrated that PANI/NiO nanocomposites could be promising materials for supercapacitors. Recently, Jadhav et al. [58] prepared PANI/MnO_2

Table 1 A comparison of the capacitive properties of CPs and carbon-based binary nanocomposites as electrodes for supercapacitors

Electrode materials	Specific capacitance (F/g) (Current density or Scan rate)	Energy density (Wh/kg)	Electrolyte	Cyclic stability	References
PANI/CNTs	30.69 mF/cm^2 (25 mV/s)	0.16 mWh/cm^2	PVA/ $NaNO_2$ gel	71% (8000)	[2]
PANI/CNTs	403.3 (1 A/g)	98.1	1 M $HClO_4$	90.2% (3000)	[26]
PANI/CNTs	1030 (5.9 A/g)	…	1 M H_2SO_4	95% (5000)	[8]
PANI/CNTs	1019.5 (10 mA/cm^2)	40.5	PVA/H_3PO_4 gel	94% (10,000)	[54]
PPy/CNTs	486.1 (0.5 A/g)	3.9	0.5 M H_2SO_4	82% (10,000)	[3]
PPy/CNTs	282 (1 A/g)	1.0	1 M KCl	63.9% (1000)	[55]
PPy/CNTs	150.8 (1 mA/cm^2)	4.5	0.5 M Na_2SO_4	101.2 (5000)	[56]
PPy/CNTs	152.8 (1 mA/cm^2)	84.9	1 M $LiClO_4$/PC	85% (5000)	[11]
PPy/CNTs	179 (1 A/g)	10.7	0.5 M Na_2SO_4	118.1 (1000)	[1]
PEDOT/CNTs	50 (100 mV/s)	…	0.5 M KCl	85% (5000)	[13]
PEDOT/CNTs	81 (0.5 A/g)	11.3	1 M $LiClO_4$	85 (1000)	[9]
PEDOT/CNTs	147 (0.5 A/g)	8.3	PVA-H_2SO_4 gel	95% (3000)	[32]
PANI/Carbon	176 mF/cm^2 (1 mA/cm^2)	24.5 μWh/cm^2	0.1 M HCl	95% (1000)	[4]
PANI/Carbon	421 (10 mV/s)	45.2	1 M H_2SO_4	83% (2500)	[12]
PPy/Carbon	419 mF/cm^2 (1 mA/cm^2)	…	1 M H_2SO_4	86.4% (3000)	[47]
PPy/Carbon	522 mF/cm^2 (0.5 mA/cm^2)	72.5 μWh/cm^2	cellulose/H_2SO_4	98% (12,000)	[48]
PEDOT/Carbon	302.5 (0.5 A/g)	30.60	1 M $EMIMPF_6$	87% (10,000)	[49]
PANI/Graphene	478 (0.5 A/g)	…	1 M NaOH	88% (2000)	[50]
PPy/Graphene	650 (0.45 A/g)	54	1 M H_2SO_4	95% (5000)	[52]
PEDOT/Graphene	174 (0.5 A/g)	810	PVA/H_3PO_4 gel	90% (5000)	[53]

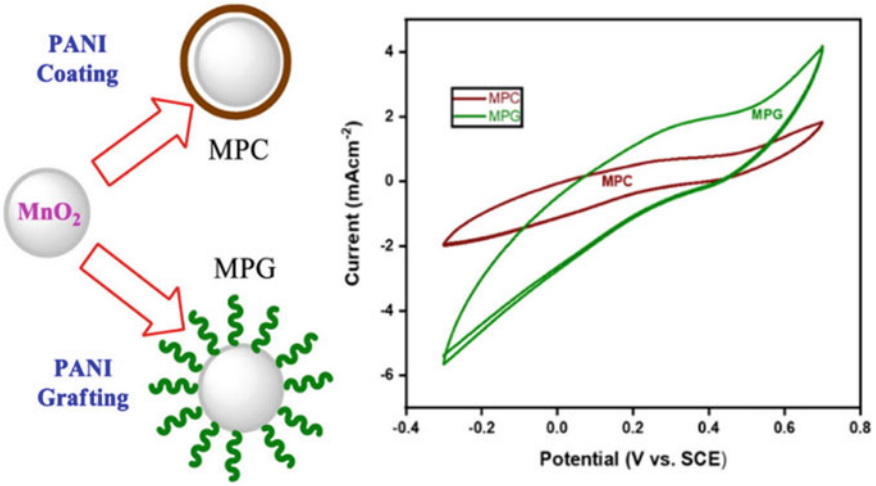

Fig. 5 Schematic representation for the preparation of PANI/MnO_2 nanocomposites via polymer coating and grafting approaches and their corresponding CVs. Adapted with permission from reference [58], Copyright (2021), Elsevier

nanocomposite polymer coating and grafting approaches. The prepared nanocomposites performed excellently as supercapacitor electrodes. The synthesis procedure for the PANI/MnO_2 nanocomposites and their corresponding CVs are shown in Fig. 5. An electrodeposition method was used to synthesize a high-performance negative electrode made of vanadium oxide (V_2O_5) and PANI nanocomposite [59]. The PANI/V_2O_5 nanocomposite-based supercapacitor operated at a longer potential window of 1.6 V and delivered a maximum specific capacitance of 443 F/g. The ability to synthesize high-performance composite electrodes using the electrodeposition method may open new possibilities for supercapacitors with high energy density.

When employing the chemical synthesis approach, PANI/TMOs nanocomposites are developed by a combination of in situ chemical oxidative polymerization with metal oxide nanoparticles [60], and in situ polymerization of monomers of PANI with metal oxides as the oxidizing agents, where metal oxides serve as the oxidizing agents in some cases [61]. Both TMOs and PANI can be synthesized simultaneously to obtain a uniform distribution of PANI/TMOs nanocomposites [62]. In-situ polymerization is a scalable and one-step method for producing widely distributed and strongly interacting polymer/TMOs nanocomposites. PANI/MnO_2 nanocomposites were synthesized via a scalable and one-step in-situ polymerization method [60]. Hu et al. [63] reported a chemical technique to create a PANI/SnO_2 nanocomposite with a unique surface structure and a synergistic impact of the complementary characteristics of both components. The energy storage capacity of the PANI/SnO_2 nanocomposite was about three times that of pure SnO_2. The FESEM images and CV curves of the SnO_2 and PANI/SnO_2 nanocomposite are shown in Fig. 6. The

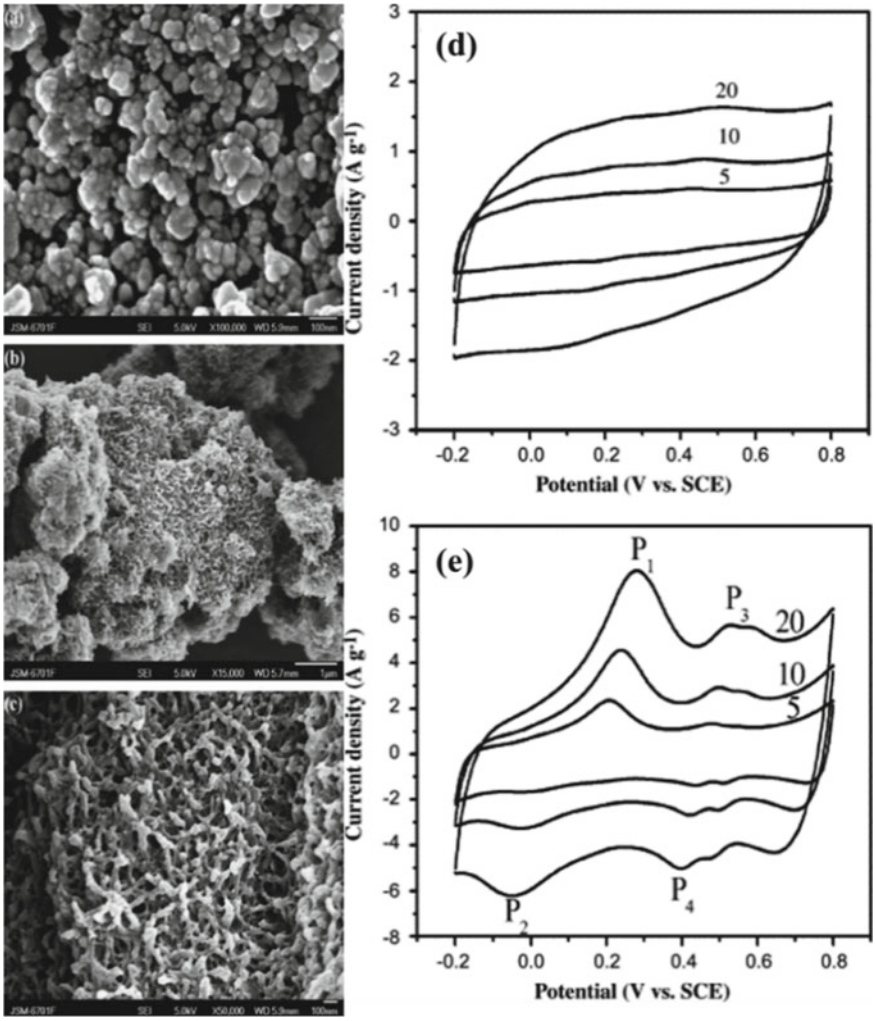

Fig. 6 FESEM images of **a** SnO_2 and **b**, **c** PANI/SnO_2 nanocomposite. CV curves of **d** pure SnO_2 and **e** PANI/SnO_2 nanocomposite at different scan rates. Adapted with permission from reference [63], Copyright (2009), Elsevier

corresponding CV curves of pure SnO2 and PANI/SnO2 nanocomposite at different scan rates are shown in Fig. 6d and Fig. 6e, respectively.

4.2.2 PPy/TMOs-Based Nanocomposites

Reversible redox reactions and high capacitance make PPy CP a good supercapacitor electrode material. It has poor electrochemical stability owing to polymer

molecule chain breakage during long-term charge and discharge. It is reported that the nanocomposites of PPy and TMOs have produced a synergetic effect on the overall performance of supercapacitors. Ruthenium, iron, copper, and cobalt ions are used for developing PPy/TMOs nanocomposites. Interchain coordination structure between a transition metal ion and the nitrogen atom of the PPy ring improves the cycle stability and rate capability of PPy by strengthening the polymer molecule chain strength during charging/discharging. As a result, PPy/TMOs nanocomposites are promising supercapacitor electrode materials for effective energy storage [64]. Yuan et al. [65] synthesized PPy/MnO_2 nanocomposites, and due to their better electrochemical performance, the nanocomposites were applied as supercapacitor electrode materials. The excellent electrochemical performances of the PPy/MnO_2 nanocomposite suggested that in-situ chemical oxidation polymerization is an effective method to develop PPy/MnO_2 nanocomposite for supercapacitors. Raja et al. [66] developed PPy/$Mn_2P_2O_7$ nanocomposite via chemical polymerization and hydrothermal methods. The synthetic approaches are summarized in Fig. 7a. The corresponding PPy/$Mn_2P_2O_7$ nanocomposite-based supercapacitor electrochemical results are shown in Fig. 7a–c. To increase pseudocapacitive performance, Zhou et al. [67] fabricated a supercapacitor electrode consisting of perfectly aligned CoO nanowires over the PPy surface. The electrode design utilized both CoO and PPy, the high electrical conductivity of PPy, and the short ion diffusion route for arranged mesoporous nanowires.

4.2.3 PEDOT/TMOs-Based Nanocomposites

Due to its fast charge/discharge kinetics, high electrical conductivity, and excellent environmental compatibility, PEDOT has recently been reported as a rapidly developing CP for supercapacitor electrodes. It is an electron-rich polymer, consequently, has low oxidation potential with a wide potential window (1.2–1.5 V), and hence exhibited a high capacitance [68]. Yang et al. [69] developed porous conducting PEDOT/MnO_2 nanocomposites as high-performance supercapacitor electrodes. Simple thermal and chemical vapor polymerization techniques produce NPs-enriched PEDOT porous structures, as shown in Fig. 8. FESEM micrographs showed uniform dispersion of MnO_2 nanoparticles into a porous matrix of PEDOT (Fig. 8a–d). The electrochemical performance of the PEDOT/MnO_2 nanocomposite-based supercapacitor is shown in Fig. 8e–h. These synergistic characteristics make the PEDOT/MnO_2 porous nanocomposite a viable electrode material for supercapacitors. According to Ranjusha et al. [70] the PEDOT/MnO_2 nanohybrid sponge may be utilized as a supercapacitor electrode. The completely functioning asymmetric coin cell was further investigated, which delivered an energy density of 200 mWh/kg and a power density of 6.4 kW/kg. Huang et al. [10] utilized CV analysis to electrochemically load hydrous RuO_2 nanoparticles into the PEDOT matrix at different potential cycles to develop a PEDOT/RuO_2 nanocomposite based supercapacitor. Tang et al. [71] demonstrated the controlled synthesis of PEDOT/MnO_2 hierarchical nanocomposites as positive electrode material for high-performing supercapacitors. Lee et al.

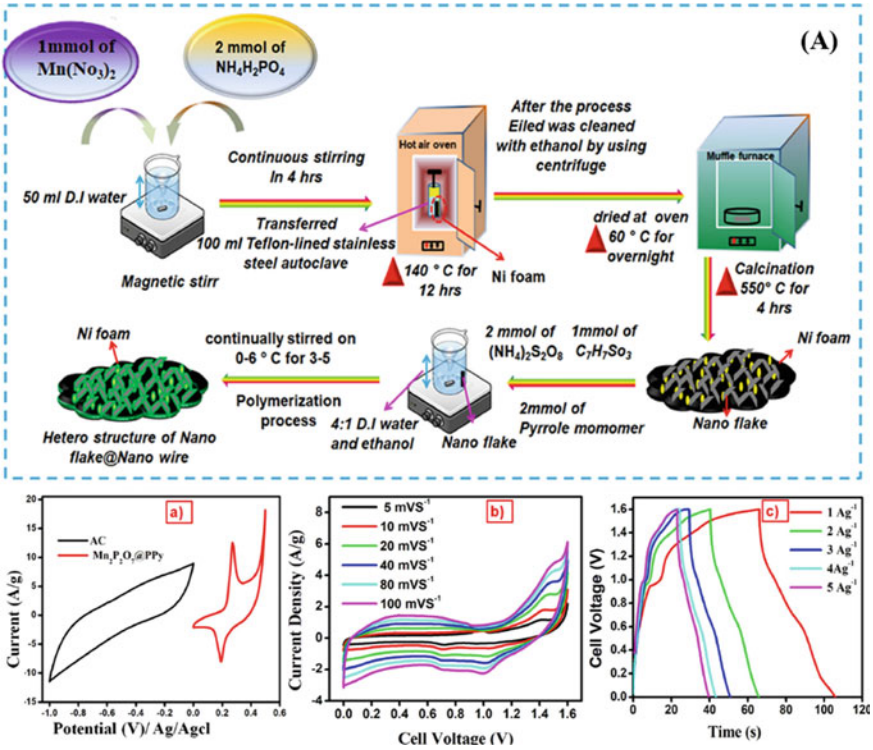

Fig. 7 (A) Schematic representation for the synthesis of $Mn_2P_2O_7$ and PPy/Mn_2P2O_7 nanocomposite. The corresponding PPy/Mn_2P2O_7 nanocomposite-based supercapacitor electrochemical results **a** comparison of the CV curves for AC and PPy/Mn_2P2O_7 recorded in three-electrode system, **b** CVs of PPy/$Mn_2P_2O_7$ nanocomposite-based supercapacitor at different scan rates, and **c** GCD profiles of PPy/Mn_2P2O_7 nanocomposite-based supercapacitor at different current densities. Adapted with permission from reference [66], Copyright (2021), Elsevier

[72] developed fabric-based PEDOT/SnO_2 nanoparticles for the high-performance supercapacitor. The dispersion of SnO_2 nano powder in aqueous PEDOT solution was used to make a composite of PEDOT/SnO_2. Ates et al. [73] reported PANI/CuO, PPy/CuO, and PEDOT/CuO nanocomposites as electrode materials for supercapacitors. The highest specific capacitance of 286.35 F/g at the scan rate of 20 mV/s was obtained for PANI/CuO as compared to PPy/CuO (20.78 F/g at 5 mV/s) and PEDOT/CuO (198.89 F/g at 5 mV/s). Table 2 summarizes the comparison of the capacitive properties of CPs and TMOs-based binary nanocomposites as electrodes for supercapacitors.

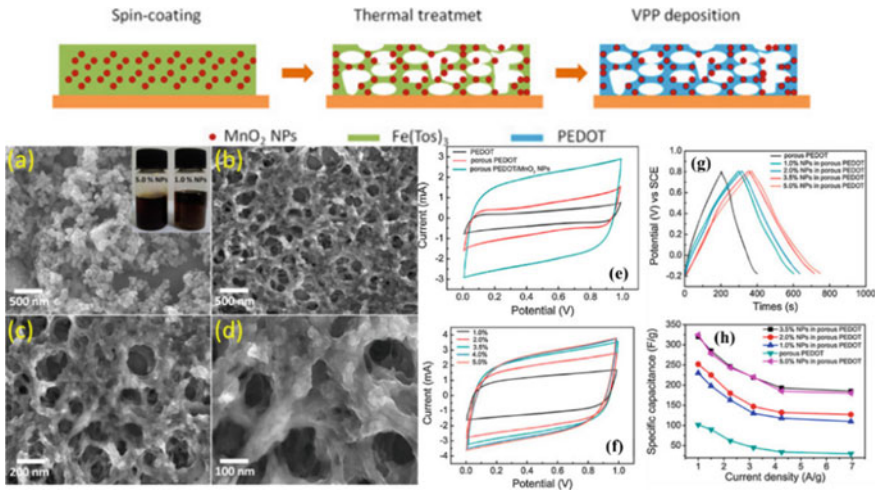

Fig. 8 Schematic representation for the synthesis of PEDOT/MnO_2 nanocomposite. **a** FESEM image of synthesized MnO_2 nanoparticles and **b–d** FESEM images of the synthesized PEDOT/MnO_2 nanocomposite at different magnifications. CVs curves of the **e** pure PEDOT, porous PEDOT, and PEDOT/MnO_2 nanocomposite electrodes recorded at a scan rate of 60 mV/s, **f** PEDOT/MnO_2 nanocomposite with different loading of MnO_2 in the nanocomposites. **g** GCD profiles of the porous PEDOT and PEDOT/MnO_2 nanocomposite electrodes with different loading of MnO_2 at a current density of 0.5 A/g. **h** Specific capacitance versus current density curves of the porous PEDOT and PEDOT/MnO_2 nanocomposites. Adapted with permission from reference [69], Copyright (2015), Elsevier

5 CPs-Based Ternary Nanocomposites for Supercapacitors

Several demerits are suffering from using single electroactive materials like carbon materials, TMOs, and CPs in supercapacitors. Therefore, several kinds of hybrid nanocomposites provide a high specific capability, energy density, power density, and cycle life electrodes with low-cost and ecologically friendly. Although binary CP-based nanocomposites have made significant progress in supercapacitor materials, their characteristics like cyclic stabilities, specific capacitance, and conductivities are still far from ideal, and the usage of binary nanocomposites cannot satisfy all the high-performance supercapacitor criteria [74]. Many methods have thus been used to prepare ternary nanocomposites by combining all three kinds of electroactive materials (i.e., carbon materials, TMOs, and CPs) to produce the perfect supercapacitors. This section thus concentrates on the recent developments of supercapacitors based on ternary nanocomposites of CPs, transitional metal oxides, and carbonaceous materials.

A ternary nanocomposite of PANI/graphene/MnO_2 was prepared on the graphene sheets coated with MnO_2 through in situ chemical oxidative polymerization [75]. The fabricated supercapacitor with PANI/graphene/MnO_2 nanocomposite electrode exhibited excellent electrochemical performance. Shafi et al. [76] reported an in situ

Table 2 A comparison of the capacitive properties of CPs and TMOs-based binary nanocomposites as electrodes for supercapacitors

Electrode materials	Specific capacitance (F/g) (Current density or Scan rate)	Energy density (Wh/kg)	Electrolytes	Cyclic stability	References
PANI/NiO	514 (1 mV/s)	17.6	1 M H_2SO_4	64% (1000)	[57]
PANI/MnO_2	417 (5 mV/s)	11.4	1 M H_2SO_4	96.4% (2000)	[58]
PANI/V_2O_5	443 (0.5 mA/cm^2)	69.2	LiCl/PVA gel	92% (500)	[59]
PANI/MnO_2	525 (2 A/g)	–	0.5 M H_2SO_4	76% (1000)	[60]
PANI/SnO_2	305.3 (5 mA/cm^2)	42.4	1 M H_2SO_4	96% (500)	[63]
PANI/CuO	286.35 (20 mV/s)	–	0.5 M H_2SO_4	81.82% (500)	[73]
PPy/MnO_2	250 (2 mV/s)	–	2 M Na_2SO_4	96.8% (400)	[65]
PPy/$Mn_2P_2O_7$	658 (1 A/g)	27.4	2 M KOH	99% (10,000)	[66]
PPy/CoO	2223 (1 mA/cm^2)	43.5	3 M NaOH	91% (20,000)	[67]
PPy/CuO	20.78 (5 mV/s)	–	0.5 M H_2SO_4	48.39% (500)	[73]
PEDOT/MnO_2	321.4 (0.5 A/g)	–	1 M H_2SO_4	90% (4000)	[69]
PEDOT/MnO_2	1068 (1 mV/s)	0.2	1 M KOH	~ 100% (1000)	[70]
PEDOT/RuO_2	653 (50 mV/s)	–	0.5 M H_2SO_4	…	[10]
PEDOT/MnO_2	449 (0.5 A/g)	47.8	0.5 M Na_2SO_4	91.3% (5000)	[71]
PEDOT/SnO_2	126 (20 mV/s)	–	2 M H_2SO_4	…	[72]
PEDOT/CuO	198.89 (5 mV/s)	–	0.5 M H_2SO_4	68.55% (500)	[73]

polymerized PANI/rGO/$LaMnO_3$ ternary nanocomposite as an efficient electrode material for supercapacitors with high energy density. The developed asymmetric supercapacitor with PANI/rGO/$LaMnO_3$ nanocomposite electrode performed better electrochemically than the symmetric supercapacitor. The exceptional performance of asymmetric supercapacitors makes them ideal for the current requirements of supercapacitors. Chen et al. [77] fabricated a flexible supercapacitor electrode based on the ternary nanocomposite PANI/CC/$NiMoO_4$ with consistent distributed dimensions acting as the principal pseudo capacitating active materials. Furthermore, a flexible all-solid-state asymmetric supercapacitor with PANI/CC/$NiMoO_4$ as the positive

electrode and commercial active carbon as the negative electrode produce maximum specific energy of 99.26 Wh/Kg and a maximum specific power of 10,667 W/Kg. The schematic representation for the synthesis PANI/CC/$NiMoO_4$ based ternary nanocomposite and the corresponding electrochemical performances of the all-solid-state asymmetric supercapacitors are shown in Fig. 9. Another research team Sha et al. [78] produced PANI/rGO/MoS_2 ternary nanocomposite using in situ polymerization technique in the presence of MoS_2 and then added well distributed GOs into PANI/MoS_2 nanocomposite, followed by a decrease in urea-reduction rGO with a hydrothermal treatment. The MoS_2 and rGO components of EDLC with the PANI pseudocapacitive component contribute to PANI/rGO/MoS_2 nanocomposite electrode's total specific capacities. PANI/rGO/Au nanoparticles were synthesized by Shayseh et al. [79] and coated on a glassy carbon electrode by CV technique as a ternary nanocomposite, and their supercapacitor performance was evaluated.

In the presence of PPy, Zhou et al. [80] produced 3D hierarchical CNTs/MnO_2 core_shell nanostructures, in which MnO_2 was precisely coated on CNTs, and a strong bush-like pseudocapacitive shell was generated to increase the specific surface area and efficiently make the ions more accessible. The developed supercapacitors retained high cycling and bending stability. These properties show that a well-designed ternary nanocomposite may be used as electrode materials for high-performance supercapacitors. PPy/graphene/MnO_x ternary nanocomposite films were electrochemically polymerized in one step using sodium p-toluene sulfonate as a supporting electrolyte [81]. The PPy/graphene/MnO_x ternary nanocomposites were made potentio-statically by adding $MnSO_4$ to the deposition solution. The MnO_x nanoparticles were produced directly on the PPy and conducting graphene, acting as spacers to keep adjacent sheets apart. A one-pot synthesis technique for a PPy/graphene/SnO_2 ternary nanocomposite supercapacitor electrode was developed by Wang et al. [82]. In addition to superior rate performance, the PPy/graphene/SnO_2 ternary nanocomposite electrode has exceptional cycle stability. A PPy/rGO/Fe_2O_3 ternary nanocomposite was prepared by two steps: one-pot chemical-microwave synthesis of Fe_2O_3/rGO binary nanohybrids and in situ oxidative polymerization [83]. This showed charge storing mechanisms in both binary and ternary nanocomposites. The ternary nanocomposites showed perfect capacitive performance at low frequencies and resistive behavior at higher frequencies. Another group, Moyseowicz et al. [84], reported a simple two-step synthesis for the synthesis of PPy/rGO/Fe_2O_3 ternary nanocomposite. It involves hydrothermally preparing a binary rGO/Fe_2O_3 composite, then polymerizing PPy on rGO/Fe_2O_3 composite surface.

A ternary nanocomposite of PEDOT/CNTs/MnO_2 in which PEDOT was used as the conductive wrapping over the CNTs/MnO_2 nanocomposite for better conductivity and exhibited a specific capacitance of 427 F/g [85]. Wang et al. [86] used PEDOT/graphene/SnO_2 as ternary nanocomposite electrode materials in supercapacitors. With improved capacitance and energy density in both acidic and neutral electrolytes, the nanocomposite PEDOT/graphene/SnO_2 outperforms its binary counterparts. These materials increased electrochemical properties are attributed to their well-designed ternary nanostructure of functional components with enhanced synergistic effects. Yan et al. [87] reported PEDOT/rGO/MnO_2 nanocomposite as

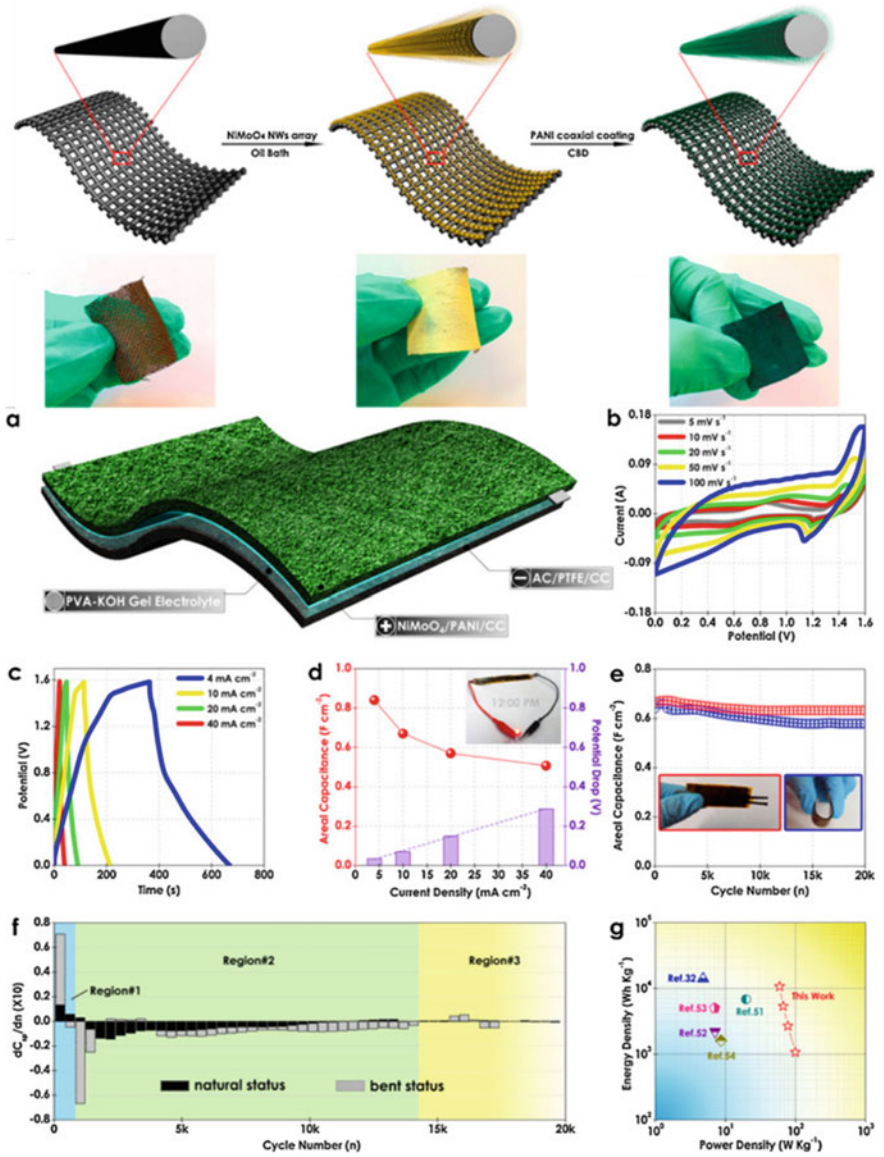

Fig. 9 Schematic representation for the synthesis PANI/CC/$NiMoO_4$ based ternary nanocomposite. **a** Schematic overview, **b** CVs at different scan rates, **c** GCD at different current densities, **d** specific capacitances at different current densities, **e** cyclic stabilities, **f** differential of cyclic specific capacitance versus cycle number, and **g** Ragone plots of PANI/CC/$NiMoO_4$ ternary nanocomposite based all-solid-state asymmetric supercapacitors. Adapted with permission from reference [77], Copyright (2015), Elsevier

supercapacitor electrode. With a specific capacitance of 169.1 F/g at 0.2 A/g, the PEDOT/rGO/MnO_2 material displayed good rate capability and outstanding cycle stability with capacitance retention of 66.2% after 2000 cycles. So, ternary nanocomposite materials are useful in supercapacitor electrodes. A comparison of the capacitive properties of CPs-based ternary nanocomposites for supercapacitors is tabulated in Table 3.

Table 3 A comparison of the capacitive properties of CPs-based ternary nanocomposites for supercapacitors

Electrode materials	Specific capacitance (F/g) (Current density or Scan rate)	Energy density (Wh/kg)	Electrolyte	Cyclic stability	References
PANI/graphene/MnO_2	395 (10 mA/cm^2)	–	1 M H_2SO_4	92% (1200)	[75]
PANI/rGO/$LaMnO_3$	111 (2.5 A/g)	50	3 M KOH	117% (100,000)	[76]
PANI/CC/$NiMoO_4$	1340 (1 mA/cm^2)	99.26	PVA/KOH gel	96.7% (2000)	[77]
PANI/rGO/MoS_2	618 (1 A/g)	–	6 M KOH	96% (2000)	[78]
PANI/rGO/AuNPs	303 (1 mA/cm^2)	–	1 M H_2SO_4	80% (20,000)	[79]
PANI/CNTs/TiO_2	270 (0.4 A/g)	13.5	1 M H_2SO_4	67% (6000)	[88]
PPy/CNTs/MnO_2	529.3 (0.1 A/g)	38.42	1 M Na_2SO_4	98.5% (1000)	[80]
PPy/graphene/MnO_x	320.6 (1 A/g)	–	1 M Na_2SO_4	93% (1000)	[81]
PPy/graphene/SnO_2	616 (1 mV/s)	19.4	1 M H_2SO_4	98% (1000)	[82]
PPy/rGO/Fe_2O_3	626.8 (1 A/g)	87.05	1 M H_2SO_4	…	[83]
PPy/rGO/Fe_2O_3	140 (0.2 A/g)	19.5	1 M Na_2SO_4	93% (5000)	[84]
PEDOT/CNTs/MnO_2	200 (5 mA/cm^2)	–	1 M Na_2SO_4	99% (1000)	[85]
PEDOT/graphene/SnO_2	184 (1 mV/s)	22	1 M H_2SO_4	100% (5000)	[86]
PEDOT/rGO/MnO_2	169.1 (0.2 A/g)	–	1 M Na_2SO_4	66.2% (2000)	[87]
PEDOT/graphite/MnO_2	195.7 (0.5 A/g)	31.4	PVA/LiCl gel	81.5% (2000)	[89]

6 Conclusion

This chapter discusses the developments of CPs-based nanocomposites for application in supercapacitors. The discussion begins with an introduction to CPs and their nanocomposites and how CPs-based nanocomposites contribute to the development of high-performance supercapacitors. As the CPs' limitations restrict its usage in supercapacitors and these shortcomings are largely mechanical due to their breakdown nature. To increase the mechanical strength and thus the functioning of the composite materials, nanocomposites of CPs with solid components such as CNTs, graphene, biomass-derived caron, and TMOs have been discussed. The processes by which these nanocomposites can be developed were discussed and introduced many types of CPs-based nanocomposite including CPs/carbon-based nanocomposites, CPs/Metals oxides-based nanocomposites, and CPs/carbon/metals based ternary nanocomposites. The literature review in this chapter clearly shows that controlling the morphology of the CPs at the nanometer scale and developing their nanocomposites may yield considerable improvements in their electrochemical performance. The cyclability of CPs-based nanocomposite is enhanced when coupled with carbon nanomaterials: pure CPs offer several thousand cycles, while their electrochemical stability rises to several tens of thousands of cycles in the case of CPs and carbon-based nanocomposite electrodes. Construction of 3D CPs-based composite materials reduces ion transport distance and electrochemical impedance to enhance material spatial order.

Acknowledgements The authors would like to acknowledge the support provided by the Deanship of Scientific Research (DSR) at King Fahd University of Petroleum & Minerals (KFUPM) for funding this work through project No. DF191038.

References

1. Y. Su, I. Zhitomirsky, Asymmetric electrochemical supercapacitor, based on polypyrrole coated carbon nanotube electrodes. Appl. Energy **153**, 48–55 (2015)
2. N.R. Aswathy, S.A. Kumar, S. Mohanty, S.K. Nayak, A.K. Palai, Polyaniline/multi-walled carbon nanotubes filled biopolymer based flexible substrate electrodes for supercapacitor applications. J. Energy Storage **35**, 102256 (2021)
3. Y. Yesi, I. Shown, A. Ganguly, T.T. Ngo, L.-C. Chen, K.-H. Chen, Directly-grown hierarchical carbon nanotube@polypyrrole core-shell hybrid for high-performance flexible supercapacitors. Chemsuschem **9**, 370–378 (2016)
4. S.S. Shah, M.A. Alfasane, I.A. Bakare, M.A. Aziz, Z.H. Yamani, Polyaniline and heteroatoms–enriched carbon derived from *Pithophora polymorpha* composite for high performance supercapacitor. J. Energy Storage **30**, 101562 (2020)
5. S.S. Shah, M.N. Shaikh, M.Y. Khan, M.A. Alfasane, M.M. Rahman, M.A. Aziz, Present status and future prospects of jute in nanotechnology: a review. Chem. Rec. **21**, 1631–1665 (2021)
6. W. Mahfoz, M.A. Aziz, S.S. Shah, A.-R. Al-Betar, Enhanced oxygen evolution via electrochemical water oxidation using conducting polymer and nanoparticle composites. Chem. Asian J. **15**, 4358–4367 (2020)

7. M.M. Hasan, T. Islam, A. Imran, B. Alqahtani, S.S. Shah, W. Mahfoz, M.R. Karim, H.F. Alharbi, M.A. Aziz, A.J.S. Ahammad, Mechanistic insights of the oxidation of bisphenol a at ultrasonication assisted polyaniline-au nanoparticles composite for highly sensitive electrochemical sensor. Electrochim. Acta **374**, 137968 (2021)
8. H. Zhang, G. Cao, Z. Wang, Y. Yang, Z. Shi, Z. Gu, Tube-covering-tube nanostructured polyaniline/carbon nanotube array composite electrode with high capacitance and superior rate performance as well as good cycling stability. Electrochem. Commun. **10**, 1056–1059 (2008)
9. X. Bai, X. Hu, S. Zhou, J. Yan, C. Sun, P. Chen, L. Li, In situ polymerization and characterization of grafted poly (3,4-ethylenedioxythiophene)/multiwalled carbon nanotubes composite with high electrochemical performances. Electrochim. Acta **87**, 394–400 (2013)
10. L.-M. Huang, H.-Z. Lin, T.-C. Wen, A. Gopalan, Highly dispersed hydrous ruthenium oxide in poly(3,4-ethylenedioxythiophene)-poly(styrene sulfonic acid) for supercapacitor electrode. Electrochim. Acta **52**, 1058–1063 (2006)
11. H. Lee, H. Kim, M.S. Cho, J. Choi, Y. Lee, Fabrication of polypyrrole (PPy)/carbon nanotube (CNT) composite electrode on ceramic fabric for supercapacitor applications. Electrochim. Acta **56**, 7460–7466 (2011)
12. D. Liu, S. Yu, Y. Shen, H. Chen, Z. Shen, S. Zhao, S. Fu, Y. Yu, B. Bao, Polyaniline coated boron doped biomass derived porous carbon composites for supercapacitor electrode materials. Ind. Eng. Chem. Res. **54**, 12570–12579 (2015)
13. C. Peng, J. Jin, G.Z. Chen, A comparative study on electrochemical co-deposition and capacitance of composite films of conducting polymers and carbon nanotubes. Electrochim. Acta **53**, 525–537 (2007)
14. S. Iqbal, S. Ahmad, Recent development in hybrid conducting polymers: synthesis, applications and future prospects. J. Ind. Eng. Chem. **60**, 53–84 (2018)
15. C.I. Awuzie, Conducting polymers. Mat. Today: Proc. **4**, 5721–5726 (2017)
16. R. Ramya, R. Sivasubramanian, M.V. Sangaranarayanan, Conducting polymers-based electrochemical supercapacitors—progress and prospects. Electrochim. Acta **101**, 109–129 (2013)
17. G.A. Snook, P. Kao, A.S. Best, Conducting-polymer-based supercapacitor devices and electrodes. J. Power Sources **196**, 1–12 (2011)
18. M.A.A. Mohd Abdah, N.H.N. Azman, S. Kulandaivalu, Y. Sulaiman, Review of the use of transition-metal-oxide and conducting polymer-based fibres for high-performance supercapacitors. Mater. Des. **186**, 108199 (2020)
19. H. Sheng, M. Wei, A. D'Aloia, G. Wu, Heteroatom polymer-derived 3D high-surface-area and mesoporous graphene sheet-like carbon for supercapacitors. ACS Appl. Mater. Interfaces **8**, 30212–30224 (2016)
20. K.D. Fong, T. Wang, S.K. Smoukov, Multidimensional performance optimization of conducting polymer-based supercapacitor electrodes, Sustain. Energy Fuels **1**, 1857–1874 (2017)
21. Q. Xiao, X. Zhou, The study of multiwalled carbon nanotube deposited with conducting polymer for supercapacitor. Electrochim. Acta **48**, 575–580 (2003)
22. S. Wang, L. Ma, M. Gan, S. Fu, W. Dai, T. Zhou, X. Sun, H. Wang, H. Wang, Free-standing 3D graphene/polyaniline composite film electrodes for high-performance supercapacitors. J. Power Sources **299**, 347–355 (2015)
23. X.-L. Song, J.-X. Guo, M.-X. Guo, D.-Z. Jia, Z.-P. Sun, L.-X. Wang, Freestanding needle-like polyaniline–coal based carbon nanofibers composites for flexible supercapacitor. Electrochim. Acta **206**, 337–345 (2016)
24. K. Shen, F. Ran, X. Zhang, C. Liu, N. Wang, X. Niu, Y. Liu, D. Zhang, L. Kong, L. Kang, S. Chen, Supercapacitor electrodes based on nano-polyaniline deposited on hollow carbon spheres derived from cross-linked co-polymers. Synth. Met. **209**, 369–376 (2015)
25. E. Frackowiak, V. Khomenko, K. Jurewicz, K. Lota, F. Béguin, Supercapacitors based on conducting polymers/nanotubes composites. J. Power Sources **153**, 413–418 (2006)
26. G. Wu, P. Tan, D. Wang, Z. Li, L. Peng, Y. Hu, C. Wang, W. Zhu, S. Chen, W. Chen, High-performance supercapacitors based on electrochemical-induced vertical-aligned carbon nanotubes and polyaniline nanocomposite electrodes. Sci. Rep. **7**, 43676 (2017)

27. H. Zhang, G. Cao, W. Wang, K. Yuan, B. Xu, W. Zhang, J. Cheng, Y. Yang, Influence of microstructure on the capacitive performance of polyaniline/carbon nanotube array composite electrodes. Electrochim. Acta **54**, 1153–1159 (2009)
28. C.-E. Zhao, J. Wu, S. Kjelleberg, J.S.C. Loo, Q. Zhang, Employing a flexible and low-cost polypyrrole nanotube membrane as an anode to enhance current generation in microbial fuel cells. Small **11**, 3440–3443 (2015)
29. A. Afzal, F.A. Abuilaiwi, A. Habib, M. Awais, S.B. Waje, M.A. Atieh, Polypyrrole/carbon nanotube supercapacitors: technological advances and challenges. J. Power Sources **352**, 174–186 (2017)
30. X. Lin, Y. Xu, Facile synthesis and electrochemical capacitance of composites of polypyrrole/multi-walled carbon nanotubes. Electrochim. Acta **53**, 4990–4997 (2008)
31. Y. Fang, J. Liu, D.J. Yu, J.P. Wicksted, K. Kalkan, C.O. Topal, B.N. Flanders, J. Wu, J. Li, Self-supported supercapacitor membranes: Polypyrrole-coated carbon nanotube networks enabled by pulsed electrodeposition. J. Power Sources **195**, 674–679 (2010)
32. X. He, W. Yang, X. Mao, L. Xu, Y. Zhou, Y. Chen, Y. Zhao, Y. Yang, J. Xu, All-solid state symmetric supercapacitors based on compressible and flexible free-standing 3D carbon nanotubes (CNTs)/poly(3,4-ethylenedioxythiophene) (PEDOT) sponge electrodes. J. Power Sources **376**, 138–146 (2018)
33. D.K. Bhat, M. Selva Kumar, N and p doped poly(3,4-ethylenedioxythiophene) electrode materials for symmetric redox supercapacitors. J. Mater. Sci. **42**, 8158–8162 (2007)
34. A. Aziz, S.S. Shah, A. Kashem, Preparation and utilization of jute-derived carbon: a short review. Chem. Rec. **20**, 1074–1098 (2020)
35. S.S. Shah, E. Cevik, M.A. Aziz, T.F. Qahtan, A. Bozkurt, Z.H. Yamani, Jute sticks derived and commercially available activated carbons for symmetric supercapacitors with bio-electrolyte: a comparative study. Synth. Met. **277**, 116765 (2021)
36. S. Adeyeye Nafiu, S.S. Shah, A. Aziz, M.N. Shaikh, Biogenic synthesis of gold nanoparticles on a green support as a reusable catalyst for the hydrogenation of nitroarene and quinolone. Chem. Asian J. **16**, 1956–1966 (2021)
37. S.S. Shah, M.A. Aziz, Agricultural product-derived carbon for energy, sensing, and environmental applications: a mini-review, Bangladesh. J. Plant Taxon **27**, 467–478 (2020)
38. A.J.S. Ahammad, P.R. Pal, S.S. Shah, T. Islam, M. Mahedi Hasan, M.A.A. Qasem, N. Odhikari, S. Sarker, D.M. Kim, M. Abdul Aziz, Activated jute carbon paste screen-printed FTO electrodes for nonenzymatic amperometric determination of nitrite. J. Electroanal. Chem. **832**, 368–379 (2019)
39. C.K. Roy, S.S. Shah, A.H. Reaz, S. Sultana, A.-N. Chowdhury, S.H. Firoz, M.H. Zahir, M.A.A. Qasem, M.A. Aziz, Preparation of hierarchical porous activated carbon from banana leaves for high-performance supercapacitor: effect of type of electrolytes on performance. Chem. Asian J. **16**, 296–308 (2021)
40. N.C. Deb Nath, S.S. Shah, M.A.A. Qasem, M.H. Zahir, M.A. Aziz, Defective carbon nanosheets derived from *Syzygium cumini* leaves for electrochemical energy-storage. ChemistrySelect **4**, 9079–9083 (2019)
41. I.A. Buliyaminu, M.A. Aziz, S.S. Shah, A.K. Mohamedkhair, Z.H. Yamani, Preparation of nano-Co_3O_4-coated *Albizia procera*-derived carbon by direct thermal decomposition method for electrochemical water oxidation. Arab. J. Chem. **13**, 4785–4796 (2020)
42. S.S. Shah, M.A. Aziz, A.K. Mohamedkhair, M.A.A. Qasem, A.S. Hakeem, M.K. Nazal, Z.H. Yamani, Preparation and characterization of manganese oxide nanoparticles-coated *Albizia procera* derived carbon for electrochemical water oxidation. J. Mater. Sci. Mater. Electron. **30**, 16087–16098 (2019)
43. A.K. Mohamedkhair, M.A. Aziz, S.S. Shah, M.N. Shaikh, A.K. Jamil, M.A.A. Qasem, I.A. Buliyaminu, Z.H. Yamani, Effect of an activating agent on the physicochemical properties and supercapacitor performance of naturally nitrogen-enriched carbon derived from *Albizia Procera* leaves. Arab. J. Chem. **13**, 6161–6173 (2020)
44. S.S. Shah, M.A.A. Qasem, R. Berni, C. Del Casino, G. Cai, S. Contal, I. Ahmad, K.S. Siddiqui, E. Gatti, S. Predieri, J.-F. Hausman, S. Cambier, G. Guerriero, M.A. Aziz, Physico-chemical

properties and toxicological effects on plant and algal models of carbon nanosheets from a nettle fibre clone. Sci. Rep. **11**, 6945 (2021)
45. T. Islam, M.M. Hasan, S.S. Shah, M.R. Karim, F.S. Al-Mubaddel, M.H. Zahir, M.A. Dar, M.D. Hossain, M.A. Aziz, A.J.S. Ahammad, High yield activated porous coal carbon nanosheets from *Boropukuria* coal mine as supercapacitor material: investigation of the charge storing mechanism at the interfacial region. J. Energy Storage **32**, 101908 (2020)
46. A.J.S. Ahammad, N. Odhikari, S.S. Shah, M.M. Hasan, T. Islam, P.R. Pal, M.A. Ahmed Qasem, M.A. Aziz, Porous tal palm carbon nanosheets: preparation, characterization and application for the simultaneous determination of dopamine and uric acid. Nanoscale Adv **1**, 613–626 (2019)
47. M. Yu, Y. Han, Y. Li, J. Li, L. Wang, Polypyrrole-anchored cattail biomass-derived carbon aerogels for high performance binder-free supercapacitors. Carbohydr. Polym. **199**, 555–562 (2018)
48. Z. Peng, C. Wang, Z. Zhang, W. Zhong, Synthesis and enhancement of electroactive biomass/polypyrrole hydrogels for high performance flexible all-solid-state supercapacitors. Adv. Mater. Interfaces **6**, 1901393 (2019)
49. J. Han, Q. Li, C. Peng, N. Shu, F. Pan, J. Wang, Y. Zhu, Increasing S dopant and specific surface area of N/S-codoped porous carbon by in-situ polymerization of PEDOT into biomass precursor for high performance supercapacitor. Appl. Surf. Sci. **502**, 144191 (2020)
50. T. Fan, S. Tong, W. Zeng, Q. Niu, Y. Liu, C.-Y. Kao, J. Liu, W. Huang, Y. Min, A.J. Epstein, Self-assembling sulfonated graphene/polyaniline nanocomposite paper for high performance supercapacitor. Synth. Met. **199**, 79–86 (2015)
51. H. Cao, X. Zhou, Y. Zhang, L. Chen, Z. Liu, Microspherical polyaniline/graphene nanocomposites for high performance supercapacitors. J. Power Sources **243**, 715–720 (2013)
52. Y. Liu, H. Wang, J. Zhou, L. Bian, E. Zhu, J. Hai, J. Tang, W. Tang, Graphene/polypyrrole intercalating nanocomposites as supercapacitors electrode. Electrochim. Acta **112**, 44–52 (2013)
53. S. Khasim, A. Pasha, N. Badi, M. Lakshmi, Y.K. Mishra, High performance flexible supercapacitors based on secondary doped PEDOT–PSS–graphene nanocomposite films for large area solid state devices. RSC Adv. **10**, 10526–10539 (2020)
54. W. Wu, X. Wang, Y. Deng, C. Zhou, Z. Wang, M. Zhang, X. Li, Y. Wu, Y. Luo, D. Chen, In situ synthesis of polyaniline/carbon nanotube composites in a carbonized wood scaffold for high performance supercapacitors. Nanoscale **12**, 17738–17745 (2020)
55. A.H.P.D. Oliveira, H.P.D. Oliveira, Carbon nanotube/ polypyrrole nanofibers core–shell composites decorated with titanium dioxide nanoparticles for supercapacitor electrodes. J. Power Sources **268**, 45–49 (2014)
56. Y. Zhu, K. Shi, I. Zhitomirsky, Polypyrrole coated carbon nanotubes for supercapacitor devices with enhanced electrochemical performance. J. Power Sources **268**, 233–239 (2014)
57. B.S. Singu, S. Palaniappan, K.R. Yoon, Polyaniline–nickel oxide nanocomposites for supercapacitor. J. Appl. Electrochem. **46**, 1039–1047 (2016)
58. S. A. Jadhav, S.D. Dhas, K.T. Patil, A.V. Moholkar, P.S. Patil, Polyaniline (PANI)-manganese dioxide (MnO_2) nanocomposites as efficient electrode materials for supercapacitors. Chem. Phys. Lett. **778**, 138764 (2021)
59. M.-H. Bai, T.-Y. Liu, F. Luan, Y. Li, X.-X. Liu, Electrodeposition of vanadium oxide–polyaniline composite nanowire electrodes for high energy density supercapacitors. J. Mater. Chem. A **2**, 10882–10888 (2014)
60. S.A. Ansari, N. Parveen, T.H. Han, M.O. Ansari, M.H. Cho, Fibrous polyaniline@manganese oxide nanocomposites as supercapacitor electrode materials and cathode catalysts for improved power production in microbial fuel cells. Phys. Chem. Chem. Phys. **18**, 9053–9060 (2016)
61. R.I. Jaidev, A.K. Jafri, S. Mishra, Ramaprabhu, polyaniline–MnO_2 nanotube hybrid nanocomposite as supercapacitor electrode material in acidic electrolyte. J. Mater. Chem. **21**, 17601–17605 (2011)
62. L. Zheng, Y. Xu, D. Jin, Y. Xie, Polyaniline-intercalated molybdenum oxide nanocomposites: simultaneous synthesis and their enhanced application for supercapacitor. Chem. Asian J. **6**, 1505–1514 (2011)

63. Z.-A. Hu, Y.-L. Xie, Y.-X. Wang, L.-P. Mo, Y.-Y. Yang, Z.-Y. Zhang, Polyaniline/SnO_2 nanocomposite for supercapacitor applications. Mater. Chem. Phys. **114**, 990–995 (2009)
64. Y. Xie, Electrochemical performance of transition metal-coordinated polypyrrole: a mini review. Chem. Rec. **19**, 2370–2384 (2019)
65. L. Yuan, C. Wan, L. Zhao, Facial in-situ synthesis of MnO_2/PPy composite for supercapacitor. Int. J. Electrochem. Sci. **10**, 9456–9465 (2015)
66. R. BoopathiRaja, S. Vadivel, M. Parthibavarman, S. Prabhu, R. Ramesh, Effect of polypyrrole incorporated sun flower like $Mn_2P_2O_7$ with lab waste tissue paper derived activated carbon for asymmetric supercapacitor applications. Surf. Interfaces **26**, 101409 (2021)
67. C. Zhou, Y. Zhang, Y. Li, J. Liu, Construction of high-capacitance 3D CoO@polypyrrole nanowire array electrode for aqueous asymmetric supercapacitor. Nano Lett. **13**, 2078–2085 (2013)
68. K.S. Ryu, Y.-G. Lee, Y.-S. Hong, Y.J. Park, X. Wu, K.M. Kim, M.G. Kang, N.-G. Park, S.H. Chang, Poly(ethylenedioxythiophene) (PEDOT) as polymer electrode in redox supercapacitor. Electrochim. Acta **50**, 843–847 (2004)
69. Y. Yang, W. Yuan, S. Li, X. Yang, J. Xu, Y. Jiang, Manganese dioxide nanoparticle enrichment in porous conducting polymer as high performance supercapacitor electrode materials. Electrochim. Acta **165**, 323–329 (2015)
70. R. Ranjusha, K.M. Sajesh, S. Roshny, V. Lakshmi, P. Anjali, T.S. Sonia, A. Sreekumaran Nair, K.R.V. Subramanian, S.V. Nair, K.P. Chennazhi, A. Balakrishnan, Supercapacitors based on freeze dried MnO_2 embedded PEDOT: PSS hybrid sponges. Microporous Mesoporous Mater. **186**, 30–36 (2014)
71. P. Tang, L. Han, L. Zhang, S. Wang, W. Feng, G. Xu, L. Zhang, Controlled construction of hierarchical nanocomposites consisting of MnO_2 and PEDOT for high-performance supercapacitor applications. ChemElectroChem **2**, 949–957 (2015)
72. M. Lee, J. Bae, High-performance fabric-based electrochemical capacitors utilizing the enhanced electrochemistry of PEDOT:PSS hybridized with SnO2 nanoparticles. Bull. Korean Chem. Soc. **36**, 2101–2106 (2015)
73. M. Ates, M.A. Serin, I. Ekmen, Y.N. Ertas, Supercapacitor behaviors of polyaniline/CuO, polypyrrole/CuO and PEDOT/CuO nanocomposites. Polym. Bull. **72**, 2573–2589 (2015)
74. Q. Meng, K. Cai, Y. Chen, L. Chen, Research progress on conducting polymer based supercapacitor electrode materials. Nano Energy **36**, 268–285 (2017)
75. B. Mu, W. Zhang, S. Shao, A. Wang, Glycol assisted synthesis of graphene–MnO_2–polyaniline ternary composites for high performance supercapacitor electrodes. Phys. Chem. Chem. Phys. **16**, 7872–7880 (2014)
76. P.M. Shafi, V. Ganesh, A.C. Bose, $LaMnO_3$/RGO/PANI ternary nanocomposites for supercapacitor electrode application and their outstanding performance in all-solid-state asymmetrical device design. ACS Appl. Energy Mater. **1**, 2802–2812 (2018)
77. Y. Chen, B. Liu, Q. Liu, J. Wang, J. Liu, H. Zhang, S. Hu, X. Jing, Flexible all-solid-state asymmetric supercapacitor assembled using coaxial $NiMoO_4$ nanowire arrays with chemically integrated conductive coating. Electrochim. Acta **178**, 429–438 (2015)
78. C. Sha, B. Lu, H. Mao, J. Cheng, X. Pan, J. Lu, Z. Ye, 3D ternary nanocomposites of molybdenum disulfide/polyaniline/reduced graphene oxide aerogel for high performance supercapacitors. Carbon **99**, 26–34 (2016)
79. J.S. Shayeh, A. Ehsani, M.R. Ganjali, P. Norouzi, B. Jaleh, Conductive polymer/reduced graphene oxide/Au nano particles as efficient composite materials in electrochemical supercapacitors. Appl. Surf. Sci. **353**, 594–599 (2015)
80. J. Zhou, H. Zhao, X. Mu, J. Chen, P. Zhang, Y. Wang, Y. He, Z. Zhang, X. Pan, E. Xie, Importance of polypyrrole in constructing 3D hierarchical carbon nanotube@MnO_2 perfect core–shell nanostructures for high-performance flexible supercapacitors. Nanoscale **7**, 14697–14706 (2015)
81. Y.S. Lim, Y.P. Tan, H.N. Lim, N.M. Huang, W.T. Tan, M.A. Yarmo, C.-Y. Yin, Potentiostatically deposited polypyrrole/graphene decorated nano-manganese oxide ternary film for supercapacitors. Ceram. Int. **40**, 3855–3864 (2014)

82. W. Wang, Q. Hao, W. Lei, X. Xia, X. Wang, Graphene/SnO_2/polypyrrole ternary nanocomposites as supercapacitor electrode materials. RSC Adv. **2**, 10268–10274 (2012)
83. R. Ghanbari, M.E. Shabestari, E.N. Kalali, Y. Hu, S.R. Ghorbani, Iron (II and III) oxides/reduced graphene oxide/polypyrrole ternary nanocomposite as electrochemical supercapacitor electrode. J. Electrochem. Soc. **168**, 030543 (2021)
84. A. Moyseowicz, A. Śliwak, E. Miniach, G. Gryglewicz, Polypyrrole/iron oxide/reduced graphene oxide ternary composite as a binderless electrode material with high cyclic stability for supercapacitors. Compos. B. Eng. **109**, 23–29 (2017)
85. Y. Hou, Y. Cheng, T. Hobson, J. Liu, Design and synthesis of hierarchical MnO_2 nanospheres/carbon nanotubes/conducting polymer ternary composite for high performance electrochemical electrodes. Nano Lett. **10**, 2727–2733 (2010)
86. W. Wang, W. Lei, T. Yao, X. Xia, W. Huang, Q. Hao, X. Wang, One-pot synthesis of graphene/SnO_2/PEDOT ternary electrode material for supercapacitors. Electrochim. Acta **108**, 118–126 (2013)
87. D. Yan, Y. Liu, Y. Li, R. Zhuo, Z. Wu, P. Ren, S. Li, J. Wang, P. Yan, Z. Geng, Synthesis and electrochemical properties of MnO_2/rGO/PEDOT:PSS ternary composite electrode material for supercapacitors. Mater. Lett. **127**, 53–55 (2014)
88. B.S. Singu, U. Male, P. Srinivasan, K.R. Yoon, Preparation and performance of polyaniline–multiwall carbon nanotubes–titanium dioxide ternary composite electrode material for supercapacitors. J. Ind. Eng. Chem. **49**, 82–87 (2017)
89. P. Tang, L. Han, L. Zhang, Facile synthesis of graphite/PEDOT/MnO_2 composites on commercial supercapacitor separator membranes as flexible and high-performance supercapacitor electrodes. ACS Appl. Mater. Interfaces **6**, 10506–10515 (2014)

Redox Active Electrolytes in Supercapacitors

Navaneeth Punnakkal, T. G. Satheesh Babu, Bipin G. Nair, and Punathil Vasu Suneesh

Abstract Supercapacitors are highly promising for future electrochemical energy storage systems due to their excellent energy density, power density, and cycling life. Most of the research in supercapacitors is focused on the development of electrode material. The incorporation of redox-active electrolytes in supercapacitors can greatly enhance charge storage. Redox-active electrolytes received considerable attention due to their ability to undergo faradaic reactions that significantly enhance energy storage performance. This chapter discusses various types of redox mediators employed to fabricate supercapacitors, their charge storage mechanism, classification, performance evaluation, advantages, and disadvantages. Various methods used for electrolyte incorporation, challenges in the development, and the future scope are also discussed in this chapter.

Keywords Redox active electrolytes · Supercapacitors · Electrochemical energy storage · Redox shuttling · Polymer gel electrolytes

1 Introduction

The scarcity of fossil fuels and the increasing demand for energy sources point out the requirement to develop suitable energy storage devices as a need of the hour. Even

N. Punnakkal · T. G. Satheesh Babu · P. V. Suneesh (✉)
Amrita Biosensor Research Lab, Amrita School of Engineering Coimbatore, Amrita Vishwa Vidyapeetham, Coimbatore 641112, India
e-mail: pv_suneesh@cb.amrita.edu

Department of Sciences, Amrita School of Engineering Coimbatore, Amrita Vishwa Vidyapeetham, Coimbatore 641112, India

T. G. Satheesh Babu
Amrita Biomedical Engineering Centre, Amrita School of Engineering Coimbatore, Amrita Vishwa Vidyapeetham, Coimbatore 641112, India

B. G. Nair
Amrita School of Biotechnology, Amrita Vishwa Vidyapeetham, Amritapuri 641112, India

S. Thomas et al. (eds.), *Nanostructured Materials for Supercapacitors*,
Advances in Material Research and Technology,
https://doi.org/10.1007/978-3-030-99302-3_23

though natural energy sources like solar and wind are suitable for future energy requirements, intermittent seasonal climate change demands suitable energy storage devices like batteries and supercapacitors to store electrical energy. Various innovations in energy storage devices have provided great convenience in day-to-day life in past decades. Batteries contributed significantly to this by storing electrical energy based on faradaic reactions, with higher energy density and acceptable power density. On the other hand, supercapacitors are a promising solution for the large energy storage requirement in consumer electronics and biomedical devices. Their low internal resistance, high cycling stability, and high capacitance allow them to be used as a stand-alone power source similar to secondary batteries to provide an extended lifetime. However, it is still necessary to optimize the energy storage performance of the supercapacitor to ensure efficient utility. A wide variety of materials have been employed to fabricate supercapacitors, which are intended to obtain high energy and high power densities. High surface area carbon materials [1], metal oxides [2], conducting polymers [3, 4], metal hydroxides [5], and carbon-metal oxide nanocomposites [6, 7] have been reported with high capacitance properties. Since the tailoring of nanostructured electrode material is comparatively easy to achieve high energy storage capacity, extensive research, a large number of research articles, book chapters, and review articles are available to showcase the progress in this area.

It is well known that the use of conventional electrolytes employed for the fabrication of supercapacitor does not contribute significantly towards the specific capacitance. Therefore, various electrolytes, including aqueous, organic, and ionic liquids, have been explored to enhance the supercapacitor performance. Among them, aqueous solutions (alkaline, acidic, neutral) are the most widely used electrolyte to fabricate supercapacitors. The major drawback associated with the system is the decomposition of water while expanding the potential window beyond 1.23 V. Organic and ionic electrolytes have emerged as an alternative to overcome the drawback associated with the aqueous electrolyte based system, and it exhibited a wide operating potential window (2.2–2.9 V) and (2.6–4.0 V) respectively [8, 9]. Even though organic and ionic liquid can significantly enhance the energy density ($E = 0.5CV^2$, C—specific capacitance, V—potential window) [10], it can not enhance the specific capacitance value.

In contrast, the use of redox mediator into these electrolytes was very effective, and significant enhancement in electrochemical properties and specific capacitance values were observed in such systems. Since carbon-based electrodes possess superior stability, high surface area, low cost, chemical inertness, and good electronic conduction, they are widely employed to fabricate supercapacitors. In addition to the inherent electrochemical double-layer capacitance of carbon-based materials, the redox reaction occurring at the electrode-electrolyte interface provides an additional contribution of pseudocapacitance, as shown in Fig. 1a. The most enlightening aspects of such systems include high energy density, power density, and specific capacitance with an overall performance comparable to batteries with safer preparation and operational conditions [11].

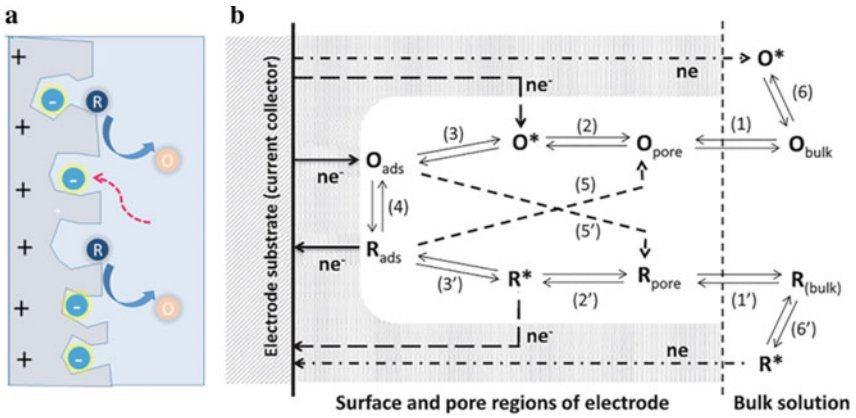

Fig. 1 Schematic illustration of redox mediator enhanced supercapacitor (**a**) and charge storage process while employing redox electrolyte in porous carbon electrode (**b**). Adapted with permission from reference [12] Copyright (2015), The Electrochemical Society

2 Mechanism of Charge Storage in Redox-Mediated Supercapacitors

The schematic illustration of the electrochemical mechanism involved and the improvement in the capacitance when redox additive is introduced into the electrolyte is depicted in Fig. 1b. The redox species in the bulk of the solution need to move inside the pores of the electrode to contribute towards the charge storage. Step (1) or (1') depicts the equilibrium during the solvation and desolvation process while entering or exiting the electrode pores. The redox molecule present in the pore attains a transition state (O^* and R^*) in step (2) or (2') prior to the electron transfer reaction taking place. The process of transition state conversion to the adsorbed state (O_{ads} and R_{ads}) is shown in steps (3) or (3').

The enhanced energy storage capacity of the system was attained through the electron transfer reaction that happened at step 4. This results in the conversion between the adsorbed redox species present on the external and internal surfaces of the electrode. It is possible that once it reaches the transition state (O^* and R^*) without invoking the adsorption, this may also exhibit the electron transfer through step (5 or 5'). In addition, it is possible that upon the electron transfer process, the adsorbed moiety (O_{ads} or R_{ads}) in the system transformed into a soluble product (O_{pore} or R_{pore}). Finally, it diffuses via the pores to the bulk of the electrolyte. Other than the electron transfer reaction inside the pores of the electrode, the outer surface is also involved in the redox process(6 or 6'). Since the outer surface area is comparatively significantly less, the contribution of this process was insignificant.

From the above discussion, it is evident that the chosen electrode material should possess sufficient porosity and must be able to retain redox species and the reaction product to obtain the best performance of the redox electrolyte in supercapacitors.

Even though the capacitance is directly related to the surface area, every part of the high surface area activated carbon does not contribute to the capacitance [13]. This is because electrolytes cannot penetrate through all the available pores, restricting the system from using all the surface area for capacitance [14]. For example, the solvated triiodide has a size of 1.8 nm; hence the electrodes with the mesoporous structure are most suitable for the electrosorption mechanism [15]. Apart from the standard redox potential of the additives, miscibility with water, environmental impact, and cost also need to be considered before being employed for practical applications. However, both organic and inorganic redox additives have been investigated and proven to be very effective with various electrolytes. The researchers have also demonstrated single and dual redox mediators by modifying electrolytes of different pH. Various redox-active electrolytes are briefly explained below.

3 Inorganic Cationic Redox Mediators

Researchers have investigated the electrochemical and pseudocapacitive behavior of various metal ions such as Ag^{+}, Cu^{2+}, and Fe^{2+} in porous carbon material. Electrochemical capacitor performance was significantly enhanced due to the inherent redox property associated with these metal ions. The pioneering work in this area of research was by Tanahashi, who utilized silver ions to improve the capacitance of carbon fiber cloth-based electrochemical capacitors. It was achieved by mixing silver nitrate, of varying concentrations, with sulphuric acid and studied the effect of silver ion concentrations. The specific capacitance of the developed supercapacitor increased with the increasing concentration of silver nitrate in the solution, and the maximum was 248 F g^{-1} at 0.5 M silver nitrate. A three-fold enhancement in capacitance was observed by employing Ag^{+}/Ag redox process compared to the zero concentration of silver nitrate. However, the high cost of silver restricts this combination towards commercialization [16].

Qiang Li et al. [17] showed an enhancement in electrochemical capacitor performance by adding Cu^{2+}ions to the sulphuric acid. However, the electrochemical process was almost irreversible, whereby the stability of the system was significantly reduced. On the other hand, the inclusion of Fe^{2+}ions into the above-mentioned electrolyte was able to overcome the drawbacks associated with the stability and exhibited a high capacity value of 223 mAh g^{-1}. The enhanced performance is attributed to the synergy between Cu^{2+} and Fe^{2+} during the electrochemical reactions.

Because of the ability to undergo (VO^{2+}/$VO_2{}^{+}$) redox reaction in combination with sulphuric acid, vanadyl sulfate is commonly employed to fabricate vanadium redox flow batteries. Due to this inherent property, the same electrolyte combination has been employed for the various supercapacitor fabrications. Senthil Kumar et al. developed an electrochemical double-layer capacitor using porous biomass-derived activated carbon with the combination of $VOSO_4$ and H_2SO_4. A substantial increase in specific capacitance value was observed when comparing the performance of

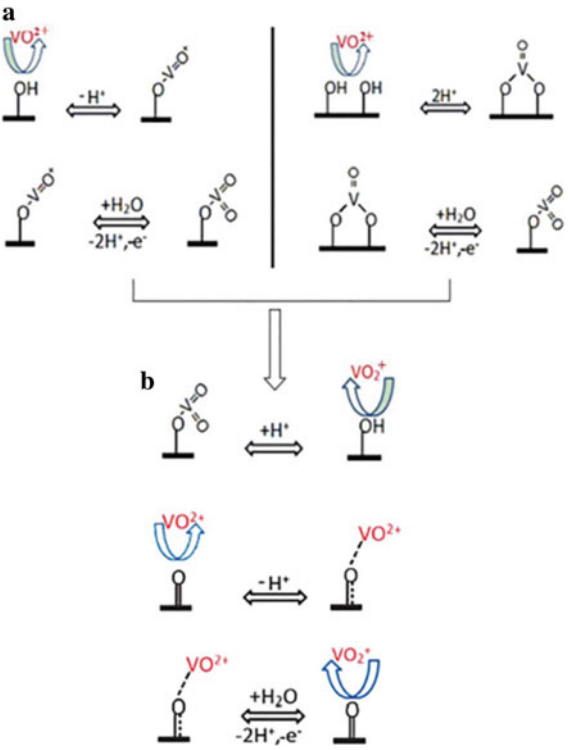

Fig. 2 The catalytic effect of hydroxyl (**a**) and carbonyl (**b**) during the VO^{2+}/VO_2^+ redox reaction. Adapted with permission from reference [18] Copyright (2013), Royal Society of Chemistry (United Kingdom)

pristine 1 M H_2SO_4. Moreover, the fabricated system could retain 97.57% of its initial capacitance even after 4000 charge-discharge cycles [18].

The catalytic reaction in the presence of different functional groups such as hydroxyl (-OH) and carbonyl (C = O) facilitates the significant enhancement in VO^{2+}/VO_2^+ redox reaction through oxygen transfer reaction (Fig. 2). In detail, when the charging happens, the adsorbed VO^{2+} present on the electrode surface replaces the H^+ ion from the -OH and leads to -O-V = bond formation. Further, by releasing H^+ and e^-, the oxygen atom is transferred, and this causes the formation of VO^{2+} on the electrode surface. Ultimately, the diffusion of VO_2^+ ions occurs into the bulk solution through the H^+ ion-exchange reaction [19, 20]. On the other hand, when considering the mechanism with the carbonyl group, the adsorbed VO^{2+} forms a transition state with carbonyl groups and then reacts with H_2O. At the same time, VO_2^+ diffuses back into the bulk electrolyte as VO_2^+ through the H^+ and e^- release. Further, the exact opposite reaction is found to happen while the discharge process takes place [18].

The potassium ferricyanide-ferrocyanide redox probe was very effective due to the fast reaction kinetics and high electrochemical reversibility. Zhang et al. discovered the improvement in capacitance of cobalt aluminium layered double hydroxide with $K_3[Fe(CN)_6]/K_4[Fe(CN)_6]$ and KOH combination [21].

During charging, Co^{2+}oxidized to Co^{3+} and Fe^{3+} reduced to Fe^{2+}, and while discharging, these reactions reversed as shown in Fig. 3. As a result, the galvanostatic charge-discharge curve obtained with Co-Al and KOH exhibited equal time for the charging and discharging process; thereby, the system shows a very high coulombic efficiency of 99.2%. Generally, when considering reversible or quasi reversible electrode processes, the discharge time is always found to be the same or slightly less than the charging time. In contrast, while mixing 0.1 M $K_4Fe(CN)_6$ or $K_3Fe(CN)_6$, the discharge time is much higher than the charging time. This clearly shows the effect of this redox pair on the electrochemical charge storage mechanism. In addition to the significant enhancement in specific capacitance with redox mediator combinations(1 M KOH − 226 F g^{-1}, 1 M KOH + K_3 Fe $(CN)_6$- 712 F g^{-1}, 1 M KOH + K_4 Fe $(CN)_6$ − 317 F g^{-1}) the authors have reported the reduction in charge transfer resistance from 3.27 to 2.96 Ω which eases the overall electrochemical process. Moreover, the underlying mechanism during the charge-discharge process is explained and proven with XRD analysis. The XRD pattern was found unchanged after several charge-discharge cycles. This indicates no intercalation of hexacyanoferrate into the electrode material, and the electrochemical reaction occurs only at the electrode-electrolyte interface. Moreover, the hexacyanoferrate enhances the rate of faradaic reactions between Co(II) and Co(III) during the charge-discharge process.

Manganese dioxide-based supercapacitor shows low cycling stability and power density due to the poor electronic conduction and low rate of faradaic processes. Maiti et al. developed a MnO_2 based symmetric supercapacitor with the addition of $K_4Fe(CN)_6$, and they found seven times improvement in energy density with a power density of 600 W kg^{-1}. The charge storage mechanism of MnO_2 based electrodes in potassium hydroxide (KOH) medium follows two simultaneous processes; i. adsorption and desorption of potassium ions on the MnO_2 surface, and ii. intercalation and deintercalation of potassium ions into the electrode structure [22].

Owing to the well-defined redox property, high specific capacitance, and low cost, $Co(OH)_2$ based systems attracted particular attention. Zhao et al. discovered a $Co(OH)_2$ + $K_3Fe(CN)_6$/KOH system capable of delivering specific capacitance of 7514 F g^{-1} with very high coulombic efficiency and cycling stability (75% specific

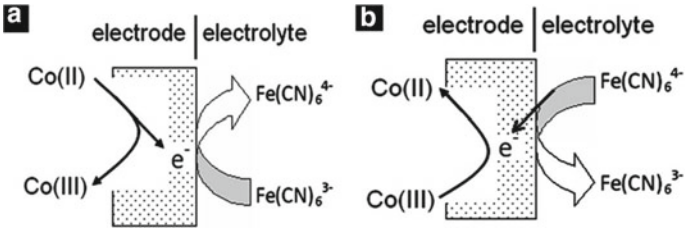

Fig. 3 The electrochemical mechanism happening at the electrode (Co-Al)-electrolyte interface during the charging (**a**) and discharging process (**b**). Adapted with permission from reference [21] Copyright (2009), Royal Society of Chemistry (United Kingdom)

capacitance retains even after 20,000 continuous cycles) [23]. The authors clearly explained the influence of $K_3Fe(CN)_6$ with the help of galvanostatic charge-discharge at a current density of 16 A g^{-1}. It was also found that while varying the concentration, the specific capacitance was increasing. Thus, even though the high concentration of redox probe causes excellent coulombic efficiency and specific capacitance, it may lead to the high concentration polarization, and low-rate capability there by the electrochemical stability of the system reduces significantly. Hence the optimization of electrolyte concentration is a crucial step in this area of research.

4 Inorganic Anionic Redox Mediators

Inorganic anionic redox mediators Br_3^-/Br^- and I_3^-/I^- have been employed for enhancing the capacitance property. The reaction of potassium iodide with iodine results in the formation of polyiodide, where the triiodide is found to be the major proportion [24]. The reaction mechanism of $Br_2$and Br^- also follows a similar mechanism of I_2 and I^- as they belong to the same group in the periodic table. Since the iodine has the ability to exhibit various valance states, it can deliver various redox reactions at the same time. Even though bromine also has the ability to show different valance states, only the −1 and 0 valance states are possible when considering the stable potential window of aqueous electrolytes. Unlike one-electron transfer reactions, interestingly I_2/I^- and Br_2/Br^- involve two-electron transfer reactions. This clearly shows the higher capacity of the system. In addition to that, the reaction rates of I_2/I^- and Br_2/Br^- were found to be very high (10^{-3}–10^{-2} cm S^{-1}) at room temperature [25]. The possible valance states and their required potentials with respect to SHE are explained in Fig. 4a, b [24].

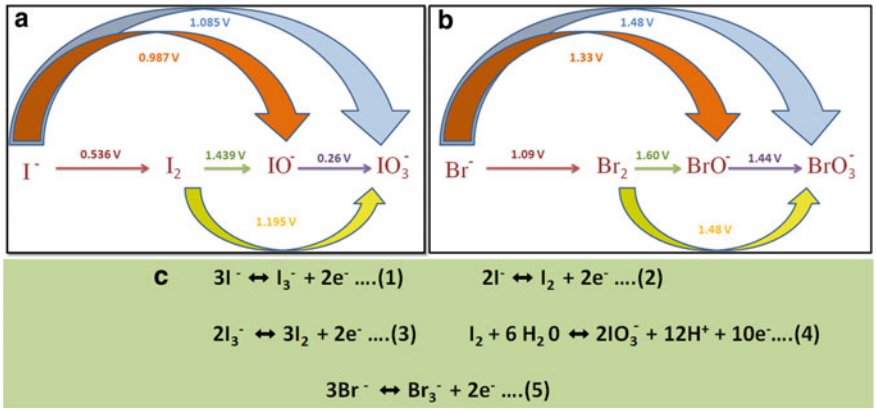

Fig. 4 Electrochemical potential is required to attain various oxidation states of iodine (**a**) and bromine (**b**). The possible redox processes when iodide and bromide based system employed as the redox additive (**c**)

The enhancement in supercapacitor performance is due to the characteristic electrochemical redox process between $3I^-/I_3^-$, $2I^-/I_2$, $2I_3^-/I_2$, I_2/IO_3^- and $3Br^-/Br_3^-$ the possible electrochemical mechanism involved is shown Fig. 4c.

Without the use of any supporting electrolyte Frackowiak et al. [26] have developed an electrochemical double-layer capacitor with potassium iodide as the electrolyte. The faradaic reaction between I_2/I_3^- and IO_3^-/I_2 contributes to the pseudocapacitance, and thereby the total capacitance of the electrode significantly improved by 10 times in one molar concentration of potassium iodide. The same research group has explained the effect of first group cations of the periodic table towards the carbon—iodide interface reaction [15]. Iodides of lithium, sodium, potassium, rubidium, and cesium were employed as the redox mediators. The capacitance was found to increase with increasing the size of cations. For example, rubidium iodide exhibits a maximum capacitance of 2272 F g^{-1}, whereas lithium iodide solution exhibits only 300 F g^{-1}. The exceptional change in capacitance with various alkali metals can be attributed to different physicochemical parameters including polarizability, size, mobility, diffusion coefficient etc.

Even though potassium iodide possesses intermediate capacitance compared to the alkali metal cations-based system, it received considerable research attention because of its low cost and high capacitance properties. Similarly, potassium bromide is also a promising redox additive in an aqueous electrolyte-based supercapacitor. Because of the Br^-/Br_3^- redox reaction, 0.5 M potassium bromide in combination with 1 M sodium sulphate significantly enhanced the supercapacitor performance (4 times the larger energy density than 1 M Na_2SO_4) with carbon nanotube-based electrodes [27].

5 Organic Redox Mediators

Even though the inorganic redox mediators can deliver excellent ionic conductivity and safe operational conditions, the lower working potential window due to the decomposition of the electrolyte restricts its application for commercial needs. The combination of organic electrolytes with organic redox-active species exhibits a wide potential window and enhanced performance. Approximately 27 times enhancement in energy density was observed when decamethyl ferrocene was used as the additive in organic medium (tetrabutylammonium perchlorate in combination with tetrahydrofuran (THF)) 36.8 Wh kg^{-1}. Also, it exhibits a considerable change in specific capacitance value from 8.3 to 61.3 Fg^{-1} [28].

Hai jun Yu et al. also developed a redox-mediated organic electrolyte by using p-phenylenediamine in combination with lithium perchlorate and acetonitrile. The supercapacitor shows very high specific capacitance (68.59 Fg^{-1}) along with an energy density of 54.46 Wh kg^{-1} and a power density of 13.11 kW kg^{-1}. The ability of p-phenylenediamine to undergo a quick redox reaction significantly enhanced the pseudocapacitive contribution in the system [29].

Since the organic additives possess structural diversity, similar to inorganic additives, the former is also considered a promising approach to enhancing supercapacitor

performance. Some of the generally used organic redox mediators are represented in Fig. 5.

In the case of organic additives, the organic compounds containing quinine, hydroquinone, amines are capable of involving in the electron transfer process. The pioneering work was based on hydroquinone combination with 1 M H_2SO_4, which was explained by Roldan et al. [30]. The excellent electrochemical activity of hydroquinone was highly promising because it involves a redox reaction with a two-electron transfer, thereby enhancing the specific capacitance value manyfolds. As a result, the fabricated capacitor exhibited a specific capacitance of 901 F g^{-1} with an energy density of 31.3 Wh kg^{-1}a three-fold enhancement in performance was observed compared to 1 M H_2SO_4 (320 F g^{-1}). However, it could retain only 65% of its initial capacitance value after 4000 cycles. Using polyaniline—graphene composite in 1 M H_2SO_4 + Hydroquinone mixture, Chen et al. showed a 92%

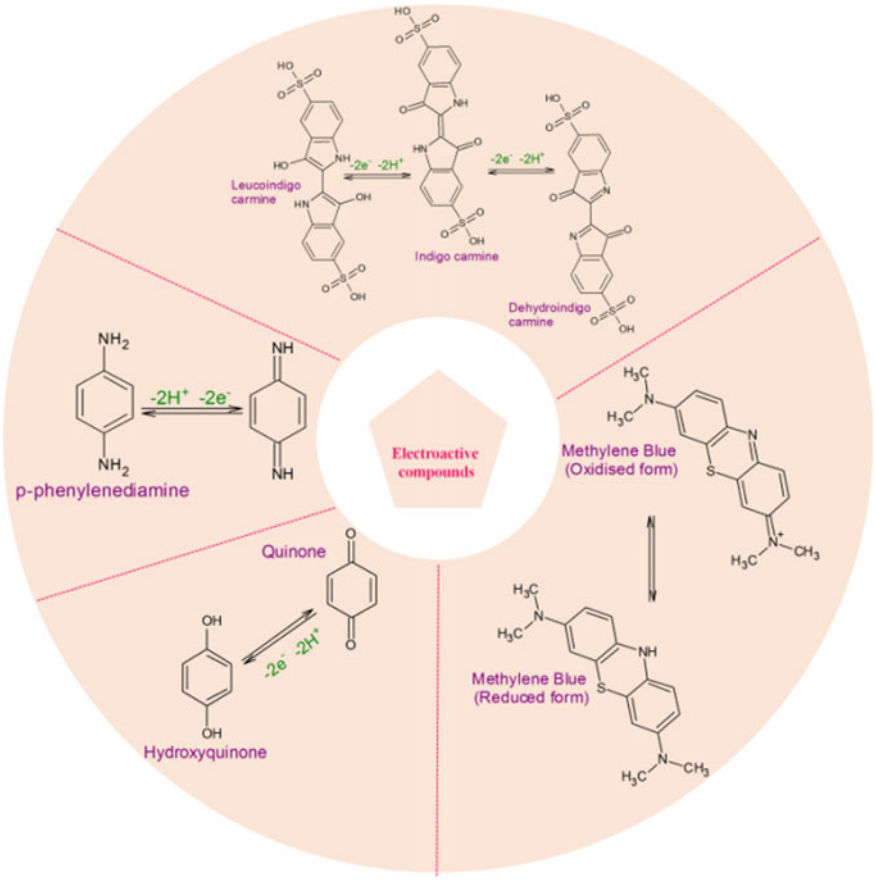

Fig. 5 Some of the commonly employed electroactive organic compounds in electrolytes for supercapacitor applications

enhancement in capacitance (288–553 F g^{-1}). In addition, the developed system showed very high cycling stability (64%) even after 50,000 cycles [31].

One major approach for developing redox species is by altering the molecular structure of hydroquinone. Gastola et al. developed hydroquinone with a brominated structure (2, 5-bromobenzene-1, 4-diol). The electrochemical performance of the developed system was studied by mixing it with KOH electrolyte.

The mechanism of the proposed approach for the synthesis of modified hydroquinone has been clearly presented in Fig. 6.

$$Q + e^- \leftrightarrow Q^- \tag{1}$$

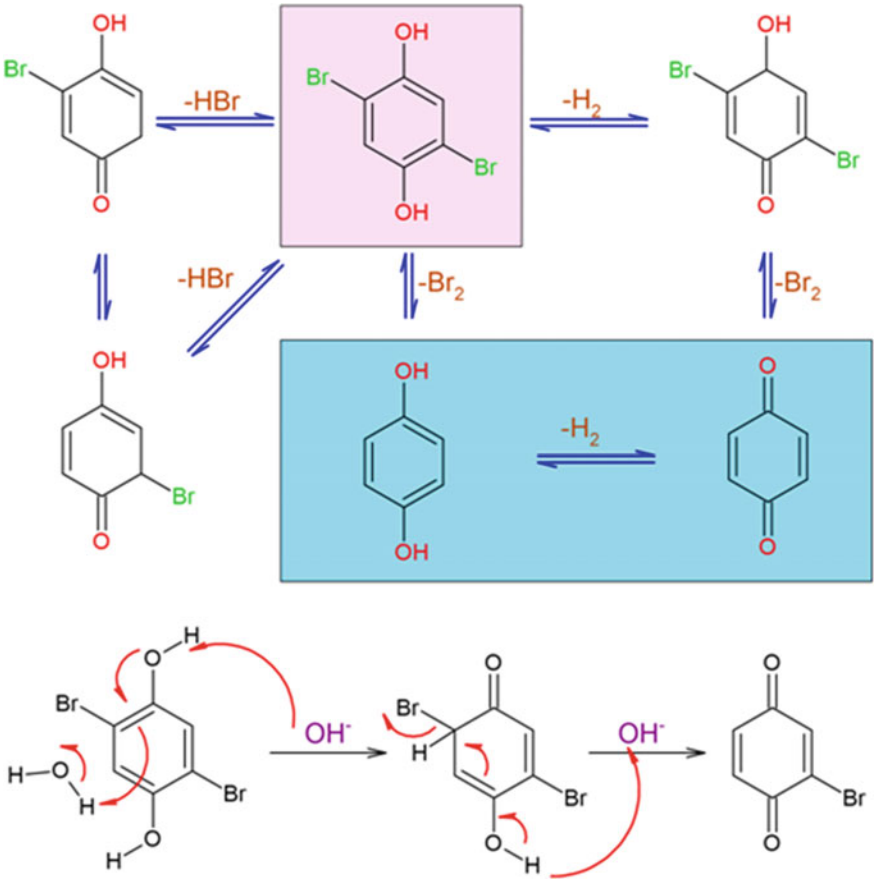

Fig. 6 Reaction mechanism and the various stages involved in the synthesis of 2, 5 dibromo benzene 1, 4 –diol used for supercapacitor application. Adapted with permission from reference [32] Copyright (2016), Elsevier

$$Q^{\cdot -} + HA \leftrightarrow A^- + HQ^{\cdot} \tag{2}$$

$$HQ^{\cdot} + e^- \leftrightarrow HQ^- \tag{3}$$

$$HQ^- + HA \leftrightarrow H_2Q + A^- \tag{4}$$

The authors have stated, there must be different faradaic reactions and pseudocapacitance contributions while carrying out the electrochemical reaction in an alkaline medium other than the quinone—hydroquinone redox process (equations 1–4). The incorporation of bromine with hydroquinone is expected to undergo extra reactions, which include,

$$2Br^- \leftrightarrow Br_{2\,aq} + 2e^- \tag{5}$$

$$Br_{2\,aq} + 2H_2O \leftrightarrow 2BrO^- + 4H^+ + 2e^- \tag{6}$$

$$Br^- + 2OH^- \leftrightarrow 2BrO^- + 4H_2O + 2e^- \tag{7}$$

$$BrO^- + 4OH^- \leftrightarrow BrO_3^- + 2H_2O + 4e^- \tag{8}$$

$$Br^- + 3H_2O \leftrightarrow BrO_3^- + 6H^+ + 6e^- \tag{9}$$

While employing the optimum ratio of brominated hydroquinone and potassium hydroxide, the activated carbon electrode exhibits a very high capacitance value of 314 F g^{-1}. The major drawback associated with the above-mentioned organic additives is that they exhibit poor electronic conductivity, which results in a lesser power density of the supercapacitors. This is because the molecules possess a smaller size, and the HOMO—LUMO gap is considerably high. Phenyldiamine is another important compound capable of delivering similar performances due to the ability to undergo p-phenylenediamine redox reaction. Jihuai Wu et al. [33] reported the effect of phenyldiamine that significant capacitance improvement (144.0–605.2 F g^{-1}) was observed while testing the composition with 0.050 g of phenylenediamine and 2 M KOH compared to the pristine KOH. A considerable variation in energy density was also observed in this system (4.458–19.862 Wh kg^{-1}).

Because of the presence of two quinones and amine groups in the indigo carmine structure, the molecule exhibits superior redox activity. The expected redox mechanism of the molecule in 1 M H_2SO_4 is shown in Fig. 5. Indigo carmine shows a leucoindigo carmine structure with oxidation/reduction at the quinine site, a two-electron transfer reaction. Similarly, with the two-electron transfer process, the molecule undergoes a redox reaction at the amine position, which leads to the conversion of indigo carmine to dehydro indigo carmine. A significant enhancement in specific capacitance (17–50 F g^{-1}) and energy density (0.6–1.7 Wh kg^{-1}) was

observed while employing the indigo carmine −1 M H_2SO_4 combination in a multi-walled carbon nanotube-based supercapacitor system [34]. m-Phenylenediamine is another promising redox material capable of enhancing the supercapacitor performance. Haijun Yu et al. [35] studied the effect of m-phenylenediamine in KOH electrolytes. Upon adding this redox mediator, the ESR value was significantly reduced (2.60–1.98 Ω cm^2) also the specific capacitance value-enhanced from 36.43 to 78.01 F g^{-1} with good capacitance retention over 1000 cycles.

Pauloet al. [36] explained the effect of methylene blue and the mechanism involved when it is acting as a redox shuttle in an activated carbon-based supercapacitor. The major drawback associated with the system is its lack of stability which can cause the secondary reaction, thereby reducing overall performance and cycle life significantly. The authors have showcased the strong interaction of methylene blue, and activated carbon causes the progressive decrement in resistance of the electrode. As a result, the energy density of the developed system has increased by more than 40%. Electron spray mass spectroscopic studies show the presence of the oxidized derivatives and the by-products formed during the demethylation after cycling. Thereby the equilibrium potential of the system constantly varies, which leads to the change in the charge storage mechanism.

6 Dual Redox Mediators

The combination of two different mediators having different redox potential opens up a new era in research. Here, the mediator with higher potential is usually employed for the positive electrode, and it undergoes an oxidation reaction. The mediator with lower potential reduces at the negative electrode, and the cation accumulation happens at the electrode surface while charging the capacitor. Researchers have employed various ways to improve the capacitance performance of a hydroquinone-based system. Nuckowska et al. have developed a dual redox mediator-based supercapacitor using Keggin-type phosphotungstate anions and hydroquinone in a molar ratio 1:1. It exhibited a high energy density and specific capacity of 20.0 Wh kg^{-1} and 40.3 mAh g^{-1}, respectively, a four-fold increase compared with a single redox additive [37]. Frackowiak et al. [38] developed a dual electrolyte of $VOSO_4$ and KI as negative and positive electrolytes, respectively. To maintain the charge balance between the two systems and to prevent mixing of both the electrolyte, a Nafion membrane was employed. Even though the system exhibited high energy density, it finds poor commercial viability due to the cost and resistance associated with the Nafion membrane. Fan et al. [39] developed a similar system with polymer gel electrolyte in place of aqueous electrolyte and without the use of Nafion membrane. It exhibited 25.4 Wh kg^{-} energy density with remarkable capacitance retention of 93.7% even after 3000 cycles.

7 Redox Mediator in a Gel Electrolyte

Fabricating the energy storage devices with gel electrolytes is a promising strategy when considering the flexibility and mechanical strength of the system for a commercial need. Gel electrolyte-based system possesses superior ionic conductivity than solid electrolytes [40]. Moreover, the application of liquid-based electrolytes is restricted because of low flexibility, corrosion, leakage, and packing issues [41]. Therefore, polymer gel electrolytes have been employed recently to avoid the drawbacks mentioned above. However, the fabricated supercapacitor prototypes were less efficient than the liquid-based system because of the less ionic movement and the less availability of ions on the electrodes. This causes a very feeble electrode-electrolyte contact area [42]. A schematic illustration of the difference in ion accessibility while using polymer and liquid electrolytes is shown in Fig. 7. Unlike gel electrolyte, in the case of liquid-based systems, ions can penetrate inside the electrodes and thereby causes good electrolyte wettability and high capacitance value.

Polyvinyl alcohol is a commonly used polymer matrix to incorporate electrolytes for gel electrolyte preparation. Yu et al. have developed a PVA—KOH-based electrolyte by varying potassium iodide (KI) composition [43]. The ionic conductivity of the electrolyte was found to increase with the amount of KI up to a particular concentration. A maximum ionic conductivity of 12.73 mS $cm^{-1}$was obtained by

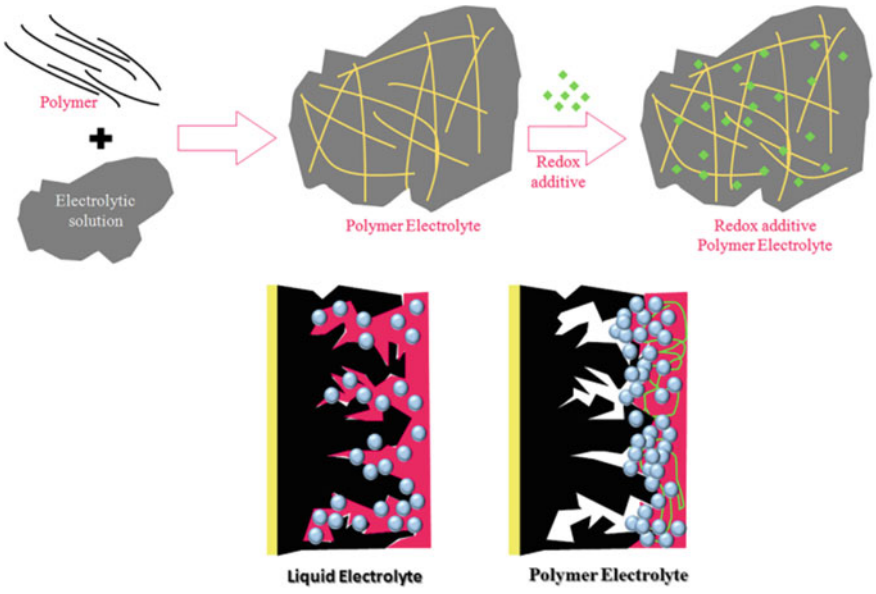

Fig. 7 Schematic representation of different stages involved in redox-active polymer gel electrolyte preparation and the difference in ion accessibility while employing liquid and polymer electrolyte. Adapted with permission from reference [11] Copyright (2013), Royal Society of Chemistry (United Kingdom)

incorporating 0.60 g of KI in the electrolyte. Further increase in KI content causes a decrease in ionic conductivity due to the free ions aggregation and the development of KI crystals. A huge change in specific capacitance (from 135.9 to 236.9 F g^{-1}), energy density (from 7.80 to 15.34 Wh kg^{-1}), and power density (from 3.98 to 4.88 W kg^{-1}) were observed compared with the PVA—KOH gel electrolyte with and without the KI additive. Also, the significant reduction in ESR value clearly explains the potential applicability of the developed system. The same research group was also developed PVA—H_2SO_4 gel electrolyte in combination with p-benzenediol. The maximum ionic conductivity of 34.8 mS cm^{-1} was observed when 0.2 g of p-benzenediol was incorporated, and they found a reduction in ionic conductivity while further increasing the additive load [44]. Similarly, Senthilkumar et al. has used the same electrolyte combination and studied the effect on activated carbon electrode material derived from biowaste [45]. The two-electron transfer reaction between quinone hydroquinone causes the specific capacitance change from 425 to 941 F g^{-1} with an energy density from 9 to 20 Wh kg^{-1}.The commonly used redox active molecule with different polymer gel electrolytes include1,4-naphthoquinone [46], indigo carmine [10], 1-butyl-3-methylimidazolium iodide (BMIMI) [47], 1-anthraquinone sulfonic acid sodium [48], alizarin red S [49], 1-ethyl-3-methylimidazolium tetrafluoroborate [50], 2-mercaptopyridine [51], $FeBr_3$ [52].

Ma et al. have developed a redox-active gel electrolyte by incorporating indigo carmine with polyvinyl alcohol and sulphuric acid. The presence of the reversible redox reaction of indigo carmine causes a drastic increase in ionic conductivity (188%) and reaches 20.27 mS cm^{-1}. This is reflected in the change in specific capacitance value (112% increase), to 382 F g^{-1} with an energy density of 13.26 Wh kg^{-1} and 80.3% of retention in capacitance value even after 3000 cycles [10]. Sun et al. have explained the effect when alizarin redS is used to add the same polymer electrolyte combination (PVA –H_2SO_4). Interestingly the ionic conductivity value reached 33.3 mS cm^{-1}. In the presence of alizarin red S, the specific capacitance value changes from 160 to 441 F g^{-1}. Moreover, the developed system exhibited 39.4 Wh kg^{-1} energy density and good cycling stability.

A completely different and novel approach has been shown by Zhou et al. [42] and Yin et al. [53]. They have developed redox additive incorporated polymer gel electrolyte in combination with suitable electroactive material and finally as the obtained gel was employed as electrode and electrolyte. Yin and co-workers have used polyethylene oxide—lithium aluminate ($LiAlO_2$) gel electrolyte in combination with NaI/I_2 as redox additive and activated carbon as electroactive material. Nafion 117 membrane was used as the separator. The specific capacitance value of the system was found to be increasing with the concentration of the redox mediator. Also, by suppressing the electrode resistance, the rate of electron transfer was significantly enhanced. A 27 fold increase in specific capacitance value was observed compared to the system with no redox additive.

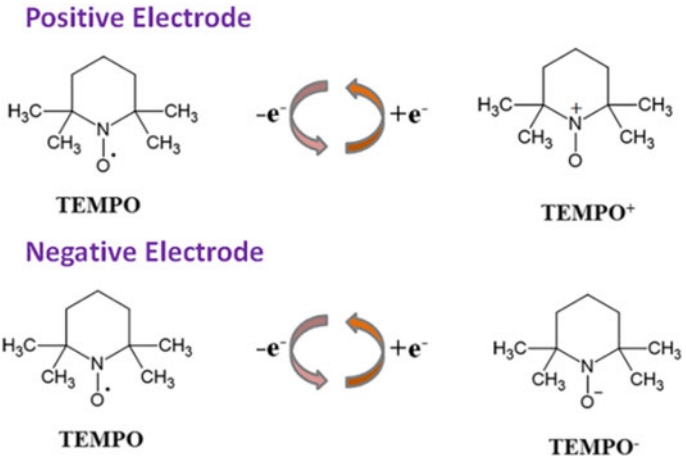

Fig. 8 Redox process involved when TEMPO used as an ambipolar redox mediator

8 Ambipolar Redox Mediator

The ambipolar redox mediator is the most suitable and desired way of implementing the redox-active mechanism in supercapacitors. Unlike dual redox mediators, this can impart simultaneous pseudocapacitance reactions for negative and positive electrodes. Lintong Hu et al. recently developed an ambipolar redox system in combination with an aqueous electrolyte and organic radical tetramethyl piperidinyloxyl (TEMPO). The fabricated EDLC with TEMPO additive exhibits a very high energy density of 51 Wh kg^{-1}, and this value was found to be 2.4 times higher than that of the supercapacitor without the presence of TEMPO. Also, it delivered promising cycling stability over 4000 cycles [54]. Since it possesses four alpha-methyl groups (steric protection) and delocalized free electrons, this radical was found to be highly stable. The significant advantage of this system is that it possesses a 10^{-2} cm s^{-1} electron transfer rate constant, which is much higher than that of normal redox mediators [55, 56]. Fabricated the supercapacitor prototype with activated carbon as positive and negative electrode material and they were separated by an ion-exchange membrane. This offers a potential way to significantly enhance the energy density of electrochemical double-layer capacitors (Fig. 8).

9 Challenges in Commercialization

Although redox-active electrolytes could enhance the overall performance of supercapacitors, the self-discharge, solubility, diffusion rate of reaction products, the toxicity of the mediator are still a concern. Furthermore, the redox shuttling process between the two electrodes leads to decreased coloumbic efficiency and causes side

reactions that restrict its development. Another major hurdle observed in this area is the aging of the supercapacitor during the functioning. Platek et al. [57] explained the factors which affect the aging mechanism which include test method, and galvanostatic cycling. These results enhanced redox side reactions and the change in carbon electrode structure.

The researchers have proposed different strategies to overcome the problem associated with the redox shuttling process. To restrict the mixing of electrolytes by allowing the process of surpassing cations and anions, commercially available ion-selective membranes have been used [58]. For example (Nafion—117) cation exchange membrane was used for developing KI/$VOSO_4$ dual redox mediator-based supercapacitor. The developed system exhibits high energy density. Likewise, in the case of $SnSO_4$/$VOSO_4$ based system, an anion exchange membrane was used. Even though the incorporation of ion-selective membrane considerably reduced the redox shuttling, it possesses drawbacks that include nafion membrane, and sulfonic acid cannot be employed in alkaline medium. Moreover, the ion-selective membrane is susceptible to the PH; this shows poor chemical stability. Also, the high cost of ion-selective membrane limits its application.

Ion exclusion membrane emerged as a promising material to overcome the drawback associated with the ion-selective membrane, which is capable of separating smaller ions despite their charges. Also, it restricts the unwanted migration of ions with a larger size. The significant advantage of the system is it possesses excellent stability in electrolytes and can be employed in electrolytes of different pH. The cost was also found significantly less compared to the ion-selective membrane. This supports the supercapacitor fabrication towards the commercial need. Similarly, various membranes have been employed in supercapacitors intended for obtaining superior performance and stability of the system. The recent works include dialysis membranes and nanofiltration membrane.

10 Conclusion

Based on the observations, the redox mediator enhanced supercapacitors are considered promising energy storage devices for future applications. Even though extensive research has been carried out in this area, most of them are studied based on electrochemical double-layer capacitor-based electrodes. The use of pseudocapacitive/battery electrode materials is expected to provide better performance. It is well known that the water-splitting reaction takes place at 1.23 V. This significantly restricts the energy density of the devices and therefore developing a suitable additive capable of extending the water splitting potential also has significant importance. Advances in redox mediators that can provide faradaic reactions lead to battery-like performance for the supercapacitors. Most of the research articles are explained the specific capacitance and energy density only by considering the mass of the electrode material. In the case of supercapacitors employing redox mediators, the mass of the redox-active molecule in the system also needs to be considered. Since most

of the reported work does not consider this during their calculations, overestimation of energy storage capacity and the specific charge is observed. Excellent energy and power densities along with superior cycling stability, show the promising application of the redox mediator-based systems for future energy storage devices.

Acknowledgements The authors thank the funding agencies Department of Science & Technology, Government of India [SP/YO/692/2018 dated 28/09/2018] and Department for Biotechnology, Ministry of Science and Technology, Government of India [102/IFD/SAN/1555/2018-2019 dated 13/08/2018] for the financial support.

References

1. L. Wan, R. Xiao, J. Liu, Y. Zhang, J. Chen, C. Du, M. Xie, A novel strategy to prepare N, S-codoped porous carbons derived from barley with high surface area for supercapacitors. Appl. Surf. Sci. **518**, 146265 (2020)
2. A. Paravannoor, S.V. Nair, P. Pattathil, M. Manca, A. Balakrishnan, High voltage supercapacitors based on carbon-grafted NiO nanowires interfaced with an aprotic ionic liquid. Chem. Commun. **51**(28), 6092–6095 (2015)
3. G.P. Krishnaa, P. Navaneeth, T. Ramachandran, T.S. Babu, P.V. Suneesh, Fabrication of polyaniline-platinum nanocomposite based flexible supercapacitor. Mater. Today: Proc. **33**, 2407–2413 (2020)
4. K.Y. Yasoda, M.S. Kumar, S.K. Batabyal, Polyaniline decorated manganese oxide nanoflakes coated graphene oxide as a hybrid-supercapacitor for high performance energy storage application. Ionics **26**(5), 2493–2500 (2020)
5. L. Gong, X. Liu, Facile synthesis and capacitive characteristics of Co (OH) 2 nanoflakes via a solid-reaction route at room temperature. Mater. Lett. **65**(13), 2025–2028 (2011)
6. R. Ranjusha, S. Ramakrishna, A.S. Nair, P. Anjali, S. Vineeth, T. Sonia, N. Sivakumar, K. Subramanian, S.V. Nair, A. Balakrishnan, Fabrication and performance evaluation of button cell supercapacitors based on MnO 2 nanowire/carbon nanobead electrodes. RSC Adv. **3**(38), 17492–17499 (2013)
7. M. Zhang, D. Yang, J. Li, Supercapacitor performances of MnO2 and MnO2/reduced graphene oxide prepared with various electrodeposition time. Vacuum **178**, 109455 (2020)
8. G. Wang, L. Zhang, J. Zhang, A review of electrode materials for electrochemical supercapacitors. Chem. Soc. Rev. **41**(2), 797–828 (2012)
9. P.J. Hall, M. Mirzaeian, S.I. Fletcher, F.B. Sillars, A.J. Rennie, G.O. Shitta-Bey, G. Wilson, A. Cruden, R. Carter, Energy storage in electrochemical capacitors: designing functional materials to improve performance. Energy Environ. Sci. **3**(9), 1238–1251 (2010)
10. G. Ma, M. Dong, K. Sun, E. Feng, H. Peng, Z. Lei, A redox mediator doped gel polymer as an electrolyte and separator for a high performance solid state supercapacitor. J. Mater. Chem. A **3**(7), 4035–4041 (2015)
11. S. Senthilkumar, R.K. Selvan, J. Melo, Redox additive/active electrolytes: a novel approach to enhance the performance of supercapacitors. J. Mater. Chem. A **1**(40), 12386–12394 (2013)
12. B. Akinwolemiwa, C. Peng, G.Z. Chen, Redox electrolytes in supercapacitors. J. Electrochem. Soc. **162**(5), A5054 (2015)
13. D. Qu, H. Shi, Studies of activated carbons used in double-layer capacitors. J. Power Sources **74**(1), 99–107 (1998)
14. J. Gamby, P. Taberna, P. Simon, J. Fauvarque, M. Chesneau, Studies and characterisations of various activated carbons used for carbon/carbon supercapacitors. J. Power Sources **101**(1), 109–116 (2001)

15. G. Lota, K. Fic, E. Frackowiak, Alkali metal iodide/carbon interface as a source of pseudocapacitance. Electrochem. Commun. **13**(1), 38–41 (2011)
16. I. Tanahashi, Capacitance enhancement of activated carbon fiber cloth electrodes in electrochemical capacitors with a mixed aqueous solution of H2SO4 and AgNO3. Electrochem. Solid State Lett. **8**(12), A627 (2005)
17. Q. Li, K. Li, C. Sun, Y. Li, An investigation of Cu2+ and Fe2+ ions as active materials for electrochemical redox supercapacitors. J. Electroanal. Chem. **611**(1–2), 43–50 (2007)
18. S. Senthilkumar, R.K. Selvan, N. Ponpandian, J. Melo, Y. Lee, Improved performance of electric double layer capacitor using redox additive (VO 2+/VO 2+) aqueous electrolyte. J. Mater. Chem. A **1**(27), 7913–7919 (2013)
19. W. Li, J. Liu, C. Yan, Reduced graphene oxide with tunable C/O ratio and its activity towards vanadium redox pairs for an all vanadium redox flow battery. Carbon **55**, 313–320 (2013)
20. W. Li, J. Liu, C. Yan, Multi-walled carbon nanotubes used as an electrode reaction catalyst for VO2+/VO2+ for a vanadium redox flow battery. Carbon **49**(11), 3463–3470 (2011)
21. L.-H. Su, X.-G. Zhang, C.-H. Mi, B. Gao, Y. Liu, Improvement of the capacitive performances for Co–Al layered double hydroxide by adding hexacyanoferrate into the electrolyte. Phys. Chem. Chem. Phys. **11**(13), 2195–2202 (2009)
22. S. Maiti, A. Pramanik, S. Mahanty, Interconnected network of MnO2 nanowires with a "cocoon-like" morphology: redox couple-mediated performance enhancement in symmetric aqueous supercapacitor. ACS Appl. Mater. Interfaces **6**(13), 10754–10762 (2014)
23. C. Zhao, W. Zheng, X. Wang, H. Zhang, X. Cui, H. Wang, Ultrahigh capacitive performance from both Co (OH) 2/graphene electrode and K 3 Fe (CN) 6 electrolyte. Sci. Rep. **3**(1), 1–6 (2013)
24. Y. Zhao, Y. Ding, Y. Li, L. Peng, H.R. Byon, J.B. Goodenough, G. Yu, A chemistry and material perspective on lithium redox flow batteries towards high-density electrical energy storage. Chem. Soc. Rev. **44**(22), 7968–7996 (2015)
25. Y. Zhao, Y. Ding, J. Song, L. Peng, J.B. Goodenough, G. Yu, A reversible Br 2/Br− redox couple in the aqueous phase as a high-performance catholyte for alkali-ion batteries. Energy Environ. Sci. **7**(6), 1990–1995 (2014)
26. G. Lota, E. Frackowiak, Striking capacitance of carbon/iodide interface. Electrochem. Commun. **11**(1), 87–90 (2009)
27. X. Tang, Y.H. Lui, B. Chen, S. Hu, Functionalized carbon nanotube based hybrid electrochemical capacitors using neutral bromide redox-active electrolyte for enhancing energy density. J. Power Sources **352**, 118–126 (2017)
28. J. Park, B. Kim, Y.-E. Yoo, H. Chung, W. Kim, Energy-density enhancement of carbon-nanotube-based supercapacitors with redox couple in organic electrolyte. ACS Appl. Mater. Interfaces **6**(22), 19499–19503 (2014)
29. H. Yu, J. Wu, L. Fan, S. Hao, J. Lin, M. Huang, An efficient redox-mediated organic electrolyte for high-energy supercapacitor. J. Power Sources **248**, 1123–1126 (2014)
30. S. Roldán, C. Blanco, M. Granda, R. Menéndez, R. Santamaría, Towards a further generation of high-energy carbon-based capacitors by using redox-active electrolytes. Angew. Chem. Int. Ed. **50**(7), 1699–1701 (2011)
31. W. Chen, R. Rakhi, H.N. Alshareef, Capacitance enhancement of polyaniline coated curved-graphene supercapacitors in a redox-active electrolyte. Nanoscale **5**(10), 4134–4138 (2013)
32. D. Gastol, J. Walkowiak, K. Fic, E. Frackowiak, Enhancement of the carbon electrode capacitance by brominated hydroquinones. J. Power Sources **326**, 587–594 (2016)
33. J. Wu, H. Yu, L. Fan, G. Luo, J. Lin, M. Huang, A simple and high-effective electrolyte mediated with p-phenylenediamine for supercapacitor. J. Mater. Chem. **22**(36), 19025–19030 (2012)
34. S. Roldán, Z. González, C. Blanco, M. Granda, R. Menéndez, R. Santamaría, Redox-active electrolyte for carbon nanotube-based electric double layer capacitors. Electrochim. Acta **56**(9), 3401–3405 (2011)
35. H. Yu, L. Fan, J. Wu, Y. Lin, M. Huang, J. Lin, Z. Lan, Redox-active alkaline electrolyte for carbon-based supercapacitor with pseudocapacitive performance and excellent cyclability. RSC Adv. **2**(17), 6736–6740 (2012)

36. P.F. Ortega, F.G. de Paula, M.C. de Castro, I. Binatti, Z. González, C. Blanco, R. Santamaría, R.L. Lavall, Mechanism and stability of a redox supercapacitor based on methylene blue: effects of degradation of the redox shuttle. ACS Appl. Energy Mater. **1**(5), 2306–2316 (2018)
37. M. Skunik-Nuckowska, K. Węgrzyn, S. Dyjak, N.H. Wisińska, P.J. Kulesza, Polyoxometalate/hydroquinone dual redox electrolyte for hybrid energy storage systems. Energy Storage Mater. **21**, 427–438 (2019)
38. E. Frackowiak, K. Fic, M. Meller, G. Lota, Cover Picture: Electrochemistry serving people and nature: high-energy ecocapacitors based on redox-active electrolytes (ChemSusChem 7/2012). Chemsuschem **5**(7), 1129–1129 (2012)
39. L.-Q. Fan, J. Zhong, J.-H. Wu, J.-M. Lin, Y.-F. Huang, Improving the energy density of quasi-solid-state electric double-layer capacitors by introducing redox additives into gel polymer electrolytes. J. Mater. Chem. A **2**(24), 9011–9014 (2014)
40. L. Zhang, S. Yang, J. Chang, D. Zhao, J. Wang, C. Yang, B. Cao, A review of redox electrolytes for supercapacitors. Front. Chem. **8**, 413 (2020)
41. H. Zheng, T. Zhai, M. Yu, S. Xie, C. Liang, W. Zhao, S.C.I. Wang, Z. Zhang, X. Lu, TiO 2@ C core–shell nanowires for high-performance and flexible solid-state supercapacitors. J. Mater. Chem. C **1**(2), 225–229 (2013)
42. J. Zhou, Y. Yin, A.N. Mansour, X. Zhou, Experimental studies of mediator-enhanced polymer electrolyte supercapacitors. Electrochem. Solid State Lett. **14**(3), A25 (2010)
43. H. Yu, J. Wu, L. Fan, K. Xu, X. Zhong, Y. Lin, J. Lin, Improvement of the performance for quasi-solid-state supercapacitor by using PVA–KOH–KI polymer gel electrolyte. Electrochim. Acta **56**(20), 6881–6886 (2011)
44. H. Yu, J. Wu, L. Fan, Y. Lin, K. Xu, Z. Tang, C. Cheng, S. Tang, J. Lin, M. Huang, A novel redox-mediated gel polymer electrolyte for high-performance supercapacitor. J. Power Sources **198**, 402–407 (2012)
45. S. Senthilkumar, R.K. Selvan, N. Ponpandian, J. Melo, Redox additive aqueous polymer gel electrolyte for an electric double layer capacitor. RSC Adv. **2**(24), 8937–8940 (2012)
46. M. Hashemi, M.S. Rahmanifar, M.F. El-Kady, A. Noori, M.F. Mousavi, R.B. Kaner, The use of an electrocatalytic redox electrolyte for pushing the energy density boundary of a flexible polyaniline electrode to a new limit. Nano Energy **44**, 489–498 (2018)
47. Q.-M. Tu, L.-Q. Fan, F. Pan, J.-L. Huang, Y. Gu, J.-M. Lin, M.-L. Huang, Y.-F. Huang, J.-H. Wu, Design of a novel redox-active gel polymer electrolyte with a dual-role ionic liquid for flexible supercapacitors. Electrochim. Acta **268**, 562–568 (2018)
48. E. Feng, G. Ma, K. Sun, Q. Yang, H. Peng, Z. Lei, Toughened redox-active hydrogel as flexible electrolyte and separator applying supercapacitors with superior performance. RSC Adv. **6**(79), 75896–75904 (2016)
49. K. Sun, F. Ran, G. Zhao, Y. Zhu, Y. Zheng, M. Ma, X. Zheng, G. Ma, Z. Lei, High energy density of quasi-solid-state supercapacitor based on redox-mediated gel polymer electrolyte. RSC Adv. **6**(60), 55225–55232 (2016)
50. H.S. Jang, C.J. Raj, W.-G. Lee, B.C. Kim, K.H. Yu, Enhanced supercapacitive performances of functionalized activated carbon in novel gel polymer electrolytes with ionic liquid redox-mediated poly (vinyl alcohol)/phosphoric acid. RSC Adv. **6**(79), 75376–75383 (2016)
51. S. Pan, J. Deng, G. Guan, Y. Zhang, P. Chen, J. Ren, H. Peng, A redox-active gel electrolyte for fiber-shaped supercapacitor with high area specific capacitance. J. Mater. Chem. A **3**(12), 6286–6290 (2015)
52. Y. Wang, Z. Chang, M. Qian, Z. Zhang, J. Lin, F. Huang, Enhanced specific capacitance by a new dual redox-active electrolyte in activated carbon-based supercapacitors. Carbon **143**, 300–308 (2019)
53. Y. Yin, J. Zhou, A.N. Mansour, X. Zhou, Effect of NaI/I2 mediators on properties of PEO/LiAlO2 based all-solid-state supercapacitors. J. Power Sources **196**(14), 5997–6002 (2011)
54. L. Hu, C. Shi, K. Guo, T. Zhai, H. Li, Y. Wang, Electrochemical double-layer capacitor energized by adding an ambipolar organic redox radical into the electrolyte. Angew. Chem. **57**(27), 8214–8218 (2018)

55. T. Suga, Y.-J. Pu, K. Oyaizu, H. Nishide, Electron-transfer kinetics of nitroxide radicals as an electrode-active material. Bull. Chem. Soc. Jpn. **77**(12), 2203–2204 (2004)
56. Y. Ding, G. Yu, A bio-inspired, heavy-metal-free, dual-electrolyte liquid battery towards sustainable energy storage. Angew. Chem. **128**(15), 4850–4854 (2016)
57. A. Platek, J. Piwek, K. Fic, E. Frackowiak, Ageing mechanisms in electrochemical capacitors with aqueous redox-active electrolytes. Electrochim. Acta **311**, 211–220 (2019)
58. K.A. Mauritz, R.B. Moore, State of understanding of Nafion. Chem. Rev. **104**(10), 4535–4586 (2004)

Supercapacitors: From Lab to Industry

Yi-Zhou Zhang and Wen-Yong Lai

Abstract The commercialization of supercapacitors start from the later half of the twentieth century, they have since found wide applications in transportation, utility grid, consumer electronics, flexible and wearable systems, energy harvesting, etc. Their superior high-power performance, excellent reliability and cycle life make them an important class of electrochemical energy storage devices; Accordingly, the global supercapacitor market is growing exponentially. Although the basic structure of a supercapacitor is simple, different products towards specific application calls for cells in different forms. This chapter focuses on manufacturing of supercapacitors from an industry point of view, mainly including their device structures, fabrication processes, and approaches to maximize performance while reducing cost.

Keywords Supercapacitors · Supercapacitor commercialization · Memory backup · Power supply · Electric vehicle · Module design

1 Introduction

The commercialization of supercapacitors can be traced back to 1957 when the General Electric patented a type of electrolytic capacitor based on porous carbon electrodes, i.e., the double-layer capacitor [1]. Then in 1970, the Standard Oil Company patented a disk-like capacitor based on carbon paste soaked in an electrolyte, which stored energy at the double-layer interface [2]. However, the patent was licensed to Nippon Electric Corporation (NEC) in 1971, which went on to manufacture the first

Y.-Z. Zhang · W.-Y. Lai (✉)
State Key Laboratory for Organic Electronics and Information Displays (SKLOEID), Institute of Advanced Materials (IAM), Nanjing University of Posts and Telecommunications, 9 Wenyuan Road, Nanjing 210023, China
e-mail: iamwylai@njupt.edu.cn

Y.-Z. Zhang
School of Chemistry and Materials Science, Institute of Advanced Materials and Flexible Electronics (IAMFE), Nanjing University of Information Science and Technology, Nanjing 210044, China

S. Thomas et al. (eds.), *Nanostructured Materials for Supercapacitors*,
Advances in Material Research and Technology,
https://doi.org/10.1007/978-3-030-99302-3_24

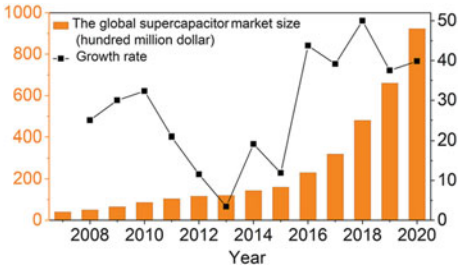

Fig. 1 The global supercapacitor market size and the corresponding growth rate (Adapted with permission from Reference [4], Copyright (2019), AIP Publishing.)

commercially successful supercapacitor. These early supercapacitors were mainly used for memory backup in consumer electronic applications. Since then, several companies represented by Panasonic started to produce supercapacitors, aiming for memory backup devices. These earlier successes drew interest towards other applications, such as in hybrid electric vehicles. Since then, the reliability and cycle life of supercapacitors has been significantly increased [3].

Nowadays, supercapacitors have gone far enough from the seminal patents in the mid-twentieth century and are widely used in applications ranging from transportation, utility grid, consumer electronics, flexible and wearable systems, energy harvesting, etc., mainly due to their superior high-power performance, excellent reliability and cycle life. Their role in shaping modern life and society has been growing continuously and exponentially. It has become one important class of electrochemical energy storage devices by itself; they are ubiquitous in our daily life and are in different forms depending on specific application scenarios. The global supercapacitor market is also rapidly growing (Fig. 1) [4]. In this chapter, we will introduce how to manufacture supercapacitors, mainly from the industry point of view, including their device structures, fabrication processes, and issues to consider when trying to maximize performance.

Although it can be assembled in different forms, the basic structure of a supercapacitor is two metal current collectors each coated with active electrode materials, separated by a separator which is a porous dielectric film. The sandwiched structure is then impregnated with an electrolyte can be an organic or aqueous solvent that contains a significant amount of ions. The basic unit can be stacked to form a flat pouch cell or rolled into a radical structure, and the size depends on the required capacitance and voltage. Presently, carbon electrodes and organic electrolytes are the standard materials choices in the industry. On the other hand, the device designs are strongly dependent on target applications and can be briefly divided into small and medium, and large cells for various applications. The steps to manufacture supercapacitors in the industry include: electrode fabrication; separator positioning; cell assembly and external connection); electrolyte impregnation; sealing of the system. The main goals of the industrialization efforts of supercapacitor manufacturing are to improve the device performance: increase the energy/power density, decrease the equivalent series resistance (ESR), and increase the robustness and cycle life of the whole cell, while reducing costs.

The application of supercapacitors can be mainly divided into two parts: (1) High-capacitance supercapacitors which are used in transport, uninterruptible power supply (UPS), lifts, etc. For these applications, supercapacitors are assembled into modules and are generally connected to an electric balancing circuit. (2) Low-capacitance supercapacitors which are used in various electronic applications, such as backup and voltage stabilization. In these applications, supercapacitors are generally in the same dimension as other electronic components such as electrolytic capacitors and dielectric capacitors, are often directly welded into the circuit board.

2 Components

2.1 Electrodes

2.1.1 Current Collector

In most commercial supercapacitors, it is necessary to deposit active materials on a metallic current collector to achieve low resistance, except for a few designs where self-supported electrodes are used without using a current collector, such as when conductive carbon cloth is used as a self-supportive electrode. In the latter case, the ESR is often too high to be efficient for obtaining a high power density. However, when considering making flexible supercapacitors, the self- supportive-electrode approach can be preferred.

The current collector connects the electrode with the outside circuit. The detachment of active material from current collector largely accounts for the increase of ESR during cycling. Optimizing the electrode material's mechanical and chemical adhesion on the current collector is an essential issue in commercial supercapacitors. Coating an activated carbon-containing aqueous or organic slurry on the current collector is the most widely adopted approach in the industry. It is also possible to directly laminate activated carbon on the current collector [5]. This method is not suitable for fabricating thick electrodes. To improve adhesion, the surface groups of activated carbon can be utilized through chemical reactions [6]. Adhesion can also be improved using physical means; for instance, plasma has been used to enhance adhesion between activated carbon and aluminum current collector [7].

The criteria for choosing a current collector include stability in the electrolyte, cost, density, and processability. First and foremost, it is critical to choose suitable current collectors depending on the target electrolytes. The most common current collector in an organic electrolyte is aluminum. It possesses low price, low density, and high electrochemical stability in common organic electrolytes. Moreover, its surface can be specially treated to increase the adhesion between itself and the active material. There are two primary forms of Al for such application: (1) Standard aluminum foil, which is low cost. However, excellent adhesion between the active material and current collector is difficult to maintain using conventional binders

such as PVDF (polyvinylidene fluoride) or PTFE (polytetrafluoroethylene). Special binders such as acetamides are often used. (2) Etched aluminum. Al can be electrochemically corroded, resulting in the so-called etched aluminum [8], which helps increase both the adhesion and porosity of the electrode. The aluminum current collector is not suitable for aqueous supercapacitors because of the usage of strong acids and bases [9]. Instead, they use nickel and stainless steel as current collectors [10]. Unavoidably, they are more costly and heavier than Al. Their ESR can be decreased by increasing the roughness of the foil and by shaping the collector into grids and introducing an underlayer.

2.1.2 Activated Carbons

Since the invention of supercapacitors, activated carbons have been the main active electrode material of commercial supercapacitors. It is thus a perfect example to show how to increase device performances through modifying materials. The early activated carbons have low pore density. Soon after, it became common knowledge that the ion-accessible surface needs to be increased to increase the capacitance. The first commercial activated carbons for supercapacitors were manufactured from the sugar industry. Thus, these carbons suffer from low purity, untuned particle size distribution, high surface functional group content, and low lifetime. Since then, researchers have tried activated carbons from different sources, trying to overcome these undesirable features. Common knowledge is that only ~20% of porosity is genuinely accessible to the ions, thus contributing to energy storage [11–13]. Many researchers focused on tuning porosity to increase the ion-accessible pore structures [14–16].

Carbon Sources

There are mainly two ways to categorize activated carbons, namely, the activation method and precursors [17]. However, it is worth mentioning that although many activated carbons have been developed in the laboratory, to upscale to the industrially relevant level is another story [18].

Supercapacitor manufacturers have used many activated carbons due to their balanced cost and performance. As shown in Fig. 2, some commercially successful carbon sources have been explored, include wood [19–21], coconuts [22], petroleum-residue [23], and carbohydrates [24, 25].

Pore sizes

Because of the energy storage mechanism, it is natural to think that the gravimetric or volumetric capacity is in proportion to the BET surface area of the carbon, which is in turn determined by the available pore volume for absorbing nitrogen molecules. However, in practice, the capacitance in neither aqueous nor organic electrolytes is proportional to the N_2 BET surface area. This is understandable because the stored ion sizes in supercapacitors are larger than the nitrogen molecule.

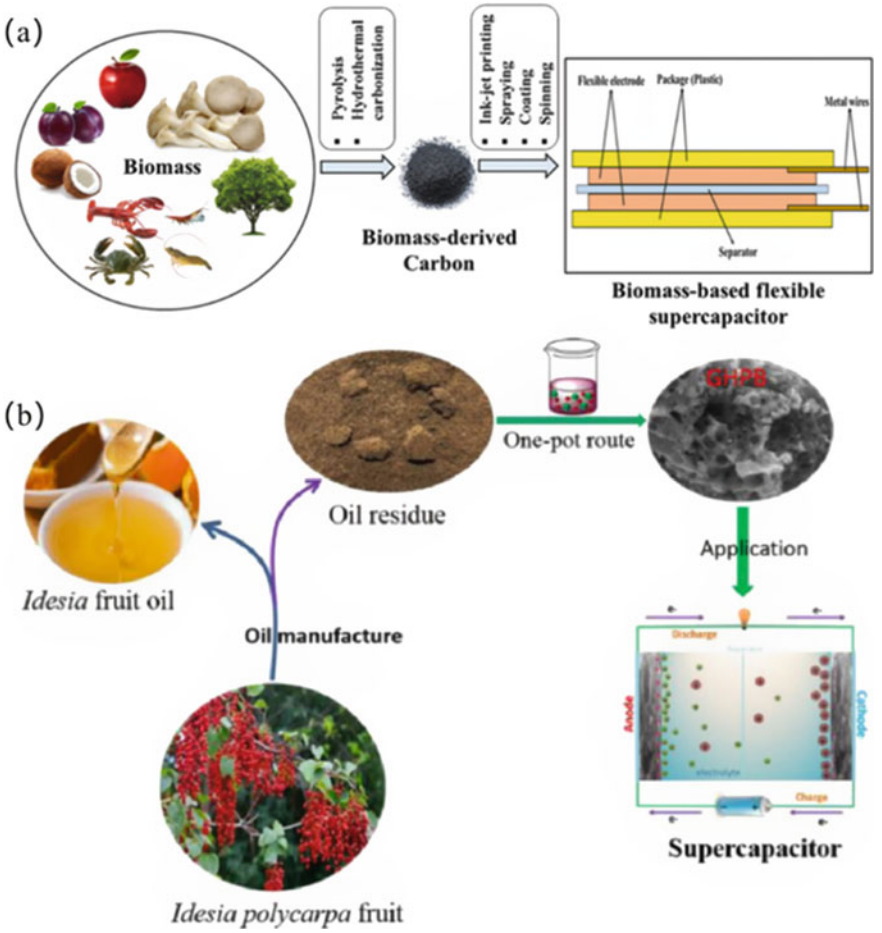

Fig. 2 Graphical representation of supercapacitor fabrication from **a** biomass (Adapted with permission from Reference [21], Copyright (2020), Springer Nature) and **b** oil residue (Adapted with permission from Reference [23], Copyright (2021), Elsevier)

There are many industrial recommendations on the pore size distribution of activated carbons for organic supercapacitors. For example, the macropore and micropore volumes should be controlled to be less than 10% and close to 50% of the total pore volume [26]; Although there is no proportionality between capacitance in organic media and BET surface area; an optimum pore size distribution can be found according to different ion sizes within electrolytes (Fig. 3) [27–29, 31].

Particle Size Distribution

Apart from pore size distribution, particle size distribution also strongly impacts performance [31]. In one representative study, a medium particle size of 4–8 μm is

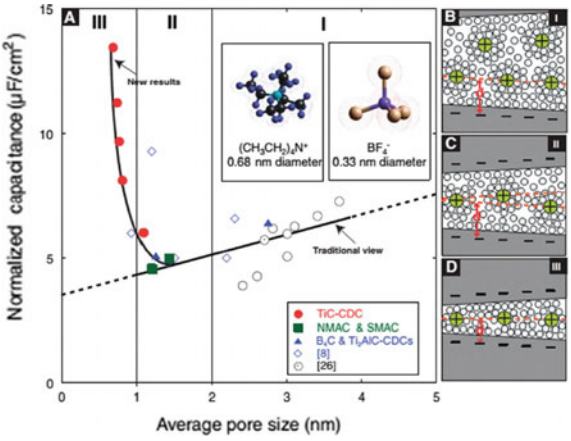

Fig. 3 **a** Plot of specific capacitance normalized by BET SSA and average pore size carbons; drawings of solvated ions residing in pores with the distance between adjacent pore walls: **b** greater than 2 nm, **c** between 1 and 2 nm, and **d** less than 1 nm, to illustrate distinguishing behavior schematically. (Adapted with permission from Reference [27], Copyright (2006), American Association for the Advancement of Science.)

needed to obtain polarizable EDLC electrodes, which helps increase the capacitance [32].

Surface Functional Group

The impact of surface groups on supercapacitor performances can be two-fold. They can impact the major performance parameters such as capacitance, resistance, operation voltage window, self-discharge, etc. First of all, surface groups can lead to redox reactions that contribute reversible pseudocapacitance [33–35], therefore adding to the total capacitance in both aqueous [36] and organic electrolytes [37]. However, residual oxygen can increase the resistance of the electrode [38–40]. Moreover, the acid functional groups are harmful in aqueous media because they facilitate gas release at low potential [41], and significantly reduce the lifetime of devices [42]. Even in organic systems, the oxygen-containing functional groups can reduce capacitance and reduce the operating voltage window of the device [43]. Therefore, in organic media, oxygen-poor carbons are generally preferred. Moreover, the amount of surface functional groups can also impact the self-discharge of supercapacitors [44].

Although the functional groups of carbon can significantly impact the performance in organic and aqueous electrolytes in complex ways, in general, oxidation of activated carbon could lead to increased capacitance while bringing about the aging problem. There are many proven surface modification methods to treat carbons, including acid treatment [45, 46], oxidizing [47–49], electrochemical [50], thermal [51], plasma [53, 54], laser [52], polishing [55], etc. However, it is worth noting that activated carbon manufacturers have a strict amount when doing such modifications to limit the aging issue of supercapacitors.

2.1.3 Binders

A binder in supercapacitors has two primary functions: connecting particles and increasing the adhesion of electrode on the current collector, which decreases the ESR and limits capacitance decrease [56]. However, the binder content must be low in the electrode mainly because most binders are insulating, high content of which can increase the ESR. As nonactive material, higher binder content can also decrease gravimetric capacitance. Moreover, the wettability of electrolytes on carbon can also increase adhesion between carbon and binder [57, 58]. PTFE (Polytetrafluoroethylene) is a popular binder in the supercapacitor industry because of its high electrochemical stability and processability in aqueous media [59]. A typical weight content is 3 and 5%. In one seminal patent [60], PTFE-carbon mixture was coated on a current collector to fabricate an EDLC device. Also popular is PVDF [61] that are dispersed in an organic solvent such as N-Methyl-2-pyrrolidone (NMP) and Dimethyl sulfoxide (DMSO), and THF (tetrahydrofuran). Other popular binders include water-soluble polymers such as PVA (polyvinyl alcohol) and CMC (carboxymethylcellulose) [62]. However, they cannot work at high voltage due to the tendency to degrade. Thus chemical modification of these binders are often necessary [63]. Another important binder is polyimide, which is particularly useful for high temperature applications.

2.1.4 Conductive Additives

A conductive additive is needed to increase the electrical conductivity of the electrode and to reduce the ESR. In 1972, carbon black was first proposed to be added to improve the conductivity of the EDLC carbon electrode [64]. This patent is the earliest of its kind to use conductive additives in the electrode formulation. Many conductive additives have since been developed, mainly including carbon black, acetylene black, Ketjenblack, carbon fibers, carbon nanotubes (CNTs), graphite, metallic fibers and particles, etc. The particle size of these conductive additives also has influence on the electrode resistance [65]. So far, manufacturers mainly use carbon blacks because of their good overall performance including electrical conductivity, purity, cost, stability, lightweight, and processability. Carbon blacks are composed of largely spherical particles with a diameter range of dozens of nm, and could form aggregates of hundreds of nm. The aggregates can then form a compact 3D conductive network. The microstructure of carbon blacks resembles that of graphite. Two types of carbon black, i.e., Ketjenblack and acetylene black, are often preferred due to their significant mesoporosity [66, 67].

2.2 Electrolyte

The electrochemical stability window of the electrolyte thus has a heavy influence on the performance of supercapacitors. Moreover, electrolytes can also influence the ESR and capacitance [70]. Critical parameters of an electrolyte include conductivity, electrochemical Stability, thermal Stability, toxicity, etc. The conductivity of an electrolyte is determined by the ion concentration, ion mobility, solvent or solvent mixtures, and temperature. The choice of salt in the electrolyte is the first important step to obtain high conductivity. The tetraalkylammonium ions are commonly used in industrial supercapacitors due to their good solubility and conductivity. These cations have shallow reduction potential, which leads to high stability. Many have studied have found out tetraalkylammonium ions can be reduced on various electrodes [69–71]. The cation RN_4^+ is often reduced to alkanes, alkenes, and trialkylamines. Common anions are BF_4^-, ClO_4^-, PF_6^-, and $SO_3CF_3^-$. The most popular ions are Et_4NBF_4 (tetraethylammonium tetrafluoroborate, $TEABF_4$) and Et_3MeNBF_4 (triethylmethylammonium tetrafluoroborate, $TEMABF_4$). Given the high conductivity in ACN compared to other solvents [72], the use of Et_4NBF_4 in ACN has rapidly become popular. However, some companies replace ACN with PC based on an environmental concern. However, the lifetime of supercapacitors based on PC is typically lower than that of ACN [73].

Regarding salt concentration, Zheng et al. [74] found that the salt concentration in can directly influence the operation voltage of supercapacitors. An example from industry shows that a capacitance of 166 F g^{-1} is raised from 103 F g^{-1} when the ratio of Et_4NBF_4 in ACN is increased from 0.1 to 1.4 M [75]. A compromise often needs to be made in the industry setting, as the electrolyte price, especially the salt, is a major part of the whole unit. Therefore, 1 M of $TEABF_4$ in CAN or PC is adopted by most companies. When choosing solvent, things to consider mainly include responsiveness to the electrode's electroactive species, its dielectric constant and its polarizability, and its stable electrochemical window. Combining these requirements, common industrial solvents in supercapacitors mainly include EC (ethylene carbonate), PC, DME (dimethoxyethane), THF (Tetrahydrofuran), ACN, DMF (Dimethylformamide), etc. The electrochemical stability of a solvent is a vital issue for industrialization and is strongly linked to impurities and to the cathodic or anodic potential [76]. Particularly, oxygen and trace water can be very harmful to many organic electrochemical systems [77]. Thus, supercapacitor solvent in the industry must have wider electrochemical potentials than the potential window of the device and very high impurity.

Electrolyte degradation

Even a pure electrolyte with high stability can still degrade through interacting with other supercapacitor components. One of the most important degradation approaches is with the trace water and surface functional groups (especially acidic ones [78]) from the activated carbon, mainly when the supercapacitor voltage is higher than

2.3 V [79]. Gasses are generated from the degradation reactions, which block pores in activated carbon and separator, and increase the ESR [80].

Gasses of propene, CO, CO_2, and hydrogen were detected up to a voltage of 2.6 V when a PC electrolyte (1 M $TEABF_4$/PC)-based supercapacitor was analyzed [81]. Similar findings were reported later by other groups and companies [82]. These studies into the degradation mechanisms of electrolytes indicate a potential failure mode of supercapacitors, i.e., the building of pressure due to the continuous production of gases. Therefore, an organic supercapacitor must be mechanically robust to resist increased inner pressure and prevent leaking. The main patented solutions are the following: gas evacuation from the inside of the device through valves [83] and membranes [84]; condense gas within the component [85]; reinforce the supercapacitor with increased thickness of cover and can; open the device via a membrane or a venting [86]; decrease the gas amount generated using chemicals [87].

Thermal stability

One significant advantage of supercapacitors is their wide working temperature range (at least −30 to 70 °C). Therefore, it is essential to keep the conductivity of different electrolytes at extreme temperatures in mind when designing cells. There are various approaches to increase conductivity at extreme temperatures. For instance, PC-based electrolytes' temperature range and conductivity can be improved by adding fluorobenzene [88] or using $EMPyrBF_4$ (ethyl methyl pyrrolidinium tetrafluoroborate) salt. A special thermal control unit can also be used to ensure the smooth operation of supercapacitors at deep space temperatures [89].

Since commercial cells mostly use high-freezing-point solvents such as PC and CAN, the main challenge is to design electrolyte mixture with low melting points and sufficient ionic conductivity while minimizing the ESR increase at lower temperatures. By adding another solvent, a wider temperature range than ACN can be obtained [90]. At high temperatures, high-power applications require high conductivity, however, high temperature also brings about accelerated aging. In practice, ACN can be used up to 80 °C, Above this temperature, PC-based electrolytes can be used, but aging can be quite serious. Other feasible solvents at high temperatures include sulfolane or EC. If an even wider temperature range is needed, ionic liquids can be used.

Non-traditional Electrolytes

A traditional solvent such as ACN has a low flash point and is toxic. Therefore, most supercapacitor manufacturers need to design cells so as to avoid electrolyte leakage. Also, the electrolyte quantity is limited in cells to avoid liquid leakage. Still ACN is still unaccepted in some countries given the strict environmental constraints. To improve PC-based supercapacitor performance is a viable option, however, it is still hard to find alternatives to ACN in terms of the combination of conductivity, thermal Stability, and electrochemical Stability [91]. However, the low flash point issue can be partially overcome by adding flame retardants [92].

Solvents can be removed altogether by using pure ionic liquids as electrolytes for supercapacitors [93]. Being solvent-free, stable over wide temperature ranges,

and non-flammable, ionic liquids seem ideal candidates, except for the relatively low conductivity [94]. Moreover, their purification is difficult [95], which, as discussed above, may compromise the lifetime of supercapacitors. This feature also results in the high price of ionic liquids, making them unsuitable for industry, except for some niche applications such as at high temperatures [96] and high voltage. There are already products that are commercially available based on DEME-BF_4, that have shown better performance than PC-based electrolytes [97].

2.3 Separator

Separators are used to separate the two electrodes from contacting each other while allowing ions to pass through. Correspondingly, their requirements include high stability (electrochemical, thermal, and chemical), high porosity, low thickness (as thin as possible but not too thin for the carbon particles to cause shortening between two electrodes), and low cost. Paper made from cellulose fibers is routinely used as supercapacitor separators. They are made from high-purity cellulose fibers (Fig. 4a), with a thickness of 15–50 μm and a low density of less than 0.85. Strong drying by thermal outgassing or acetone washing is needed to rid such separators of any water contamination in supercapacitors [98, 99].

However, these paper separators have one important drawback: when exposed to a high voltage of over 3 V, oxidative deterioration happens, leading to a significant decrease in strength and even destruction of the paper [100]. However, such voltage is often reached or approached in practice, and researchers are working on increasing the working voltage to maximize energy density and power density. Thus polymeric separators have been developed in the industry [101]; some typical examples include: Glass fiber-based separators [102, 103]; porous polypropylene films [104–106] (Fig. 4b); multilayer separator [107], with the second layer of electrospun ultrafine fibers deposited on one standard polymeric separator, such structure can help reduce short circuits between electrodes; separators based on thermoplastic

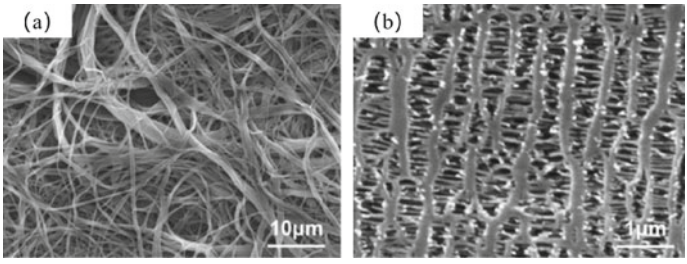

Fig. 4 SEM images of the surface of different separators. **a** Cellulose. **b** Porous polypropylene. (Adapted with permission from Reference [99], Copyright (2021), Springer Nature.)

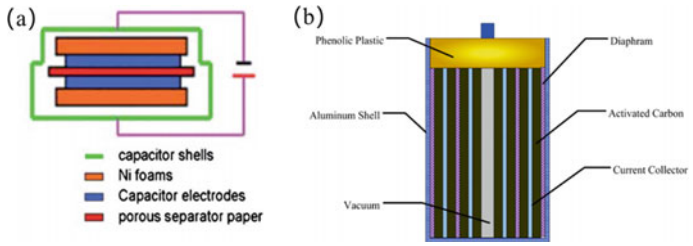

Fig. 5 **a** Coin-type cell construction (Adapted with permission from Reference [110], Copyright (2011), The Royal Society of Chemistry.) and **b** wound-type cell construction. (Adapted with permission from Reference [111], Copyright (2015), PLOS.)

resin and pulp fibers [108, 109], which have excellent mechanical strength, ion, and liquid permeability, yet also high price; PTFE- and polyimide-based based separators.

3 Cell Design and Assembly

According to applications, small supercapacitors (coin type) and large ones (hundreds of F) have different architectures.

3.1 Small-Size Supercapacitors

These refer to welded components for electronic applications, such as energy storage units for wireless communication sensors, actuators, and toys, backup power for memory boards, power management for laptop computers, a power system for portable and mobile applications such as LED flashes. Cells for these applications typically have less than 1 F capacitance. These supercapacitors can have two appearances [110, 111]: Coin cells (Fig. 5a) and Wound cells (Fig. 5b).

3.2 Large Cells

Large cell structure and construction are less standardized than their small-size counterparts: each manufacturer uses its own designs. But generally, there are two forms: the high-power cells, for use in electric vehicles; and energy cells for stationary applications such as uninterrupted power supply (UPS).

Fig. 6 Pouch cells from GTCAP (**a** 6000 F, 4.0 V, **b** 2000 F, 4.0 V)

3.2.1 High-Power Cells

The high-power requirements call for low ESR, thus cell design is relatively simple. Main designs include wound cell and bipolar design. The spiral wound cell roll electrodes with the huge surface area into a small case. The large electrode area can significantly reduce the capacitor's internal resistance, and the case greatly simplifies the capacitor sealing. In a spiral wound design, only the outside components require sealing. On contrary, each cell needs sealing around the electrodes in the bipolar design. However, in a wound design, only the outer can require sealing. Because of targeted heavy-duty applications, high reliability is emphasized, i.e., these cells must resist high pressure and remain fully sealed. The cover and can commonly use aluminum.

3.2.2 Energy Cells

The assembly of these energy cells is inspired by electrolytic capacitors. Because of the emphasis on energy density, the ESR of this type of cell is higher. Typically, they are based on PC electrolytes, and the electrode thickness is generally higher than power-type cells to increase energy density.

Pouch cell designs are commonly adopted for EDLC energy cells. This design, like in Li-ion cell phones, enables high energy density and easy flat-mode integration in applications such as cell phones (GTCAP, Fig. 6) and electronics. However, due to the light packing, these cells cannot resist mechanical shocks, they are sensitive to heat, gas, and water thus has limited long-term utility.

4 Module Design

Supercapacitor modules are needed for specific applications where high voltage and high power output are needed. By combining several units in series, higher voltages and energy density can be achieved. Such application often calls for high individual voltage. In a supercapacitor module, only unit cells contain active materials. Thus, the energy/power densities of the module are always lower than unit cell values. Manufacturers tend to design their modules with minimized passive materials versus

the cells while considering safety, environmental, and aging performances. Geometry can also be an important design factor. The passive components within a module are detailed as follows.

4.1 Metallic Interconnects Between Cells

It is often necessary to connect unit cells to increase the voltage (connected in series) or capacitance (connected in parallel). When designing interconnects, the cell geometry and terminal positioning on the cells must be taken into consideration. For example, flat interconnect strips can be used if cell terminals are flat [112]; while rolled or tubular modules call for more complex strip geometries [113]. The connection between the cells and the interconnect strip can be achieved by welding [114], brazed [115], screwed [116], etc. Meanwhile, the connecting strips also help thermal dissipation of the module.

4.2 Electric Terminal for Module

The connection between terminals of the first and last cells must have low resistance to constrain heat generation. One common approach is to weld the module terminals directly on the first and the last cell of the module [117].

4.3 Insulator for Module

Many commercial insulating materials can be readily used. For instance, Polyimide and PTFE can be used for small thickness scenarios. Interestingly, one of the useful insulator materials is an elastomer filled with carbon black. The elastomer layer fulfills several functions simultaneously [118]. Apart from insulation, it can also absorb shock through compression and promote heat exchange between the module and the environment.

4.4 Cell Balancing

To obtain high module durability and safety, thermal modeling of the supercapacitor cell is important, to ensure the supercapacitor module is within a suitable temperature range [119, 120]. Voltage balancing between cells to a cell is needed to distribute stored charges across cells evenly. Moreover, since cell capacitance, series resistance, and self-discharge cannot be fully equal because of variations in processing and aging

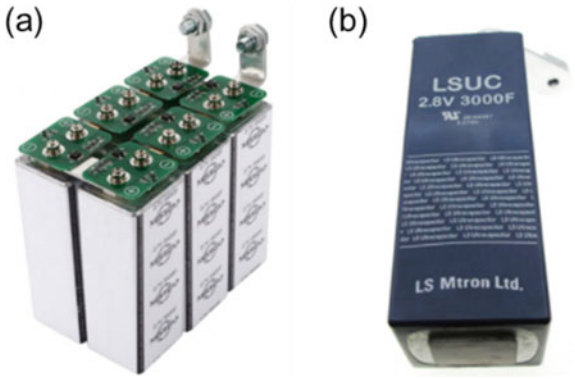

Fig. 7 Module enclosure of **a** Jiashengtai electronics (16 **V**/500 F), and **b** LSUC (3000 F/2.8 V)

[121], in the absence of balancing electronics, cell overvoltage could lead to a risk of cell overvoltage to excessive aging. Voltage balancing can be achieved by driving a bypass current in/out of cells when the voltage passes beyond a threshold voltage. To enhance the balancing effect, one balancing circuit per cell can be connected in series into a balancing system.

4.5 Module Enclosure

Figure 7 shows some aluminum encloses various modules. Such enclosure also enables simple cooling through air ventilation. Although such a heavy enclosure significantly lowers the gravimetric energy/power densities of the modules, security is of paramount importance for urban transport applications.

5 Summary

There are mainly two families of commercial supercapacitors, i.e., the small cells that have are mature for years and are widely used in mobile applications, consumer electronics, toys, backup, etc.; and large cells that are based on low-cost materials to be competitive for new markets such as automotive and grid utility. Besides cost, innovative ways of using supercapacitors in new applications also drive the industry development of supercapacitors. For instance, energy density is important in electric vehicle application besides the traditional advantages of long cycle life and high power density. New issues and designs are necessary to meet this new demand. Specifically, in a conventional symmetric supercapacitor, the energy density can be increased by increasing the operating voltage. To do so, one can change the capacitance ratio of two electrodes; match the electrolyte ion sizes to the electrode; match the pore size distribution of electrodes to the electrolyte ions by changing electrolyte

conditions. Lastly, cell and module designs are critical issues for successfully taking the supercapacitor from lab to industry.

References

1. H.E. Becker, Low voltage electrolytic capacitor. US2800616 for General Electric (1957)
2. D.I. Boos, Electrolytic capacitor having carbon paste electrodes. US3536963 for Standard Oil Co. (1970)
3. W. Raza, F. Ali, N. Raza, Y. Luo, K.H. Kim, J. Yang, S. Kumar, A. Mehmood, E.E. Kwon, Recent advancements in supercapacitor technology. Nano Energ. **52**, 441–473 (2018)
4. S. Huang, X. Zhu, S. Sarkar, Y. Zhao, Challenges and opportunities for supercapacitors. APL Mater. **7**, 100901 (2019)
5. C. Portet, P.L. Taberna, P. Simon, E. Flahaut, Modification of Al current collector/active material interface for power improvement of electrochemical capacitor electrodes. J. Electrochem. Soc. **153**(4), A649 (2006)
6. K. Babel, K. Jurewicz, KOH activated carbon fabrics as supercapacitor material. J. Phys. Chem. Solids **65**(2), 275–280 (2004)
7. E. Adhamash, R. Pathak, K. Chen, M.T. Rahman, A. El-Magrous, Z. Gu, S. Lu, Q. Qiao, Y. Zhou, High-energy plasma activation of renewable carbon for enhanced capacitive performance of supercapacitor electrode. Electrochim. Acta **362**, 137148 (2020)
8. R.S. Kühnel, A. Balducci, Comparison of the anodic behavior of aluminum current collectors in imide-based ionic liquids and consequences on the stability of high voltage supercapacitors. J. Power Sour. **249**, 163–171 (2014)
9. R.E. Isley, Manufacturing of industrial supercapacitors. US3656027 for Stan- dard Oil Co. (1972)
10. N.A. Salleh, S. Kheawhom, A.A. Mohamad, Characterizations of nickel mesh and nickel foam current collectors for supercapacitor application. Arab. J. Chem. **13**(8), 6838–6846 (2020)
11. D. Qu, H. Shi, Studies of activated carbons used in double-layer capacitors. J. Power. Sour. **74**, 99–107 (1998)
12. W.G. Pell, B.E. Conway, N. Marincic, Analysis of non-uniform charge/discharge and rate effects in porous carbon capacitors containing sub-optimal electrolyte concentrations. J. Electroanal. Chem. **491**, 9–21 (2000)
13. C. Vix-Guterl, E. Frackowiak, K. Jurewicz, M. Friebe, J. Parmentier, F. Béguin, Electrochemical energy storage in ordered porous carbon materials. Carbon **43**, 1293–1302 (2005)
14. J. Zhao, Y. Jiang, H. Fan, M. Liu, O. Zhuo, X. Wang, Q. Wang, L. Yang, Y. Wang, Z. Hu, Porous 3D few-layer graphene-like carbon for ultrahigh-power supercapacitors with well-defined structure–performance relationship. Adv. Mater. **29**(11), 1604569 (2017)
15. K. Xie, X. Qin, X. Wang, Y. Wang, H. Tao, Q. Wu, Z. Hu, Carbon nanocages as supercapacitor electrode materials. Adv. Mater. **24**(3), 347–352 (2012)
16. J. Zhao, H. Lai, Z. Lyu, Y. Jiang, K. Xie, X. Wang, Z. Hu, Hydrophilic hierarchical nitrogen-doped carbon nanocages for ultrahigh supercapacitive performance. Adv. Mater. **27**(23), 3541–3545 (2015)
17. M.M. Johns, W.E. Marshall, C.A. Toles, The effect of activation method on the properties of pecan shell-activated carbons. J. Chem. Technol. Biotechnol. Int. Res. Process Environ. Clean Technol. **74**(11), 1037–1044 (1999)
18. V.V.N. Obreja, On the performance of supercapacitors with electrodes based on carbon nanotubes and carbon activated material—a review. Physica E **40**, 2596–2605 (2008)
19. H. Benaddi, T.J. Bandosz, J. Jagiello, J.A. Schwarz, J.N. Rouzaud, D. Legras, F. Béguin, Surface functionality and porosity of activated carbons obtained from chemical activation of wood. Carbon **38**(5), 669–674 (2000)

20. S. Yorgun, N. Vural, H. Demiral, Preparation of high-surface area activated carbons from Paulownia wood by $ZnCl_2$ activation. Microporous Mesoporous Mater. **122**(1–3), 189–194 (2009)
21. N. Bora, R. Narzari, N. Bhuyan, R. Kataki, *Bioenergy-byproducts based electrodes for flexible supercapacitors in biorefineries: a step towards renewable and clean energy* (Springer, Singapore, 2020), pp. 437–464
22. K. Yang, J. Peng, C. Srinivasakannan, L. Zhang, H. Xia, X. Duan, Preparation of high surface area activated carbon from coconut shells using microwave heating. Bioresour. Technol. **101**(15), 6163–6169 (2010)
23. S. Yao, Z. Zhang, Y. Wang, Z. Liu, Z. Li, Simple one-pot strategy for converting biowaste into valuable graphitized hierarchically porous biochar for high-efficiency capacitive storage. J. Energ. Storage **44**, 103259 (2021)
24. S. Sharma, S.E. Chun, Electrochemical immunoassay based on indium tin oxide activity toward a alkaline phosphatase. J. Electrochem. Sci. Technol. **10**(4), 387–393 (2019)
25. J. Han, K. Lee, M.S. Choi, H.S. Park, W. Kim, K.C. Roh, Chlorella-derived activated carbon with hierarchical pore structure for energy storage materials and adsorbents. Carbon Lett. **29**(2), 167–175 (2019)
26. K. Murakami, Y. Mogi, K. Tabayashi, T. Shimoyama, K. Yamada, Y. Shinozaki, Carbonaceous material, its production process and electric double layer capacitor employing it. EP1049116 for Asahi Glass Co, Adchemco Corp and JFE Chemical (2000)
27. J. Chmiola, G. Yushin, Y. Gogotsi, C. Portet, P. Simon, P.-L. Taberna, Anomalous increase in carbon capacitance at pore sizes less than 1 nanometer. Science **313**, 1760–1763 (2006)
28. C. Largeot, C. Portet, J. Chmiola, P.-L. Taberna, Y. Gogotsi, P. Simon, Relation between the ion size and pore size for an electric double-layer capacitor. J. Am. Chem. Soc. **130**, 2730–2731 (2008)
29. C. Vix-Guterl, S. Saadallah, K. Jurewicz, E. Frackowiak, M. Reda, J. Parmentier, F. Beguin, Supercapacitor electrodes from new ordered porous carbon materials obtained by a templating procedure. Mater. Sci. Eng. B **108**(1–2), 148–155 (2004)
30. E. Raymundo-Piñero, M. Cadek, F. Béguin, Tuning carbon materials for supercapacitors by direct pyrolysis of seaweeds. Adv. Funct. Mater. **19**(7), 1032–1039 (2009)
31. S. Kondrat, C.R. Perez, V. Presser, Y. Gogotsi, A.A. Kornyshev, Effect of pore size and its dispersity on the energy storage in nanoporous supercapacitors. Energ. Environ. Sci. **5**(4), 6474–6479 (2012)
32. K. Kierzek, G. Gryglewicz, Activated carbons and their evaluation in electric double layer capacitors. Molecules **25**(18), 4255 (2020)
33. Y.H. Lee, K.H. Chang, C.C. Hu, Differentiate the pseudocapacitance and double-layer capacitance contributions for nitrogen-doped reduced graphene oxide in acidic and alkaline electrolytes. J. Power Sour. **227**, 300–308 (2013)
34. D. Qu, Studies of the activated carbons used in double-layer supercapacitors. J. Power Sour. **109**(2), 403–411 (2002)
35. A. Śliwak, B. Grzyb, J. Ćwikła, G. Gryglewicz, Influence of wet oxidation of herringbone carbon nanofibers on the pseudocapacitance effect. Carbon **64**, 324–333 (2013)
36. G. Sahoo, S.R. Polaki, S. Ghosh, N.G. Krishna, M. Kamruddin, K.K. Ostrikov, Plasma-tuneable oxygen functionalization of vertical graphenes enhance electrochemical capacitor performance. Energ. Storage Mater. **14**, 297–305 (2018)
37. T. Lin, I.W. Chen, F. Liu, C. Yang, H. Bi, F. Xu, F. Huang, Nitrogen-doped mesoporous carbon of extraordinary capacitance for electrochemical energy storage. Science **350**(6267), 1508–1513 (2015)
38. M.G. Sullivan, R. Kötz, O. Haas, Thick active layers of electrochemically modified glassy carbon. Electrochemical impedance studies. J. Electrochem. Soc. **147**, 308–317 (2000)
39. L. Jiang, J. Wang, X. Mao, X. Xu, B. Zhang, J. Yang, S. Hou, High rate performance carbon nano-cages with oxygen-containing functional groups as supercapacitor electrode materials. Carbon **111**, 207–214 (2017)

40. R. Zhang, X. Jing, Y. Chu, L. Wang, W. Kang, D. Wei, H. Li, S. Xiong, Nitrogen/oxygen co-doped monolithic carbon electrodes derived from melamine foam for high-performance supercapacitors. J. Mater. Chem. A **6**(36), 17730–17739 (2018)
41. S.T. Mayer, R.W. Pekala, J.L. Kaschmitter, The aerocapacitor: an electrochemical double-layer energy-storage device. J. Electrochem. Soc. **140**, 446–451 (1993)
42. B. Pillay, J. Newman, The influence of side reactions on the performance of electrochemical double-layer capacitors. J. Electrochem. Soc. **143**, 1806–1814 (1996)
43. S. Kerisit, B. Schwenzer, M. Vijayakumar, Effects of oxygen-containing functional groups on supercapacitor performance. J. Phys. Chem. Lett. **5**(13), 2330–2334 (2014)
44. Q. Zhang, C. Cai, J. Qin, B. Wei, Tunable self-discharge process of carbon nanotube based supercapacitors. Nano Energ. **4**, 14–22 (2014)
45. L.Z. Fan, S. Qiao, W. Song, M. Wu, X. He, X. Qu, Effects of the functional groups on the electrochemical properties of ordered porous carbon for supercapacitors. Electrochim. Acta **105**, 299–304 (2013)
46. J.M. Boyea, R.E. Camacho, S.P. Sturano, W.J. Ready, Carbon nanotube-based supercapacitors: technologies and markets. Nanotech. L. Bus. **4**, 19 (2007)
47. Z. Wang, Z. Wu, G. Di Benedetto, J.L. Zunino III., S. Mitra, Microwave synthesis of highly oxidized and defective carbon nanotubes for enhancing the performance of supercapacitors. Carbon **91**, 103–113 (2015)
48. D. Hulicova-Jurcakova, M. Seredych, G.Q. Lu, T.J. Bandosz, Combined effect of nitrogen-and oxygen-containing functional groups of microporous activated carbon on its electrochemical performance in supercapacitors. Adv. Funct. Mater. **19**(3), 438–447 (2009)
49. J. Cherusseri, K.K. Kar, Ultra-flexible fibrous supercapacitors with carbon nanotube/polypyrrole brush-like electrodes. J. Mater. Chem. A **4**(25), 9910–9922 (2016)
50. M. Zhu, C.J. Weber, Y. Yang, M. Konuma, U. Starke, K. Kern, A.M. Bittner, Chemical and electrochemical ageing of carbon materials used in supercapacitor electrodes. Carbon **46**(14), 1829–1840 (2008)
51. V. Ruiz, C. Blanco, E. Raymundo-Piñero, V. Khomenko, F. Béguin, R. Santamaría, Effects of thermal treatment of activated carbon on the electrochemical behaviour in supercapacitors. Electrochim. Acta **52**(15), 4969–4973 (2007)
52. J.B. In, B. Hsia, J.H. Yoo, S. Hyun, C. Carraro, R. Maboudian, C.P. Grigoropoulos, Facile fabrication of flexible all solid-state micro-supercapacitor by direct laser writing of porous carbon in polyimide. Carbon **83**, 144–151 (2015)
53. S. Hussain, R. Amade, E. Jover, E. Bertran, Nitrogen plasma functionalization of carbon nanotubes for supercapacitor applications. J. Mater. Sci. **48**(21), 7620–7628 (2013)
54. E. Adhamash, R. Pathak, K. Chen, M.T. Rahman, A. El-Magrous, Z. Gu, Y. Zhou, High-energy plasma activation of renewable carbon for enhanced capacitive performance of supercapacitor electrode. Electrochim. Acta **362**, 137148 (2020)
55. R.M. Wigntman, M.R. Deakin, P.M. Kovach, W.G. Kuhr, K.J. Stutts, Methods to improve electrochemical reversibility at carbon electrodes. J. Electrochem. Soc. **131**, 1578–1583 (1984)
56. Z. Zhu, S. Tang, J. Yuan, X. Qin, Y. Deng, R. Qu, G.M. Haarberg, Effects of various binders on supercapacitor performances. Int. J. Electrochem. Sci **11**(10), 8270–8279 (2016)
57. D. Qu, Studies of the activated carbons used in double-layer supercapacitors. J. Power. Sour. **109**, 403–411 (2002)
58. W. Qiao, Y. Korai, I. Mochida, Y. Hori, T. Maeda, Preparation of an activated carbon artifact: oxidative modification of coconut shell-based carbon to improve the strength. Carbon **40**, 351–358 (2002)
59. L. Bonnefoi, P. Simon, J.F. Fauvarque, C. Sarrazin, J.F. Sarrau, A. Dugast, Electrode compositions for carbon power supercapacitors. J. Power Sour. **80**(1–2), 149–155 (1999)
60. M. Vijayakumar, A. Bharathi Sankar, D. Sri Rohita, T.N. Rao, M. Karthik, Conversion of biomass waste into high performance supercapacitor electrodes for real-time supercapacitor applications. ACS Sustain. Chem. Eng. **7**(20), 17175–17185 (2019)

61. Y. Gao, Graphene and polymer composites for supercapacitor applications: a review. Nanoscale Res. Lett. **12**(1), 1–17 (2017)
62. F. Markoulidis, C. Lei, C. Lekakou, D. Duff, S. Khalil, B. Martorana, I. Cannavaro, A method to increase the energy density of supercapacitor cells by the addition of multiwall carbon nanotubes into activated carbon electrodes. Carbon **68**, 58–66 (2014)
63. C. Benoit, D. Demeter, D. Bélanger, C. Cougnon, A redox-active binder for electrochemical capacitor electrodes. Angew. Chem. **128**(17), 5404–5407 (2016)
64. V.P. Zykov, A.A. Panov, P.A. Prudnikov, M.I. Khlopin, A.D. Shlyapnikov, Electrolytic capacitor and a method of manufacturing the same. US3675087 (1972)
65. A.G. Pandolfo, G.J. Wilson, T.D. Huynh, A.F. Hollenkamp, The influence of conductive additives and inter-particle voids in carbon EDLC electrodes. Fuel Cells **10**(5), 856–864 (2010)
66. D. Tashima, K. Kurosawatsu, M. Taniguchi, M. Uota, M. Otsubo, Basic characteristics of electric double layer capacitor mixing ketjen black as conductive filler. Electr. Eng. Jpn. **165**(1), 1–8 (2008)
67. D. Tashima, H. Yoshitama, M. Otsubo, S. Maeno, Y. Nagasawa, Evaluation of electric double layer capacitor using Ketjenblack as conductive nanofiller. Electrochim. acta **56**(24), 8941–8946 (2011)
68. W.C. West, M.C. Smart, E.J. Brandon, L.D. Whitcanack, G.A. Plett, Double-layer capacitor electrolytes using 1, 3-D ioxolane for low temperature operation. J. Electrochem. Soc. **155**(10), A716 (2008)
69. Y. Matsuda, M. Morita, M. Ishikawa, M. Ihara, New electric double-layer capacitors using polymer solid electrolytes containing tetraalkylammonium salts. J. Electrochem. Soc. **140**(7), L109 (1993)
70. S.D. Ross, M. Finkelstein, R.C. Petersen, Mechanism of the electroreduction of benzyltriethylammonium nitrate in dimethylformamide at aluminum and platinum cathodes. J. Am. Chem. Soc. **92**, 6003–6006 (1970)
71. E.K. Humphreys, P.K. Allan, R.J. Welbourn, T.G. Youngs, A.K. Soper, C.P. Grey, S.M. Clarke, A neutron diffraction study of the electrochemical double layer capacitor electrolyte tetrapropylammonium bromide in acetonitrile. J. Phys. Chem. B **119**(49), 15320–15333 (2015)
72. J. Krummacher, C. Schütter, S. Passerini, A. Balducci, Characterization of different conductive salts in ACN-based electrolytes for electrochemical double-layer capacitors. ChemElectroChem **4**(2), 353–361 (2017)
73. P. Liu, M. Verbrugge, S. Soukiazian, Influence of temperature and electrolyte on the performance of activated-carbon supercapacitors. J. Power Sour. **156**(2), 712–718 (2006)
74. J.P. Zheng, T.R. Jow, The effect of salt concentration in electrolytes on the maximum energy storage for double layer capacitors. J. Electrochem. Soc. **144**, 2417–2420 (1997)
75. C.J. Farahmandi, J.M. Dispennette, Manufacturing of industrial supercapacitors. WO9611486 for Maxwell Tech. (1998)
76. D. Aurbach, *Nonaqueous Electrochemistry*. Chapter 4. (CRC Press, 1999)
77. F.A. Cotton, G. Wilkinson, *Advanced Inorganic Chemistry*. (Wiley, New York,1966), p. 240
78. V. Ruiz, T. Huynh, S.R. Sivakkumar, A.G. Pandolfo, Ionic liquid-solvent mixtures as supercapacitor electrolytes for extreme temperature operation. RSC Rdv. **2**(13), 5591–5598 (2012)
79. Y. Liu, B. Soucaze-Guillous, P.L. Taberna, P. Simon, Understanding of carbon-based supercapacitors ageing mechanisms by electrochemical and analytical methods. J. Power Sour. **366**, 123–130 (2017)
80. R. German, A. Sari, P. Venet, M. Ayadi, O. Briat, J.M. Vinassa, Prediction of supercapacitors floating ageing with surface electrode interface based ageing law. Microelectron. Reliab. **54**, 1813–1817 (2014)
81. D. Hulicova, M. Kodama, H. Hatori, Electrochemical performance of nitrogen-enriched carbons in aqueous and non-aqueous supercapacitors. Chem. Mater. **18**(9), 2318–2326 (2006)

82. S. Ishimoto, Y. Asakawa, M. Shinya, K. Naoi, Electrochemical performance of nitrogen-enriched carbons in aqueous and non-aqueous supercapacitors. J. Electrochem. Soc. **156**, 563–571 (2009)
83. Y. Kanbe, M. Oya, Electric double layer capacitor. JP2000216068 for NEC (2000)
84. O. Caumont, J.M. Depond, A. Jourdren, P. Azais, Device to prevent overpressure in a supercapacitor. WO2009112718 for Batscap (2009)
85. R.O'D. Petersen, R.C. Kullberg, L. Toia, S. Rondena, B.J. Mio, Metal getter systems WO2008033560 for SAES Getters (2008)
86. T.R. Beatty Rupture diaphragm for galvanic cell. CA1209201 for Union Carbide Corp. (1984)
87. T. Fujino, Locality information retrieval system. US7224274 for Honda Motor. (2007)
88. K. Abe, Nonaqueous electrolytes and advances in additives, in *Electrolytes for Lithium and Lithium-Ion Batteries.* (Springer, New York, NY, 2014), pp. 167–207
89. M. Ayadi, O. Briat, A. Eddahech, R. German, G. Coquery, J.M. Vinassa, Thermal cycling impacts on supercapacitor performances during calendar ageing. Microelectron. Reliab. **53**(9–11), 1628–1631 (2013)
90. E. Perricone, M. Chamas, J.C. Leprêtre, P. Judeinstein, P. Azais, E. Raymundo-Pinero, F. Béguin, F. Alloin, Safe and performant electrolytes for supercapacitor. Investigation of esters/carbonate mixtures. J. Power Sour. **239**, 217–224 (2013)
91. M. Arulepp, L. Permann, J. Leis, A. Perkson, K. Rumma, A. Jänes, E. Lust, Influence of the solvent properties on the characteristics of a double layer capacitor. J. Power Sour. **133**, 320–328 (2004)
92. T. Ye, D. Li, H. Liu, X. She, Y. Xia, S. Zhang, H. Zhang, D. Yang, Seaweed biomass-derived flame-retardant gel electrolyte membrane for safe solid-state supercapacitors. Macromolecules **51**(22), 9360–9367 (2018)
93. M. Salanne, Ionic liquids for supercapacitor applications. Ionic Liquids **II**, 29–53 (2017)
94. T. Abdallah, D. Lemordant, B. Claude-Montigny, Are room temperature ionic liquids able to improve the safety of supercapacitors organic electrolytes without degrading the performances? J. Power Sour. **201**, 353–359 (2012)
95. A. Eftekhari, Supercapacitors utilising ionic liquids. Energ. Storage Mater. **9**, 47–69 (2017)
96. A.J. Rennie, N. Sanchez-Ramirez, R.M. Torresi, P.J. Hall, Ether-bond-containing ionic liquids as supercapacitor electrolytes. J. Phys. Chem. Lett. **4**(17), 2970–2974 (2013)
97. S. Zhang, S. Brahim, S. Maat, High-voltage operation of binder-free CNT supercapacitors using ionic liquid electrolytes. J. Mater. Res. **33**(9), 1179–1188 (2018)
98. Y.M. Shulga, S.A. Baskakov, Y.V. Baskakova, Y.M. Volfkovich, N.Y. Shulga, E.A. Skryleva, Y.N. Parkhomenko, K.G. Belay, G.L. Gutsev, A.Y. Rychagov, V.E. Sosenkin, Supercapacitors with graphene oxide separators and reduced graphite oxide electrodes. J. Power Sour. **279**, 722–730 (2015)
99. M. Wu, C. Yang, H. Xia, J. Xu, Comparative analysis of different separators for the electrochemical performances and long-term stability of high-power lithium-ion batteries. Ionics **27**(4), 1551–1558 (2021)
100. T. Tsukuda, M. Midorikawa, T. Sato, Separator for electric double layer capacitor. WO2007061108, for Mitsubishi Paper Mills (2007)
101. B. Szubzda, A. Szmaja, M. Ozimek, S. Mazurkiewicz, Appl. Phys. A **117**(4), 1801–1809 (2014)
102. D. Xu, G. Teng, Y. Heng, Z. Chen, D. Hu, Eco-friendly and thermally stable cellulose film prepared by phase inversion as supercapacitor separator. Mater. Chem. Phys. **249**, 122979 (2020)
103. B.K. Deka, A. Hazarika, O. Kwon, D. Kim, Y.B. Park, H.W. Park, Multifunctional enhancement of woven carbon fiber/ZnO nanotube-based structural supercapacitor and polyester resin-domain solid-polymer electrolytes. Chem. Eng. J. **325**, 672–680 (2017)
104. N. Wang, G. Han, Y. Xiao, Y. Li, H. Song, Y. Zhang, Polypyrrole/graphene oxide deposited on two metalized surfaces of porous polypropylene films as all-in-one flexible supercapacitors. Electrochim. Acta **270**, 490–500 (2018)

105. N. Wang, G. Han, H. Song, Y. Xiao, Y. Li, Y. Zhang, H. Wang, Integrated flexible supercapacitor based on poly (3, 4-ethylene dioxythiophene) deposited on Au/porous polypropylene film/Au. J. Power Sour. **395**, 228–236 (2018)
106. N. Wang, X. Wang, Y. Zhang, W. Hou, Y. Chang, H. Song, Y. Zhao, G. Han, All-in-one flexible asymmetric supercapacitor based on composite of polypyrrole-graphene oxide and poly (3, 4-ethylenedioxythiophene). J. Alloys Compd. **835**, 155299 (2020)
107. K.D. Verma, P. Sinha, S. Banerjee, K.K. Kar, M.K. Ghorai, in *Handbook of Nanocomposite Supercapacitor Materials I*. (Springer, Cham, 2020), pp. 315–326
108. T. Kobayashi, N. Kimura, JP2006144158 for Japan Vilene (2006)
109. N. Oya, Y. Asano, S. Yao, JP2003229329 for Ube Industries (2003)
110. J. Mu, C. Shao, Z. Guo, M. Zhang, Z. Zhang, P. Zhang, B. Chen, Y. Liu, Solvothermal synthesis and electrochemical properties of 3D flower-like iron phthalocyanine hierarchical nanostructure. Nanoscale **3**(12), 5126–5131 (2011)
111. K. Wang, L. Li, H. Yin, T. Zhang, W. Wan, Thermal modelling analysis of spiral wound supercapacitor under constant-current cycling. PLOS One **10**(10), e0138672 (2015)
112. O. Caumont, J.-M. Depond, A.-C. Juventin, Module pour ensembles de stockage d'energie electrique a barrette de liaison plate. EP2198472 for Batscap. (2008)
113. H. Goesmann, M. Setz, Electrical capacitor module for automobile use has a number of capacitors mounted in line together with connections. DE102004039231 for EPCOS (2006)
114. O. Caumont Olivier, A.-C. Juventis-Mathes, K. Le Bras, J.-M. Depond, Module pour ensemble de stockage d'energie electrique. EP2145360 for Batscap. (2008)
115. O. Caumont, P. Paillard, G. Saindrenan, Method of producing electrical connections for an electrical energy storage unit by means of diffusion brazing. WO2007147978 for Batscap and Ecole Polytechnique del'Université de Nantes (2007)
116. H.Goesmann, Capacitor module with capacitor cells comprising double layer capacitors having adjacent fastening plates fastened to a substrate plate. DE102004030801 for EPCOS (2005)
117. M. Setz, S. Nowak, A. Hoerger, Capacitor and capacitor module. WO2006005277 for EPCOS (2006)
118. C.S. Luo, P. Wan, H. Yang, S.A.A. Shah, X. Chen, Healable transparent electronic devices. Adv. Funct. Mater. **27**(23), 1606339 (2017)
119. H. Gualous, H. Louahlia-Gualous, R. Gallay, A. Miraoui, Supercapacitor thermal modeling and characterization in transient state for industrial applications. IEEE Trans. Ind. Appl. **45**(3), 1035–1044 (2009)
120. M. Al Sakka, H. Gualous, J. Van Mierlo, H. Culcu, Thermal modeling and heat management of supercapacitor modules for vehicle applications. J. Power Sour. **194**(2), 581–587 (2009)
121. G. Navarro, J. Nájera, J. Torres, M. Blanco, M. Santos, M. Lafoz, Development and experimental validation of a supercapacitor frequency domain model for industrial energy applications considering dynamic behaviour at high frequencies. Energies **13**(5), 1156 (2020)

Recent Development in Flexible Supercapacitors

Anuj Kumar, Felipe De Souza, Ali Panhwar, and Ram K. Gupta

Abstract Energy has remained one of the top priorities of researchers for its maximum conservation due to the rapidly depleting conventional energy resources. The recent developments in the field of energy storage have compelled researchers to explore the power and potential of supercapacitors. These efforts have revealed the hidden yet unique benefits of supercapacitors for producing highly advanced and smart flexible wearable devices and consumer electronics. The ongoing researches have explored the performance, potential, and capacity of supercapacitors in comparison with conventional capacitors. In this chapter, different types of materials and methods utilized to facilitate energy storage have been discussed. In particular, the use of graphene with metal oxides, chalcogenides, and conductive polymer materials along with mechanisms have also been emphasized in detail. Additionally, the recent advancements on various supercapacitors and their possible applications, including sensors, smart, flexible devices, consumer electronics, hybrid vehicles, advanced energy storage systems, heavy machinery, power grid systems, etc. were considered as the heart of this chapter. Further, the prospects of supercapacitor-based devices which hold promising innovations in advanced energy storage processes are also systematically highlighted.

Keywords Supercapacitor · Flexible devices · Energy density · Power density · 2D materials

A. Kumar (✉)
Nano-Technology Research Laboratory, Department of Chemistry, GLA University, Mathura, Uttar Pradesh 281406, India
e-mail: anuj.kumar@gla.ac.in

F. De Souza · A. Panhwar · R. K. Gupta (✉)
Kansas Polymer Research Center, Pittsburg State University, Pittsburg, KS 66762, USA
e-mail: ramguptamsu@gmail.com

R. K. Gupta
Department of Chemistry, Pittsburg State University, Pittsburg, KS 66762, USA

S. Thomas et al. (eds.), *Nanostructured Materials for Supercapacitors*,
Advances in Material Research and Technology,
https://doi.org/10.1007/978-3-030-99302-3_25

1 Introduction

Energy is the most valuable commodity in the world today. It is the strength of energy that has driven economic and social progress in societies and has determined the quality of life. The importance of energy can be seen through the extensive innovative developments in technology and its use in everyday life. For instance, in developed countries like Canada, reliable and affordable energy is the driving force behind the production and distribution of services that enrich and extend life. Be it power computers, communications, transportation, or cutting-edge medical equipment; energy is the mainspring behind every revolutionary innovation [1]. Broadly, energy sources are of two types; renewable and non-renewable. Despite a lot of progression in the non-renewable energy sector, crude oil and coal are the most dominant form of non-renewable energy source that is used in industry, agriculture, trade, and transportation [2]. However, the world is rapidly moving towards renewable energy sources, mainly solar, wind, and hydroelectric energies. These are considered safe and reliable for long-term use compared to the rapidly depleting non-renewable sources. According to a study, renewable energy share would be equal to two-thirds of the total global primary energy supply in 2050 [3]. Along with the escalation in the use of renewable energy, there have been efforts to store energy on chemical and electrical levels, which employs supercapacitors in electrical devices, machines, and appliances. These are lightweight and environment-friendly and show high performance in less charging time than conventional batteries [4].

Energy storage is one of the most difficult yet invaluable aspects of energy production and consumption practices. Energy is required in the transportation, industry, and overall economic activity of a country; therefore, its preservation and storage are immensely important [5]. Energy storage in the grids is also considered to be the reason for making the grids systems more efficient and reliable in the long term. Once energy is stored and appropriately utilized, economic and environmental security can strengthen a country that is directly related to the energy storage mechanisms [6]. Since the non-renewable sources are depleting and the renewable ones are still in the initial phases, there is a capacity to introduce other methods of energy storage. These methods are of various types, and they are creating strides in the energy sector. They can be categorized as mechanical storage, electrical/electromagnetic storage, electrochemical storage, thermal storage, and chemical storage. The mechanical storage includes spring, flywheel energy storage, pumped hydro energy storage, fireless locomotive, hydraulic accumulator thermal expansion, solid mass gravitational [7]. The capacitor, supercapacitor, superconducting magnetic energy storage is a type of electrical/electromagnetic storage. Electrochemical storage contains rechargeable batteries, flow batteries, ultra-batteries, liquid air energy storage, liquid nitrogen system. Thermal storage incorporates cryogenic energy storage, steam accumulator, and chemical storage covers biofuels, eutectic system, hydrated salts, hydrogen storage, vanadium pentoxide.

There are various types of energy storage methods used across the globe, and the most frequently and extensively used are batteries. Batteries have been used in a

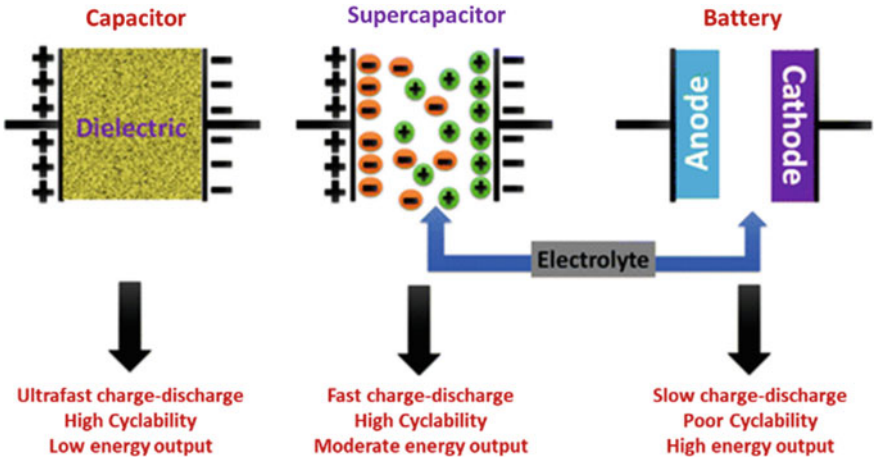

Fig. 1 Difference between capacitor, supercapacitor, and battery charge–discharge capabilities. Adapted with permission from reference [9], Copyright 2018, Springer Nature

wide variety of applications that extend from toys to medical implants. The energy storage in the battery has a few drawbacks that include heating problems, gasification, risk of explosion, danger to the atmosphere, shorter lifecycle, lower power density, and longer charging time. Supercapacitors can be an alternative to batteries with the characteristics of both the batteries and the capacitor. In the last few years, there has been significant progress in the field of supercapacitors for commercial applications [8]. The supercapacitor, as compared to batteries and capacitors, has superior capacitance, longer lifecycle, reduced charging time, lightweight, and has no significant impact on the environment (Fig. 1) [9].

2 Importance of Flexible/Wearable Devices

Over the past few decades, flexible and wearable devices have been used to preserve energy and innovatively use them. These electronics have inspired many developers to create innovative technologies in more advanced ways. Unlike the conventional silicon-based inventions, flexible and wearable electronic devices reflect more reliable and superior qualities like high flexibility, ultra-lightweight, easy processability, adaptability to roll-to-roll production procedures, and acceptance by the users who find them more convenient than the traditional devices [10]. These devices are continuously being evolved into the best versions possible. For this, the bendability and flexibility of these devices are frequently measured to determine their quality and longevity. The curvature radius of these devices is observed, which should bear approximately 80% bending and remain intact, i.e., from 100 mm up to 1 mm. Similarly, if the curvature radius declines to 1 mm or less than that, then the device

is recognized as an ultra-flexible substrate. This observation, however, determines whether the device is reliable or not for energy storage [11]. The most important aspect of these flexible wearable devices is that they are much different in durability and adaptability in terms of performance and adjusting to the emerging needs of the consumer market. Especially, when the world is moving towards energy conservation, these devices are meant to make this job easier. They are unbreakable as they incorporate a glass-free active matrix display which is unique and convenient. Also, they can be easily manufactured at a low cost along with creating minimum waste [12]. Similarly, these devices have a maximum processing temperature of 100 °C which is best for the lower-cost production of flexible substrates. Hence, the flexible wearable devices are of immense advantage for the manufacturers and the consumers both.

Recently, there has been much innovation in the field of consumer electronics in which many flexible and bendable devices are being created. These devices offer unmatched pliability and a robust structure that is not just safe but durable as well. For instance, sensors, bendable display screens, electronics made with durable plastics, etc., have become popular in the consumer markets. The most striking aspect of flexible devices is that they ensure thin, lightweight wearables, yet robust enough to be durable, as they have a perfect form factor to be adjusted in any shape. Also, they prove to be immensely comfortable for the user. The futuristic applications of these devices include 3D printed flexible batteries for wrist bands, etc. Similarly, electric car companies like Tesla incorporate flexible devices for their future electronic car productions. These are also being further investigated to be used in healthcare systems as conventional treatment and disease tracking devices. Thus, the future holds immense opportunities for the applications of flexible wearable devices.

Flexible supercapacitors are considered as a promising energy storage technology for future textiles, automobiles, gadgets, electronics, etc. [13]. The importance of flexible supercapacitors can be reflected in the fact that they are much in demand than ever before. This is because they are new, lightweight, cost-friendly, and environment-friendly. These are largely incorporated in the production of display technologies, touch screens and sensors, and other bendable electronics. Another aspect of their importance is that electrodes in flexible supercapacitors are composed of a carbon network, which can be binder-free and conductive. These properties of carbon networks also remove the need to use metal foils in the devices [14]. Similarly, the combination of the carbon network and the pseudocapacitive materials, created with the doping of polymers in the carbon chains (polyaniline or polythiophene), is known to increase the capacitance of the flexible electrodes. Hence, these properties of the supercapacitors make them unique and of high utility [15]. Simply put, when compared with conventional capacitors, supercapacitors exhibit high power density, prominently increased capacitance, a good low-temperature performance, which make them durable, enhance energy density, improve current discharge ability, offer longer life, promote fast charging speed, along with convenient detection [16]. That is why they are frequently used in flexible wearable devices and other electronic gadgets for more convenience. They are also important for hybrid vehicles for supplementary storage of battery life and energy.

3 Materials and Charge Storage Mechanisms

As compared to conventional batteries, capacitors are known to be of much prominence in terms of being able to store energy for shorter periods, i.e., for quick use of any device. Also, they have less energy per unit weight, which makes them quite slow during the performance. However, the higher specific powers and faster response make them better than batteries. Comparatively, supercapacitors have more power and response times than capacitors [17]. The mechanism of batteries and capacitors differ due to the difference in energy storage electrodes and their materials. These differences of mechanism include (a) the faradic charge storage, i.e., of batteries, and (b) the non-faradic or the capacitive charge storage in pseudocapacitors, which are caused by electrostatic interactions in the electrodes. Supercapacitors are electrochemical devices for storing energy in an efficient way [18]. However, the materials used for energy storage include nanostructured materials that have higher reaction rates due to the additional electrode surface area and short path lengths. These nanoscale materials are needed for batteries so that the solid-state ionic diffusions must be avoided for uninterrupted charge storage. In supercapacitors, carbonaceous materials are used to store charge energy, such as graphite, graphene, carbon nanotubes (CNTs), activated carbon (AC), carbon fibercloth, conducting polymers, transition-metal oxides, sulfides, etc. Precisely, supercapacitors use electrodes, electrolytes, and separators that collectively work to store energy [19].

The hybrid supercapacitors are the combinations of electrochemical double-layer capacitors (EDLCs) and pseudocapacitors and therefore have an enhanced performance rate. Hybrid supercapacitors have elevated chances of amplified energy density, extensive life cycle, rapid kinetics, better security, and low expenditure on preparation [20]. These supercapacitor systems also have non-aqueous redox materials that are responsible for furthering the energy storage process. There are two types of hybrid supercapacitors; (a) symmetric and (b) asymmetric. The difference between these two types is based on the electrode material. The symmetric hybrid supercapacitor has similar electrodes while asymmetric has dissimilar types. The most unique and popular application of hybrid supercapacitors is vehicles. They are incorporated in hybrid vehicles that create reduced environmental pollution and offer high energy storage capacity. Therefore, to generate maximum performance of the vehicles or electric devices, the combination of high-energy–density lithium-ion batteries and high-power density supercapacitors is the perfect way to make the electrodes work best for reliable power generation and storage applications [21]. One of the distinctive features of hybrid supercapacitors includes a higher capacitance than the normal capacitors and a higher working voltage. They also exhibit a very low current leakage as compared to EDLCs. Hybrid supercapacitors are normally safe; however, the electrolytes in them can be flammable and harmful. That is why they require a specific temperature to avoid too much heat for possible damage. Despite that, they are more efficient and reliable in terms of durability and performance of the devices.

4 Flexible Supercapacitors

Flexible supercapacitors are immensely important when it comes to lightweight, portable electronic devices. These supercapacitors are installed in the devices for maximum energy storage with the least inconvenience. Flexible supercapacitors incorporate the combination of the flexible electrode and the substrate material, which creates structural flexibility with high power density. These abilities of these supercapacitors make them unique and perfect for innovative portable devices. Flexible supercapacitors are produced with various materials; however, the ones made from activated carbon showed high capacitance as the activated carbon is responsible for reducing resistance [22]. For a successful design of a flexible supercapacitor, it is important to synthesize EDLCs and the pseudocapacitors along with the synthesis of electrodes and electrolytes. These will ensure the stable design and maximum performance of a flexible supercapacitor. Flexible supercapacitors are bendable, and their electrodes are also adjustable to this bendability. For flexible supercapacitors, the most popular design is free-standing films with a large scale up to several centimeters. The active electrode materials used in them are usually larger than the planar configuration, which is the actual reason for high capacitance. Hence, with high capacitance come much stronger mechanical properties. The flexibility of the flexible supercapacitors can be achieved by using free-standing electrode films, flexible current collector substrates, and gel polymer-based electrolytes, such as carbon-based cloths, metal foils, fibers, wires, and tapes (Fig. 2). These materials enhance the potential of the supercapacitors in terms of energy storage, and they are also the most feasible for flexible wearable devices [23].

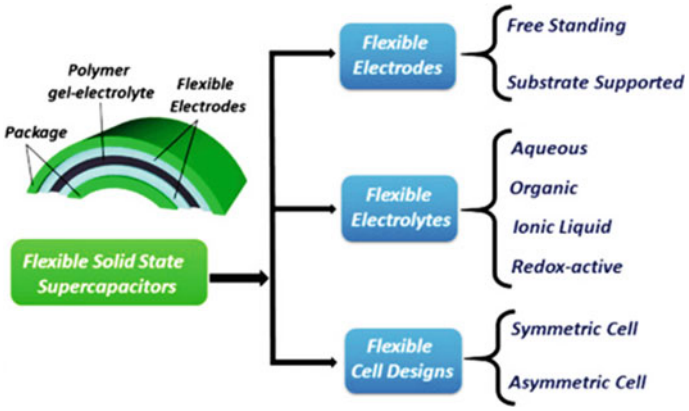

Fig. 2 Photographic view of the construction of flexible solid-state supercapacitors. Adapted with permission from reference [24], Copyright 2018, Elsevier

4.1 Allotropes of Carbon for Flexible Supercapacitors

Various allotropes of carbons such as graphene, carbon nanotubes are used to maximize the energy storage capacity in flexible supercapacitors. Graphene is a thin layer of pure carbon in a hexagonal honeycomb-like structure, tightly bonded together. Graphene has enhanced the capability and performance of carbon-based supercapacitors. For example, they can charge within seconds and discharge tens of thousands of charging cycles [25]. Graphene-based electrodes have been tested to make them more responsive in terms of the energy storage process.

Over the years, various graphene materials have been synthesized to increase the potential of supercapacitors. These materials include graphene films, graphene fibers, and 3D porous graphene frameworks, which exhibit more power storage and less energy wastage. These materials can be deformed in a controlled environment to be adjusted into portable, flexible devices. This feature of graphene supercapacitors has increased their application, for instance, in solar cells and similar self-powering devices.

4.1.1 Graphene-Based Flexible Supercapacitors

The overall potential and performance of a supercapacitor are determined by its charge storage mechanism, which incorporates either EDLCs or redox reactions. While EDLCs store charges more like normal capacitors, the pseudocapacitors work more like batteries. However, carbonaceous materials are the ones that dominate the energy storage process as compared to the above-mentioned materials. But, for this elevated performance, the carbonaceous materials require graphene and carbon nanotubes which increase their potential manifold, especially in flexible electrodes. There has been extensive research on these carbonaceous materials as they have outstanding electrical and electrochemical properties, especially graphene.

Graphene-based electrodes as well as the electrolytes, are highly flexible, be it symmetric or asymmetric in nature and structure. This is because graphene contains prominent physical features, such as good mechanical strength, high specific surface area, good chemical stability, high electrical conductivity, thermal conductivity, and mechanical flexibility for flexible supercapacitor devices, which makes it a suitable electrode material. These features are responsible for creating a highly flexible and thin film of graphene-based electrode materials (as demonstrated in (Fig. 3) that can be worn on the body or in wearable electronic devices. One of the main composites graphene-based flexible supercapacitors include pure graphene-based electrode materials that are graphene-based or reduced multilayer graphene oxide film-based flexible electrodes, prepared by chemical reduction of graphene oxide (GO). This method is conducted through organic reducing agents, resulting in identical flexible graphene electrodes or combining flexible devices with ultra-thin and optically transparent features [26]. Besides, pure graphene is also responsible for delivering

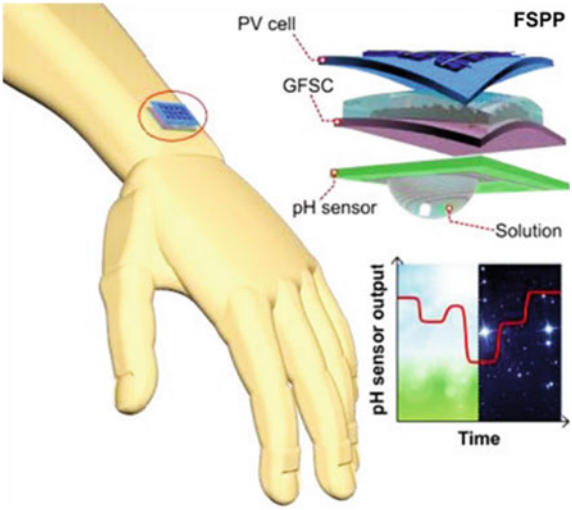

Fig. 3 Graphene-Ag-3D graphene foam electrodes used in Flexible self-charging SC [29]. Adapted from reference [29]. This is an open-access article distributed under the terms of the Creative Commons CC-BY license

normalized capacitance of 80 μF/cm, which is quite efficient in a flexible supercapacitor (FSC). Also, graphene is best when prepared as a porous flexible paper through vacuum filtration, which can be directly used as a supercapacitor electrode without even using a binder [27]. This electrode has high capacitance (468 F/g at a scan rate of 2 mV/s), and an exceptional cycling performance [28]. Some of the prominent composites of graphene-based FSCs are discussed below.

4.1.2 Metal Oxide/Graphene Composites For Flexible Supercapacitors

Metal oxides are used for the synthesis of composite materials in which the metal oxide nanoparticles' size and morphology change drastically. These changes improve the availability of sorptive sites for sorbate molecules, which enhances the capacitance [30]. Graphene, being a carbon monolayer, is unique for its functional properties. Especially when combined with metal nanoparticles like metal oxides, the efficiency of graphene-based FSC increased manifold. For instance, metals such as silver (Ag), manganese (Mn), gold (Au), nickel (Ni), copper (Cu), palladium (Pd), platinum (Pt), ruthenium (Ru), and rhodium (Rh); and oxides like MnO_2, ZnO, TiO_2, SnO_2, Fe_3O_4, Co_3O_4, Cu_2O, NiO, RuO_2, and SiO_2 are the prominent materials [31].

Metal oxides are suitable materials that show enhanced electrochemical properties for sensors or biosensors. They can construct a 3D conductive pathway for clearing charge transfer ways in a porous form. These pathways help to improve the sensitivity of the electrochemical sensors and devices. Due to this ability of metal oxides, they are beneficial for supercapacitors [32]. The creation of graphene nanoparticles is a diverse process that results in the synthesis of various graphene composites. For instance, as Fig. 4 shows, different techniques of creating graphene composites result

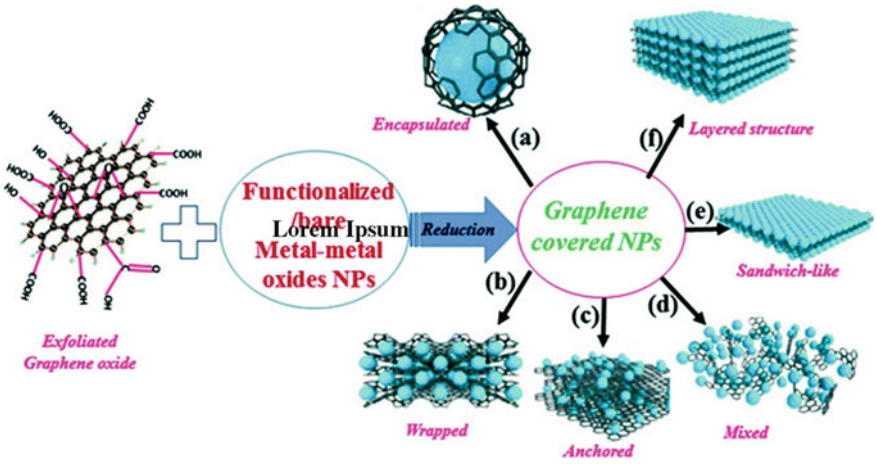

Fig. 4 Pictorial view of techniques used for the creation of graphene–nanoparticles (NPs) composites and different structures of (**a**) encapsulated-graphene nanoparticless, (**b**) wrapped-graphene nanoparticles, (**c**) graphene-nanosheets to which NPS are anchored, (**d**) mixed graphene–NP structures, (**e**) sandwich structures of graphene nanoparticle, and (**f**) layered graphene nanoparticle. Adapted with permission from reference [33], Copyright 2021, Springer Nature

in different types of graphene-based nanoparticles. These nanoparticles are all equally effective and efficient for enhancing the supercapacitor's potential.

Manganese oxide usually contains negative charges that need to be made positive to suit the graphene-based FSC. For this, the incorporation of manganese dioxide in hexadecyltrimethylammonium bromide will increase capacitance rapidly as compared to that of neat manganese dioxide. This can be done through the process of micro-emulsion. Similarly, ammonia-doped rGO and $Cu(ClO_4)_2$ suspension in ethanol was employed to fabricate N-doped porous rGO/copper oxide composite. This is done via the one-pot technique, which involves the application of a direct current voltage. This technique is more favorable compared to others as it does not use any additives or surfactants in the process. Besides, this technique can be used for maximizing the performance of other metal ions and conducting substrates as well. Similarly, a simple hydrothermal method was used to fabricate MnO_2 nanorods (MnO_2 NRs) of 20–40 nm diameter [34]. The electrodes made with MnO_2 NRs@rGO normally showed a higher specific capacitance of 759 F/g at 2 A/g, when operated at a potential of 0.9 V in 1 M Na_2SO_4. Along with this, it also displayed increased specific energy i.e. 64.6 Wh/kg, when a specific power of 15 kW/kg was applied. This material was found to be highly efficient for FSC applications with a life cycle of 88%. This material also exhibited excellent performance in hybrid SCs. Figure 5 demonstrated a well-defined mechanism of reduced-graphene oxide when combined with copper oxide in a hydrothermal process. This process helped to synthesize the two materials of high-performance SCs. In another study, iron oxide (Fe_3O_4) was reported to have superior supercapacitative performance. The prepared material was characterized by various techniques such as field emission scanning electron microscopy, X-ray

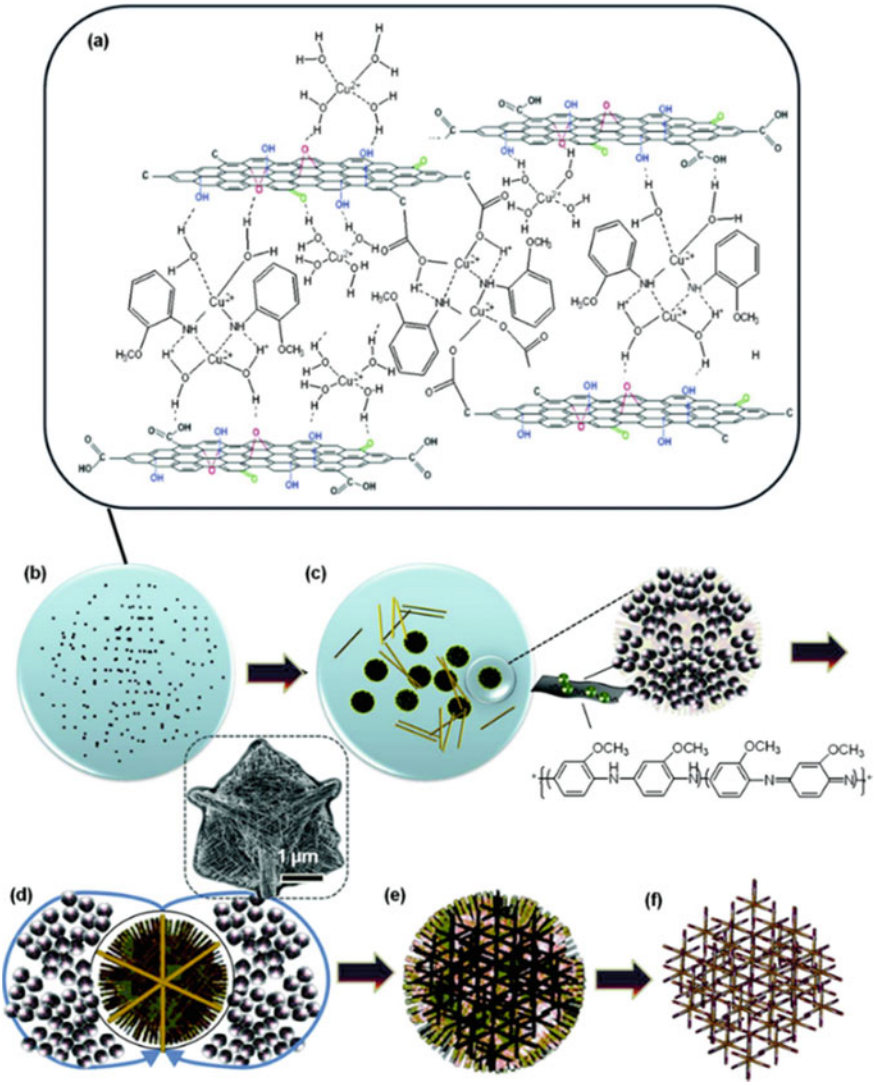

Fig. 5 Multistep sequential growth mechanism of 3D rGO-conjugated Cu_2O-nanowire mesoporous hybrids in the presence of graphene oxide and o-anisidine in a one-pot hydrothermal treatment. Adapted with permission from reference [36], Copyright 2012, American Chemical Society

diffraction, cyclic voltammetry, galvanostatic charge–discharge, and electrochemical impedance spectroscopy. The results indicated that iron oxide when combined with nitrogen-doped graphene displayed high supercapacitative performance [35].

4.1.3 Other Carbon/Graphene-Based Composites for Flexible Supercapacitors

Carbon is an ideal choice for supercapacitors material because of its good electrical conductivity. It also has high chemical stability along with a large surface area and mechanical strength. Besides, carbon is also known to support high electron mobility and high adaptability. Some of the common carbon-based graphene composites include activated carbon, carbon nanotubes, and carbon nanofibers. Activated carbons like coal, wood, etc. are highly electrically stable towards supercapacitors' performance. These materials, when treated under hydrothermal carbonization process at 700–1200 °C, exhibit promising characteristics in terms of significant specific surface area (2000 to 3000 m^2/g), balanced micro-mesoporosity, high electrical conductivity, and high specific capacitance (up to 270 F/g). Activated carbons can also be extracted from hydrochars via the hydrothermal carbonization process [37]. These chemically activated carbons were found to be suitable for graphene-based FSCs. Moreover, the blending of activated carbons with several activating agents like zinc chloride, phosphoric acid, sodium hydroxide, etc., can maximize their surface area.

Carbon nanotubes are rolled-up graphenes with in-plane properties that make them the strongest fibers. Despite that, they can be easily bent and twisted as they also retain flexibility and high pliability. CNTs have been recognized as excellent anode materials for supercapacitor electrodes [38]. CNTs can stack up in a nested structure of tubes inside the multi-walled nanotubes (MWNTs), displaying the notable mechanical and electrical properties in a supercapacitor. Hence, CNTs are more sensitive to tube orientations which reinforces the overall performance of a graphene-based supercapacitor [39]. CNTs are also widely used for FSCs due to the high absorption ability towards different molecules/biomolecules which make them excellent agents to be used in highly selective and sensitive biological and chemical sensors [40]. Carbon nanofibers are used for graphene-based FSCs owing to their capabilities of high surface area and good electrical conductivity. However, although their surface area and structure are quite stable, they can still be modified through surface etching and using chemical activation methods and doping agents.

4.2 Chalcogenides-Based Flexible Supercapacitors

Chalcogenides are chemical compounds in column VI of the periodic table, and chalcogenide materials consist of at least one chalcogen ion. These compounds form covalent glasses that intervene between the fabrication processes of glass oxides and polymers. Similarly, metal chalcogenide-based flexible supercapacitors, which include transition metals like Cu, Ni, Fe, and Co, have been of much significance in the production of flexible supercapacitors, mainly due to their anisotropic property [41]. The structure and properties of these transition metal chalcogenides resemble semi-metal pristine graphene. Their band-gap values range between 0 and 2 eV, which

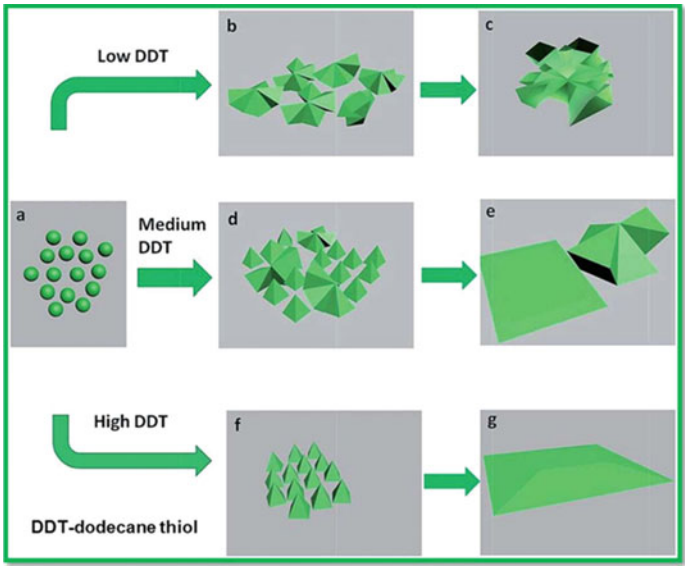

Fig. 6 Schematic illustration for the formation of 3-D Ni_3S_4 nanosheet frames and Ni_3S_4 sheets. Adapted with permission from reference [42], Copyright 2010, Royal Society of Chemistry

makes them flexible. Therefore, different industrially important materials have been produced owing to their highly trimmable and adaptive structures. These productions are demonstrated in Fig. 6, in which different forms of chalcogenides-based supercapacitors are shown, incorporated in various products.

The chalcogenides-based FSCs are known for not just having a high specific power but their ability to endure continued stability and life cycle make them unique among researchers. These FSCs portray a high tolerance relative rate towards batteries, making them applicable to a wide range of devices such as electric tools, consumer electronics, hybrid electronic vehicles, buffer power systems, etc. [43]. Apart from these applications, chalcogenides-based FSCs have been researched and found to be most suitable for producing solar cells, fuel cells, LEDs, Li-ion batteries, sensors, electro-catalysts, memory devices, and thermoelectric devices. Chalcogenides are responsible for making the supercapacitors more efficient due to their properties of unmatched flexibility, long life cycles, catalytic power, higher conductivity, reduced resistance, very low current and ohmic loss, short passage length that supports electron movements, and projecting quantum-sized effects. They also show great conductivity, enhanced mechanical and thermal stability, and higher electrochemical activity, creating strong bond structures for composite supercapacitors. These structures are created by lead and cadmium chalcogenides, which are grafted on pyrolytic graphite surfaces. Hence, a successive ionic layer adsorption process helps the FSC to optimize its capacitance power [44].

In recent studies, the replacement of Se atom by Te in SnSe significantly enhanced the thermoelectric performance of pristine SnSe [45]. Through an experiment to

fabricate a spray-painted 3D binder-free electrode by painting the ink using the SnSe nanocrystals, it is typically seen that the created electrodes show enhanced reversible capacity of 676 mAh/g after 80 discharge–charge cycles at a current density of 200 mA/g. The coulombic efficiency of 90% was obtained. Due to these properties of high charge and conductivity, FSCs become stronger and durable when these materials are installed in them. Hence, metal chalcogenides have gained much attention for being fitting material for supercapacitor electrodes. This prominence is because they possess not only rich redox chemistry but also better mechanical and thermal stability and conductivity.

4.2.1 Chalcogenides and Their Composites for Flexible Supercapacitors

Chalcogenides, especially transition metal ones, are used in high-performance logic devices and mono-layered nanosheets. These are considered to be ideal for bigger electronics that are flexible and transparent. The pliability of these layers can be viewed through the highly flexible thin-film transistors in which showcase better electrical performance with a remarkably high mechanical flexibility, good voltage, and desirable mobility. Some of the composites of chalcogenide materials for flexible supercapacitors are discussed below.

Copper chalcogenide-based materials have high intrinsic conductivity and a fast charge transfer rate. It has been observed that copper chalcogenide prepared by an in-situ oxidative polymerization approach project a superior specific capacity of 171 mF/cm^2 with excellent cycling stability, which is useful for fabricating chalcogenide-based nanosheets [46]. These nanosheets are synthesized using a one-step solvothermal process that eventually increases the capacitance. A successive ionic layer adsorption and reaction (SILAR) process is used to prepare thin electrode films for supercapacitors by combining the reduced-graphene oxide and copper sulfide materials. This process is shown in Fig. 7.

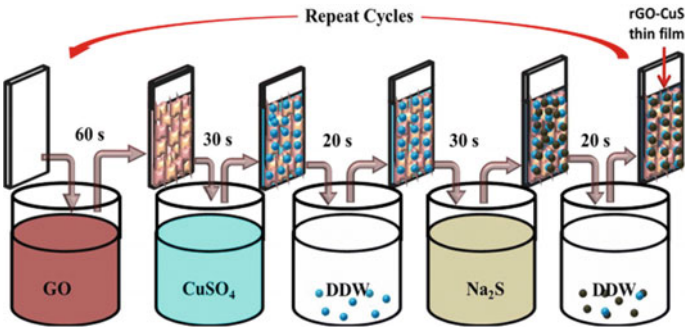

Fig. 7 Step by step process for the preparation of rGO-CuS thin film electrode by using SILAR process. Adapted with permission from reference [47], Copyright 2020, Springer Nature

Selenides are essential materials used for making Li-ion batteries, just as reduced graphene oxide/cobalt selenide(rGO/$CoSe_2$) composites [48]. These two materials provide stable anode material, which ensures strong electrochemical performance in individual selenides. Resultantly, the advanced energy-saving systems produced in the markets turn out to be highly efficient and reliable [49]. Besides, the high electrical conductivity of selenides can act as free passages for smooth and fast electron transfer when incorporated in electrode structures. Similarly, they have a rough nano-rod structure that enables large active surface areas and rapid ion channels for uninterrupted ion transport. Combining all these factors form an ultra-high specific capacity for the FSCs. For instance, the combination of Co-Cd-Se and a Fe anode was used to build a battery-supercapacitor hybrid (BSH) system to show a prominent power density that regulates the life cycles of the electrode materials. This is done by mixing Co-Cd selenide (Co-Cd-Se) nanorods, fabricated on nickel foam via a two-step hydrothermal route. The obtained selenide shows a specific capacity of 124 mAh/g at a high current density of 20 A/g, and 95.3% capacity retention can be obtained after cycling 1000 times at 2 A/g [50]. Thus, this feature projects the superiority of metal selenides in increasing performance in an FSC [51].

Sulfur chalcogenides are a low-cost and environment-friendly cathode material. Sulfur possesses advantages that are much preferred by researchers and manufacturers of smart electrical devices. For the production of high-performance 3D electrodes in the pseudocapacitors and EDLCs, sulfur is used through a solution-based activation process. This process is efficient as it helps in manufacturing scalable and mass production of electronics [51]. For sulfur-chalcogenide batteries, a flexible cathode reflects excellent features as compared to conventional cathodes. These include (1) high content of active materials, (2) mechanically robust structure to adjust volumetric changes, (3) long-range interpenetrated conductive framework, (4) porous structure for electrolyte infiltration, and (5) a 3D scaffold to improve areal sulfur loading. With the help of Cu_2S nanorods, a highly efficient cathode substrate for FSCs can be created. This is done through a direct synthesis process in which ammonium sulfide is applied to the Cu_2S solution. At room temperature, the created Cu_2S electrode exhibits excellent specific capacitance and superior rate retention performance. It also demonstrates a higher specific capacitance of 750 mF/cm^2 at a current density of 2 mA/cm^2 with an excellent rate and cycling retention of 82.3% at a current density of 40 mA/cm^2, and 90.5% at 20,000 cycles, respectively [52]. Due to these features of a sulfur chalcogenide-based electrode, the flexible supercapacitor can enhance its performance. Telluride-based reduced graphene oxide composites are perfect anode materials for the smooth working of a flexible supercapacitor. Especially in the form of hybrid powder, telluride chalcogenides combined with iron become spherical-like fine-sized anode materials. These powders can be made hybrid by mixing them with reduced graphene oxide as their hybrid forms show higher conductivity and Na-ion storage capacity [53]. Besides, telluride-based materials have an excellent electrochemical performance. These materials are synthesized by conversion reactions through which the creation of hybrid metal telluride powders becomes feasible.

Manganese has unique polymorph crystals, which are very good conductors for electrolytes. These crystals (α-MnS, β-MnS, and γ-MnS) are undoubtedly among the best materials for supercapacitor electrodes. These are made to perform through a one-pot template-free solvothermal method in which hollow α-MnS spheres are created which have a porous shell. This combination creates a stable specific capacity of 430 mAh/g after 20 cycles at a current density of 0.2 A/g [54]. As compared to the theoretical capacity of pure MnS nanoparticles and graphene, this capacitance is much higher. Hence, with the addition of this MnS, the efficiency of an FSC increases.

Cobalt can be used to produce high-performance metal sulfides like CoS_2, Co_3S_4, CoS, and Co_9S_8, which are promising anode materials with high potential capacities. Many cobalt sulfides have nanostructures like hollow spheres, cotton-like, rode-like, yolk-shell microspheres, hollow nanospheres, etc. These structures are synthesized to form high electrochemical performance in an SC. It is due to the porous and rough nanostructure of these materials, which becomes suitable for diffusing lithium-ions during the charge/discharge process. Nickel sulfide (NiS) composites for the graphene-based SCs are synthesized through a two-step method that results in the creation of Ni_3S_2-rGO. This process creates a nanoslice structure of NiS, which shows a high-performance rate when used in an SC. It is because nickel sulfides have varying molecular formulas and crystal forms, which influence the formation of Ni_3S_4 nanoprisms for graphene.

4.3 Metal Oxide-Based Flexible Supercapacitors

Single metal oxide like MnO_2 and compound metal oxides like $NiCo_2O_4$ constitute the organic constituents. These have large-conductance changes associated with their transformation. In this regard, transition metal oxides are chosen for flexible supercapacitors because they have a good (a) charge storage material and capacity, (b) proper structure for making graphene more efficient, and (c) mechanical properties to support graphene-based electrodes [55]. Due to these properties, the transition metal oxides can turn into various forms and structures that support the mechanism of different types of supercapacitors, i.e., symmetric or asymmetric, etc., as projected in Fig. 8.

Nickel oxide (NiO) appears the most promising element for being installed in an SC among all metal oxides, which is because of its easy oxidation process. This process involves a hydrothermal method through which the elements show very high capacitance, i.e., 1016 F/g, and excellent cycling stability even after 5000 cycles with capacitance retention of 94.9%. These materials show very impressive charge transport and electrolyte diffusion in a 3D conductive graphene sheet [57].

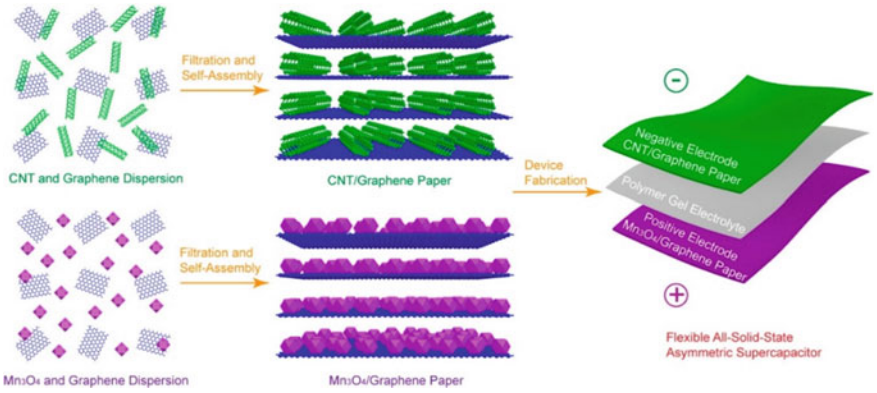

Fig. 8 Flexible SC based on transition metal-oxide electrode. Adapted with permission from reference [56], Copyright 2012, American Chemical Society

4.3.1 Metal Oxides and Their Composites for Flexible Supercapacitor

One of the best choices for strengthening the mechanism of graphene is the use of metal oxide composites. These composites also increase the interaction between metal matrix and graphene, making them more stable and reliable [58]. Some of these metal oxide composites include are as follows.

Magnesium composite for graphene is created by the combination of two techniques, such as hot-pressed sintering and ball-milling. Through these techniques, the mechanical characteristics of the composite are also enhanced. In the aerospace and automotive industries, magnesium and its alloys have a huge application due to their outstanding damping capacity and low mass density.Hence, the addition of graphene enhances the mechanical strength and chemical properties of all materials along with increasing the capacitance capability of an SC.

Copper-graphene composite is combined with graphene oxide (GO) through a laser vapor deposition process. This process makes the graphene electrode more active and electrically charged. Nickel-graphene composites are carbon-stable materials. They are used in graphene sheets through the process of nickel-plating using $NiSO_4$ solution. The microstructure of Ni-graphene composites is usually used as catalysts for capacitance increase as they have a permeable shape, particular big region, and they can constantly absorb Ni particles on the film surface of graphene. Tungsten oxide composites are electrochemically stable n-type metal oxide. It has effective applications in gas detectors, energy storage devices, photo-catalyst, and electrochromic tungsten oxide products. Nanostructured tungsten oxides as electrode components are seen to exhibit refined electrochemical competence, mainly due to their low charge movement resistance and significant surface area.

Titanium di-oxide composite has been considered to be one of the best compounds for super-capacitor electrodes. It is because of their unique features of having high chemical stability, non-toxicity, low manufacture cost, easy availability, and a large

surface area. Thus, titanium dioxide composite is best suited for the production of large energy storage devices, especially due to its highly enhanced power sensitivity rate. In contrast to other noble metals or nanostructures of metal oxides, copper oxide composite is one of the low price intercalation materials, which is due to its impressive features like best capacitive properties, easy availability, low price, and less toxicity. It has a wide application stream, such as being in active anode materials, superconductors, sensors, and heterogeneous catalysts. Hence, the graphene–Cu–O composite is created through a hydrothermal method which is guided by ammonium solution present in the supercapacitors. Zinc is an element that is used as a composite for the graphene electrodes for their ability to change the power and performance of the electrode materials. When combined with reduced-graphene oxide, the zinc oxide nanoparticles strengthen the graphene material for the electrodes that show a high electric charge rate and specific current. Also, zinc has a low resistance and improved ion diffusion capacity, ultimately responsible for enhanced capacitance.

Manganese monoxides are crystalline with a high specific thickness and manageable particle size and morphology. This makes them good electrical conductors, which ultimately enhance the speed, capacity, and cycling strength of the electrode materials. Similarly, the structure of compounds based on MnO_2 can be further enhanced by using conductive substances like conductive polymers, nanofibers/spheres, flexible metal substrates, and carbon nanotubes [59]. To sum up, metal oxide-graphene-based composites have enormous utilizations. These show unique characteristics like being highly accessible for metal matrix nanocomposites, which increase the performance of SCs.

4.4 Conducting Polymer-Based Flexible Supercapacitors

Conducting polymers (CPs) are known for their intrinsic properties of formed structures and compositions through controlled synthesis processes. These are typically formed by chemical or electrochemical polymerization methods. Figure 9 shows these different methods, which result in various conducting polymer composites for electrode materials. Due to the outstanding processability, insulating nature, and low-cost qualities, CPs are used in the manufacturing of many devices.

CPs exhibit reliable characteristics that are needed for stable electrochemical energy storage. However, they have low stability under charge/discharge situations. Therefore, with the inclusion of graphene to change the molecular conformation and orientation of CP chains, a positive effect on the composites is observed. In other words, the combination of CP and Gr creates a high surface area, structural uniformity, a short distance for ion transfer, considerable structural diversity, and a controllable morphology. Hence, through asymmetric configurations, CPs can expand the voltage of the supercapacitor to achieve maximum potential energy, which makes it more effective in its overall performance.

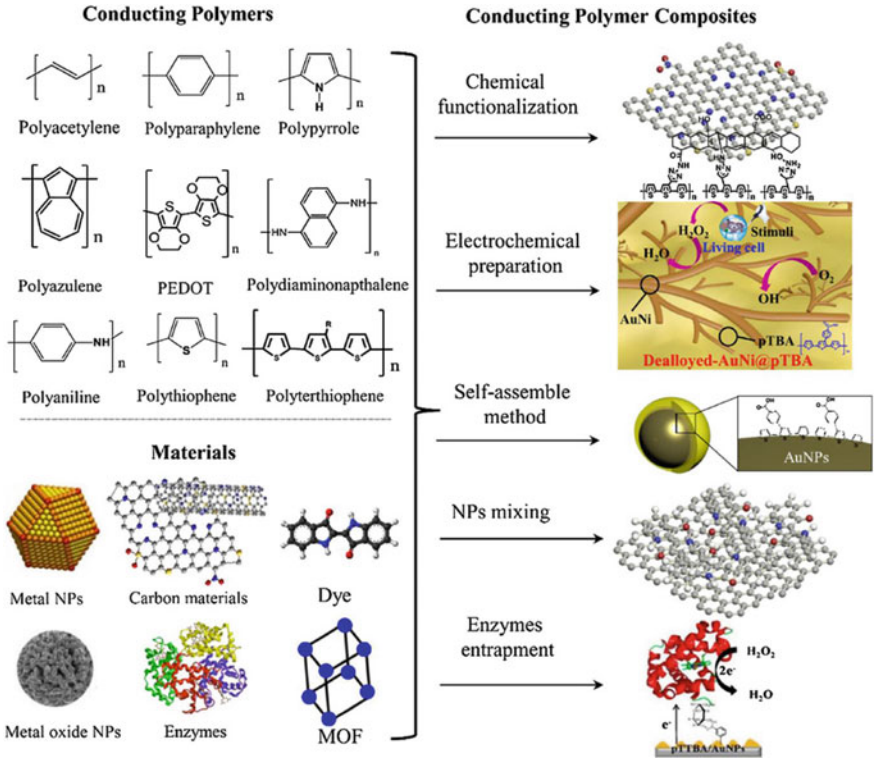

Fig. 9 Composite materials for various conducting polymers. Adapted with permission from reference [60] Copyright 2017, Elsevier

4.4.1 Conducting Polymer and Its Composites for Flexible Supercapacitor

Conductive polymers can be useful in various commercial applications such as supercapacitors and solar energy conversion devices. Such polymers with electrical conductivity mainly include polyacetylene, which is considered important owing to their exceptional chemical and electrical properties. The conducting polymer-based composites of graphene are responsible for high load-bearing membrane applications. These membranes are made with layered graphene polymer films and are created by either covalent or non-covalent nanosheets with 2D models for polymer ornaments. These composites increase the solubility of graphene materials. Through a sonochemical process, the conducting polymers can be combined to fill the pores of activated carbon powder. This method increases the capacitance of electrodes three times. Some of the composites of conducting polymer are as follows. Thermally reduced graphene nano-fillers have a potentially high capability to impart conductivity to polymers compared to carbon nanotubes. During the process, the conductive fillers were added into the non-mixable polymer blend, resulting in the

selective localization of the nano-fillers. That is how they maintain their conductivity, enhanced by the nano-fillers, which results in high-performance electrodes. Graphene nanoparticles are created by various methods, including the combination of rGO and thermally reduced graphene nano-fillers, which enhance the filler quality for high performance.

Carbon-based polymer nanocomposites are highly responsible for enhancing the capacitance in photovoltaic (PV) cells and supercapacitors. It happens because, in a solar cell, merely a conductive electrode is enough for producing energy output. For instance, materials like Indium tin oxide (ITO) and fluorine tin oxide (FTO) work well as conductive electrodes for PV devices. For the creation of carbon-based polymer nanocomposites, a smooth process of the dispersion of nanoparticles in a polymer matrix must happen uninterruptedly. This process will determine the success of the nano-composites creation, which occurs through a solution mixing method, resulting in the strengthening of the fillers. During this process, the physical properties of carbon-based polymer nanocomposites can be changed. It is usually due to the nano-filler dispersion capacity and the capacity of carbon nanotubes as fillers. The high-filler content composites in carbon-based polymers are used in many applications, in many forms. This is due to the high mechanical and electrical properties of these carbon-based polymer nanocomposites.

Carbon nanotubes (CNTs) are often used as the material for the double-layered electrochemical supercapacitors owing to their high surface area, strong electrical properties, good mechanical strength, and good spatial structure. CNTs help increase composites' conductivity by 10^6 S/m, which is the best rate among all nanocomposites. Similarly, graphene-based polymer composites also have a remarkable electrical conductivity, as they have a combination of reduced graphene oxides and graphites.

Di-electric polymer composites are composites that have low thermal conductivity but have significant thermal insulation. However, the thermal conductivity of polymeric materials can be increased by adding boron nitride, silicon nitride, and aluminum oxide fillers. Factors like intrinsic thermal conductance matrix and filler size or type define the conductivity and thermal capacity of the polymers. Also, with surface treatment methods, not just the thermal conductivity of filler particles can be improved, but the polymer matrix and the filler can be smoothly synthesized and combined. This process is demonstrated in Fig. 10, in which the thermal resistance decreases while the conductivity of the electrode increases.

Silica–carbon-epoxy resin composite is known for its high conductivity. Adding this composite into the polymer materials can enhance the conductivity of all other composites. Hence, the introduction of silica increases the conductivity of the composites due to strong conductive networks made of carbon black particles, which become activated with the addition of silica. Therefore, silica can increase the performance of electrodes in a flexible supercapacitor. Similarly, as shown in Fig. 11, sulfuric acid and potassium permanganate oxidation combination result in the creation of graphite oxide, which has the same effect as that of silica–carbon composite on the graphene electrodes.

Conductive polymers have become an important aspect of the development of electrochemical electrode materials as they can be obtained with low cost, high

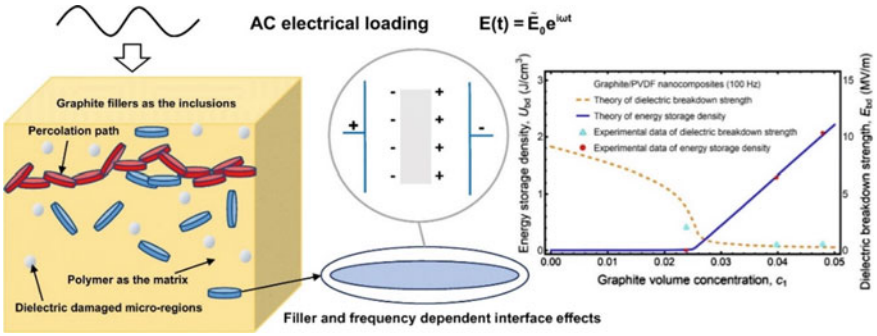

Fig. 10 Overview of the dielectric breakdown strength and energy storage density in polymer composites. Adapted with permission from reference [59] Copyright 2020, Elsevier

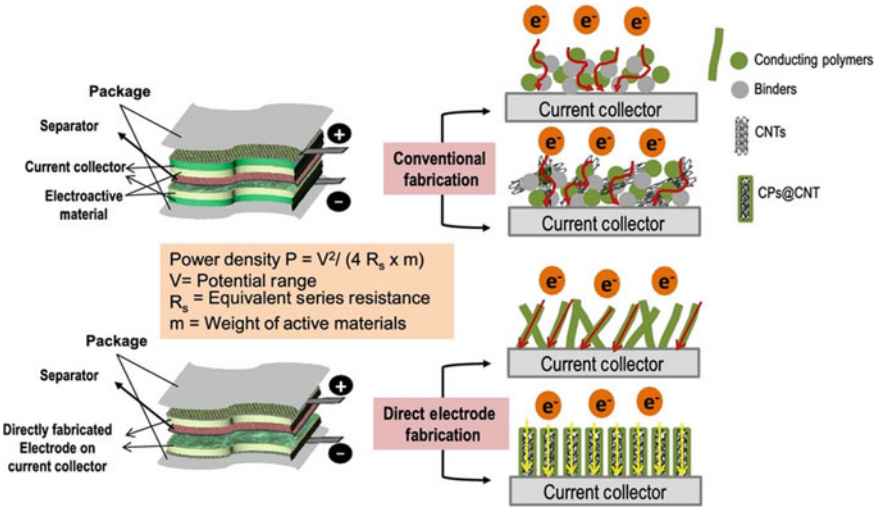

Fig. 11 Schematic diagram of the CPs-based flexible electrode fabrication process. Adapted from reference [61]. This is an open-access article distributed under the terms of the Creative Commons CC-BY license

conductivity, high environmental stability, high charge storage capacity, and excellent reversibility. These features have made them highly in-demand among the manufacturers of electronics. However, for further improvement in the future, 3D conductive polymer-based composite materials will be required, which could reduce the ion transport distances and the electrochemical resistivity. Thus, the conductive polymers can be further optimized for effective flexible supercapacitors in the future, making the SCs much more efficient and durable. Figure 12 shows some of the applications of flexible supercapacitors in terms of charge storage and distribution. Flexible supercapacitor used in the devices includes wearable wristband with LED

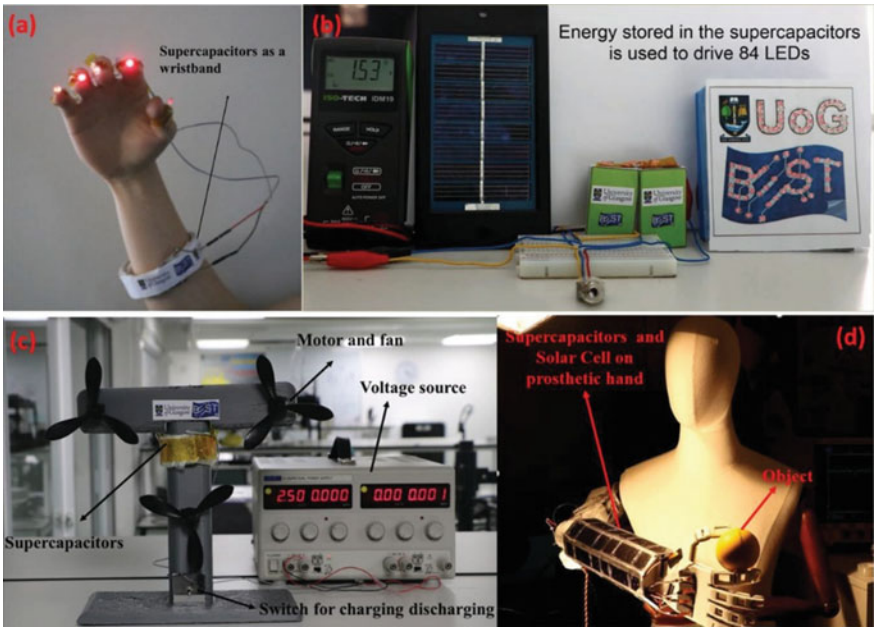

Fig. 12 Pictorial illustration for the application of FSC in various devices. Adapted from reference [62]. This is an open-access article distributed under the terms of the Creative Commons CC-BY license

lights, self-powered power pack system, and FSC used with addition to the solar cell for the operation of the prosthetic hand.

5 Conclusion

Energy is one of the most important things for human survival, and therefore, efforts have been put into place for its maximum conservation as the non-renewable sources of energy are rapidly depleting. With recent innovative upgrades in the field of energy storage, flexible electronics have been created that work with FSCs. These FSCs work with the help of many electrode materials that are responsible for enhancing their conductivity and performance in flexible devices. For instance, graphene, carbon nanotubes (CNTs), activated carbon (AC), carbon fiber-cloth, conducting polymers, transition-metal oxides, etc., are the materials used for increasing electrode power. These composites are responsible for managing the life cycles, conductivity, electrical ability, and durability of the anode charges in an SC. Various materials and innovative methods are being employed for enhancing the performances of FSCs and FSC-based devices for future application. For instance, big companies like electric vehicles, electronic wearable devices, and smart and flexible screen manufacturers are already

incorporating supercapacitor technology for better device performance. Hence, the advanced SCs will be incorporated in the new rail transit systems, smart meters and trackers, hybrid automotive, power grid tools, wind turbines, and military machinery, which will significantly boost the use of FSCs in the future.

References

1. M. Javid, Review article-renewable energies. Energy Proc. **74**, 1289–1297 (2015)
2. O.P. Asantewaa, A.-S. Samuel, A review of renewable energy sources, sustainability issues and climate change mitigation. Cogent Eng. **3**, 1–14 (2016)
3. G. Dolf, B. Francisco, S. Deger, D. Bazilian Morgan, W. Nicholas, G. Ricardo, The role of renewable energy in the global energy transformation. Energy Strateg Rev. **24**, 38–50 (2019)
4. P.G. Gautham, S. Nidheesh, T. Simran, B.K.B. Rakshitha, Supercapacitor technology and its applications: a review. IOP Conf. Ser. Mater. Sci. Eng. **561**, 1–11 (2019)
5. R.A. Kumar, D.K. Priyalakshmi, R. Saroj, An overview of energy storage and its importance in Indian renewable energy sector: part I—technologies and comparison. J. Energy Storage **13**, 10–23 (2017)
6. Z. Ahmed, A.L. Shaqsi, S. Kamaruzzaman, A.-H. Amer, Review of energy storage services, applications, limitations, and benefits. Energy Rep. **6**, 288–306 (2020)
7. A. Maryam, S. Ramteen, X. Johnson Jeremiah, A. Keoleian Gregory, The role of energy storage in deep decarbonization of electricity production. Nat. Commun. **10**, 3413 (2019)
8. C. Chukwuka, K.A. Folly, Batteries and super-capacitors. in *IEEE Power and Energy Society Conference and Exposition in Africa: Intelligent Grid Integration of Renewable Energy Resources*, *PowerAfrica* (2012)
9. M. Ram Bhagat, S. Vikrant, S. Raj Kishore, S. Gurmeet, Efficient, sustainable, and clean energy storage in supercapacitors using biomass-derived carbon materials. in *Handbook of Ecomaterials.* (2019), pp. 855–880
10. G. Yiding, Z. Ting, C. Hao, P. Wang Feng, G.C. Yueming, L. Shibin, Mini review on flexible and wearable electronics for monitoring human health information. Nanoscale Res. Lett. **14**, 1–15 (2019)
11. H.S. Alireza, R. Seeram, A.A. Gerhard, Recent progress in flexible-wearable solar cells for self-powered electronic devices. Energy Environ. Sci. **13**, 685–743 (2020)
12. P. Taniya, S. Guneet, K. Dinesh, S. Mandeep, D.R. Sundar, High-performance flexible supercapacitors based on electrochemically tailored three-dimensional reduced graphene oxide networks. Sci. Rep. 1–13 (2018)
13. H. Nicholas, Y. Sheng, B. Stephen, ScienceDirect the good, the bad and the porous : a review of carbonaceous materials for flexible supercapacitor applications. Energy Rep. **6**, 148–156 (2020)
14. X. Shi Shan, Y.C. Chengjun, D. Li Jia, L.B. Hongda, K. Feiyu, Flexible supercapacitors. Particuology **11**, 371–377 (2013)
15. P. Soubantika, R. Karthik, R.K. Gupta, G. Arunava, Flexible supercapacitors: a materials perspective. Front Mater. **5**, 1–9 (2019)
16. H. Shifei, Z. Xianglin, S. Samrat, Z. Yufeng, Challenges and opportunities for supercapacitors. APL Mater. **7**, 100901 (2019)
17. S. Theresa, K. Mario, S. Michael, P. Ralf, E. Igor, I. Adriana, B. Andreas, P. De Leon, U.M. Carlos, Understanding the charge storage mechanism of conductive polymers as hybrid battery-capacitor materials in ionic liquids by: in situ atomic force microscopy and electrochemical quartz crystal microbalance studies. J. Mater. Chem. A **6**, 17787–17799 (2018)
18. F. Krzysztof, P. Anetta, P. Justyna, M. Jakub, S. Adam, B. Paulina, Revisited insights into charge storage mechanisms in electrochemical capacitors with Li_2SO_4 -based electrolyte. **22**, 1–14 (2019)

19. G. Ander, G. Eider, A. Jon, M. Roman, Review on supercapacitors : technologies and materials. **58**, 1189–1206 (2016)
20. M. Aqib, A.M. Basheer, D. Kalim, T. Jagannathan, A review on recent advances in hybrid supercapacitors: design, fabrication and applications. Renew. Sustain. Energy Rev. **101**, 123–145 (2019)
21. P. Théophile, M. Tedjani, D. Sylvain, F. Damien, U. Wilfried, Sizing of lithium-ion battery/supercapacitor hybrid energy storage system for forklift vehicle. Energies **13**, 4518 (2020)
22. N.A. Echeverry-Montoya, J.J. Prías-Barragán, L. Tirado-Mejía, C. Agudelo, G. Fonthal, H. Ariza-Calderón, Fabrication and electrical response of flexible supercapacitor based on activated carbon from bamboo. Phys. Status Solidi. Curr. Top Solid State Phys. **14**, 1600258 (2017)
23. C. Jayesh, P. Deepak, S.K. Kowsik, T. Jayan, Z. Lei, Flexible supercapacitor electrodes using metal-organic frameworks. Nanoscale **12**, 17649–17662 (2020)
24. P. Dubal Deepak, Advances in flexible supercapacitors for portable and wearable smart gadgets. in *Emerging Materials for Energy Conversion and Storage* (Elsevier Inc., 2018), pp. 209–246
25. H. Chi-yuen, K. Chi-wai, M. Chee-leung, C. Kam-hong, Flexible energy storage system—an introductory. Processes **7**, 922 (2019)
26. A. Gowrisankar, T. Saravanakumar, T. Selvaraju, in *Graphene-Based Composite Materials For Flexible Supercapacitors.* (Elsevier Inc., 2020)
27. X. Jinghao, W. Tao Peng, X.C. Zhengmei, L. Xiaoping, N. Shuangxi, Nanocellulose-graphene composites: a promising nanomaterial for flexible supercapacitors. Carbohydr Polym. **207**, 447–459 (2019)
28. Y. Shihong, T. Hao, G. Zhenzhen, L. Bai Wenlong, W.J. Liang, Z. Xiaogang, Fabrication of flexible nanoporous nitrogen-doped graphene film for high-performance supercapacitors. J. Solid State Electrochem. **21**, 1653–1663 (2017)
29. M. Libu, N.C. García, D. Wenting, D. Ravinder, Flexible self-charging supercapacitor based on graphene-Ag-3D graphene foam electrodes. Nano Energy **51**, 604–612 (2018)
30. K. Azmatullah, J.E. Szulejko, S. Pallabi, K.K. Hyun, E. Wonsik, S.B. Ambade, H.T. Hee, The effect of diverse metal oxides in graphene composites on the adsorption isotherm of gaseous benzene. Environ. Res. **172**, 367–374 (2019)
31. N. Debabrata, M.V. Balaji, K. Bhowmick Anil, B. Debes, Metal/metal oxide decorated graphene synthesis and application as supercapacitor: a review. J. Mater. Sci. **55**, 6375–6400 (2020)
32. A. Saleh Tawfik, F. Ganjar, Recent trends in the design of chemical sensors based on graphene–metal oxide nanocomposites for the analysis of toxic species and biomolecules. TrAC—Trends Anal. Chem. **120**, 115660 (2019)
33. K. Anish, J. Mohammad, N. Bernaurdshaw, M. Asiri Abdullah, in Graphene Functionalization Strategies: From Synthesis to Applications (Springer, 2019)
34. J. Sarika, R.S. Kalubarme, T. Chiaki, B.B. Kale, G. Vijay, F. Akira, S.W. Gosavi, Manganese dioxide/ reduced graphene oxide composite an electrode material for high-performance solid state supercapacitor. Electrochim. Acta **299**, 34–44 (2019)
35. C.B. Meng, A.N.H. Nabilah, A.M.A.A. Mohd, S. Yusran, Supercapacitive performance of N-doped graphene/Mn_3O_4/Fe_3O_4 as an electrode material. Appl. Sci. **9**, 1040 (2019)
36. D. Suzi, T. Verawati, F.H. Ming, R. Tan Hui, C. Sayle Dean, O. Malini, M. Subodh, W. Jun, S.C. Haur, Reduced graphene oxide conjugated Cu_2O nanowire mesocrystals for high-performance NO_2 gas sensor. J. Am. Chem. Soc. **134**, 4905–4917 (2012)
37. C. Engin, B. Dustin, O. Oluwatosin, L. Ross, S. Kaushlendra, S. Litha, M. Sabolsky Edward, Performance of activated carbons synthesized from fruit dehydration biowastes for supercapacitor applications. Environ. Prog. Sustain. Energy **38**, 0–2 (2019)
38. K. Sonia, I. Nazmul, Organic and medicinal chem IJ carbon nanotubes-properties and applications. Org. Med. Chem. Int. J. **7**, 1–6 (2018)
39. A. Kinloch Ian, S. Jonghwan, L. Jun, J. Young Robert, M. Ajayan Pulickel, Composites with carbon nanotubes and graphene: an outlook. **553**, 547–553 (2018)

40. W. Wang Zhuqing, W.J. Shasha, Y. Along, W. Gang, Carbon nanofiber-based functional nanomaterials for sensor applications. Nanomaterials **9**, 1045 (2019)
41. T. Jayaraman, K. Karuppasamy, D. Govindarajan, R.A. ul Hassan Sarwar, A. Prabhakarn, S. Kirubanandam, K. Parasuraman, K.H. Seok, Recent advances in metal chalcogenides (MX; X = S, Se) nanostructures for electrochemical supercapacitor applications: a brief review. Nanomaterials **8**, 256 (2018)
42. W. Lina, L. Jiajia, A. Li, Z. Li, X. Dai Baosong, J.M. Meng, X.S. Zhao, C. Chuanbao, Z. Jiatao, Z. Hesun, Rigid three-dimensional Ni_3S_4 nanosheet frames: controlled synthesis and their enhanced electrochemical performance. RSC Adv. **5**, 8422–8426 (2015)
43. W. Enli, J. Jingsha, L. Shaowen, L. Dan, G. Shufang, D. Fei, Y. Xuemin, Open a novel preparation of nano-copper chalcogenide (Cu2S) -based flexible counter electrode. Sci. Rep. 1–9 (2019)
44. B. Daniele, C. Daling, Z. Haiguang, R. Federico, V. Alberto, Direct measurement of electronic band structure in single quantum dots of metal chalcogenide composites. **1801668**, 1–9 (2018)
45. S. Weiran, G. Minxuan, W. Jinping, G. Jianfeng, F. Chenwei, A. Eric, L. Handong, W. Zhiming, Tin selenide (SnSe): growth, properties, and applications. Adv. Sci. **5**, 1700602 (2018)
46. L.Y. Woo, K.B. Sung, H. John, L. Juwon, P. Sangyeon, J.H. Sik, W. Dongmok, C. Seungnam, S.J. Inn, K.J. Min, A pseudo-capacitive chalcogenide-based electrode with dense 1-dimensional nanoarrays for enhanced energy density in asymmetric supercapacitors. J. Mater. Chem. A **4**, 10084–10090 (2016)
47. B. Malavekar Dhanaji, C. Lokhande Vaibhav, J. Mane Vikas, B. Kale Shital, N. Bulakhe Ravindra, U.M. Patil, I. Insik, C.D. Lokhande, Facile synthesis of layered reduced graphene oxide–copper sulfide (rGO-CuS) hybrid electrode for all solid-state symmetric supercapacitor. J. Solid State Electrochem. **24**, 2963–2974 (2020)
48. C.J. Sang, L.S. Yeon, L.J. Kul, K.Y. Chan, Iron telluride-decorated reduced graphene oxide hybrid microspheres as anode materials with improved na-ion storage properties. ACS Appl. Mater. Interf. **8**, 21343–21349 (2016)
49. G. Pengbiao, Z. Shasha, T. Hao, Z. Rongmei, Z. Li, C. Shuai, Transition metal sulfides based on graphene for electrochemical energy storage. **1703259**, 1–26 (2018)
50. Q. Fu Lijun, H.R. Qunting, V.V. Kondratiev, W. Yuping, Composites of metal oxides and intrinsically conducting polymers as supercapacitor electrode materials: the best of both worlds? J. Mater. Chem. A **7**, 14937–14970 (2019)
51. J.G. Hwa, B. Seungmin, L. Seungyeol, K.S. Wook, Metal oxide/graphene composites for supercapacitive electrode materials. Chem.–An Asian J. **11**, 949–964 (2016)
52. G. Hongcai, X. Fei, C.C. Bun, D. Hongwei, Flexible all-solid-state asymmetric supercapacitors based on free-standing carbon nanotube/graphene and Mn_3O_4 nanoparticle/graphene paper electrodes. ACS Appl. Mater. Interf. **4**, 7020–7026 (2012)
53. H.S. Zakir, I. Muhammad, H.S. Babar, O.W. Chun, U. Kefayat, A review on graphene based transition metal oxide composites and its application towards supercapacitor electrodes. SN Appl. Sci. **2**, 764 (2020)
54. Z. Chen, J. Xiaoteng, S. Kewei, Y. Changchun, G. Wallace Gordon, W. Caiyun, Conducting polymer composites for unconventional solid-state supercapacitors. J. Mater. Chem. A **8**, 4677–4699 (2020)
55. N.M. Halappa, G.N. Ganesh, S.Y. Bo, Applications of conducting polymer composites to electrochemical sensors: a review. Appl. Mater. Today **9**, 419–433 (2017)
56. Hongcai Gao, Fei Xiao, Chi Bun Ching, and Hongwei Duan, Flexible All-Solid-State Asymmetric Supercapacitors Based on Free-Standing Carbon Nanotube/Graphene and Mn3O4 Nanoparticle/Graphene Paper Electrodes, ACS Appl. Mater. Interfaces 2012, 4, 12, 7020–7026
57. B. Velram, L. Kin-tak, H. David, B. Debes, Graphene-based materials and their composites : a review on production, applications and product limitations. Compos. Part B **142**, 200–220 (2018)
58. M. Muhazri Abd, M. Rashid Norhana, A. Farhana, 22. in *Carbon-Based Polymer Nanocomposite for Photovoltaic Devices*. Elsevier Inc. (2018)

59. X. Xiaodong, X. Bai-Xiang, X. Xiazi, J. Weng George, Modeling the dielectric breakdown strength and energy storage density of graphite-polymer composites with dielectric damage process. Mater. Des. **189**, 108531 (2020)
60. M.H. Naveen, N.G. Gurudatt, Y.B. Shim, Applications of conducting polymer composites to electrochemical sensors: a review. Appl. Mater. Today **9**, 419–433 (2017)
61. S. Indrajit, G. Abhijit, C.L. Chyong, C.K. Hsien, Conducting polymer-based flexible supercapacitor. Energy Sci. Eng. **3**, 2–26 (2015)
62. M. Libu, N.W. Taube, N.C. García, D. Ravinder, Graphene-graphite polyurethane composite based high-energy density flexible supercapacitors. Adv. Sci. **6**, 1802251 (2019)

Flexible Supercapacitors

Hazar Guemiza, Thuan-Nguyen Pham-Truong, Cédric Plesse, Frédéric Vidal, and Pierre-Henri Aubert

Abstract For decades, supercapacitors (SCs) have emerged as a promising technology providing the necessary power that was lacking to batteries and many efforts have been devoted to developing new materials, to design (nano) architectures that considerably improve their performances: energy, density, lifetime, decreased cost, renewable. This success pushes the supercapacitor technology to the next challenges, i.e. development of high-performing flexible SCs to power up imprinted, portable electronics and more recently wearable devices such as light-emitting diodes or flexible screens. This book chapter puts a focus on the strategies to develop electrode (nano-)materials, with help of chemistry, material science, and engineering tools. It will pave the way toward the development of flexible SCs with the perspectives of future research on stretchable SCs, which represents a new target and a real breakthrough in the field of energy storage.

Keywords Flexible supercapacitors · Flexible electrodes · Carbonaceous materials · Conducting polymers · Transition metal oxides · MXenes · Metal and covalent organic frameworks

1 Introduction

Energy storage devices are playing an important part in our lives. In 1990, lithium-ion batteries with high energy densities (180 Wh/kg) were introduced by Sony and are now indispensable in our everyday life. Since then, a lot of efforts have been dedicated to the improvement of their performances [1], especially to increase their energy density and to decrease their charging time. Hence, it is very beneficial for the development of automotive systems and to improve their integration in portable consumer electronic devices (cell phones, tablets, etc.) and their miniaturization (Internet of things, IoT). Energy storage devices require to charge/discharge in a given time that

H. Guemiza · T.-N. Pham-Truong · C. Plesse · F. Vidal · P.-H. Aubert (✉)
CY Cergy Paris Université, LPPI, 5 mail Gay Lussac, site de Neuville, 95000 Cergy-Pontoise, France
e-mail: pierre-henri.aubert@cyu.fr

S. Thomas et al. (eds.), *Nanostructured Materials for Supercapacitors*,
Advances in Material Research and Technology,
https://doi.org/10.1007/978-3-030-99302-3_26

fundamentally governs two key parameters: specific energy (Wh/kg or Wh/l) and specific power (W/kg or W/l). Whilst batteries offer high energy densities (20–150 Wh/kg), they are unable to charge/discharge at a high power rate. Supercapacitors (SCs) appear as ideal solutions thanks to their high power density (1-10 kW/kg) and long cycling lifetime (>1 000 000 cycles) [2]. Since the past decade, intensive investments have been focused on the improvement of their performances [3–6], working mainly on the design of electrodes materials and electrolytes. Commercially available SCs are using carbon materials with highly developed specific surface area to store charges. They operate on the principle of an Electrical Double-Layer Capacitor (EDLC) that can release all its harvested energy within short times, typically from a few seconds to a few minutes, which is complementary to batteries. This behavior is directly related to the faster ion motion at the electrode/electrolyte interface of SCs compared to the much slower bulk insertion reactions with charge transfer in batteries. SCs are almost maintenance-free and display a longer shelf and cycle life, so they are often favored in many electronic applications [7]. Commercially available SCs are commonly found in different configurations such as flat with a single pair of electrodes, wound in a cylindrical case, or stacked in a rectangular case. However, these available packagings are rigid, stiff, and not compliant, making them unsuitable as energy storage devices for the growing and fast-evolving field of flexible electronic systems, including roll-up, bendable displays, portable electronic papers, and wearable personal multi-media [8]. Consequently, significant efforts are nowadays brought to develop flexible, conformable, and even stretchable SCs.

In this chapter, we will focus on the recent developments of active materials suitable for flexible supercapacitors. After an introduction, classical consideration on supercapacitors will be briefly mentioned and will put the first bases on the specifications for SCs flexibility. The following sections will describe the methodologies to obtain flexible SCs from classical carbonaceous materials, typically activated carbons, carbon nanotubes, graphene, and of course their mixtures. Then conducting polymers, metal oxide, as well as emerging material such as Metal Organic Frameworks and MXenes, will be addressed. Finally, a conclusion with perspectives will open the future orientations on the topic.

2 General Considerations on Supercapacitors

2.1 Conventional Supercapacitors

Conventional electrochemical capacitors (Fig. 1a) consist of two metal foils (current collectors), each of them coated with active material of electrodes (positive and negative) separated by an ion-permeable membrane (separator) and an organic or aqueous electrolyte. The expression of capacitance at each electrode (+ or −) is given by the expression:

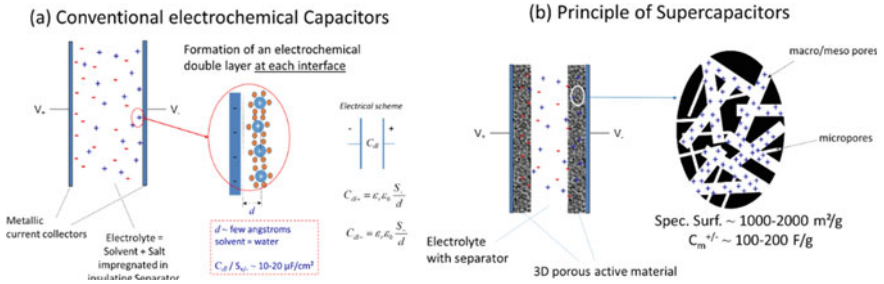

Fig. 1 Schematic representations of conventional electrochemical capacitors **a** with planar electrodes and formation of double-layer capacitance and supercapacitors **b** where the porous material at each electrode increases the specific surface. Usually macro (>50 nm) and meso (2–50 nm) pores are accessible by ions whilst micro pores (<2 nm) aren't, except in specific cases where the geometry of ions fits the micropore size

$$C_{dl}^{+/-} = \varepsilon_r \varepsilon_0 S^{+/-}/d \tag{1}$$

where ε_r is the relative permittivity of electrolyte, ε_0 is vacuum permittivity, S is surface of electrode and d is electrochemical double layer thickness. With classical values (solvent = water, and d = few Angtröms) the typical surface double layer capacitances are in the range of 10–20 $\mu F\,cm^{-2}$ [9]. Thus the only lever to increase the ion storage at the interface is the available surface area of the active material. For this, SCs are a class of electrochemical capacitors where an electrode is made of 3D porous material typically activated carbon (Fig. 1b) exhibiting 1000–2000 $m^2\,g^{-1}$ according to their preparation. According to these specifications, the specific capacitance $C_m^{\pm}$ of an electrode can reach theoretically 200 $F\,g^{-1}$ but experimentally, the real surface area of activated carbons seen by ions is lower, limiting the capacitance to 100 $F\,g^{-1}$.

The specific energy stored in a supercapacitor is given by the relation $E_m = 1/2\ C_{sc} \times \Delta V^2_{max}$ where C_{sc} is the specific capacitance ($F\,g^{-1}$) of the SC ($C_{sc} = 1/4\ C_{m\pm}$), ΔV_{max} is the maximum voltage supported by the SC, usually limited by the electrochemical window (EW) of the electrolyte (1.2–1.8 V in aqueous media, 2.7 V in organic solvent like acetonitrile). To improve the performances (specific energy E_m and specific power $P_m = E_m$/ discharge _time), state-of-the-art researches focus on three main areas:

- Electrode material by increasing the specific capacitance of 3D materials: this trend focuses first on the improvement and control of the pore size of the materials [2, 10] leading to the use of other forms of carbon materials such as Carbon Derived Carbides (CDCs) [11–13]. The latter exhibits more control in the pore size distribution. Hence, the specific surface area is considerably increased, as long as ionic species are correctly selected [14]. Other materials of interest are carbon onions, carbon nanotubes (CNTs) such as multi- and single-walled [15–18]. More interestingly, vertically aligned CNTs [16, 19–22] afford straight diffusion paths to the ionic species, clearly improving the rates of charge/discharge.

In addition, graphene has already proven its suitability as an electrode material with enhanced performance [23–28]. These materials are certainly the most promising in their category since they afford good interface with electrolyte (both sides are free for ions adsorption in contrast with CNTs), have high electronic conductivities, and are easily solution-processable to be cast as electrode materials. CNTs and graphene are usually combined [29–31] to improve ionic pathways inside 3D porous nanocomposites. Finally, to enhance the specific capacitance, nothing is more effective than adding redox reactions at the interface; hence pseudo-capacitive materials such as metal oxides or conducting polymers have demonstrated their potentialities in this field as long as they are mixed as composite electrodes with carbon materials (activated carbons, CNTs or graphene with Polypyrrole, Polythiophenes, Polyaniline [32–44].

- Electrolytes to increase the EW by use of organic-based electrolytes. Typically, the replacement of water has considerably increased the potential window but often at the expense of specific capacitance that drops due to the lower permittivity of these solvents compared to that of water. If acetonitrile, propylene carbonate, γ-butyrolactone [45–47] have advantageously replaced water, they still come up against safety considerations due to flammability and/or leakages issues. Ionic liquids are also interesting with even larger EW (up to 5 V) [48]. For a long time they suffered from high cost and high viscosities but recent research tends to demonstrate their potential interest in EDLCs [2, 49, 50]. Nowadays, a general trend in electrolyte research is focused on polyelectrolytes [51], gel-based electrolytes, quasi-solid, and all-solid electrolytes [52–54].
- Electrical Serial Resistance (ESR) to improve power capabilities. If ESR is mainly depending on a good ionic conductivity (>1 mS/cm) of the electrolyte, all interfacial issues are also of interest to decrease ESR: [55] manufacture of electrodes, interfacial resistance between the active material and the electrolyte, or with the current collector are all parameters that have to be taken into consideration.

2.2 Structural and Architectural Insight for Flexible Supercapacitors

All the above-mentioned aspects contribute to intensive research focusing on the improvement of energy storage performances. However, as mentioned earlier, the mechanical properties of the resulting devices must also be considered to answer to the growing need for soft electronics for which the rigid bulky cases of commercially available SCs appear unsuitable. The development of flexible SCs combining not only excellent electrochemical performance but also high mechanical integrity when bending, folding, or even rolling with a compact lightweight design has become a crucial target. To illustrate this, Fig. 2 shows the number of publications on this rapidly growing field (source: Web of Science, keywords: supercapacitors and (flexible < or > stretchable < or > wearable). Among the 1900 papers, 39 are reviews and 84 are highly cited in the field. The topic unites materials, nanoscience, electrochemistry, physics,

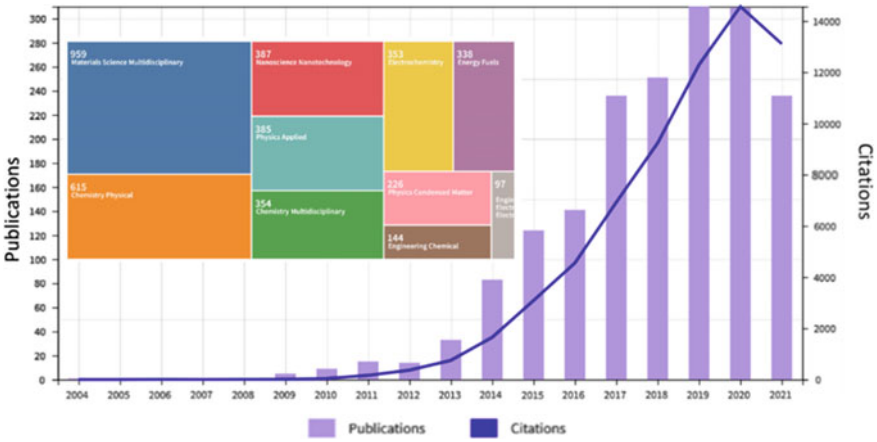

Fig. 2 Bibliometrics on the topic "supercapacitors" using the keywords "flexible", "wearable", "stretchable"

and engineering domains. Since 2015, >100 publications per year are produced (>300 since 2019) and the total citation reaches 15 000 per year.

The development of flexible energy storage devices requires considering several elements. Firstly, all materials, being inorganic or organic, can support bending to some extent. This ability is correlated to the material's mechanical properties but also, and most importantly, to the thickness of the material. Indeed, bendability and flexibility increase significantly with the reduction of the thickness as experienced when comparing a stiff, bulky, and poorly deformable aluminum piece with bendable and rollable aluminum foil while they both present the same Young's modulus. It can be explained by estimating the strain (ε) experienced by a material in the bending direction which can be calculated by the ratio of the thickness of the layer h to twice the radius of curvature, $2r$ [56]. Significantly decreasing the thickness of the layer will proportionally decrease the resulting strain leading to the possibility of large bending deformations even for stiff materials.

However, when considering electrochemical devices such as SCs, this simple solution reaches rapidly some limits. Indeed, SCs are composed of multiple layers (current collectors, active material, separator + electrolyte, encapsulating layers, etc.) which can limit the accessible decrease of thickness. Moreover, if bendability and flexibility could be achieved by the development of ultrathin multilayer SCs, the resulting energy stored per surface area would become too low for many practical applications. It is then necessary to consider also the mechanical properties of each component. Among them, the active layer materials are the main focus of research efforts since they are mostly made of stiff carbon microstructures that need to remain thick enough for large energy storage per surface area. Consequently, they can easily break, crack or peel away from the current collector, upon repetitive bending, twists or stretching, a non-reversible process, except in a few cases like with self-healable

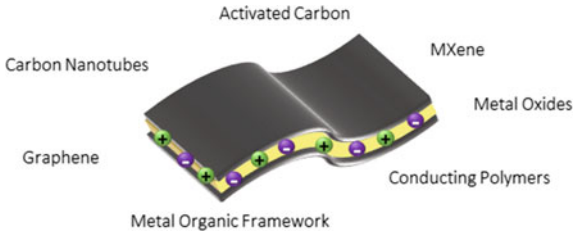

Fig.3 Summary of nanomaterials for flexible supercapacitors

materials [51, 57, 58]. For the development of high-performance flexible supercapacitors, novel configuration designs are required but also novel electrode materials, with or without binder and/or inert conductive additives, since their mechanical flexibility would be not only an extra advantage but becomes a prerequisite [59]. The following parts will then present the recent developments of flexible electrode materials for the very active field of flexible SCs. More specifically, it will focus on carbon-based materials (activated carbon (AC), CNTs, graphene, and their composites), electronic conducting polymers, metal oxide, and metal–organic framework (MOF) (Fig. 3). Finally, general considerations on the future of flexible SCs, i.e. turning flexible devices into stretchable ones, will be discussed.

3 From Material Engineering to Fabrication of Flexible Supercapacitors

3.1 Carbone-Based Materials

Carbon materials have a variety of geometric shapes from a macroscopic point of view, such as zero-dimensional fullerene or carbon nanoparticles, one-dimensional CNTs or carbon fibers (CFs), and two-dimensional graphene or graphite sheets. Carbon nanoparticles, graphene, and CNTs have been widely used for the fabrication of freestanding SC. With their high-developed surface, intrinsic conductivity, and high aspect ratio they are naturally good candidates for flexible electrodes. Intrinsically, casual material developed for rigid SCs can be used to develop flexible SCs prototypes as long as the symmetric configuration (Al/AC||membrane||AC/Al) is sandwiched inside a flexible encapsulation such as transparent tape [60]. If performances are maintained compared to rigid devices, the application requires to store more energy and for that point of view, the nano structuration, or addition of extra-active material is important. For example, flax is a waste product in the industry and can be recycled to produce flexible carbon fibers after the pyrolysis step [61], keeping the mechanical properties of the initial flax (Fig. 4a–b). The pyrolyzed flax has intrinsically EDLCs behavior but exhibits low capacitances near 1 F g^{-1}. Nevertheless, the material has good capacitance retention (100% after 8 000 cycles) and the authors

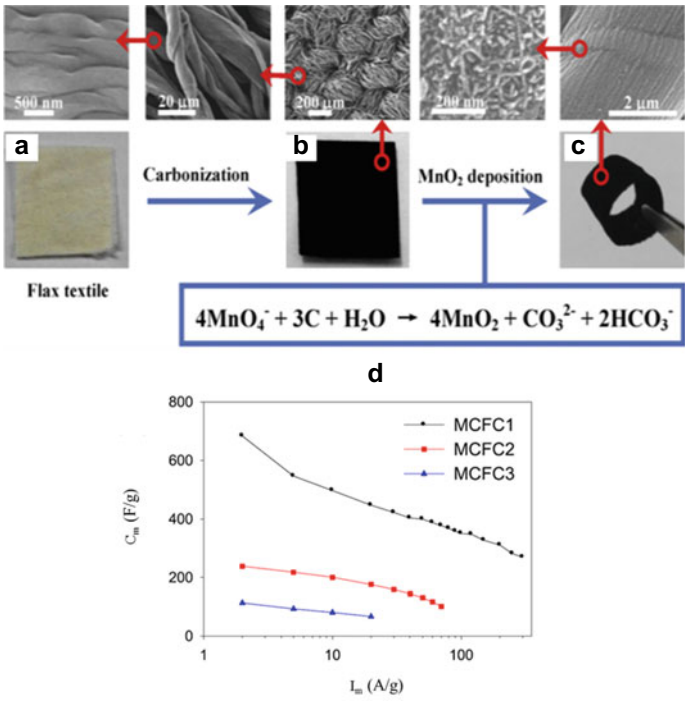

Fig. 4 **a** Flax textile before **a**, after **b** carbonization and **c** after MnO_2 deposition. Top SEM pictures enlarge the surface of the carbonized flax and MnO_2-decorated flax. **d** Evolution of specific capacitance C_m (F g^{-1}) upon gravimetric current I_m (A g^{-1}) for different MnO_2 loadings. Reproduced with permission [61]. Copyright 2015, Elsevier

added pseudocapacitive material, such as MnO_2 fabricated in situ from $KMnO_4$ treatment onto the pyrolyzed flax fibers. Such composition still maintains the flexibility of the electrode since the electrode can be entirely rolled-up (Fig. 4c). and they observed, of course, a huge improvement in the capacitance (684 F g^{-1}). Moreover, different MnO_2-modified materials (MCFC1 MCFC2 and MCFC3, Fig. 4d) with increased MnO_2 composition show extremely high rate capabilities with c.a. 300F g^{-1} @300A/s. If the study concludes that carbon cloth derived from flax can offer a low-cost material for the facile, cost-efficient and large-scale fabrication of binder-free electrode materials, it also highlights that after a first modification (pyrolysis of a flax) the carbonaceous flax is still flexible.

Activation of carbon fibers is also an interesting route. Carbon cloths (CC) are inexpensive and conductive textiles and are good candidates as a substrate for assembling EDLCs due to their very good mechanical properties and electrochemical compatibility. However, the wide possibility of application is significantly hampered by their low specific capacitance. It is possible to increase the capacitance by several

techniques, mainly using thermal activation, such as for common carbonaceous materials. Thus Wang et al. [62] have increased 800 folds the areal capacitance of commercial carbon-cloths by thermal activation to reach up to 933 mF cm^{-2} with $NaBF_4$ electrolyte. BET experiment shows that the heat treatment allows generating macropores (1^{-2} nm) by oxidation of carbon in the structure of CC, with a specific BET surface passing from 28 m^2 g^{-1} to 698 m^2 g^{-1}. Moreover, the increased surface area is mainly contributed by micropores. Here, not only focusing on the enhancement of capacitance performances, the authors play with the macroporosity of the CC to stack 2 × 4 electrodes to build 3.3 F cm^{-2} flexible SC with energy and power densities of 740 μWh/cm^2 and 9000 μW/cm^2. Good capacitance retention (95.2%) is observed after 10 000 charge/discharge cycles, showing outstanding cycle durability of the flexible SC. No bending tests were done but the work offers a foolproof and scalable method to prepare flexible electrode materials for wearable energy storage devices. One particularity of carbonaceous materials stands in the possibility to prepare inks, then to obtain thin films via different techniques like vacuum filtration through membranes, spraying, casting, printing on flexible substrates, etc. In this context, flexible electrodes can be prepared with CNTs or graphene or a mix of both. Single-walled Carbon nanotube (SWCNT) thin-film electrodes and flexible SCs were described by Yuksel et al. [63] Typically SWCNTs were filtered on polydimethylsiloxane substrates by vacuum filtration followed by a stamping method. The binder-free electrodes were assembled in a symmetric configuration with gel electrolyte ($TBAPF_6$:PMMA:PC:ACN)[1] in a ratio of 3:7:20:70) to achieve a solid-state SC. With a specific capacitance of 34.2 F g^{-1}, the power density of the SC reaches 41.5 kW kg^{-1} and shows good capacity retention (94%) upon cycling. Concerning the mechanical tests, SWCNT bucky-paper electrodes do not show any change of resistivity when submitted to bending stress. Moreover, the CV test exhibit the same rectangular shape upon bending at different radius curvature, from $r =$ infinite (flat) to $r = 13$ mm then 9 mm and finally 6 mm. Additionally, the low content of SWCNTs allows good optical transparency of 82% and opens the route to capacitive transparent electrodes for the next generation of flexible displays. Xi et al. [64] fabricated micro-SC with interdigitated electrodes made of CNT fibers. The *in-plane* arrangement of the SC device is interesting for printing technologies that are cost-effective and allow the large-scale production of printable organic electronics. CNT fibers and yarns were obtained by CVD [65] using a mixture of ethanol, ferrocene, and thiophene at 1150 °C. Assembling onto polydimethylsiloxane (PDMS) as multiple parallel digit electrodes (Fig. 5a), they obtained a solid-state, flexible, "on-chip" SC with H_2SO_4/PVA gel electrolyte. The as-fabricated SCs have demonstrated high flexibility such as folding, rolling, and twisting. For example, after 1 000 bending cycles (curvature radius of 5 mm, parallel to the digits, Fig. 5b) the specific capacitance of the device (11.23 F g^{-1}) is constant even at a smaller radius of 2.5 mm.

Numerous studies report CNT as an active material of flexible SC, one can cite also the work of Hu et al. [66] who prepare SCs of classical cellulosic paper or Sun

[1] $TBAPF_6$: tetrabutylammoniumhexafluorophosphate, PMMA: poly(methyl methacrylate), PC: propylene carbonate and ACN:acetonitrile.

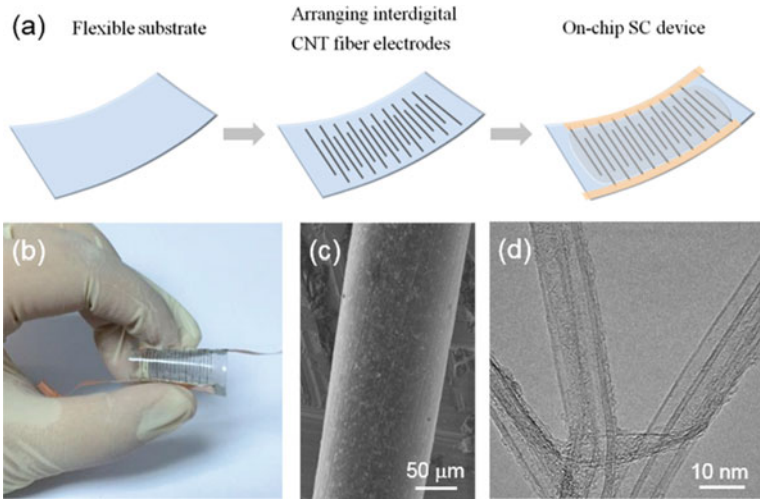

Fig. 5 **a** Fabrication process of all-solid-state supercapacitors, **b** optical picture of supercapacitors, and **c** SEM **d** TEM images of CNT. Reproduced with permission [64], Copyright 2016, Elsevier

et al. [67] who prepared asymmetric fiber-shaped solid-state supercapacitor (FSSC) with AC@CF (negative electrode) and CNT@CF (positive electrode). The FSSC was 8.5 cm long, 2.4 mm thick affording 400mF@5 mA. The bending test demonstrated 80% capacitance retention after 1000 cycles and 100% retention upon repetitive torsion test. This work demonstrates that FSSC would have wide applications for portable devices, smart electronics, implantable medical devices, etc., and highlights the importance of interfacial modification between the fiber current collector and active material, which applies to most of the fiber-shaped solid-state supercapacitors.

Graphene-based materials have proven to be promising for use as an electrode in supercapacitors [24, 26, 68, 69] with their impressive physical and chemical properties: large specific surface area (up to 3100 $m^2.g^{-1}$), good electronic/mechanical properties, and chemical stability, when rolled or stacked. Using chemical activation of exfoliated graphite oxide, a capacitance of 200 F g^{-1} for a single electrode can be reached; graphene-based wearable energy devices are obtained according to different fabrication, such as freestanding electrodes, substrate supported, and graphene-coated conductive/nonconductive substrate electrodes [70]. El-Kady et al. [7] used a standard Light Scribe DVD optical drive to reduce graphene oxide (GO) films to reduced graphene oxide (rGO). The produced films show high electrical conductivity of 1738 S m^{-1} and specific surface area 1520 m^2 g^{-1}, and they are self-standing and mechanically robust. This particularity makes them flexible and they can be used directly as electrodes without the need for binders nor current collectors. The electrode show excellent capacitance of 4.85 mF cm^{-2} (265 F g^{-1}) but, more impressive, the capacitance retention is 40% @1000A g^{-1}!! Flexible SC devices were produced with these electrodes and have an ultrahigh energy density of 1.36 mWh cm^{-3} (associated with ionic liquid), a value that is approximately 2 times

higher than that of the AC-based SCs; also, they possess a high power density of 20 W cm^{-3} to correspond to c.a. 20 times higher compared to that of the AC-based SCs. Mechanical tests were also performed on the corresponding SCs: for example, the measure of capacitance by cyclic voltammetry didn't show any difference when the SC was bent with angles ranging from 0, 30°, 60°…180°. It means that both energy and power capabilities are maintained upon repetitive mechanical strain indicating that they could be used in high-power, flexible electronics.

One of the drawbacks of graphene is the stacking of nanosheets into nanopellets that deny the accessibility of ionic species to the whole surface. To prevent the re-staking after the dispersion/deposition process, the incorporation of nanomaterials as spacers to improve the 3D porous graphene structure has been envisaged. Xu et al. [71] have developed free-standing, mechanically flexible, and binder-free 3D sandwich-type network film electrodes. The active material, i.e. reduced graphene oxide (rGO), is mixed to wrapped helical carbon nanotubes (HCNT) intimately elaborated by a synergistic and applicable self-assembly strategy (Fig. 6a). The resulting architecture efficiently prevents the self-restacking of the rGO sheets with interlayered HCNT acting as conducting spacers. This rGO/HCNT film has excellent mechanical properties and can be bent, twisted, rolled, or folded (Fig. 6b) without visible cracks. The electrode structure provides direct channels for electrolyte ions and ensures high-rate performance. In addition, the HCNT help for the formation of interconnected 3D conducting network architecture to guaranty a highly robust

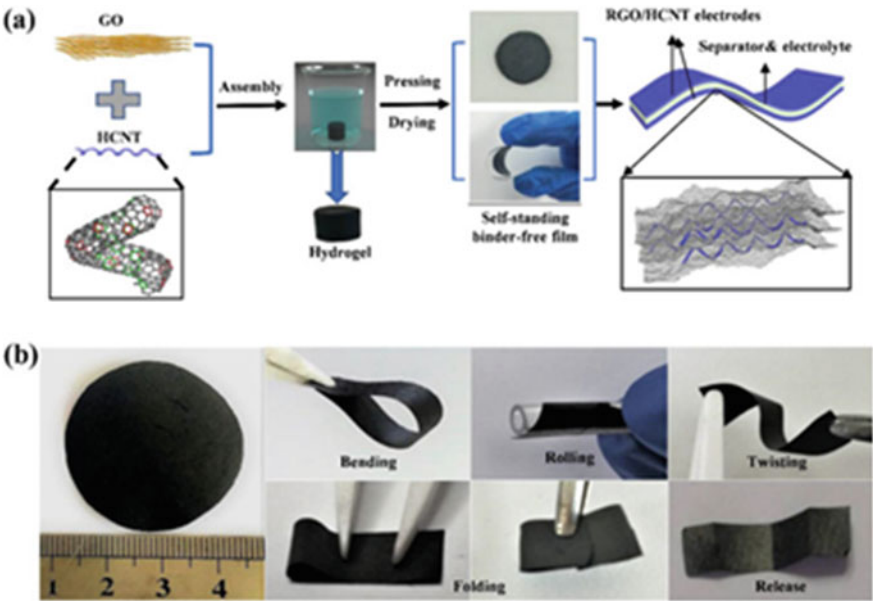

Fig. 6 **a** Schematic illustration for the construction of RGO/HCNT hybrid film. **b** Pictures of the appearance and flexibility testing (bending, rolling, twisting, and folding) of the obtained RGO/HCNT hybrid film. Reproduced from Xu et al. [71] with permission. Copyright 2020, Elsevier

conducting pathway by improving electronic transport while maintaining the architectural integrity. As a result, the as-prepared rGO/HCNT electrodes show excellent electrochemical characteristics, yielding the specific capacitances of 336 F g^{-1} at a current density of 0.25 A g^{-1}, and it offers the energy density of 7.5 Wh kg^{-1} with the corresponding power density of 100 W kg^{-1} as well as excellent cycling stability at approximately 89.5% capacitance retention for 3000 cycles. This novel HCNT materials and design provide a way for the next-generation wearable energy device.

Jiang et al. [72] reports an interesting strategy to form densely packed graphene nanomesh/CNT films (GNCN). The method consists in etching the graphene sheets and subsequently mixing them with CNTs before forming the film by vacuum filtration. The ionic transport is improved in the cross-plane diffusion path but also the in-plane diffusion since CNT act as a spacer between the rGO sheets (Fig. 7a). Furthermore, CNTs significantly improve the hybrid film's electrical and mechanical properties (Fig. 7b and insert) and the GNCN film can be bent and twisted. The GNCN electrode film has a specific capacitance of 294 F g^{-1} (331 F cm^{-3}) at 5 mV s^{-1}, which is better than the rGO alone (185 F g^{-1}) and stands for the best reported combined gravimetric/volumetric values at this stage. The excellent rate capability (200 F g^{-1} at 2 V/s) is confirmed by electrochemical impedance spectroscopy (EIS) and outstanding cycling performance (93% capacitance retention after 5000 cycles) is also reported.

Weng et al. [73] show a simple and scalable method to fabricate graphene cellulose paper (GCP) by vacuum filtration of graphene nanosheets suspension throughout a piece of filter paper. GCP electrode membranes show good electrochemical conductivity and high stability with a decrease of only 6% after being bent 1000 times and a high gravimetric capacitance of 120 F g^{-1} of graphene, with retention > 99% capacitance over 5000 cycles. In addition, the mechanical flexibility of the GCP membrane was examined by using tensile and fatigue tests, stress–strain curve, and in situ resistance change ($\Delta R/R$). The GCP membrane can withstand stress as high as 8.67 MPa with a 3% elongation which is three times higher than that of the G-paper (0.76%), which broke at 5.13 MPa. These findings show that flexible Poly-SCs made of GCP material could be useful as energy storage devices for a variety of flexible, rechargeable, and portable micropower sources. Moreover, Xu et al. [74] have demonstrated the fabrication of flexible solid-state supercapacitors based on 3D graphene hydrogel films with a highly interconnected 3D network structure. Briefly, a modified hydrothermal reduction method was used to prepare graphene hydrogel in the presence of a 2 M ascorbic acid aqueous solution. The mixture was sealed in a Teflon-lined autoclave and kept at 180 °C for 2 h. Once cooled, the as-prepared graphene hydrogel was removed and soaked overnight in a 1 M H_2SO_4 aqueous solution all night. The as-synthesized graphene hydrogel film has a high specific surface area (414 m^2 g^{-1}), with exceptional electrical conductivity of 192 S m^{-1}, and mechanical robustness. All these features make it very promising for flexible SCs. The fabrication of a flexible solid-state SC device using these 3D graphene hydrogels yielded outstanding capacitive performance in H_2SO_4/PVA gel electrolyte. The as-assembled SC achieves a high specific capacitance of 186 F g^{-1} at 1 A g^{-1}, good stability, a high energy density of about 6.5 Wh kg^{-1}, and excellent

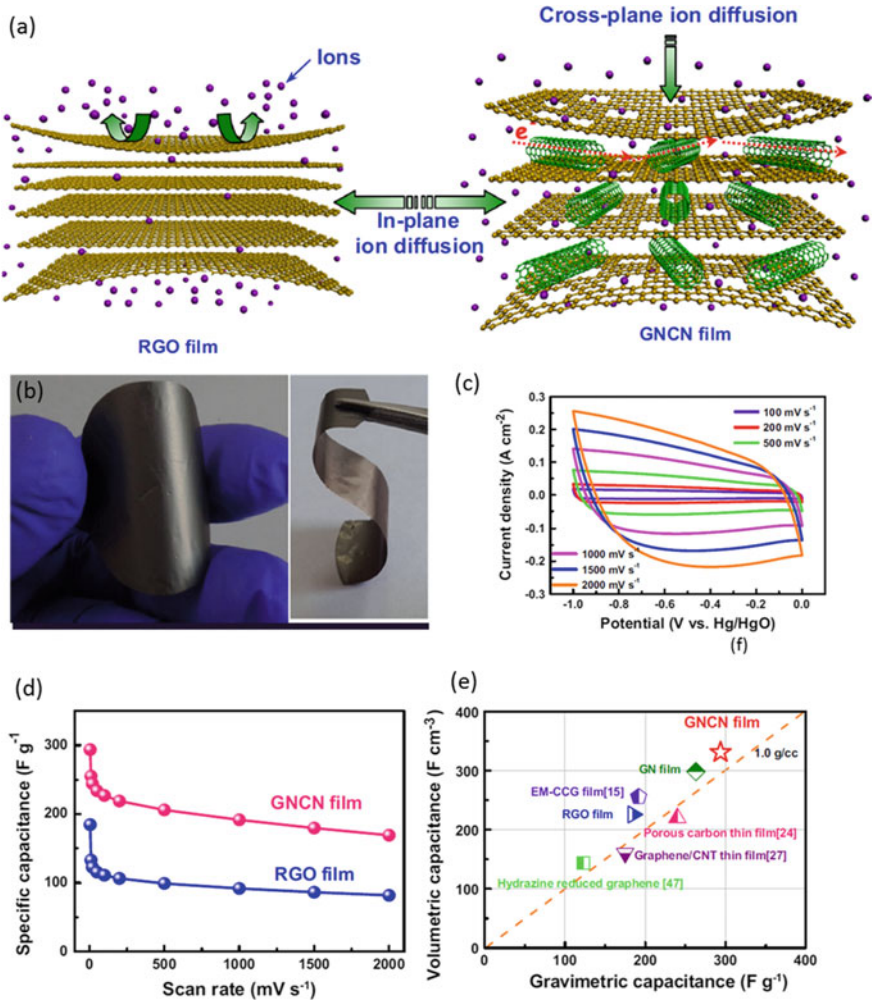

Fig. 7 **a** illustration of the ion diffusion (in-plane and cross (plane) behavior for the rGO film and porous GNCN. **b** Pictures of the GNCN film obtained showing excellent flexibility; **c** Cyclic voltammetry experiments of the GNCN film at low and high scan rates. **d** Evolution of GNCN capacitance as a function of scan rate, compared to rGO films. **e** Volumetric versus gravimetric capacitance comparison of GNCN film electrodes with other carbon electrodes in aqueous electrolytes. Reproduced with permission [72]. Copyright 2015, Elsevier

flexibility, making graphene hydrogel's 3D network structure promising materials for high-performance flexible energy storage devices. Additionally, the use of solid-state ionic liquid electrolytes can also improve the energy density of graphene-based SCs. Tamilarasan et al. [75] reported a mechanically stable, flexible graphene-based all-solid-state SCs with ionic liquid incorporated polyacrylonitrile (PAN/[BMIM][TFSI]) electrolyte (Fig. 8). The as-fabricated SCs exhibit a specific capacitance of

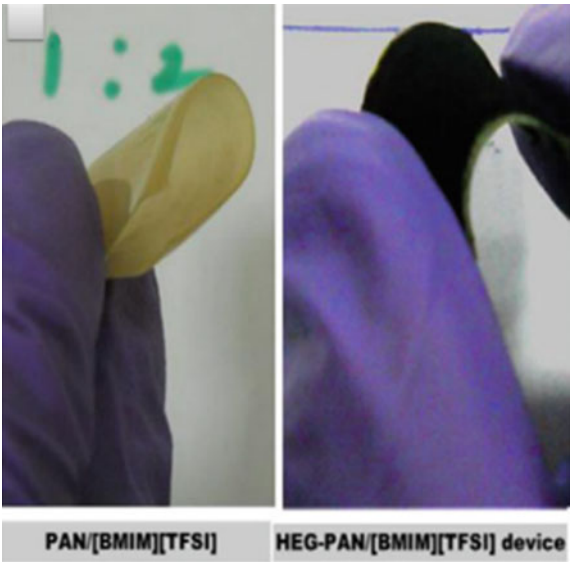

Fig. 8 Images of PAN/[BMIM][TFSI] and the fabricated supercapacitor device which demonstrate their flexibility. Reproduced with permission [75], Copyright 2013, Elsevier

98 F g^{-1} at 10 A g^{-1} with good cyclic stability. Moreover, by expanding the potential window to 3 V, the as-fabricated flexible SCs achieved a high energy density of 32.3 Wh kg^{-1}.

3.2 Conducting Polymers and Their Composites

Since their first discovery in the late 1970s by Shirakawa et al. [76] who were awarded Nobel Prize in Chemistry 2000, conducting polymers have been widely investigated and applied in a large spectrum of applications, ranging from electrochemical/bio sensor [77], organic electronic [78], electrochromic devices [79] and more importantly in the electrochemical energy storage system [80–84]. From a structural standpoint, ECP's backbone is generally built with an alternating system of a single and double bond, resulting in a continuous network of the delocalized electron. Accordingly, in the past few decades, different physical–chemical properties of different conducting polymers have been reported. Indeed, they all have tunable conductivity depending on the doping state (10^{-15} to 10^{5} S cm^{-1}) [85], reversible redox behavior, ion-electrical conversion capability, and processability. Commonly, ECPs can be synthetized either by chemical polymerization and electropolymerization. And last but not least, important flexibility compared to inorganic materials make them capable of being employed in lab-on-skin, implanted, or wearable devices. As typical representatives, polyaniline (PANI), polythiophene and their derivatives (PEDOT, P3HT, etc.), or polypyrrole (PPy) are currently receiving intensive attention for responding

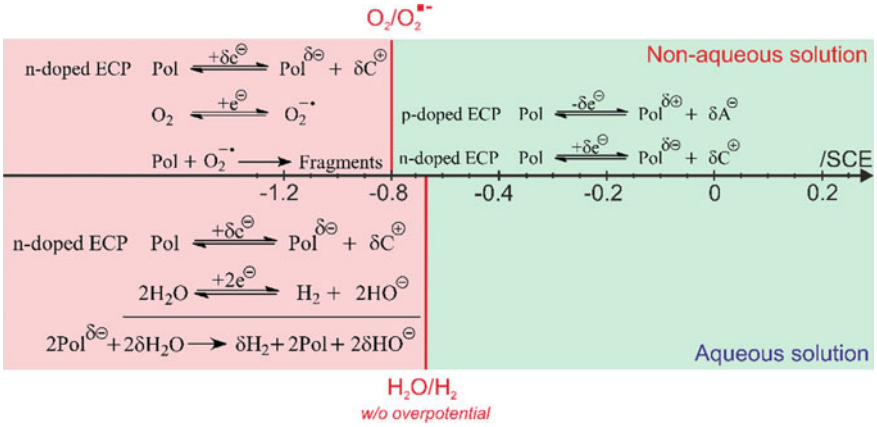

Fig. 9 Doping of *n*-type and *p*-type ECPs where δ reflects the doping level

to the requirement of flexible systems, especially in the field of SCs. From an electrochemical standpoint, conducting polymers can undoubtedly be classified into two main categories, n-doped, and p-doped ECPs, depending on the doping process as shown in Fig. 9. Nevertheless, n-doped conducting polymers cannot, up-to-date, be used as standalone materials for fabrication of n-doped ECPs supercapacitors due to their compacity, low cycling stability, and high sensibility with humidity and oxygen (Fig. 9). Indeed, due to the stability problem, *p*-doped ECPs are dominantly exploited in supercapacitor applications. Upon doping process, positive charges are generated on the polymer backbone with a doping level ranging from 30–50% per monomer unit. Accordingly, counter anions need to diffuse from the bulk solution into the film to stabilize the formed charges, leading to the formation of polaron (radical cation) and bipolaron (di-cation). As a consequence, ECPs store charges using pseudocapacitive phenomenon.

Theoretically, significant specific capacitance could be therefore obtained, e.g. 750 F g^{-1} (PANI), 620 F g^{-1} (PPy), 485 F g^{-1} (PTh), and 210 F g^{-1} (PEDOT). However, it is worth noting that polymer chains usually form densely packed structures, which limit the diffusion of ions back and forth within the matrix, resulting in non-accessible and/or irreversible doping regions. Consequently, a dramatic decrease in gravimetric capacitance and increase in ionic resistance is commonly observed. A typical example that could be cited is the early works from Wallace et al. [86] on the preparation of flexible supercapacitor from drop-casted polyaniline onto Au coated PVDF membrane. It was demonstrated a drastic decrease in specific capacitance from 253 to 134 F g^{-1} in 1 M H_2SO_4 after 10 000 cycles at $v = 100$ mV s^{-1}; i.e. 55% capacitance retention.

Generally, to overcome these issues, many efforts have been focused on improving the nano structuration of ECP layers, the interfaces of ECP/solution, or coupling ECPs with other materials to afford more performing composites. In the same study, Nafion® was used as a protection layer for the PANI layer. A

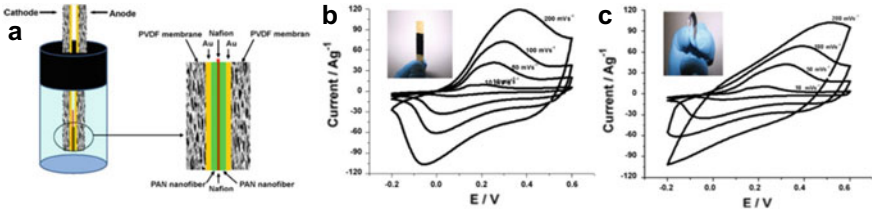

Fig. 10 **a** scheme of an electrochemical cell for capacitance measurement of symmetric PAN nanofiber/Nafion electrode. (**b** and **c**) Digital photographs and cyclic voltammograms of PAN nanofibers on gold-coated PVDF membrane in 1.0 M H_2SO_4 at various scan rates: **b** Planar electrode and **c** twist electrode. Reproduced with permission [86], Copyright 2010, Elsevier

simple casting of 2 μL of Nafion (0.25%wt in ethanolic solution) on 1 × 1 cm PANI/Au/PVDF surface is enough to enhance the stability of the electrode up to 84% in capacitance retention (237 to 178 F g^{-1} under the same experimental conditions). Afterward, the assembly of 2 electrodes results in a symmetrical cell, i.e. PVDF/Au/PANI/Nafion/PANI/Au/PVDF (Fig. 10a). The specific capacitance of the resulting cell in 1 M of sulfuric acid reaches 269 and 248 F g^{-1} at $v = 10$ and 100 mV s^{-1}, respectively. The capacitance retention is about 90 and 65% after 3500 and 10 000 cycles which is reasonable for further developing stable flexible SCs. Nevertheless, upon bending, the electron transfer kinetic of PANI is lowered, resulting from a broadening of peak-to-peak separation. Indeed, upon bending, most of the stress is in the layers owing lower Young's modulus [87], which is the active material film (PANI/Nafion) rather than on stiffer layers (0.1 μm thick Au and PVDF substrate), thus the electrochemical behavior could not endure important bending deformation [88]. In parallel with tailoring the ECP/solution interface, it was recently found that combining PANI with CNTs and graphene can reduce the volume change upon charging and had a good effect on the electrochemical properties of the flexible ECP-based supercapacitors. For example, Yan et al. [89] coated graphene nanosheets (GNS) and carbon nanotubes (CNT) mixture (mass ratio of 99:1) with PANI via in situ polymerization from aniline solution (0.93 g vs 0.195 g of GNS/CNTs) in presence of ammonium persulfate (APS) as oxidant (molar ratio of 1:1). As-prepared PANI/GNS/CNTs exhibited a specific capacitance of 1035 F g^{-1} in 6 M KOH at v = 1 mV s^{-1} (vs. 115, 780, and 1046 F g^{-1} for PANI, PANI/CNTs, and PANI/GNS, respectively). Even though PANI/GNS/CNTs exhibits slightly lower capacitance compared to PANI/GNS, excellent cycling stability is obtained with capacitance retention of 94% over 1000 cycles (vs. 52, 67% for PANI/GNS and PANI/CNTs). This phenomenon could be explained by the synergetic effect by mixing graphene/CNTs which has also been reported elsewhere [90, 91]. In another approach, Wang et al. [92] prepared rGO@PS[2] membrane by mixing aqueous suspensions of rGO and of PS together followed by filtration through PVDF membrane. Once dried, freestanding rGO/PS film was collected by peeling from the PVDF membrane. Afterward, *in-situ* polymerization of aniline in presence of rGO/PS film was performed in presence of

[2] PS = Polystyrene.

APS as an oxidative agent. Finally, polystyrene was removed from the film by chemical etching in tetrahydrofuran (THF), leading to the generation of freestanding 3D rGO/PANI film. The flexibility was visually demonstrated by rolling the membrane without damaging the integrity of the film. In terms of storage performance, 3D rGO/PANI membrane exhibits a specific capacitance of 740 F g^{-1}@0.5 A g^{-1}, which is 7.4, 3.9, and 2.4 times higher than rGO, 3D rGO, and PANI, respectively. Moreover, an energy density of 65.94 Wh kg^{-1}@power density of 0.2 kW kg−1 and 34 Wh kg^{-1}@4 kW kg^{-1} were achieved. Besides, capacitance retention of 87% was obtained after 1 000 cycles at 10 A g^{-1}. In complement with PANI, Liu et al. [93] report the fabrication of all-solid-state flexible supercapacitors based on all conducting polymer electrodes, i.e. poly(3,4-ethylenedioxythiophene): polystyrene sulfonate (PEDOT:PSS) and polypyrrole (PPy). Two different approaches were proposed to prepare two electrodes (Fig. 11a). Briefly, PEDOT:PSS was incorporated as a component in PEDOT:PSS/PVA hydrogel electrode noted (EG-PCPPH), resulting from a physical cross-linked structure using 3 cycles of freezing–thawing with a mixture of 0.5 − 0.65 wt% of PEDOT:PSS and 5% of PVA (degree of polymerization = 2000). For preparing PPy/PVA electrode (CCPH-PPy), vapor phase polymerization was applied where $FeCl_3$ saturated PVA hydrogel film (CCPH) was rapidly placed in a pyrrole vapor saturated chamber. A trilayer asymmetric flexible supercapacitor (AFSCs) with a thickness of 0.4 mm (Fig. 11c) was fabricated with a CCPH layer in a sandwich between 2 ECP-based electrodes (Fig. 11a). Remarkably, the device shows good mechanical durability and flexibility, with a tensile strength of 22.3 MPa and an

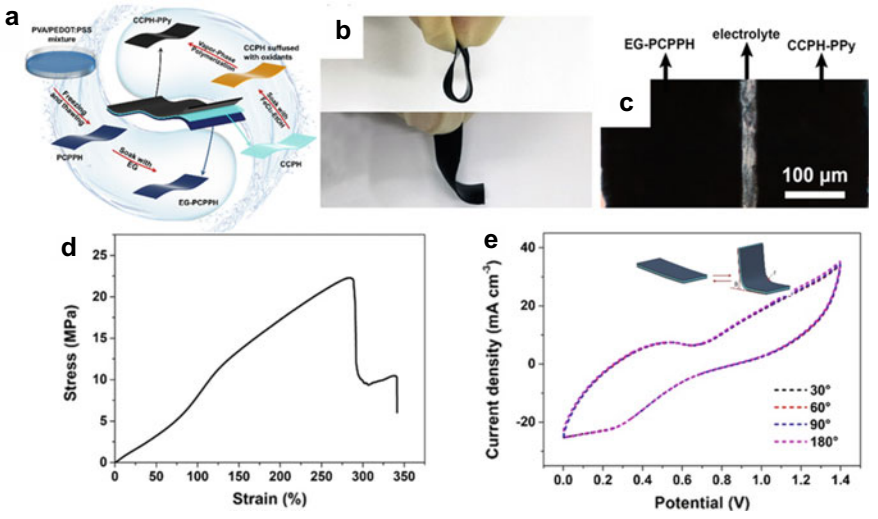

Fig. 11 **a** Illustration of the preparation process of the all-solid-state integrated AFSCs. **b** Digital photos of AFSC demonstrating flexibility. **c** Cross-section of the AFSC by optical microscopy. **d** Tensile stress − strain curve of the AFSC. **e** CV curves of AFSC under various bending states at a scan rate of 60 mV s^{-1} Reproduced with permission Copyright 2021, Elsevier

elongation at a break of 286% (Fig. 11d). Furthermore, the SC is very malleable that can be easily rolled or bent (Fig. 11b). From an electrochemical standpoint, 1.46 F cm^{-3}@20 mA cm^{-3} and 58.5 mF cm^{-2}@0.8 mA cm^{-2} were achieved as volumetric and areal capacitances. Interestingly, the electrochemical behaviors remain intact in the function of bending angle (Fig. 11e) and the capacitance retention is 88.1% over 10 000 charge–discharge cycles and > 98% over 1 000 bending cycles ($\theta = 90°$, bending radius = 5 mm) at 100 mA cm^{-3}. Moreover, volumetric energy density is obtained at 397.99 and 322.6 μWh.cm^{-3} at power density of 14.13 and 73.04 mW cm^{-3}, respectively. Last but not least, 2 ECP-electrodes are perfectly interchangeable without differentiation.

The combination of good electrochemical and mechanical properties has been also explored by the preparation of graphene/polymer composites. Wang et al. [94] have fabricated a Graphene/Polyaniline composite paper by in situ electropolymerizations of aniline monomers into PANI film for high-performance flexible electrode. Graphene/PANI composite paper shows a favorable tensile strength of 12.6 MPa and a stable large electrochemical capacitance of 233 F g^{-1} for gravimetric capacitance and 135 F cm^{-3} for volumetric capacitances, which outperforms many other currently available carbon-based flexible electrodes and is hence particularly promising for flexible supercapacitors.

As a step forward, electrodeposition of ECPs could efficiently reduce the problems of interfacial resistance without the need for polymeric binder. Lin et al. [95] report the development of an all-solid-state supercapacitor from rGO@PANI@carbon woven fabric (CWF), prepared through a two-step method. Firstly, the PANI layer was electrochemically deposited onto CWF substrate by chronoamperometry at 0.65 V/SCE, leading to a deposition of a dark green film with a coated weight of 2.2 mg cm^{-2}. After that, controllable graphene wrapping was deposited by facile impregnation method by dipping the PANI/CWF substrate successively into Poly (allylamine hydrochloride) (PAH), GO suspension, and HI/EtOH solution, respectively (Fig. 12a), leading to the formation of rGOx-PANI/CWF electrode where x (0.5 – 5 mg ml^{-1}) represents the concentration of GO suspension. In presence of PAH linker, rGO nanosheets combine well with the PANI particles (Fig. 12b) with an increase in the electrode's conductivity and limiting the volume change during the charge/discharge process. In terms of electrochemical characteristics, the specific capacitance of the optimized electrode, rGO-1/PANI/CWF, is 571 F g^{-1}@1A g^{-1} (areal capacitance of 812 F cm^{-2}) along with superior stability, i.e. 89% in capacitance retention after 5000 cycles at 10 A g^{-1}. Afterward, the assembled solid-state supercapacitor, which is built from 2 plates of rGO-1/PANI/CWF separated by a gel electrolyte, has excellent flexibility where the SCs can easily be twisted and bent (Fig. 12c). Moreover, the electrochemical response shows a negligible change from a normal state to deformed states (Fig. 12d), and the cycling stability was tested in the bent state (bent angle of 180°) for 5 000 cycles at 10 A g^{-1}, resulting in capacitance retention of 82% (Fig. 12e). As key parameters, energy and power density are reported in the Ragone plot where high energy density of 20.6 Wh kg^{-1} (28.2 μWh cm^{-2})@ 0.13 kW kg^{-1} (0.12 mW cm^{-2}).

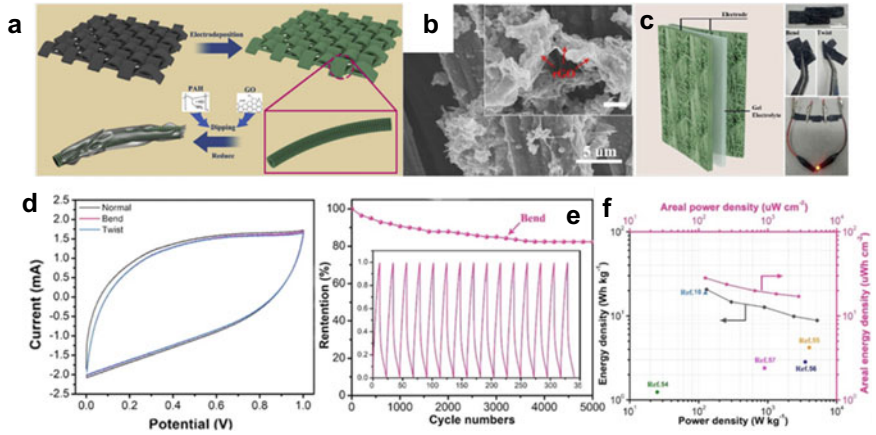

Fig. 12 **a** Preparation process of the graphene-enveloped CWF/PANI. **b** SEM images of rGO@PANI carbon fabric electrode. **c** Schematic of flexible solid-state supercapacitor (FSC) assembled with two identical PANI-rGO-1 hybrid textiles with a gel electrolyte and digital photos of the as-prepared solid-state flexible supercapacitance, including a photograph of a LED powered by three devices in series. **d** CV curves under different deformation states. **e** Cycling stability of FSCs at 10 A g^{-1} **f** FSCs data compared to data from other all-solid-state SCs in a Ragone plot. Reproduced with permission [95], Copyright 2018, Elsevier

Zhou et al. [96] developed flexible all-solid-state supercapacitors by using electrochemical deposited PPy@CNTs as freestanding electrodes using chronoamperometry (E_{dep} = 0.7 V/AglAgCl for 200 s). The resulting PPy@CNTs films reach a specific capacitance of 331.4 F g^{-1} @5 mV s^{-1}. The symmetrical device exhibits high stability during 10 000 charge/discharge cycles with capacitance retention of 65.6% at 2 A g^{-1}. They have also exhibited nearly unchanged capacitive behavior upon bending to 120°, folding into an 'S' shape in a twisted state. These characteristics provide them for many potential applications in flexible electronics and energy storage textiles.

In summary, even though numerous investigations reported using conducting polymers as active materials alone or as a component in composites to develop flexible supercapacitors, promising results (high energy density at high power density, superior capacitance) are highlighted in the literature, the reported storage performances show a large discrepancy, ranging from ~ 10^2 to ~ 10^3 F g^{-1} under the same discharge rate. Indeed, the morphological properties of ECP layers have a great impact on their electrochemical behaviors. As prospective directions, a reliable model correlation between morphology, processing methods, and storage performance must be established. Moreover, cycling stability at a low discharge rate is likely to remain their fatal weakness. Besides, new conducting polymers or new substituents on existing ECPs or combining different ECPs as a copolymer with enhanced accessibility of ions as well as improved stability and strengthened adhesion to the substrate could be further explored.

3.3 Metal Oxides and Composites

Transition metal-based materials, e.g. metal oxides (TMO), metal dichalcogenide (TMD), and metal phosphides (TMP), attract significant attention for electrochemical storage systems thanks to their abundancy, their well-defined redox properties, diversity in composition and morphology, high theoretical specific capacitance alongside with superior energy density. However, based on their chemical nature, severe drawbacks could be undoubtedly listed as low electrical conductivity, uncontrollable volume change during the charge–discharge process as well as sluggish ion diffusion in the core of the materials. Besides, Young's moduli of these materials are extremely high (> > 1 GPa) for consideration as materials alone for flexible supercapacitors. Therefore, intensive investigations are urgently required to tailor the physical–chemical properties of these materials using designing new compositions and novel nano structuration, making them more electrochemically/mechanically controllable. Up-to-date, a wide range of transition metals has been already investigated (Ti, V, Mn, Fe, Co, Ni, Cu, Zn, Mo, Ru) in their oxide/dichalcogenide/phosphide form towards the fabrication of supercapacitors, and some of them have even been applied in flexible supercapacitors by combining with other materials. In this context, MnO_2 and RuO_2 have demonstrated a high capacitance through the transformation between their different valence states [97] but their structural instability [98], on the other hand, results in short cycle life. In addition, NiO, Co_3O_4, ZnO, and CuO-based materials, pave the way for the fabrication of flexible electrodes owning high energy and power densities [99, 100], but their poor cycling stability and retention rate limit their practical uses [98]. Among different oxides, RuO_2 was originally regarded to be one of the ideal supercapacitor electrode materials, thanks to its good chemical stability, high theoretical capacitance, large voltage window, good electronic conductivity, and reversibility [98, 101]. It is worth noting that RuO_2 nanoparticles agglomerate into larger particles during the manufacturing, charging, and discharging processes. Consequently, the latter affects the electrochemical performance of the RuO_2 electrode [101]. For resolving these problems, Ruiyi et al. [98] recently reported the synthesis of atomically dispersed RuO_2-tryptophan functionalized graphene quantum dot-graphene hybrid (AD-RuO_2-Trp-GQD-G) as shown in Fig. 13a. In a multistep process, AD-RuO_2-Trp-GQD-G was obtained by pyrolyzing a ruthenium complex, Ru^{3+}-tryptophan@GQD-G, under an inert atmosphere followed by re-oxidation in the air at 200 °C for 2 h in sequence. The resulted material exhibits a high capacitance of 503.7 F g^{-1} @1 A g^{-1} in 1 M H_2SO_4 compared to those of the graphene (160 F g^{-1}) and G-Trp-GQD (192F g^{-1}). Moreover, AD-RuO_2-Trp-GQD-G shows superior capacitance retention of 55.5% when the discharge rate increases from 1 A g^{-1} to 25 A g^{-1}, resulting from an extremely fast faradaic process as all of Ru sites are exposed to the solution. Indeed, well-defined redox behavior of RuO_2 from voltammograms at different scan rates are obtained. Afterwards, assembled device was prepared by 3D printer from which the current collector (thickness after drying = 20 μm) are interdigitatedly printed onto flexible PET substrate followed by superposing a layer of active material (thickness = 2 mm). Lately, a layer of

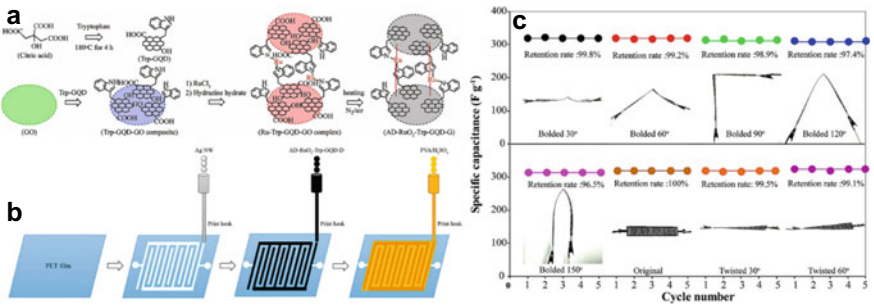

Fig. 13 **a** Illustration for the synthesis of Trp-GQD and AD-RuO2-Trp-GQD-G B) Preparation of the symmetrical flexible supercapacitor, **c** Digital photographs of the supercapacitor and its specific capacitances at the current density of 1 A g^{-1} for 5-cycles Reproduced with permission [98], Copyright 2021, Elsevier

gel electrolyte (PVA/H_2SO_4) was printed to cover the whole device (Fig. 13b). The resulted device displays high capacitance of 354 F g^{-1} at 0.5 A g^{-1} and an energy density of 33 Wh kg^{-1}@52 kW kg^{-1}. Furthermore, as the atomic RuO_2 species are stably embedded in the composite, their stability over cycling is remarkably enhanced compared to other reported works on RuO_2-based materials, i.e. 99.5% capacitance retention after 10,000 cycles at 10 A g^{-1}. More importantly, the electrochemical responses of flexible supercapacitor versus mechanical constraints were tested at different bending/twisting angles. Hence, the capacitance retention remains > 99% (Fig. 13c). This approach is outperforming several flexible systems which are mainly based on RuO_2 nanoparticles, aggregates, or bulky ones [102–105]. Although several studies on using RuO_2 have been reported in the literature as aforementioned, RuO_2 tends to be replaced by other transition metals due to their high cost. In this context, MnO_2 based materials have been widely investigated due to their interesting properties, such as high theoretical specific capacitance, good chemical, and thermal stability, natural abundance, environmental friendliness, and low cost [106]. However, MnO_2 possesses low electric conductivity (10^{-5} to 10^{-6} S cm^{-1}), implying a severe problem to achieve excellent electrochemical performance. Consequently, improving the electrical conductivity of MnO_2-based electrodes becomes crucial, leading to the development of MnO_2 based composites with an electrically conductive material.

Moving forward to this direction, He et al. [107] developed a freestanding, three-dimensional Graphene/MnO_2 composite network with a large MnO_2 loading up to 92.9% (9.8 mg cm^{-2}) of the entire electrode's mass. Starting from lightweight (0.75 mg cm^{-2}), ultrathin (<200 μm), highly conductive (55 S cm^{-1}), and flexible 3D graphene electrode, electrochemical deposition of MnO_2 was performed in aqueous by pulsed square wave technique (pulse period of 2 ms for a duration ranging from 15 to 1440 min with a current density of 0.5 mA cm^{-2}). After that, the as-prepared electrode was annealed at 300 °C under an inert atmosphere to generate a crystalline structure. From a large range of mass loading, the highest specific capacitance was

achieved at 465 F g^{-1}@2 mV s^{-1} with a mass loading of 0.1 mg cm^{-2}. Nevertheless, from a practical standpoint, the performance of the device not only depends on the specific capacitance per gram of the active material but critically on the total mass (including 2 electrodes, separator, current collector, electrolyte, etc.), hence a mass loading of 0.4 mg cm^{-2} ($C_{sp/entire\ electrode}$ = 110 F g^{-1} and $C_{sp/entire\ cell}$ = 30 F g^{-1} vs. 50 F g^{-1} and 13.6 F g^{-1} for 0.1 mg cm^{-2}) was chosen as the most balanced value for fabrication of lightweight (<10 mg), thin (<1 mm) and flexible SCs. The resulting symmetrical devices exhibit good stability over cycling with capacitance retention of 82% after 5 000 cycles at a current density of 1.5 mA cm^{-2}. Moreover, an energy density of 6.8 Wh kg^{-1}@62 W kg^{-1} and 3.75 Wh kg^{-1}@2.5 kW kg^{-1} are achieved. It is widely known that depending on the deposition conditions, a large spectrum of morphology could be obtained using electrochemical methods. Accordingly, different works on electrochemical deposition of MnO_2 for flexible SCs have also been reported with high storage performance, e.g. MnO_2 nanoflowers/graphene fiber ($C_{sp(cell)}$ = 9.6 mF cm^{-2}) [108], MnO_2 nanospheres/CNT paper (C_{sp} = 486.6 F g^{-1}@0.5 A g^{-1}) [109], In parallel, other methods are also investigated for preparing MnO_2 nanostructured, such as hydrothermal (MnO_2 nanosheets on nanocarbon based film with specific capacitance of 324 F g^{-1}@1.9 A g^{-1} [110], 634.5 F g^{-1}@2.5 A g^{-1} [111], 520 F g^{-1}@0.5 A g^{-1}, [112], 560 F g^{-1}@0.2 A g^{-1}, [113] and solvothermal (3D MnO_2 microspheres with Csp = 129 F g^{-1}@0.5 A g^{-1} ([114]), MnO_2 NPs/C fibers (803.6 mAh g^{-1}@20 mV s^{-1}) [115].

3.4 MXene and Composites

MXene refers to a novel class of 2D inorganic materials ranging from transition metal carbides, carbonitrides to nitrides [70, 114]. With a general formula of $M_{n+1}X_nT_x$, where M is a transition metal (Mo, V, Nb, Ta, and Ti), X is a carbon or Nitrogen, T_x represents the surface groups (=O, −OH, −Cl, and −F) and $1 < n < 4$ (e.g. Ti_3C_2, Ti_3CN, Nb_2C, and Ti_4N_3) [70]. MXenes have attracted tremendous interest in different fields such as catalysis, electromagnetic interference shielding, and reinforcement for composites, energy storage, and many other applications [70, 116]. The synthesis of MXene consists mainly of the exfoliation of MAX using fluoride contained substance (Fig. 14) [117]. Interestingly, MXene is recognized as a flexible 2D material with plentiful surface-active groups (–OH, –F, or –O), as well as good electrical conductivity and due to its ultrahigh density, an MXene can provide far larger volumetric capacitance than graphene. These properties are attained due to: (1) the presence of a conductive inner transition metal carbide layer that provides fast electron transport to electrochemically active sites; (2) electroactive transition metal oxide-like surface generated during the synthesis; layered structure with pre-intercalated solvent molecules, thus enables fast ion transport [118]. Due to their unique structure, MXenes are particularly attractive for energy storage applications. Up-to-date, titanium carbide $Ti_3C_2T_x$ has been the most extensively explored MXene, with high volumetric capacitances of 900 F cm^{-3}, a high electronic conductivity up

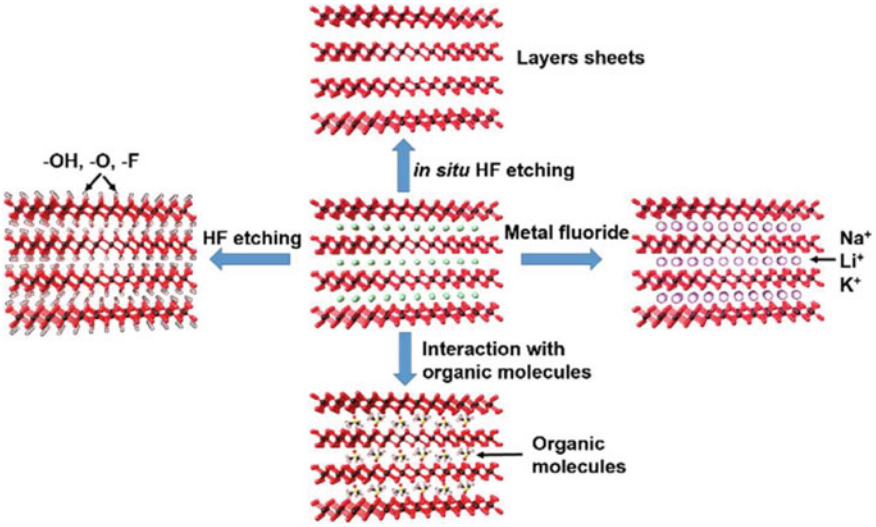

Fig. 14 Schematic illustration of different MXene syntheses from MAX via different routes. Reproduced with permission [117], Copyright 2017, Royal Society of Chemistry

to ≈10 000 S.cm^{-1}, and a TiO_2-like surface, resulting in ultrahigh volumetric capacitance (≈1500 F cm^{-3}) in $Ti_3C_2T_x$ hydrogel films and high areal capacitance (≈61 mF cm^{-2}) in $Ti_3C_2T_x$ MSCs.

To get insight into the origin of the resulting capacitance of $Ti_3C_2T_x$, Lukatskaya et al. [119] reported the use of *in-situ* X-ray absorption spectroscopy (XAS) to probe the storage mechanism of this material in 1 M H_2SO_4 aqueous electrolyte. A linear relationship between the Ti edge energy (resulting from Ti K-edge XANES spectra) with applied electrochemical potential proves a change in the Ti oxidation state of $Ti_3C_2T_x$ during charge/discharge, concluding that the predominant electrochemical behavior of $Ti_3C_2T_x$ is pseudocapacitive with proton-coupled electron transfer mechanism. More importantly, the average Ti oxidation state in $Ti_3C_2T_x$, is closer to + 2 than + 4 (from 2.33 to 2.43 or 0.1e per Ti atom). A simplified presentation of the redox process at MXene surface can be shown as $Ti_3C_2O_x(OH)_yF_z + \delta e- + \delta H^+ \rightarrow Ti_3C_2O_{x-\delta}(OH)_{y+\delta}F_z$, confirming the crucial role of oxide groups at the surface. Moreover, the role of OH-terminal groups could be further extended in a flexible system. Thin-film of pristine $Ti_3C_2T_x$ MXene was demonstrated to have sufficient mechanical strength to handle with a tensile strength of 22 ± 2 MPa (thickness of 3.3 μm) and Young's modulus of 3.5 GPa. However, the stiffness was increased by adding poly(vinyl alcohol) at 60 wt% (tensile stress of 91 ± 10 MPa). It is worth noting that this phenomenon is not completely attributed to the MXene or PVA itself (tensile stress = 30 ± 5 MPa/ 12 μm thick film) but correspond probably to the interaction between OH-terminal groups of MXene and PVA, resulting to a transfer of some stress into the interfacial bonding [120]. It is worth noting that the strain to failure is also increased about 4 times, thus more flexible and stronger materials are

achieved. Consequently, MXenes have been advantageously used in flexible supercapacitors with/without additional binders. Binder-free $Ti_3C_2T_x$ MXene/CNT yarn prepared by biscrolling method was reported by Wang et al. [121] Indeed, MXene suspension was drop-casted onto 5 layer-stacked vertically aligned CNTs (350 μm in height/sheet). One end of the CNT substrate is then fixed to an electric motor which is in charge for twisting the substrate into yarn with a rate of 2000 turns m^{-1}, leading to Mxene/CNT yarn with a mass loading of 97.4%. As prepared fiber was directly electrochemically tested in electrolyte without any current collector. Specific capacitances of 523 F g^{-1}, 118 mF cm^{-1}, 3188 mF cm^{-2} and 1083 F cm^{-3} @2 mA cm^{-2} was achieved which outperform other fibered structures [122–125]. Moreover, flexible SCs can be easily built by twisting 2 fibers of PVA-covered MXene/CNTs with an energy density of 8.54 mWh cm^{-3}@530 mW cm^{-3}. The resulted devices exhibit strong stability over 0.8 V voltage. To further improve the interaction with MXene as well as increase the interlayer distance of MXene, Yan et al. [126] proposed novel approach for self-assembling of titanium carbide MXene and rGO by means of electrostatic interactions. Reduced graphene oxide was first mixed with poly(diallyldimethylammonium chloride) – PDDA (0.01 wt%) to afford a positively charged rGO mixture. Then, negatively charged and delaminated $Ti_3C_2T_x$ MXene was added into PDDA@rGO suspension, large aggregates of MXene/rGO were obtained followed by vacuum-assisted filtration to afford freestanding and flexible film. With only 5% of rGO within the materials, the electrochemical performance is strongly enhanced. Accordingly, a specific capacitance of 335.4 F g^{-1} (1 040 F cm^{-3}@2 mV s^{-1}) along with superior rate capability (100 F g^{-1} at 10 V s^{-1}, i.e. 30% in capacitance retention) were observed. The improvement in rate capability can be attributed to the increase in interlayer spacing of MXene in presence of rGO. However, a further increase in rGO leads to a decrease in specific capacitance which is evidenced by a drop in electrical conductivity of the composite. Furthermore, remarkable stability was achieved with no degradation after 20 000 cycles. For practical use, a symmetrical device was built and displays a gravimetric energy density of 10.5 Wh kg^{-1}@80.3 W kg^{-1} (and retain at 3.3 Wh kg^{-1}@24 kW kg^{-1}), an ultrahigh volumetric energy density of 32.6 Wh L^{-1}, and a maximum power density of 74.4 kW L^{-1}.

Even though massive investigations have been devoted to the development of more and more performing electrode materials, there are still many challenges that hinder the practical use of MXene based materials. From the synthesis standpoint, the exfoliation of bulk MXene into stable 2D layers are mainly occurred in HF and more recently LiF/HCl to reduce the toxicity of HF. However, more eco-friendly approaches with fluoride-free substances need to be developed. As aforementioned about the importance of surface functional groups, seeking for new synthesis procedure that can improve the quantity and homogeneity of surface functions is still open for further studies. Finally, the porosity and electrochemical surface area of pristine MXene are relatively low which requires an improvement. Countless efforts have been put on combining other materials with MXene to increase interlayer spacing but the addition of those materials leads to a decrease in electrical conductivity of MXene, thus decreasing the storage performance.

3.5 Metal–Organic Frameworks and Composites

Since their first discovery in the 2000s, Metal–organic frameworks (MOFs) have excited the scientific community as new class of porous materials synthetized from metal–organic complexation with ultra-high specific surface area (up to 6000 $m^2\ g^{-1}$) and unlimited possibilities of designing their physicochemical structure by changing the structure of ligands as well as the metallic centers. Depending on the coordination number of involved transition metal, the resulted MOF could take different geometries. Although significant specific surface is obtained, most of reported MOF cannot be electrochemically exploited, resulting from a low electrical conductivity, ranging from fS to mS cm^{-1} [127]. Up to date, most of reported works on fabrication of (flexible) supercapacitors using metal organic frameworks are based on their composites with other materials. Up-to-date, most of reported works on fabrication of (flexible) supercapacitors using metal organic frameworks are based on their composites with other materials. Various porous MOFs were synthesized in the past few years using distinct synthetic methods like hydrothermal/solvothermal [128, 129], electrochemical [130], mechanochemical [131, 132], microwave healing/ultrasound irradiation [133], depending upon the targeted proprieties and the desired final structure. Among various MOF-based SCs, they can be classified into three categories: (1) SCs that are fabricated by using pristine MOFs [134], (2) MOF-based composites [135] and (3) porous carbon derived from pyrolyzed MOF [136]. Even though it is derived from MOF, generated porous carbon-based materials will not be treated in this subsection. The first pristine MOF used as supercapacitor electrode was Co8-MOF-5 [137]. MOF-5 electrode showed typical electric double layer capacitors behavior in acetonitrile at low scan rate, due to the influence of carbon black additives. The electrode exhibited low specific capacitance (3.27 F g^{-1}@25 mV s^{-1}) due to its low electronic conductivity limited by the particular MOF and the electrolyte used, which may be solved by a specific tuning of the MOF structure and the use of suitable electrolytes. Recently, 2D conducting MOFs were reported with enhanced specific capacitor. Sheberla et al. [138] reported novel MOF, $Ni_3(HITP)_2$, from the complexation of Ni^{2+} and hexaaminotriphenylene (HATP), leading to ultrahigh electrically conductive of 2 S cm^{-2} for bulk pellet and 40 S cm^{-1} for thin film configuration. Later, they demonstrated the use of reported MOF to supercapacitor application with a specific capacitance of 111 F g^{-1} at 50 mA g^{-1} (or 18 μF cm^{-2} once normalized with specific surface area) [134], paving the way for possible application in flexible supercapacitors. However, none of state-of-the-art MOF can be used for flexible SCs in their pristine form. Accordingly, to further improve the electrical conductivity and flexibility, conducting polymers were widely used to combine with MOF, resulted to ECP@MOF composites. Among them, Polypyrrole (PPy) polyaniline (PANI), poly (3,4-ethylenedioxythiophene) (PEDOT) etc. are commonly chosen [139]. Conducting polymer can be physically mixed with MOF nanoparticles. However, the dispersion of MOF nanoparticles in the polymer still not uniform and the composite still has a poor charge transfer [5]. To overcome this problem, a

more effective method is to grow or deposit polymers on MOFs and form a conductive network connecting all particles [5]. Wang et al .[140] develop PANI@ZIF67 deposited onto carbon cloth as an electrode for flexible and all-solid-state SC by electrochemically interweaving MOF particles with polyaniline (PANI) chains. When compared to the pristine MOF architecture, the presence of PANI allowed not only an addition of pseudocapacitance contribution but more importantly and easy electron and electrolyte transport across the interwoven hybrid structure connecting all the MOF crystals together. Consequently, PANI-ZIF-67-CC exhibits high areal capacitance of 2146 mF cm^{-2} at 10 mV s^{-1} [140]. Instead of PANI, flexible MOFs-based supercapacitors can also be prepared by fabricating an in-situ network of ZIF-67 particles connected by conductive PPy tubes [141]. The obtained MOF–PPy (ZIF–PPy) hybrid showed a specific surface area of 1545.2 $m^2.g^{-1}$ and good electric conductivity. This result makes the MOF–PPy hybrid an ideal supercapacitor electrode candidate. They exhibited a specific capacitance of 554.4 F g^{-1}@0.5 A g^{-1} and excellent stability in a three-electrode system. This hybrid structure allowed for faster electron transfer between the MOF and PPy, resulting in a continuous conducting network connecting all MOF nanoparticles. Apart from previously mentioned works, countless efforts have been given for coupling MOF with conducting polymer for flexible supercapacitors by changing the nature of MOF and ECP or by modulating the morphology of resulted composites for achieving improved storage performance [5, 142–144]. In parallel with conducting polymer, nanocarbons (graphene, CNTs) were also intensively investigated in preparing composite with metal organic framework [145, 146]. However, flexible supercapacitors from this family of composites are still very scanty. As a typical example, 2D-Ni MOF and Co MOF was coupled with rGO through self-assembled approach to afford flexibles ASC with a high volumetric energy density of 1.87 mWh cm^{-3} a power density of 250 mW cm^{-3} [147]. Schematic procedure for synthetizing 2D-MOF/rGO paper is displayed in the (Fig. 15a). Owning positive −Ni(Co) surface terminated groups, resulted 2D-MOFs are intrinsically positively charged while GO are negatively charged due to the presence of oxygenated groups (Fig. 15b). Once mixed together, electrostatic interactions lead to the formation of self-assembled composites. After vacuum filtration, flexible membrane were obtained as shown in the (Fig. 15c). Afterward, electrochemical behaviors of freestanding papers with 40 wt% of GO was tested in 1 M H_2SO_4, resulted to a specific capacitance of 656.6 and 570.8 F cm^{-2}@1 mA cm^{-2} for Co-MOF/G and Ni-MOF/G, respectively. Afterwards, Co-MOF/G and Ni-MOF/G were used as positive and negative electrodes for fabrication of asymmetric SCs (Fig. 15d), leading to an areal capacitance of 426.5 mF cm^{-2} as well as volumetric capacitance of 22.45 F cm^{-3}@1.2 mA cm^{-2}. Rate capability was evaluated by changing the discharge rate from 1.2 to 14.4 mA cm^{-2} with a capacitance retention of 21% (4.7 F cm^{-3}). Moreover, specific capacitance of the device remained intact with different bending angle, ranging from 0° to 180° as well as after 100 bending cycles (94%) or 3000 charge–discharge cycles at 2.4 mA cm^{-2} (97.5%). More importantly, this approach allows to achieve editable device which can be cut into desired shape without damaging its storage performance.

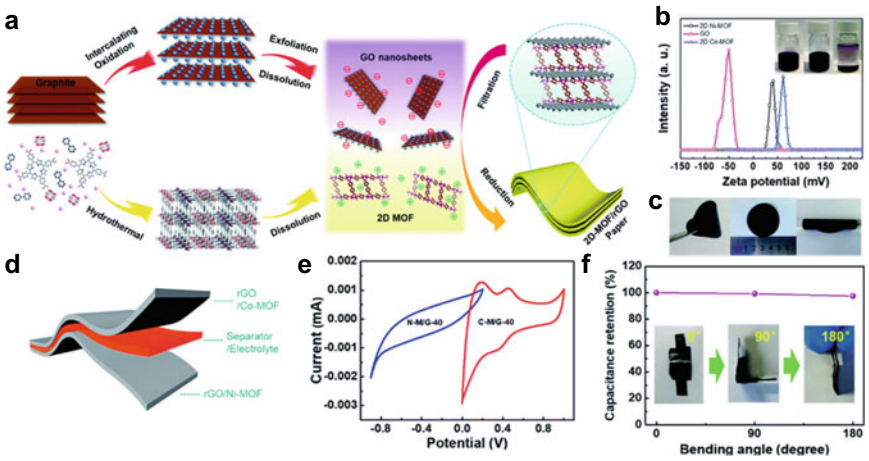

Fig. 15 **a** Schematic route for synthesis of 2D-MOF/rGO paper. **b** Zeta potential and (inset) photograph of 2D Ni-MOF, Co-MOF and GO suspension. **c** Photographs of freestanding and flexible 2D-MOF/rGO paper. **d** Assembly scheme for fabricating ASCs. **e** Voltammograms of N-M/G-40 and the C-M/G-40 electrodes at $v = 10$ mV s^{-1}. **f** Capacitance retention with different bending angles. Reproduced with permission [147]. Copyright 2018, Royal Society of Chemistry

4 Conclusions and Prospects

In conclusion, the development of flexible electronics involves developing highly flexible energy storage devices, with energy/power density and rate performance at least similar to conventional power sources. The key point to address is the mechanical properties of the device that is mainly achieved by engineering stiff (nano)materials onto flexible substrates or by intimately mixing these materials into intrinsically flexible materials (e.g. CNTs or graphene with other components such as ECPs, MXenes, MOF, MO, etc.). The latter approach is a win–win concept since both electrochemical performances and mechanical properties are improved at the same time by maintaining a robust 3D framework and providing a maximum accessible surface area for the pathway of electrolyte ions, hence improving the capacitance. Generally, an additional binder is no more necessary and efforts made on the development of new electrolytes (such as polymer electrolytes, gels, etc.) help for the improvement of mechanical properties of the assembled device. The table below summarizes some of the performances of relevant works referenced in the Chapter:

Materials	Capacitance	Capacitance retention	Capacitance retention upon deformation	Energy/power density	Reference
MCFC	684 F g^{-1} at 2 A g^{-1}	94% 1000 cycles	n.d.*	46.54 Wh kg^{-1} 45.50 kW kg^{-1}	[61]
TACC	3291 mF cm^{-2}	95% 10,000 cycles	n.d.*	740 μWh cm^{-2} 9000 μ W cm^{-2}	[62]
SWCNT	34.2 F g^{-1}. at 0.63 A g^{-1}	94% 500 cycles	Any change of resistivity when submitted to bending stress	18.0 kWh kg^{-1} 21.1 kW kg^{-1}	[63]
CNT fibers	11.23 F g^{-1} at 0.075 A g^{-1}	>2000 cycles	High flexibility	n.d.*	[64]
SWNT	115.83 F g^{-1}	n.d*	n.d.*	48.86 Wh/kg	[66]
a-FSSC	111 mF cm^{-2}	110% 5000 cycles	80% after 1000 bending cycles	25.l mWh cm^{-2} 0.48 mW cm^{-2}	[67]
LSG-EC	3.67 mF cm^{-2}	96.5% after 10,000 cycle5	95% after >1000 cycles	1.36 mWh cm^{-3}	[7]
rGO/HCNT	336 F g^{-1} at 0.25 A g^{-1}	89.5% 3000 cycles	98.8% of the initial specific capacitance can be retained at 180°	7.5 Wh kg^{-1} 100 W kg^{-1}	[71]
GNCN electrode	294 F g^{-1} at 5 mV s^{-1}	93% 5000 cycles	n.d.*	26 Wh L^{-1}	[72]
GCP electrode	81 mF cm^{-2}	99% 5000 cycles	Resistance of the GCP membrane increased only 6% after 1000 cycles	n.d.*	[73]

(continued)

(continued)

Materials	Capacitance	Capacitance retention	Capacitance retention upon deformation	Energy/power density	Reference
Graphene hydrogel	186 F g^{-1} at 1 A g^{-1}	70% retention @20 A g^{-1}	n.d.*	6.5 Wh kg^{-1}	[74]
Graphene	98 F g^{-1} at 10 A g^{-1}	92% 1000 cycles	n.d.*	32.3 Wh kg^{-1} 82 kW/kg	[75]
PVDF/Au/PANI⁺Nafion	269 F g^{-1} at l0 mV s^{-1}	90% 3500 cycles	n.d.*	n.d.*	[86]
GNS/CNT/PANI	1035 F g^{-1} at 1 mV s^{-1}	94 % 1000 cycles	n.d.*	n.d.*	[89]
rGO/PANI	740 F g^{-1} at 0.5 A g^{-1}	87% 1000 cycles	n.d.*	65.94 Wh kg^{-1} 0.2 kW kg^{-1}	[92]
EG-PCPPH/CCPH-PPy	58.5 mF cm^{-2}	88.1% 10,000 cycles	98% after 1000 bending cycles	397.99 μWh cm^{-3} 14.13 mW cm^{-3}	[93]
rGO/PANI/CWF	790 F cm^{-2} at 1 A cm^{-2}	82% 3000 cycles	n.d*	20.6 Wh kg^{-1} 0.13 kW kg^{-1}	[95]
PPy@CNTs films	331.4 F g^{-1} at 5mV s^{1}	65.6% 10,000 cycles	unchanged capacitive behavior upon bending to 120°	n.d.*	[96]
AD-Ru02-Trp-GQD-G	354 F g^{-1} at 0.5 A g^{-1}	99.5% after 10,000 cycles	96% of the initial specific capacitance can be retained at 150°	332 Wh Kg^{-1} 52 kW kg^{-1}	[98]
3D graphene/MnO2	465 F g^{-1} at 2 mV s^{-1}	82% after 5000 cycles	92% after 200 bending	62 W/kg 6.8 Wh/kg	[107]
BMX yarn	523 F g^{-1}	n.d.*	100% after 1000 bending cycle	61.6 mWh cm^{-3} 5428 mW cm^{-3}	[121]
MXene/rGO	335.4 F g^{-1}	61%	n.d.*	32.6 Wh L^{-1} 74.4 kW L^{-1}	[126]
PAM-ZIF-67- CC	2146 mF cm^{-2}	80% after 2000 cycles	n.d.*	16 μWh cm^{-3} 0.833 W cm^{-3}	[141]

(continued)

(continued)

Materials	Capacitance	Capacitance retention	Capacitance retention upon deformation	Energy/power density	Reference

*n.d. = no data

Flexible power sources' application areas and lifetime are depending on their mechanical deformation and the electrical property retention under deformation. They should be able to endure high strain induced by external mechanical deformation like bending, compressing, stretching, folding, and twisting with keeping electrochemical performance stability and structural integrity. However, while flexibility enables numerous new applications for energy storage devices, some limits already appear in terms of mechanical robustness and conformability. Indeed, concave surfaces, moving textiles like a garment of sails require more than just flexibility and bending. In this case, stretchability becomes the new target and stretchable electronics can be considered as a technological breakthrough. These devices can achieve highly stable performance under strain and be reversibly stretched while maintaining functionality, such as light-emitting [148, 149] or light-harvesting [150] or transistor [151]. In comparison with the field of flexible devices, stretchable electronics are pushing further the strain or deformation that the device can experience, operate under or conform to. Developing similarly wearable energy storage devices such as stretchable supercapacitors (SSCs) becomes essential for powering those abovementioned systems. To guarantee the sustainable operation of a (wearable) electronic device, suitable SSC power sources must supply stable and persistent current/voltage output whatever the input deformation conditions that can be bending, twisting, stretching, or even scratching which requires the SSCs devices to be at least flexible, stretchable to be comfortably implemented onto clothes or on human bodies [8, 152]. To date, research efforts in stretchable SCs have been devoted mostly to some points: (i) The design and configuration of all stretchable components, from electrodes, current collectors, and (electro)active materials. The quasi-infinite combinations of (nano)composite materials and the numerous possibilities of electrode designs (planar, coaxial, 3D, etc.) result in substantial differences in both the final mechanical properties and electrochemical performances of the SSCs compared to the classical SCs. (ii) all components of the SSCs must be compliant with stretchability, whatever the configuration (coaxial, 2D, or 3D) of the SSC to maintain power delivery performances upon any deformation. (iii) The compliance with other functionalities such as lightweight, thinness, or in some cases, for "on skin" development, transparency.

The latter point remains one of the main challenges in the next decade. To date, the research has mainly focused on the electrode components, responsible for the electrochemical and mechanical performances. So, priority was mainly devoted to preparing stretchable electrodes, with rational material selection and novel structure designs [153, 154].

In addition to intrinsically stretchable devices where the components are made inherently stretchable, extrinsic stretchability can be obtained thanks to the device design. The field of textile appears especially promising for this purpose since it adds a level of control on the final mechanical properties by adapting the textile construction itself such as the numerous possibilities of knitting or weaving yarns. Providing that yarns are made electroactive, elementary linear functional yarns can be assembled into large-area products by taking advantage of the tremendous progress made in recent years in the field of technical textiles [155].

References

1. J.B. Goodenough, Y. Kim, Challenges for rechargeable Li batteries. Chem. Mater. **22**, 587–603 (2010). https://doi.org/10.1021/cm901452z
2. P. Simon, Y. Gogotsi, Materials for electrochemical capacitors. Nat. Mater. **7**, 845–854 (2008). https://doi.org/10.1038/nmat2297
3. Z.S. Iro, C. Subramani, S.S. Dash, A brief review on electrode materials for supercapacitor. Int. J. Electrochem. Sci. **11**, 10628–10643 (2016). https://doi.org/10.20964/2016.12.50
4. M. Vangari, T. Pryor, L. Jiang, Supercapacitors: review of materials and fabrication methods. J. Energy Eng. **139**, 72–79 (2013). https://doi.org/10.1061/(asce)ey.1943-7897.0000102
5. J. Cherusseri, D. Pandey, K. Sambath Kumar, J. Thomas, L. Zhai, Flexible supercapacitor electrodes using metal-organic frameworks. Nanoscale **12**, 17649–17662 (2020). https://doi.org/10.1039/d0nr03549a
6. Y. Sui, J. Zhou, X. Wang, L. Wu, S. Zhong, Y. Li, Recent advances in black-phosphorus-based materials for electrochemical energy storage. Mater. Today. **42**, 117–136 (2021). https://doi.org/10.1016/j.mattod.2020.09.005
7. M.F. El-Kady, V. Strong, S. Dubin, R.B. Kaner, Laser scribing of high-performance and flexible graphene-based electrochemical capacitors. Science **335**, 1326–1330 (2012). https://doi.org/10.1126/science.1216744
8. T. Chen, L. Dai, Flexible supercapacitors based on carbon nanomaterials. J. Mater. Chem. A. **2**, 10756–10775 (2014). https://doi.org/10.1039/c4ta00567h
9. J. Gamby, P.L. Taberna, P. Simon, J.F. Fauvarque, M. Chesneau, Studies and characterisations of various activated carbons used for carbon/carbon supercapacitors. J. Power Sources. **101**, 109–116 (2001). https://doi.org/10.1016/S0378-7753(01)00707-8
10. S. Zhu, P.L. Taberna, N. Zhao, P. Simon, Salt-template synthesis of mesoporous carbon monolith for ionogel-based supercapacitors. Electrochem. Commun. **96**, 6–10 (2018). https://doi.org/10.1016/j.elecom.2018.09.003
11. L. Trognko, P. Lecante, N. Ratel-Ramond, P. Rozier, B. Daffos, P.L. Taberna, P. Simon, TiC-carbide derived carbon electrolyte adsorption study by ways of X-ray scattering analysis. Mater. Renew. Sustain. Energy. **4** (2015). https://doi.org/10.1007/s40243-015-0059-4
12. M. Naguib, O. Mashtalir, J. Carle, V. Presser, J. Lu, L. Hultman, Y. Gogotsi, M.W. Barsoum, Two-dimensional transition metal carbides. ACS Nano **6**, 1322–1331 (2012). https://doi.org/10.1021/nn204153h
13. V. Presser, M. Heon, Y. Gogotsi, Carbide-derived carbons - from porous networks to nanotubes and graphene. Adv. Funct. Mater. **21**, 810–833 (2011). https://doi.org/10.1002/adfm.201002094
14. K. Xu, H. Shao, Z. Lin, C. Merlet, G. Feng, J. Zhu, P. Simon, Computational insights into charge storage mechanisms of supercapacitors. Energy Environ. Mater. **3**, 235–246 (2020). https://doi.org/10.1002/eem2.12124

15. E. Frackowiak, K. Metenier, V. Bertagna, F. Beguin, Supercapacitor electrodes from multiwalled carbon nanotubes. Appl. Phys. Lett. **77**, 2421–2423 (2000). https://doi.org/10.1063/1.1290146
16. B. Kim, H. Chung, W. Kim, High-performance supercapacitors based on vertically aligned carbon nanotubes and nonaqueous electrolytes, Nanotechnology. **23** (2012). https://doi.org/10.1088/0957-4484/23/15/155401
17. M. Kaempgen, C.K. Chan, J. Ma, Y. Cui, G. Gruner, Printable thin film supercapacitors using single-walled carbon nanotubes. Nano Lett. **9**, 1872–1876 (2009). https://doi.org/10.1021/nl8038579
18. H. Pan, J. Li, Y.P. Feng, Carbon nanotubes for supercapacitor. Nanoscale Res. Lett. **5**, 654–668 (2010). https://doi.org/10.1007/s11671-009-9508-2
19. M.R. Arcila-Velez, J. Zhu, A. Childress, M. Karakaya, R. Podila, A.M. Rao, M.E. Roberts, Roll-to-roll synthesis of vertically aligned carbon nanotube electrodes for electrical double layer capacitors. Nano Energy **8**, 9–16 (2014). https://doi.org/10.1016/j.nanoen.2014.05.004
20. P. Lv, P. Zhang, F. Li, Y. Li, Y. Feng, W. Feng, Vertically aligned carbon nanotubes grown on carbon fabric with high rate capability for super-capacitors. Synth. Met. **162**, 1090–1096 (2012). https://doi.org/10.1016/j.synthmet.2012.04.029
21. F. Nassoy, M. Pinault, J. Descarpentries, T. Vignal, P. Banet, P.E. Coulon, T.G. de Monsabert, H. Hauf, P.H. Aubert, C. Reynaud, M. Mayne-L'hermite, Single-step synthesis of vertically aligned carbon nanotube forest on aluminium foils. Nanomaterials **9**, 1–18 (2019). https://doi.org/10.3390/nano9111590
22. T. Vignal, P. Banet, M. Pinault, R. Lafourcade, J. Descarpentries, L. Darchy, H. Hauf, C. Reynaud, M. Mayne-L'Hermite, P.H. Aubert, Electropolymerized poly(3-methylthiophene) onto high density vertically aligned carbon nanotubes directly grown on aluminum substrate: application to electrochemical capacitors. Electrochim. Acta. **350** (2020). https://doi.org/10.1016/j.electacta.2020.136377
23. J. Xia, F. Chen, J. Li, N. Tao, Measurement of the quantum capacitance of graphene. Nat. Nanotechnol. **4**, 505–509 (2009). https://doi.org/10.1038/nnano.2009.177
24. X. Cao, Y. Shi, W. Shi, G. Lu, X. Huang, Q. Yan, Q. Zhang, H. Zhang, Preparation of novel 3D graphene networks for supercapacitor applications. Small **7**, 3163–3168 (2011). https://doi.org/10.1002/smll.201100990
25. J.J. Yoo, K. Balakrishnan, J. Huang, V. Meunier, B.G. Sumpter, A. Srivastava, M. Conway, A.L. Mohana Reddy, J. Yu, R. Vajtai, P.M. Ajayan, Ultrathin planar graphene supercapacitors. Nano Lett. **11**, 1423–1427 (2011). https://doi.org/10.1021/nl200225j
26. C. Liu, Z. Yu, D. Neff, A. Zhamu, B.Z. Jang, Graphene-based supercapacitor with an ultrahigh energy density. Nano Lett. **10**, 4863–4868 (2010). https://doi.org/10.1021/nl102661q
27. S.R.C. Vivekchand, C.S. Rout, K.S. Subrahmanyam, A. Govindaraj, C.N.R. Rao, Graphene-based electrochemical supercapacitors. J. Chem. Sci. **120**, 9–13 (2008). https://doi.org/10.1007/s12039-008-0002-7
28. Q. Ke, J. Wang, Graphene-based materials for supercapacitor electrodes—a review. J. Mater. **2**, 37–54 (2016). https://doi.org/10.1016/j.jmat.2016.01.001
29. Y. Cheng, S. Lu, H. Zhang, C.V. Varanasi, J. Liu, Synergistic effects from graphene and carbon nanotubes enable flexible and robust electrodes for high-performance supercapacitors. Nano Lett. **12**, 4206–4211 (2012). https://doi.org/10.1021/nl301804c
30. J. Liu, L. Zhang, H. Bin Wu, J. Lin, Z. Shen, X.W. Lou, High-performance flexible asymmetric supercapacitors based on a new graphene foam/carbon nanotube hybrid film. Energy Environ. Sci. **7**, 3709–3719 (2014). https://doi.org/10.1039/c4ee01475h
31. D. Yu, K. Goh, H. Wang, L. Wei, W. Jiang, Q. Zhang, L. Dai, Y. Chen, Scalable synthesis of hierarchically structured carbon nanotube-graphene fibres for capacitive energy storage. Nat. Nanotechnol. **9**, 555–562 (2014). https://doi.org/10.1038/nnano.2014.93
32. W.A. Wampler, K. Rajeshwar, R.G. Pethe, R.C. Hyer, S.C. Sharma, Composites of polypyrrole and carbon black: Part III. Chemical synthesis and characterization. J. Mater. Res. **10**, 1811–1822 (1995). https://doi.org/10.1557/JMR.1995.1811

33. A. Izadi-Najafabadi, D.T.H. Tan, J.D. Madden, Towards high power polypyrrole/carbon capacitors. Synth. Met. **152**, 129–132 (2005). https://doi.org/10.1016/j.synthmet.2005.07.094
34. D. Wang, F. Li, J. Zhao, W. Ren, Z. Chen, J. Tan, Z. Wu, I. Gentle, G.Q. Lu, H. Cheng, Fabrication of graphene/polyaniline performance flexible electrode electropolymerization for high- composite paper via in situ anodic. ACS Nano **3**, 1745–1752 (2009). https://doi.org/10.1021/nn900297m
35. H.P. Cong, X.C. Ren, P. Wang, S.H. Yu, Flexible graphene-polyaniline composite paper for high-performance supercapacitor. Energy Environ. Sci. **6**, 1185–1191 (2013). https://doi.org/10.1039/c2ee24203f
36. Y. Han, L. Dai, Conducting polymers for flexible supercapacitors. Macromol. Chem. Phys. **220**, 1–14 (2019). https://doi.org/10.1002/macp.201800355
37. J.H. Fan, M.X. Wan, D.B. Zhu, B.H. Chang, Z.W. Pan, S.S. Xe, Synthesis, characterizations, and physical properties of carbon nanotubes coated by conducting polypyrrole. J. Appl. Polym. Sci. **74**, 2605–2610 (1999). Doi https://doi.org/10.1002/(Sici)1097-4628(19991209)74:11<2605::Aid-App6>3.0.Co;2-R
38. K.H. An, K.K. Jeon, J.K. Heo, S.C. Lim, D.J. Bae, Y.H. Lee, High-capacitance supercapacitor using a nanocomposite electrode of single-walled carbon nanotube and polypyrrole. J. Electrochem. Soc. **149**, A1058 (2002). https://doi.org/10.1149/1.1491235
39. C. Zhou, S. Kumar, C.D. Doyle, J.M. Tour, Functionalized single wall carbon nanotubes treated with pyrrole for electrochemical supercapacitor membranes. Chem. Mater. **17**, 1997–2002 (2005). https://doi.org/10.1021/cm047882b
40. Y. Gao, Graphene and polymer composites for supercapacitor applications: a review. Nanoscale Res. Lett. **12**, 1–17 (2017). https://doi.org/10.1186/s11671-017-2150-5
41. K. Lota, V. Khomenko, E. Frackowiak, Capacitance properties of poly(3,4-ethylenedioxythiophene)/carbon nanotubes composites. J. Phys. Chem. Solids. **65**, 295–301 (2004). https://doi.org/10.1016/j.jpcs.2003.10.051
42. W.-C.C. Chen, T.-C.C. Wen, H. Teng, Polyaniline-deposited porous carbon electrode for supercapacitor. Electrochim. Acta. **48**, 641–649 (2003). https://doi.org/10.1016/S0013-4686(02)00734-X
43. W.C. Chen, T.C. Wen, Electrochemical and capacitive properties of polyaniline-implanted porous carbon electrode for supercapacitors. J. Power Sources. **117**, 273–282 (2003). https://doi.org/10.1016/S0378-7753(03)00158-7
44. C. Downs, J. Nugent, P.M. Ajayan, D.J. Duquette, K.S.V. Santhanam, Efficient polymerization of aniline at carbon nanotube electrodes. Adv. Mater. **11**, 1028–1031 (1999). https://doi.org/10.1002/(SICI)1521-4095(199908)11:12%3c1028::AID-ADMA1028%3e3.0.CO;2-N
45. R. Kötz, M. Hahn, P. Ruch, R. Gallay, Comparison of pressure evolution in supercapacitor devices using different aprotic solvents. Electrochem. Commun. **10**, 359–362 (2008). https://doi.org/10.1016/j.elecom.2007.12.016
46. R. Newell, J. Faure-Vincent, B. Iliev, T. Schubert, D. Aradilla, A new high performance ionic liquid mixture electrolyte for large temperature range supercapacitor applications (−70 to 80 °C) operating at 3.5V cell voltage. Electrochim. Acta. **267**, 15–19 (2018). https://doi.org/10.1016/j.electacta.2018.02.067
47. L. Dagousset, G. Pognon, G.T.M. Nguyen, F. Vidal, S. Jus, P.H. Aubert, Self-standing gel polymer electrolyte for improving supercapacitor thermal and electrochemical stability. J. Power Sour. **391**, 86–93 (2018). https://doi.org/10.1016/j.jpowsour.2018.04.073
48. H. Ohno, *Electrochemical aspects of ionic liquids* (John Wiley, Wiley, Hoboken, NJ, USA, 2011)
49. J.S. Wilkes, M.J. Zaworotko, Air and water stable 1-ethyl-3-methylimidazolium based ionic liquids. J. Chem. Soc. Chem. Commun. **13**, 965–967 (1992). https://doi.org/10.1039/c39920000965
50. M. Galiński, A. Lewandowski, I. Stępniak, Ionic liquids as electrolytes. Electrochim. Acta. **51**, 5567–5580 (2006). https://doi.org/10.1016/j.electacta.2006.03.016
51. Y. Huang, M. Zhong, Y. Huang, M. Zhu, Z. Pei, Z. Wang, Q. Xue, X. Xie, C. Zhi, A self-healable and highly stretchable supercapacitor based on a dual crosslinked polyelectrolyte. Nat. Commun. **6**, 1–8 (2015). https://doi.org/10.1038/ncomms10310

52. E. Kovalska, C. Kocabas, Organic electrolytes for graphene-based supercapacitor: liquid, gel or solid. Mater. Today Commun. **7**, 155–160 (2016). https://doi.org/10.1016/j.mtcomm.2016.04.013
53. B. Asbani, C. Douard, T. Brousse, J. Le Bideau, High temperature solid-state supercapacitor designed with ionogel electrolyte. Energy Storage Mater. **21**, 439–445 (2019). https://doi.org/10.1016/j.ensm.2019.06.004
54. B.G. Choi, S.J. Chang, H.W. Kang, C.P. Park, H.J. Kim, W.H. Hong, S. Lee, Y.S. Huh, High performance of a solid-state flexible asymmetric supercapacitor based on graphene films. Nanoscale **4**, 4983–4988 (2012). https://doi.org/10.1039/c2nr30991b
55. K.B. Li, D.W. Shi, Z.Y. Cai, G.L. Zhang, Q.A. Huang, D. Liu, C.P. Yang, Studies on the equivalent serial resistance of carbon supercapacitor. Electrochim. Acta. **174**, 596–600 (2015). https://doi.org/10.1016/j.electacta.2015.06.008
56. E. Dauzon, X. Sallenave, C. Plesse, F. Goubard, A. Amassian, T.D. Anthopoulos, Pushing the limits of flexibility and stretchability of solar cells: a review. Adv. Mater. **33**, 2101469 (2021). https://doi.org/10.1002/adma.202101469
57. S. Wang, N. Liu, J. Su, L. Li, F. Long, Z. Zou, X. Jiang, Y. Gao, Highly stretchable and self-healable supercapacitor with reduced graphene oxide based fiber springs. ACS Nano **11**, 2066–2074 (2017). https://doi.org/10.1021/acsnano.6b08262
58. R. Jia, L. Li, Y. Ai, H. Du, X. Zhang, Z. Chen, G. Shen, Self-healable wire-shaped supercapacitors with two twisted NiCo2O4 coated polyvinyl alcohol hydrogel fibers. Sci. China Mater. **61**, 254–262 (2018). https://doi.org/10.1007/s40843-017-9177-5
59. W.K. Chee, H.N. Lim, Z. Zainal, N.M. Huang, I. Harrison, Y. Andou, Flexible graphene-based supercapacitors: a review. J. Phys. Chem. C. **120**, 4153–4172 (2016). https://doi.org/10.1021/acs.jpcc.5b10187
60. N.A. Echeverry-Montoya, J.J. Prías-Barragán, L. Tirado-Mejía, C. Agudelo, G. Fonthal, H. Ariza-Calderón, Fabrication and electrical response of flexible supercapacitor based on activated carbon from bamboo. Phys. Status Solidi Curr. Top. Solid State Phys. **14**,1600258 (2017). https://doi.org/10.1002/pssc.201600258
61. S. He, W. Chen, Application of biomass-derived flexible carbon cloth coated with MnO2 nanosheets in supercapacitors. J. Power Sour. **294**, 150–158 (2015). https://doi.org/10.1016/j.jpowsour.2015.06.051
62. Q. Wang, W. Ren, F. Gao, C. Qiu, Q. Wang, F. Gao, C. Zhao, Thermally activated multilayered carbon cloth as flexible supercapacitor electrode material with significantly enhanced areal energy density. Chem Electro Chem (2019). https://doi.org/10.1002/celc.201801642
63. R. Yuksel, Z. Sarioba, A. Cirpan, P. Hiralal, H.E. Unalan, Transparent and flexible supercapacitors with single walled carbon nanotube thin film electrodes. ACS Appl. Mater. Interfaces. **6**, 15434–15439 (2014). https://doi.org/10.1021/am504021u
64. S. Xi, Y. Kang, S. Qu, S. Han, Flexible supercapacitors on chips with interdigital carbon nanotube fiber electrodes. Mater. Lett. **175**, 126–130 (2016). https://doi.org/10.1016/j.matlet.2016.03.143
65. X.H. Zhong, Y.L. Li, Y.K. Liu, X.H. Qiao, Y. Feng, J. Liang, J. Jin, L. Zhu, F. Hou, J.Y. Li, Continuous multilayered carbon nanotube yarns. Adv. Mater. **22**, 692–696 (2010). https://doi.org/10.1002/adma.200902943
66. S. Hu, R. Rajamani, X. Yu, Flexible solid-state paper based carbon nanotube supercapacitor. Appl. Phys. Lett. **100**, 1–5 (2012). https://doi.org/10.1063/1.3691948
67. X. Lu, Y. Bai, R. Wang, J. Sun, A high-performance flexible and weavable asymmetric fiber-shaped solid-state supercapacitor enhanced by surface modifications of carbon fibers with carbon nanotubes. J. Mater. Chem. A. **4**, 18164–18173 (2016). https://doi.org/10.1039/c6ta08233e
68. Y. Wang, Z. Shi, Y. Huang, Y. Ma, C. Wang, M. Chen, Y. Chen, Supercapacitor devices based on graphene materials. J. Phys. Chem. C. **113**, 13103–13107 (2009). https://doi.org/10.1021/jp902214f
69. Y. Han, Y. Ge, Y. Chao, C. Wang, G.G. Wallace, Recent progress in 2D materials for flexible supercapacitors. J. Energy Chem. **27**, 57–72 (2018). https://doi.org/10.1016/j.jechem.2017.10.033

70. M.R. Benzigar, V.D.B.C. Dasireddy, X. Guan, T. Wu, G. Liu, Advances on emerging materials for flexible supercapacitors: current trends and beyond. Adv. Funct. Mater. **30**, 2002993 (2020). https://doi.org/10.1002/adfm.202002993
71. D. Xu, C. Xuan, X. Li, Z. Luo, Z. Wang, T. Tang, J. Wen, M. Li, J. Xiao, Novel helical carbon nanotubes-embedded reduced graphene oxide in three-dimensional architecture for high-performance flexible supercapacitors. Electrochim. Acta. **339**, 135912 (2020). https://doi.org/10.1016/j.electacta.2020.135912
72. L. Jiang, L. Sheng, C. Long, Z. Fan, Densely packed graphene nanomesh-carbon nanotube hybrid film for ultra-high volumetric performance supercapacitors. Nano Energy **11**, 471–480 (2015). https://doi.org/10.1016/j.nanoen.2014.11.007
73. Z. Weng, Y. Su, D.W. Wang, F. Li, J. Du, H.M. Cheng, Graphene-cellulose paper flexible supercapacitors. Adv. Energy Mater. **1**, 917–922 (2011). https://doi.org/10.1002/aenm.201100312
74. G.H. Films, Y. Xu, Z. Lin, X. Huang, Y. Liu, Y. Huang, X. Duan, Flexible solid-state supercapacitors based on three-dimensional 4042–4049 (2013)
75. P. Tamilarasan, S. Ramaprabhu, Graphene based all-solid-state supercapacitors with ionic liquid incorporated polyacrylonitrile electrolyte. Energy **51**, 374–381 (2013). https://doi.org/10.1016/j.energy.2012.11.037
76. H. Shirakawa, E.J. Louis, A.G. MacDiarmid, C.K. Chiang, A.J. Heeger. Synthesis of electrically conducting organic polymers: halogen derivatives of polyacetylene, (CH)x. J. Chem. Soc. Chem. Commun. 578–580 (1977). https://doi.org/10.1039/C39770000578
77. H. Yoon, J. Jang, Conducting-polymer nanomaterials for high-performance sensor applications: issues and challenges. Adv. Funct. Mater. **19**, 1567–1576 (2009). https://doi.org/10.1002/adfm.200801141
78. M. Hamedi, R. Forchheimer, O. Inganäs, Towards woven logic from organic electronic fibres. Nat. Mater. **6**, 357–362 (2007). https://doi.org/10.1038/nmat1884
79. P.M. Beaujuge, J.R. Reynolds, Color control in pi-conjugated organic polymers for use in electrochromic devices. Chem. Rev. **110**, 268–320 (2010). https://doi.org/10.1021/cr900129a
80. Q. Meng, K. Cai, Y. Chen, L. Chen, Research progress on conducting polymer based supercapacitor electrode materials. Nano Energy **36**, 268–285 (2017). https://doi.org/10.1016/j.nanoen.2017.04.040
81. G.A. Snook, P. Kao, A.S. Best, Conducting-polymer-based supercapacitor devices and electrodes. J. Power Sour. **196**, 1–12 (2011). https://doi.org/10.1016/j.jpowsour.2010.06.084
82. M.E. Abdelhamid, A.P. O'Mullane, G.A. Snook, Storing energy in plastics: a review on conducting polymers and their role in electrochemical energy storage. RSC Adv. **5**, 11611–11626 (2015). https://doi.org/10.1039/c4ra15947k
83. L. Pan, H. Qiu, C. Dou, Y. Li, L. Pu, J. Xu, Y. Shi, Conducting polymer nanostructures: template synthesis and applications in energy storage. Int. J. Mol. Sci. **11**, 2636–2657 (2010). https://doi.org/10.3390/ijms11072636
84. J. Yang, Y. Liu, S. Liu, L. Li, C. Zhang, T. Liu, Conducting polymer composites: Material synthesis and applications in electrochemical capacitive energy storage. Mater. Chem. Front. **1**, 251–268 (2017). https://doi.org/10.1039/c6qm00150e
85. A.G. MacDiarmid, Synthetic metals: a novel role for organic polymers. Synth. Met. **125**, 11–22 (2001). https://doi.org/10.1016/S0379-6779(01)00508-2
86. B.C. Kim, J.S. Kwon, J.M. Ko, J.H. Park, C.O. Too, G.G. Wallace, Preparation and enhanced stability of flexible supercapacitor prepared from Nafion/polyaniline nanofiber. Synth. Met. **160**, 94–98 (2010). https://doi.org/10.1016/j.synthmet.2009.10.011
87. H. Gleskova, S. Wagner, Z. Suo, Failure resistance of amorphous silicon transistors under extreme in-plane strain. Appl. Phys. Lett. **75**, 3011–3013 (1999). https://doi.org/10.1063/1.125174
88. L. Mao, Q. Meng, A. Ahmad, Z. Wei, Mechanical analyses and structural design requirements for flexible energy storage devices. Adv. Energy Mater. **7**, 1–19 (2017). https://doi.org/10.1002/aenm.201700535

89. J. Yan, T. Wei, Z. Fan, W. Qian, M. Zhang, X. Shen, F. Wei, Preparation of graphene nanosheet/carbon nanotube/polyaniline composite as electrode material for supercapacitors. J. Power Sour. **195**, 3041–3045 (2010). https://doi.org/10.1016/j.jpowsour.2009.11.028
90. A.Y. Lo, L. Saravanan, C.M. Tseng, F.K. Wang, J.T. Huang, Effect of composition ratios on the performance of graphene/carbon nanotube/manganese oxide composites toward supercapacitor applications. ACS Omega **5**, 578–587 (2020). https://doi.org/10.1021/acsomega.9b03163
91. A. Ansaldo, P. Bondavalli, S. Bellani, A.E. Del Rio Castillo, M. Prato, V. Pellegrini, G. Pognon, F. Bonaccorso, High-power grapheneCarbon nanotube hybrid supercapacitors. Chem. Nano. Mat. **3**, 436–446 (2017). https://doi.org/10.1002/cnma.201700093
92. S. Wang, L. Ma, M. Gan, S. Fu, W. Dai, T. Zhou, X. Sun, H. Wang, H. Wang, Free-standing 3D graphene/polyaniline composite film electrodes for high-performance supercapacitors. J. Power Sour. **299**, 347–355 (2015). https://doi.org/10.1016/j.jpowsour.2015.09.018
93. Q. Liu, J. Qiu, C. Yang, L. Zang, G. Zhang, E. Sakai, H. Wu, S. Guo, Robust quasi-solid-state integrated asymmetric flexible supercapacitors with interchangeable positive and negative electrode based on all-conducting-polymer electrodes. J. Alloys Compd. **887**, 161362 (2021). https://doi.org/10.1016/j.jallcom.2021.161362
94. D.W. Wang, F. Li, J. Zhao, W. Ren, Z.G. Chen, J. Tan, Z.S. Wu, I. Gentle, G.Q. Lu, H.M. Cheng, Fabrication of graphene/polyaniline composite paper via in situ anodic electropolymerization for high-performance flexible electrode. ACS Nano **3**, 1745–1752 (2009). https://doi.org/10.1021/nn900297m
95. Y. Lin, H. Zhang, W. Deng, D. Zhang, N. Li, Q. Wu, C. He, In-situ growth of high-performance all-solid-state electrode for flexible supercapacitors based on carbon woven fabric/ polyaniline/ graphene composite. J. Power Sour. **384**, 278–286 (2018). https://doi.org/10.1016/j.jpowsour.2018.03.003
96. Y. Zhou, X. Hu, Y. Shang, C. Hua, P. Song, X. Li, Y. Zhang, A. Cao, Highly flexible all-solid-state supercapacitors based on carbon nanotube/polypyrrole composite films and fibers. RSC Adv. **6**, 62062–62070 (2016). https://doi.org/10.1039/c6ra07297f
97. L. Chen, J. Huang, R. Zeng, Y. Xiong, J. Wei, K. Yuan, Y. Chen, Regulating voltage window and energy density of aqueous asymmetric supercapacitors by pinecone-like hollow Fe2O3/MnO2 nano-heterostructure. Adv. Mater. Interfaces. **7**, 1–9 (2020). https://doi.org/10.1002/admi.201901729
98. L. Ruiyi, H. Keyang, Y. Yongqiang, Z. Haiyan, L. Zaijun, Atomically dispersed RuO2-tryptophan functionalized graphene quantum dot-graphene hybrid with double Schottky heterojunctions for high performance flexible supercapacitors. Chem. Eng. J. **426**, 130893 (2021). https://doi.org/10.1016/j.cej.2021.130893
99. S. Prabhu, S. Sohila, D. Navaneethan, S. Harish, M. Navaneethan, R. Ramesh, Three dimensional flower-like CuO/Co3O4/r-GO heterostructure for high-performance asymmetric supercapacitors, Elsevier B.V., (2020) https://doi.org/10.1016/j.jallcom.2020.156439
100. V.E. Gurenko, V.I. Popkov, A.A. Lobinsky, Synthesis of NiO granular nanospheres as a novel material for high-performance supercapacitors. Mater. Lett. **279**, 128478 (2020). https://doi.org/10.1016/j.matlet.2020.128478
101. B. Asbani, K. Robert, P. Roussel, T. Brousse, C. Lethien, Asymmetric micro-supercapacitors based on electrodeposited Ruo2 and sputtered VN films. Energy Stor. Mater. **37**, 207–214 (2021). https://doi.org/10.1016/j.ensm.2021.02.006
102. S. Cho, J. Kim, Y. Jo, A.T.A. Ahmed, H.S. Chavan, H. Woo, A.I. Inamdar, J.L. Gunjakar, S.M. Pawar, Y. Park, H. Kim, H. Im, Bendable RuO2/graphene thin film for fully flexible supercapacitor electrodes with superior stability. J. Alloys Compd. **725**, 108–114 (2017). https://doi.org/10.1016/j.jallcom.2017.07.135
103. V.K.A. Muniraj, C.K. Kamaja, M.V. Shelke, RuO2·nH2O nanoparticles anchored on carbon nano-onions: an efficient electrode for solid state flexible electrochemical supercapacitor. ACS Sustain. Chem. Eng. **4**, 2528–2534 (2016). https://doi.org/10.1021/acssuschemeng.5b01627

104. K. Brousse, S. Pinaud, S. Nguyen, P.F. Fazzini, R. Makarem, C. Josse, Y. Thimont, B. Chaudret, P.L. Taberna, M. Respaud, P. Simon, Facile and scalable preparation of ruthenium oxide-based flexible micro-supercapacitors. Adv. Energy Mater. **10**, 1–9 (2020). https://doi.org/10.1002/aenm.201903136
105. Y. Chang, W. Zhou, J. Wu, G. Ye, Q. Zhou, D. Li, D. Zhu, T. Li, G. Nie, Y. Du, J. Xu, High-performance flexible-film supercapacitors of layered hydrous RuO2/poly(3,4-ethylenedioxythiophene)-poly(styrenesulfonate) through vacuum filtration. Electrochim. Acta. **283**, 744–754 (2018). https://doi.org/10.1016/j.electacta.2018.06.044
106. M. Huang, F. Li, F. Dong, Y.X. Zhang, L.L. Zhang, MnO2-based nanostructures for high-performance supercapacitors. J. Mater. Chem. A. **3**, 21380–21423 (2015). https://doi.org/10.1039/c5ta05523g
107. Y. He, W. Chen, X. Li, Z. Zhang, J. Fu, C. Zhao, E. Xie, Freestanding three-dimensional graphene/Mno2 composite networks as ultralight and flexible supercapacitor electrodes. ACS Nano **7**, 174–182 (2013). https://doi.org/10.1021/nn304833s
108. Q. Chen, Y. Meng, C. Hu, Y. Zhao, H. Shao, N. Chen, L. Qu, MnO2-modified hierarchical graphene fiber electrochemical supercapacitor. J. Power Sour. **247**, 32–39 (2014). https://doi.org/10.1016/j.jpowsour.2013.08.045
109. Y. Jin, H. Chen, M. Chen, N. Liu, Q. Li, Graphene-patched CNT/MnO2 nanocomposite papers for the electrode of high-performance flexible asymmetric supercapacitors. ACS Appl. Mater. Interfaces. **5**, 3408–3416 (2013). https://doi.org/10.1021/am400457x
110. Q. Wang, Y. Ma, X. Liang, D. Zhang, M. Miao, Flexible supercapacitors based on carbon nanotube-MnO2 nanocomposite film electrode. Chem. Eng. J. **371**, 145–153 (2019). https://doi.org/10.1016/j.cej.2019.04.021
111. N. Yu, H. Yin, W. Zhang, Y. Liu, Z. Tang, M.Q. Zhu, High-performance fiber-shaped all-solid-state asymmetric supercapacitors based on ultrathin MnO2 nanosheet/carbon fiber cathodes for wearable electronics. Adv. Energy Mater. **6**, 1–9 (2016). https://doi.org/10.1002/aenm.201501458
112. D. Zhou, H. Lin, F. Zhang, H. Niu, L. Cui, Q. Wang, F. Qu, Freestanding MnO2 nanoflakes/porous carbon nanofibers for high-performance flexible supercapacitor electrodes. Electrochim. Acta. **161**, 427–435 (2015). https://doi.org/10.1016/j.electacta.2015.02.085
113. X. Dong, X. Wang, J. Wang, H. Song, X. Li, L. Wang, M.B. Chan-Park, C.M. Li, P. Chen, Synthesis of a MnO 2-graphene foam hybrid with controlled MnO 2 particle shape and its use as a supercapacitor electrode. Carbon N. Y. **50**, 4865–4870 (2012). https://doi.org/10.1016/j.carbon.2012.06.014
114. F. Liao, X. Han, D. Cheng, Y. Zhang, X. Han, C. Xu, H. Chen, MnO2 hierarchical microspheres assembled from porous nanoplates for high-performance supercapacitors. Ceram. Int. **45**, 1058–1066 (2019). https://doi.org/10.1016/j.ceramint.2018.09.285
115. S. Sun, G. Jiang, Y. Liu, Y. Zhang, J. Zhou, B. Xu, Growth of MnO2 nanoparticles on hybrid carbon nanofibers for flexible symmetrical supercapacitors. Mater. Lett. **197**, 35–37 (2017). https://doi.org/10.1016/j.matlet.2017.03.092
116. Z. Fan, Y. Wang, Z. Xie, X. Xu, Y. Yuan, Z. Cheng, Y. Liu, A nanoporous MXene film enables flexible supercapacitors with high energy storage. Nanoscale **10**, 9642–9652 (2018). https://doi.org/10.1039/c8nr01550c
117. N.K. Chaudhari, H. Jin, B. Kim, D. San Baek, S.H. Joo, K. Lee, MXene: an emerging two-dimensional material for future energy conversion and storage applications. J. Mater. Chem. A. **5**, 24564–24579 (2017). https://doi.org/10.1039/C7TA09094C
118. M.R. Lukatskaya, S. Kota, Z. Lin, M.Q. Zhao, N. Shpigel, M.D. Levi, J. Halim, P.L. Taberna, M.W. Barsoum, P. Simon, Y. Gogotsi, Ultra-high-rate pseudocapacitive energy storage in two-dimensional transition metal carbides. Nat. Energy. **2**, 1–6 (2017). https://doi.org/10.1038/nenergy.2017.105
119. M.R. Lukatskaya, S.M. Bak, X. Yu, X.Q. Yang, M.W. Barsoum, Y. Gogotsi, Probing the mechanism of high capacitance in 2D titanium carbide using in situ X-ray absorption spectroscopy. Adv. Energy Mater. **5**, 2–5 (2015). https://doi.org/10.1002/aenm.201500589

120. Z. Ling, C.E. Ren, M.Q. Zhao, J. Yang, J.M. Giammarco, J. Qiu, M.W. Barsoum, Y. Gogotsi, Flexible and conductive MXene films and nanocomposites with high capacitance. Proc. Natl. Acad. Sci. U. S. A. **111**, 16676–16681 (2014). https://doi.org/10.1073/pnas.1414215111
121. Z. Wang, S. Qin, S. Seyedin, J. Zhang, J. Wang, A. Levitt, N. Li, C. Haines, R. Ovalle-Robles, W. Lei, Y. Gogotsi, R.H. Baughman, J.M. Razal, High-performance biscrolled MXene/Carbon nanotube yarn supercapacitors. Small **14**, 1–9 (2018). https://doi.org/10.1002/smll.201802225
122. C. Choi, K.M.K.J.K.M. Kim, K.M.K.J.K.M. Kim, X. Lepró, G.M. Spinks, R.H. Baughman, S.J. Kim, Improvement of system capacitance via weavable superelastic biscrolled yarn supercapacitors. Nat. Commun. **7**, 1–8 (2016). https://doi.org/10.1038/ncomms13811
123. Q. Zhang, X. Wang, Z. Pan, J. Sun, J. Zhao, J. Zhang, C. Zhang, L. Tang, J. Luo, B. Song, Z. Zhang, W. Lu, Q. Li, Y. Zhang, Y. Yao, Wrapping aligned carbon nanotube composite sheets around vanadium nitride nanowire arrays for asymmetric coaxial fiber-shaped supercapacitors with ultrahigh energy density. Nano Lett. **17**, 2719–2726 (2017). https://doi.org/10.1021/acs.nanolett.7b00854
124. H. Yang, H. Xu, M. Li, L. Zhang, Y. Huang, X. Hu, Assembly of NiO/Ni(OH)2/PEDOT nanocomposites on contra wires for fiber-shaped flexible asymmetric supercapacitors. ACS Appl. Mater. Interfaces. **8**, 1774–1779 (2016). https://doi.org/10.1021/acsami.5b09526
125. W. Cai, T. Lai, J. Lai, H. Xie, L. Ouyang, J. Ye, C. Yu, Transition metal sulfides grown on graphene fibers for wearable asymmetric supercapacitors with high volumetric capacitance and high energy density. Sci. Rep. **6**, 1–9 (2016). https://doi.org/10.1038/srep26890
126. J. Yan, C.E. Ren, K. Maleski, C.B. Hatter, B. Anasori, P. Urbankowski, A. Sarycheva, Y. Gogotsi, Flexible MXene/graphene films for ultrafast supercapacitors with outstanding volumetric capacitance. Adv. Funct. Mater. **27**, 1–10 (2017). https://doi.org/10.1002/adfm.201701264
127. L.S. Xie, G. Skorupskii, M. Dincă, Electrically conductive metal-organic frameworks. Chem. Rev. **120**, 8536–8580 (2020). https://doi.org/10.1021/acs.chemrev.9b00766
128. Y. Qi, F. Luo, Y. Che, J. Zheng, Hydrothermal synthesis of metal-organic frameworks based on aromatic polycarboxylate and flexible bis(imidazole) ligands. Cryst. Growth Des. **8**, 606–611 (2008). https://doi.org/10.1021/cg700758c
129. W. Xuan, R. Ramachandran, C. Zhao, F. Wang, Influence of synthesis temperature on cobalt metal-organic framework (Co-MOF) formation and its electrochemical performance towards supercapacitor electrodes. J. Solid State Electrochem. **22**, 3873–3881 (2018). https://doi.org/10.1007/s10008-018-4096-7
130. N. Campagnol, E. Rezende Souza, D.E. De Vos, K. Binnemans, J. Fransaer, Luminescent terbium-containing metal–organic framework films: new approaches for the electrochemical synthesis and application as detectors for explosives. Chem. Commun. **50**, 12680–12683 (2014). https://doi.org/10.1039/c4cc05742b
131. M. Klimakow, P. Klobes, A.F. Thünemann, K. Rademann, F. Emmerling, Mechanochemical synthesis of metal-organic frameworks: a fast and facile approach toward quantitative yields and high specific surface areas. Chem. Mater. **22**, 5216–5221 (2010). https://doi.org/10.1021/cm1012119
132. D. Chen, J. Zhao, P. Zhang, S. Dai, Mechanochemical synthesis of metal–organic frameworks. Polyhedron **162**, 59–64 (2019). https://doi.org/10.1016/j.poly.2019.01.024
133. N.A. Khan, S.H. Jhung, Synthesis of metal-organic frameworks (MOFs) with microwave or ultrasound: rapid reaction, phase-selectivity, and size reduction. Coord. Chem. Rev. **285**, 11–23 (2015). https://doi.org/10.1016/j.ccr.2014.10.008
134. D. Sheberla, J.C. Bachman, J.S. Elias, C.J. Sun, Y. Shao-Horn, M. Dincă, Conductive MOF electrodes for stable supercapacitors with high areal capacitance. Nat. Mater. **16**, 220–224 (2017). https://doi.org/10.1038/nmat4766
135. Z. Wang, Y. Liu, C. Gao, H. Jiang, J. Zhang, A porous Co(OH)2 material derived from a MOF template and its superior energy storage performance for supercapacitors. J. Mater. Chem. A. **3**, 20658–20663 (2015). https://doi.org/10.1039/c5ta04663g
136. R.R. Salunkhe, Y. Kamachi, N.L. Torad, S.M. Hwang, Z. Sun, S.X. Dou, J.H. Kim, Y. Yamauchi, Fabrication of symmetric supercapacitors based on MOF-derived nanoporous carbons. J. Mater. Chem. A. **2**, 19848–19854 (2014). https://doi.org/10.1039/c4ta04277h

137. R. Díaz, M.G. Orcajo, J.A. Botas, G. Calleja, J. Palma, Co8-MOF-5 as electrode for supercapacitors. Mater. Lett. **68**, 126–128 (2012). https://doi.org/10.1016/j.matlet.2011.10.046
138. D. Sheberla, L. Sun, M.A. Blood-Forsythe, S. Er, C.R. Wade, C.K. Brozek, A. Aspuru-Guzik, M. Dincă, High electrical conductivity in Ni3(2,3,6,7,10,11- hexaiminotriphenylene)2, a semiconducting metal-organic graphene analogue. J. Am. Chem. Soc. **136**, 8859–8862 (2014). https://doi.org/10.1021/ja502765n
139. C.W. Kung, P.C. Han, C.H. Chuang, K.C.W. Wu, Electronically conductive metal-organic framework-based materials. APL Mater. **7**, 110902 (2019). https://doi.org/10.1063/1.5125487
140. L. Wang, X. Feng, L. Ren, Q. Piao, J. Zhong, Y. Wang, H. Li, Y. Chen, B. Wang, Flexible solid-state supercapacitor based on a metal-organic framework interwoven by electrochemically-deposited PANI. J. Am. Chem. Soc. **137**, 4920–4923 (2015). https://doi.org/10.1021/jacs.5b01613
141. X. Xu, J. Tang, H. Qian, S. Hou, Y. Bando, M.S.A. Hossain, L. Pan, Y. Yamauchi, Three-dimensional networked metal-organic frameworks with conductive polypyrrole tubes for flexible supercapacitors. ACS Appl. Mater. Interfaces. **9**, 38737–38744 (2017). https://doi.org/10.1021/acsami.7b09944
142. B. Wang, S. Liu, L. Liu, W.W. Song, Y. Zhang, S.M. Wang, Z.B. Han, MOF/PEDOT/HPMo-based polycomponent hierarchical hollow micro-vesicles for high performance flexible supercapacitors. J. Mater. Chem. A. **9**, 2948–2958 (2021). https://doi.org/10.1039/d0ta10603h
143. D. Mohanadas, M.A.A. Mohd Abdah, N.H.N. Azman, T.B.S.A. Ravoof, Y. Sulaiman, Facile synthesis of PEDOT-rGO/HKUST-1 for high performance symmetrical supercapacitor device. Sci. Rep. **11**, 1–13 (2021). https://doi.org/10.1038/s41598-021-91100-x
144. C. Zhu, Y. He, Y. Liu, N. Kazantseva, P. Saha, Q. Cheng, ZnO@MOF@PANI core-shell nanoarrays on carbon cloth for high-performance supercapacitor electrodes. J. Energy Chem. **35**, 124–131 (2019). https://doi.org/10.1016/j.jechem.2018.11.006
145. K. Jayaramulu, M. Horn, A. Schneemann, H. Saini, A. Bakandritsos, V. Ranc, M. Petr, V. Stavila, C. Narayana, B. Scheibe, Š Kment, M. Otyepka, N. Motta, D. Dubal, R. Zbořil, R.A. Fischer, Covalent Graphene-MOF Hybrids for High-Performance Asymmetric Supercapacitors. Adv. Mater. **33**, 2004560 (2021). https://doi.org/10.1002/adma.202004560
146. S. Li, C. Shi, Y. Pan, Y. Wang, 2D/2D NiCo-MOFs/GO hybrid nanosheets for high-performance asymmetrical supercapacitor. Diam. Relat. Mater. **115**, 108358s (2021). https://doi.org/10.1016/j.diamond.2021.108358
147. J. Cheng, S. Chen, D. Chen, L. Dong, J. Wang, T. Zhang, T. Jiao, B. Liu, H. Wang, J.J. Kai, D. Zhang, G. Zheng, L. Zhi, F. Kang, W. Zhang, Editable asymmetric all-solid-state supercapacitors based on high-strength, flexible, and programmable 2D-metal-organic framework/reduced graphene oxide self-assembled papers. J. Mater. Chem. A. **6**, 20254–20266 (2018). https://doi.org/10.1039/c8ta06785f
148. W. Kim, S. Kwon, Y.C. Han, E. Kim, K.C. Choi, S.-H. Kang, B.-C. Park, Reliable actual fabric-based organic light-emitting diodes: toward a wearable display. Adv. Electron. Mater. **2**, 1600220 (2016). https://doi.org/10.1002/aelm.201600220
149. M.K. Choi, J. Yang, K. Kang, D.C. Kim, C. Choi, C. Park, S.J. Kim, S.I. Chae, T.-H. Kim, J.H. Kim, T. Hyeon, D.-H. Kim, Wearable red–green–blue quantum dot light-emitting diode array using high-resolution intaglio transfer printing. Nat. Commun. **6**, 7149 (2015). https://doi.org/10.1038/ncomms8149
150. N. Zhang, J. Chen, Y. Huang, W. Guo, J. Yang, J. Du, X. Fan, C. Tao, A wearable all-solid photovoltaic textile. Adv. Mater. **28**, 263–269 (2016). https://doi.org/10.1002/adma.201504137
151. S.H. Chae, W.J. Yu, J.J. Bae, D.L. Duong, D. Perello, H.Y. Jeong, Q.H. Ta, T.H. Ly, Q.A. Vu, M. Yun, X. Duan, Y.H. Lee, Transferred wrinkled Al2O3 for highly stretchable and transparent graphene–carbon nanotube transistors. Nat. Mater. **12**, 403–409 (2013). https://doi.org/10.1038/nmat3572

152. T. An, W. Cheng, Recent progress in stretchable supercapacitors. J. Mater. Chem. A. **6**, 15478–15494 (2018). https://doi.org/10.1039/C8TA03988G
153. C. Yu, C. Masarapu, J. Rong, B.Q.M. Wei, H. Jiang, Stretchable supercapacitors based on buckled single-walled carbon nanotube macrofilms. Adv. Mater. **21**, 4793–4797 (2009). https://doi.org/10.1002/adma.200901775
154. Z. Niu, H. Dong, B. Zhu, J. Li, H.H. Hng, W. Zhou, X. Chen, S. Xie, Highly stretchable, integrated supercapacitors based on single-walled carbon nanotube films with continuous reticulate architecture. Adv. Mater. **25**, 1058–1064 (2013). https://doi.org/10.1002/adma.201204003
155. G.B. Tsaeghi, B. Malengier, K.A. Fante, A.B. Nigusse, L. Van Langenhove, Integration of conductive materials with textile structures, an overview. Sensors **20**, 6910 (2020). https://doi.org/10.3390/s20236910

Supercapacitors: Future Direction and Challenges

Rasmita Barik, Vaishali Tanwar, and Pravin P. Ingole

Abstract The development of high-potential energy storage (ES) devices via advanced technologies is at the forefront of the current research scenario related to science and technology. Supercapacitors (SCs) or Electrochemical capacitors with longer durability and faster capability of charge storage are proved as emerging candidates in the energy domain. However, SCs are not a viable option in comparison to batteries and fuel cells for practical applications. There is also an urgent requirement of fabrication methods, which must be encountered to provide a suitable SC electrode. Herein, in this book chapter, a brief description of the various challenges experienced in terms of the manufacturing of the devices and market applications will be critically examined, and potential solutions towards the future technology will be provided. A major part will focus on the already developed and reported supercapacitor material and technologies. The book chapter will be able to impart a better understanding of the challenges at different stages of the research, manufacturing, and practical implication of SC in the market. Finally, a conclusive outlook of how the above-mentioned discussion will provide critical insights and generate opportunities to increase the potential scope of new-generation SCs has been discussed.

Keywords Supercapacitors · Energy material · Strategy · Future aspect · Hybrid supercapacitors · Micro-supercapacitors · Photo supercapacitors · Wearable and flexible supercapacitors

R. Barik (✉) · V. Tanwar · P. P. Ingole
Department of Chemistry, Indian Institute of Technology, Delhi, New Delhi 110016, India
e-mail: rasmita.barik@chemistry.iitd.ac.in

V. Tanwar
e-mail: vaishali.tanwar@chemistry.iitd.ac.in

P. P. Ingole
e-mail: ppingole@chemistry.iitd.ac.in

S. Thomas et al. (eds.), *Nanostructured Materials for Supercapacitors*,
Advances in Material Research and Technology,
https://doi.org/10.1007/978-3-030-99302-3_27

1 Introduction

Depletion of fossil fuels and natural resources due to globalization, industrialization, and significant enhancement in the use of electronic equipment (hybrid vehicles, electric vehicles, mobiles, laptops) with high rise population explosion has created an alarming situation for the whole world. On the other hand, the world's population is consistently increasing and is expected to be 9.4–10.2 billion by 2050 and to fulfill their energy demand the convenient and efficient energy storage devices such as supercapacitors and batteries are solicited [1–6]. The discovery of advanced energy storage devices/energy material/technique/devices is indisputably one of the great challenges in the twenty-first century to meet the need of modern society**.**

Electrochemical Supercapacitors (ECs) or Ultracapacitors, is the most enthusiastic research field for the current generation after battery research. Supercapacitors form a bridge between traditional capacitors and batteries. Capacitors do not store the energy as chemical energy, but rather by positioning opposite electrical charges near each other. The first-ever patent for supercapacitor was filed by H. I. Becker in 1957 (U.S. Patent 2,800,616), however, the device was never marketed. Although the concept of traditional capacitors was acquainted by Hermann von Helmholtz in 1879, the commonly used supercapacitor technology was invented by Robert A. Rightmire, who was working as a chemist at Standard Oil Company, Ohio in 1962 with Donald L. Boos [1–6]. This technology emerged in several other industries based on supercapacitors and the rapid growth can be well observed by advanced electronic devices. Electrochemical supercapacitors of SOHIO have progressed through several generations. While the supercapacitors are initially used in power devices for volatile clock chips and computer memories as complementary metal-oxide-semiconductor (CMOS).

ECs offer several advantages over other capacitors such as high energy density, high power density, stable cycle life, continuous longer charge–discharge cycles, low cost, environmental friendliness, and easy maintenance [7, 8]. Although they are capable to provide higher power density (PD) than batteries, their commercial liability is very low. Therefore, it is necessary to enhance the energy density (ED) by developing highly active electrode materials and widening the operating voltage window [9–27]. The physical charge storage of ECs does not rely on chemical reaction rates, which limits its application. Further, the search for novel, smart, flexible supercapacitors is an ongoing process. Apart from that, several disadvantages such as quick charging–discharging restrict the practical implication of SCs in applications. Moreover, unfortunately, the traditional ECs are bulky, and thereby can't be utilized in advanced electronic devices [1, 5, 9–12].

However, until the 1990s electrochemical supercapacitor technology was unable to draw attention, in the advance energy sector. Considering recent times, the demand for high-speed/power rechargeable energy storage devices with high performance is continuously increasing as shown in Fig. 1, and has motivated a lot of researchers to develop new advanced materials. The smart mobile devices, roll-up displays,

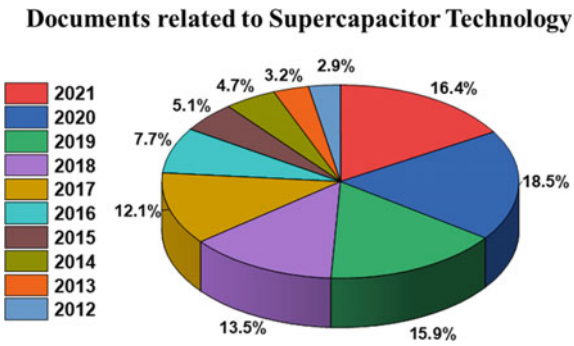

Fig. 1 Publication or Technology or patent of supercapacitor technology from last decade (*Data source* Scopus)

implantable biosensors have drawn huge attention with the use of organic light-emitting diode (OLED) in TV panels, smartphones, in the automobile industry as electric or hybrid vehicles and in wearable devices (smartwatch, different sensors) has forced the new generation to find out alternative energy sources apart from the conventional sources.

To fabricate a better performing electrochemical supercapacitor it is requisite to examine the storage mechanism. Apart from that, the development of advanced, and improved technology in such a manner that the state-of-the-art materials in SCs can replace the world-renowned batteries. Despite, numerous advantages such as long cycling life, safety, high efficiency, and high stability, why are supercapacitors lacking behind the batteries, and are incapable of substituting the batteries? Following this, the first crucial need is to understand the mechanism of ECs. Supercapacitors store electrical charge following the Faradic and/or electrostatic process at a surface-electrolyte interface. The specific or high capacitance is obtained due to the high surface area of the active materials such as metal oxides/sulfides/different carbon sources/polymers. The supercapacitors can produce higher energy density which is far greater than that of regular capacitors. The capacitance C (Farad, F) is calculated from the equation [10–12].

$$C = \frac{\varepsilon S}{d} \tag{1}$$

where ε is the dielectric constant of the insulating separators (F M^{-1}), S is the area of the electrodes (m^2) and d is the distance between the two electrodes (m).

The energy stored in supercapacitor devices is given by the following equation

$$E = \frac{1}{2} C V^2 \tag{2}$$

where, E = Energy density in W h kg^{-1}/W h cm^{-1}, C = Capacitance in F g^{-1}/F cm^{-2}, V = voltage in Volt.

Furthermore, EC devices show high power density with enhanced ultra-high energy density. However, the EC devices having high equivalent series resistance and low ion diffusion rate exhibits lower power density. The following relation shows the relation between power density (P), cell voltage (V), and resistance (R).

$$P = \frac{V^2}{4RS} \tag{3}$$

Therefore, to increase power density an appropriate electrolyte with reduced equivalent inner resistance is much needed. Electrochemical impedance spectroscopy (EIS) is one of the most commonly used techniques for the investigation of supercapacitors. It shows the charging of supercapacitors with a particular amplitude and a supplied potential. Frequency is directly proportional to applied potential, which is a major tool for supercapacitor study. Lower the frequency response better will be the capacitive behavior [10–13]. So, to boost the capacitance of EC's the cell applied voltage, electrolyte stability, selecting proper electrode materials and working substrate are playing an important character.

In this book chapter, we have briefly discussed the future perspective and mechanism of supercapacitors starting from the historical background. We have also discussed the key features of supercapacitors. In the second part, the development of the currently applicable devices along with their future scopes are discussed. While in third part the future aspects of supercapacitor technology with respect to energy material, device fabrication, industrial standard, and market values of SCs with respect to its consistency and reliability and how they will impact the future research are presented.

2 Current Research

The researchers and scientific community have shown keen interest in the supercapacitor and its development. They are constantly trying to establish the concept of ECs based on the charge-storage mechanism. The total charge storage is based on charge transfer reaction or faradic process (intercalation/deintercalation reaction) and non-faradic (electric double layer effect by electrode/electrolyte interface) [14, 15]. The total charge storage mechanism developed by Dunn gives a new direction towards fundamental supercapacitor research [16, 17]. The need for an alternative advanced energy storage device with higher charge storage capacity than the currently established technologies is paving the way towards real-time application.

In the early years of the SC, the research was more focused on developing electrode materials with high operating cell voltage (~4 V) by using novel and emerging electrolytes. The prime focus in earlier decades was based on the fabrication of symmetric/asymmetric supercapacitors and (Pseudo/Double layer) capacitors. With numerous progress, real ECs devices are fabricated (shown in Fig. 2) and named as hybrid supercapacitors, flexible supercapacitors, microsupercapacitors (MSC),

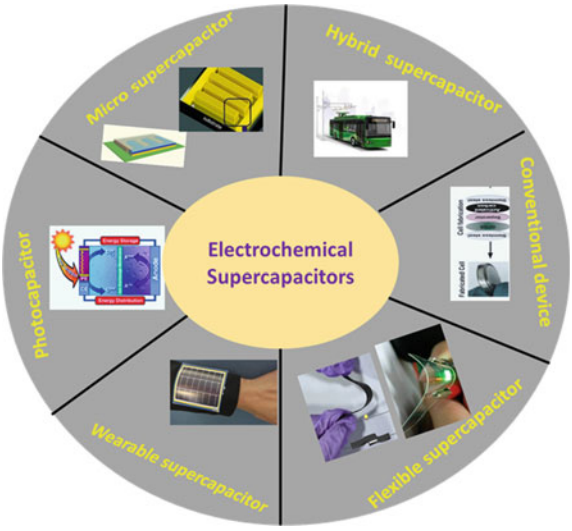

Fig. 2 Currently developed supercapacitor devices

photocapacitors, wearable capacitors, etc. With the rapid improvement, the flexible, multifunctional, miniature, with lightweight and deformable micro-energy storage and devices, integrated into the circuit, has become extremely important from the viewpoints of both basic research and practical applications.

2.1 Conventional Supercapacitors

It's very well known that supercapacitors are of two types; one is pseudocapacitors and the other is double-layer capacitors. While according to device fabrication methods, asymmetric and symmetric supercapacitors are fabricated. Still, lots of research going on metal oxide/sulfides, high surface area, and porous carbon-based materials like graphene, carbon nanotubes, activated carbon, etc.

The metal oxides or metal-based energy materials or conducting polymers show pseudo-capacitance behavior while the carbon or carbon-based, or carbon-derived materials show electric double layer behavior. Some of the new materials such as MXene [18, 19], metal-organic framework (MOFs) [20, 21], tertiary composites [22], metal oxides/sulfides [23] have gain attention. While the role of electrolytes still needs to be optimized. The discovery of MXene has shown some new promise for the development of supercapacitor devices and we can expect this will abolish all the energy problems. Transition metal carbides, carbonitrides and nitrides belongs to the MXene family with formula the $M_{n+1}X_nT_x$ ($n = 1$–3), where M signifies transition metals like Sc, Ti, Zr, Hf, V, Nb, Ta, Cr, Mo ….), X for carbon/nitrogen and T_x for hydroxyl/oxygen/fluorine groups with several MXene compositions [19]. Some of them show extraordinary electrochemical behavior as a supercapacitor. It is

quite helpful in developing electrochemical flow capacitors, however, reaching the maximum cell voltage can be achieved through the ionic liquid rather than aqueous or organic electrolytes.

2.2 *Hybrid Supercapacitors*

Supercapacitor technology is still behind the batteries and fuel cells concerning their energy density. So, to achieve higher voltage, the concept of the hybrid-structured capacitor is developed, which consists of two electrodes with distinctive mechanisms. Here, one electrode is a battery-type faradaic electrode as an energy source, and the other is a capacitive electrode as a power source [24, 25]. Similar to rechargeable batteries, they play a crucial role in consumer electronics, automotive, aerospace, and stationary markets. There are primarily two types of devices for reversible electrochemical energy storage, secondary batteries, and electrochemical capacitors. The former offers a high energy density, while the latter offers high power and high cyclability. The current dominant energy storage technology is the lithium-ion battery (LIB), which is based on a Li-containing ceramic oxide cathode and a graphite anode. Then only the hybrid supercapacitors will be able to fulfill the high energy and power density and it is well understood from Fig. 3 [26].

The latest use of hybrid supercapacitors is in the emergency door operation and eviction slide operation in the Airbus A380 jumbo jet. The e-bus developed in China by a hybrid configuration of $Ni(OH)_2$-AC. With only 90s charging it can cover a 7.9 km distance with a maximum speed of 44.8 km h^{-1} and an average speed of 22 km h^{-1}. In addition, the tramcar working on EDLC configuration with charging time of 30 s and distance range of 3–5 km has been developed by CSR Co. Ltd. (Chinese) [11].

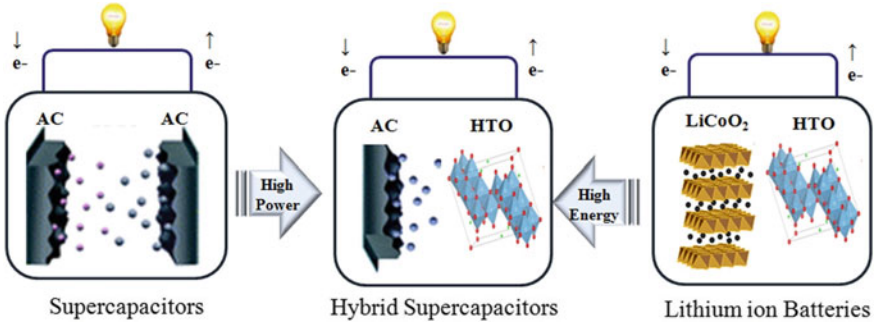

Fig. 3 Concept of different supercapacitors. Activated Carbon (AC) as both cathode and anode is called supercapacitor, while AC cathode with battery-type anode (HTO) called hybrid supercapacitor. When Li based material as cathode and HTO as anode is used called Lithium ion batteries. Adapted from Reference [26], Copyright-The Authors (2018), Springer Nature. Distributed under a Creative Commons Attribution License 4.0 (CC BY)

2.3 Microsupercapacitors

Another intriguing type of SC is micro-supercapacitors (MSCs), which are used as power sources in a wide range of applications. While for the hybrid vehicle, implantable biochips and advanced electronic devices miniaturized power source devices are necessary which provide them required higher power and energy for a longer time. However, they often possess a relatively low (ED) and limited mechanical stretchability. In addition to that, they inevitably suffer from frequent replacement due to their short life span, especially in biomedical and sensor fields. Moreover, micro-batteries are not competent in the cases where high power is needed. Although it has been reported that high power can be output to integrated systems through series and/or parallel connection of batteries, it will inevitably increase the device volume. Recently, renowned metal-free MSCs developed by the Kamboj group have gained substantial attention [28]. The MSC chips are developed by using Laser irradiation (LI) of rGO or ErGO with computer-controlled laser writing methods, which may be helpful for future research.

A metal-free LIG-MSC can be stable up to 100,000 cycles as they have a unique structure, interconnected highly conducting graphene sheets that facilitate ion and electron diffusion. The complete graphitization process is achieved by the combination of electro-reduction and LI reduction, but this process is not so easy and still has challenges to overcome [29–31]. The MSCs reduce the material cost by up to 90% during commercialization. In Fig. 4, the micro supercapacitor developed with different electrode materials shows the bearable current is achieved as compared to commercial electronics and it satisfies the current threshold. So, one can hope for future opportunities on the MSCs [30].

2.4 Photo Supercapacitors (PSC)

Another class of emerging dual-functional devices is photo supercapacitors which consist of hybridization of energy harvesting devices like solar cells, and energy storage system like SCs into a single unit. This kind of integration helps us to increase the efficiency, flexibility, and portability of the fabricated device. Moreover, the integration of a solar cell or dye-sensitized solar cell with a supercapacitor module termed as “self-charging power unit”, can also yield stable power output by simultaneously compensating for the power fluctuation in the commercialized solar cell [32, 33].

Photo capacitors have tremendous potential in flexible electronic, and optoelectronic devices, and as a sustainable self-powered system in portable electronics. However, the integration of supercapacitors with an energy harvester requires a proper power management strategy. Nonetheless, to grasp the full potential of PSC several challenges including the manufacturing and designing of photo capacitors must be addressed. The hybridized devices should be efficiently able to integrate

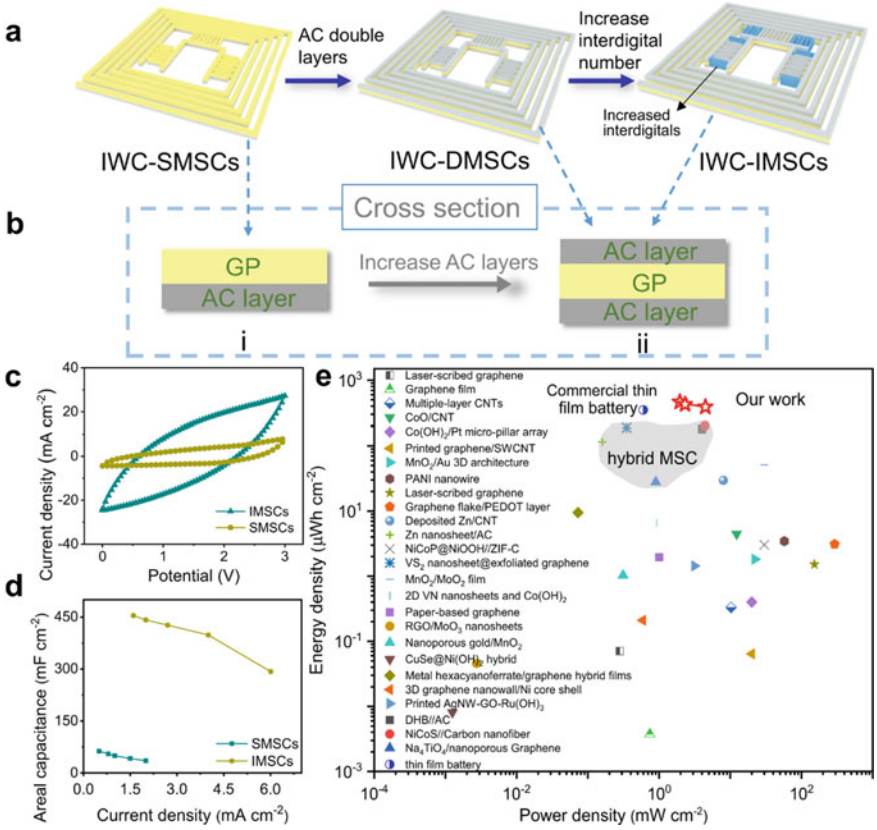

Fig. 4 Schematic representation of Microsupercapacitors and its cross section with comparison cyclic voltammetry curves, rate capacity curves and Ragone plots. "Adapted from Reference [30], Copyright-The Authors (2021), Springer Nature. Distributed under a Creative Commons Attribution License 4.0 (CC BY)"

the individual performance of each unit. This includes that PSC should have similar energy storage capacity and durability as that of a viable supercapacitor, and consequent efficiency should be the same as a commercial solar cell. An inevitable goal would be to eliminate the excess circuitry and consider the reduction of resistive losses in the device. In that regard, a variety of supercapacitor electrode materials are being constantly investigated, to establish which combinations are best suited for such a device. The fabrication of the photo supercapacitor and its design with solid-state electrolyte and electrodes are well studied [34] (Fig. 5).

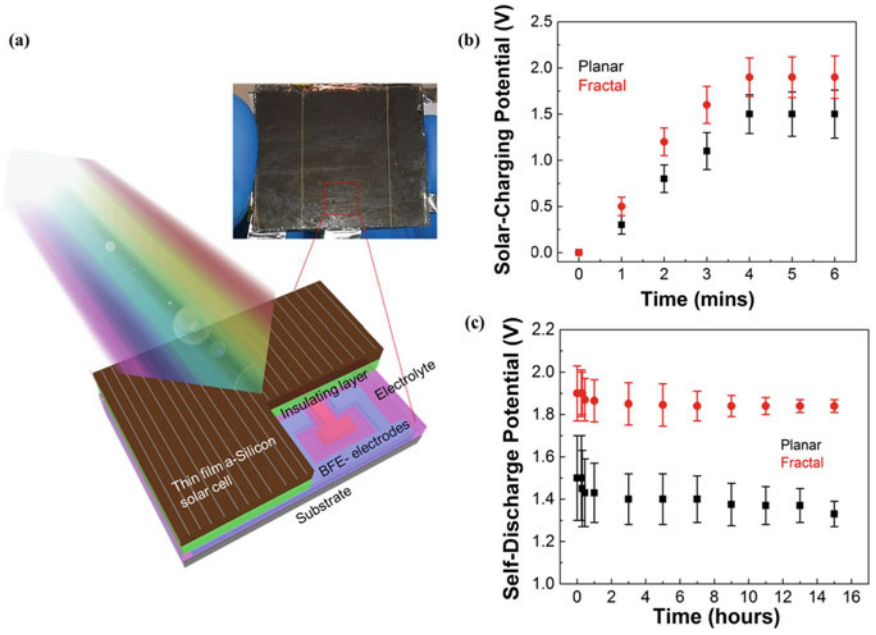

Fig. 5 Schematic presentation of thin film amorphous silicon solar cell with solar charging performance and self-discharge performance. "Adapted from Reference [34], Copyright-The Authors (2017), Springer Nature. Distributed under a Creative Commons Attribution License 4.0 (CC BY)"

2.5 Wearable Supercapacitors

Over the years, flexible and wearable electronic devices, including portable mobile phones, laptops, health monitors, watch bands, electronic sensors have shown an emerging growth in the consumer market sector and are focused to develop flexible, light-weight supercapacitors having [32, 33] promising electrochemical and mechanical performance. Apart from that, the high specific capacitance, storage rate, and improved delamination property, structural flexibility, and appreciable conductivity of electrodes fabricated from the conducting polymers make them suitable for the construction of wearable or stretchable hybrid supercapacitor devices [35]. Flexible MSCs can be employed as the most capable energy storage devices [35–38]. The wearable supercapacitors recently (Fig. 6) developed has shown promising result for the future scope [36]. This will help us to store charges without using bulk storage devices.

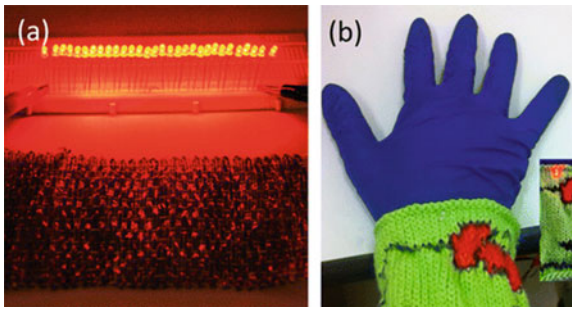

Fig. 6 Photographs of the energy storage textiles made of yarns. **a** The 15 cm × 10 cm woven clothes can light 30 LEDs. **b** A wristband knitted with a pattern (inset shows the pattern powering a LED). Adapted with permission from reference [36], Copyright (2015), American Chemical Society

3 Energy and Electrode Materials

Regardless of the type of device fabrication, the electrochemical performance is mainly determined by charge storage mechanism or faradic process taking place at the interface, one is an electric double layer (EDLC) and the other is pseudo capacitors as presented in Fig. 7. Battery type/supercapattery/hybrid capacitors are recently developed novel supercapacitors. While coming from the material point of view, the search for stable, highly efficient, and promising energy material is still in a nascent stage. The discovery of graphene, MXene, and metal-organic framework gives some hope, but still, they are yet not well established. The detailed study with respect to mathematical modeling and theoretical simulation will be helpful for the establishment of supercapacitor industries. The solution to the high-cost ionic electrolyte or the toxic organic electrolyte is essential to be found out. Supercapattery is an efficient battery-type material, which helps in eradicating the slow kinetics, low cycling stability and diminished performance of ESCs. Due to the intercalating faradic process, they possess high (ED) when compared to EDLC however, they suffer at cost of providing longer cyclic stability, which restricts their overall performance, and practical applications [39]. The Li-ion capacitors (hybrid capacitors)

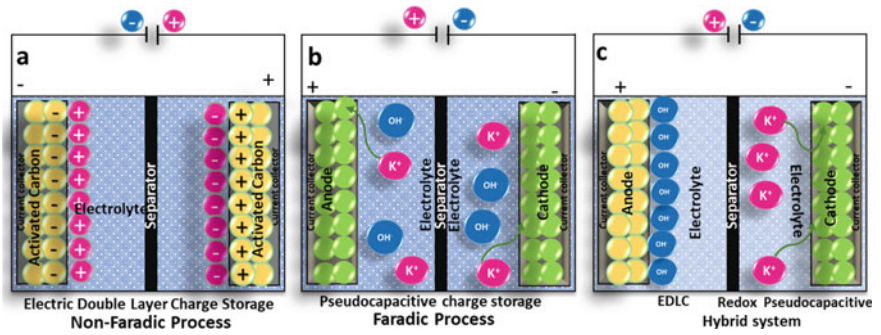

Fig. 7 Schematics presentation of types of supercapacitors: **a** EDLC, **b** pseudocapacitor, and **c** hybrid system

discovered in 2007 has shown promising performance in the field of hybrid capacitors, which further gives hope for the next generation to work on Li-ion capacitor, Na-ion capacitor along with mixed composites hybrid materials. Based on these distinct mechanisms, varied electrode materials are being used for the SCs and how they will be beneficial in the future are discussed. There is an urgent need for the configuration of flexible, lightweight, portable/wearable asymmetric supercapacitor (ASC) devices. The most used ASCs are having major issues such as low mass loadings or the weight of current collector (not flexible or hard, low width) are not favorable for true electrochemical performance, and hence are far from practical implications. However, profound knowledge in synergistic effects/material interactions/supercapacitor technology and optimization of different physical parameters such as mass loading, material composition is required to ensure high-performing ASCs [2, 40].

3.1 EDLC Materials

In EDLC, the storing mechanism involves the formation of two layers in which one is a Helmholtz inner layer and another Helmholtz outer layer. While the EDLC is formed at charged Helmholtz inner monolayer over the surface of electrodes without faradic process or charge transfer between electrodes and electrolytes. The Helmholtz outer layer is formed due to the electrostatic interactions of the opposite charge at the Helmholtz inner layer. However, the enhanced specific capacitance of EDLC is attributed to the surface area of the electrode materials. Carbon nanotubes (CNTs), graphene, graphite, activated carbon– or carbon-based materials show EDLC [41]. Due to the adsorption of electrolytic ions forming a double layer have better storage durability since no faradic processes are involved, which eliminates the adverse effect of the faradic process, and is safer and faster during the discharging–charging process. Using stable, safe high voltage electrolytes, EDLC can be commercialized due to its low economic cost, and wide availability [42].

3.2 Pseudo Capacitor Materials

Pseudo capacitor materials gained recognition as efficient SC electrode materials owing to their enormous surface area, intrinsic conductivity, and highly porous structural organization. Metal oxides (generally transition metal oxides (TMOs)) are used as pseudocapacitors, due to the reversibly fast redox reactions taking place over their interfacial surface region. Out of the widely used TMOs some metal oxides like ruthenium oxide (RuO_2), manganese dioxide (MnO_2), nickel oxide (NiO), cobalt oxide (Co_3O_4), and iron oxide (Fe_2O_3, Fe_3O_4) are very well-acknowledged. These metal oxide-based materials can contribute towards the high-capacity rate, appropriate energy/power density values and perform efficiently as energy storage systems

mainly due to their unique mechanism, which consists of simultaneous adsorption/desorption of electrolytic ion and/or its intercalation. They are proficient as highly efficient SC electrodes and can be utilized as rechargeable batteries or hybrid capacitors.

Indeed, these materials will become more alluring and are expected to provide new growth horizons for energy storage. Exploration in materials will improve the energy densities and overall rate performances and a device based on the pseudocapacitive materials is realized. Figure 8 shows the power density and energy density relationship of asymmetric, symmetric systems, batteries, and other supercapacitors, etc. Another class of electroactive materials that are widely recognized in recent years as SC, on account of their much high energy density, when compared to TMOs are conducting polymers. These are economically viable, easily accessible materials having lesser equivalent series resistance (ESR) that serves as a significant solution in the current research scenario for the development of SC devices [43]. However, they store charges via faradic reactions in the matrix of the polymer and suffer from disadvantages like poor cyclic stability. Some of the important most commonly used conducting polymers (CPs) are polyaniline (PANi), polypyrrole (PPy), and polythiophenes (PTh). Primarily, to enhance the overall performance of the CP-based supercapacitor electrodes, certain properties are needed to be addressed are the crystallinity, and morphology of the as-generated microstructures done usually via modifying the method of polymerization, oxidation rate, type of surfactant's used, and its composition. Besides that, a few other important properties such as thermal durability, and mechanical strength are usually required to meet practical implementation in the market sector.

Apart from the charge storage mechanism the ECs involve symmetric or asymmetric type device fabrication [44]. Symmetric supercapacitors are made of two analogous electrode configurations. Mostly, it involves carbon as active material which shows larger cycle stability due to the interfacial mechanism. The asymmetric

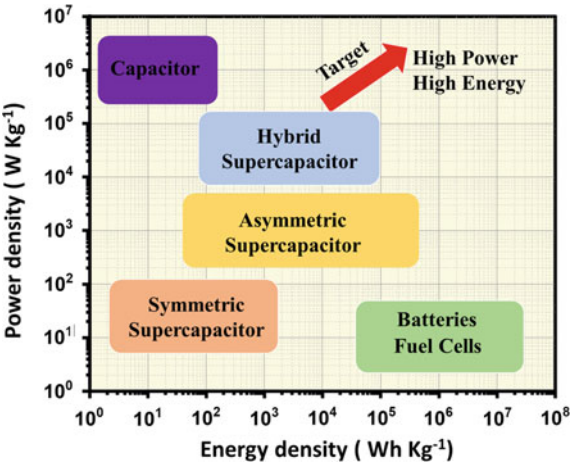

Fig. 8 Energy density and power density of different energy storage devices

system (ASC) is of two dissimilar electrode configuration systems, one is active electrode material, and the other is mostly carbon material with different surface functional groups. In addition to this, the choice of positive and negative electrode need to be optimized with respect to the applied potential window [40].

Still, the ASC has several drawbacks like mediocre electrical conductivity which inhibits the Van der Waal forces and reduces the ion transport. Novel materials such as metal-organic frameworks (MOFs), MXenes, metal nitrides, covalent organic frameworks (COFs), metal sulfide, etc. emerged as the electroactive material for asymmetric systems. There is a thorough study on asymmetric supercapacitors by Kaipannan et al. 2019 as presented in Fig. 9 [45]. Their asymmetric supercapacitor is fabricated by using nickel hexacyanoferrate-derived $Ni(OH)_2$ nanosheets. They have used bio-activated carbon as a carbon source for negative electrodes and they showed how to fabricate the symmetric device and how it can be commercialized. The proper cell assembly, packaging, and application like glowing of LED proved the development of a new supercapacitor electrode material which give a high voltage of 9.6 V, and we can hope this work will help researchers to establish their work on a practical scale.

However, there are enormous number of studies based on the supercapacitor technology, electrode material, electrolyte, device system, and charge storage mechanism in literature. But there are a few critical features that require more attention for the road of commercialization. To manufacture or fabricate a device there are several steps to be achieved. Firstly, a proper electrode should be manufactured with an

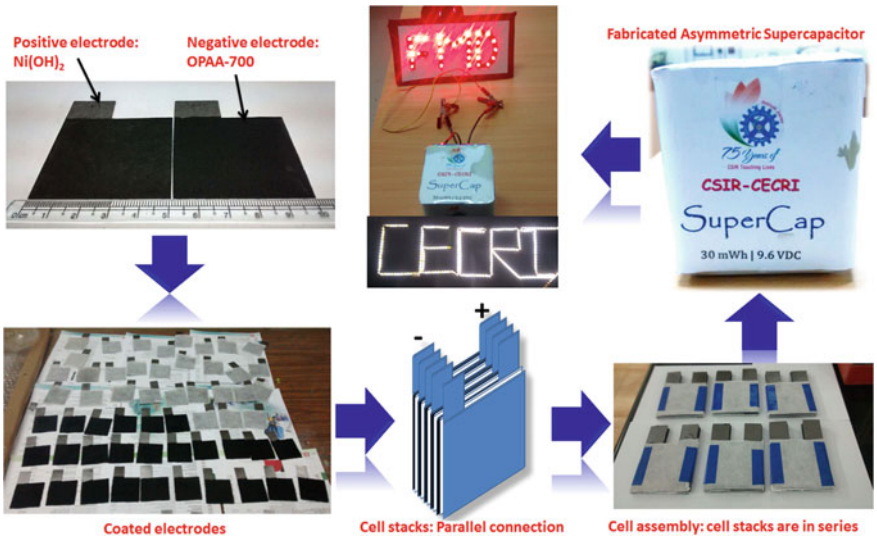

Fig. 9 A step-by-step fabrication of asymmetric supercapacitor device. "Adapted from Reference [45], Copyright-The Authors (2019), Springer Nature. Distributed under a Creative Commons Attribution License 4.0 (CC BY)"

insulating separator soaked in highly conducting electrolytes. Secondly, electrode assembling followed by electrolyte impregnation is the most crucial task.

3.3 Composite Materials

Over the years, varied active materials are being explored vigorously to facilitate the electrochemical efficiency and performance of the SC. Nonetheless, there are numerous associated technical challenges still hampering the progress of ECs and cannot fulfill the practical implications. Compositing EDLC materials with pseudocapacitive materials (metal oxide, and CPs) is a propitious approach to comprehend their synergism for the enhanced energy-storage capacity. These composites can profitably diminish the supposed bridging gap between the metal-ion batteries and SCs. An extensive exploration of these newly emerging composites, having characteristic morphology, and unique architectures arrangement, will impart prospective research for the development of efficient SCs. Moreover, tailoring of electrode materials according to a particular type of electrolyte utilized is also required, and the capability of electrode material in keeping with suitable electrolytes is also required. One such class of materials is metal-organic frameworks (MOFs), having characteristic porosity and tunable pore structure with a regular 3D framework with exceptionally large surface area. But MOFs tend to suffer from insufficient electrical conductivity, to overcome this composite of MOFs with varied carbonaceous materials like carbon nanotubes (CNTs), graphene oxide, etc., is a considerate approach to boost the electronic conductivity. In addition to that, breakthroughs have been achieved in SC applications via novel materials for SC electrodes like MXenes, Metal nitrides/sulfides, Covalent organic framework (COFs). These materials have been studied for the fabrication of highly advanced and efficient supercapacitors [46].

3.4 Electrolyte

The electrolyte is one of the most crucial and substantial components in SC, it is responsible for efficient transportation of charges between the cathode and the anode and affects the cyclic durability, energy/power density, and capacitance rate. As already stated, the development of these newly recognized electrolytes like Ionic liquids (ILs), redox-active, all-solid-state electrolytes has been a solicited solution to storage capacity, an optimal operational voltage of the SCs. Mostly aqueous, organic, inorganic, solid-state redox-active electrolytes are used and need to be modified to prevent poorer electrical conductance, insufficient electrochemical durability, flammable nature, and voltage leak problems. Numerous characterization methods (in situ FT-IR, NMR, Raman) together with theoretical, and modeling simulations are studied or opted for innovative electrolytes [47]. Furthermore, to construct flexible SC devices based on the various polymer-based electrolytes it is condemning to

estimate the mechanical performance of the electrolyte. Lastly, to accomplish excellent performance, and expand SC technologies in the consumer sector of the market, harmony between the newly emerging electrolytes and novel electroactive materials is of paramount importance.

3.5 Current Collector (CC)

Apart from the electrode, and electrolyte, a suitable CC is also a prime requisite for the proficient performance of SCs. Practically speaking, electrochemical performance is affected by the thickness of the substrates. Usually, in the laboratory, the substrates are used only 2–3 mg cm^{-2} of mass loading which exhibits high specific capacitance while coming to industrial-scale the value become worsen and it hampers the overall rate performance of the fabricated SC device.

Again, the electrocatalyst is uniformly coated on a CC's surface, a CC must possess a low contact resistance or charge transfer resistance, along with reasonable electrical conductivity [48]. The CC must be thin with insubstantial weight having vigorous stability, mechanical resistance, and flexibility. Over the years, the majority of current collectors in SC technologies are developed with aluminum, however, due to their high charge transfer resistance alternative sources like carbon cloth, copper foil, nickel foam, are required to diminish the contact resistance, without hampering the overall cost and performance efficacy of SC.

According to Ref. [49], the Cu wire can be a very good substrate for wearable supercapacitors with a flexible textile substrate (Fig. 10a) [49]. Hopefully, this study will diminish the use of carbon sources as negative electrodes will abolish the use

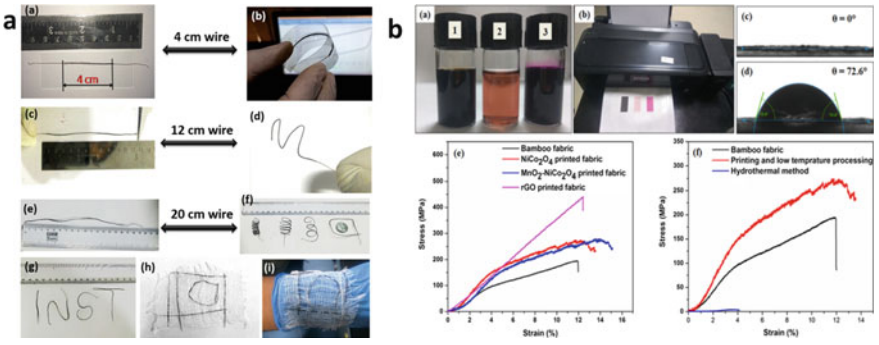

Fig. 10 **a** Flexibility and scalability of textile material for its possible application in textile/wearable devices. "Adapted from Reference [49], Copyright-The Authors (2019), Springer Nature. Distributed under a Creative Commons Attribution License 4.0 (CC BY)". **b** Photograph of printed inks on fabric substrates, with contact angle for stress–strain curves of different fabrics and with different processing methods. "Adapted from Reference [50], Copyright-The Authors (2020), Springer Nature. Distributed under a Creative Commons Attribution License 4.0 (CC BY)"

of liquid electrolytes and the issue of flexible current collectors. Again, the study of ink-printed fabric substrate (Fig. 10b) will also be a good help for the development of flexible substrate. These studies positively bring some new futuristic material for commercialization [50].

4 Future Perspective with the Current Situation

With several expectations in the energy sector, supercapacitors are the most promising and simplistic devices. Initial research was focused only on the development of new energy materials along with the established supercapacitor techniques. With time, it is clearly understood that these are not only the problems, and the supercapacitor technology needs more modifications.

4.1 Supercapacitor Research Advantages and Disadvantages

The supercapacitor can enhance the battery life with a combination of fuel cells which will be beneficial for enhancing efficiency. But the use of organic electrolytes or high-cost electrolytes makes the system unstable and unsafe. The high cost, the voltage drop in aqueous electrolytes, are considerable issues for the large-scale commercialization of supercapacitors [51, 52]. There are several features of ECS like voltage drop, stability, cost, safety still needs to be either modified or new materials/technology needs to be invented. The development of some new materials like highly stable textile materials as working electrodes, solid-state electrolytes, new computational tools are developed, and they give us hope for the future.

4.1.1 New or Futuristic Materials or Substrates and Their Future Aspects

The carbon-free GMS (graphene mesosponge) sheets (less carbon content i.e. 4% of the number present in conventional activated carbons) modified with Al_2O_3 show a high voltage of 3.5 V at ambient temperature with green electrolyte. Hopefully, more research will be done with this material so that the activated carbon and multi-walled carbon nanotubes-free [53] high-voltage supercapacitors can be developed. The toxicity of carbon will be abolished along with no expensive electrolyte or hectic assembling of hybrid type supercapacitors fabricated system will be avoided. Along with MXene, MOFs/COFs should be explored more for the establishment of supercapacitor technology.

4.1.2 Substrates and Conducting Sources

For commercial supercapacitors, the foremost important electrode material precursor is carbon and their allotropes like carbon nanotubes and graphene along with polymers owing to their high conductivity. It is very well known that the carbons and polymers (specially polyaniline) are having high surface area and high conductivity with porous structure, which facilitates the conductivity of the supercapacitor electrode material [54]. This metal-free supercapacitor research gives new directions to the current research. The development of graphene hydrogels [55], 3D Printed materials [56], and favorable carbon sources (Biomass [57]/waste rice [58]/Spent Tea Waste [59, 60]/leaves [61], conducting polymers [62, 63], different peels, woods, etc.) based materials give a new direction to supercapacitor research.

4.2 Technology and Real Devices

The invention of smart supercapacitors or self-healing (identify the damage and immediately repair themselves) supercapacitors are utmost needed [36, 64]. The self-healing of a supercapacitor is one of the best solutions to the current problems of faster charging-discharging problem Although it's a biological phenomenon, the Fe_3O_4@Au/polyacrylamide (MFP) hydrogel-based electrodes and electrolyte materials developed by Yu and his group [64] shows this kind of unique behavior. Also, the development of some smart shape fiber or electrochromic supercapacitors is another necessity for industrial application. The high electrical conducting, more stretchable, good energy storage capability flexible fiber polymers with multi-functionalities, are used in the development of smart shape-memory supercapacitors [32, 65].

Mostly the wearable and flexible supercapacitors are emerged with superior electrochemical and mechanical performances. Despite several advantages, these are also having some lacuna like the need for carbon sources for enhancement of conductivity, and optimization of electrodes for the device fabrication. Colossal substantial efforts are made to develop highly conductive energy storage electrodes with high energy density but still, it is highly enticing to commercialize the material. However, the shortage or production of conductive yarns for industrial-scale limits the wide-scale application of textiles. Despite the achievements made in flexible and wearable MScs some issues need to be addressed. Photocapacitors have emerged as advanced, encouraging self-sufficient energy devices which unite the greener solar cells and supercapacitors for simultaneous energy conversion and storage. It is one of the greener devices which may be helpful for the remediation of energy scarcity by converting light into an electrical signal.

4.3 Industrial Precautions or Technical Challenges

Over the years, the fabrication/development of supercapacitors as per the industrial standards is the most important factor for its research. SCs are capable to deliver massive power within a limited span of time-long life with a faster discharge rate but suffer lesser stability. Therefore, the high durability performance without any loss in charge storage ability is inevitably required. In the last three decades, many other applications have developed such as portable wireless communication, power sources for industries, power generation systems, and hybrid electric vehicles. There are several supercapacitor industries currently trying to improve the electrical parameters of supercapacitors such as Panasonic, Cooper, Fuji Heavy Industries, Maxwell, AVX corporation, Elna (USA), Power Systems (Japan), EL Technology (Russia) LS EPCOS (Germany), Cable (South Korea), Cap-XX (Australia), Tavrima (Canada) and many more.

For the laboratory scale research or publishing the data, the low mass loading, aqueous electrolyte, expensive non-abundant material can be accepted, but when coming to the storage device system the reverse would be expected. The manufacturing cost should be reduced by avoiding low-cost material as it is almost 10 times higher than batteries and electrolytes. Another critical thing is to analyze the design, and charge storage mechanism of supercapacitors via theoretical aspect or computational view [5, 66]. A continuing expansion of the global supercapacitor market (Fig. 11) can be observed that China has surpassed all other countries. However, from laboratory to industrial scale supercapacitor fabrication is still the major barrier. The supercapacitor was commercialized with a maximum voltage of 2.7 V, maximum power density of 23,275 Wh kg^{-1} and working efficiency of 95% [20].

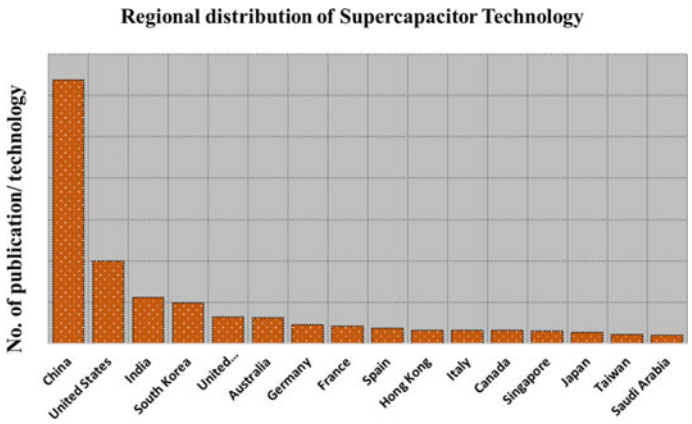

Fig. 11 Distribution of supercapacitor technology worldwide. (*Data source* Scopus)

4.3.1 Computational Tools

The fundamental knowledge, which will provide a comprehensible understanding of the structural organization of these advanced materials, is also vital. Recently, computational techniques such as molecular dynamic (MD) simulation/modeling, density functional theory (DFT) have been developed to rationalize a better performing SC device and thus provide a thorough understanding of the charge storage mechanism [67]. These DFT studies elaborate the perception about the capacitance contribution due to the pore size in double-layer materials and solvation of electrolytic ions in the charging and discharging mechanism of SCs. The MD simulations can quantify various models associated with interfacial contact of electrode and electrolyte. Nonetheless, these technologies still lack admiration for the highly advanced and novel composite SC materials based on the pseudocapacitive and EDLC type. Therefore, an extensive conception of the charge storage mechanism for SC based on these simulation techniques might help to develop new-generation devices with significantly high and improved performance.

4.3.2 Consistency Detection

The advance, stable, high current, and faster charging–discharging supercapacitors are essential for technical execution. So, consistency is one of the most important factors for supercapacitor technology. Even though overcharging and unstable ECs have created life-threatening problems. Proper sealing or packaging is vital to prevent the performance loss of supercapacitors. There are several parameters such as weighing, appearance, charge–discharge curve, open-circuit voltage, and internal resistance, which are inconsistent. So, after normalizing this characteristic information of dynamic data in power performance and life cycle of supercapacitors can be enhanced [66, 68].

4.3.3 Reliability of Supercapacitors

Reliability is another important property that is necessarily required for the commercialization of supercapacitors. The basic properties like mechanism, design, statistics based on operation data need to be evaluated carefully for real-time application. It is a known fact that sometimes the fabricated device does not perform well while its root cause and failure should be analyzed. While the life span and life cycle cost of electrical ECs, ambiguities in cost data and technical parameters must be carefully analyzed. The failure of commercialized capacitors always faces capacitance loss, series resistance, leakage, and opening of capacitors [69, 70]. Although some statistical models may help develop test groups and lifetime of supercapacitors as suggested by Kobyashi et al. 1984 Weibull cycle life [68]. The electrochemical supercapacitor functionality is mostly dependent on the circuit, so with the dead circuit, the supercapacitor may collapse. The control of electrolyte flow, cell rupture, and

packaging will control the failure or death of the supercapacitor. The cell reliability assessment further generates hope for future application.

4.3.4 Protocols

There are some protocols or procedures for any industrial application. Similarly, supercapacitor technology should follow some standard rules like the basic mechanism of the component and materials, the reliability, degradation performance, life span of the device, the physical phenomena like temperature resistance, voltage resistance, engineering of the device, electronics parts, performance of all components, device physics, and failure mechanisms. Before final application, the device must be tested extensively. The lifetime of the supercapacitors must be studied and estimated. The safety parameters and care must be taken for circuit designing and following safety parameters which leads to the success of supercapacitors for potential application and the future perspective aspect.

4.4 Strategies

The bigger electric vehicles or e-buses introduced by Aowei Technology Co., Ltd. (Shanghai, China) and "Capabus" in 2006 the worldwide research is motivated for basic research with practical visions, which further symbolizes the bright prospects of supercapacitors. Some common terms associated with supercapacitor technology like self-discharge, packaging, high voltage, temperature resistance, advanced energy storage low-cost materials has gained serious attention and some basic strategy should be followed. Therefore, a well-organized strategy is much needed for the development of supercapacitor technology to solve the practical energy issue from the future perspective.

First, SCs technology should be developed identical to a wearable supercapacitor, photo supercapacitors, hybrid supercapacitors, so that further commercialization will be feasible. The natural unending sources such as water, solar, air must be helpful in the development of energy storage devices. The miniaturized electrochemical storage device in form of micro supercapacitor (MSC), wearable, self-healing, supercapacitor offers a larger power density which may be simple for transportation. The flexible/wearable devices should be designed by following computational tools and industrial protocols. The fundamental knowledge and charge storage mechanism should be well understood by the researchers so that the failure, short circuit, self-discharge, series resistance will be avoided.

Then moving on to data analysis, it should be perfect and well-studied. Some low-cost energy material synthesis techniques likely electrospinning, microwave, hydrothermal, coprecipitation should be developed or followed to avoid multiple chaotic steps. This will further support the MXene, MOFs to abolish conductivity, inhibit the aggregation, volume expansion, structural scaffolds, etc. issues. For the

commercialization point, the reliable electrochemical analysis data should come from the two electrode or asymmetric device system with higher mass loading and flexible electrode, which can further reinforce the large-scale industrial production of SCs without capacitance loss. The solid-state electrolytes or aqueous binders will be favorable for better supercapacitor fabrication. The development of non-flammable and non-toxic electrolytes will be a boon for supercapacitor technology.

Further, the problem associated with supercapacitors like self-discharge, voltage loss or low voltage, resistance, packaging, electrolyte, stability, sustainability, and flexibility should be resolved for the appropriate SC technology. Self-discharge which means the loss of stored energy at higher temperatures is the biggest drawback for supercapacitors. The parasitic redox reactions occurred at the electrode and electrolyte interface and the short circuit may cause self-discharge. That problem will be diminished using some battery material as for Lithium-ion battery. The coupling of the supercapacitor will provide a larger density which will minimize the self-discharge. Still, the coupling is not easier, but with this self -discharge can be controlled [42].

Energy is directly proportional to the capacitance and square of the applied voltage. Therefore, a strategy is needed for the increase in both capacitance and voltage. While another most important parameter, the equivalent series resistances (ESR) of the device/cell should be controlled. ESR of supercapacitor should be very low, by controlling the surface of the active material and current collectors, which also minimizes the Ohmic drop. Once the operation voltage is too high especially in an aqueous electrolyte, the electrolyte decomposed so fast leading to self-discharge. Restrained self-discharge can be achieved through the migration of charges in the obstructed electric double layer. EDL between two electrodes is hindered, the suppressed self-discharge is achieved [71, 72]. There are lots of techniques that are evaluated but now it's time to standardize the evaluation procedures with respect to the industrial application for determining the capacitance and resistance of devices by achieving higher energy and power density.

In the aspect of safety operation, high/low-temperature supercapacitor devices will be more helpful. The performance of conventional capacitors due to sluggish ion and charge transport often deteriorates with decreasing or increasing temperature. The commercial supercapacitors developed by AVX Corporation can be reached up to 175 °C. But by increasing the ionic mobility of ionic liquid electrolytes, they can be stable up to 200 °C [72]. So, research can be focused on the use of solid-state electrolytes [73] and 3D-printed aerogel for low-temperature supercapacitors [74].

The supercapacitors should be moisture free and proper sealing must be done to avoid performance failure. They must be prevented from impurities (air and water) from further degradation and surface oxidation on electrodes, or short circuit in cells. The multiple connections of supercapacitors to achieve high voltage must be avoided which may enhance the resistance and overall efficiency of the device. Therefore, packaging plays a vital role that needs to be carefully managed. The use of polymeric material with electrical insulation and moisture resistance property may provide mechanical stability/flexibility.

5 Concluding Remarks

The exhilarating development of energy storage devices like supercapacitors and batteries has dragged the attention of energy storage research from the last two decades, with numerous applications such as portable electronic devices, hybrid electric vehicles, industrial-scale power production, and energy management. In this view, this chapter deals with the advanced energy storage materials development towards the preparation of electrodes for supercapacitors for commercialization. After a short introduction to energy storage systems/devices, the history and mechanism of supercapacitors are discussed. Then the current research going on with the development of various supercapacitors and their future aspects are discussed and explained. The portable and flexible cutting-edge electronics are strongly required to develop next-generation reasonable, ultra-flexibility, small dimension, and sustainable energy storage systems. Enormous studies are still going on. The MXene, MOFs, COFs, metal oxides/sulfides needs more attention and care before further processing. One important aspect of data interpretation should be perfect and with respect to theoretical calculation. Also, computational tools should be obtained before expansion. We have summarized the future perspective of supercapacitors in Fig. 12. The knowledge of the mechanism, types of supercapacitors, and device fabrication is

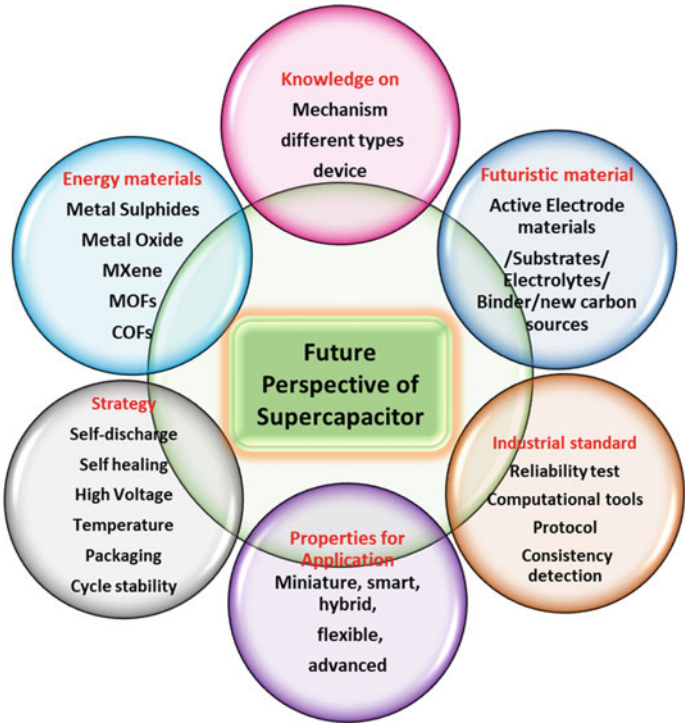

Fig. 12 Future perspective of supercapacitors

much needed or the preliminary requirements of supercapacitor technology development. The industrial standards must be followed with some unique strategies. The miniature, hybrid, smart, flexible supercapacitors can be developed with the current technology and energy materials. So, we can expect a proper strategy for the development of energy material and electrolytes, and by following industrial protocol, the recently developed supercapacitors will be established.

Acknowledgements The authors are thankful to IIT Delhi for their permission to write the book chapter. RB is grateful to Institute Postdoctoral Fellowship provided by IIT Delhi. VT is thankful to MHRD for PMRF Fellowship. PPI is thankful to the Ministry of Science and Technology, India for the financial support under the grant Materials for energy storage (DST-MES) vide sanction order No. DST/TMD/MES/2K17/99(G).

References

1. F. Wang, X. Wu, X. Yuan, Z. Liu, Y. Zhang, L. Fu, Y. Zhu, Q. Zhou, Y. Wu, W. Huang, Latest advances in supercapacitors: from new electrode materials to novel device designs. Chem. Soc. Rev. **46**(22), 6816–6854 (2017)
2. W. Guo, C. Yu, S. Li, J. Qiu, Toward commercial-level mass-loading electrodes for supercapacitors: opportunities, challenges and perspectives. Energy Environ. Sci. **14**(2), 576–601 (2021)
3. N. Wu, X. Bai, D. Pan, B. Dong, R. Wei, N. Naik, R.R. Patil, Z. Guo, Recent advances of asymmetric supercapacitors. Adv. Mater. **8**, 2001710 (2021)
4. C. Lethien, J.L. Bideau, T. Brousse, Challenges and prospects of 3D micro-supercapacitors for powering the internet of things. Energy Environ. Sci. **12**(1), 96–115 (2019)
5. S. Huang, X. Zhu, S. Sarkar, Y. Zhao, Challenges and opportunities for supercapacitors. APL Mater. **7**(10), 100901 (2019)
6. X.Y. Yu, X.W. Lou, Mixed metal sulfides for electrochemical energy storage and conversion. Adv. Energy Mater. **8**(3), 1–37 (2018)
7. C. Zhao, W. Zheng, A review for aqueous electrochemical supercapacitors. Front. Energy Res. **3**, 23 (2015)
8. Q. Gou, S. Zhao, J. Wang, M. Li, J. Xue, Recent advances on boosting the cell voltage of aqueous supercapacitors. Nano-Micro Lett. **12**(1), 1–22 (2020)
9. R. Barik, P.P. Ingole, Challenges and prospects of metal sulfide materials for supercapacitors. Curr. Opin. Electrochem. **21**, 327–334 (2020)
10. P. Simon, Y. Gogotsi, Perspectives for electrochemical capacitors and related devices. Nat. Mater. **19**, 1151–1163 (2020)
11. J. Ding, W. Hu, E. Paek, D. Mitlin, Review of hybrid ion capacitors: from aqueous to lithium to sodium. Chem. Rev. **118**(14), 6457–6498 (2018)
12. A. Eftekhari, The mechanism of ultrafast supercapacitors. J. Mater. Chem. A **6**(7), 2866–2876 (2018)
13. T.S. Mathis, N. Kurra, X. Wang, D. Pinto, P. Simon, Y. Gogotsi, Energy storage data reporting in perspective-guidelines for interpreting the performance of electrochemical energy storage systems. Adv. Energy Mater. **9**(39), 1–13 (2019)
14. J. Wang, J. Polleux, J. Lim, B. Dunn, Pseudocapacitive contributions to electrochemical energy storage in TiO_2(anatase) nanoparticles. J. Phys. Chem. C **111**(40), 14925–14931 (2007)
15. S. Ardizzone, G. Fregonara, S. Trasatti, "Inner" and "Outer" active surface of RuO, electrodes. Electrochem. Acta **35**, 263–267 (1990)

16. J.J.S. Teles, E.R. Faria, D.V. Franco, L.M. Da Silva, Inner and outer surface areas, electrochemical porosity, and morphology factor of mixed oxide-covered mesh electrodes with a nominal composition of MOME-$Sn_{0.5}Ir_xRu_{(0.5-x)}O_2$. Int. J. Electrochem. Sci. **12**, 1755–1773 (2017)
17. P. Yu, C. Li, X. Guo, Sodium storage and pseudocapacitive charge in textured $Li_4Ti_5O_{12}$ thin films. J Phys. Chem. C **118**(20), 10616–10624 (2014)
18. B. Anasori, M.R. Lukatskaya, Y. Gogotsi, 2D metal carbides and nitrides (MXenes) for energy storage. Nat. Rev. Mater. **2**(2), 16098 (2017)
19. M. Hu, H. Zhang, T. Hu, B. Fan, X. Wang, Z. Li, Emerging 2D MXenes for supercapacitors: status, challenges and prospects. Chem. Soc. Rev. **49**(18), 6666–6693 (2020)
20. D.-G. Wang, Z. Liang, S. Gao, C. Qu, R. Zou, Metal-organic framework-based materials for hybrid supercapacitor application. Coord. Chem. Rev. **404**, 213093 (2020)
21. S. Zheng, Q. Li, H. Xue, H. Pang, Q. Xu, A highly alkaline-stable metal oxide@metal-organic framework composite for high-performance electrochemical energy storage. Nat. Sci. Rev. **7**, 305–314 (2020)
22. D. Chen, Q. Wang, R. Wang, G. Shen, Ternary oxide nanostructured materials for supercapacitors: a review. J. Mater. Chem. A **3**(19), 10158–10173 (2015)
23. W. Cai, T. Lai, J. Lai, H. Xie, L. Ouyang, J. Ye, C. Yu, Transition metal sulfides grown on graphene fibers for wearable asymmetric supercapacitors with high volumetric capacitance and high energy density. Sci. Rep. **6**, 26890 (2016)
24. D.P. Chatterjee, A.K. Nandi, A review on the recent advances in hybrid supercapacitors. J. Mater. Chem. A **9**(29), 15880–15918 (2021)
25. L. Dong, Y. Wang, Y. Wu, L. Yang, W. Wenjian, W.G. Wang, Multivalent metal ion hybrid capacitors: a review with a focus on zinc-ion hybrid capacitors. J. Mater. Chem. A **7**(23), 13810–13832 (2019)
26. S.-H. Lee, J.-H. Kim, J.-R. Yoon, Laser scribed graphene cathode for next generation of high performance hybrid supercapacitors. Sci. Rep. **8**, 8179 (2018)
27. R. Barik, A.K. Yadav, S.N. Jha, D. Bhattacharyya, P.P. Ingole, Two-dimensional tungsten oxide/selenium nanocomposite fabricated for flexible supercapacitors with higher operational voltage and their charge storage mechanism. ACS Appl. Mater. Interfaces **13**, 8102–8119 (2021)
28. N. Kamboj, T. Purkait, M. Das, S. Sarkar, K.S. Hazra, R.S. Dey, Ultralong cycle life and outstanding capacitive performance of a 10.8 v metal free micro-supercapacitor with highly conducting and robust laser-irradiated graphene for an integrated storage device. Energy Environ. Sci. **12**(8), 2507–2517 (2019)
29. J. Chmiola, C. Largeot, P.-L. Taberna, P. Simon, Y. Gogotsi, Monolithic carbide-derived carbon films for micro-supercapacitors. Science **328**(5977), 480–483 (2010)
30. C. Gao, J. Huang, Y. Xiao, G. Zhang, C. Dai, Z. Li, Y. Zhao, L. Jiang, L. Qu, A seamlessly integrated device of micro-supercapacitor and wireless charging with ultrahigh energy density and capacitance. Nat. Commun. **12**(1), 1–10 (2021)
31. C. Zhang, Z. Peng, C. Huang, B. Zhang, C. Xing, H. Chen, H. Cheng, J. Wang, S. Tang, High-energy all-in-one stretchable micro-supercapacitor arrays based on 3D laser-induced graphene foams decorated with mesoporous ZnP nanosheets for self-powered stretchable systems. Nano Energy **81**, 105609 (2021)
32. K. Guo, N. Yu, Z. Hou, L. Hu, Y. Ma, H. Li, T. Zhai, Smart supercapacitors with deformable and healable functions. J. Mater. Chem. A **5**(1), 16–30 (2017)
33. T. Miyasaka, T.N. Murakami, The photocapacitor: an efficient self-charging capacitor for direct storage of solar energy. Appl. Phys. Lett. **85**(17), 3932–3934 (2004)
34. V.L. Thekkekara, M. Gu, Bioinspired fractal electrodes for solar energy storages. Sci. Rep. **7**, 4558 (2017)
35. J. Gong, J.-C. Li, J. Yang, S. Zhao, Z. Yang, K. Zhang, J. Bao, H. Pang, M. Han, High-performance flexible in-plane micro-supercapacitors based on vertically aligned CuSe@$Ni(OH)_2$ hybrid nanosheet films. ACS Appl. Mater. Interfaces **10**(44), 38341–38349 (2018)

36. Y. Huang, H. Hu, Y. Huang, M. Zhu, W. Meng, C. Liu, Z. Pei, C. Hao, Z. Wang, C. Zhi, From industrially weavable and knittable highly conductive yarns to large wearable energy storage textiles. ACS Nano **9**(5), 4766–4775 (2015)
37. R. Jia, G. Shen, F. Qu, D. Chen, Flexible on-chip micro-supercapacitors: Efficient power units for wearable electronics. Energy Storage Mater. **27**, 169–186 (2020)
38. N. Yu, H. Yin, W. Zhang, Y. Liu, Z. Tang, M.-Q. Zhu, High-performance fiber-shaped all-solid-state asymmetric supercapacitors based on ultrathin MnO_2 nanosheet/carbon fiber cathodes for wearable electronics. Adv. Energy Mat. **6**, 1501458 (2016)
39. L. Yu, G.Z. Chen, Supercapatteries as high-performance electrochemical energy storage devices. Electrochem. Energ. Rev. **3**(2), 271–285 (2020)
40. N. Choudhary, C. Li, J. Moore, N. Nagaiah, L. Zhai, Y. Jung, J. Thomas, Asymmetric supercapacitor electrodes and devices. Adv. Mater. **29**(21), 1605336 (2017)
41. H. Jiang, P.S. Lee, C. Li, 3D carbon based nanostructures for advanced supercapacitors. Energy Environ. Sci. **6**(1), 41–53 (2013)
42. A. González, E. Goikolea, J.A. Barrena, R. Mysyk, Review on supercapacitors: Technologies and materials. Renew. Sustain. Energy Rev. **58**, 1189–1206 (2016)
43. Q. Meng, K. Cai, Y. Chen, L. Chen, Research progress on conducting polymer based supercapacitor electrode materials. Nano Energy **36**, 268–285 (2017)
44. Y. Shao, M.F. El-Kady, J. Sun, Y. Li, Q. Zhang, M. Zhu, H. Wang, B. Dunn, R.B. Kaner, Design and mechanisms of asymmetric supercapacitors. Chem. Rev. **118**(18), 9233–9280 (2018)
45. S. Kaipannan, S. Marappan, Fabrication of 9.6 v high performance asymmetric supercapacitors stack based on nickel hexacyanoferrate-derived $Ni(OH)_2$ nanosheets and bioderived activated carbon. Sci. Rep. **9**, 1104 (2019)
46. X. Gao, Y. Dong, S. Li, J. Zhou, L. Wang, B. Wang, MOFs and COFs for batteries and supercapacitors. Electrochem. Energ. Rev. **3**, 81–126 (2020)
47. B. Pal, S. Yang, S. Ramesh, V. Thangadurai, R. Jose, Electrolyte selection for supercapacitive devices: a critical review. Nanoscale Adv. **1**, 3807–3835 (2019)
48. G.F. Yang, K.Y. Song, S.K. Joo, A metal foam as a current collector for high power and high capacity lithium iron phosphate batteries. J. Mater. Chem. A **2**, 19648–19652 (2014)
49. T. Purkait, G. Singh, D. Kumar, M. Singh, R.S. Dey, High-performance flexible supercapacitors based on electrochemically tailored three-dimensional reduced graphene oxide networks. Sci. Rep. **8**, 640 (2018)
50. P. Sundriyal, S. Bhattacharya, Textile-based supercapacitors for flexible and wearable electronic applications. Sci. Rep. **10**, 13259 (2020)
51. A. Du Pasquier, I. Plitz, S. Menocal, G. Amatucci, A comparative study of Li-ion battery, supercapacitor and nonaqueous asymmetric hybrid devices for automotive applications. J. Power Sources **115**(1), 171–178 (2003)
52. V. Paladini, T. Donate, A. Risi, D. Laforgia, Super-capacitors fuel-cell hybrid electric vehicle optimization and control strategy development. Energy Convers. Manag. **48**(11), 3001–3008 (2007)
53. K. Nomura, H. Nishihara, N. Kobayashi, T. Asada, T. Kyotani, 4.4 V Supercapacitors based on super-stable mesoporous carbon sheet made of edge-free graphene walls. Energy Environ. Sci. **12**(5), 1542–1549 (2019)
54. F. Li, X. Wang, R. Sun, A metal-free and flexible supercapacitor based on redox-active lignosulfonate functionalized graphene hydrogels. J. Mater. Chem. A **5**(39), 20643–20650 (2017)
55. N. Blomquist, T. Wells, B. Andres, J. Bäckström, S. Forsberg, H. Olin, Metal-free supercapacitor with aqueous electrolyte and low-cost carbon materials. Sci. Rep. **7**, 1–7 (2017)
56. X. Aeby, A. Poulin, G. Siqueira, M.K. Hausmann, G. Nyström, Fully 3d printed and disposable paper supercapacitors. Adv. Mater. **2101328**, 1–9 (2021)
57. Z. Zhang, S. Yang, H. Li, Y. Zan, X. Li, Y. Zhu, M. Dou, F. Wang, Sustainable carbonaceous materials derived from biomass as metal-free electrocatalysts. Adv. Mater. **31**(13), 1805718 (2019)

58. K.K. Yadav, R. Wadhwa, N. Khan, M. Jha, Efficient metal-free supercapacitor based on graphene oxide derived from waste rice. Current Res. Green Sustain. Chem. **4**, 100075 (2021)
59. C. Peng, X.-b. Yan, R.-t.Wang, J.-w. Lang,Y.-j. Ou, Q.-j. Xue, Promising activated carbons derived from waste tea-leaves and their application in high performance supercapacitors electrodes. Electrochim. Acta **87**, 401–408 (2013)
60. S. Bhoyate, P.K. Kahol, R.K. Gupta, Nanostructured materials for supercapacitor applications. SPR Nanosci. **5**, 1–29 (2019)
61. M. Biswal, A. Banerjee, M. Deo, S. Ogale, From dead leaves to high energy density supercapacitors. Energy Environ. Sci. **6**(4), 1249–1259 (2013)
62. N. Kurra, R. Wang, H.N. Alshareef, All conducting polymer electrodes for asymmetric solid-state supercapacitors. J. Mater. Chem. A **3**(14), 7368–7374 (2015)
63. Y. Wang, Y. Ding, X. Guo, G. Yu, Conductive polymers for stretchable supercapacitors. Nano Res. **12**(9), 1978–1987 (2019)
64. H. Qin, P. Liu, C. Chen, H.-P. Cong, S.-H. Yu, A multi-responsive healable supercapacitor. Nat. Commun. **12**(1), 4297 (2021)
65. X. Wang, Q. Lu, C. Chen, M. Han, Q. Wang, H. Li, Z. Niu, J. Chen, A consecutive spray printing strategy to construct and integrate diverse supercapacitors on various substrates. ACS Appl. Mater. Interfaces **9**(34), 28612–28619 (2017)
66. M. Yassine, D. Fabris, Performance of commercially available supercapacitors. Energies **10**(9), 1340 (2017)
67. D.A.C. da Silva, A.J.P. Neto, A.M. Pascon, E.E. Fileti, L.R.C. Fonseca, H.G. Zanin, Combined density functional theory and molecular dynamics simulations to investigate the effects of quantum and double-layer capacitances in functionalized graphene as the electrode material of aqueous-based supercapacitors. J. Phys. Chem. C **125**(10), 5518–5524 (2021)
68. M. Kobayashi, N. Colaneri, M. Boysel, F. Wudl, A.J. Heeger, The electronic and electrochemical properties of poly(isothianaphthene). J. Chem. Phys. **82**(12), 5717–5723 (1984)
69. A. Muzaffar, M.B. Ahamed, K. Deshmukh, J. Thirumalai, A review on recent advances in hybrid supercapacitors: design, fabrication and applications. Renew. Sustain. Energy Rev. **101**, 123–145 (2019)
70. J. Liu, Y. Zhou, Z. Xie, Y. Li, Y. Liu, J. Sun, Y. Ma, O. Terasaki, L. Chen, Conjugated copper–catecholate framework electrodes for efficient energy storage. Angew. Chem. Int. Ed. **59**, 1081–1086 (2020)
71. A. Borenstein, O. Hanna, R. Attias, S. Luski, T. Brousse, D. Aurbach, Carbon-based composite materials for supercapacitor electrodes: a review. J. Mater. Chem. A **5**(25), 12653–12672 (2017)
72. R.S. Borges, A.L.M. Reddy, M.-T.F. Rodrigues, H. Gullapalli, K. Balakrishnan, G.G. Silva, P.M. Ajayan, Supercapacitor operating at 200 degrees celsius. Sci. Rep. **3**, 2572 (2013)
73. L.W. Le Fevre, A. Ejigu, R. Todd, A.J. Forsyth, R.A.W. Dryfe, High temperature supercapacitors using water-in-salt electrolytes: stability above 100 °C. Chem. Commun. **57**(43), 5294–5297 (2021)
74. B. Yao, H. Peng, H. Zhang, J. Kang, C. Zhu, G. Delgado, D. Byrne, S. Faulkner, M. Freyman, X. Lu, M.A. Worsley, J.Q. Lu, Y. Li, Printing porous carbon aerogels for low temperature supercapacitors. Nano Lett. **21**(9), 3731–3737 (2021)